U.S. Army Corps of Engineers
Walla Walla District

Lower Snake River Programmatic Sediment Management Plan, Final Environmental Impact Statement

Appendix F - Hydrology and Hydraulics, Lower Granite Reservoir Sedimentation Analysis and Lewiston Levee Flood Risk Analysis

August 2014







Lower Snake River Programmatic Sediment Management Plan Environmental Impact Statement

Appendix F

Hydrology and Hydraulics
Lower Granite Reservoir Sedimentation Analysis and Lewiston Levee Flood Risk Analysis

Part 1

Prepared by:

U.S. Army Corps of Engineers
Walla Walla District

August 2014

Table of Contents

1. Introduction and Findings 13
1.1. Project Setting 14
1.2. Scope of the Hydraulics and Hydrology Investigation 16
1.3. Major Findings of the Hydraulics and Hydrology Analysis 17
2. Multivariate Discharge Frequency Analysis 22
2.1. Discharge and Stage Data 23
2.2. Historic Floods at Lower Granite 25
2.3. Discharge Characteristics of the Tributary Rivers 27
2.4. Correlation of Tributary Discharges 33
2.5. Regional Skew Comparison 40
2.6. Climatic Patterns 43
2.7. Univariate Flood Frequency Analysis 53
2.8. Joint Probability-Multivariate Analysis of Coincident Discharge 56
2.9. Joint Probability of Exceedance for Flow Distribution 65
2.10. Simplified Multivariate Analysis of Total Probability 70
2.11. Extended Multivariate Analysis of Total Probability 71
2.12. Summary of the Discharge Frequency Analysis 77
3. Variability of Observed Stage at the Confluence 78
4. Fixed-Bed Hydraulic Modeling of Flood Stage 82
4.1. Channel Elevation Data 83
4.2. Overbank and Floodplain Elevation Data 85
4.3. Top-of-Levee Elevation Data 85
4.4. Bridge Geometric Data 86
4.5. Reservoir Water Control 86
4.6. Channel Characterization 90
4.7. Historic one-dimensional hydraulic models 91
4.8. Hydraulic Model Reach and Cross Section Development 94
4.9. HEC-RAS Model Calibration 98
4.10. Empirical Estimates of Manning's n 104
4.11. Confluence Junction Headloss 107
5. Flood Risk Analysis – Existing Channel Condition 110

5.1. Exceedance Discharges for the FDA Analysis 110
5.2. Discharge Uncertainty 112
5.3. Index Sections 112
5.4. Downstream Boundary Condition 112
5.5. Index Rating Curves 113
5.6. Stage Uncertainty 115
5.7. Hydraulic Flow Resistance 116
5.8. Water Surface Profiles 116
5.9. Comparison with the SPF Water Surface Profile 117
5.10. Assurance - Conditional Non-Exceedance Probabilities – 2009 Fixed-Bed Model 121
5.11. Potential for Geotechnical Failure of the Levees 125
5.12. Potential for Induced Flooding 125
5.13. SPF in the Flood Risk Analysis 129
5.14. Summary of the Risk Analysis of Current Condition 130
5.15. Flood Risk Analysis of Future Channel Conditions and Channel Modification Alternatives 130
6. Potential Inundation Area of the Lewiston Levee System 131
6.1. Potential Inundation of Lewiston South of the Clearwater River 131
6.2. Potential Inundation of Lewiston North of the Clearwater River 132
7. Lower Granite Reservoir Sedimentation 137
7.1. Sediment Ranges 137
7.2. Sediment Range Analysis 143
7.3. Net Sediment Accumulation Volume 148
7.4. Dredge Material Volumes 151
7.5. Total Sediment Accumulation Volume 152
7.6. Sediment Yield Estimate 154
7.7. Sediment Distribution in Lower Granite Reservoir 154
7.8. Sediment Accumulation at the Mouth of the Palouse River 156
8. Lower Granite Reservoir Bed Material 159
8.1. Sediment Core Survey 159
8.2. Sediment Core Observations 164
8.3. Sediment Core Analysis 166
8.4. Spatial Variation of Grain Size 167

8.5. Grain Size Distributions 173
9. Sediment Load at Lower Granite Reservoir 176
9.1. Historic Sediment Load Measurements 179
9.2. 2008-2010 Sediment Load at Anatone and Spalding 182
9.3. Time Series Trend in Sediment Load 185
9.4. Sediment Load Estimation 189
9.5. Sediment Load Relationships 190
9.6. Snake River Suspended Sediment Load and Bedload Relationships 192
9.7. Clearwater River Suspended Sediment Load and Bedload Relationships 199
9.8. Sediment Load Regression Analysis with 2011 Data Included 205
9.9. Reduced Major Axis (RMA) Regression 205
9.10. Sediment Unit Weight 207
9.11. Comparison of Sediment Load Estimates with Measured Sediment Accumulation 209
9.12. Uncertainty of Sediment Load Volume Estimates 211
9.13. Effective Discharge 213
9.14. Sediment Load Grain Size Distributions 217
9.15. Sediment Load Characteristics for Sediment Transport Modeling 222
9.16. Sediment Load in Snake and Clearwater River Tributaries 229
9.16.1. Regression Analysis of Tributary Sediment Loads 230
9.16.2. Salmon River and Lower Snake River Sediment Loads 236
9.16.3. Clearwater River Sediment Loads 240
9.16.4. Mass Balance of the Tributary basin Sediment Loads 243
9.16.5. Trends in Sediment Load in the Tributary Basins 244
9.17. Sediment Load in the Palouse River 249

List of Figures

Figure 1. Lower Snake River PSMP Project Area. 14
Figure 2. Lower Granite Reservoir, Idaho and Washington. 15
Figure 3. Lower Snake River sediment delivery watershed. 15
Figure 4. Flowchart of tributary discharges at the confluence of the Snake River and Clearwater River. 23
Figure 5. Hydrograph of the December 1933 flood on the Clearwater River. 26
Figure 6. Hydrograph of the May 1948 flood on the Clearwater River. 27
Figure 7. Correlation Anatone maximum day discharge and Spalding coincident discharge. 36

Figure 8. Correlation Spalding maximum day discharge and Anatone coincident discharge. 37
Figure 9. Correlation Lower Granite maximum day discharge and Dworshak outflow coincident discharge. 37
Figure 10. Correlation Lower Granite maximum day discharge and Hells Canyon outflow coincident discharge. 38
Figure 11. Correlation Lower Granite maximum day discharge and the coincident discharge at Weiser on the Snake River. 38
Figure 12. Translocated 72hr PMP Rainfall Distribution. 39
Figure 13. Pacific Northwest region from the regional skew map in Bulletin 17B[23]. 43
Figure 14. Multivariate ENSO Index 1950 – 2010. 44
Figure 15. Comparison of the annual peak discharges are Spalding with the SST-CTI. 45
Figure 16. Comparison of the annual peak discharges are Spalding with the ENSO MEI. 46
Figure 17. Regression of SST-CTI with Spalding annual peak discharge. 48
Figure 18. Regression of ENSO-MEI with Spalding annual peak discharge. 49
Figure 19. Regression of ENSO-MEI with Anatone annual peak discharge. 49
Figure 20. Regression of ENSO-MEI with the Salmon River at Whitebird annual peak discharge. 50
Figure 21. 1974 flood hydrograph for the Salmon River at Whitebird. 50
Figure 22. Annual maximum discharge for Salmon River at Whitebird. 51
Figure 23. Annual flood volume for Salmon River at Whitebird. 51
Figure 24. Day of annual maximum discharge for Salmon River at Whitebird 52
Figure 25. Annual flood duration for Salmon River at Whitebird. 52
Figure 26. Beginning day of the annual flood for Salmon River at Whitebird. 53
Figure 27. Flowchart of the Monte Carlo simulation of the multivariate analysis of conditional probabilities for coincident discharge. 61
Figure 28. LP3 distribution of Anatone annual maximum day discharge. 63
Figure 29. LP3 distribution of Spalding coincident daily average discharge. 64
Figure 30. LP3 distribution of Spalding annual maximum day discharge. 64
Figure 31. LP3 distribution of Anatone coincident daily average discharge. 65
Figure 32. Joint probability of exceedance of the Snake and Clearwater River at Lower Granite. 67
Figure 33. Histogram of Flow-Split values for the 1 percent probability of exceedance for total discharge. 69
Figure 34. Proportion of flow contributed by the Snake River during the annual maximum daily discharge at Lower Granite. 69
Figure 35. Location of the confluence stage gage. 79
Figure 36. Lower Granite total inflow hydrograph during 1997 winter and spring floods. 80
Figure 37. Stage and discharge relationships in Lower Granite Reservoir during the 1997 flood. 80
Figure 38. Lewiston confluence stage during the high discharge of January 1997. 81
Figure 39. Stage and discharge relationships in Lower Granite Reservoir during the 1997 spring flood. 81
Figure 40. Hourly difference of instantaneous stage at the confluence. 82
Figure 41. Sediment range locations in Lower Granite Reservoir. 87
Figure 42. Sediment range cross sections near the confluence. 88
Figure 43. 2009 USGS multibeam echosounding survey bathymetry. 88

Figure 44. Comparison of 2009 MBES bathymetry and 2009 sediment range elevations. 89
Figure 45. Elevation difference by water depth. 89
Figure 46. 2010 LiDAR elevation coverage of the Lewiston levee floodplain. 90
Figure 47. Historic water surface elevation estimates at the confluence during the Standard Project Flood. 93
Figure 48. Shift in Lower Granite SPF hinge point 1974 -2009 (profile). 94
Figure 49. Shift in Lower Granite SPF hinge point 1974 -2009 (plan). 94
Figure 50. 2009 HEC-RAS model of Lower Granite confluence. 97
Figure 51. Lower Granite forebay boundary condition. 97
Figure 52. Ineffective flow areas near Silcott Island. 98
Figure 53. Stage board at the confluence of the Snake and Clearwater Rivers. 102
Figure 54. Stage board at the East Lewiston Pump Station. 102
Figure 55. Sheet pile wall at Hells Gate Marian, RM 142.95. 103
Figure 56. ADH water surface profile locations. 108
Figure 57. Comparison of 1D and 2 D simulated water surface profiles at the confluence (Lower Granite to Clearwater River). 108
Figure 58. Comparison of 1D and 2 D simulated water surface profiles at the confluence (Lower Granite to Snake River). 109
Figure 59. Index section at the levee low point on the Clearwater River at confluence. 113
Figure 60. HEC-RAS 2009 fixed-bed steady flow profiles for Clearwater River. 117
Figure 61. HEC-RAS 2009 fixed-bed steady flow profiles for Snake River above confluence. 118
Figure 62. HEC-RAS 2009 fixed-bed steady flow profiles for Snake River below the confluence (Lower Granite Reservoir). 118
Figure 63. Levee low point during SPF discharge. 120
Figure 64. Comparison of 8 June 2010 profiles for calibrated and historic Manning's *n* values. 120
Figure 65. Comparison of SPF profiles for calibrated and historic Manning's *n* values. 121
Figure 66. Simulated moderate debris blockage at the CPRR bridge Clearwater RM 0.6. 127
Figure 67. Simulated agressive debris blockage at the CPRR bridge Clearwater RM 0.6. 128
Figure 68. Simulated deck blockage at the CPRR bridge Clearwater RM 0.6. 128
Figure 69. Inundation surface for breach of left bank levee at RM 3.7 at peak of SPF. 133
Figure 70. Inundation surface for breach of left bank levee at RM 1.9 at peak of SPF. 134
Figure 71. Inundation surface for breach of right bank levee at RM 3.1 at peak of SPF. 135
Figure 72. Inundation surface for breach of right bank levee at RM 0.9 at peak of SPF. 136
Figure 73. Sediment range locations in Lower Granite Reservoir. 139
Figure 74. Sediment range cross sections near the confluence. 140
Figure 75. Rectification of sediment range elevation points. 142
Figure 76. Comparison of 1995 and 1997 sediment ranges at Clearwater RM 0.28. 144
Figure 77. Comparison of 1997 and 2009 sediment ranges at Clearwater RM 0.28. 145
Figure 78. Comparison of 1974 and 2009 sediment ranges at Snake RM 137.69. 145
Figure 79. Equilbrium section at Snake RM 137.69. 146
Figure 80. Comparison of 1974 and 2009 sediment ranges at Snake RM 123.30. 146
Figure 81. Comparison of 1974 and 2009 sediment ranges at Clearwater RM 6.37. 147

Figure 82. Comparison of 1974 and 2009 sediment ranges at Snake RM 147.47. 147
Figure 83. Distribution of sediment volume in Lower Granite between 1995 and 1997. 155
Figure 84. Distribution of sediment volume in Lower Granite between 2009 and 2010. 155
Figure 85. Mean active bed elevation change in Lower Granite below the confluence. 156
Figure 86. Palouse River sediment delivery watershed. 157
Figure 87. Palouse River Sediment Ranges. 158
Figure 88. 2010 sediment core locations on the Clearwater River. 160
Figure 89. 2010 sediment core locations on the Snake River. 161
Figure 90. Sediment core acquisition with vibratory corer at Lower Granite. 163
Figure 91. Sediment core inspection and subsampling. 163
Figure 92. Sediment core acquired at Clearwater RM 0.28. 164
Figure 93. Comparison of 1974-2009 sediment ranges at Clearwater RM 0.28. 165
Figure 94. Silt sediment core tube obtained near Lower Granite Dam. 165
Figure 95. Uniform silt sediment near the bottom of core sample obtained near Lower Granite Dam. 166
Figure 96. Spatial variation of sediment core D_{50} in Lower Granite Reservoir. 168
Figure 97. Spatial variation of sediment core D_{90} in Lower Granite Reservoir. 169
Figure 98. Spatial variation of sediment core D_{50} in the Clearwater River. 169
Figure 99. Spatial variation of sediment core D_{90} in the Clearwater River. 170
Figure 100. Map of sediment core surface D_{50} in the Snake River above the confluence. 170
Figure 101. Map of sediment core surface D_{50} in the Snake River below the confluence. 171
Figure 102. Map of sediment core surface D_{50} in the Snake River below Red Wolf Bridge. 171
Figure 103. Map of sediment core surface D_{50} in the Snake River above Silcott Island. 172
Figure 104. Map of sediment core surface D_{50} in the Snake River at Silcott Island. 172
Figure 105. Map of sediment core surface D_{50} in the Clearwater River below RM 1.6. 173
Figure 106. Grain size distribution Snake RM 138.94. 175
Figure 107. Lower Snake River sediment delivery watershed. 176
Figure 108. Lower Granite Reservoir sediment delivery watershed. 177
Figure 109. Primary sediment monitoring stations on the Snake and Clearwater Rivers. 178
Figure 110. Snake River at Anatone measured sediment load 1972-1979. 181
Figure 111. Clearwater River at Spalding measured sediment load 1972-1979. 182
Figure 112. Snake River at Anatone measured sediment load 2008-2009. 183
Figure 113. Clearwater River at Spalding measured sediment load 2008-2010. 184
Figure 114. Comparison of suspended sediment concentration at Snake River at Anatone for the periods 1972-1979 and 2008-2011. 187
Figure 115. Comparison of suspended sand concentration at Snake River at Anatone for the periods 1972-1979 and 2008-2011. 187
Figure 116. Residuals of suspended sediment concentration at Snake River at Anatone. 188
Figure 117. Residuals of suspended sand concentration at Snake River at Anatone. 188
Figure 118. Comparison of suspended sediment concentration at Clearwater River at Spalding for the periods 1972-1979 and 2008-2010. 189
Figure 119. Snake River at Anatone suspended sediment load regression fit. 195
Figure 120. Snake River at Anatone suspended sediment load regression residuals. 195

Figure 121. Snake River at Anatone suspended sediment load 1974 – 2010. 196
Figure 122. Snake River at Anatone suspended sand load regression fit. 198
Figure 123. Snake River at Anatone bedload regression fit. 198
Figure 124. Clearwater River at Spalding suspended sediment load regression fit. 200
Figure 125. Clearwater River at Spalding suspended sediment load regression residuals. 201
Figure 126. Clearwater River at Spalding suspended sediment load 1974 – 2010. 202
Figure 127. Clearwater River at Spalding suspended sand load regression fit. 204
Figure 128. Clearwater River at Spalding bedload regression fit. 204
Figure 129. Comparison of RMA regression with OLS regression for suspended sediment load. 206
Figure 130. Consolidated unit weights of submerged silt and clay deposits. 209
Figure 131. Effective discharge Snake River at Anatone. 215
Figure 132. Sediment flow-duration Snake River at Anatone. 215
Figure 133. Effective discharge Clearwater River at Spalding. 215
Figure 134. Sediment flow-duration Clearwater River at Spalding. 216
Figure 135. Effective discharge Lower Granite Reservoir. 216
Figure 136. Sediment flow-duration Lower Granite Reservoir. 217
Figure 137. Variation of percent fines with discharge for Snake River at Anatone. 219
Figure 138. Variation of percent fines with discharge for Clearwater River at Spalding. 219
Figure 139. Bedload grain size parameters Snake River at Anatone. 221
Figure 140. Bedload grain size parameters Clearwater River at Spalding. 221
Figure 141. Average bedload grain size distribution for the Snake River and Clearwater River. 222
Figure 142. Snake River percent suspended sand relationship for sediment transport modeling. 226
Figure 143. Clearwater River percent suspended sand relationship for sediment transport modeling. 226
Figure 144. Snake River total sediment rating curve for HEC-RAS sediment transport modeling. 228
Figure 145. Clearwater River total sediment rating curve for HEC-RAS sediment transport modeling. 228
Figure 146. Sediment load measurement sites. 229
Figure 147. Regression fit of measured suspended sediment load for Salmon River. 231
Figure 148. Prediction intervals and confidence intervals for the suspended sediment load measurements in the Salmon River. 231
Figure 149. Flow-duration-frequency curves for Salmon River at Whitebird. 232
Figure 150. Flow-duration-frequency curves for Clearwater River at Orofino. 232
Figure 151. Relative suspended sediment loads of the Lower Granite sediment yield watershed. 235
Figure 152. Relative suspended sand loads of the Lower Granite sediment yield watershed. 235
Figure 153. Discharge of Snake River above Lower Granite Reservoir WY 2009-2011. 238
Figure 154. Comparison of measured suspended sediment loads on the Snake River 2008-2011. 238
Figure 155. Comparison of measured suspended sand loads on the Snake River 2008-2011. 239
Figure 156. Difference in computed suspended sediment loads of the Salmon River and Snake River, WY 1974-2011. 239
Figure 157. Comparison of measured suspended sediment loads on the upper Clearwater River 2009-2011. 241
Figure 158. Comparison of measured suspended sand loads on the upper Clearwater River 2009-2011. 241

Figure 159. Comparison of measured suspended sediment loads on the middle Clearwater River 2009-2011. 242
Figure 160. Comparison of measured suspended sediment loads on the lower Clearwater River 2008-2011. 242
Figure 161. Comparison of suspended sediment loads in the Salmon River. 245
Figure 162. Regression residuals for suspended sediment concentration for the Salmon River at Whitebird. 245
Figure 163. Regression residuals for suspended sand concentration for the Salmon River at Whitebird. 246
Figure 164. Comparison of suspended sediment load in the Selway River. 247
Figure 165. Regression residuals for suspended sediment concentration for the Selway River near Lowell. 248
Figure 166. Comparison of suspended sediment load in the Lochsa River. 249
Figure 167. Palouse River suspended sediment load regression curves. 250

List of Tables

Table 1. Elements of the PSMP hydraulics and hydrology report. 17
Table 2. USGS stream gage stations used in the Lower Granite flood risk analysis. 24
Table 3. Lower Granite annual maximum day discharges. 30
Table 4. Annual peak discharge at Anatone on the Snake River and Spalding on the Clearwater River.. 31
Table 5. Lower Granite reduction rate of maximum day discharge. 32
Table 6. Coincident average daily discharges of the tributaries to Lower Granite Reservoir. 33
Table 7. Contribution of regulated discharge to the Standard Project Flood..... 39
Table 8. Change in station skew and LP3 weighted skew at unregulated discharge sites. 42
Table 9. Univariate LP3 discharge frequencies for Lower Granite tributaries..... 55
Table 10. Summary of discharge flow conditions at Lower Granite. 59
Table 11. Frequencies of flow conditions at Lower Granite. 59
Table 12. Lower Granite maximum day and coincident daily discharge data for total probability-multivariate analysis. 60
Table 13. Condition discharge frequency series for Lower Granite..... 62
Table 14. Comparison of total probability-mulitvariate and univariate discharge frequency estimates for Lower Granite. 63
Table 15. Proportion of discharge from the Snake and Clearwater Rivers for the annual maximum daily discharge at Lower Granite. 68
Table 16. . Comparison of the simplified total probability-mulitvariate and univariate discharge frequency estimates for Lower Granite. 70
Table 17. Salmon River at Whitebird maximum day discharge and tributary coincident discharges (Condition 1). 72
Table 18. Clearwater River at Orofino maximum day discharge and tributary coincident discharges (Condition 2). 72
Table 19. Lower Granite maximum day tributary coincident discharges (Condition 3). 73
Table 20. Frequencies of flow conditions at Lower Granite for the extended multivariate analysis. 73
Table 21. Comparison of the extended total probability mulitvariate and univariate discharge frequency estimates for Lower Granite. 75
Table 22. Extended total probability mulitvariate with increased maximum discharge at Whitebird. 76
Table 23. Extended total probability mulitvariate with reduced region skew. 76
Table 24. HEC-RAS 2009 model calibration data for 8 June 2010. 103
Table 25. HEC-RAS 2009 model calibration data for 8 June 2010 104
Table 26. HEC-RAS 2009 model calibrated hydraulic resistance factors. 104
Table 27. Manning n values for sand and gravel bed material from EM 1110-2-1601. 106
Table 28. HEC-RAS annual maximum daily average steady flow discharges for FDA risk analysis. 111
Table 29. HEC-RAS estimated annual peak steady flow discharges for FDA risk analysis. 111
Table 30. Discharges and forebay elevations used in HEC-RAS modeling of the curve extensions for the FDA index sections. 115
Table 31. HEC-RAS 2009 Fixed-Bed Water Surface Profile - Clearwater River near the Confluence..... 119
Table 32. HEC-RAS 2009 Fixed-Bed Water Surface Profile - Snake River near the Confluence. 119

Table 33. Conditional non-exceedance probabilities at Clearwater RM 0.3 curve extension method 1. 122
Table 34. Conditional non-exceedance probabilities at Clearwater RM 0.3 curve extension method 2. 122
Table 35. Levee freeboard for 1-percent annual chance exceedance flood – Clearwater River. 124
Table 36. Levee freeboard for 1 percent annual chance exceedance flood – Snake River. 125
Table 37. Effect of spillway on conditional non-exceedance probabilities. 126
Table 38. Sediment range acquisitions, Snake River at Lower Granite Reservoir. 141
Table 39. Sediment range acquisitions, Clearwater River at Lower Granite Reservoir. 142
Table 40. Sediment accumulation volume 1974-2009, Snake River above confluence. 149
Table 41. Sediment accumulation volume 1974-2009, Snake River below confluence. 150
Table 42. Sediment accumulation volume 1974-2009, Clearwater River above confluence. 151
Table 43. Estimated dredge volumes at the confluence of the Snake and Clearwater Rivers. 152
Table 44. Summary of Sediment Accumulation in Lower Granite Reservoir. 153
Table 45. Sediment accumulation volumes at the mouth of the Palouse River. 157
Table 46. Top ranked measured suspended sediment load Snake River at Anatone. 184
Table 47. Top ranked measured suspended sediment load Clearwater River at Spalding. 185
Table 48. Results of Mann-Whitney-Wilcoxon test for step-trend for suspended sediment in the Snake River at Anatone. 189
Table 49. Snake River at Anatone suspended sediment load regression coefficients. 196
Table 50. Snake River at Anatone suspended sediment load estimate 1974-2010. 196
Table 51. Snake River at Anatone suspended sand load regression coefficients. 197
Table 52. Snake River at Anatone suspended sand load estimate 1974-2010. 197
Table 53. Snake River at Anatone bedload regression coefficients. 197
Table 54. Snake River at Anatone bedload estimate 1974-2010. 197
Table 55. Clearwater River at Spalding suspended sediment load regression coefficients. 201
Table 56. Clearwater River at Spalding suspended sediment load estimate 1974-2010. 202
Table 57. Clearwater River at Spalding suspended sand load regression coefficients. 202
Table 58. Clearwater River at Spalding suspended sand load estimate 1974-2010. 203
Table 59. Clearwater River at Spalding bedload regression coefficients. 203
Table 60. Clearwater River at Spalding bedload estimate 1974-2010. 203
Table 61. Snake River at Anatone suspended sediment load estimate with 2011 sediment load data added to the regression. 205
Table 62. Comparison of Lower Granite Reservoir estimated sediment load and measured sediment accumulation. 211
Table 63. Calibration of sediment unit weight. 211
Table 64. Monte Carlo analysis of sediment volume. 213
Table 65. Snake River at Anatone suspended sediment average grain size distribution. 220
Table 66. Clearwater River at Spalding suspended sediment average grain size distribution. 220
Table 67. Snake River combined suspended sediment and bedload rating table for HEC-RAS sediment transport modeling. 225
Table 68. Clearwater River combined suspended sediment and bedload rating table for HEC-RAS sediment transport modeling. 225
Table 69. Snake River grain size fractions for sediment transport modeling. 227

Table 70. Clearwater River grain size fractions for sediment transport modeling. 227
Table 71. HEC-RAS sediment load series summary and volume verification. 228
Table 72. Total suspended sediment load WY 2009-2011 Snake and Clearwater River tributaries. 233
Table 73. Total suspended sand load WY 2009-2010 Snake and Clearwater River tributaries. 234
Table 74. Relative contributions of tributaries to total Load at Lower Granite Reservoir. 234
Table 75. Relative contribution of tributary basins WY 2009, 2010 and 2011. 237
Table 76. Mass balance and watershed sediment yield for Lower Granite Reservoir WY 2009-2011. 243
Table 77. Mann-Whitney-Wilcoxon test for step-trend for suspended sediment in the Salmon River at Whitebird. 246
Table 78. Mann-Whitney-Wilcoxon test for step-trend for suspended sediment in the Selway River near Lowell. 248
Table 79. Sediment yield of the Palouse River basin 2009-2011. 250

THIS PAGE INTENTIONALLY LEFT BLANK

1. Introduction and Findings

Flood risk in the Lewiston, Idaho levee system is a serious concern which is largely defined by the magnitude and rate of sediment accumulation. The Lewiston levees at the confluence of the Snake and Clearwater Rivers are part of the Lower Granite project. Without the levees, downtown Lewiston would be flooded by the normal backwater of Lower Granite Dam which is located 32 miles downstream. Approximately 80 million cubic yards (mcy) of sediment has accumulated in Lower Granite Reservoir since the reservoir was first filled in April 1975. Over the 37 year period, sediment from the Snake and Clearwater Rivers has progressively raised the predicted water surface elevations at the confluence so that the risk of overtopping the Lewiston levees during extreme floods has increased.

While there has not yet been a flood that has approached the flow capacity of the levee channels since construction of the reservoir, it was not known at the beginning of this study whether the current level of flood risk at the Lewiston levees is acceptable, both from viewpoint of the affected community and the requirements of U.S. Army Corps of Engineers (USACE) policy. The primary objective of this hydraulics and hydrology (H&H) analysis is to determine the current level of flood risk and predict the change in flood risk caused by continued sedimentation in Lower Granite Reservoir. Secondary, but important objectives, of the H&H analysis were to examine the impacts of sedimentation on navigation, reservoir operations and fisheries habitat.

Sedimentation analyses of natural river and reservoir systems are rarely simple. When performed as part of a flood risk analysis, interrelationships between hydrology, hydraulics, sedimentation, and flood risk compound so that the analysis is complex. The analysis is made more complex by the physical setting at the confluence of two rivers and that some methodology is not well detailed in existing USACE engineering guidance. At times it was necessary to develop new methodology for uncommon aspects of sedimentation analysis and flood risk.

Sufficient detail is included in the report so that the analysis should be transparent to independent reviewers who participate in the USACE review process. This report is also intended to document the data, procedures and results of the study with sufficient detail so that USACE H&H engineers can efficiently update the sedimentation and risk analysis in future years. It is also intended that the report satisfy the requirements of a Stage 2 (feasibility level) sedimentation study as required by USACE engineering regulations[1].

[1] USACE (1995) *Engineering Regulation 1110-2-8153 Sedimentation Investigations,* U.S. Army Corps of Engineers, Washington, DC.

1.1. Project Setting

The focus of the sedimentation and risk analysis is Lower Granite Reservoir at the confluence of the Snake and Clearwater Rivers in Idaho and Washington. Lower Granite is the most upstream dam on the USACE Lower Snake River lock and dam system (Figure 1). Total watershed area upstream from Lower Granite Dam is 102,000 square miles, but only part of this area delivers sediment to the lower Snake River. Lower Granite Reservoir (Figure 2) receives sediment from 27,000 square miles of forest, range and agricultural land, bounded by the Hells Canyon Complex of dams on the Snake River and Dworshak Dam on the North Fork of the Clearwater River (Figure 3). The size of the sediment delivery watershed of the lower Snake River reservoir system increases to 32,000 square miles at the mouth of the Snake River on the Columbia River. Physical characteristics of the reservoir system are further described in the main body of the Programmatic Sediment Management Plan Environmental Impact Statement (PSMP-EIS) and in the official water control manual for the Lower Granite Lock and Dam project[2].

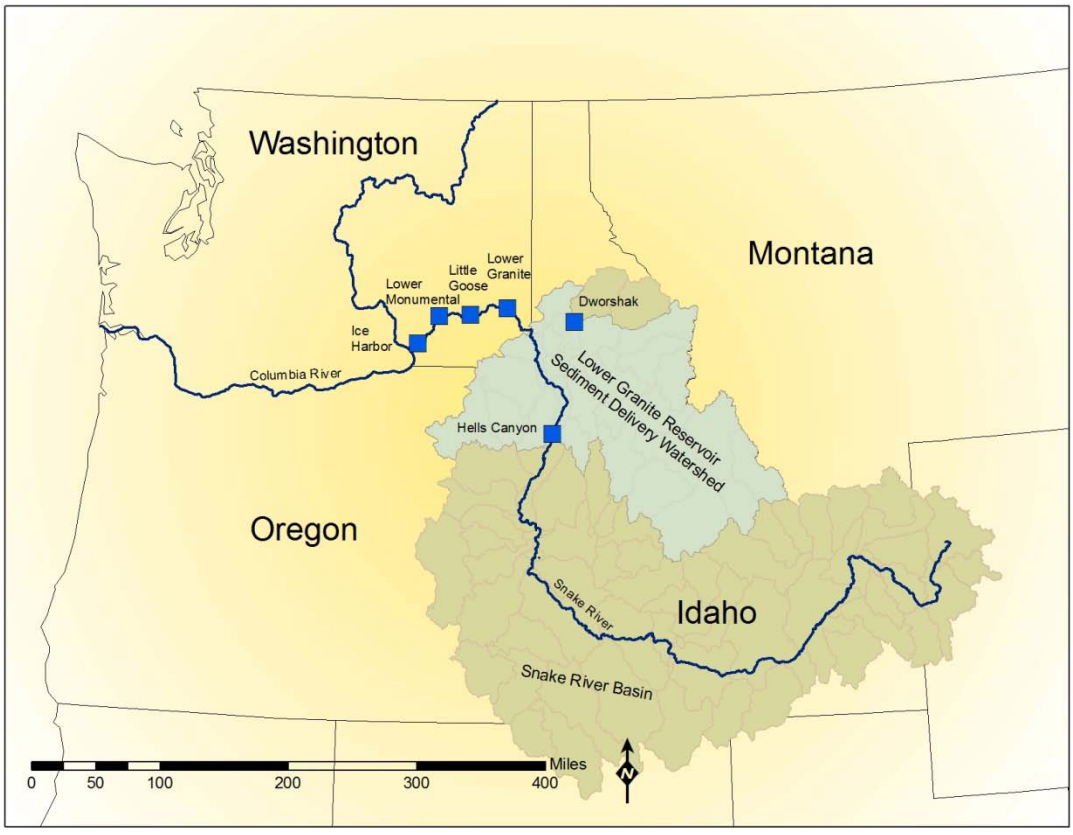


Figure 1. Lower Snake River PSMP Project Area.

[2] USACE (1987). *Water Control Manual for Lower Granite Lock and Dam, Snake River, Oregon, Washington and Idaho*, U.S. Army Corps of Engineers, Walla Walla District, Walla Walla, WA.

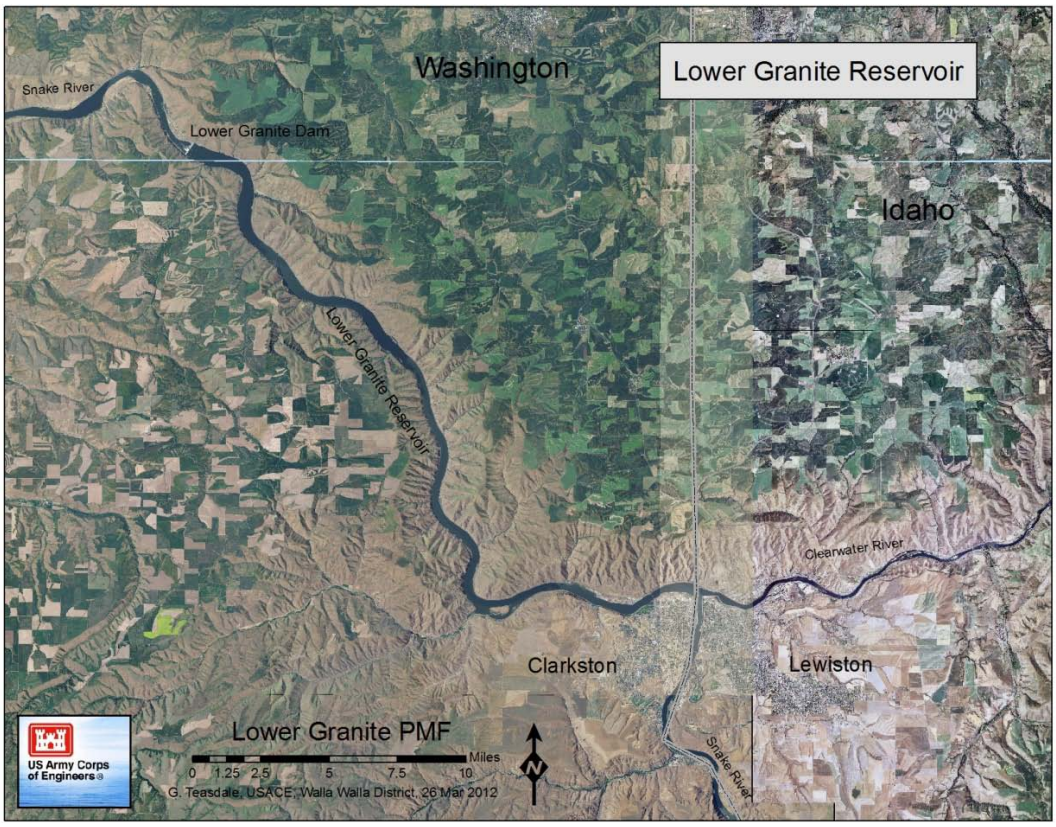


Figure 2. Lower Granite Reservoir, Idaho and Washington.

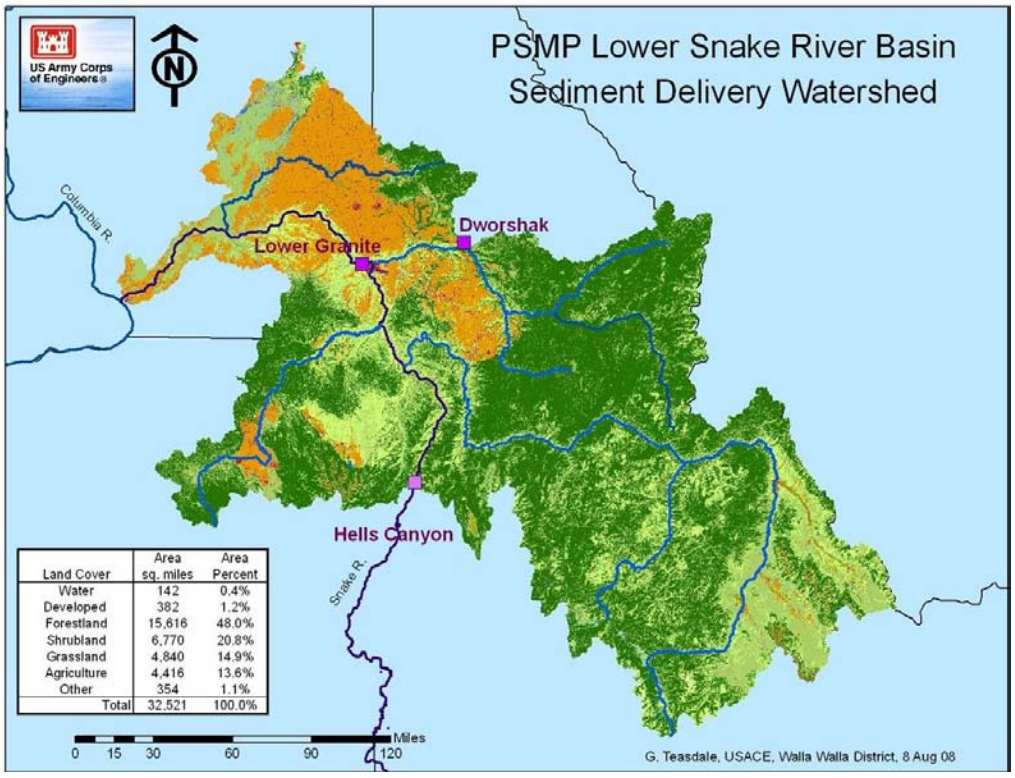


Figure 3. Lower Snake River sediment delivery watershed.

1.2. Scope of the Hydraulics and Hydrology Investigation

Much was learned about the hydrology, hydraulics and sedimentation of the Lower Snake River system over the four and half years of the study. With the assistance of the U.S. Geological Survey (USGS) and the USACE Engineering Research and Development Center - Coastal Hydraulics Laboratory (ERDC-CHL), multiple high-resolution bathymetries of Lower Granite Reservoir were collected that directly recorded the state and development of sand bedforms. With USACE (Corps) funding, USGS scientists in Idaho helped plan and then perform an unprecedented multi-year campaign of sediment load measurements throughout the Snake and Clearwater River basins. Also for the first time, full depth sediment cores were sampled throughout Lower Granite Reservoir by a team of USGS scientists from Texas. The Corps also funded independent assessments of sediment yield from forest and agricultural watersheds by research scientists and engineers at the U.S. Forest Service (USFS), Washington State University, and the University of Idaho. Nearly all analyses in this hydraulics and hydrology report were performed by the USACE Walla Walla District.

The report is organized in 18 sections in three parts that follow the H&H analysis process (Table 1). Part 1 describes the hydrologic data which supports the flood risk analysis, and steps through the process that produces the primary flood risk analysis of the existing channel condition. Readers who are mostly interested in the current level of flood risk at the Lewiston Levees will find that Part 1 contains most of the information and results that supports this aspect of the flood risk analysis.

Part 2 describes the sediment transport analysis and the mobile-bed hydraulic modeling that was performed to evaluate the risk of flooding at the Lewiston Levees for the future channel condition. Part 2 also includes the analysis of alternatives for sediment management within Lower Granite Reservoir and the analysis of flood risk due to wind waves at the confluence.

Part 3 describes the impact of recent sedimentation on the navigation channels and includes an extended analysis of the effect of sand bedforms on flow resistance in Lower Granite Reservoir. Part 3 also includes a description of the multi-dimensional hydraulic modeling of environmental flows and a description of the initial modeling of the effect of potential climate change on sediment yield in the Snake and Clearwater River basins.

Elements of the PSMP Hydraulics and Hydrology Analysis		
Part 1	1	Introduction and major findings
	2	Multivariate discharge frequency analysis
	3	Stage variability at the confluence
	4	Fixed-bed hydraulic modeling of flood stage
	5	Flood risk analysis of the existing channel condition
	6	Potential inundation area of the Lewiston levee system
	7	Sediment accumulation in Lower Granite Reservoir
	8	Characterization of the bed material of Lower Granite Reservoir
	9	Analysis of sediment load at Lower Granite Reservoir
Part 2	10	Sediment transport analysis of Lower Granite Reservoir
	11	Mobile-bed flood risk analysis of the future channel condition
	12	Alternatives for sediment management in Lower Granite Reservoir
	13	Flood risk due to wind waves at the confluence
	14	Summary of the flood risk analysis
Part 3	15	Evolution of sand bedforms
	16	Sediment deposition in navigation channels
	17	Hydraulic modeling of environmental flows
	18	Effect of climate change on watershed sediment yield

Table 1. Elements of the PSMP hydraulics and hydrology report.

1.3. Major Findings of the Hydraulics and Hydrology Analysis

Major findings of the hydraulics and hydrology analysis are summarized below. The findings emphasize the most important outcomes of the overall flood risk analysis.

1. Based on probabilistic analysis of flood risk, the current risk of overtopping the Lewiston Levees by extreme flood discharge is likely acceptable to reviewing authorities and the affected community because of high assurance probability (conditional nonexceedance probability)[3] and low long-term risk probabilities[4] (Section 5).

2. Probabilistic analysis with sediment transport and mobile-bed hydraulic models showed that the risk of overtopping the Lewiston levees for the most likely channel condition in 50 years would likely be seen by reviewing authorities as marginally acceptable. Under conservative, but still plausible, assumptions

[3] Assurance, also called the conditional non-exceedance probability, is the probability that a target stage, such as the top of a levee, will not be exceeded during the occurrence of a specified flood.

[4] Long-term risk is the probability of one or more exceedances of a selected target or capacity in a specified duration.

about the hydraulic response the channel, the flood risk for the future channel condition is unacceptable (Section 11).

3. Deterministic hydraulic analysis with new calibrated HEC-RAS models of Lower Granite Reservoir showed that the freeboard during the Standard Project Flood (SPF) is currently greater than four feet (Section 11.6). The Lewiston Levees were constructed as a part of the Lower Granite Dam project and were designed with 5 feet of freeboard during the SPF. A direct comparison of the historic and current freeboard values may be misleading. There has been substantial loss of freeboard due to sediment accumulation, and if current modeling methods were used in the past they would have shown that the original freeboard was greater. When computed by traditional (historic) methods, freeboard during the SPF for the current channel condition is now less than 2 feet at the confluence (Section 4.7). As a matter of policy interpretation, it is unclear if the original SPF criteria must be satisfied to comply with current USACE engineering regulations and policy for dam safety (Section 5.13). If so, the selection of alternatives for reservoir sediment management cannot be based solely on the probabilistic analysis of flood risk.
4. The probabilistic basis of the flood risk analysis is conditioned by the need to assume that Lower Granite Dam is operated in accordance with the authorized water control manual. Flood flows can overtop the Lewiston Levee system if the dam is misoperated and the forebay elevation is allowed to remain too high during a flood to safely pass flood flows. The potential to induce flooding by misoperation is discussed in Section 5.12.
5. About 80 million cubic yards (mcy) of sediment has accumulated in Lower Granite Reservoir since 1974. Average annual sediment accumulation is about 2.2 million cubic yards per year (Section 7.5).
6. Sediment inflows (load) into Lower Granite Reservoir have not decreased since the 1970's and based on the recent sediment load measurements may be increasing in the Snake River (Section 9). Much more sediment is delivered by the Snake River than the Clearwater River (Section 9). The largest single source of sediment is the Salmon River basin. The amount of sediment delivered by basins where cultivated agriculture is prevalent is a relatively small proportion of the total sediment load at Lower Granite Reservoir.
7. Episodic wildfires and landslides in forest and range lands are the main sources of sediment in Lower Granite Reservoir. Current watershed sediment management practices cannot achieve substantial and reliable reductions in sediment load from these sources. Erosion of the silt soils of the cultivated agricultural land supplies very small amounts of the sand size material that has

the greatest effect on flood risk at the Lewiston levee system (USFS and WSU/UI reports).

8. The inability to reliably reduce sediment supply at the scale that affects Lower Granite Reservoir does not mean that effective watershed sediment management is unimportant in local watersheds and streams within the basin. The Corp's study of watershed sediment yield was not an exhaustive analysis of all aspects of watershed sediment management; it was pursued until it was evident that watershed sediment management was not a reliable means to reduce the rate of sediment accumulation in Lower Granite Reservoir that heightens the risk of flooding at Lewiston. Further cooperative research and evaluation of sediment load and yield throughout the lower Snake River basin would be beneficial to the federal, state and tribal entities that bear responsibility for sediment management.
9. Historic sediment accumulation was simulated with good accuracy with the HEC-RAS sediment transport model. Sediment accumulation for the next 50 years was simulated to produce the geometry of the future channel condition (Section 10).
10. Uncertainty in the hydraulic response of the future channel condition is due to phenomena of sand bedforms. The analysis shows that sand bedforms will likely washout during extreme flood discharges and reduce the flow resistance of the channel, thereby passing flood water at a lesser stage than if the dunes remained fully formed. However, the transition from a channel with large sand dunes (lower bed regime) to a channel with washed-out bedforms (upper bed regime) cannot be precisely predicted with existing data and computational methods (Section 14). Further study and analysis of bedforms and flow resistance in Lower Granite Reservoir is recommended in future work for the Programmatic Sediment Management Plan. Faced with this important uncertainty, whether to use the credible future channel condition or the conservative future channel condition to define the level of flood risk at the Lewiston Levees is likely a decision to be made by jointly considering USACE policy and community tolerance of flood risk.
11. Wind waves at the confluence are an important element of flood risk (Section 13). Wind waves do not control the risk of overtopping the Lewiston Levees for the existing channel condition, but have greater effect on flood risk for the future channel condition.
12. Potential alternatives for management of sediment within Lower Granite Reservoir include dredging, construction of spur dikes, reservoir drawdown, and trapping of sediment upstream from the confluence (Section 12). Periodic dredging is a reliable short-term action to maintain navigation channel depths

under current reservoir operations. About 0.7 mcy per year of sand must be dredged to maintain the authorized navigation channel depth and maintain the current hydraulic capacity of the levees (Section 9).

13. Spur dikes in the turning basin of the Clearwater River and near the confluence are the most feasible long-term solution that can reduce the amount of dredging needed to maintain depth in the navigation channels and port areas (Section 12.1). Spur dikes would not completely eliminate the need for periodic dredging at the ports.

14. Periodic drawdown of the reservoir as a means to erode sediment from the confluence area appears feasible, but to be the most effective would have to occur during a period of high seasonal discharge (Section 12.2). This method of sediment management should be tested to prove reliability and evaluate possible adverse impacts on infrastructure in Lower Granite Reservoir.

15. Construction of a sediment trap upstream from the Lewiston levee system on the Snake River could intercept sand bedload and reduce the rate of increase in flood risk at the levees (Section 12.3). About 0.6 mcy of sand could be extracted from the trap each year, potentially for commercial use or for the construction of shallow water habitat in the reservoir. Trapping of sand on the Snake River would also reduce sediment deposition at the Port of Clarkston. The feasibility of this management alternative should be further evaluated.

16. Adding height to the lowest segments of the Lewiston levee is a reliable action that can maintain the current level of flood risk reduction or recover the flood risk reduction provided by the original SPF design (Section 11.6). A detailed design and cost estimate for adding height to the lowest segments of the Lewiston levee should be developed as a contingency action.

17. Dredging of large volumes of sediment to increase the hydraulic capacity of the levee system is plausible (Section 12.6), but would only be an effective long-term solution if followed by periodic dredging of approximately 0.7 mcy per year of sand to maintain the recovered capacity.

18. The most effective strategy for managing sediment in Lower Granite Reservoir is likely a combination of alternatives. A reasonable priority would be 1) short term dredging actions, 2) design and construction of spur dikes, 3) experimental drawdowns of the reservoir to promote transport of sediment, 4) construction of a experimental sediment trap on the Snake River. Raising the height of the lowest segments of the levees is a valid contingency action if other sediment management alternatives are not implemented.

19. The bathymetry data acquired in this study enabled the development of higher resolution one and two dimensional hydraulic models of Lower Granite Reservoir that are useful for simulation and study of environmental flows (Section 17).
20. The basin-scale modeling of sediment yield is further evidence that wildfires and climate change can significantly increase sediment delivery to Lower Granite Reservoir (Section18).

2. Multivariate Discharge Frequency Analysis

Reliable frequency relationships for the joint discharge of the Snake and Clearwater Rivers in Lower Granite Reservoir are necessary for the analysis of flood risk at the confluence. The complexity of joint frequency analyses that involves discharges that are substantially correlated is recognized in Corps engineering guidance, but a general method for computing joint frequency relationships is not yet available[5]. This section describes the discharge frequency analysis for the assessment of flood risk at the Lewiston Levee system and presents a general Monte Carlo approach for computing joint discharge frequency relationships for multiple correlated tributaries. Frequency analyses for Corps projects are required to follow Bulletin 17B procedures[6,7]. It is recognized that the Log Pearson Type 3 (LP3) distribution and Bulletin 17B are not the only statistical approaches that can be used to estimate discharge frequencies[8]. Nonetheless, the Bulletin 17B procedure is robust and widely accepted[9] in the U.S., and is the fundamental statistical model that is used to define the uncertainty of discharge in this study.

Total flow at the confluence and Lower Granite Reservoir is the combined discharge of the Snake and Clearwater Rivers. About 64 percent of the annual maximum discharge comes from the Snake River and 36 percent is from the Clearwater. Annual maximum discharges typically occur April through June. The largest contributions of flow to the Snake River above the confluence at the time of the annual maximum discharge come from Salmon River basin and the outflow of Hells Canyon Dam on the Snake River with lesser contributions from the Grande Ronde and the Imnaha Rivers. Most of the flow in the Clearwater River during the annual peak originates in the Lochsa, Selway and South Fork of the Clearwater River basins with

[5] USACE (1993). *Chapter 11, Engineer Manual 1110-2-1415 Hydrologic Frequency Analysis*. U.S. Army Corps of Engineers, Washington, DC.

[6] USACE (1994). ER 1110-2-1450 Hydrologic Frequency Estimates, U.S. Army Corps of Engineers, Washington, DC.

[7] USGS (1982). *Hydrology Subcommittee of the Interagency Advisory Committee on Water Data, Bulletin 17B 1982 (Mar), Guidelines for Determining Flood Flow Frequency*, U.S. Department of Interior, Geological Survey, Office of Water Data Coordination,Reston, VA.

[8] Hoskin, R.R.M and Wallis, J.R. (1997). *Regional Frequency Analysis*, Cambridge University Press, Cambridge, UK.

[9] Stedinger, J.R. and Griffis, V.W. (2008). "Flood Frequency Analysis in the United States: time to update.", *Journal of Hydrologic Engineering*, 13(4), 199-287.

lesser contributions from the lower tributaries. Figure 4 is a schematic of the tributary network and stream gages of the Snake and Clearwater River basins above confluence.

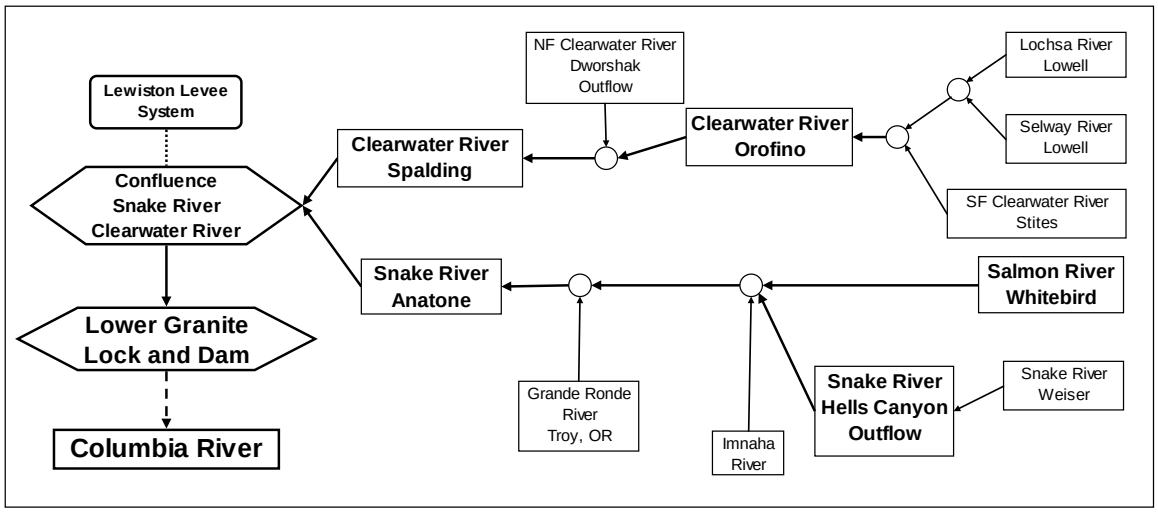


Figure 4. Flowchart of tributary discharges at the confluence of the Snake River and Clearwater River.

2.1. Discharge and Stage Data

Discharge data for the analysis was obtained from the USGS National Water Information System (NWIS)[10] accessed via the HEC-DSSVue program[11]. Stage data was obtained from the USACE Northwest Division (NWD) Water Control Database[12]. Stream and stage gages employed in the study are listed in Table 2. The period of record extends back to the early 1900's at some gages on the main tributary rivers. Other gages were installed near the time that Dworshak Dam was constructed on the North Fork of the Clearwater River. Regulation of the Clearwater River by Dworshak Dam[13] began in water year 1972. All the stream gages are considered reliable and are used routinely in Corps water management operations. Most of the USGS data are also reported in the Corps water management database.

[10] http://waterdata.usgs.gov/nwis.

[11] USACE (2010). HEC-DSSVue Version 2.0, February 2010, Hydrologic Engineering Center, U.S. Army Corps of Engineers, Davis, CA, www.hec.usace.army.mil.

[12] http://www.nwd-wc.usace.army.mil/report.htm.

[13] Regulation of the North Fork Clearwater River at Ahsahka began on Sept. 27, 1971, when diversion tunnel at Dworshak Dam was closed (USGS NWIS). Lower Granite first reached full pool in Feb 18, 1975.

Stream Gage and River Stage Stations		
Station	Name	Period
	Snake River Basin Discharge Data	
13269000	Snake River at Weiser, Id	1910 - 2010
13290450	Snake River at Hells Canyon Dam Id-Or State Line	1965 - 2010
13292000	Imnaha River at Imnaha, Or	1928 - 2010
13317000	Salmon River at White Bird Id	1910 - 2010
13333000	Grande Ronde River at Troy, Or	1944 - 2010
13334300	Snake River near Anatone, Wa	1958 - 2010
	Clearwater River Basin Discharge Data	
13336500	Selway River near Lowell, Id	1911 - 2010
13337000	Lochsa River near Lowell, Id	1910 - 2010
13338500	SF Clearwater River at Stites, Id	1911 - 2010
13339000	Clearwater River at Kamiah, Id	1910 - 1965
13340000	Clearwater River at Orofino, Id	1930 - 2010
13341000	NF Clearwater River at Ahsahka, Id	1926 - 1968
13341050	Clearwater River near Peck, Id	1964 - 2010
13340600	NF Clearwater River near Canyon Ranger Station, Id	1967 - 2010
13342500	Clearwater River at Spalding, Id	1910 - 2010
	Stage Data	
SRCI	SRCI:Snake River At Lewiston Control Point (HLIRXZZAZD water surface elevation)	1990 - 2010
CRLI	CRLI:Clearwater River At Lewiston (HLIRXZZAZD water surface elevation)	1990 - 2010
LWG	LWG:Lower Granite Dam & Lake On Snake River (HFIRXZZAZD forebay elevation)	1975 - 2010

Table 2. USGS stream gage stations used in the Lower Granite flood risk analysis.

The meaning of certain terms in the analysis of joint and multivariate frequency should be defined at the onset:

Annual Peak Discharge is the single greatest instantaneous discharge recorded at a stream gage location in a given water year. A water year begins on October 1 and ends on September 30. Frequency analysis in this study is based on the annual maximum series.

Average Daily Discharge is the average discharge recorded at a stream gage site over a given day. The day period is assumed to begin and end at midnight, 00:00 AM or 24:00 AM.

Maximum Day Discharge is the greatest daily average discharge recorded at a stream gage site or computed for a specified location in a given water year.

Coincident Discharge is the discharge that occurs at one location at the same time as either an annual peak discharge or maximum day discharge at another location. The site of the maximum discharge is called the primary discharge (or gage) and the site of the coincident discharge is called the secondary or complementary discharge (or gage) When several tributaries combine, there are several coincident discharges associated with a single primary discharge. The sum of the coincident average daily discharges

should be approximately equivalent to the primary maximum day discharge if all sources of flow are included.

All measured and recorded discharges are somewhat uncertain[14]. Values given in the gage records were assumed to be accurate unless by inspection they were clearly erroneous. Uncertainty of the discharge record is incorporated at later stages in the risk analysis.

The discharge records were complete for the regulated period and could be used without augmentation or extended interpolation. An exception was the record of outflow discharges for Dworshak Dam. The outflow for Dworshak dam is not measured directly at a USGS stream gage station, but the average daily outflow may be computed as the difference between the USGS stream gage near Peck (13341050) and the USGS stream gage at Orofino (13340000). The average daily outflow for Dworshak dam is also reported in the NWD database. The outflow computed from the USGS stream gage data was more consistent than values reported in the Corps database and was used in the analysis. The original discharge data may be obtained through the USGS NWIS website and is archived in a HEC-DSS database that is a part of the digital data appendix to this report.

2.2. Historic Floods at Lower Granite

Annual maximum discharges in Lower Granite have occurred in May and June since 1972 and are produced by snowmelt or a combination of rainfall and snowmelt[15] and is typical of the Pacific Northwest[16,17]. Significant flood events in 1894, 1933, 1948 and 1956 are discussed in the water control manuals for Lower Granite Lock and Dam[18]

[14] Rantz, S.E. (1982) *Measurement and Computation of Streamflow: Volume 1. Measurement of Stage and Discharge, Water Supply Paper 2175*. U.S. Geological Survey, Washington DC.

[15] USACE (1963). Lower Granite Lock and Dam, Design Memorandum No. 1, Hydrology, U.S. Army Corps of Engineers, Walla Walla, WA.

[16] MacDonald, L. H. and J. A. Hoffman; "Causes of peak flows in northwestern Montana and northeastern Idaho"; Water Resources Bulletin; 31(1), 79-95, 1995.

[17] Ferguson, S.A. (2000). "The spatial and temporal variability of rain-on-snow", in *Proceedings of the International Snow Science Workshop*, 1-6 October 2000, Big Sky, Montana. American Avalanche Association.

[18] USACE (2003) *Water Control Manual for Lower Granite Lock and Dam, Snake River Oregon, Washington, Idaho*, U.S. Army Corps of Engneers, Walla Walla, WA.

and Dworshak Dam[19]. Large early winter floods sometimes occur in the Clearwater River basin and can peak rapidly. The hydrograph of the December 1933 flood on the Clearwater River in Figure 5 reached a maximum discharge of 172,000 cfs in four days. In contrast, the hydrograph of the May 1948 flood on the Clearwater in Figure 6 rose to a peak 177,000 cfs over a period of about two weeks.

The 1948 flood was a significant flood on the Snake River below the confluence because the flow contributed by the Salmon and middle Snake River was substantial, while in 1933 the tributary flows from the Snake were relatively low. These historical floods indicate that while winter floods on the Clearwater River can rise rapidly, the water level at the confluence is more easily controlled with normal spillway gate operations because total flow at Lower Granite is moderate. Large spring snowmelt floods typically rise gradually, allowing time for progressive lowering of the spillway gates to control the water level at the confluence. The difference between these floods suggests that the potential for a flood to be caused by misoperation may be more likely during winter floods that have higher meteorological uncertainty and shorter warning times.

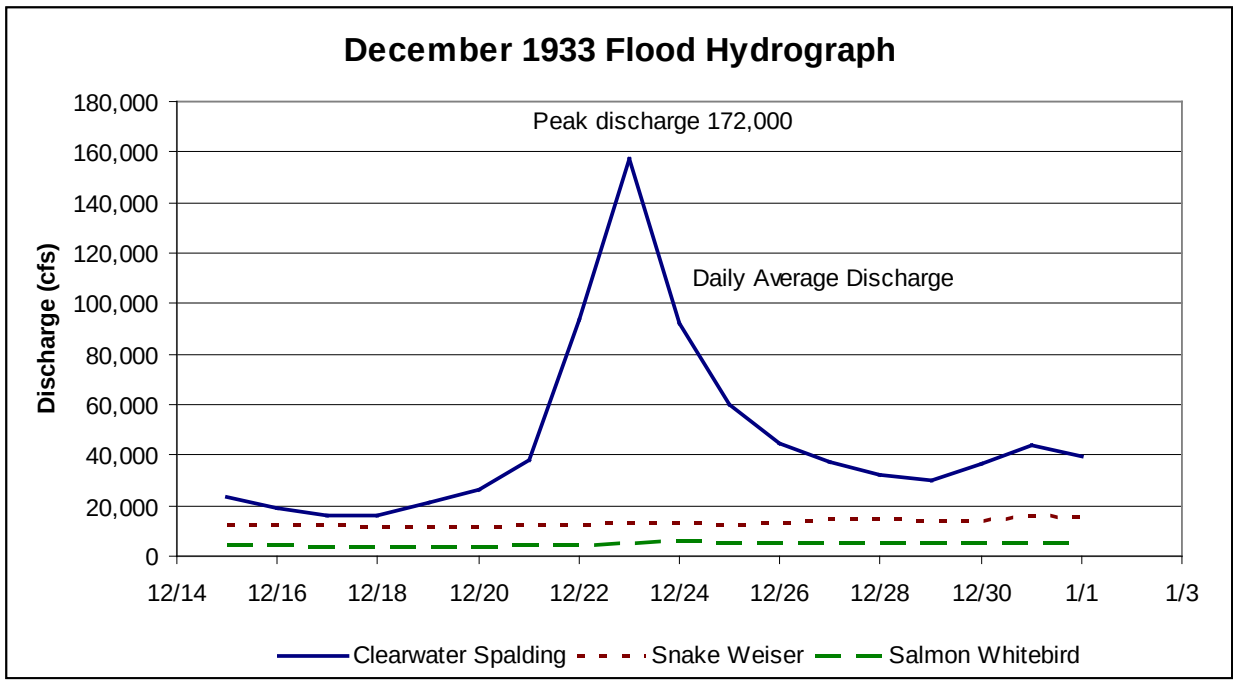


Figure 5. Hydrograph of the December 1933 flood on the Clearwater River.

[19] [19] USACE (1986) *Water Control Manual for Dworshak Dam and Reservoir, Clearwater River, Idaho*, U.S. Army Corps of Engneers, Walla Walla, WA.

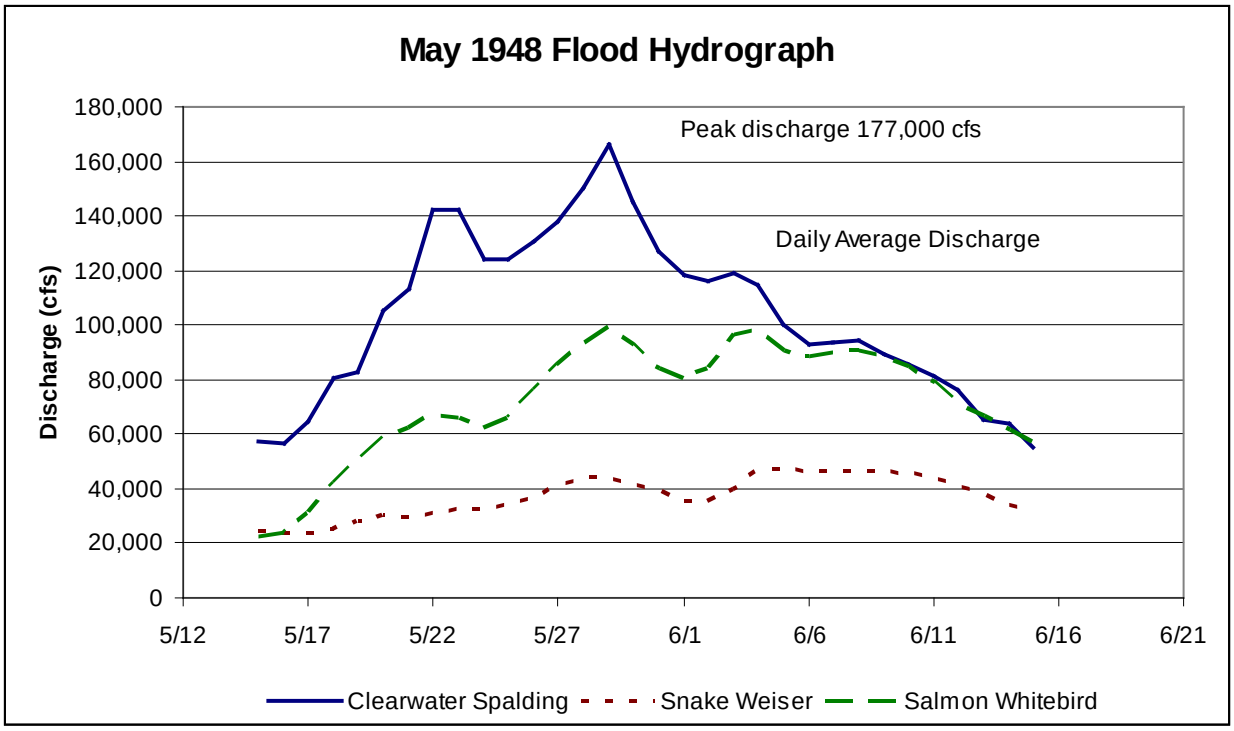


Figure 6. Hydrograph of the May 1948 flood on the Clearwater River.

2.3. Discharge Characteristics of the Tributary Rivers

Total discharge in Snake River below Lower Granite Reservoir is not measured directly at the confluence because of the backwater effect of Lower Granite Dam. Total inflow to Lower Granite at the confluence in this study is computed as the sum of the discharges recorded at the Anatone gage (USGS 13334300) at River Mile 167.2 on the Snake River (28 miles upstream from the confluence) and the Spalding gage (USGS 13342500) at River Mile 11.6 on the Clearwater River. Negligible flow is contributed by the small creeks and direct runoff areas between the gage locations and the confluence during the time of the maximum day discharge. Table 3 summarizes the maximum day total discharge for the confluence since 1972 and also lists the component flows from the Snake and Clearwater Rivers. On average, 65 percent of the maximum day discharge in Lower Granite is contributed by the Snake River and 35 percent is produced by the Clearwater River. Only in 1988 was the contribution from the Clearwater River larger than that from the Snake River.

Annual instantaneous peak discharge is not measured directly in Lower Granite and cannot be computed reliably from the sum of the instantaneous annual peaks at the Anatone and Spalding gages because in many years the timing of the annual peak discharges do not coincide. Table 4 compares the magnitude and timing of annual peak discharges at the Anatone gage and the Spalding gage. Peaks discharges occurred on the same day only four years out of 38 and were separated by a single day

only 7 times in the record. The timing of the peak flows is important because comparison of instantaneous discharge with daily moving average discharges in Table 5 shows that in many years the maximum annual daily average discharge rises and diminishes significantly within 3 to five days.

Even if the instantaneous peaks coincided, or if an approximate coincident instantaneous peak discharge could be determined from the record of 15-minute interval discharges at the complementary gage, hydraulic attenuation of the instantaneous peaks between the stream gages and the confluence cannot be computed accurately because of incomplete historic channel data. For this risk analysis, it is necessary to derive discharge and stage frequency statistics from the records of maximum day discharge and the coincident average daily discharges. Comparisons of the 15-minute discharge records and the stage recorded at the confluence show that the travel times of flood peaks from the Anatone and Spadling sites to the confluence is less than less than 6 hours on both rivers— so the sum of the maximum daily discharges at the gages is good approximation of maximum day discharge at the confluence. The travel time of flood waves was confirmed by routing of peak floods with hydraulic models developed from cross sections measured in 2010.

Flood risk analysis is typically based on the instantaneous peak discharge. Peak factors derived from the ratios of instantaneous peak discharges to daily average discharges are applied at later stages in the analysis to examine the effect of adopting daily average discharges as the basis of the frequency computations. Use of maximum day discharges also avoids the need to model hydraulic attenuation and circumvents some minor conceptual difficulties with using instantaneous discharges, which theoretically have no flood volume, in an analysis of overtopping risk.

Regulation of the Snake River by Hells Canyon Dam and other dams and reservoirs on the middle and upper Snake River have a substantial effect on the instantaneous peak and maximum day discharges at Lower Granite. Regulation of the North Fork of the Clearwater has a lesser influence on total discharge at Lower Granite, but significantly diminishes peak discharges on the Lower Clearwater River. Table 6 gives the relative contributions of the main tributary rivers to the annual maximum day discharge at Lower Granite. About 75 percent of the total maximum day discharge derives from unregulated watersheds. On average, the outflow from Hells Canyon Dam contributes about 19 percent of the flow and the outflow from Dworshak Dam contributes about 6 percent. The sum of the coincident average daily flows at the gage sites on the tributary rivers is within 5 percent of the total maximum daily flow at Lower Granite, which shows there is negligible attenuation of high discharges between the gage locations and the confluence. This is expected because of the moderately steep gradient and canyon topography of the tributary rivers.

While flow regulation does not dominate the annual peak discharge at Lower Granite, its effect should be treated in a manner that is compatible with the assumptions and approach taken in the risk analysis, particularly when estimating the extreme magnitude of low probability discharges. Ideally, the probabilities of project misoperation and structural limitations would be evaluated and incorporated into the risk analysis, but a detailed study of project operations was beyond the scope and practical limitations of this risk analysis. The approach here is to place the hydrologic uncertainty of regulated discharges in context of total probability and incorporate the regulated discharges as elements in a Monte Carlo analysis.

Lower Granite Annual Maximum Day Discharge							
			Annual	Average Daily Discharge		Proportion of Total Flow	
			Maximum Day	Snake	Clearwater	Snake	Clearwater
Water			Lower Granite	Anatone	Spalding	Anatone	Spalding
Year	Date	Rank	cfs	cfs	cfs	%	%
1972	2-Jun-72	4	227,200	135,000	92,200	59.4%	40.6%
1973	19-May-73	34	95,800	61,800	34,000	64.5%	35.5%
1974	18-Jun-74	1	312,000	191,000	121,000	61.2%	38.8%
1975	7-Jun-75	15	187,500	116,000	71,500	61.9%	38.1%
1976	11-May-76	14	188,800	118,000	70,800	62.5%	37.5%
1977	3-May-77	39	61,400	32,900	28,500	53.6%	46.4%
1978	9-Jun-78	21	145,000	93,000	52,000	64.1%	35.9%
1979	25-May-79	23	139,000	78,600	60,400	56.5%	43.5%
1980	12-Jun-80	26	130,800	92,400	38,400	70.6%	29.4%
1981	10-Jun-81	18	175,500	120,000	55,500	68.4%	31.6%
1982	18-Jun-82	11	205,800	145,000	60,800	70.5%	29.5%
1983	29-May-83	13	195,400	141,000	54,400	72.2%	27.8%
1984	31-May-84	2	252,700	177,000	75,700	70.0%	30.0%
1985	8-Jun-85	27	126,700	71,600	55,100	56.5%	43.5%
1986	1-Jun-86	7	214,800	154,000	60,800	71.7%	28.3%
1987	1-May-87	32	102,500	53,100	49,400	51.8%	48.2%
1988	7-May-88	37	87,600	43,100	44,500	49.2%	50.8%
1989	22-Apr-89	29	123,300	76,600	46,700	62.1%	37.9%
1990	30-May-90	28	125,200	63,300	61,900	50.6%	49.4%
1991	20-May-91	30	121,100	72,200	48,900	59.6%	40.4%
1992	2-May-92	38	82,300	47,000	35,300	57.1%	42.9%
1993	21-May-93	17	183,400	118,000	65,400	64.3%	35.7%
1994	11-May-94	35	94,400	64,300	30,100	68.1%	31.9%
1995	5-Jun-95	20	151,300	118,000	33,300	78.0%	22.0%
1996	10-Jun-96	9	206,800	148,000	58,800	71.6%	28.4%
1997	18-May-97	3	231,800	152,000	79,800	65.6%	34.4%
1998	27-May-98	5	218,000	166,000	52,000	76.1%	23.9%
1999	27-May-99	16	185,300	131,000	54,300	70.7%	29.3%
2000	23-Apr-00	31	113,700	68,200	45,500	60.0%	40.0%
2001	16-May-01	36	94,200	54,200	40,000	57.5%	42.5%
2002	31-May-02	24	138,100	84,200	53,900	61.0%	39.0%
2003	31-May-03	8	211,000	147,000	64,000	69.7%	30.3%
2004	29-May-04	25	137,900	69,500	68,400	50.4%	49.6%
2005	20-May-05	22	139,100	94,600	44,500	68.0%	32.0%
2006	21-May-06	12	203,600	144,000	59,600	70.7%	29.3%
2007	13-May-07	33	102,400	59,000	43,400	57.6%	42.4%
2008	20-May-08	10	205,900	130,000	75,900	63.1%	36.9%
2009	31-May-09	19	172,100	109,000	63,100	63.3%	36.7%
2010	6-Jun-10	6	216,100	159,000	57,100	73.6%	26.4%
	Average		161,679	105,092	56,587	63.7%	36.3%

Table 3. Lower Granite annual maximum day discharges.

Annual Peak Discharges Snake River and Clearwater River at Lower Granite					
Water Year	Date	Snake Anatone Annual Peak cfs	Date	Clearwater Spalding Annual Peak cfs	Difference day
1972	3-Jun-72	138,000	2-Jun-72	94,200	1
1973	18-May-73	63,700	18-May-73	36,900	0
1974	18-Jun-74	195,000	16-Jun-74	131,000	2
1975	8-Jun-75	119,000	3-Jun-75	79,300	5
1976	15-May-76	124,000	11-May-76	78,700	4
1977	7-Jun-77	38,000	2-May-77	31,700	36
1978	9-Jun-78	99,300	7-Jun-78	58,800	2
1979	25-May-79	82,000	24-May-79	66,900	1
1980	12-Jun-80	92,400	26-May-80	52,300	17
1981	10-Jun-81	122,000	19-Jun-81	66,400	-9
1982	18-Jun-82	148,000	17-Jun-82	66,300	1
1983	31-May-83	150,000	29-May-83	61,000	2
1984	31-May-84	183,000	31-May-84	81,500	0
1985	11-Apr-85	82,700	8-Jun-85	60,800	-58
1986	1-Jun-86	159,000	30-May-86	70,600	2
1987	13-May-87	57,900	1-May-87	52,000	12
1988	26-May-88	58,400	10-May-88	46,300	16
1989	22-Apr-89	77,600	8-May-89	52,900	-16
1990	31-May-90	68,800	29-May-90	70,500	2
1991	19-May-91	78,500	19-May-91	67,200	0
1992	1-May-92	48,400	1-May-92	42,200	0
1993	21-May-93	119,000	16-May-93	71,500	5
1994	10-May-94	68,100	15-May-94	41,800	-5
1995	5-Jun-95	122,000	7-May-95	55,300	29
1996	10-Jun-96	151,000	9-Feb-96	92,800	122
1997	2-Jan-97	179,000	17-May-97	85,100	-135
1998	27-May-98	169,000	23-May-98	56,800	4
1999	27-May-99	152,000	26-May-99	63,100	1
2000	23-Apr-00	68,900	22-Apr-00	46,000	1
2001	17-May-01	65,500	15-May-01	44,700	2
2002	31-May-02	86,200	15-Apr-02	69,400	46
2003	31-May-03	156,000	30-May-03	68,300	1
2004	31-May-04	77,700	29-May-04	71,300	2
2005	20-May-05	107,000	17-May-05	52,200	3
2006	21-May-06	147,000	20-May-06	67,000	1
2007	15-May-07	62,700	13-May-07	46,000	2
2008	21-May-08	143,000	19-May-08	79,800	2
2009	7-Jun-09	126,000	31-May-09	67,000	7

Table 4. Annual peak discharge at Anatone on the Snake River and Spalding on the Clearwater River.

Lower Granite Annual Maximum Day Discharge Reduction Rate				
	Annual	Reduction from Maximum Day		
	Maximum Day	3-Day	5-Day	7-Day
	Discharge	Average	Average	Average
Date	cfs	cfs	cfs	cfs
2-Jun-72	227,200	2.3%	5.7%	8.5%
19-May-73	95,800	0.8%	3.7%	8.6%
18-Jun-74	312,000	1.5%	3.1%	5.8%
7-Jun-75	187,500	3.1%	5.8%	7.3%
11-May-76	188,800	5.2%	9.1%	11.1%
3-May-77	61,400	9.6%	16.1%	20.2%
9-Jun-78	145,000	2.7%	5.9%	9.1%
25-May-79	139,000	2.4%	4.7%	7.7%
12-Jun-80	130,800	1.9%	5.0%	6.4%
10-Jun-81	175,500	4.4%	10.1%	12.7%
18-Jun-82	205,800	2.5%	4.7%	6.7%
29-May-83	195,400	1.2%	3.1%	6.1%
31-May-84	252,700	8.3%	13.8%	17.3%
8-Jun-85	126,700	6.0%	11.3%	15.0%
1-Jun-86	214,800	0.3%	1.3%	3.1%
1-May-87	102,500	4.8%	9.7%	14.2%
7-May-88	87,600	1.8%	3.4%	9.3%
22-Apr-89	123,300	2.6%	6.9%	11.2%
30-May-90	125,200	10.5%	16.2%	19.9%
20-May-91	121,100	4.2%	9.8%	13.2%
2-May-92	82,300	2.8%	9.2%	13.1%
21-May-93	183,400	1.6%	4.1%	7.3%
11-May-94	94,400	2.9%	2.6%	4.9%
5-Jun-95	151,300	1.5%	4.3%	6.3%
10-Jun-96	206,800	1.6%	4.0%	6.2%
18-May-97	231,800	3.0%	6.1%	8.7%
27-May-98	218,000	6.7%	11.4%	12.8%
27-May-99	185,300	5.0%	9.4%	11.8%
23-Apr-00	113,700	2.2%	4.6%	6.3%
16-May-01	94,200	2.6%	7.4%	11.8%
31-May-02	138,100	3.6%	7.1%	10.0%
31-May-03	211,000	7.2%	11.9%	16.4%
29-May-04	137,900	4.4%	9.8%	13.9%
20-May-05	139,100	5.0%	7.5%	8.7%
21-May-06	203,600	3.4%	5.3%	7.4%
13-May-07	102,400	3.0%	4.8%	8.0%
20-May-08	205,900	2.9%	8.4%	14.8%
31-May-09	172,100	2.4%	4.1%	6.1%
6-Jun-10	216,100	1.2%	5.9%	11.5%

Table 5. Lower Granite reduction rate of maximum day discharge.

		Annual	Coincident Average Daily Discharge						
		Maximum Day	Salmon	Clearwater	Snake	Grande	NF Clearwater		Tributary
		Lower Granite	Whitebird	Orofino	Hells Canyon	Ronde	Dworshak	Imnaha	Total
Date	Rank	cfs	Percent	Percent	Percent	Percent	Percent	Percent	Percent
18-Jun-74	1	312,000	41.0%	24.5%	13.3%	5.1%	12.4%	1.2%	97.4%
31-May-84	2	252,700	34.1%	26.0%	26.9%	6.0%	3.7%	1.2%	97.9%
18-May-97	3	231,800	42.7%	33.7%	14.2%	6.5%	0.3%	1.2%	98.5%
27-May-98	4	218,000	19.7%	16.5%	42.8%	7.5%	5.9%	2.2%	94.6%
6-Jun-10	5	216,100	36.6%	23.9%	24.6%	8.5%	0.7%	1.4%	95.7%
1-Jun-86	6	214,800	44.1%	23.3%	19.3%	4.4%	4.3%	1.2%	96.5%
31-May-03	7	211,000	42.8%	28.6%	19.9%	5.7%	1.2%	1.2%	99.4%
10-Jun-96	8	206,800	45.8%	23.7%	21.0%	3.7%	4.1%	0.9%	99.2%
20-May-08	9	205,900	42.4%	34.3%	7.8%	8.7%	0.9%	2.3%	96.4%
18-Jun-82	10	205,800	44.2%	26.4%	18.1%	5.3%	3.1%	1.2%	98.3%
21-May-06	11	203,600	44.4%	25.4%	15.3%	6.5%	2.8%	1.6%	95.9%
29-May-83	12	195,400	43.8%	24.3%	20.2%	6.0%	3.2%	1.6%	99.1%
11-May-76	13	188,800	31.4%	35.6%	21.5%	7.7%	2.0%	1.3%	99.4%
7-Jun-75	14	187,500	38.5%	32.4%	15.3%	5.9%	3.8%	1.6%	97.4%
27-May-99	15	185,300	41.1%	29.0%	13.0%	6.2%	0.4%	1.6%	91.3%
21-May-93	16	183,400	35.0%	25.7%	20.7%	6.8%	9.5%	1.3%	99.1%
10-Jun-81	17	175,500	35.8%	23.0%	24.4%	5.5%	7.7%	0.9%	97.4%
31-May-09	18	172,100	42.7%	33.3%	12.4%	6.9%	2.8%	1.2%	99.4%
5-Jun-95	19	151,300	45.5%	21.2%	26.3%	6.8%	0.1%	1.6%	101.6%
9-Jun-78	20	145,000	47.2%	31.0%	13.4%	4.4%	5.3%	1.2%	102.5%
20-May-05	21	139,100	33.7%	23.2%	29.9%	6.0%	6.7%	1.6%	101.2%
25-May-79	22	139,000	37.8%	34.0%	9.2%	7.6%	8.4%	1.4%	98.4%
31-May-02	23	138,100	37.9%	36.6%	15.0%	6.9%	1.2%	1.3%	98.9%
29-May-04	24	137,900	26.5%	33.1%	13.1%	8.2%	13.1%	1.4%	95.2%
12-Jun-80	25	130,800	26.1%	21.1%	35.8%	4.6%	8.5%	1.3%	97.3%
8-Jun-85	26	126,700	26.1%	27.9%	19.7%	7.2%	14.9%	1.5%	97.3%
30-May-90	27	125,200	27.0%	36.6%	12.0%	4.6%	6.1%	1.8%	88.0%
22-Apr-89	28	123,300	22.2%	37.1%	25.2%	9.7%	-0.2%	1.4%	95.4%
20-May-91	29	121,100	20.3%	34.8%	15.4%	13.8%	1.7%	1.7%	87.6%
23-Apr-00	30	113,700	20.5%	25.9%	28.4%	8.1%	13.7%	1.5%	98.1%
1-May-87	31	102,500	29.6%	38.5%	8.0%	8.4%	8.8%	1.3%	94.6%
13-May-07	32	102,400	36.0%	31.5%	14.6%	5.4%	9.5%	1.3%	98.2%
19-May-73	33	95,800	38.3%	34.4%	10.8%	6.5%	0.6%	1.7%	92.3%
11-May-94	34	94,400	29.8%	31.0%	24.7%	6.7%	0.2%	1.3%	93.8%
16-May-01	35	94,200	33.1%	39.0%	16.9%	7.5%	1.5%	1.1%	99.0%
7-May-88	36	87,600	14.6%	21.1%	26.3%	4.1%	27.6%	0.6%	94.3%
2-May-92	37	82,300	25.4%	27.2%	24.8%	3.9%	14.6%	0.6%	96.5%
3-May-77	38	61,400	22.6%	44.3%	17.8%	4.9%	2.0%	0.6%	92.1%
Average		159,955	34.4%	29.5%	19.4%	6.5%	5.6%	1.4%	96.7%

Table 6. Coincident average daily discharges of the tributaries to Lower Granite Reservoir.

2.4. Correlation of Tributary Discharges

Correlation between magnitudes of the discharges in the tributary rivers is an important element of a multivariate joint probability analysis. In a long series of events, tributary discharges that tend to peak at about the same time will on average produce greater total combined maximum flows than those whose peaks are independent and tend to compensate. The aim of the correlation analysis presented in this section is to investigate the dependency between the tributary flows that produce maximum discharges at the confluence. This is a form of spatial dependency analysis similar to

that used in the analysis of the joint probability of storm surge, wind waves and river stage in coastal environments[20].

Spatial association of the tributary rivers is constrained by the stream network (Figure 4). In this risk analysis, only the correlation of flows upstream of the confluence need be evaluated to the extent that defines the limits of flow regulation. Correlation between paired gages is defined by the standard correlation coefficient computed for the sequence of maximum day discharges at one gage with the coincident daily average discharges at the complementary gage. A single correlation coefficient describes the correlation of the entire sequence of flows. Of interest is how correlation changes with flow magnitude. The full sequence flows that includes many relatively high probability-low discharges might show strong correlation, whereas the largest flows might show little or no correlation. It is the correlation of the relatively high discharges that have the most influence on the discharge-exceedance probabilities in the risk analysis. Correlation coefficients may be repeatedly computed for the joint series of ranked discharges as the least ranked (smallest discharge of the primary gage left in the sequence) pairs are removed. To form the correlation plot, the sequence of correlation coefficients may then be plotted against the minimum discharge of the primary gage in the paired series.

The value of the correlation plot is as an indicator of whether two stream gage stations are positively dependent (augmenting), independent (neutral) or negatively dependent (compensating). The correlation plot is an objective means to ascertain how far upstream in a regulated flow network the tributary flows remain correlated. Flows that are substantial and correlated must be treated appropriately in the frequency analysis so as not to underestimate or overestimate their effect on the joint probability of flood risk. Correlation plots that show increasing correlation with discharge indicate a relatively strong dependence between the paired gages at more extreme flows. Correlation plots that show decreasing or even negative correlation trends suggest that the gages become increasing less dependent or compensating as discharge at the primary gage increases.

Figure 7 shows that coincident average daily discharge at Spalding correlates well with the maximum day discharge at Anatone and becomes more strongly correlated at high discharges. Figure 8 shows that coincident average daily discharge at Anatone correlates well with the maximum day discharge at Spalding, but becomes less correlated at higher discharges. This can be explained by the relative size and

[20] Hawkes, P. and Svensson, C. (2005). Joint Probability: *Dependence Mapping and Best Practice: Technical Report on Dependence Mapping, R&D Technical Report FD2308/TR1*, Defra / Environment Agency Flood and Coastal Defence R&D Programme, London.

location of the Snake and Clearwater River basins. High discharges on the Snake River indicate that the lower Snake basin, including the Clearwater basin, is experiencing widespread snowmelt or a large regional rain storm in addition to snowmelt. The smaller Clearwater River basin can be influenced by more localized rain and snowmelt events that do not extend across the Salmon and Grande Ronde River basins or the regulated regions of the middle and upper Snake River.

Figure 9 shows that the outflow of Dworshak Dam becomes more correlated with total annual maximum day inflow to Lower Granite as the coincident release increases though the magnitude of the release from Dworshak is relatively low. Some positive correlation is expected because flow from Dworshak is a component of the total flow at Lower Granite. The degree of correlation is dependent on the magnitude of the discharge from Dworshak relative to the total flow. A positive correlation is likely because of the need to maintain reserve storage in Dworshak for late season flood events.

Figure 10 shows that the outflow of Hells Canyon Dam is well correlated when the complete series of annual discharges are included in the computation of the correlation coefficient, but becomes negatively correlated at high discharge. It appears, and makes sense, that projects in the upper and middle Snake River are operated so they tend to mitigate flood flows in the lower Snake basin and Clearwater basin. The negative correlation of middle Snake River flows at higher discharge is confirmed in the correlation plot in Figure 11 for the Snake River at Weiser above Brownlee Reservoir. These correlation plots show that the frequency characteristics of the regulated flows of the Snake River have relatively little influence in a conservative analysis of flood risk at the confluence. Diminished influence of discharge in the Snake River above Hells Canyon is supported by the analysis of large storms. In the translocated 72-hour rainfall distribution in Figure 12, the relative rainfall depth decreases to less than 10 percent in the regulated middle Snake River tributary area even when the winter maximized (1909) storm is centered on the Salmon River basin.

It is again worthwhile to note that regulated discharge is a low percentage of the total annual maximum day inflow to Lower Granite. Previous modeling of Standard Project Floods (SPF) on in the Lower Columbia River basin[21] (Table 7) found that regulated flow is about 25 percent of the total SPF discharge in the lower Snake River. Similarly, tributary hydrographs for the SPF at Lower Granite in Design Memorandum 1

[21] USACE (1969). *Lower Columbia River Standard Project Flood and Probable Maximum Flood*, U.S. Army Engineering Division, North Pacific, Portland, OR.

(DM1) for Lower Granite Dam[22] show that the regulated Snake River at Brownlee produces about 15 percent of the total discharge during the peak of SPF hydrograph below the confluence.

It is noted that the number of values decrease in the computation of correlation coefficients as pairs are eliminated, so a correlation plot is an indicator of the relative importance of the correlation of two stream gages and not an absolute measure of correlation; a single valid value of the correlation coefficient must be selected for the joint flood risk analysis. Correlation between the gages in the joint probability analysis is computed with the full sequence of paired values for the period of regulation by Dworshak Dam (1972-2010). This is the first correlation coefficient depicted in each of the correlation plots.

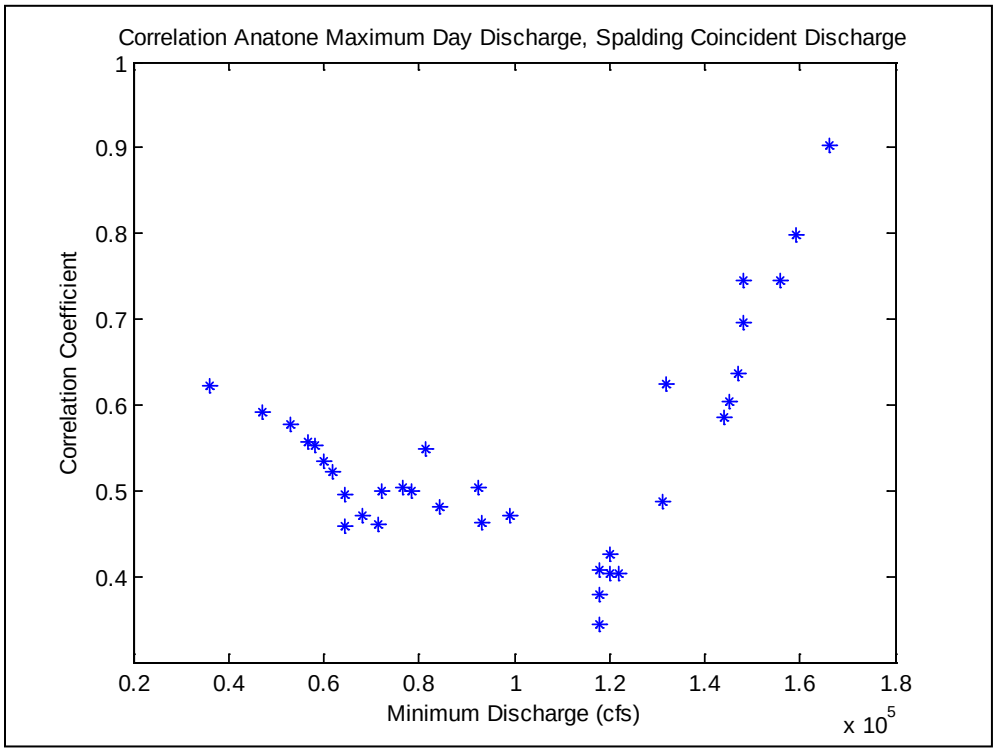


Figure 7. Correlation Anatone maximum day discharge and Spalding coincident discharge.

[22] USACE (1963). Lower Granite Lock and Dam, Design Memorandum No. 1, Hydrology, U.S. Army Corps of Engneers, Walla Walla, WA.

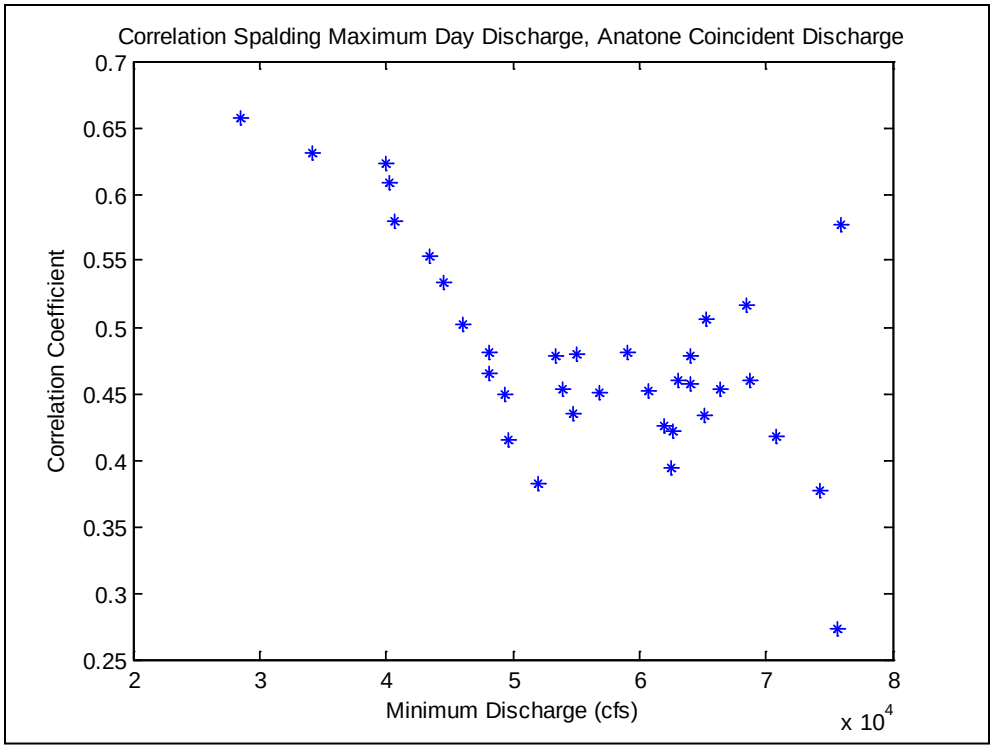


Figure 8. Correlation Spalding maximum day discharge and Anatone coincident discharge.

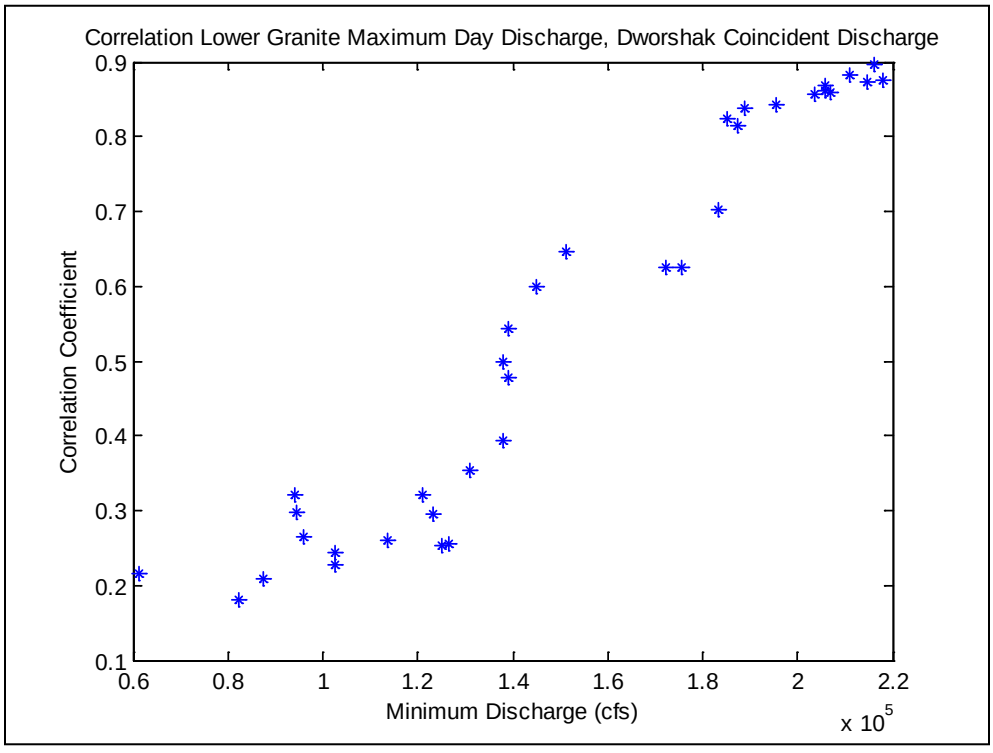


Figure 9. Correlation Lower Granite maximum day discharge and Dworshak outflow coincident discharge.

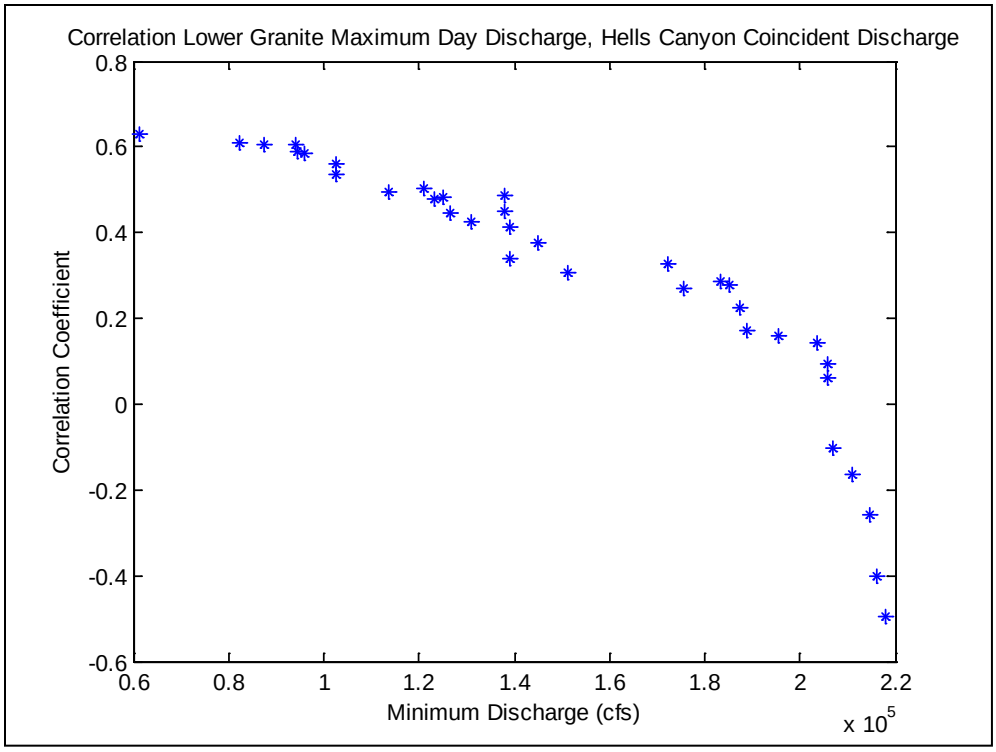


Figure 10. Correlation Lower Granite maximum day discharge and Hells Canyon outflow coincident discharge.

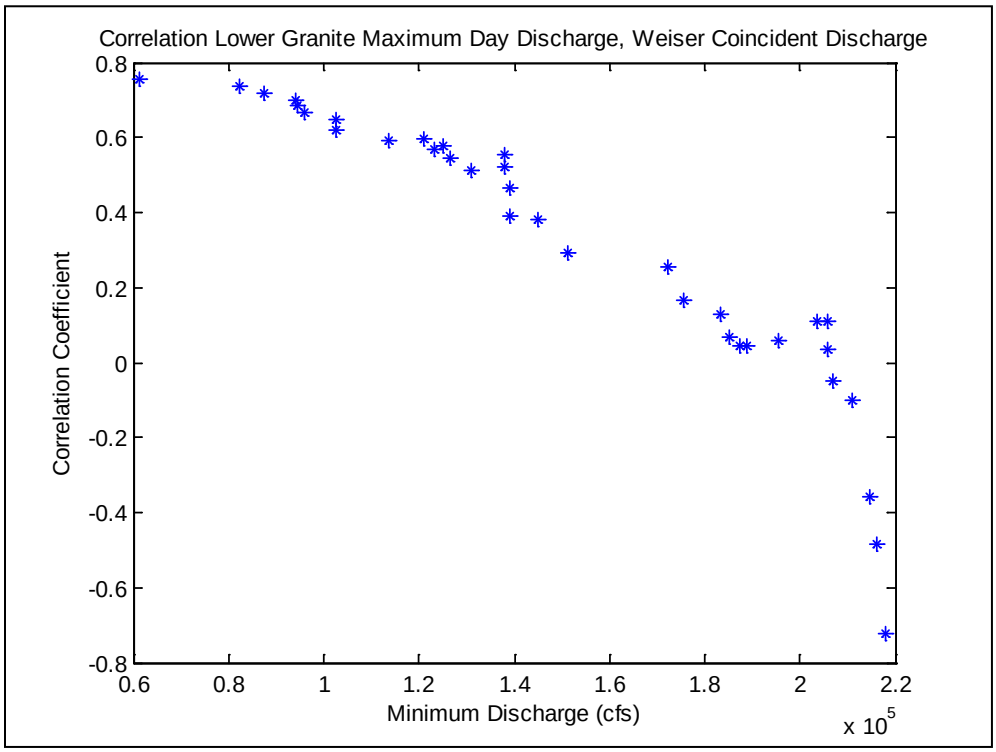


Figure 11. Correlation Lower Granite maximum day discharge and the coincident discharge at Weiser on the Snake River.

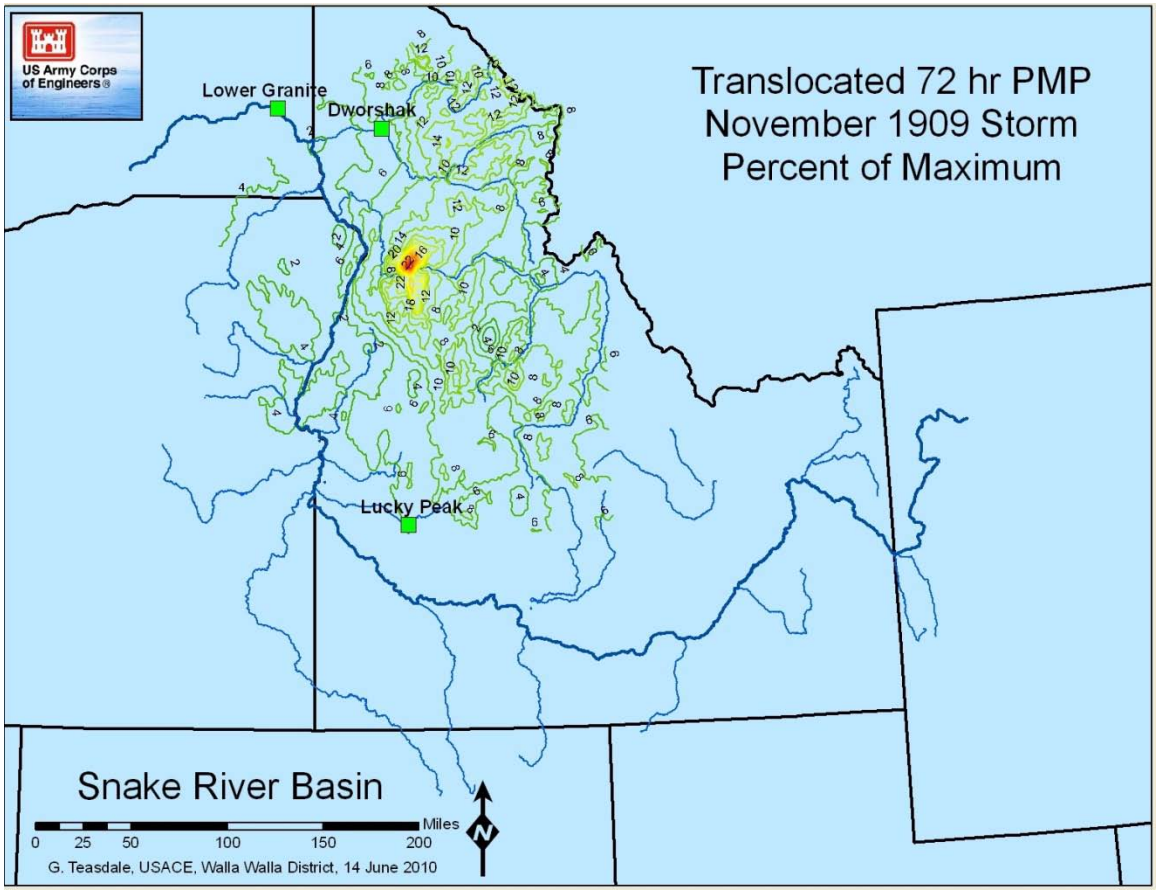


Figure 12. Translocated 72hr PMP Rainfall Distribution.

Standard Project Flood Discharges (USACE 1969 Analysis)					
River	Location	Peak Date	Unregulated cfs	Regulated cfs	Percent of Regulated SPF
Snake	Weiser	10-Jun	213,000	73,000	24%
Snake	Brownlie	10-Jun	215,000	77,500	25%
Clearwater	Dworshak	1-Jun	55,600	4,000	1.3%
Other unregulated			239,400	226,500	74%
Snake	Ice Harbor	10-Jun	510,000	308,000	100%

Table 7. Contribution of regulated discharge to the Standard Project Flood.

2.5. Regional Skew Comparison

Extreme values of the Log Pearson Type 3 annual peak discharge frequency distribution are influenced by the skew parameter[23,24]. Flood skew is ultimately bounded by the distribution of rainfall and weather events that generate runoff and is subsequently altered by watershed storage processes[25]. Watershed processes that increase storage tend to decrease skew. It is increasingly recognized that the existing generalized regional skew map in Bulletin 17B should be updated with the now longer record of discharge data using more accurate computational methods[26]. It is also seen that other aspects of flood frequency distribution selection and fitting should be addressed including the effect of outliers, climate change and flow regulation[27]. A comprehensive review of the new regional skew estimation methods and their application was beyond the scope of this study. Such an effort is considerably more complex that previous methods[28,29]. Instead, station skews were compared to the regional skew from Bulletin 17B and the sensitivity of the flood frequency statistics to the weighted skew value was evaluated. This approach is justified by the long period of record for the primary stream gages. The influence of regional skew in the weighted skew computation of Bulletin 17B decreases as the length of the gage record increases because it diminishes the station mean square error. The long gage record can also

[23] USGS (1982). *Hydrology Subcommittee of the Interagency Advisory Committee on Water Data, Bulletin 17B 1982 (Mar), Guidelines for Determining Flood Flow Frequency*, U.S. Department of Interior, Geological Survey, Office of Water Data Coordination,Reston, VA.

[24] Griffis, V.W and Stedinger, J.R. (2007). "Log-Pearson Type 3 distribution and its application in flood frequency analysis. I: distribution characteristics.", *Journal of Hydrologic Engineering*, 12(5), 482-491.

[25] McCuen, R.H. and Smith, E. (2008). "Origin of flood skew", *Journal of Hydrologic Engineering*, 13(9), 771-115.

[26] Stedinger, J.R. and Griffis, V.W. (2008). "Flood Frequency Analysis in the United States: time to update. ", *Journal of Hydrologic Engineering*, 13(4), 199-287.

[27] England, J.F. and Cohn, T.A. (2007). "Scientific and Practical Considerations Related to Revising Bulletin 17B: The Case for Improved Treatment of Historical Information and Low Outliers", in *World Environmental and Water Resources Congress 2007*, ASCE, New York.

[28] Reis, D. S., Jr., Stedinger, J.R., and Martins, E.S. (2005), "Bayesian generalized least squares regression with application to log Pearson type 3 regional skew estimation", *Water Resources Research*, 41, W10419, doi:10.1029/2004WR003445.

[29] Veilleux, A.G. and Stedinger, J.R. (2010). "Bayesian GLS analysis of California regional skew", in *World Environmental and Water Resources Congress 2010*, ASCE, New York.

show trends in skew values over the period of record may indicate changes in climate or watershed characteristics.

The regional skew depicted in Bulletin 17B for the lower Snake River and Clearwater River basins is uniformly -0.3 across the Clearwater River and Salmon River basins and is between -0.3 and -0.2 in the Grande Ronde basin (Figure 13). These values of skew reflect the snowmelt dominated period of peak runoff. The mean square error of the regional skew for all locations associated with the national map is 0.302 in units of base 10 logarithm (log) of discharge in cfs. In separate work at about the same time as Bulletin 17B was developed, USGS in Idaho developed seasonal regional skew maps and similarly found a uniform value of -0.3 to be an appropriate regional skew for snowmelt floods[30] in the study region. The mean square error for the seasonal snowmelt skew for the USGS 1981 maps[31] is 0.15, about half the error of the national skew map in Bulletin 17B.

Frequency factors for the LP3 distribution are based on a skew value that is a weighted combination of the regional skew and the skew computed from the discharge record (station skew) according to the conditional formulas described in the Bulletin 17B procedure. To study the influence of skew on flood discharge estimates, station skews and weighted skews were computed for different periods of record for the primary unregulated tributary discharges to Lower Granite. Table 8 summarizes the effect of the changes in skew and the influence of regional skew on 1-percent exceedance discharge. The three primary unregulated stations were compared in the analysis: the Clearwater River at Orofino, the Salmon River at Whitebird and the Grande Ronde River at Troy. The data from each station was separated into four series: the first half of the full period of record, the last half of the record, the period of regulation at Dworshak Dam, and the full period of record. The mean square error of the regional skew used in the computations in this table was the Bulletin 17B value of 0.302. The difference between peak discharges computed with the station skew and the weighted skew were about 1 percent for Orofino and Whitebird, and less than about 5 percent for Troy.

Table 8 shows that the station skews and weighted skews changed substantially over the latter half of the record compared to first half. The general trend is for the station skew to increase (become less negative). This means that the LP3 distribution

[30] Kjelstrom, L.C., and Moffatt, R.L. (1981), *A method of estimating flood-frequency parameters for streams in Idaho: U.S. Geological Survey Open-File Report 81-909,* U.S. Geological Survey, Boise, ID. Also in *Appendix B Hydraulic Design Manual*, Idaho Department of Transportation, 2009.

[31] Berenbrock, C. (2002). *Estimating the Magnitude of Peak Flows at Selected Recurrence Intervals for Streams in Idaho*, Water-Resources Investigations Report 02–4170, U.S. Geological Survey, Boise, ID.

has become more positively skewed in the latter part of the record and that peak discharges become greater for a given exceedance probability. The one-percent exceedance discharge estimates at Whitebird is about 12 percent greater based on the latter half of the record compared to an estimate based on the full period of record. The discharge estimates at Orofino are less affected by the period of record and the discharge estimate at Troy is somewhat more affected. Possible causes of the positive trend in station skew include long term climate cycles, the decrease in the storage of precipitation in the winter snowpack of the Pacific Northwest caused by climate warming and the changes in forest land cover due the increased prevalence of severe wildfire in forestlands of the Clearwater River and Salmon River basins.

The period of regulation at Dworshak (1972- 2010) produces the greatest discharge estimates of the four series at Whitebird and Orofino. For reasonable conservatism and because of possible non-stationary due to climate and watershed change during the 50-year forward-looking analysis period adopted for the study, the 1972-2010 stream gage record was selected as the basis of the flood frequency analysis for the evaluation of flood risk at the confluence.

A weighted skew was used throughout the analysis to conform to Bulletin 17B procedures. In a comparison not shown in Table 8, use of a 0.15 mean square error for the regional skew from the USGS seasonal analysis decreased the peak discharges for Orofino and Whitebird by about 1 percent and the peak discharge for Troy about 5 percent. The Bulletin 17B mean square error produced the more conservative estimate of peak discharge so it was used throughout the risk analysis.

					Based on Log10 of Discharge in cfs						1-Percent Exceedance		Percent Change Discharge	
		Period	Years of	Mean			Station	Weighted	Percent Change Skew		Station	Weighted	Compared to Full Period	
River	Gage	Water Year	Record	cfs	Mean	St. Dev.	Skew	Skew	Station	Weighted	cfs	cfs	Station	Weighted
Clearwater	Orofino	1965 - 1987	23	54543	4.737	0.118	-0.116	-0.194	57%	42%	100,330	98,773	0.8%	0.5%
Clearwater	Orofino	1988 -2010	23	51126	4.709	0.125	-0.003	-0.126	-96%	-8%	99,889	97,318	0.4%	-0.9%
Clearwater	Orofino	1972 -2009	38	52150	4.717	0.126	0.006	-0.088	-109%	-36%	102,490	100,450	3.0%	2.3%
Clearwater	Orofino	1965 - 2010	46	52807	4.723	0.121	-0.074	-0.137	--	--	99,517	98,237		
Salmon	Whitebird	1912 - 1961	48	59643	4.776	0.143	-0.486	-0.426	23%	13%	114,150	115,820	-11.6%	-10.7%
Salmon	Whitebird	1962 - 2009	48	59432	4.774	0.186	-0.343	-0.330	-13%	-12%	144,430	145,030	11.9%	11.8%
Salmon	Whitebird	1972 -2009	38	57722	4.761	0.197	-0.211	-0.240	-47%	-36%	154,400	152,910	19.6%	17.8%
Salmon	Whitebird	1912 - 2009	96	59537	4.775	0.165	-0.395	-0.376	--	--	129,070	129,750		
Grande Ronde	Troy	1945 - 1977	33	14728	4.168	0.185	0.019	-0.089	-93%	-167%	39,899	38,570	-13.6%	-12.6%
Grande Ronde	Troy	1978 - 2009	32	14863	4.172	0.209	0.454	0.158	68%	20%	53,339	48,129	15.5%	9.0%
Grande Ronde	Troy	1972 -2009	38	14633	4.165	0.213	0.196	0.033	-28%	-75%	49,099	46,310	6.3%	4.9%
Grande Ronde	Troy	1945 - 2009	65	14795	4.170	0.196	0.270	0.132	--	--	46,198	44,151		

Table 8. Change in station skew and LP3 weighted skew at unregulated discharge sites.

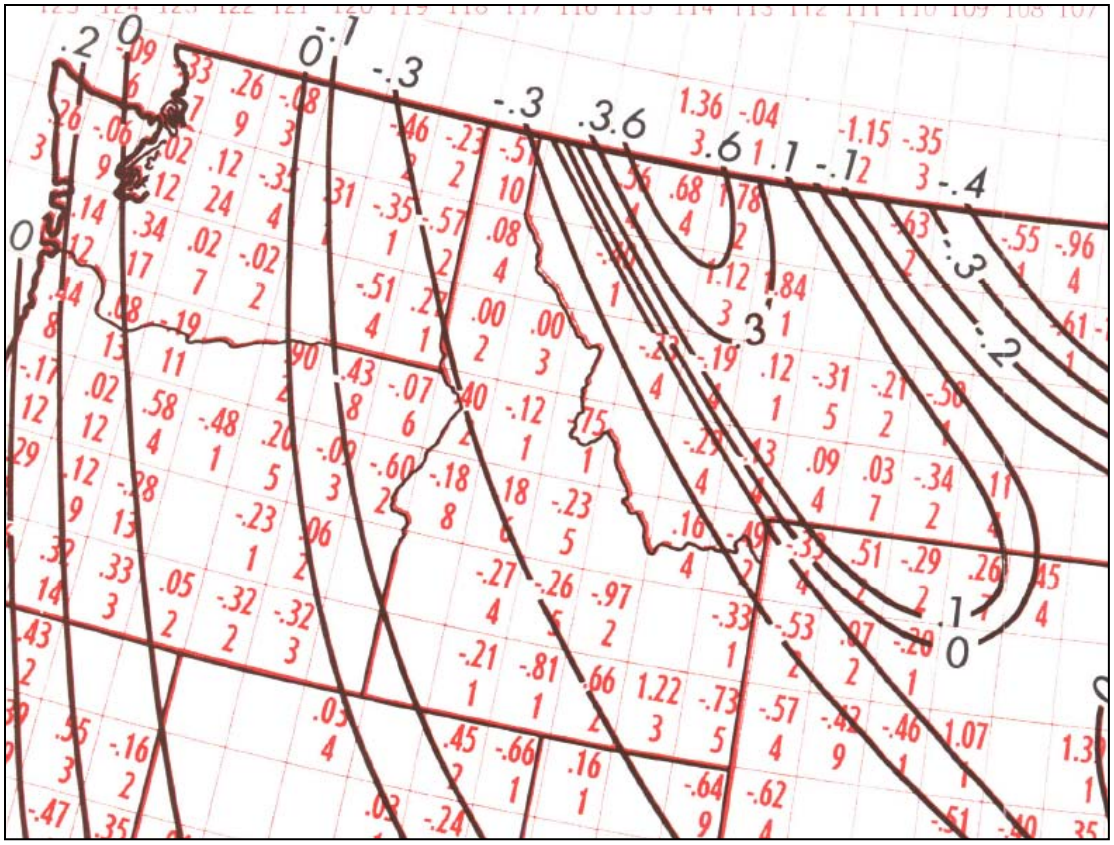


Figure 13. Pacific Northwest region from the regional skew map in Bulletin 17B[23].

2.6. Climatic Patterns

Climatic patterns influence stream flows in the Pacific Northwest[32] and may impose variability in extreme discharges that affect flood risk[33]. These include the interannual El Niño/ Southern Oscillation (ENSO) and the Pacific Decadal Oscillation (PDO)[34]. A consensus approach that incorporates climate variables into Bulletin 17B

[32] Piechota, T.C. and Dracup, J.A. (1999) Implications of the El Niño-Southern Oscillation for Long-Range Streamflow Forecasting: The Columbia River Basin, in Preparing for the 21st Century Proceedings of 29th Annual Water Resources Planning and Management Conference.

[33] IPCC (2007). Contribution of Working Group II to the Fourth Assessment Report of the Intergovernmental Panel on Climate Change, 2007, M.L. Parry, O.F. Canziani, J.P. Palutikof, P.J. van der Linden and C.E. Hanson (eds)

Cambridge University Press, Cambridge, United Kingdom and New York, NY, USA.

[34] Piechota, T.C., J.D. Garbrecht, and J.M. Schneider, (2006). Climate variability and climate change, Climate Variations, Climate Change, and Water Resources Engineering, eds. J.D. Garbrecht and T.C. Piechota, American Society of Civil Engineers, Reston, VA, pp. 19-33, 2006.

flood frequency analysis has yet to develop[35,36]. To better understand the potential impacts of climate patterns on extreme discharges in the lower Snake River basin, the Multivariate ENSO index (MEI) and the Sea Surface Temperature (SST) Cold Tongue index (CTI) are compared to the long-term record of discharges at the primary stream gages.

El Niño/Southern Oscillation (ENSO) is the most important coupled ocean-atmosphere phenomenon that causes global climate variability on interannual time scales[37]. The multivariate ENSO Index (MEI) is based on the six main observed variables over the tropical Pacific: sea-level pressure, surface wind, sea surface temperature (SST), surface air temperature, and total cloudiness fraction of the sky. The ENSO-MEI index is updated frequently by NOAA. Figure 14 is a plot of the MEI since 1950. Strong La Niña conditions are indicated by the current MEI (2010) which has not been this low since 1975. The region of equatorial cold Pacific Sea Surface Temperature (SST) is commonly referred to as the "cold tongue." The cold tongue index (CTI) is the average SST anomaly over 6N-6S, 180-90W.

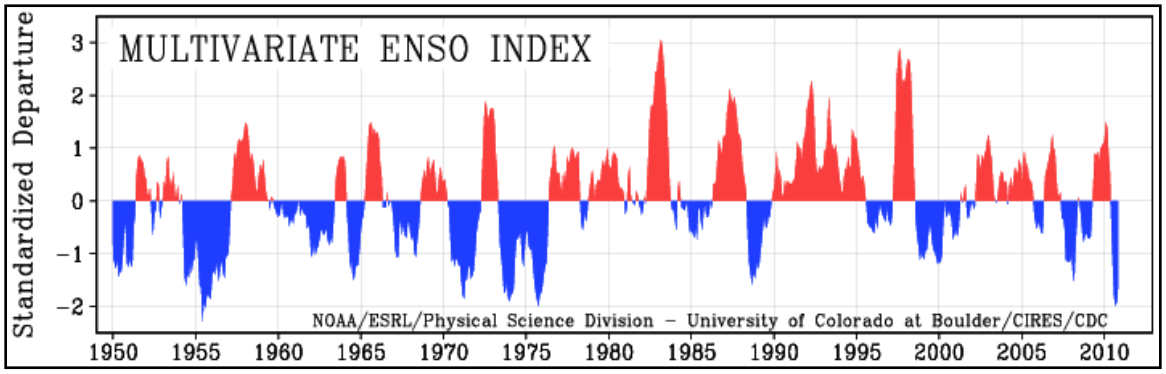


Figure 14. Multivariate ENSO Index 1950 – 2010.

The Pacific Northwest is more likely to be wetter than normal in the late fall and early winter with the presence of a well-established La Niña. On average, La Niña winters are warmer than normal in the southeastern U.S. and colder than normal in the

[35] Griffis, V.W. and Stedinger, J.R. (2007). "Incorporating climate change and variability into Bulletin 17B LP3 model", in *World Environmental and Water Resources Congress 2007*, ASCE, NY.

[36] Brekke, L.D., Kiang, J.E., Olsen, J.R., Pulwarty, R.S., Raff, D.A., Turnipseed, D.P., Webb, R.S., and White, K.D., 2009, Climate change and water resources management—A federal perspective: U.S. Geological Survey Circular 1331, 65 p. (Also available online at http://pubs.usgs.gov/circ/1331/.)

[37] NOAA (2010). http://www.esrl.noaa.gov/psd/enso/enso.mei_index.html.

Pacific Northwest. According to the National Centers for Environmental Prediction, this century's previous La Niñas began in 1903, 1906, 1909, 1916, 1924, 1928, 1938, 1950, 1954, 1964, 1970, 1973, 1975, 1988, and 1995. These events typically continued into the following spring. Since 1975, La Niñas have been only half as frequent as El Niños.

The plots in Figure 15 and Figure 16 compare the CTI and MEI with the annual peak discharge at Spalding. Large peak discharges are associated with antecedent negative values of the CTI and MEI. The period of regulation of the lower Clearwater River began in 1972, so maximum peak discharges after this time are not as high as in the earlier record.

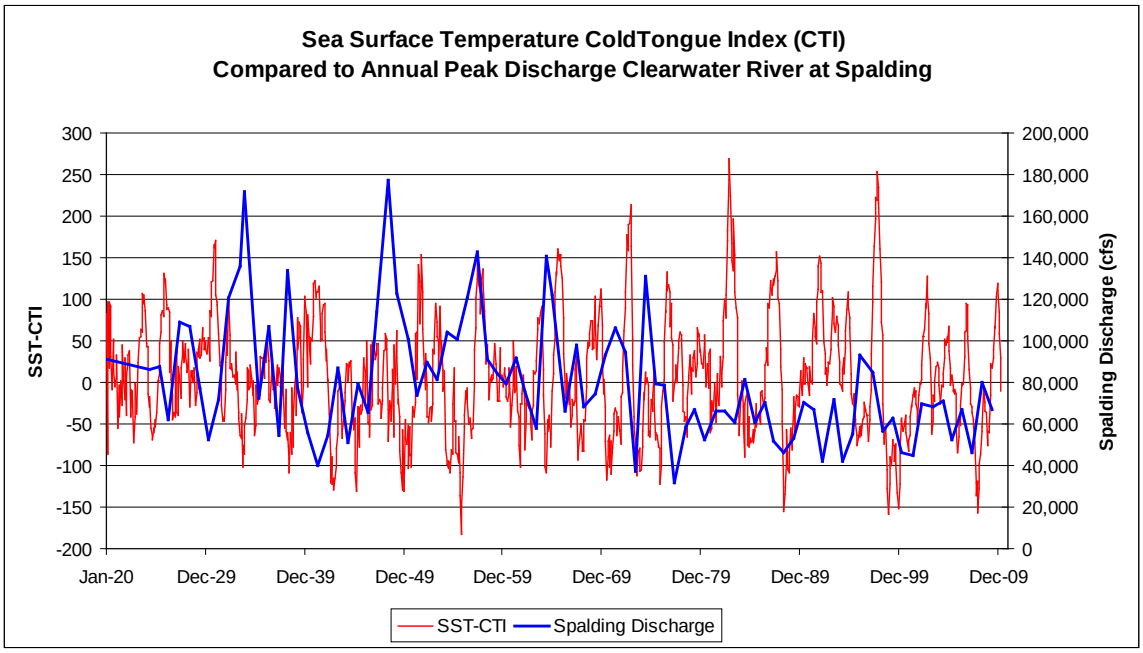


Figure 15. Comparison of the annual peak discharges are Spalding with the SST-CTI.

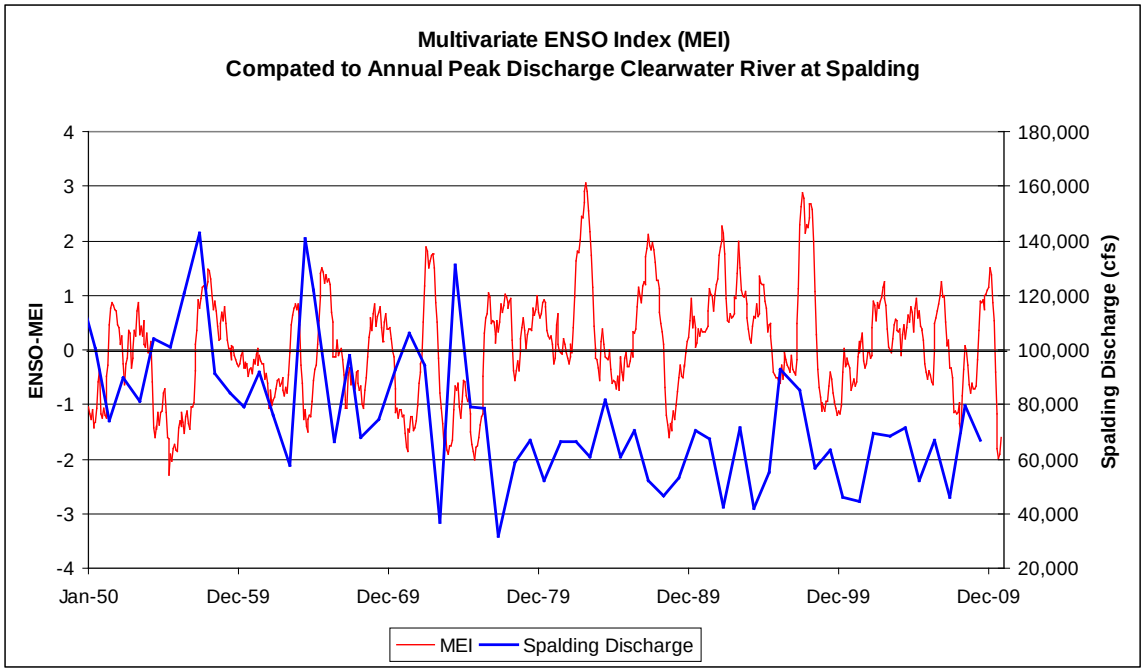


Figure 16. Comparison of the annual peak discharges are Spalding with the ENSO MEI.

A regression and trend analysis with annual peak discharge was developed by computing average values of CTI and MEI for various beginning times and durations prior to the occurrence of the annual peak discharge at Spalding and Anatone, then fitting a log-linear relationship to the CTI/MEI versus discharge data. The significance of the trend was tested with the nonparametric Mann-Kendall taub method[38].

In Figure 17 and Figure 18, lower CTI and MEI values are significantly correlated with higher peak discharges at Spalding. The strongest correlation occurs for a 3 month averaging period ending 6 months before the peak for both the SST and MEI. At Anatone, lower MEI is also significantly correlated in Figure 19 with higher peak discharge, but less so than at Spalding. The strongest correlation also occurs for a 3 month averaging period ending 6 months before the peak. The Salmon River at Whitebird correlates well in Figure 20 with MEI for a 2 month averaging period ending 6 months before the peak.

The Salmon River is the largest source of unregulated flow to Granite Reservoir. Trends in annual peak discharge and flood volume for the Salmon River would indicate non-stationary in the discharge series that should be considered in the risk analysis.

[38] Helsel, D.R., and Hirsch, R.M. (2002) "Trend Analysis", *Statistical Methods in Water Resources, Book 4, Hydrologic Analysis and Interpretation, Techniques of Water-Resources Investigations of the United States Geological Survey*, U.S. Geological Survey, Reston, VA.

The discharge record for Whitebird since 1920 was evaluated for trends in several flood variables including annual peak discharge, annual flood volume, annual flood duration, and the day of the peak discharge. Flood hydrographs for each year, such as that in Figure 21, were examined and the beginning and ending dates of the annual flood visually selected. Flood parameters were computed with a Matlab script. The significance of the trends is identified with the nonparametric Mann-Kendall taub test. Plots of the time series of the flood variables are shown in Figure 22 through Figure 26.

There are no significant trends in annual maximum discharge, flood volume or day of the annual maximum discharge. Interestingly, there is a significant increasing trend in the annual flood duration even though there is no overall trend in the beginning date of the flood. A climatic pattern is evident in these last two variables with beginning date of the flood reaching a maximum at about 1970, and decreases thereafter. The shift to an earlier starting date and shorter day lengths may account for the longer duration of floods in this snowmelt dominated basin. These flood variables may be linked to the frequency and extent of wildfire in the Salmon River basin, which in turn may be affected by climatic patterns. It should be noted that the selection of beginning and ending dates of the annual flood is subjective and will vary among analysts, but if a consistent method is employed, significant trends should be identified.

The gage record for the Clearwater River at Orofino did not show trends in the flood variables, but the useable gage record was relatively short (1965 - 2009). The longer gage record for the Lochsa River at Lowell (1930 - 2009) did not show significant trends in any of the flood variables. No trends in the flood variables were detected in the gage record for the Grande Ronde River at Troy (1940 - 2009).

Several observations can be made from the regression and trend analysis:

- Peak Annual Discharges at Lower Granite Reservoir and other Idaho Rivers show a correlation with ENSO-MEI and SST-CTI.
- An increased chance of flood conditions can be expected when low average ENSO-MEI are computed 6 months in advance of the flood without knowing snowpack conditions.
- Flood magnitudes are scattered about the MEI regression line so flood magnitude cannot be predicted with much accuracy.
- Climate factors that affect ENSO-MEI likely affect the occurrence and magnitude of NWW floods.
- Nothing in the trend analysis suggests that a significant shift has occurred that invalidates the use of historical peak discharge data in the flood risk at the confluence.

The dependence between peak discharges, water supply and climatic patterns is being studied by the Corps and other federal agencies[39]. The analysis here suggests that this work could produce data and findings that are important for the evaluation of flood risk at the confluence. Though there are as yet no generally accepted methods to directly incorporate climate change in Corps flood risk analysis, an attempt should be made and the approach taken in Section 2.8 is to examine the influence of potential climate change on the discharge exceedance probabilities used in the risk analysis.

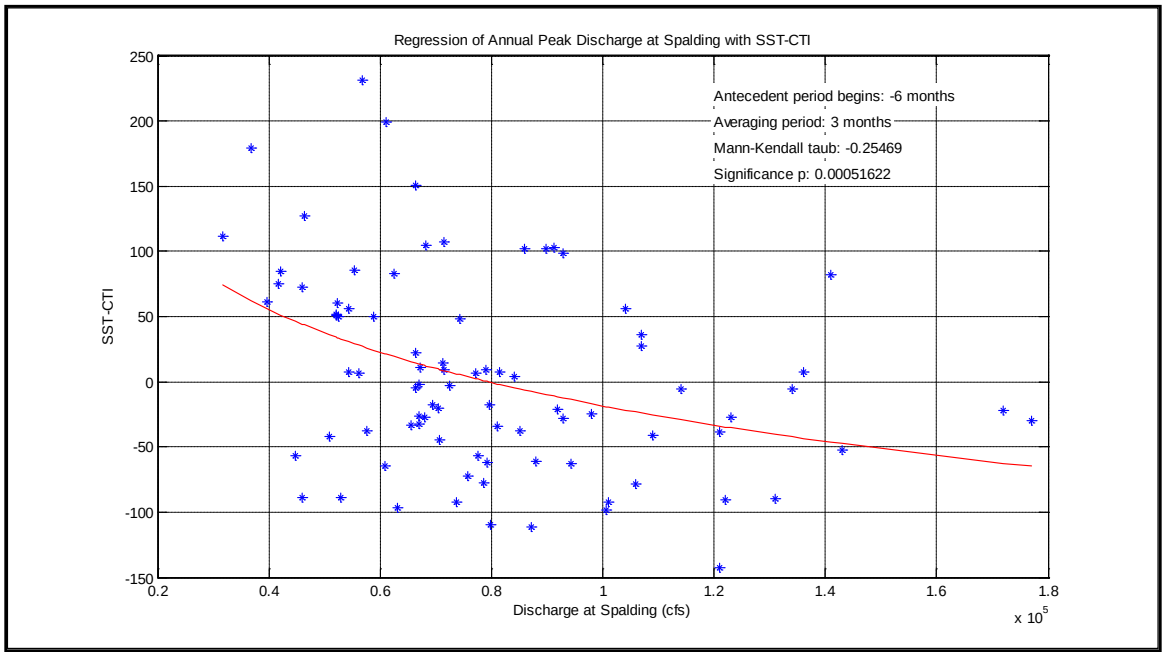


Figure 17. Regression of SST-CTI with Spalding annual peak discharge.

[39] Brekke, L.D., Kiang, J.E., Olsen, J.R., Pulwarty, R.S., Raff, D.A., Turnipseed, D.P., Webb, R.S., and White, K.D. (2009), *Climate change and water resources management—A federal perspective: U.S. Geological Survey Circular 1331*, 65 p. (online at http://pubs.usgs.gov/circ/1331/.)

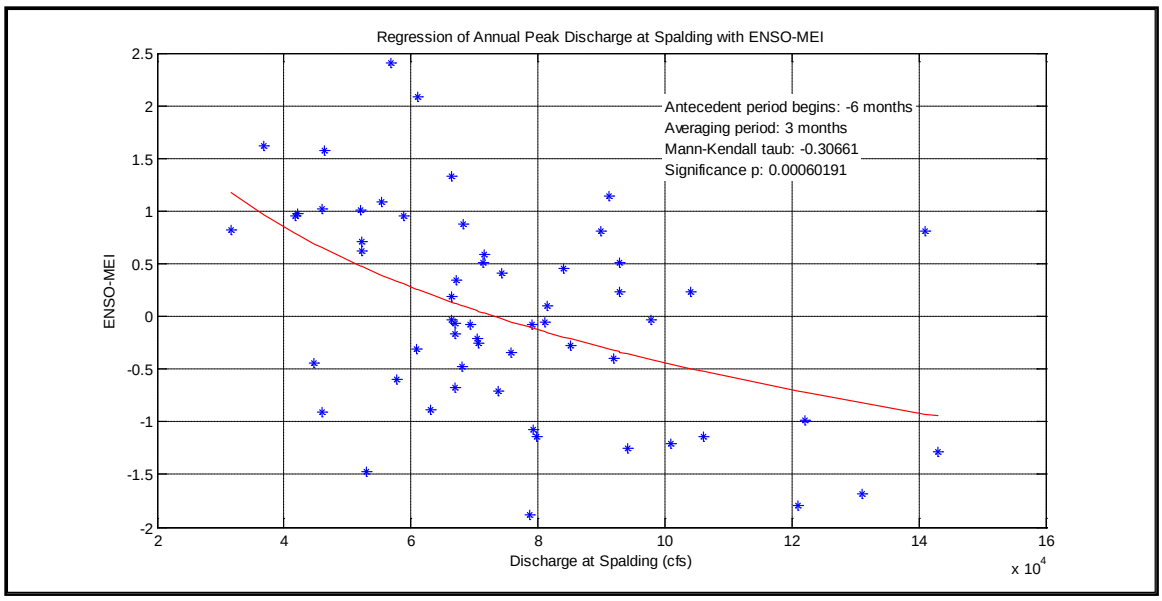


Figure 18. Regression of ENSO-MEI with Spalding annual peak discharge.

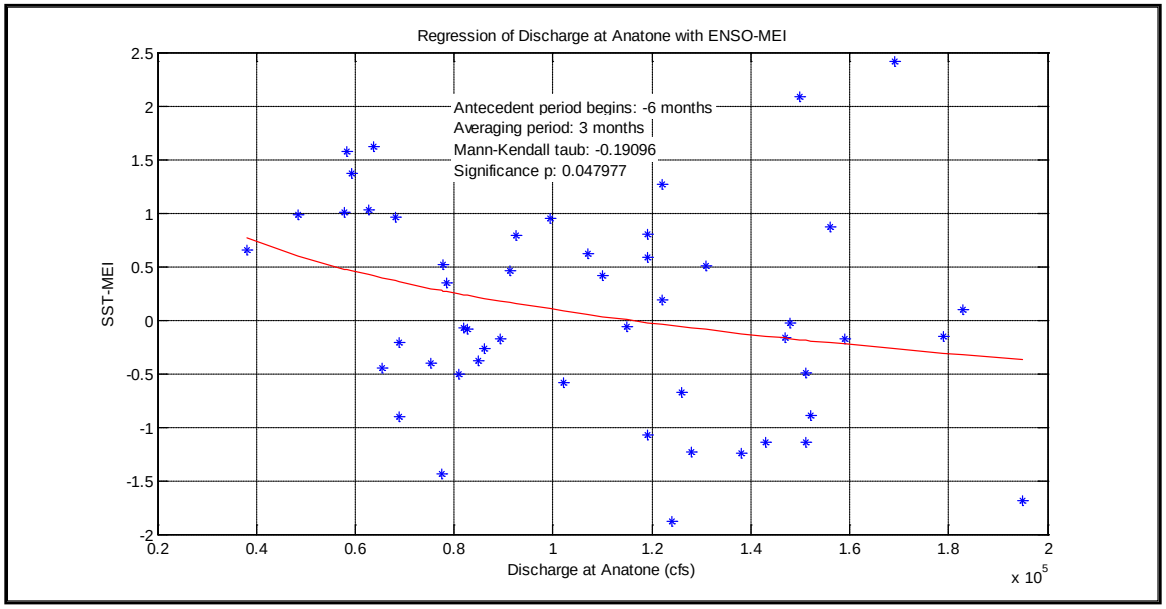


Figure 19. Regression of ENSO-MEI with Anatone annual peak discharge.

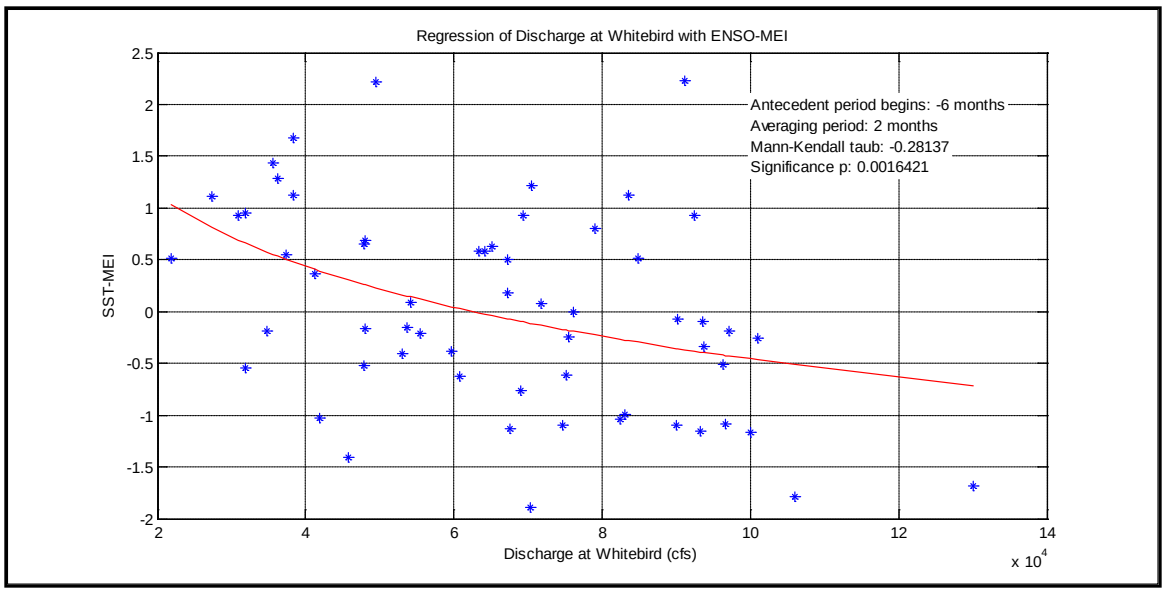


Figure 20. Regression of ENSO-MEI with the Salmon River at Whitebird annual peak discharge.

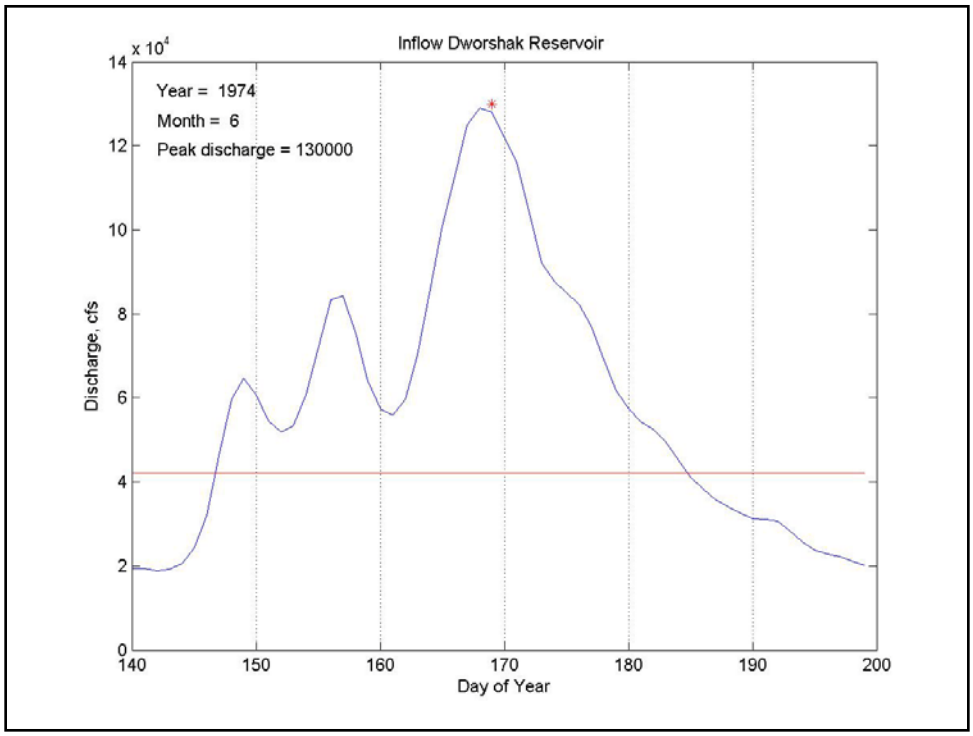


Figure 21. 1974 flood hydrograph for the Salmon River at Whitebird.

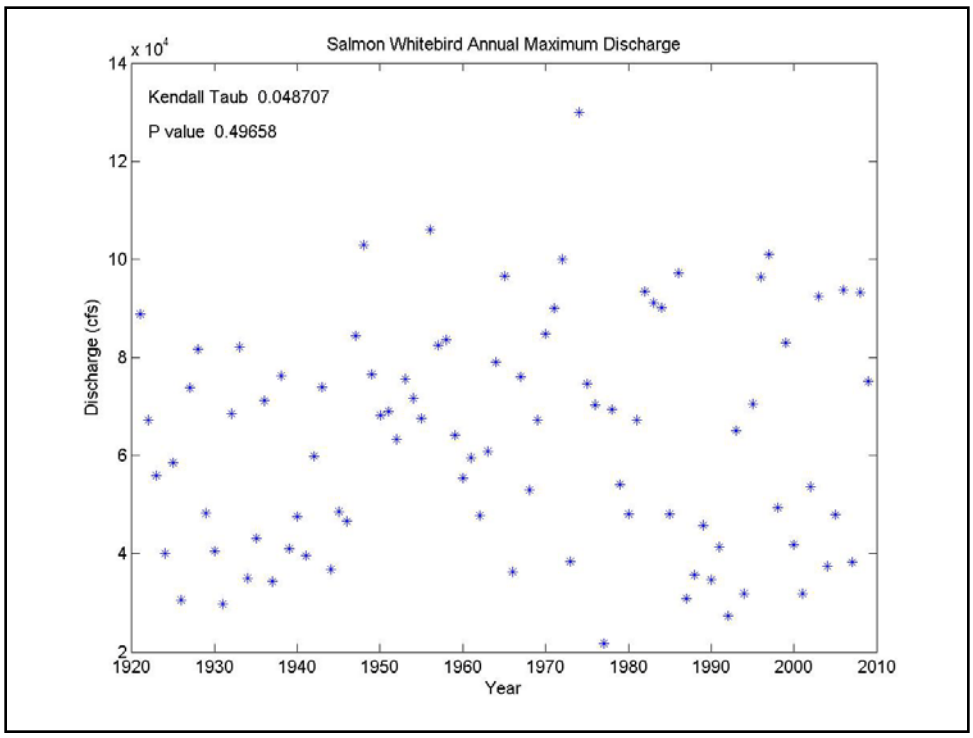


Figure 22. Annual maximum discharge for Salmon River at Whitebird.

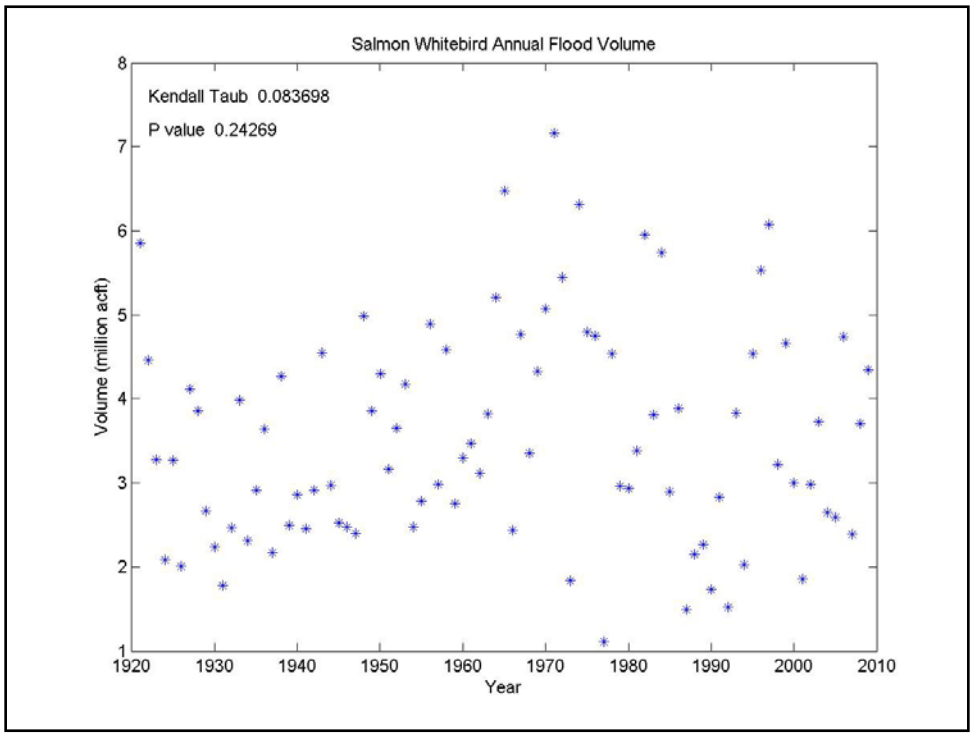


Figure 23. Annual flood volume for Salmon River at Whitebird.

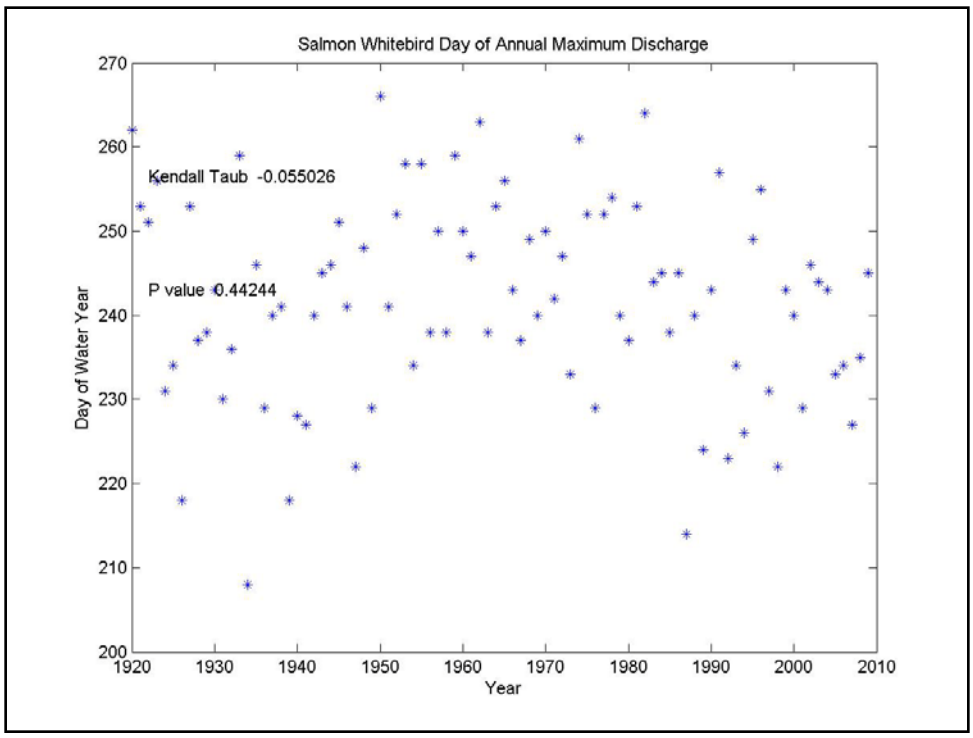


Figure 24. Day of annual maximum discharge for Salmon River at Whitebird

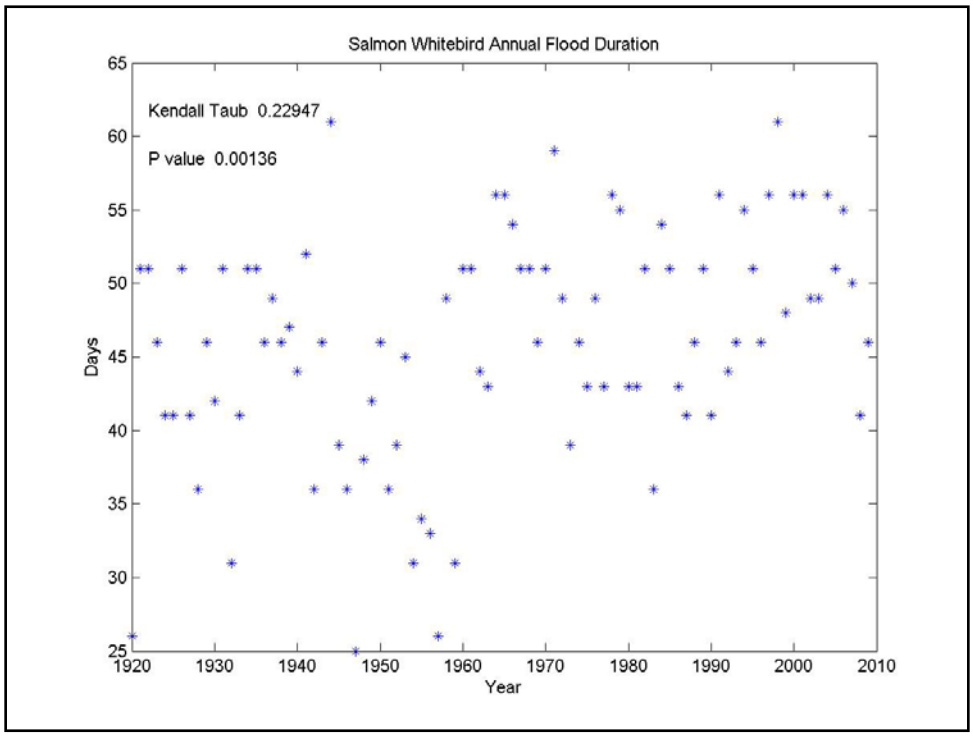


Figure 25. Annual flood duration for Salmon River at Whitebird.

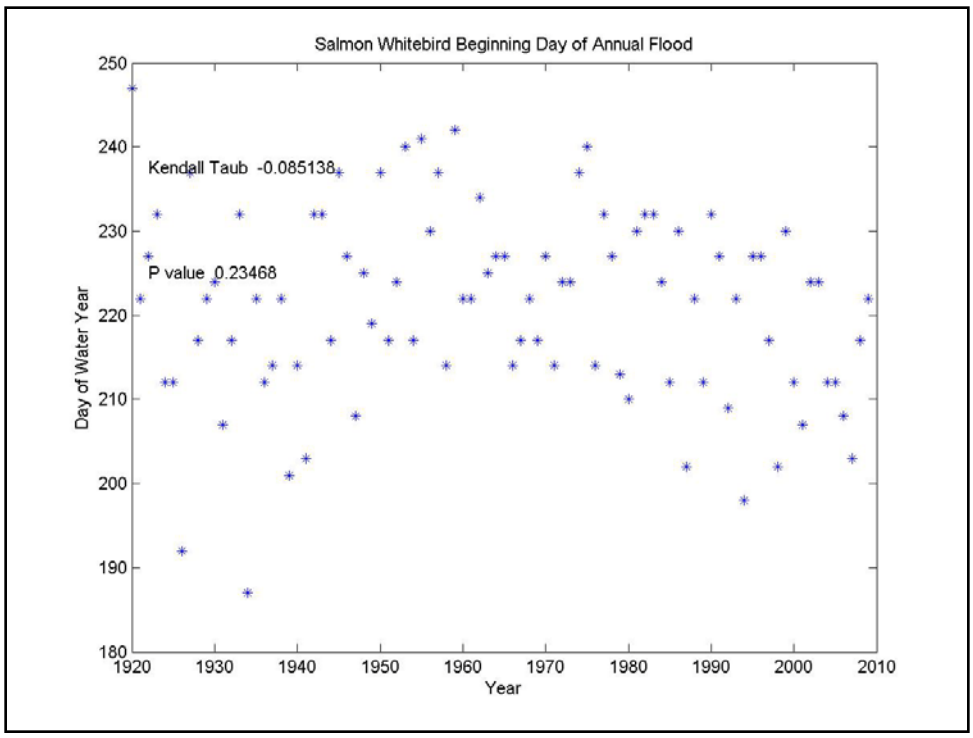


Figure 26. Beginning day of the annual flood for Salmon River at Whitebird.

2.7. Univariate Flood Frequency Analysis

The objective of a flood frequency analysis is to develop a statistical relationship between the magnitude of high discharge and the frequency (annual probability) that that discharge will be exceeded[40,41]. A general flood frequency analyses may incorporate the effect of several discharge sources in a joint multivariate analysis, or more typically, the frequency analysis evaluates the effect of a single (univariate) source that dominates the flood hydrograph. Both multivariate and univariate analyses were applied to the flood frequency analysis of the combined discharge of the Snake and Clearwater Rivers to examine different aspects of levee overtopping risk. This section presents the results of a conventional univariate flood frequency analysis that follows the Bulletin 17B procedures required by USACE engineering regulations[42]. Flood

[40] Beard, L.R. (1962*) Statistical Methods in Hydrology*. U.S. Army Corps of Engineers, Sacramento, CA.

[41] USACE (1993). Engineer Manual 1110-2-1415 Hydrologic Frequency Analysis. U.S. Army Corps of Engineers, Washington, DC.

[42] USACE (1994). ER 1110-2-1450 Hydrologic Frequency Estimates, U.S. Army Corps of Engineers, Washington, DC.

frequency computations were performed with the Hydrologic Engineering Center – Statistical Software Package[43] (HEC-SSP) version 2.0, October 2010.

Bulletin 17B discharge frequency estimates of the annual peak (instantaneous) discharges were computed for the Salmon River at Whitebird, the Clearwater River at Orofino, and the Snake River at Anatone for the period encompassing water year 1972 through 2010. A constant value of regional skew of -0.3 and regional mean square error of 0.302 was used in the weighted skew computation. The LP3 distribution fit the unregulated and partially regulated discharge reasonably well. Only one outlier was identified and that occurred in the regulated discharge for the Clearwater River at Spalding. No outliers were eliminated in the computation. The median probability (computed) annual peak discharge estimates are listed in Table 9 for exceedance probabilities that range from 99 percent to 0.05 percent. Annual maximum daily frequency estimates computed using Bulletin 17B procedures are also listed. The estimates for annual peak discharge exceeded the annual maximum daily average by 7 percent for the Clearwater River at Orofino to about 2% for the Snake River at Anatone. Table 9 also lists the Bulletin 17B frequency estimates for the total annual maximum daily discharge at Lower Granite below the confluence in which the average daily flow is computed as the sum of the Anatone and Spalding average daily discharges. It can be seen in Table 9 that the sum of the annual maximum daily flows for Anatone and Spalding exceed the annual maximum daily flow for Lower Granite by between 8 percent and 12 percent for exceedance probabilities less than 1 percent. This is because annual maximum daily discharges at Anatone and Spalding do not always occur on the same day. Discharge frequency plots and tabulations for the Bulletin 17B analysis produced by HEC-SSP are included in the digital data appendix to this report.

Bulletin 17B procedures and software compute expected probability discharges and confidence limit discharges in addition to the median (computed) probability discharge estimate. The appropriate discharge to use in a Monte Carlo analysis of flood risk is the median probability[44] because the Monte Carlo procedure accounts for the statistical uncertainty in the frequency estimates. The annual maximum day discharge frequency estimates for Lower Granite in Table 9 is the best estimate of the total probability discharge frequency for the confluence.

It is important to recognize that the annual peak frequency distributions for Anatone and Spalding are not used directly in the flood risk analysis of the confluence

[43] USACE (2010). HEC-SSP Statistical Software Package User's Manual, CPD-86, Hydrologic Engineering Center, Davis, CA.

[44] USACE (1006). *EM 1110-2-1619 Risk-based analysis for flood damage reduction studies*. U.S. Army Corps of Engineers, Washington DC.

because the annual peaks in each river occur on different days and so cannot be summed to give the total discharge at Lower Granite that is needed for hydraulic modeling and the computation of flood stage. Assuming a peak adjustment of about 5 percent to the annual maximum daily discharge for Lower Granite, addition of the peak discharge frequency values would produce estimates that are between 7 percent and 10 percent higher than the adjusted annual maximum day frequency estimates for Lower Granite. The summed peak frequency value is useful because it provides an upper bound on the total-probability frequency discharge estimates for the regulated period in Lower Granite. Similarly, the Whitebird and Orofino annual peak frequencies are useful because as the main sources of unregulated discharge they demonstrate a logical consistency in the discharge data. The unregulated Whitebird and Orofino annual maximum day frequency distributions are important because they are used in the Monte Carlo computation of joint frequencies described below.

The frequency estimates for the Grande Ronde at Troy and the Imnaha River were not included in Table 9 because contributions from these rivers have not dominated the maximum annual discharge at Lower Granite in the period of record. The same is true for the regulated discharges for the Snake River at Hells Canyon and the outflow of Dworshak Reservoir. These sources are important coincident tributary flows in the Monte Carlo joint frequency analysis.

Annual Peak Discharge and Annual Maximum Day Frequencies for Tributaries to Lower Granite Reservoir (1972-2010)[1]										
		Discharge in Cubic Feet Per Second (cfs)								
		Salmon River at Whitebird		Clearwater River at Orofino		Snake River at Anatone		Clearwater River at Spalding		**Lower Granite**
Return Period	Percent Exceedance	Annual Peak Median Probability	Maximum Day Median Probability	Annual Peak Median Probability	Maximum Day Median Probability	Annual Peak Median Probability	Maximum Day Median Probability	Annual Peak Median Probability	Maximum Day Median Probability	**Maximum Day Median Probability**
2000	0.05	210,640	203,331	128,511	121,062	324,826	315,828	146,078	140,202	**407,704**
1000	0.1	197,321	190,882	122,170	114,933	307,568	298,886	139,220	133,277	**389,118**
500	0.2	183,846	178,225	115,740	108,735	289,763	281,412	132,242	126,269	**369,770**
303	0.33	173,925	168,857	111,011	104,190	276,387	268,285	127,096	121,128	**355,111**
250	0.4	170,131	165,271	109,185	102,436	271,243	263,239	125,106	119,143	**349,447**
200	0.5	165,741	161,119	107,060	100,396	265,269	257,380	122,787	116,831	**342,849**
100	1	151,766	147,836	100,311	93,935	245,891	238,376	115,405	109,511	**321,281**
50	2	137,475	134,182	93,346	87,289	225,624	218,511	107,757	101,971	**298,445**
25	4	122,755	120,041	86,082	80,382	204,247	197,571	99,747	94,124	**274,019**
10	10	102,302	100,266	75,779	70,625	173,635	167,618	88,319	83,016	**238,360**
5	20	85,560	83,970	67,083	62,429	147,721	142,299	78,609	73,662	**207,444**
2	50	59,488	58,407	52,793	49,040	105,645	101,291	62,506	58,318	**155,449**
1.25	80	40,179	39,347	41,199	38,247	72,927	69,536	49,280	45,874	**112,935**
1.11	90	32,342	31,591	36,067	33,490	59,217	56,280	43,371	40,360	**94,357**
1.05	95	26,869	26,171	32,257	29,966	49,478	46,891	38,959	36,261	**80,796**
1.01	99	18,685	18,075	26,048	24,234	34,654	32,651	31,717	29,563	**59,393**
[1]Discharge at Anatone and Spalding are partially regulated by Snake River dams and Dworshak Dam										

Table 9. Univariate LP3 discharge frequencies for Lower Granite tributaries.

2.8. Joint Probability-Multivariate Analysis of Coincident Discharge

The goal of a comprehensive risk analysis is to recognize and account for the uncertainty in all key variables that affect flood risk at a particular location[45]. In the present analysis, the key variables related to discharge are the magnitude, frequency and distribution of flows between the Snake and Clearwater Rivers during annual maximum flow conditions in Lower Granite Reservoir. The annual maximum flow (peak discharge) is an appropriate variable in this setting because the Corps' approach to risk analysis is based on the probability that a discharge of a given magnitude will overtop the Lewiston levees and cause flood damage. The risk analysis is implemented through a Monte Carlo analysis of the key flood variables via the HEC-FDA software[46]. Use of the FDA software requires the input of discharge frequency and stage-discharge relationships in order to execute the probabilistic analysis. The previous sections showed that univariate frequency statistics can be developed for the main tributary inflows to Lower Granite with Bulletin 17 B methods. However, since that the tributary sources are partially correlated and annual peak discharges occur at different times, the annual peaks cannot be simply summed to characterize the discharge frequency at the confluence of the Snake and Clearwater Rivers.

A further limitation of the univariate analysis is that the Lower Granite annual maximum day frequency does not give the conditional probabilities of the division of flow between the Snake and Clearwater Rivers. The conditional probabilities of the flow split must be obtained from a multivariate analysis. It will be shown below, using the principle of total probability, that the univariate frequency estimate for Lower Granite is closely approximated by the joint probability-multivariate Monte Carlo analysis of the coincident tributary flows. The joint probability-multivariate analysis developed here is a conceptually consistent and practical extension of the Bulletin 17B method that satisfies the requirements of the engineering regulations.

The theorem of total probability[47] states that:

$$P[A] = P[A \mid B]P[B] + P[A \mid B^C]P[B^C] \qquad 1.1$$

[45] USACE (2006). *ER 1105-2-101 Risk Analysis for Flood Damage Reduction Studies*, U.S. Army Corps of Engineers, Washington, DC.

[46] USACE (2008). *HEC-FDA Flood Damage Reduction Analysis, User's Manual Version 1.2.4*, Hydrologic Engineering Center, U.S. Army Corps of Engineers, Davis, CA.

[47] Ang, A.H-S. and Tang,W. A. (2007) *Probability Concepts in Engineering, Emphasis on Applications in Civil and Environmental Engineering, 2nd Ed.*, Wiley.

where $P[A]$ is the total probability of event A, $P[B]$ is the probability of event B, $P[A|B]$ is the conditional probability of event A given the occurrence of event B and $P[B^C]$ is the probability of all events that are not event B.

In the present context, this principle means that frequency distribution of maximum annual discharges at Lower Granite is the sum of the probabilities associated with the tributary discharges. The first term on the right hand side of equation 1.1 can be viewed as the component probability of one discharge source and the second term is viewed as contributions of all other sources. The right hand side of equation 1.1 can include as many terms as significant sources. The joint probability analysis must account for all flows that significantly affect the total probability. At Lower Granite, a annual maximum daily discharge can occur one of three ways:

1. The annual maximum discharge at Lower Granite is the sum of the maximum annual discharge of the Snake at Anatone plus the coincident discharge of the Clearwater at Spalding.
2. The annual maximum discharge at Lower Granite is the sum of the maximum annual discharge of the Clearwater at Spalding plus the coincident discharge of the Snake at Anatone.
3. The annual maximum discharge at Lower Granite occurs when the annual maximum discharge occurs neither at Anatone or Spalding. In this case the maximum discharge at Lower Granite is the sum of the flows at Anatone and Spalding.

The set of three conditions is exhaustive, ignoring very unusual conditions such as the inadvertent release of flood discharge by Dworshak Dam or the Hells Canyon Dam. It is possible that conditions 1 and 2 are not mutually exclusive because the annual maximum discharge at Anatone and Spalding could occur on the same day.

The total probability of equation 1.1 can be reformulated to give:

$$P\left[LG_{\max}\right] = P\left[LG_{\max} \mid A_{\max}\right]P\left[A_{\max}\right] + P\left[LG_{\max} \mid S_{\max}\right]P\left[S_{\max}\right] + P\left[LG_{\max} \mid AS_{\max}\right]P\left[AS_{\max}\right] \quad 1.2$$

where LG_{max} is the annual maximum discharge at Lower Granite, A_{max} is the annual maximum discharge at Anatone, S_{max} is the annual maximum discharge at Spalding, and AS_{max} is the sum of the Anatone and Spalding discharges when the sum is the annual maximum discharge at Lower Granite.

The probabilities $P[A_{max}]$, $P[S_{max}]$ *and* $P[AS_{max}]$ can be estimated by the frequencies of their occurrence in the stream gage record. Table 10 lists the combined discharges for each condition for the period 1972 to 2010. There were 19 years in the record where the maximum annual daily discharge at Lower Granite was produced by annual maximum daily discharge at Anatone plus the coincident average daily discharge at

Spalding (Condition 1). Similarly, there were 12 years in the record where the maximum annual daily discharge at Lower Granite was produced by annual maximum daily discharge at Spalding plus the coincident average daily discharge at Anatone (Condition 2). There were 5 years in the record where the average daily discharges of Anatone and Spalding produced the maximum annual daily discharge at Lower Granite and neither Anatone nor Spalding was an annual maximum daily discharge. There were 3 years when maximum annual discharges occurred at Anatone and Spalding on the same day and their total produced the maximum annual discharge at Lower Granite (intersection of condition 1 and 2). The ties could be considered a separate component of probability, but since there are so few, for simplicity two of the ties were assigned to condition 1 and one of the ties was assigned to condition 2.

The tally of the flow conditions and the frequencies of occurrence are listed in Table 11. Annual probabilities of the occurrence of a specific flow conditions are estimated as the frequencies of occurrence computed as the adjusted counts of the conditions divided by the total number of years in the record. By this method, the probability of $P[A_{max}]$ is 0.538, $P[S_{max}]$ is 0.308 and $P[AS_{max}]$ is 0.154.

The conditional probabilities $P[LG_{max}|A_{max}]$, $P[LG_{max}|S_{max}]$ and $P[LG_{max}|AS_{max}]$ are not as easily obtained. A multivariate analysis is necessary because marginal frequency distributions for both the annual maximum daily discharge of the primary station and the coincident average daily discharge of the complementary gage must be used in the computation of conditional probability. The analysis is made more complex because the discharges are partially correlated. Analytical bivariate distributions and fitting procedures are available[47], but none are based on the log Pearson Type 3 distribution and Bulletin 17B procedures. A practical alternative is to fit LP3 distributions to the annual maximum daily discharge and coincident average daily discharge data, then employ Monte Carlo simulation to compute the conditional probabilities. Such an approach is consistent both with the requirement to use Bulletin 17B procedures and the Monte Carlo approach taken in HEC-FDA.

In the univariate frequency analysis the annual maximum daily average discharge series is well represented by the LP3 distribution. It could be expected that the LP3 distribution would fit the coincident average daily flow series reasonably well because of the correlation between the primary and complementary discharges shown previously. It should be recognized that the LP3 distribution is being fit to the coincident discharges at the complimentary station that occur on the same days as the annual maximum daily average discharges at the primary station. A distribution is not being fit to the complete series of average daily discharges at the complementary station.

Summary of Discharge Conditions at Lower Granite				
Year	Anatone Max Day plus Spalding Coincident	Spalding Max Day plus Anatone Coincident	Sum of Anatone and Spalding	Condition
1972	227,200	227,200	227,200	1,2
1973	95,800	95,400	95,800	1
1974	312,000	298,000	312,000	1
1975	183,800	176,200	187,500	3
1976	188,600	188,800	188,800	2
1977	58,400	61,400	61,400	2
1978	145,000	137,000	145,000	1
1979	139,000	134,300	139,000	1
1980	130,800	127,200	130,800	1
1981	175,500	125,400	175,500	1
1982	205,800	196,500	205,800	1
1983	193,800	188,800	195,400	3
1984	252,700	252,700	252,700	1,2
1985	105,400	126,700	126,700	2
1986	213,500	207,400	214,800	3
1987	101,100	102,500	102,500	2
1988	85,200	87,600	87,600	2
1989	123,300	115,000	123,300	1
1990	117,200	125,200	125,200	2
1991	121,100	120,400	121,100	1
1992	82,300	67,800	82,300	1
1993	183,400	180,800	183,400	1
1994	94,400	83,600	94,400	1
1995	151,300	123,400	151,300	1
1996	206,800	177,200	206,800	1
1997	210,200	231,400	231,800	3
1998	218,000	218,000	218,000	1,2
1999	174,300	182,800	185,300	3
2000	113,700	111,600	113,700	1
2001	93,800	94,200	94,200	2
2002	138,100	122,400	138,100	1
2003	211,000	189,000	211,000	1
2004	131,700	137,900	137,900	2
2005	135,700	122,500	139,100	3
2006	203,600	199,700	203,600	1
2007	100,600	102,400	102,400	2
2008	205,300	205,900	205,900	2
2009	170,300	172,100	172,100	2
2010	216,100	213,200	216,100	1

Table 10. Summary of discharge flow conditions at Lower Granite.

Frequencies of Lower Granite Flow Conditions			
Condition	Count	Adjusted Count	Frequency
1. Anatone max day plus Spalding coincident	19	21	0.538
2. Spalding max day plus Anatone coincident	11	12	0.308
Intersection 1 and 2	3	0	0.000
3. Anatone plus Spalding is Lower Granite max day	6	6	0.154
Total	39	39	1.000

Table 11. Frequencies of flow conditions at Lower Granite.

The Monte Carlo analysis of the multivariate conditional probability was implemented through custom Matlab® scripts. A flow chart of the computational process is shown in Figure 27. The coincident discharge data for the three conditional probability analyses are listed in Table 12. A critical element of the Monte Carlo simulation is to account for correlation among the discharge series. Correlated random normal deviates are obtained via Cholesky factorization with the expression[48]:

$$Z_{correlated} = \rho\, Z_{random1} + \left(1-\rho^2\right)^{0.5} Z_{random2} \qquad 1.3$$

where $Z_{random1}$ is a first random sample of normal deviates, $Z_{random2}$ is a second sample of random deviates, ρ is the correlation coefficient of the two discharge series, and $Z_{correlated}$ is the correlated sample of random deviates. Random normal deviates were generated by the default algorithm in Matlab. Test data sets confirmed that the Monte Carlo procedure correctly simulated the Bulletin 17B procedure and the LP3 distribution.

Lower Granite Total Probability-Multivariate Maximum Day and Coincident Daily Discharge Data								
Flow Condition 1			Flow Condition 2			Flow Condition 3		
Date	Anatone Max Day Discharge cfs	Spalding Coincident Day Discharge cfs	Date	Spalding Max Day Discharge cfs	Anatone Coincident Day Discharge cfs	Date	Spalding Coincident Day Discharge cfs	Anatone Coincident Day Discharge cfs
2-Jun-72	135,000	92,200	11-May-76	70,800	118,000	7-Jun-75	116,000	71,500
19-May-73	61,800	34,000	3-May-77	28,500	32,900	29-May-83	141,000	54,400
18-Jun-74	191,000	121,000	8-Jun-85	55,100	71,600	1-Jun-86	154,000	60,800
9-Jun-78	93,000	52,000	1-May-87	49,400	53,100	18-May-97	152,000	79,800
25-May-79	78,600	60,400	7-May-88	44,500	43,100	27-May-99	131,000	54,300
12-Jun-80	92,400	38,400	30-May-90	61,900	63,300	20-May-05	94,600	44,500
10-Jun-81	120,000	55,500	27-May-98	52,000	166,000			
18-Jun-82	145,000	60,800	16-May-01	40,000	54,200			
31-May-84	177,000	75,700	29-May-04	68,400	69,500			
22-Apr-89	76,600	46,700	13-May-07	43,400	59,000			
20-May-91	72,200	48,900	20-May-08	75,900	130,000			
2-May-92	47,000	35,300	31-May-09	63,100	109,000			
21-May-93	118,000	65,400						
11-May-94	64,300	30,100						
5-Jun-95	118,000	33,300						
10-Jun-96	148,000	58,800						
23-Apr-00	68,200	45,500						
31-May-02	84,200	53,900						
31-May-03	147,000	64,000						
21-May-06	144,000	59,600						
6-Jun-10	159,000	57,100						
Condition 1: Anatone maximum day discharge, Spalding coincident discharge Condition 2: Spalding maximum day discharge, Anatone coincident discharge Condition 3: Lower Granite maximum day discharge, Anatone plus Spalding								

Table 12. Lower Granite maximum day and coincident daily discharge data for total probability-multivariate analysis.

[48] Jorion, P. (2006). *Chapter 12 Monte Carlo Methods, Value at Risk, 3rd Ed.* . McGraw-Hill

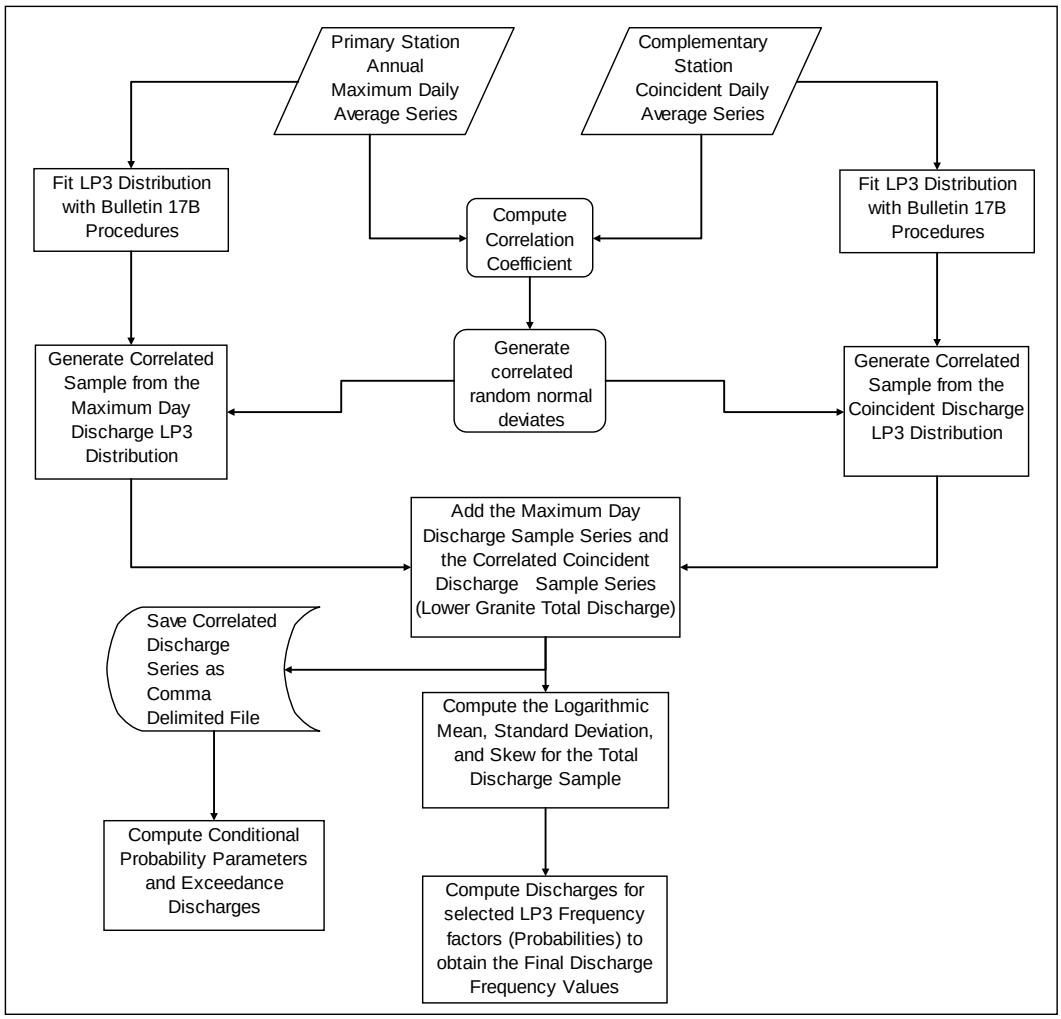


Figure 27. Flowchart of the Monte Carlo simulation of the multivariate analysis of conditional probabilities for coincident discharge.

Monte Carlo simulations of length n = 100,000 were performed for each of the three flow conditions in the total probability formulation (equation 1.2). The conditional discharge frequencies from the three simulations are listed in Table 13. The fitted distributions were plotted with the original data to verify the fit. The plots in Figure 29 through Figure 37 demonstrate a reasonable fit of the LP3 distributions for Anatone and Spalding even though a reduced number of values were used to obtain the distribution parameters (as compared to complete annual series).

Discharge frequencies obtained from each simulation was multiplied by the probability components in Table 11 and summed to obtain the final exeedance discharges. For example to obtain the final 1-percent exceedance discharge the calculation is:

$$Q_{1\%LG} = Q_{1\%Condition1}P[A_{\max}] + Q_{1\%Condition2}P[S_{\max}] + Q_{1\%Condition3}P[AS_{\max}]$$

$$Q_{1\%LG} = 344{,}493(0.5385) + 298{,}476(0.3077) + 271{,}233(0.1538) = 319{,}063\,\text{cfs}$$

The final total probability exceedance discharges of the multivariate joint probability analysis listed in Table 14 compare very well with the total probability univariate exceedance discharges. A good agreement is expected because the univariate and multivariate analyses are based on the same data. The univariate 1-percent chance exceedance discharge estimate was 321,300 as compared to 318,400 from the multivariate analysis. Differences between the univariate and multivariate estimates varied from about -1 percent for the 1 percent exceedance discharge to about 4 percent for the 0.05 percent exceedance discharge. Differences were greater for exceedances greater than 50 percent, but high exceedance discharges (low magnitude) are unimportant in an analysis of flood risk. The differences between the univariate and multivariate discharges are attributed to the randomness of the Monte Carlo simulation, treatment of ties between Condition 1 and Condition 2, and numerical algorithm error.

Lower Granite Univariate and Multivariate Discharge Frequency Estimates				
		Annual Maximum Day (cfs)		
Return Period	Percent Exceedance	Multivariate Condition 1 Probability	Multivariate Condition 2 Probability	Multivariate Condition 3 Probability
2000	0.05	460,165	419,256	303,189
1000	0.1	433,892	390,930	296,666
500	0.2	407,394	362,891	289,686
303	0.33	388,066	342,775	284,316
250	0.4	380,591	335,071	282,171
200	0.5	371,879	326,148	279,622
100	1	344,493	298,476	271,233
50	2	316,464	270,757	262,001
25	4	287,517	242,773	251,679
10	10	247,019	204,738	235,647
5	20	213,449	174,209	220,637
2	50	159,780	127,326	192,310
1.25	80	117,990	92,497	164,989
1.11	90	100,142	78,077	151,290
1.05	95	87,204	67,794	140,343
1.01	99	66,792	51,854	120,825
Condition 1: Anatone maximum day discharge, Spalding coincident discharge Condition 2: Spalding maximum day discharge, Anatone coincident discharge Condition 3: Lower Granite maximum day discharge, Anatone plus Spalding				

Table 13. Condition discharge frequency series for Lower Granite

Lower Granite Univariate and Multivariate Estimates of Total Probability				
		Annual Maximum Day (cfs)		
Return Period	Percent Exceedance	Univariate Total Probability	Multivariate Joint Probability	Difference
2000	0.05	407,704	423,427	3.9%
1000	0.1	389,118	399,561	2.7%
500	0.2	369,770	375,592	1.6%
303	0.33	355,111	358,169	0.9%
250	0.4	349,447	351,443	0.6%
200	0.5	342,849	343,615	0.2%
100	1	321,281	319,063	-0.7%
50	2	298,445	294,021	-1.5%
25	4	274,019	268,236	-2.1%
10	10	238,360	232,260	-2.6%
5	20	207,444	202,481	-2.4%
2	50	155,449	154,799	-0.4%
1.25	80	112,935	117,377	3.9%
1.11	90	94,357	101,222	7.3%
1.05	95	80,796	89,407	10.7%
1.01	99	59,393	70,508	18.7%

Table 14. Comparison of total probability-mulitvariate and univariate discharge frequency estimates for Lower Granite.

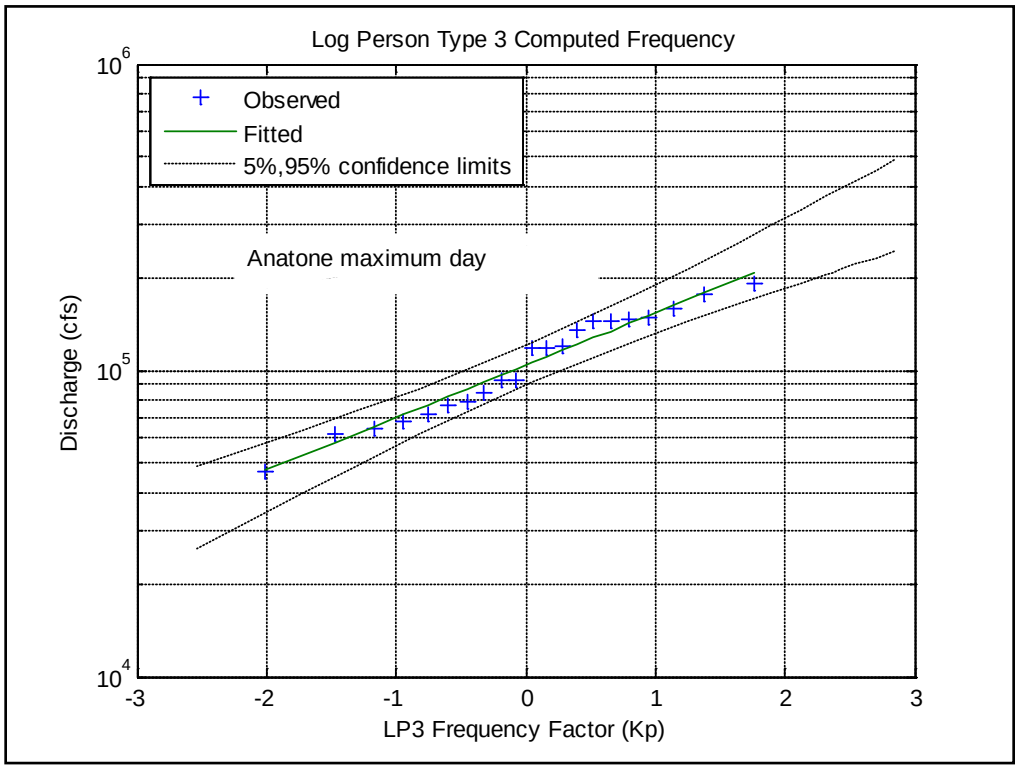


Figure 28. LP3 distribution of Anatone annual maximum day discharge.

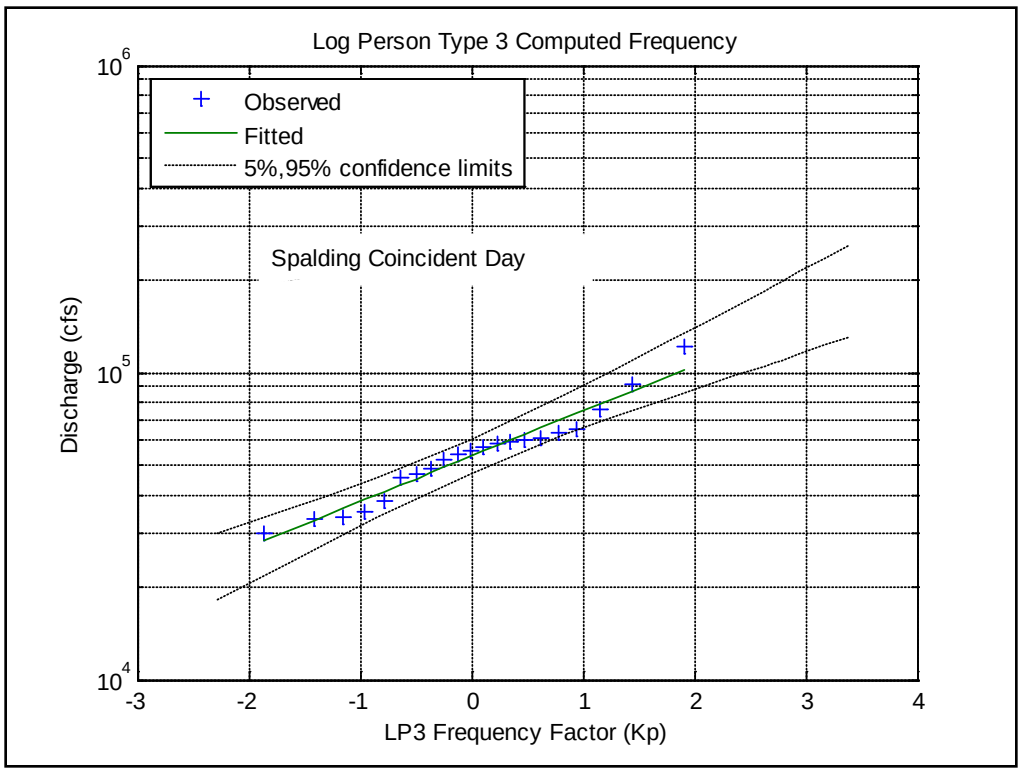


Figure 29. LP3 distribution of Spalding coincident daily average discharge.

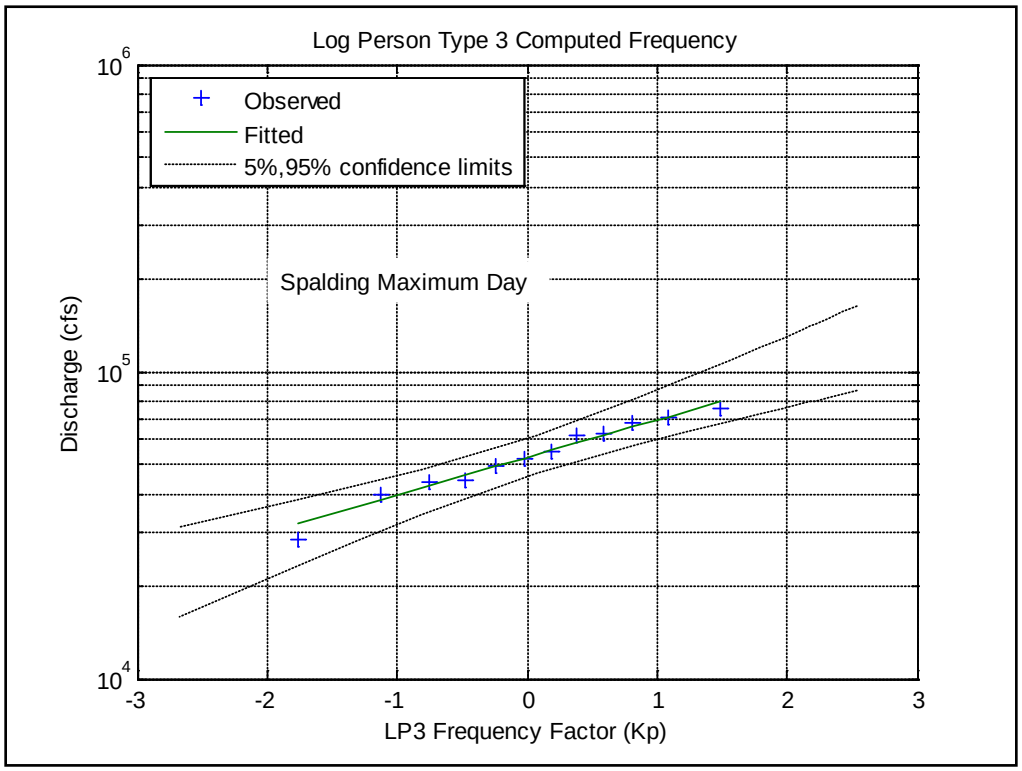


Figure 30. LP3 distribution of Spalding annual maximum day discharge.

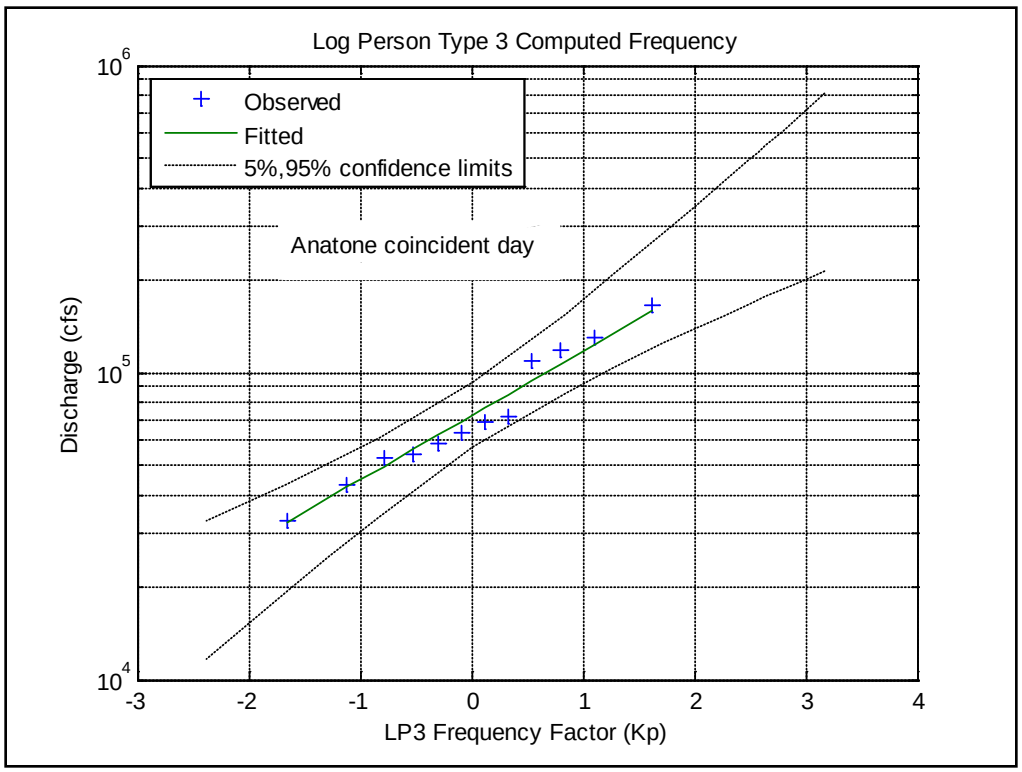


Figure 31. LP3 distribution of Anatone coincident daily average discharge.

2.9. Joint Probability of Exceedance for Flow Distribution

The comparison above demonstrated good agreement between the univariate and multivariate estimates of the total probability discharge frequencies for the annual maximum daily average discharge in Lower Granite based on data from the period 1972 through 2010. The univariate estimate would be sufficient if it was only necessary to estimate the discharge frequencies of total flow below the confluence. Because of the merging flows of the Snake and Clearwater Rivers, hydraulic modeling of the confluence requires probabilistic information about the distribution of discharges between the rivers (flow splits). The necessary information can be obtained from a Monte Carlo multivariate analysis.

Paired sample series were generated during the Monte Carlo simulation for each of the flow conditions (Figure 27). Each sample series contains a sequence of paired discharge values for the Snake River and the Clearwater River. The relative difference between each discharge and the combined total is an estimate of the split of flow at that total discharge. The separate conditional sample series can be combined into a single composite series in proportion to their contribution to total probability from Table 11. Since the order of the values in the conditional series is random, a composite series can be constructed simply by combining the first *nP* values in each conditional series, where *n* is the number of values in the series and *P* is the proportion of total probability for the

particular conditional series. The composite series is then evaluated to determine the exceedance probabilities of specific combinations of discharges from the Snake and Clearwater Rivers. Two types of frequency analysis can be performed with the composite series. A Type 1 analysis gives the joint exceedance probability of a particular split of flow and a Type 2 analysis gives the most likely distribution of flow for a given exceedance probability of total discharge.

To compute the Type 1 joint probability of exceedance for flow distribution, a count is made in the composite series of the number of the paired discharges that both exceed specified threshold values. The count is then divided by the total number of paired values in the composite series to obtain a probability of exceedance. For example, assuming a Snake River discharge of 200,000 cfs and a Clearwater River discharge of 100,000 cfs, there were 896 pairs in a composite series of 100,000 in which the Anatone value exceeded 200,000 cfs and the Spalding value exceeded 100,000 cfs. The exceedance probability is computed as 896/100,000 or 0.00896, which is equivalent to a return interval 112 years.

It is important to recognize the Type 1 exceedance probability of flow distribution is not the same as the exceedance probability of the total discharge. In Table 14 the exceedance probability for a total maximum daily average flow of 300,000 is about 0.02 or a return interval of 50 years. Other less likely combinations of discharge can also sum to a total discharge of 300,000 cfs. For example, the flow combination 295,000 cfs at Anatone and 5,000 cfs at Spalding has a total flow of 300,000 cfs, but in the composite series this combination has an exceedance probability of 0.00126 or a return interval of 793 years.

There are many possible combinations of discharges that have about the same joint probability of exceedance. If a joint probability of exceedance is computed for each pair in the composite series, lines of equal probability may be plotted as in Figure 32. It is seen that in this figure the discharge pair (200000, 100000) plots somewhat above the 1 percent exceedance line. The lines of equal probability have a curvature that is dependent on the parent marginal distributions, log Pearson Type 3 in this case, and have lower probabilities as total discharge increases. Mathematical relationships for the lines of equal probability can be derived for analytical multivariate distributions and copula models[49,50,51]. A copula model was developed to compute the joint probability of

[49] Yue, S. (2001). "The bivariate lognormal distribution to model a multivariate flood episode", *Hydrological Processes*, 14, 2575-2588.

[50] Zhang, L, Singh, V.P. (2006). "Bivariate flood frequency analysis using the copula method", Journal of Hydrologic Engineering, 11(2), 150-164.

[51] Salvadori, G. (2004). "Bivariate return periods via 2-copulas", *Statistical Methodology*, 1, 129-144.

exceedance of flow distribution of the Snake and Clearwater Rivers. Computation and plotting of the exceedance probabilities was performed with custom Matlab scripts.

The analysis of the joint probability of exceedance shows that the chance of standard project floods (SPF) occurring simultaneously on the Snake and Clearwater Rivers is very low. The SPF for the Snake River is 295,000 cfs and the SPF for the Clearwater River is 150,000 cfs. Figure 32 shows that simultaneous occurrence of the SPF discharges greatly exceeds 0.1 percent (1000 years). This example is more illustrative than exact, but there is little doubt that the probability of a simultaneous occurrence is very low and requires significant extrapolation of the historic data. Another use of the Type 1 joint exceedance probability is in evaluating the possibility of simultaneous discharges that produce high sediment loads. Sediment transport is a nonlinear threshold phenomenon. Minimal sediment transport can be expected until the critical discharge (shear stress) in the channel bed is exceeded. Sediment transport is discussed more in Section 10.

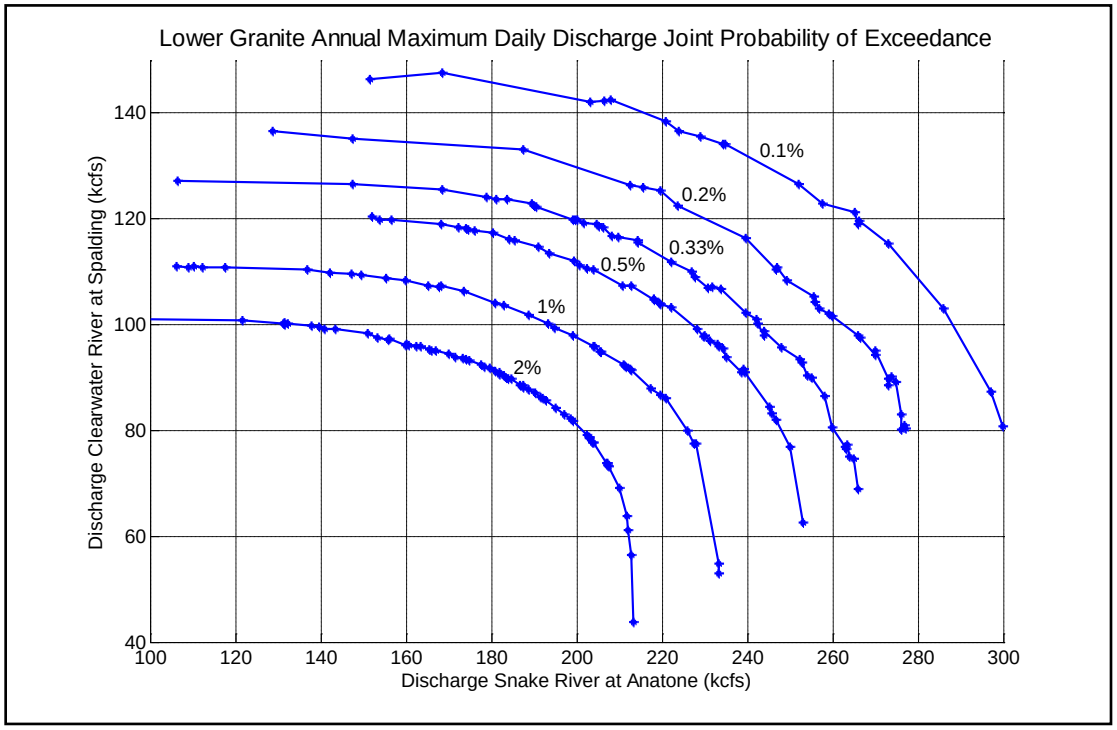


Figure 32. Joint probability of exceedance of the Snake and Clearwater River at Lower Granite.

In a Type 2 analysis the most likely distribution of flow (flow split) is derived for a given exceedance probability of total discharge. The composite flow series is first sorted by total flow in descending order and the empirical probability of exceedance computed with the Weibull plotting formula. The flow-split for each pair in the series is

computed as the proportion of flow of one of the discharges relative to the total discharge. The Anatone discharge was selected as the basis of the flow-split computation because it is usually the largest contributor to total flow. The flow-split nearest the desired exceedance probability could be selected directly from the ranked composite series, but a better approach is to compute the median flow-split over a narrow interval centered on the desired exceedance probability. The width of interval is selected by trial to give a reasonable number of values for the computation of the median value. Intervals of between ±1 percent to ±5 percent of the desired exceedance probability produced reasonable results for a composite series of 100,000 values. Intervals are wider for lower exceedance probabilities because there are fewer values of extreme discharges in the composite series. The results of the Type 2 analysis for the annual maximum daily discharge at Lower Granite are summarized in Table 15. The distribution of flow between the Snake and Clearwater Rivers is relatively uniform at 70 percent and 30 percent across the range of exceedance probabilities.

When the flow-split is defined as the Snake River discharge divided by the total discharge, the distribution of flow-split values are positively skewed for higher exceedance probabilities and become less skewed at lower exceedance probabilities. Figure 33 is a histogram of flow-split values for the 1 percent probability of exceedance for total discharge at Lower Granite. The median value for the 1 percent total discharge exceedance probability flow split is 0.70 or 70 percent of the flow comes from the Snake River during a total annual maximum daily discharge that has a exceedance probability of 1 percent. The other 30 percent comes from the Clearwater River. Based on this analysis, a flow distribution of 70 percent for the Snake River and 30 percent for the Clearwater River was used in the hydraulic analysis of the confluence.

The simulated flow distributions compare favorably with the flow-splits computed for the higher ranked discharges in stream gage record listed in Table 3. The plot of the flow-splits computed from the gage record in Figure 34 show an increasing trend with total discharge.

Proportion of Discharge from the Snake and Clearwater Rivers for Annual Maximum Daily Discharge at Lower Granite						
Exceedance Probability	2.0%	1.0%	0.50%	0.33%	0.20%	0.10%
Return period, years	50	100	200	300	500	1000
Snake River	0.701	0.702	0.709	0.685	0.691	0.673
Clearwater River	0.299	0.298	0.291	0.315	0.309	0.327
Lower Granite	1.000	1.000	1.000	1.000	1.000	1.000

Table 15. Proportion of discharge from the Snake and Clearwater Rivers for the annual maximum daily discharge at Lower Granite.

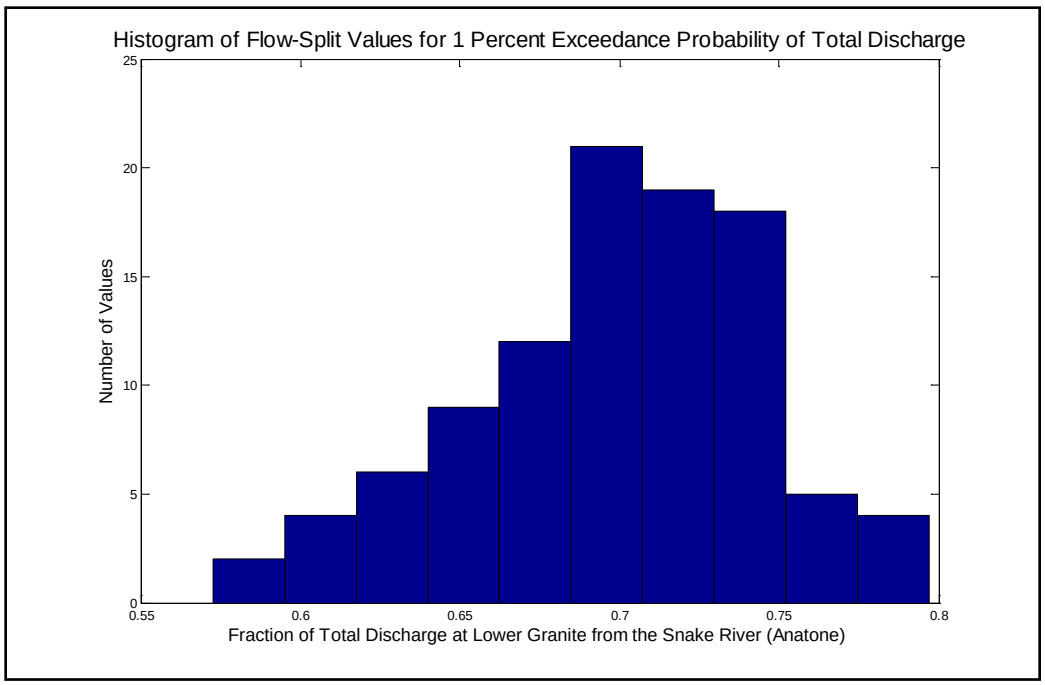


Figure 33. Histogram of Flow-Split values for the 1 percent probability of exceedance for total discharge.

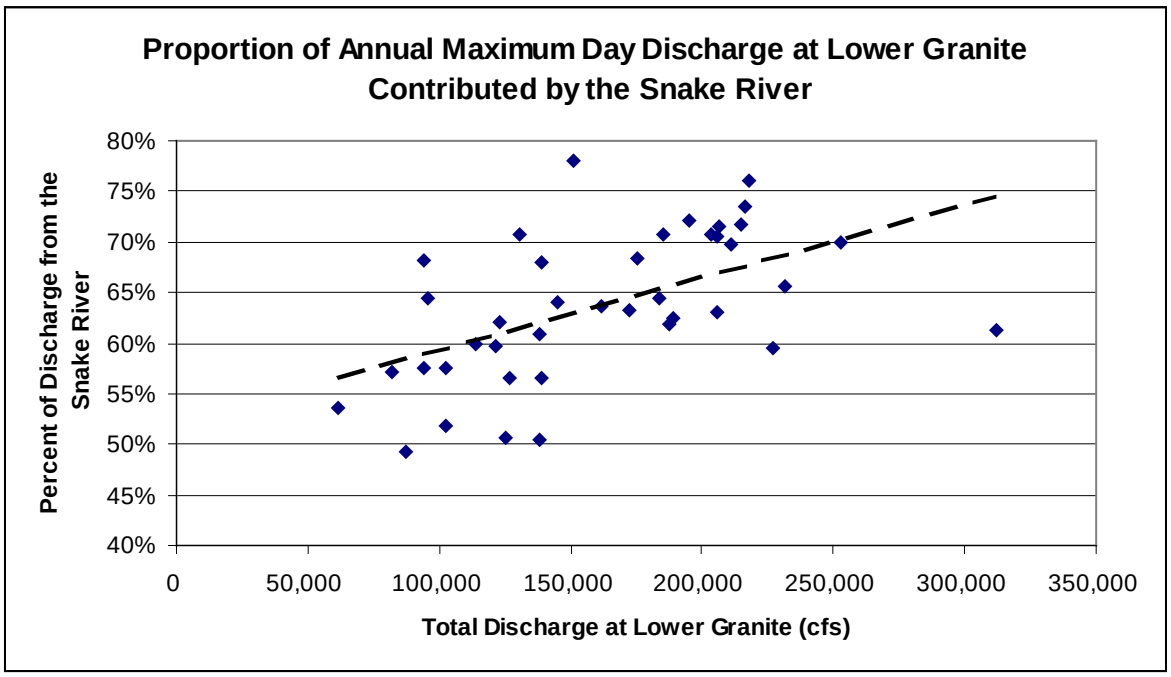


Figure 34. Proportion of flow contributed by the Snake River during the annual maximum daily discharge at Lower Granite.

2.10. Simplified Multivariate Analysis of Total Probability

A total probability multivariate analysis of the Snake and Clearwater River discharges at the confluence can also be developed solely from the coincident discharges series listed in Table 3. In this case, there is only one condition: the annual maximum daily discharge in Lower Granite is the sum of the coincident discharge at Anatone and Spalding. This simpler analysis is not as appealing from a conceptual viewpoint as the analysis above because neither coincident discharge series is exclusively a maximum annual discharge series. This raises theoretical problems similar to concerns expressed about mixed populations in annual discharge frequency analysis. In the previous analysis only condition 3, which was relatively infrequent, suffered from this deficiency. Results of the simplified multivariate Monte Carlo analysis for the coincident discharges in Table 3 are listed in Table 16. The multivariate discharge frequency estimates are generally higher by a few percentage points than the previous analysis. The accuracy is of the simpler method is likely adequate for flood risk analysis given the uncertainty of less well defined variables. The previous multivariate analysis acknowledged the importance of primary and complimentary stations in the assessment of conditional and total probability for discharge frequency relationships.

Lower Granite Univariate and Multivariate Estimates of Total Probability				
		Annual Maximum Day (cfs)		
Return Period	Percent Exceedance	Univariate Total Probability	Multivariate Joint Probability	Difference
2000	0.05	407,704	435,316	6.8%
1000	0.1	389,118	412,026	5.9%
500	0.2	369,770	388,293	5.0%
303	0.33	355,111	370,824	4.4%
250	0.4	349,447	364,032	4.2%
200	0.5	342,849	356,092	3.9%
100	1	321,281	330,950	3.0%
50	2	298,445	304,935	2.2%
25	4	274,019	277,761	1.4%
10	10	238,360	239,223	0.4%
5	20	207,444	206,820	-0.3%
2	50	155,449	154,200	-0.8%
1.25	80	112,935	112,637	-0.3%
1.11	90	94,357	94,785	0.5%
1.05	95	80,796	81,833	1.3%
1.01	99	59,393	61,439	3.4%

Table 16. . Comparison of the simplified total probability-mulitvariate and univariate discharge frequency estimates for Lower Granite.

2.11. Extended Multivariate Analysis of Total Probability

The multivariate Monte Carlo analysis of total probability can be extended upstream to the point where regulated and unregulated discharges are separate flow streams. This is advantageous because the influence of the regulated flow source can be represented as a separate discharge frequency distribution and the extreme discharges of the unregulated tributaries will be better characterized by the Bulletin 17B LP3 distribution. It also allows adjustments for possible climate change applied directly to the unregulated sources to evaluate the effect on the total probability discharge exceedance.

The Monte Carlo multivariate analysis is performed with a procedure that is similar to that for the Anatone and Spalding discharges but is based on the six tributary stream gate stations above Anatone and Spalding shown in Figure 4. The flow conditions that comprise the total probability of the annual maximum day discharge at Lower Granite are:

1. The annual maximum discharge at Lower Granite is the sum of the annual maximum day discharge of the Salmon River at Whitebird plus the coincident discharges of the Clearwater at Orofino, Dworshak outflow, Snake at Hells Canyon, Imnaha River, and Grande Ronde River at Troy.
2. The annual maximum discharge at Lower Granite is the sum of the annual maximum day discharge of the Clearwater River at Orofino plus the coincident discharges of the Salmon at Whitebird, Dworshak outflow, Snake at Hells Canyon, Imnaha River, and Grande Ronde River at Troy.
3. The annual maximum discharge at Lower Granite occurs when the annual maximum discharge occurs neither at Whitebird or Orofino. In this case the maximum discharge at Lower Granite is the sum of the flows at Salmon at Whitebird, Clearwater at Orofino, Dworshak outflow, Snake at Hells Canyon, Imnaha River, and Grande Ronde River at Troy.

Discharge data for the three flow conditions is listed in Table 17, Table 18 and Table 19.

There were 13 years in the record where the maximum annual daily discharge at Lower Granite was produced by annual maximum daily discharge at Whitebird plus the coincident tributary discharges (Condition 1). Similarly, there were 11 years in the record where the maximum annual daily discharge at Lower Granite was produced by annual maximum daily discharge at Orofino plus the coincident tributary discharges (Condition 2). There were 7 years in the record where the average daily discharges of the tributaries produced the maximum annual daily discharge at Lower Granite and neither Whitebird nor Orofino was an annual maximum daily discharge. There were 8 years when maximum annual discharges occurred at Whitebird and Orofino on the same day and their total produced the maximum annual discharge at Lower Granite

(intersection of condition 1 and 2). The 4 ties were assigned each to condition 1 and condition 2. The tally of the flow conditions and the frequencies of occurrence are listed in Table 20.

Condition 1 Discharge Data Multivariate Analysis of Total Maximum Daily Discharge at Lower Granite							
	Max Day (cfs)	Coincident Average Daily Discharge (cfs)					Total (cfs)
	Salmon	Clearwater	Grande Ronde	Imnaha	NF Clearwater	Snake	Lower
Date	Whitebird	Orofino	Troy	Imnaha	Dworshak	Hells Canyon	Granite
2-Jun-72	67,300	59,200	14,600	2,430	3,700	40,500	187,730
18-Jun-74	67,300	59,200	14,600	2,430	3,700	40,500	187,730
7-Jun-75	28,600	13,900	2,980	437	1,000	13,100	60,017
9-Jun-78	52,000	49,200	10,800	1,990	9,700	12,800	136,490
10-Jun-81	57,300	86,500	10,800	2,490	5,800	35,500	198,390
31-May-84	47,500	89,700	11,400	3,100	1,900	39,300	192,900
1-Jun-86	39,500	30,300	8,560	1,380	9,000	8,210	96,950
30-May-90	47,200	25,600	16,200	2,060	6,600	16,600	114,260
21-May-93	28,700	22,400	3,600	585	11,100	18,500	84,885
5-Jun-95	60,000	73,300	12,700	3,300	200	44,700	194,200
10-Jun-96	50,600	52,300	9,510	1,800	1,700	20,700	136,610
18-May-97	45,600	36,500	11,300	1,890	18,000	18,000	131,290
16-May-01	32,300	36,900	5,480	1,290	9,700	14,900	100,570
31-May-03	70,700	87,200	17,900	4,680	1,900	16,100	198,480
20-May-05	62,000	82,100	22,600	3,790	1,300	47,931	219,721
21-May-06	90,300	51,700	13,200	3,170	5,600	31,200	195,170
31-May-09	73,500	57,300	11,900	2,120	4,800	21,400	171,020
Condition 1: Whitebird maximum day discharge,other coincident daily discharge							
Condition 2: Orofino maximum day discharge, other coincident daily discharge							
Condition 3: Lower Granite maximum day discharge, tributary flows coincident daily discharge							

Table 17. Salmon River at Whitebird maximum day discharge and tributary coincident discharges (Condition 1).

Condition 2 Discharge Data Multivariate Analysis of Total Maximum Daily Discharge at Lower Granite							
	Max Day (cfs)	Coincident Average Daily Discharge (cfs)					Total (cfs)
	Clearwater	Salmon	Grande Ronde	Imnaha	NF Clearwater	Snake	Lower
Date	Orofino	Whitebird	Troy	Imnaha	Dworshak	Hells Canyon	Granite
19-May-73	98,500	81,200	13,100	2,380	14,000	20,600	229,780
11-May-76	129,000	78,700	16,000	3,660	39,300	33,200	299,860
3-May-77	73,600	55,200	9,950	2,540	6,100	28,300	175,690
25-May-79	68,600	39,700	6,070	1,730	5,000	12,400	133,500
18-Jun-82	66,700	44,800	10,700	1,850	15,000	38,900	177,950
29-May-83	86,200	65,800	15,100	3,030	9,300	68,000	247,430
1-May-87	94,800	50,000	9,390	2,590	9,200	41,400	207,380
20-May-91	33,800	45,800	5,700	2,220	7,600	15,000	110,120
2-May-92	64,200	47,200	12,500	2,400	17,400	38,000	181,700
27-May-99	68,900	32,100	10,300	2,410	200	39,800	153,710
31-May-02	94,800	49,100	7,550	1,870	8,500	43,400	205,220
29-May-04	98,900	78,100	15,000	2,710	700	33,000	228,410
13-May-07	31,200	36,700	7,040	1,030	1,400	15,900	93,270
20-May-08	90,300	60,400	12,100	2,610	2,500	41,900	209,810
5-Jun-10	46,900	32,300	8,370	2,280	9,300	41,600	140,750
Condition 1: Whitebird maximum day discharge,other coincident daily discharge							
Condition 2: Orofino maximum day discharge, other coincident daily discharge							
Condition 3: Lower Granite maximum day discharge, tributary flows coincident daily discharge							

Table 18. Clearwater River at Orofino maximum day discharge and tributary coincident discharges (Condition 2).

Condition 3 Discharge Data Multivariate Analysis of Total Maximum Daily Discharge at Lower Granite							
	Coincident Average Daily Discharge (cfs)						Total (cfs)
	Salmon	Clearwater	Grande Ronde	Imnaha	NF Clearwater	Snake	Lower
Date	Whitebird	Orofino	Troy	Imnaha	Dworshak	Hells Canyon	Granite
12-Jun-80	34,100	27,600	6,020	1,650	11,100	46,800	127,270
8-Jun-85	33,100	35,400	9,110	1,900	18,900	24,900	123,310
7-May-88	12,800	18,500	3,580	493	24,200	23,000	82,573
22-Apr-89	27,400	45,700	12,000	1,690	50	31,100	117,940
11-May-94	28,100	29,300	6,330	1,270	200	23,300	88,500
27-May-98	43,000	35,900	16,300	4,860	12,800	93,400	206,260
23-Apr-00	23,300	29,500	9,180	1,690	15,600	32,300	111,570
Condition 1: Whitebird maximum day discharge,other coincident daily discharge							
Condition 2: Orofino maximum day discharge, other coincident daily discharge							
Condition 3: Lower Granite maximum day discharge, tributary flows coincident daily discharge							

Table 19. Lower Granite maximum day tributary coincident discharges (Condition 3).

Frequencies of Lower Granite Flow Conditions			
Condition	Count	Adjusted Count	Frequency
1. Whitebird max day plus Orofino coincident	13	17	0.436
2. Orofino max day plus Whitebird coincident	11	15	0.385
Intersection 1 and 2	8	0	0.000
3. Tributary sum is Lower Granite max day	7	7	0.179
Total	39	39	1.000

Table 20. Frequencies of flow conditions at Lower Granite for the extended multivariate analysis.

The Monte Carlo analysis for each flow condition was performed with Matlab scripts by the process depicted in Figure 27 except that the inputs included the data from all 6 tributary stations. Correlations used in generation of the discharge series were those between the primary station and the complementary tributary stations. The regulated discharges at Dworshak and Hells Canyon were simulated by fitting LP3 distributions to the historic coincident discharges. The Monte Carlo analysis generates implausibly high discharges for the regulated sources unless upper values are censured. Censuring may be included in Monte Carlo analysis by various methods[52]. The method used here was to limit generated extreme values to a specific discharge. The limit for both Dworkshak and Hells Canyon was 1.25 times the maximum historic regulated release. For Dworshak, the maximum historic release was 39,300 cfs and for Hells Canyon the maximum historic release was 98,100 cfs. In lieu of an extensive study of misoperation processes and probabilities at the projects, it is assumed that these upper limits are reasonably conservative.

[52] Gentle, J.E. (1998). *Random Number Generation and Monte Carlo Methods*, Springer, New York.

Results of the extended multivariate analysis are summarized in Table 21. The multivariate estimates of total discharge frequencies greater than the 1-percent exceedence level are between 4 and 5 percent lower than the estimates of total discharge frequencies from the univariate analysis of annual maximum daily discharges are Lower Granite. The differences can be attributed to the discharge from the ungaged small tributary streams and groundwater inflow downstream from the tributary stream gages stations. The discharges and percentage differences in Table 21 may also be compared to the two-station multivariate estimate in Table 14. An important use of the extended multivariate analysis is to provide independent corroboration of the univariate analysis and multivariate analysis based solely on the Anatone and Spalding gage data Because the Spalding and Anatone data is not used in the extended analysis a large difference between the results of the analyses would indicate inconsistencies in the extreme discharges in the gage records.

The extended multivariate analysis can be modified to demonstrate the effect of climate change on the discharge frequencies. The Monte Carlo analysis for flow conditions 1 and 2 were repeated with discharge data that included an additional extreme discharge event that was twice the historic annual maximum daily discharge. At Whitebird the historic maximum daily discharge 129,000 cfs occurred on 18 June 1974, so an additional annual maximum daily value of 258,000 cfs was added to the Whitebird data series at a future nominal date of 18 June 3074. The date assigned to the augmentation discharge is unimportant in the analysis; it needs only to be included in the data. Coincident daily discharges were kept the same as the 18 June 1974 values. Similarly, at Orofino the historic maximum daily discharge 81,200 cfs occurred on 2 June 1972 so an additional annual maximum daily value of 162,400 cfs was added to the Whitebird data at a future nominal date of 2 June 2072.

A doubling of the flow at Whitebird produces a total flow of 428,860 cfs at Lower Granite, which is slightly more than the Standard Project Flood at Lower Granite of 420,200 cfs. Table 21 shows that a partially regulated SPF discharge of 420,000 cfs has an exceedance probability of less than 0.05 percent (2000 years). Table 22 shows that if a discharge at Whitebird produces an SPF at Lower Granite, the exceedance probability of the SPF is only increased to just over 0.2 percent (500 to 1000 years). The addition of a discharge to the Orofino data that was twice the historic annual maximum Orofino (81,200 cfs to 162,400 cfs) reduced the probably of exceedance of the SPF to between 0.05 to 0.1 percent (1000 to 2000 years). Even when additional discharges that are twice the historic maximums are added to the Whitebird and Orofino data in the same simulation, the probability of exceedance of the SPF only increased to between 0.333 to 0.2 percent (300 to 500 years).

Two conclusions are made from this analysis: 1) An extreme increase in discharge is required at the most likely source – the Salmon River at Whitebird to

produce the SPF in Lower Granite, and 2) the SPF event has a very low exceedance probability indicating that a discharge at the level of the SPF will have very little effect on the computation of conditional non-exceedance probabilities at the Lewiston levee system.

Potential effect of climate change can also be evaluated within the multivariate Monte Carlo analysis by changing the LP3 regional skew value. The regional skew analysis in Section 2.5 showed that station skew values have tended to increase (become less negative) over the gage record. The extended Monte Carlo analysis for the three flow conditions using the original unaltered discharge data was repeated with a regional skew value of 0.0 instead of the Bulletin 17B regional skew of -0.3. Table 23 shows that increasing the regional skew by 0.3 increased the discharges of the exceedance probabilities by about 6 percent.

Lower Granite Univariate and Multivariate Discharge Frequency Estimates				
		Annual Maximum Day (cfs)		
Return Period	Percent Exceedance	Univariate Total Probability	Multivariate Joint Probability	Difference
2000	0.05	407,704	392,851	-3.6%
1000	0.1	389,118	373,537	-4.0%
500	0.2	369,770	353,811	-4.3%
303	0.33	355,111	339,257	-4.5%
250	0.4	349,447	333,589	-4.5%
200	0.5	342,849	326,956	-4.6%
100	1	321,281	305,896	-4.8%
50	2	298,445	283,997	-4.8%
25	4	274,019	260,984	-4.8%
10	10	238,360	228,040	-4.3%
5	20	207,444	199,992	-3.6%
2	50	155,449	153,523	-1.2%
1.25	80	112,935	115,684	2.4%
1.11	90	94,357	99,003	4.9%
1.05	95	80,796	86,693	7.3%
1.01	99	59,393	66,867	12.6%

Table 21. Comparison of the extended total probability mulitvariate and univariate discharge frequency estimates for Lower Granite.

Lower Granite Univariate and Multivariate Discharge Frequency Estimates				
		Annual Maximum Day (cfs)		
Return Period	Percent Exceedance	Univariate Total Probability	Multivariate Joint Probability	Difference
2000	0.05	407,704	466,158	14.3%
1000	0.1	389,118	437,605	12.5%
500	0.2	369,770	409,091	10.6%
303	0.33	355,111	388,471	9.4%
250	0.4	349,447	380,537	8.9%
200	0.5	342,849	371,319	8.3%
100	1	321,281	342,539	6.6%
50	2	298,445	313,394	5.0%
25	4	274,019	283,620	3.5%
10	10	238,360	242,519	1.7%
5	20	207,444	208,930	0.7%
2	50	155,449	156,112	0.4%
1.25	80	112,935	115,691	2.4%
1.11	90	94,357	98,595	4.5%
1.05	95	80,796	86,254	6.8%
1.01	99	59,393	66,850	12.6%

Table 22. Extended total probability mulitvariate with increased maximum discharge at Whitebird.

Lower Granite Univariate and Multivariate Discharge Frequency Estimates				
		Annual Maximum Day (cfs)		
Return Period	Percent Exceedance	Univariate Total Probability	Multivariate Joint Probability	Difference
2000	0.05	407,704	423,539	3.9%
1000	0.1	389,118	400,034	2.8%
500	0.2	369,770	376,383	1.8%
303	0.33	355,111	359,160	1.1%
250	0.4	349,447	352,504	0.9%
200	0.5	342,849	344,751	0.6%
100	1	321,281	320,398	-0.3%
50	2	298,445	295,489	-1.0%
25	4	274,019	269,761	-1.6%
10	10	238,360	233,718	-1.9%
5	20	207,444	203,739	-1.8%
2	50	155,449	155,440	0.0%
1.25	80	112,935	117,274	3.8%
1.11	90	94,357	100,738	6.8%
1.05	95	80,796	88,630	9.7%
1.01	99	59,393	69,257	16.6%

Table 23. Extended total probability mulitvariate with reduced region skew.

2.12. Summary of the Discharge Frequency Analysis

Reliable frequency relationships for the joint discharge of the Snake and Clearwater Rivers in Lower Granite Reservoir are essential for the evaluation of the risk of overtopping levees at the confluence. This section presented a generally applicable method of computing marginal and total probability discharge frequency relationships for correlated tributary flows using Monte Carlo simulation and Bulletin 17B log Pearson Type 3 frequency distributions. The total probability multivariate method was shown to produce frequency estimates that closely agreed with total probability univariate estimates, both with discharge data from the two primary stations (Anatone and Spalding) and in an extended analysis of the regulated and unregulated tributary sources (Whitebird, Orofino, Troy, Imnaha, Dworshak and Hells Canyon).

An analysis of the correlation between the tributaries identified the appropriate primary and secondary gages to be used as the basis of the joint probability analysis. Stream gage data for these stations was reviewed and synthesized. An evaluation of the trends in the station skew of the annual peak discharge showed that the period of regulation of the Clearwater River by Dworshak Dam 1972 – 2010 was selected as the basis of the flood frequency analysis because it produced the most conservative LP3 parameters and the greatest partially regulated discharge frequency estimates. This period of record also includes large historic discharges.

The influence of cyclic climatic patterns was examined with a regression and trend analysis between annual peak discharges of the primary stream gage stations and the SST-CTI and ENSO-MEI indices. Significant trends exist between peak discharge and the climatic indices, indicating that climatic patterns likely influence flood risk at the confluence. Nothing in the trend analysis suggests that a significant shift has occurred that invalidates the use of historical peak discharge data in the flood risk at the confluence.

The univariate analysis of the sum of the Anatone and Spalding discharges provides the best estimate of the partially regulated discharge frequency of the annual maximum daily flow in Lower Granite. Empirical peaking factors can be applied to adjust the annual maximum daily flow to the instantaneous annual peak flow. However, the univariate analysis does not provide information about the distribution of flows between the Snake and Clearwater Rivers – information that is essential for hydraulic modeling of stage at the confluence. Correlated discharge series are a product of the Monte Carlo multivariate analysis that can be further evaluated to determine the exceedance probabilities of specific flow combinations (Type 1 analysis) and the likely (median) flow-split for a specified exceedance probability of total discharge (Type 2 analysis). The Type 2 analysis provides the best estimate of the distribution of flow between the Snake and Clearwater Rivers for hydraulic modeling.

The extended multivariate Monte Carlo analysis simulated the tributary discharges at the point of separation between regulated and unregulated flows. This allowed climate forcing to be applied to the unregulated sources to evaluate possible effects on the discharge frequency estimates. Doing so directly links the climate change scenario to the discharge frequency estimate, and ultimately the risk analysis, with a minimum of assumptions. As the primary unregulated tributaries, the Salmon River (Whitebird) and the Clearwater River (Orofino) are expected to be the source of extreme flows affected by climate change. Both the univariate and multivariate analyses showed that the Standard Project Flood of 420,000 cfs at Lower Granite has a very low exceedance probability in the range of 0.2 percent to 0.1 percent (500 – 1000 years) even if an event of the magnitude of the SPF was included in the discharge series.

3. Variability of Observed Stage at the Confluence

An important consideration in the evaluation of flood risk at the confluence levees is the uncertainty in estimates of computed water surface elevations (stage) due to hydraulic factors such as sediment bed forms, sediment transport rate, wind waves, spillway control at Lower Granite Dam, and unsteady flow effects[53]. This section describes how uncertainty in stage was evaluated for the range of discharges actual observed in the reservoir. In addition to observed or normal variability, stage for a given discharge can vary because of changes in sediment bedforms at very high discharges. This element of the uncertainty in stage is discussed in Section 10.

Water surface elevations are measured at the confluence by an electronic stage gage that is maintained by the Corps. The confluence gage (Figure 35) is located where the left-bank levee on the Clearwater River joins the right-bank levee on the Snake River. It is located near the low point of the top-of-levee profile. The gage transmits instantaneous water levels (not time-averaged) once every hour to NWD water management database.

The variability of stage at high discharge is of the most concern in the flood risk analysis. Unfortunately this means that the variability of stage can only be evaluated for very few observed discharges. Total discharge in Lower Granite Reservoir during the high discharge year of 1997 reached a maximum winter average daily discharge of 210,200 cfs on January 2 and a maximum spring average daily discharge of 231,800 cfs on May 18 (Figure 36). The maximum discharge on May 18 was the second highest

[53] USACE (1006). "Chapter 5, Uncertainty of stage-discharge function", *EM 1110-2-1619 Risk-based analysis for flood damage reduction studies*. U.S. Army Corps of Engineers, Washington DC.

discharge of record after the reservoir reached full pool in 1975. The greatest annual maximum daily discharge occurred on 31 may 1984, but the confluence stage data at this time is unreliable. Stage measurements at the confluence during the high discharge of January 1997 (SRCI) are compared in Figure 37 with the total inflow to Lower Granite Reservoir, the outflow of Lower Granite Dam and the water surface elevation of the forebay at Lower Granite. The separate view of the stage measurements in Figure 38 show that total variability in stage is less than 1 foot. The abrupt peak in stage appears to have been caused by a relatively rapid change in outflow at the dam, perhaps during adjustment of spillway gate setting. Stage variability during the peak discharge in May 1997 in Figure 39 is less. The hourly differences of instantaneous stage for all discharges since 1990 plotted in Figure 40 indicate that the variability in stage tends to decrease with discharge. This relationship is due to regulation of the reservoir, cyclic hydropower releases, greater sampling of wave run-up at lower discharges (Section 13), and data quality. The few large differences of about 2 feet or more in the plot are attributed to uncorrected errors in the recorded data.

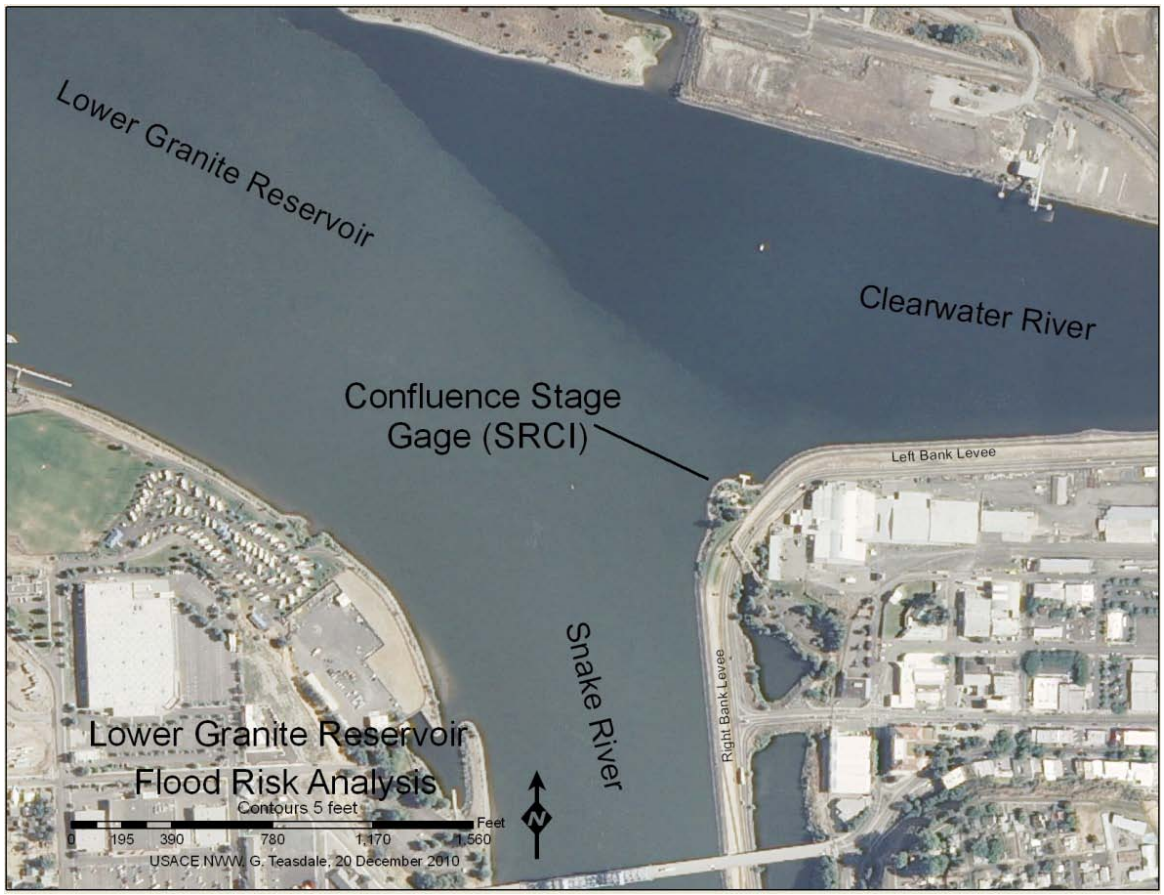


Figure 35. Location of the confluence stage gage.

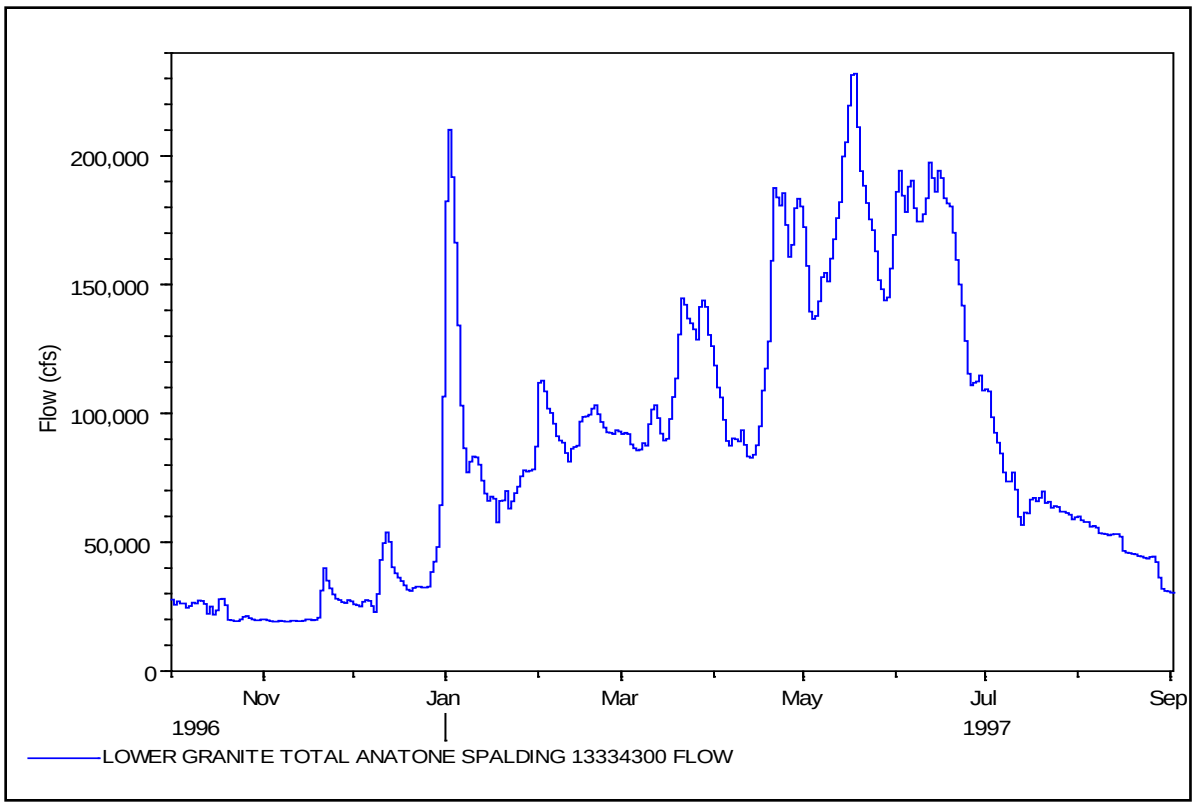


Figure 36. Lower Granite total inflow hydrograph during 1997 winter and spring floods.

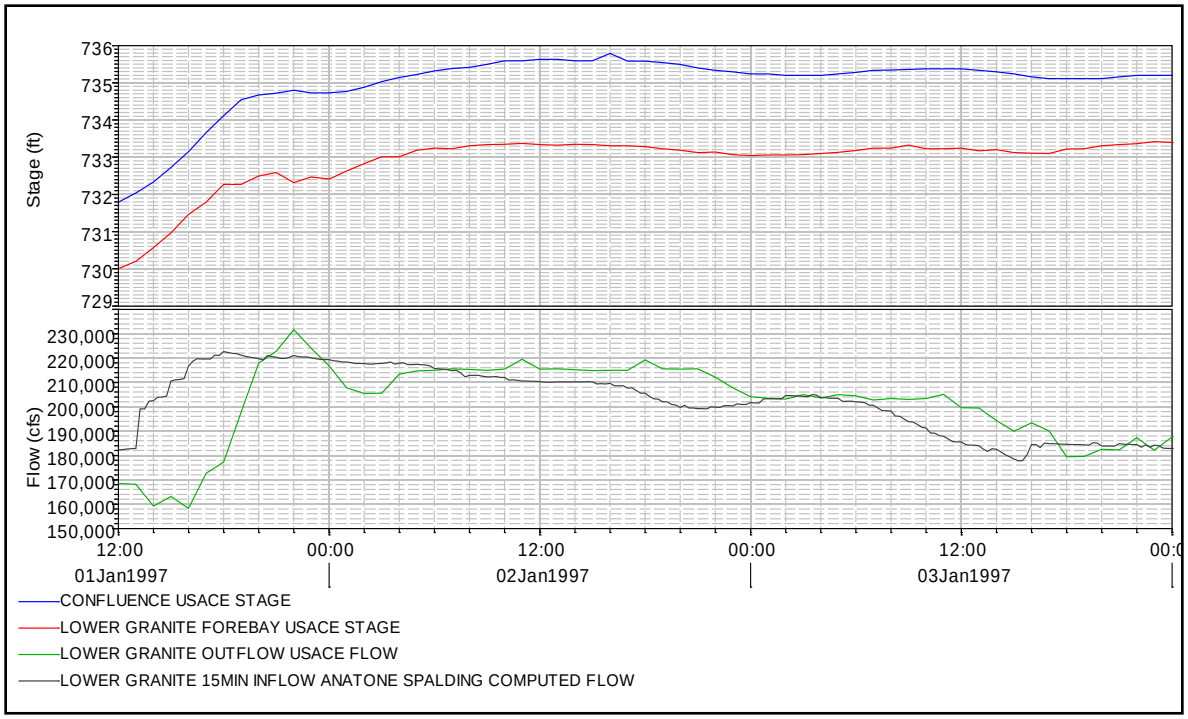


Figure 37. Stage and discharge relationships in Lower Granite Reservoir during the 1997 flood.

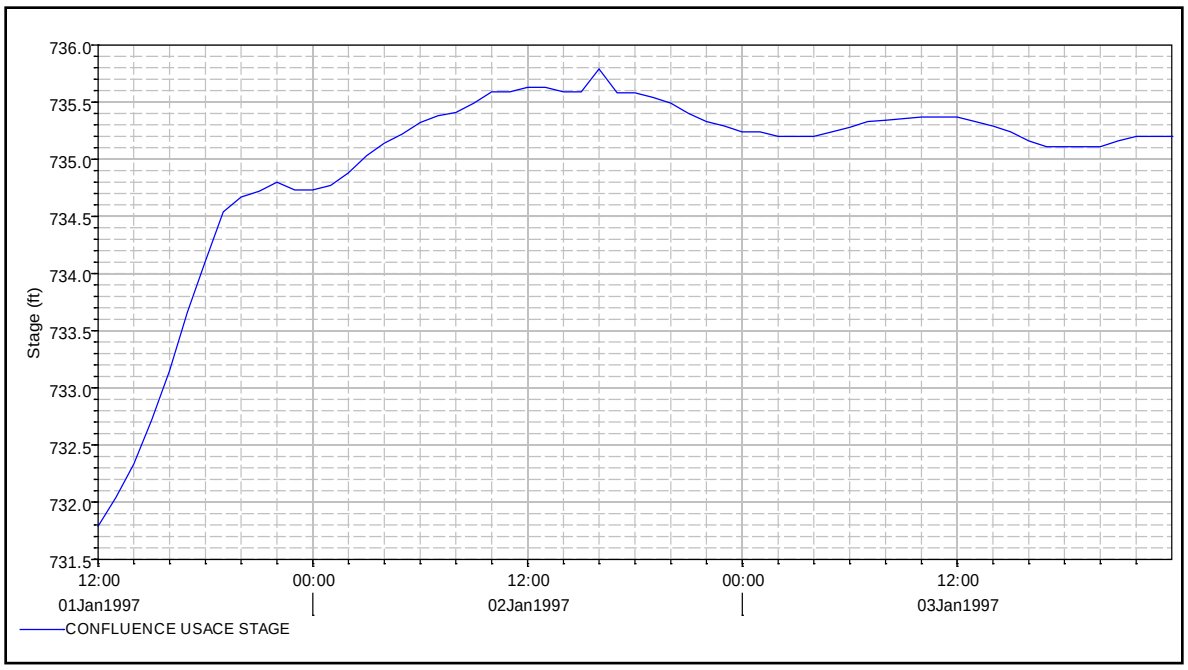


Figure 38. Lewiston confluence stage during the high discharge of January 1997.

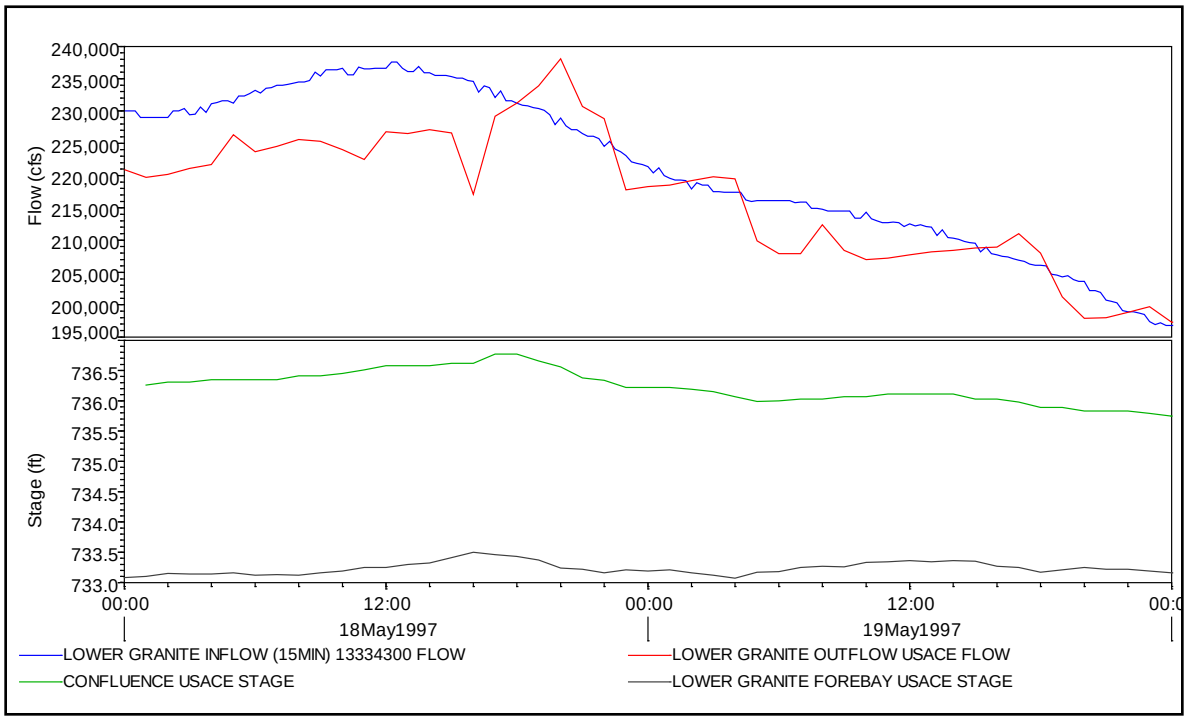


Figure 39. Stage and discharge relationships in Lower Granite Reservoir during the 1997 spring flood.

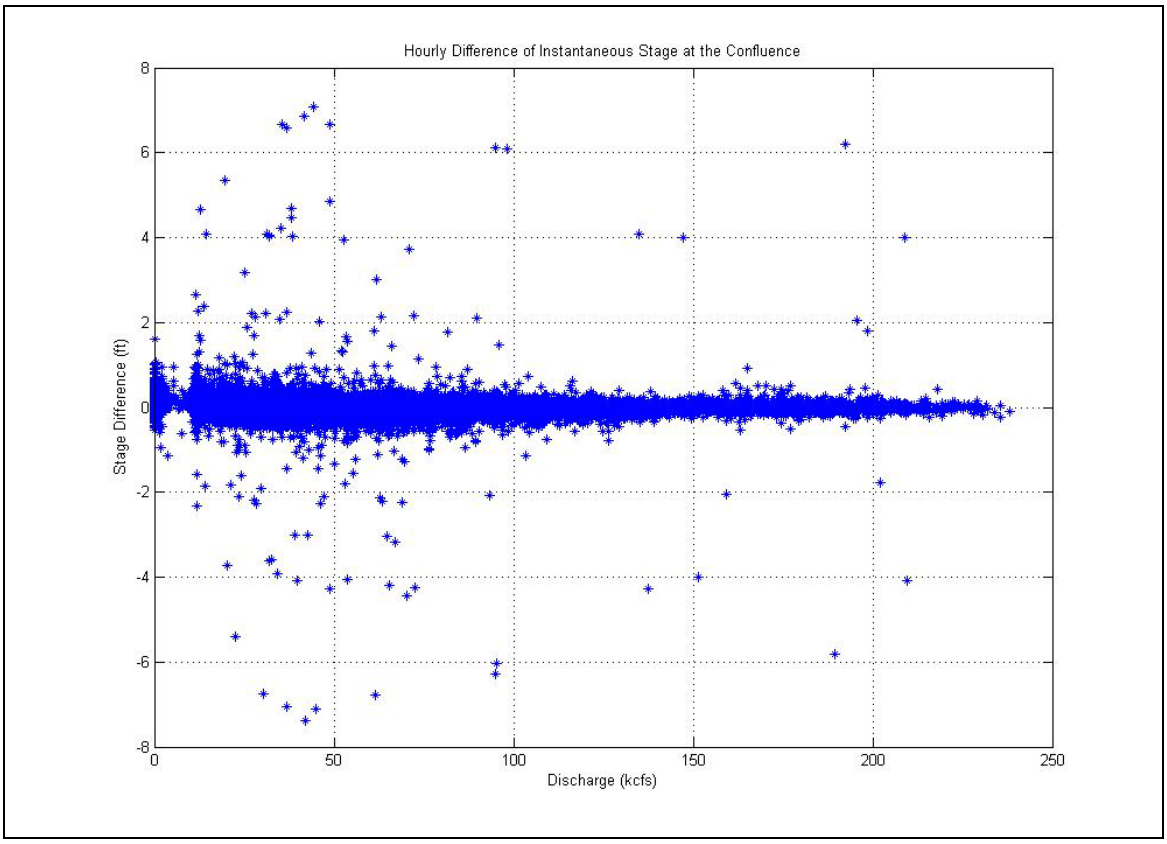


Figure 40. Hourly difference of instantaneous stage at the confluence.

4. Fixed-Bed Hydraulic Modeling of Flood Stage

This section describes development and application of the one-dimensional model of the Snake and Clearwater Rivers in Lower Granite Reservoir that was developed for the flood risk analysis with the HEC-RAS 4.1 software[54]. The frequency characteristics of water level (stage) define the probability that flood flows will overtop the crest of a levee. Two components of probability must be specified to define the probability of overtopping. The first component of probability is defined by the exceedance probability of the discharge; the second results from random fluctuation of stage at a given level of discharge. The median stage height for a flood risk analysis is normally computed with hydraulic models from the median discharges associated with specified discharge exceedance probabilities. Stage exceedance probabilities could be

[54] Brunner, G.W., (2010). *HEC-RAS River Analysis System User's Manual, Version 4.1*, January 2010. Hydrologic Engineering Center, U.S. Army Corps of Engineers, Davis, CA.

derived directly from stage measurements, but stage datasets for channels are seldom sufficient for this purpose.

Median stage can be viewed as the stage that would be observed 50 percent of the time given the random fluctuations caused by effects not completely correlated with discharge. Commonly, water surface profiles of the median stage are computed with one-dimensional fixed-bed hydraulic models. Estimation of stage variability that is not related to discharge variation was discussed in Section 3.

Open channel hydraulic models can be classified according to the degree of simplification of the hydrodynamic processes of water and sediment movement within the model formulation[55]. One-dimensional, fixed-bed models, such as those developed with HEC-RAS, do not directly simulate the lateral or vertical movement of water, or the movement of sediment within a given channel cross section or river reach. One-dimensional, mobile bed models can be developed with HEC-RAS to simulate sediment transport, deposition and scour along the channel.

One-dimensional models perform well where gradually varying flows are confined to a single channel and only average water surface elevations and mean velocities are needed to define flood potential. Two-dimensional (multi-dimensional) models are more accurate when simulation of lateral flows becomes important as in floodplains, multithread channels and where large flows merge, such as at the confluence of the Clearwater and Snake Rivers. Two-dimensional models, such as the Adaptive Hydraulics Model (ADH)[56], can be run in fixed-bed and mobile-bed mode. Both one and two dimensional models, and fixed-bed and mobile-bed models, are used in this risk analysis to investigate the hydrodynamics of the confluence and show the effect that model assumptions have on the conditional non-exceedance probabilities for overtopping of the levees.

4.1. Channel Elevation Data

Sediment ranges (cross sections) have been measured in Lower Granite Reservoir every two to three years since the pool was filled in February 1975 (Figure 41). There are 66 sediment ranges between Lower Granite Dam at River Mile (RM) 107.73 to RM 148.83 on the Snake River above Asotin, WA, and 33 sediment ranges

[55] USACE (1963). EM 1110-2-1416 *River Hydraulics*, U.S. Army Corps of Engineers, Washington, DC.

[56] Berger, R.C., Tate, J.N., Brown, G.L., Savant, G. (2010). Adaptive Hydraulics Users Manual, AdH Version 3.2, Coastal and Hydraulics Laboratory, Engineering Research and Development Center, U.S. Army Corps of Engineers, Vicksburg, MS.

on the Clearwater from the confluence to RM 7.85. The sediment ranges extend beyond the M1 profile (backwater) zone of Lower Granite Dam on both the rivers. At the SPF discharge backwater extends to about Snake RM 146.3 near Asotin and about Clearwater RM 3.9. Sediment ranges near confluence of the Clearwater and Snake Rivers are spaced close together and give a good record of sediment accumulation and changes in channel geometry. The use of sediment ranges for measurement of sediment accumulation is discussed in Section 7. The most recent complete set of sediment ranges at the time of this analysis was acquired in 2009[57]. In future years, sediment ranges will likely be replaced with more detailed bathymetry acquired with multi-beam echo-sounding instruments.

The sediment range cross sections are measured with acoustic methods that meet or exceed the accuracy standards and procedures specified in the Corps hydrographic surveying manual[58]. The performance standards require at least a 95 percent root-mean-square (RMS) of 0.5 feet for depths less than 15 feet, 1.0 ft RMS in depths up to 40 feet, and 2.0 ft RMS for depths greater than 40 feet. Accuracy reported at the 95 percent confidence level means that 95 percent of the elevations in the dataset will have an error with respect to true ground elevation that is equal to or smaller than the reported value. Manual soundings in near shore areas must have accuracies greater than 0.1 foot. Positions are logged by kinematic GPS survey that is tied to a network of bench marks established by the Corps. Elevation data was processed by the contract hydrographic surveyor with Hypack 2009. Densely spaced bottom transects have historically been are acquired of the navigation channel near the confluence, but do not extend across the full width of the channel.

Recent sediment range data was delivered by the surveying contractor as ascii point data projected to the Washington State Plane System South NAD83 and NAVD88 in units of U.S. survey feet. Older sediment range data is projected to the NAD27 Washington State Plane System South and NGVD29 datum or was in station-elevation (GR) format. At the confluence NAVD88 elevations are 3.24 feet higher than the NGVD29 datum.

High-resolution multibeam echosounding bathymetry was acquired in 2009 by USGS[59] of the upper reach of Lower Granite Reservoir from just below Silcott Island at

[57] RSI (2009). *Lower Granite Sediment Range Survey*, Contract No. W912EF-08-D-0011, Task Order No. 16, Surveying, Inc, Sept 2009.

[58] USACE (2002). *EM 1110-2-1003 Hydrographic Surveying*, U.S. Army Corps of Engineers, Washington, DC.

[59] The U.S. Geological Survey in Idaho performed the bathymetric survey work under a MIPR agreement with NWW. Original bathymetric data is available from USGS.

about RM 130 to about RM 142 near Swallows Nest Park on the Snake River, and from the confluence to about RM 2.0 on the Clearwater River (Figure 43). The processed elevation coordinate data was delivered in the UTM 11 NAD83 and NAVD88 projection in units of meters then reprojected to Washington State Plane South coordinate system. Both the MBES bathymetry and the 2009 sediment ranges were acquired during low flows in late summer and autumn of 2009.

Elevations of the 2009 MBES bathymetry were compared to coincident points in the 2009 sediment ranges. Figure 44 shows that the average difference elevation difference between the MBES data and the sediment range elevations was -0.22 feet (MBES lower). Figure 45 shows that the difference in elevation is somewhat related to depth. The agreement between the two data sources satisfies the accuracy requirements hydrographic surveying standards so the MBES data was used without adjustment. The close agreement between the independently measured elevation datasets validates the use of both datasets in the hydraulic analysis.

4.2. Overbank and Floodplain Elevation Data

Floodplain and overbank elevations for the hydraulic model were extracted from LiDAR elevation data acquired in 2010 under contract for the Corps. The resolution of the LiDAR data is 3.28 feet (1 meter) and covered the near shore area from Lower Granite Dam to just upstream of Asotin on the Snake River, and from the confluence to upstream of the levee system in Lewiston. Figure 46 shows the LiDAR coverage of the floodplain behind the Lewiston levees. The 2009 MBES bathymetry and the 2010 LiDAR elevation data were merged for extraction of georeferenced cross sections and for generation of gridded data for two dimensional models of the channel and floodplain.

4.3. Top-of-Levee Elevation Data

The crest elevation profiles of the Lewiston levees were verified by field survey in May 2010. The tops of the levees were surveyed at approximately 100 ft intervals. Cross sections of the levee were measured at 500 ft intervals and where the levees changed configuration or composition. Side shots were taken on utilities or signs that marked where utilities crossed the levees. The datum for the survey is NAD 83\2007 and NAVD 88 in U.S feet[60]. The 2010 top-of-levee profile agreed closely with elevations measured in a 1991 levee survey and indicated no settlement or displacement of the levees.

[60] RSI (2010*). Lewiston Levee System Profile and Cross Section Survey*, Contract No. W912EF-08-D-0011, Task Order No. 27, Rogers Surveying, Inc, June 2010.

4.4. Bridge Geometric Data

Bridge geometries for the hydraulic model were obtained from design and as-built construction drawing or photographs. Design drawings for Memorial Bridge on the US HW 12 that crosses the Clearwater River at RM 1.99 were provided by the Idaho Transportation Department. Geometry for the Camas Prairie Railroad Bridge at RM 0.6 on the Clearwater River and the Southway Bridge at RM 141.2 on the Snake River was obtained from drawings archived by the Corps. Plans for the US HW 12 bridge across the Snake River at RM 139.5 were obtained from the Washington State Department of Transportation. Bridge plans for Red Wolf Bridge across the Snake at RM 137.3 could not be located, so pier geometry and locations for were estimated from photographs. The bottom chord of Red Wolf Bridge is well above potential flood water elevations.

4.5. Reservoir Water Control

The water surface elevation at the confluence during high discharge is controlled by spillway gate settings and releases at Lower Granite Lock and Dam. The spillway of Lower Granite Dam is located about mid-river and has a total length of 512 feet between abutment centerlines, including seven intermediate piers, and consists of eight gate-controlled bays, each 50 feet wide. Piers that are 14 feet wide separate the bays. Elevation of the spillway crest is 681 feet. Spillway discharges are controlled by eight tainter gates each 50 feet wide by 60.15 feet high. The gates are operated by electric hoist units mounted above the gates, with one motor and two hoist units per gate. Operation of the gates may be by manual control through pushbutton stations located near each hoist, but normally gates are remotely controlled from the powerhouse control room. One spare hoist motor is provided for maintenance and emergency use, and all spillway gates can be operated with emergency power supplied by a diesel generator set.

Operation of Lower Granite Reservoir during flood conditions is specified in the Water Control Manual for Lower Granite Dam[61]. A flood period is defined as a period when Lower Granite inflow is greater than 120,000 cfs or flow at The Dalles (Oregon) is greater than 450,000 cfs and when these flows have the potential to increase substantially and to remain above the indicated levels for at least 24 hours because of past or forecasted near future meteorological events.

For rising inflows during a flood period, the forebay at Lower Granite Dam will be drawn down to elevation 734 feet (NGVD29) at a rate not to exceed 0.5 foot per hour.

[61] USACE (2003). *Water Control Manual for Lower Granite Lock and Dam, Snake River Oregon, Washington, and Idaho*, U.S. Army Corps of Engineers, Walla Walla District, February 2003.

On a rising hydrograph, the forebay elevation will be maintained near 734 feet until the 3-day forecast of the sum of flows at Spalding and Anatone exceeds 300,000 cfs, at which time the forebay at Lower Granite may be drawn down to elevation 725 feet (NGVD29) at a rate not to exceed 0.5 foot per hour. The forebay at the dam will be drawn down to 724 feet (NGVD29) for the SPF inflow of 420,000 cfs.

These control specifications define the downstream water elevation for one-dimensional hydraulic modeling of the confluence. The conversion from NGVD29 to NAVD88 at Lower Granite Dam for use in the model was computed with CorpsCon[62] software and is the NGVD29 elevation in feet plus 3.40 feet.

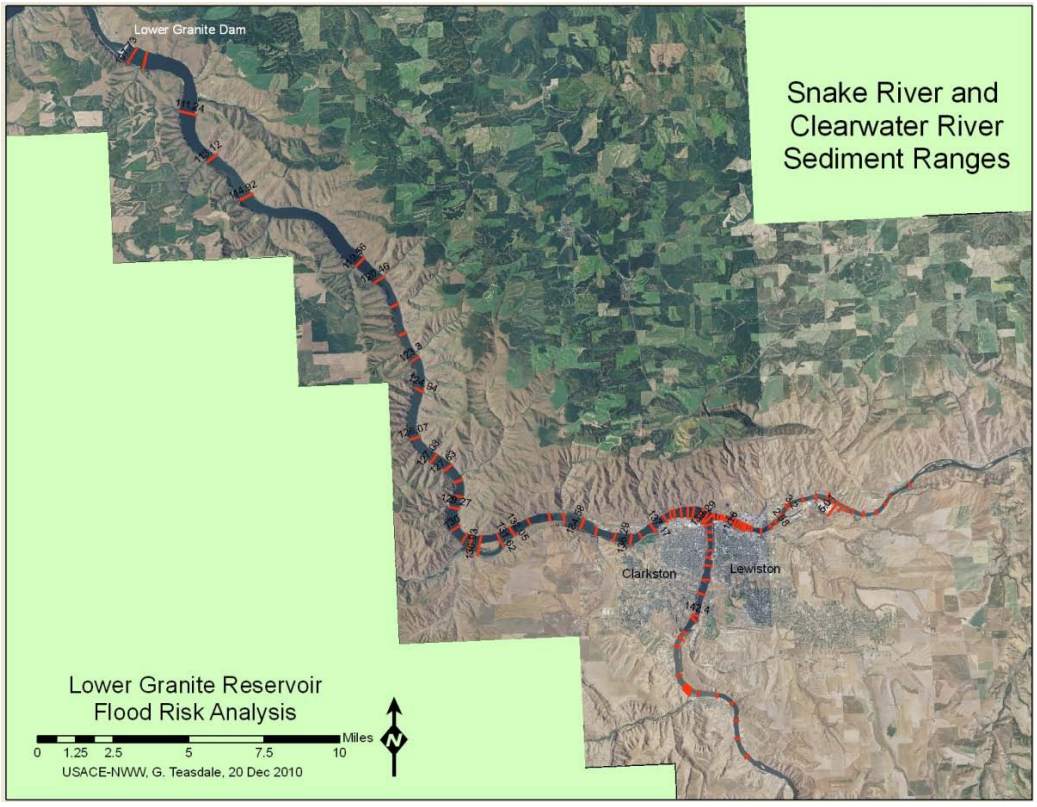


Figure 41. Sediment range locations in Lower Granite Reservoir.

[62] USACE (2004). *Corpscon Version 6.0 Technical Docmentation and Operating Instructions*. U.S. Army Corps of Engineeres, Topographic Engineering Center, Alexandria, VA.

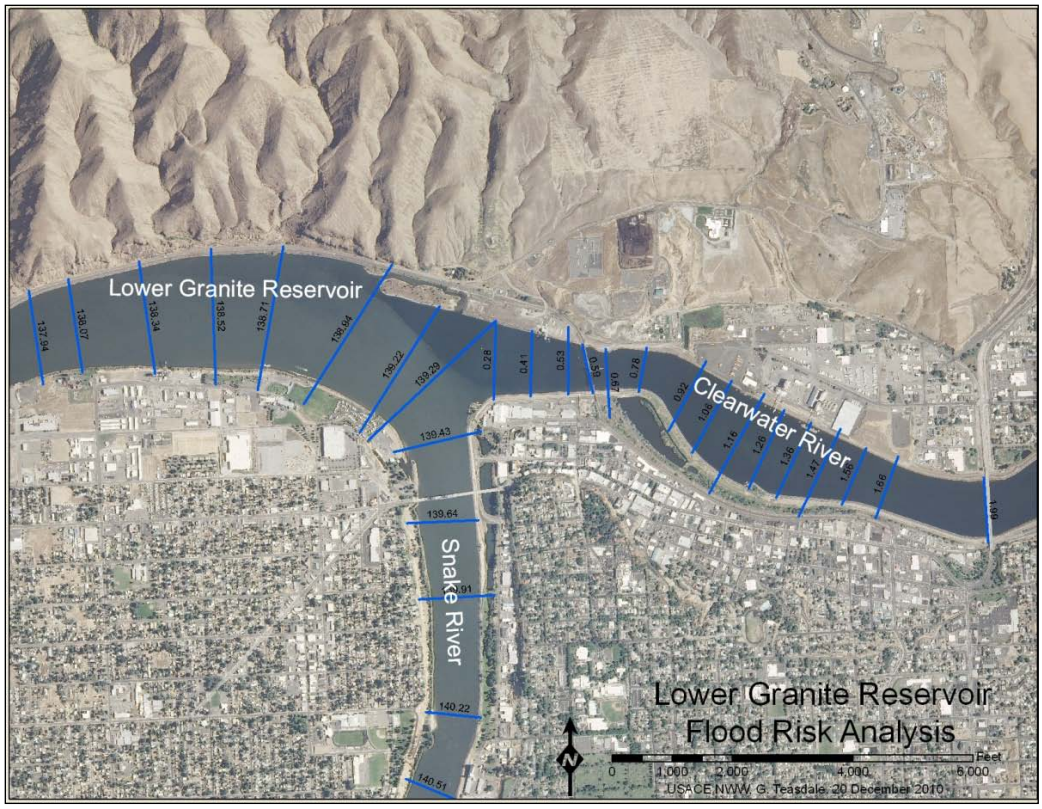


Figure 42. Sediment range cross sections near the confluence.

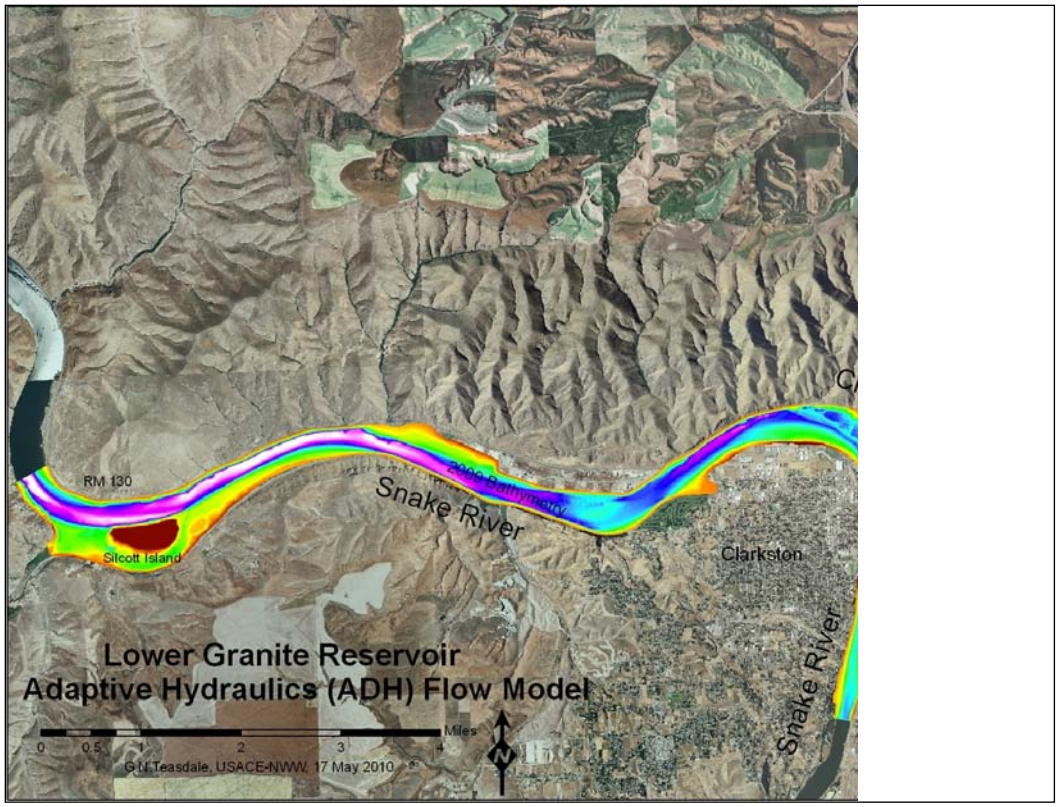


Figure 43. 2009 USGS multibeam echosounding survey bathymetry.

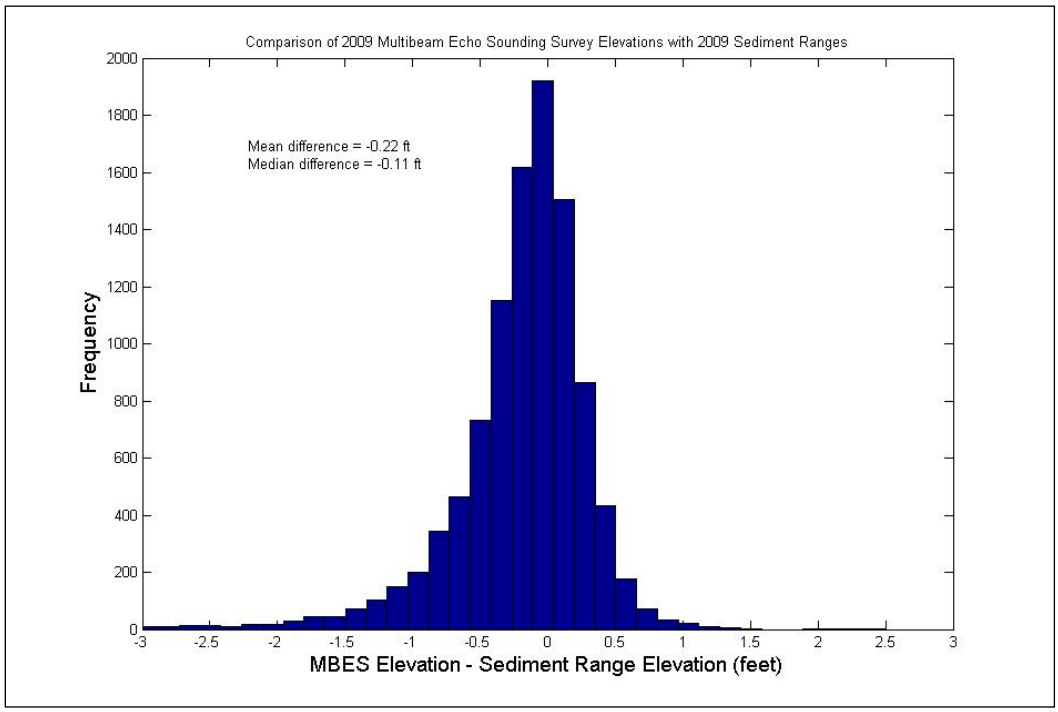


Figure 44. Comparison of 2009 MBES bathymetry and 2009 sediment range elevations.

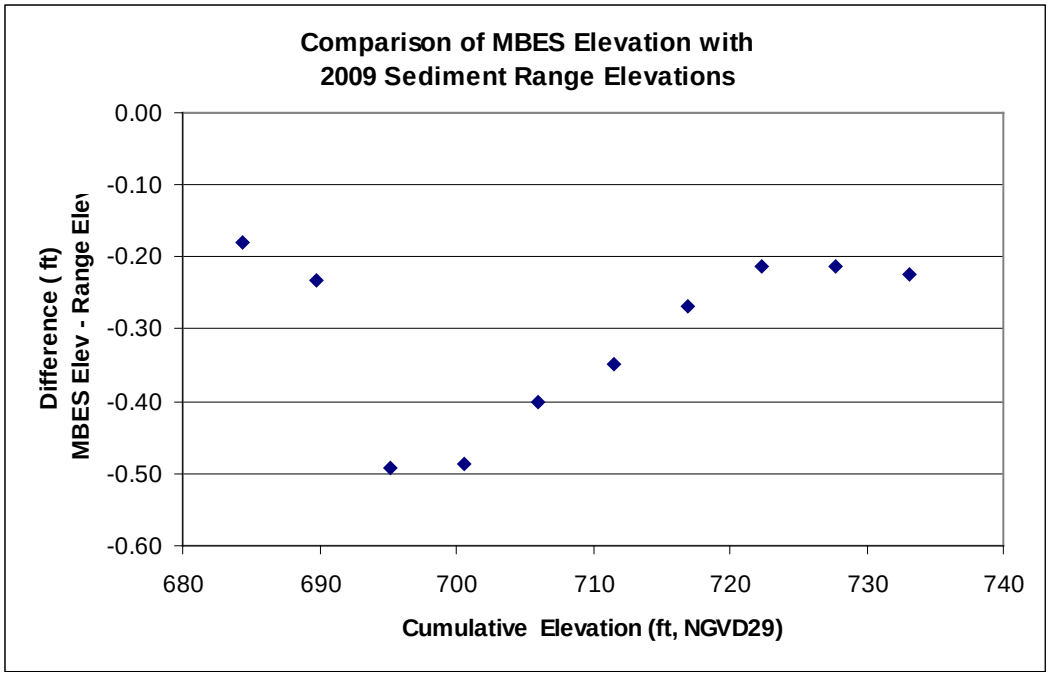


Figure 45. Elevation difference by water depth.

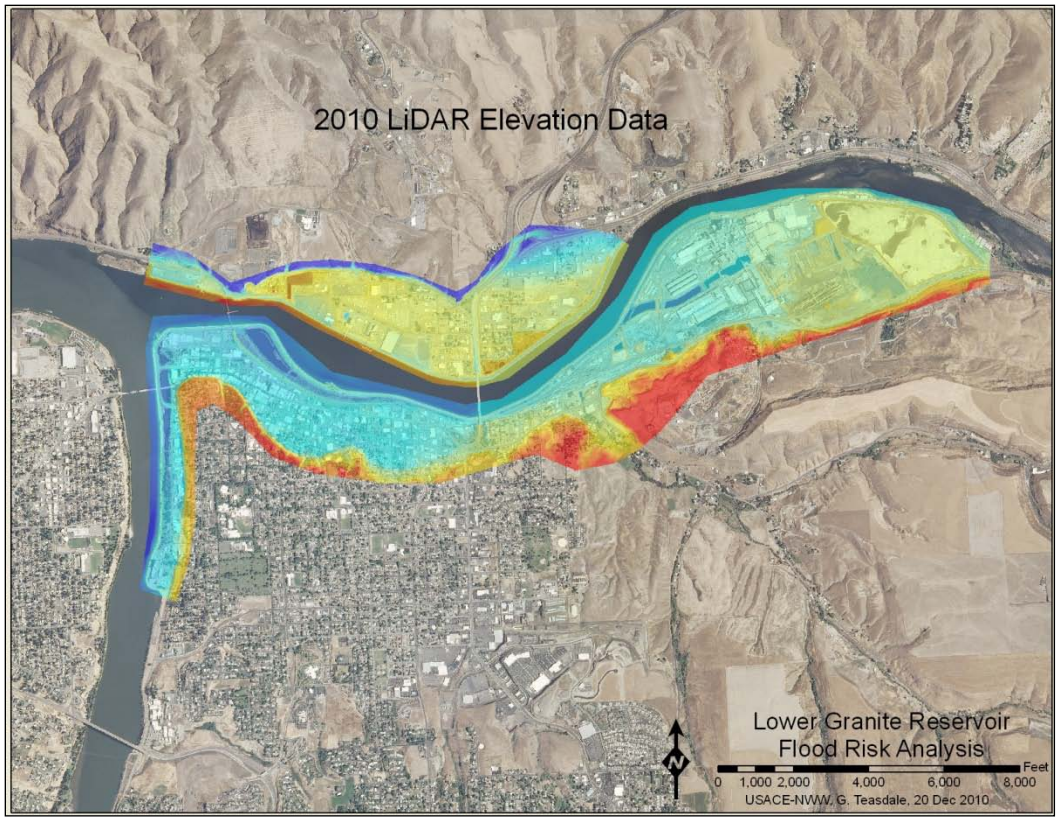


Figure 46. 2010 LiDAR elevation coverage of the Lewiston levee floodplain.

4.6. Channel Characterization

Three distinct transitions of bed material are observed in the bathymetry data shown in Figure 43. The channels of the Snake River and Clearwater River above Lower Granite Reservoir are gravel-cobble and transport relatively high amounts of suspended sand and silt. As the sand settles from suspension in the backwater of Lower Granite Dam, the channels transition from relatively stable gravel beds to beds that are dominated by ripple and dune bedforms. Below Silcott Island, the bed material changes from sand to mostly silt as the reservoir becomes wider and deeper.

The Snake and Clearwater Rivers are single-tread channels through the backwater zone. Merging flows at the confluence have partially reworked the original bed topography and maintain two distinct thalwegs for about 0.25 mile downstream. The Snake River channel below the confluence has a single main thalweg. Pre-dam island and bars have been submerged by backwater except for Silcott Island. The back channel around the Silcott Island is relatively shallow and does not contribute significantly to the total conveyance of the reservoir.

4.7. Historic one-dimensional hydraulic models

Hydraulic models of Lower Granite Reservoir have been updated periodically following the acquisition of new sediment range data. Early models were developed with the HEC2 model software (now considered legacy software) while later models were developed as non-georeferenced models with earlier versions of HEC-RAS. With the acquisition of the recent sediment range data and high resolution bathymetry, it is not necessary to use historic model geometry in the hydraulic modeling for the risk analysis. The historic models help document the historic channel and show the hydraulic effects of sediment accumulation throughout the life of the project. Previous hydraulic models are discussed in prior reports including:

- U.S. Army Corps of Engineers, *Walla Walla District, Lower Granite Lock and Dam, Design Memorandum Number 1, Hydrology*, Walla Walla, Washington, December 1963.
- U.S. Army Corps of Engineers, Walla Walla District, *Sedimentation Study, Interim Report, Lower Granite Project, Snake River, Washington and Idaho*, Walla Walla, Washington, February 1984.
- U.S. Army Corps of Engineers, Walla Walla District, *Lower Granite Sedimentation Study, Preliminary Evaluation and Progress Report*, Walla Walla, Washington, December 1992.

For this study, the historic models were reconstructed and adjusted to the NAVD88 elevation datum, and recast on the cutlines of the current georeferenced HEC-RAS model so that changes in water surface elevation near the confluence due to sediment accumulation could be evaluated. Model estimates for the SPF water surface elevation at the confluence of the Snake and Clearwater Rivers (RM 139.29) for 1974 through 1999 are plotted in Figure 47 along with the annual maximum daily discharge. Locations and numbers of cross sections in the fixed-bed one-dimensional models are similar, so a change in water surface elevation results only from a change in channel geometry brought about by sediment accumulation or removal. The water surface elevations were computed with similar assumptions for hydraulic roughness, expansion/contraction coefficients, boundary conditions, and cross section skew.

Cross section conveyance is changed mostly by sediment erosion, sediment deposition and dredging. Sediment erosion and deposition varies with discharge, sediment load and pool operations. Drawdown of Lower Granite Reservoir in 1992 substantially eroded the bed of cross sections in the upper part of the reservoir as evidenced by the vertical shift in the water surface elevation for that year in Figure 47. Dredging of the navigation channel also changed the conveyance of some cross sections, but has had a relatively minor effect since 1997. Beginning in 2003, the upward trend of the SPF water surface elevation stabilized which suggests a tendency

towards a dynamic balance of channel conveyance and sediment load under the prevailing flow regime. This apparent stability underscored the need to incorporate mobile-bed dynamics in hydraulic models of the confluence. Previous mobile-bed modeling with HEC6[63] was difficult and inconclusive because of the limited information that was available to characterize sediment load and the bed sediment[64]. The present investigation included 4 years of sediment load measurements and characterization of bed sediment throughout Lower Granite Reservoir to provide data that is necessary for mobile-bed modeling.

Another way to examine the effect of sediment accumulation on the hydraulics of the confluence is to compare the SPF water surface profiles over the life of Lower Granite Reservoir. Flood control specifications in Section 4.5 require that the forebay of Lower Granite Dam be drawn down as discharge increases to the SPF level. This creates an SPF water surface profile that has a "hinge point", or a point of constant elevation, within the profile. Water surface elevations near the dam are lower during the peak of the flood while the water surface at the confluence is higher. Figure 48 and Figure 49 show that the location of the hinge point has shifted further downstream because of sediment accumulation. In 1974, the hinge point was near the confluence; by 2009 the hinge point had shifted downstream about 4.6 miles. The location of the hinge point is important in flood risk management because facilities located upstream of a hinge point experience rising waters during a flood while locations downstream are exposed to decreasing water levels. Thus, upstream locations prepare for possible flooding while downstream locations could face problems caused by foundation settlement and bank instability.

It is important to note that the water surface elevations depicted in Figure 47 are based on fixed bed modeling and do not explicitly reflect the effect of sediment transport during the SPF flood. The SPF discharge of 420,000 cfs is about twice that of recent annual maximum daily discharges in Lower Granite. Sand deposited by lesser flows will remobilize at the higher SPF discharge unless incoming sediment load is so great that it overwhelms transport capacity (supply-limited versus transport-limited). Channel scour and fill are not simulated directly in the fixed-bed models so the possibility of added hydraulic resistance due to sediment transport phenomena, such as the formation of sand dunes and sediment bulking, was implicitly incorporated into the historic fixed-bed

[63] USACE (1993). HEC6 *Generalized Computer Program "Scour and Deposition in Rivers and Reservoirs", User's Manual*, Hydrologic Engineering Center, U.S. Army Corps of Engineers, Davis, CA.

[64] USACE (2002). *Appendix A Hydrologic Analysis, Dredged Material Management Plan and Environmental Impact Statement*, Walla Walla District, U.S. Army Corps of Engineers, Walla Walla, WA.

models by adjustment of hydraulic roughness parameters. Flow resistance at high discharge is discussed in Section 10.

The latest version of HEC-RAS has improved capabilities to model sediment erosion and deposition and was used for one-dimensional mobile-bed modeling of flood discharges at the confluence. The historic channel geometry provided a starting point for long-term modeling of sediment transport in Lower Granite Reservoir. The long-term modeling produced a reasonable match of the channel geometry measured in 2009. Final hydraulic modeling of the confluence during the SPF flood and in the flood risk analysis was based on one-dimensional HEC-RAS models developed from the 2009 channel geometry and was run in both fixed-bed and mobile-bed modes. Development of the 2009 fixed-bed model geometry is discussed below. Mobile-bed modeling of SPF hydrograph and the sediment transport analysis is discussed in Section 10.

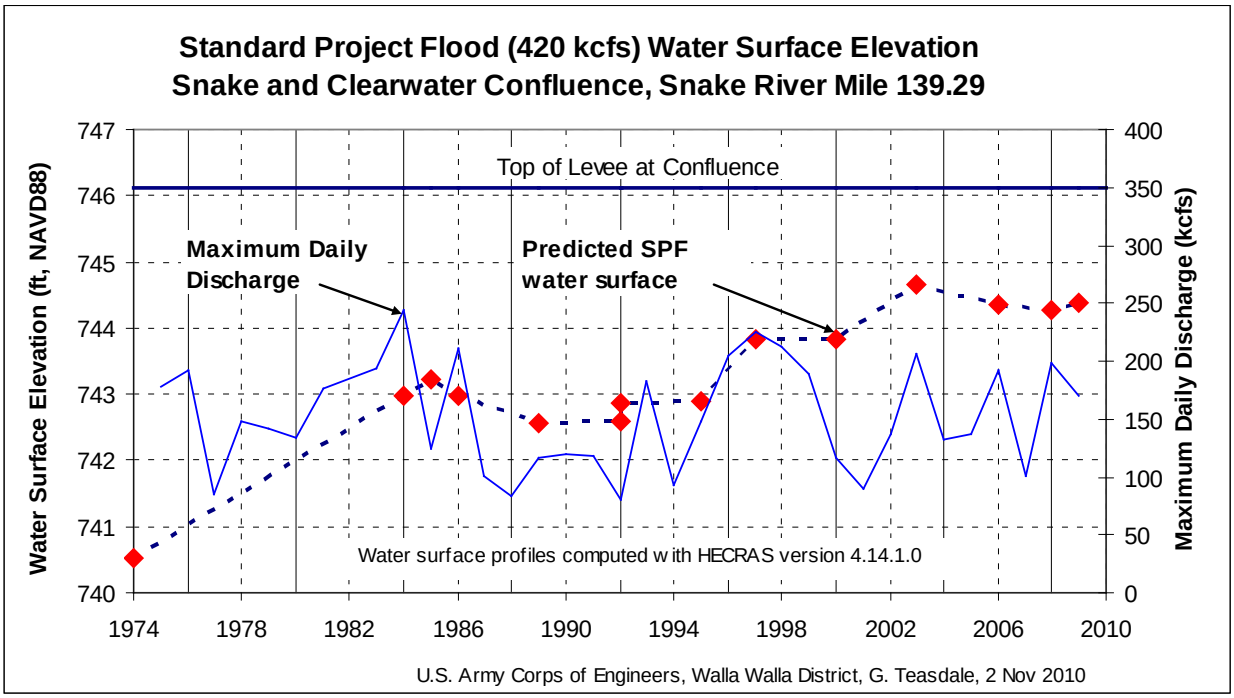


Figure 47. Historic water surface elevation estimates at the confluence during the Standard Project Flood.

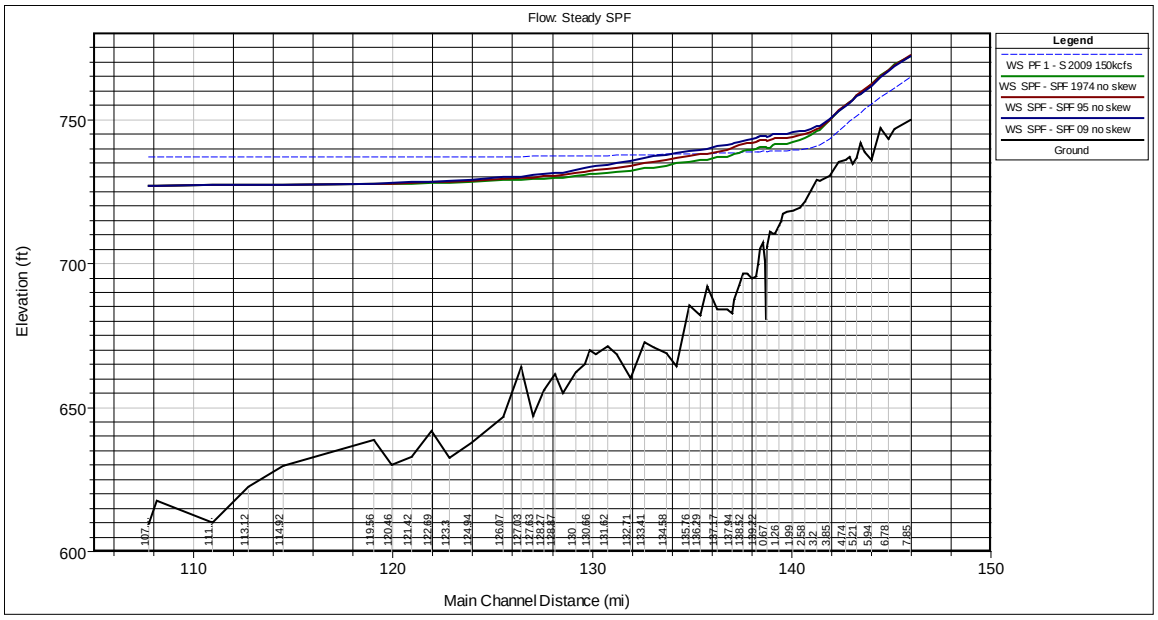


Figure 48. Shift in Lower Granite SPF hinge point 1974 -2009 (profile).

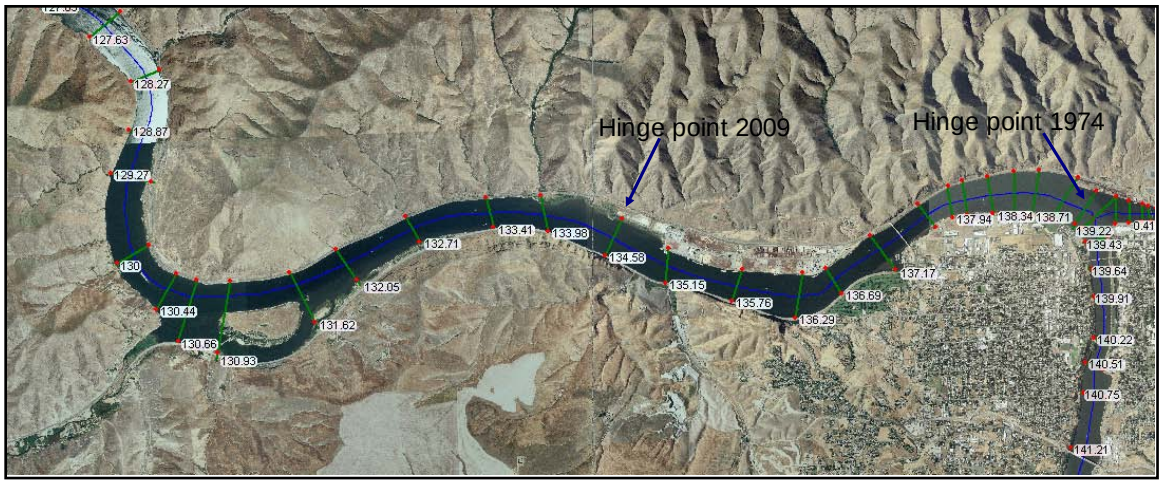


Figure 49. Shift in Lower Granite SPF hinge point 1974 -2009 (plan).

4.8. Hydraulic Model Reach and Cross Section Development

Many different hydraulic models of Lower Granite Reservoir were developed during the study to investigate hydrodynamic and sediment transport characteristics of the confluence. Georeferenced cross sections of the channels and overbanks were extracted from the digital elevation models (DEM) and Triangulated Irregular Networks (TIN) produced from the 2009 sediment ranges and the merged high-resolution 2009 bathymetry and 2010 LiDAR elevation data. Georeferenced import files for the

HECRAS model were developed using the standard tools available in the USACE HEC-GeoRAS extension[65] for the ESRI ArcView software.

The final HEC-RAS model of Lower Granite used in the flood risk analysis is composed of three reaches: Clearwater-Lewiston, Snake-Clarkston, and Snake-Lower Granite. The confluence of the Snake and Clearwater River is represented as the only junction in the model. Flows throughout the model domain remain subcritical up to the SPF discharge, so the only necessary boundary condition is the water surface elevation of the forebay of Lower Granite Dam. The levees in Lewiston on the right and left banks of the Clearwater River and on the right bank of the Snake River at represented as levee features. Areas behind the levees are represented as storage areas.

Preliminary versions of the model included Lower Granite Dam represented as an inline structure with controllable spillway gates. Initial testing showed that the elevations required for flood control could be correctly simulated when the geometry of the spillway and gates were configured as described in the water control manual and design memoranda. To simplify the final HEC-RAS model, the inline dam structure was removed and the downstream water elevation at RM 107.43 was specified as shown in Figure 51.

Cross section cutlines in the area covered by the high-resolution bathymetry were defined by straight lines digitized perpendicular to the channel alignment and were extracted at a close spacing of 100 feet to capture the hydraulic detail of the channel bottom. Cutlines extended beyond the maximum water levels produced by the SPF (no vertical extension errors). Initial tests with trial channel geometries showed that the cross section spacing could be increased to 400 feet (Figure 50, except near bridges, without incurring conveyance ratio warnings during model runs or reducing significant hydraulic detail.

Beyond the high-resolution bathymetry coverage, channel cross sections were derived from the 2009 sediment range cross section data. Spacing of the sediment ranges varied from several hundred feet in the Clearwater and Snake Rivers above the confluence to 4.6 miles in Lower Granite Reservoir. Extraction of the cross sections was a multi-step process in which initial overbank cross sections were first extracted from the LiDAR DEM, followed by the merging of station-elevation data derived from the sediment ranges into the channel section. The sediment range elevation points were cosine adjusted to the straight cutline so as not to artificially increase cross section conveyance. Where necessary, skew angles were set in the model geometry for cross sections derived from the sediment ranges. Conveyance ratio warnings were issued for

[65] Ackerman, C.T., 2005. *HEC-GeoRAS User's Manual, Version 4, September 2005*. Hydrologic Engineering Center, U.S. Army Corps of Engineers, Davis, CA.

a few of the widely spaced sediment range cross sections in the lower part of Lower Granite reservoir (below Silcott Island) and for many of the cross sections on the Snake and Clearwater Rivers above the levee system. Interpolated cross sections were initially added to eliminate the warnings, but did not significantly change the computed water surface elevation in the levee segment. Interpolated cross sections were removed from the final model.

Cross sections for the fixed-bed model were thinned to less than 500 points using the HEC-RAS point filter tools. Further reductions in point density did not significantly reduce model computation time for the steady flow profiles runs used in the risk analysis. Model run times were short; about 15 seconds for the eight profiles required for FDA. Cross section point density was reduced to less than 100 to decrease computation time in long-duration sediment simulations. Expansion and contraction coefficients were kept at default settings of 0.1 for contraction and 0.3 for expansion.

Ineffective flow areas were manually set guided by indications of shallow and occluded areas in NAIP aerial imagery, and by positions of elevation breaks in the cross sections. The largest ineffective flow adjustments were in the vicinity of Silcott Island in Lower Granite Reservoir (Figure 52). Computed water surface profiles were only slightly influenced by the selection of ineffective flow areas because of the large available conveyance and relatively low mean velocities even at the SPF discharge.

Top-of-levee elevations were initially set by manually matching the levee crest in the extracted cross section. Final levee elevations were set by adjusting the initial levee elevations to match the elevation of the nearest point in the top-of-levee profile survey.

Bridges were defined with the HEC-RAS bridge editor based on the information described in Section 4.4.

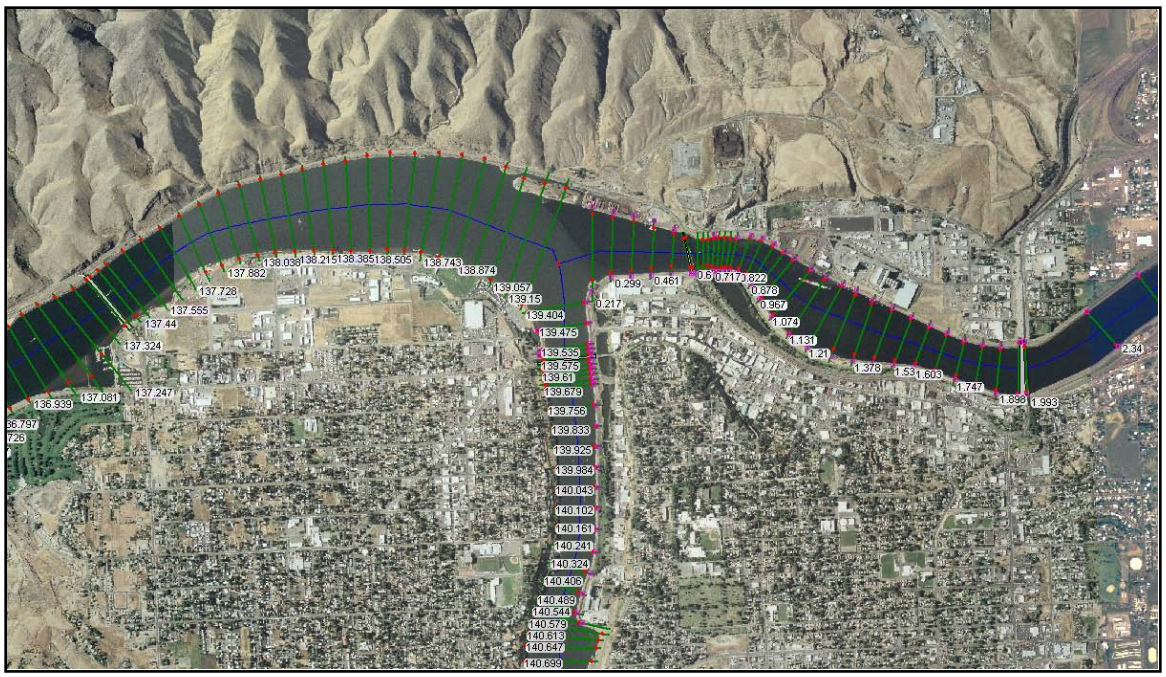


Figure 50. 2009 HEC-RAS model of Lower Granite confluence.

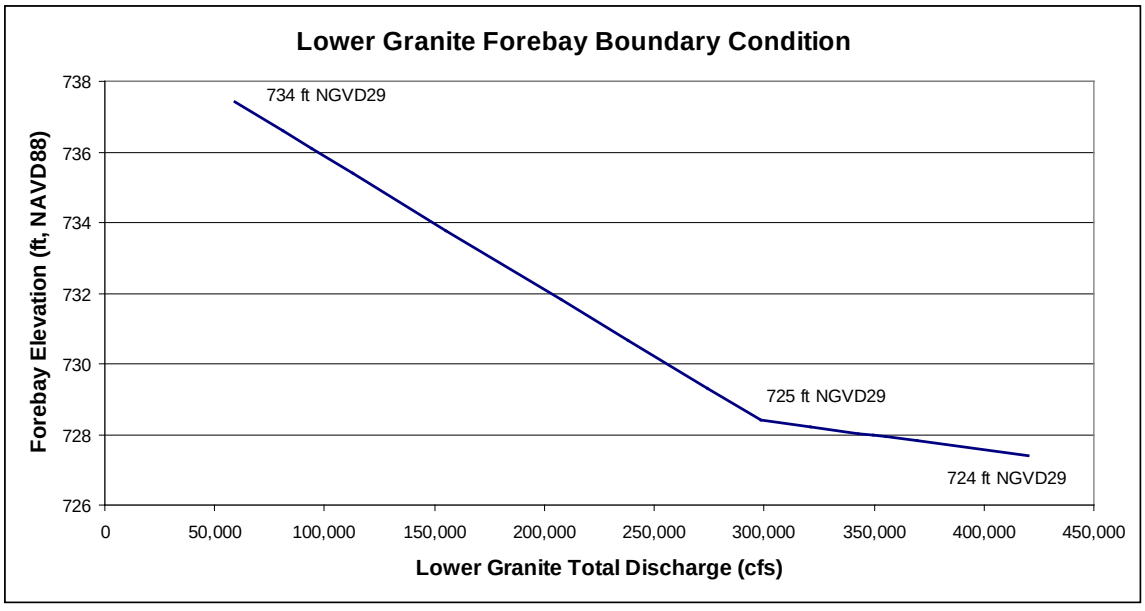


Figure 51. Lower Granite forebay boundary condition.

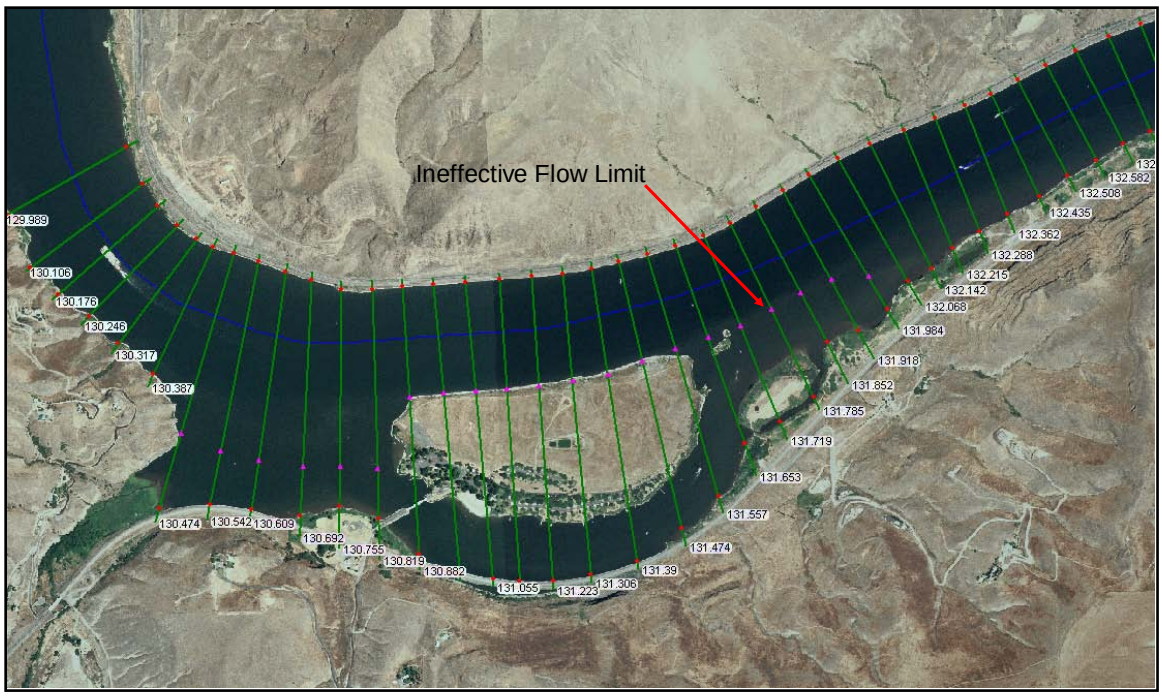


Figure 52. Ineffective flow areas near Silcott Island.

4.9. HEC-RAS Model Calibration

One-dimensional fixed-bed models are calibrated primarily by adjusting hydraulic resistance factors (Manning's *n*) until model output agrees with measured water surface profiles. For flood simulations, the model should be calibrated to historic discharges that are of a magnitude that is near the discharge that is intended to be simulated[54]. High discharges have the most influence on the outcome of a flood risk analysis, but are often not in the historic record. The maximum annual daily average discharge since the pool was raised in Lower Granite was 252,700 cfs which occurred in 1984. This discharge has a frequency of between 4 percent and 10 percent (the empirical probability is 5 percent by the Weibull plotting position) which is very much less than the capacity of the levee channel. Therefore, it is necessary to extrapolate hydraulic resistance characteristics beyond the historic dataset to simulate the infrequent high discharges required by the flood risk analysis.

An added complication for Lower Granite is that model geometries based on recent channel measurements cannot be calibrated to historic water surface profiles because sediment accumulation has changed the conveyance of the channel. Nor can historic models be used to determine Manning's *n* values for the 2009 hydraulic model because the 2009 model represents the channel geometry at higher resolution.

Manning's *n* values must usually be increased to account for more widely spaced cross sections because less real expansion and contraction headloss is accounted for in the model. This latter assertion is easily demonstrated by comparing non-uniform high resolution and low resolution models developed from the same channel elevation dataset.

Calibration of the 2009 one-dimensional fixed-bed HEC-RAS model of Lower Granite involves two elements. First, the 2009 model is calibrated by adjusting the hydraulic resistance factors (Manning's *n*) so that the water surface profiles output by the model closely match the water surface profile of the high discharge that occurred in early June 2010. Second, the hydraulic resistance of the channels for extreme discharges is estimated by empirical methods that are recommended in Corps guidance and the hydraulic engineering literature.

It is important to note that only the hydraulic resistance of the segments of the Snake and Clearwater Rivers adjacent to and below the levee system in Lewiston affect the water surface elevation at the levee system (in addition to pool control and discharge). This is because flows remain subcritical and pool control at Lower Granite Dam creates an M1 backwater profile under all flows of interest in the risk analysis. Therefore, it is not essential to accurately calibrate the segments of the model above about RM 5.0 on the Clearwater and above about RM 140.6 on the Snake River for the flood risk analysis. Furthermore, because of pool control at Lower Granite Dam, hydraulic resistance factors have a decreasing affect on the water surface profile with decreasing distance to the dam. Thus, it is more important to accurately estimate the hydraulic resistance above about Silcott Island (RM 130) on the Snake River than below. This was a primary reason for acquiring high resolution bathymetry of this reach in 2009.

As discussed in Section 2.1, water discharges are recorded at the USGS Anatone stream gage on the Snake River and at the USGS Spalding stream gage on the Clearwater River. Total discharge below the confluence is the sum of the Anatone and Spalding discharges. Water surface elevations are recorded at the Lower Granite Dam forebay (Station LWG), at the confluence of the Snake and Clearwater Rivers (Station SRCI) and at the East Lewiston Pump Station at RM 2.9 on the Clearwater River (Station CRLI). There is not a permanent stage gage on the Snake River above the confluence within the backwater zone of Lower Granite Dam. The stage gages at the confluence and the East Lewiston Pump station are equipped with permanent stage boards (Figure 53, Figure 54) and electronic level recorders. Instantaneous levels are transmitted every hour via radio frequency to the Corps data management system.

Data used in the calibration of the HEC-RAS 2009 one-dimensional fixed-bed model is summarized in Table 24. Discharges and water surface elevations were average over a two hour period on 8 June 2010 beginning at 8:00 am and ending at

10:00 am. Both discharge and water surface elevations were relatively constant during the period. Average discharge in Lower Granite was 214,000 cfs, which is equivalent to about an 18 percent exceedance for the annual maximum daily discharge. Discharges were obtained from the online USGS NWIS 15 minute discharge record. The sum of the Anatone and Spalding discharges was about 6 percent less than the outflow discharge of Lower Granite during this period, which is reasonable since the forebay elevation was increasing slightly. Stage elevation data in the Corps database are recorded in NGVD29 datum. The stage elevations were adjusted to the NAVD88 datum using conversions obtained with the Corpscon 6.0 program.

At the confluence, the bank water surface elevation listed in Table 24 is visually calibrated to the external gage board (Figure 53). Readings of the stage board are relatively unaffected by turbulence and under calm wind conditions provide a good estimate of the mean water surface elevation of the confluence. The computed difference between the energy grade line and water surface elevation at the confluence for the measured discharge is less than 0.1 foot, so the confluence stage elevation was accepted as the water surface calibration elevation without adjustment.

At the East Lewiston Pump Station (Clearwater RM 2.9), the bank water surface elevation at in Table 24 is as reported in the Corps database which has been visually calibrated to the external gage board (Figure 54). Turbulence eddies and surface waves significantly influence the visual reading of the gage board at higher discharge, so the reported gage value was not adjusted for velocity head. This stage measurement provides an approximate calibration value and was used to judge the reasonableness of the selected Manning's *n* values.

The bank water surface level at Snake RM 142.95 was manually referenced to the top of a sheet pile wall at the outlet of the Hells Gate Marina boat basin. A field survey was later performed to determine the elevation of the sheet pile. Water at the base of the sheet pile wall (river side) is shielded from turbulence eddies and was relatively static during the measurement. Therefore, the measured water surface elevation was adjusted downward by a velocity head of 0.5 feet to obtain an estimate of the elevation of the free-flowing water surface.

Manning's *n* values in the HEC-RAS 2009 model were adjusted to obtain a reasonable match of the measured water surface elevation. Computed water surface elevations and measured elevations are compared in Table 25. The computed water surface level at the confluence was within 0.01 feet of the measured elevation. At Snake RM 142.95 the difference between the computed water surface and the calibration value was .02 feet. At Clearwater RM 2.9 the computed water surface was within 0.09 feet of the approximate calibration value. Hydraulic resistance factors for the Clearwater are likely somewhat conservative because the approximate calibration water surface elevation incorporates a portion of the channel velocity head.

Calibrated Manning's *n* values for each reach are listed in Table 26. A constant Manning's *n* value of 0.022 was assigned to for the main channel in Lower Granite. Based on channel conditions observed in the high resolution bathymetry, there is little justification for a non-uniform hydraulic resistance value below the confluence. On the Snake River, the selected Manning's *n* values varied from 0.023 at the confluence to 0.024 to the calibration point. Above the calibration point, Manning's *n* was increased to a maximum of 0.035 based on a visual assessment of the main river channel.

The selected Manning's *n* values for the Clearwater River varied from 0.023 to 0.032 at RM 7.85. The Manning's *n* values were held constant at 0.023 in the predominantly sand bed channel between the confluence and RM 1.99. Above Memorial Bridge at RM 1.99, the Manning's *n* was increased 0.028 up to the East Lewiston Pump Station gage at RM 2.89. Upstream of the pump station the Manning's *n* was increased to 0.032 based on observation of the gravel bed channel.

Manning's *n* factors for banks and overbanks were set to 0.04 for all cross sections in each reach. Bank points were set at the 99% percent water surface elevation in all cross sections except within the levee system. Bank points for cross sections within the levee system were set at the approximate toe of the levee as indicated by slope breaks in the cross section. The position of bank points and Manning's n values for overbanks had negligible effect on the computed water surface elevations for all discharges including the SPF.



Figure 53. Stage board at the confluence of the Snake and Clearwater Rivers.



Figure 54. Stage board at the East Lewiston Pump Station.

Lower Granite 2009 HEC-RAS Model Calibration Data 8 June 2010							
	Elevations in feet NGVD 29			NAVD88 ft	Discharge in cfs		
	Forebay	RM 139.3	RM 2.9	RM 142.95	Snake	Clearwater	Total
Time	LWG	SRCI	CRLI	Hells Gate	Anatone	Spalding	Inflow
08-Jun-2010 08:00	733.47	736.38	737.60		154,000	59,600	213,600
08-Jun-2010 08:15					154,000	59,600	213,600
08-Jun-2010 08:30					154,000	59,600	213,600
08-Jun-2010 08:45					154,000	59,300	213,300
08-Jun-2010 09:00	733.48	736.40	737.64		155,000	59,800	214,800
08-Jun-2010 09:15					154,000	60,700	214,700
08-Jun-2010 09:30				742.18	153,000	61,100	214,100
08-Jun-2010 09:45					154,000	61,400	215,400
08-Jun-2010 10:00	733.52	736.43	737.70		153,000	61,700	214,700
Average NGVD29	733.49	736.40	737.65		153,889	60,311	214,200
Difference NGVD29 NAVD88	3.41	3.28	3.27				
Average NAVD88	736.90	739.68	740.92	742.18			

Table 24. HEC-RAS 2009 model calibration data for 8 June 2010.



Figure 55. Sheet pile wall at Hells Gate Marian, RM 142.95.

HEC-RAS 2009 Model Calibration Results for 8 June 2010					
	Elevation (feet, NAVD88)			Difference	
Location	Water Surface	Energy Grade	Measured	feet	Percent
Clearwater RM 0.21	739.67	739.74	739.68	-0.01	-0.002%
Clearwater RM 2.9	741.01	741.56	740.92	0.09	0.012%
Snake River RM 142.95	742.20	743.60	742.18	0.02	0.003%

Table 25. HEC-RAS 2009 model calibration data for 8 June 2010

HEC-RAS 2009 Model Hydraulic Calibrated Resistance Factors					
			Manning's *n*		
River	Reach	River Mile	Left Bank	Channel	Right Bank
Clearwater	Lewiston	7.85	0.04	0.032	0.04
Clearwater	Lewiston	4.74	0.04	0.032	0.04
Clearwater	Lewiston	4.3	0.04	0.030	0.04
Clearwater	Lewiston	3.2	0.04	0.030	0.04
Clearwater	Lewiston	2.89	0.04	0.028	0.04
Clearwater	Lewiston	1.99	0.04	0.028	0.04
Clearwater	Lewiston	1.974	0.04	0.023	0.04
Clearwater	Lewiston	0.217	0.04	0.023	0.04
Snake	Clarkston	148.83	0.04	0.035	0.04
Snake	Clarkston	147.47	0.04	0.035	0.04
Snake	Clarkston	146.87	0.04	0.026	0.04
Snake	Clarkston	144.73	0.04	0.026	0.04
Snake	Clarkston	143.69	0.04	0.024	0.04
Snake	Clarkston	142.005	0.04	0.024	0.04
Snake	Clarkston	141.949	0.04	0.023	0.04
Snake	Clarkston	139.404	0.04	0.023	0.04
Snake	Lower Granite	139.254	0.04	0.022	0.04
Snake	Lower Granite	107.43	0.04	0.022	0.04

Table 26. HEC-RAS 2009 model calibrated hydraulic resistance factors.

4.10. Empirical Estimates of Manning's n

Bed mobility and hydraulic resistance of the channels in Lower Granite Reservoir are discussed in Section 10. At this point it adds perspective to compare the calibrated Manning's *n* values with empirical formula from Corps guidance[66],[67] and the hydraulic engineering literature.

Flow resistance results from the combined effect of grain roughness, bed forms, channel obstructions, variation in cross section, and vegetation. Grain roughness dominates hydraulic resistance in fixed-bed sand and gravel that have negligible bed

[66] USACE (1994). Chapter 5, "Methods for predicting n values for the Manning equation", *EM 1110-2-1601 Hydraulic Design of Flood Control Channels*, U.S. Army Corps of Engineers, Washington, DC.

[67] USACE (2010)."Stable channel design functions', *HEC-RAS River Analysis System Hydraulic Reference Manual, Ver. 4.1*, January 2010, Hydrologic Engineering Center, U.S. Army Corps of Engineers, Davis, CA.

and channel irregularities. Manning's *n* values for grain roughness in fixed-beds can be computed with the Strickler and Keulegan equations. Manning's *n* values computed with these equations are minimum values which are then increased for other elements of hydraulic resistance.

The Strickler equation is,

$$n = Ck_s^{1/6}$$

where C is a coefficient that takes the value 0.034 for natural sediments and k_s is the roughness height of the bed sediment, estimated as the median sediment grain size (D_{50}) in units of feet. The sediment cores survey discussed in Section 8 showed that the median surface sediment grain size in the Snake and Clearwater Rivers near the confluence is about 0.3 mm. Substituting this grain size into the Strickler equation gives,

$$n = Ck_s^{1/6} = 0.034\left(\frac{0.3\,\text{mm}}{25.4\frac{\text{mm}}{\text{in}}\cdot\frac{12\,\text{in}}{\text{ft}}}\right)^{1/6} = 0.011$$

Manning's *n* based on the Keulegan equation for fully rough (turbulent) flow is a function of roughness height and hydraulic radius (R) is,

$$n = \frac{1.486}{32.6\log_{10}\left(\frac{12.2R}{k_s}\right)}R^{1/6}$$

The hydraulic radius at RM 2.89 on the Clearwater River during the 8 June 2010 calibration discharge was approximately 13 feet. Assuming that k_s is 0.3 mm (0.001 ft) and the hydraulic radius is 13 feet, Manning's *n* for grain roughness according to the Keulegan equation is,

$$n = \frac{1.486}{32.6\log_{10}\left(\frac{12.2(13)}{0.001}\right)}(13)^{1/6} = 0.013$$

The Keulegan equation also varies according to the Froude number of the flow. The Strickler and Keulegan equations are compared for various sediment grain sizes and Froude number in Table 5-5 of EM 1110-2-1601 included here as Table 27. The Froude number has a small effect for sand material and Manning's *n* for small to medium gravel remain below 0.02 for low Froude numbers.

Table 5-5
n Values Calculated by Strickler and Keulegan Equations

Effective Roughness				Keulegan Equation R, ft				
k_s, mm	k_s, ft	Strickler $n = 0.034 \cdot k_s^{1/6}$	F	1	5	10	20	50
			8	0.012	0.013	0.014	0.015	0.016
0.10	0.0003281	0.009	1.88	0.010	0.011	0.012	0.013	0.014
			0.2	0.009	0.011	0.011	0.012	0.013
			8	0.017	0.017	0.018	0.019	0.020
1.00	0.003281	0.013	1.88	0.013	0.014	0.015	0.015	0.017
			0.2	0.012	0.013	0.014	0.015	0.016
			8	0.019	0.019	0.020	0.020	0.021
2.13	0.007	0.015	1.88	0.014	0.015	0.016	0.017	0.018
			0.2	0.013	0.015	0.015	0.015	0.018
			8	0.026	0.025	0.025	0.025	0.026
10	0.03281	0.019	1.88	0.018	0.018	0.019	0.019	0.020
			0.2	0.016	0.017	0.017	0.018	0.019
			8	0.049	0.037	0.035	0.034	0.033
64	0.20997	0.026	1.88	0.026	0.024	0.024	0.025	0.025
			0.2	0.022	0.022	0.022	0.022	0.023
			8	0.060	0.042	0.039	0.037	0.036
100	0.3281	0.028	1.88	0.029	0.026	0.026	0.026	0.027
			0.2	0.024	0.023	0.023	0.024	0.024

Table 27. Manning n values for sand and gravel bed material from EM 1110-2-1601.

Manning's *n* for plane bed (upper regime) gravel bed channels can be computed with the Limerinos equation,

$$n = \frac{0.0926 R^{1/6}}{1.16 + 2.0 \log_{10}\left(\frac{R}{D_{84}}\right)}$$

where *R* is the hydraulic radius (feet) and D_{84} is the 84th percentile grain size. Above RM 2.89 the Clearwater River is a gravel-bed channel that has a D_{84} of about 64 mm (0.21 ft) and a hydraulic radius of 10 feet, the grain size by the Limerinos equation is,

$$n = \frac{0.0926(10)^{1/6}}{1.16 + 2.0 \log_{10}\left(\frac{10}{0.21}\right)} = 0.030$$

The Limerinos equation is intended for channels that have a planar bed, so the equation gives an estimate of the Manning's *n* associated with grain roughness. The total Manning's *n* should be higher for the gravel channels entering Lower Granite Reservoir.

The empirical equations for Manning's *n* show that the calibration of the HEC-RAS fixed-bed hydraulic model to the 8 June 2010 high discharge produced reasonable

hydraulic resistance factors. The analysis also shows that the Manning's *n* associated with grain roughness of the sand-bed channels is about half the total Manning's *n* determined by calibration. Grain roughness would not increase during greater discharges unless grain size of the bedload increases dramatically. An increase in Manning's *n* at higher discharge, if any, must be caused by changes in bed irregularities due to the growth and decay of bed forms. This is an essential consideration for the risk analysis to be addressed in Section 10 with the aid of the Brownlie regime relationships for hydraulic resistance.

4.11. Confluence Junction Headloss

Headloss across tributary junctions in one-dimensional models may be computed by either the energy equation or momentum equation in HEC-RAS. Differences between the methods were less 0.3 feet at the SPF discharge. Water surface profiles computed with the one-dimensional HEC-RAS model were compared to the water surface computed with the two-dimensional ADH model for similar conditions of discharge and flow resistance. The longitudinal observation arcs on the ADH model shown in Figure 56 are compared in Figure 57 and Figure 58 with the corresponding HEC-RAS water surface elevations. Junction headloss was computed in HEC-RAS with the energy method. The headloss across the junction computed with HEC-RAS is slightly greater than that computed with ADH. Therefore, the HEC-RAS one-dimensional model produces a somewhat more conservative simulation of water surface elevations for the risk analysis. The ADH model was not used to compute water surface profiles for the FDA risk analysis.

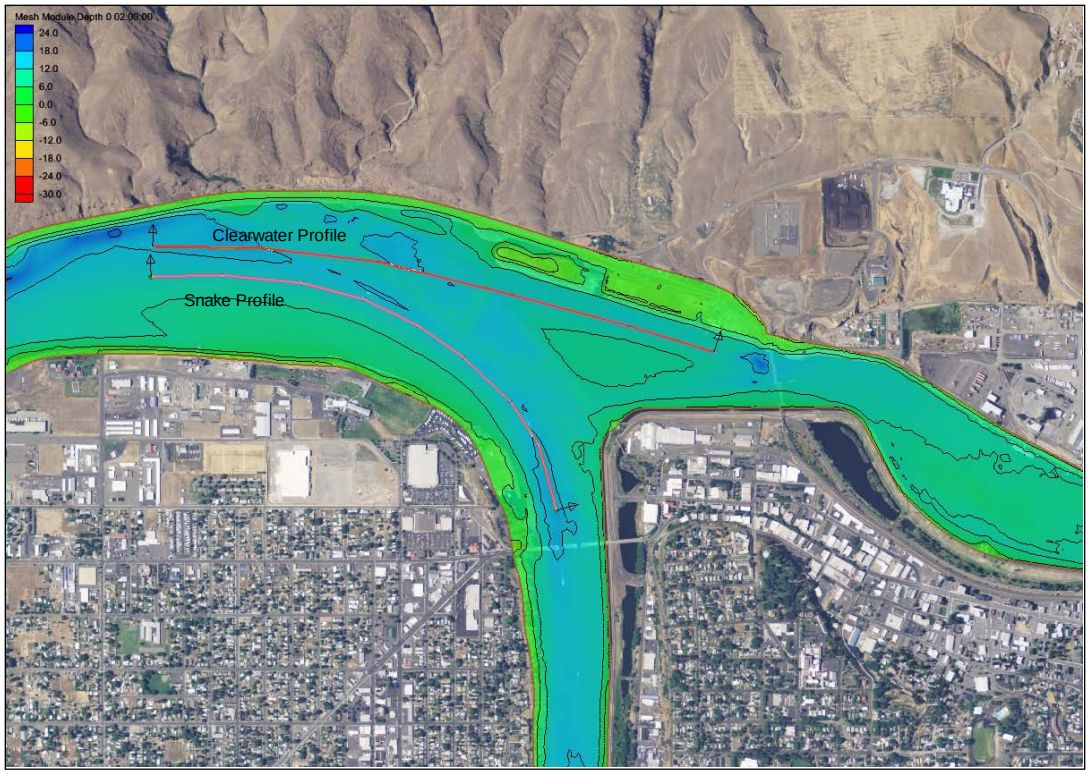


Figure 56. ADH water surface profile locations.

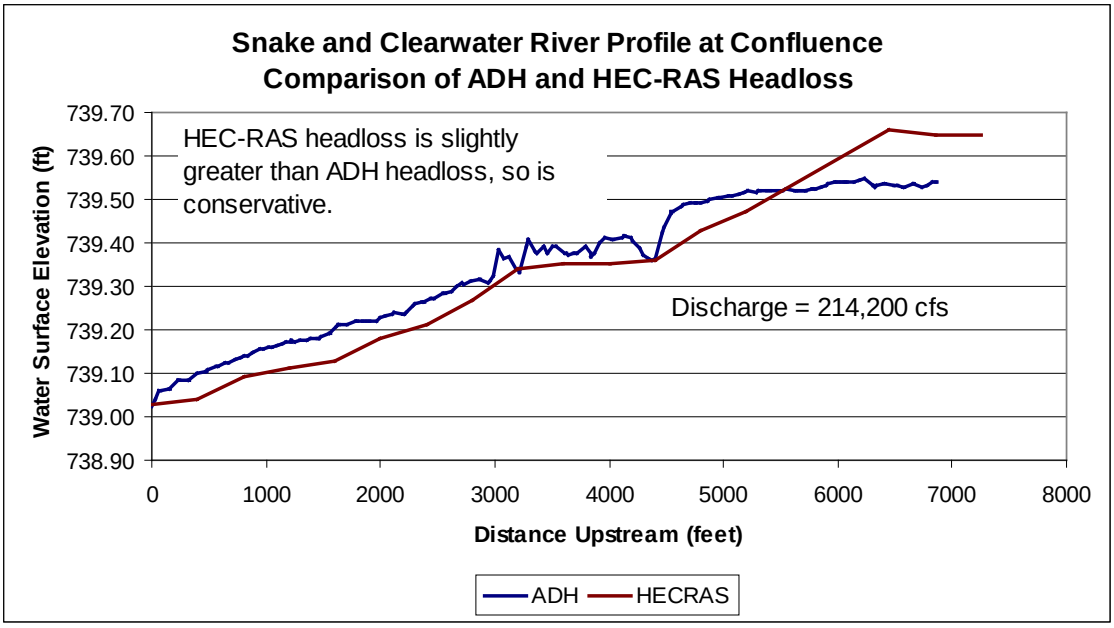


Figure 57. Comparison of 1D and 2 D simulated water surface profiles at the confluence (Lower Granite to Clearwater River).

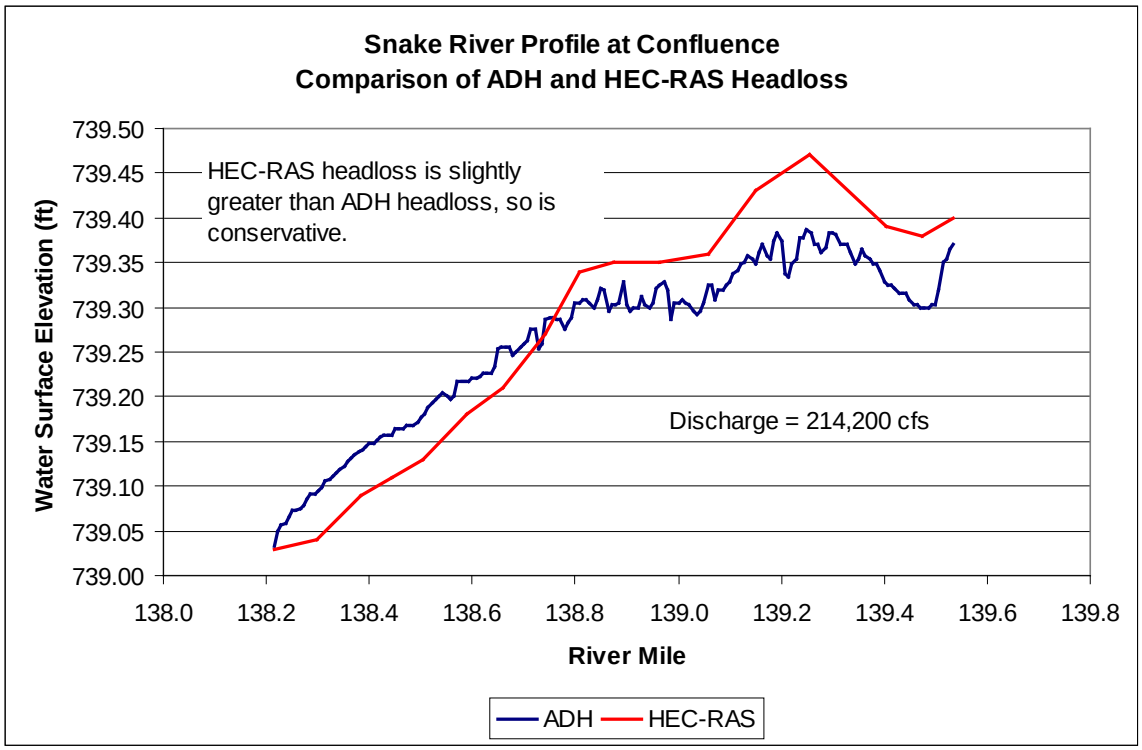


Figure 58. Comparison of 1D and 2 D simulated water surface profiles at the confluence (Lower Granite to Snake River).

5. Flood Risk Analysis – Existing Channel Condition

Probabilistic flood risk analysis for Corps projects is performed with the Hydrologic Engineering Center - Flood Damage Assessment Program (FDA) software[68]. The FDA risk analysis explicitly incorporates uncertainty in discharge-frequency, stage-discharge, and stage-damage relationships in the economic and performance analyses of alternative plans. The process uses Monte Carlo simulation to compute the expected value of damage and damage reduced, while explicitly accounting for the impact of uncertainty. This section describes the FDA flood risk analysis for the current channel in 2009 with no channel modifications and conservative assumptions concerning channel flow resistance. This channel condition is important because it defines the current level of overtopping risk at the Lewiston levee system. The flood risk analysis of the future channel condition and the channels modified with spur dikes follows the sediment transport analysis. Section 14 summarizes the flood risk analyses for all the alternatives.

5.1. Exceedance Discharges for the FDA Analysis

The FDA analysis requires water surface profiles for a range of discharge exceedance frequencies. The standard set of profiles includes discharges for exceedance probabilities 0.5, 0.2, 0.1, 0.04, 0.02, 0.01, 0.004, and 0.002[69]. The final discharge exceedance values for the HEC-RAS and FDA analysis are developed in three steps:

1. The medium probability annual maximum day flow-frequency curves for the Lower Granite Reservoir below the confluence were obtained from the univariate LP3 analysis discussed in Section 2.7 and are listed in Table 28.

2. The total flow of Lower Granite below the confluence was apportioned to the Snake River above the confluence and the Clearwater River. As shown in the joint probability analysis (Section 2.9), the Snake River is assigned 70 percent of the total discharge and the Clearwater River is

[68] USACE (2008). *HEC-FDA Flood Damage Reduction Analysis, User's Manual Version 1.2.4*, Hydrologic Engineering Center, U.S. Army Corps of Engineers, Davis, CA.

[69] USACE (2008). *HEC-FDA Flood Damage Reduction Analysis, User's Manual Version 1.2.4*, Hydrologic Engineering Center, U.S. Army Corps of Engineers, Davis, CA.

assigned 30 percent. The analysis showed that the flow split is nearly constant across the range of exceedance discharges.

3. The maximum day exceedance discharges (Table 28) were adjusted with peaking factors to approximate the instantaneous annual peak exceedance discharge required for the FDA analysis. Based on comparison of annual peaks with maximum day discharges (Section 2.1) peaking factors of 1.02 for the Snake River and 1.06 for the Clearwater River were applied to the univariate flow-frequency analysis. This adjustment is somewhat subjective, but because the extreme discharges are dominated by seasonal snowmelt it is reasonable that the annual peak discharges are not much greater than the maximum day discharges. The composite peaking factor for Lower Granite Reservoir below the confluence is 1.032, so the peak adjustment does not have a large influence on the outcome of the flood risk analysis.

The final annual peak exceedance discharges used in the FDA analysis are summarized Table 29, which also gives the downstream boundary conditions (forebay elevations) for the HEC-RAS models defined by flood control operations in the water control manual (Figure 51). The values in Table 29 were used throughout the flood risk analysis, for the current condition (year 2009) and the 50-year channel (year 2060) condition, with and without the spur dike alternative.

HEC-RAS Annual Maximum Average Daily Steady Flow Discharges for FDA Risk Analysis												
			Exceedance Probability (Percent)									
River	Reach	RS	50	20	10	4	2	1	0.4	0.2	0.1	SPF
Clearwater	Lewiston	7.85	46,635	62,233	71,508	82,206	89,533	96,384	104,834	110,931	116,735	125,000
Snake	Clarkston	148.83	108,814	145,211	166,852	191,813	208,911	224,897	244,613	258,839	272,382	295,000
Snake	Lower Granite	139.254	155,449	207,444	238,360	274,019	298,445	321,281	349,447	369,770	389,118	420,000
Lower Granite forebay elevation (feet)			733.78	732.00	730.66	729.32	728.40	728.21	727.98	727.81	727.60	727.40

Table 28. HEC-RAS annual maximum daily average steady flow discharges for FDA risk analysis.

HEC-RAS Estimated Annual Peak Steady Flow Discharges for FDA Risk Analysis												
			Exceedance Probability (Percent)									
River	Reach	RS	50	20	10	4	2	1	0.4	0.2	0.1	SPF
Clearwater	Lewiston	7.85	49,433	65,967	75,799	87,138	94,905	102,167	111,124	117,587	123,739	125,000
Snake	Clarkston	148.83	110,991	148,115	170,189	195,650	213,089	229,394	249,505	264,016	277,830	295,000
Snake	Lower Granite	139.254	160,423	214,082	245,988	282,788	307,995	331,562	360,629	381,603	401,569	420,000
Lower Granite forebay elevation (feet)			733.78	732.00	730.66	729.32	728.40	728.21	727.98	727.81	727.60	727.40

Table 29. HEC-RAS estimated annual peak steady flow discharges for FDA risk analysis.

5.2. Discharge Uncertainty

In FDA, the exceedance probability functions with uncertainty were computed with the analytical fit to the discharge data imported from the water surface profiles generated by the HEC-RAS models. The equivalent period of record length was 39 years which is the length of the gage record used to generate the maximum day discharge-frequency statistics (1972-2010). The gage records for both the Snake River at Anatone and the Clearwater River at Spalding are actually much longer, but as the report discusses in Section 2.5, the 39 year period since construction of the dam provides conservative frequency estimates. Since total flow in the reservoir is the sum of the Snake and Clearwater River flows the 39 year period of record is acceptable in the FDA analysis because by the linearity principle the expected value of a sum of two independent variables is the sum of the expected values of the variables.

5.3. Index Sections

The FDA software computes flood risk at designed locations called index sections. To simplify the discussion, a single index section RM 0.3 on the Clearwater River is evaluated. This location is a critical low point in the left-bank levee and is shown in Figure 59. Overtopping at this location will flood the interior of the levee system as described in Section 6. Additional index sections are included in the extended flood risk analysis of the future channel condition and alternative channel modifications discussed in Part 2.

5.4. Downstream Boundary Condition

It is important to recognize that the specification of exact forebay elevations in Table 29 for the exceedance discharges conditions the probabilistic risk analysis. This is because the spillway at Lower Granite Reservoir can be operated so that the water surface elevation at the confluence for the 1-percent chance flood (or any other discharge) can be made the same as for the SPF or even cause overtopping of the levee. Control of the reservoir in this manner would violate the prescribed control strategy for Lower Granite Dam. Large flood events in the lower Snake River basin are the result of regional snowmelt and rainfall events which can be reliably forecast in advance of the flood. It is unlikely that water managers would fail to follow proper flood control procedures. The appropriate assumption for the flood risk analysis is that the reservoir will be operated according to the authorized water control manual. Operation of the spillway at Lower Granite Dam is currently not impaired by sediment or expected to be affected by sedimentation during the 50-year planning period. Therefore, sedimentation should not significantly change the risk of flooding due to possible misoperation.

Though not included directly in the probabilistic risk analysis, the risk of misoperation is an important element of flood risk that should not be neglected.

Misoperation of the dam during flood events is evaluated as a separate scenario of flood risk analysis along with potential blockage of the Camas Prairie Railroad Bridge in Section 5.12. The Hydrologic Engineering Center is considering methodology to incorporate the uncertainty of reservoir operation directly in the probabilistic risk analysis. Alternative methods may be applied in future evaluations.



Figure 59. Index section at the levee low point on the Clearwater River at confluence.

5.5. Index Rating Curves

The FDA software computes the uncertainty of the flood water surface elevation at an index location by sampling the probability distributions of both discharge and stage. In the Monte Carlo analysis, the median probability stage associated with a particular discharge is obtained from a stage-discharge rating curve specified in the FDA input. In this study, the stage-stage discharge rating curves for the index locations were imported from the HEC-RAS water surface profile. Since the Monte Carlo simulation randomly selects discharges from within the band of uncertainty defined by

the software, the selected discharge can exceed the largest discharges in median probability exceedance discharges listed in Table 29. It is therefore necessary to extend the rating curve at each index location to provide an appropriate stage for the high discharge values.

Rating curves are readily extended in a typical flood risk analysis where the stage discharge relationship is defined by the discharge of a single unregulated river channel. However, in this flood risk analysis there is currently no completely satisfactory basis to extend the rating curves for the FDA simulation because of the joining flows of the Snake and Clearwater Rivers. This is because the FDA Monte Carlo analysis evaluates the extreme discharges for the Snake and Clearwater Rivers independently without regard for the correlation of high discharges or variation in the distribution of flow between each tributary. As discussed above, the flow split in Lower Granite during extreme discharge is approximately 30 percent from the Clearwater River and 70 percent from the Snake River, but they do vary and ideally this variability should be recognized as an additional source of uncertainty in the Monte Carlo analysis. Since the levees are at the confluence of the Snake and Clearwater Rivers, the flow split at high discharge partially determines the water surface elevation that is being simulated by FDA at the index locations. The current FDA software cannot simulate the simultaneous combining of the tributary flows that determine the water surface profile so the risk probabilities for very extreme flows are somewhat biased.

Furthermore, the maximum discharge computed by the FDA simulation for the Clearwater River was about 160,000 cfs, which when divided by the flow-split of 0.3 gives a total discharge in Lower Granite of 533,000 cfs. The water surface profile for this total discharge would on average include 373,000 cfs from the Snake River. Similarly, the maximum discharge computed by the FDA simulation for the Snake River was about 359,000 cfs, which with a flow-split of 0.7 gives a total discharge of 513,000 cfs. The lower total discharge for the Snake River FDA simulation is counter intuitive. Both total discharge values are greater than the 420,000 kcfs SPF and exceed the capacity of the levee channels. At these high discharges the spillway would be operated in free-flow condition. There is an approximate free-flow rating curve for the spillway, but the actual water surface elevation at the confluence is uncertain because inundation of the confluence would create a highly two-dimensional flow field that is not modeled accurately with the HEC-RAS one-dimensional hydraulic model. This latter concern becomes important if flood damages are being computed, which they are not in this flood risk analysis.

While the bias has no real effect on project performance when the water surface profile is below the top of the levee, it will have more of an effect for the most extreme discharges when the water surface is near the overtopping level. In this study, it is reasonable to extend the rating curves to the computed maximum values if it is

assumed that the complementary flow is limited to an appropriately high value. An appropriate choice is the SPF of 420,000 cfs which is passed at a forebay elevation of 727.4 ft NAVD88. Alternatively, the FDA index section rating curves can be extended assuming the 30/70 flow-split discussed above with forebay water surface elevations obtained from the free-flow rating curve for the spillway. The FDA flood risk analysis was performed with both approaches. Steady flow discharges and forebay elevations used in computing the water surface profile are listed in Table 30.

River	Reach	RS	CWR Ext Curve 1	SR Ext Curve 1	CWR Ext Curve 2	SR Ext Curve 2
Clearwater	Lewiston	7.85	160,000	61,000	160,000	153,857
Snake	Clarkston	148.83	260,000	359,000	373,333	359,000
Snake	Lower Granite	139.254	420,000	420,000	533,333	512,857
Lower Granite forebay elevation (feet)			727.4	727.4	733.9	732.4

Table 30. Discharges and forebay elevations used in HEC-RAS modeling of the curve extensions for the FDA index sections.

5.6. Stage Uncertainty

Based on the available water surface measurements, the observed uncertainty in stage at high discharge at the confluence of the Clearwater and Snake Rivers is discussed in Section 3 and is less than 1 foot. A common assumption in flood risk analysis is to estimate the standard deviation of stage uncertainty as the total range of variability divided by 4. This gives a standard deviation of the uncertainty of approximately 0.25 feet, which is implausibly low for the unobserved higher discharges adopted in the flood risk analysis. The minimum standard deviation for stage uncertainty in the risk analysis was assumed to be 0.5 feet. It should be noted that the procedures and stage uncertainty plot in Chapter 5 of EM 1110-2-1619 cannot be applied directly because of the backwater effect of Lower Granite and the convergence of flow at the confluence. The uncertainty of stage assumed in this analysis is within the range listed in Table 5-2 of EM 1110-2-1619.

Flood risk was also computed assuming an implausibly large standard deviation of stage of 2.0 ft. This was done to demonstrate a simple approach that conservatively bounds the uncertainty that might be attributed the mobile bed dynamics in lieu of the more rigorous analysis of sediment transport and flow resistance. Uncertainty in stage caused by bed dynamics and bedform development is more appropriately represented by varying the hydraulic roughness factors (Manning's *n*) in the hydraulic model by the methods discussed in Section 10.

Variation in stage for a given discharge is also caused by the regulation of the spillway at Lower Granite Dam. As discussed in Section 5.4, the water control manual specifies a well defined response to forecast flood conditions. Single-value rating

curves at the index sections with added stage uncertainty represent this condition. Conceptually, stage-frequency statistics could be defined in the FDA analysis to incorporate stage uncertainty due to misoperation of the spillway gates, but lacking support of an actual analysis of operational risk the approach would be speculative.

5.7. Hydraulic Flow Resistance

As discussed in Section 10, two mobile-bed conditions are evaluated in the flood risk analysis: the lower bed regime with higher hydraulic flow resistance and upper bed regime with lower hydraulic flow resistance. As shown in Section 10, the flow resistance for upper bed regime conditions is represented in the HEC-RAS model by the calibrated Manning's *n* factors given in Table 26 which are 0.022 to 0.023 in the reservoir below the confluence and variable from 0.023 to 0.035 above the confluence. Greater hydraulic roughness of the lower bed regime produces a higher water surface in the flood risk analysis. Hydraulic roughness for the lower bed regime is conservatively represented, as shown in Section 10, by the Manning's *n* values assumed in the traditional fixed-bed analysis discussed in Section 4.7. The historic analysis assumed that Manning's *n* of the channel throughout the reservoir was 0.028 and that the Manning's *n* of the Snake and Clearwater Rivers above the confluence was 0.03.

5.8. Water Surface Profiles

The water surface profiles for the FDA analysis of the current condition were computed with the HEC-RAS 2009 fixed-bed model described in Section 4. The model was run in steady flow mode using the discharges and downstream boundary water surface elevations listed in Table 29 and for the high discharges that extended the stage-discharge curves listed in Table 30. Figure 60, Figure 61 and Figure 62 are plots of the water surface profiles obtained from the calibrated model for three discharges: the 8 June 2010 calibration discharge, the 1 percent exceedance discharge, and the SPF for the Clearwater River (Lewiston Reach), the Snake River above the confluence (Clarkston Reach) and the Snake River below the confluence (Lower Granite Reach). Water surface profiles used in the FDA flood of all the alternatives risk analysis are included in the digital data appendix. Hydraulic parameters from the water surface profile computations for the Clearwater River and Snake River near the confluence are listed in Table 31 and Table 32. The water surface for the SPF is below the top-of-levee elevations by at least 4 feet. Top-of-levee elevations near the confluence were confirmed in the 2010 field survey (Section 4.3) and are shown in Figure 63 and Figure 59.

5.9. Comparison with the SPF Water Surface Profile

The SPF water surface profile computed with the HEC-RAS 2009 high-resolution fixed-bed model is significantly different than the HEC-RAS model developed from the sediment range cross sections discussed in Section 4.7. The levee margin (freeboard) computed with the 2009 high-resolution model is about 4 feet at the confluence for the SPF, while the 2009 sediment range model computed a margin of about 2 feet. The difference is due to the resolution of the cross section spacing and the Manning's *n* values used in the two models. The Manning's *n* values adopted in the 2009 sediment range model were the same as used in the historical models. The historical models reflect a deterministic modeling philosophy that is currently less favored than the risk-based approach. Previous models assumed conservative values of Manning's *n* so that the computed water surface profile was high enough to account for uncertainties in the hydraulic data, computation methods and stage variability. This uncertainty is now directly included in the probabilistic FDA Monte Carlo analysis. The levee margin at the confluence reduces to about 1.8 feet if the historic Manning's *n* are assumed in the HEC-RAS 2009 high-resolution fixed-bed model. Water surface profiles computed with calibrated and historic Manning's *n* values are compared in Figure 64 and Figure 65 for the calibration discharge on 8 June 2010 and the SPF.

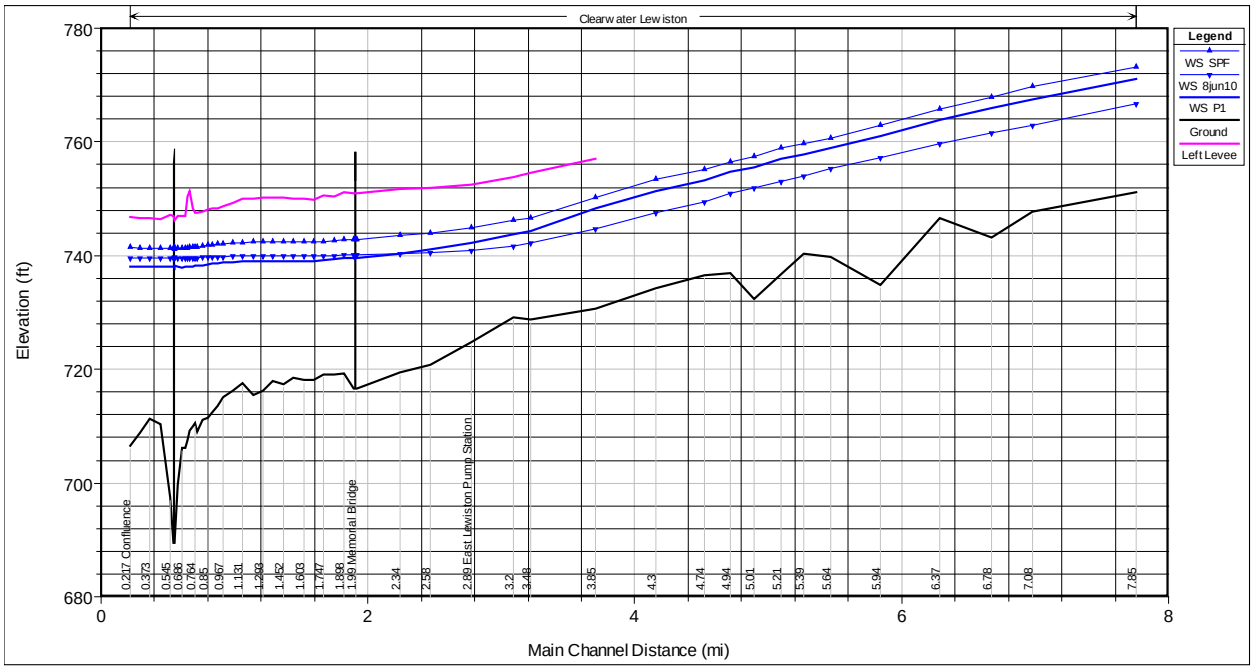


Figure 60. HEC-RAS 2009 fixed-bed steady flow profiles for Clearwater River.

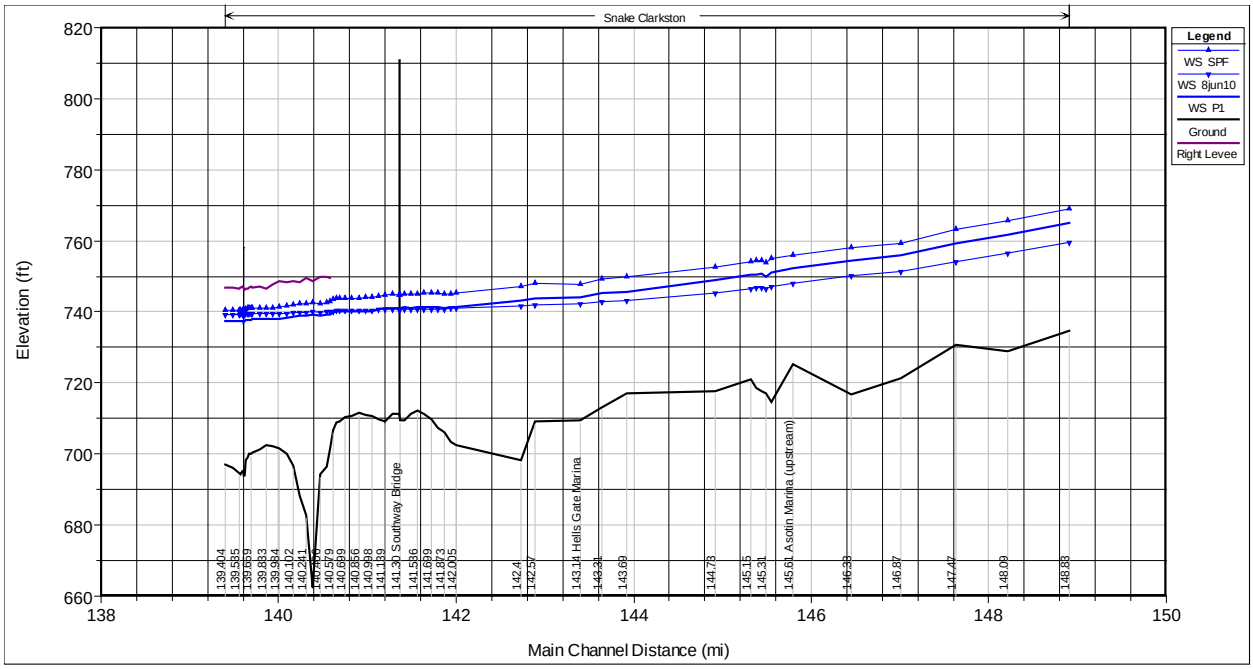


Figure 61. HEC-RAS 2009 fixed-bed steady flow profiles for Snake River above confluence.

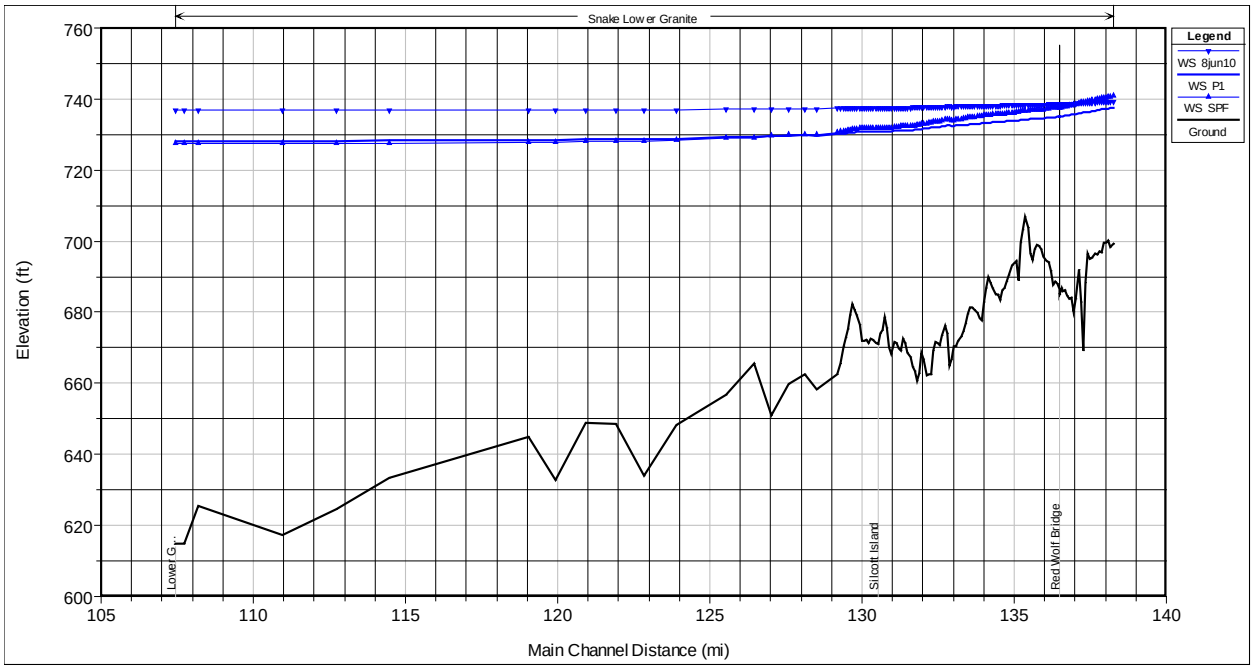


Figure 62. HEC-RAS 2009 fixed-bed steady flow profiles for Snake River below the confluence (Lower Granite Reservoir).

HEC-RAS 2009 Fixed-Bed Water Surface Profile for Upper Bed Regime (Calibrated Manning's *n*) - Clearwater River near the Confluence											
				Water Surface		Mean			Levee Elevations		Levee Freeboard	
			Discharge	Elevation	Energy	Velocity		Left	Right	Left	Right
Reach	River Sta	Profile	cfs	ft NAVD88	Slope	ft/s	Froude No.	ft NAVD88	ft NAVD88	ft	ft
Lewiston	0.217	8-Jun-10	60,311	739.67	0.000017	2.04	0.08	746.56	758.95	6.89	19.28
Lewiston	0.217	P1	102,167	738.16	0.000064	3.73	0.15	746.56	758.95	8.40	20.79
Lewiston	0.217	SPF	125,000	741.57	0.000055	3.87	0.14	746.56	758.95	4.99	17.38
Lewiston	0.299	8-Jun-10	60,311	739.66	0.000024	2.43	0.09	746.57	759.21	6.91	19.55
Lewiston	0.299	P1	102,167	738.13	0.000087	4.44	0.17	746.57	759.21	8.44	21.08
Lewiston	0.299	SPF	125,000	741.52	0.000077	4.64	0.17	746.57	759.21	5.05	17.69
Lewiston	0.373	8-Jun-10	60,311	739.66	0.000027	2.66	0.10	746.41	756.90	6.75	17.24
Lewiston	0.373	P1	102,167	738.13	0.000098	4.84	0.19	746.41	756.90	8.28	18.77
Lewiston	0.373	SPF	125,000	741.51	0.000088	5.08	0.18	746.41	756.90	4.90	15.39
Lewiston	0.461	8-Jun-10	60,311	739.66	0.000028	2.85	0.10	746.23	753.76	6.57	14.10
Lewiston	0.461	P1	102,167	738.13	0.000102	5.17	0.19	746.23	753.76	8.10	15.63
Lewiston	0.461	SPF	125,000	741.50	0.000095	5.48	0.19	746.23	753.76	4.73	12.26
Lewiston	0.545	8-Jun-10	60,311	739.67	0.000022	2.81	0.09	747.88	754.89	8.21	15.22
Lewiston	0.545	P1	102,167	738.19	0.000074	5.02	0.17	747.88	754.89	9.69	16.70
Lewiston	0.545	SPF	125,000	741.53	0.000075	5.47	0.17	747.88	754.89	6.35	13.36
Lewiston	0.59	8-Jun-10	60,311	739.67	0.000023	2.96	0.09	746.70	745.28	7.03	5.61
Lewiston	0.59	P1	102,167	738.17	0.000079	5.28	0.17	746.70	745.28	8.53	7.11
Lewiston	0.59	SPF	125,000	741.51	0.000082	5.78	0.18	746.70	745.28	5.19	3.77
Lewiston	0.6	8-Jun-10	60,311	740.35	0.000022	2.96	0.09	746.23	753.06	5.88	12.71
Lewiston	0.6	P1	102,167	738.92	0.000075	5.26	0.17	746.23	753.06	7.31	14.14
Lewiston	0.6	SPF	125,000	742.30	0.000078	5.77	0.18	746.23	753.06	3.93	10.76
Lewiston	0.65	8-Jun-10	60,311	740.29	0.000041	3.87	0.12	746.36	748.40	6.07	8.11
Lewiston	0.65	P1	102,167	738.71	0.000140	6.92	0.23	746.36	748.40	7.65	9.69
Lewiston	0.65	SPF	125,000	742.05	0.000144	7.56	0.24	746.36	748.40	4.31	6.35
Lewiston	0.686	8-Jun-10	60,311	740.29	0.000046	4.00	0.13	746.52	746.74	6.23	6.45
Lewiston	0.686	P1	102,167	738.70	0.000163	7.21	0.25	746.52	746.74	7.82	8.04
Lewiston	0.686	SPF	125,000	742.05	0.000161	7.77	0.25	746.52	746.74	4.47	4.69

Table 31. HEC-RAS 2009 Fixed-Bed Water Surface Profile - Clearwater River near the Confluence.

HEC-RAS 2009 Fixed-Bed Water Surface Profile for Upper Bed Regime (Calibrated Manning's n) - Snake River near the Confluence											
				Water Surface		Mean			Levee Elevations		Levee Freeboard	
			Discharge	Elevation	Energy	Velocity		Left	Right	Left	Right
Reach	River Sta	Profile	cfs	ft NAVD88	Slope	ft/s	Froude No.	ft NAVD88	ft NAVD88	ft	ft
Clarkston	139.404	8-Jun-10	153,889	739.38	0.000074	5.27	0.17		747.02		7.64
Clarkston	139.404	P1	229,394	737.44	0.000208	8.43	0.28		747.02		9.58
Clarkston	139.404	SPF	295,000	740.57	0.000238	9.69	0.31		747.02		6.45
Clarkston	139.475	8-Jun-10	153,889	739.38	0.000080	5.54	0.18		746.93		7.55
Clarkston	139.475	P1	229,394	737.45	0.000224	8.87	0.29		746.93		9.48
Clarkston	139.475	SPF	295,000	740.58	0.000256	10.18	0.32		746.93		6.35
Clarkston	139.535	8-Jun-10	153,889	739.38	0.000075	5.79	0.18		746.49		7.11
Clarkston	139.535	P1	229,394	737.47	0.000203	9.17	0.29		746.49		9.02
Clarkston	139.535	SPF	295,000	740.54	0.000246	10.72	0.32		746.49		5.95
Clarkston	139.55	8-Jun-10	153,889	739.42	0.000070	5.64	0.17		746.61		7.19
Clarkston	139.55	P1	229,394	737.59	0.000189	8.90	0.28		746.61		9.02
Clarkston	139.55	SPF	295,000	740.70	0.000228	10.40	0.31		746.61		5.91
Clarkston	139.565	8-Jun-10	153,889	739.37	0.000086	6.03	0.19		746.95		7.58
Clarkston	139.565	P1	229,394	737.47	0.000235	9.57	0.30		746.95		9.48
Clarkston	139.565	SPF	295,000	740.54	0.000280	11.14	0.34		746.95		6.41

Table 32. HEC-RAS 2009 Fixed-Bed Water Surface Profile - Snake River near the Confluence.

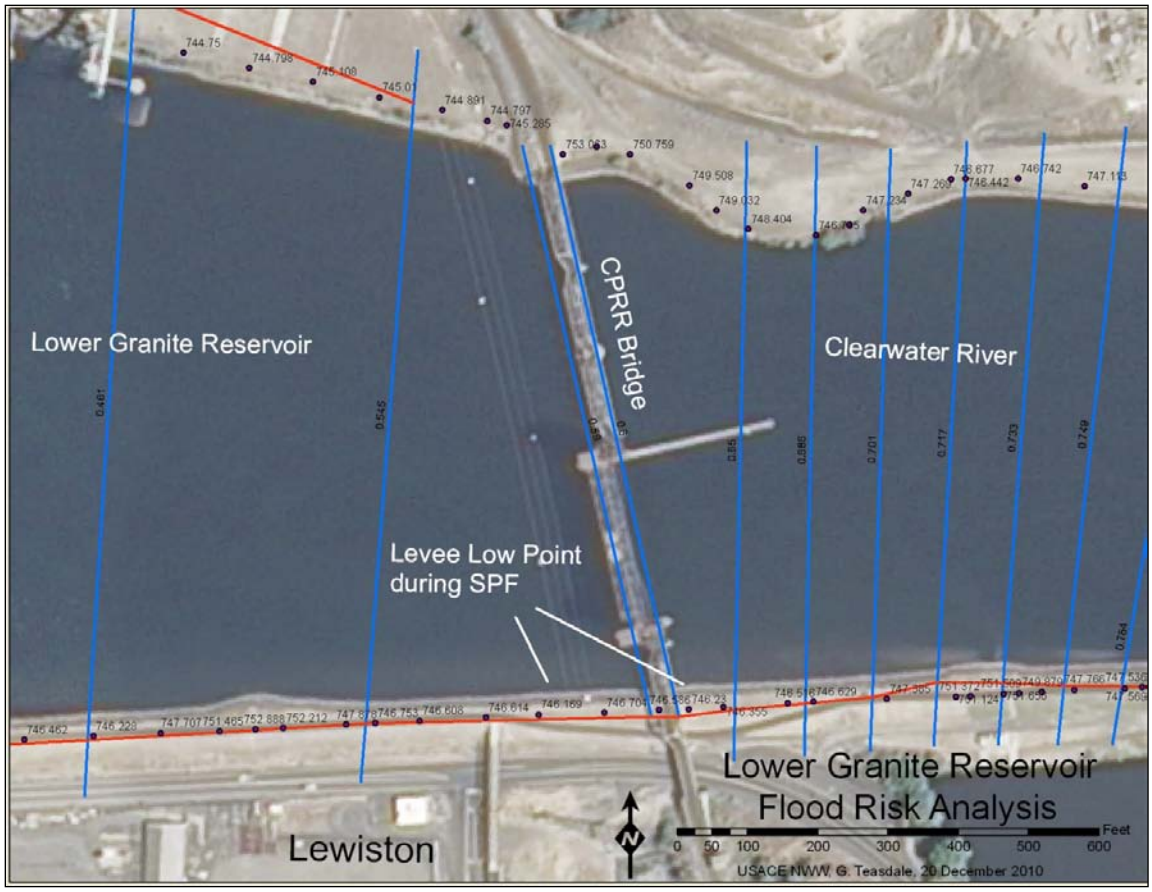


Figure 63. Levee low point during SPF discharge.

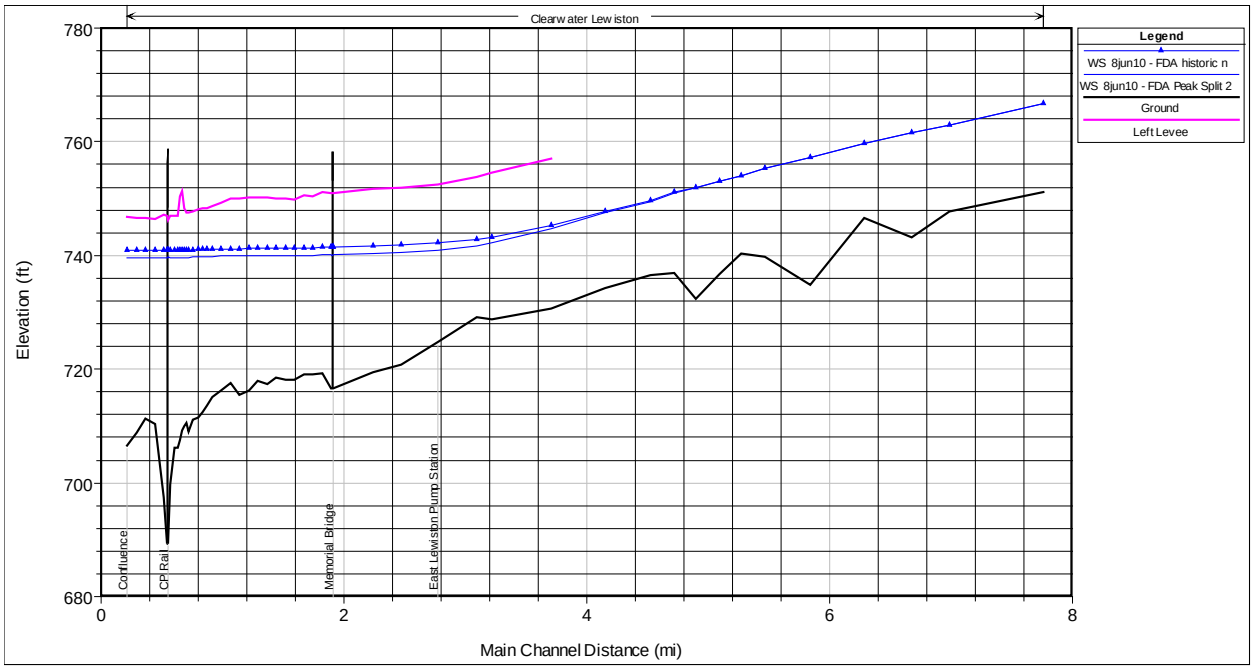


Figure 64. Comparison of 8 June 2010 profiles for calibrated and historic Manning's *n* values.

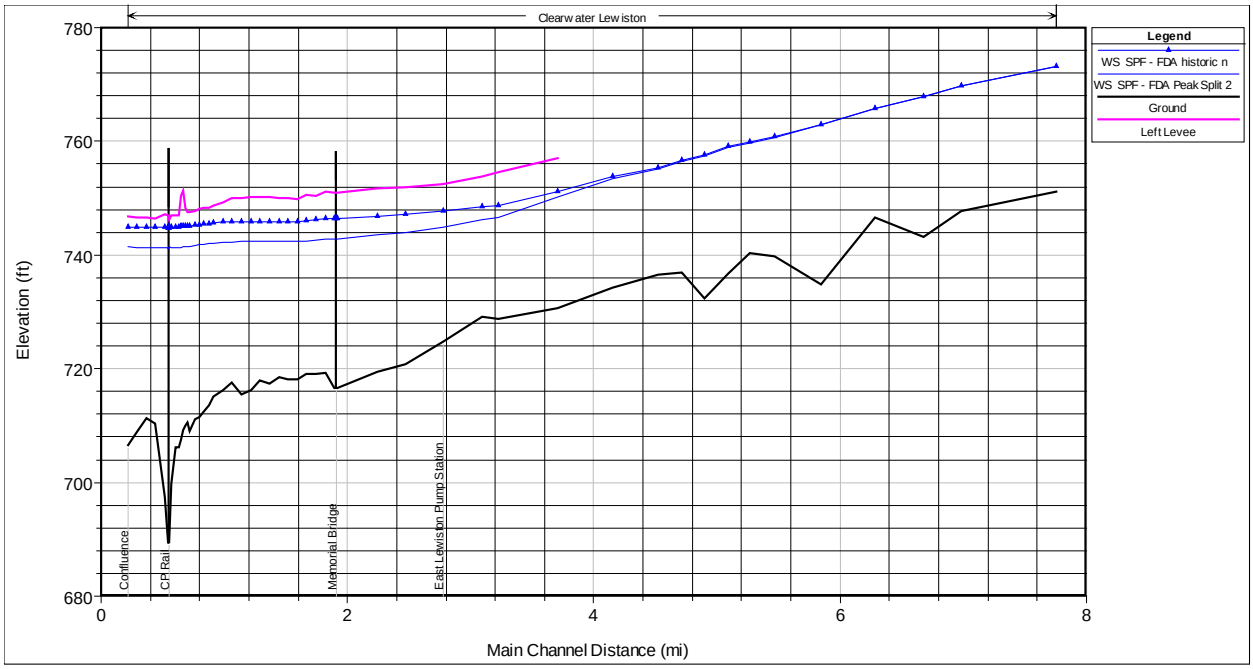


Figure 65. Comparison of SPF profiles for calibrated and historic Manning's *n* values.

5.10. Assurance - Conditional Non-Exceedance Probabilities – 2009 Fixed-Bed Model

Assurance or conditional annual non-exceedance probability (CNP) is an index of the likelihood that a specified target, such as the crest of a levee, will not be exceeded given the occurrence of a hydrometeorological event[70]. This element of risk is called *assurance* in recent Corps guidance[71]. The term CNP is used in this report because this is how it is reported by the FDA software. Water surface elevations computed with the HEC-RAS 2009 fixed-bed model are well below the top of the levees throughout the Lewiston levee system for discharges up to the SPF, so conditional non-exceedance probabilities are expected to be high (high *assurance*, low risk).

The water surface profile data computed with calibrated and historic Manning's *n* values were input into the FDA program and the Monte Carlo simulation was run with stage uncertainty at two levels as defined by standard deviations of 0.5 and 2.0 feet, and for the two curve extension methods discussed above. Results are summarized in Table 33 and Table 34. Curve extension method 1 limits the total discharge in Lower Granite Reservoir to 420 kcfs and curve extension method 2 defines the total discharge

[70] USACE (1996). EM 1110-2-1619 *Risk-Based Analysis for Flood Damage Reduction Studies*, U.S. Army Corps of Engineers, Washington, DC.

in Lower Granite reservoir by the 30 percent and 70 percent flow-splits. Conditional non-exceedance probabilities for the 1-percent chance exceedance discharge exceed 99 percent for all computation alternatives except for the lower regime bed condition with a 2.0 standard deviation of stage uncertainty which exceeded 97 percent. The greatest 50-yr long-term risk was 5.1 percent for the lower bed regime condition with a 2.0 standard deviation of stage uncertainty and curve extension method 2. It should be recognized that the 50-yr long-term risk values have little practical meaning because, as Section 10 shows, sediment accumulation continues to change the channel condition during the 50-year future analysis period. This long-term risk values are only meaningful if the hydraulic capacity of the channel is maintained to preserve the 2009 channel conveyance. The FDA analysis of the future channel condition and channel modification alternatives are discussed in Section 10.

Year 2009 Conditional Non-Exceedance Probabilities and Long-term Risk at Clearwater RM 0.3, Curve Extension 1								
	Standard	50-year	Flood Frequency					
	Deviation	Long-Term	10.0%	4.0%	2.0%	1.0%	0.4%	0.2%
Hydraulic Resistance	Stage (ft)	Risk	Conditional Non-Exceedance Probabilities					
Upper Regime	0.5	0.0050	1.0000	1.0000	1.0000	1.0000	1.0000	1.0000
Lower Regime	0.5	0.0050	1.0000	1.0000	1.0000	1.0000	1.0000	1.0000
Upper Regime	2.0	0.0053	1.0000	1.0000	0.9999	0.9998	0.9993	0.9987
Lower Regime	2.0	0.0267	0.9999	0.9994	0.9960	0.9862	0.9623	0.9394

Table 33. Conditional non-exceedance probabilities at Clearwater RM 0.3 curve extension method 1.

Year 2009 Conditional Non-Exceedance Probabilities and Long-term Risk at Clearwater RM 0.3, Curve Extension 2								
	Standard	50-year	Flood Frequency					
	Deviation	Long-Term	10.0%	4.0%	2.0%	1.0%	0.4%	0.2%
Hydraulic Resistance	Stage (ft)	Risk	Conditional Non-Exceedance Probabilities					
Upper Regime	0.5	0.0050	1.0000	1.0000	1.0000	1.0000	0.9999	0.9996
Lower Regime	0.5	0.0294	1.0000	1.0000	0.9995	0.9938	0.9412	0.8268
Upper Regime	2.0	0.0093	1.0000	1.0000	0.9998	0.9987	0.9892	0.9689
Lower Regime	2.0	0.0510	0.9999	0.9994	0.9951	0.9775	0.9033	0.7925

Table 34. Conditional non-exceedance probabilities at Clearwater RM 0.3 curve extension method 2.

To place the CNP values in perspective, the levee system evaluation requirements for the National Flood Insurance Program (NFIP) require that a levee must provide at least a 90 assurance (CNP) of excluding the 1 percent annual chance exceedance flood for all reaches of the system[71]. In addition, riverine levees must provide a minimum freeboard of three feet above the median water surface level (base

[71] USACE (2010). EC 1110-2-6067 *USACE Process for the National Flood Insurance Program (NFIP) Levee System Evaluation*, U.S. Army Corps of Engineers, Washington, DC.

flood) of the 1 percent annual chance exceedance flood. An additional one foot above the minimum is required within 100 feet in either side of structures, such as bridges, or wherever the flow is constricted. If the top of levee elevation is less than the required freeboard above the 1 percent annual chance exceedance flood stage, then the levee can only be in accordance with NFIP levee system evaluation requirements if the assurance (CNP) is 95 percent or greater. Top-of-levee elevation shall not be less than two feet above the 1 percent annual chance exceedance flood elevation, even if assurance is 95 percent or greater.

Levee freeboard for 1 percent annual chance exceedance flood for the calibrated Manning's *n* and historic Manning's *n* are listed in Table 35 for the Lewiston Levee system on the Clearwater River and in Table 36 for the Snake River. The hydraulic capacity of the Lewiston levees satisfies both the NFIP assurance and freeboard requirements for levee system evaluation even with very conservative assumptions about flow resistance and stage uncertainty. The freeboard for the 1 percent annual chance exceedance flood exceeds 8 feet near the confluence for the calibrated Manning's *n* model, which is sufficient to accommodate the possibility of wind waves (Section 13) at the peak of the flood that are expected to not exceed a maximum wave height of 3 feet.

HEC-RAS 2009 Fixed-Bed Levee Freeboard - 1 Percent Exceedance Discharge						
			Upper Bed Regime Calibrated Manning's *n* Levee Freeboard		Lower Bed Regime Historic Manning's *n* Levee Freeboard	
River	Reach	River Mile	Left ft	Right ft	Left ft	Right ft
Clearwater	Lewiston	0.22	8.4	20.8	5.7	18.1
Clearwater	Lewiston	0.30	8.4	21.1	5.7	18.3
Clearwater	Lewiston	0.37	8.3	18.8	5.5	16.0
Clearwater	Lewiston	0.46	8.1	15.6	5.3	12.9
Clearwater	Lewiston	0.55	9.7	16.7	6.9	13.9
Clearwater	Lewiston	0.59	8.5	7.1	5.8	4.3
Clearwater	Lewiston	0.60	7.3	14.1	4.5	11.4
Clearwater	Lewiston	0.65	7.7	9.7	4.8	6.9
Clearwater	Lewiston	0.69	7.8	8.0	5.0	5.2
Clearwater	Lewiston	0.70	8.7	8.5	5.8	5.7
Clearwater	Lewiston	0.72	12.3	7.7	9.5	4.8
Clearwater	Lewiston	0.73	12.8	7.9	10.0	5.1
Clearwater	Lewiston	0.75	8.9	8.2	6.1	5.3
Clearwater	Lewiston	0.76	8.7	8.8	5.9	6.0
Clearwater	Lewiston	0.79	8.9	12.9	6.0	10.0
Clearwater	Lewiston	0.82	8.9	12.9	6.0	10.1
Clearwater	Lewiston	0.85	9.2	12.1	6.3	9.3
Clearwater	Lewiston	0.88	9.3	9.2	6.5	6.4
Clearwater	Lewiston	0.91	9.2	9.6	6.4	6.8
Clearwater	Lewiston	0.97	9.4	10.0	6.6	7.2
Clearwater	Lewiston	1.07	9.7	10.2	6.9	7.4
Clearwater	Lewiston	1.13	10.5	10.1	7.7	7.3
Clearwater	Lewiston	1.21	10.5	9.8	7.7	7.0
Clearwater	Lewiston	1.29	10.7	10.1	7.9	7.3
Clearwater	Lewiston	1.38	10.7	10.0	7.9	7.2
Clearwater	Lewiston	1.45	10.4	9.9	7.6	7.1
Clearwater	Lewiston	1.53	10.5	10.0	7.6	7.2
Clearwater	Lewiston	1.60	10.2	10.1	7.4	7.2
Clearwater	Lewiston	1.67	10.4	10.0	7.6	7.1
Clearwater	Lewiston	1.75	10.9	10.3	8.0	7.4
Clearwater	Lewiston	1.82	10.6	10.7	7.7	7.8
Clearwater	Lewiston	1.90	11.1	10.3	8.2	7.5
Clearwater	Lewiston	1.97	11.1	10.0	8.2	7.1
Clearwater	Lewiston	1.99	10.9	10.4	8.0	7.5
Clearwater	Lewiston	2.34	10.9	10.9	8.3	8.3
Clearwater	Lewiston	2.58	10.6	12.2	8.1	9.8
Clearwater	Lewiston	2.89	10.1	10.9	8.0	8.7
Clearwater	Lewiston	3.20	9.8		8.2	
Clearwater	Lewiston	3.48	10.2		8.8	
Clearwater	Lewiston	3.85	8.7		8.2	

Table 35. Levee freeboard for 1-percent annual chance exceedance flood – Clearwater River.

HEC-RAS 2009 Fixed-Bed Levee Freeboard - 1 Percent Exceedance Discharge						
			Calibrated Manning's *n* Levee Freeboard		Historic Manning's *n* Levee Freeboard	
River	Reach	River Mile	Left ft	Right ft	Left ft	Right ft
Snake	Clarkston	139.40		9.6		6.7
Snake	Clarkston	139.48		9.5		6.5
Snake	Clarkston	139.54		9.0		6.1
Snake	Clarkston	139.55		9.0		6.1
Snake	Clarkston	139.57		9.5		6.5
Snake	Clarkston	139.58		8.6		5.6
Snake	Clarkston	139.60		8.9		5.9
Snake	Clarkston	139.61		8.6		5.6
Snake	Clarkston	139.63		8.7		5.8
Snake	Clarkston	139.66		9.0		6.1
Snake	Clarkston	139.68		9.2		6.2
Snake	Clarkston	139.76		8.7		5.7
Snake	Clarkston	139.83		9.1		6.1
Snake	Clarkston	139.93		9.7		6.6
Snake	Clarkston	139.98		9.7		6.7
Snake	Clarkston	140.04		9.9		6.9
Snake	Clarkston	140.10		9.7		6.7
Snake	Clarkston	140.16		9.6		6.6
Snake	Clarkston	140.24		10.5		7.4
Snake	Clarkston	140.32		9.7		6.8
Snake	Clarkston	140.41		11.2		8.0
Snake	Clarkston	140.49		10.8		7.7
Snake	Clarkston	140.54		10.5		7.4

Table 36. Levee freeboard for 1 percent annual chance exceedance flood – Snake River.

5.11. Potential for Geotechnical Failure of the Levees

The potential for geotechnical failure can be incorporated into the FDA probabilistic analysis. The Lewiston Levees were designed and constructed to provide a high degree of reliability and do not present a significant risk of geotechnical failure prior to overtopping. Geotechnical characteristics of the Lewiston Levee system are discussed in the geotechnical section of the EIS.

5.12. Potential for Induced Flooding

The flood risk conditional nonexceedance probabilities (assurance) values above were computed with the important assumption that the spillway at Lower Granite Dam is operated in accordance with the water control manual. It is possible to cause backwater behind the dam to overtop the levees in Lewiston even during modest inflows by improperly adjusting the spillway gates. However, induced flooding is unlikely given

the progressive procedures prescribed in the water control manual, the prolonged characteristics of the snowmelt flood hydrograph, and equipment redundancy at the dam.

At present, there are no methods in Corps engineering guidance to evaluate the risk associated with misoperation in an FDA analysis. A simple approach is to assume a scenario that forebay elevations are higher than those specified in the water control manual and evaluate the change in CNP. The FDA analysis was repeated assuming that the forebay elevations were 4 feet and 6 feet higher than allowed by the water control manual. Table 37 shows that significantly higher pools have a small effect on the CNP's for the levee at the confluence. Under the conservative assumptions of the calibrated Manning's *n* values and a 2 ft standard deviation of stage uncertainty, the long-term 50 year risk increases to 7.8 percent and the CNP for the 1- percent exceedance discharge decreases to 98.1 percent.

Conditional Non-Exceedance Probabilities at Clearwater RM 0.3 - Effect of Spillway Misoperation									
	Standard	Pool	50-year	Flood Frequency					
	Deviation	Rise	Long-Term	10.0%	4.0%	2.0%	1.0%	0.4%	0.2%
Hydraulic Resistance	Stage (ft)	ft	Risk	Conditional Non-Exceedance Probabilities					
Calibrated Mannings n	0.5	0.0	0.005	1.0000	1.0000	1.0000	1.0000	1.0000	1.0000
Calibrated Mannings n	0.5	4.0	0.0184	1.0000	1.0000	0.9998	0.9940	0.9661	0.8871
Calibrated Mannings n	0.5	6.0	0.0248	1.0000	1.0000	0.9997	0.9952	0.9518	0.8508
Calibrated Mannings n	2.0	6.0	0.0776	0.9985	0.9978	0.9944	0.9812	0.9201	0.8203

Table 37. Effect of spillway on conditional non-exceedance probabilities.

The forebay elevation would have to rise by 14 feet from the forebay elevation specified in the water control manual to about 742.5 ft NAVD88 during the peak of the 1-percent annual chance exceedance flood to induce flooding at the confluence. Lower Granite Reservoir has limited storage so if the spillway gates were completely blocked, the rise would occur in about 4 hours at steady inflow of 331,560 cfs . The uniform gate opening for all 8 – 50ft wide tainter gates is about 28 feet during the 1 percent exceedance discharge. About 0.25 acres of impervious debris would have to impinge upon and block the gates to induce the flooding. This analysis suggests that normal flood control operations at Lower Granite Dam do not significantly affect flood risk at the confluence, and that extreme misoperation or blockage of the spillway gates would be necessary to induce flooding in Lewiston.

Overtopping could potentially be induced by blockage of the Camas Prairie Rail Road Bridge at Clearwater RM 0.6 by floating debris. Methods have been developed to evaluate the potential for debris to accumulate at bridges[72], but flood risk from debris

[72] FHWA (2005). *Hydraulic Engineering Circular No. 9 Debris Control Structures, Evaluation and Countermeasures, 3rd Ed.*, U.S Department of Transportation, Federal Highway Administration. Washington, DC.

blockage is difficult to quantify. The effect of debris blockage at the CPRR Bridge was modeled in HEC-RAS by placing "blocked obstructions" between the banks and the adjacent piers (Figure 66). A navigation guide wall (Figure 63) reduces the potential to block the middle piers. The moderate amount of blockage assumed in the analysis raised the upstream water surface during the SPF by about 0.3 feet and did not significantly change the CNP values upstream of the CPRR. In a second scenario, the more aggressive blockage depicted in Figure 67 raised the upstream water surface of the SPF by about 1 foot. In a third scenario, the bottom chord of the deck was lowered to an elevation 735 feet to simulate blockage by floating debris across the full width of the channel to a depth of about 6 feet below the SPF water surface. This amount of blockage raised the upstream water surface during the SPF by about 1.5 feet. In all three scenarios, the higher water surface during the SPF was contained within the levees. This analysis suggests that a plausible amount of blockage at the CPRR Bridge does not greatly increase the risk of induced flooding in the Lewiston levee system. The effect of debris blockage on the water surface profile is likely adequately represented in the 2.0 ft standard deviation of stage assumed in the conservative FDA analysis discussed above.

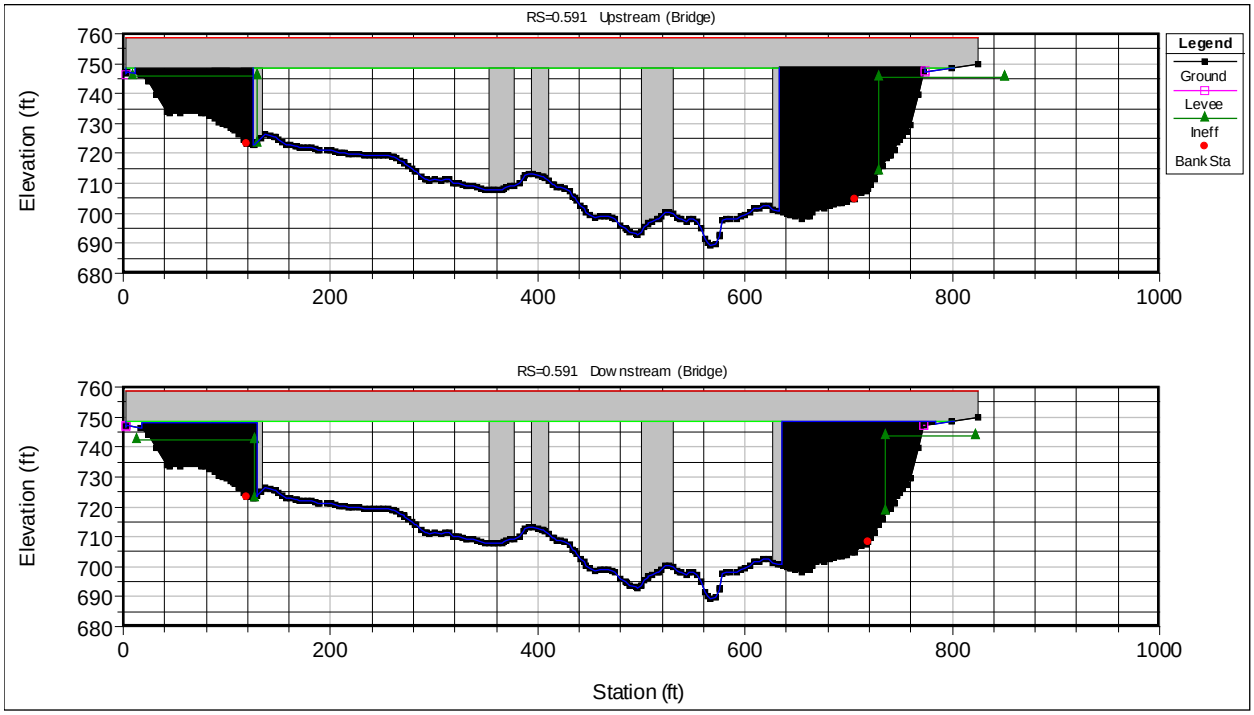


Figure 66. Simulated moderate debris blockage at the CPRR bridge Clearwater RM 0.6.

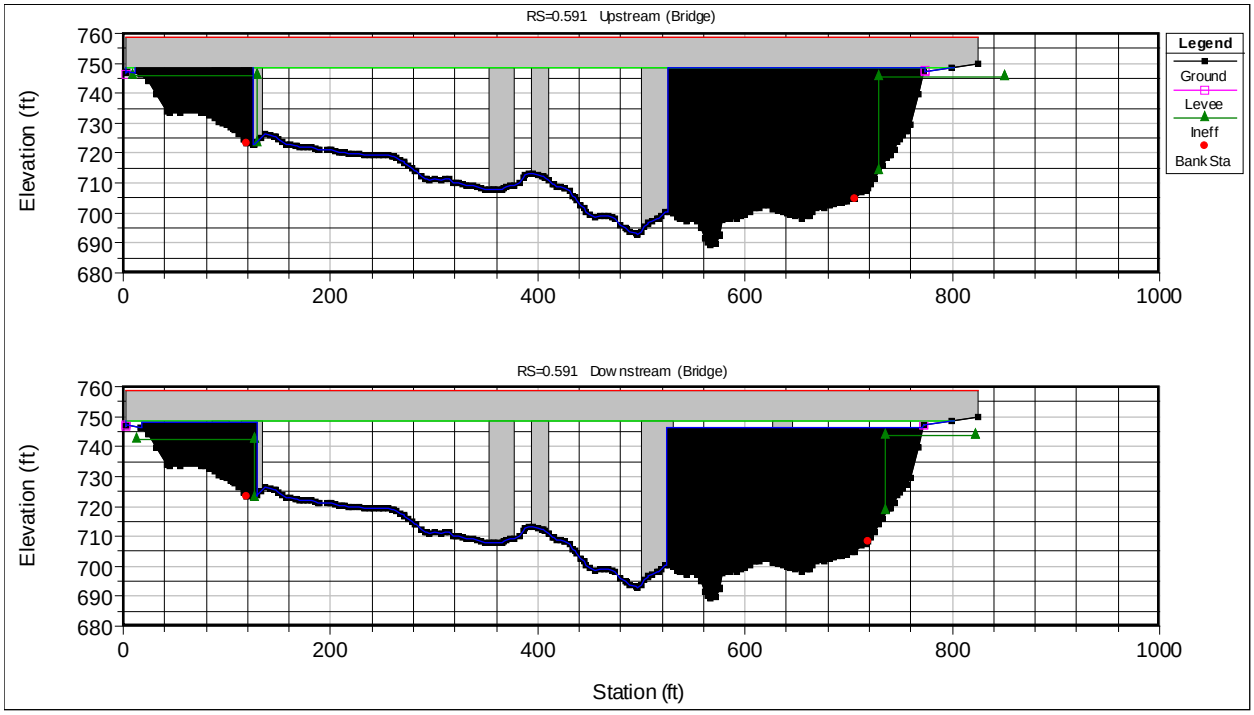


Figure 67. Simulated agressive debris blockage at the CPRR bridge Clearwater RM 0.6.

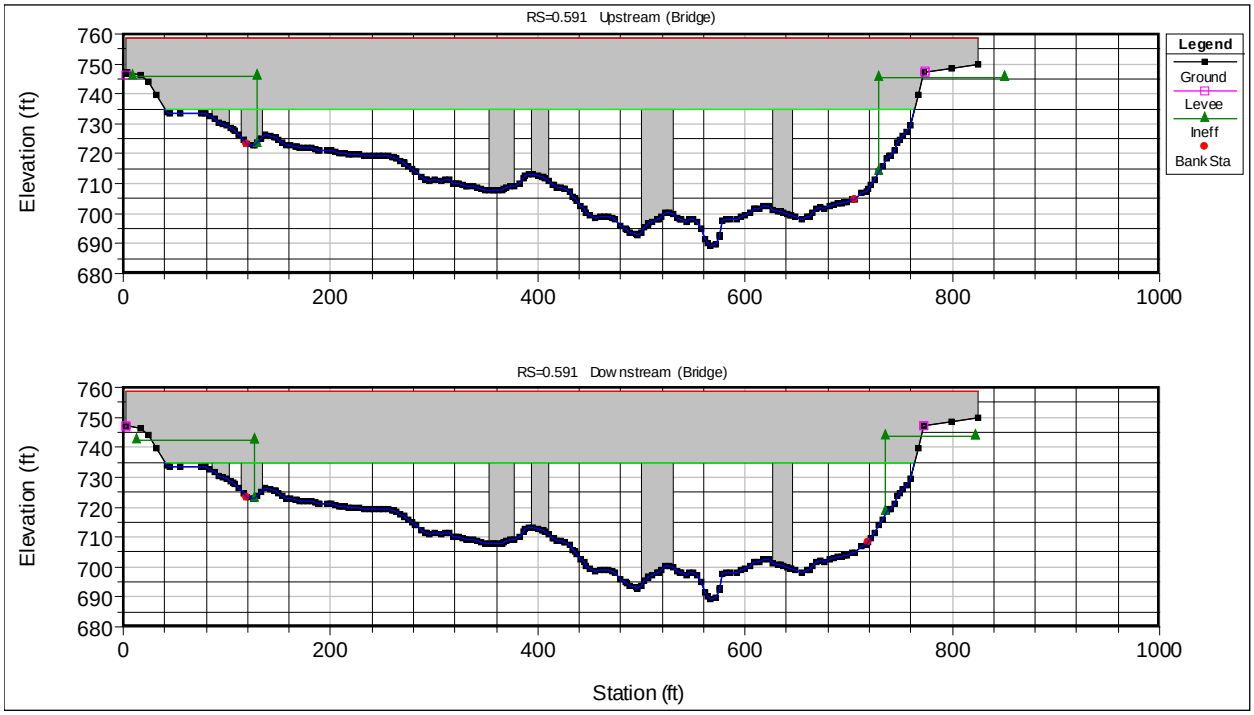


Figure 68. Simulated deck blockage at the CPRR bridge Clearwater RM 0.6.

5.13. SPF in the Flood Risk Analysis

It is important to recognize that the SPF does not enter directly into the computation of flood risk under current Corps guidance, which does not consider the SPF to be a valid project performance target, having been superseded by the risk-based guidance[73]. In part, this is because the magnitude of the SPF is determined by deterministic hydrologic modeling with a pre-selected fixed set of extraordinary watershed input conditions and not derived from a flood frequency analysis of stream gage records (or other probabilistic basis). Strictly speaking, the SPF has no firm probabilistic basis because parametric uncertainty is not (usually) included in its derivation. In a large watershed, there may be several equally valid sets of hydrologic data that produce an SPF of a given magnitude. The approximate exceedance frequency of an SPF may be inferred from a discharge frequency analysis of stream gage records, as was done in Section 2.7, but the SPF magnitude is a deterministic value that is defined directly by the hydrologic assumptions employed in its derivation. The SPF is best considered a flood scenario of the kind discussed by Morgan and Henrion[74]. Under current guidance, a full range of floods, including those that would exceed the SPF, is to be used in formulation and evaluation of alternatives.

Engineering Regulation 1105-2-101 acknowledges that the SPF is defined in legacy regulations and guidance documents. It is noted that in certain regions of the United States, there is a significant history of projects that were planned, designed and constructed based on the SPF, and strong local identification with the concept continues to be prevalent. As a consequence, while current guidance on project formulation and selection governs, the SPF may have a useful role for application in risk analysis, for comparing new project proposals with nearby existing projects that were based on the SPF, and as a check and validation of floods computed from statistical frequency analysis. This is the approach taken in this report.

[73] USACE (2006). ER 1105-2-101 *Risk Analysis for Flood Damage Reduction Studies*, U.S. Army Corps of Engineers, Washington, DC.

[74] Morgan, G., and Henrion, M. (1990). *Uncertainty, a Guide to Dealing with Uncertainty in Quantitative Risk and Policy Analysis*. Cambridge University Press, New York, NY.

5.14. Summary of the Risk Analysis of Current Condition

This section described the FDA flood risk analysis for the current channel condition based on the one-dimensional HEC-RAS 2009 fixed-bed model with no channel modifications. This channel condition is important because it defines the current level of overtopping risk at the Lewiston levee system. It was shown that the probabilistic risk analysis as currently implemented by the HEC-FDA software cannot directly evaluate all the important elements that affect flood risk at the Lewiston levees. Site specific conditions including bed dynamics at high discharge, joining of the tributary flows and potential misoperation of the spillway cannot be directly incorporated into the analysis. Conservative approximate methods were applied to overcome the limitations. The final results show a high level of assurance and low long-term risk for the existing channel condition. Overall, the conclusion that may be made from the risk analysis of current condition is that the conditional non-exceedance values listed in Table 33 and Table 34 are very high, even for the 0.2 percent annual chance exceedance flood. The Lewiston levee system currently exceeds the minimum requirements for levee system evaluation under the National Flood Insurance Program. Immediate drastic measures, such as raising the levees in Lewiston or massive dredging of the confluence area to recover conveyance, are not warranted based on the current level of flood risk. However, the flood risk is not fixed and will increase with future sediment accumulation during the 50-year planning period.

5.15. Flood Risk Analysis of Future Channel Conditions and Channel Modification Alternatives

Sediment dynamics were not incorporated directly in the above flood risk analysis of current conditions except as represented by varying the hydraulic roughness (Manning's *n*) in the hydraulic model. Short-term, the most important aspect of sediment movement is its effect on the hydraulic resistance of the reservoir and river channels. Long-term, sediment deposition and scour alters the conveyance throughout the system. The effect of sediment on hydraulic resistance was implicit in the fixed-bed model calibration of Manning's *n* for the high discharge event of 8 June 2010. It is evident from the historical sediment ranges and sediment load measurements that events such as that on 8 June 2010 transport substantial amounts of sediment into the reservoir. Sediment was being transported at a relatively high rate as bedload during the calibration event and roughness due to bed forms influenced the water surface that was the basis for calibration. The sediment dynamics alter channel hydraulic roughness as flows increase to the extreme discharges adopted in the flood risk analysis.

In the analysis of current conditions, the effect of prior sediment accumulation is integrated into the HEC-RAS model used for the FDA analysis because the model geometry was developed from the recent surveyed channel cross sections and high-

resolution bathymetry. The 2009 cross sections and multibeam echosounding bathymetry are a good representation of the near-term channel geometry because the amount of sediment transported into the reservoir in a single year would not substantially alter the conveyance of the channel system. Over the 50-year planning period, sediment will continue to accumulate so that the current model geometry no longer provides a valid representation of the hydraulic performance of the levee system. To define the future hydraulic condition of the levee system, the sediment impacts must be predicted through sediment load estimation and sediment transport modeling. Following sections describe the methods of estimating of future sediment load and the sediment transport modeling that define the future channel geometry and hydraulic resistance. After describing the basis for prediction of the future channel change, the flood risk analysis is extended in Section 11 to the future channel condition which includes proposed channel modifications (spur dikes) that help manage sediment accumulation near the confluence.

6. Potential Inundation Area of the Lewiston Levee System

The previous sections showed a low risk that floodwaters would overtop the levees in Lewiston under current channel conditions. Flooding behind the levees can also be caused by structural failure of the levee embankment. If overtopping or breaching were to occur, large areas of the central business district in Lewiston and in the Port of Lewiston would be flooded. To better recognize the impact of flooding behind the levees, potential inundation areas caused by breaching of the Snake and Clearwater River were mapped with a terrain elevation grid derived from the 2010 LiDAR data. Figure 69 through Figure 72 show the inundation depths during the peak of the SPF for areas behind the levees in Lewiston and North Lewiston.

6.1. Potential Inundation of Lewiston South of the Clearwater River

The SPF water surface profile on the Clearwater River drops about 7 feet between RM 3.85 and RM 0.28. Since the left bank levee on the Clearwater River is continuous, a breach at the upper end of the levee system would flood the entire interior area. If a breach occurs at the upstream end of the left levee at RM 3.7 (Figure 69), the water surface elevation of the inundation is determined by the SPF water surface elevation in the channel, which is 748.4 ft at that point. This elevation is high enough that flood waters admitted by the breach will pass through downtown Lewiston and overtop the Snake River levee from the interior side. Average water depth in the flooded area is about 9.8 ft and the total flood area is 533 ac of the business and

residential area of downtown Lewiston. In an emergency, flooding caused by a breach in the upper left bank levee might be contained by construction of a temporary flood barrier near Memorial Bridge where the width of the flooded area narrows to less than 200 feet and the flood water is less than 5 feet deep.

A breach in the lower segment of the left bank levee will only flood the area downstream of Memorial Bridge during the SPF (and lesser floods). Figure 70 shows the inundation surface that would occur if the levee was breached at the upper end of the toe drain at RM 1.9 where the SPF water surface elevation is 742.8 ft. Average water depth in the flooded area is about 7.5 ft and the total flood area is 360 ac. It may be possible to contain floodwaters from a breach in the levee above the CPRR Bridge by raising a temporary flood barrier at both ends of the railroad embankment that passes through downtown Lewiston. The top of the railroad embankment is several feet above the flood water surface along a substantial length of its alignment.

6.2. Potential Inundation of Lewiston North of the Clearwater River

In North Lewiston, a breach in the upper right bank levee segment at RM 3.1 during the SPF would flood the interior area to an elevation of 745.5 ft. Total flooded area in Figure 71 is 336 ac and the average flood depth is 7.6 ft. The embankment of the approach to Memorial Bridge on U.S. Highway 12 is higher than adjacent terrain and may provide an alignment for a temporary flood barrier to isolate floodwaters caused by a breach in the upper levee.

A breach in the lower right bank levee segment in North Lewiston during the SPF, shown in Figure 72, would flood a 290 ac area to an average depth of 4.8 ft. The approach to Memorial Bridge might afford an opportunity to isolate floodwaters originating in a breach in the lower levee segment from flooding North Lewiston to the east of U.S. Highway 12.

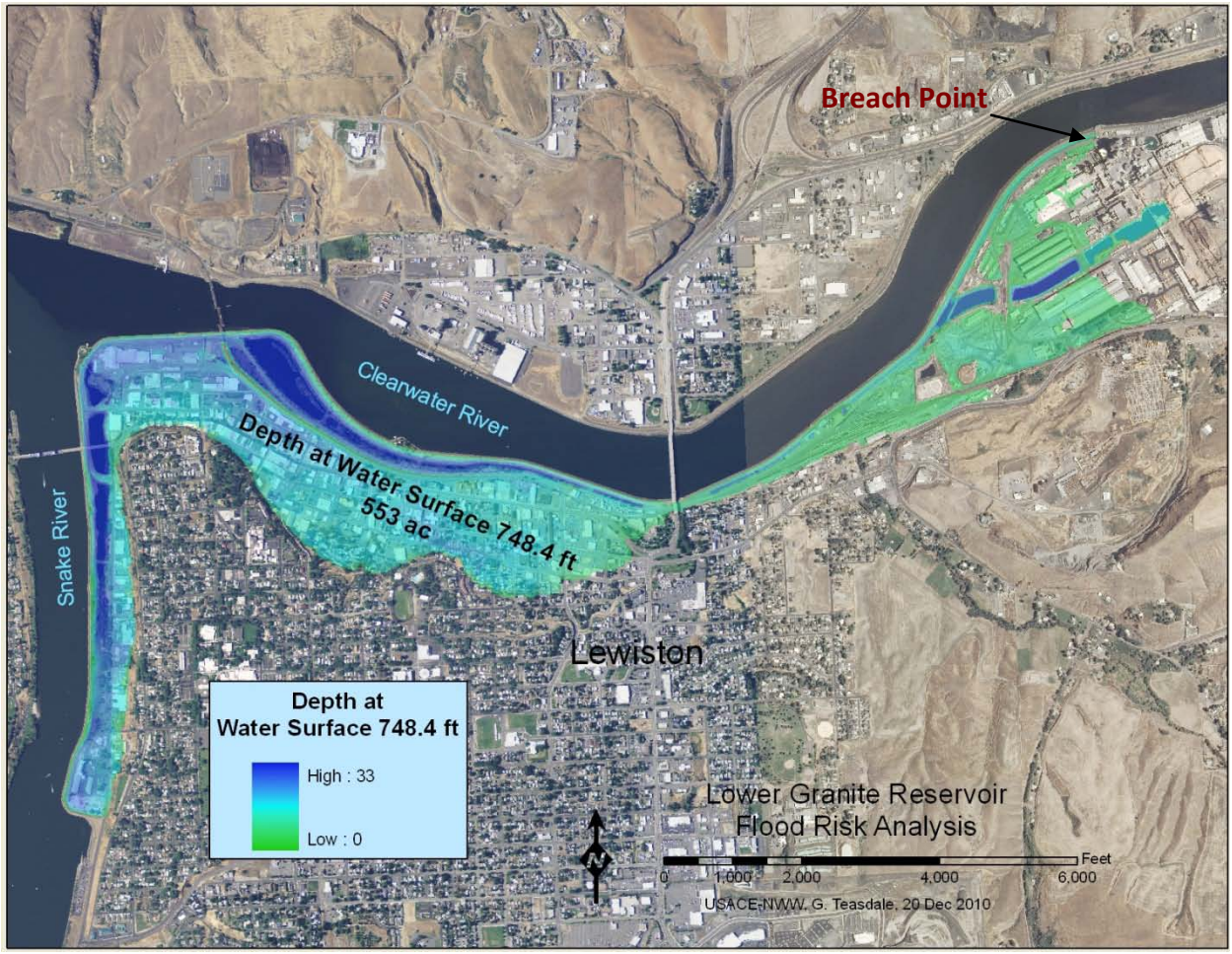


Figure 69. Inundation surface for breach of left bank levee at RM 3.7 at peak of SPF.

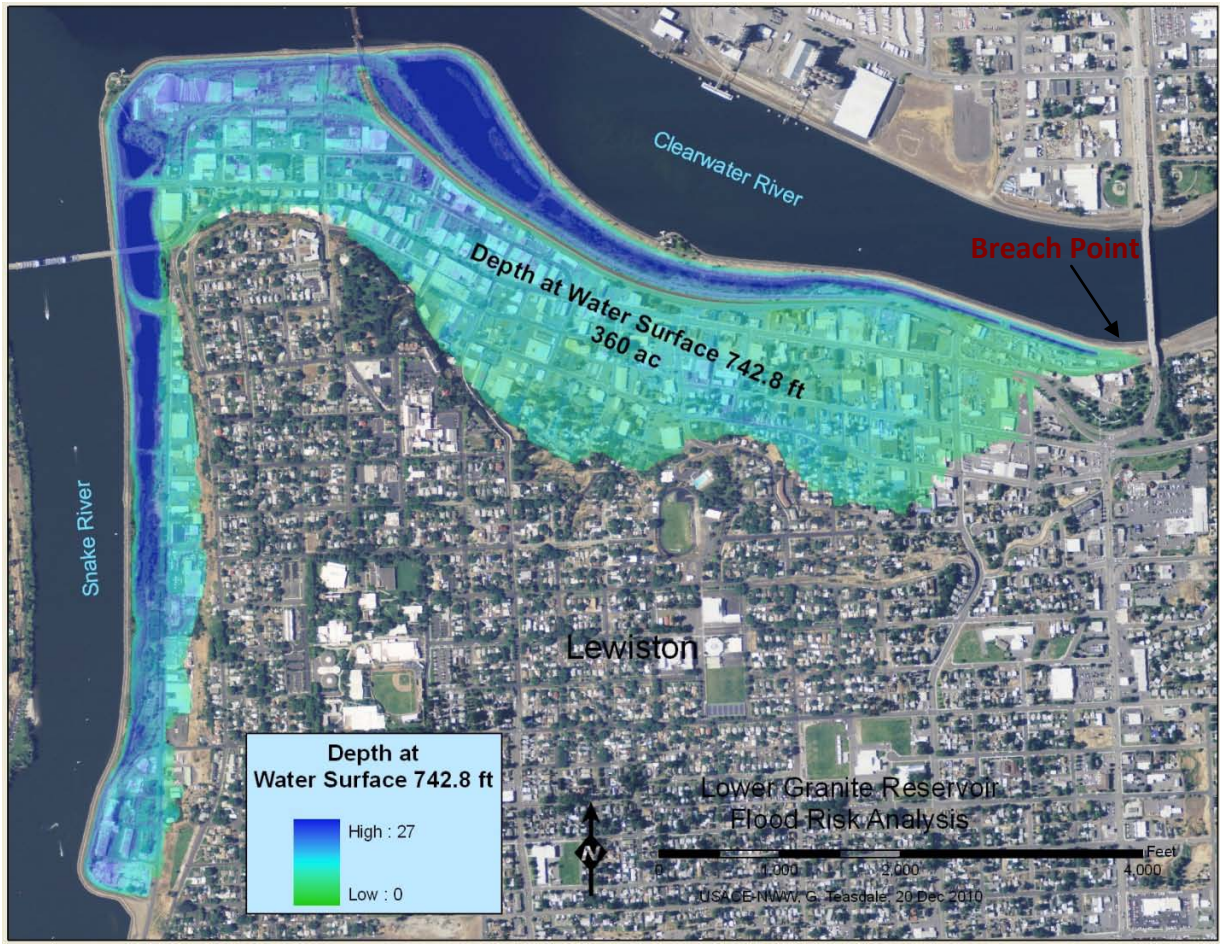


Figure 70. Inundation surface for breach of left bank levee at RM 1.9 at peak of SPF.

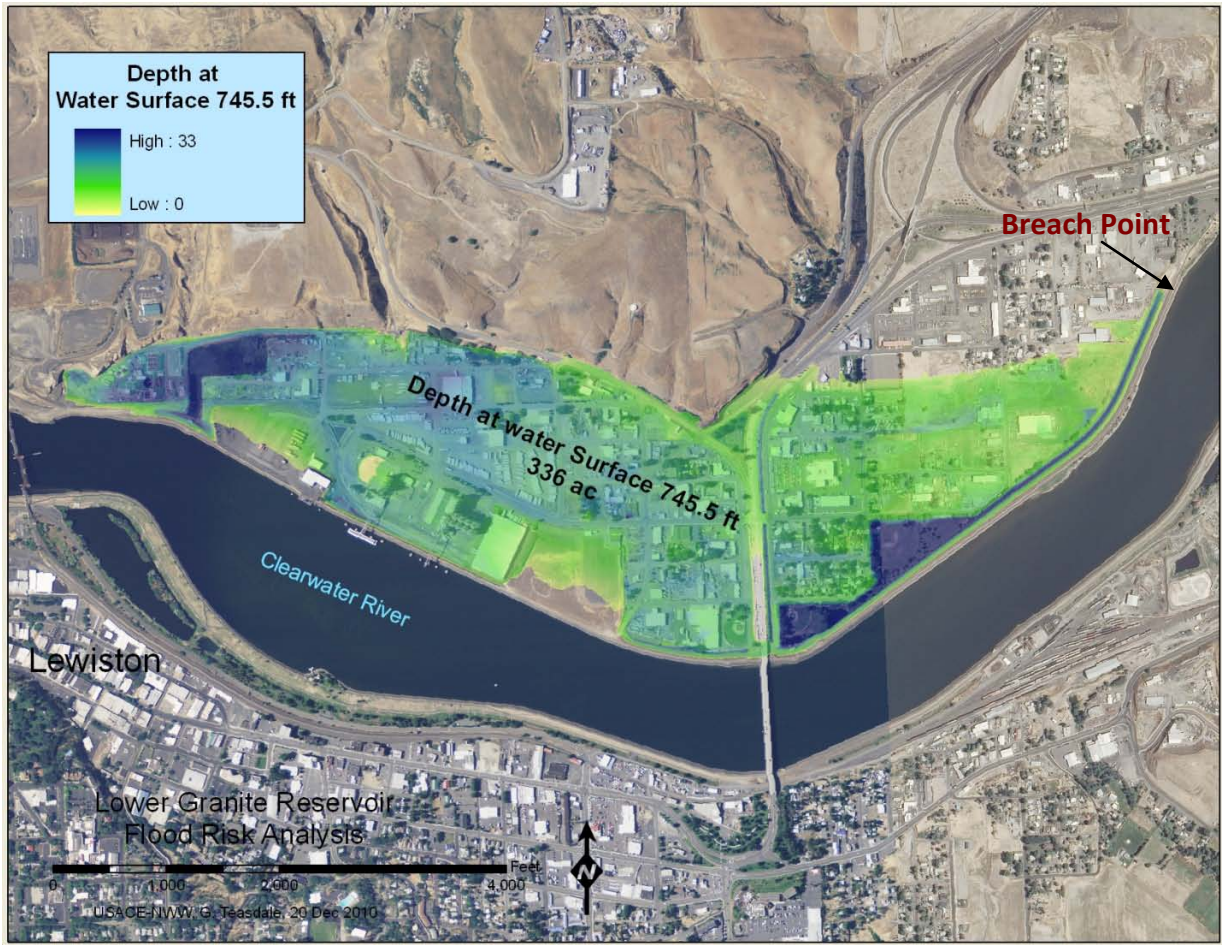


Figure 71. Inundation surface for breach of right bank levee at RM 3.1 at peak of SPF.

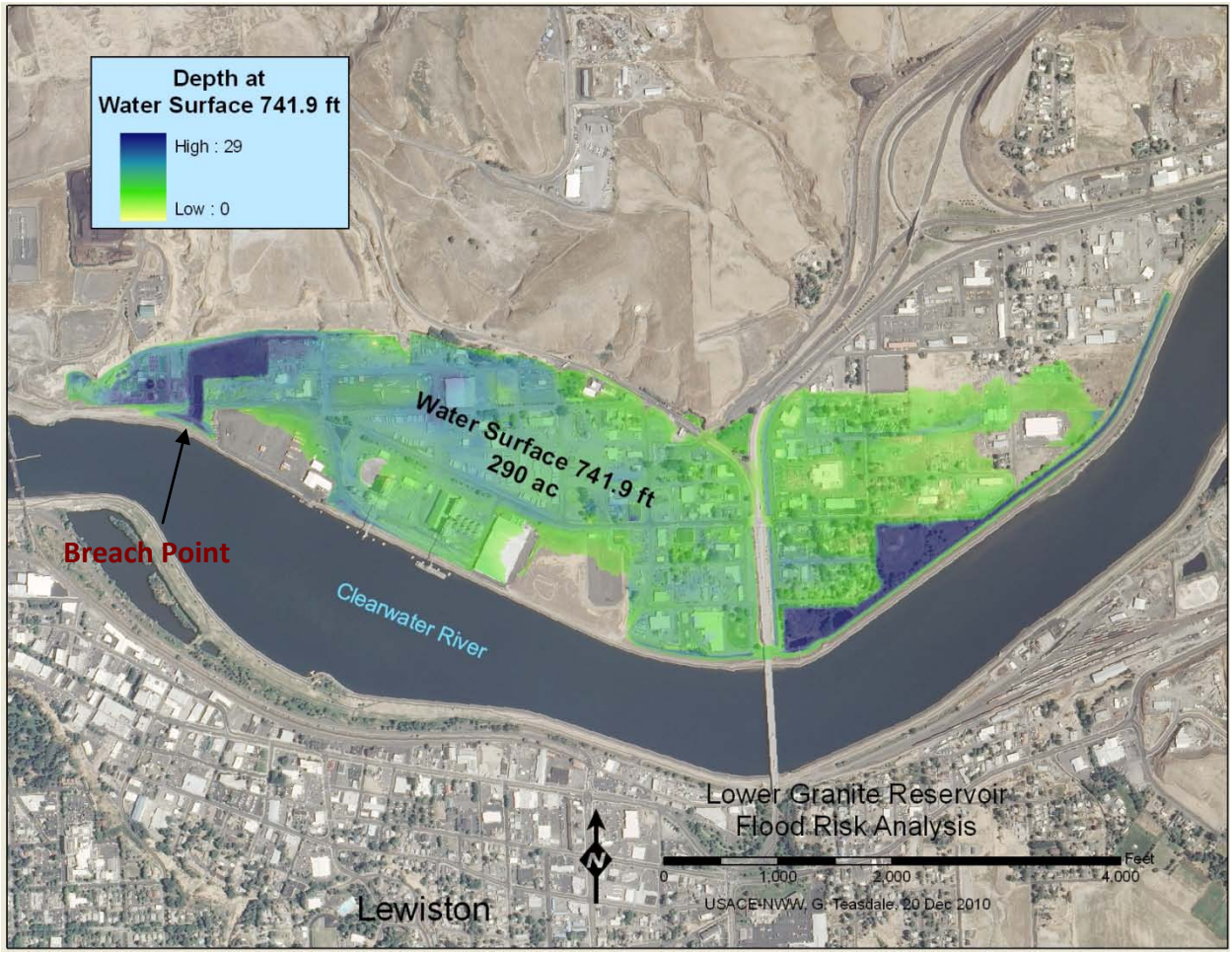


Figure 72. Inundation surface for breach of right bank levee at RM 0.9 at peak of SPF.

7. Lower Granite Reservoir Sedimentation

Sediment carried by the Snake and Clearwater Rivers deposits upon reaching the backwater of Lower Granite Dam causing the water surface elevation to rise as sediment accumulates on the bed of the reservoir and tributary channels. Historical sediment ranges in Lower Granite Reservoir record the timing, amount and distribution of sediment deposition since the pool was raised. Information derived from sediment ranges include sediment accumulation estimated by the difference in sediment ranges surveyed at different times, operational life of the reservoir estimated from the rate of sediment accumulation, and watershed sediment yield computed from the change in reservoir sediment volume. This section discusses the analysis of the sediment ranges of the Snake and Clearwater Rivers in Lower Granite Reservoir and characterization of reservoir sedimentation.

7.1. Sediment Ranges

Riverine sediment ranges are linear referenced or georeferenced elevation transects of the channel bed that cross perpendicular to the average direction of flow. Sediment ranges serve a dual purpose of monitoring change in bed elevation and providing cross section geometry for hydraulic modeling. Sediment range surveys are intended to be repeatable. The endpoints of sediment ranges are permanently marked with survey monuments so that bed elevation measurements can be acquired at the same location in subsequent surveys.

Sediment ranges are located throughout Lower Granite reservoir (Figure 41) and have been measured on a cycle of two to three years since the pool was filled in February 1975. There are a total of 66 sediment ranges between Lower Granite Dam at River Mile (RM) 107.73 to RM 148.83 on the Snake River above Asotin, WA, and 33 sediment ranges on the Clearwater from the confluence to RM 7.85. Sediment ranges near confluence of the Clearwater and Snake Rivers are spaced close together to give a good record of sediment accumulation and changes in channel geometry (Figure 74). Sediment ranges are positioned above the M1 profile (backwater) zone of Lower Granite Dam on both the rivers so that the condition of the inflow channels can be monitored. At the SPF discharge, backwater extends to about Snake RM 146.3 near Asotin and about Clearwater RM 3.9 near the paper mill in Lewiston.

Sediment ranges were surveyed in 1974, 1976, 1977, 1979, 1982, 1983, 1984, 1985, 1986, 1987, 1989, 1992, 1995, 1997, 2000, 2003, 2006, 2008, 2009, and 2010. The number of sediment ranges surveyed in a given year varied depending on funding and project requirements. Sediment range acquisitions for the Snake and Clearwater

are listed in Table 38 and Table 39. The most recent synoptic set of sediment ranges at the time of this analysis was acquired in 2009[75]. A partial set of sediment ranges near the confluence were surveyed in the autumn of 2010 and the remaining sediment ranges were surveyed in January 2011. The 2010 and 2011 sediment ranges are not completely synoptic because a moderate discharge event occurred in December 2010 that likely brought some sediment into the upper reaches of the reservoir. The 2010 and 2011 sediment ranges were not used in hydraulic modeling for the risk analysis because the 2009 high-resolution bathymetry provides greater detail and its accuracy was validated with the 2009 sediment ranges. Also, the surveys in 2010 and 2011 were acquired with somewhat different equipment and methods than previous years and have not yet been fully evaluated. Nevertheless, the 2010 and 2011 sediment ranges were used to update sediment accumulation volumes.

Prior to 1992, sediment ranges for Lower Granite Reservoir were developed and archived in station-elevation (GR) format. Later sediment range data is ascii-xyz (northing, easting, elevation) format. Sediment ranges prior to 2008 are projected to NAD1927 State Plane Washington South (FIPS_4602), NGVD 29 in units of U.S. Survey feet. Beginning in 2008, sediment range data is projected to NAD1983 State Plane Washington South (FIPS 4602), NAVD 88 in units of U.S. Survey feet. The difference is vertical datums is important because, for instance, at the confluence NAVD 88 elevations are 3.24 feet higher than the NGVD29 datum.

Sediment ranges are currently measured with acoustic methods that meet or exceed the accuracy standards and procedures specified in the Corps hydrographic surveying manual[76]. The performance standards require at least a 95 percent root-mean-square (RMS) of 0.5 feet for depths less than 15 feet, 1.0 ft RMS in depths up to 40 feet, and 2.0 ft RMS for depths greater than 40 feet. Accuracy reported at the 95 percent confidence level means that 95 percent of the elevations in the dataset will have an error with respect to true ground elevation that is equal to or smaller than the reported value. Manual soundings in near shore areas must have accuracies greater than 0.1 foot. Positions are logged by kinematic GPS survey that is tied to a network of bench marks established by the Corps. Elevation data was processed by the contractor with Hypack 2009. Performance requirements and data formats are detailed in the District project specifications for sediment range surveys. It is difficult to judge the absolute accuracy of earlier sediment range data, though unpublished analysis and file notes suggest the accuracy is likely between 0.5 feet and 1 foot.

[75] RSI (2009). *Lower Granite Sediment Range Survey*, Contract No. W912EF-08-D-0011, Task Order No. 16, Surveying, Inc, Sept 2009.

[76] USACE (2002). *EM 1110-2-1003 Hydrographic Surveying*, U.S. Army Corps of Engineers, Washington, DC.

Horizontal positions of surveyed sediment range elevation points depart to some extent from the transect line, as in Figure 75. Survey tracks that depart more than about 10 feet from the sediment range line are resurveyed. In subsequent processing, surveyed points are rectified (cosine corrected) to the straight alignment of the range line during conversion to station-elevation format to eliminate errors in the computation of range distance and cross section area. Rectified sediment range data was used in the hydraulic modeling and accumulation volume computations.

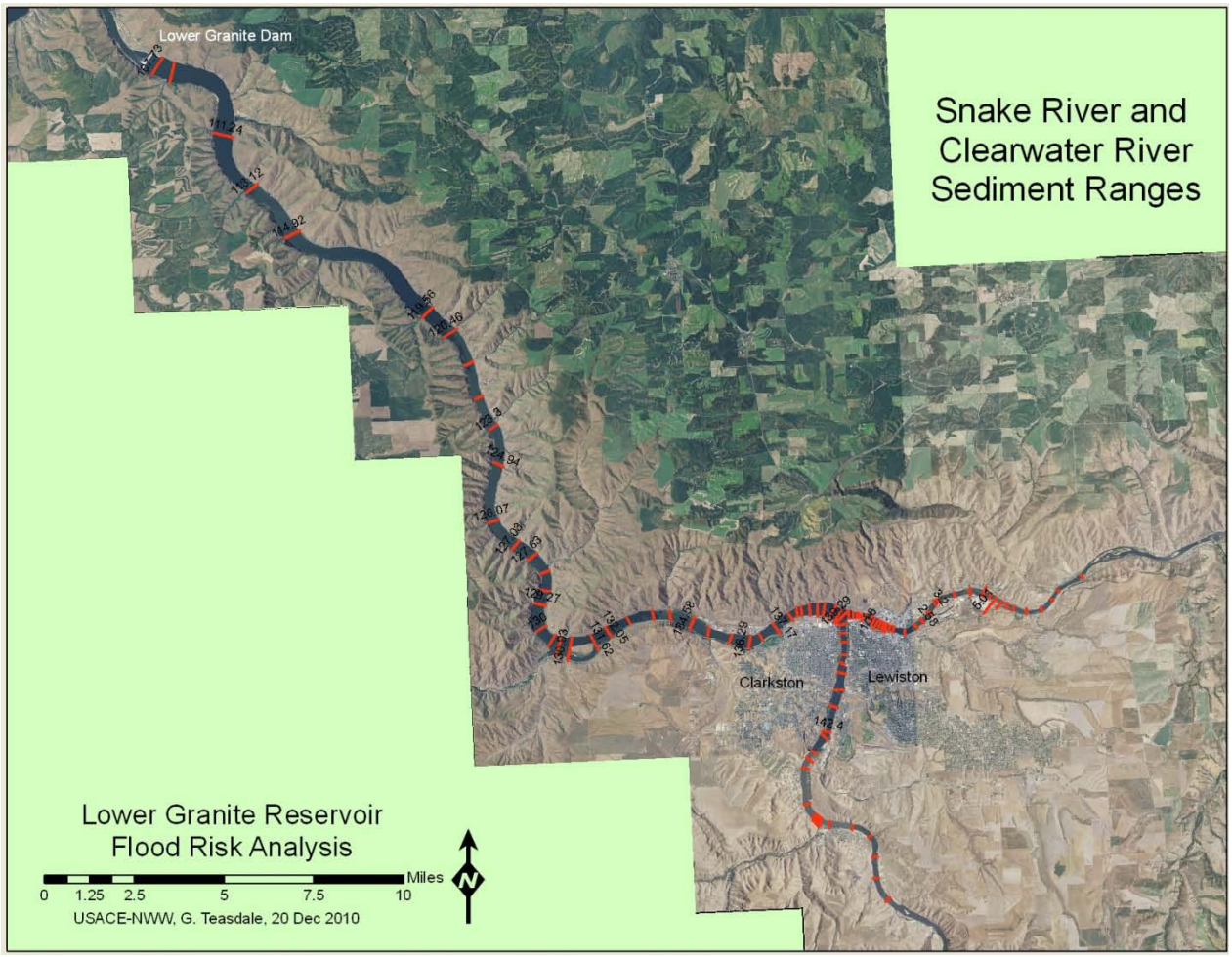


Figure 73. Sediment range locations in Lower Granite Reservoir.

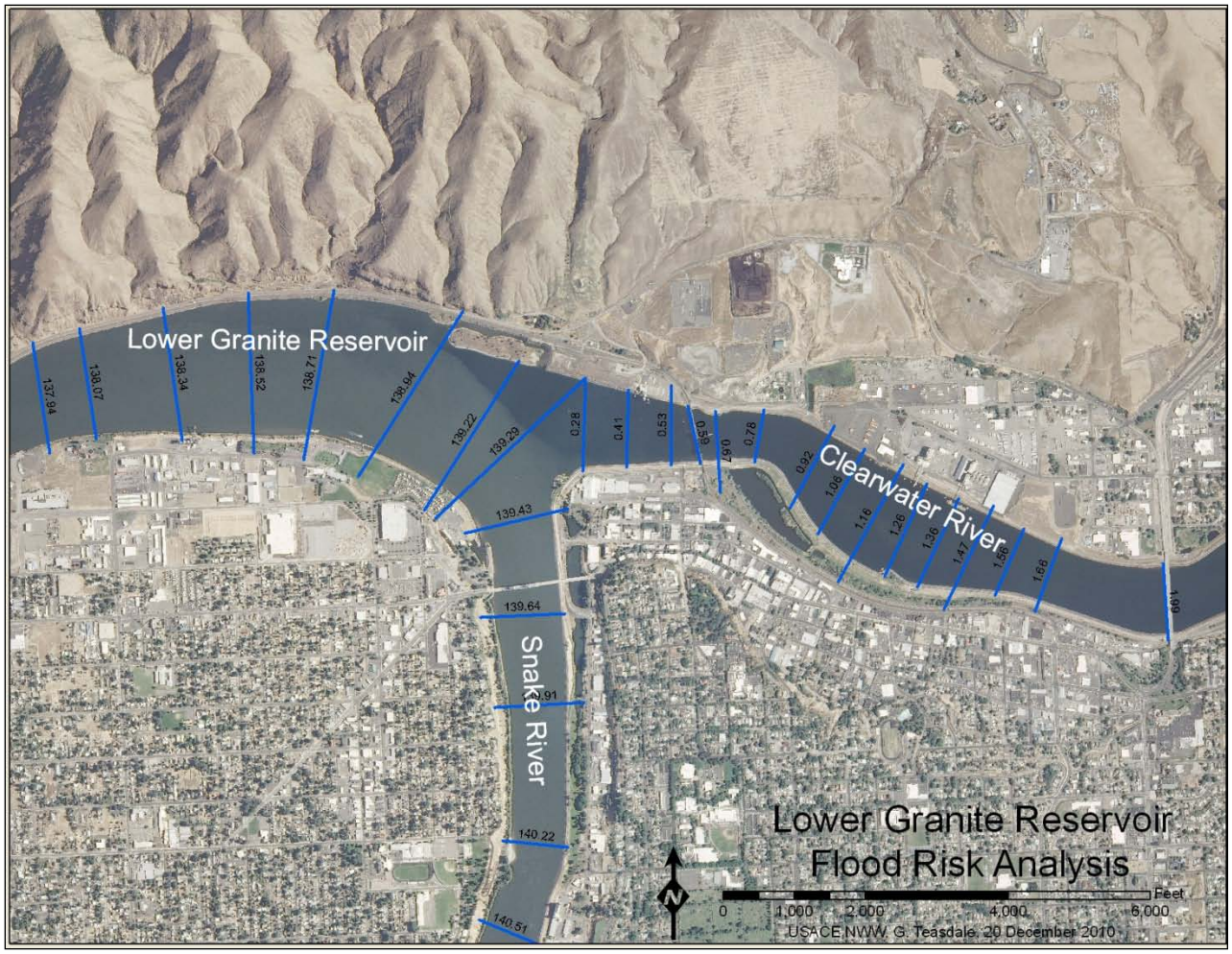


Figure 74. Sediment range cross sections near the confluence.

Lower Granite Reservoir Sediment Ranges: Snake River																					
Sediment	x signifies that the sediment range was surveyed in a the given year																				
Range	1974	1976	1977	1979	1982	1983	1984	1985	1986	1987	1989	1992	1995	1997	2000	2003	2006	2008	2009	2010	2011
107.73	x	x	x	x	x	x	x	x	x	x	x	x	x	x	x	x	x	x	x		x
108.31	x	x	x	x	x	x	x	x	x	x	x	x	x	x	x	x	x	x	x		x
111.24	x	x	x	x	x	x	x	x		x	x	x	x	x	x	x	x	x	x		x
113.12	x	x	x	x	x	x	x	x	x	x	x	x	x	x	x	x	x	x	x		x
114.92	x	x	x	x	x	x	x	x	x	x	x	x	x	x	x	x	x	x	x		x
119.56	x	x	x	x	x	x	x	x	x	x	x	x	x	x	x	x	x	x	x		x
120.46	x	x	x	x	x	x	x	x	x	x	x	x	x	x	x	x	x	x	x		x
121.42							x	x	x	x	x	x	x	x	x	x	x	x	x		x
122.69	x	x	x	x	x	x	x	x	x	x	x	x	x	x	x	x	x	x	x		x
123.30							x	x	x	x	x	x	x	x	x	x	x	x	x		x
124.94	x	x	x	x	x	x	x	x	x	x	x	x	x	x	x	x	x	x	x		x
126.07							x	x	x	x	x	x	x	x	x	x	x	x	x		x
127.03	x	x	x	x	x	x	x	x	x	x	x	x	x	x	x	x	x	x	x		x
127.63							x	x	x	x	x	x	x	x	x	x	x	x	x		x
128.27							x	x	x	x	x	x	x	x	x	x	x	x	x		x
128.87	x	x	x	x	x	x	x	x	x	x	x	x	x	x	x	x	x	x	x		x
129.27							x	x	x	x	x	x	x	x	x	x	x	x	x		x
130.00							x	x	x	x	x	x	x	x	x	x	x	x	x	x	
130.44	x	x	x	x	x	x	x	x	x	x	x	x	x	x	x	x	x	x	x	x	
130.66	x	x	x	x	x	x	x	x	x	x	x	x	x	x	x	x	x	x	x	x	
130.93	x	x	x	x	x	x	x	x	x	x	x	x	x	x	x	x	x	x	x	x	
131.62	x	x	x	x	x	x	x	x	x	x	x	x	x	x	x	x	x	x	x	x	
132.05							x	x	x	x	x	x	x	x	x	x	x	x	x	x	
132.71							x	x	x	x	x	x	x	x	x	x	x	x	x	x	
133.41							x	x	x	x	x	x	x	x	x	x	x	x	x	x	
133.98							x	x	x	x	x	x	x	x	x	x	x	x	x	x	
134.58							x	x	x	x	x	x	x	x	x	x	x	x	x	x	
135.15	x	x	x	x	x	x	x	x	x	x	x	x	x	x	x	x	x	x	x	x	
135.76							x	x	x	x	x	x	x	x	x	x	x	x	x	x	
136.29	x	x	x	x	x	x	x	x	x	x	x	x	x	x	x	x	x	x	x	x	
136.69							x	x	x	x	x	x	x	x	x	x	x	x	x	x	
137.17	x	x	x	x	x	x	x	x	x	x	x	x	x	x	x	x	x	x	x	x	
137.69							x	x	x		x		x	x	x	x	x	x	x	x	
137.94							x	x	x		x		x	x	x	x	x	x	x	x	
138.07							x	x	x		x		x	x	x	x	x	x	x	x	
138.34	x	x	x	x	x	x	x	x	x		x		x	x	x	x	x	x	x	x	
138.52							x	x	x		x		x	x	x	x	x	x	x	x	
138.71							x	x	x		x		x	x	x	x	x	x	x	x	
138.94							x	x	x		x		x	x	x	x	x	x	x	x	
139.22	x	x	x	x	x	x	x	x	x		x		x	x	x	x	x	x	x	x	
139.29							x	x	x		x		x	x	x	x	x	x	x	x	
139.43	x	x	x	x	x	x	x	x	x		x		x	x	x	x	x	x	x	x	
139.64							x	x	x		x		x	x	x	x	x	x	x	x	
139.91	x	x	x	x	x	x	x	x	x		x		x	x	x	x	x	x	x	x	
140.22	x	x	x	x	x	x	x	x	x		x	x	x	x	x	x	x	x	x	x	
140.51	x	x	x	x	x	x	x	x	x		x	x	x	x	x	x	x	x	x	x	
140.75	x	x	x	x	x	x	x	x	x		x	x	x	x	x	x	x	x	x	x	
141.21	x	x	x	x	x	x	x	x	x		x	x	x	x	x	x	x	x	x	x	
141.78	x	x	x	x	x	x	x	x	x		x	x	x	x	x	x	x	x	x	x	
142.40	x	x	x	x	x	x	x	x	x		x	x		x	x	x	x	x	x	x	
142.57	x	x	x	x	x	x	x	x	x		x	x		x	x	x	x	x	x	x	
143.14	x	x	x	x	x	x	x	x	x		x	x		x	x	x	x	x	x	x	
143.31	x	x	x	x	x	x	x	x	x		x	x		x	x	x	x	x	x	x	
143.69	x	x	x	x	x	x	x				x	x		x	x	x	x	x	x	x	
144.73	x	x	x	x	x	x	x				x	x		x	x	x	x	x	x	x	
145.15	x	x	x	x	x	x	x				x	x		x	x	x	x	x	x	x	
145.22	x	x	x	x	x	x	x				x	x		x	x	x	x	x	x	x	
145.27	x	x	x	x	x	x	x				x	x		x	x	x	x	x	x	x	
145.31	x	x	x	x	x	x	x				x	x		x	x	x	x	x	x	x	
146.33	x	x	x	x	x	x	x				x	x		x	x	x	x	x	x	x	
145.38	x	x	x	x	x	x	x				x	x		x	x	x	x	x	x	x	
145.61	x	x	x	x	x	x	x				x	x		x	x	x	x	x	x	x	
146.87	x	x	x	x	x	x	x				x			x	x	x	x	x	x		x
147.47	x	x	x	x	x	x	x							x	x	x	x	x	x		x
148.09	x	x	x	x	x	x	x							x	x	x	x	x	x		x
148.83	x	x	x	x	x	x	x							x	x	x	x	x	x		x

Table 38. Sediment range acquisitions, Snake River at Lower Granite Reservoir.

Lower Granite Reservoir Sediment Ranges: Clearwater River																					
Sediment Range	x signifies that the sediment range was surveyed in a the given year																				
	1974	1976	1977	1979	1982	1983	1984	1985	1986	1987	1989	1992	1995	1997	2000	2003	2006	2008	2009	2010	2011
0.28							x	x	x	x	x		x	x	x	x	x	x	x	x	
0.41								x	x	x	x		x	x	x	x	x	x	x	x	
0.53							x	x	x	x	x		x	x	x	x	x	x	x	x	
0.59								x	x		x		x	x	x	x	x	x	x	x	
0.67	x	x	x	x	x	x	x	x	x		x		x	x	x	x	x	x	x	x	
0.78	x	x	x	x	x	x	x	x	x		x		x	x	x	x	x	x	x	x	
0.92	x	x	x	x	x	x	x	x	x		x		x	x	x	x	x	x	x	x	
1.06								x	x		x	x	x	x	x	x	x	x	x	x	
1.16	x	x	x	x	x	x	x	x	x		x		x	x	x	x	x	x	x	x	
1.26								x	x		x	x	x	x	x	x	x	x	x	x	
1.36								x	x		x	x	x	x	x	x	x	x	x	x	
1.47	x	x	x	x	x	x	x	x	x		x		x	x	x	x	x	x	x	x	
1.56								x	x		x		x	x	x	x	x	x	x	x	
1.66	x	x	x	x	x	x	x	x	x		x		x	x	x	x	x	x	x	x	
1.99								x	x		x	x	x	x	x	x	x	x	x	x	
2.34	x	x	x	x	x	x	x	x	x			x			x	x	x	x	x		x
2.58	x	x	x	x	x	x	x					x			x	x	x	x	x		x
2.89	x	x	x	x	x	x	x					x			x	x	x	x	x		x
3.20	x	x	x	x	x	x	x					x			x	x	x	x	x		x
3.48	x	x	x	x	x	x	x					x			x	x	x	x	x		x
3.85	x	x	x	x	x	x	x					x			x	x	x	x	x		x
4.30	x	x	x	x	x	x	x					x			x	x	x	x	x		x
4.74	x	x	x	x	x	x	x								x	x	x	x	x		x
4.94	x	x	x	x	x	x	x								x			x	x		x
5.01	x	x	x	x	x	x	x								x	x	x	x	x		x
5.21	x	x	x	x	x	x	x								x	x	x	x	x		x
5.39	x	x	x	x	x	x	x								x	x	x	x	x		x
5.64	x	x	x	x	x	x	x								x	x		x	x		x
5.94	x	x	x	x	x	x	x								x	x		x	x		x
6.37	x	x	x	x	x		x								x	x		x	x		x
6.78	x	x	x	x	x	x	x								x	x		x	x		x
7.08	x	x	x	x	x	x	x								x	x		x	x		x
7.85	x	x	x	x	x	x	x								x	x		x	x		x

Table 39. Sediment range acquisitions, Clearwater River at Lower Granite Reservoir.

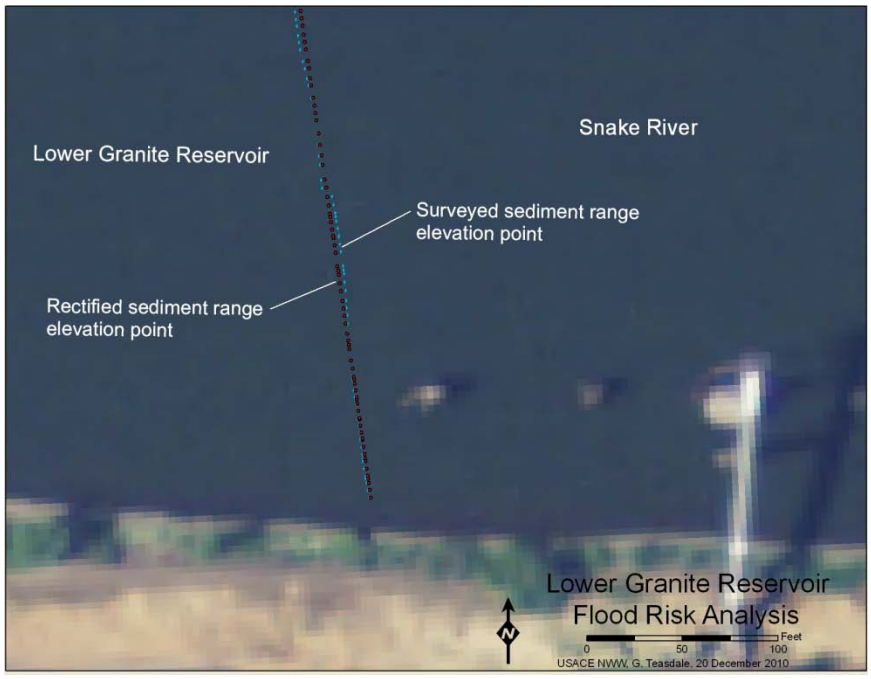


Figure 75. Rectification of sediment range elevation points.

7.2. Sediment Range Analysis

Changes in the bed of Lower Granite Reservoir are quantified by comparing the time sequence of sediment ranges. At-a-station hydraulic and sediment parameters were computed from the sediment range cross section data with custom Matlab scripts. Plots generated by the scripts, such as Figure 76 for the 1995 and 1997 sediment ranges at Clearwater RM 0.28, give a visual comparison of the cross sections and the values of the computed sediment parameters. Cross section plots in these figures are oriented facing downstream so that the left bank is on the left side of the figure. Sediment parameters include total deposition area, erosion area, net change area, average deposition depth, and average erosion depth.

The extent of the individual cross sections that were measured in near shore areas varied between surveys because of water level conditions and the presence of obstructions, so the computed change was limited to the mean active channel width as defined by the 2009 sediment ranges. Also, since it was desired to compute average erosion depths and deposition depth at each cross section, it was necessary to interpolate one of the sediment range cross sections to match the elevation point positions of the second cross section. Both operations were implemented in the script.

The visual plots can be evaluated qualitatively. The sediment range at RM 0.28 exhibits both deposition and erosion, a characteristic that is common to cross sections above Silcott Island. The average deposition depth of 4.6 feet across the left part of the section occurred during large runoff events in 1996 and 1997. On the right side of the section the thalweg of the Clearwater River has been further eroded since 1995, promoted in part by the colder and generally less turbid flow of the Clearwater River. In subsequent years, the cross section at RM 0.28 is more stable; Figure 77 shows only about 0.9 feet of deposition between 1997 and 2009. This is evidence that after initial filling, the cross section is tending towards a state of equilibrium with prevailing discharge and sediment load. Qualitative and quantitative evaluation of two dimensional bed changes in the sediment range plots helps corroborate the results of sediment transport modeling.

Some sediment ranges, such as at Snake RM 137.69 in Figure 78, are stable and have not changed much since 1974. Bedload moves through this reach as sand waves, leaving dunes of various heights expressed in the 2009 bathymetry after flows recede (Figure 79). This physical evidence demonstrates a dynamic equilibrium with the prevailing discharge and sediment regimes, which implies that the hydraulic parameters of this sediment range describe the attributes of a self-maintaining cross section at this location in the reservoir. Further validation is that the hydraulic properties of this section are similar to those predicted by the equilibrium hydraulic geometry relationship in Section 10.

Sediment ranges below Silcott Island are mostly depositional as the reservoir widens and deepens. Figure 80 shows that sediment accumulates on the inside of the bend at Sediment range Snake RM 123.3 while the outside of the bend is stable.

Sediment ranges in the gravel-bed segments of the Snake and Clearwater Rivers above the backwater zone, such as those in Figure 81 and Figure 82, show little change since 1976. This is evidence that gravel transport and deposition is a minor fraction of the total sediment load and has a negligible effect on the hydraulic capacity of the levee channels over the time frame adopted in the risk analysis.

An extensive set of sediment range plots similar to those above are included in the digital appendix to this report. Sediment parameters derived from the analysis of the time sequence of change at the sediment ranges provide the data needed to determine the amount and rate of sediment accumulation over the life of the reservoir, the results of which are presented below.

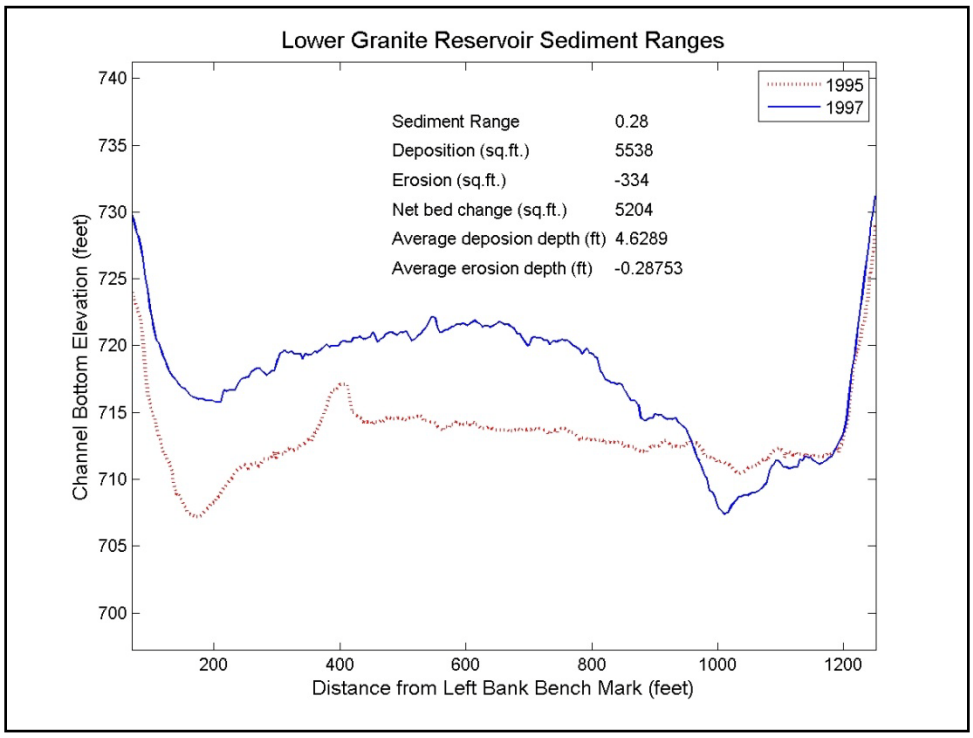


Figure 76. Comparison of 1995 and 1997 sediment ranges at Clearwater RM 0.28.

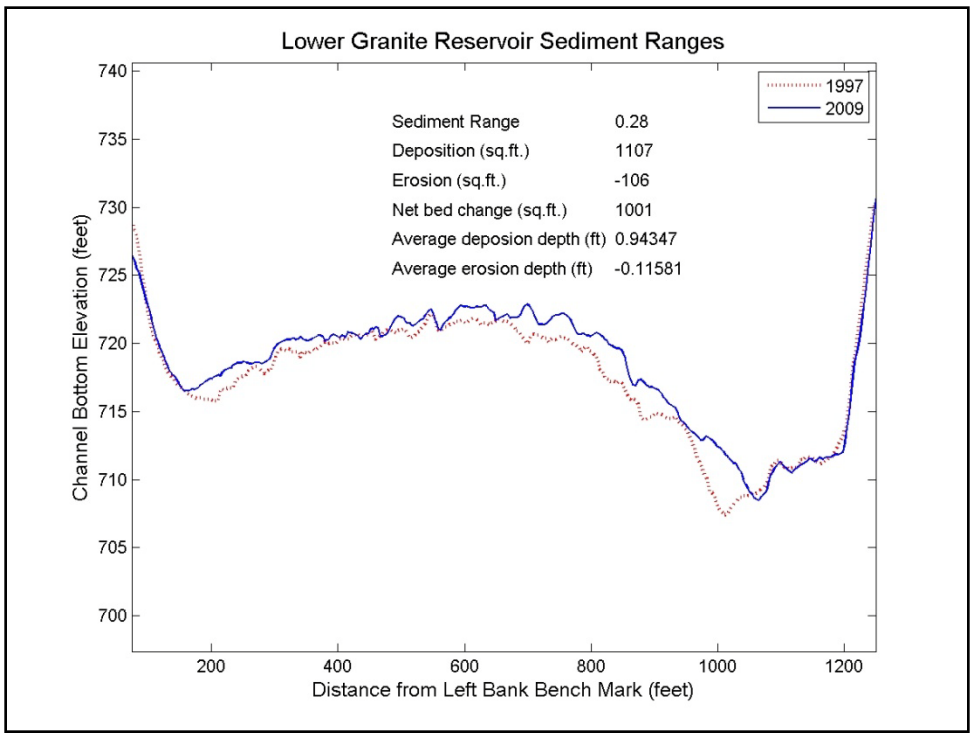


Figure 77. Comparison of 1997 and 2009 sediment ranges at Clearwater RM 0.28.

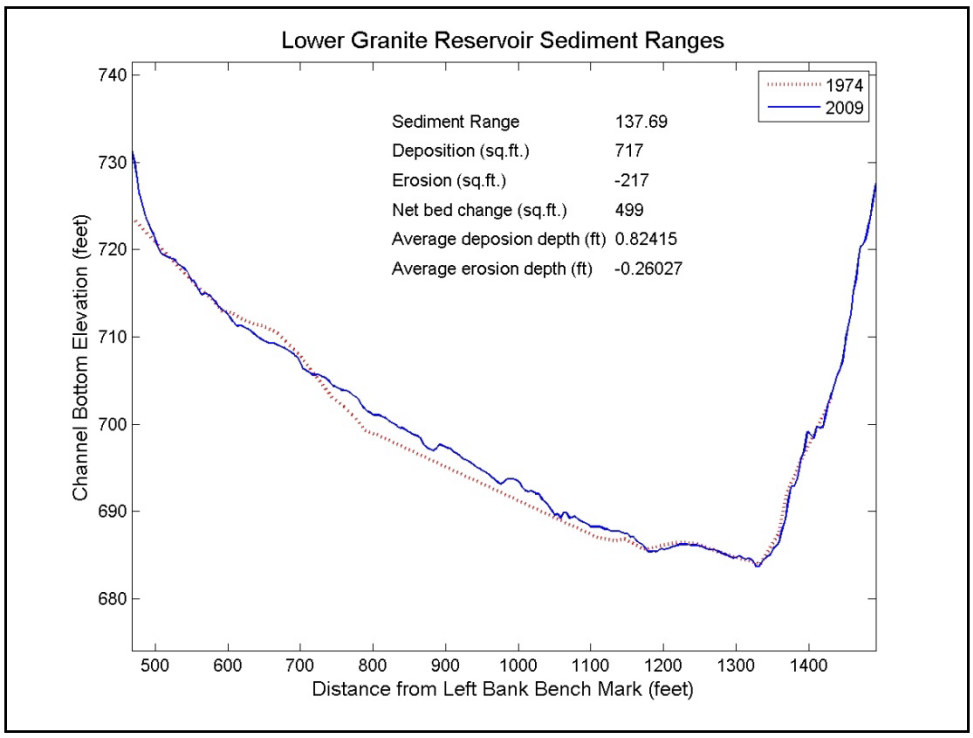


Figure 78. Comparison of 1974 and 2009 sediment ranges at Snake RM 137.69.

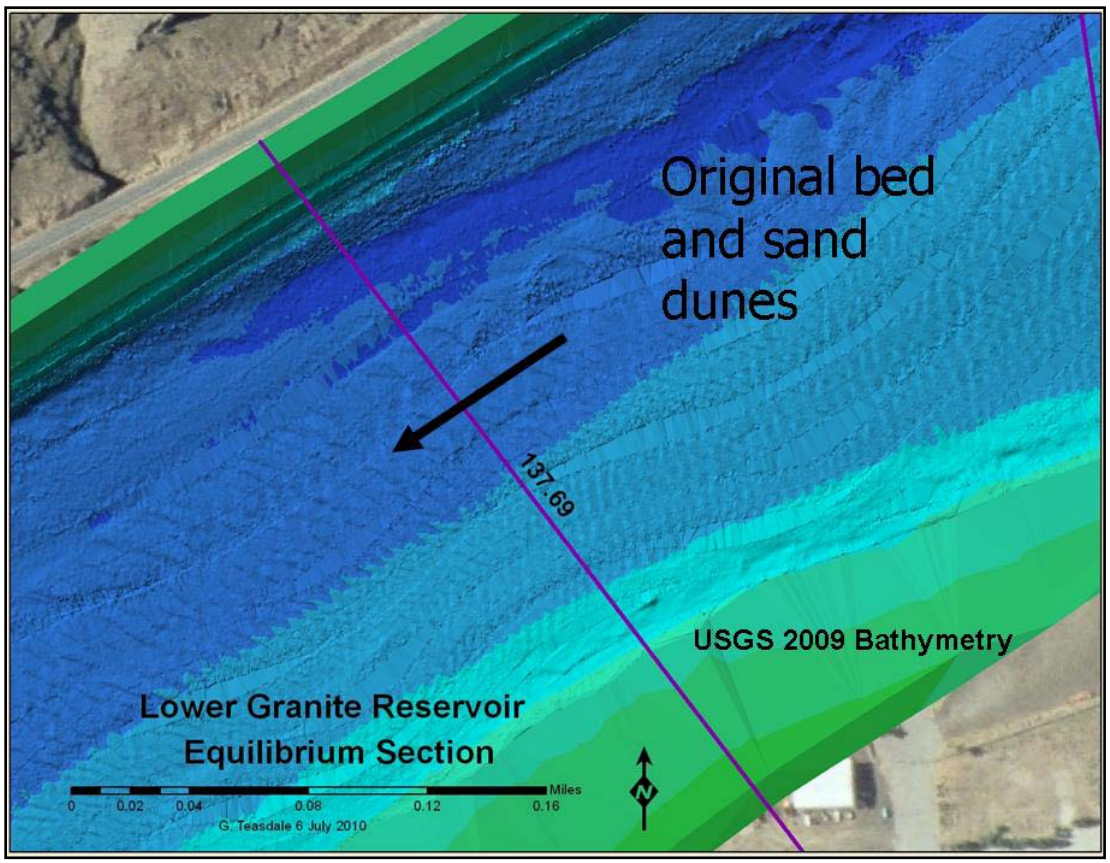


Figure 79. Equilbrium section at Snake RM 137.69.

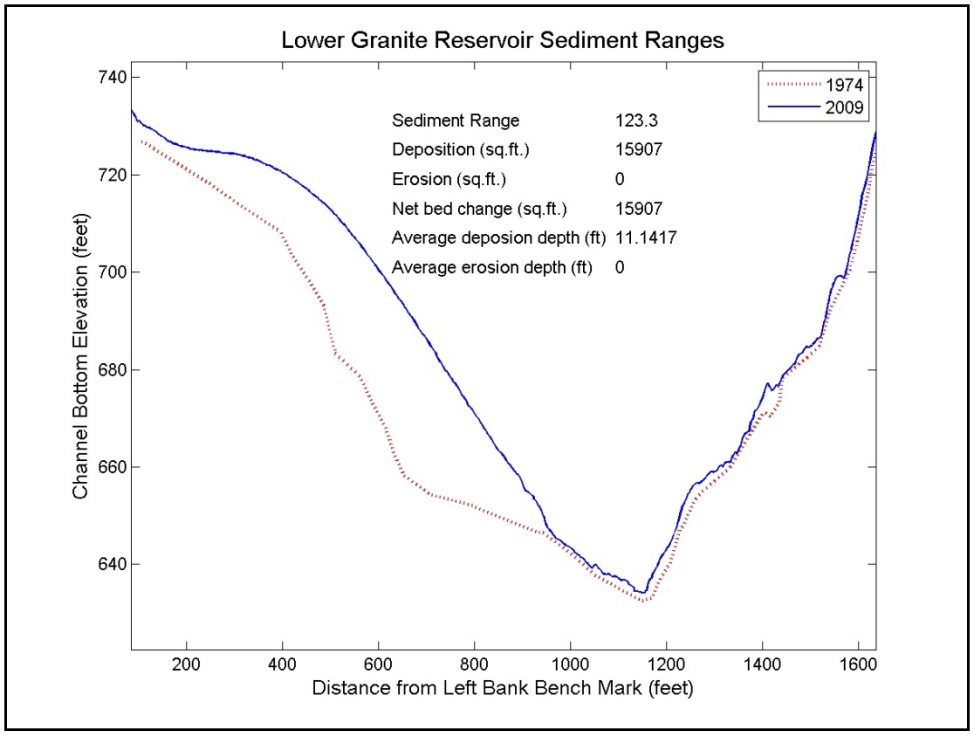


Figure 80. Comparison of 1974 and 2009 sediment ranges at Snake RM 123.30.

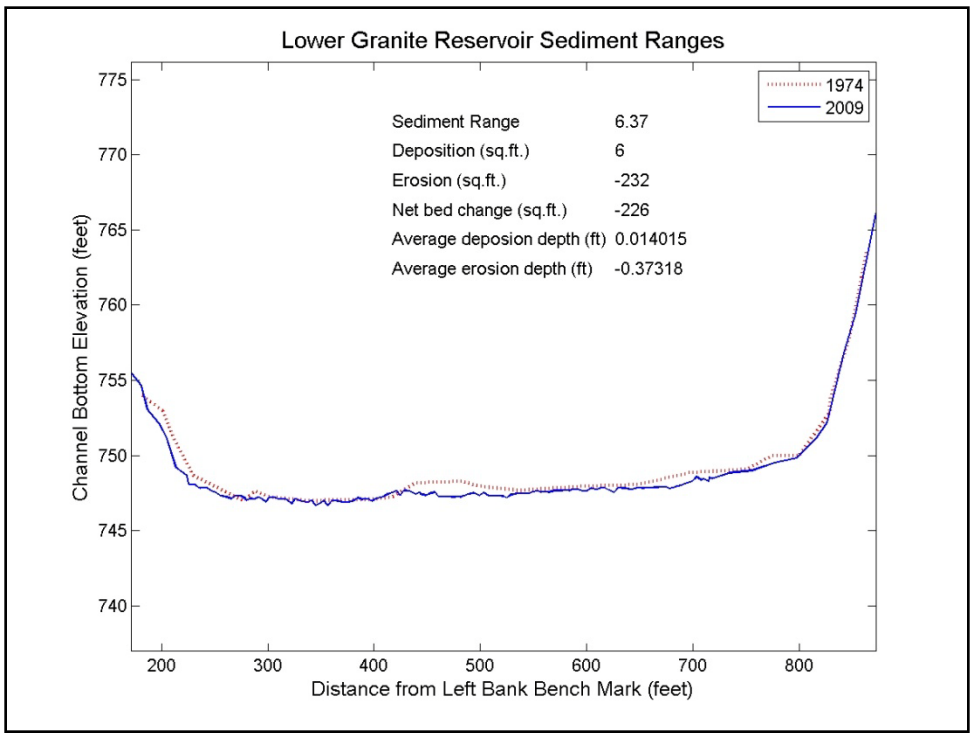


Figure 81. Comparison of 1974 and 2009 sediment ranges at Clearwater RM 6.37.

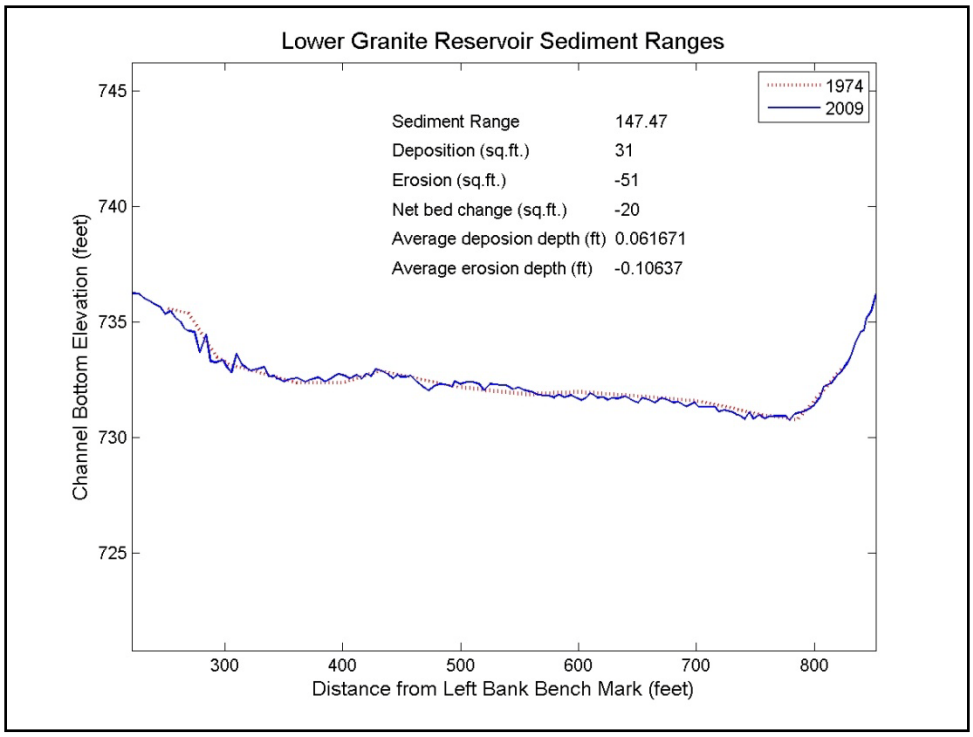


Figure 82. Comparison of 1974 and 2009 sediment ranges at Snake RM 147.47.

7.3. Net Sediment Accumulation Volume

The rate and volume of sediment accumulation in Lower Granite Reservoir is derived from the net change in cross sectional area between successive sediment range surveys. Sediment volume was computed by the average end-area method by the expression,

$$V_{reach} = \frac{A_{net1} + A_{net2}}{2} \times L_{reach}$$

where V_{reach} is the volume of the reach, A_{net1} is the net change in cross sectional area between first survey and second survey at the upstream cross section, A_{net2} is the net change in cross sectional area between first survey and second survey at downstream cross section, and L_{reach} is the distance between the cross sections. Reach lengths between cross section were measured in GIS and differ somewhat from reach lengths computed from the nominal river mile designations of the sediment ranges.

Computation of changes in sediment volumes is not limited to consecutive sediment range surveys and sediment volume changes may be determined between any set of historic sediment range surveys. The computation of the volume of sediment accumulated in Lower Granite Reservoir between 1974 and 2009 is summarized in Table 40, Table 41 and Table 42 for the Snake River above the confluence, the Snake River in Lower Granite, and the Clearwater River above the confluence. The total sediment accumulation obtained by summing the far right column of the three tables is 74.6 million cubic yards (mcy). This computation provides an estimate of the net sediment accumulation in Lower Granite Reservoir and does not account for the volume of sediment removed from the confluence area by dredging. Total dredge volume from 1982 – 2006 is approximately 4.8 mcy.

Lower Granite 1974-2009 Sediment Accumulation Volume							
River Mile	Reach Length ft	Average Deposition ft	Average Erosion ft	Deposition Area ft2	Erosion Area ft2	Net Change Area ft2	Sediment Volume cy
148.83	3,652	0.20	-0.15	112	-151	-39	
148.09	3,046	0.01	-0.58	5	-259	-254	-19,788
147.47	3,268	0.06	-0.11	31	-51	-20	-15,415
146.87	2,971	0.65	-0.07	233	-21	213	11,695
146.33	3,446	0.76	-0.06	473	-74	399	33,674
145.61	1,339	0.11	-0.13	79	-89	-10	24,879
145.38	279	0.17	-0.49	85	-233	-148	-3,914
145.31	278	0.20	-0.52	78	-185	-107	-1,317
145.27	291	1.55	-0.47	627	-189	438	1,704
145.22	352	1.17	-0.22	687	-113	574	5,447
145.15	2,100	0.28	-0.38	199	-270	-71	3,278
144.73	5,244	1.79	-0.02	1,120	-11	1,109	40,351
143.69	1,531	0.23	-0.38	156	-256	-100	97,923
143.31	1,266	0.56	-0.10	415	-54	361	7,393
143.14	2,698	0.48	-0.19	348	-117	230	13,872
142.57	841	0.67	-0.06	653	-53	600	41,505
142.4	3,841	0.37	-0.41	318	-293	25	9,736
141.78	2,664	0.61	-0.03	463	-24	439	32,993
141.21	2,499	3.07	-0.14	3,660	-155	3,506	194,634
140.75	1,326	4.97	-0.19	5,889	-164	5,725	427,145
140.51	1,325	3.09	-0.28	2,088	-181	1,907	187,439
140.22	1,956	1.76	-0.50	1,080	-294	786	66,084
139.91	1,277	0.26	-0.35	173	-212	-39	27,079
139.64	1,351	0.94	-0.14	770	-111	659	14,655
139.43	739	0.64	-0.23	561	-212	349	25,209

Table 40. Sediment accumulation volume 1974-2009, Snake River above confluence.

Lower Granite 1974-2009 Sediment Accumulation Volume							
River Mile	Reach Length ft	Average Deposition ft	Average Erosion ft	Deposition Area ft2	Erosion Area ft2	Net Change Area ft2	Sediment Volume cy
139.29	618	6.32	-0.08	14,520	-178	14,342	275,441
139.22	1,054	6.81	-0.17	13,131	-331	12,800	310,495
138.94	1,325	4.22	-0.40	6,455	-626	5,829	363,651
138.71	972	5.22	-0.24	8,300	-368	7,932	337,608
138.52	1,100	5.11	-0.16	8,757	-261	8,496	295,790
138.34	1,201	3.82	-0.10	5,886	-158	5,728	289,683
138.07	679	1.91	-0.25	2,443	-312	2,130	174,719
137.94	1,232	2.17	-0.26	2,645	-283	2,362	56,472
137.69	2,654	0.82	-0.26	717	-217	499	65,281
137.17	2,584	6.75	-0.23	19,667	-295	19,372	976,613
136.69	1,863	5.27	-0.02	6,433	-27	6,407	1,233,548
136.29	2,868	9.75	-0.05	18,873	-101	18,772	868,822
135.76	3,362	4.26	-0.27	5,621	-316	5,304	1,278,523
135.15	2,784	6.39	-0.67	7,382	-851	6,531	736,851
134.58	3,334	1.87	-0.39	3,201	-621	2,580	469,655
133.98	2,536	2.14	-0.11	2,587	-209	2,378	306,101
133.41	3,689	5.28	-0.01	6,003	-7	5,995	393,240
132.71	3,462	6.92	-0.01	7,485	-6	7,479	920,524
132.05	2,491	8.77	-0.02	11,831	-30	11,801	1,236,249
131.62	3,185	5.42	-0.29	10,732	-447	10,285	1,018,987
130.93	1,661	8.86	-0.12	11,307	-122	11,185	1,266,225
130.66	1,155	7.53	-0.08	20,591	-202	20,389	971,054
130.44	2,350	13.16	-0.28	23,697	-535	23,162	931,476
130	3,612	10.78	-0.10	14,305	-154	14,151	1,623,791
129.27	2,125	11.11	-0.03	15,621	-39	15,582	1,988,728
128.87	2,762	4.79	-0.27	5,923	-336	5,587	832,969
128.27	3,015	4.77	0.00	5,556	0	5,556	569,970
127.63	2,982	9.09	0.00	12,767	-6	12,761	1,022,666
127.03	4,813	12.16	-0.03	21,256	-39	21,217	1,876,345
126.07	8,587	12.85	-0.10	20,476	-129	20,347	3,704,278
124.94	5,662	6.15	-0.29	8,228	-314	7,914	4,494,029
123.3	4,867	11.14	0.00	15,907	0	15,907	2,497,815
122.69	5,217	4.25	-0.32	5,448	-366	5,081	1,891,807
121.42	5,329	7.21	-0.01	10,647	-12	10,635	1,518,265
120.46	4,575	16.31	-0.01	33,909	-26	33,883	4,393,575
119.56	24,162	10.46	0.00	20,807	0	20,807	4,633,567
114.92	9,158	5.36	-0.17	12,217	-363	11,854	14,613,617
113.12	9,414	5.00	-0.10	9,210	-152	9,058	3,546,642
111.24	14,698	2.43	-0.21	6,777	-518	6,259	2,670,243
108.31	2,328	4.04	-0.10	12,570	-228	12,342	5,062,898
107.73	1,500	3.96	-0.06	12,093	-139	11,954	1,047,499

Table 41. Sediment accumulation volume 1974-2009, Snake River below confluence.

Lower Granite 1974-2009 Sediment Accumulation Volume							
River Mile	Reach Length ft	Average Deposition ft	Average Erosion ft	Deposition Area ft2	Erosion Area ft2	Net Change Area ft2	Sediment Volume cy
7.85	3,940	0.91	-0.18	558	-183	374	0
7.08	1,673	1.05	-0.02	672	0	672	76,340
6.78	2,245	0.10	-0.96	43	-505	-461	6,531
6.37	2,516	0.01	-0.37	6	-232	-226	-28,582
5.94	2,082	0.02	-1.49	6	-755	-748	-45,405
5.64	1,022	0.34	-0.20	329	-162	167	-22,399
5.39	1,078	0.13	-1.02	151	-771	-620	-8,567
5.21	1,049	0.54	-0.37	692	-261	431	-3,765
5.01	871	0.19	-0.87	138	-587	-450	-358
4.94	962	0.50	-0.11	385	-77	308	-2,280
4.74	1,652	0.57	-0.16	513	-161	352	11,768
4.3	2,276	0.03	-0.75	14	-730	-716	-11,128
3.85	2,425	0.09	-0.12	41	-100	-59	-32,649
3.48	710	0.19	-0.16	122	-115	7	-2,313
3.2	1,385	0.06	-0.25	40	-209	-170	-2,134
2.89	1,861	0.02	-0.28	11	-187	-175	-8,850
2.58	1,170	0.03	-0.36	15	-266	-251	-14,681
2.34	2,157	0.07	-0.18	50	-134	-85	-7,266
1.99	1,897	0.19	-0.35	156	-282	-126	-8,437
1.66	610	0.29	-0.20	202	-133	69	-2,032
1.56	601	0.77	-0.07	651	-52	599	7,543
1.47	494	1.61	-0.07	1,693	-74	1,619	24,665
1.36	486	5.05	0.00	5,581	0	5,581	65,924
1.26	536	5.23	-0.08	5,865	-69	5,796	102,466
1.16	587	6.53	-0.05	8,736	-68	8,668	143,608
1.06	576	3.33	-0.02	3,671	-20	3,651	133,890
0.92	828	1.59	-0.23	1,352	-204	1,148	51,203
0.78	519	0.06	-0.59	20	-317	-297	13,050
0.67	663	1.03	-0.22	411	-104	307	95
0.53	623	1.81	-0.30	1,199	-207	993	15,960
0.41	624	3.94	-0.06	3,774	-52	3,722	54,425
0.28	630	7.05	-0.12	8,243	-130	8,113	136,766

Table 42. Sediment accumulation volume 1974-2009, Clearwater River above confluence.

7.4. Dredge Material Volumes

The confluence area has been periodically dredged to maintain the authorized navigation channel and access to the port facilities. Relatively small amounts of sediments are dredged from public recreation areas and irrigation intakes for wildlife management areas. Prior to 1990, dredging was performed to recover channel conveyance. About 4.8 million cubic yards of material has been dredged from the confluence area. Table 43 lists the approximate quantities of material dredged from the

confluence area and ports since 1982[77]. Dredge material was disposed in-water in the lower part of Lower Granite Reservoir to construct in-water habitat. The disposed material is placed between the established sediment ranges and so is not measured in the historic sediment ranges (Section 12.8). Dredge material amounts to only about 6 percent of the net sediment accumulation, so does not significantly affect the hydraulic computations for the risk analysis; particularly, since the dredge material was deposited well below Silcott Island were sediment accumulation has less effect on the flood water surface at the confluence.

Year	Location	Volume Cubic Yards
1982	Port of Lewiston – Lower Granite	256,200
1982	Port of Clarkston – Lower Granite	5,000
1985	Confluence of Clearwater and Snake	771,000
1986	Port of Lewiston – Lower Granite	378,000
1988	Confluence of Clearwater and Snake	916,000
1989	Confluence of Clearwater and Snake	993,500
1992	Confluence of Clearwater and Snake	520,700
1997	Port of Lewiston – Lower Granite	3,700
1998	Confluence of Clearwater and Snake	68,700
1998	Confluence of Clearwater and Snake	215,200
1998	Port of Clarkston – Lower Granite	12,200
2000	Confluence of Clearwater and Snake	118,000
2006	Confluence of Clearwater and Snake	553,229
	Total	4,811,429

Table 43. Estimated dredge volumes at the confluence of the Snake and Clearwater Rivers.

7.5. Total Sediment Accumulation Volume

Cumulative and total gross sediment volume from 1974 to 2010 was computed from successive sediment range surveys and adjusted for dredge volumes to estimate the total sediment inflow into Lower Granite Reservoir. The computations of cumulative gross sediment volume are summarized in Table 44. Total gross sediment accumulation from 1974 to 2010 is 79.8 mcy. The cumulative estimate through 2009 (76.5 mcy) agrees well with the net accumulation volume computed from the difference of the 1974 and 2009 cross sections when the dredge material volume is added (total 79.5 mcy). The difference, 3.0 mcy, is about 4 percent of the total gross sediment volume and is attributed to survey measurement error, cross section interpolation,

[77] USACE (2002) *Dredged Material Management Plan and Environmental Impact Statement, McNary and Lower Snake River Reservoirs,* Walla Walla District, U.S. Army Corps of Engineers.

errors in dredge volume estimates, and consolidation of silt sediment in the lower part of Lower Granite Reservoir. Average annual inflow of deposited sediment into Lower Granite Reservoir is 2.22 mcy per year. Annual sediment loads vary significantly between sediment range surveys.

Cumulative gross sediment volumes are separated by reach in Table 44. Very little sediment has accumulated in the Snake and Clearwater Reaches upstream from the confluence, though it is important to note that sediment has been dredged from the navigation channel and turning basin at the Port of Lewiston on the Clearwater River. It is difficult to accurately estimate the volume of sediment removed from the Clearwater River from dredging project records. About 62.2 mcy or 78 percent of the total sediment inflow has accumulated below Silcott Island. About 16 percent of the total sediment inflow has accumulated in Lower Granite Reservoir between the confluence and Silcott Island. Sections 7 and 8 show that bed material above Silcott Island is mostly sand and that the 16 percent accumulation volume above Silcott Island agrees well with the percentage of sand measured in the incoming sediment load.

The total accumulation rate below the confluence is about 2.1 mcy per year. Current available storage in Lower Granite Reservoir below the confluence based on the sediment range cross sections is about 398,000 acre feet, which gives a nominal reservoir life of about 300 years at an accumulation rate of 2.1 mcy/yr. Operational life would be less and is difficult to predict because of the uncertainty in long-term sediment load discussed in Section 8. The simulation of sediment accumulation and distribution within the reservoir over the next 100 years is discussed in Section 10.

Lower Granite Cumulative Gross Sediment Accumulation 1974 - 2010

	Sediment Volume (million cubic yards)								
Range Survey Period	Snake Above Confluence[1]	Clearwater Above Confluence[2]	Snake Confluence to Silcott[3]	Snake Below Silcott[4]	Snake Below Confluence[5]	Dredge Volume	Period Total Volume	Average Annual Volume	Cumulative Total Volume
1974-1995	0.50	0.51	7.50	32.91	40.41	2.060	43.48	2.07	43.48
1995-1997	-0.15	0.51	2.09	10.24	12.33	0.030	12.71	6.36	56.19
1997-2000	0.43	0.04	0.93	6.26	7.19	0.118	7.78	2.59	63.98
2000-2003	0.34	0.04	1.29	3.82	5.10	0.000	5.48	1.83	69.45
2003-2006	-0.17	-0.06	-0.44	3.15	2.71	0.553	3.03	1.01	72.49
2006-2009	0.10	0.02	0.51	3.35	3.86	0.000	3.98	1.33	76.47
2009-2010	0.26	-0.03	0.60	2.53	3.13	0.000	3.36	3.36	79.83
Total, mcy	1.30	1.03	12.48	62.26	74.74	2.761	79.83		
Percent of total	1.6%	1.3%	15.6%	78.0%	93.6%	3.5%	100.0%		
Average, mcy/yr	0.04	0.03	0.35	1.73	2.08	0.08		2.22	

[1]Snake River mile 148,83 - 139.43, [2]Clearwater River Mile 0.28 - 1.66
[3]Snake River mile 139.29 - 130.66, [4]Snake River mile 130.66 - 107.73, [5]Snake River mile 139.29 - 107.73

Table 44. Summary of Sediment Accumulation in Lower Granite Reservoir.

7.6. Sediment Yield Estimate

Sediment yield for the area above Lower Granite Reservoir can be estimated from the gross sediment accumulation volume if a trapping efficiency is applied. Assuming a trapping efficiency of 80 percent and an average sediment unit weight of 70 lb ft^{-3}, the average annual sediment yield for the 27,130 acre watershed that contributes sediment directly to Lower Granite Reservoir is computed,

$$\text{Sediment yield}, S_V = \frac{2.22\,\frac{\text{mcy}}{\text{yr}}}{0.80} \times 70\,\frac{\text{lb}}{\text{ft}^3} \times \frac{27\times10^6\,\frac{\text{ft}^3}{\text{mcy}}}{2000\,\frac{\text{lb}}{\text{ton}}} \times \frac{1}{27{,}130\,\text{mi}^2} \times \frac{1\,\text{mi}^2}{640\,\text{ac}}$$

$$\text{Sediment Yield}, S_V = 0.15\,\frac{\text{ton}}{\text{ac}\cdot\text{yr}}$$

On average, the total sediment yield of sand and silt is approximately 0.15 U.S. tons per acre per year or about 97 tons per square mile (33 metric tons per square kilometer). This estimate agrees well with the measured sediment load discussed in Section 9.

7.7. Sediment Distribution in Lower Granite Reservoir

Sediment distribution between successive sediment range surveys in Lower Granite Reservoir can be plotted by river mile as in Figure 84 which shows that most of the sediment load delivered in 1996 and 1997 was deposited below Snake RM 130 and that sediment was eroded between RM 137 and 138. Sediment delivered in 2010 followed a similar pattern in Figure 84 except that sediment was eroded between RM 132 and 134.

Several sediment range surveys can be compared by referencing the mean active bed change to an index year. In Figure 85, the change in mean active bed elevation for sediment range surveys from 1995 to 2006 are compared to the mean active bed in 2009. The plots show that sediment accumulated below RM 130 all through the period, and that above Silcott Island the rate of accumulation has diminished and that some sediment range cross sections above about RM 132 have lost sediment. The bed difference plots suggest that upper reach of Lower Granite Reservoir between Silcott Island and the confluence is tending towards a morphological equilibrium under the prevailing discharge and sediment regimes.

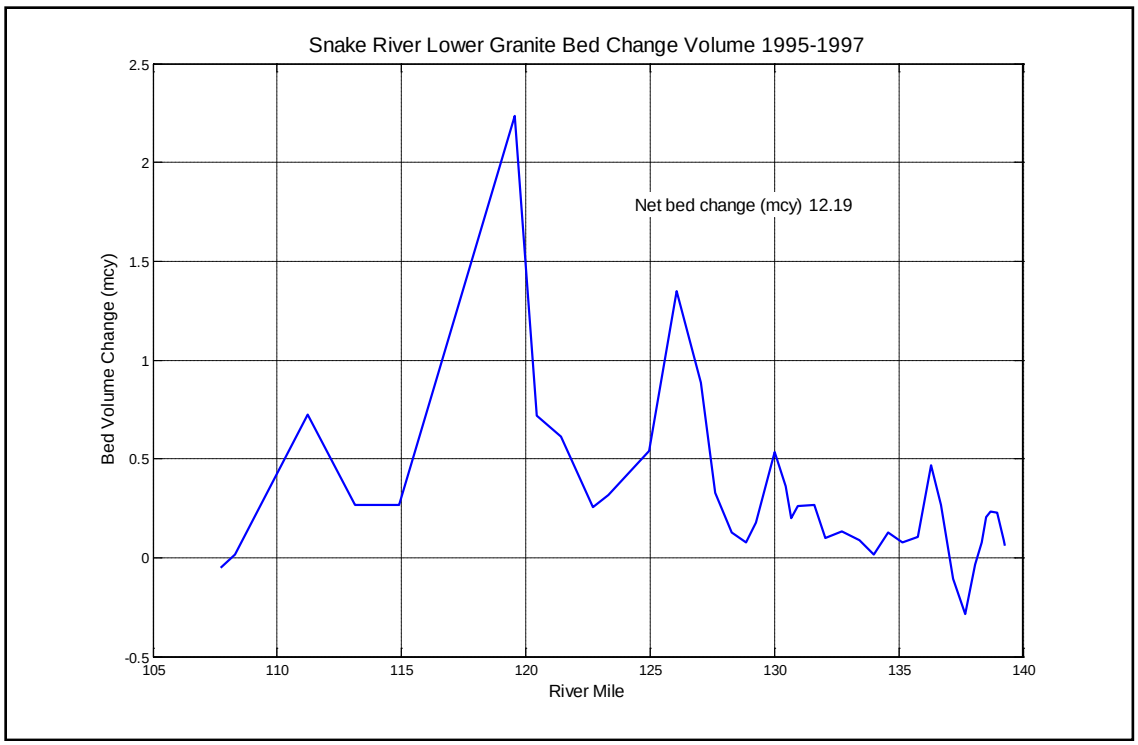


Figure 83. Distribution of sediment volume in Lower Granite between 1995 and 1997.

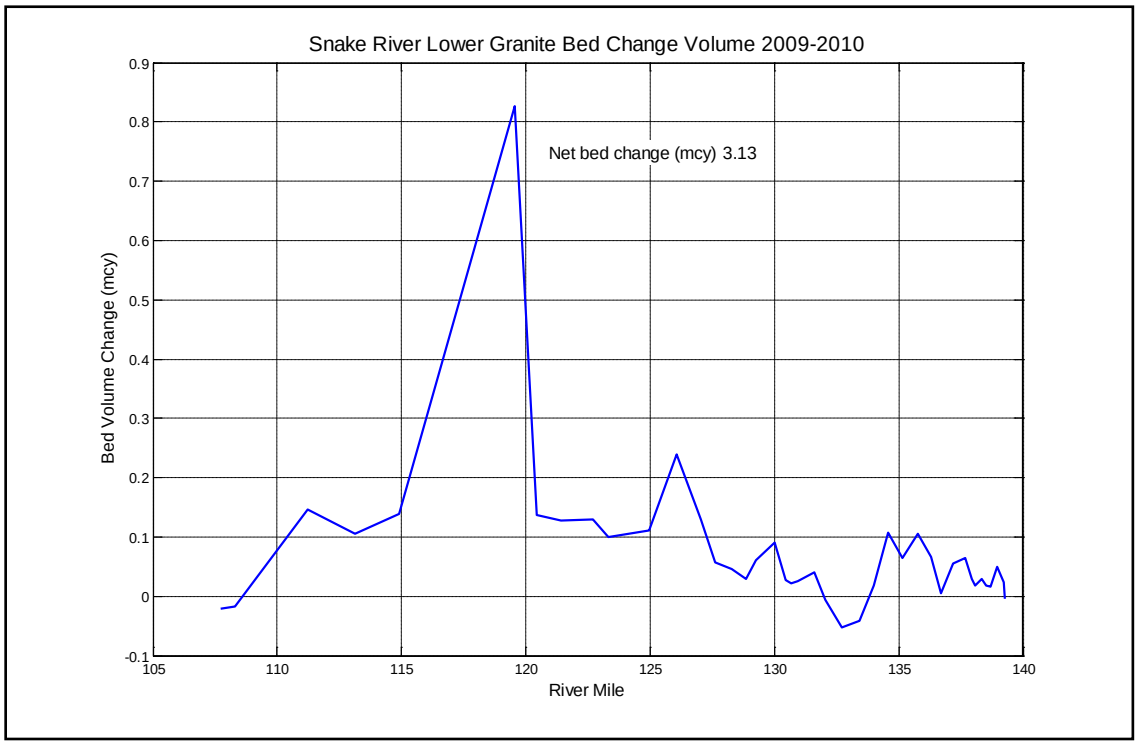


Figure 84. Distribution of sediment volume in Lower Granite between 2009 and 2010.

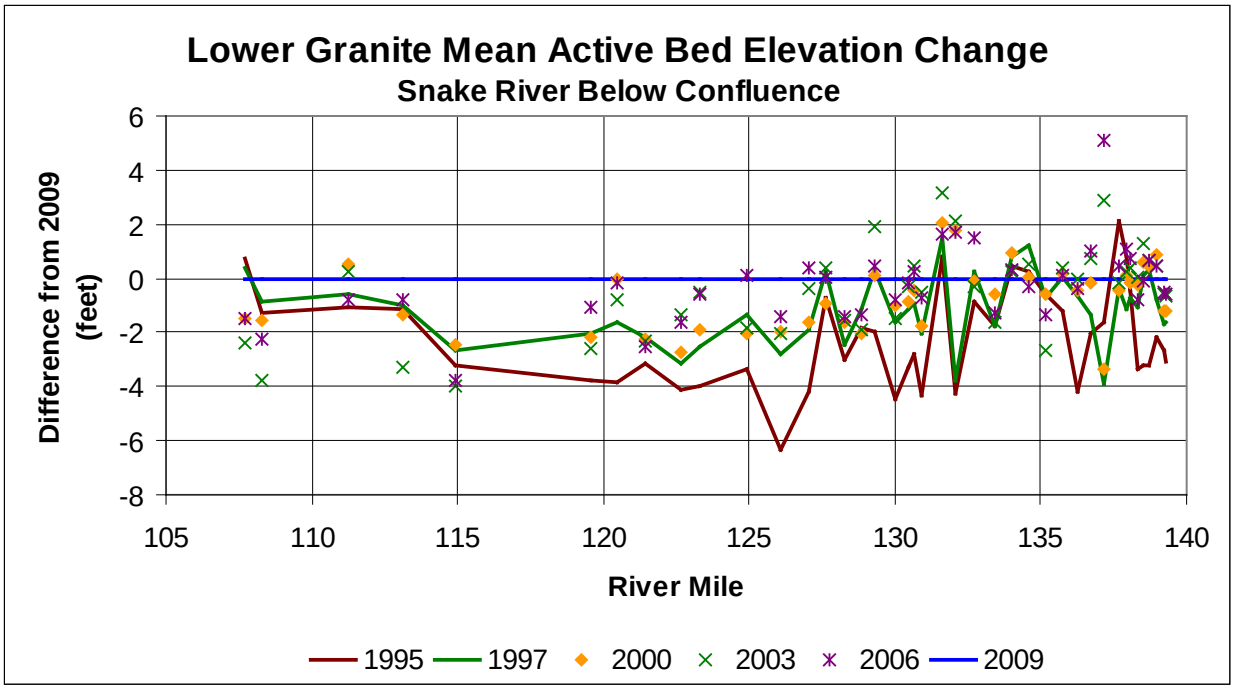


Figure 85. Mean active bed elevation change in Lower Granite below the confluence.

7.8. Sediment Accumulation at the Mouth of the Palouse River

The Palouse River is a direct tributary to Lower Monumental Reservoir. The sediment delivery watershed is about 2,790 miles, exclusive of the area of the watershed above Rock Lake (Figure 86). Sediment ranges have been periodically surveyed at the mouth of the Palouse River since 1969 (Figure 87). The sediment ranges were last surveyed in 2005.

Sediment accumulation at the mouth of the Palouse River was determined by methods similar to those described for Lower Granite Reservoir and is summarized by period in Table 45. Total accumulation since 1969 is about 24 mcy or an average annual accumulation of 0.67 mcy per year. The rate of accumulation has decreased with time. Average annual accumulation was about 1 mcy per year from 1969 to 1984. Later sediment ranges showed that the rate of accumulation decreased by about 50 percent. The timing of the decrease coincides with the wider adoption of effective soil conservation practices[78]. The current sediment yield of the Palouse River basin at Lower Monumental Reservoir is estimated at 0.25 U.S. tons per acre per year by calculation:

[78] Michalson, E. L., Papendick, R. I., and Carlson, J. (1998). *Conservation Farming in the United States: The methods and accomplishments of the STEEP program*, CRC Press, Boca Raton, Fla.

$$\text{Sediment yield}, S_L = 0.47\frac{\text{mcy}}{\text{yr}} \times 70\frac{\text{lb}}{\text{ft}^3} \times \frac{27\times10^6\frac{\text{ft}^3}{\text{mcy}}}{2000\frac{\text{lb}}{\text{ton}}} \times \frac{1}{2{,}780\ \text{mi}^2} \times \frac{1\ \text{mi}^2}{640\ \text{ac}}$$

$$\text{Sediment yield}, S_L = 0.25\frac{\text{ton}}{\text{ac}\cdot\text{yr}}$$

Sediment loads in the Palouse River were measured at Hooper, WA by USGS in 2009, 2010 and 2011 as part of the study and are discussed in Section 9.

Palouse River Sediment Accumulation Volume (1969-2005)		
Period	Cumulative Volume mcy	Mean Annual Accumulation mcy/yr
1969-1973	4.18	1.04
1973-1984	11.57	1.05
1984-1994	3.09	0.31
1994-2005	5.18	0.47
Average	24.02	0.67

Table 45. Sediment accumulation volumes at the mouth of the Palouse River.

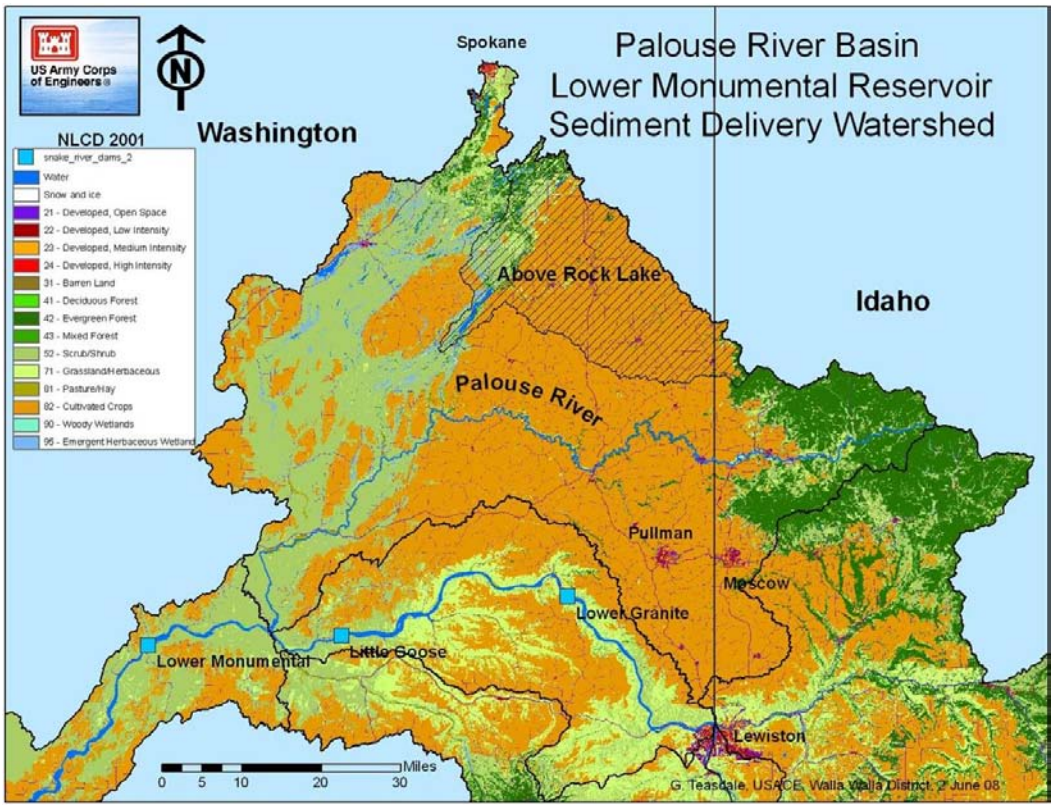


Figure 86. Palouse River sediment delivery watershed.

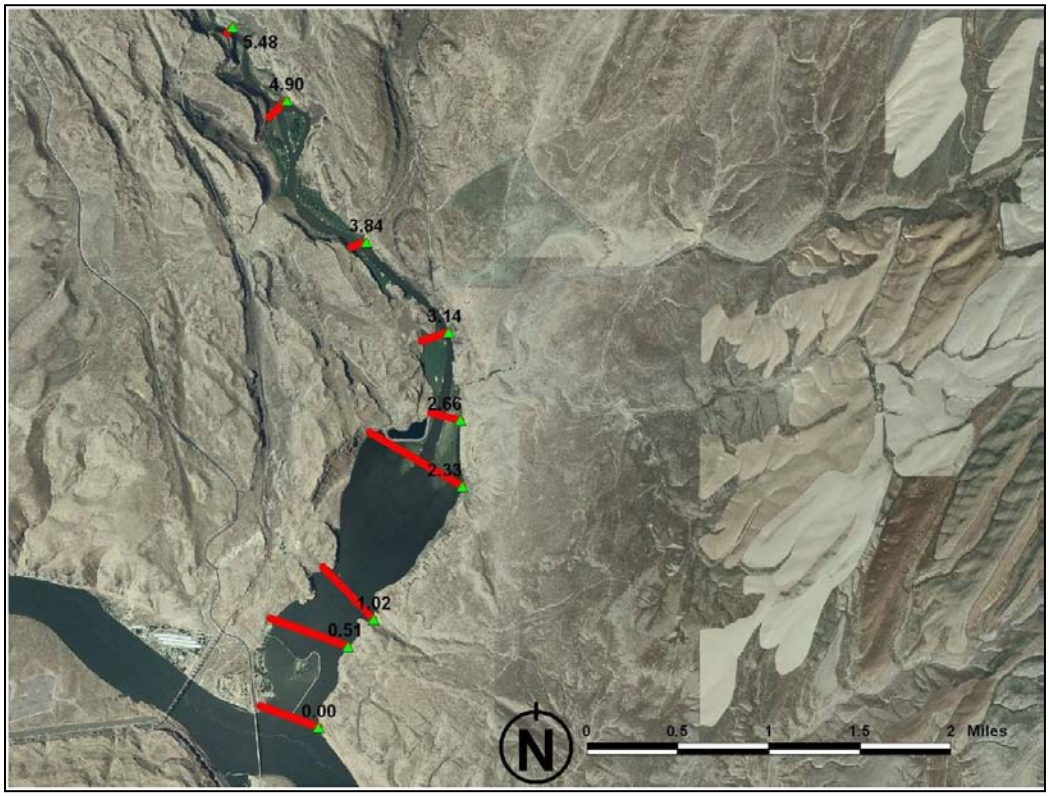


Figure 87. Palouse River Sediment Ranges.

8. Lower Granite Reservoir Bed Material

Sediment accumulation in Lower Granite Reservoir varies with time and spatial extent. The previous section showed that about 80 million cubic yards of sediment has accumulated in Lower Granite Reservoir since 1974 and that annual sediment volumes differ between years. Annual sediment volumes are variable because the inflow discharge and sediment load vary with weather, watershed conditions and reservoir operation. Sediment depth and texture are variable within Lower Granite Reservoir because of differential settling of the different size fractions of the incoming sediment load. Previous sections described the discharge regime of Lower Granite Reservoir. This section describes the spatial variation of grain size of bed sediment within the reservoir and the backwater zones of the Snake and Clearwater Rivers. It is important to understand how grain size varies within the reservoir to correctly model sediment transport.

Previous characterizations of bed sediment[79,80,81,82] indicated that sand dominates the bed in the upper reach of Lower Granite Reservoir and that deposits below about RM 130 are mostly silt. Most sediment samples in the previous studies were obtained from the bed surface obtained from relatively shallow depths and the data coverage was too sparse to support a detailed sediment transport analysis. Consequently, an extensive, synoptic sediment coring survey of Lower Granite Reservoir was performed as part of the PSMP EIS to characterize the grain size distribution of the bed for sediment transport modeling.

8.1. Sediment Core Survey

During the spring and summer of 2010, the U.S. Geological Survey (USGS) extracted sediment cores at the historic sediment range locations in deep and shallow water areas throughout Lower Granite Reservoir and the backwater zones of the Snake

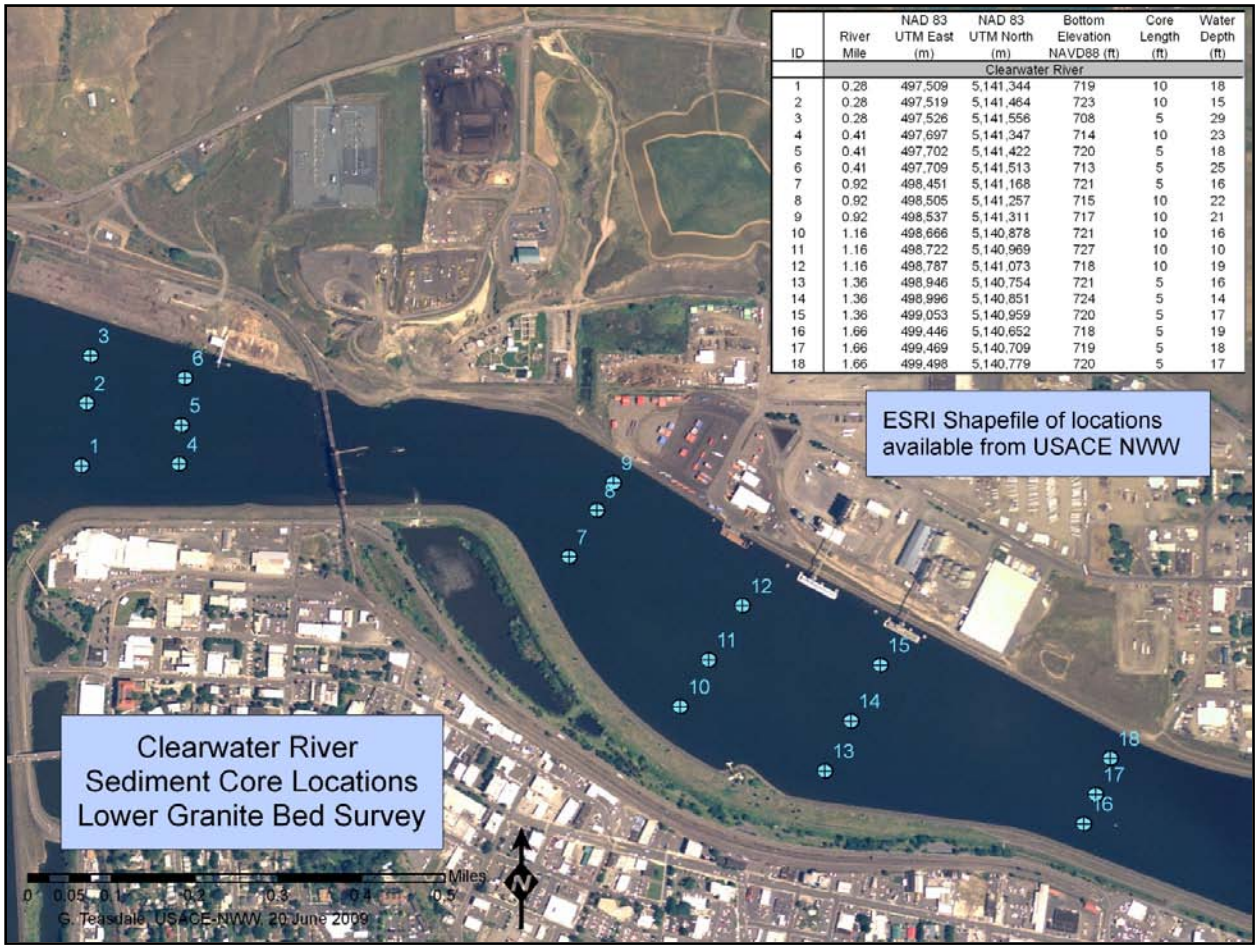
[79] USACE (1988). *Report of 1988 Post-Dredging Sediment Sampling Lower Granite Pool*, Walla Walla District, U.S. Army Corps of Engineers.

[80] Bennett, D.H., M.A. Madsen, T.J. Dresser, Jr., and T.S. Curet. (1994). *Monitoring fish community activity at disposal and reference sites in the Lower Granite Reservoir, Idaho-Washington Year 5* (1992). Department of Fisheries and Wildlife Resources, University of Idaho.

[81] CH2MHill (1997). "Sediment Sampling Particle Size Sampling Task", *Lower Snake River Juvenile Salmon Migration Feasibility Study*, Contract DACW68-94-D-0006. Walla Walla District, U.S. Army Corps of Engineers.

[82] PNNL (2004). *Sediment Inventory and Analysis for Lower Granite, John Day, and the Dalles Reservoirs*, Pacific Northwest National Laboratory, Richland, WA.

and Clearwater Rivers. Sediment cores were obtained between Snake RM 107.73 and RM 141.78 and between Clearwater RM 0.00 and RM 1.66. The sediment coring locations on the Clearwater River and Snake River are shown in Figure 88 and Figure 89. Of the 89 coring locations, 64 yielded useable sediment cores; original gravel and cobble beds were encountered at the other locations.



ID	River Mile	NAD 83 UTM East (m)	NAD 83 UTM North (m)	Bottom Elevation NAVD88 (ft)	Core Length (ft)	Water Depth (ft)
	Clearwater River					
1	0.28	497,509	5,141,344	719	10	18
2	0.28	497,519	5,141,464	723	10	15
3	0.28	497,526	5,141,556	708	5	29
4	0.41	497,697	5,141,347	714	10	23
5	0.41	497,702	5,141,422	720	5	18
6	0.41	497,709	5,141,513	713	5	25
7	0.92	498,451	5,141,168	721	5	16
8	0.92	498,505	5,141,257	715	10	22
9	0.92	498,537	5,141,311	717	10	21
10	1.16	498,666	5,140,878	721	10	16
11	1.16	498,722	5,140,969	727	10	10
12	1.16	498,787	5,141,073	718	10	19
13	1.36	498,946	5,140,754	721	5	16
14	1.36	498,996	5,140,851	724	5	14
15	1.36	499,053	5,140,959	720	5	17
16	1.66	499,446	5,140,652	718	5	19
17	1.66	499,469	5,140,709	719	5	18
18	1.66	499,498	5,140,779	720	5	17

Figure 88. 2010 sediment core locations on the Clearwater River.

Three types of sediment coring equipment were used in the survey. The choice of coring equipment depended on bed material. Gravity and piston corers were used to sample the silt deposits below Silcott Island, while the denser sand deposits in the upper reaches of the reservoir were sampled with a vibratory corer. Technical protocols of coring and sampling are described in separate publications by USGS[83,84].

[83] Van Metre, P.C., Wilson, J.T., Fuller, C.C., Callender, E., and Mahler, B.J., 2004, Methods, Site Characteristics, and Age Dating of Sediment Cores for 56 U.S. Lakes and Reservoirs Sampled by the USGS National Water-Quality Assessment Program, 1993-2001: U.S. Geol. Surv. SIR 2004-5184, 120 p. [Scientific Investigations Report].

Maximum length of the sediment cores was approximately 12 feet and the maximum water depth was approximately 120 feet.

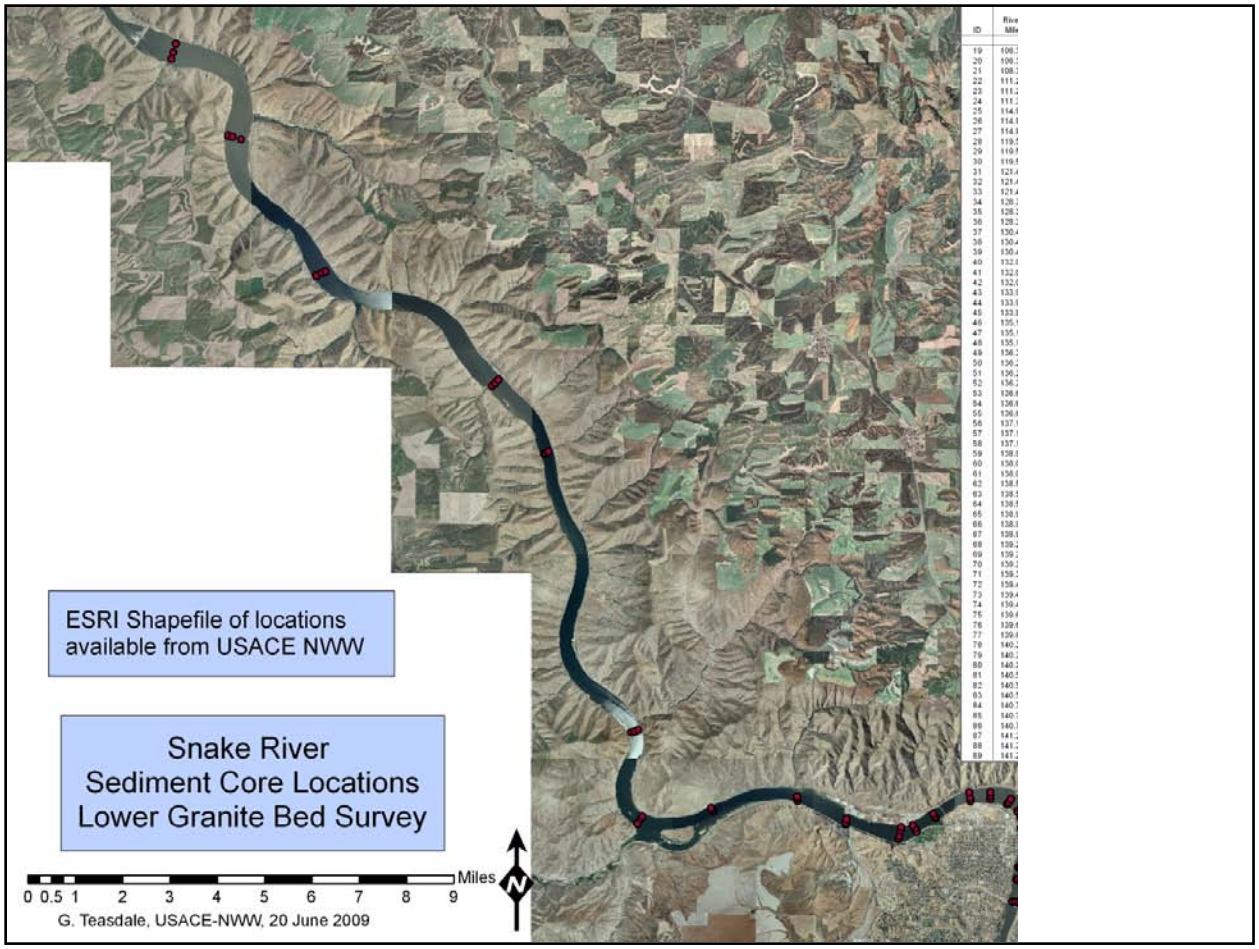


Figure 89. 2010 sediment core locations on the Snake River.

All the coring was conducted from a pontoon boat that was equipped with an A-frame hoist and electric winch. Coring positions were located by GPS and depths were determined with an electronic sounder. All sediment cores were 67 mm in diameter and of a length determined by the depth of penetration. The rigid barrels of the corers were lined with a clear polybuterate tube that encased and preserved the stratigraphy of the sediment and core. With the gravity corer, the weight of the heavy steel barrel drives the sampler into the bed sediment. A check valve in the top of the liner releases water

[84] Barton, G., 2003, Characterization of channel substrate, and changes in suspended-sediment transport and channel geometry in White Sturgeon spawning habitat in the Kootenai River near Bonners Ferry, Idaho, following closure of Libby Dam: U.S. Geological Survey, 33 p.

during penetration, and then closes to retain sediment during extraction. The piston corer is also driven by the weight of the barrel, but retention of the sample is enhanced by a piston inside the barrel. The piston is connected by a cable to a trigger arm which holds the corer until it contacts the bed. After contact, the arm releases the corer barrel allowing it to descend past the piston into the sediment. This produces a weak vacuum below the piston which enhances the recovery of the saturated sediment.

The vibratory corer drives the core barrel into the sand bed by combined action of weight and high frequency vibration. The weighted electric powered vibratory head is clamped to the top of an aluminum barrel that holds the plastic liner. The vibratory sampler is lowered to the river bed in a deployable stand by means of an electric winch (Figure 90). After the stand contacts the bed, the vibrating core barrel is driven through the sand for the full length of the barrel or until stopped (refusal) by the coarse material of the original river bed. A reed-type check valve is fitted to the bottom of the tube to retain the loose sand sample as it is withdrawal from the bed. Strata in vibratory core samples are preserved, but the sediment is consolidated during acquisition so that bulk densities are altered.

Approximate depths of penetration and other aspects of the sample acquisition are noted in the field sheets. The plastic liners were removed from the corer barrel, trimmed to length, labeled, and stored on the coring boat. On shore, the liner tubes were cut lengthwise, the opened core photographed, and the strata described. Half of the split core was archived for possible future analysis (Figure 91). Subsamples were selected from the core at distinct strata for grain distribution analysis. Major and trace element concentrations in selected subsamples will be determined using USGS analytical methods[85]. A duplicate set of sediment samples were collected from each sediment core for independent analysis by the Corps.

[85] Arbogast, B.F.E., 1996, Analytical methods manual for the Mineral Resource Surveys Program, U.S. Geological Survey, Open File Report, U.S. Geol. Surv., v. 96-0525.

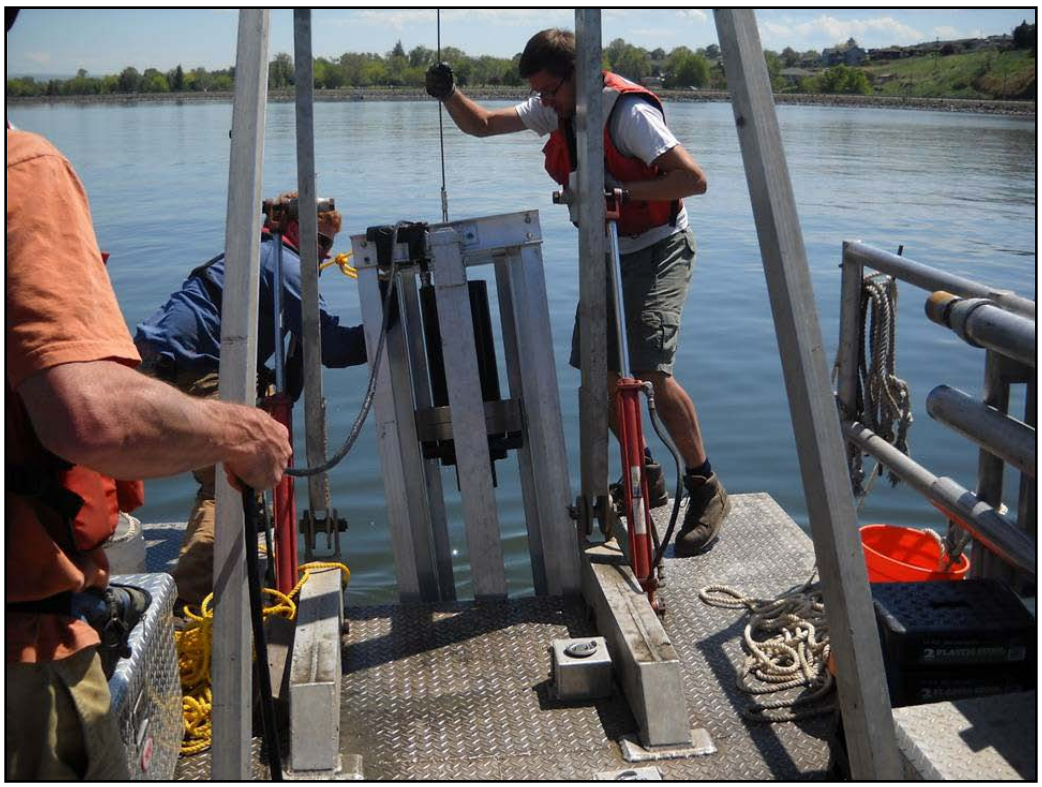


Figure 90. Sediment core acquisition with vibratory corer at Lower Granite.



Figure 91. Sediment core inspection and subsampling.

8.2. Sediment Core Observations

Sediment stratification and textural changes was evident in some cores. Distinct strata mark significant sediment events and indicate the sediment transport processes that dominated the events. A crucial core for the sediment transport analysis was acquired at Clearwater RM 0.28 and is shown in Figure 92. This core was extracted from the mound of sediment deposited by the 1996 and 1997 floods (see Section 7.1). The strata in the sample show that the material deposited by these sediment events was silt and very fine sand. As important, is the finding that the core contained no coarse sand or gravel, indicating that these large sediment events did not carry coarse grained material into the confluence. While this was expected from sediment transport theory, this and similar cores are physical evidence of the applicability of empirical sediment transport relationships. Field notes indicate that the core penetrated the full depth of the deposit, about 7 feet at the location where the sample was obtained (Figure 93).

Sediment cores acquired with the piston and gravity corers below Silcott Island were mostly homogeneous silt (Figure 94 and Figure 95). Most cores penetrated the full depth to the original sand and gravel bed. Subtle variation in color and texture in the cores is evidence of oxidation and biological processes. Bulk density of the silt core increased with depth. Sediment at the surface layer appeared weakly flocculated.

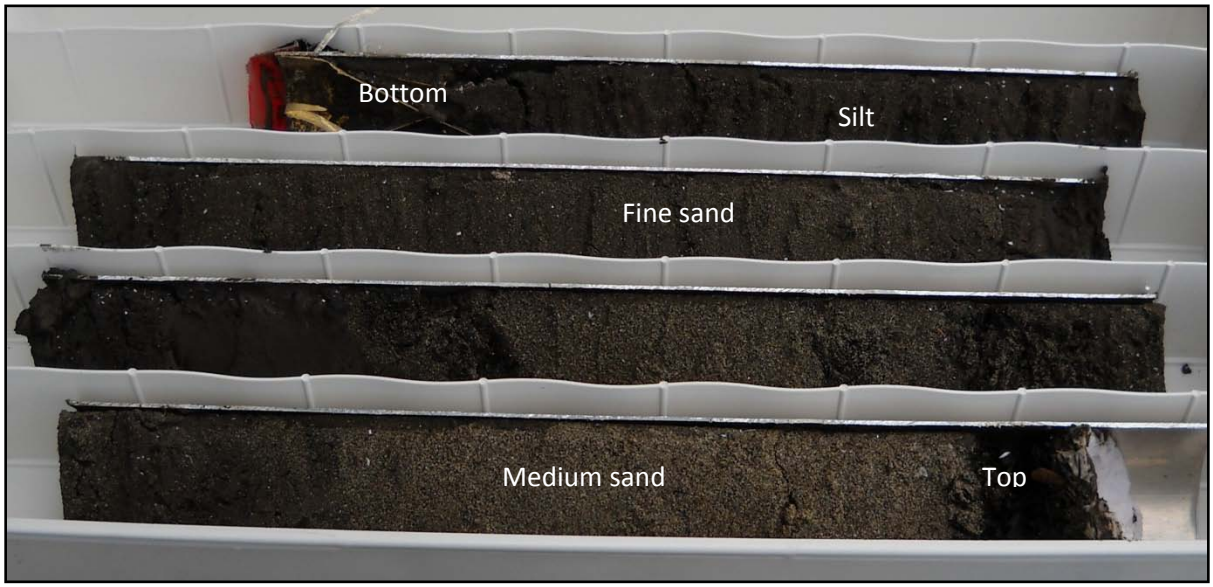


Figure 92. Sediment core acquired at Clearwater RM 0.28.

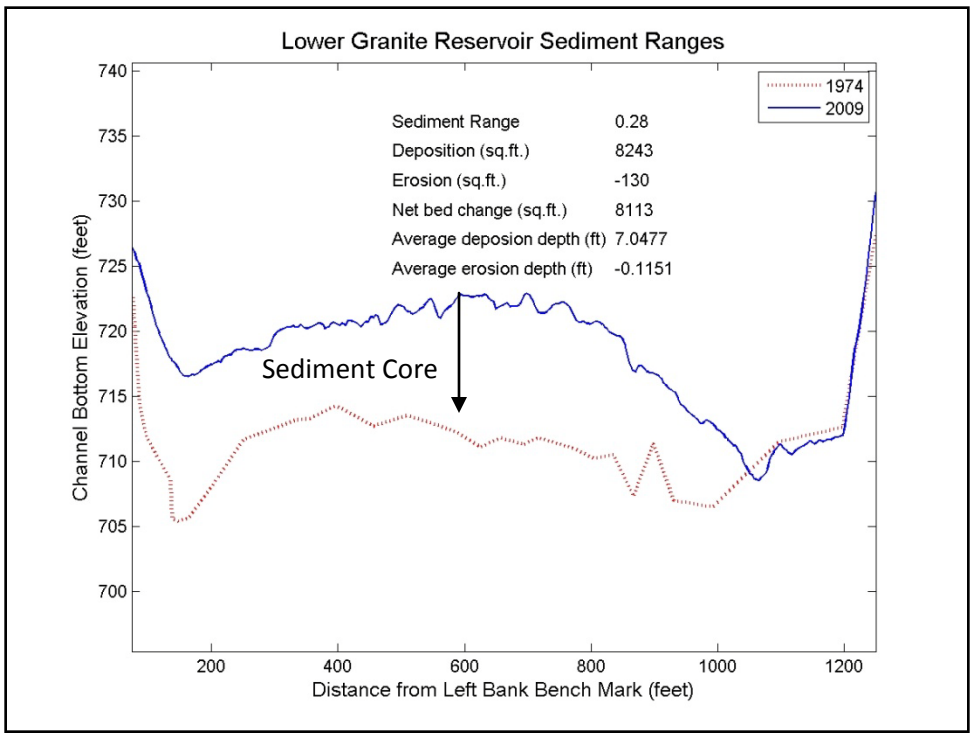


Figure 93. Comparison of 1974-2009 sediment ranges at Clearwater RM 0.28.



Figure 94. Silt sediment core tube obtained near Lower Granite Dam.



Figure 95. Uniform silt sediment near the bottom of core sample obtained near Lower Granite Dam.

8.3. Sediment Core Analysis

Subsamples of sediment were taken from distinct strata in the sediment cores and were sent to the USGS Cascades Volcano Observatory Sediment Laboratory[86] for grain size distribution analysis. In each core, a subsample was obtained at least from the surface layer. Additional subsamples were selected from lower strata based on textural changes. At least three subsamples were selected from most cores. Grain size distributions were determined by USGS standard methods equivalent to ASTM C136. The laboratory reported the passing weights and percentages for standard sieve sizes that ranged from 0.001 mm to 16 mm.

[86] http://vulcan.wr.usgs.gov/Projects/SedLab/framework.html

8.4. Spatial Variation of Grain Size

Grain size distributions of the bed material are summarized by spatial location in Lower Granite Reservoir and by the relative position of the subsample within the bed. Figure 96 shows the median grain size (D_{50}) for the sediment cores from the Snake River in Lower Granite Reservoir between the dam and RM 142. The variation of grain size with depth is indicated by the individual D_{50} for subsamples at levels 1, 2 and 3. Level 1 is at the surface, level 2 is at the first distinct strata below the surface layer and level 3 is the next distinct strata below level 2. The depths of level 2 and deeper are relative and can occur at different depths within the bed.

Above Silcott Island, the maximum D_{50} is less than 0.4 mm and all but two subsamples are less than 0.35 mm. Sediment in this size range classifies as medium sand. An abrupt transition to finer material occurs near Silcott Island. Below Silcott Island the D_{50} is less than 0.1 mm (very fine sand) and below RM 125 it is less than 0.05 mm (coarse silt). Very important observations from Figure 96 are that sediment of the surface layer (level 1) throughout the upper reach of Lower Granite Reservoir is medium sand and the maximum D_{50} of the surface layer does not begin to decrease until river mile 132. This indicates that the existing flow regime is capable of transporting the incoming sediment load through the upper reach. Furthermore, the D_{50} of the surface layers are generally coarser than the D_{50} of the subsurface layers. In the presence of stratification, lower strata precede upper strata in time, so this is evidence that coarser material is being transported over previously deposited finer material, a finding that is expected for an over-fit channel that is tending towards equilibrium geometry. Some level 1 subsamples from the upper reach had D_{50} sizes in the silt and fine sand range because are from cores obtained from near-shore areas and shallow benches.

The 90^{th} percentile (D_{90}) grain size diameters for Lower Granite Reservoir and the Snake River to RM 142 are shown in Figure 97. Spatial trends for D_{90} are similar to those for D_{50}. Below the confluence the maximum D_{90} is less than 0.5 mm (medium sand). Below Silcott Island the maximum D_{90} of the surface layer gradually transitions from fine sand to silt. The two level 3 subsamples from cores near Lower Granite Dam that have D90 grain sizes were likely obtained from original bed material.

The D_{50} and D_{90} grain size diameters for the surface layer in backwater zone of the Clearwater River below RM 1.6 in Figure 98 and Figure 99 are not significantly different from those in the upper reach of Lower Granite Reservoir. Both the D_{50} and D_{90} grain size plots show a slight trend to finer material in the downstream direction. This trend is expected because the turning basin at Clearwater RM 1.2 accumulates sediment and has been periodically dredged to maintain the navigation channel.

Sediment core locations and the D_{50} of the surface layer are mapped Figure 100 through Figure 105. As indicated in the plots above, the D_{50} grain size varies

depending on position in the cross section. Finer sediment accumulates along the channel margins, but there is a continuous thread of medium sand through the upper reach of Lower Granite. By comparison with the high-resolution bathymetry, there is an indication that grain size correlates with the presence and size of sand bed forms. The accuracy of the GPS measurements of the core locations does not permit a precise analysis of the correlation between grain size and bed form.

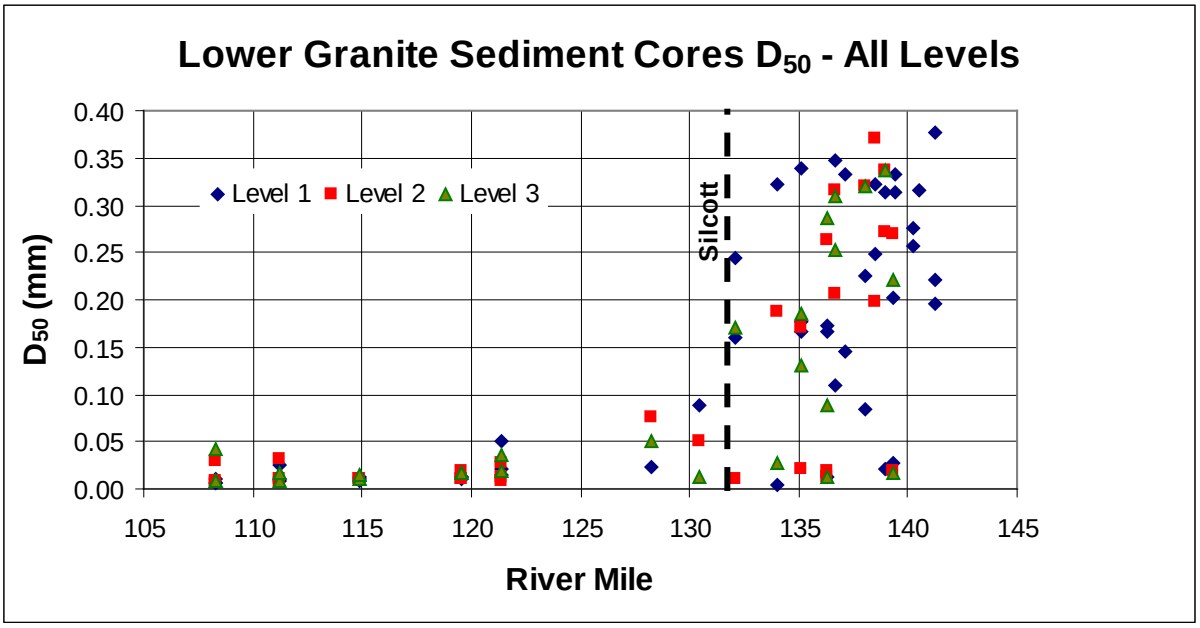


Figure 96. Spatial variation of sediment core D_{50} in Lower Granite Reservoir.

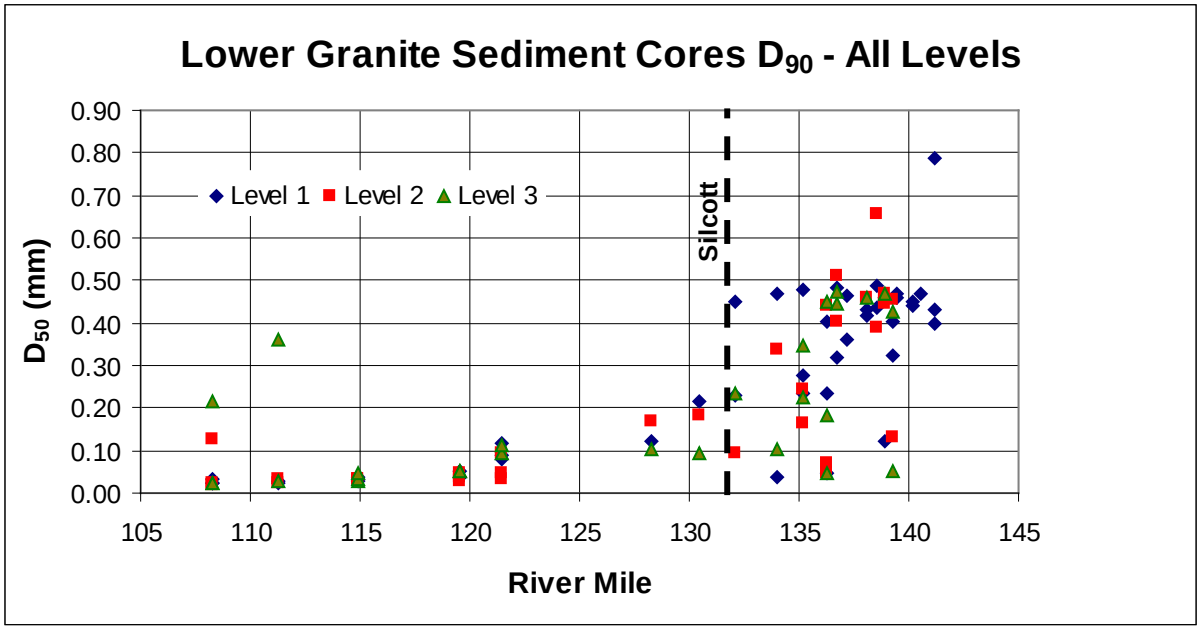


Figure 97. Spatial variation of sediment core D_{90} in Lower Granite Reservoir.

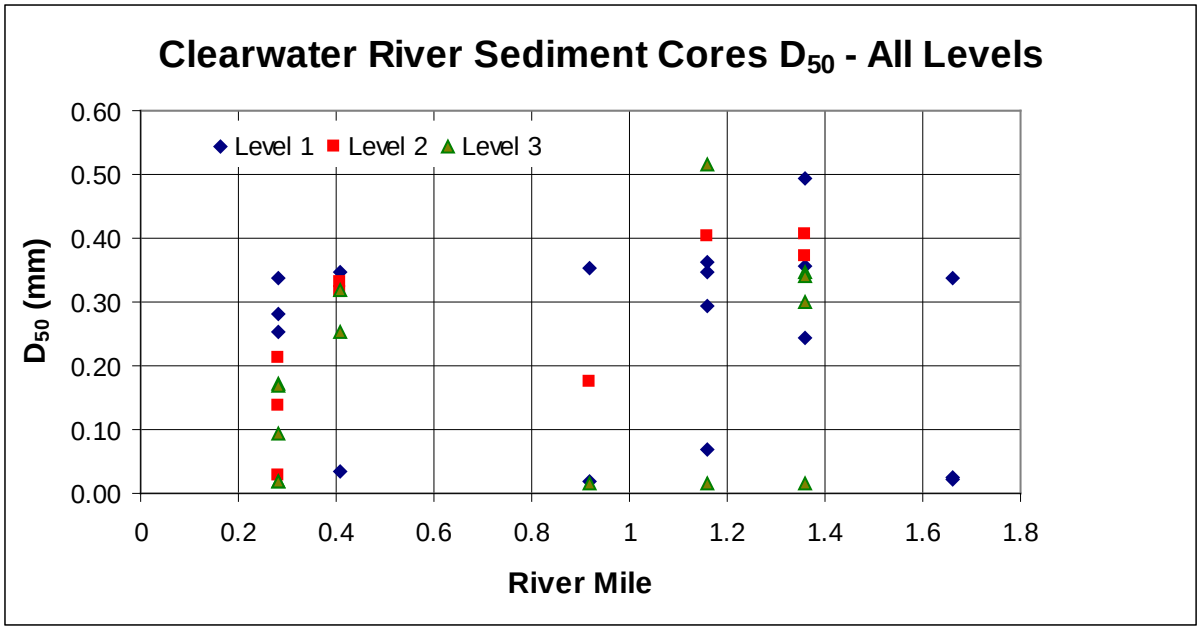


Figure 98. Spatial variation of sediment core D_{50} in the Clearwater River.

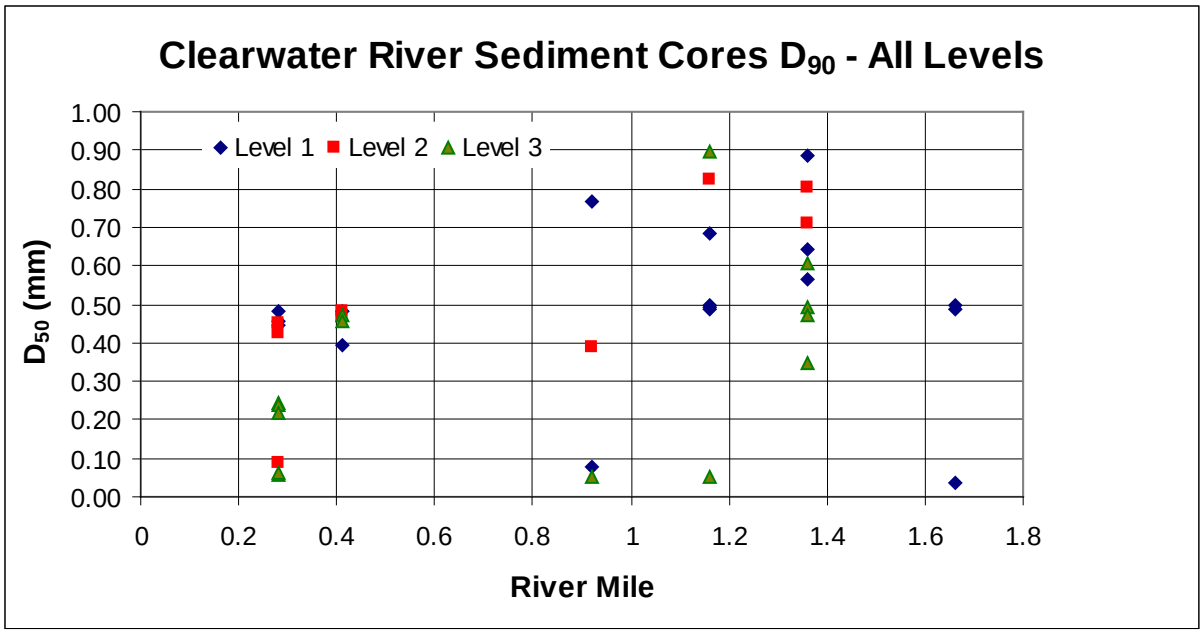


Figure 99. Spatial variation of sediment core D_{90} in the Clearwater River.



Figure 100. Map of sediment core surface D_{50} in the Snake River above the confluence.



Figure 101. Map of sediment core surface D_{50} in the Snake River below the confluence.

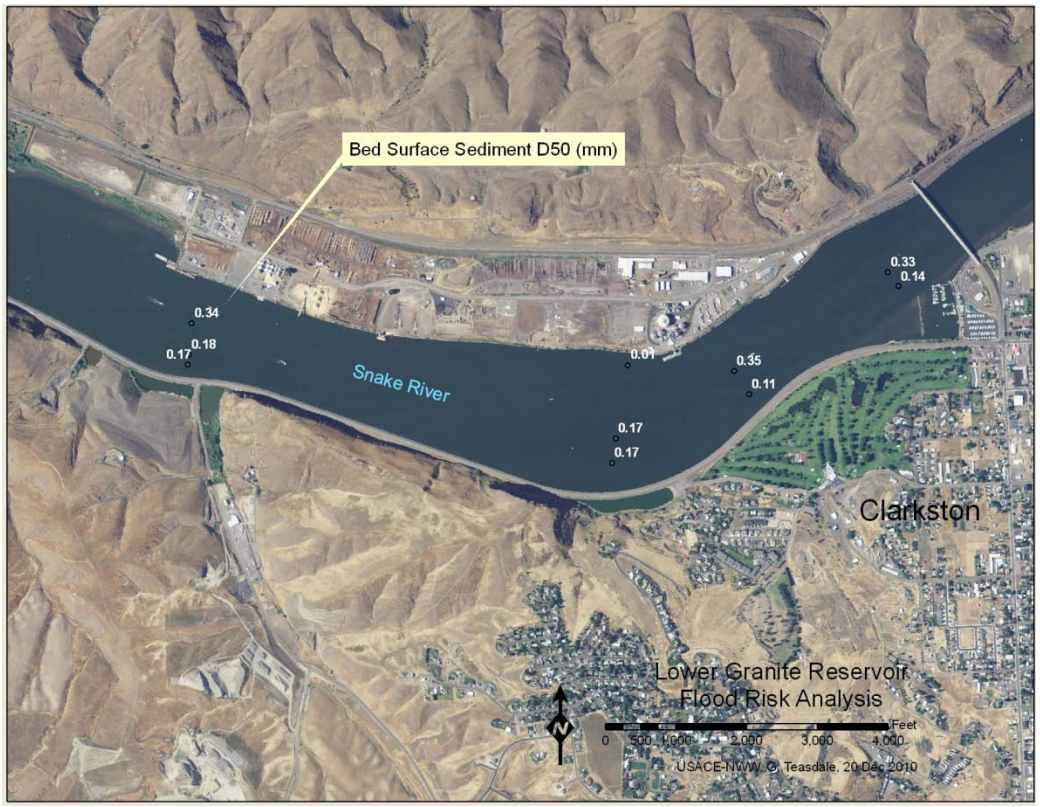


Figure 102. Map of sediment core surface D_{50} in the Snake River below Red Wolf Bridge.

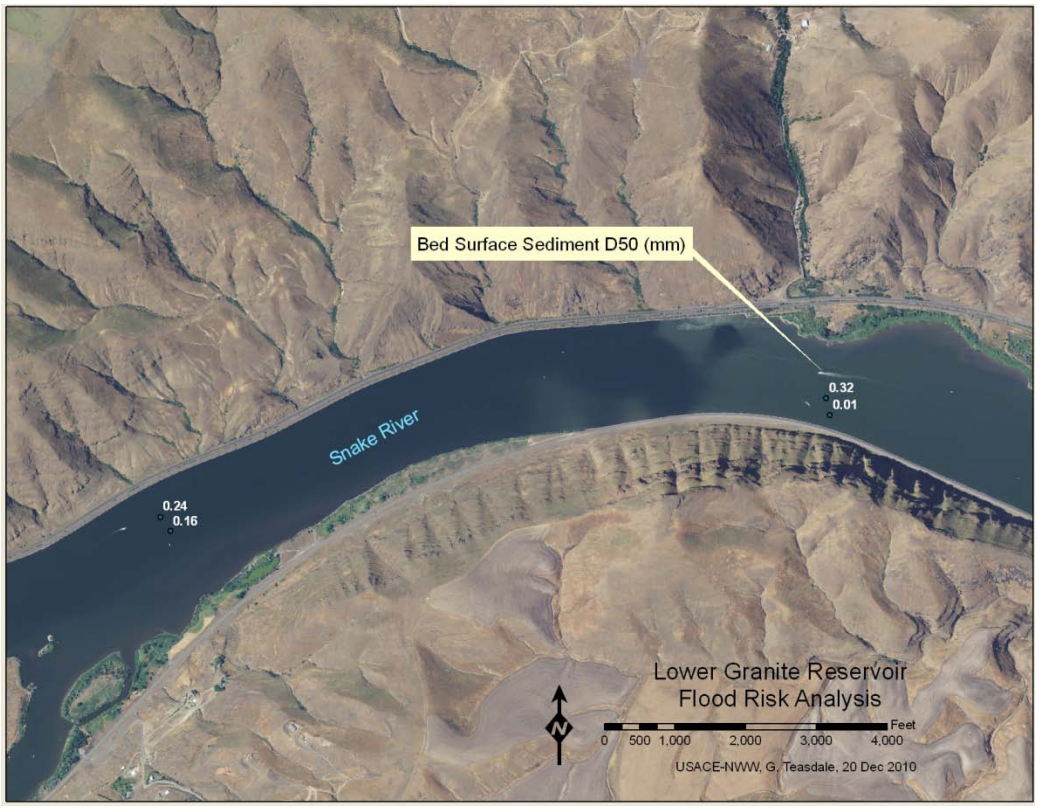


Figure 103. Map of sediment core surface D_{50} in the Snake River above Silcott Island.

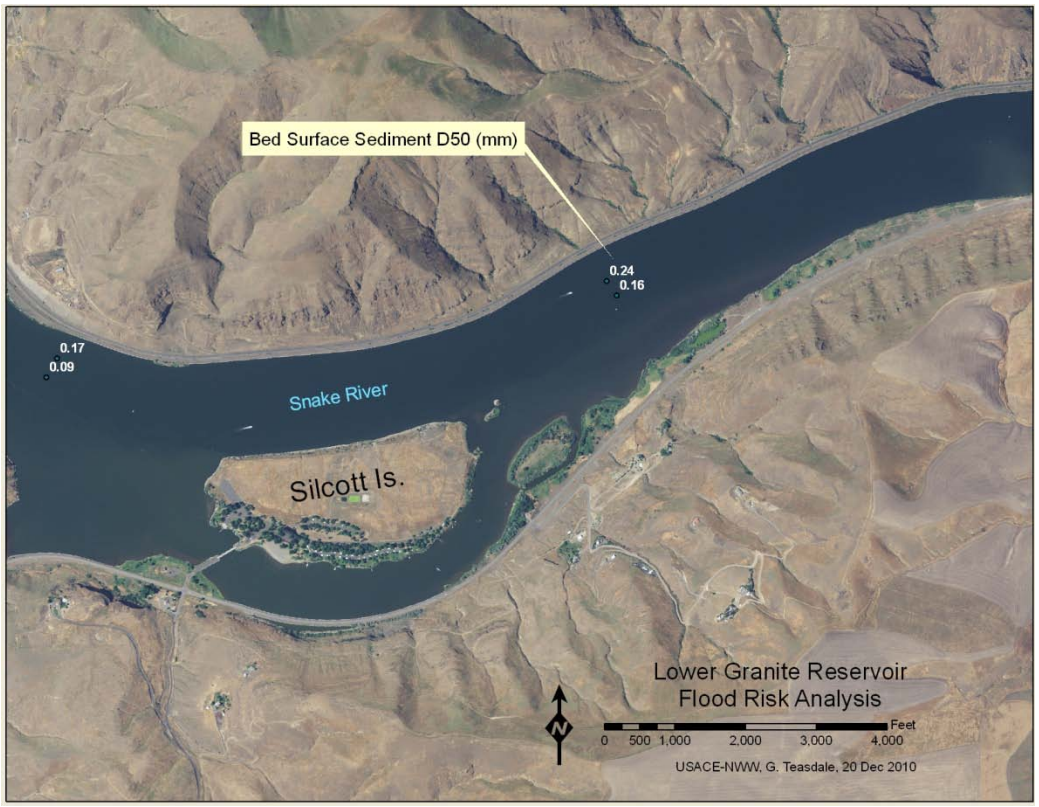


Figure 104. Map of sediment core surface D_{50} in the Snake River at Silcott Island.



Figure 105. Map of sediment core surface D_{50} in the Clearwater River below RM 1.6.

8.5. Grain Size Distributions

The D_{50} and D_{90} grain size diameters for the surface layer in backwater zone of the Clearwater River below RM 1.6 in Figure 98 and Figure 99 are not significantly different from those in the upper reach of Lower Granite Reservoir. Both the D_{50} and D_{90} grain size plots show a slight trend to finer material in the downstream direction. This trend is expected because the turning basin at Clearwater RM 1.2 accumulates sediment and has been periodically dredged to maintain the navigation channel.

Lower Granite Reservoir Snake River Bed Surface Grain Size Distribution											
				D16	D50	D75	D84	D90	Dg	Sg	Dm
Rank	River Mile	Core ID	Level ID	mm	mm	mm	mm	mm	mm	mm	mm
1	141.21	87.0	1.0	0.26	0.38	0.50	0.66	0.79	0.40	0.63	0.43
2	136.69	54.0	1.0	0.26	0.35	0.43	0.46	0.48	0.35	0.44	0.36
3	135.15	48.0	1.0	0.25	0.34	0.42	0.45	0.48	0.34	0.45	0.35
4	139.43	72.0	1.0	0.25	0.33	0.41	0.45	0.47	0.33	0.45	0.33
5	137.17	57.0	1.0	0.25	0.33	0.41	0.44	0.46	0.33	0.43	0.33
6	133.98	44.0	1.0	0.20	0.32	0.41	0.44	0.47	0.30	0.50	0.33
7	138.52	63.0	1.0	0.17	0.32	0.42	0.46	0.49	0.29	0.54	0.34
8	140.51	81.0	1.0	0.19	0.32	0.40	0.44	0.47	0.30	0.51	0.32
9	138.94	65.0	1.0	0.19	0.31	0.40	0.43	0.46	0.29	0.50	0.31
10	139.43	73.0	1.0	0.18	0.31	0.40	0.44	0.46	0.29	0.51	0.31
11	140.22	80.0	1.0	0.15	0.28	0.38	0.42	0.45	0.26	0.52	0.28
12	140.22	78.0	1.0	0.15	0.26	0.36	0.41	0.44	0.25	0.50	0.27
13	138.52	62.0	1.0	0.15	0.25	0.35	0.40	0.44	0.25	0.50	0.26
14	132.05	41.0	1.0	0.15	0.24	0.36	0.41	0.45	0.25	0.51	0.27
15	138.07	59.0	1.0	0.11	0.23	0.34	0.39	0.43	0.22	0.53	0.24
16	141.21	89.0	1.0	0.13	0.22	0.33	0.39	0.43	0.22	0.51	0.24
17	139.29	71.0	1.0	0.14	0.20	0.28	0.35	0.40	0.22	0.46	0.23
18	141.21	88.0	1.0	0.14	0.19	0.26	0.34	0.40	0.21	0.45	0.22
19	135.15	47.0	1.0	0.13	0.18	0.22	0.24	0.28	0.18	0.33	0.20
20	136.29	49.0	1.0	0.13	0.17	0.21	0.22	0.23	0.17	0.30	0.17

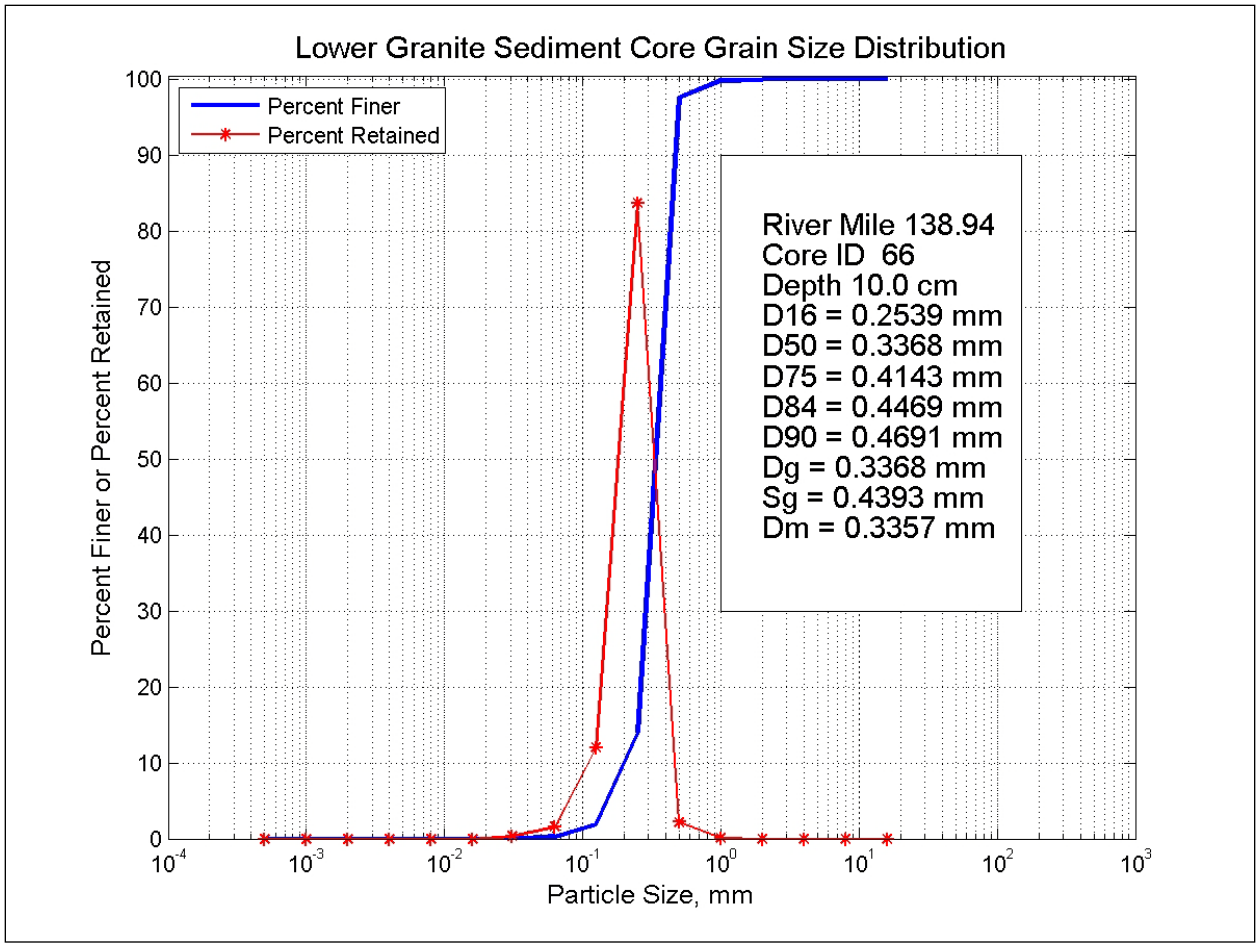


Figure 106. Grain size distribution Snake RM 138.94.

9. Sediment Load at Lower Granite Reservoir

The sediment transport model of Lower Granite Reservoir requires sediment load time series for the Snake and Clearwater Rivers as upstream boundary conditions. This section discusses how the sediment load time series were developed from current and historic sediment load measurements. Nearly all the sediment load to Lower Granite Reservoir is delivered by the Snake and Clearwater Rivers. The small tributary creeks that flow directly into Lower Granite Reservoir contribute small amounts of sediment. As discussed in Section 1, the 102,600 square mile Snake and Clearwater River drainage is partially regulated by large reservoirs. The dams in the Hells Canyon complex on the Snake River and Dworshak Dam on the North Fork of the Clearwater River trap sediment that is larger than all but the finest silt and clay particles. The total area of the watershed that contributes sediment directly to the dams on the lower Snake River is 32,500 sq. mi. (Figure 107). About 27,140 square miles of the Snake and Clearwater River watershed delivers sediment directly to Lower Granite Reservoir.

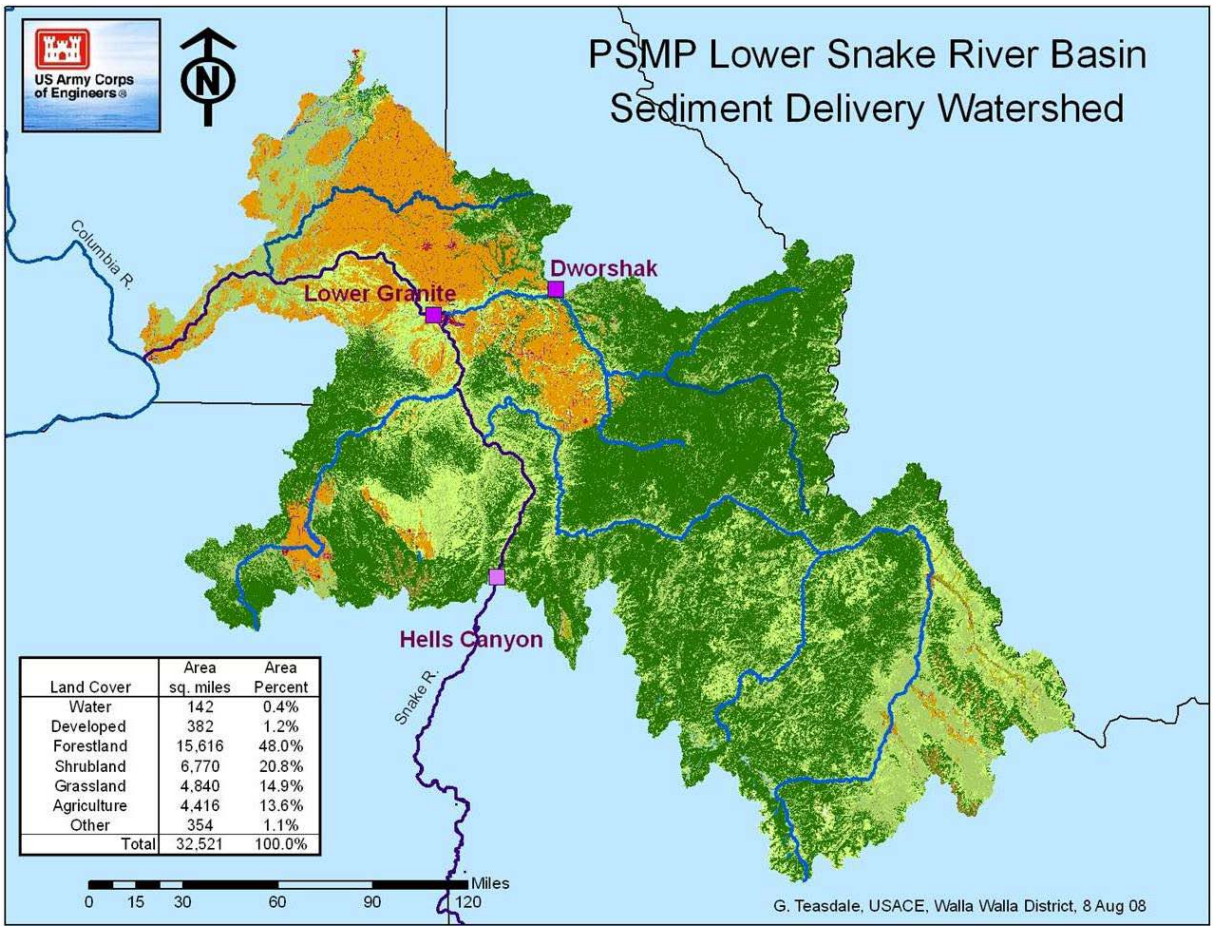


Figure 107. Lower Snake River sediment delivery watershed.

Sediment load was measured during the current investigation at each of the locations shown as solid boxes in schematic in Figure 108. The primary sediment load measurement sites are at the stream gage stations at Anatone (USGS 13334300, RM 167) on the Snake River and at Spalding (USGS 13342500, RM 11.6) on the Clearwater River. Sediment load was monitored at Anatone and Spading (Figure 88) in a previous study during the 1970's. Sediment load at Anatone and Spalding is summed to estimate the sediment load at Lower Granite. Both rivers are free-flowing between the stream gages and the backwater of Lower Granite Reservoir and the historic sediment ranges showed no significant sediment accumulation or scour in these reaches.

Suspended sediment load and bedload were measured at Anatone and Spalding from 2008 through 2010 using conventional sampling methods. The current measurements can be directly compared to historic sediment load measurements obtained by similar methods at these sites. Suspended sediment was also measured with surrogate electronic techniques during part of the period. In 2009, conventional suspended sediment sampling was extended to the upstream tributary locations to better characterize sediment sources in the watershed.

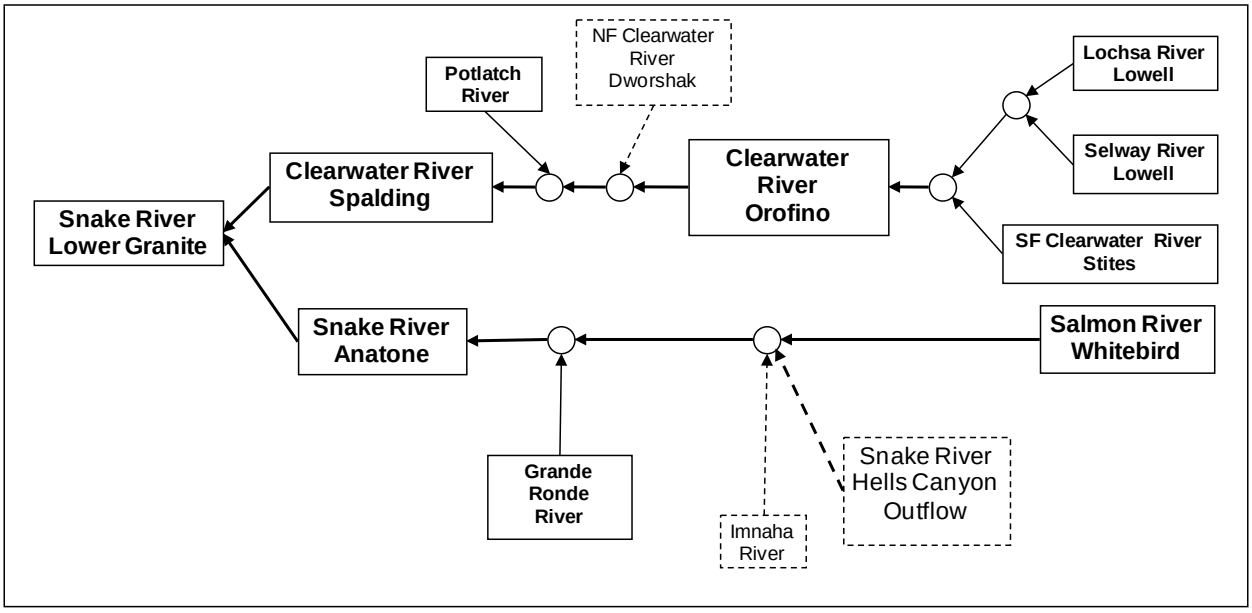


Figure 108. Lower Granite Reservoir sediment delivery watershed.

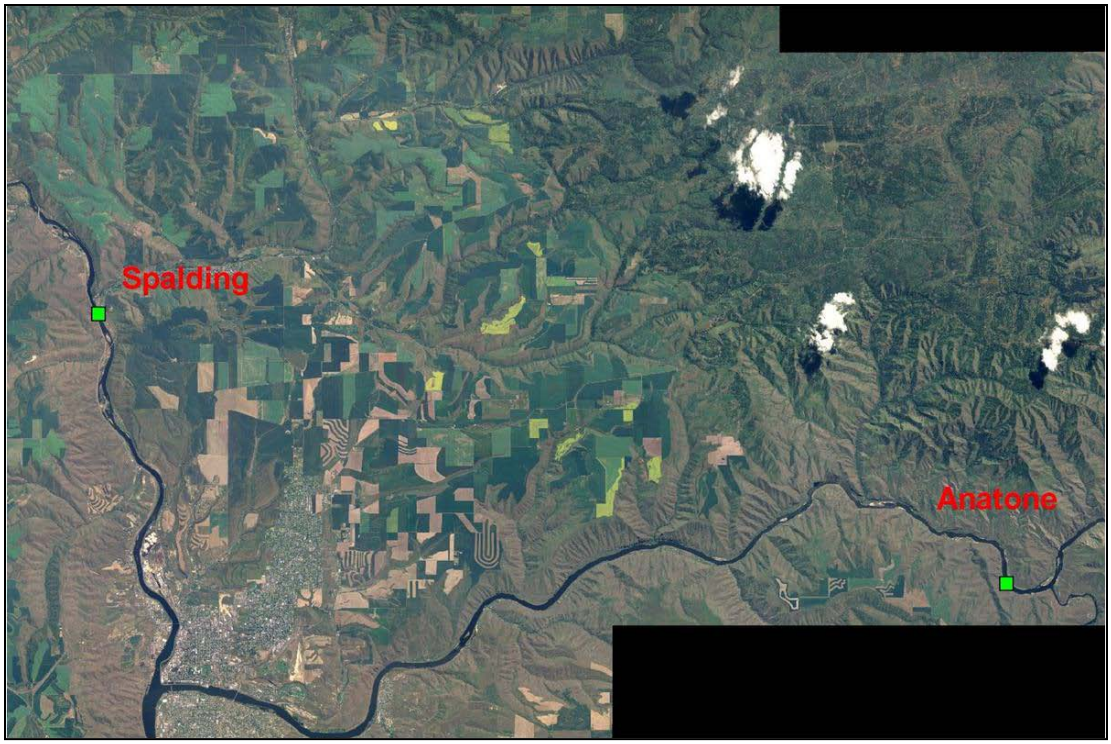


Figure 109. Primary sediment monitoring stations on the Snake and Clearwater Rivers.

9.1. Historic Sediment Load Measurements

The U.S. Geological Survey measured sediment load in the Snake River at Anatone and in the Clearwater Rivers at Spalding[87] from 1972 to 1979. Suspended sediment and bedload were measured with conventional sampling methods[88] equivalent to those employed in the current study. Suspended sediment was measured with P-61 or P-63 samplers and bedload was measured with Helley-Smith sampler with a 6 inch by 6 inch orifice. Some bedload samples in 1972 were obtained with a Helley-Smith sampler that had a 3 inch by 3 inch orifice. The intensive 1970's study measured sediment across a broad range of flows that varied from very low flow drought conditions to very high snowmelt discharges. The 1970's dataset has been cited in many sediment transport studies[89] and it provides a high quality reference to evaluate time trends in sediment load and grain size at Lower Granite.

Sediment load measured during the 1970's study is plotted with the historic daily discharge series in Figure 110 and Figure 111. The sediment load measurements are distributed through the seasonal hydrograph and characterize the natural variability of the sediment load. Discharge and sediment load are plotted on logarithmic scales to better depict the range of sediment load measurements. The plots visually accentuate bedload mass, which is a relatively minor fraction of total sediment load.

At Anatone, the maximum measured suspended load was 268,000 U.S. tons per day (tpd) on 19 June 1974 at a discharge of 191,000 cfs. The suspended sediment concentration was 512 mg/L, 52 percent of which was silt or finer. Both the suspended sediment concentration and the discharge during this event were the maximum values in the set of 69 measurements. The suspended sand load at this discharge is much less than that predicted by equilibrium sediment transport functions, which indicates that transport is limited by the available supply of sediment. Supply limited conditions for the transport of sand, silt and clay sediment are not uncommon in regulated gravel-bed river systems.

A total of 75 suspended sediment samples were measured at Spalding. The maximum measured suspended load was 139,000 tpd on 8 May 1979 at a discharge of 47,800 cfs. The suspended sediment concentration was 1070 mg/L, 98 percent of which

[87] Jones, M.L and H.R. Seitz. (1980). Sediment Transport in the Snake and Clearwater Rivers in the Vicinity of Lewiston, Idaho, Water Resources Investigations Open File Report 80-690, U.S. Geological Survey, Lakewood, CO.

[88] Edwards, T.K. and G. D. Glysson (1999). Field Methods for Measurement of Fluvial Sediment, U.S. Geological Survey, Techniques of Water-Resources Investigations, Book 3, Chapter C2. U.S. Geological Suvey, Reston, VA.

[89] For example, Bravo-Espinosa, M., Osterkamp, W.R., Lopes, V.L. (2003) "Bedload transport in alluvial channels", *J. Hydraulic Engineering*. 129(10), 783-795.

was silt or finer. The maximum sediment load measured at Spalding is somewhat incongruous in that it occurred at a relatively moderate discharge. The high percentage of fine material in the sediment load during this event indicates that the sediment was generated by surface erosion in the agricultural areas of the lower Clearwater basin. Supply limited conditions for sand, silt and clay are again indicated.

There were 63 bedload measurements at Anatone and 78 bedload measurements at Spalding. Maximum measured bedload at Anatone was 5,600 tpd on 14 April 1976 at a discharge of 94,800 cfs and the maximum bedload measured at Spalding was 3,700 tpd on 20 June 1974 at a discharge of 110,000 cfs. Suspended sediment is the largest fraction of the total sediment load at both sites. During this period, bedload averaged 64 percent sand at Anatone and 85 percent sand at Spalding. Bedload amounts were between 2 and 10 percent of the suspended load and averaged about 5 percent[87].

Sediment measurements obtained for the Clearwater River in 1974 were made immediately before and after the extreme regulated discharge of record that occurred during an inadvertent release from Dworshak Reservoir at the height of a regional snowmelt flood. A peak discharge of 131,000 cfs occurred on 16 June 1974. The following day on 17 June 1974, a bedload of 1,130 tpd was measured in the Clearwater River at a discharge of 124,000 cfs. Three days later, a bedload of 3,670 tpd was measured at a discharge of 110,000 cfs. A suspended sediment load of 41,300 tpd was measured on 18 June 1974 at a discharge of 117,000 cfs. About 43 percent of the suspended sediment load was silt and clay.

The bedload and suspended sediment loads measured during June 1974 should be similar to the sediment load that would be expected during the Standard Project Flood (SPF) on the Clearwater River. This event was a large snowmelt flood and the bedload transport should have been active on most of the gravel bars in the Lower Clearwater River. The 131,000 cfs discharge is about 87 percent of the Standard Project Flood (SPF) discharge of 150,000 cfs for the Clearwater River at Lewiston and was the largest flood since the pool of Lower Granite was raised. The probability analysis in Section 2.9 showed that during the joint SPF when the Snake and Clearwater Rivers total 420,000 cfs the most likely contribution from the Clearwater River is approximately 125,000 cfs. Bedloads measured during June 1974 were not extraordinary. Thus, it is reasonable to conclude that bedload in the Clearwater River is a relatively minor component of the total sediment load that would be expected during the SPF for Lower Granite. Furthermore, it will be shown below that the suspended sediment load carried by this flood was also not extraordinary in the Clearwater River. This is important because sediment loads for the mobile bed hydraulic model are estimated from relationships developed from the historic sediment measurements and

the estimates are more accurate when the estimates are within the range of the original data. Development of the sediment load relationships is discussed in Section 9.

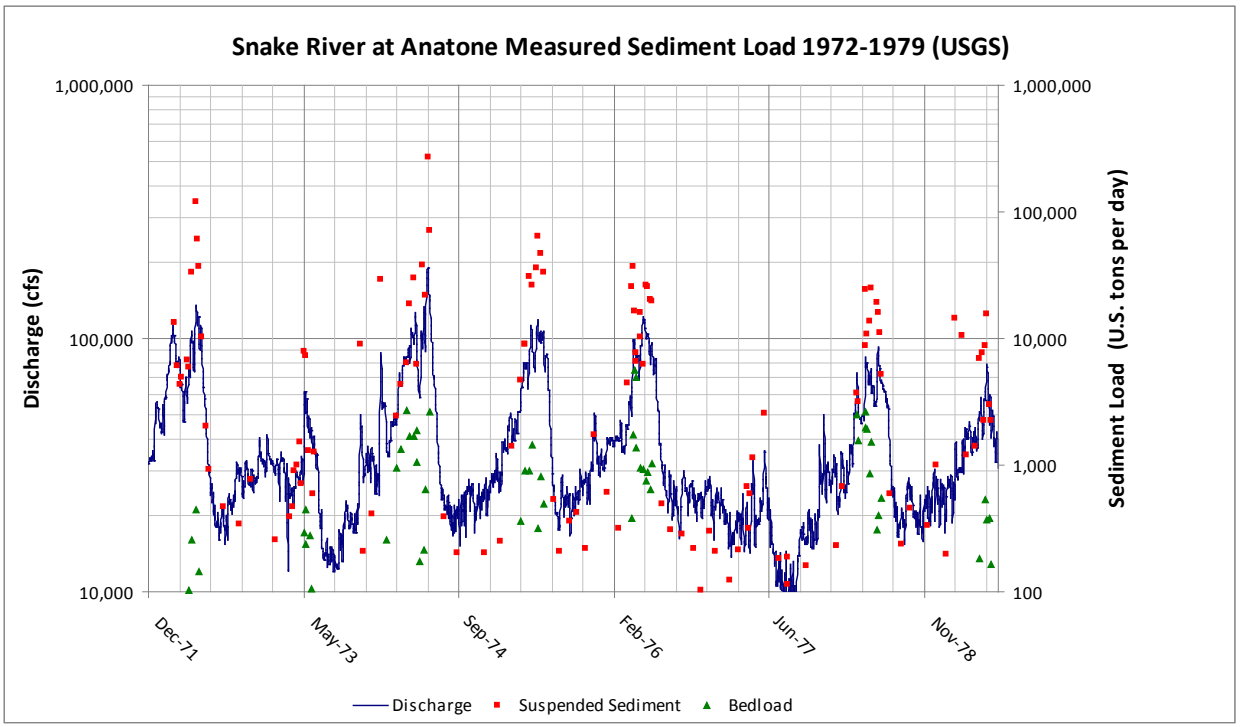


Figure 110. Snake River at Anatone measured sediment load 1972-1979.

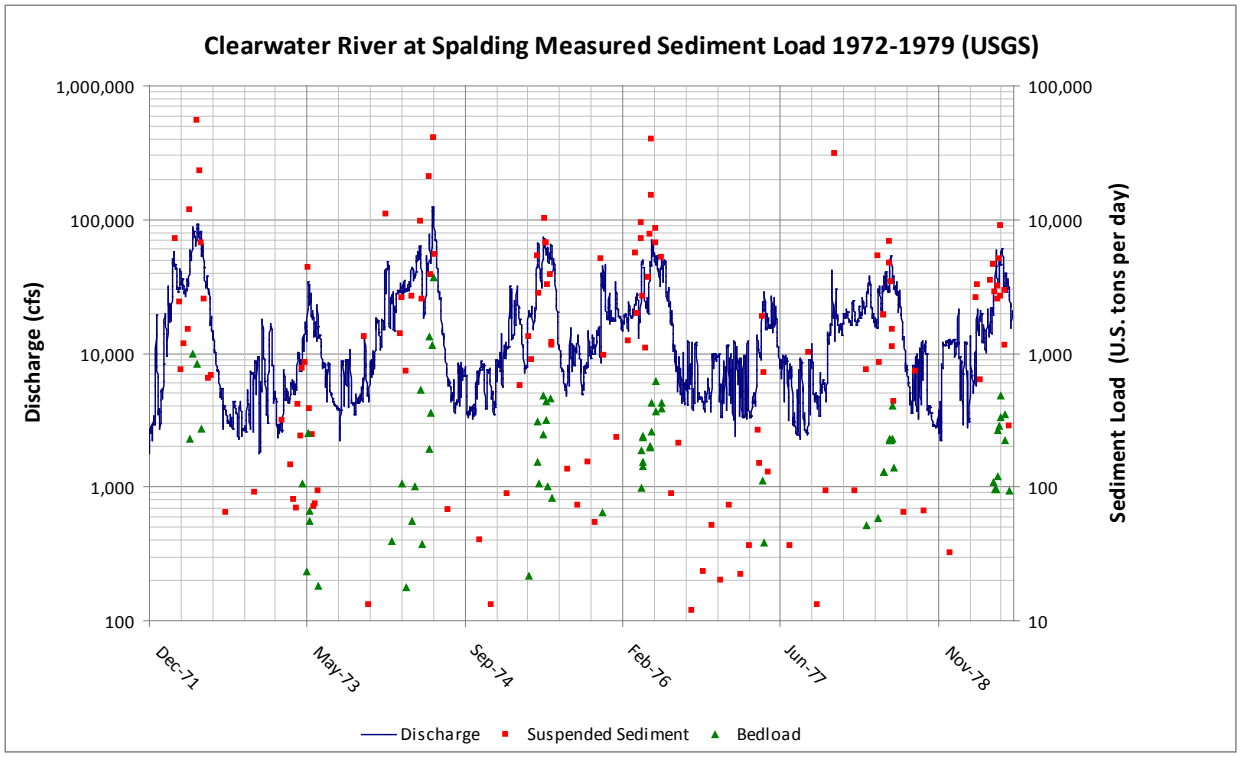


Figure 111. Clearwater River at Spalding measured sediment load 1972-1979.

9.2. 2008-2010 Sediment Load at Anatone and Spalding

Sediment load was again measured for the Corps by USGS at Anatone and Spalding from 2008 through 2011. A total of 38 suspended sediment measurements were obtained at each site. Suspended sediment load and bedload measurements are plotted with the discharge series in Figure 112 and Figure 113. The measurements are well distributed through the seasonal hydrographs. The maximum suspended load measured at Anatone was 173,000 U.S. tons per day (tpd) on 6 June 2010 at a discharge of 155,000 cfs. The suspended sediment concentration was 414 mg/L, 44 percent of which was silt or finer. As with the historic data, the maximum suspended sediment concentration occurred when the discharge was also the maximum value in the recent set of measurements.

The maximum suspended load measured at Spalding was 44,700 tpd on 19 May 2008 at a discharge of 78,900 cfs. The suspended sediment concentration was 210 mg/L, 42 percent of which was silt or finer. The maximum suspended sediment concentration occurred at the maximum discharge in the recent set of measurements. Similar to the historic data, most of the total sediment load at both sites is suspended sediment.

The number of bedload measurements totaled 13 at Anatone and 17 at Spalding. Bedload measurements for 2010 and 2011 were not available at the time this report

was written. Maximum bedload measured at Anatone was 300 tpd on 10 June 2008 at a discharge of 73,200 cfs. Maximum bedload measured at Spalding was 840 tpd on 19 May 2008 at a discharge of 82,900 cfs. During this period, bedload averaged 62 percent sand at Anatone and 63 percent sand at Spalding. Bedload amounts were between 2 and 10 percent of the suspended load and averaged about 6 percent.

Suspended sediment loads for the 1972-1979 and 2008-2010 periods are combined and ranked in order of decreasing sediment load in Table 46 and Table 47 to show the top twenty suspended sediment loads. The ranges of discharge given in the tables are those that carry most of the sediment load into Lower Granite Reservoir. In this range, the silt or clay fraction amounts to about 61 percent in the Snake River and 56 percent in the Clearwater River.

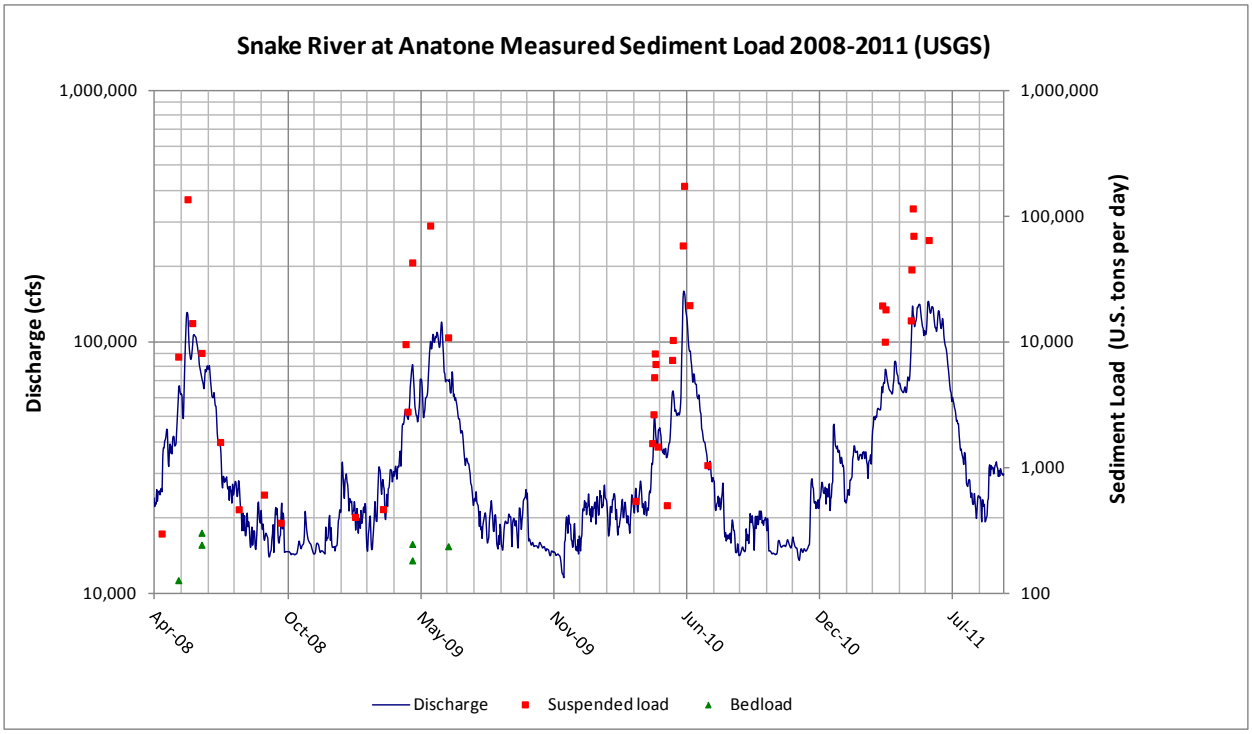


Figure 112. Snake River at Anatone measured sediment load 2008-2009.

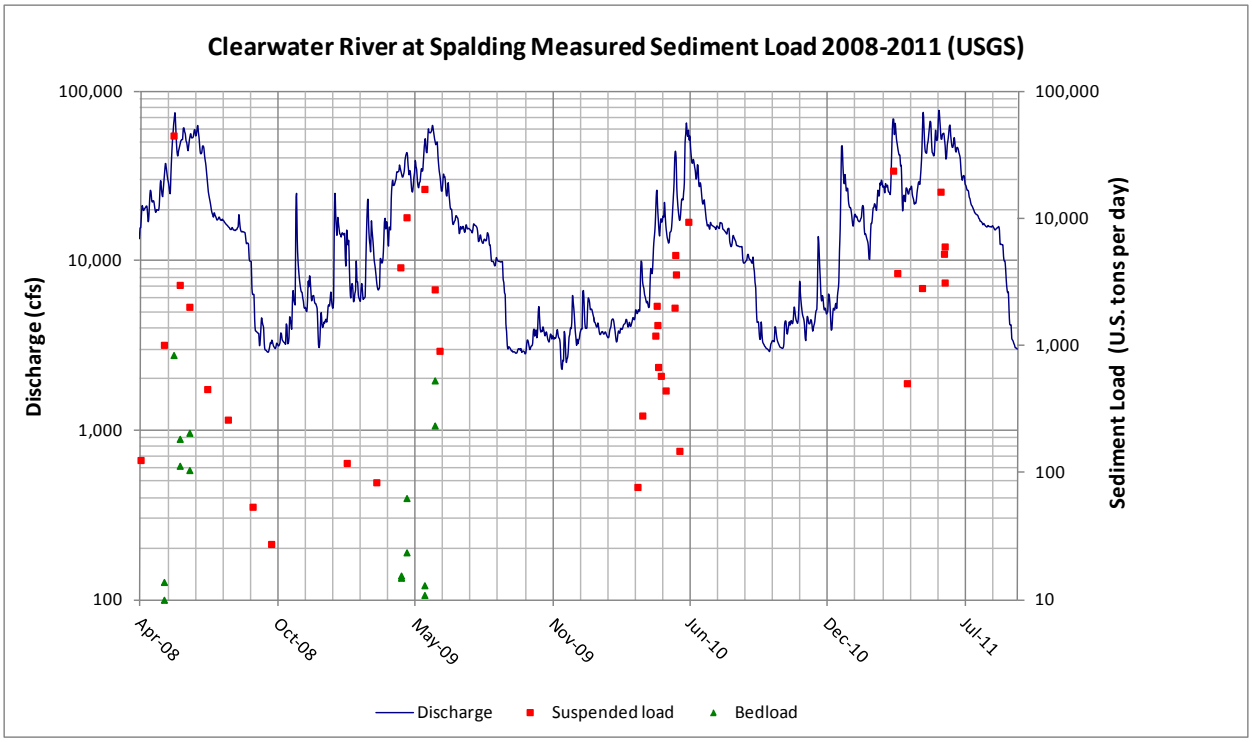


Figure 113. Clearwater River at Spalding measured sediment load 2008-2010.

Ranked Measured Suspended Sediment Loads at Snake River at Anatone							
Rank	Date	Discharge cfs	Suspended Sediment Concentration mg/L	Suspended Sediment Load US ton/day	Percent Finer than Silt <0.062 mm	Sand Concentration mg/L	Sand Load US ton/day
1	6/19/1974	191,000	521	268,250	52	250.1	128,760
2	6/6/10	155,000	414	172,982	44	231.8	96,870
3	5/20/08	129,000	389	135,272	53	182.8	63,578
4	6/2/1972	133,000	338	121,182	73	91.3	32,719
5	5/16/11	141,000	301	114,407	46	162.5	61,780
6	5/20/2009	103,000	301	83,574	49	153.5	42,623
7	6/26/74	141,000	186	70,697	57	80.0	30,400
8	5/17/2011	126,000	204	69,290	54	93.8	31,873
9	6/9/11	145,000	164	64,103	43	93.5	36,539
10	6/4/2010	105,000	205	58,025	42	118.9	33,654
11	6/18/1975	91,700	187	46,225	74	48.6	12,019
12	4/23/2009	86,200	183	42,523	60	73.2	17,009
13	6/4/1974	107,000	133	38,362	66	45.2	13,043
14	4/13/1976	98,400	141	37,401	68	45.1	11,968
15	5/14/2011	102,000	136	37,394	52	65.3	17,949
16	6/5/1975	104,000	128	35,885	64	46.1	12,919
17	5/14/1975	93,900	123	31,134	75	30.8	7,784
18	5/25/1976	102,000	95	26,121	54	43.7	12,016
19	5/27/1976	102,000	94	25,846	54	43.2	11,889
20	4/7/1976	61,800	152	25,322	80	30.4	5,064
	Average	115,900	220	75,200	58	96	34,023

Table 46. Top ranked measured suspended sediment load Snake River at Anatone.

Ranked Measured Supended Sediment Loads at Clearwater River at Spalding							
Rank	Date	Discharge cfs	Suspended Sediment Concentration mg/L	Suspended Sediment Load US ton/day	Percent Finer than Silt <0.062 mm	Sand Concentration mg/L	Sand Load US ton/day
1	5/8/1979	47,800	1070	137,873	98	21.4	2,757
2	6/1/1972	96,700	209	54,481	56	92.0	23,971
3	5/19/08	78,900	210	44,665	42	121.8	25,906
4	6/18/1974	117,000	131	41,317	43	74.7	23,551
5	5/11/1976	80,200	185	39,996	49	94.4	20,398
6	12/14/1977	27,000	426	31,006	98	8.5	620
7	4/1/2011	60,500	145	23,648	63	53.7	8,750
8	6/5/74	68,700	113	20,927	54	52.0	9,626
9	5/19/2009	60,600	104	16,989	50	52.0	8,495
10	6/9/2011	72,200	83	16,154	65	29.1	5,654
11	5/12/76	69,000	81	15,066	36	51.8	9,642
12	1/19/1974	28,000	144	10,869	97	4.3	326
13	4/23/09	56,300	67	10,168	72	18.8	2,847
14	4/6/1976	36,800	96	9,523	91	8.6	857
15	6/7/2010	54,300	64	9,368	40	38.4	5,621
16	5/23/1979	55,100	60	8,912	31	41.4	6,149
17	5/24/1976	59,300	53	8,472	24	40.3	6,439
18	5/6/1976	53,600	53	7,658	47	28.1	4,059
19	6/6/1978	55,000	46	6,820	42	26.7	3,956
20	6/10/1975	59,100	42	6,691	31	29.0	4,617
	Average	61,805	169	26,030	56	44	8,712

Table 47. Top ranked measured suspended sediment load Clearwater River at Spalding.

9.3. Time Series Trend in Sediment Load

The suspended sediment concentrations for the 1972-1979 and 2008-2010 periods for Anatone and Spalding are plotted in Figure 114, Figure 115 and Figure 118. Power regression lines were fit to the data from each period. Regression lines that are significantly different between periods indicate that the sediment load rating curve has changed, possibly because of altered watershed conditions or climate cycles.

In Figure 114, the regression line for the 2008-2010 data at Anatone plots somewhat above the regression line for the 1972-1979 data, indicating that suspended sediment loads in the Snake River may have generally increased. The plot of suspended sand fraction of Figure 115 also indicates that the sand load (which is part of the total suspended sediment load) has increased. The characterization of sediment yield in the Salmon River discussed in the EIS suggests that increased frequency and extent of wildfire have increased sediment loads.

A test for a step-trend[90,91] may be performed with the measured suspended sediment and suspended sand concentration data. Effects of the exogenous variable discharge are removed by applying a regression of the power relationship to the concentration data. Residual concentrations, computed as the difference of the measured concentration and regression estimate, appear to increase with time in Figure 116 and Figure 117. The significance and strength of the trend is determined with the non-parametric Mann-Whitney-Wilcoxon rank sum test computed with the R statistical package[92]. Results of the Mann-Whitney-Wilcoxon test summarized in Table 48 indicate the step trend in suspended sediment and suspended sand are both significant at 0.01 level. The magnitude of the shift in concentration is 13 mg/L for suspended sediment and 10 mg/L for suspended sand, which indicates that the trend is mostly due to an increase in suspended sand load. Note that the median values reported in the table are the median of the difference between a sample drawn from the 1974-1979 data and a sample from the 2008-2011 data[92]. The present and historic sediment rating curves for the Clearwater River at Spalding in Figure 118 are not significantly different. Other methods of trend analysis are available[93].

An important finding from this data is that there is no evidence that annual sediment loads to Lower Granite Reservoir are decreasing. Moreover, a comparison of past and present measured sediment data for the Snake River indicates an increasing trend, particularly in suspended sand load. It may be that with additional measurements of sediment load the increase in trend may weaken and become insignificant, and there is no absolute assurance that methods of sample collection and analysis were the same in both periods which weakens the statistical analysis. Also, suspended sand concentrations are greatest near the bed, which makes suspended sand measurements especially sensitive to methodology. Nonetheless, increasing sediment load has serious management implications for Lower Granite Reservoir and an engineering judgment must be made in consideration of the existing data. For planning purposes and flood risk analysis, the expectation should be that sediment inflows to Lower

[90] Helsel, D.R. and Hirsch, R.M. (2002) *Statistical Methods in Water Resources Techniques of Water Resources Investigations, Book 4, chapter A3*. U.S. Geological Survey. 522 pages.

[91] McCuen, R.H. (2002) *Modeling Hydrologic Change: Statistical Methods*, CRC Press, Baca Raton.

[92] http://www.r-project.org/

[93] Kundzewicz, Z.W. and Robson, A.J. (2004) "Change detection in hydrologic records- a review of the methodology." *Hydrologic Sciences*, 49(1).

Granite Reservoir are increasing and that alternatives for sediment management must take this into account.

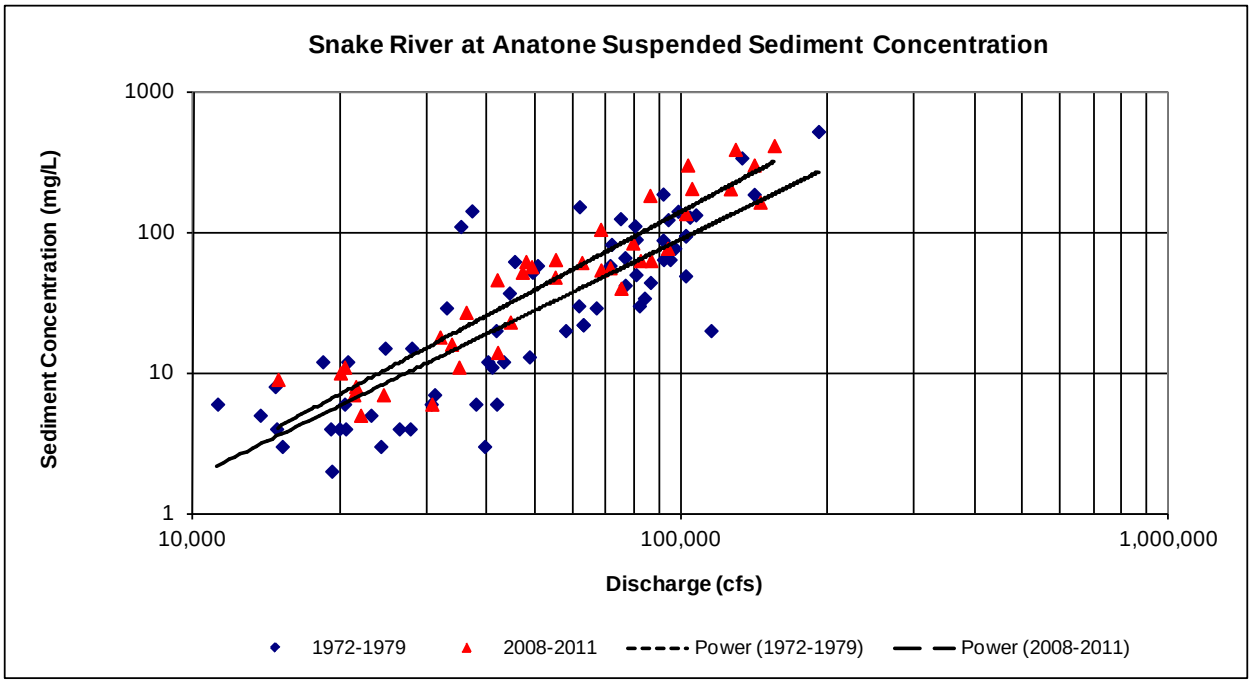


Figure 114. Comparison of suspended sediment concentration at Snake River at Anatone for the periods 1972-1979 and 2008-2011.

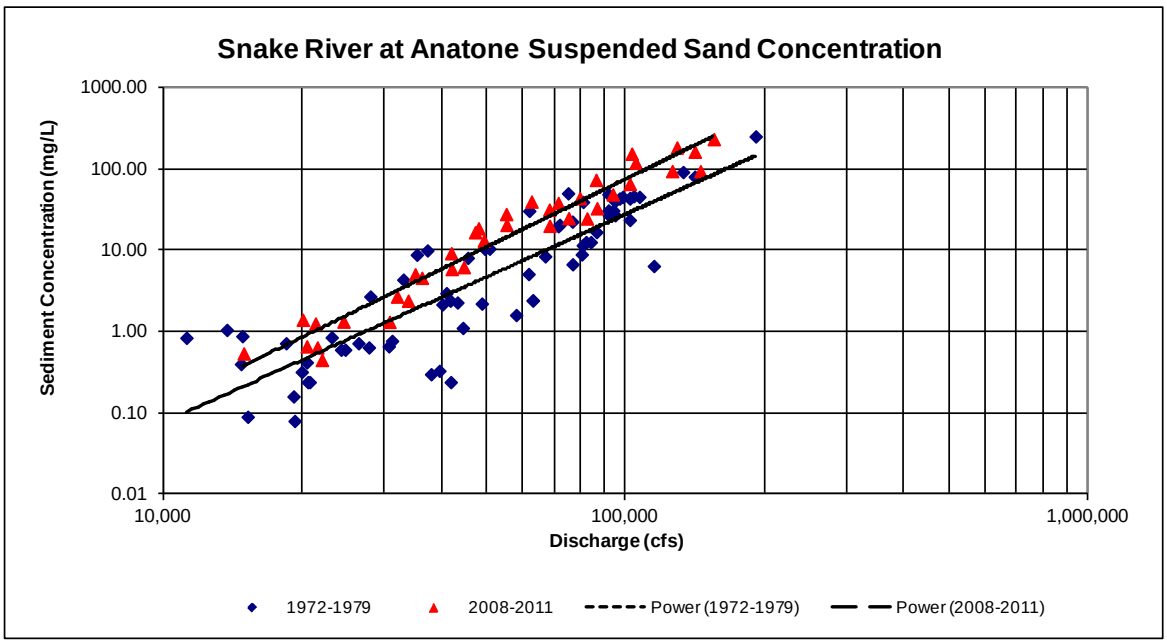


Figure 115. Comparison of suspended sand concentration at Snake River at Anatone for the periods 1972-1979 and 2008-2011.

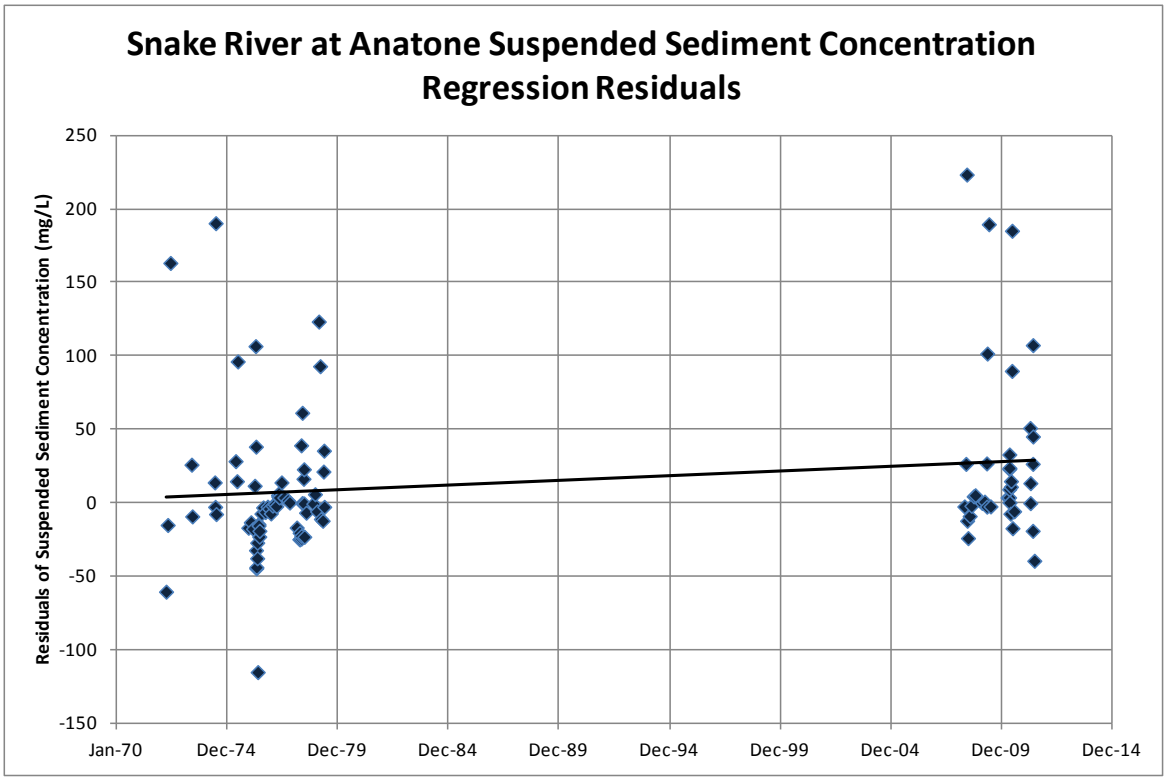


Figure 116. Residuals of suspended sediment concentration at Snake River at Anatone.

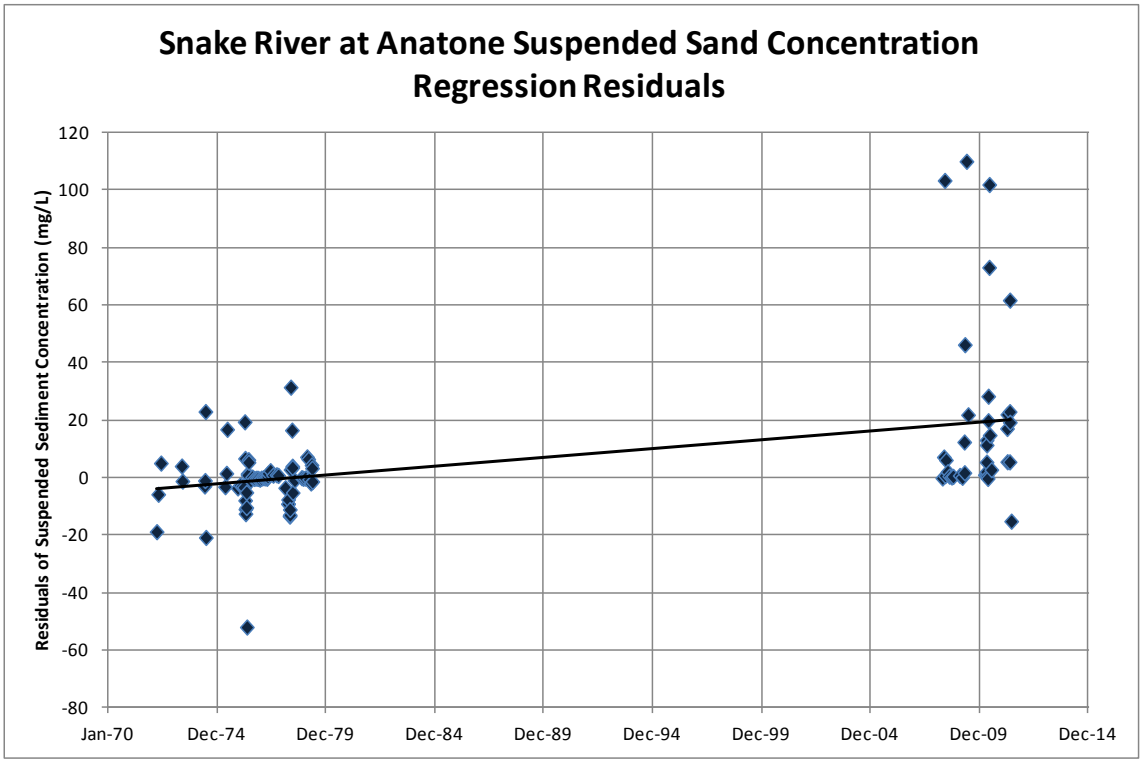


Figure 117. Residuals of suspended sand concentration at Snake River at Anatone.

Mann-Whitney-Wilcoxon Test for Step Trend Snake River at Anatone Suspended Sediment Measurements 1974-1979 and 2008-2011					
			95 percent Confidence Interval		
			Low	High	Median
Data	W	P-value	mg/L	mg/L	mg/L
Suspended sediment concentration	900	0.0075	3	24	13
Suspended sand concentration	519	<0.0001	5	16	10

Table 48. Results of Mann-Whitney-Wilcoxon test for step-trend for suspended sediment in the Snake River at Anatone.

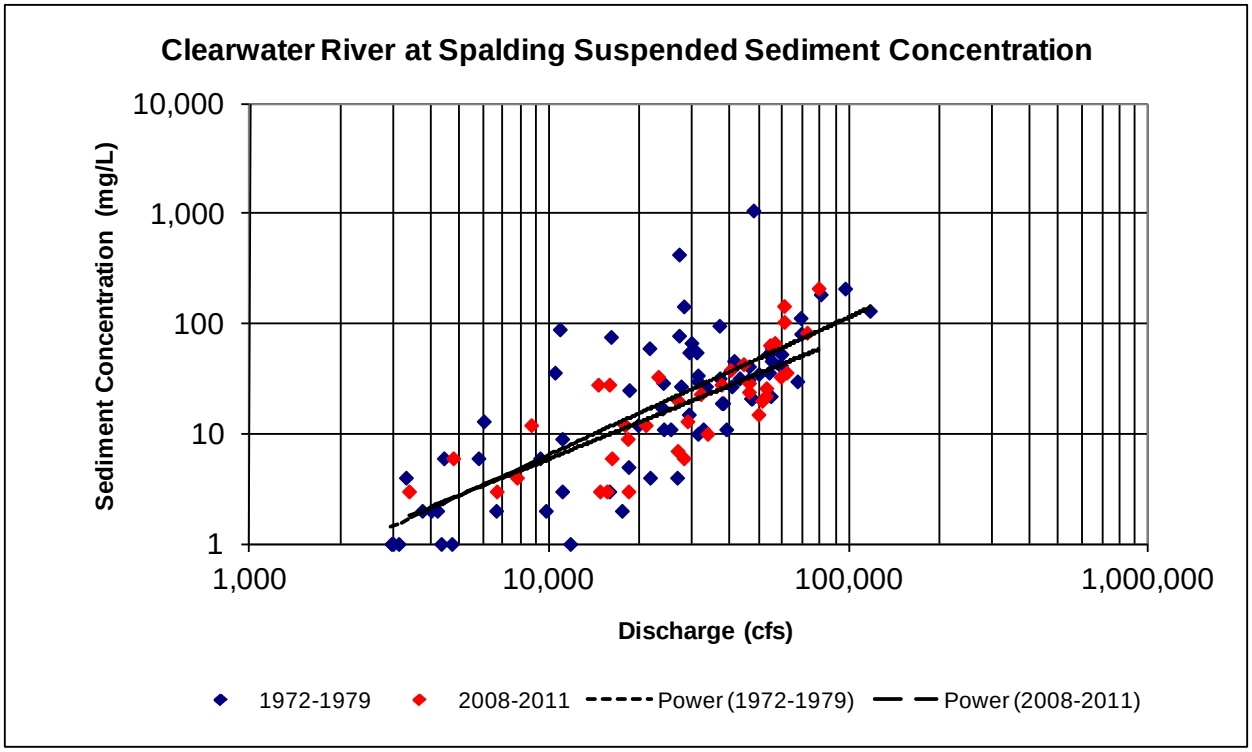


Figure 118. Comparison of suspended sediment concentration at Clearwater River at Spalding for the periods 1972-1979 and 2008-2010.

9.4. Sediment Load Estimation

The primary objective of the sediment load analysis discussed below is to estimate the sediment load that can be expected during the 50-year future analysis period of the EIS. Credible estimates of sediment load are needed for the mobile-bed modeling of sediment accumulation in Lower Granite Reservoir and the planning of sediment management measures. The approach to developing the sediment load time series involves a number of steps including:

1. Fit mathematical relationships to the measured sediment load data,

2. Apply the load relationships to the historic discharge series to produce an estimate of the historic sediment load at Lower Granite Reservoir,
3. Convert the estimated sediment load to an equivalent sediment volume and compare the estimate with the measured sediment accumulation in Lower Granite Reservoir. Good agreement will validate load estimation method.
4. Estimate the uncertainty in predictions of future sediment load based on natural variability and uncertainty of the mathematical sediment load model.
5. Derive representative sediment grain size characteristics for the sediment load series from measured grain size distributions.
6. Develop sediment load rating tables for the HECRAS sediment transport model.

9.5. Sediment Load Relationships

Sediment concentration or load is commonly related to water discharge with statistical regression methods to produce mathematical relationships that can estimate historic sediment loads or predict future loads[94]. Sediment load is directly computed from sediment concentration and water discharge with the conversion equation,

$$Q_s = Q_w C_s k \qquad 9\text{-}1$$

where Q_s is the sediment discharge (U.S. tons per day), Q_w is the water discharge (cfs), C_s is the sediment concentration (mg/L), and k is the constant 0.0027 based on the U.S. customary units.

Sediment load computed by equation 9-1 is a rate, which implies that the water discharge and sediment concentration are averaged over the same time period. In practice, it is difficult to obtain true average values of either sediment concentration or discharge with conventional sediment sampling methods, and both measurements generally have variability that is not quantified. Nonetheless, the estimation of sediment load for daily periods and longer from relationships developed from short-term measurements is widely applied in practice, and this approach will be used here. It will be shown below that sediment loads estimated by this method are validated by the historic sediment accumulation measurements.

[94] Gray, J.R and Simoes, F.J.M. (2008). "Estimating sediment discharge." *Sedimentation Engineering, Processes, Measurements, Modeling and Practice*, ASCE Manuals and Reports of Engineering Practice No. 110

A sediment transport curve is fit to measured concentration or load data with univariate or multivariate linear regression techniques or other computational methods[95]. Three methods of mathematical load estimation were used in this analysis. These include 1) the bias-corrected transformed power function, 2) the nonlinear power function, and 3) the minimum variance unbiased estimator (MVUE). A fourth method, Reduced Major Axis (RMA) regression[96] was also tested.

The simplest and most commonly employed relationship for load estimation in sediment transport modeling is a power equation fit to the measured sediment concentration or load data and the water discharge recorded at the time of the sediment load measurement. The power function takes the form[88],

$$Q_s = aQ_w^{\ b} \qquad 9\text{-}2$$

where Q_s is the sediment discharge (U.S. tons per day), Q_w is the water discharge (cfs), and the coefficients a and b are derived by the regression analysis. The power function is typically derived by linear regression after the variables are transformed to logarithms. Power relationships plot as straight lines in log space, and as shown in Figure 114 and Figure 118, provide a reasonable fit of the measured suspended sediment concentration data to average daily discharge for the Snake and Clearwater Rivers.

A downward bias of the sediment load estimate results upon re-transformation of the regression equation back to original units. A bias correction is applied to adjust sediment concentration or load estimates for the effect of the log transformation. Several methods of bias correction are available[97]; the method developed by Duan[98] was employed in this analysis for linear regression of the power function. The Duan bias-corrector is computed as the average of the re-transformed residuals and is a constant coefficient that is a multiplier to the power regression coefficient. In this study, least squares regression and bias correction of the transformed variables were performed with custom Matlab scripts.

[95] Kondolf, G.M. Piegay, H. (2003) *Tools in Fluvial Geomorphology*, Wiley, New York

[96] McArdle, B.H. (1988) "The structural relationship: regression in biology", *Canadian Journal of Zoology*, 66, 2329-2339.

[97] Craig A. Stow, Kenneth H. Reckhow, Song S. Qian, S.S. (2006) “A Bayesian approach to retransformation bias in transformed regression.” *Ecology*, 87(6) (Jun., 2006), pp. 1472-1477.

[98] Duan, N. (1983). “Smearing estimate: a nonparametric retransformation method.” *Journal of the American Statistical Association,* 78(383), 605-610.

Nonlinear regression of sediment concentration and daily discharge was performed with the Levenberg–Marquardt (LM) algorithm which combines gradient descent minimization with the Gauss-Newton method. A bias correction for logarithmic transformation is not needed for the nonlinear analysis. The nonlinear regression was performed with standard curve fitting algorithms available in Matlab. The LM algorithm is widely implemented in commercial and public domain statistical packages[99].

The minimum variance unbiased estimator (MVUE) is increasingly employed in water quality studies[100] and is incorporated into the LOADEST software developed by USGS[101]. The MVUE maximum likelihood estimator for load is,

$$L_{MVUE} = \exp\left(a_o + \sum_{j=1}^{M} a_j X_j \right) g_m\left(m, s^2, V\right) \qquad 9\text{-}3$$

where L_{MVUE} is the maximum likelihood estimate of instantaneous load, m is the number of degrees of freedom, s^2 is the residual variance, and V is a function of the explanatory variables. The model coefficients, a_0 and a_j, are estimated by maximum likelihood and the bias correction factor is $g_m(m,s^2,V)$. The MVUE estimates of sediment load were performed with custom Matlab scripts and the results from test datasets agreed well with the LOADEST software.

9.6. Snake River Suspended Sediment Load and Bedload Relationships

Sediment load relationships were derived by the methods discussed above from the combined 1972-1979 and 2008-2010 suspended sediment and bedload data measured on the Snake River at Anatone. The regression lines and suspended sediment measurements are plotted in Figure 119. All regression lines follow the general trend of the data and provide a good visual fit of the logarithms of the data. Residuals of the fit of the power equation in Figure 120 do not depart significantly from normality, indicating that confidence intervals and prediction intervals based on the regression statistics should be reasonable. Regression coefficients for the relationships are listed in Table 49. The MVUE analysis method does not directly produce a single

[99] For example the R statistical computing environment, http://www.r-project.org/

[100] Cohn, T.A., Delong, L.L., Gilroy, E.J., Hirsch, R.M., and Wells, D.K. (1989) "Estimating constituent loads." Water Resources Research, 25(5), p. 937-942.

[101] Runkel, R.L., Crawford, C.G., and Cohn, T.A. (2004) *Load Estimator (LOADEST): A FORTRAN Program for Estimating Constituent Loads in Streams and Rivers*, U.S. Geological Survey, Reston, VA.

coefficient and exponent for a power relationship, so an approximate coefficient and slope for the MVUE estimator were derived by fitting a power equation to MVUE estimates for the measured data and discharges. The approximate parameters for the MVUE estimator were only used to visually compare the regression lines; MVUE load predictions were estimated with the actual MVUE algorithm.

The slopes and intercepts of the bias-corrected power equation and the MVUE estimator in log space are nearly equivalent. The slope of the nonlinear fit of the power equation is significantly different and produces greater load estimates for higher discharges. As expected, the unadjusted power equation regression line plots below the corrected power equation. From the regression statistics, the coefficient of determination (R^2) for the unadjusted power equation of load is 0.94. Coefficients of determination for load are somewhat inflated because discharge is a parameter in the computation of load from sediment concentration. A power equation fit to the suspended sediment concentration and discharge data produced an R^2 of 0.86. High coefficients of determination are not uncommon in regressions of suspended sediment for rivers that carry a high percentage of fine material.

Total sediment load for was estimated for the period 1 October 1974 through 30 September 2010 with each of the regression equations and the average daily discharge series. Total sediment load of the Snake and Clearwater Rivers from this period can be directly compared to the total volume of sediment accumulated in Lower Granite Reservoir since the pool was raised. The sediment load series is plotted with water discharge and the measured sediment load data in Figure 121 and summary statistics for the total load are listed in Table 50. Estimates of mean daily sediment load do not vary greatly between the three estimation methods. The unadjusted power equation estimates is given only for reference. As suggested by the regression plot, the maximum daily sediment load of 220,100 tons per day for nonlinear power equation is higher than the estimates for the bias-corrected power equation and the MVUE estimator. Total sediment volumes, computed assuming and sediment unit weight of 70 pounds per cubic foot (pcf), were 63.8, 63.1 and 62.4 million cubic yards (mcy) for the bias-corrected power equation, MVUE estimator and the nonlinear power equation. Good agreement between the estimators increases confidence in the estimates and indicates that uncertainty in the long-term load estimate due to the form of the estimator (epistemic uncertainty) is not overwhelming.

Alternate load equations were tested including a piecewise fit of the load data and multiple regressions with tributary flows. Some of the more complex formulations produced marginal improvements in the coefficient of determination. Even so, the single discharge parameter load equations are adequate for estimation of long-term

sediment load and the sediment transport computations in this study and are similar to approaches adopted in other investigations of sediment load in the region[102].

Regression relationships were also developed for the sand fraction of the suspended load and bedload. Regression coefficients and total load statistics for the sand fraction and bedload are summarized in Table 51 through Table 54. Suspended sand is about 43 percent of the total suspended load and bedload is about 6 percent of the total suspended load. The computed sand fraction agrees well with the 39 percent average measured sand fraction from Table 46. Sediment volume was computed assuming a sediment bulk unit weight of 90 pounds per cubic foot. The regression estimators fit the suspended sand data reasonably well (R^2 for load 0.92) in Figure 122 but provide only an approximate fit of the bedload data (R^2 for load 0.66) in Figure 123. The regression fit of the bedload data is adequate for the purposes of the study since bedload is a small fraction of the suspended load.

The bedload sampler with the 6 inch by 6 inch orifice likely samples a portion of the sandload also sampled by the P-61 and P-63 suspended samplers which can sample within about 3 inches of the bed surface. In computation of total load, the sand load attributed to bedload should be adjusted to account for the overlap in the sample estimates so that the total sand load is not overestimated. This sand load adjustment is discussed in Section 9.15. Also bedload transport is very sensitive to local bed shear stress, so the transport of larger grain size fractions at the Anatone site are likely not representative of coarse faction transport at the upper limit of backwater.

[102] King, J.G.,Emmett, W. W.,Whiting, P. J., Kenworthy, R. P., Barry, J. J. (2004) *Sediment transport data and related information for selected coarse-bed streams and rivers in Idaho. Gen. Tech. Rep. RMRS-GTR-131*. Fort Collins, CO: U.S. Department of Agriculture, Forest Service, Rocky Mountain Research Station.

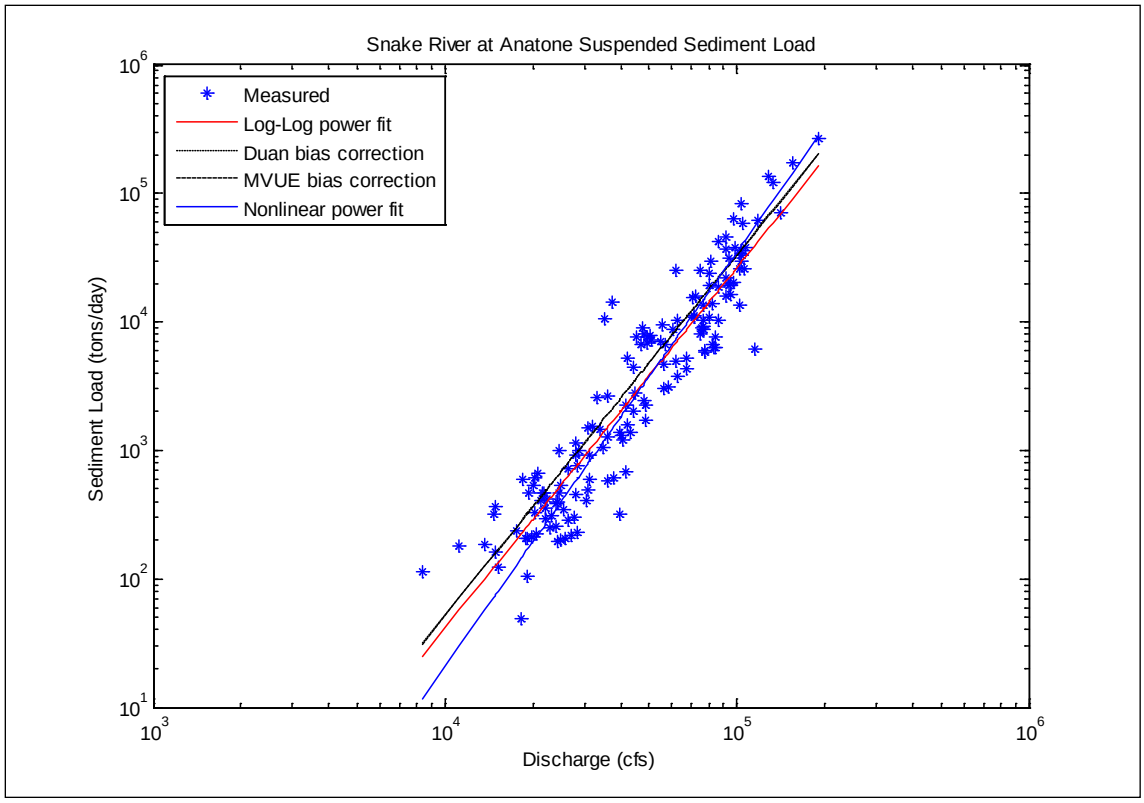


Figure 119. Snake River at Anatone suspended sediment load regression fit.

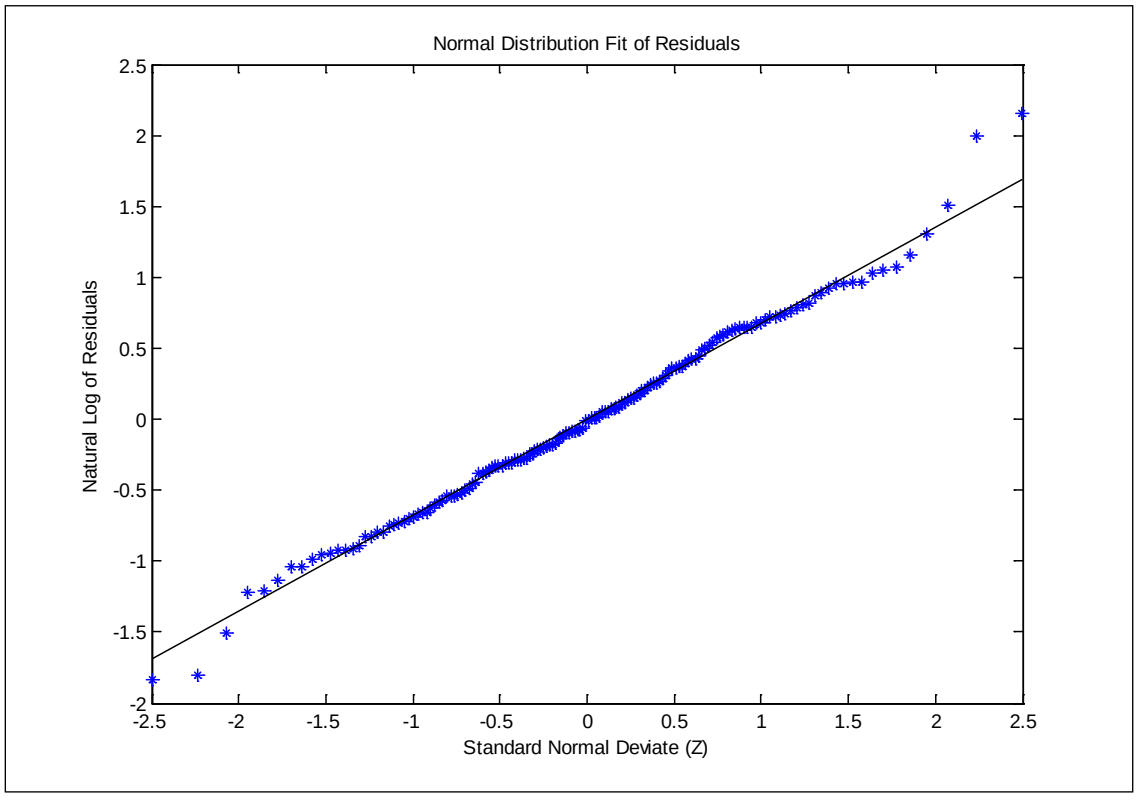


Figure 120. Snake River at Anatone suspended sediment load regression residuals.

Snake River at Anatone Suspended Sediment Load Regression Coefficients						
Power			Nonlinear		MVUE	
A	B	BCF	A	B	A	B
2.49E-10	2.8051	1.2687	2.63E-12	3.2247	3.12E-10	2.8054

Table 49. Snake River at Anatone suspended sediment load regression coefficients.

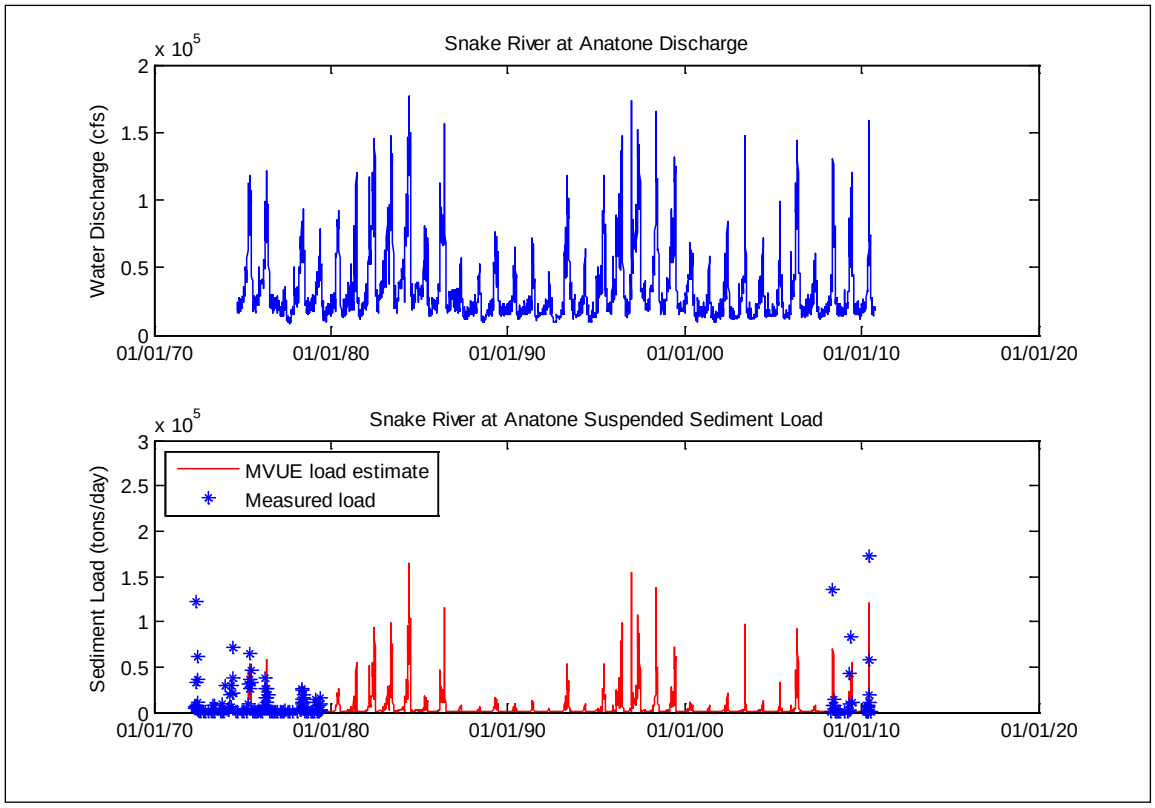


Figure 121. Snake River at Anatone suspended sediment load 1974 – 2010.

Snake River at Anatone Suspended Sediment Load Estimates (1974-2010)				
	Unadjusted Power	Bias Corrected Power	MVUE	Nonlinear Power
Maximum, tpd	131,100	166,324	163,769	220,124
Minimum, tpd	26	34	33	12
Mean, tpd	3,612	4,583	4,532	4,483
Median, tpd	494	626	620	360
St. Dev., tpd	9,419	11,950	11,801	13,726
Total, ton	4.750E+07	6.026E+07	5.960E+07	5.894E+07
Volume[1], mcy	50.3	63.8	63.1	62.4
Yield, mcy/yr	1.4	1.8	1.8	1.7
[1]Sediment unit weight 70 lb/cu.ft.				

Table 50. Snake River at Anatone suspended sediment load estimate 1974-2010.

Snake River at Anatone Suspended Sand Load Regression Coefficients						
Power			Nonlinear		MVUE	
A	B	BCF	A	B	A	B
3.56E-14	3.4861	1.6357	1.07E-13	3.4288	5.61E-14	3.4880

Table 51. Snake River at Anatone suspended sand load regression coefficients.

Snake River at Anatone Suspended Sand Load Estimates (1974-2010)				
	Unadjusted Power	Bias Corrected Power	MVUE	Nonlinear Power
Maximum, tpd	70,155	114,750	111,310	105,769
Minimum, tpd	2	3	3	3
Mean, tpd	1,205	1,970	1,934	1,883
Median, tpd	68	111	110	115
St. Dev., tpd	4,031	6,593	6,442	6,185
Total, ton	1.584E+07	2.591E+07	2.543E+07	2.477E+07
Volume, mcy	13.0	21.3	20.9	20.4
Yield, mcy/yr	0.4	0.6	0.6	0.6
[1]Sediment unit weight 90 lb/cu.ft.				

Table 52. Snake River at Anatone suspended sand load estimate 1974-2010.

Snake River at Anatone Bedload Regression Coefficients						
Power			Nonlinear		MVUE	
A	B	BCF	A	B	A	B
1.46E-11	2.7595	1.8140	4.73E-03	1.0743	2.74E-11	2.7674

Table 53. Snake River at Anatone bedload regression coefficients.

Snake River at Anatone Bedload Estimates (1974-2010)				
	Unadjusted Power	Bias Corrected Power	MVUE	Nonlinear Power
Maximum, tpd	4,430	8,036	8,640	2,054
Minimum, tpd	1	2	2	79
Mean, tpd	126	229	256	351
Median, tpd	18	33	35	242
St. Dev, tpd	323	587	653	285
Total, ton	1.662E+06	3.016E+06	3.372E+06	4.611E+06
Volume, mcy	1.4	2.5	2.8	3.8

Table 54. Snake River at Anatone bedload estimate 1974-2010.

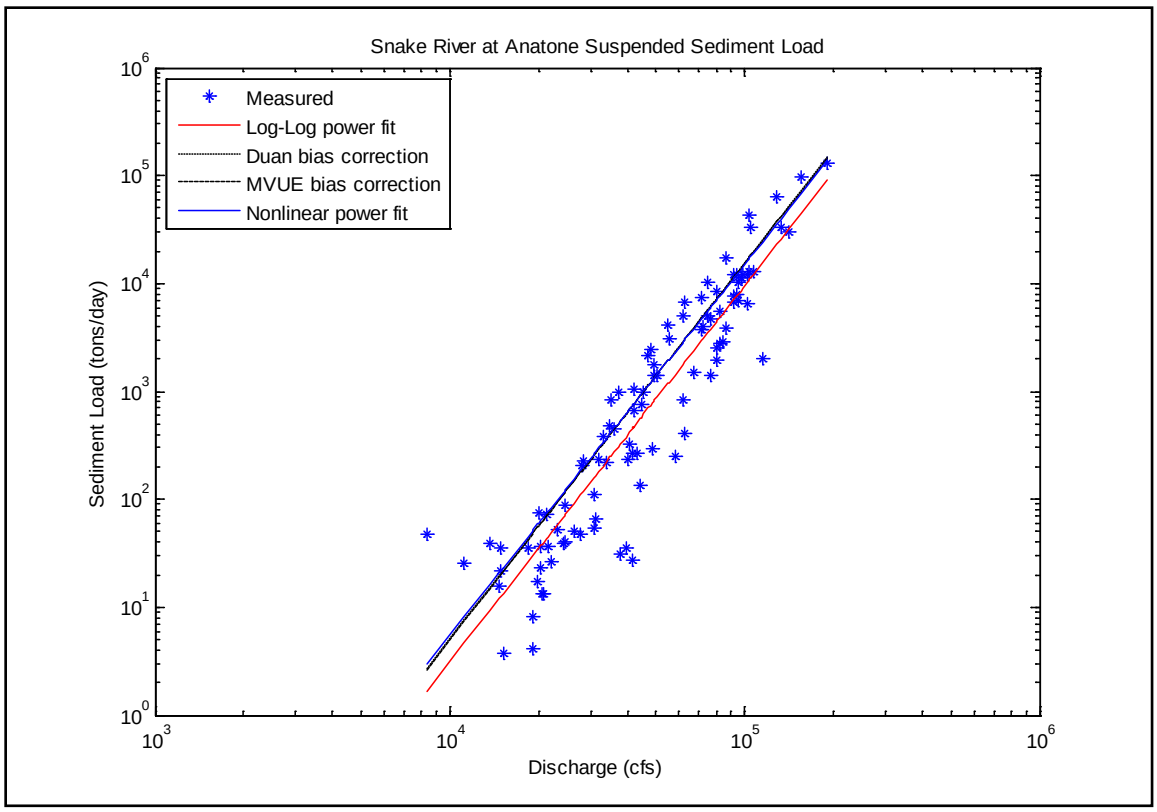


Figure 122. Snake River at Anatone suspended sand load regression fit.

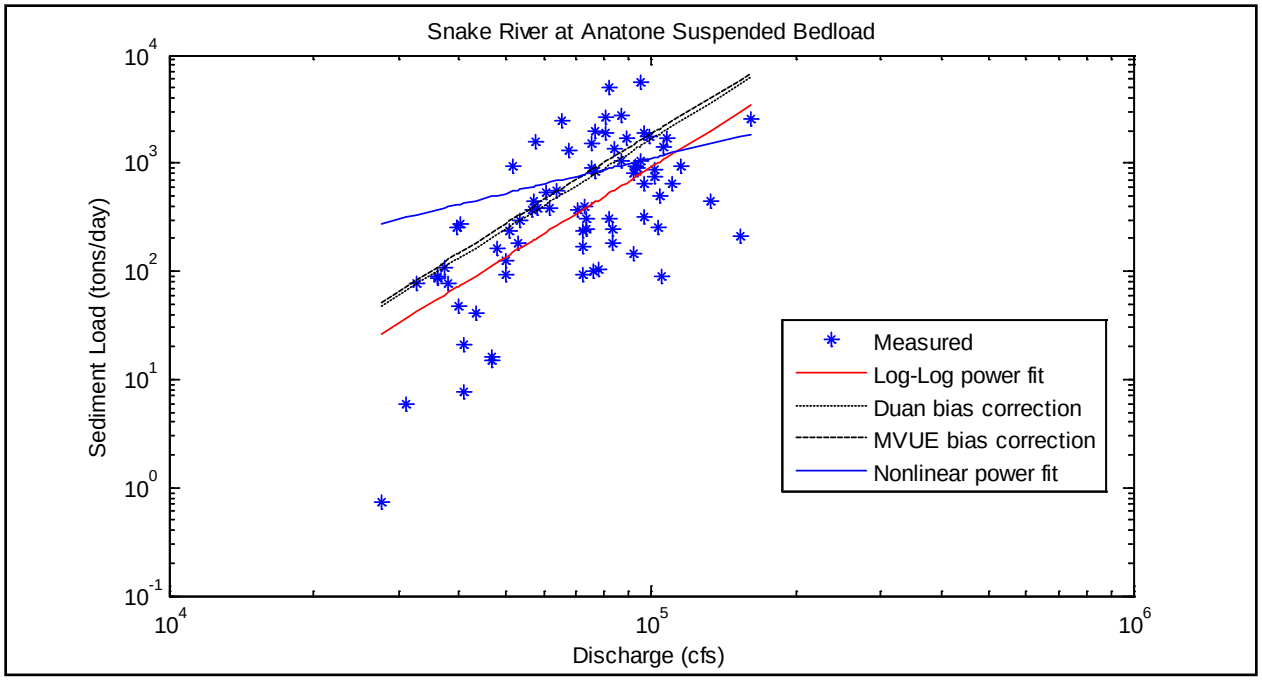


Figure 123. Snake River at Anatone bedload regression fit.

9.7. Clearwater River Suspended Sediment Load and Bedload Relationships

Sediment load relationships were derived for the Clearwater River from the combined 1972-1979 and 2008-2010 suspended sediment and bedload data measured at Spalding. The regression lines plotted in Figure 124 and provide a reasonable visual fit of the logarithms of the suspended sediment measurements, though there is considerable scatter in the data. Residuals of the fit of the power equation in Figure 125 are mostly normal except for extreme values. Confidence intervals and prediction intervals based on the regression statistics should be reasonable for the range of discharges that produce most of the annual sediment load. The five upper extreme values in Figure 125 have empirical plotting positions that are less than about 3 percent exceedance (33 years return interval).

Regression coefficients for the Clearwater River suspended sediment relationships are listed in Table 55. The slopes and intercepts of the bias-corrected power equation, the MVUE estimator and the nonlinear fit of the power equation are nearly equivalent in log space. Again, the unadjusted power equation regression line plots below the corrected power equation. The R^2 for the unadjusted power equation of load is 0.88 and is 0.70 for the concentration relationship. The coefficients of determination are lower for the Clearwater River than the Snake River because the Clearwater data is more scattered about the regression lines.

The total sediment load time series for the Clearwater River was estimated for the period 1 October 1974 through 30 September 2010 and is plotted with water discharge and the measured sediment load data in Figure 126. Summary statistics for the total suspended sediment load are listed in Table 56. Estimates of mean daily sediment load vary somewhat between the three estimation methods; the MVUE and nonlinear power equation estimates are about 15 and 7 percent lower than the adjusted power equation estimate. Total sediment volumes, again computed assuming a sediment unit weight of 70 pounds per cubic foot (pcf), were 19.2, 16.3 and 17.8 million cubic yards (mcy) for the bias-corrected power equation, MVUE estimator and the nonlinear power equation. There is reasonably good agreement between the estimators for long-term load estimation.

Regression coefficients and total load statistics for the sand fraction and bedload are summarized in Table 57 through Table 60. Suspended sand is about 30 percent of the total suspended load and bedload is about 5 percent of the total suspended load. The computed sand fraction is less than the 44 percent average measured sand fraction from Table 47 (but the values in Table 47 are not weighted by flow). Sediment volume was computed assuming a sediment bulk unit weight of 90 pounds per cubic foot. The regression estimators fit the suspended sand data reasonably well (R^2 for load 0.90) in Figure 127 and also provide a reasonable fit of the bedload data (R^2 for load 0.77) in

Figure 128. The fit of the bedload data is adequate for the purposes of the study since bedload is a small fraction of the suspended load.

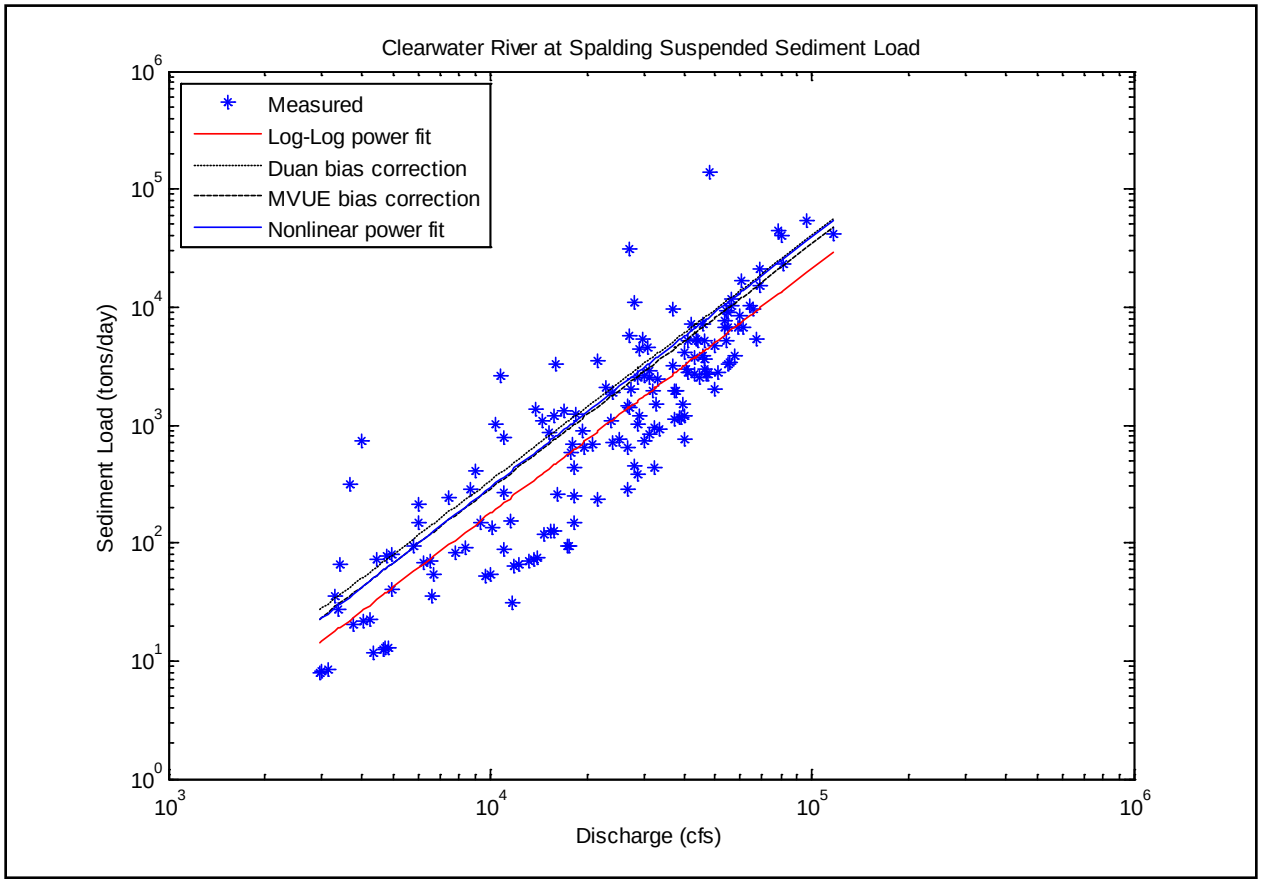


Figure 124. Clearwater River at Spalding suspended sediment load regression fit.

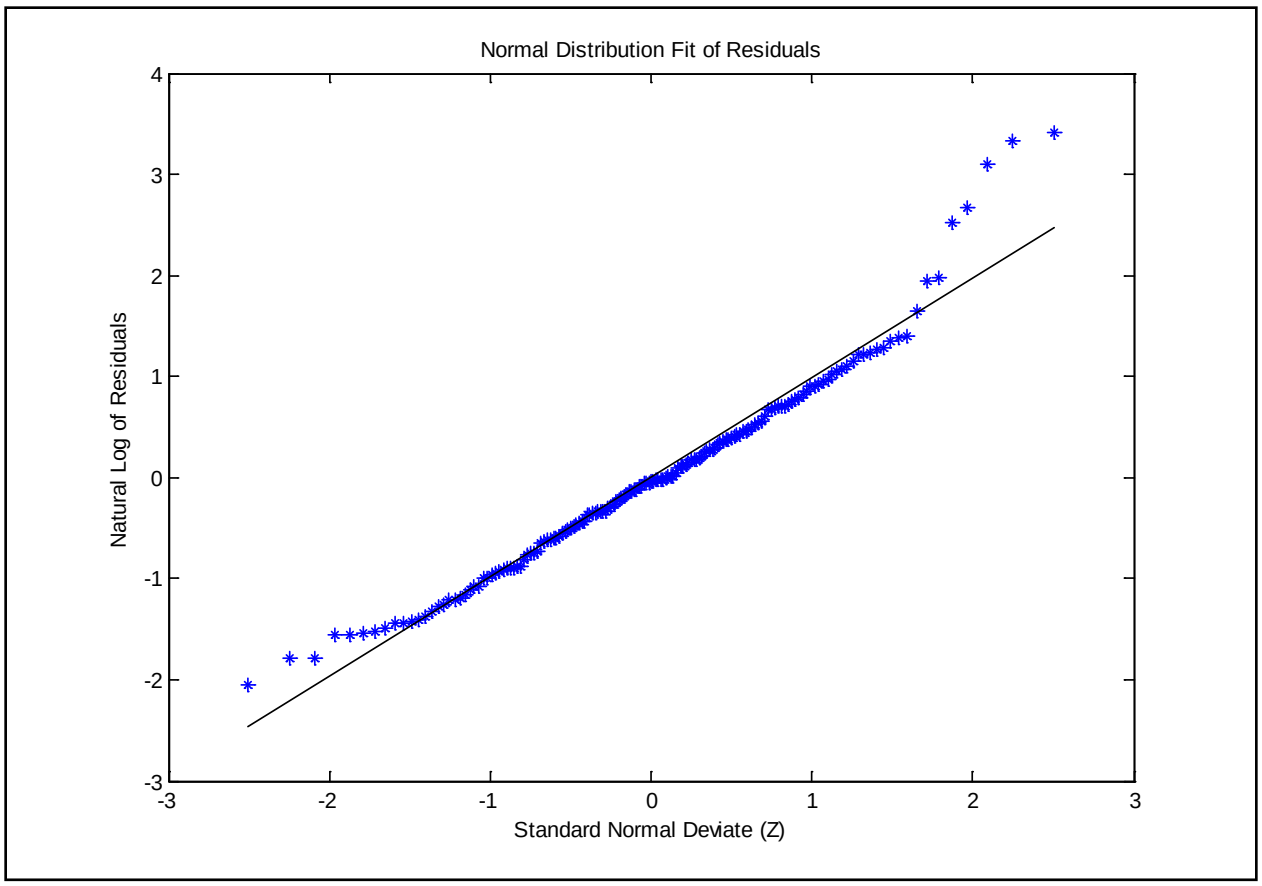


Figure 125. Clearwater River at Spalding suspended sediment load regression residuals.

Clearwater River at Spalding Suspended Sediment Load Regression Coefficients						
Power			Nonlinear		MVUE	
A	B	BCF	A	B	A	B
8.94E-07	2.0748	1.9011	9.48E-07	2.1238	1.42E-06	2.0766

Table 55. Clearwater River at Spalding suspended sediment load regression coefficients.

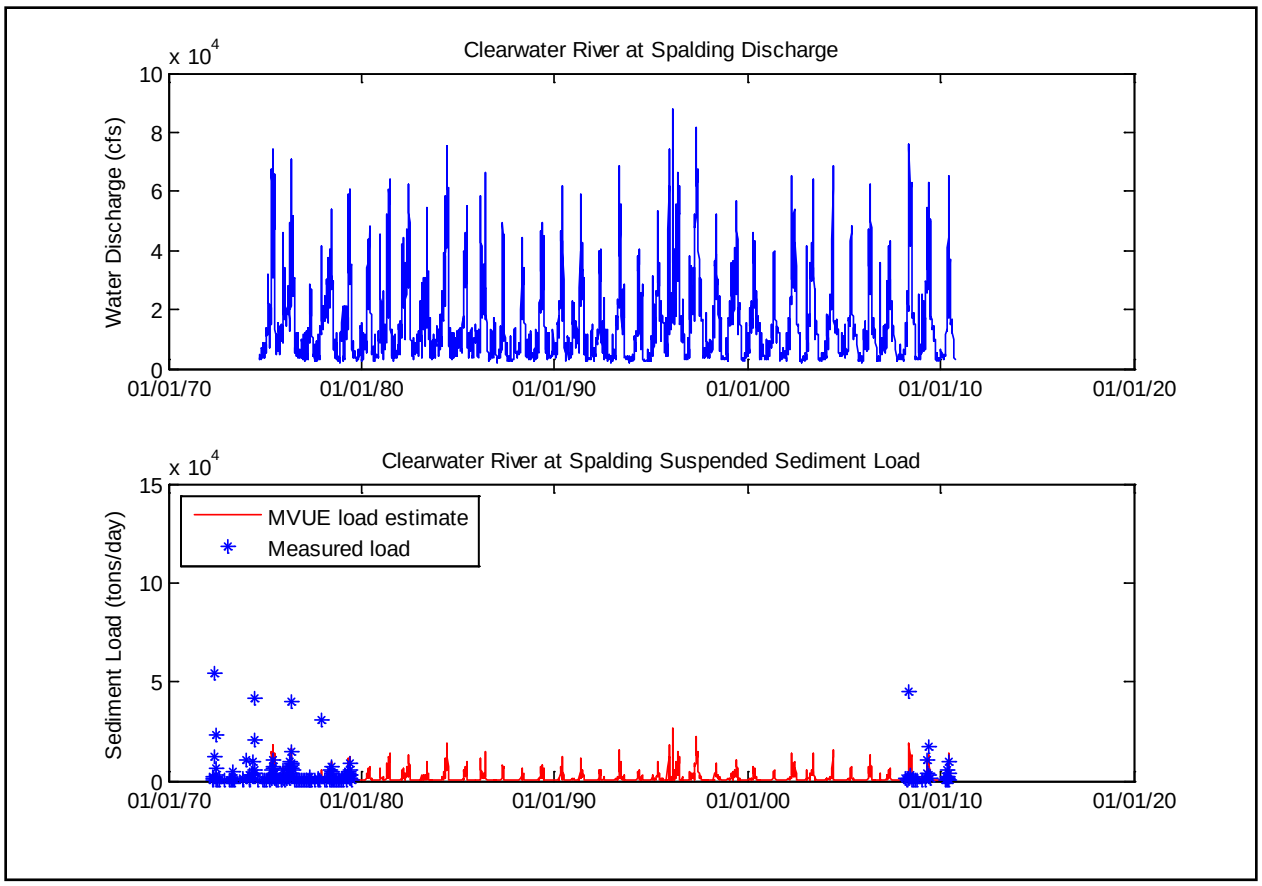


Figure 126. Clearwater River at Spalding suspended sediment load 1974 – 2010.

Clearwater River at Spalding Suspended Sediment Load Estimates (1974-2010)				
	Unadjusted Power	Bias Corrected Power	MVUE	Nonlinear Power
Maximum, tpd	16,259	30,910	26,184	30,121
Minimum, tpd	7	13	11	10
Mean, tpd	725	1,378	1,174	1,279
Median, tpd	189	360	307	316
St. Dev, tpd	1,362	2,589	2,203	2,463
Total, ton	9.534E+06	1.812E+07	1.544E+07	1.682E+07
Volume, mcy	10.1	19.2	16.3	17.8
Yield, mcy/yr	0.3	0.5	0.5	0.5
[1]Sediment unit weight 70 lb/cu.ft.				

Table 56. Clearwater River at Spalding suspended sediment load estimate 1974-2010.

Clearwater River at Spalding Suspended Sand Load Regression Coefficients						
Power			MVUE		Nonlinear	
A	B	BCF	A	B	A	B
1.82E-10	2.7983	1.2428	1.87E-08	2.4104	2.24E-10	2.8019

Table 57. Clearwater River at Spalding suspended sand load regression coefficients.

Clearwater River at Spalding Suspended Sand Load Estimates (1974-2010)				
	Unadjusted Power	Bias Corrected Power	MVUE	Nonlinear Power
Maximum, tpd	12,498	15,532	15,913	15,494
Minimum, tpd	0	0	0	2
Mean, tpd	290	361	372	502
Median, tpd	31	38	39	88
St. Dev, tpd	749	931	960	1,104
Total, ton	3.816E+06	4.743E+06	4.898E+06	6.601E+06
Volume, mcy	3.1	3.9	4.0	5.4
Yield, mcy/yr	0.1	0.1	0.1	0.2
[1]Sediment unit weight 90 lb/cu.ft.				

Table 58. Clearwater River at Spalding suspended sand load estimate 1974-2010.

Clearwater River at Spalding Bedload Regression Coefficients						
Power			MVUE		Nonlinear	
A	B	BCF	A	B	A	B
3.91E-05	1.4603	1.1377	1.19E-08	2.2109	4.22E-05	1.4634

Table 59. Clearwater River at Spalding bedload regression coefficients.

Clearwater River at Spalding Bedload Estimates (1974-2011)				
	Unadjusted Power	Bias Corrected Power	MVUE	Nonlinear Power
Maximum, tpd	650	740	724	1,018
Minimum, tpd	3	3	3	0
Mean, tpd	57	65	64	40
Median, tpd	28	32	31	9
St. Dev, tpd	75	85	84	80
Total, ton	7.551E+05	8.591E+05	8.355E+05	5.222E+05
Volume, mcy	0.62	0.71	0.69	0.43

Table 60. Clearwater River at Spalding bedload estimate 1974-2010.

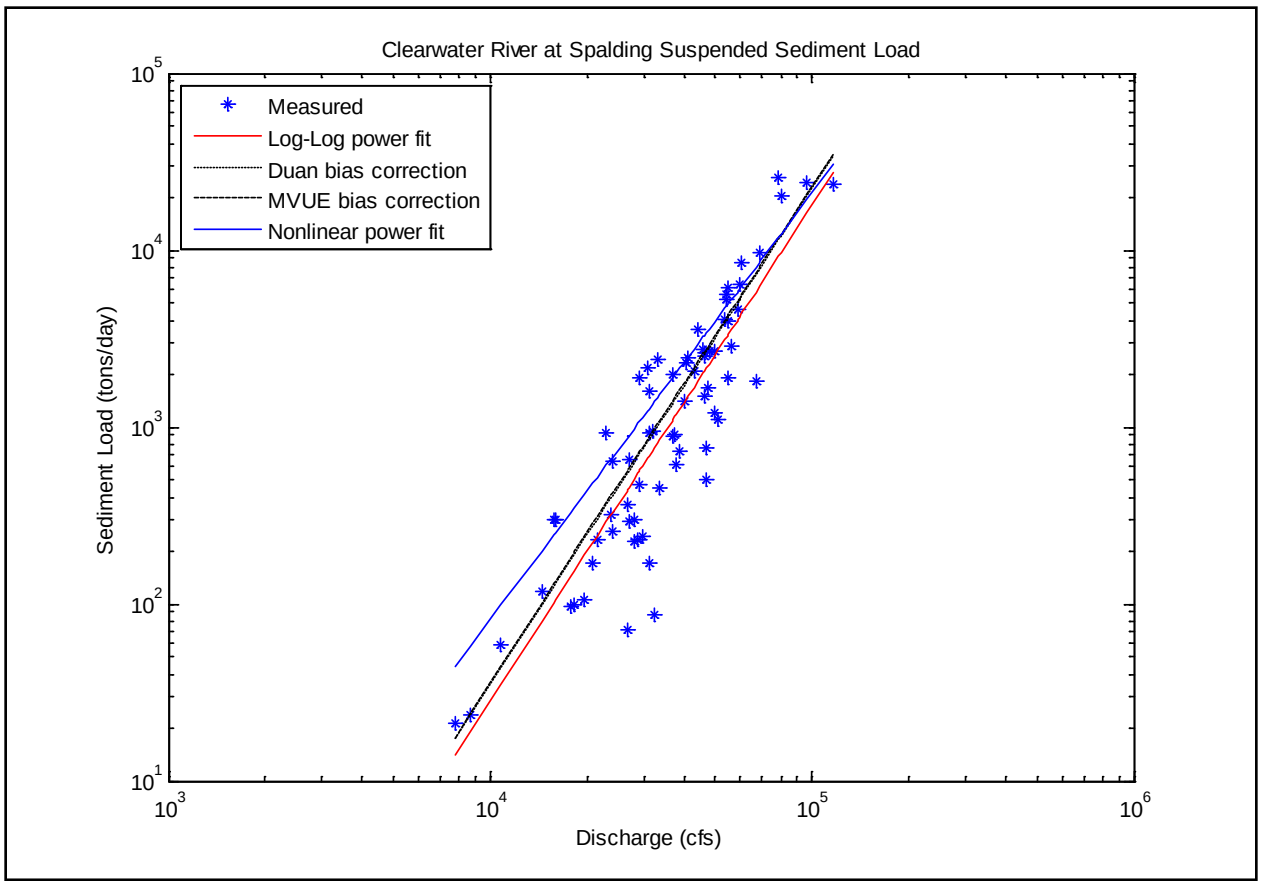


Figure 127. Clearwater River at Spalding suspended sand load regression fit.

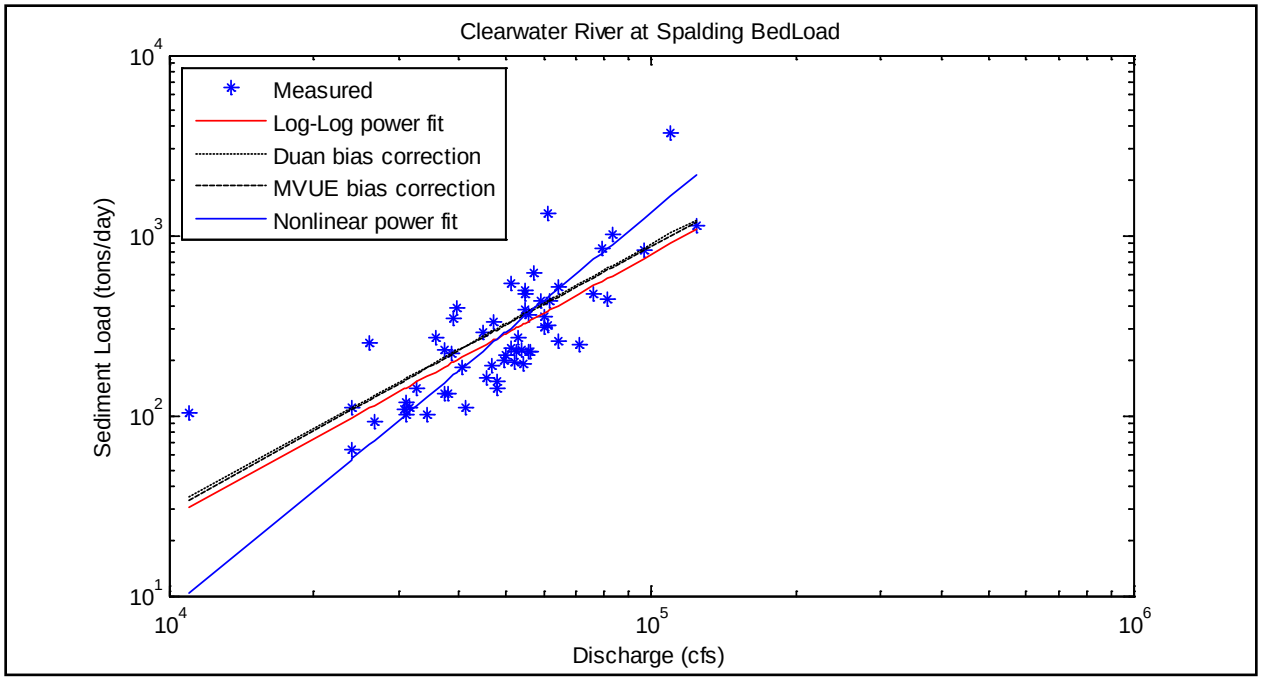


Figure 128. Clearwater River at Spalding bedload regression fit.

9.8. Sediment Load Regression Analysis with 2011 Data Included

Measured sediment load data for 2011 was unavailable when the sediment load regression analysis described above was performed. The sediment regression equations are used to define the sediment load boundary conditions for the sediment transport analysis and extensive sediment transport modeling and analysis was performed based on regression equations derived from the 1974 to 2010 data. To confirm that this modeling remains valid, the sediment load regression analysis was repeated with the additional 2011 data. Table 61 summarizes the suspended sediment load estimates for the Snake River at Anatone for 1974-2010 based on a regression equation derived with the complete set of measured sediment load data from 1974 to 2011. The total volumes for estimates by the MVUE and Bias Corrected methods differ by less than 1 percent from the values listed in Table 50 that are based only on the 1974 to 2010 data. The differences between the load estimates are negligible, so the sediment transport analysis is valid and was not repeated with the 2011 data incorporated into the load estimates.

Snake River at Anatone Suspended Sediment Load Estimates (1974-2010) Sediment Load Data 1974-2011				
	Unadjusted Power	Bias Corrected Power	MVUE	Nonlinear Power
Maximum, tpd	133,583	168,715	166,712	217,074
Minimum, tpd	26	33	33	12
Mean, tpd	3,654	4,614	4,569	4,405
Median, tpd	494	623	617	351
St. Dev., tpd	9,565	12,081	11,953	13,514
Total, ton	4.804E+07	6.067E+07	6.008E+07	5.793E+07
Volume[1], mcy	50.8	64.2	63.6	61.3
[1]Sediment unit weight 70 lb/cu.ft.				

Table 61. Snake River at Anatone suspended sediment load estimate with 2011 sediment load data added to the regression.

9.9. Reduced Major Axis (RMA) Regression

Reduced major axis regression (RMA) may be appropriate when both the dependent and independent variables include measurement error[96,103] as do water discharge and sediment load measurements. Both RMA and ordinary least squares

[103] Parker, G., Wilcock, P. R., Paola, C., Dietrich, W. E., and Pitlick, J. (2007). "Physical basis for quasi-universal relationships describing bankfull hydraulic geometry of single-thread gravel bed rivers." *J. Geophys. Res*., 112, F04005.

(OLS) regressions were performed with measured suspended sediment loads for the Snake River at Anatone using the procedure developed by Legendre[104] for the R statistical computing system. The data were transformed to logarithms. Regression lines for both OLS and RMA are shown in Figure 129. The results of the OLS regression are identical to the power equation fit without bias adjustment discussed above. The difference between the RMA and OLS regression lines is negligible, so RMA was not used to estimate sediment loads for the sediment transport modeling.

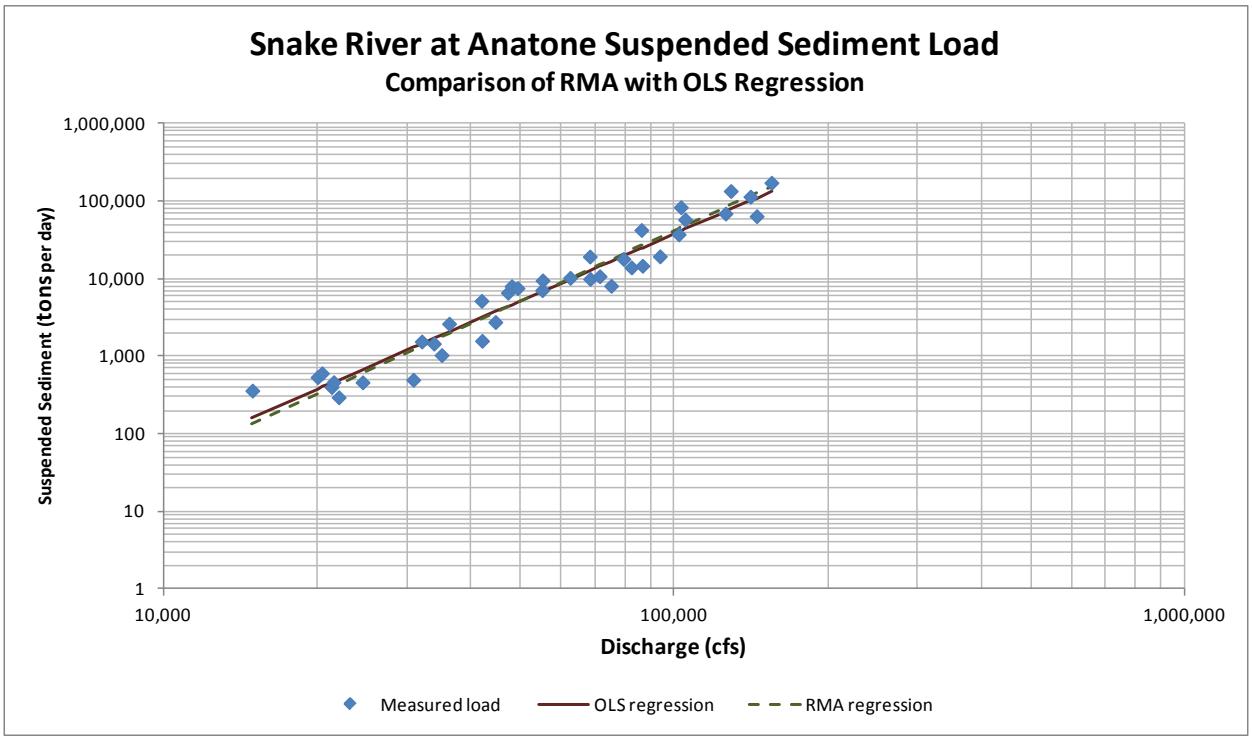


Figure 129. Comparison of RMA regression with OLS regression for suspended sediment load.

[104] Legendre, P. (2008). *Model II Regression User's Guide, R Edition*, www.r-project.org.

9.10. Sediment Unit Weight

Reservoir sediment volume is computed by multiplying the accumulated sediment load by the bulk unit weight of the settled and consolidated sediment. Sediment unit weight is estimated using the relationship[105,106].

$$\gamma_{dc} = \gamma_{di} + B \log_{10} T \qquad 9\text{-}4$$

where γ_{dc} is the consolidated unit weight (lb/ft^3), γ_{di} is the initial unit weight (lb/ft^3) at the end of one year, B is a coefficient of consolidation, and T is the age of the deposit in years.

The initial unit weight and coefficient of consolidation of silt deposits that are always or nearly always submerged is 65 lb/ft^3 and 5.7. Substituting these values in equation 1.4 and assuming a consolidation period of 10 years gives a consolidated silt unit weight of,

$$\gamma_{dc} = 65 + 5.7 \log_{10} 10 = 70.7 \frac{\text{lb}}{\text{ft}^3}$$

By a similar computation, after 37 years (1974 to 2010) the consolidated unit weight of deposited silt would be 73.9 lb/ft^3. For deposited clay, the initial unit weight and coefficient of consolidation of submerged deposits are 30 lb/ft^3 and 16.0. The consolidated unit weight after 10 years is,

$$\gamma_{dc} = 30 + 16 \log_{10} 10 = 46 \frac{\text{lb}}{\text{ft}^3}$$

After 37 years the consolidated unit weight of deposited clay would be 55.1 lb/ft^3. The consolidated unit weights for silt and clay for the life of the reservoir are plotted in Figure 130. Deposited sand material does not consolidate with time and has a bulk unit weight of approximately 93 lb/ft^3.

Assuming an equal initial thickness of sediment is deposited each year, an average consolidated unit weight may be computed by integrating equation 1.4 and dividing by the total number of years. The integral is,

[105] USACE (1995) *EM 1110-2-4000 Sedimentation Investigations of Rivers and Reservoirs*. U.S. Army Corps of Engineers, Washington, DC.

[106] ASCE (2008) *Sedimentation Engineering, Processes, Measurements, Modeling and Practice*, ASCE Manuals and Reports of Engineering Practice No. 110

$$\int \gamma_{di} + B\log_{10} T \cdot dT = \int \gamma_{di} + \frac{B}{\ln 10}\ln T \cdot dT = \gamma_{di} T + \frac{B}{\ln 10} T(\ln T - 1) + C$$

Which when evaluated over the integral from 1 to T becomes,

$$\int_1^T \gamma_{di} + B\log T \cdot dT = (T-1)\gamma_{di} + T\frac{B}{\ln 10}\ln T - (T-1)\frac{B}{\ln 10}$$

Therefore, the average unit weight of the deposited sediment is,

$$\gamma_{da} = \frac{(37-1)65 + 37\frac{5.7}{\ln 10}\ln 37 - (37-1)\frac{5.7}{\ln 10}}{37} = 69.8\frac{\text{lb}}{\text{ft}^3}$$

By this method, the average unit weight of deposited silt is approximately 70 lb/ft^3 and similarly the average unit weight of deposited clay is approximately 48 lb/ft^3.

The sediment core survey described in Section 8 investigated the variability of grain size in the sediment deposited in Lower Granite Reservoir. The survey found that sediment deposits above Silcott are heterogeneous and there is insufficient data to map the spatial variation of the bulk density of the deposits. An average unit weight of 70 lb/ft^3 is assumed to be representative of deposited sediment composed of mostly silt and clay and an average unit weight of 90 lb/ft^3 is assumed to be representative of sediment that is mostly sand. Limited measurements of the bulk densities of samples from sediment cores indicate these are reasonable values for sediment deposited in Lower Granite Reservoir.

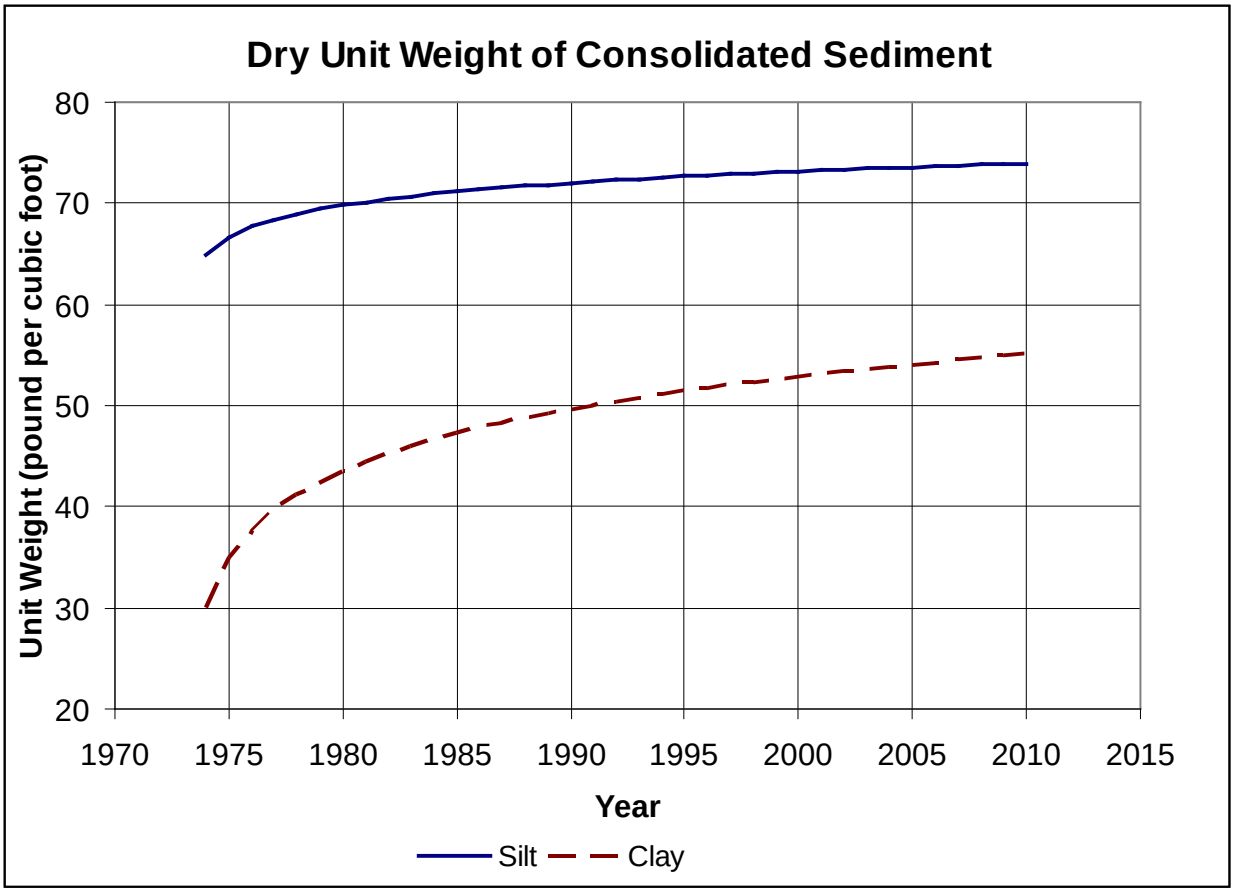


Figure 130. Consolidated unit weights of submerged silt and clay deposits.

9.11. Comparison of Sediment Load Estimates with Measured Sediment Accumulation

The computed estimates of sediment load volumes for the Snake and Clearwater Rivers can be compared to the measured volume of sediment that has accumulated in Lower Granite Reservoir since 1974. The evaluation of sediment load estimators in Sections 9.6 and 9.7 showed that both the bias-corrected power equation and the minimum variance unbiased estimator (MVUE) provided reasonable fits of the measured suspended sediment data. As discussed in Section 7, total measured sediment accumulation in Lower Granite Reservoir from 1974 to 2010 is 79.8 million cubic yards.

Computed sediment load estimates and the measured accumulation volume are compared in Table 62. Total sediment inflow Lower Granite Reservoir is estimated as the sum of the Snake and Clearwater load estimates. The estimated total sediment load volume and the measured accumulation volume agree extraordinarily well. The

difference between the MVUE estimate of suspended sediment and the measured accumulation is about 0.5 percent and the estimate from the bias-corrected power equation (BCP) is within 4 percent of the measured accumulation volume. The average of the MVUE and BCP estimates is within 2 percent of the accumulation volume. Total sediment load at Anatone and Spalding includes both suspended sediment and bedload. As suggested above it, is questionable whether bedload estimates at Anatone and Spalding provide good estimates of bedload entering Lower Granite Reservoir. When bedload is added to the suspended sediment load estimate at Lower Granite Reservoir, the average estimate of total sediment load is about 6 percent greater than the measured sediment accumulation volume. This suggests that bedload estimated at Anatone and Spalding is a negligible fraction of the total sediment load at Lower Granite.

Sediment volumes are directly dependent on the value of bulk unit weight assumed in the conversion from load to volume. The sediment volumes in Table 62 were computed assuming a unit weight of 70 lb/ft^3 for total suspended load and 90 lb/ft^3 for bedload (Section 9.10). If the unit weights are increased by 10 lb/ft^3 for both the suspended load and bedload, the computed total average sediment volume is about 7 percent less than the measured accumulation volume. Similarly, if the unit weights are decreased by 10 lb/ft^3 for both the suspended load and bedload, the computed total average sediment volume is about 23 percent more than the measured accumulation volume. Considering the effect of sediment consolidation, an error in the estimate should tend toward greater sediment unit weights.

The good agreement between the computed and measured sediment volumes validates the sediment load relationships for use in sediment transport modeling and planning of sediment management measures. It is recognized that the assumed sediment unit weight in the volume computation can act as a calibration parameter in the validation of the sediment load estimators. However, as shown in Section 9.10, the assumed sediment unit weights are realistic. These values of sediment unit weight are used consistently in the sediment transport analysis.

Calibration of sediment unit weight illustrates the sensitivity of the load validation to the assumed unit weight. In Table 63, the assumed unit weight of silt and clay sediment is determined by trial to be 67 lb/ft^3 to achieve a close match of the measured sediment accumulation. The silt and clay faction in this computation was computed as the difference between the separate regression estimates of total suspended sediment load and suspended sand. The suspended sand fraction is 32 percent of the total sediment load by weight and after calibration is 38 percent of the total sediment load by volume. The assumed unit weight of the silt and clay fraction only has to be varied by a modest amount to obtain near perfect agreement between the computed and measured sediment volumes.

The close agreement between the sediment volumes computed from the load regressions and measured sediment volumes indicates a high sediment trapping efficiency in Lower Granite Reservoir. Sediment loads that pass Lower Granite Dam have not been measured so trapping efficiency cannot be estimated directly from a measured sediment mass balance. Sediment transport simulations discussed in Section 10 indicate that the simulated trapping efficiency for total sediment load is about 80 percent and is sensitive to the particular transport function selected for the simulation. Trapping efficiencies for coarse silt (0.0625 mm) and sand are near 100 percent. Sediment loads that pass Lower Granite Dam should measured in future studies.

Comparison of Lower Granite Reservoir Estimated Sediment Load and Measured Sediment Accumulation							
	Suspended Sediment (70 lb/ft^3)			Bedload (90 lb/ft^3)			
	Bias Corrected Power Equation mcy	MVUE mcy	Average mcy	Bias Corrected Power mcy	MVUE mcy	Average mcy	Total Sediment mcy
Snake River at Anatone	63.76	63.07	63.42	2.48	2.78	2.63	66.05
Clearwater River at Spalding	19.18	16.34	17.76	0.71	0.69	0.70	18.46
Total	82.94	79.41	81.18	3.19	3.47	3.33	84.51
Lower Granite Reservoir measured sediment accumulation							79.83
Percent Difference	3.9%	-0.5%	1.7%				5.9%

Table 62. Comparison of Lower Granite Reservoir estimated sediment load and measured sediment accumulation.

Calibration of Lower Granite Reservoir Estimated Sediment Load and Measured Sediment Accumulation Relationship										
	Suspended Silt and Clay (67 lb/ft^3)			Suspended Sand (90 lb/ft^3)			Bedload (90 lb/ft^3)			
	Bias Corrected Power Equation	MVUE	Average	Bias Corrected Power Equation	MVUE	Average	Bias Corrected Power	MVUE	Average	Total Sediment
Snake River at Anatone, ton	34,347,685	34,167,670	34,257,678	25,908,632	25,428,921	25,668,777	3,015,722	3,372,256	3,193,989	63,120,444
Clearwater River at Spalding, ton	13,381,086	10,545,732	11,963,409	4,743,149	4,897,502	4,820,326	859,103	835,541	847,322	17,631,057
Total, ton	47,728,771	44,713,403	46,221,087	30,651,782	30,326,423	30,489,103	3,874,826	4,207,797	4,041,312	80,751,501
Snake River at Anatone, mcy	37.97	37.78	37.87	21.32	20.93	21.13	2.48	2.78	2.63	61.63
Clearwater River at Spalding, mcy	14.79	11.66	13.23	3.90	4.03	3.97	0.71	0.69	0.70	17.89
Total, mcy	52.77	49.43	51.10	25.23	24.96	25.09	3.19	3.46	3.33	79.52
Lower Granite Reservoir measured sediment accumulation, mcy										79.83
Percent Difference										-0.4%

Table 63. Calibration of sediment unit weight.

9.12. Uncertainty of Sediment Load Volume Estimates

The sediment load regression relationships in Sections 9.6 and 9.7 exhibit statistical uncertainty because of the scatter in the measured sediment load data. The uncertainty of the estimate of load at a particular value of discharge can be modeled with the equation for the prediction interval of the regression relationship. The prediction interval is a representation of the range of values that an individual value of

the dependent variable y may take on for a give value of the dependent value x_o. The prediction interval is computed[107],

$$y_t = \hat{y} \pm ts\left(1 + \frac{1}{n} + \frac{(x_o - \bar{x})^2}{S_{xx}}\right) \qquad 9\text{-}5$$

where y_t is the predicted value of the dependent variable for a selected value t from the t -distribution and a selected value of the independent variable x_o, $\hat{y}$ is the mean value of the predicted value for value x_o from the linear regression equation, $\bar{x}$ is the mean of the independent data, S_{xx} is the error sum of squares from the regression, and n is the number of data pairs (sample size) used in the regression. In the present context, the independent variable is water discharge and the dependent variable is suspended sediment load estimated by the log-log fit of the power equation, without the bias correction applied.

The prediction interval equation 1-5 can be employed in a Monte Carlo analysis to estimate long-term load estimates for particular exceedance probabilities. In the procedure, the value of the t is replaced with a randomly selected value of the normal variate z for each discharge in the time series of daily discharges and the predicted load is computed with equation 1-5. The substitution of z for t is acceptable for relatively large data sample sizes as is the case with the Anatone and Spalding suspended sediment data. All predicted daily values of sediment load in the series are summed to compute a long-term realization of total sediment load. The computations are repeated in the Monte Carlo analysis for many repetitions of the discharge series. Each realization produces an estimate of long term total load that includes the uncertainty of the load regression equation and sample data. The full set of total load estimates are ranked and empirical frequencies for particular values of total load determined according to Weibull plotting position.

The results of the Monte Carlo simulation of total suspended sediment load, after conversion to sediment volume, for the Snake River at Anatone and the Clearwater River at Spalding are summarized in Table 64. The discharge series is for water years 1974 – 2010 and the number of realizations was 10,000. As expected, the median probability (0.5) value of total sediment volume 80.03 million cubic yards (mcy) is very close to the measured accumulation volume. Since this is a fixed historic discharge series, the practical meaning of exceedance loads in Table 64 is that if the historic sequence was repeated innumerable times, it could be expected that 5 percent of the total sediment load volumes would be greater than or equal to 83.89 mcy because of

[107] Hirsch, R.M., Helsel, D.R., Cohn, T.A., Gilroy, E.J. (1993) "Statistical Analysis of Hydrologic Data", *Handbook of Hydrology*, D.R. Maidment, Ed., McGraw-Hill, NY.

natural variability in the sediment load. The Monte Carlo analysis of total sediment load can be extended to include variability in the discharge time series, although just re-sequencing the discharge values would not change the long-term total load.

The percent differences from the median value listed in Table 64 vary over a relatively small range. This indicates that uncertainty in the load predictions should not have a large effect on the prediction of total sediment load for sediment transport modeling and sediment management planning for the future 50-year time period in the EIS. However, if the hydrologic conditions of the watersheds of the Snake and Clearwater Rivers change significantly in the future, the altered sediment supply may not be adequately represented by the historic sediment load data and the regression relationships derived from this data would not be valid.

Monte Carlo Sediment Volume Exceedance (1974-2010)				
Exceedance Probability	Anatone Sediment Volume mcy	Spalding Sediment Volume mcy	Total Sediment Volume mcy	Percent Difference
0.1	62.05	16.02	78.07	-2.5%
0.2	62.54	16.19	78.72	-1.6%
0.5	63.52	16.51	80.03	0.0%
0.8	64.54	16.86	81.40	1.7%
0.9	65.08	17.04	82.12	2.6%
0.95	65.54	17.19	82.73	3.4%
0.99	66.40	17.49	83.89	4.8%

Table 64. Monte Carlo analysis of sediment volume.

9.13. Effective Discharge

Effective discharge is the prevailing discharge that transports the most sediment over a long period of time[108,109] and is a useful reference for planning sediment management measures. The sediment load time series computed above for the Snake River at Anatone and Clearwater River at Spalding can be analyzed in a manner similar to a flow duration curve to determine the effective discharge and the discharge exceedance band that transports most of the sediment.

[108] Wolman, M. G., and Miller, J. P. (1960) "Magnitude and frequency of forces in geomorphic processes." *Journal of Geology*, 68, 54–74.

[109] Emmett, W. W., and Wolman, M. G. (2001). "Effective discharge andgravel-bed rivers." *Earth Surface Processes and Landforms*, 26, 1369–1380.

Effective discharge histograms and flow-duration curves for Snake and Clearwater Rivers and Lower Granite Reservoir are shown in Figure 131 through Figure 136. The effective discharge for the Snake River at Anatone is about 90,000 cfs (Figure 131). The sediment flow duration curve for Anatone in Figure 132 shows that 75 percent of the daily flows carry less than 10 percent of the total load. About 80 percent of the sediment load in the Snake River is carried by discharges between 40,000 and 140,000 cfs.

The effective discharge for the Clearwater River at Spalding is about 45,000 cfs (Figure 133). The sediment flow duration curve for Spalding in Figure 134 shows that 68 percent of the daily flows deliver less than 10 percent of the total load. About 80 percent of the sediment load in the Snake River is carried by discharges between 15,000 and 60,000 cfs.

Daily discharge and sediment load for the Snake and Clearwater Rivers are summed to estimate the total sediment load delivered to Lower Granite Reservoir. The effective discharge for Lower Granite Reservoir is about 115,000 cfs (Figure 135). The sediment flow duration curve for Lower Granite in Figure 136 shows that 70 percent of the daily flows deliver less than 10 percent of the total load. About 80 percent of the sediment load in the Snake River is carried by discharges between 50,000 and 190,000 cfs. These curves demonstrate that very high flows do not contribute significantly to the total accumulated load in Lower Granite Reservoir because they are relatively infrequent

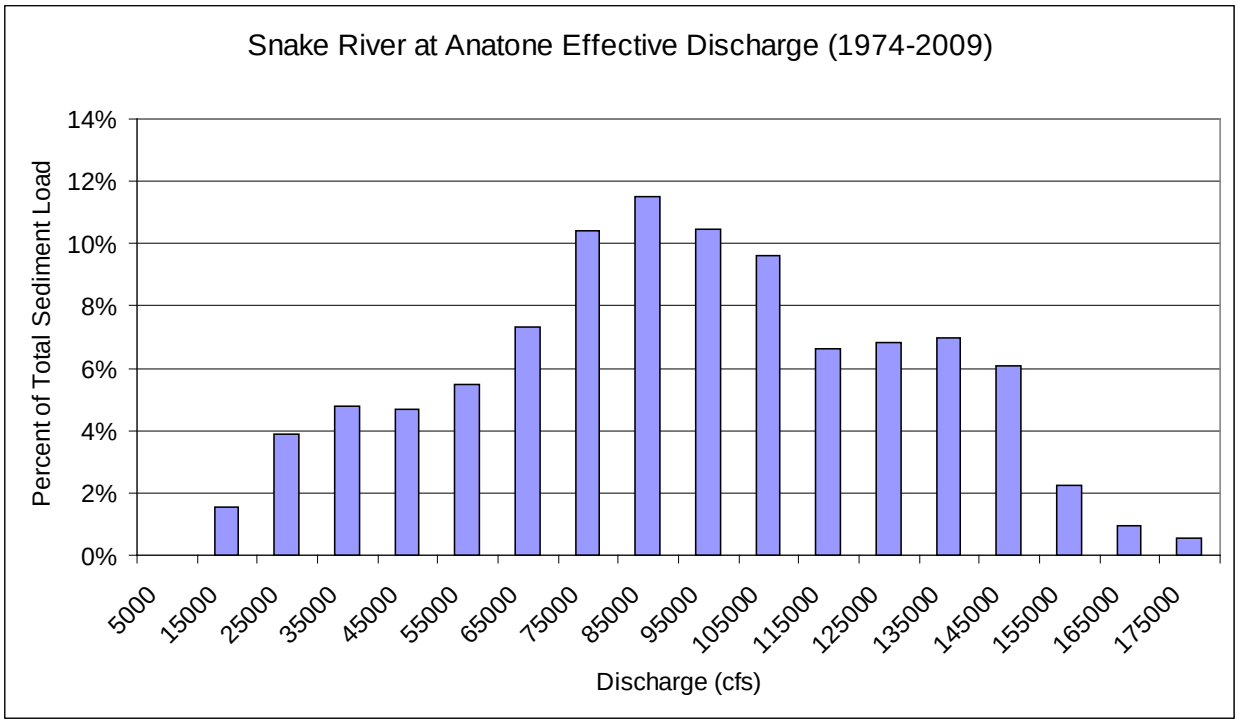


Figure 131. Effective discharge Snake River at Anatone.

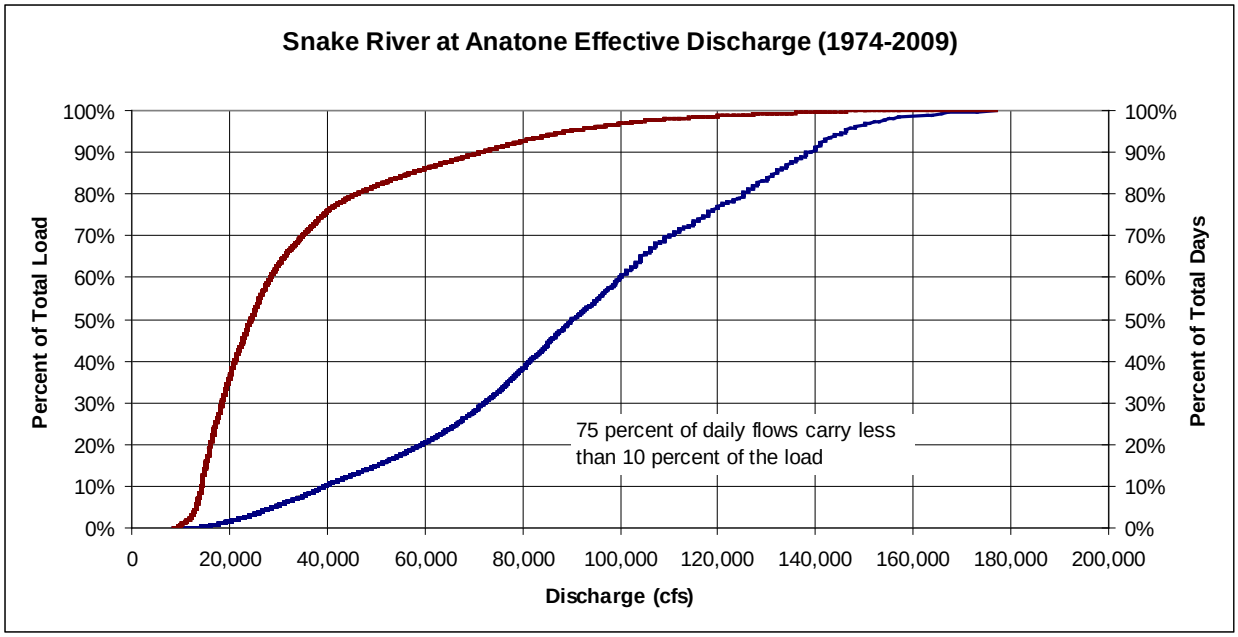


Figure 132. Sediment flow-duration Snake River at Anatone.

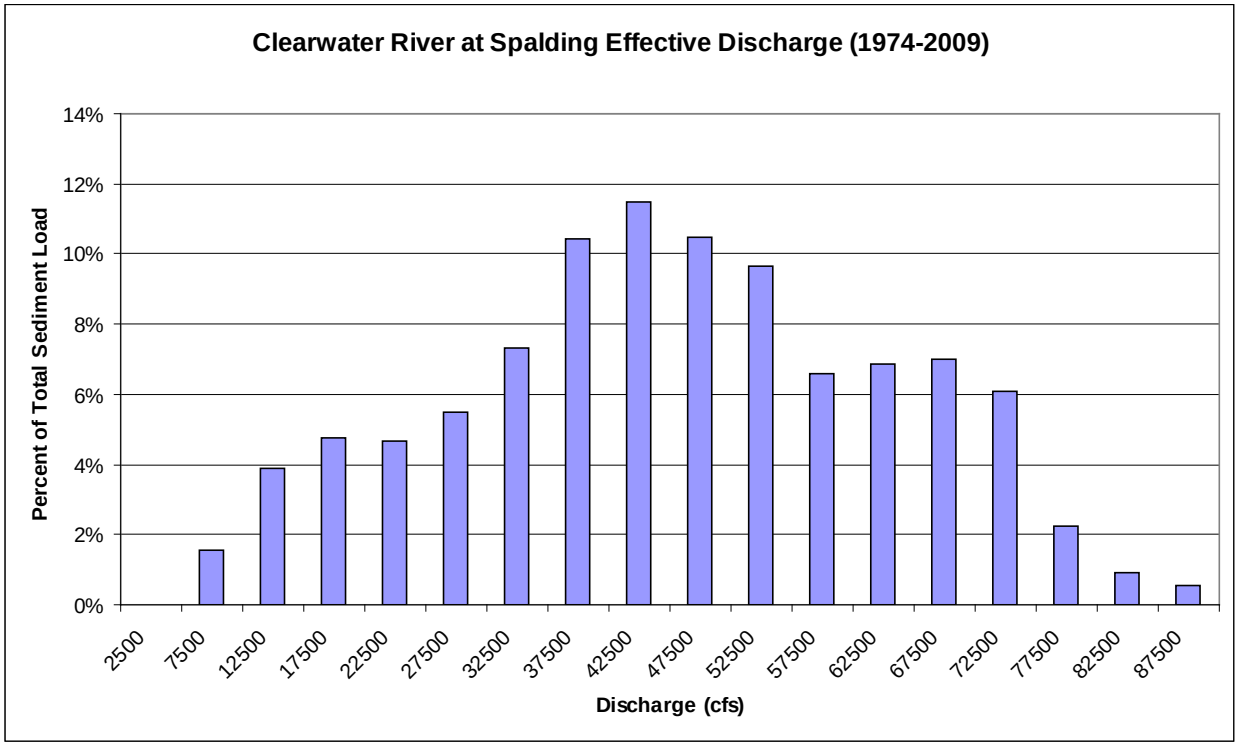


Figure 133. Effective discharge Clearwater River at Spalding.

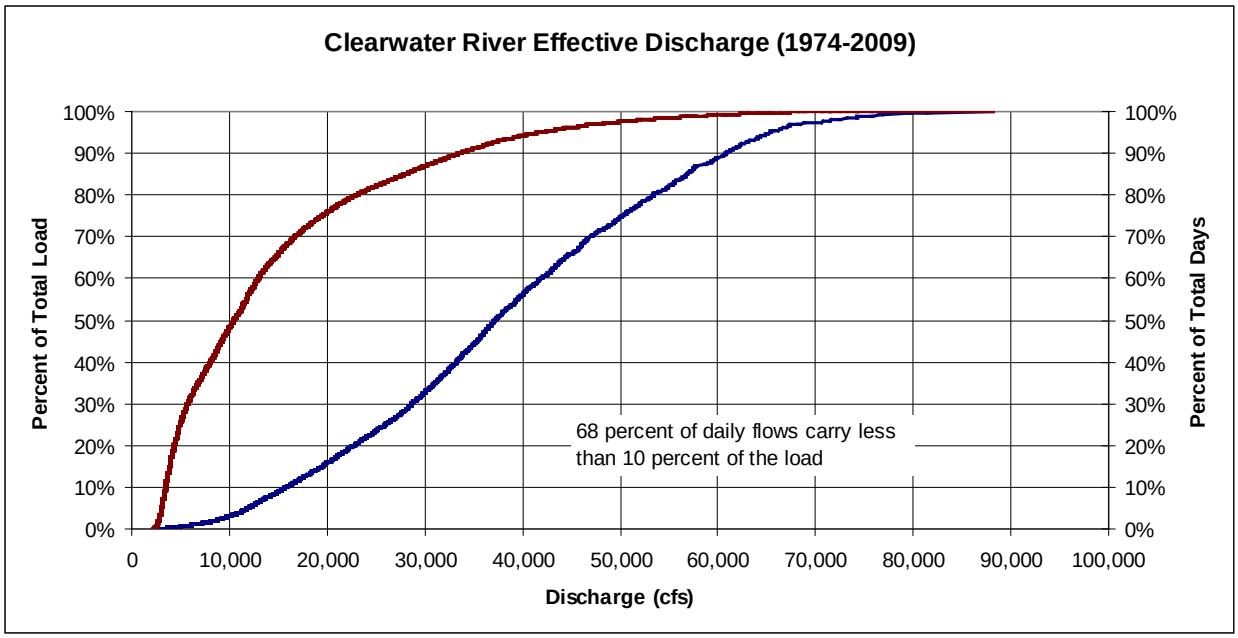


Figure 134. Sediment flow-duration Clearwater River at Spalding.

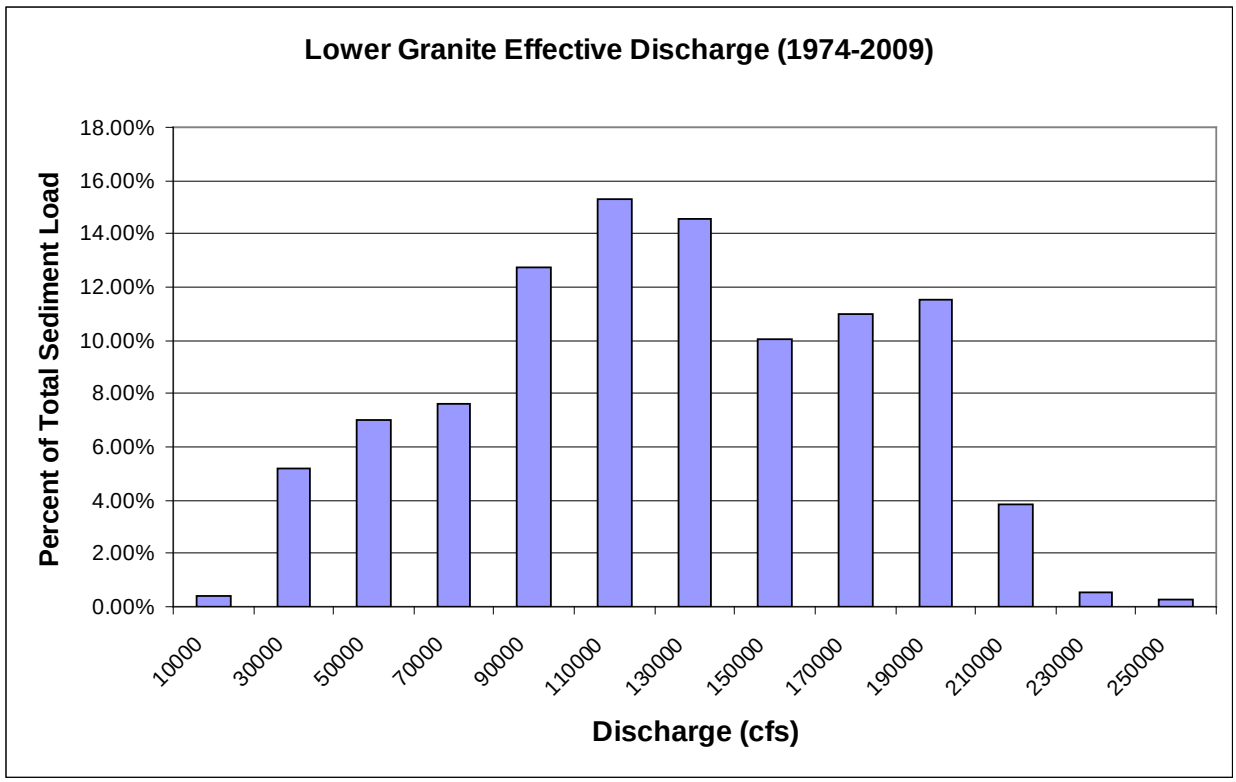


Figure 135. Effective discharge Lower Granite Reservoir.

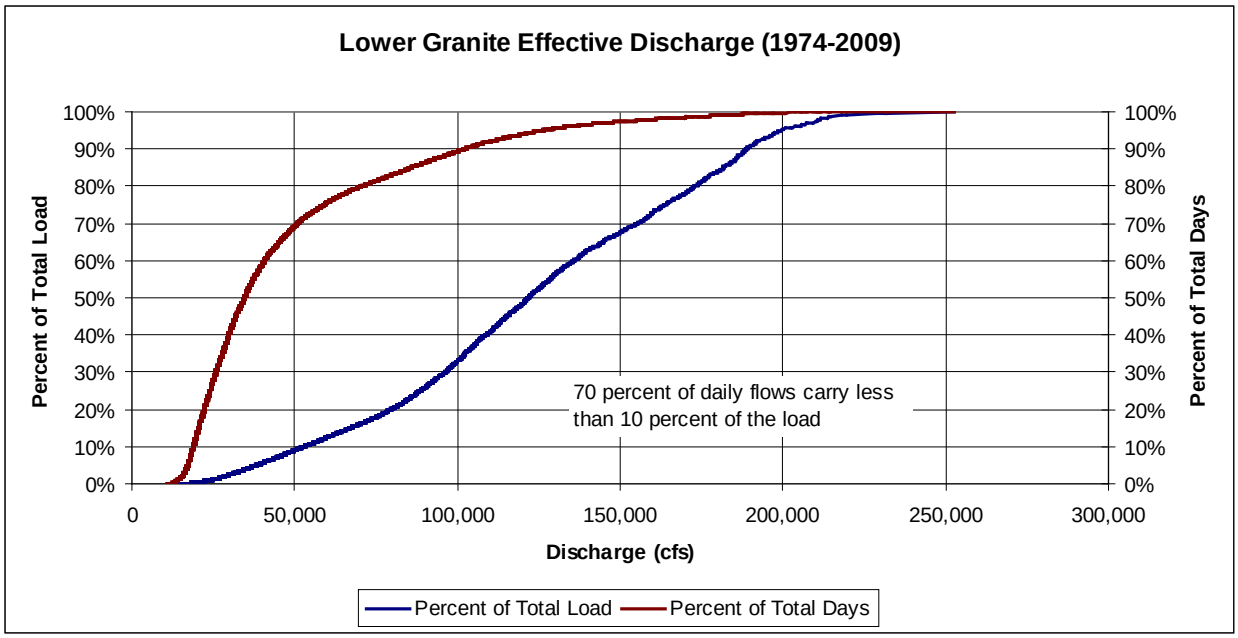


Figure 136. Sediment flow-duration Lower Granite Reservoir.

9.14. Sediment Load Grain Size Distributions

Sediment grain size fractions were measured for the suspended sediment and bedload samples collected by USGS in the studies discussed in Sections 9.6 and 9.7. The fraction of fine material (sand break) was determined for nearly all sediment samples (Table 46 and Table 47). The fine fraction is the percent of total sediment load that is silt and clay. The upper limit of the silt class is 0.062 mm. Complete grain size distributions were determined for many samples in the 1972-1979 sediment data and for selected samples in the 2008-2010 samples.

The percent fine sediment for the Snake River at Anatone for the periods 1972-1979 and 2008-2010 are plotted with discharge in Figure 137. Percent fines in the suspended sediment decrease somewhat with increasing discharge and averages about 60 percent in the range of discharges that transport most of the sediment (Section 9.13). In other words, a greater percentage of sand is being transported at higher discharges, even though the total silt load increases. The recent suspended sediment measurements suggest that the percent fines has decreased since the 1970's, which agrees with the apparent trend in increasing sand load seen in Figure 115.

The relationship between percent fines and discharge for the Clearwater River at Spalding is plotted in Figure 138. The fraction of fine material decreases with increasing discharge at a rate that is somewhat greater than at Anatone and has an average of about 50 percent of total load in the range of discharges that produce most of the sediment load.

Average grain percent-finer size distributions for the measured suspended sediment data are summarized in Table 65 and Table 66 for the Snake River at Anatone and the Clearwater River at Spalding. The average distributions are listed for 1972-1979 data, the more recent data, and the combined data. Suspended sediment at Anatone is less than 1 percent coarse sand, 5 percent medium sand, 8 percent fine sand, and 10 percent very fine sand. The Anatone data suggests that the grain size distribution of suspended sediment in the Snake River is becoming coarser, but there are too few measurements in the recent dataset to confirm a statistical difference.

Suspended sediment at Spalding is less than 2 percent coarse sand, 10 percent medium sand, 10 percent fine sand, and 9 percent very fine sand. There is no indication that the suspended sediment grain size distribution of the Clearwater River has changed since the 1970's.

Bedload grain size distributions were also measured at Anatone and Spalding during the studies in 1972-1979 and 2008-2010. The grain size distributions vary greatly between measurements and there is almost no correlation of grain size parameters with discharge. Bedload median diameter (D_{50}) and the 90th percentile diameter (D_{90}) for Anatone and Spalding are plotted in Figure 139 and Figure 140. The upper range of bedload D_{50} and D_{90} are approximately 60 mm and 100 mm at both sites. Low D_{50} and D_{90} at high discharges are likely because of the transport of sand delivered from tributary sources and perhaps the difficulty of positioning the sampler on the bed in high velocity flows. Average percent-finer bedload distributions are plotted in Figure 141. The bedload distributions are bimodal, a characteristic of the Snake River and Clearwater River bedload and bed material that has been noted in previous reports[110]. About 70 percent of the bedload is sand and 50 percent of the bedload is in the size range measured by the suspended sediment samplers. It is important to note that the bedload distributions were obtained from the bedload samples and not from material obtained from the beds of the Snake and Clearwater Rivers.

[110] Thomas, W.A. (1982) "Mathematical Modelling of Sediment Movement", *Gravel-bed Rivers,* R.D. Hey, J.C. Bathurst and C.R. Thorne Ed., Wiley, NY.

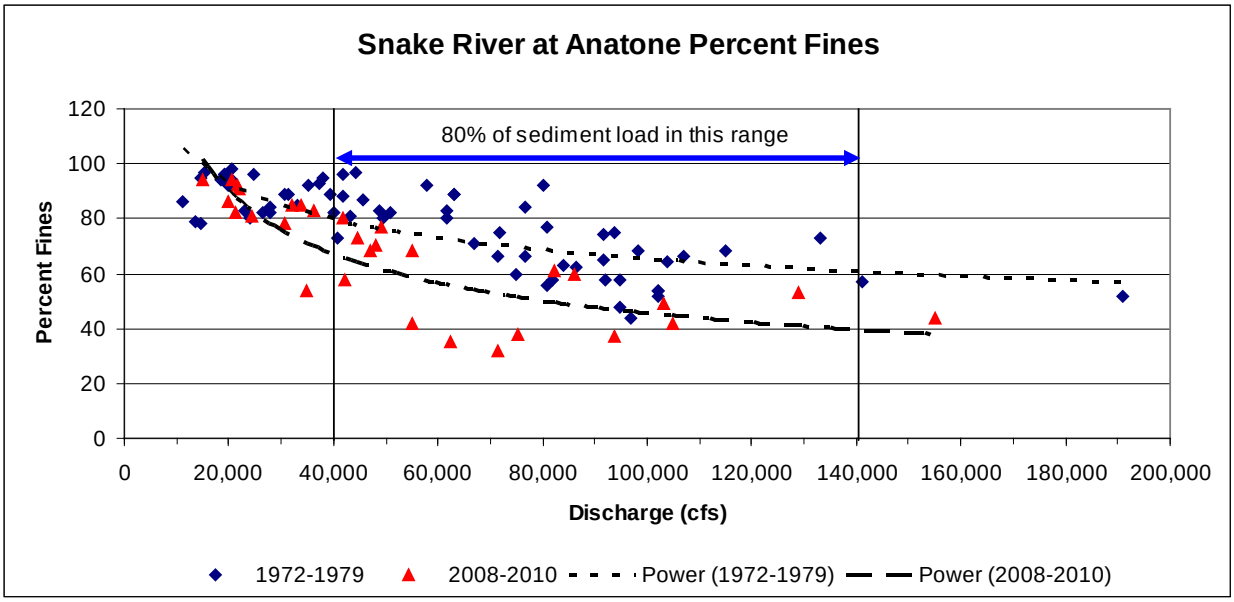


Figure 137. Variation of percent fines with discharge for Snake River at Anatone.

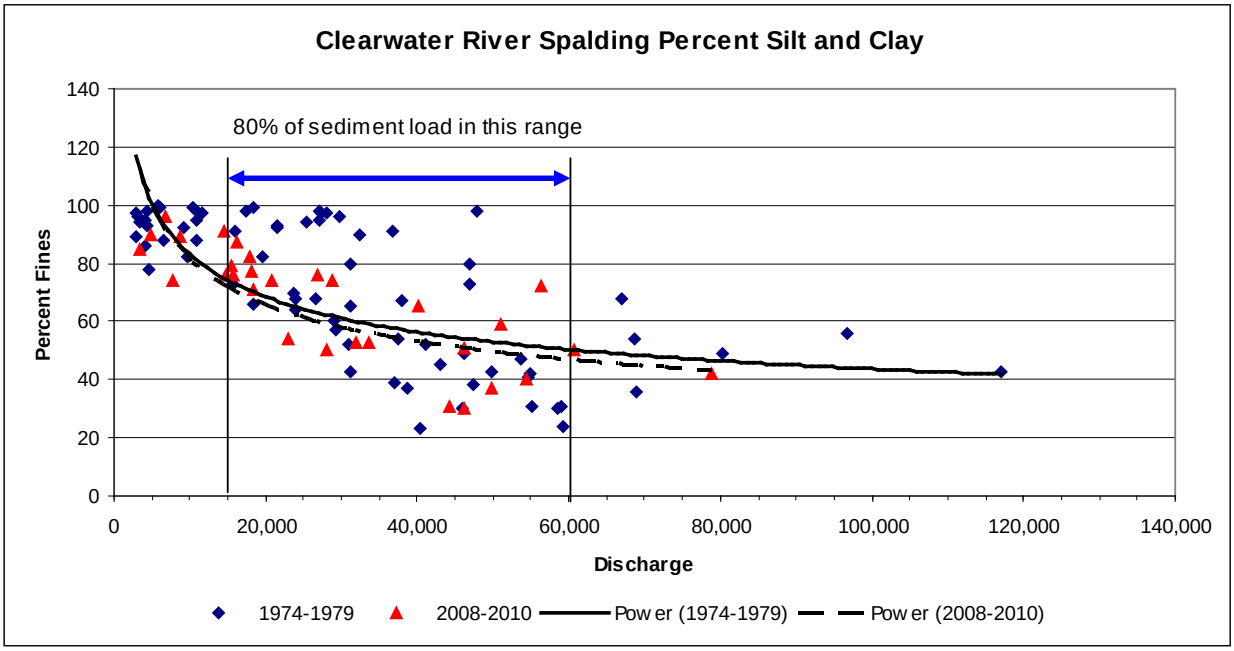


Figure 138. Variation of percent fines with discharge for Clearwater River at Spalding.

Snake River at Anatone Suspended Sediment Average Percent-Finer Grain Size Distribution				
Particle Size mm	Class	1972-2010 Fraction Average	1972-1979 Fraction Average	2010 Fraction Average
2.0	Very Coarse Sand	100.0	100.0	100.0
1.0	Coarse Sand	100.0	100.0	99.9
0.50	Medium Sand	99.3	99.5	98.0
0.25	Fine Sand	94.3	95.2	87.3
0.125	Very Fine Sand	86.5	87.6	78.0
0.062	Silt and Clay	76.8	77.7	70.2

Table 65. Snake River at Anatone suspended sediment average grain size distribution.

Clearwater River at Spalding Suspended Sediment Average Percent-Finer Grain Size Distribution				
Particle Size mm	Class	1972-2010 Fraction Average	1972-1979 Fraction Average	2008-2010 Fraction Average
2.0	Very Coarse Sand	100	100	100
1.0	Coarse Sand	100	100	100
0.50	Medium Sand	97.9	97.9	97.7
0.25	Fine Sand	87.5	87.3	88.4
0.125	Very Fine Sand	77.9	77.9	77.9
0.062	Silt and Clay	68.9	69.6	65.9

Table 66. Clearwater River at Spalding suspended sediment average grain size distribution.

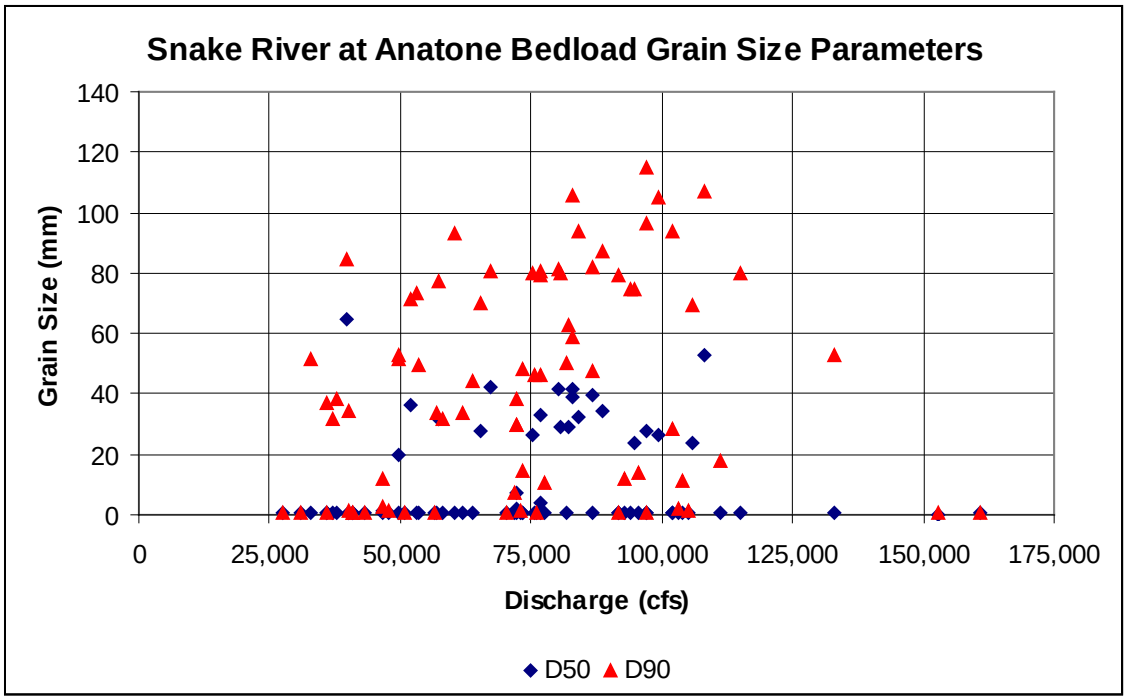


Figure 139. Bedload grain size parameters Snake River at Anatone.

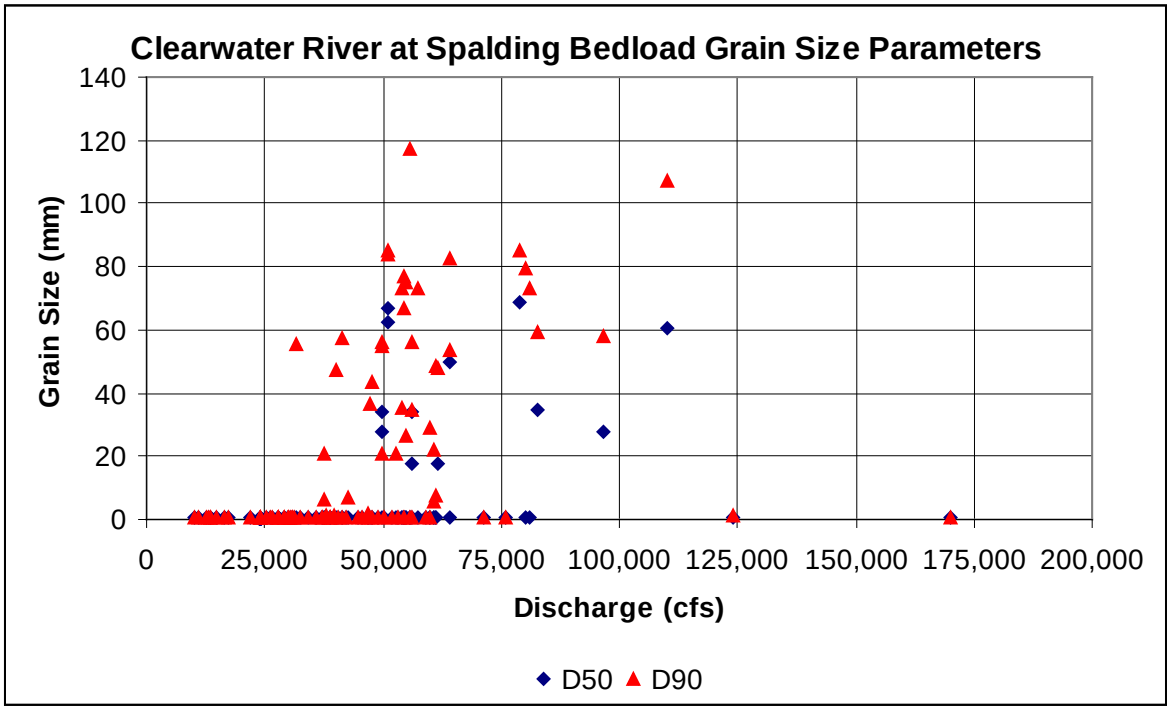


Figure 140. Bedload grain size parameters Clearwater River at Spalding.

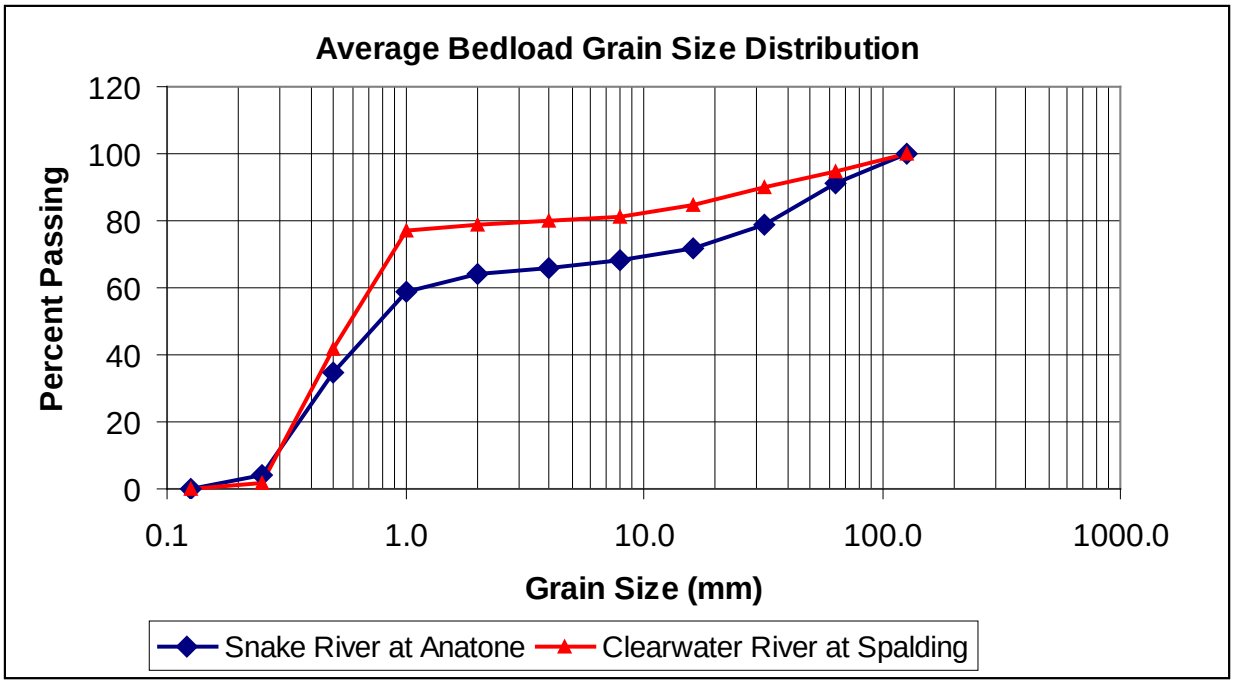


Figure 141. Average bedload grain size distribution for the Snake River and Clearwater River.

9.15. Sediment Load Characteristics for Sediment Transport Modeling

The previous sections demonstrated that sediment volumes estimated with the load regression relationships developed from the USGS sediment data agreed well with the measured volume of sediment that has accumulated in Lower Granite Reservoir since 1974. The good agreement between the estimated and measured sediment accumulation validates the use of the load relationships for simulation of sediment load in sediment transport modeling and sediment management planning for the 50-year future analysis period for the EIS.

Sediment load is input as a boundary condition in sediment transport modeling with HEC-RAS. Water discharge rates for sediment transport modeling in HEC-RAS are specified as quasi-steady flow time series. A quasi-steady flow series is a series of discrete discharges that are constant over regular or irregular time steps. Daily time intervals were used in the simulations in this analysis. The sediment load time series is specified either as discrete load amounts for every discharge in the time series or as a sediment rating curve (rating table). A sediment rating table contains total sediment load rates (tons per day) and grain size fractions for the range of the discharges in the discharge series. Sediment loads for long simulations in this analysis were specified with rating curves developed from sediment load relationships and average grain size distributions described above.

Sediment rating tables for the Snake River and Clearwater River reaches of the HEC-RAS model of Lower Granite Reservoir are shown in Table 67 and Table 68. The procedure used to develop the rating tables is performed in the following steps:

1. Select sufficient discrete discharge values across the range of discharges in the time series to characterize the nonlinear sediment load relationship. A total of 19 (line 1) points were selected for both the Snake and Clearwater Rivers (line 2). The range of discharge for the Snake River was from 0 to 180,000 cfs in 10,000 cfs increments and the range for the Clearwater River was 0 to 90,000 cfs in 5,000 cfs increments. Several discharge values are skipped in Table 67 and Table 68 so the tables are readable.
2. Compute total suspended loads for each discharge value in the rating tables with the bias-corrected log-log power relationships in Sections 9.6 and 9.7 (line 3).
3. Compute bedloads for each discharge value in the rating tables with the bias-corrected log-log power relationships developed in Sections 9.6 and 9.7 (line 4).
4. Sum the suspended load and bedload to obtain total sediment load for each value of discharge (line 8).
5. Compute the sand fraction with the linear regression relationships shown in Figure 142 and Figure 143 (line 5). An alternative would be to compute the suspended sand fraction from the regression relationships presented in Sections 9.6 and 9.7. The first method was preferred in this analysis because of the more linear relationship of sand fraction with discharge.
6. Compute the bedload fraction by dividing line 4 by line 8.
7. Apportion load fractions by grain size for each discharge value according to the average grain size distributions for the suspended loads and bedloads presented in Section 9.14. The sand contribution from bedload is adjusted to account for overlap in the sample zone near the bed. Both the suspended sediment samples and bedload samples had significant fractions of fine sand and medium sand. Grain size fractions less than coarse sand in the bedload are likely also sampled by the suspended sampler since the Helley-Smith orifice extends 6 inches up from the surface of the bed and the P-61 sampler nozzle can sample within about 3 inches of the bed. The bedload fraction of total load for sediment transport modeling was adjusted to remove the fraction less than coarse sand as shown in Table 69 and Table 70.

To illustrate the computation of load fractions, the coarse silt, very fine sand, coarse sand and fine gravel fractions are computed for a discharge of 50,000 cfs for the Snake River as follows,

$$F_{cm} = 0.25(0.772) = 0.193$$

$$F_{vfs} = 0.50(.207) = 0.104$$

$$F_{cs} = 0.05(0.207) + 0.12(0.0206) = 0.013$$

$$F_{fg} = 0.10(0.0206) = 0.002$$

Total load sediment rating curves for the Snake River and Clearwater Rivers as represented in the HEC-RAS rating tables are plotted in Figure 144 and Figure 145. The 19 discharge points adequately represent the curvature of the load relationship so linear interpolations between values in the loads are acceptable. The relationships for percent fines are also shown on the plots.

To confirm the performance of the sediment rating tables in HEC-RAS, the tabulated sediment load and load fractions were simulated for the 1974-2010 daily time series and the total load was summed for the period. The total HEC-RAS sediment load is summarized in Table 71. Load proportions are 77 percent for the Snake River and 22 percent for Clearwater River which agrees with the proportions estimated from the sediment load measurements. Total combined load is 78 million tons or a volume 75.4 mcy at an average unit weight of 76.6 lb/ft^3. The simulated volume is about 5.6 percent less than the total accumulation of 79.83 mcy measured in the sediment ranges. The average unit weight is computed,

$$\gamma_{avg} = \left[70\frac{\text{lb}}{\text{ft}^3}(1-0.332)\right]_{silt} + \left[90\frac{\text{lb}}{\text{ft}^3}(0.332)\right]_{sand} = 76.64\frac{\text{lb}}{\text{ft}^3}$$

An exact match of the measured accumulation results if the unit weight of silt is assumed to be 63 lb/ft^3. The good agreement between the simulated loads and the measured sediment accumulation volumes validates the use of the HEC-RAS sediment rating curves (tables) for sediment transport modeling.

Snake River Combined Suspended Sediment and Bedload Rating Table for HEC-RAS Sediment Transport Modeling											
1. HEC-RAS Table Set No.	1	2	3	4	5	6	15	16	17	18	19
2. Discharge, cfs	0	10,000	20,000	30,000	40,000	50,000	140,000	150,000	160,000	170,000	180,000
3. Suspended Load, US ton/day	0	53	367	1,145	2,565	4,797	86,158	104,555	125,304	148,533	174,363
4. Bedload, US ton/day	0	1	8	25	54	101	1,725	2,087	2,494	2,948	3,452
5. Suspended Fines, percent	88.8%	88.8%	86.0%	83.1%	80.2%	77.2%	50.8%	47.9%	45.0%	42.0%	39.1%
6. Suspended Sand, percent	8.9%	8.9%	11.9%	14.8%	17.8%	20.7%	47.2%	50.1%	53.1%	56.0%	59.0%
7. Coarse Bedload, percent	2.21%	2.21%	2.14%	2.10%	2.08%	2.06%	1.96%	1.96%	1.95%	1.95%	1.94%
8. Total Load, US ton/day	0	54	375	1,169	2,620	4,898	87,883	106,642	127,798	151,481	177,815
9. Clay	0.000	0.000	0.000	0.000	0.000	0.000	0.000	0.000	0.000	0.000	0.000
10. Very fine silt (VFM)	0.222	0.222	0.215	0.208	0.200	0.193	0.127	0.120	0.112	0.105	0.098
11. Fine silt (FM)	0.222	0.222	0.215	0.208	0.200	0.193	0.127	0.120	0.112	0.105	0.098
12. Medium silt (MM)	0.222	0.222	0.215	0.208	0.200	0.193	0.127	0.120	0.112	0.105	0.098
13. Coarse silt (CM)	0.222	0.222	0.215	0.208	0.200	0.193	0.127	0.120	0.112	0.105	0.098
14. Very fine sand (VFS)	0.045	0.045	0.059	0.074	0.089	0.104	0.236	0.251	0.265	0.280	0.295
15.Fine sand (FS)	0.022	0.022	0.030	0.037	0.044	0.052	0.118	0.125	0.133	0.140	0.147
16. Medium sand (MS)	0.018	0.018	0.024	0.030	0.036	0.041	0.094	0.100	0.106	0.112	0.118
17. Coarse sand(CS)	0.007	0.007	0.009	0.010	0.011	0.013	0.026	0.027	0.029	0.030	0.032
18. Very coarse sand (VCS)	0.001	0.001	0.001	0.001	0.001	0.001	0.001	0.001	0.001	0.001	0.001
19. Very fine gravel (VFG)	0.001	0.001	0.001	0.001	0.001	0.001	0.001	0.001	0.001	0.001	0.001
20. Fine gravel (FG)	0.002	0.002	0.002	0.002	0.002	0.002	0.002	0.002	0.002	0.002	0.002
21. Medium gravel (MG)	0.004	0.004	0.004	0.004	0.004	0.004	0.003	0.003	0.003	0.003	0.003
22. Coarse gravel (CG)	0.006	0.006	0.006	0.006	0.006	0.006	0.006	0.006	0.006	0.006	0.006
23. Very coarse gravel (VCG)	0.005	0.005	0.005	0.005	0.005	0.005	0.004	0.004	0.004	0.004	0.004

Table 67. Snake River combined suspended sediment and bedload rating table for HEC-RAS sediment transport modeling.

Clearwater River Combined Suspended Sediment and Bedload Rating Table for HEC-RAS Sediment Transport Modeling											
1. HEC-RAS Table Set No.	1	2	3	4	5	6	15	16	17	18	19
2. Discharge, cfs	0	5,000	10,000	15,000	20,000	25,000	70,000	75,000	80,000	85,000	90,000
3. Suspended Load, US ton/day	0	80	338	785	1,426	2,265	19,180	22,131	25,302	28,694	32,307
4. Bedload, US ton/day	0	3	7	13	20	27	122	134	148	161	175
5. Suspended Fines, percent	86.0%	86.0%	83.5%	80.4%	77.2%	73.8%	42.9%	39.5%	36.0%	32.5%	29.1%
6. Suspended Sand, percent	10.9%	10.9%	14.5%	18.0%	21.5%	25.0%	56.4%	59.9%	63.4%	66.9%	70.4%
7. Coarse Bedload, percent	3.1%	3.1%	2.1%	1.6%	1.4%	1.2%	0.6%	0.6%	0.6%	0.6%	0.5%
8. Total Load, US ton/day	0	83	345	798	1,445	2,292	19,301	22,266	25,450	28,855	32,482
9. Clay	0.000	0.000	0.000	0.000	0.000	0.000	0.000	0.000	0.000	0.000	0.000
10. Very fine silt (VFM)	0.215	0.215	0.209	0.201	0.193	0.185	0.107	0.099	0.090	0.081	0.073
11. Fine silt (FM)	0.215	0.215	0.209	0.201	0.193	0.185	0.107	0.099	0.090	0.081	0.073
12. Medium silt (MM)	0.215	0.215	0.209	0.201	0.193	0.185	0.107	0.099	0.090	0.081	0.073
13. Coarse silt (CM)	0.215	0.215	0.209	0.201	0.193	0.185	0.107	0.099	0.090	0.081	0.073
14. Very fine sand (VFS)	0.055	0.055	0.072	0.090	0.107	0.125	0.282	0.300	0.317	0.335	0.352
15.Fine sand (FS)	0.027	0.027	0.036	0.045	0.054	0.062	0.141	0.150	0.159	0.167	0.176
16. Medium sand (MS)	0.022	0.022	0.029	0.036	0.043	0.050	0.113	0.120	0.127	0.134	0.141
17. Coarse sand(CS)	0.008	0.008	0.009	0.010	0.012	0.014	0.029	0.030	0.032	0.034	0.036
18. Very coarse sand (VCS)	0.001	0.001	0.001	0.001	0.001	0.001	0.000	0.000	0.000	0.000	0.000
19. Very fine gravel (VFG)	0.001	0.001	0.001	0.001	0.001	0.001	0.000	0.000	0.000	0.000	0.000
20. Fine gravel (FG)	0.005	0.005	0.004	0.003	0.002	0.002	0.001	0.001	0.001	0.001	0.001
21. Medium gravel (MG)	0.007	0.007	0.004	0.003	0.003	0.003	0.001	0.001	0.001	0.001	0.001
22. Coarse gravel (CG)	0.007	0.007	0.004	0.003	0.003	0.003	0.001	0.001	0.001	0.001	0.001
23. Very coarse gravel (VCG)	0.007	0.007	0.004	0.003	0.003	0.003	0.001	0.001	0.001	0.001	0.001

Table 68. Clearwater River combined suspended sediment and bedload rating table for HEC-RAS sediment transport modeling.

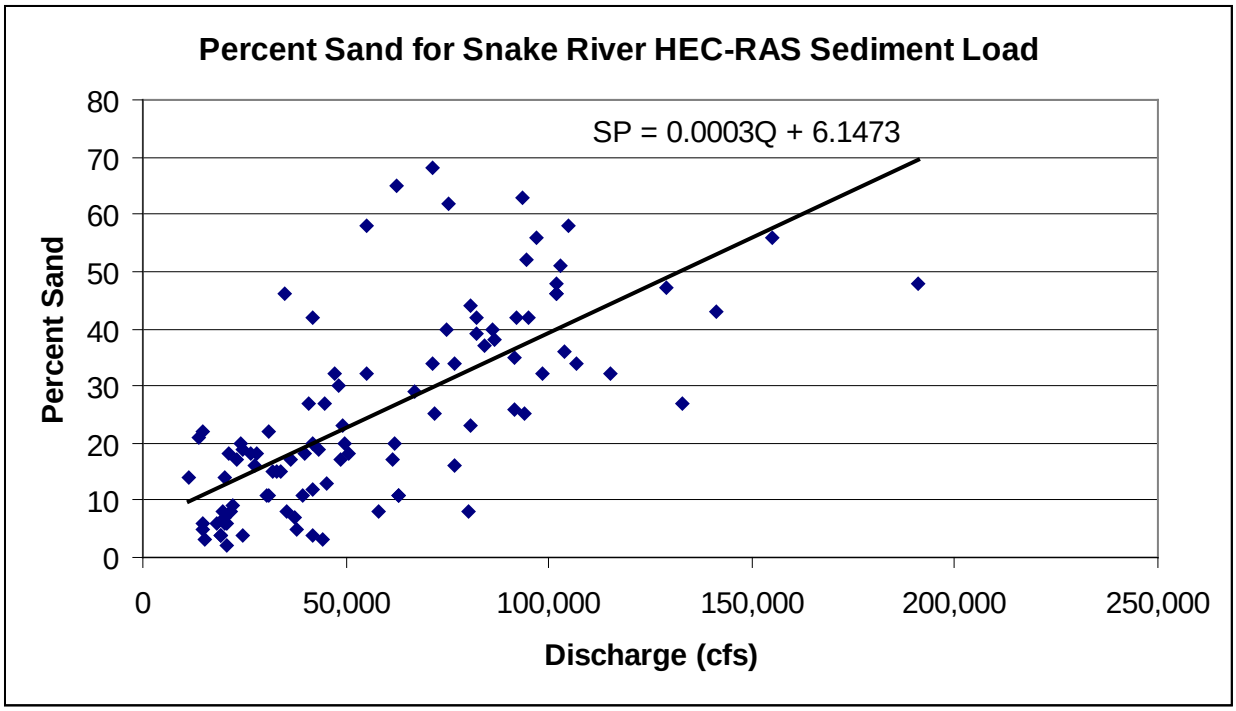


Figure 142. Snake River percent suspended sand relationship for sediment transport modeling.

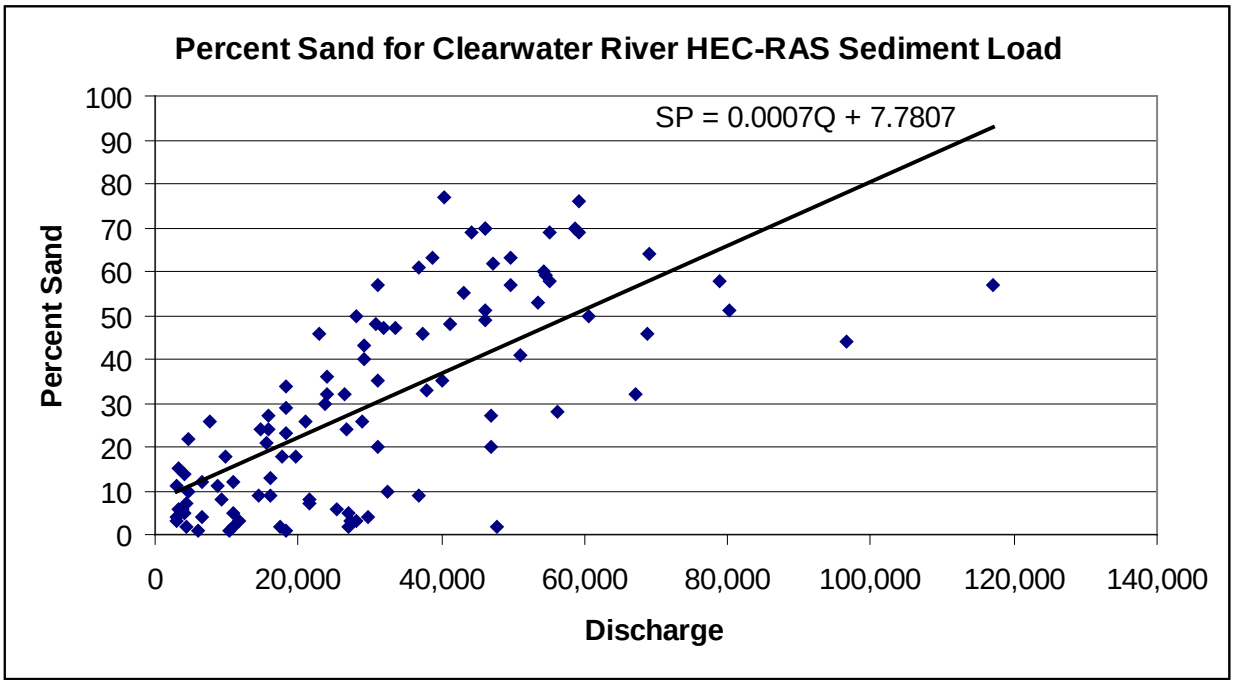


Figure 143. Clearwater River percent suspended sand relationship for sediment transport modeling.

Snake River Grain Size Fractions for Sediment Transport Modeling					
Size Class	Suspended Silt	Suspended Sand	Average Bedload	Adjusted Bedload	Size mm
Clay	0.00				0.004
VFM	0.25				0.008
FM	0.25				0.016
MM	0.25				0.032
CM	0.25				0.0625
VFS		0.50	0.04		0.125
FS		0.25	0.31		0.25
MS		0.20	0.24		0.5
CS		0.05	0.05	0.12	1
VCS			0.02	0.05	2
VFG			0.02	0.05	4
FG			0.04	0.10	8
MG			0.07	0.17	16
CG			0.12	0.29	32
VCG			0.09	0.22	64
SC					128
LC					256
SB					512
MB					1024
LB					2048
Total	1.00	1.00	1.00	1.00	

Table 69. Snake River grain size fractions for sediment transport modeling.

Clearwater River Grain Size Fractions for Sediment Transport Modeling					
Size Class	Suspended Silt	Suspended Sand	Average Bedload	Adjusted Bedload	Size mm
Clay	0.00				0.004
VFM	0.25				0.008
FM	0.25				0.016
MM	0.25				0.032
CM	0.25				0.0625
VFS		0.50	0.02		0.125
FS		0.25	0.40		0.25
MS		0.20	0.35		0.5
CS		0.05	0.02	0.09	1
VCS			0.01	0.04	2
VFG			0.01	0.04	4
FG			0.04	0.17	8
MG			0.05	0.22	16
CG			0.05	0.22	32
VCG			0.05	0.22	64
SC					128
LC					256
SB					512
MB					1024
LB					2048
Total	1.00	1.00	1.00	1.00	

Table 70. Clearwater River grain size fractions for sediment transport modeling.

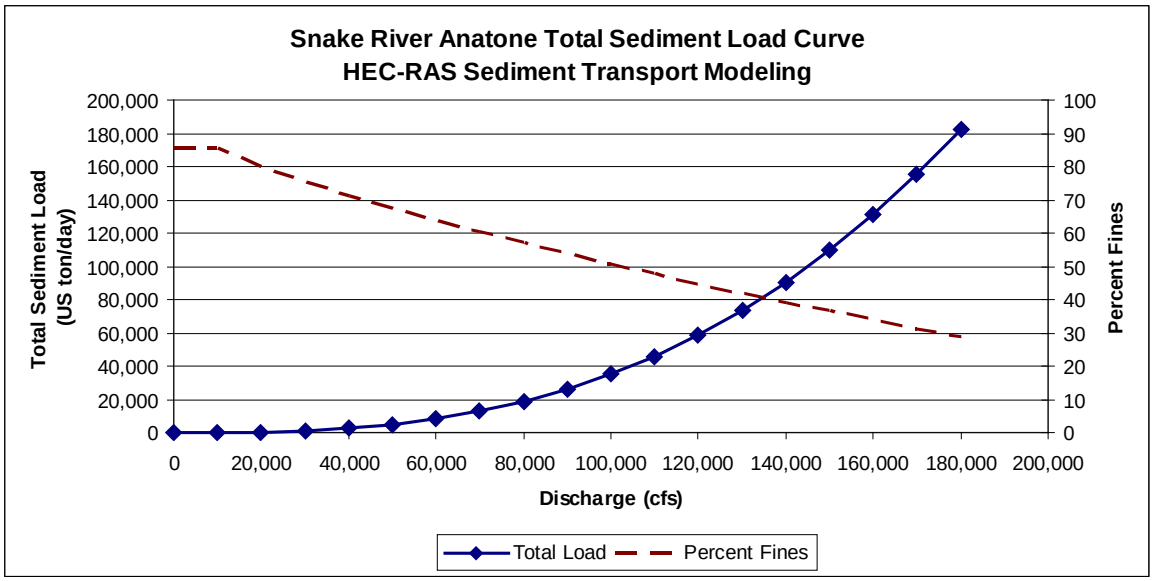


Figure 144. Snake River total sediment rating curve for HEC-RAS sediment transport modeling.

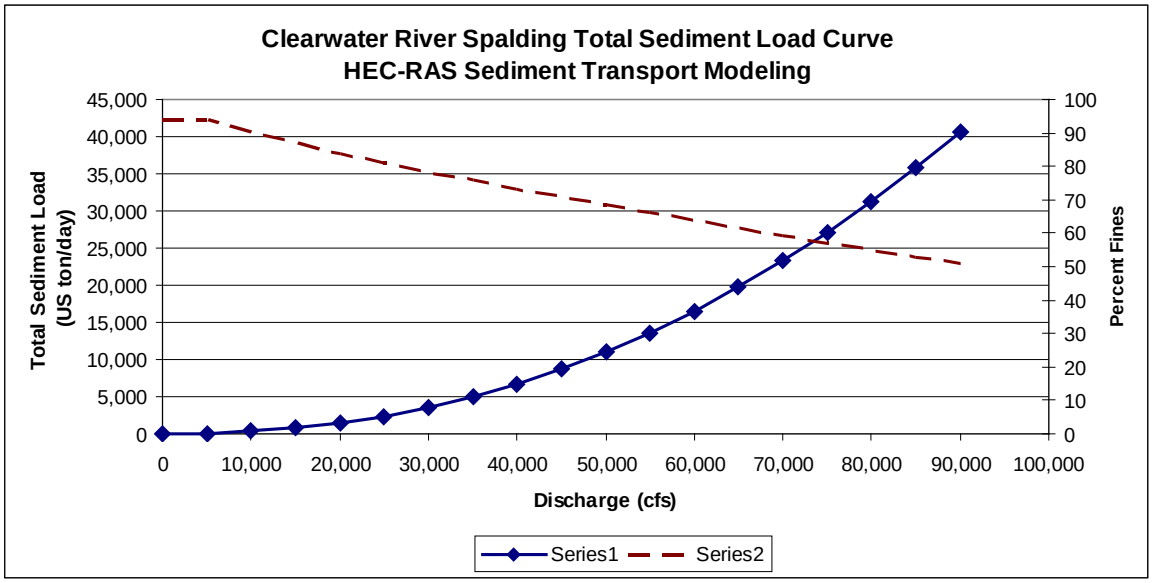


Figure 145. Clearwater River total sediment rating curve for HEC-RAS sediment transport modeling.

HEC-RAS Sediment Load 1974-2010			
	Snake River	Clearwater River	Lower Granite
Sum of load, ton	59,979,760	18,029,700	78,009,460
Mean load, tpd	4,562	1,371	3,824
Mean percent sand	33.1%	33.4%	33.2%
Mean unit weight, lb/ft^3	76.63	76.68	76.64
Total volume, mcy	57.98	17.42	75.40

Table 71. HEC-RAS sediment load series summary and volume verification.

9.16. Sediment Load in Snake and Clearwater River Tributaries

Suspended sediment load and bedload was measured by USGS in 2009, 2010 and 2011 at 11 locations on the rivers of the Snake and Clearwater River basins shown in Figure 146. Sediment load was also measured on the Palouse River. The intent of the sediment measurement campaign was to identify the relative proportion of load delivered by the tributaries. All the sediment load measurement sites are at USGS stream gage stations except for the sites at Harpster, Kooskia and near the mouth of the Grande Ronde River. Suspended sediment and bedload were measured from bridges according to standard USGS protocols[111].

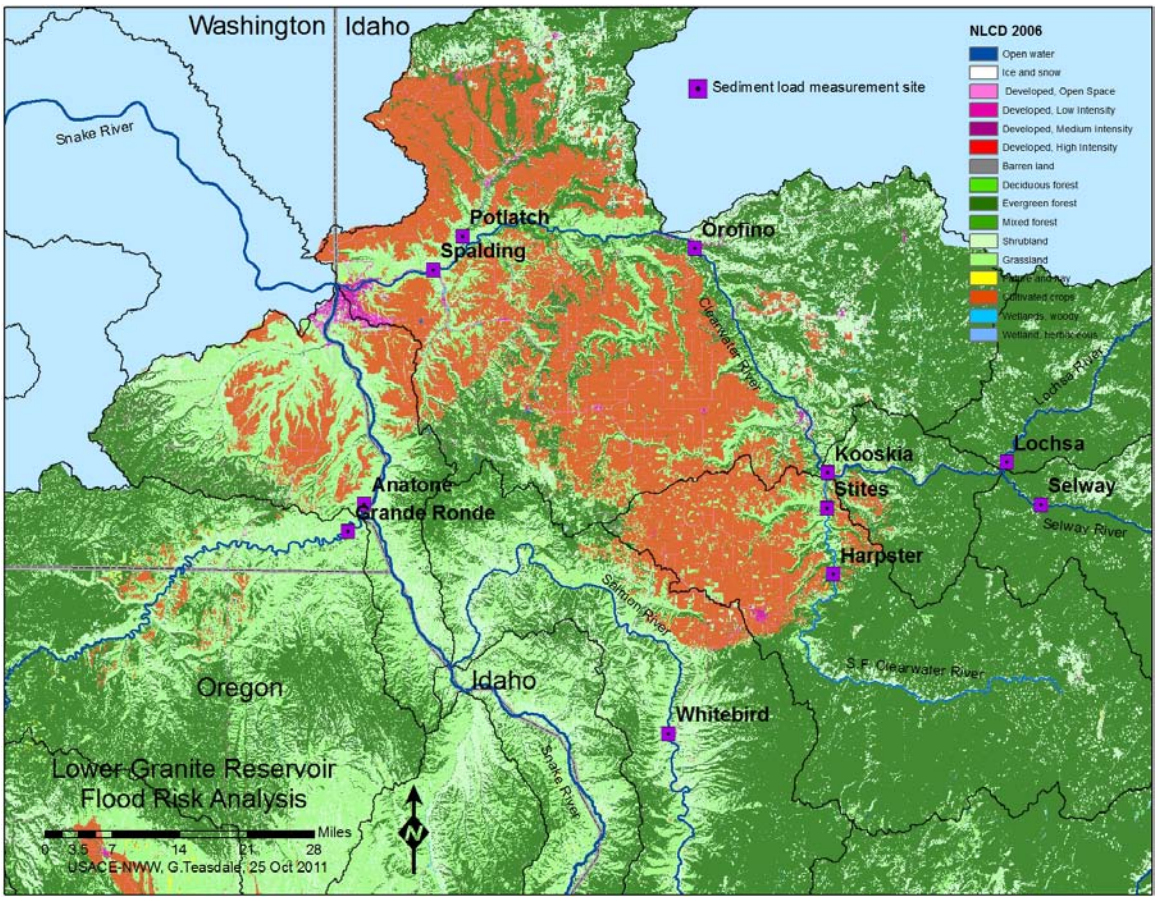


Figure 146. Sediment load measurement sites.

[111] Edwards, T.K. and Glysson, G. D. (1999). *Field Methods for Measurement of Fluvial Sediment, Techniques of Water-Resources Investigations, Book 3, Chapter C2*, U.S. Geological Survey, Reston, VA.

9.16.1. Regression Analysis of Tributary Sediment Loads

Regression relationships were fit to the suspended sediment data using methods similar to those described in Sections 9.6 and 9.7. The number of suspended sediment samples varied from 36 to 42 at each site. Similar to the sediment load measurements at Anatone and Spalding, the sediment load data of the tributaries were best fit by the adjusted power and the MVUE regression lines. Fitted regression lines of the suspended sediment load in the Salmon River at Whitebird are shown in Figure 147. Considerable scatter exists about the regression lines and the prediction intervals are broad (Figure 148), so the load estimates based on the regression are not precise. The more extensive sediment datasets for Anatone and Spalding show substantial annual variability, so sediment loads would have to be measured over a much longer period of time to substantially reduce the uncertainty in the load estimates.

Even though the specific load estimates have substantial statistical uncertainty, the relative contributions of the tributaries provide the best available means to the rank the tributary basins as sources of sediment supplied to Lower Granite Reservoir, provided that climate and watershed conditions remain relatively unchanged. Since sediment concentration (and load) is reasonably correlated with water discharge in the tributaries, a substantial change in the annual flow of the tributaries would have to occur to dramatically change the relative ranking of the proportional sediment loads. The daily discharges of the tributaries for water years 2009, 2010 and 2011 were representative of the typical seasonal flows of these basins. This is evident from the flow-duration-frequency curves in Figure 149 and Figure 150 for the Salmon River at Whitebird and the Clearwater River at Orofino for WY 2009, 2010 and 2011. The curves show low, medium and high seasonal flow duration patterns compared to the long-term curves for these sites.

Total suspended sediment loads and suspended sand loads for the tributary basins for water years 2009 through 2011 are summarized in Table 72 and Table 73. Relative proportions and ranking of the tributary suspended sediment and suspended sand loads are listed in Table 74. Proportional suspended sediment loads and suspended sand loads are arranged schematically in Figure 151 and Figure 152. The relative proportions Lower Granite Reservoir do not sum to 100 percent at Lower Granite because the tributary basins are nested and the estimates are based on individual regression equations. A sediment mass balance for the tributaries is estimated from this information below.

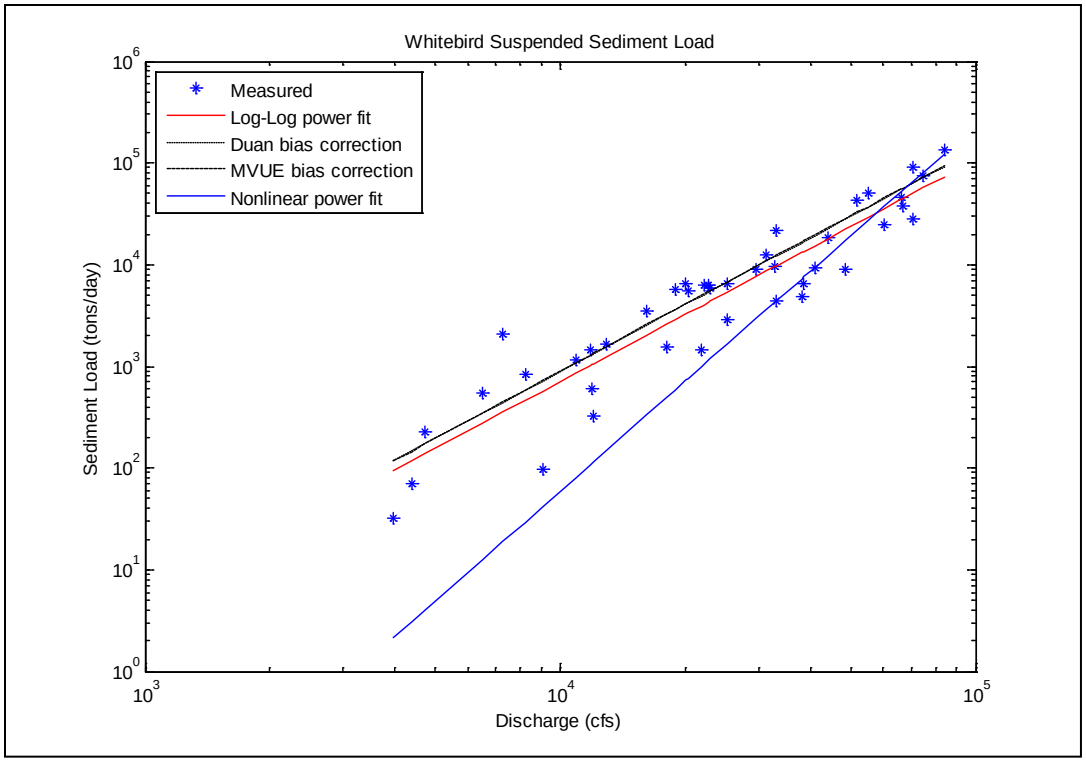


Figure 147. Regression fit of measured suspended sediment load for Salmon River.

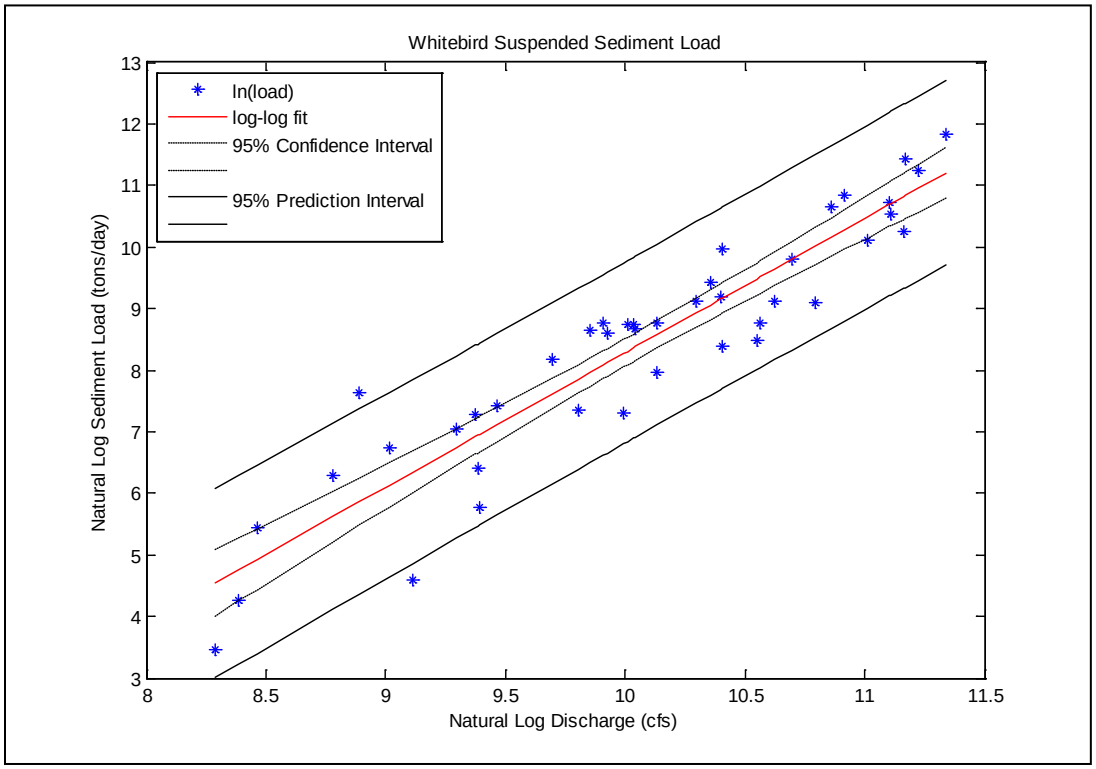


Figure 148. Prediction intervals and confidence intervals for the suspended sediment load measurements in the Salmon River.

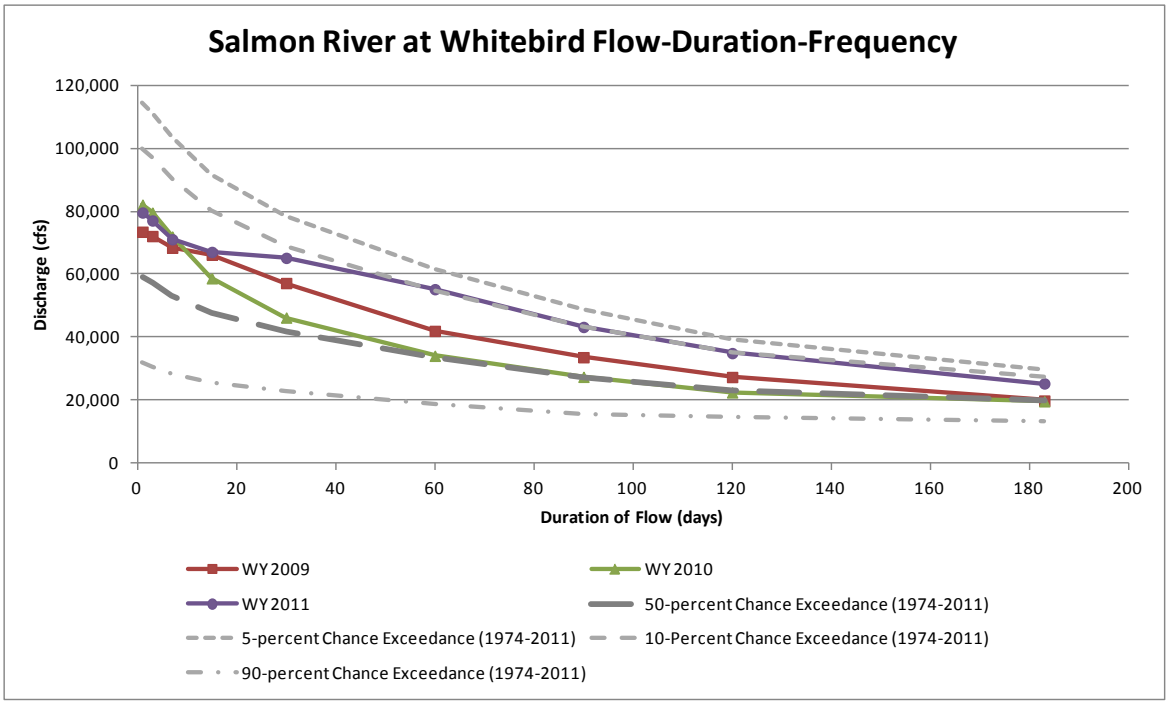


Figure 149. Flow-duration-frequency curves for Salmon River at Whitebird.

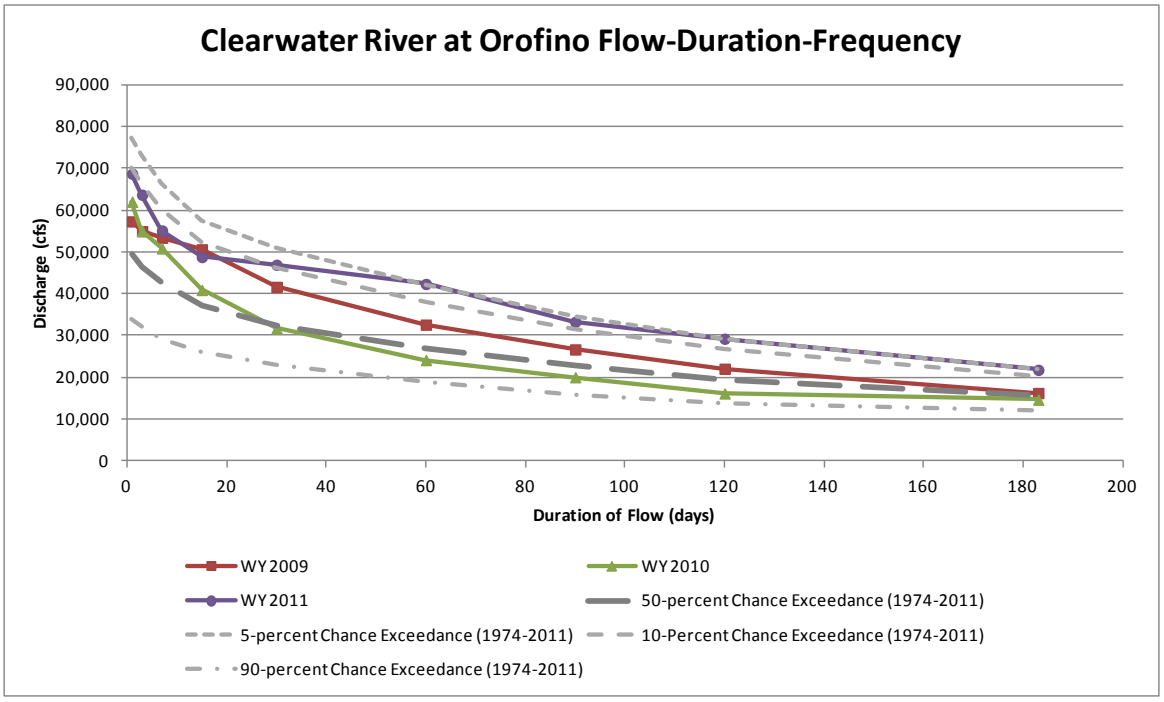


Figure 150. Flow-duration-frequency curves for Clearwater River at Orofino.

	Total Suspended Sediment Load Water Year 2009-2011					Bias Adjusted Power fit As Percent Lower Granite
Site	Discharge Volume maf	Unadjusted Power fit tons	Bias Adjusted Power fit tons	MVUE Adjusted Power fit tons	Nonlinear Power fit tons	
Selway River nr Lowell	8.73	257,565	359,154	381,618	433,876	3.6%
Lochsa River nr Lowell	6.19	108,676	132,258	136,537	134,014	1.3%
Total	14.91	366,241	491,412	518,154	567,890	
Clearwater River at Kooskia	14.91	339,094	432,626	446,879	430,827	4.3%
S.F. Clearwater at Harpster	2.50	125,936	152,876	151,886	148,170	1.5%
S.F. Clearwater at Stites	2.50	132,487	169,738	167,759	138,498	1.7%
Average	2.50	129,212	161,307	159,822	143,334	1.6%
Total	17.42	468,306	593,933	606,702	574,161	
Clearwater River at Orofino	20.89	632,876	932,406	920,221	1,119,883	9.2%
Potlatch River nr Spalding	1.10	178,885	285,316	294,166	543,152	2.8%
Total	21.99	811,761	1,217,722	1,214,386	1,663,036	
Clearwater River at Spalding	35.31	990,707	1,262,662	1,272,674	843,771	12.5%
Salmon River at Whitebird	27.22	4,311,763	5,406,912	5,468,692	4,039,680	53.5%
Grande Ronde River at mouth	7.35	427,543	589,980	571,459	378,008	5.8%
Total	34.58	4,739,306	5,996,892	6,040,151	4,417,688	
Snake River at Anatone	79.49	8,059,119	8,848,463	8,873,099	9,260,038	87.5%
Lower Granite total	114.79	9,049,826	10,111,125	10,145,773	10,103,809	100.0%

Table 72. Total suspended sediment load WY 2009-2011 Snake and Clearwater River tributaries.

	Suspended Sand Load Water Year 2009-2011					Bias
Site	Discharge Volume maf	Unadjusted Power fit tons	Bias Adjusted Power fit tons	MVUE Adjusted Power fit tons	Nonlinear Power fit tons	Adjusted Power fit Percent Lower Granite
Selway River nr Lowell	8.73	157,077.73	233,502.36	246,371.35	314,623.18	4.4%
Lochsa River nr Lowell	6.19	55,636.38	70,020.58	72,325.28	76,659.91	1.3%
Total	14.91	212,714	303,523	318,697	391,283	
Clearwater River at Kooskia	14.91	163,263	216,552	219,342	255,388	4.0%
S.F. Clearwater at Harpster	2.50	65,285	80,146	79,119	91,051	1.5%
S.F. Clearwater at Stites	2.50	53,636	69,412	67,724	78,569	1.3%
Average	2.50	59,461	74,779	73,422	84,810	1.4%
	17.42	222,724	291,331	292,763	340,197	
Clearwater River at Orofino	20.89	283,217	453,867	433,489	618,995	8.5%
Potlatch River nr Spalding	1.10	11,700	19,254	18,323	77,905	0.4%
Total	21.99	294,917	473,121	451,812	696,900	
Clearwater River at Spalding	35.31	384,963	510,067	518,453	340,860	9.5%
Salmon River at Whitebird	27.22	2,749,688	3,491,306	3,549,937	2,558,606	65.2%
Grande Ronde River at mouth	7.35	68,475	118,012	109,115	101,426	2.2%
Total	34.58	2,818,162	3,609,318	3,659,052	2,660,033	
Snake River at Anatone	79.49	4,440,921	4,846,599	4,855,906	4,497,167	90.5%
Lower Granite total	114.79	4,825,884	5,356,666	5,374,360	4,838,027	100.0%

Table 73. Total suspended sand load WY 2009-2010 Snake and Clearwater River tributaries.

Relative Contribution of Sediment Load by Tributary Basins WY 2009 - 2011				
	Percent of Total at Lower Granite		Suspended	Suspended
Site	Suspended Sediment	Suspended Sand	Sediment Rank	Sand Rank
Snake River at Anatone	87.5%	90.5%	1	1
Salmon River at Whitebird	53.5%	65.2%	2	2
Clearwater River at Spalding	12.5%	9.5%	3	3
Clearwater River at Orofino	9.2%	8.5%	4	4
Grande Ronde River at mouth	5.8%	2.2%	5	7
Clearwater River at Kooskia	4.3%	4.0%	6	6
Selway River nr Lowell	3.6%	4.4%	7	5
Potlatch River nr Spalding	2.8%	0.4%	8	11
S.F. Clearwater at Stites	1.7%	1.3%	9	10
S.F. Clearwater at Harpster	1.5%	1.5%	10	8
Lochsa River nr Lowell	1.3%	1.3%	11	9
Lower Granite total	100.0%	100.0%		

Table 74. Relative contributions of tributaries to total Load at Lower Granite Reservoir.

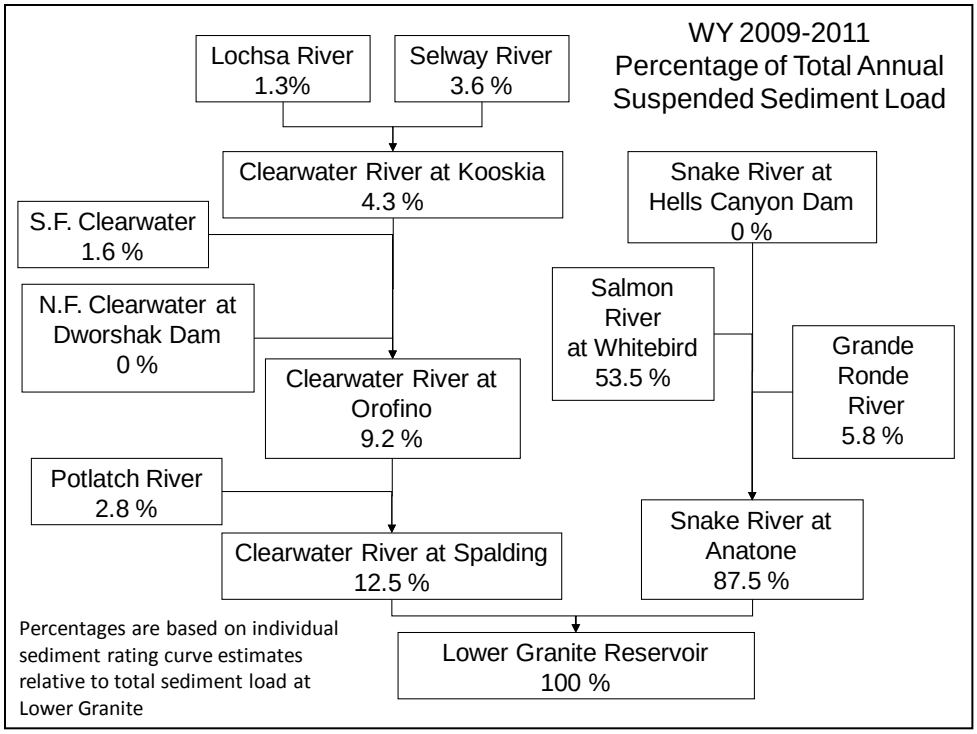


Figure 151. Relative suspended sediment loads of the Lower Granite sediment yield watershed.

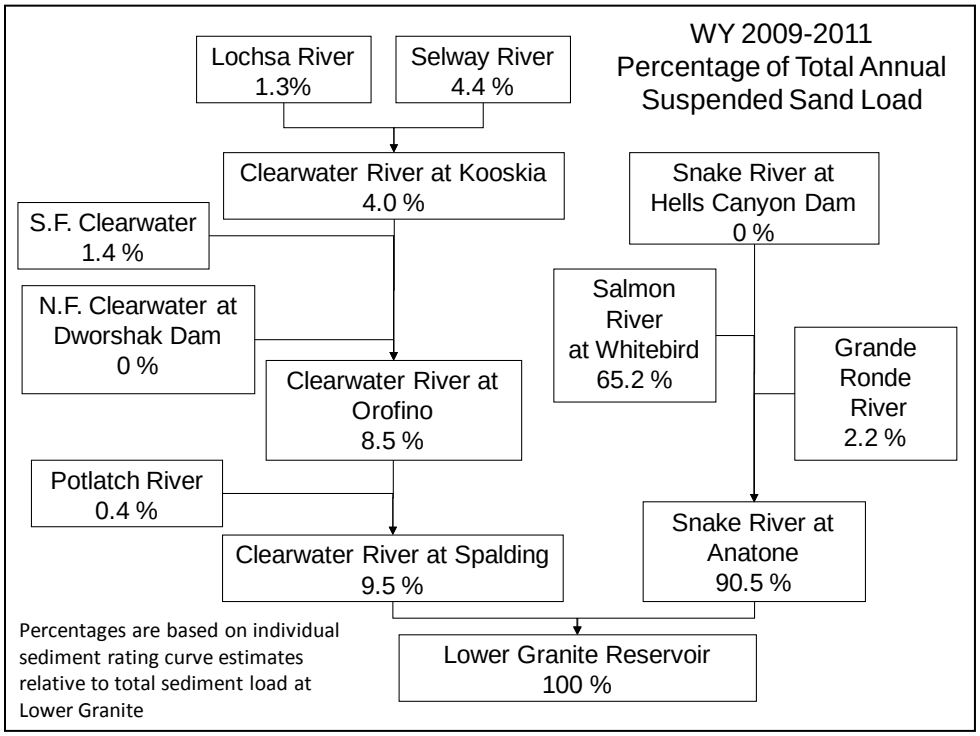


Figure 152. Relative suspended sand loads of the Lower Granite sediment yield watershed.

9.16.2. Salmon River and Lower Snake River Sediment Loads

The Salmon River basin contributes the largest proportion of sediment load to Lower Granite, both as total suspended sediment and suspended sand. For the period WY 2009 – 2011, the computed total suspended sediment load in the Salmon River at Whitebird was 53.5 percent of the total load at Lower Granite while the Snake River at Anatone is 87.5 percent of the total. During this period the sediment load in the Grande Ronde River was a relatively minor proportion of the total load (5.8 percent), so it appears that 28 percent of the sediment load in the Snake River was supplied by the Hells Canyon reach of the Snake River and other tributaries in the lower Snake River basin upstream from Anatone. Statistical imprecision of the regression equations, timing and magnitude of the discharges of the tributaries and the Snake River affect the relative proportions.

The proportional loads of the tributary basins listed in Table 75 vary each water year. It is notable that the computed suspended sand load of the Salmon River in WY 2009 was 107 percent of the suspended sand load at Lower Granite while the suspended sediment load in the Salmon River accounted for 88 percent of the suspended sediment load in the Snake River at Anatone. The discharge hydrographs in Figure 153 show that the discharge of the Salmon River was a greater proportion of the total discharge of the Snake River in WY 2009 and therefore transported more sediment than normal into the Snake River above Anatone. In contrast, the proportional load from the Salmon River is much reduced in WY 2011 when higher discharges were released from the Hells Canyon Reach early in the year while flows in the Salmon River were low. These relationships are seen in the comparison of the measured suspended load data for Snake, Salmon and Grande Ronde Rivers in Figure 154 and Figure 155. Maximum measured daily suspended sand loads of the Salmon River at Whitebird equaled or exceeded the maximum measured suspended sand loads at Anatone in all three years.

Preliminary sediment transport modeling with approximate channel geometries suggests that not all the suspended sediment that passes the Salmon River at Whitebird is transported past the Anatone gage in a single season. Sediment loads measured at Anatone are higher in subsequent years because of the transient sediment temporarily stored in the 70 miles of river channel between Whitebird and Anatone. In many years, the computed suspended sediment load of the Salmon River exceeds the computed suspended load of the Snake River. Figure 156 is a plot of the difference between computed suspended sediment loads at Anatone and Whitebird from 1974 to 2011. It shows that sediment loads in the Salmon River should regularly exceed sediment loads in the Snake River when discharge in the Snake River is relatively low. When sediment load is computed for many water years so that differences between water years are averaged, the suspended sediment load in the Salmon River is about

71 percent of the total load in the Snake River at Anatone. Similarly, over many years the computed suspended sediment load in the Grande Ronde River is about 8 percent of the total suspended sediment load at Anatone. The remaining proportion, about 21 percent, of the suspended sediment load at Anatone is a measure of the statistical uncertainty of the regression relationships or from other sediment sources in the Lower Snake River.

Since the regression equations were developed from recent data, the relative proportions of the lower Snake River tributaries may be affected by land disturbance caused by recent fires in Hells Canyon which could increase the amount of sediment delivered to this reach. Other sources may include the net erosion and downstream transport of material from sandbars in the Snake River below Hells Canyon Dam. A recent study by Idaho Power Company found that this is not a likely dominant long-term source of sediment[112]. This study also found that Brownlee Reservoir traps virtually all sediment larger than fine sand (0.25 mm). Additional investigation of sediment yield and transport in the Snake River above Anatone should be performed in future studies for the PSMP.

Relative Contribution of Sediment Load by Tributary Basins WY 2009-2011								
	WY 2009		WY 2010		WY 2011		WY 2009-2011	
Site	Suspended Sediment	Suspended Sand	Suspended Sediment	Suspended Sand	Suspended Sediment	Suspended Sand	Suspended Sediment	Suspended Sand
Salmon River at Whitebird	73.4%	107.2%	60.9%	68.8%	43.5%	51.7%	53.5%	65.2%
Grande Ronde River at mouth	9.4%	4.3%	6.2%	2.4%	4.4%	1.5%	5.8%	2.2%
Snake River at Anatone	83.4%	85.5%	89.5%	93.0%	88.4%	91.2%	87.5%	90.5%
Lochsa River nr Lowell	1.8%	2.2%	1.2%	1.2%	1.1%	1.1%	1.3%	1.3%
Selway River nr Lowell	5.6%	8.5%	3.5%	4.1%	2.8%	3.2%	3.6%	4.4%
Clearwater River at Kooskia	6.4%	7.4%	4.2%	3.7%	3.5%	3.2%	4.3%	4.0%
S.F. Clearwater at Harpster	2.1%	2.4%	1.1%	1.0%	1.4%	1.4%	1.5%	1.5%
S.F. Clearwater at Stites	2.3%	2.1%	1.2%	0.8%	1.6%	1.2%	1.7%	1.3%
Clearwater River at Orofino	12.8%	14.0%	8.8%	7.5%	8.0%	7.1%	9.2%	8.5%
Potlatch River nr Spalding	3.3%	0.5%	0.2%	0.0%	3.5%	0.4%	2.8%	0.4%
Clearwater River at Spalding	16.6%	14.5%	10.5%	7.0%	11.6%	8.8%	12.5%	9.5%
Lower Granite Reservoir total	100.0%	100.0%	100.0%	100.0%	100.0%	100.0%	100.0%	100.0%

Table 75. Relative contribution of tributary basins WY 2009, 2010 and 2011.

[112] Parkinson, S, Anderson, K., Conner, J. and Milligan, J. (2003). Sediment Transport, Supply and Stability in the Hells Canyon Reach of the Snake River, Technical Report Appendix E.1-1, Hells Canyon Complex, FERC No. 1971, Idaho Power Company, Boise, ID.

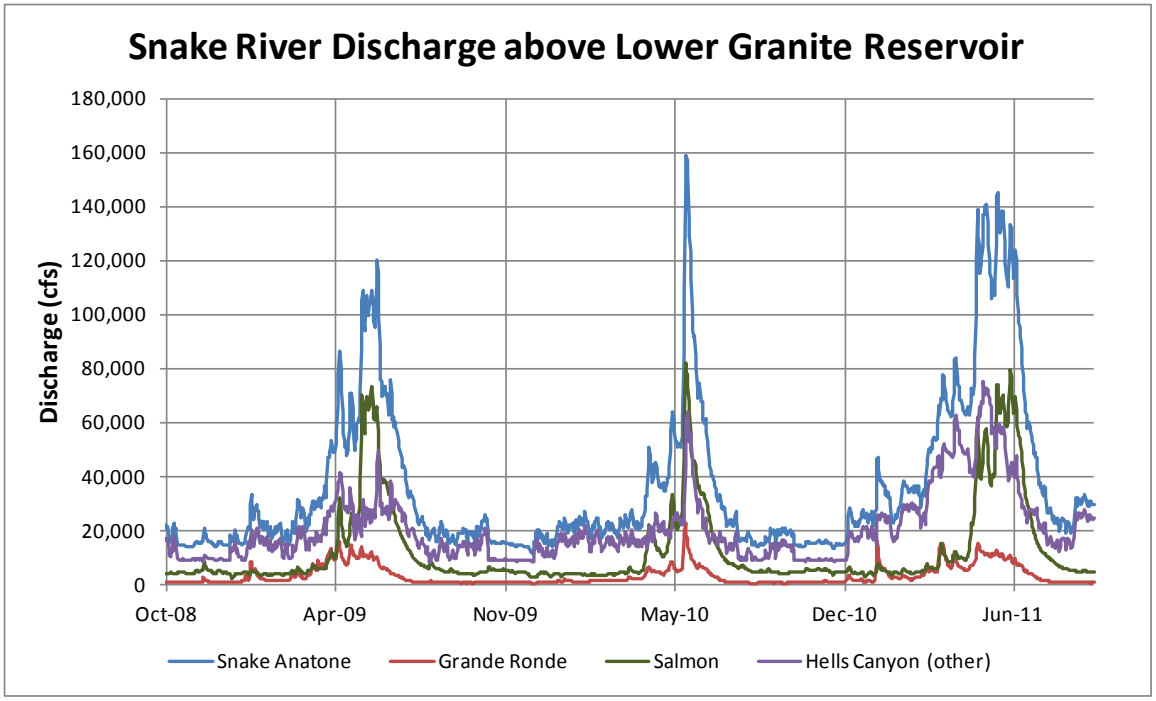


Figure 153. Discharge of Snake River above Lower Granite Reservoir WY 2009-2011.

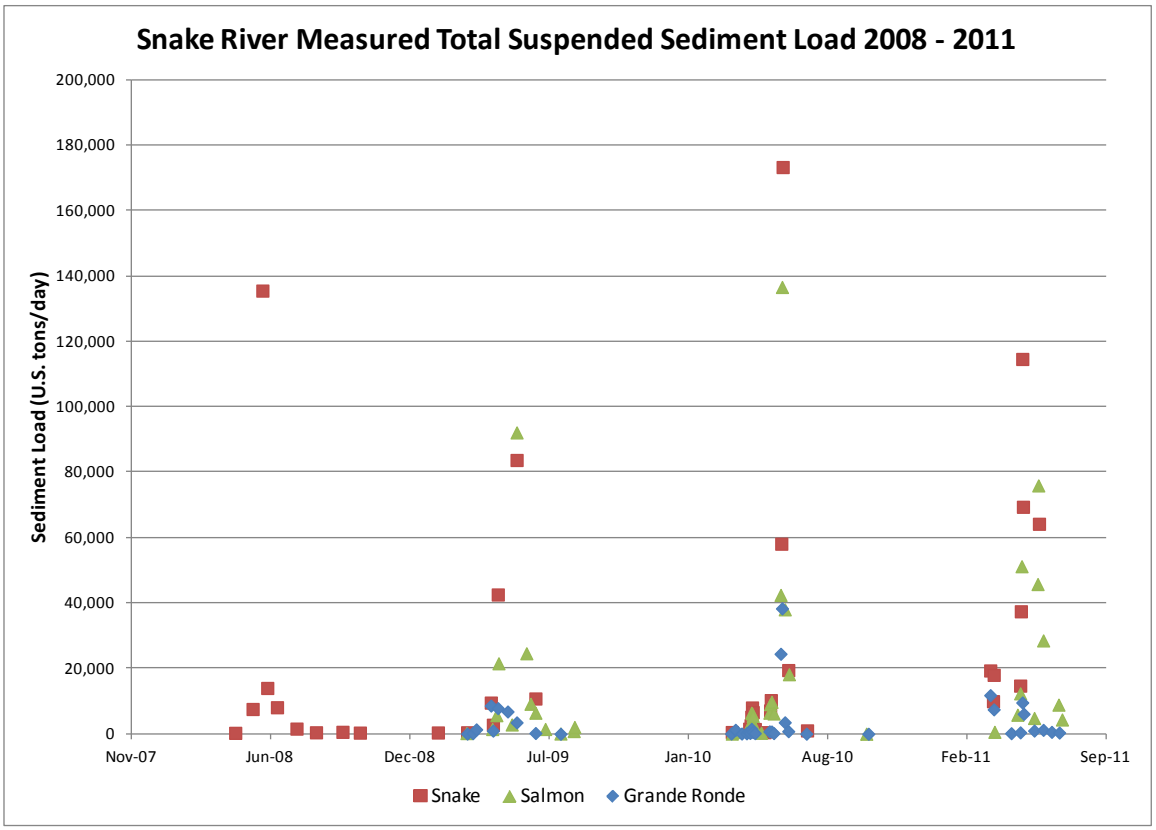


Figure 154. Comparison of measured suspended sediment loads on the Snake River 2008-2011.

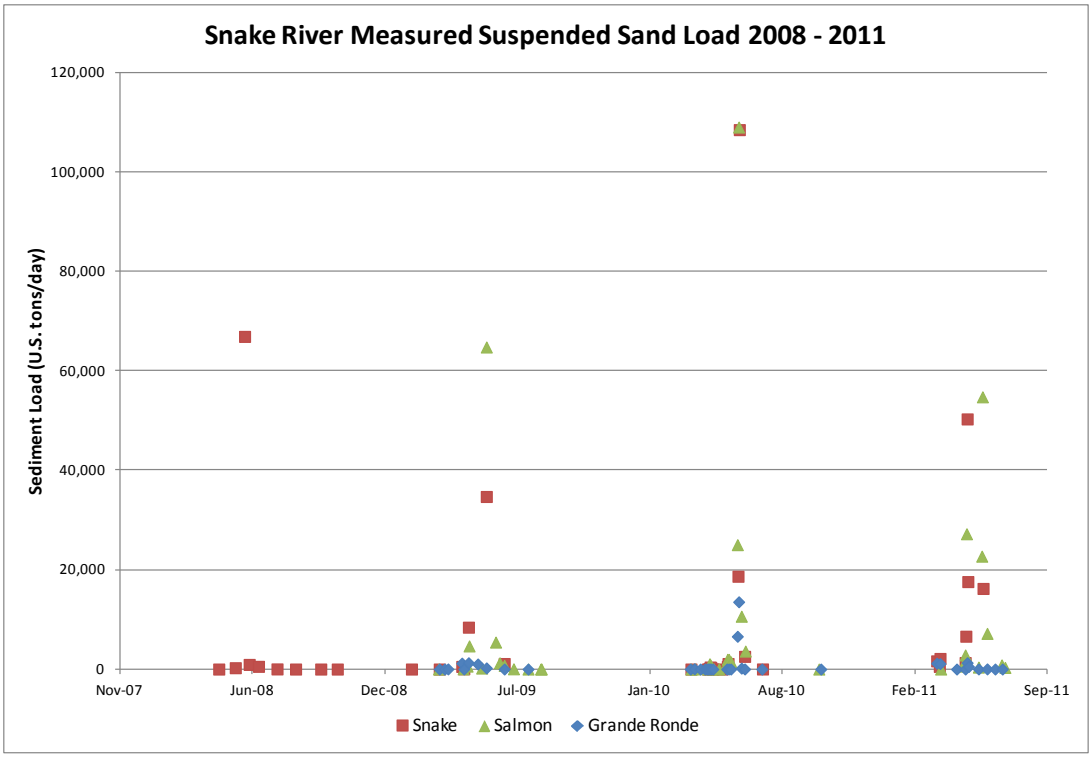


Figure 155. Comparison of measured suspended sand loads on the Snake River 2008-2011.

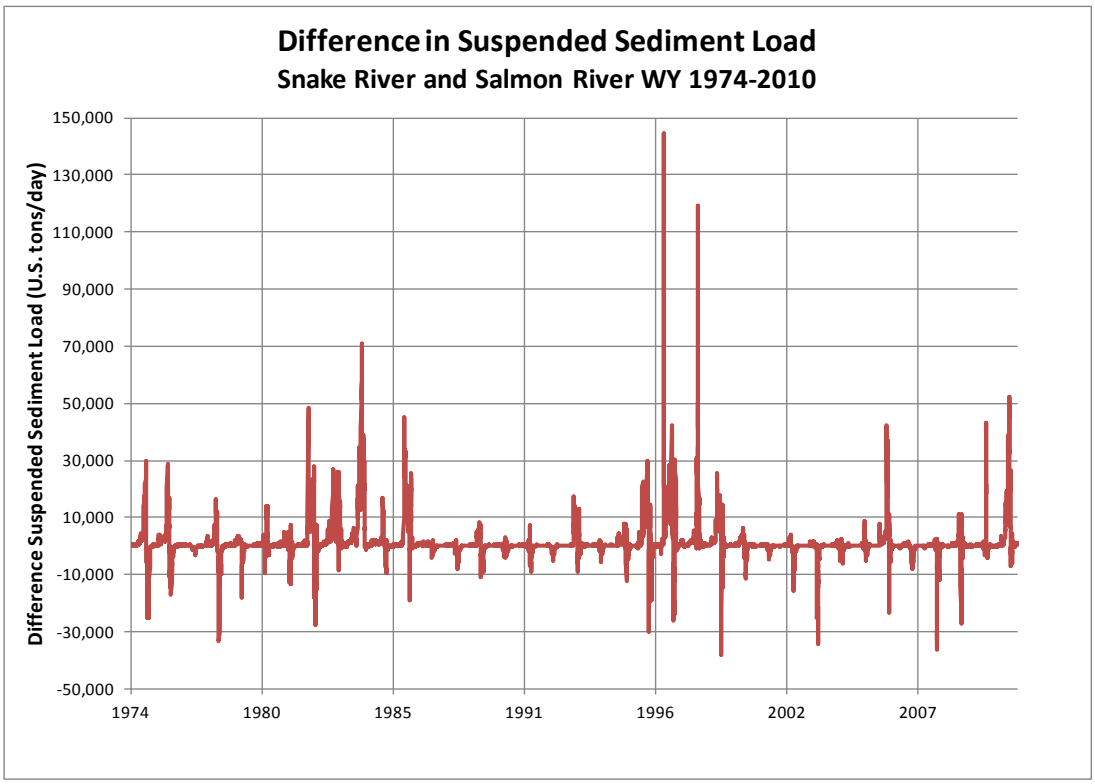


Figure 156. Difference in computed suspended sediment loads of the Salmon River and Snake River, WY 1974-2011.

9.16.3. Clearwater River Sediment Loads

The regression analysis of measured sediment load showed that the Clearwater River basin contributed 12.5 percent of the total computed suspended load at Lower Granite Reservoir during WY 2009, 2010 and 2011 (Figure 151 and Table 72). The Selway River basin was the largest contributor of suspended sediment at 3.6 percent of the total at Lower Granite. Proportional loads mostly increase downstream, indicating that transient storage of sediment is less than in the Clearwater River than in the Snake River. The sum of the proportional loads for the Lochsa River and Selway River is slightly higher than the computed load at Kooskia (0.6 percent) which indicates some transient storage in the Clearwater River above Kooskia. This relationship is seen in the measured suspended sediment loads in Figure 157 and Figure 158. The measured maximum daily suspended sediment loads in the Selway exceeds those at Kooskia in 2009. The measured maximum daily suspended sand loads in the Selway exceeds those at Kooskia in all three years.

The difference between the proportional load in the Clearwater River at Orofino and the sum of the proportional loads for S.F of Clearwater River and at Kooskia indicate that about 3 percent of the suspended sediment load is supplied by other subbasins in the middle Clearwater River. The comparison of the measured suspended sediment loads for the middle Clearwater River in Figure 159 show that the suspended sediment loads at Orofino exceeded those at Kooskia except in 2010 when the maximum measured daily loads were nearly equal.

Below Orofino, the computed proportional load of the Potlatch River for the period 2009-2011 was 2.8 percent. The relatively large computed proportional load for this basin was influenced by high suspended sediment loads measured during a substantial low elevation runoff event in January 2011 during which the measured maximum daily suspended sediment load was 152,000 tons per day (Figure 160). Winter runoff events are not uncommon in the lower Clearwater River basin, but the duration of the events are relatively short so that the total loads from these basins do not comprise a large percentage of the total sediment load at Lower Granite. The proportional load at Spalding is 0.5 percent greater than the sum of the proportional loads for the Potlatch River and Orofino which indicates that the other subbasins of the Lower Clearwater contributed small amounts of sediment during this period.

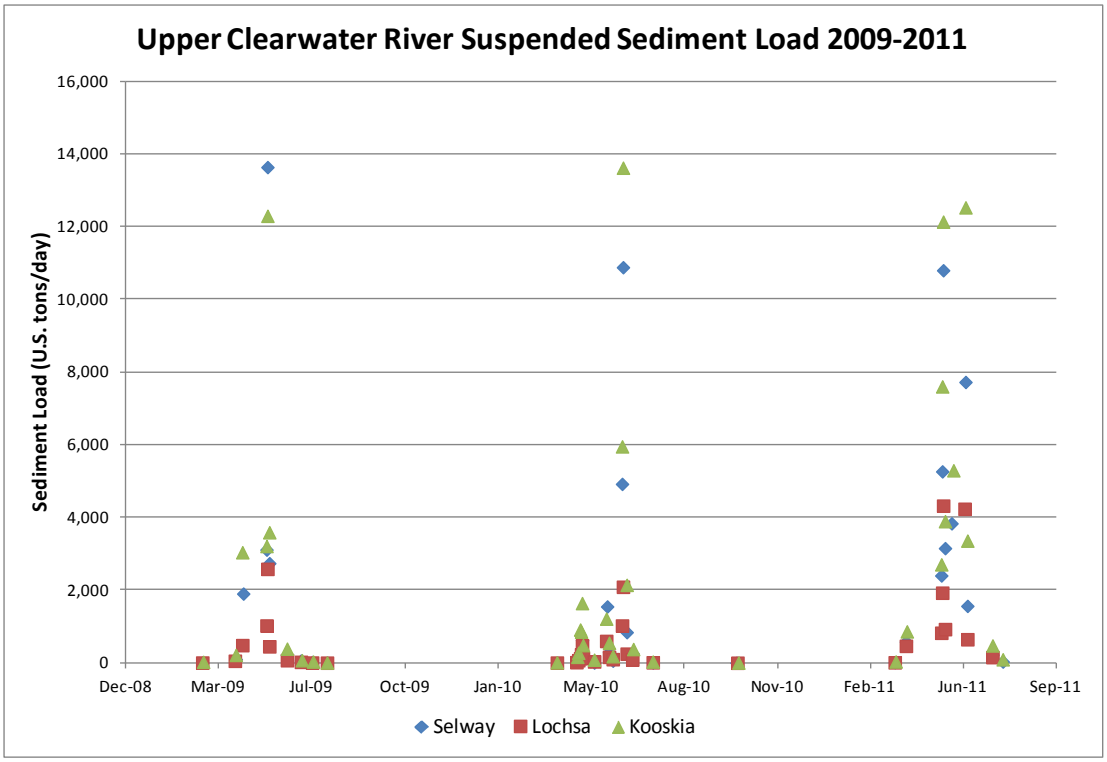


Figure 157. Comparison of measured suspended sediment loads on the upper Clearwater River 2009-2011.

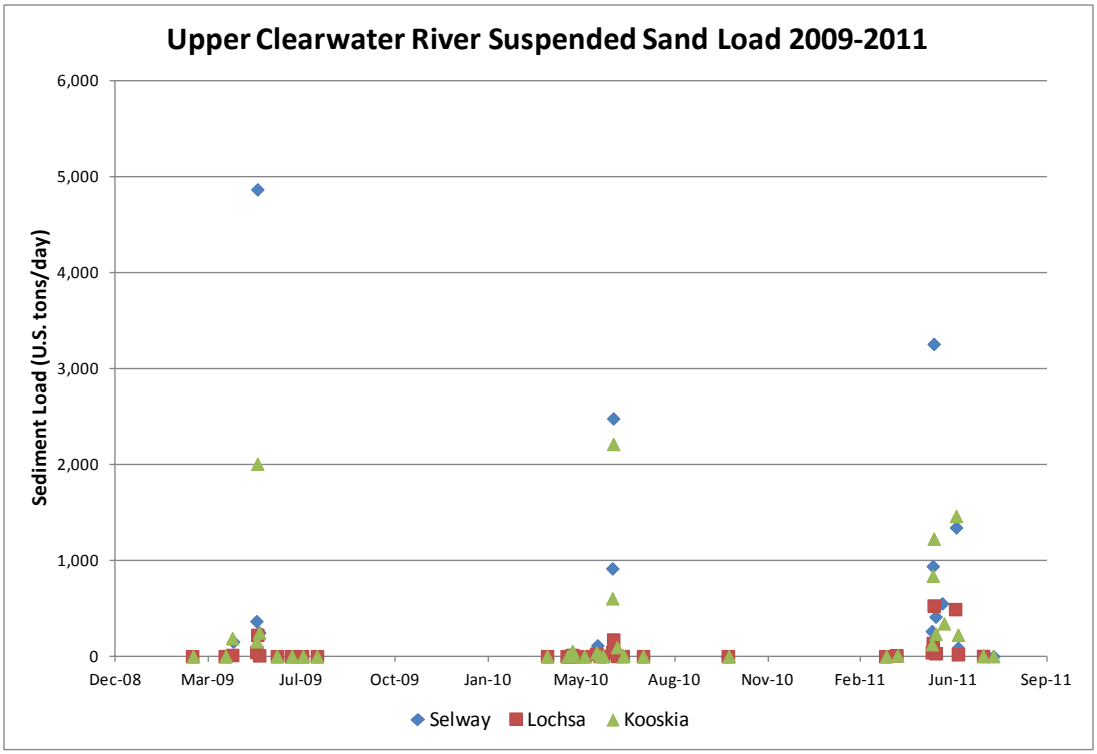


Figure 158. Comparison of measured suspended sand loads on the upper Clearwater River 2009-2011.

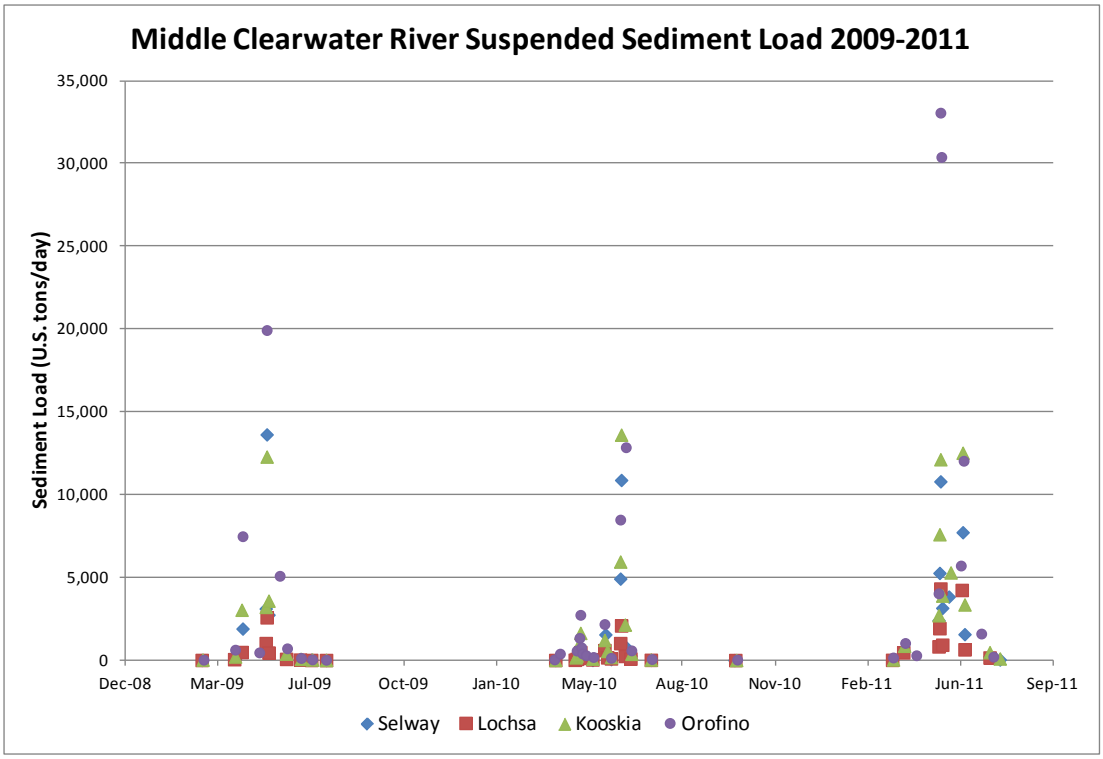


Figure 159. Comparison of measured suspended sediment loads on the middle Clearwater River 2009-2011.

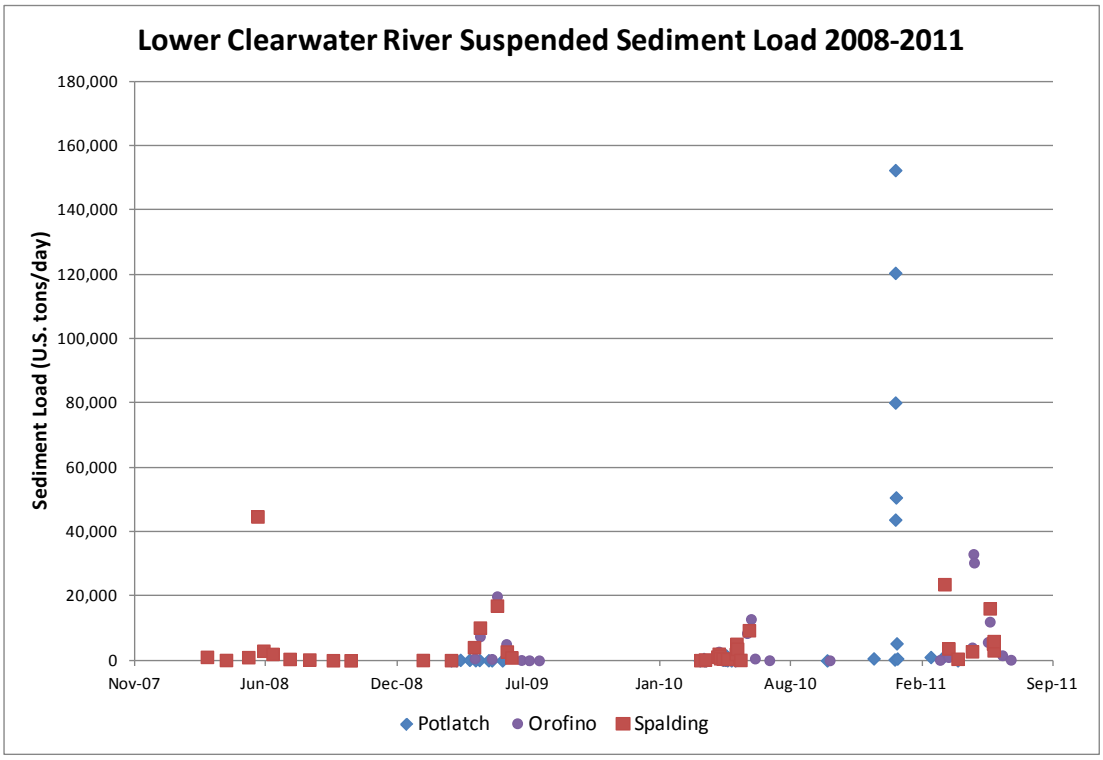


Figure 160. Comparison of measured suspended sediment loads on the lower Clearwater River 2008-2011.

9.16.4. Mass Balance of the Tributary basin Sediment Loads

A sediment mass balance for Lower Granite Reservoir was derived with the regression relationships for tributary basins. The basins are nested so sediment loads for subbasins that were not directly measured are estimated by the difference between aggregate and subordinate basins. The mass balance for the period 2009-2011is summarized in Table 76. As discussed above, the negative yield of the unmeasured subbasins in the middle Clearwater Basin, which amounts to 0.6 percent of the total load at Lower Granite, is likely a result of statistical precision of the regression equations, transient sediment storage and contributions from unmeasured tributaries. Sediment yields (specific yields) of the tributary basins varied from 0.03 to 0.7 U.S. tons per acre per year. The average sediment yield of the Potlatch River basin was 0.25 tons/ac/yr, which is close to the 0.22 ton/ac/yr determined by aerial assessment of ephemeral gully erosion in the Potlatch River basin[113,114].

Total Suspended Sediment Mass Balance Water Years 2009-2011							
Source Watershed	Suspended Sediment tons	Watershed Area mi2	Sediment Yield ton/mi^2/yr	Sediment Yield ton/ac/yr	Percent of Spalding	Percent of Anatone	Percent of Lower Granite
Selway River	359,154	1,916	62.5	0.10	28.4%		3.6%
Lochsa River	132,258	1,178	37.4	0.06	10.5%		1.3%
Lower Middle Fork (computed)[1]	-58,786	313	-62.6	-0.10	-4.7%		-0.6%
S.F. Clearwater above Harpster	152,876	878	58.0	0.09	12.1%		1.5%
Lower S.F. Clearwater (computed)[2]	16,862	291	19.3	0.03	1.3%		0.2%
Above Orofino (computed)[3]	330,043	931	118.1	0.18	26.1%		3.3%
Potlatch River	285,316	594	160.2	0.25	22.6%		2.8%
Lower Clearwater (computed)[4]	44,940	738	20.3	0.03	3.6%		0.4%
Total at Spalding	1,262,662	6,839	61.5	0.10	100.0%		12.5%
Salmon River at Whitebird	5,406,912	13,424	134.3	0.21		61.1%	53.5%
Grande Ronde River at mouth	589,980	4,101	48.0	0.07		6.7%	5.8%
Lower Snake River (computed)[5]	2,851,571	2,108	451.0	0.70		32.2%	28.2%
Total at Anatone	8,848,463	19,633	150.2	0.23		100.0%	87.5%
Total at Lower Granite	10,111,125	27,137	124.2	0.19			100.0%

[1] Kooskia - (Selway + Lochsa)
[2] Stites - Harpster
[3] Orofino - (Kooskia + Stites)
[4] Spalding - (Orofino + Potlatch)
[5] Anatone - (Whitebird + Grande Ronde)
[6] Anatone + Spalding

Table 76. Mass balance and watershed sediment yield for Lower Granite Reservoir WY 2009-2011.

[113] Teasdale, G.N. (2005) *Satellite and Aerial Imaging in Characterization, Hydrologic Analysis and Modeling of Inland Watersheds and Streams*, Ph.D. thesis, Department of Civil and Environmental Engineering, Washington State University, Pullman, WA.

[114] Teasdale, G.N. and Barber, M.E. (2008). "Aerial assessment of ephemeral gully erosion from agricultural regions of the Pacific Northwest", *Journal of Irrigation and Drainage Engineering*, 134(6), 807-814.

9.16.5. Trends in Sediment Load in the Tributary Basins

The U.S. Forest Service (USFS) measured suspended sediment load in the Salmon River and Clearwater River basins during the 1990's[115]. While sampling methods used by the USFS likely varied from USGS protocols, the methodology should be sufficiently similar so that past and present suspended sediment concentrations may be compared to reveal possible trends in sediment yield of the basins.

In May and June 1997, the USFS measured suspended sediment in the Salmon River near Shoup, ID. The measurement site at Shoup is 145 miles upstream of Whitebird. Suspended sediment in the Salmon River was measured periodically by USGS at Whitebird from 1974 through 2008 with a gap in data collection between 1994 and 2000. The sand fraction was determined for many of the samples. This data is available through the National Water Information System (NWIS)[116]. The sampling method is uncertain. Reduced variability in the early data suggests that data collection methods were different than for the current study. The historic suspended sediment load measurements are plotted with the 2009 through 2011 data in Figure 161. Power relationships were fit to the measured suspended sediment loads for both periods. The power relationship for 2009-2011 at Whitebird plots above the power relationship for the 1974-2008 data. A power relationship for the 1997 data at Shoup plots well above the relationships for Whitebird, which is expected because the tributary watershed area at Shoup is smaller than at Whitebird and the discharge in May and June 1997 was extraordinarily high in the Salmon River.

A Mann-Whitney-Wilcoxon step-trend test was performed with the Salmon River suspended sediment and suspended sand concentration residuals using procedures that are similar to the trend analysis for the Snake River at Antone suspended sediment. Regression residuals for suspended sediment and suspended sand are plotted in Figure 162 and Figure 163. Results of the step-trend tests in Table 77 indicate a weak trend of increasing suspended sand load at a significance level of 0.05.

[115] King, J.G., Emmett, W.W., Whiting, P.J., Kenworthy, J.J., and Barry, J.J. (2004). Sediment Transport Data and Related Information for Selected Coarse-bed Streams and Rivers in Idaho, General Technical Report RMRS GTR-131, Rocky Mountain Research Station, U.S. Forest Service, Fort Collins, CO. 26 p.

[116] http://nwis.waterdata.usgs.gov/nwis

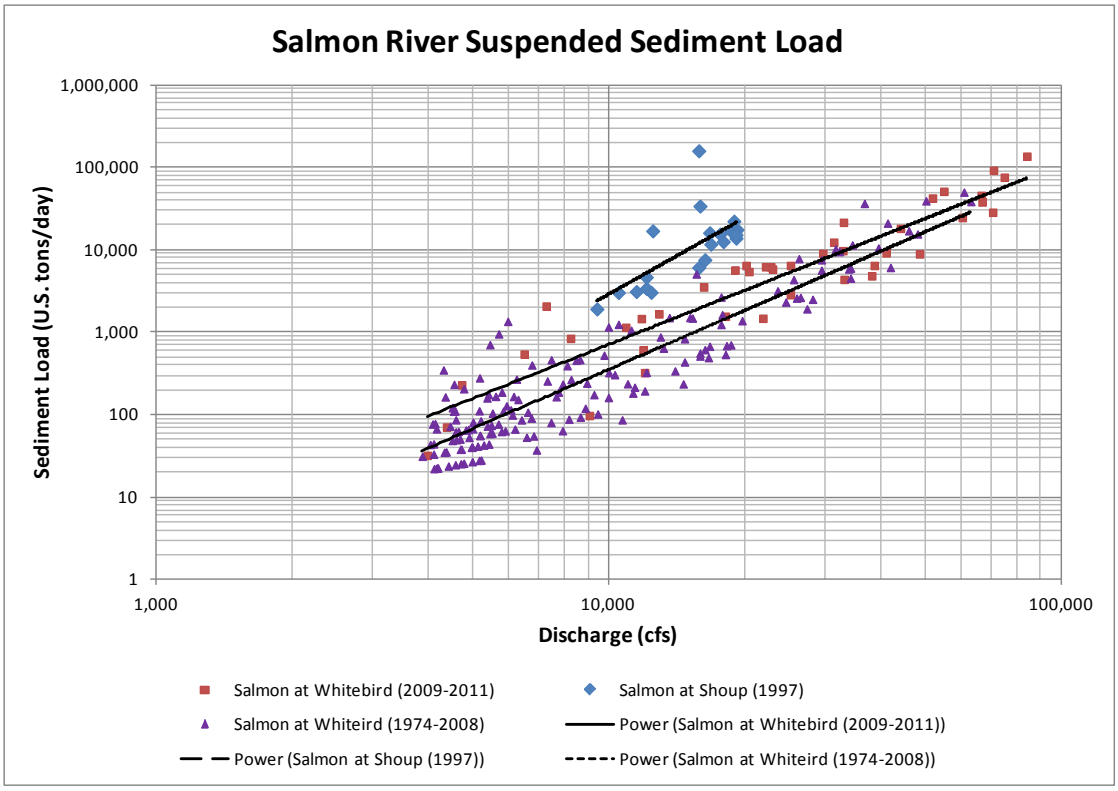


Figure 161. Comparison of suspended sediment loads in the Salmon River.

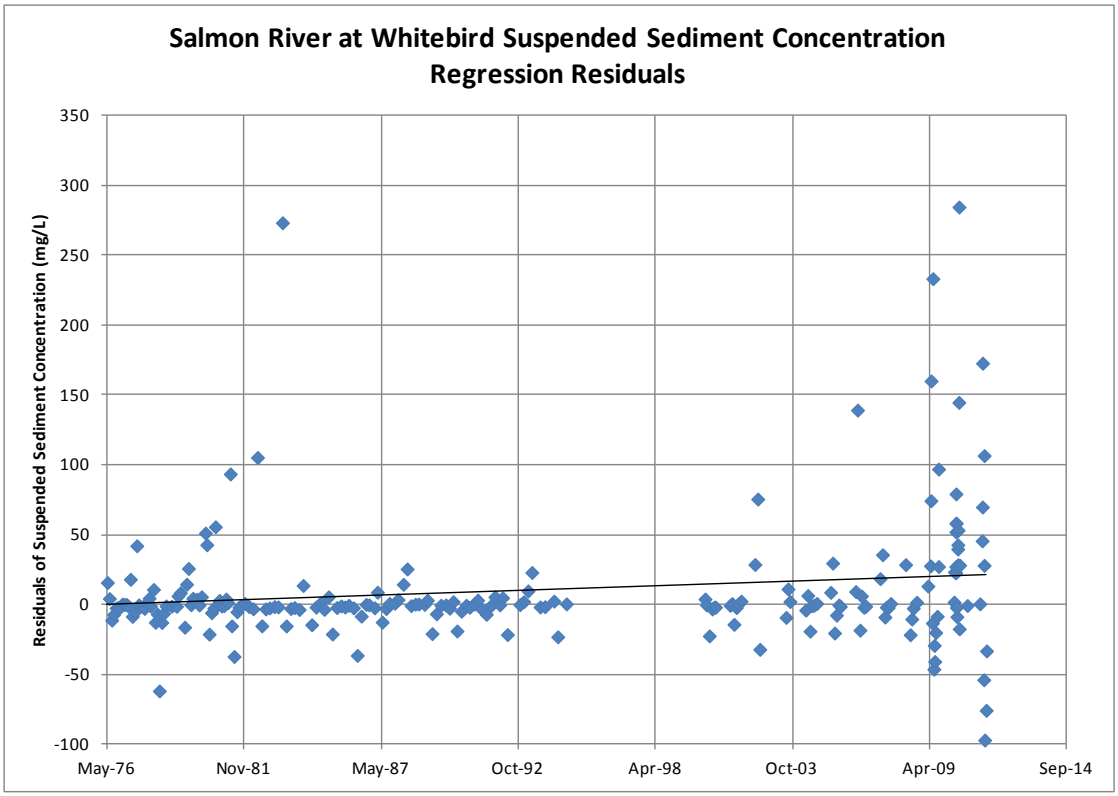


Figure 162. Regression residuals for suspended sediment concentration for the Salmon River at Whitebird.

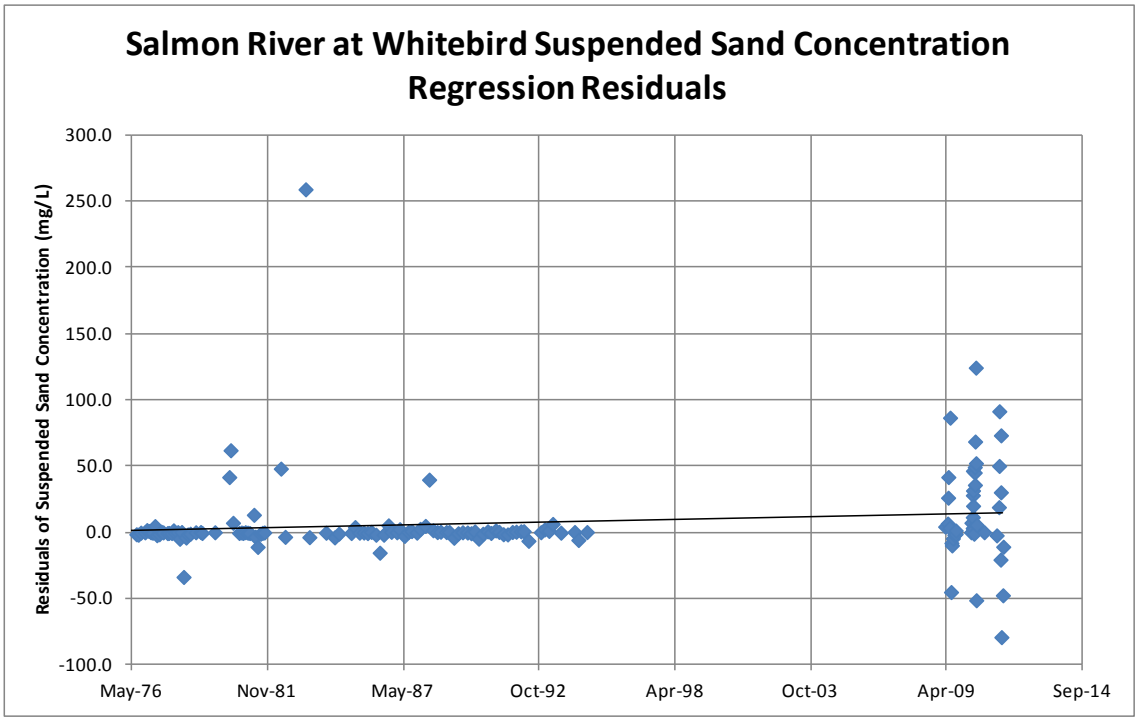


Figure 163. Regression residuals for suspended sand concentration for the Salmon River at Whitebird.

Mann-Whitney-Wilcoxon Test for Step Trend Salmon River at Whitebird Suspended Sediment Measurements 1974-2008 and 2008-2011					
			95 percent Confidence Interval		
			Low	High	Median
Data	W	P-value	mg/L	mg/L	mg/L
Suspended sediment concentration	5608	0.055	0	9	3
Suspended sand concentration	1747	0.0032	2	19	6

Table 77. Mann-Whitney-Wilcoxon test for step-trend for suspended sediment in the Salmon River at Whitebird.

The USFS measured suspended sediment loads on the Selway River near Lowell in 1994, 1995 and 1997, and on the Lochsa River near Lowell in 1994 and 1995. Sediment loads in the Selway River measured by USGS from 2009 to 2011plot somewhat above the USFS data in Figure 164. Regression residuals of suspended sediment concentration for the Selway River are plotted in Figure 165 and the results of the Mann-Whitney-Wilcoxon test for step-trend are summarized in Table 78. Only the measurements from 2009-2011 within the range of discharges in the 1994-1997 data were plotted and used in the step-trend analysis. The step-trend test for suspended sediment was significant at the 0.05 level and indicated a small increase in sediment

load. The step-trend for suspended sand was not significant at the 0.05 level. There is no apparent trend in measured sediment loads for the Lochsa River in Figure 166.

The analysis of the step-trend in the Salmon River and Selway River sediment load is based on relatively few years of samples, so is not a rigorous confirmation of an increasing trend in sediment yield. However, the apparent increasing trends in these headwater basins have important implications for future sediment delivery at Lower Granite Reservoir. The apparent increasing trend of sediment load in the Salmon River at Whitebird substantiates the apparent trend at Anatone on the Snake River. Though the data are few, the appropriate engineering judgment is that the data do not show a decreasing trend in sediment load and more likely indicate that sediment yields in these large headwater basins are increasing.

Sediment yield may increase because of land disturbance caused by recent fire, landslides and climate variability. The effect of fire and landslides on sediment yield in forestland is characterized in other studies of the EIS. The potential impact of climate variability on sediment yield in the lower Snake and Clearwater basins is examined in Section 18.

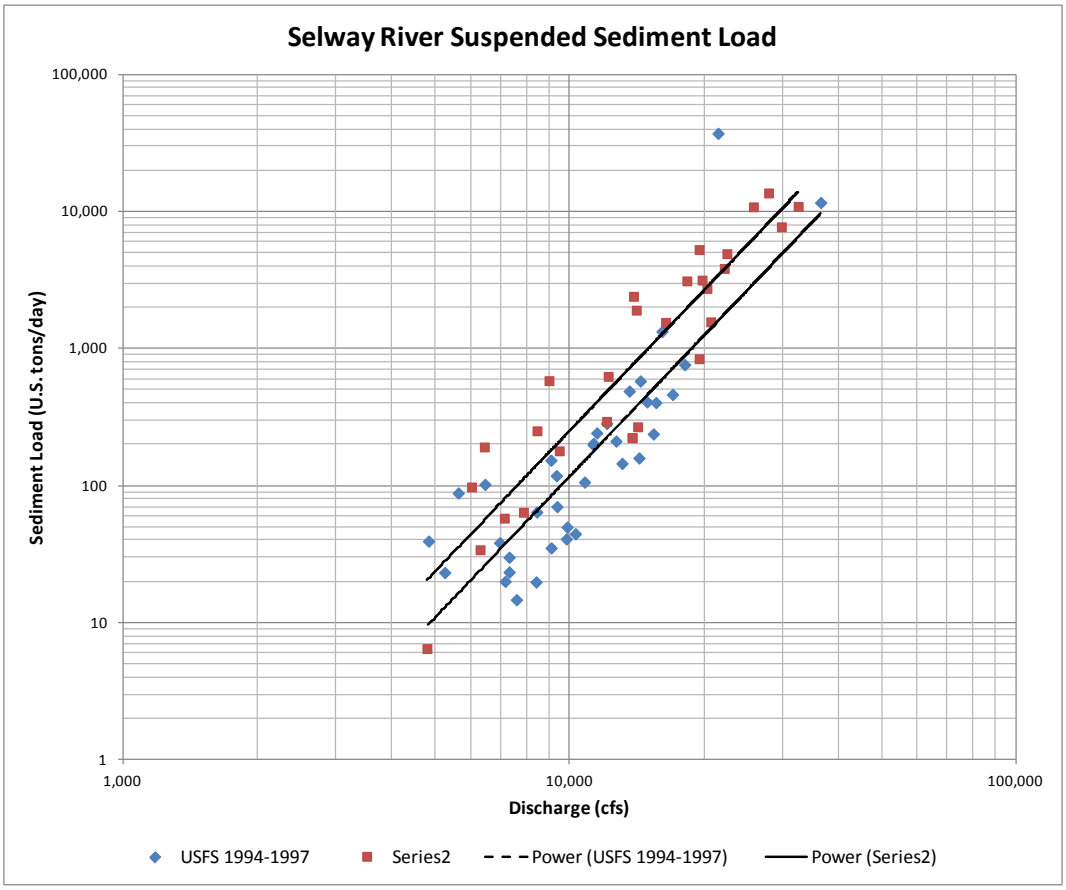


Figure 164. Comparison of suspended sediment load in the Selway River.

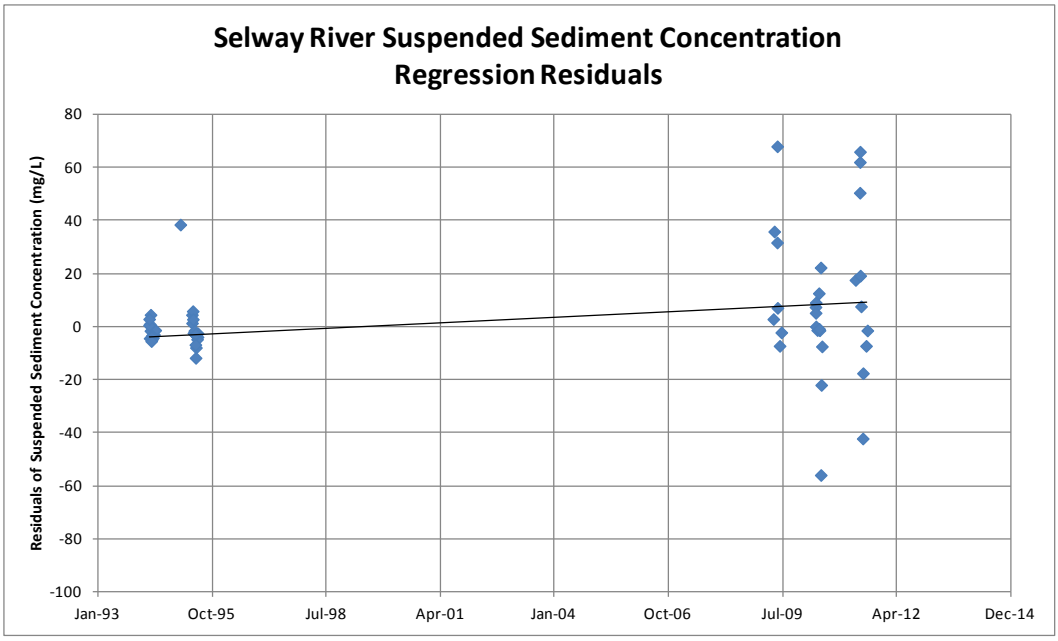


Figure 165. Regression residuals for suspended sediment concentration for the Selway River near Lowell.

Mann-Whitney-Wilcoxon Test for Step Trend Selway River Suspended Sediment Measurements 1994-1997 and 2008-2011					
			95 percent Confidence Interval		
			Low	High	Median
Data	W	P-value	mg/L	mg/L	mg/L
Suspended sediment concentration	312	0.0085	2	14	7
Suspended sand concentration	553	0.29			

Table 78. Mann-Whitney-Wilcoxon test for step-trend for suspended sediment in the Selway River near Lowell.

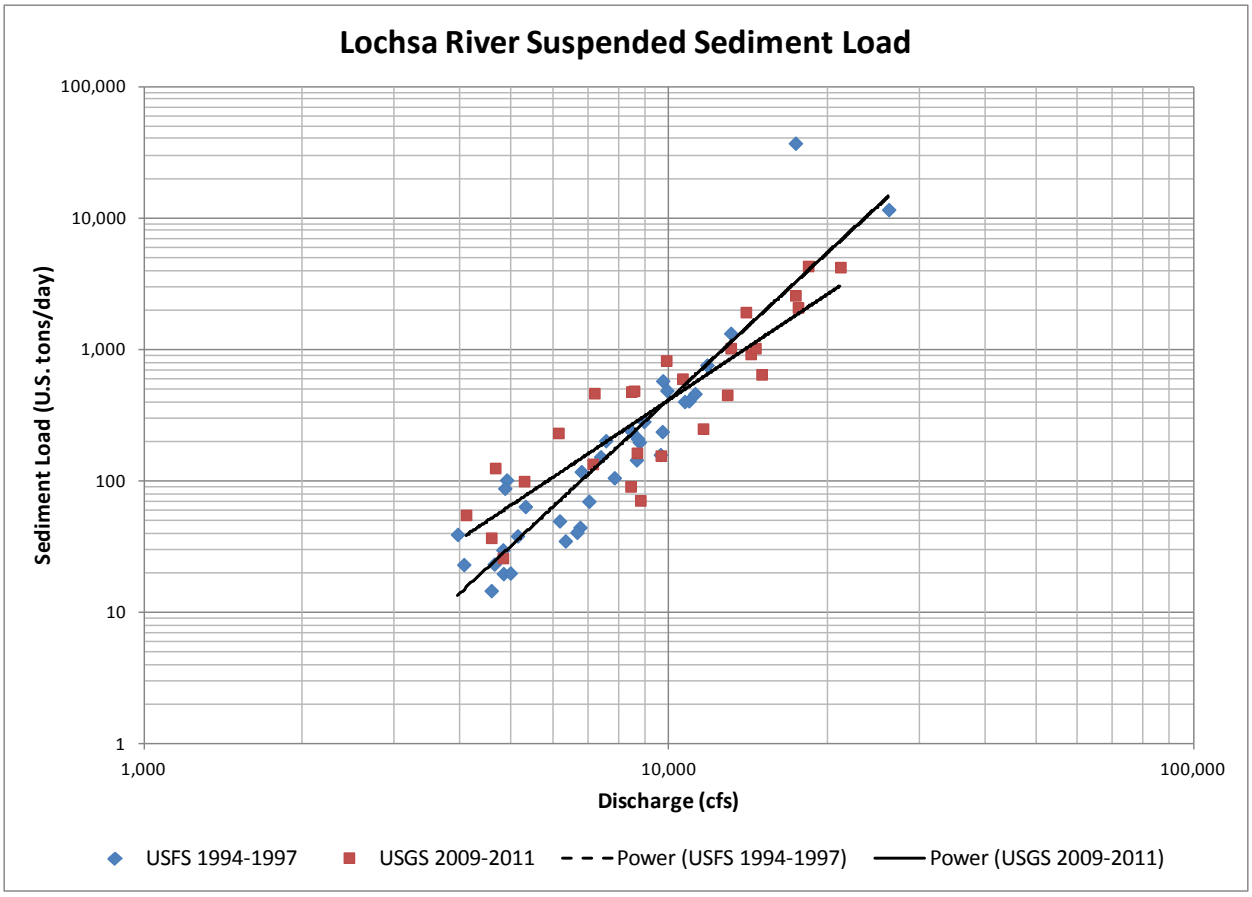


Figure 166. Comparison of suspended sediment load in the Lochsa River.

9.17. Sediment Load in the Palouse River

Sediment load in the Palouse River was measured by USGS at the stream gage at Hooper in 2009, 2010 and 2011. The measured suspended sediment loads are plotted in Figure 167 with suspended sediment loads for the period 1992 through 2004 obtained from NWIS database. Power relationships fit to the data by ordinary least squares regression for both periods show that sediment rating curve for the Palouse River at this location has not changed significantly.

Sediment loads and yield were estimated for the Palouse River with the same methods as described above. Total volume of suspended sediment for the period 2009-2011 was 10.7 mcy. The estimate by the adjusted power relationship agreed closely with the MVUE estimate. Suspended sand was about 41 percent of the total suspended sediment volume. Sediment yield for the period 2009-2011 is summarized in Table 79. Yield of suspended sediment was 0.42 U.S. tons per acre per year and is 68 percent more than the 0.25 tons per acre per year estimated by sediment accumulation in

Section 7. The difference can be attributed to uncertainty in both estimation methods and the likelihood that very fine sediment does not settle at the mouth of the Palouse.

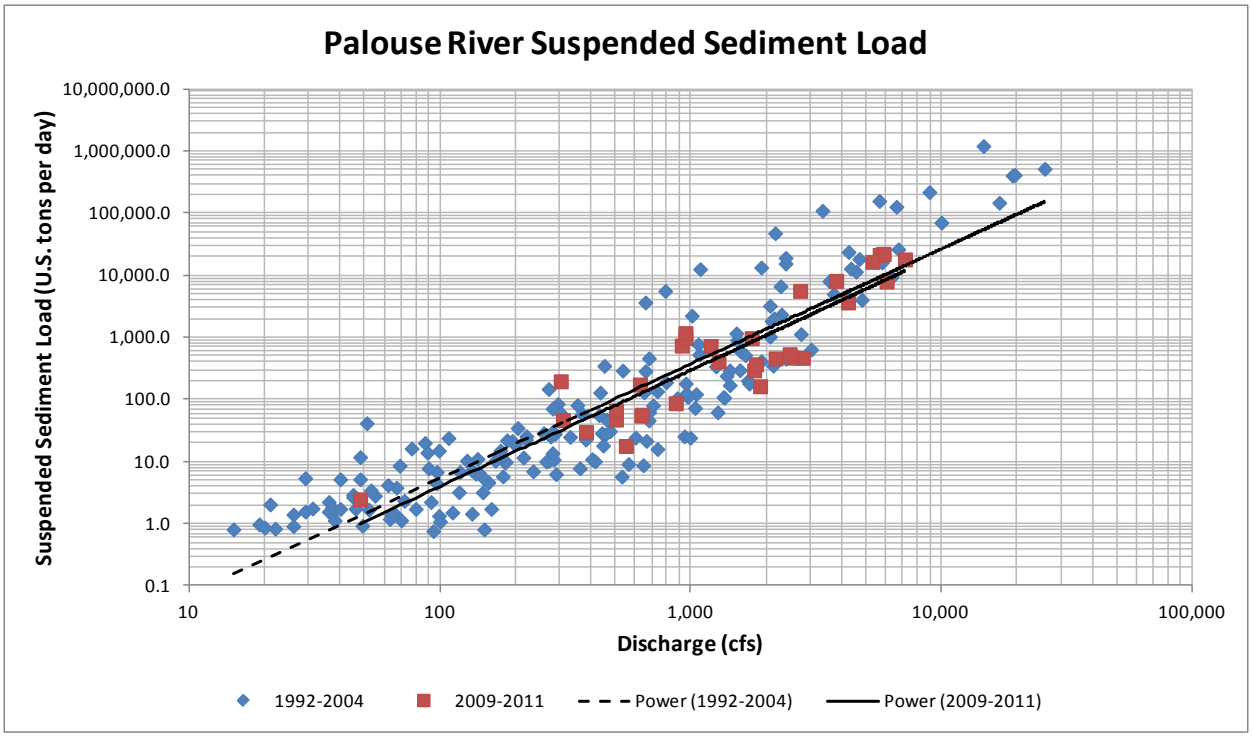


Figure 167. Palouse River suspended sediment load regression curves.

Site	Area mi^2	Average Annual Sediment Yield 2009-2011			
		Suspended Sediment		Suspended Sand	
		Yield ton/mi^2/yr	Yield ton/ac/yr	Yield ton/mi^2/yr	Yield ton/ac/yr
Palouse River at Hooper	1,962	270.5	0.42	18.2	0.03

Table 79. Sediment yield of the Palouse River basin 2009-2011.

Lower Snake River Programmatic Sediment Management Plan Environmental Impact Statement

Appendix F

Hydrology and Hydraulics
Lower Granite Reservoir Sedimentation Analysis and Lewiston Levee Flood Risk Analysis

Part 2

Prepared by:

U.S. Army Corps of Engineers
Walla Walla District

August 2014

Table of Contents

10. Sediment Transport Analysis of Lower Granite Reservoir 9
10.1. Alluvial Hydraulic Geometry and Bed Transitions 10
10.2. Implications of Equilibrium Hydraulic Geometry 21
10.3. Approach to Sediment Transport Modeling 21
10.4. Characterization of the Model Domain 23
10.5. Flow Characterization 24
10.6. Mobile-bed Channel Characteristics 25
10.7. Underwater Video Mapping Survey 31
10.8. Bedforms and Hydraulic Resistance 35
10.9. Mobile-bed Flow Resistance 40
10.10. Conceptual Effect of Sediment Accumulation on Flood Water Surface 54
10.11. Selection of Sediment Transport Function 58
10.12. Simulation of Historic Sediment Accumulation 58
10.13. Simulation of Future 50-year Sediment Accumulation 71
11. Mobile-bed Flood Risk Analysis of the Future Channel 87
11.1. Partial Mobile-Bed approach 87
11.2. Index Sections for the FDA Flood Risk Analysis 98
11.3. Conditional Non-Exceedance Probabilities – 2060 Partial Mobile-Bed Analysis of Upper and Lower Bed Regime 99
11.4. Balanced Hydrograph Development 100
11.5. Full Mobile-Bed Approach 104
11.6. Conditional Non-Exceedance Probabilities – 2060 Full Mobile-Bed Analysis of Upper and Lower Bed Regime 110
11.7. Added Levee Height for SPF Freeboard 110
11.8. Summary of the Flood Risk Analysis for the year 2060 future Channel Condition 113
12. Alternatives for Sediment Management in Lower Granite Reservoir 115
12.1. Sediment Management with Spur Dike Fields 115
12.2. Flood Risk Analysis of Current and Future Channels with Spur Dikes 123
12.3. Seasonal Drawdown of Reservoir Water Surface 126
12.4. Sediment Trap in the Snake River 133
12.5. Extreme Drawdown During Floods 136

12.6. Dredging to Preserve the 2009 Level of Flood Risk Reduction 137
12.7. Dredging to Recover Hydraulic Capacity 138
12.8. Stability of Dredge Material Placement 140
12.9. Management of Sediment at Boat Basins in Lower Granite Reservoir 144
13. Flood Risk due to Wind Waves at the Confluence 149
13.1. Computational Method for Wave Height, Run-up and Set-up 149
13.2. Fetch Length and Depth 150
13.3. Wind Speed Frequency Analysis 151
13.4. Significant Wave Height 155
13.5. Wind Set-up at the Confluence 156
13.6. Wave Run-up and Overtopping Rate 160
13.7. Summary of the Wind Wave Analysis 163
14. Summary of the Flood Risk Analysis 164

List of Figures

Figure 1. Removal of the WWP Dam on the Clearwater River February 1973. 12
Figure 2. Approximate location of hydraulic geometry sand transition on the Clearwater River. 16
Figure 3. Approximate location of hydraulic geometry sand transition on the Snake River. 17
Figure 4. Equilibrium hydraulic geometry of Lower Granite Reservoir 8 June 2010. 19
Figure 5. Equilibrium hydraulic geometry of Lower Granite Reservoir of 8 June 2010 at the SPF discharge (D_{50} = 0.3 mm). 19
Figure 6. Equilibrium hydraulic geometry of Lower Granite Reservoir for the SPF discharge during the SPF (D_{50} = 0.3 mm). 20
Figure 7. Equilibrium hydraulic geometry of Lower Granite Reservoir for the SPF discharge during the SPF (D_{50} = 0.5 mm). 20
Figure 8. Sediment transport model domain in upper Lower Granite Reservoir. 23
Figure 9. Channel Froude number during SPF and 1-percent exceedance discharge. 24
Figure 10. Mean velocity during 50-percent and 1-percent exceedance discharges. 25
Figure 11. Mean bed shear stress during 50-percent and 1-percent exceedance discharges. 25
Figure 12. Sand transition at Clearwater River Mile 1.66. 27
Figure 13. Sand transition at Snake River Mile 141.21. 28
Figure 14. Silt transition at Snake River Mile 130.66 September 2009. 29
Figure 15. Silt transition at Snake River Mile 128.87 September 2011. 30
Figure 16. Sediment encroachment in 2009 on navigation channels at the confluence. 31
Figure 17. Underwater video image at gravel-cobble bed to sand bed transition Snake RM 141.21. 32
Figure 18. Underwater video image at gravel-cobble bed to sand bed transition Clearwater RM 1.66. 33
Figure 19. Underwater video image of sand bed at Snake RM 139.23. 33

Figure 20. Sediment facies map of confluence Snake RM 139.3. 34
Figure 21. Sediment facies map of confluence near Port of Wilma Snake RM 135. 34
Figure 22. Sand dunes on the Snake River in Lower Granite Reservoir. 37
Figure 23. Profile of sand dunes in Figure 22. 38
Figure 24. Bed profile transect Snake River Mile 134.58 - 137.94, bathymetry 2009. 38
Figure 25. Bed profile plot Snake River Mile 134.58 - 137.94, bathymetry 2009. 39
Figure 26. Bed profile transect Snake River Mile 134.58 - 137.94, USGS 1970 DRG. 39
Figure 27. Lower Granite Reservoir sediment grain size for Brownlie regime analysis. 44
Figure 28. Brownlie hydraulic radius for Lower Granite Reservoir 8 June 2010 at 213,500 cfs. 45
Figure 29. Manning's *n* for Lower Granite Reservoir 8 June 2010 at 213,500 cfs. 45
Figure 30. Sediment concentration for Lower Granite Reservoir 8 June 2010 at 213,500 cfs. 46
Figure 31. Brownlie hydraulic radius for Lower Granite Reservoir SPF at 420,000 cfs. 49
Figure 32. Manning's *n* for Lower Granite Reservoir SPF at 420,000 cfs. 49
Figure 33. Sediment concentration for Lower Granite Reservoir SPF at 420,000 cfs. 50
Figure 34. Brownlie hydraulic radius for Lower Granite Reservoir 2-percent exceedance discharge at 308,000 cfs. 50
Figure 35. Brownlie hydraulic radius for Lower Granite Reservoir 1-percent exceedance discharge at 331,600 cfs. 51
Figure 36. Comparison of depths predicted by Engelund-Hansen method. 53
Figure 37. Backwater and free channel flow water surface profiles for the Snake River in Lower Granite Reservoir. 54
Figure 38. SPF water surface profile with 2.42 sediment accumulation near the confluence. 56
Figure 39. SPF water surface profile with 2.49 mcy sediment accumulation at mid reservoir. 56
Figure 40. SPF water surface profile with 23.5 mcy sediment accumulation at mid reservoir. 57
Figure 41. SPF Water surface profile with 171.9 mcy sediment accumulation below RM 130. 57
Figure 42. 1974 HEC-RAS model domain. 60
Figure 43. 1974 HEC-RAS cross sections at confluence of Snake and Clearwater Rivers. 60
Figure 44. Typical 1974 cross section at Snake RM 138.94. 61
Figure 45. Measured and sediment accumulation simulated with Ackers-White and Toffaleti functions 1974-2009. 63
Figure 46. Sediment volume simulated with candidate transport functions. 63
Figure 47. Measured and simulated bed change 1974-2009. 64
Figure 48. Segment of 1974 sediment transport model above Silcott Island. 65
Figure 49. Bend at Snake River RM 123.3. 65
Figure 50. Centennial Island at Snake RM 120. 66
Figure 51. Simulated Ackers-White bed change Clearwater River. 68
Figure 52. Simulated Ackers-White bed change Snake River upstream of confluence. 69
Figure 53. Simulated sediment passing with Ackers-White and Toffaleti functions 1974-2009. 69
Figure 54. Simulated and actual wetted-area in Lower Granite Reservoir. 70
Figure 55. Simulated and actual hydraulic radius in Lower Granite Reservoir. 70
Figure 56. Thinned cross section at Snake River 139.057. 72
Figure 57. Sediment accumulation simulated with Ackers-White and Toffaleti functions 2010-2060. 74

Figure 58. Simulated sediment passing with Ackers-White and Toffaleti functions 2010-2060. 75
Figure 59. Simulated Lower Granite Reservoir Bed Change 2010-2060. 77
Figure 60. Effect of cross section spacing on simulated bed change. 77
Figure 61. Simulated Ackers-White 2010-2060 bed change Clearwater River. 78
Figure 62. Simulated Ackers-White 2010-2060 bed change Snake River upstream of confluence. 78
Figure 63. Ackers-White sediment accumulation volumes in Lower Granite Reservoir with alternative sediment loads. 79
Figure 64. Toffaleti sediment accumulation volumes in Lower Granite Reservoir with alternative sediment loads. 79
Figure 65. Simulated Bed change in Lower Granite Reservoir for alternative sediment loads. 80
Figure 66. Simulated wetted-area in Lower Granite Reservoir in 2060. 81
Figure 67. Simulated wetted-area Silcott to the confluence in 2060. 82
Figure 68. Simulated hydraulic radius in Lower Granite Reservoir in 2060. 82
Figure 69. Simulated hydraulic radius Silcott to the confluence in 2060. 83
Figure 70. Effect of cross section spacing on long-term simulation of sediment accumulation. 83
Figure 71. 50-year and 100-year sediment accumulation volumes in Lower Granite Reservoir. 85
Figure 72. 50-year and 100-year sediment accumulation volumes from Silcott to the confluence in Lower Granite Reservoir. 85
Figure 73. 50-yr and 100-year mean effective bed change and surface D50 for Lower Granite Reservoir RM 125 to the confluence. 86
Figure 74. HEC-RAS 2060 upper regime fixed-bed steady flow profiles for Clearwater River. 89
Figure 75. HEC-RAS 2060 upper regime fixed-bed steady flow profiles for Snake River above confluence. 90
Figure 76. HEC-RAS 2060 upper regime fixed-bed steady flow profiles for Snake River below the confluence (Lower Granite Reservoir). 90
Figure 77. HEC-RAS 2060 upper regime fixed-bed steady flow profiles for Clearwater River near the CPRR bridge. 91
Figure 78. HEC-RAS 2060 upper regime fixed-bed steady flow profiles for Snake River near Interstate Bridge. 91
Figure 79. HEC-RAS 2060 lower regime fixed-bed steady flow profiles for Clearwater River. 94
Figure 80. HEC-RAS 2060 lower regime fixed-bed steady flow profiles for Clearwater River near CPRR Bridge. 94
Figure 81. HEC-RAS 2060 lower regime fixed-bed steady flow profiles for Snake River above confluence. 95
Figure 82 HEC-RAS 2060 lower regime fixed-bed steady flow profiles for Snake River near Interstate Bridge. 95
Figure 83. FDA Index cross section locations. 98
Figure 84. 1974 Flood Hydrograph at Lower Granite Reservoir. 102
Figure 85. Volume-frequency curves for Lower Granite Reservoir. 102
Figure 86. Balanced hydrograph floods for Lower Granite Reservoir. 103
Figure 87. Deposition and scour during 1-percent exceedance balanced hydrograph. 106
Figure 88. Sediment discharge at peak of 1-percent exceedance balanced hydrograph. 107

Figure 89. Longitudinal cumulative mass change at peak of 1-percent exceedance balanced hydrograph. 107
Figure 90 Longitudinal cumulative mass change at peak of 0.2-percent exceedance balanced hydrograph for the upper regime bed condition. 108
Figure 91. Longitudinal cumulative mass change at peak of 0.2-percent exceedance balanced hydrograph for the upper regime bed condition. 108
Figure 92. Location of potential spur dikes in Lower Granite Reservoir. 117
Figure 93. Spur dike at Clearwater RM 1.131 represented in HEC-RAS. 118
Figure 94. Ackers-White sediment accumulation volumes at year 2060 in Lower Granite Reservoir with and without spur dikes. 119
Figure 95. Ackers-White sediment bed change at year 2060 in Lower Granite Reservoir with and without spur dikes. 119
Figure 96. Ackers-White sediment accumulation volumes at year 2060 in Clearwater River with and without spur dikes. 120
Figure 97. Ackers-White sediment bed change at year 2060 in the Clearwater River with and without spur dikes. 120
Figure 98. Ackers-White sediment accumulation volumes at year 2060 in Lower Granite Reservoir with half-height spur dikes. 121
Figure 99. Ackers-White sediment bed change at year 2060 in the Lower Granite Reservoir with half-height spur dikes. 122
Figure 100. Erosion and deposition predicted by an ADH 2D model of a confluence spur dike field. 125
Figure 101. Erosion and deposition predicted by an ADH 2D model of a Clearwater turning basin spur dike field. 126
Figure 102. February-March 2010 Drawdown Scenario. 130
Figure 103. May-June 2010 Drawdown Scenario. 130
Figure 104. March-April 2011 Drawdown Scenario. 131
Figure 105. March 17, 1992 aerial photograph of confluence during drawdown. 132
Figure 106. Lower Granite Reservoir drawdown sediment accumulation. 132
Figure 107. Clearwater River drawdown sediment accumulation. 133
Figure 108. Location of a potential sediment trap on the Snake River. 134
Figure 109. Snake River sediment trap mass analysis, WY 2010-2011. 135
Figure 110. Snake River sediment trap efficiency. 135
Figure 111. Conceptual extreme drawdown of forebay for flood control. 136
Figure 112. Flood water surface profile for extreme forebay drawdown. 137
Figure 113. Dredging priority areas for flow conveyance. 139
Figure 114. Removal of the submerged island at the Port of Wilma. 140
Figure 115. Dredge material placement site at Snake RM 117. 141
Figure 116. Shallow water habitat site before dredge material placement. 142
Figure 117. Shallow water habitat site after dredge material placement. 143
Figure 118. 2D velocity field at the dredge material placement site at 200 kcfs. 143
Figure 119. Shields-Parker sedimentation diagram for RM 117 at 200 kcfs. 143
Figure 120. Comparison of bed elevation transects at the dredge material placement site at RM 117. 144

Figure 121. Sediment deposition at inlet to the Asotin Boat Basin. 145
Figure 122. Sand bar at the inlet to the Asotin Boat Basin. 146
Figure 123. Silt deposits in the Asotin Boat Basin. 146
Figure 124. Velocity vectors and eddy at the inlet of the Asotin Boat Basin. 147
Figure 125. Potential spur dike extension at the inlet of the Asotin Boat Basin. 147
Figure 126. Potential relief channel at the Asotin Boat Basin. 148
Figure 127. Confluence fetch diagram. 151
Figure 128. 2-minute annual maximum wind speed at the Lewiston Airport. 152
Figure 129. Frequency curve for 2-minute duration maximum annual seasonal (Nov-Jun) wind speed at the Lewiston, ID Airport. 153
Figure 130. Correlation between annual maximum discharge and wind speed. 154
Figure 131. Stage and discharge in Lower Granite Reservoir February 5-9, 2008. 156
Figure 132. Wind set-up conditions in Lower Granite Reservoir February 6-9, 2008. 157
Figure 133. Wind set-up derived from HEC-RAS computation of water surface at the confluence. 158
Figure 134. ACES wave run-up diagram. 161
Figure 135. Geometry of the levee at Clearwater RM 0.21. 161
Figure 136. FDA Index Cross sections at the Lewiston levee system. 164

List of Tables

Table 1. Comparison of stage-discharge predictors for sand bed channels. 53
Table 2. Change in water surface due to conceptual sediment accumulation. 55
Table 3. Bed material designations in 2009 initial sediment transport geometry. 73
Table 4. HEC-RAS annual peak steady flow discharges for FDA risk analysis. 88
Table 5. HEC-RAS 2060 Fixed-Bed Upper Regime Water Surface Profile - Clearwater River near the Confluence. 92
Table 6. HEC-RAS 2060 Fixed-Bed Upper Regime Water Surface Profile - Snake River near the Confluence. 93
Table 7. HEC-RAS 2060 Fixed-Bed Lower Regime Water Surface Profile - Clearwater River near the Confluence. 96
Table 8. HEC-RAS 2060 Fixed-Bed Lower Regime Water Surface Profile - Snake River near the Confluence. 97
Table 9. Year 2060 fixed-bed conditional non-exceedance probabilities at Clearwater RM 0.3. 99
Table 10. Year 2060 fixed-bed conditional non-exceedance probabilities at Snake RM 139.58. 100
Table 11. Volume-duration-frequency statistics for Lower Granite Reservoir. 103
Table 12. Discharge ratios for proportioning the Lower Granite Reservoir balanced hydrograph. 103
Table 13. Bed material designations for the balanced hydrograph sediment transport model. 106
Table 14. Water surface elevations at Clearwater RM 0.217 for partial and full mobile-bed computation methods. 109
Table 15. Water surface elevation difference at Clearwater RM 0.217 for partial and full mobile-bed computation methods. 110

Table 16. Added height to Clearwater River levee to provide 5 ft freeboard during SPF. 112
Table 17. Added height to Snake River levee to provide 5 ft freeboard during SPF. 113
Table 18. Upper bed regime water surface elevations at Clearwater RM for simulations with spur dikes. 123
Table 19. Lower bed regime water surface elevations at Clearwater RM for simulations with spur dikes. 123
Table 20. Year 2009 CNP and LTR for channel with spur dikes at Clearwater RM 0.3. 124
Table 21. Year 2060 CNP and LTR for channel with spur dikes at Clearwater RM 0.3. 124
Table 22. Fetch lengths at the confluence of the Snake and Clearwater Rivers. 150
Table 23. Annual maximum 2-minute duration wind speed. 153
Table 24. Wind speed - frequency values for the Lewiston, ID Airport. 154
Table 25. Significant wave height and period at confluence computed with ACES. 155
Table 26. Water surface elevations at Clearwater RM 0.21 for year-2009 and year-2060. 162
Table 27. Wave run-up at the confluence for the year-2009 channel. 163
Table 28. Wave run-up at the confluence for the year 2060 channel. 163
Table 29. Channel configurations evaluated for the Lewiston levee flood risk analysis. 165
Table 30. Lewiston levee CNP and LTR evaluations for year 2009 channel condition. 167
Table 31. Lewiston levee CNP and LTR evaluations for year 2060 channel condition. 168

THIS PAGE INTENTIONALLY LEFT BLANK

10. Sediment Transport Analysis of Lower Granite Reservoir

About 80 million cubic yards of sediment has accumulated in Lower Granite Reservoir since 1974. Sediment deposition in the reservoir is variable and the historic sediment ranges (Section 6) showed that relatively narrow channel cross sections in the upper segment of the reservoir have not changed significantly since the construction of Lower Granite lock and dam, which indicates these sections are tending towards dynamic equilibrium with the prevailing sediment load and discharge. Other segments, particularly those below RM 130, continue to accumulate sediment because nearly all the sand and coarse silt sediment load is retained in the backwater of Lower Granite Dam. The analysis of measured sediment load (Section 8) showed that sediment loads have not diminished with time and may be increasing. The fixed-bed hydraulic modeling (Section 3) showed that historic sediment deposition has decreased the hydraulic capacity of the Snake and Clearwater River channels in Lower Granite Reservoir. Together, these analyses demonstrate the likelihood that sediment will continue to accumulate in Lower Granite Reservoir during the 50-year future analysis period and that the hydraulic capacity of the levee system will continue to decrease because of sediment accumulation.

Key concerns in the flood risk analysis are how the reservoir channel will change during the 50-year future analysis period and how the expected sediment deposition will alter flood risk. Several channel configurations are in this part of the hydraulics and hydrology report (H&H) evaluated to characterize the epistemic uncertainty of the channel simulation. Epistemic uncertainty is the uncertainty due to lack of knowledge of the system process or the model that represents the process[1]. The main sources of epistemic uncertainty in this flood risk analysis include the future sediment loads, the sediment transport models that predict the future channel condition, and hydraulic response of the channel to extreme discharges. Several aspects of future sediment accumulation are examined including, 1) the temporal and spatial distribution of the sediment, the effect of sediment accumulation on flow resistance, 2) the response of the channel bed to extreme flows, 3) the hydraulic capacity of the future channel, 4) the effect of continued sediment accumulation on the water surface profile of the reservoir, 5) the change in flood risk reduction afforded by the Lewiston levees, and 6) the potential of structures and operations to manage sediment accumulation. All these aspects are evaluated below with sediment transport simulations, mobile-bed hydraulic analysis, and equilibrium hydraulic geometry analysis.

[1]Schult, M.T., Bridges, T.S.,Mitchell, K.N., and Harper, B.K. (2010) *Decision Making Under Uncertainty, ERDC TR-10-12*, Engineering Research and Development Center, U.S. Army Corps of Engineers, Washington, DC.

10.1. Alluvial Hydraulic Geometry and Bed Transitions

It was noted in the fixed-bed hydraulic modeling (Section 3) that it certain that sediment deposited near the confluence will remobilize during the extreme, low frequency discharges that define long-term flood risk. Extreme flows greater than about a 2-percent chance exceedance discharge have not occurred in Lower Granite Reservoir since the pool was raised, so there has been no direct observation of sediment movement during large flood events. For a given discharge and channel geometry, particle size has the greatest influence on mobility of cohesionless sediments. Other factors such as water temperature, surface armoring and consolidation of deposited sediment have much less influence, particularly for sand sediment.

The sediment core survey (Section 7) showed that sand and silt accumulate in the backwater zone of Lower Granite and that there is no identifiable gravel fraction. All the channel surveys undertaken in this study: sediment range surveys, high resolution bathymetry, sediment coring survey, and underwater video mapping, confirm that sand and silt, but not gravel, are transported through the confluence and into the upper segment of Lower Granite Reservoir. This observation is consistent with fluvial mechanics because transport energy is not sufficient to carry gravel sediment very far into the backwater zone of Lower Granite Reservoir under the regulated flow regime.

Sediment dynamics in Lower Granite Reservoir can be viewed within the context of general relationships for alluvial channels. The shape and hydraulic properties of alluvial channels adjust to variations in discharge and sediment load. This principle is expressed in the widely applied qualitative relationship for channel adjustment proposed by Lane[2]:

$$QS \approx Q_s D_{50}$$

where Q is water discharge, S is channel slope, Q_s is sediment discharge, and D_{50} is the median diameter of the bed sediment load. Though simple, this relationship is a powerful predictor of likely trends in channel adjustment.

According to Lane's relationship, if discharge increases while sediment load and sediment size remains the same, then channel slope must decrease to maintain equilibrium. An increase in slope also results if the incoming sediment load increases while water discharge and sediment size remain constant. Self-forming channels adjust bed slope by erosion (degradation) or deposition (aggradation) of channel bed material. If all other factors are held constant, a decrease in discharge or an increase in sediment

[2] Lane, E.W. (1955). "The importance of fluvial morphology in hydraulic engineering." Proceedings of ASCE, 81(745), 1-17.

load will cause an increase in channel slope by bed aggradation. In Lower Granite Reservoir, Lane's relationship predicts a rise in water surface at the upper end of the reservoir due to long-term sediment accumulation. Lane's relationship by itself does not predict the functional geometry of the channel or the rate of channel change. Lane's relationship is the starting point for further analysis[3]. The morphodynamics[4] of Lower Granite Reservoir must be predicted with more complex empirical and analytical methods.

Alluvial dynamic equilibrium is expressed in the relationships of hydraulic geometry, which represent the tendency for self-formed channels to attain geometries of similar average widths, depths, slopes, meander geometry, and bed features when subject to similar regimes of flow, sediment grain size and sediment load[5]. Hydraulic geometry relationships provide a simple, yet well-founded, empirical means to assess sediment impacts and potential future conditions in Lower Granite Reservoir. A hydraulic geometry assessment is an informative and useful introduction to the more involved, but less transparent, sediment transport analysis that follows. The key ideas are 1) the point along the river profile where the actual geometry of the Lower Granite channels first becomes similar to that predicted by equilibrium hydraulic geometry relationships for sand bed channels should indicate where the transition from gravel-bed to sand bed occurs, and 2) appropriate hydraulic geometry relationships approximate the geometry of the equilibrium channel that would form in the upper segment of the reservoir given sufficient time and accumulated sediment for the channel to become self-forming.

It is recognized that hydraulic geometry relationships are developed from stable alluvial channels that have formed under relatively constant sediment and discharge regimes. Use of equilibrium hydraulic geometry relationships in an analysis of non-equilibrium reservoir conditions is justified because sand bed channels respond quickly to an imbalance of hydrodynamic forces and sediment load through the process sediment transport[6]. It is possible for sand channels to attain temporary equilibrium as long as discharge and sediment load are relatively constant during the time it takes for

[3] Dust, D. and Wohl, E. (2012) "Conceptual model for complex river responses using an expanded Lane's relationship." Geomorphology, Vol. 139-140, p.109-121

[4] Morphodynamics is the complex response of an alluvial channel to sediment load and water discharge as either or both vary through time.

[5] Leopold, L.B and Maddock, T., Jr. (1953) "The Hydraulic Geometry of Stream Channels and Some Physiographic Implications", *Professional Paper 252*, U.S. Geological Survey, Washington, DC.

[6] Vanoni, A. *et al*. (1975) "Chapter II, Sediment transportation mechanics", *ASCE Manual 54 Sedimentation Engineering*, American Society of Civil Engineers, New York.

the channel to adjust to the prevailing condition. Rapid and dramatic reestablishment of channel equilibrium was observed following removal of the Washington Water Power Dam at Lewiston on the Clearwater in 1973 (Figure 1). The large sand deposit behind the dam was eroded and transported past the confluence mostly within a single season[7].

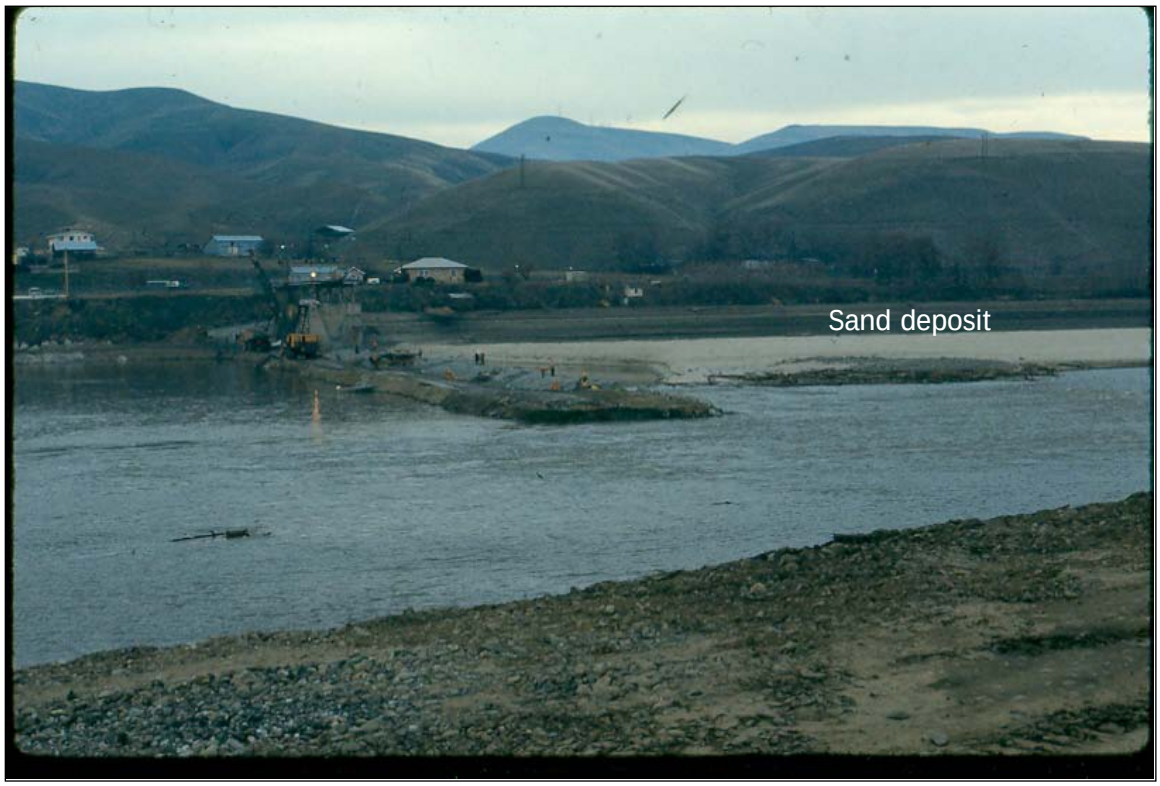


Figure 1. Removal of the WWP Dam on the Clearwater River February 1973.

Many mathematical relationships have been proposed for the hydraulic geometry of alluvial channels. Two formulations that are based on extensive field data and sedimentation mechanics are discussed below.

Parker[8] analyzed an extensive set of gravel-bed and sand-bed streams and developed the following dimensionless hydraulic geometry relationships for bankfull sand channel geometry:

[7] Williams, D.T. (1977) *Effects of Dam Removal: An Approach to Sedimentation, TP-50*, Hydrologic Engineering Center, U.S. Army Corps of Engineers, Davis, CA.

[8] Parker, G. (2008). "Transport of gravel and sediment mixtures." *Sedimentation Engineering, Processes, Measurements, Modeling and Practice*, ASCE Manuals and Reports of Engineering Practice No. 110

Bankfull width: $B = 0.274\hat{Q}^{0.565}D_{50}$ **10-1**

Bankfull depth: $H = 3.01\hat{Q}^{0.321}D_{50}$ **10-2**

Channel slope: $S = 6.42\hat{Q}^{-0.397}$ **10-3**

Dimensionless discharge is: $\hat{Q} = \frac{Q_{bf}}{\sqrt{gD_{50}}D_{50}^{2}}$ **10-4**

Dimensionless (Shields) shear stress: $\tau^{*}_{bf\,50} = \frac{\tau_{bf}}{\gamma(S_g - 1)D_{50}} = 1.86$ **10-5**

where B is the stable width, H is the stable depth, Q is the bankfull discharge, D_{50} is the median diameter of the bed surface material, γ is the unit weight of water, S_g is the specific gravity of the sediment, and g is the acceleration of gravity. Consistent U.S. customary or SI units can be used in the equations. The equations above were expressed in dimensional form in this report. Recently, Wilkerson and Parker reformulated the sand-bed hydraulic geometry relationships to include the particle Reynolds number[9], but the simpler relationships above are sufficient for the analysis here.

Lee and Julien[10,11] also developed hydraulic geometry relationships for alluvial channels from an extensive dataset of 1,125 measurements that include braided gravel bed channels. The regression equations were tested for channels widths ranging from 0.2 m to 1,100 m (1 ft – 3600 ft), channel depths range from .01 m to 16 m (.03 ft – 52 ft), and channel slopes from 0.0001 to 0.08. The relationships for bankfull width and bankfull depth in SI units are:

[9] Wilkerson, G.V., G. Parker. (2011) "Physical basis for quasi-universal relationships describing bankfull hydraulic geometry of sand-bed rivers", *Journal of Hydraulic Engineering*, 137(7), 739-753.

[10] Lee, J., P.Y. Julien. (2006). "Downstream hydraulic geometry of alluvial channels." *Journal of Hydraulic Engineering*, 132(12), 1347-1352.

[11] Julien, P.Y. and J. Wargadalam. (1995). "Alluvial channel geometry: theory and applications.", Journal of Hydraulic Engineering, 121(4), 312 – 325.

Bankfull width: $W = 3.004Q^{0.426}D_{50}{}^{-0.002}S^{-0.153}$ [SI] **10-6**

Bankfull Depth: $H = 0.201Q^{0.336}D_{50}{}^{-0.025}S^{-0.060}$ [SI] **10-7**

where Q is the bankfull discharge (m^3 s^{-1}), D_{50} is the median grain size of the bed material (m), and S is the channel slope (m/m). Coefficients of determination (R^2) from a validation dataset of 360 measurements were 0.87 for the width relationship and 0.93 for the depth relationship. Lee and Julien also proposed a relationship for stable slope (S) that includes terms for sediment size and Shields parameter (dimensionless critical shear stress):

$$S = 4.981Q^{-0.346}D_{50}{}^{0.955}\tau_{50}^{*\ 0.966} \quad \text{[SI]} \quad \textbf{10-8}$$

where τ_{50}* is the dimensionless shear stress (Shields) parameter:

$$\tau_{50}^{*} = \frac{\rho gRS}{(\rho_s - \rho)gD_{50}} \quad \text{[dimensionless]} \quad \textbf{10-9}$$

and ρ_s is the sediment density, ρ is the density of water, and g is the acceleration of gravity.

The Parker and Lee-Julien hydraulic geometry relationships include median sediment size as a parameter. This allows the relationships to be used to estimate the location where gravel channels transition to sand channels.

Gravel-bed channels transition to sand-bed channels as the longitudinal slope (energy gradient) of the channel decreases. The transition from gravel-bed to sand-bed in the Snake and Clearwater Rivers can be approximately located by comparing general hydraulic geometry relationships for sand bed channels with the properties of the channels of Lower Granite Reservoir. To conduct this analysis for typical seasonal discharges, it is necessary to define a dominant discharge for which to compute the actual and predicted geometry. The peak discharge of 8 June 2010 has an exceedance of about 18 percent for the annual maximum daily discharge, so on average this flow would occur about once every 5 to 6 years. Channel forming discharges are usually in the range of 2 to 5 years, so 8 June provides a reasonable discharge at which to compare the mean dimensions of the channels in Lower Granite with those predicted by the hydraulic geometry relationships.

The peak discharge in the Clearwater River on 8 June was 60,300 cfs and the sediment core survey shows that the median grains size of the beds of the Clearwater and Snake Rivers near the confluence is about 0.3 mm. Substituting this discharge and sediment size into the Parker relationships gives a mean depth of 15.0 feet, a mean width of 900 feet and a bed shear stress of 1.6 lb-ft^2. Multiplying the mean depth by the mean width gives a mean wetted channel area of 13,500 ft^2. Similarly, the Lee-Julien relationships give a mean depth of 16.2 feet, a mean width of 850 feet which when multiplied gives a mean wetted channel area of 13,800 ft^2. The average channel slope for the likely area of the sand transition from the HEC-RAS model was used in the Lee-Julien relationships.

The constant values of wetted-area and bed shear stress are plotted in Figure 2 along with the actual wetted-area and bed shear stress of the Clearwater River computed with the HEC-RAS 2009 fixed-bed model. The line for the Lee-Julien prediction for wetted-area is indistinguishable from the Parker prediction at the scale of the plot, so is not shown. The plots show that wetted-area increases and bed shear stress decreases in the downstream direction because of the backwater of Lower Granite Dam.

The plots in Figure 2 indicate that the wetted-area and bed shear stress of the Clearwater River become equal to the equilibrium hydraulic geometry at about RM 2.34. This location is just upstream from Memorial Bridge and agrees well with the observation of the beginning of sand bedforms on the Clearwater River. Downstream from this point the channel deepens and widens, and the shear stress reduces. This segment of the channel is not self-formed and it has an over fitted geometry that is the result of the backwater. The difference between the equilibrium parameter lines and the actual hydraulic parameters suggest that sediment transport equilibrium cannot be maintained and sand must accumulate on the bed. Hydraulic calculations show that this is the location in the channel where shear velocity becomes approximately equal to the settling velocity of medium sand past the peak of a typical seasonal hydrograph. This is also the location of the navigation turning basin at the Port of Lewiston between RM 1.0 and about RM 1.6 where it is known that sand accumulates in the turning basin and must be dredged to maintain the navigation channel. The channel cross section again narrows at the CPRR Bridge at RM 0.6. At this point, the actual wetted area decreases to about the equilibrium value and the ratio of shear velocity to settling velocity again increases. The sediment ranges show that sand does not accumulate at this location.

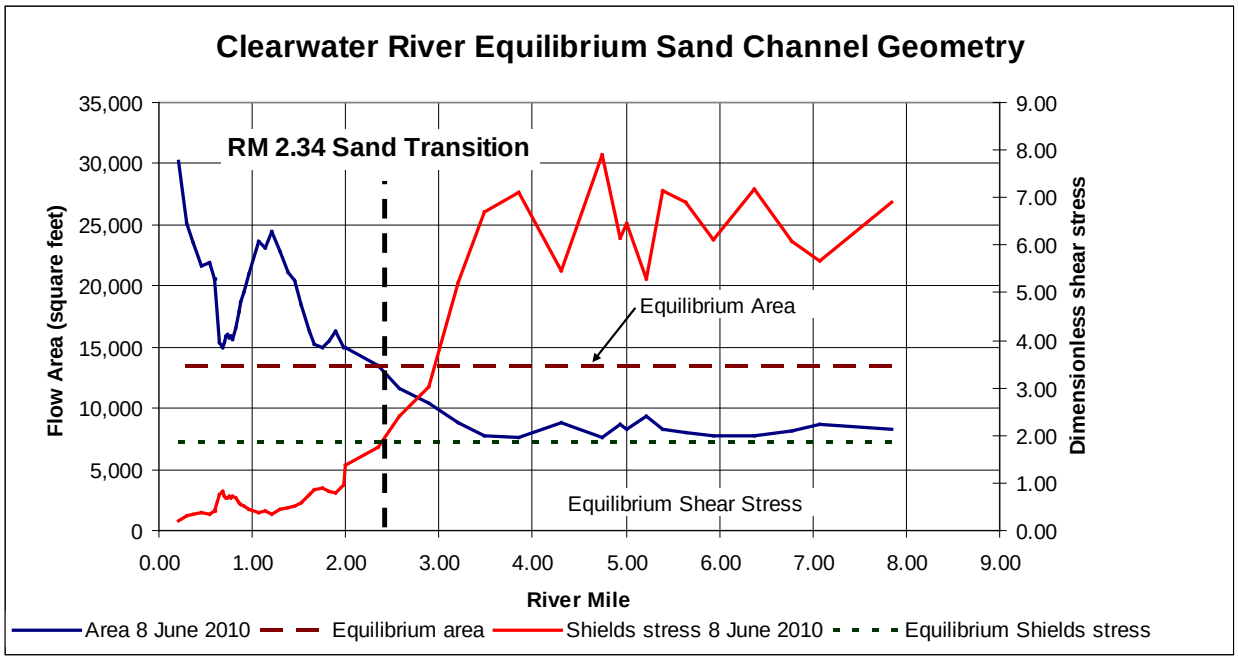


Figure 2. Approximate location of hydraulic geometry sand transition on the Clearwater River.

An important aspect of Figure 2 is that the wetted-area upstream from the transition point is less than the predicted equilibrium geometry and that the actual bed shear stress is significantly higher than the equilibrium shear stress. This means that sand load is suspended upstream of the transition point and that bedload is insufficient to produce dunes of significant magnitude to impact hydraulic resistance. This also implies that sand that is deposited on the bed during the rising or falling limbs of the hydrograph is swept from the bed at higher discharge. These implications of equilibrium hydraulic geometry are supported by the lack of residual sand bedforms in the low flow high-resolution bathymetry immediately below Memorial Bridge at RM 1.99.

A similar hydraulic geometry analysis for the Snake River is plotted in Figure 3. This plot shows that the sand transition occurs between RM 141.2 and about 142.5, which also agrees with the appearance of sand bedforms in the low flow high-resolution bathymetry. Again, the wetted-area is less and the bed shear stress is greater upstream from the transition point, indicating that sand is carried in suspension.

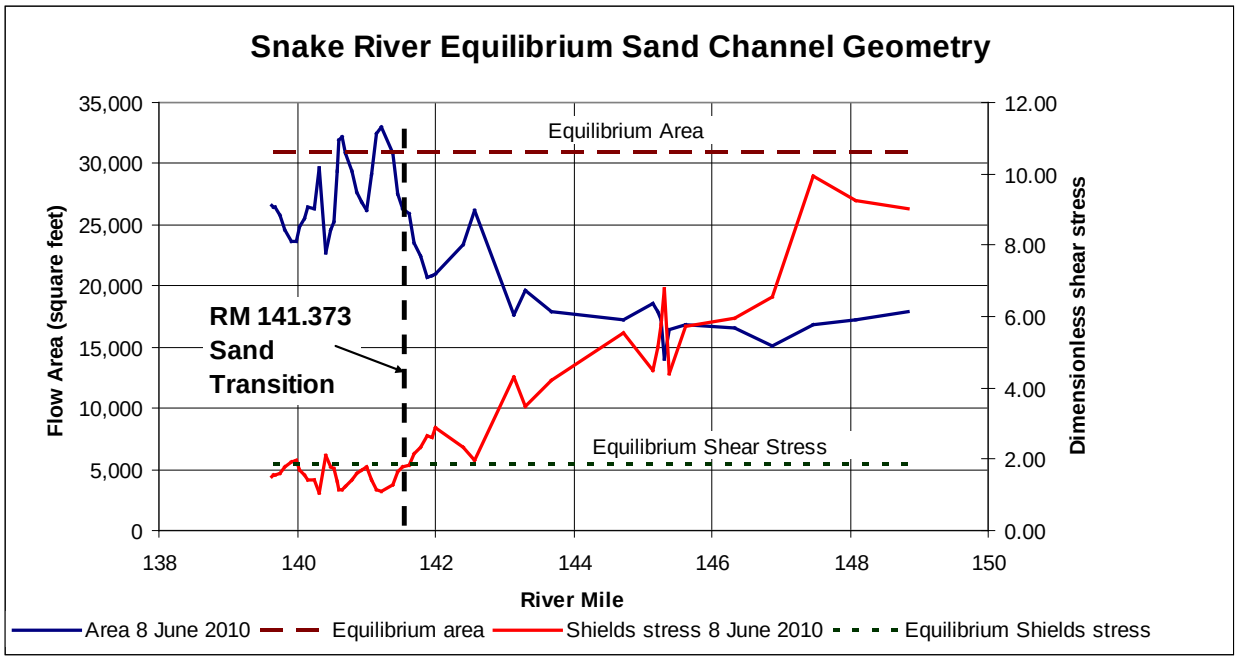


Figure 3. Approximate location of hydraulic geometry sand transition on the Snake River.

Equilibrium hydraulic geometry was also computed for the Lower Granite channel below the confluence. As would be expected, the equilibrium geometry does not indicate a sand transition in Lower Granite for the 8 June discharge because sand transitions occurred in both the Snake and Clearwater Rivers above the confluence. The actual bed shear stress plotted in Figure 4 is considerably lower than the equilibrium bed shear stress at all points in the profile. Importantly, the actual wetted-area in Lower Granite approaches the predicted equilibrium wetted-area upstream of about RM 132. This corresponds to the upper reach of Lower Granite Reservoir where large dunes are observed in the high-resolution bathymetry and there are cross sections in the historic sediment ranges where sediment has not significantly accumulated or scoured since the pool was raised. Disparity between the equilibrium bed shear stress and the equilibrium wetted area would be expected because of the over fit channel. Most of the sediment is transported in the deepest part of the channel where the bed shear stress is greater than the section mean computed with the HEC-RAS model. Though not shown on the plot, the equilibrium wetted-area predicted by the Lee-Julien relationship plots nearer the actual wetted-area (about 50,000 ft^2) even though the slope assumed in the computation is outside the range of the regression data.

The difference between the predicted equilibrium wetted-area and the actual wetted-area computed with the HEC-RAS 2009 model gives an estimate of the volume that would accumulate as equilibrium geometry is attained. Based on the Parker relationships the total required accumulation between RM 132 above Silcott Island to

the confluence is about 18 million cubic yards. This is equivalent to about 8 feet of uniform deposition throughout the upper reach of Lower Granite Reservoir and is about the amount of sediment load that is expected in an 8 year period. Based on the Lee-Julien relationships, the total required accumulation is 0.7 mcy, equivalent to about an average deposition depth of 0.3 feet. This latter estimate indicates that the upper reach of Lower Granite Reservoir is in approximate equilibrium under the prevailing discharge and sediment regime, which provides plausible support for the stability seen in recent model estimates of the SPF water surface elevation at the confluence, recalling that this analysis did not account for sediment mobility.

The equilibrium hydraulic geometry analysis can be extended to greater discharges. At the extreme SPF discharge, the hydraulic geometry relationships for Lower Granite plotted in Figure 5 show that bed shear stress in the reach above Silcott Island (RM 130) exceeds the equilibrium value for the 8 June discharge and that the wetted-area of the channel approaches the predicted equilibrium area of 8 June. This is an important outcome because it indicates that during the SPF flood, sand should be scoured from the upper reach of Lower Granite Reservoir and transported below Silcott Island to be deposited deeper in the reservoir where it has less effect on the water surface elevation at the confluence. Scouring will occur if the incoming sediment load does not exceed the transport capacity of the Lower Granite Reservoir channel. If incoming sediment load equals transport capacity, then the equilibrium geometry should be approximately maintained (bed shear stress still exceeds the equilibrium value) or somewhat decreased, but should produce no drastic changes in the conveyance of the Lower Granite channel.

If the duration of the peak of the SPF is sufficient, a larger equilibrium channel will be formed through the accumulated sand deposits in the upper reach of Lower Granite Reservoir, further increasing the flood capacity at the confluence over that indicated by the fixed-bed model. Figure 6 shows the equilibrium geometry predicted by the Parker relationships during the SPF. The actual bed shear stress and the actual (before scour) wetted-area cross the equilibrium lines at about RM 126, indicating that the sand transition would move from the river channels above the confluence to below Silcott island during the SPF discharge. This is a compelling observation that suggests that flood capacity at the confluence will increase during the SPF and that the fixed-bed model is conservative for extreme discharges. Scour during the SPF would likely be limited to the depth of the original gravel channel.

Sediment size affects the hydraulic geometry predictions; larger grain size increases the equilibrium bed shear stress and decreases the equilibrium wetted-area. In Figure 7, the hydraulic geometry relationships for Lower Granite are plotted for a D_{50} of 0.5 mm. The plots indicate the sand transition begins at about RM 132. Jointly, the

plots in Figure 6 and Figure 7 indicate that sand size bed material may be sorted through the upper reach of Lower Granite during extreme discharges.

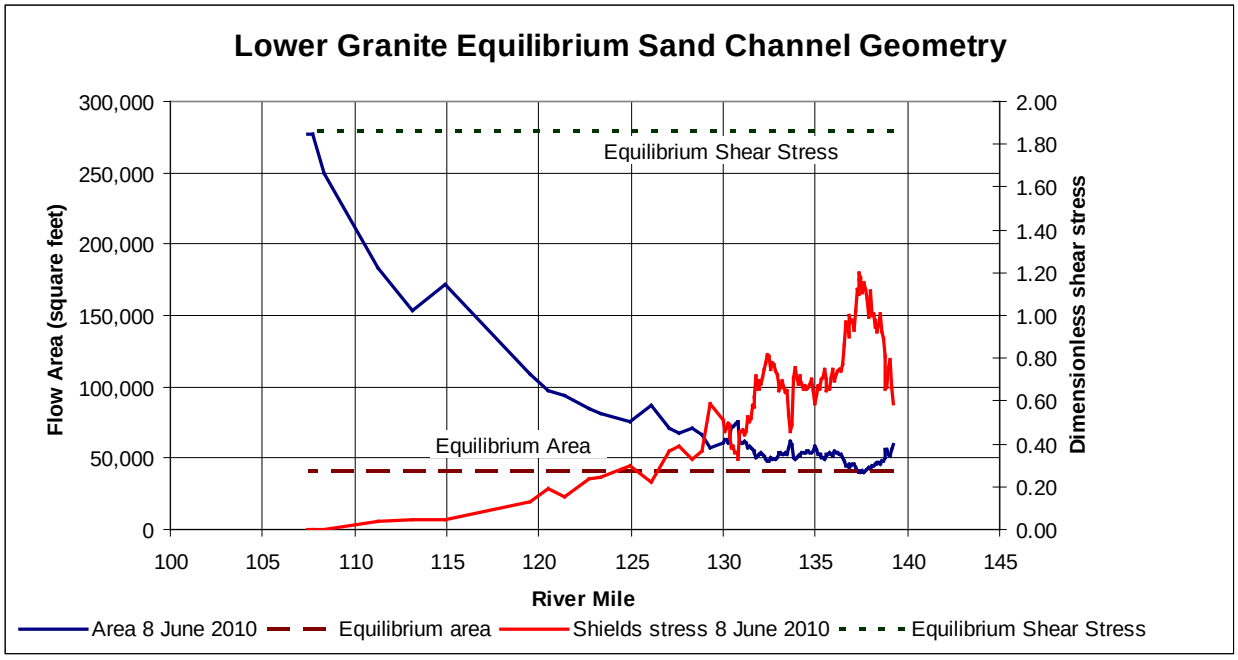


Figure 4. Equilibrium hydraulic geometry of Lower Granite Reservoir 8 June 2010.

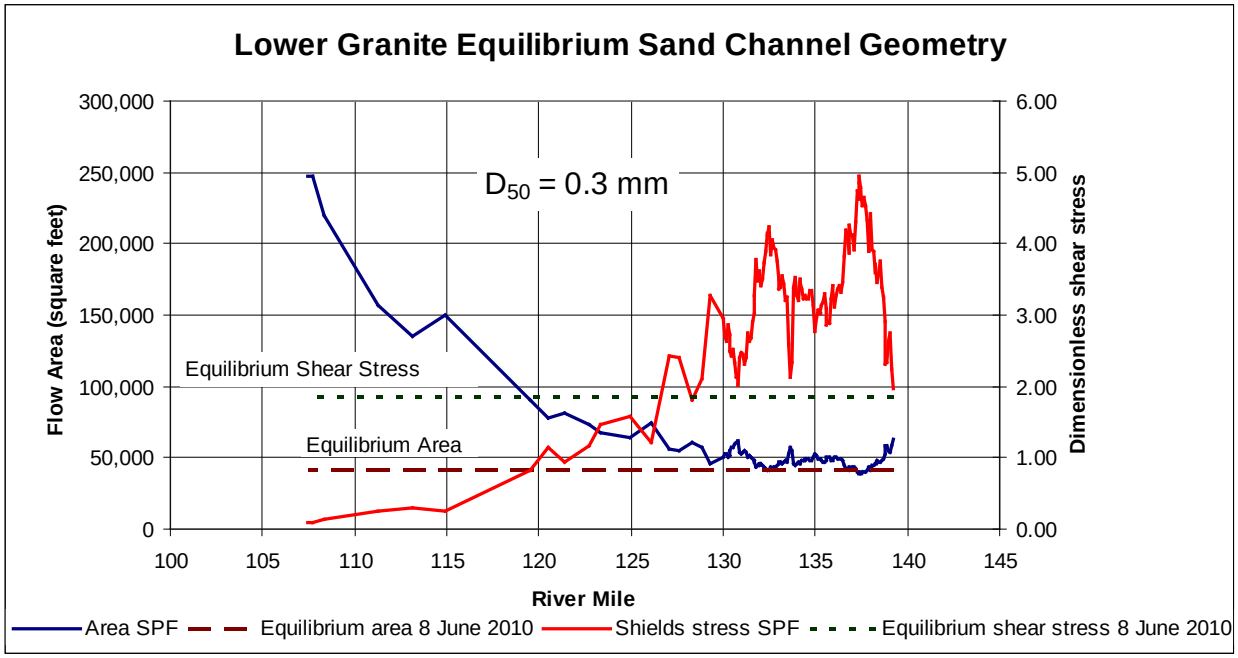


Figure 5. Equilibrium hydraulic geometry of Lower Granite Reservoir of 8 June 2010 at the SPF discharge (D_{50} = 0.3 mm).

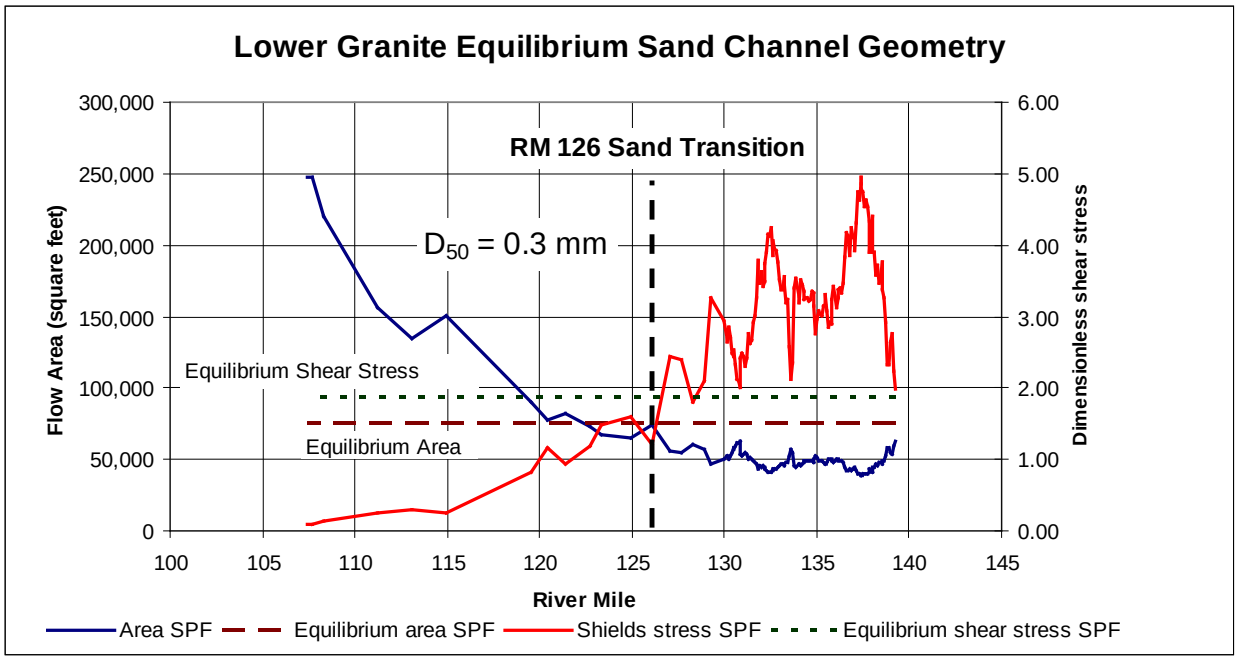


Figure 6. Equilibrium hydraulic geometry of Lower Granite Reservoir for the SPF discharge during the SPF (D_{50} = 0.3 mm).

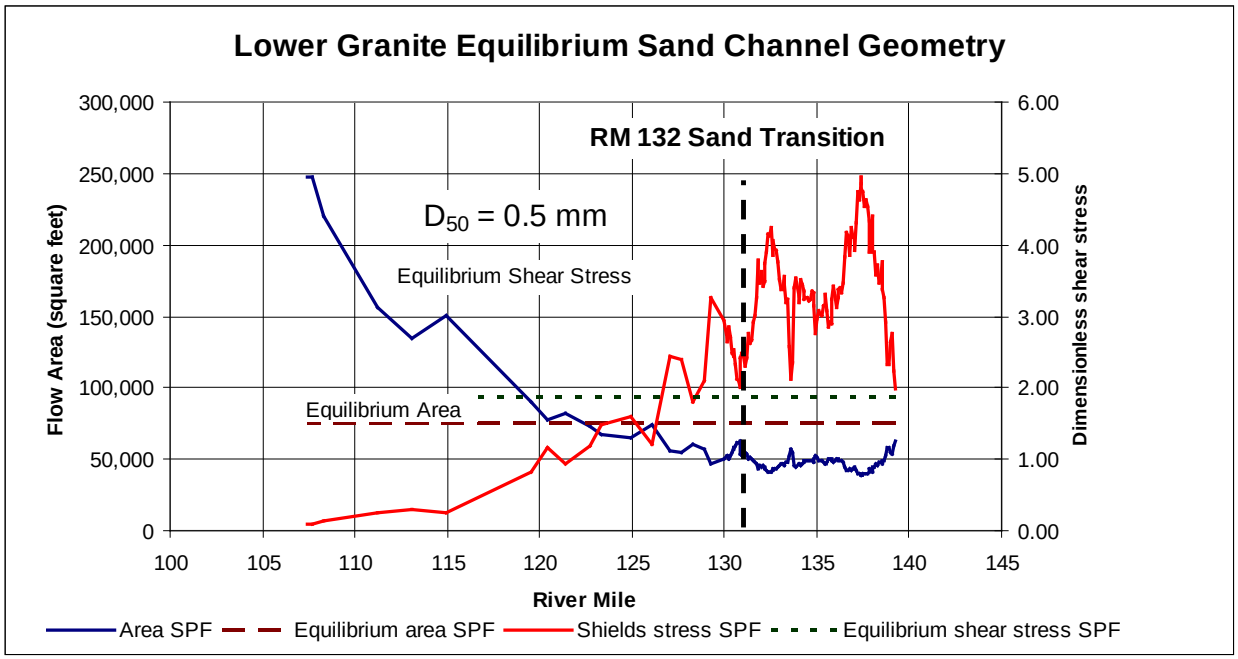


Figure 7. Equilibrium hydraulic geometry of Lower Granite Reservoir for the SPF discharge during the SPF (D_{50} = 0.5 mm).

10.2. Implications of Equilibrium Hydraulic Geometry

The hydraulic geometry assessments performed with the Parker and Lee-Julien relationships yield an informative view of the sediment dynamics of Lower Granite Reservoir. Given the current flood control operations of Lower Granite Dam, during the SPF (or other extreme discharge), fluvial sediment transport processes should form an approximate equilibrium channel that maintains and perhaps increases the conveyance of the upper reach of Lower Granite Reservoir. Sediment eroded from the confluence area will likely be deposited deeper in reservoir where it has less effect on the flood water surface at the Lewiston levees. Unlike freely flowing channels, in Lower Granite Reservoir the forebay elevation at the dam controls the energy gradeline of the water surface so that sediment deposited deeper in the reservoir has less influence on the flood water surface at the confluence. This relatively simple, yet well founded, assessment of the effect of sediment mobility during the SPF strongly suggests that the flood risk analysis of current conditions based on the HEC-RAS 2009 fixed-bed model is conservative and that sediment mobility during extreme discharge events do not significantly heighten flood risk even if sediment loads are substantial. Additionally, the prediction of seasonal equilibrium geometry for Lower Granite suggests that some filling of the channel above Silcott Island should be expected in the future under the prevailing flow regime, but that accumulation is not without limit. The seasonal analysis suggests that the cross section geometry of Lower Granite below the confluence is approaching an equilibrium condition. These findings contrast with previous evaluations of sediment impacts in Lower Granite Reservoir.

Primary uncertainties in the assessment of future and extreme hydraulic geometries are the unknown magnitude, timing and size of the incoming sediment load; hydrologic uncertainties have been addressed in previous sections. Quantity and size of sediment load and characteristics of the antecedent bed determines where deposition begins during extreme events and how much it influences the elevation of the water surface at the confluence. A more complex modeling assessment of sediment load and transport is needed to address these uncertainties. Unavoidably, sediment transport modeling introduces additional uncertainty into the flood risk analysis. The data and reasoning to support development of sediment transport models for Lower Granite Reservoir are presented in the sections below.

10.3. Approach to Sediment Transport Modeling

The hydraulic analysis of future condition is performed with mobile-bed sediment transport models that take into account the sediment volume that is expected to accumulate during the 50-year planning period. The purpose of sediment transport modeling for the flood risk analysis in this assessment is not to develop a precise

simulation of the long-term sediment distribution within the reservoir. Instead, the primary objective is to predict with reasonable confidence the hydraulic conveyance of the Lower Granite Reservoir channel at the end of the 50-year analysis period with and without sediment management actions and features. Sediment dynamics in the upper segment of Lower Granite Reservoir are complex because of the merging partially regulated flows of the Snake and Clearwater Rivers, which often have different water temperatures and variable sediment loads. Ideally, sediment transport and accumulation in the upper reach of the reservoir would be simulated with depth-averaged two-dimensional or three-dimensional models[12], but doing so is not feasible with current modeling technology for the long durations necessary to predict a 50-year future channel condition.

In practice, long-duration sediment transport modeling is performed with one-dimensional hydraulic models coupled with conventional sediment transport functions[13]. Several one-dimensional sediment transport modeling systems are suitable for this analysis including the USACE HEC-RAS system which evolved from HEC6, the proprietary HEC6T[14], the U.S Bureau of Reclamation SRH 1D[15], and the proprietary MIKE 11[16].

Sediment transport modeling for this study was performed with HEC-RAS because it includes sediment transport functions suitable for the analysis of Lower Granite Reservoir and is approved for USACE hydraulic analysis. Sediment deposition and scour in Lower Granite Reservoir has been modeled in previous studies, the earliest being the work by Emmett and Thomas in the early 1970's when the levee system was being constructed[17]. Use of HEC-RAS for mobile-bed modeling also ensures compatibility with the fixed-bed hydraulic modeling (Section 3) for the FDA flood risk analysis. Sediment transport modeling in HEC-RAS does not incorporate

[12] Spasojevic, M and F.M. Holly, Jr. (2008). "Two and three-dimensional numerical simulation of mobile-bed hydrodynamics and sedimentation." *Sedimentation Engineering, Processes, Measurements, Modeling and Practice*, ASCE Manuals and Reports of Engineering Practice No. 110.

[13] Thomas, W.A. and Chang, H. (2008). "Computational modeling of sedimentation processes." *Sedimentation Engineering, Processes, Measurements, Modeling and Practice*, ASCE Manuals and Reports of Engineering Practice No. 110.

[14] http://www.mbh20.com.

[15] http://www.usbr.gov/pmts/sediment.

[16] http://www.mikebydhi.com.

[17] Emmett, W.W. and Thomas, W.A. (1978): "Scour and deposition in Lower Granite Reservoir, Snake and Clearwater Rivers near Lewiston, Idaho, U.S.A.", *Journal of Hydraulic Research*, 16:4, 327-345.

uncertainty directly in sediment deposition and scour computations. As with fixed-bed modeling, the uncertainty of the stage prediction is applied directly in the FDA flood risk computation after development of an appropriate calibrated deterministic model.

10.4. Characterization of the Model Domain

The model domain for the mobile-bed model is the same as for the fixed-bed model and extends from Lower Granite Dam to RM 7.85 on the Clearwater River and RM 148.83 on the Snake River. The initial geometry for most of the mobile-bed simulations were derived from the 2009 sediment range cross sections and the high-resolution bathymetry. Some simulations were also performed with the September 2011 high-resolution bathymetry. The elevation data sources and model domain in the upper reach of Lower Granite Reservoir are shown in Figure 8. An initial step in mobile-bed modeling is to characterize the hydrodynamics and bed sediment of the channels within the model domain. Characterization of the model domain guides the selection of appropriate sediment transport functions and the bed roughness coefficients (Manning's *n*) that control hydraulic resistance during the simulation of sediment transport.

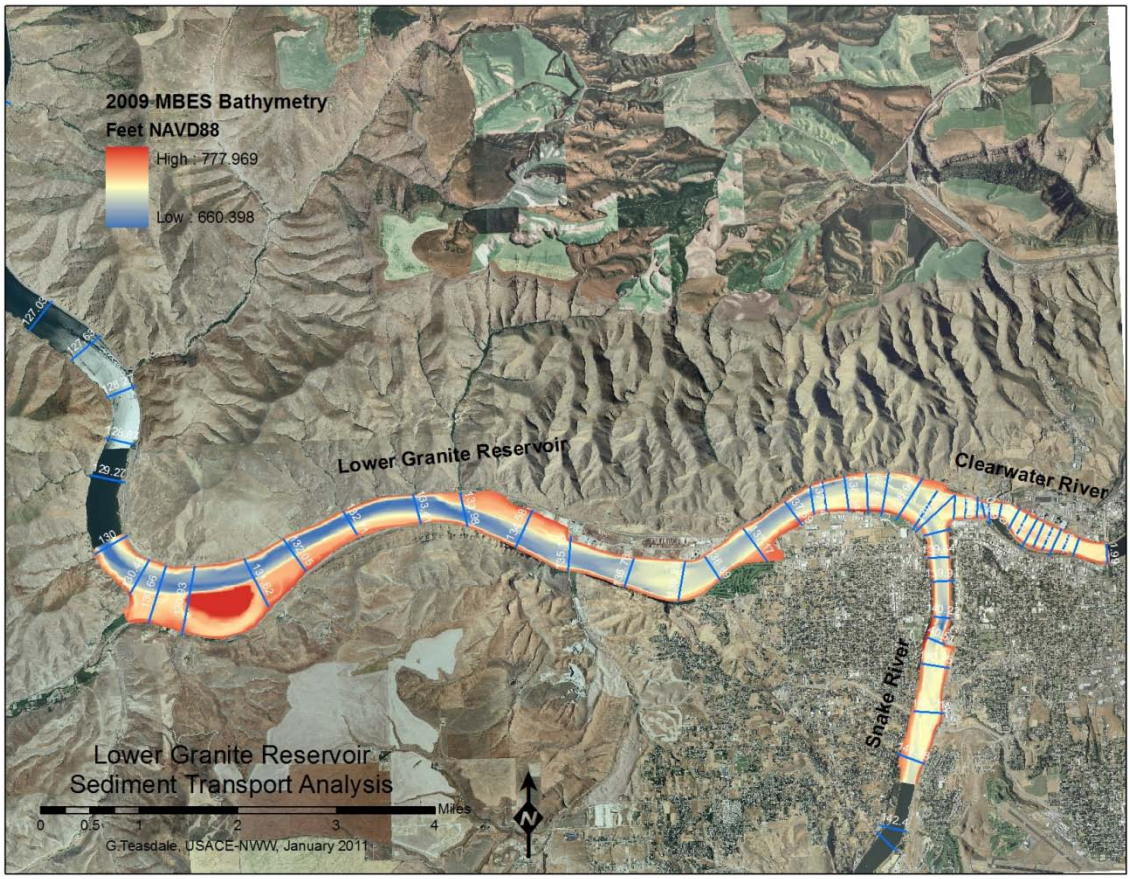


Figure 8. Sediment transport model domain in upper Lower Granite Reservoir.

10.5. Flow Characterization

Flow throughout the model domain is gradually varied and the water surface is classified as an M1 backwater profile[18] for discharges up to and including the Standard Project Flood (SPF). Channel Froude numbers for the Clearwater River and the Snake River in Lower Granite Reservoir computed with the fixed-bed hydraulic model are plotted in Figure 9 for the SPF and 1-percent exceedance discharges. Channel Froude numbers remain well below supercritical for all cross sections and conditions of flow and are less than about 0.3 in the backwater zone. Mean channel velocities and mean bed shear stress for the 50-percent and 1-percent exceedance discharges are plotted in Figure 10 and Figure 11. Within Lower Granite Reservoir, the mean channel velocity peaks at about 9.2 ft s^{-1} and the mean bed shear stress reaches a maximum of about 0.34 lb ft^{-2} at Snake RM 137.4 during the 1-percent discharge. The mean channel velocity and mean bed shear stress during the 1-percent discharge at RM 137.4 is about 2 times the channel velocity and 4 times the bed shear stress during the 50-percent discharge.

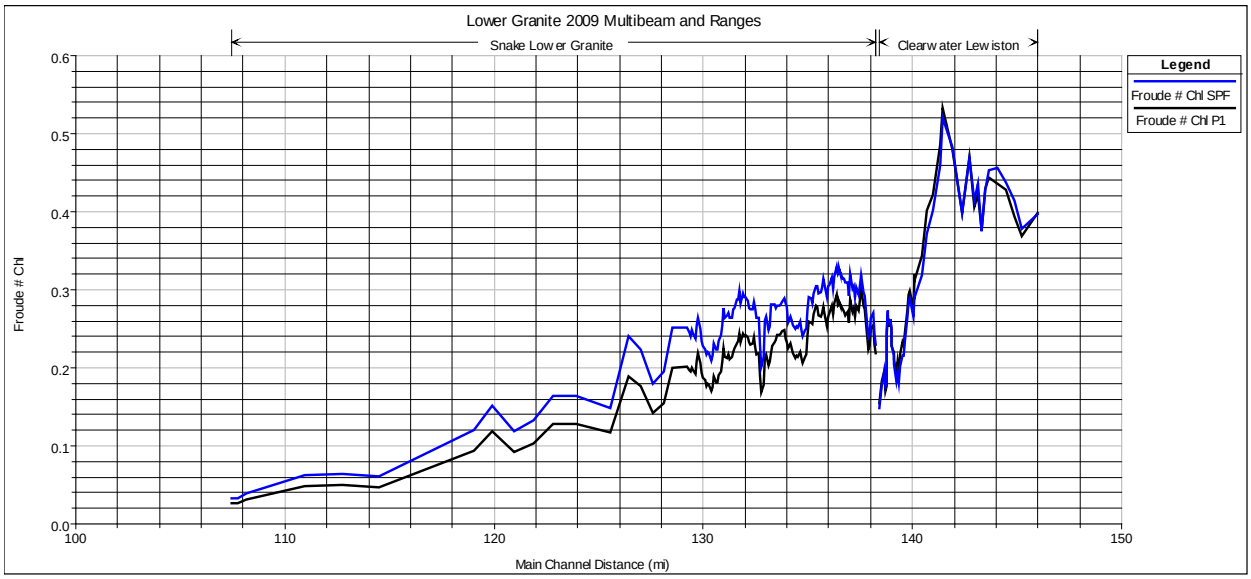


Figure 9. Channel Froude number during SPF and 1-percent exceedance discharge.

[18]Chow, V.T. (1959). *Open Channel Hydraulics*, McGraw-Hill.

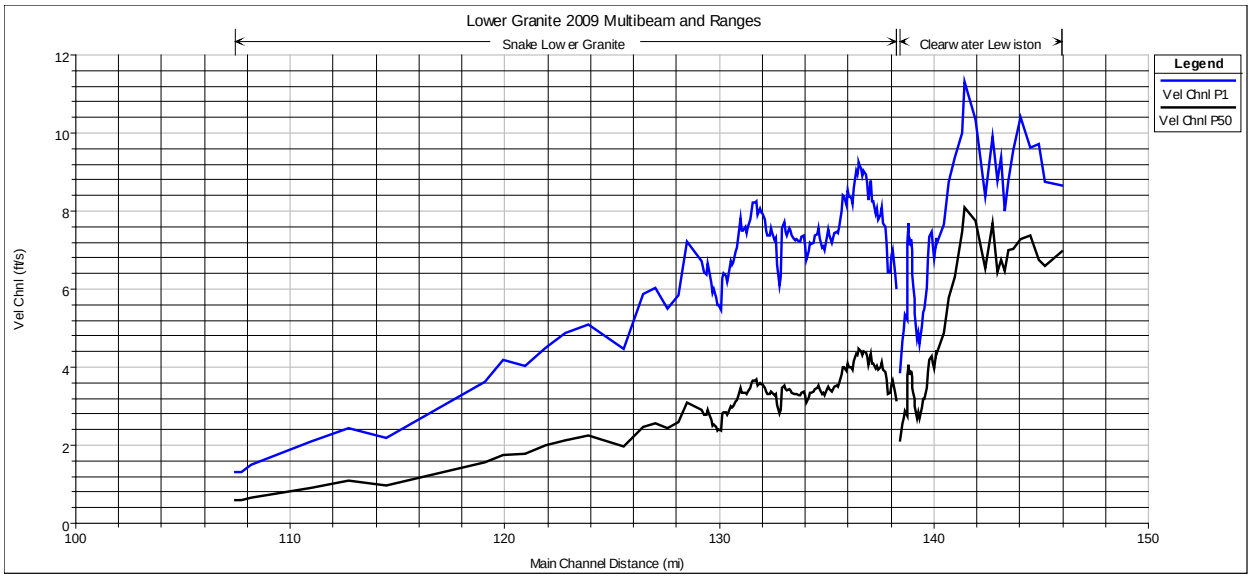


Figure 10. Mean velocity during 50-percent and 1-percent exceedance discharges.

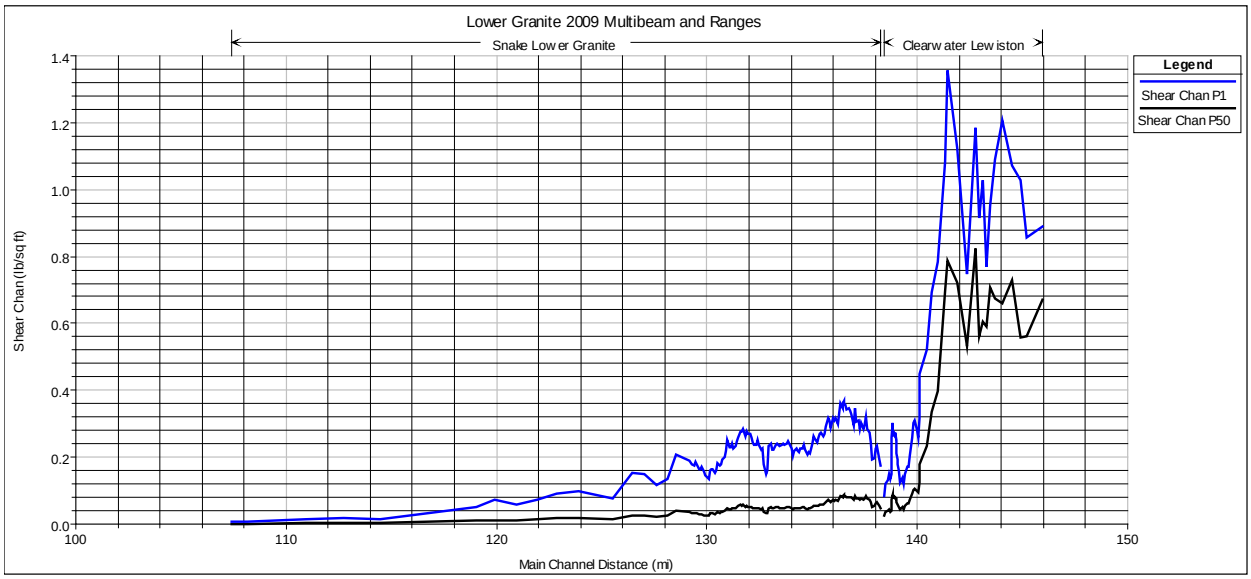


Figure 11. Mean bed shear stress during 50-percent and 1-percent exceedance discharges.

10.6. Mobile-bed Channel Characteristics

Sediment load and bed sediment characteristics influence flow resistance and guide the selection of sediment transport functions. The Snake and Clearwater Rivers in and upstream of Lower Granite Reservoir are confined by steep canyon topography, roads and the levee system, so there are no appreciable bank and floodplain sources of sediment. The plan-form and general shape of the run-of-the-river reservoir channel is

controlled by topography and cannot be substantially altered under the reduced hydraulic gradient in the backwater zone of the dam. Elements of the imposed topography includes canyon bends, original islands, bridge structures, constructed revetments, armored channel beds, bedrock protrusions, and constrictions between resistant banks in the original channel.

Mobile-bed hydraulic resistance factors and sediment transport functions are different for gravel beds, sand beds and silt beds, so it is necessary to identify transitions between bed types in the model domain. Three transitions of bed material in Lower Granite Reservoir channels are identified by sediment transport principles, the equilibrium hydraulic analysis above, and analysis of the bathymetric data. Transitions from gravel-cobble beds to sand beds occur in the Clearwater River at about RM 1.66 (Figure 12) and between the Snake River RM 141.5 and RM 142.5 (Figure 13). The moderately sloped (5 ft/mile) gravel-bed channels above the backwater zone transport the sand and silt loads in suspension. The bed load measurements, sediment cores and the historic sediment range cross sections show that negligible amounts of gravel are transported into Lower Granite under the prevailing partially regulated flow regime.

As the sand settles from suspension in the backwater zone, the channels change from armored and stable (threshold) gravel-cobble beds to beds in which bedload moves predominately as sand waves (bedforms). During the peak seasonal flows very little sand accumulates in the Snake River channel upstream of the confluence. As flow declines, sand settles from suspension to form a persistent dune field that begins below Southway Bridge and transits to the confluence without significantly altering the relatively stable mobile-bed hydraulic conveyance of the reach. Dredging is not necessary to maintain navigation of the Snake River above the confluence, though deposition of fine sediment impairs use of the boat basins and launches in Chief Looking Glass Park (Asotin), Swallows Nest Park (Clarkston) and Confluence Park (Clarkston).

On the Clearwater River, dunes begin to form below Memorial Bridge and substantial amounts of sand accumulate in the commercial navigation channel and towboat turning basin within the Lewiston levee system at the Port of Lewiston. Sediment deposits that encroached into the 14 foot deep navigation channel in 2009 are mapped in Figure 16.

Sand from the Snake and Clearwater Rivers is transported through the upper reach of Lower Granite Reservoir as both bedload (sand waves) and suspended load. Fine sand and silt deposit in the margins of the reservoir and impair commercial navigation at the Port of Clarkston below the confluence. The amount of sand in suspension decreases with downstream distance as the energy slope of the reservoir decreases. Sand dunes are largest in the stable segment near the Port of Wilma, then decrease in size as the channel approaches Silcott. Sand bedforms diminish and are

not observable in the high-resolution bathymetry where the channel widens and deepens below Silcott Island. This indicates a transition from a bed dominated by sand to a bed that is predominately silt. A silt transition is observed at about RM 130.6 in the 2009 low flow bathymetry (Figure 14). High discharge during 2011 extended sand waves further into the reservoir and the silt transition now occurs at about RM 128.8 (Figure 15). Sediment transport computations show a transition from sand-bed to silt-bed below Silcott at about RM 129. Sediment transport modeling also shows that most coarse and medium size silt is retained in the reservoir below Silcott. Some fine silt and most clay size material passes through the Lower Granite lock and dam.

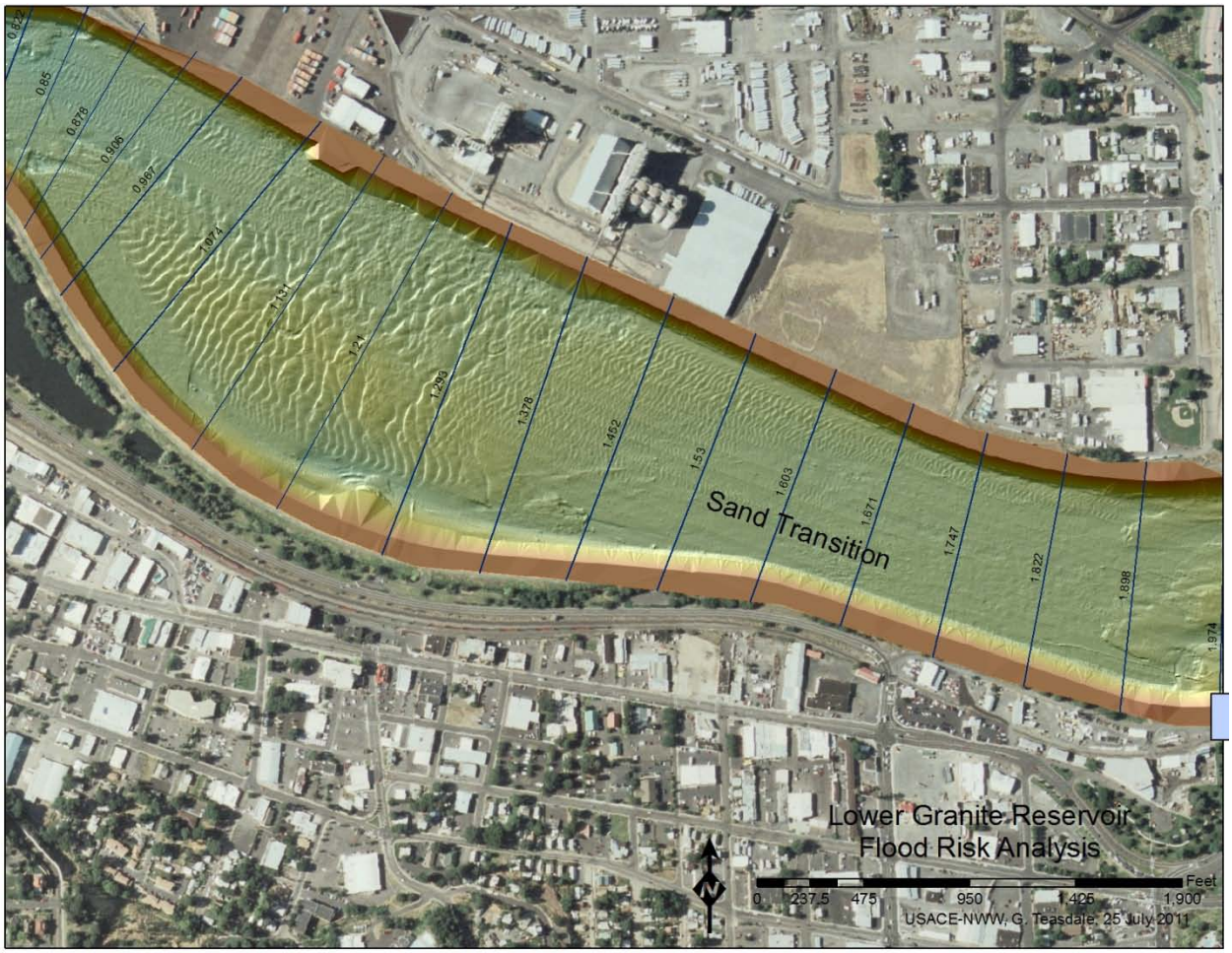


Figure 12. Sand transition at Clearwater River Mile 1.66.

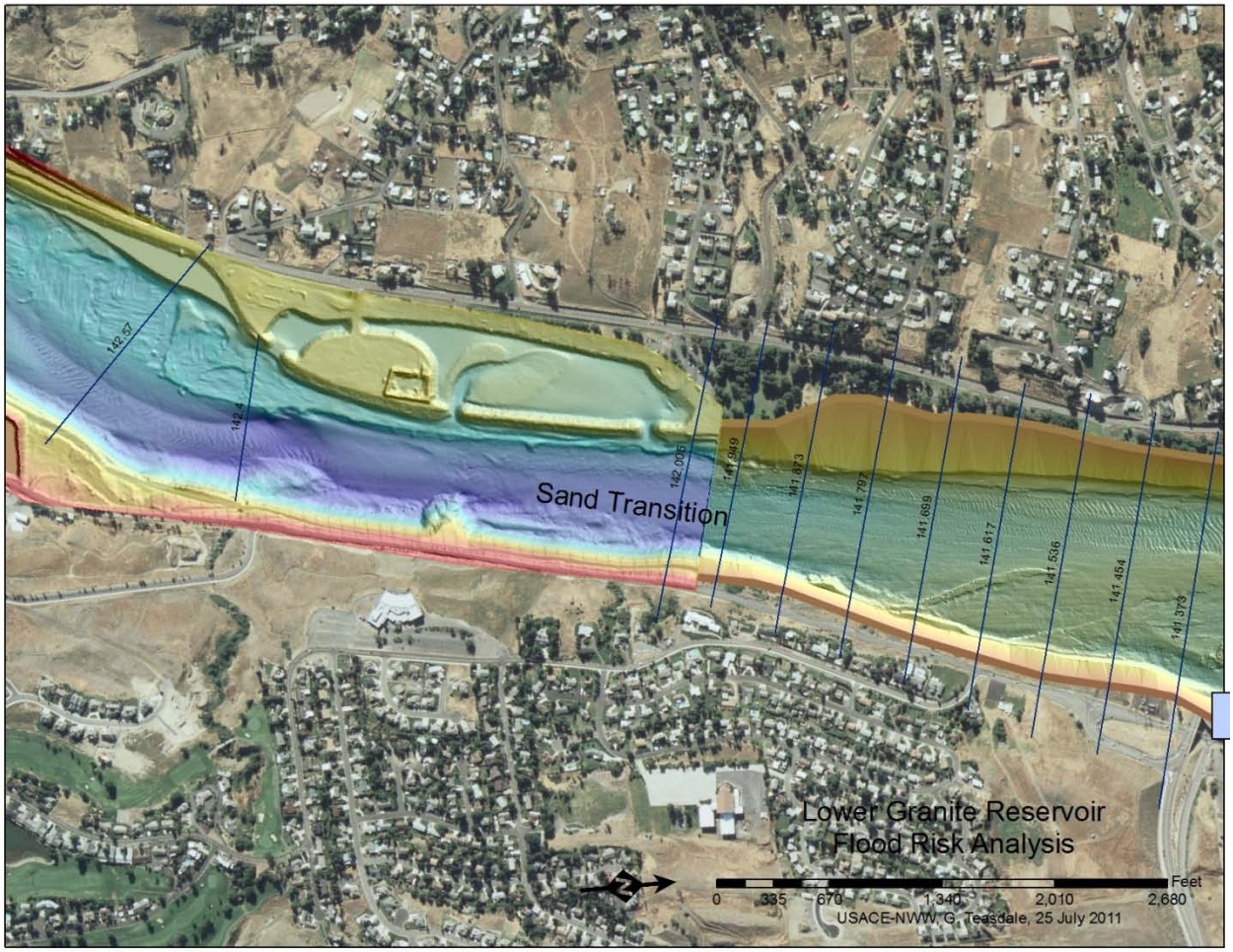


Figure 13. Sand transition at Snake River Mile 141.21.

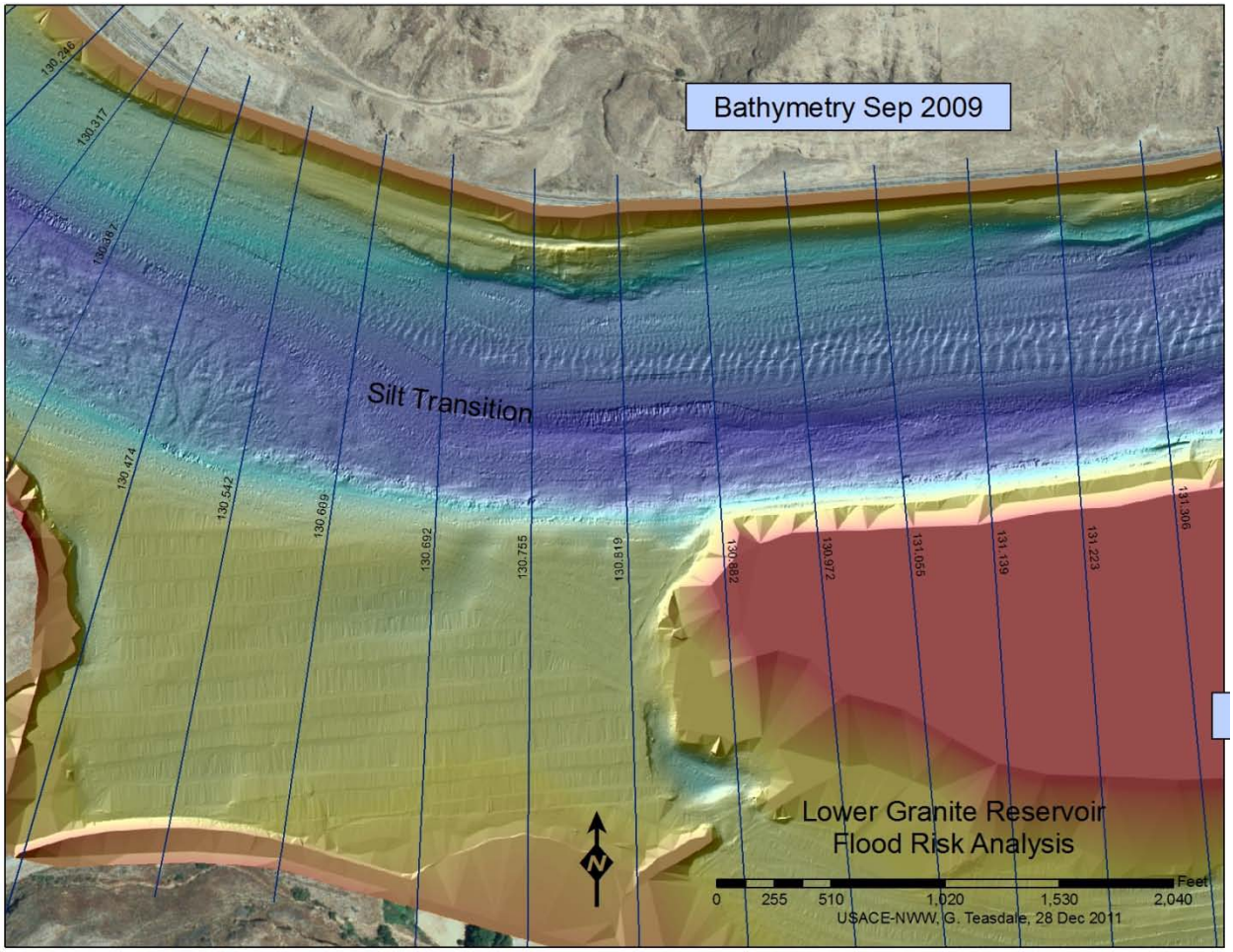


Figure 14. Silt transition at Snake River Mile 130.66 September 2009.

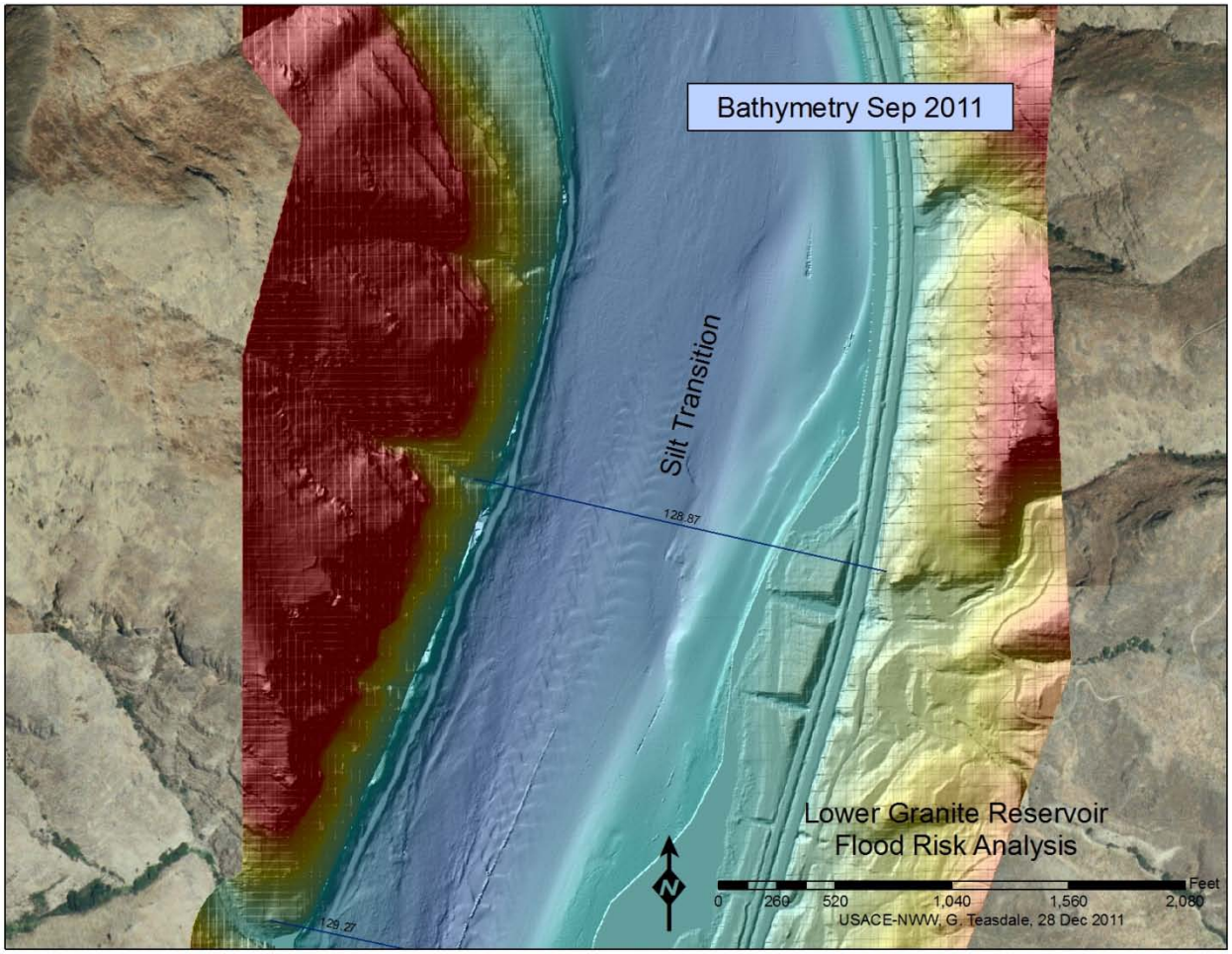


Figure 15. Silt transition at Snake River Mile 128.87 September 2011.

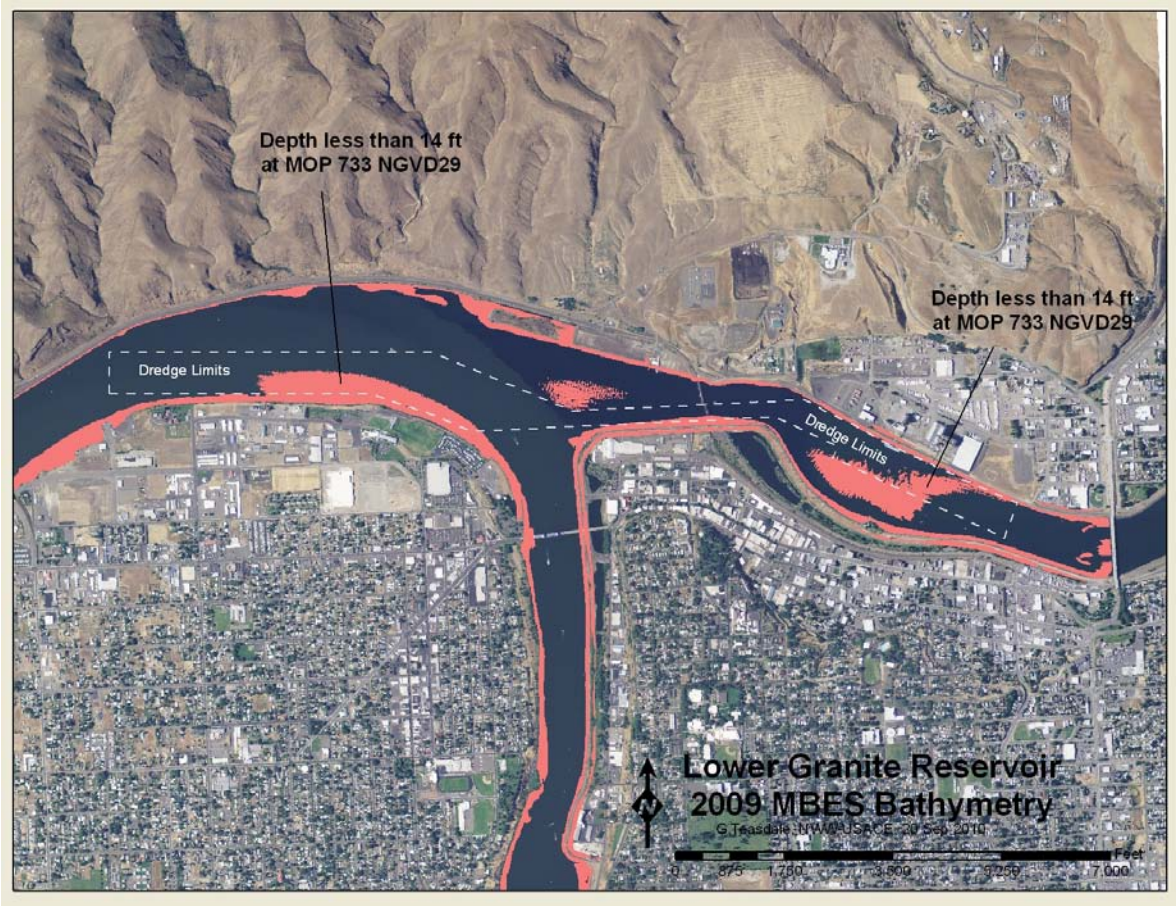


Figure 16. Sediment encroachment in 2009 on navigation channels at the confluence.

10.7. Underwater Video Mapping Survey

The bed-material transitions and bed types are confirmed by the USGS sediment coring data discussed in Section 7 and an underwater video mapping survey performed by USGS in 2009 and 2010. In the mapping survey, video clips of the bed surface were acquired with an underwater video camera at the locations of sediment range cross sections. Examples of still image captures of the video imagery are in Figure 17, Figure 18 and Figure 19. The converging red lines in the images are laser lines that aid in judging the proximity of the camera to the bed. Geographic coordinates, time, image identification number, and depth in meters are imprinted on the image. Figure 17 was acquired at Snake RM 141.21 and shows gravel and cobble in the bed material transition zone. Gravel and cobble material in the bed transition zone at Clearwater RM 1.66 is seen in Figure 18 . A typical video image of sand that deposited in the confluence at Snake RM 139.23 is in Figure 19.

A bed sediment (facies) GIS data layer was developed by USGS for Lower Granite Reservoir by interpretation of the video imagery and bathymetry. Bed sediment was classified into categories of bedrock, gravel-cobble, sand and silt with coarse and

fine subcategories based on qualitative interpretation of particle size. The difference between gravel-cobble and sand is readily apparent, but the difference between fine sand and silt is difficult to distinguish in images acquired in deeper water. Classifications of silt in the USGS data layer below Silcott conflict somewhat with the sediment core data, which was not available at the time USGS developed the facies map. Maps images made from the USGS facies data layer in Figure 20 and Figure 21 show that the differences in surface bed material follow the lines of flow in the reservoir. Bed features that existed before the reservoir was filled can be observed in the historic sediment ranges, high-resolution bathymetry and facies map. The persistence of these features indicates that sand bedload is selectively transported in the deeper portions of the channel.



Figure 17. Underwater video image at gravel-cobble bed to sand bed transition Snake RM 141.21.



Figure 18. Underwater video image at gravel-cobble bed to sand bed transition Clearwater RM 1.66.



Figure 19. Underwater video image of sand bed at Snake RM 139.23.

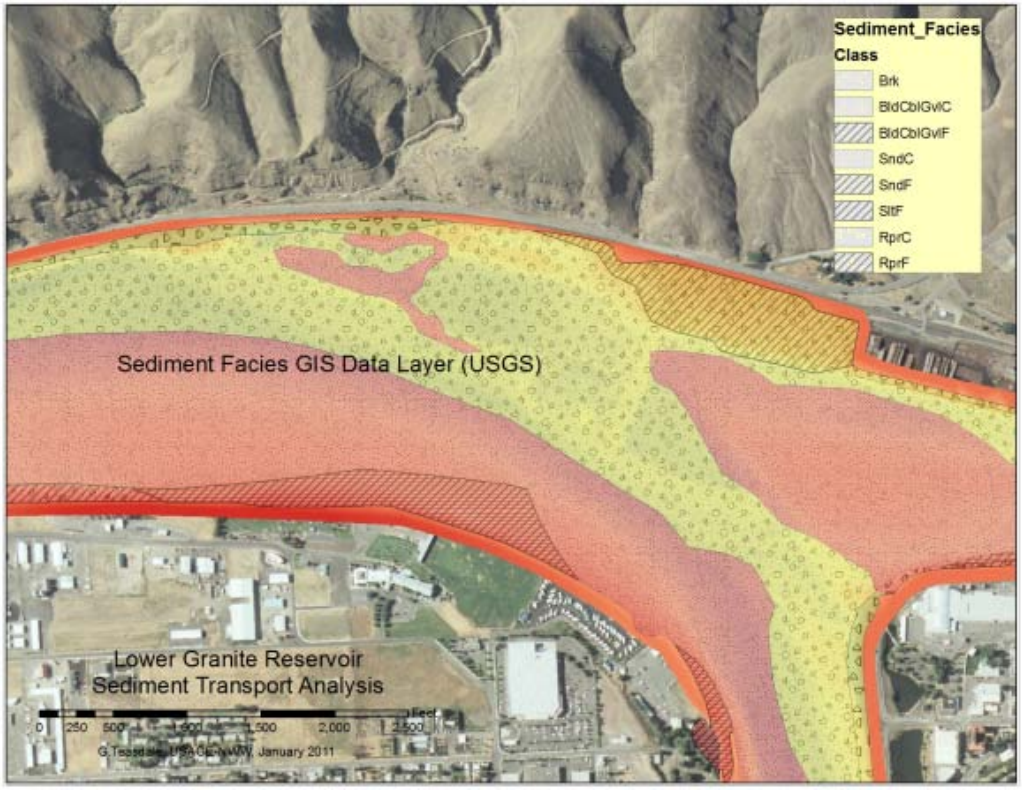


Figure 20. Sediment facies map of confluence Snake RM 139.3.

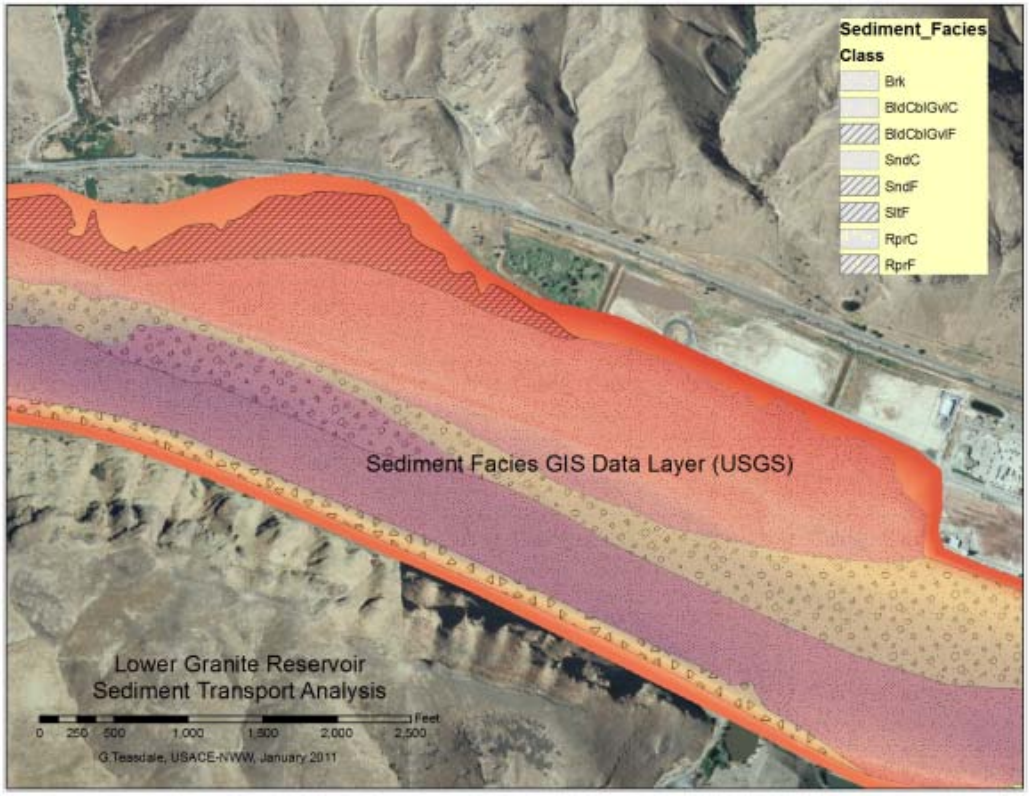


Figure 21. Sediment facies map of confluence near Port of Wilma Snake RM 135.

10.8. Bedforms and Hydraulic Resistance

The hydraulic resistance (roughness or flow resistance) of a mobile bed can change dramatically during the rise and fall of a flood hydrograph. The effect of variable flow resistance on the peak water surface elevation (flood stage) is an important consideration in flood modeling, particularly when evaluating the capacity of levees and dikes in sand bed channels[19,20]. Flow resistance in Lower Granite Reservoir varies as sand bedforms change with discharge. Mobile boundary flow resistance is the combined effect of flow resistance due to shear stress on the individual sediment grains (grain or skin resistance) and resistance to flow induced by pressure differential and energy loss in the eddies that form downstream of bedforms (form drag) [21,22]. Boundary channel properties including bank roughness, channel bends and channel transitions (expansion and contraction) also affect hydraulic resistance but are relatively invariant during normal flows compared to changes in flow resistance produced by bed mobility. All components of roughness may change significantly with the rise of stage in a large flood. Sand bedforms (sand waves) are also prevalent in coastal inlets and navigation channels[23] and share many similarities in development and hydrodynamic performance as riverine sand bedforms.

Separation of the sources of hydraulic resistance is important in mobile bed analysis because the component of bed shear stress that is attributable to form resistance does not directly contribute to sediment transport[24]. In the case of Lower Granite Reservoir, the effect of bedforms on hydraulic resistance must be understood to correctly model the flood water surface during extreme flows when the sand bed of the main channel is very mobile. Erroneous roughness values in the hydraulic model of a

[19] Julien, P.Y. and G.J. Klaassen (1995). "Sand-dune geometry of large rivers during floods", *Journal of Hydraulic Engineering*, 121(9), 657-663.

[20] Julien, P.Y., G.J.Klaassen, W.B.M. Ten Brinke and A.W.E Wilbers (2002). "Case Study: Bed Resistance of Rhine River during 1998 Flood" , *Journal of Hydraulic Engineering*, 128(12), 1042-1050.

[21] Einstein, H.A. and N.L. Barbarossa. (1952) "River Channel Roughness", *Trans. ASCE*, 117, 1121-1146.

[22] Van Rijn, L.C. (2007). "Unified View of Sediment Transport by Currents and Waves. I: Initiation of Motion, Bed Roughness, and Bed-Load Transport", *Journal of Hydraulic Engineering*, 133(6), 649-667.

[23] Whitmeyer, S.J. and FitzGerald, D. (2006). *Sand Waves That Impede Navigation of Coastal Inlet Navigation Channels*, CHETN-V-68, U.S. Army Corps of Engineers, Engineering Research and Development Center, Vicksburg, MS.

[24] Einstein, H.A. (1950). "The Bedload Function for Bedload Transportation in Open Channel Flows." Technical Bulletin No. 1023, U.S.D.A., Soil Conservation Service, 1-71.

levee channel could lead to an incorrect characterization of the flood reduction capacity of the levee system.

Evolving sand bedforms generally follow an often observed progression: 1) flow upon a static bed in which there is negligible sediment movement, 2) formation of ripples as the bed becomes mobile, 3) development of mega-ripples and dunes with large rates of sediment transport, 4) washed-out of dunes and formation of a plane bed with active sediment transport, 5) formation of antidunes with high rates of transport, and 6) formation of a chute and pool bed that verge on debris flows[21,25]. Dunes are the ultimate bedform in many large sand-bed rivers when flows are subcritical, resulting in surface water waves that are out of phase with the bed sand waves[19,26]. Such is the case in Lower Granite Reservoir during typical seasonal discharges.

Channels that do not progress beyond the formation of dunes are said to be in the lower bedform regime[25]. Large dunes in the lower bed regime impose the greatest amount of form resistance. As discharge approaches critical flow (high Froude number), an indefinite threshold of shear stress is crossed and dunes begin to diminish. Sufficiently high discharges cause dunes to washout, forming a mobile planar bed which imposes dramatically less form resistance. At even higher discharges, anti-dunes form that are in phase with water surface waves. A channel that forms a plane mobile bed or anti-dunes during high discharge is said to be in the upper bed regime. Chutes and pools form at extremely high discharges and are also considered to be in the upper flow regime. The transition between lower and upper regime occurs over a range of flows and cannot be precisely predicted. In practice, semi-empirical relationships, such as those discussed below, are used to predict the formation of bedforms and the likely bed regime at particular discharges.

Ripples and dunes remain on the surface of the channel bed after flows decrease and become part of the low-flow static bed geometry. The 2009 high resolution bathymetry was acquired during the low discharge period in late summer and early fall. A field of primary dunes near the Port of Wilma is seen in the bathymetry image in Figure 22. Primary dunes are large dunes that dominate the bedform population during the rising stage of the flood hydrograph. Primary dunes typically have wavelengths in excess of 60 ft and increase 2–3 times in length during the floods. The bed profile in Figure 23 shows that the height (amplitude) of the largest dunes is about 4 ft and the average wavelength is about 120 ft. Secondary dunes generally develop on top of large dunes during the falling stage of the hydrograph and are typically less than 50 ft in

[25] Simons, D.B. and F. Senturk (1976). *Sediment Transport Technology*, Water Resources Publications, Littleton, CO.

[26] Wright, S. and G. Parker. (2004) "Flow resistance and suspended load in sand-bed rivers: simplified stratification model", *Journal of Hydraulic Engineering*, 130(8), 796-805.

length[19]. It is evident in Figure 22 that the sizes of the dunes vary greatly across the channel. Size and orientation of dunes vary throughout the upper reach of Lower Granite Reservoir even though the peak discharge is essentially the same at all locations in the reach. The bed profile depicted in Figure 24 and plotted in Figure 25 shows that larger dunes evolve upstream and downstream from the channel highpoint near RM 136.3. The historic topographic map in Figure 26 shows that the highpoint point is a submerged island that existed prior to the construction of Lower Granite Dam. Secondary flow patterns, the gradually varied water surface profile and conditions of partial transport (supply limited) heighten the variability in the spatial distribution of bedforms.

A more extensive analysis of sand wave development in Lower Granite Reservoir is presented in Section 15, including comparisons of bathymetry datasets acquired at high and low discharges. That section shows that the existence and prevalence of large sand bedforms in Lower Granite Reservoir are well documented by the field surveys undertaken in this study.

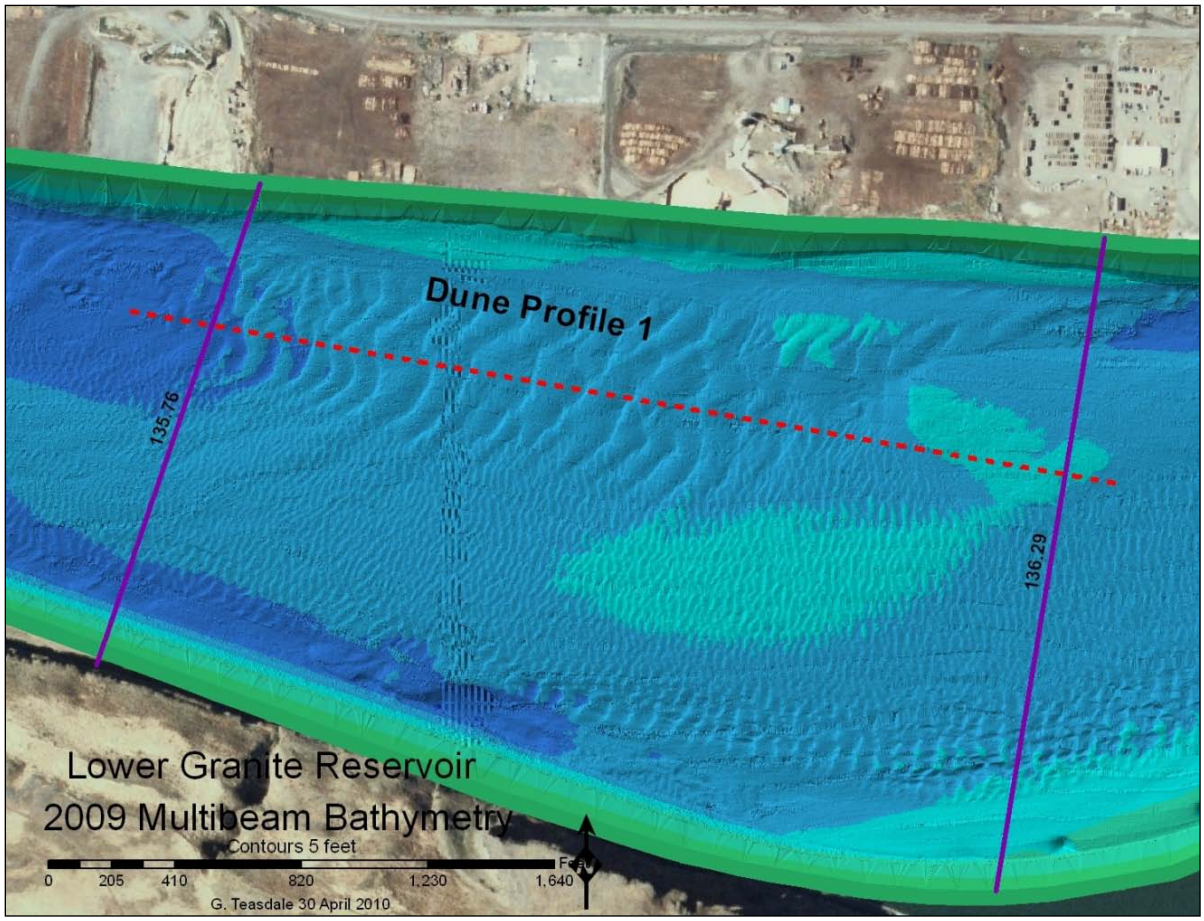


Figure 22. Sand dunes on the Snake River in Lower Granite Reservoir.

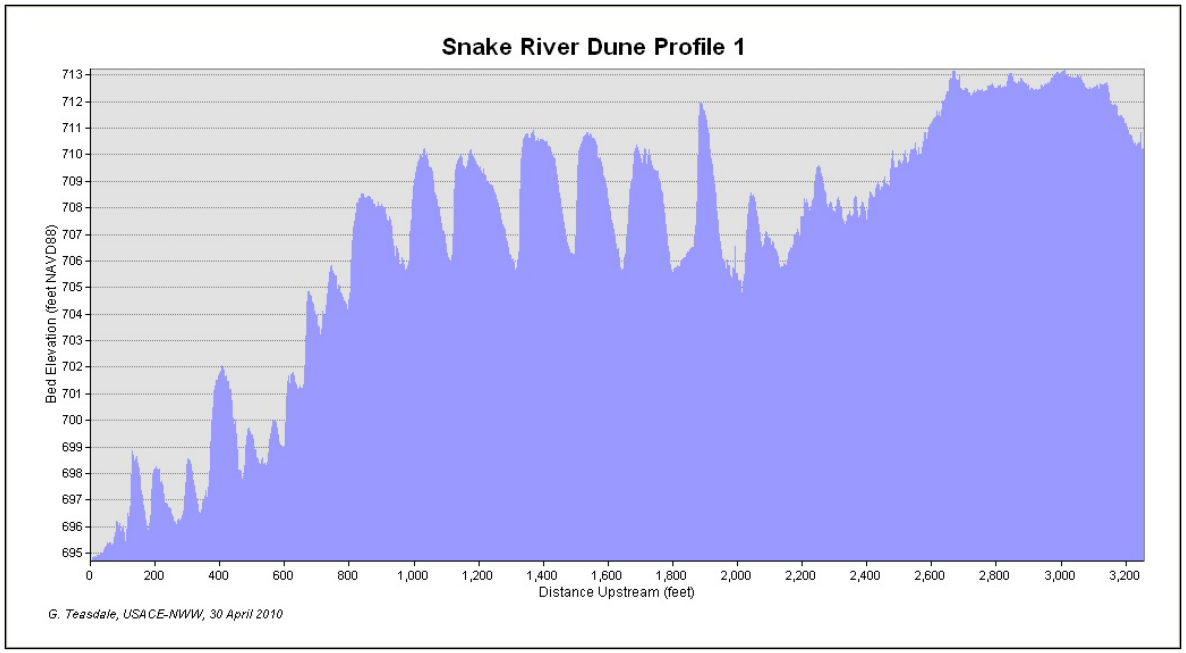


Figure 23. Profile of sand dunes in Figure 22.

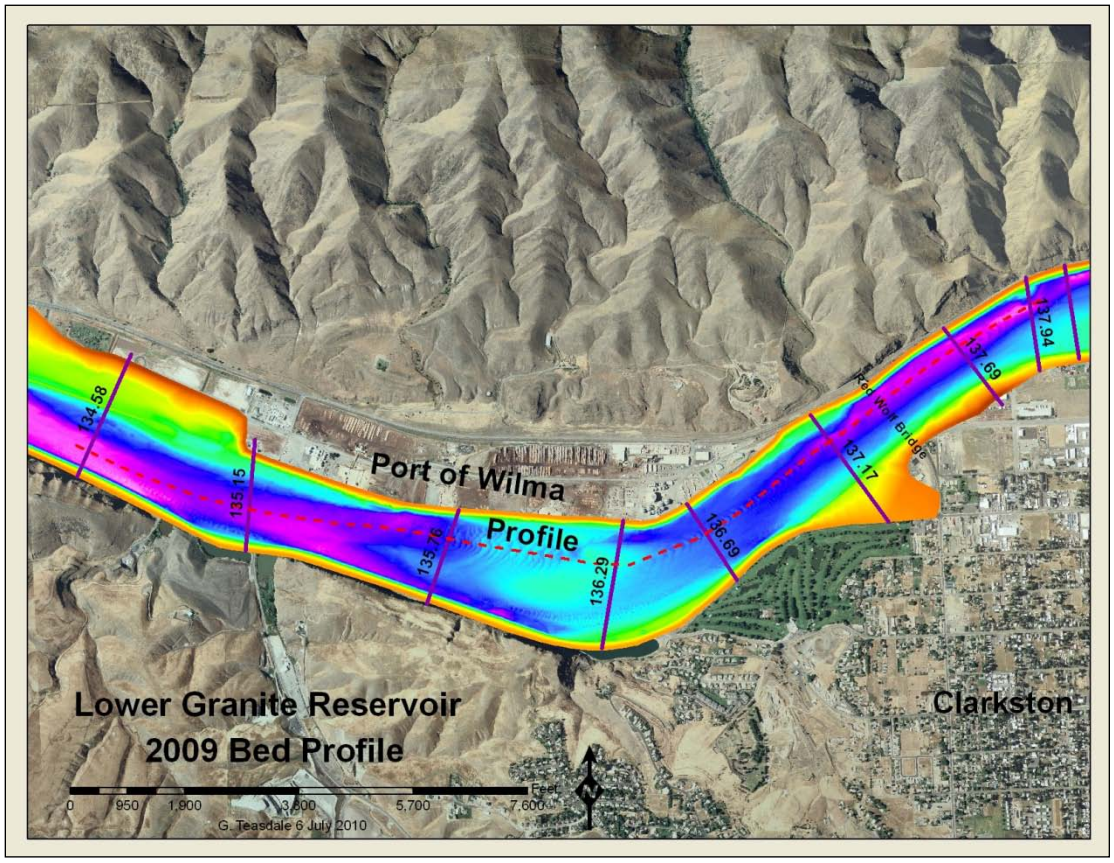


Figure 24. Bed profile transect Snake River Mile 134.58 - 137.94, bathymetry 2009.

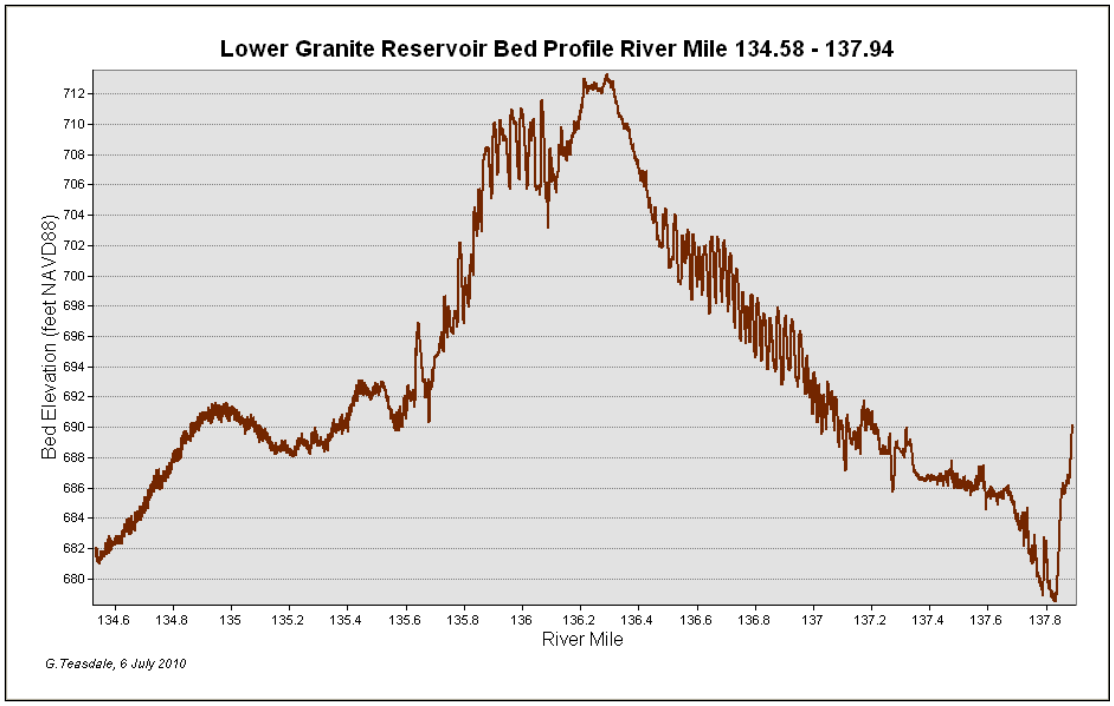


Figure 25. Bed profile plot Snake River Mile 134.58 - 137.94, bathymetry 2009.

.

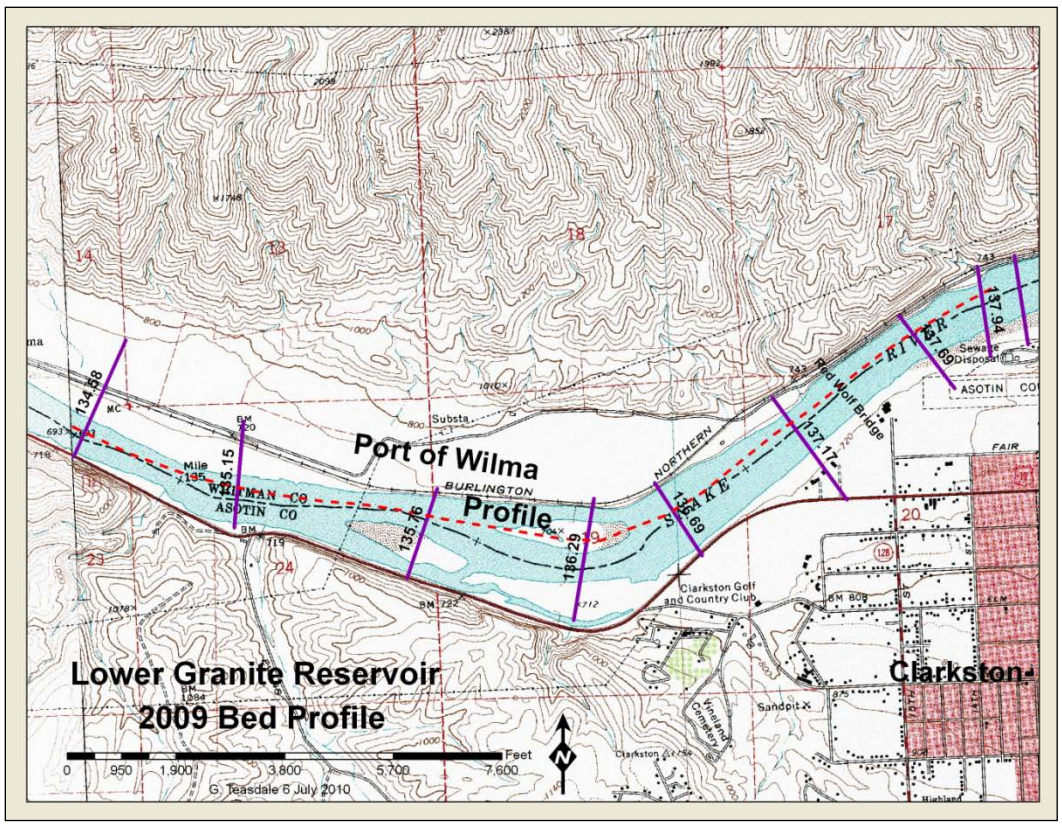


Figure 26. Bed profile transect Snake River Mile 134.58 - 137.94, USGS 1970 DRG.

10.9. Mobile-bed Flow Resistance

Operational multidimensional hydraulic modeling software cannot yet accurately simulate the physical processes that produce the morphology and variation of sand dunes in complex riverine or estuary channels, and currently there is no practical methodology by which flow resistance may be estimated from a spatially diverse dune field directly from measurements of mobile bedforms. In practice, hydraulic resistance must be estimated from empirical relationships for mobile-bed channels. Many empirical relationships have been developed that can estimate hydraulic resistance in sand-bed channels and these are often linked to stage-discharge predictors and bed transport functions. Methods include those by Brownlee[27], Engelund[28], Nelson and Smith[29], Van Rijn[22], Julien et al [30,31], and Wright and Parker[26]. Mobile-bed resistance formulations generally include a method to predict bed regime as a function of discharge because of its prominent effect on hydraulic resistance.

The effect of bedforms on flow resistance in Lower Granite can be demonstrated with the Nelson-Smith bed shear stress partition directly from measured bedform dimensions and flow measurements. In a formulation presented by Garcia[35], bed shear due to bedforms may be computed with the relationship

$$\tau_{bf} = \tau_b - \tau_{bs} = \frac{1}{2} C_D \frac{\Delta}{\lambda \kappa^2} \left[\ln\left(30 \frac{\Delta}{k_s} \right) - 1 \right]^2 \tau_{bs}$$

where τ_b is the total bed shear stress, τ_{bs} is the bed shear stress due to skin friction and τ_{bf} is the bed shear due to bedforms. Other parameters include the dune height Δ, dune length λ, the von Karmen coefficient κ (0.41), and grain roughness height k_s is estimated as 2.5 D_{50}. For example, the total bed shear stress at Snake RM 136 near the peak of the seasonal discharge on June 8, 2010 was 0.07 lb/ft^2 at the location where the dune height was 4 ft, dune wavelength was 120 ft, and the median grain size was 0.3 mm.

[27] Brownlie, W.R. (1983). "Flow depth in sand-bed channels", *Journal of Hydraulic Engineering*, 109(7), 959-990.

[28] Engelund, F. (1966). Hydraulic resistance of alluvial streams", *Journal of the Hydraulics Division*, ASCE 100, 1631-1648.

[29] Nelson, J.M, Smith, J.D. (1989) "Flow in meandering channels with natural topography." River meandering, S. Ikeda and G. Parker, eds. *Water Resources Monograph No. 12*, American Geophysical Union, Washington D.C., 69-102.

[30] Julien, P.Y., Klaassen, G.J. (1995) "Sand dune geometry of large rivers during floods." *Journal of the Hydraulic Engineering*, 121(9), 657-663.

[31] Julien, P.Y., Klaassen, G.J., Ten Brinke, W.B.M., Wilbers, A.W.E. (2000) "Case study: bed resistance of Rhine River during 1998 flood." *Journal of the Hydraulic Engineering*, 128(12), 1042-1050.

By direct solution of the Smith-Nelson relationship, bedforms are shown to account for approximately 66 percent of the total bed shear stress. Relationships such as the Nelson-Smith partition cannot be used to directly estimate stage because total bed shear stress must be known to partition the shear stress into components.

Other empirical relationships can estimate stage in a mobile bed channel for a given discharge and do not depend on direct measurement of bedforms. Brownlee developed a method based on an extensive dataset of sediment measurements from laboratory and natural channels including large sand-bed rivers[32], and is a method described in USACE engineering guidance[33] and incorporated into HEC-RAS stable channel design functions (Copeland method)[34]. Brownlie's method can be expressed as a set of equations for the hydraulic radius and Manning's *n* value for the lower and upper bed regimes,

$$R_{lower} = 0.3724 q_*^{0.6539} S^{-0.2542} \sigma^{0.1050} d_{50}$$

$$R_{upper} = 0.2836 q_*^{0.6248} S^{-0.2877} \sigma^{0.0813} d_{50}$$

$$q_* = \frac{q}{\left(g d_{50}^{\ 3}\right)^{0.5}}$$

$$n_{lower} = \left[1.6940 \left(\frac{R}{d_{50}} \right)^{0.1374} S^{0.1112} \sigma^{0.1605} \right] 0.034 \left(d_{50}\right)^{0.167}$$

[32] Brownlie, W.R. (1985). "Compilation of Alluvial Channel Data", *Journal of Hydraulic Engineering*, 111(7), 1115-1119.

[33] USACE (1994). Chapter 5, "Methods for predicting n values for the Manning equation", *EM 1110-2-1601 Hydraulic Design of Flood Control Channels*, U.S. Army Corps of Engineers, Washington, DC.

[34] USACE (2010)."Stable channel design functions', *HEC-RAS River Analysis System Hydraulic Reference Manual, Ver. 4.1*, January 2010, Hydrologic Engineering Center, U.S. Army Corps of Engineers, Davis, CA.

$$n_{upper} = \left[1.0213 \left(\frac{R}{d_{50}} \right)^{0.0662} S^{0.0395} \sigma^{0.1282} \right] 0.034 (d_{50})^{0.167}$$

where n is the Manning's roughness factor for the lower and upper regimes, R is the hydraulic radius of the channel (ft), d_{50} is the median grain size of the sediment (ft), S is the bed slope in uniform flow or the slope of the energy grade line in gradually varied flow, σ is the geometric standard deviation of the sediment mixture (mm), q is the specific discharge ($ft^2\ s^{-1}$), and g is the acceleration of gravity ($ft\ s^{-2}$).

Brownlie found that the transition from lower to upper regime is a function of grain Froude number,

$$\text{If } F_g \leq \frac{1.74}{S^{1/3}}, \text{ then the channel is in lower regime}$$

$$\text{If } F_g > \frac{1.74}{S^{1/3}}, \text{ then the channel is in upper regime}$$

The grain Froude number is computed,

$$F_g = \frac{V}{\left[(s_s - 1) g d_{50} \right]^{0.5}}$$

where F_g is the grain Froude number, V is the flow velocity ($ft\ s^{-1}$), s_s is the specific gravity of the sediment particles, g is the acceleration of gravity ($ft^3\ s^{-1}$). The maximum slope at which lower regime occurred in Brownlie's dataset was about 0.006 (0.6%); there is a high degree of certainty that channels with bed gradients greater than 0.6% will be in upper regime. Brownlie's journal paper[32], engineering guidance developed by USACE and sedimentation engineering texts present additional details of Brownlie's method[33,35,36].

Brownlie's empirical relationships were used to predict the bed regime and mobile bed properties of Lower Granite Reservoir during extreme discharges. With Brownlie's relationships, the regime hydraulic radius is computed for a given discharge,

[35] Garcia, M.H. (2008). "Sediment Transport and Morphodynamics." *Sedimentation Engineering, Processes, Measurements, Modeling and Practice*, ASCE Manuals and Reports of Engineering Practice No. 110.

[36] Chang, H. (1988). *Fluvial Processes in River Engineering*. Krieger Publishing Company, Malabar Florida.

energy gradient, and sediment size. The hydraulic radius is approximately equivalent to the average flow depth in a relatively wide reservoir channel. The likely bed regime is indicated using the slope test of the grain Froude number. With the likely bed regime identified, Manning's *n* and equilibrium sediment concentration are computed for the likely regime. The predicted regime hydraulic radius is compared to the actual hydraulic radius to determine the expected response of the Lower Granite Reservoir channel to the extreme discharge. Channels that have cross section geometries near equilibrium for a specified discharge will have a hydraulic radius that is about same as the hydraulic radius predicted by the Brownlie relationships for one or the other regime.

Brownlie's relationships are currently not incorporated into the sediment transport functions of HEC-RAS. A custom Matlab script was developed to implement the method. It was assumed in the analysis that the energy grade slope from the fixed-bed HEC-RAS model could be used directly in the Brownlie analysis. A more exact method would iterate the energy grade slope in the hydraulic model until the hydraulic radii converged. This was not necessary for the accuracy needed in this study since the energy grade line is largely controlled by the elevation of the forebay at Lower Granite Dam. Sediment D_{50} grain sizes used in the analysis were guided by the sediment core data and are plotted in Figure 27. The D_{50} for the SPF is somewhat larger than the normal gradation to reflect the possibility that the bed material will coarsen during the extreme event.

As a reference, the Brownlie regime analysis was first performed for the 213,600 cfs discharge on 8 June 2010 in Lower Granite Reservoir to which the 2009 fixed-bed hydraulic model was calibrated. This is a typical seasonal peak discharge that was very likely in the lower bed regime. Figure 28 is a plot of the upper and lower regime hydraulic radii computed with the Brownlie relationships. The actual hydraulic radius on 8 June 2010 computed from the calibrated fixed-bed HEC-RAS model closely matches the lower regime hydraulic radius predicted by the Brownlie equation for the reach of Lower Granite Reservoir above Silcott (RM 130). The upper regime hydraulic radius is substantially less than the actual hydraulic radius, so the channel at this discharge rate is not in upper regime. By the grain Froude number test, the Brownlie relationships predict that lower regime will occur throughout Lower Granite Reservoir.

The indication that the reach above Silcott is in lower regime agrees with the observation of dune bedforms in the 2009 bathymetry throughout this reach following the somewhat less flows in 2008 and 2009. Below Silcott the actual hydraulic radius is greater than the hydraulic radius for lower regime, indicating that the lower part of the reservoir is deeper than would be required to form an equilibrium channel in lower regime. This agrees with the previous comparisons with equilibrium hydraulic geometry relationships.

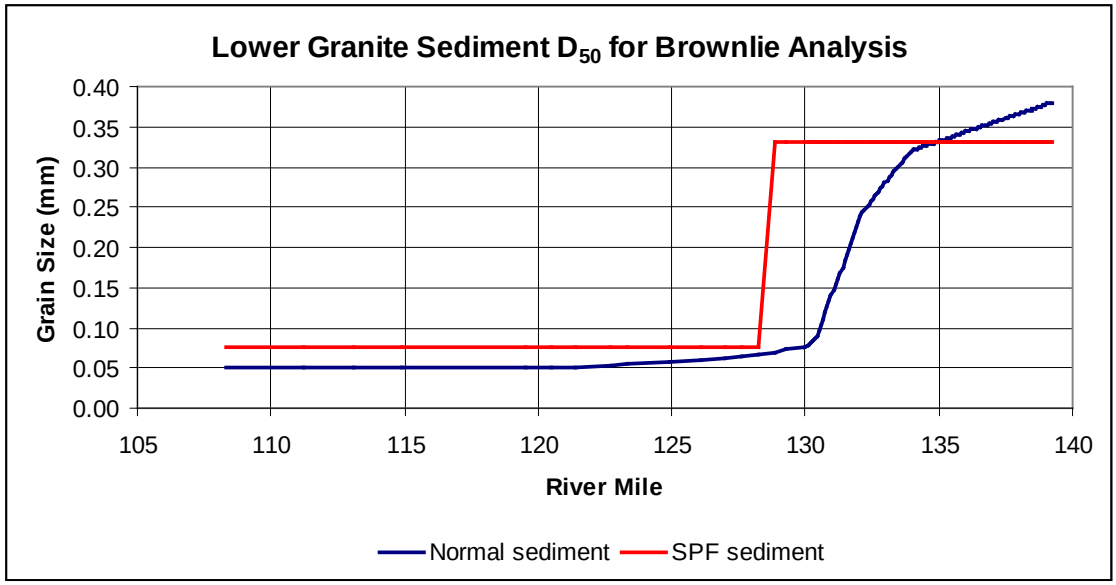


Figure 27. Lower Granite Reservoir sediment grain size for Brownlie regime analysis.

Manning's *n* values for Lower Granite Reservoir for a discharge of 213,500 cfs were computed with the Brownlie relationships and plotted in Figure 29. The Manning's *n* predicted by the lower regime equation for the reach above Silcott, is between 0.022 and 0.024, which agrees well with the Manning's *n* value of 0.023 for the calibrated model. Manning's *n* values for the upper regime are substantially less than those for lower regime.

Brownlie also developed sediment transport functions for lower and upper regime flow. Sediment concentrations were computed for Lower Granite Reservoir for a discharge of 213,500 cfs and plotted in Figure 30. Maximum equilibrium sediment concentrations are about 150 mg/L if the bed remains in lower regime and about 350 mg/L if the bed transitions to upper regime.

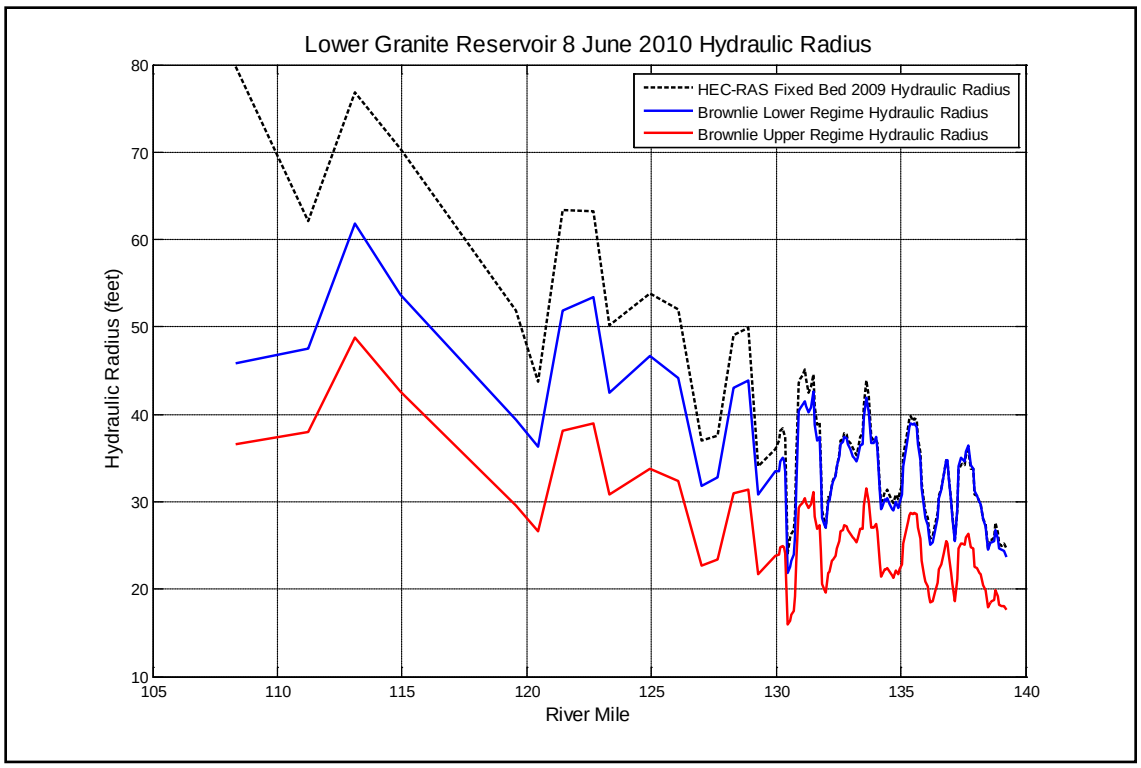


Figure 28. Brownlie hydraulic radius for Lower Granite Reservoir 8 June 2010 at 213,500 cfs.

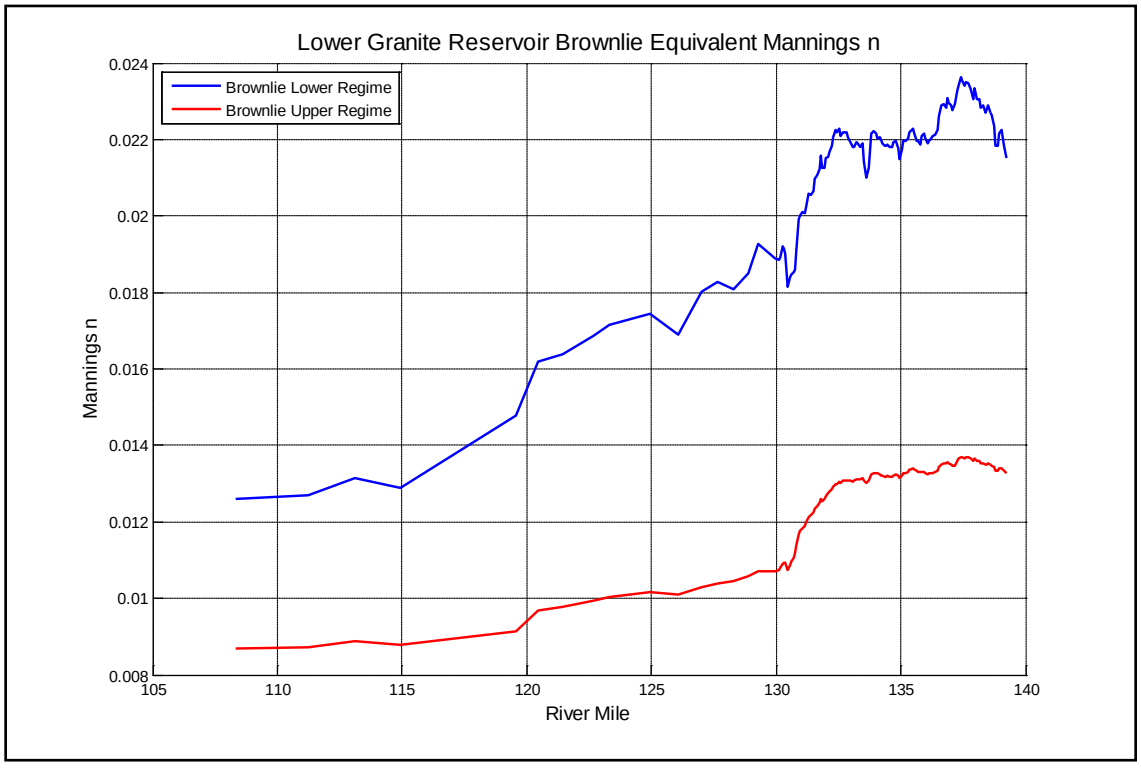


Figure 29. Manning's *n* for Lower Granite Reservoir 8 June 2010 at 213,500 cfs.

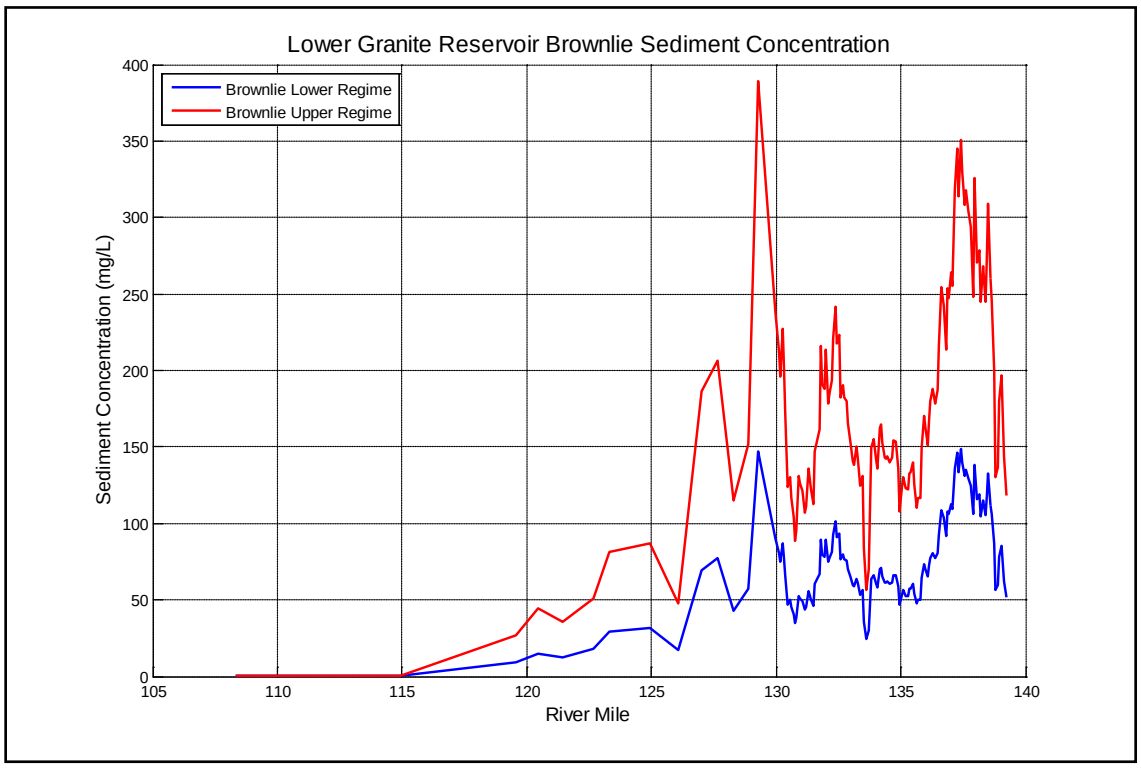


Figure 30. Sediment concentration for Lower Granite Reservoir 8 June 2010 at 213,500 cfs.

The Brownlie analysis of bed regime was repeated for the SPF discharge with somewhat larger D_{50} sediment sizes to reflect possible coarsening of the sediment load during the extreme event. The actual fixed-bed hydraulic radius during the 420,000 cfs discharge lies between the hydraulic radii plotted in Figure 31 for the lower and upper regime for the reach above Silcott. Manning's *n* values for the upper and lower bed regimes computed with the Brownlie relationships are plotted in Figure 32. The Manning's *n* values for the reach above Silcott are about 0.026 in lower regime and reduce to about 0.014 in upper regime. The Manning's n value for the lower regime is slightly less than the 0.028 value adopted in the more conservative fixed-bed hydraulic model in the FDA analysis in Section 3.

The plots indicate two possible responses of the sand bed during the rising limb of the SPF hydrograph. If the bed remains in lower regime during the SPF, as bedforms increase in size the water surface elevation could rise between 2 and 4 ft based on the greater Manning's *n* value over that computed by the fixed-bed model based on the calibrated Manning's *n*. The alternative response is that the bed would transition to upper regime, bedforms would washout, and the SPF water surface level would be less based on the lesser Manning's *n* value than that computed by the calibrated fixed-bed

model. The latter of these alternatives is more plausible. Sand that was deposited at lesser flows will remobilize during the SPF; it is unlikely that the bed would remain fixed.

Further, the particle Froude number test for the SPF discharge indicates that most of the reach above Silcott would transition to upper bed regime during the SPF. At the SPF discharge of 420,000 cfs, 88 percent of the cross sections above RM 130 are predicted to be in upper regime, 6 percent are in transition between regimes, and 6 percent are in lower regime. To enter upper regime, the channel above Silcott must transition from lower bed regime during the rising limb of the SPF hydrograph, thus bedforms should grow in size before the transition to upper regime, which may indicate general elevation of the bed after the bedforms washout. But, by the Brownlie relationship, upper regime requires a hydraulic radius that is less than that computed with the fixed bed model so the effect of any bed elevation is likely compensated and the net result is a lowering of the flood water surface.

Sediment concentrations predicted by the Brownlie relationships are plotted in Figure 33. Maximum equilibrium sediment concentrations are about 1,300 mg/L if the bed remains in lower regime and about 3,500 mg/L when the bed is in upper regime. For comparison, the expected concentration of the sediment load entering Lower Granite Reservoir at the SPF discharge is about 700 mg/L based on the sediment load analysis in Section 8.

The Brownlie regime analysis was repeated for the 2-percent (50-year) and 1-percent (100-year) exceedance discharges. Brownlie hydraulic radii plotted in Figure 34 and Figure 35 show an increasing likelihood that the bed will transition to upper regime as flows increase to the SPF discharge. During the 2-percent discharge of 308,000 cfs, 39 percent of the cross sections above RM 130 are predicted to be in upper regime, 17 percent were identified as in transition between regimes, and 45 percent were expected be in lower regime. When the discharge is increased to 331,600 cfs for the 1-percent discharge, 56 percent of the cross sections above RM 130 are in upper regime, 18 percent are in transition between regimes, and 25 percent are in lower regime.

The implications of the Brownlie regime analysis of Lower Granite Reservoir during extreme discharges are significant for the flood risk analysis. Under extreme discharge, the mobile-bed Lower Granite Reservoir channel could respond in three ways:

1. The reach above Silcott could transition from lower bed regime to upper regime for discharges greater than about the 1-percent exceedance discharge even if a considerable volume of sediment accumulated in the rising limb of the hydrograph. As the flow enters upper regime during extreme discharges, the Manning's *n* roughness value would dramatically decrease as the dunes washout and the mobile bed becomes planar. The stage at the confluence during upper regime flow would be considerably less than that predicted by the fixed bed

model. Lowering of the forebay elevation at Lower Granite Dam in advance of an extreme flood would help promote this response.

2. Since the water surface elevation of Lower Granite Reservoir is controlled by the forebay elevation at Lower Granite Dam, it is possible that lower regime flow will persist during extreme discharges because the actual hydraulic radius is greater than the hydraulic radius for upper regime flow. In this condition, shear stress at the bed would not be great enough to washout the dunes to enter upper regime flow. If this occurs, the reach above Silcott could scour slightly to attain the hydraulic radius predicted by the Brownlie lower regime relationship. This is plausible because bed shear stress is higher than the shear stress when the sediment was deposited and equilibrium sediment concentrations predicted by the Brownlie sediment transport function are several times greater than the expected sediment load concentration based on the sediment load analysis in Section 8, recalling that sand transport into Lower Granite Reservoir is supply limited because the upstream channels have gravel and cobble beds.
3. If Lower Granite Reservoir remains in lower regime because of the over-fit channel, the water surface elevation could rise slightly to attain the hydraulic radius predicted by the Brownlie lower regime relationship. Currently, this is less plausible than response 2 unless the gradation of the sediment load during the extreme event is substantially coarser than the historic sediment load (which changes the Brownlie predictions). Since the forebay elevation remains constant, a higher water surface in the reach above Silcott is accompanied by an increase in the energy gradient which would increase bed shear stress and act to counter the rising water surface.

Channel responses 1 and 2 indicate that the flood risk analysis in Section 3 based on the fixed-bed hydraulic analysis of the current condition is reasonable and somewhat conservative. Responses 1 and 2 are not significantly altered by the amount of sediment that accumulates in Lower Granite Reservoir in the near term. Brownlie's relationships characterize the equilibrium channel, so the upper channel in Lower Granite Reservoir would adjust to form an equilibrium channel at extreme discharges regardless of the amount of sediment that has been deposited in lesser flows. Response 3 becomes more plausible in the future as the reservoir below Silcott fills with sediment and the flood water surface profile changes from an M1 profile to an M2 profile.

In Section 12, the Brownlie relationships are adapted to develop a spatial analysis of the bed regime in Lower Granite Reservoir. Other methods are also presented that corroborate the insights gained from the Brownlie regime relationships.

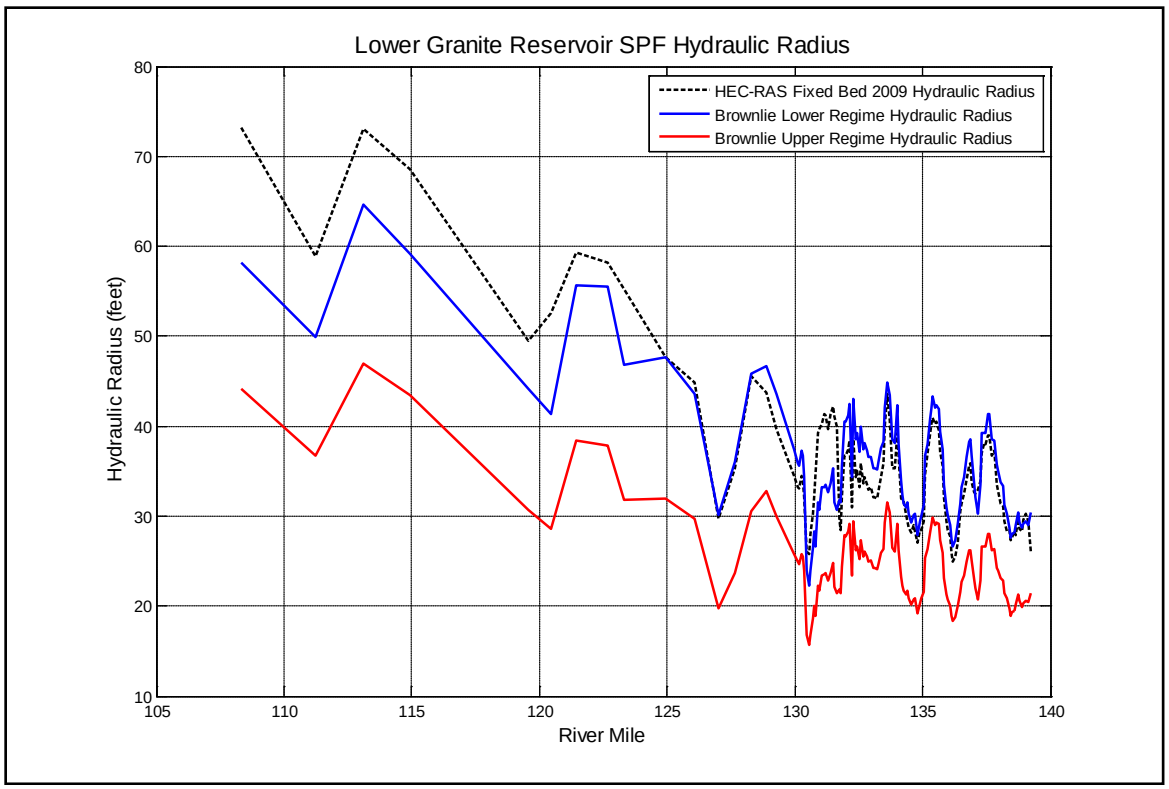


Figure 31. Brownlie hydraulic radius for Lower Granite Reservoir SPF at 420,000 cfs.

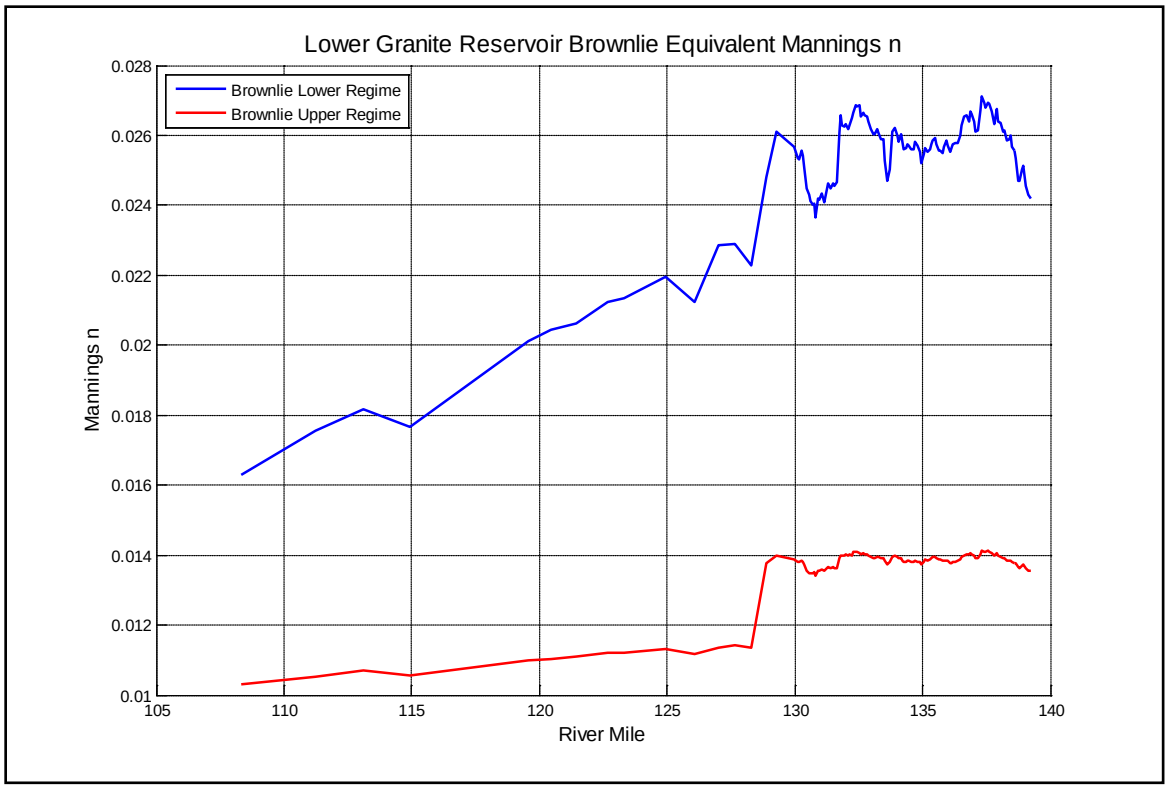


Figure 32. Manning's *n* for Lower Granite Reservoir SPF at 420,000 cfs.

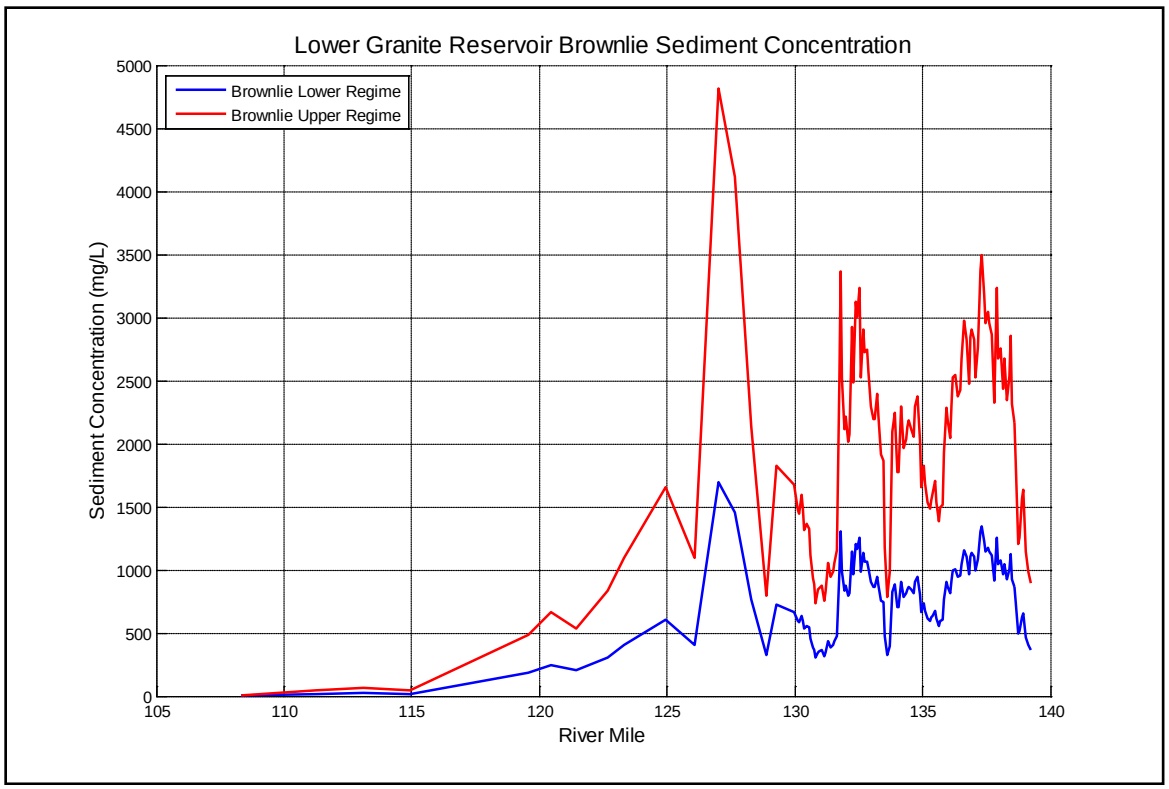


Figure 33. Sediment concentration for Lower Granite Reservoir SPF at 420,000 cfs.

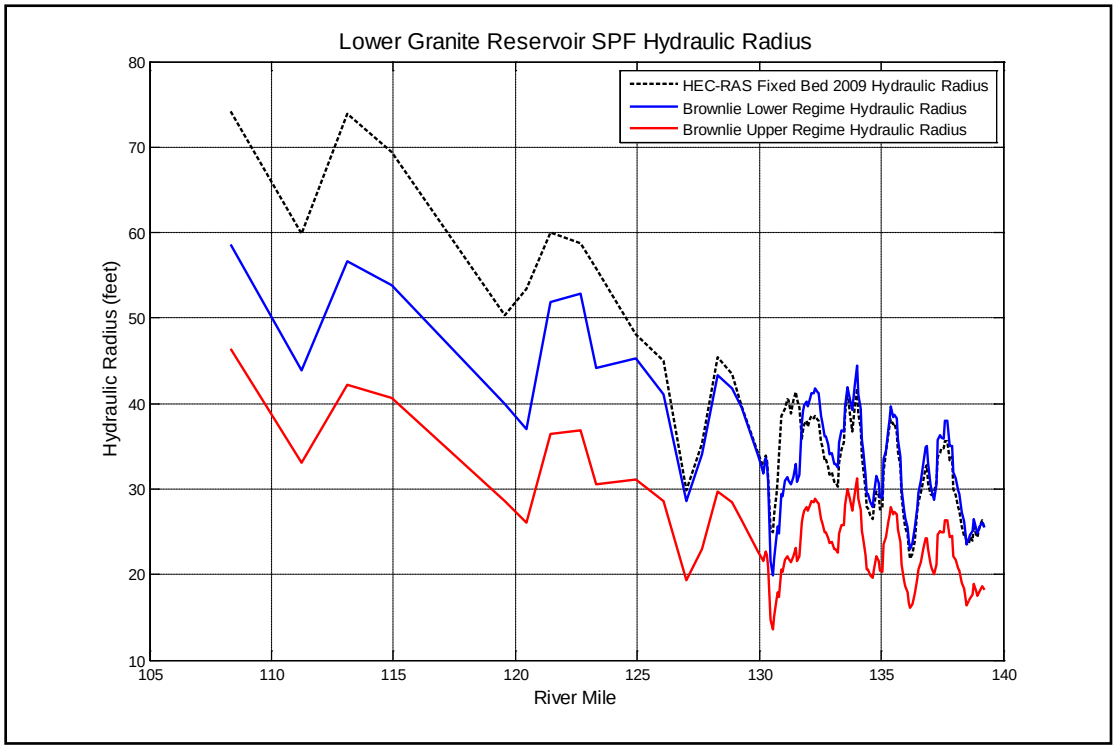


Figure 34. Brownlie hydraulic radius for Lower Granite Reservoir 2-percent exceedance discharge at 308,000 cfs.

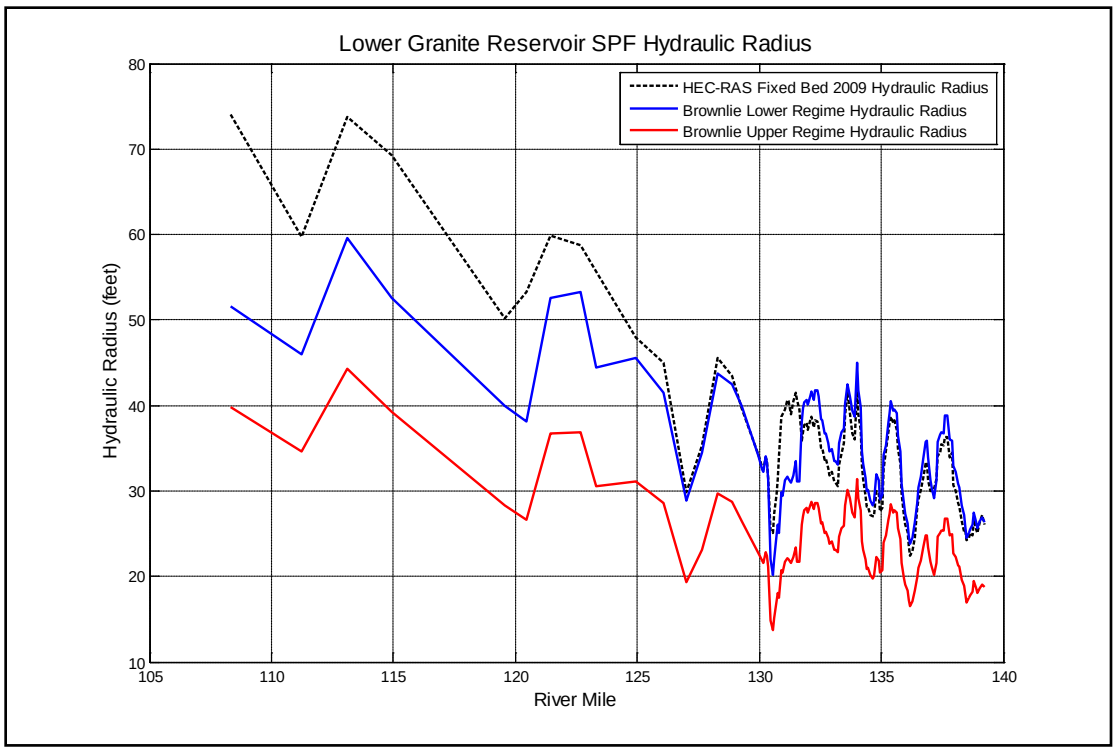


Figure 35. Brownlie hydraulic radius for Lower Granite Reservoir 1-percent exceedance discharge at 331,600 cfs.

The Brownlie relationships for bed regime and flow resistance are well established in sedimentation engineering practice and they are appropriate for the analysis of bed regime in Lower Granite Reservoir. Other relationship such as the Engelund and Hansen method[28] and the Wright and Parker method[26] can also be applied. In the lower bed regime, Engelund and Hansen partitioned the shear stress for grain friction with the relationship

$$\tau_s^* = 0.06 + 0.4\left(\tau^*\right)^2$$

where τ_s* is the dimensionless bed shear stress for grain friction and τ* is the total dimensionless bed shear stress. The relationship for shear stress associated with grain friction developed by Wright and Parker is

$$\tau_s^* = 0.05 + 0.4\left(\tau^* F^{0.7}\right)^{0.8}$$

where F is the Froude number of the flow. The Wright and Parker method also accounts the effect of stratification in suspended sediment concentration which appears to delay the onset of transition to upper bed regime in large sand bed rivers that have low energy gradients. The method applied by Julien et al computes representative dune heights and wavelengths which are then used as parameters in a relationship for dune roughness height. All methods represent lower bed regime conditions.

Water depth was computed with the Engelund-Hansen, Wright-Parker and Julien et al relationships for Snake River Mile 137.63 at a discharge of 214,200 cfs and compared to the actual depth from the calibrated HEC-RAS model and the depth obtained with the Brownlie relationship. The depth obtained from the calibrated HEC-RAS model is the best estimate of the actual depth for the 2009 mobile bed channel condition. The cross section at RM 137.63 provides a good basis for comparison because it is an equilibrium cross section as described in Section 8. Iterative calculations required to implement the Engelund-Hansen, Wright-Parker and Julien et al methods are described in the citations and are not repeated here. Hydraulic parameters and computed flow depths are summarized in Table 1..

Water depths computed for the mobile bed with the Brownlie and Engelund-Hansen agree well with the depth obtained with the calibrated HEC-RAS model. Depths predicted by the Wright-Parker and Julien et al methods are about 10 feet deeper than the actual depth at this flow rate. The likely reason for the deeper depths obtained from the Wright-Parker and Julien et al methods is that they represent fully transport limited (equilibrium) bedload conditions for large sand bed rivers where bedforms reach maximum development across the channel. The condition of partial transport in Lower Granite Reservoir appears to be better represented by the Brownlie and Engelund-Hansen methods. Depths for all cross sections in Lower Granite Reservoir for the discharge on 8 June 2010 were computed with the Engelund-Hansen method for lower regime in a manner similar to the Brownlie analysis above. Differences between the actual (calibrated model) hydraulic radius and the predicted hydraulic radius are plotted in Figure 36. As with the Brownlie method, the Engelund-Hansen method indicates that the channel in the upper segment of the reservoir has a near equilibrium geometry for the prevailing sediment load and discharge.

Estimates by the mobile-bed stage-discharge predictors discussed above carry added uncertainty beyond that inherent to the methods when applied to the gradually varied flow profile of Lower Granite Reservoir. The methods were developed from field data that were acquired when flows were approximately steady and normal. As shown in Figure 37, flow depths in the M1 backwater profile of Lower Granite Reservoir are substantially greater than the depths for equivalent discharges in a free-flowing channel. In practice, it is not unusual to apply mobile bed relationships developed for normal flow conditions in an analysis of gradually varied flow. The good agreement between depths determined with the Brownlie and Engelund-Hansen relationships with the actual depths indicates the added uncertainty is not extraordinary.

Method	Discharge cfs	Top Width ft	Slope ft/ft	D_{50} mm	Depth ft
Calibrated HEC-RAS	214,200	1106	0.000049	0.33	39.6
Brownlie	214,200	1106	0.000049	0.33	37.6
Engelund-Hansen	214,200	1106	0.000049	0.33	39.4
Wright-Parker	214,200	1106	0.000049	0.33	48.1
Julien et al.	214,200	1106	0.000049	0.33	48.4

Table 1. Comparison of stage-discharge predictors for sand bed channels.

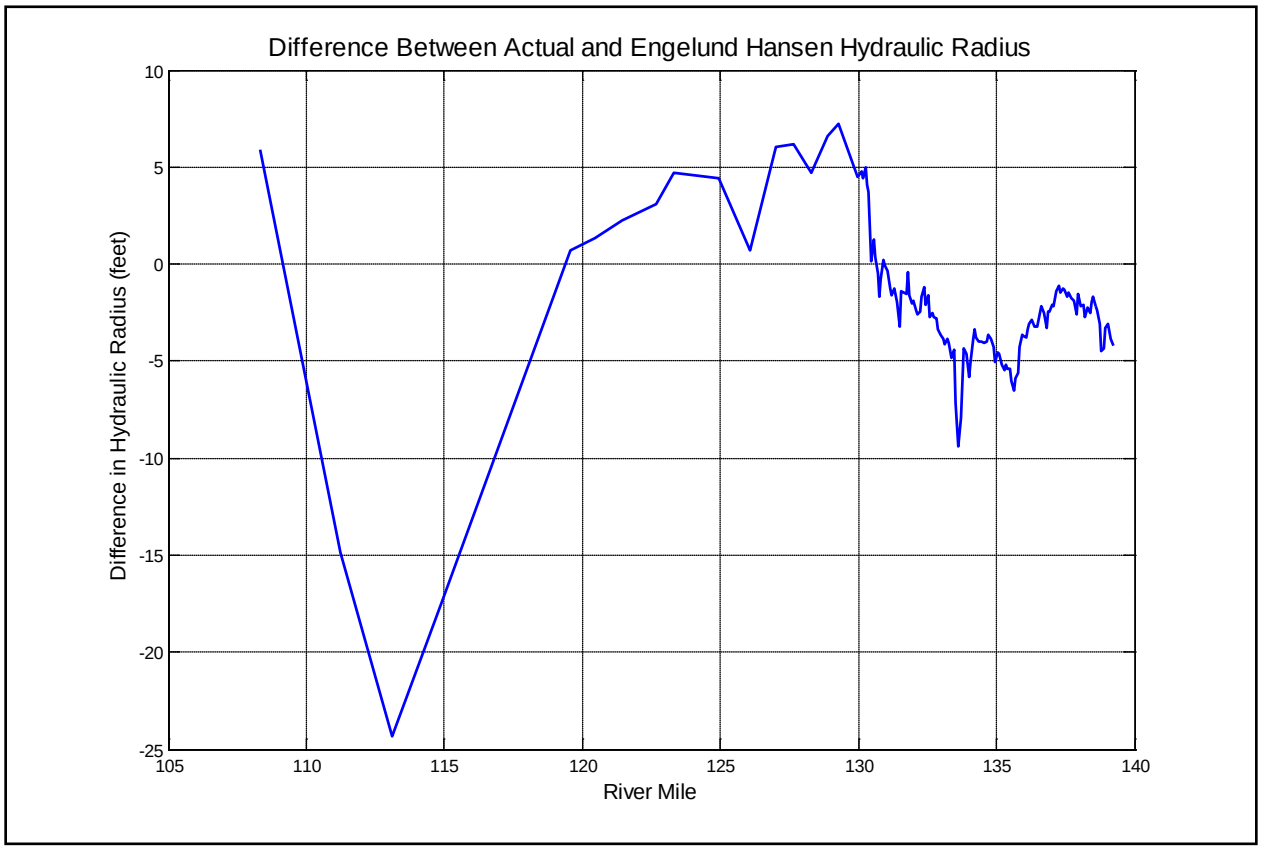


Figure 36. Comparison of depths predicted by Engelund-Hansen method.

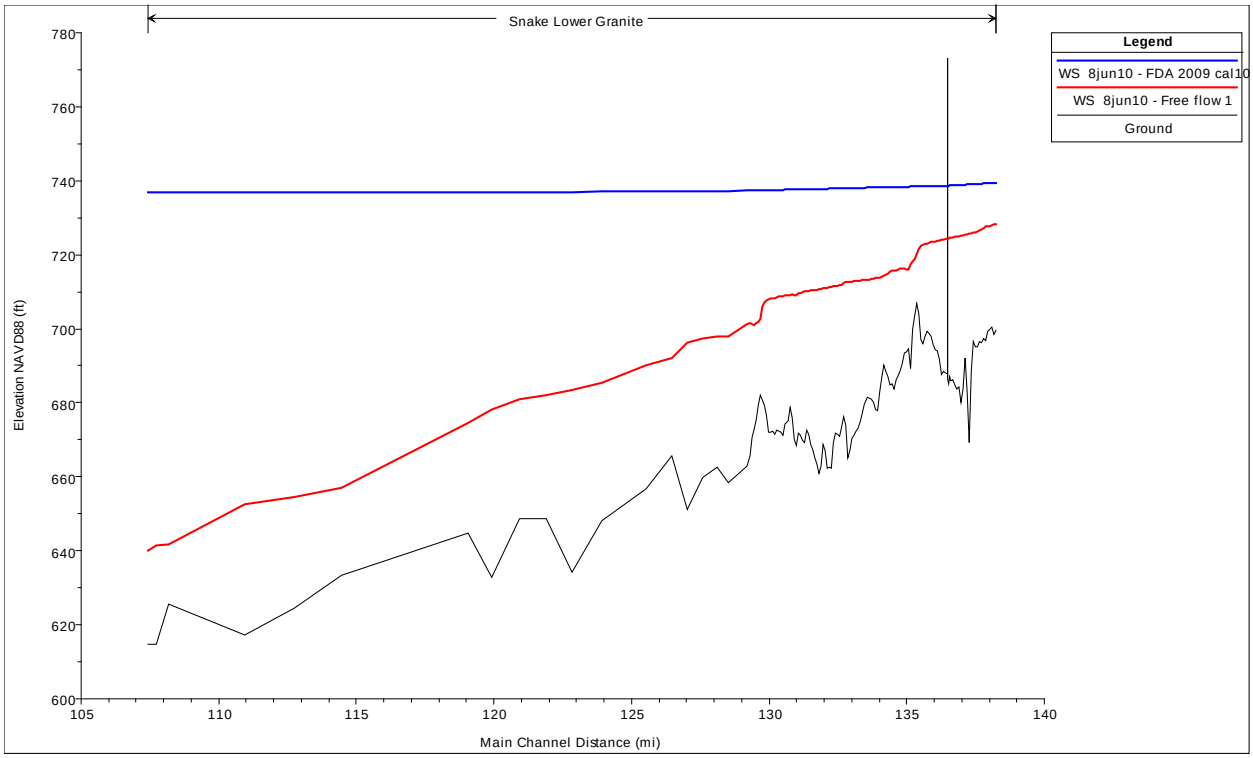


Figure 37. Backwater and free channel flow water surface profiles for the Snake River in Lower Granite Reservoir.

10.10. Conceptual Effect of Sediment Accumulation on Flood Water Surface

For sediment management planning, it is important to know the effect of large volumes of sediment accumulation on the water surface profile of Lower Granite Reservoir when the sediment is placed at different locations in the reservoir. The HEC-RAS modeling system provides a convenient method to specify hypothetical sediment depths in selected cross sections. Figure 38 through Figure 41 show the water surface profiles for the SPF (420 kcfs) for several sediment placement scenarios. Table 2 compares the water surface elevation at the confluence (RM 139.25) for the different scenarios and two steady flow discharge rates 200 kcfs and the SPF 420 kcfs. The water surface elevations were computed with a fixed-bed HEC-RAS model developed from September 2011 bathymetry. The water surface elevations are approximate because mobile-bed effects are neglected, but the relative comparison of the water surface elevations will demonstrate the effect of the sediment placement.

When 2.42 million cubic yards (mcy) of sediment is placed near the confluence, which is equivalent to about the average annual sediment load, the water surfaces for the 200 kcfs and SPF discharges rise by 0.3 and 1.4 ft. The placement of a similar volume of sediment near the middle of the reservoir has negligible effect on the water

surface at the confluence. Moreover, the table shows that it requires over 23 mcy of sediment placed in the middle segment of the reservoir to raise the water surface at the confluence by about the same amount as the smaller amount placed at the confluence. When a very large volume of sediment, 172 mcy, is distributed between RM 130 and Lower Granite Dam the 200 kcfs water surface rises by less than 1 ft and the SPF water surface rises by about 3 ft.

Even though this conceptual modeling neglects sediment dynamics and mobile-bed effects on the flood water surface, it shows the importance of sediment distribution within the reservoir for managing the flood water surface at the confluence. Since sediment accumulation within the reservoir is unavoidable, sediment management methods discussed later in this section are intended to promote the transport of sediment beyond the confluence so the effect on the flood water surface at the confluence and the associated flood risk are lessened.

Sediment Location	Added Sediment mcy	Water Surface Elevation (ft) 200 kcfs	SPF - 420 kcfs
2011 condition	0	739.4	741.5
Near confluence	2.42	739.7	742.8
Mid Reservoir	2.49	739.4	741.5
RM130 - 119	23.47	739.7	742.6
RM130 - 107	171.85	740.3	744.6

Table 2. Change in water surface due to conceptual sediment accumulation.

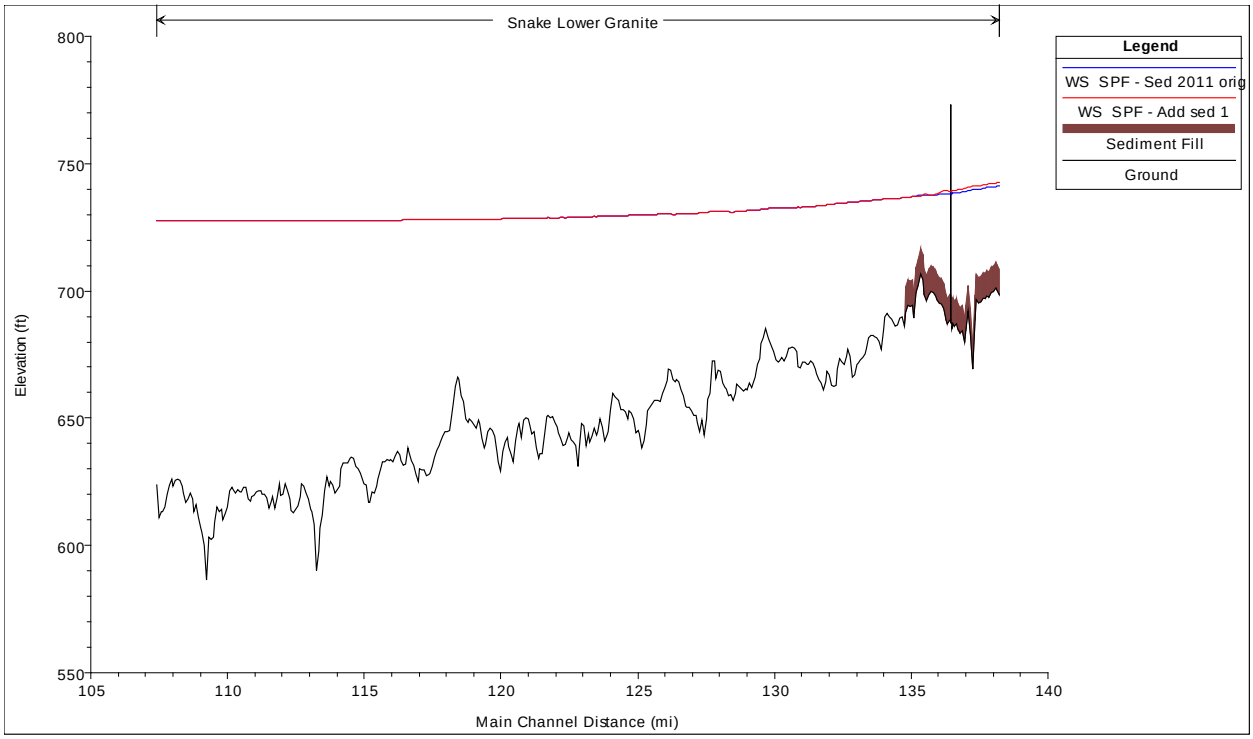


Figure 38. SPF water surface profile with 2.42 sediment accumulation near the confluence.

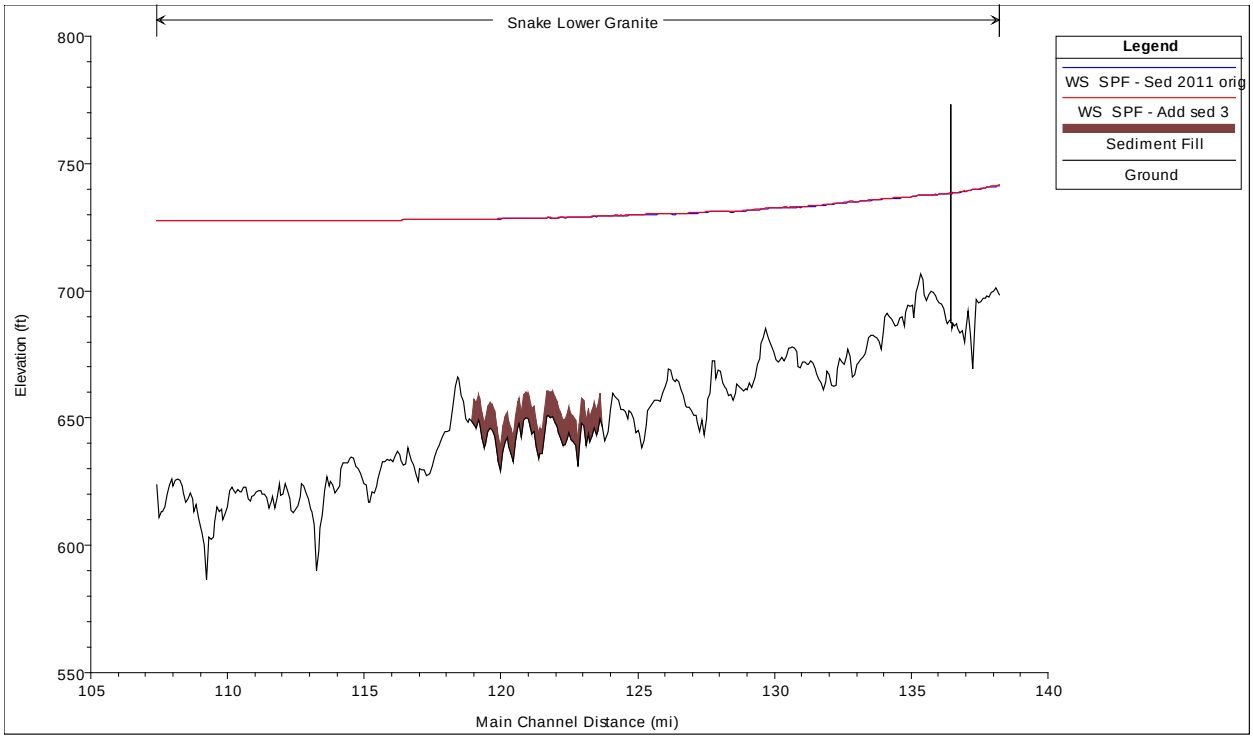


Figure 39. SPF water surface profile with 2.49 mcy sediment accumulation at mid reservoir.

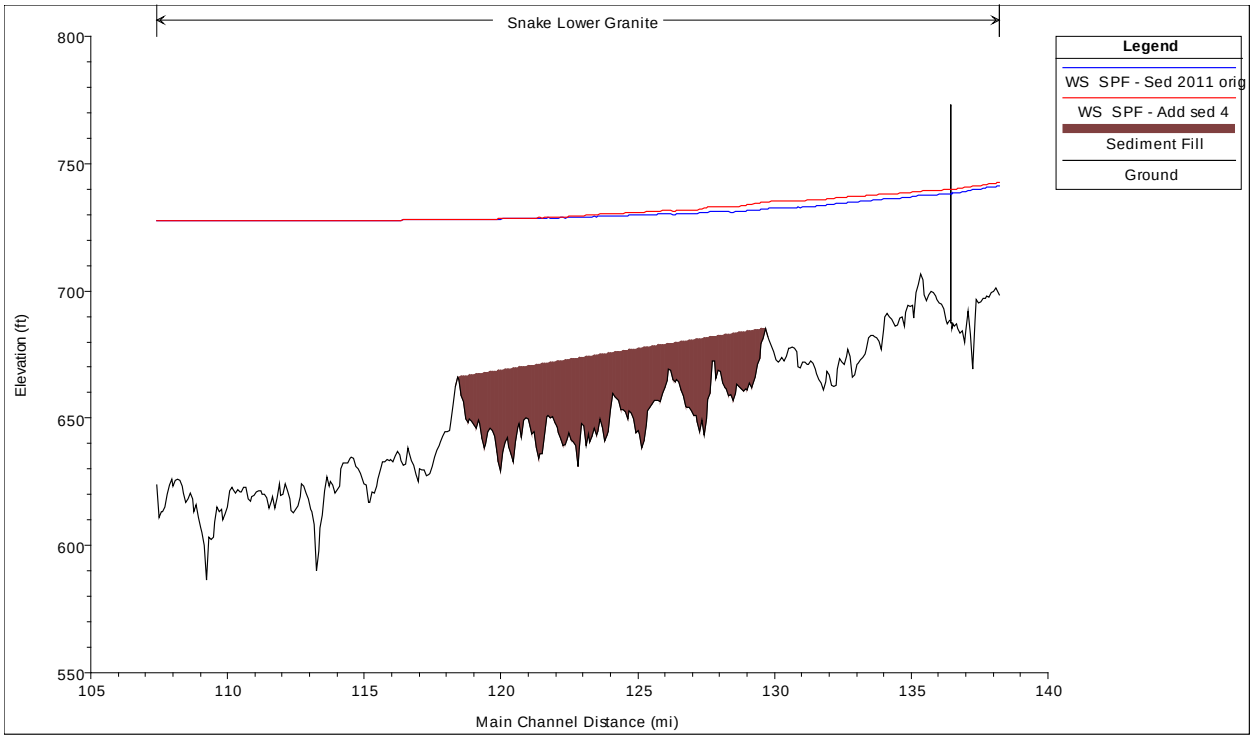


Figure 40. SPF water surface profile with 23.5 mcy sediment accumulation at mid reservoir.

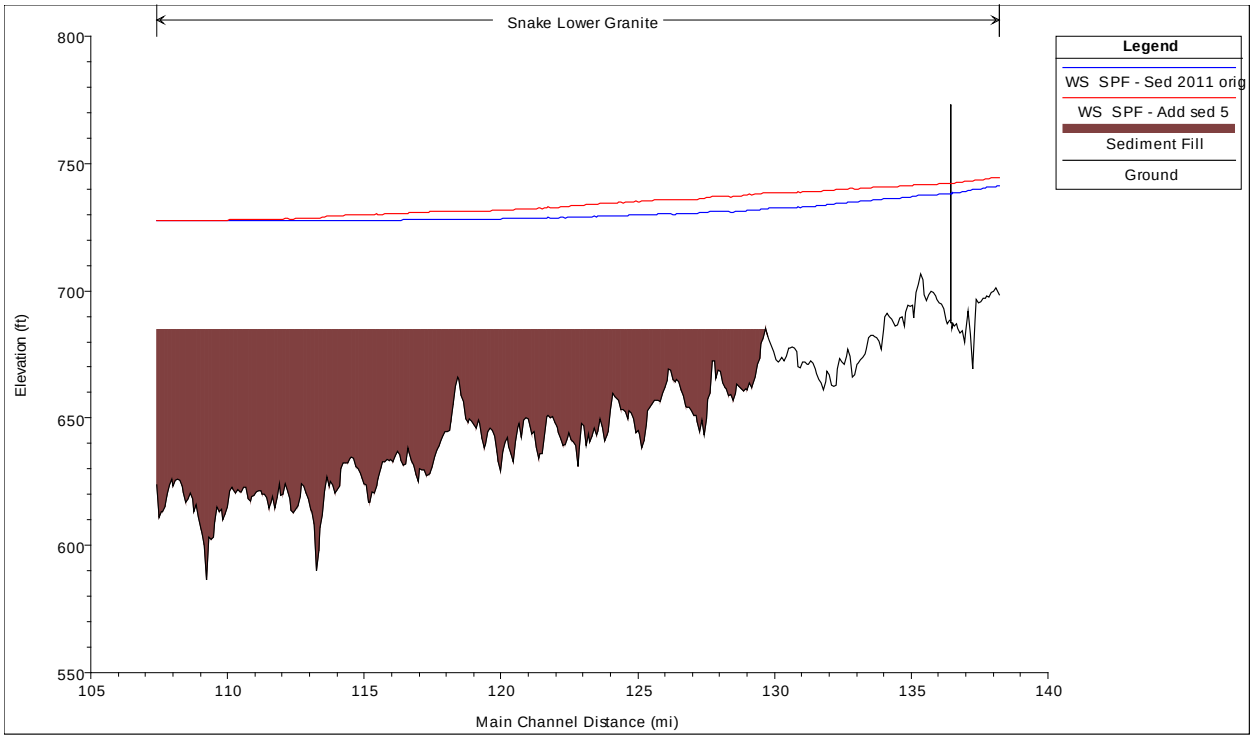


Figure 41. SPF Water surface profile with 171.9 mcy sediment accumulation below RM 130.

10.11. Selection of Sediment Transport Function

Sediment transport functions are developed from laboratory and natural channels that are free to adjust in response to changes in flow rate, bed material grain size and sediment load. Conventional sediment transport functions are partly empirical so they are most reliable when applied to conditions that are similar to those for which they were developed. Bed conditions and sediment size vary throughout Lower Granite Reservoir, so a single sediment transport function would not be expected to perform well for all segments of the reservoir and the Snake and Clearwater Rivers above the confluence.

Sediment transport functions are selected based on modeling objectives, range of applicability, and if available, measured sediment data. The sediment transport model for Lower Granite Reservoir is intended to predict the conveyance at the end of the 50-year future analysis period. A reasonable criterion for selection of a sediment transport function for this study is to select the function that best predicts the historic sediment accumulation. A transport function that predicts past sediment accumulation well should also reliably predict future sediment accumulation under similar conditions of discharge and sediment load. The historic sediment range data and accumulation volumes evaluated in Section 6 provide the data needed to assess candidate sediment transport functions.

Currently, HEC-RAS includes seven sediment transport functions: Ackers-White, Engelund-Hansen, Laursen (Copeland), Meyer-Peter-Muller, Toffaleti, Yang, and Wilcock. Details on the formulation of these functions and range of applicability are described in USACE guidance[37,38] and sedimentation references[35,36]. Of these, the Meyer-Peter-Muller and Wilcock functions are best suited to model gravel transport and were not considered appropriate for this analysis. The remaining transport functions were considered potential candidates.

10.12. Simulation of Historic Sediment Accumulation

Historic sediment accumulation was simulated for the period 1 October 1974 to 30 September 2009. The initial model geometry was developed from the 1974 sediment ranges, and is one of the historic models discussed in Section 3. The 1974

[37] USACE (2010). *HEC-RAS River Analysis System, Hydraulic Reference Manual*, Ver. 4.1, U.S. Army Corps of Engineers, Washington, D.C.

[38] USACE (1995). *EM 1110-2-4000, Sedimentation Investigations of Rivers and Reservoirs*, U.S. Army Corps of Engineers, Washington, D.C.

model domain (Figure 42) consists of 99 cross sections, 33 on the Clearwater River between the confluence and RM 7.85 and 66 on the Snake River between the dam at RM 107.73 and upstream of Asotin, WA at RM 148.83. A single junction at the confluence joins the Snake and Clearwater Rivers (Figure 43). Cross sections in Lower Granite Reservoir, such as that at Snake RM 138.94 in Figure 44, generally define the bottom topography reasonably well for the sounding methods employed at that time. Cross section spacing between the confluence and RM 130 at Silcott averages 2,200 ft and averages 6,900 ft below RM 130. Bridges were not represented in the geometry because preliminary modeling showed they have little effect on the energy gradient for typical seasonal flows. Channel Manning's *n* values were held constant at 0.028 in all simulations to conservatively represent lower regime flow. Overbank Manning's *n* was set to a constant value of 0.04, but overbank flow is minimal in all simulations. Contraction and expansion coefficients were set at 0.1 and 0.3.

It is known from the comparison of historic sediment ranges that the bed has not scoured below the depth of the 1974 channel, so the bed gradations at all cross sections were set to a coarse well-graded sediment distribution comprised of mostly cobble. Sediment bed stations were set to the full width of the cross section. The sediment load for the Snake and Clearwater Rivers was input as a sediment rating curve developed from the adjusted power fit of the measured sediment data as described in Section 6. Unit weights of sediment were 90 lb ft^{-3} for sand, 60 or 70 lb ft^{-3} for silt and 30 lb ft^{-3} for clay.

Daily quasi-unsteady flow time series for the Snake and Clearwater Rivers for the full time period (12783 daily values) were derived from USGS stream gage records. Based on preliminary tests, the sediment computation interval was set at 6 hours. The downstream boundary condition was represented as a stage time series that was held constant at 739.41 ft NAVD88, except for the drawdown study period between 28 February 1992 and 6 April 1992. Downstream stage elevations for the drawdown period were set to the actual daily average water surface elevations at the forebay of Lower Granite Dam reported in the NWD water management database. Dredging volumes were not removed in the simulations because the total dredging volume for the period was only about 6 percent of the total accumulated sediment volume and the locations of the dredging was not clear in the project records. The temperature time series for the sediment transport analysis was held constant at 50 degrees Fahrenheit.

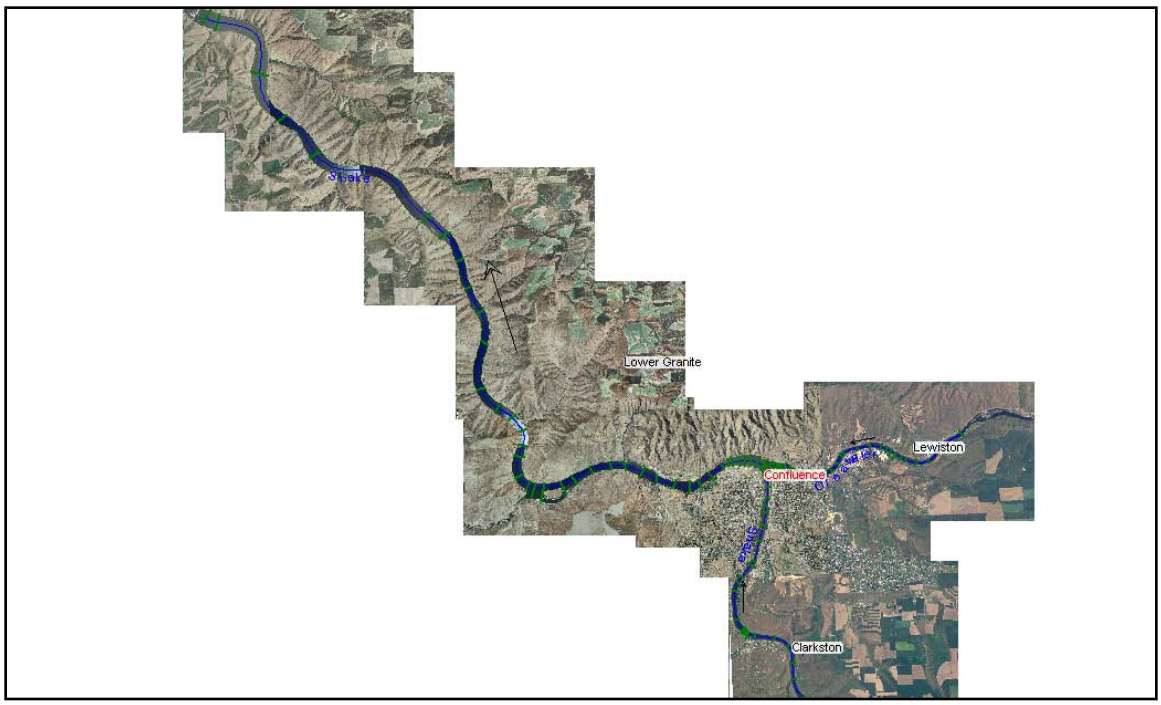


Figure 42. 1974 HEC-RAS model domain.

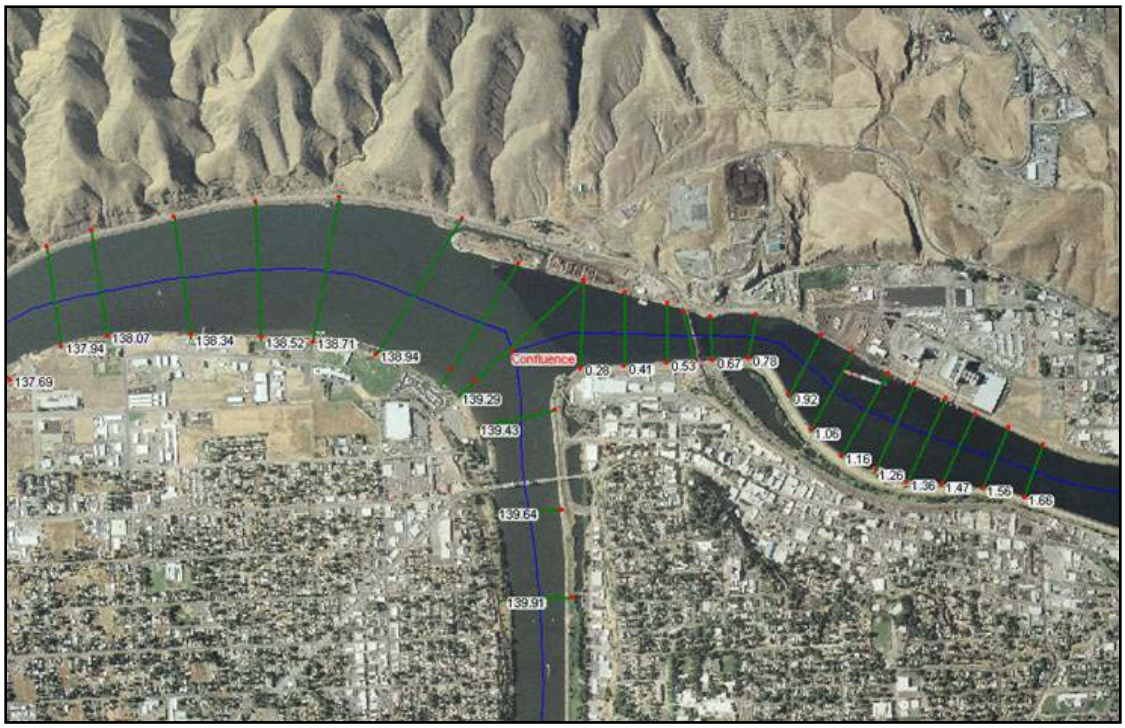


Figure 43. 1974 HEC-RAS cross sections at confluence of Snake and Clearwater Rivers.

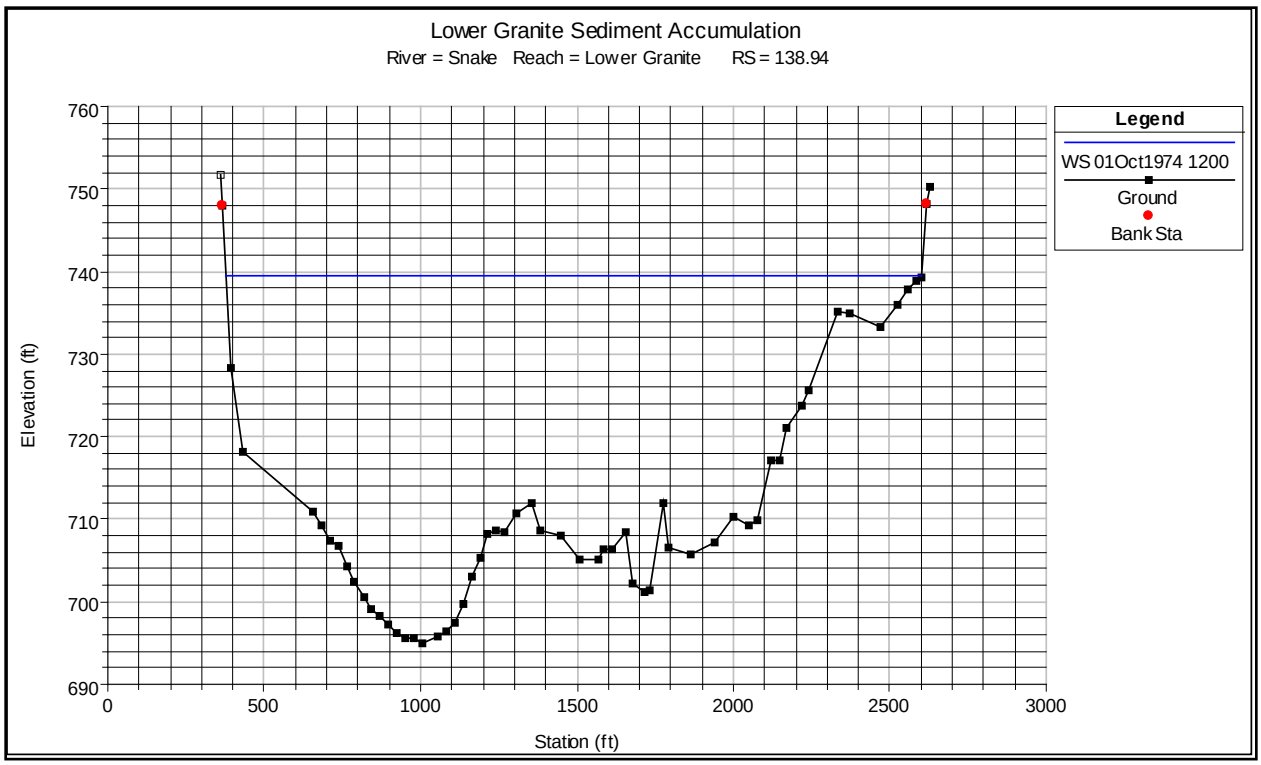


Figure 44. Typical 1974 cross section at Snake RM 138.94.

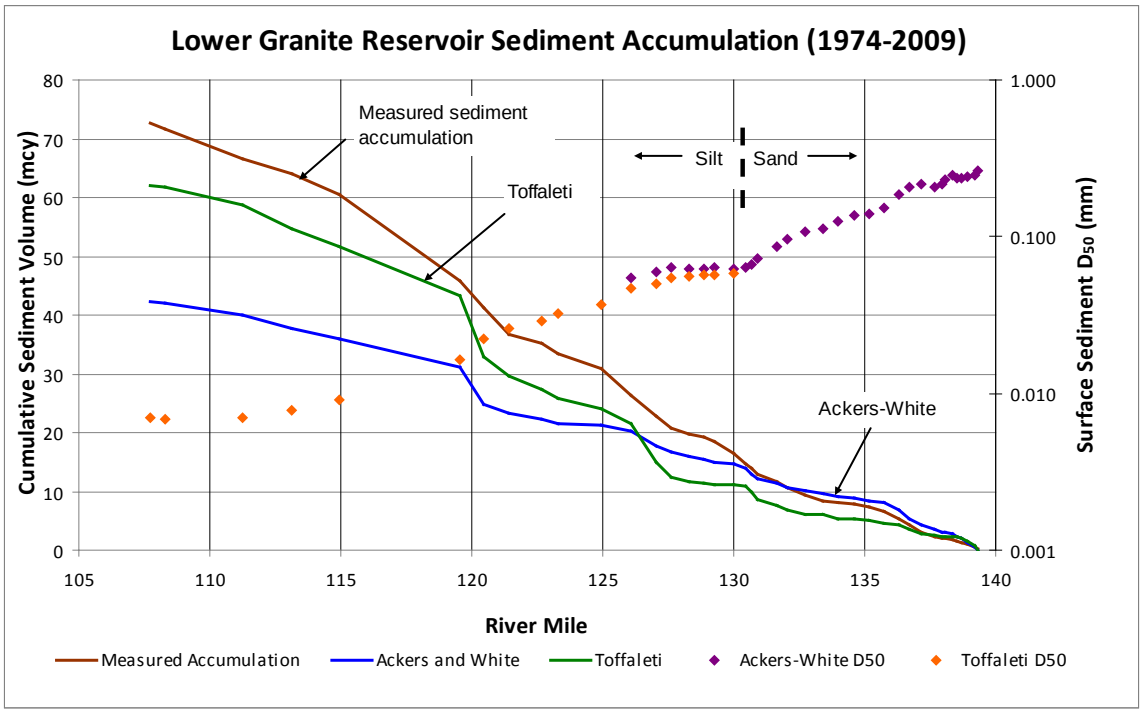
Numerous trial simulations of the 1974-2009 period were performed with HEC-RAS 4.1.0 and the candidate transport functions including: Ackers-White, Engelund-Hansen, Laursen (Copeland), Toffaleti, and Yang. Plots of the invert change, cumulative mass bed change, longitudinal cumulative mass bed change, and d_{50} of the surface cover were compared to the actual sediment accumulation measured by the sediment ranges. Various options in the sediment computation settings were selected in several tests when instabilities appeared with some transport functions, but the default settings were acceptable for best performing functions. The Ackers-White and Toffaleti transport functions reproduced the historical accumulation better than the other transport functions. The longitudinal cumulative mass bed change for these transport functions are plotted with the measured accumulation as volumes in Figure 45.

The longitudinal volume accumulation curve from the Ackers-White simulation agrees with the measured accumulation curve reasonably well in upper segment of Lower Granite Reservoir between the confluence and Silcott (RM 130). Below RM 130, the Ackers-White function estimated less sediment accumulation than was measured. Sediment accumulation predicted by the Toffaleti simulation more closely matches the measured accumulation in the reservoir below RM 130, but underestimates sediment accumulation in segment above RM 130. The Toffaleti accumulation curve plots above

the Ackers-White curve because the Toffaleti function provides more realistic simulation of the retention of silt in the lower reservoir[39].

It can be expected that the transport functions are more effective simulating sediment transport in the different segments of the reservoir. The Ackers-White transport total load function was developed from shallow flume data for various bed conditions and is best applied to sands and coarse silt[37], so it could be expected that Ackers-White would simulate the transport of coarser sand material in the conditions of partial transport in the upper segment of the reservoir. The Toffaleti function was developed with mixed natural sediments from large, deep rivers, so it could be expected to better simulate transport in the deeper lower segment of the reservoir. The simulated surface sediment D_{50} from the Ackers-White transport function reproduces the observed transition from sand to silt near RM 130.

Other transport functions did not match the actual accumulation curve as well. For comparison, the accumulated sediment volume curves computed by all the candidate transport functions are plotted Figure 46. The Engelund-Hansen and Yang functions overestimate sediment accumulation in the reservoir above Silcott and accumulation above Silcott is underestimated by the Laursen-Copeland function.



[39] Emmett and Thomas used the Toffaleti function for the upper reach of the reservoir in the 1978 sediment transport study.

Figure 45. Measured and sediment accumulation simulated with Ackers-White and Toffaleti functions 1974-2009.

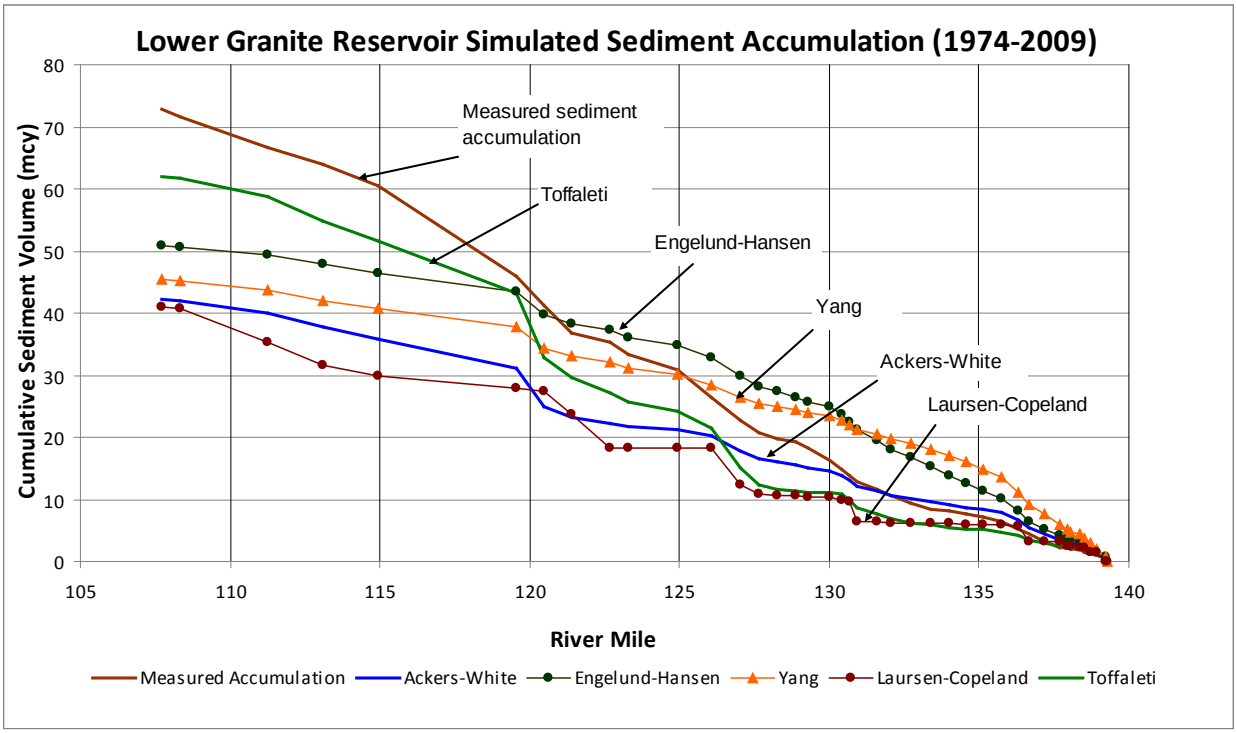


Figure 46. Sediment volume simulated with candidate transport functions.

Simulated changes in bed elevation are compared with measured bed changes in Figure 47. The simulated bed change is represented as the HEC-RAS mean effective channel change and is compared to the mean active bed difference between the 1974 and 2009 sediment ranges. The two measures of bed change are computed somewhat differently, but are similar enough to judge the efficacy of the sediment transport functions.

Consistent with the volume accumulation curves, the Ackers-White function estimated the actual bed change reasonably well in the upper segment of the reservoir, but underestimates bed change in the lower reservoir. The greatest discrepancy in the upper reach is in the segment immediately above Silcott Island which was underestimated by the Ackers-White function. The aerial image in Figure 48 indicates that sediment accumulation in the cross sections at RM132.05 and 132.71 is likely promoted by a change in energy gradient caused by the secondary circulation at the upstream end of the island. Secondary circulations are not simulated in one-dimensional hydraulic models. Addition of ineffective flow areas to the model upstream of the island did not significantly alter the simulated bed change. The 1974 cross section geometry also does not represent the small island. Significant differences below Silcott

between the bed change computed by the Toffaleti function and the measured bed change occur at RM 123.3 and RM 120. A bend at RM 123.3 (Figure 49) likely has secondary circulation that may increase the local sediment deposition and a small island (Centennial Island) at RM 120 (Figure 50) likely increases local sediment deposition. Underestimation of bed change below Silcott may in part be due to differences between actual channel geometry and the channel geometry represented in the model based on the relatively widely spaced cross sections (see Section 12).

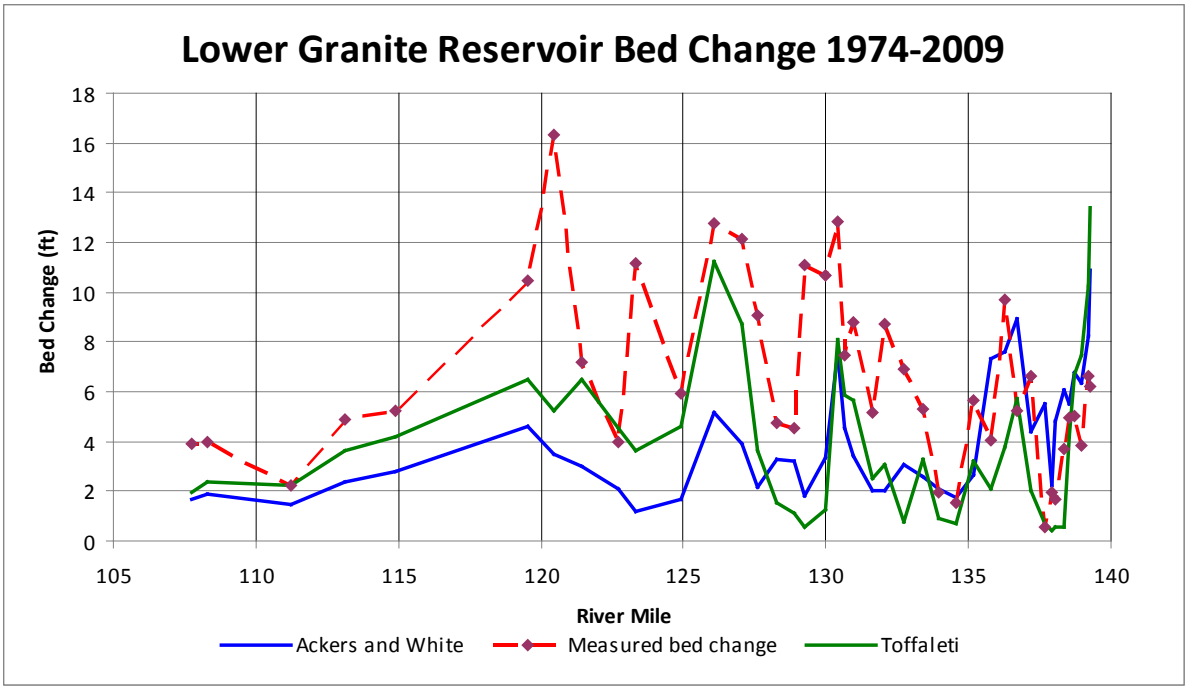


Figure 47. Measured and simulated bed change 1974-2009.

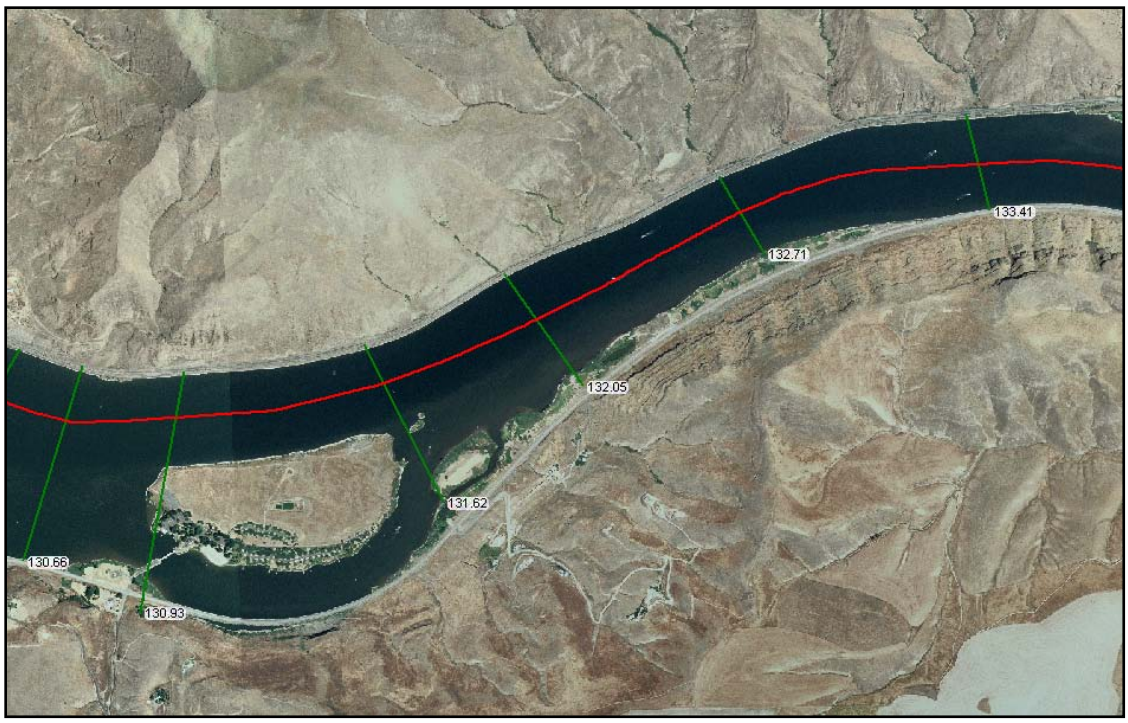


Figure 48. Segment of 1974 sediment transport model above Silcott Island.

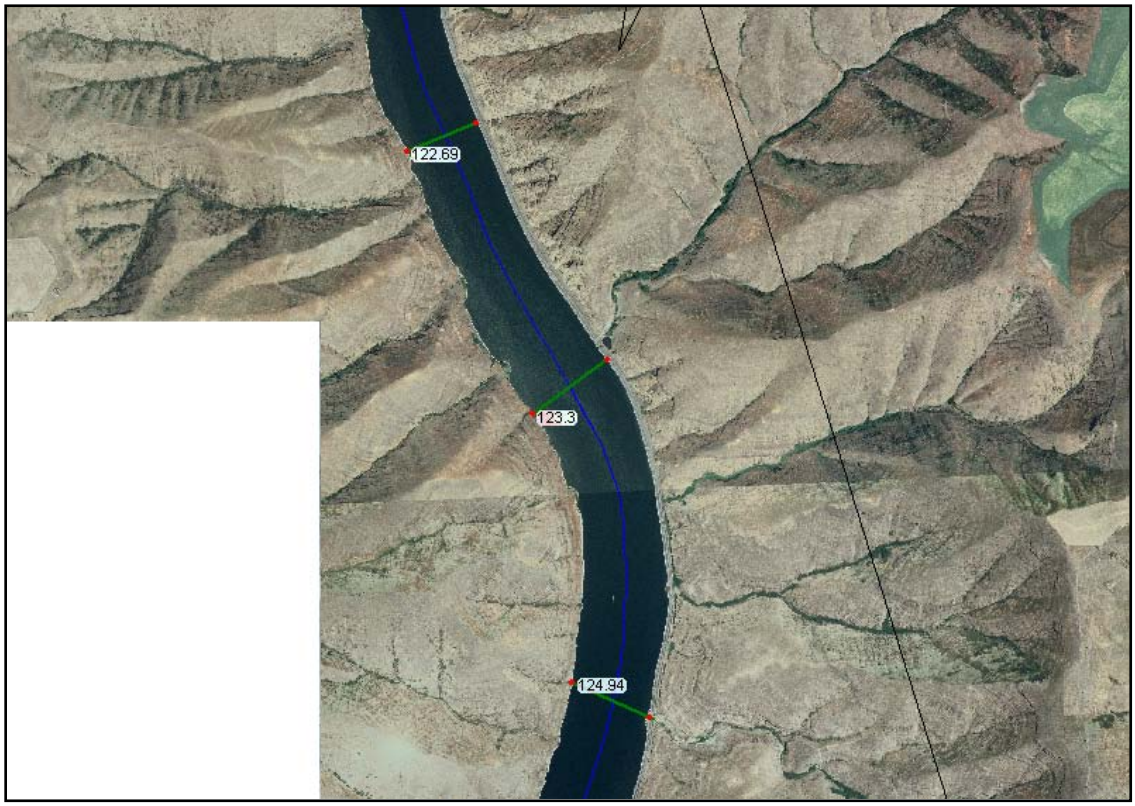


Figure 49. Bend at Snake River RM 123.3.

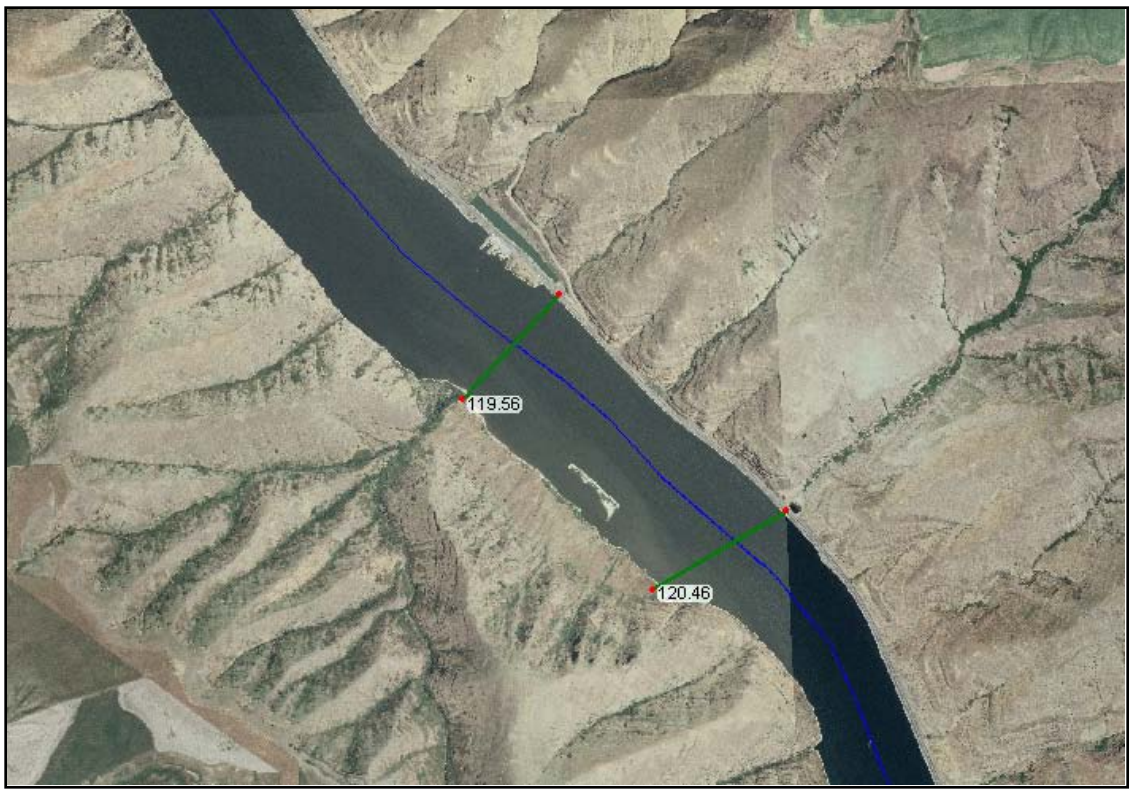


Figure 50. Centennial Island at Snake RM 120.

The Ackers-White transport function also performed very well in the simulation of long-term bed elevation change and surface median sediment size of the Snake and Clearwater Rivers upstream from the confluence. Simulated mean effective bed elevation changes for 1974-2009 are compared with the actual mean bed elevation changes in Figure 51 and Figure 52. On the Clearwater River (Figure 51), the Ackers-White function correctly computed very little accumulation upstream from Memorial Bridge at RM 2. About 8 ft of accumulation was computed for the turning basin and compares well with the 6 ft of measured accumulation. Sediment has been dredged from the turning basin, so the actual accumulation should be less than the computed amount. Negligible accumulation was computed for the channel through the constriction at the CPRR Bridge and is followed by substantial accumulation in the segment between the railroad bridge and the confluence. The computed accumulation near the confluence is greater than the measured accumulation, but not extraordinarily so considering the duration of the simulation. Sediment has also been dredged from the confluence so the measured accumulation should be less than the computed amount.

On the Snake River above the confluence (Figure 52), negligible accumulation was computed for the channel above about RM 143 near Hells Gate Marina. The Ackers-White function correctly computed the 5 ft bed change upstream from the

channel constriction caused by the levee, though the maximum accumulation is offset by one cross section. There is very little accumulation, computed or measured, immediately upstream from the confluence.

Ideally, the Ackers-White transport function would be used to simulate transport in the upper segment of the reservoir and the Toffaleti function would be used to simulate transport in the lower reservoir during the same sediment transport simulation so that mass continuity is maintained. Currently, HEC-RAS does not allow selection of more than a single transport function in a single simulation. For this particular model, the curve of cumulative mass passing a particular cross section (mass-out curve) for the Ackers-White simulation in Figure 53 intersects the Toffaleti mass-out curve at RM 130 and RM 127. This means that an equivalent total mass load is passed by both simulations to the lower reservoir at these locations and that these locations would be appropriate locations to pass the simulation from the Ackers White function to the Toffaleti function. The location at RM 130 is preferred because the sediment mass-passing in each grain size class for both simulations is about the same.

Since the transfer between transport functions cannot be made within a single simulation, an alternative is to switch between cross section geometries (HEC-RAS merge) at a point where the mass-out curves intersect. For this particular model, this would mean that cross sections produced by the Ackers-White function would be used above RM 130 and cross sections produced by the Toffaleti function would be used at or below RM 130. The locations where the mass-out curves cross are not unique and would change with different sediment load, discharge series and duration of the simulation. Also for this particular model, it is noted that the longitudinal accumulation volume curve for Ackers-White simulation crosses the Toffaleti accumulation volume curve at about RM 126 at the end of the simulation period, which suggests that cross sections produced by the Toffaleti function should only be used below this point for a conservative representation of total accumulation in flood modeling.

Channel cross sections produced by the Ackers-White and Toffaleti functions at the end of the 1974-2009 simulation were exported from the sediment transport model and compared to the actual channel 2009 cross sections. Sediment deposition and scour in HEC-RAS is spread evenly across the active width of the cross section so the adjusted channel is not expected to reproduce specific bed features. In this study, the efficacy of the simulated cross section geometries is judged based on how well the simulated geometry reproduces the flood water surface profile computed with the actual 2009 geometry. The most relevant cross sections properties are the wetted channel area, hydraulic radius and the water surface at the confluence.

A composite model was developed with the simulated Ackers-White cross sections for all segments above RM 130 and the Toffaleti cross sections at and below RM 130. The steady-state water surface profile for the 1-percent exceedance discharge

(331,600 cfs) was computed for the composite geometry and the actual 2009 geometry. The wetted-area and hydraulic radius of the composite model of Lower Granite Reservoir compares favorably with the actual 2009 geometry in Figure 54 and Figure 55. The average difference between the composite model and actual wetted-area and hydraulic radius was less than 2 percent. The water surface elevation for the 1-percent exceedance discharge computed by the composite model was 740.78 ft at the confluence which agrees very well with the 740.62 ft elevation computed with the actual geometry.

The efficacy with which the Ackers-White and Toffaleti transport functions reproduce the historic long-term accumulation of sediment in the varied channels of the Snake and Clearwater Rivers upstream from the confluence and in the reservoir below the confluence justifies the use of the Ackers-White and Toffaleti functions in the simulation of the 50-year future channel condition.

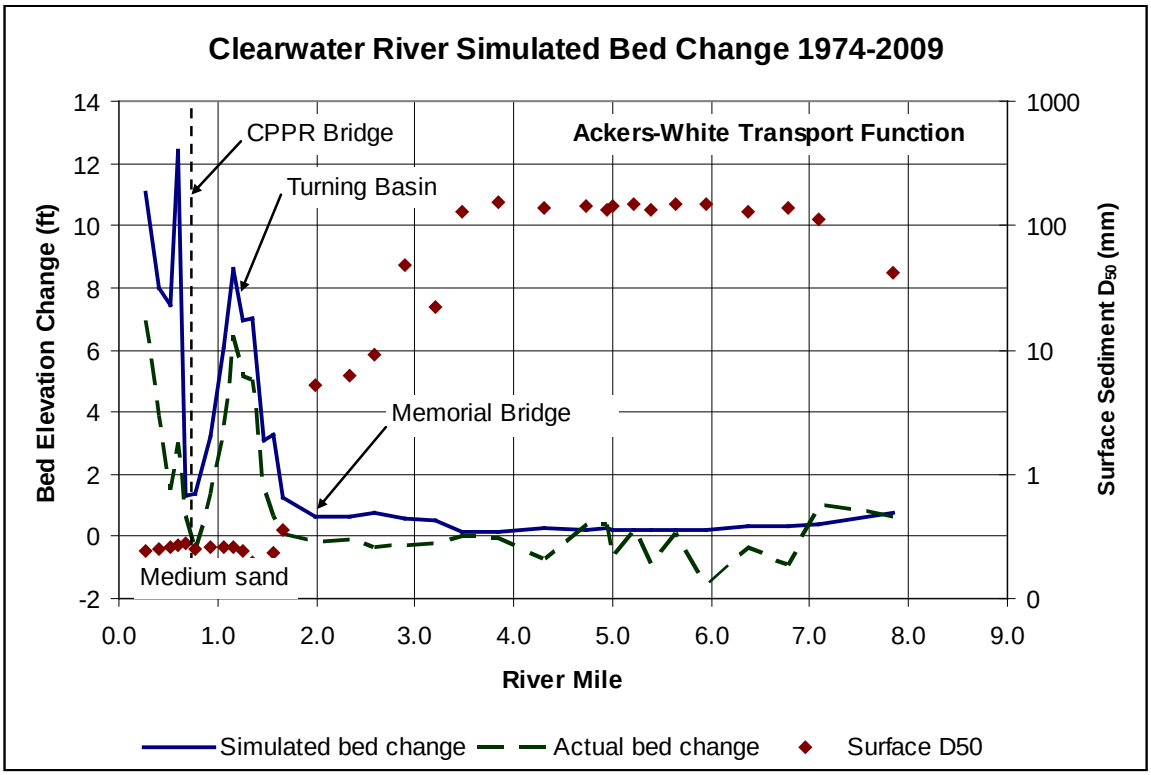


Figure 51. Simulated Ackers-White bed change Clearwater River.

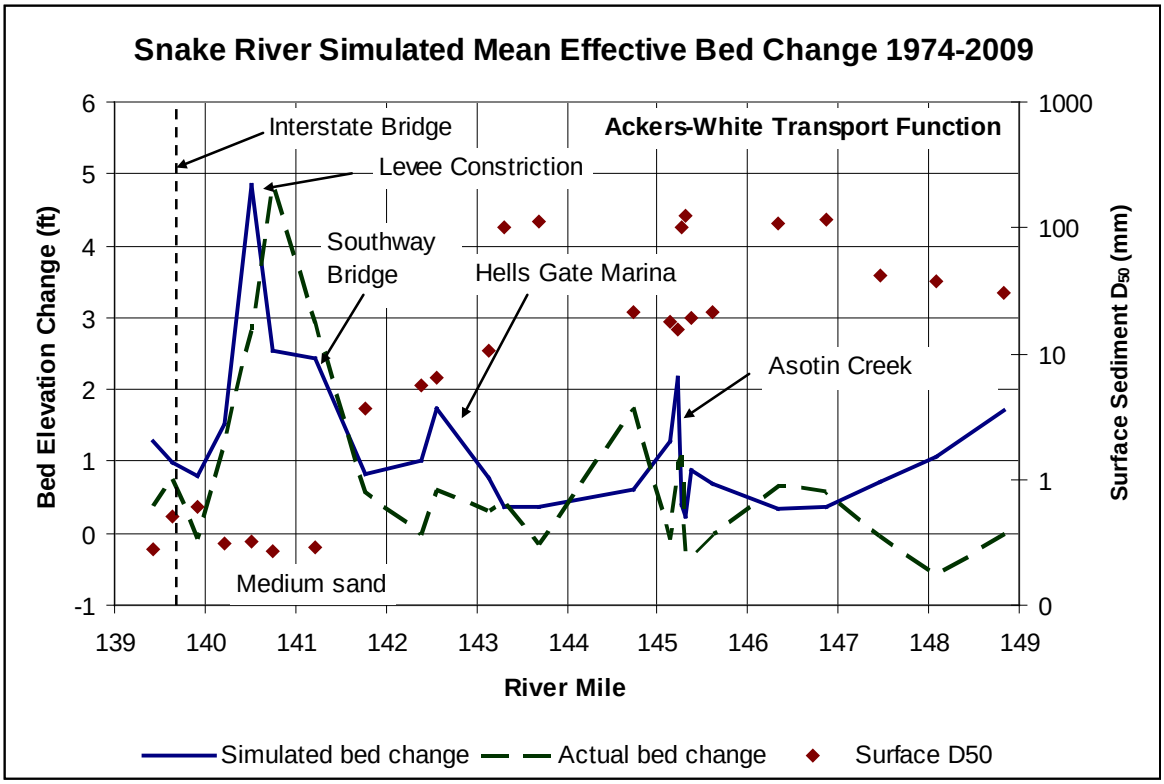


Figure 52. Simulated Ackers-White bed change Snake River upstream of confluence.

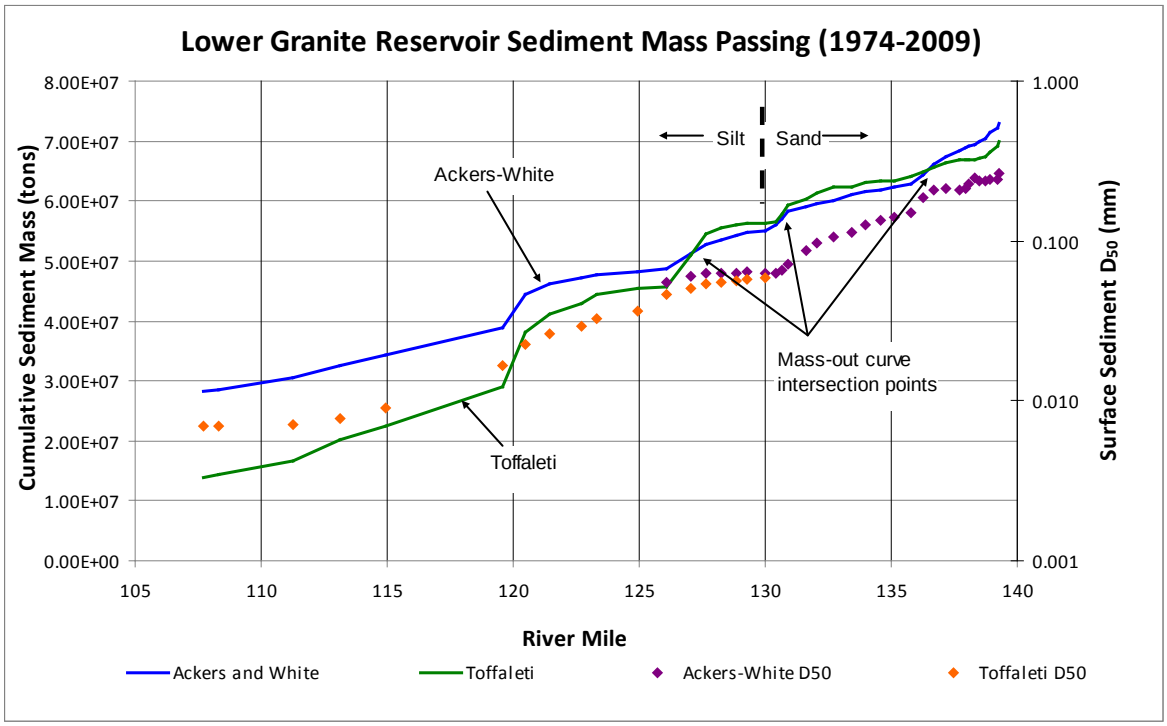


Figure 53. Simulated sediment passing with Ackers-White and Toffaleti functions 1974-2009.

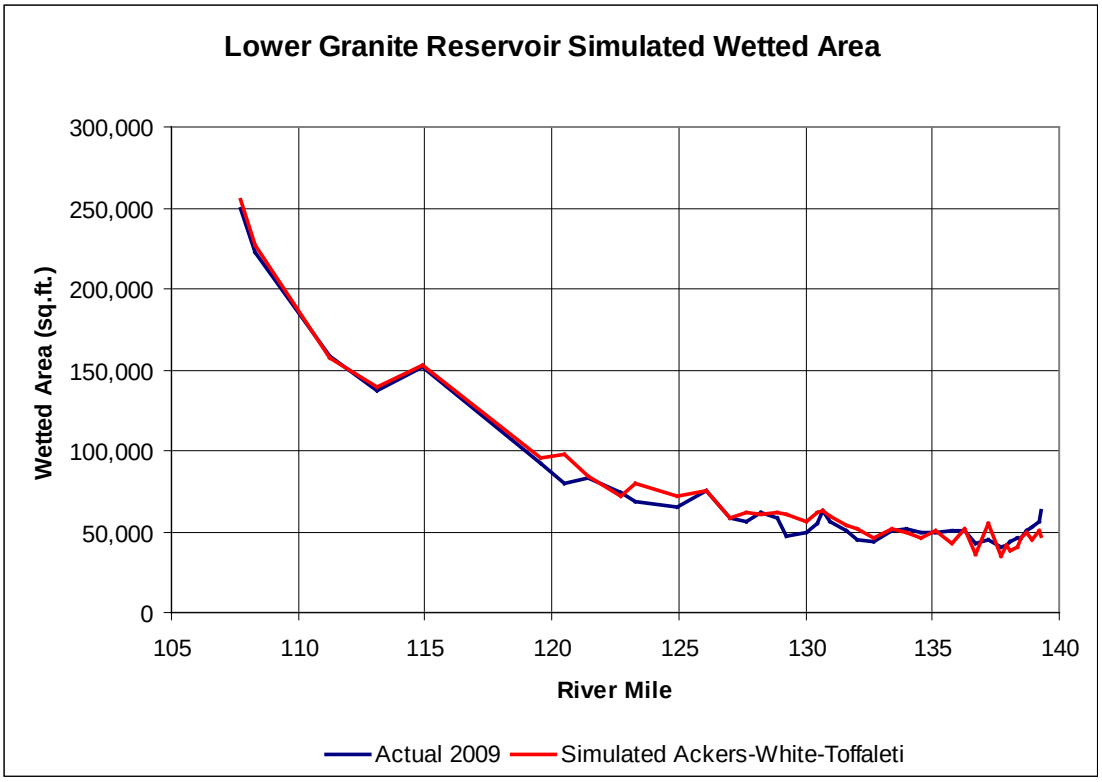


Figure 54. Simulated and actual wetted-area in Lower Granite Reservoir.

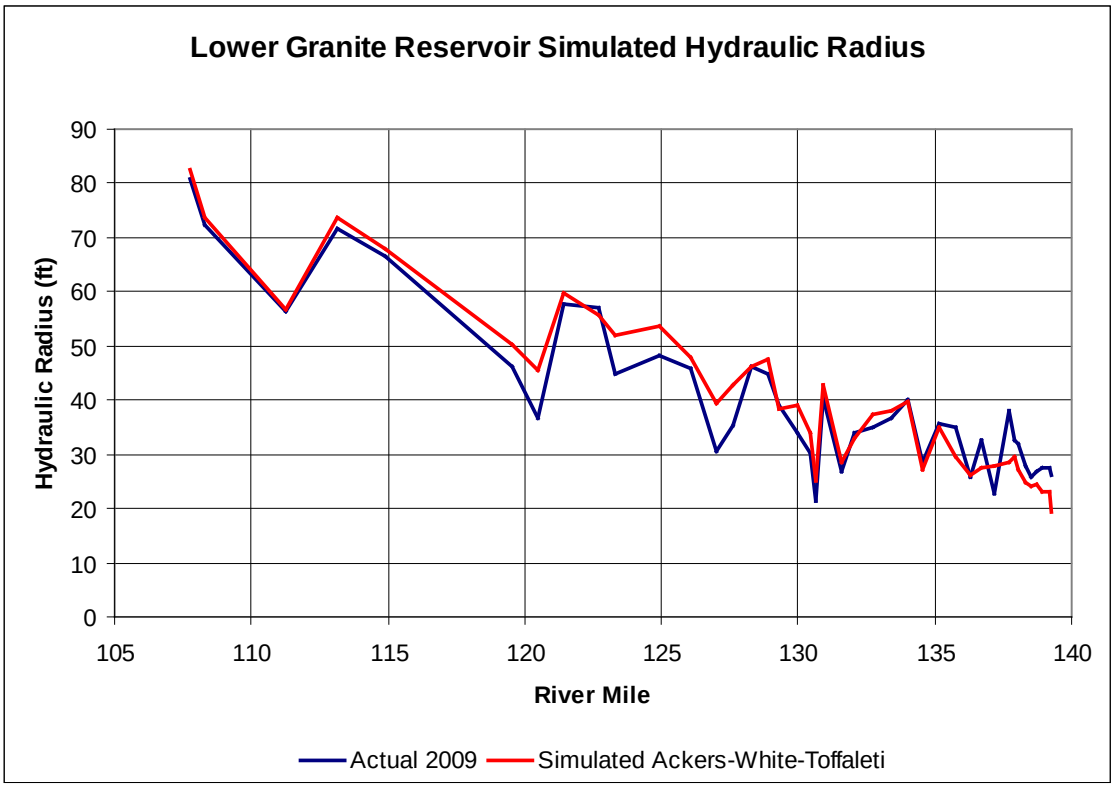


Figure 55. Simulated and actual hydraulic radius in Lower Granite Reservoir.

10.13. Simulation of Future 50-year Sediment Accumulation

The flood risk at the end of the future 50-year analysis period must be evaluated for the channel conditions expected at that time. Sediment will continue to accumulate in Lower Granite Reservoir, so the cross section geometry must be adjusted for the expected accumulation. The previous section showed that historic sediment accumulation was simulated well with the HEC-RAS Ackers-White and Toffaleti transport functions and that the flood water surface elevation at the confluence computed with simulated cross section geometry at the end of the 1974-2009 period agreed well with the water surface elevation computed with the actual 2009 cross section geometry. The successful simulation of the historic sediment accumulation is appropriate justification to use HEC-RAS and the Ackers-White and Toffaleti transport functions to simulate the channel geometry at the end of the 50-year analysis period.

The initial model geometry for mobile-bed simulation of the future channel condition was developed from the 2009 multibeam echosounding (MBES) bathymetry and 2009 sediment ranges. The initial geometry model is the same as the calibrated fixed-bed model of the current condition described in Section 3. The 2009 model domain (Figure 42) consists of 252 cross sections, 52 on the Clearwater River between the confluence and RM 7.85 and 60 on the Snake River above the confluence at RM 139.404 to RM 148.83 and 140 on the Snake River between the Dam at RM 107.73 and the confluence. Cross section spacing varies from 400 ft in the segments covered by the MBES bathymetry to several thousand feet in segments represented by the sediment range cross sections. A spacing of 400 ft between cross sections in the upper segment of Lower Granite Reservoir gave the best representation of measured variability bed change and is 3 to 4 times the wavelength of the largest bedforms. A spacing of 400 ft is about twice the travel distance required for medium sand to settle through the full depth of the water column during typical peak discharges. Sediment transport solutions obtained from models with cross sections spaced less than 400 ft in Lower Granite Reservoir appear to be influenced by erosion and deposition limiters in the HEC-RAS sediment transport algorithms.

Cross sections from the 2009 fixed-bed model were thinned to 50 bed points to reduce sediment transport computation runtimes. The thinned cross sections, such as that at Snake RM 139.057 in Figure 56, conform well to the original cross section, so the change in hydraulic properties is negligible. Bridges were not represented in the geometry because initial tests showed they did not significantly affect sediment transport. Levees were included in the cross section geometry. Channel Manning's *n* values were set depending on the modeling objective and varied from the calibrated values at low and moderate discharges in the simulation of future accumulation to 0.026 and 0.028 to represent the lower regime flow resistance at extreme discharges (Section 10.9). Overbank Manning's *n* was set to a constant value of 0.04, but overbank flow is

minimal. Contraction and expansion coefficients were set at 0.1 and 0.3. A single junction at the confluence joins the Snake and Clearwater Rivers (Figure 43).

Initial bed material gradations for the sediment transport model were guided by the sediment core survey and ranged from small boulder and large cobble in the segments of the Snake and Clearwater Rivers above the backwater zone to sand in the upper segment of Lower Granite Reservoir to silt in the lower segment of Lower Granite Reservoir. Bed material designations for the 2009 sediment transport model are listed in Table 3. Transients in the simulation caused by bed initialization (warm-up) occurred in the first several years, but did not significantly affect the simulated long-term geometry. The sediment loads for the Snake and Clearwater Rivers were input as a sediment rating curves developed from the adjusted power fit of the measured sediment data as described in Section 8. Unit weights of sediment were 90 lb ft^{-3} for sand, 60 or 70 lb ft^{-3} for silt and 30 lb ft^{-3} for clay.

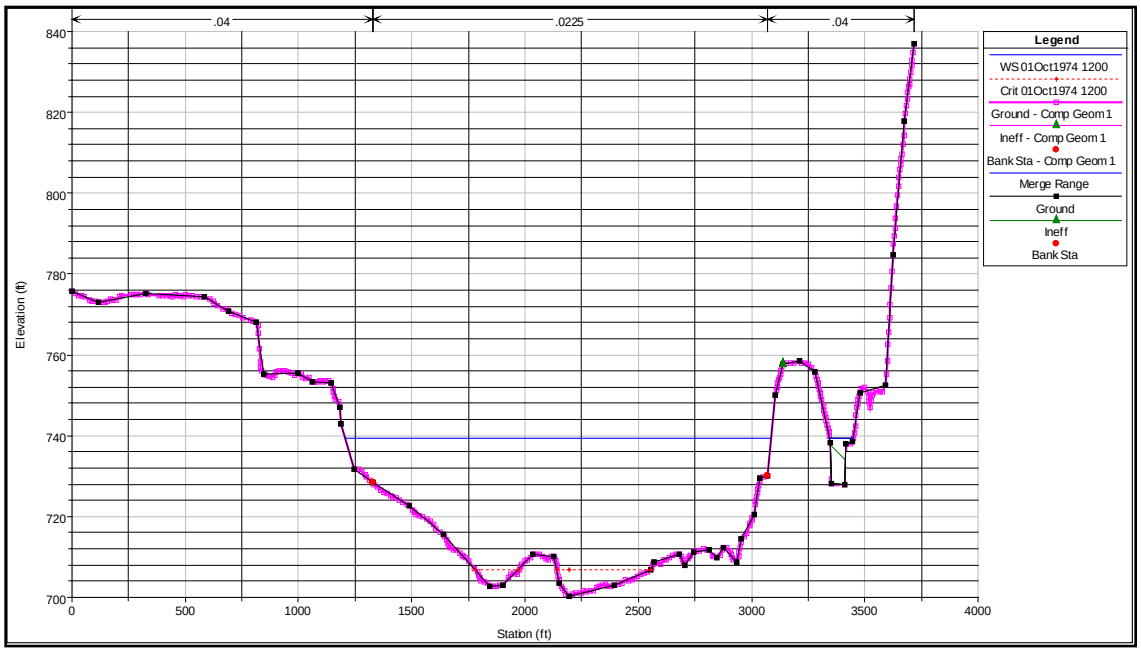


Figure 56. Thinned cross section at Snake River 139.057.

Bed Material Designation in 2009 Initial Sediment Transport Geometry					
River	Reach	Upstream Station	Downstream Station	Bed Material	D_{50} mm
Clearwater	Lewiston	7.850	1.603	Large Cobble	128
Clearwater	Lewiston	1.530	0.967	Medium Sand	0.5
Clearwater	Lewiston	0.906	0.545	Large Cobble	128
Clearwater	Lewiston	0.461	0.217	Medium Sand	0.5
Snake	Clarkston	148.83	142.005	Small boulder	512
Snake	Clarkston	141.949	139.404	Large Cobble	128
Snake	Lower Granite	139.254	134.066	Medium Sand	0.5
Snake	Lower Granite	133.997	130.106	Fine Sand	0.25
Snake	Lower Granite	129.989	107.43	Silt	0.016

Table 3. Bed material designations in 2009 initial sediment transport geometry.

Daily quasi-unsteady flow time series for the Snake and Clearwater Rivers for the future 50-year period is comprised of the historic discharge record from 1 October 1974 through 30 September 2010 for the first 36 years plus the repeated period 1 October 1974 to 30 September 1988 for the latter 14 years (18263 daily values). All discharge values were derived from the USGS stream gage records at Anatone and Spalding. Based on preliminary tests, the sediment computation interval was set at 6 hours. The downstream boundary condition was represented as a stage time series that was held constant at 739.41 ft NAVD88, The drawdown period between 28 February 1992 and 6 April 1992 was not included. The temperature time series for the sediment transport analysis was held constant at 50 degrees Fahrenheit.

Longitudinal sediment accumulation curves for the 2010-2060 period computed with the Ackers-White and Toffaleti transport functions are plotted in Figure 57. Total accumulated sediment at RM 130 in Lower Granite Reservoir by the Ackers-White function is 16.6 mcy, or about 0.33 mcy per year. The predicted volume and accumulation rate agrees very well with the historic 12.5 mcy measured accumulation volume and 0.35 mcy per year accumulation rate. The accumulation rates could be made to match with slight adjustment of the assumed unit weights of deposited sediment.

The Toffaleti accumulation curve intersects the Ackers-White curve at about RM 120 and intersections of the mass-out curves in Figure 58 occur near RM 130 and RM 120. Total mass inflow and the sediment load grain size distribution into Lower Granite is about the same with both transport functions, so this indicates that the Toffaleti sediment accumulation curve can be used to estimate the total accumulation and distribution of sediment in the lower Reservoir below the mass-out intersection points. As discuss in Section 10.12, switching between transport curves produces the most plausible distribution of sediment and adjusted cross section geometry within the reservoir.

Total sediment accumulation at RM 107.73 from the Toffaleti curve over the 50 year period is 83.9 mcy. The predicted 1.7 mcy per year total accumulation rate agrees reasonably well with the historic 2.1 mcy per year accumulation rate. The accumulation rates could be made to match by assuming smaller, yet plausible, unit weights for silt deposited in the lower reservoir.

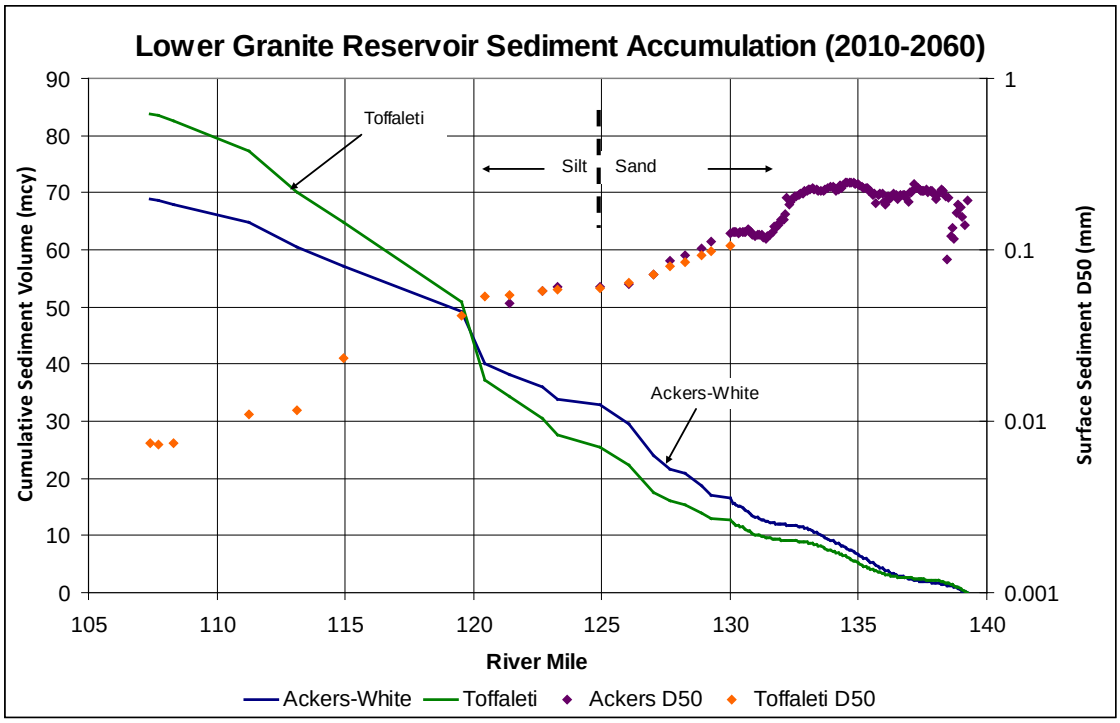


Figure 57. Sediment accumulation simulated with Ackers-White and Toffaleti functions 2010-2060.

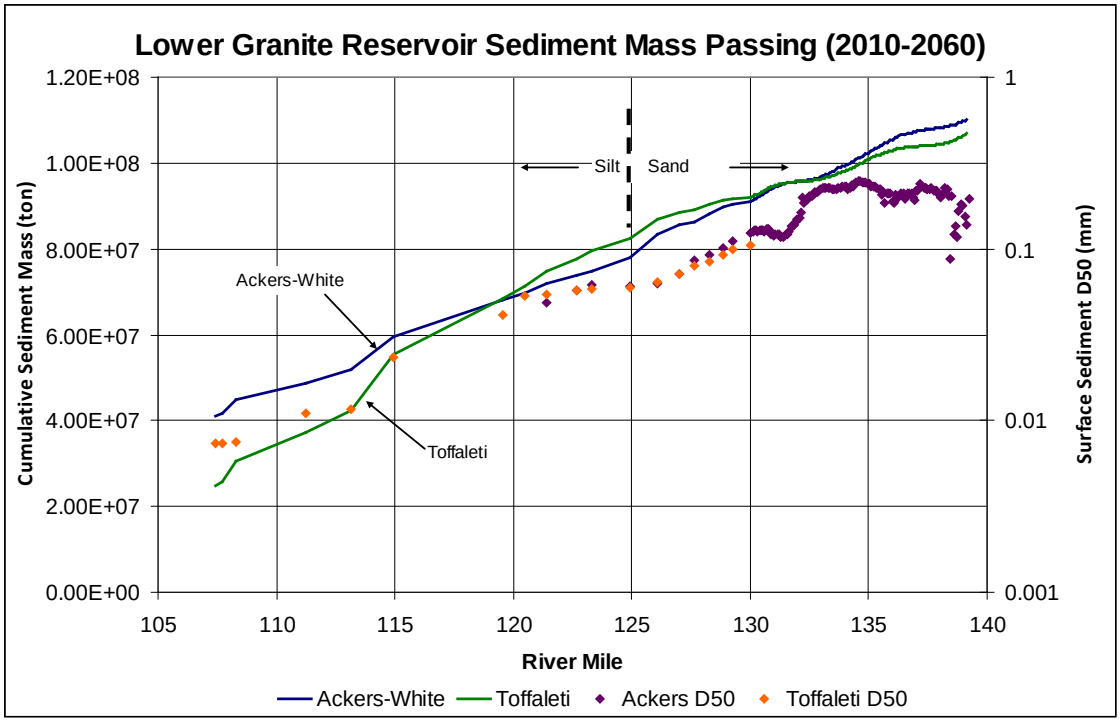


Figure 58. Simulated sediment passing with Ackers-White and Toffaleti functions 2010-2060.

Mean effective bed change curves for 2010-2060 in Lower Granite Reservoir period for the Ackers-White and Toffaleti transport functions are plotted in Figure 59. In the sand bed segment above Silcott, bed change varies from less than 1 ft between RM 137 and RM 137 and near RM 132 to over 15 feet at 133.7. The average bed change in Lower Granite Reservoir computed with the Ackers-White function above RM 130 is 6.0 feet. Average bed change increases to 6.8 ft between RM 130 and RM 120 and to 7.3 ft between RM 120 and RM 107. The effect of cross section spacing on the long-term simulated bed change is seen in Figure 60. The 1600 ft cross section interval decreased the variability of the bed change. More importantly, the greater cross section spacing cause a shift of the relatively large accumulation of sediment near RM 134 downstream where it has less hydraulic effect on the flood water surface at the confluence.

The mean effective bed change for 2010-2060 for the Clearwater River simulated with the Ackers-White transport function is plotted in Figure 61. Negligible bed change occurred above Clearwater RM 2. No dredging was assumed in the 50 year simulation, so about 6 feet of sand accumulated in the turning basin. Maximum bed change occurred in the deep thalweg at the CPRR Bridge. Accumulation at this location is unrealistic because of secondary flows near the bridge piers. Between 5 and 9 feet of sediment accumulated in the segment between the confluence and the CPRR bridge. Total accumulated sediment volume in the Clearwater River reach is 1.9 mcy.

The mean effective bed change for 2010-2060 for the Snake River above the confluence simulated with the Ackers-White transport function is plotted in Figure 62. Simulated bed change was less than 2 ft above RM 141.5. The simulation predicts accumulation of between 3 and 5 feet of sand above the constriction at the upper end of the levee at RM 140.5. Maximum bed change occurred at RM 140.2 in the deep thalweg at this location. The simulation predicts the accumulation of between 1 ft and 5 feet of sand in the segment between the confluence and Interstate Bridge. Total accumulated sediment volume in the Snake River reach above the confluence is 2.9 mcy.

The accumulation volumes and bed elevation changes discussed above are computed with the expected sediment loads based on the regression analysis of measured sediment data. Sediment loads at Lower Granite Reservoir may be greater or less than the expected load because of climate variation or other factors. To better understand the effect of altered sediment loads on sediment accumulation and distribution in the reservoir, the HEC-RAS sediment transport simulations were repeated with sediment load increased to 125 percent and decreased to 75 percent. The altered sediment loads were input by multiplying the sediment rating curves (tables) for the Snake and Clearwater River boundary conditions by factors of 1.25 and 0.75.

Cumulative sediment volumes Lower Granite Reservoir for the alternative sediment loads are plotted in Figure 63 and Figure 64. At RM 130, the Ackers-White transport function computed a total cumulative volume of 12.1 mcy for the 75 percent load and a volume of 20.9 mcy for the 125 percent load. At RM 107, the Toffaleti transport function computed a total cumulative volume of 62.9 mcy for the 75 percent load and a volume of 105.4 mcy for the 125 percent load. Proportionately, the alternative loads produced volumes that are close to the 0.75 and 1.25 factors applied to the sediment load rating tables.

Distribution of the sediment grain size within the reservoir changes somewhat under the alternative loads. The Ackers-White mean effective channel bed change and surface sediment D_{50} are plotted in Figure 65 for the Lower Granite Reservoir between RM 125 and the confluence. With increased sediment load the surface sediment becomes coarser near RM 132 and the channel continues to aggrade as sand is carried further into the reservoir. The transport of sand deeper into the reservoir was observed in the bathymetry acquired during the high discharge and low flow periods in 2011 and is discussed in Section 12. Overall, the pattern of channel adjustment for the three load alternatives is similar. The adjusted channel in the segments from RM 130 to RM 132 and near RM 136 attained relative stability at 75 percent load and remain stable even though sediment load is increased.

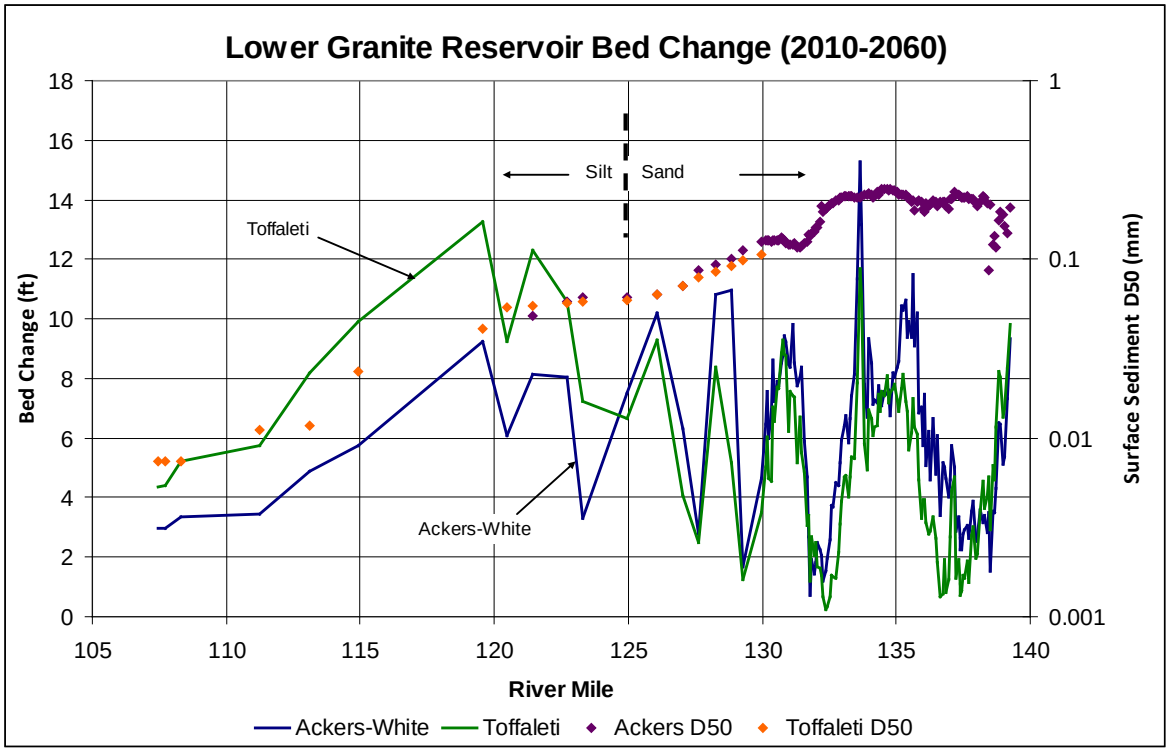


Figure 59. Simulated Lower Granite Reservoir Bed Change 2010-2060.

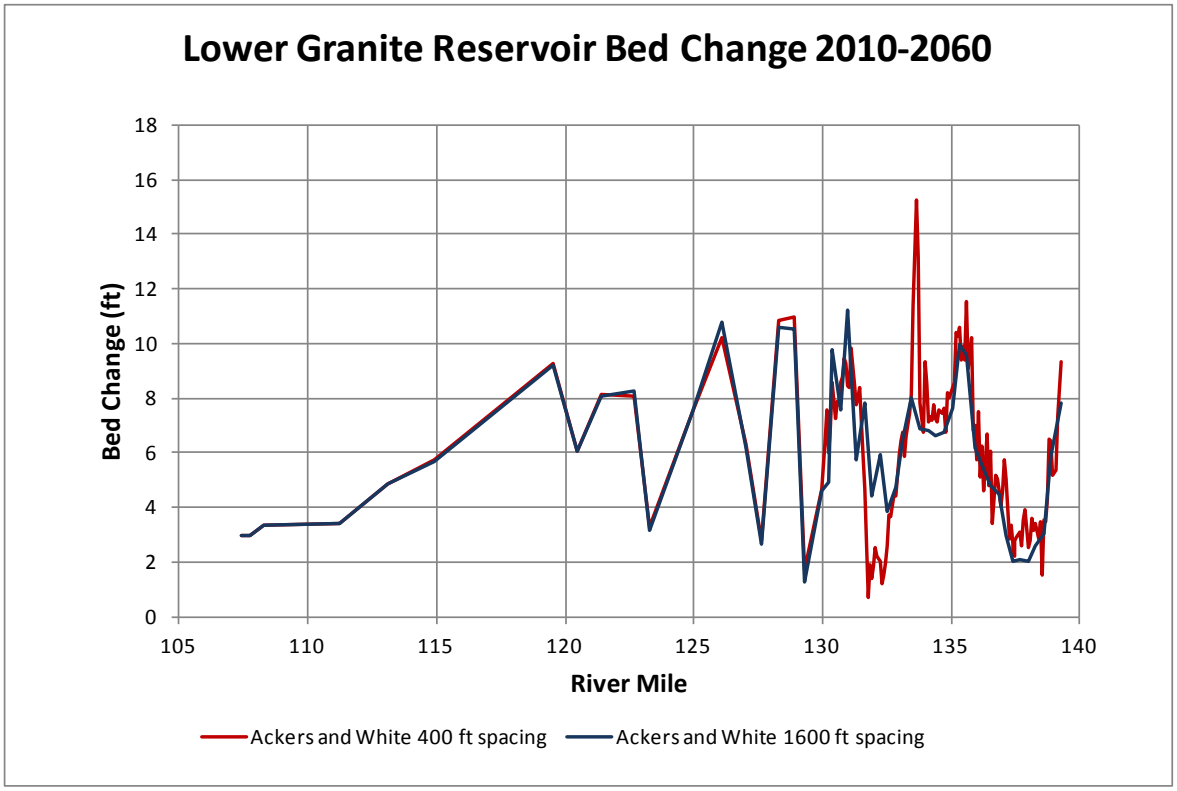


Figure 60. Effect of cross section spacing on simulated bed change.

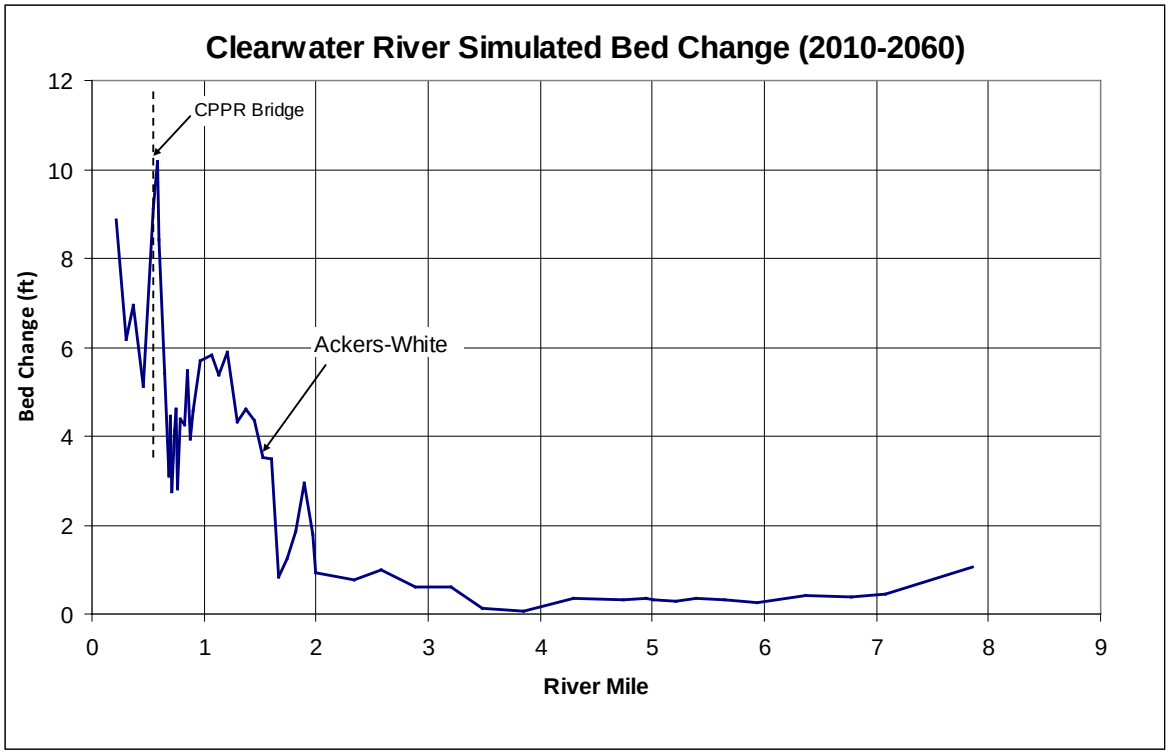


Figure 61. Simulated Ackers-White 2010-2060 bed change Clearwater River.

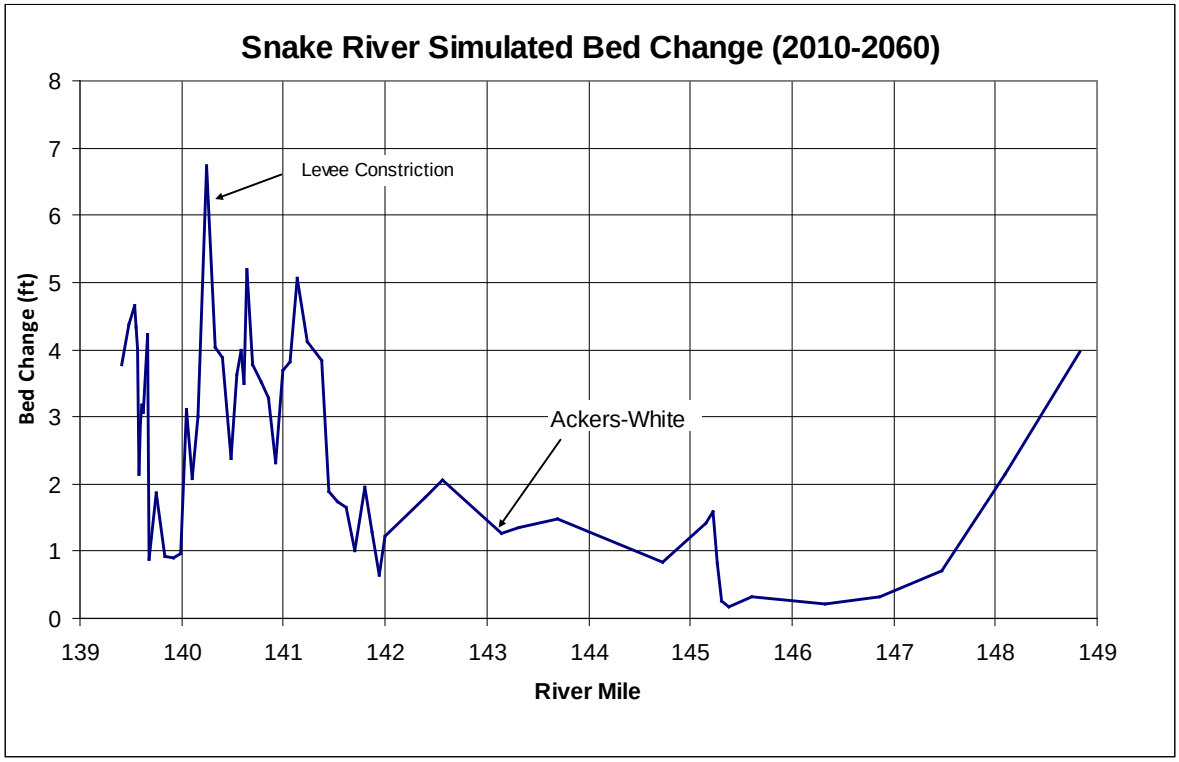


Figure 62. Simulated Ackers-White 2010-2060 bed change Snake River upstream of confluence.

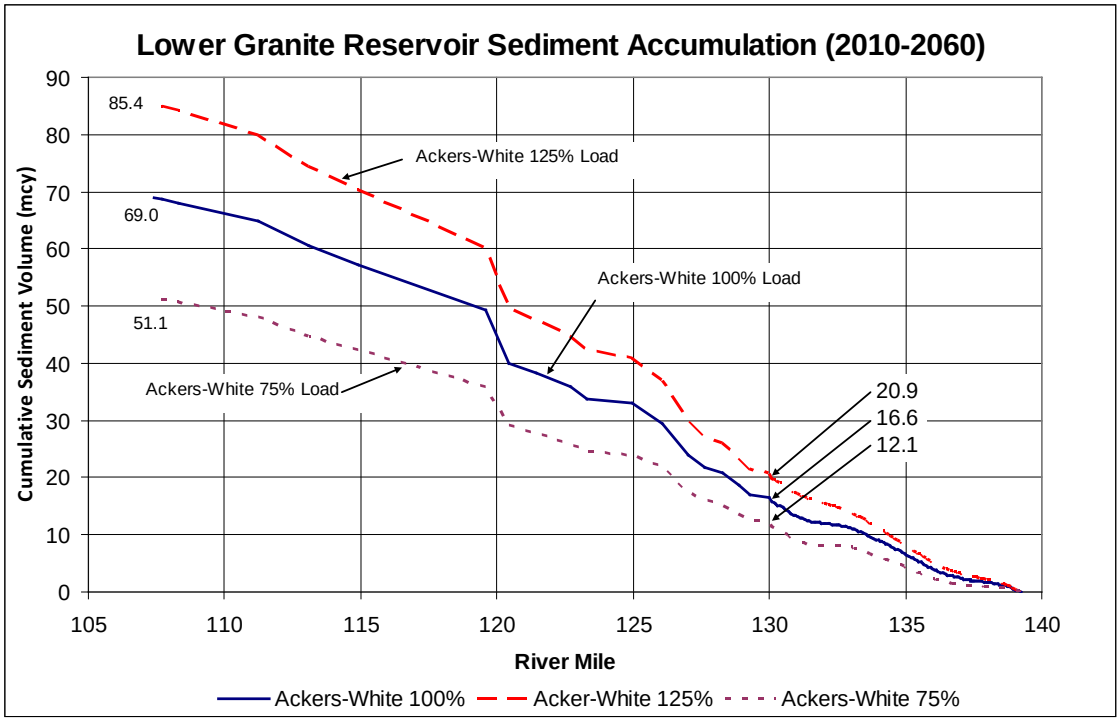


Figure 63. Ackers-White sediment accumulation volumes in Lower Granite Reservoir with alternative sediment loads.

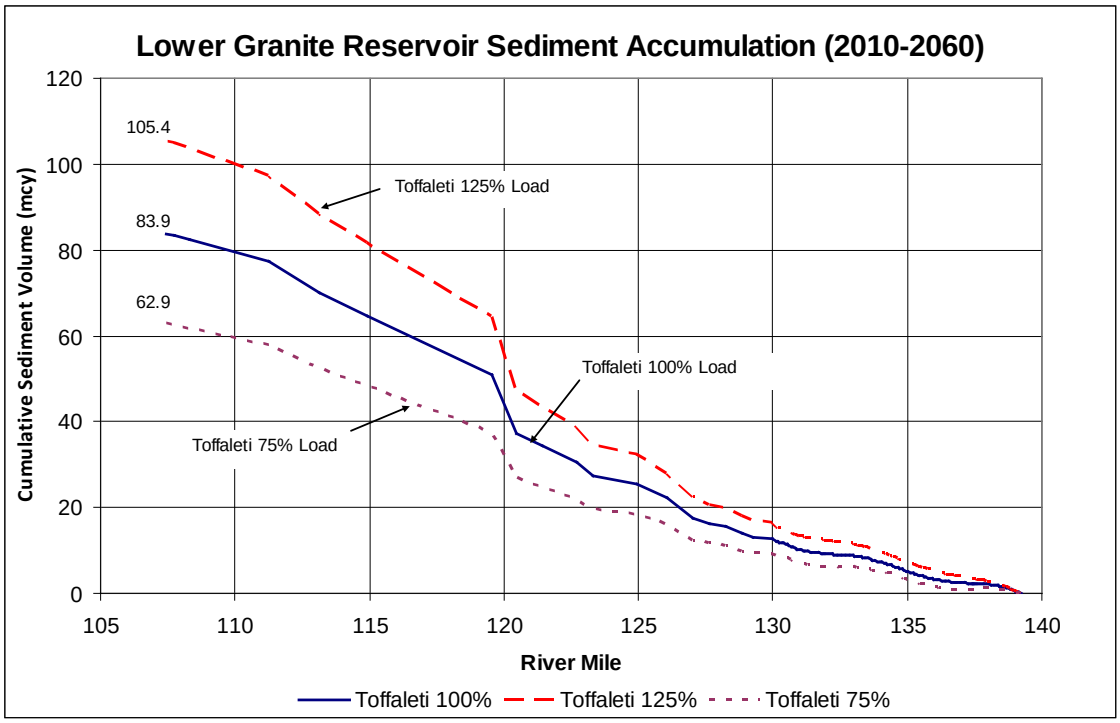


Figure 64. Toffaleti sediment accumulation volumes in Lower Granite Reservoir with alternative sediment loads.

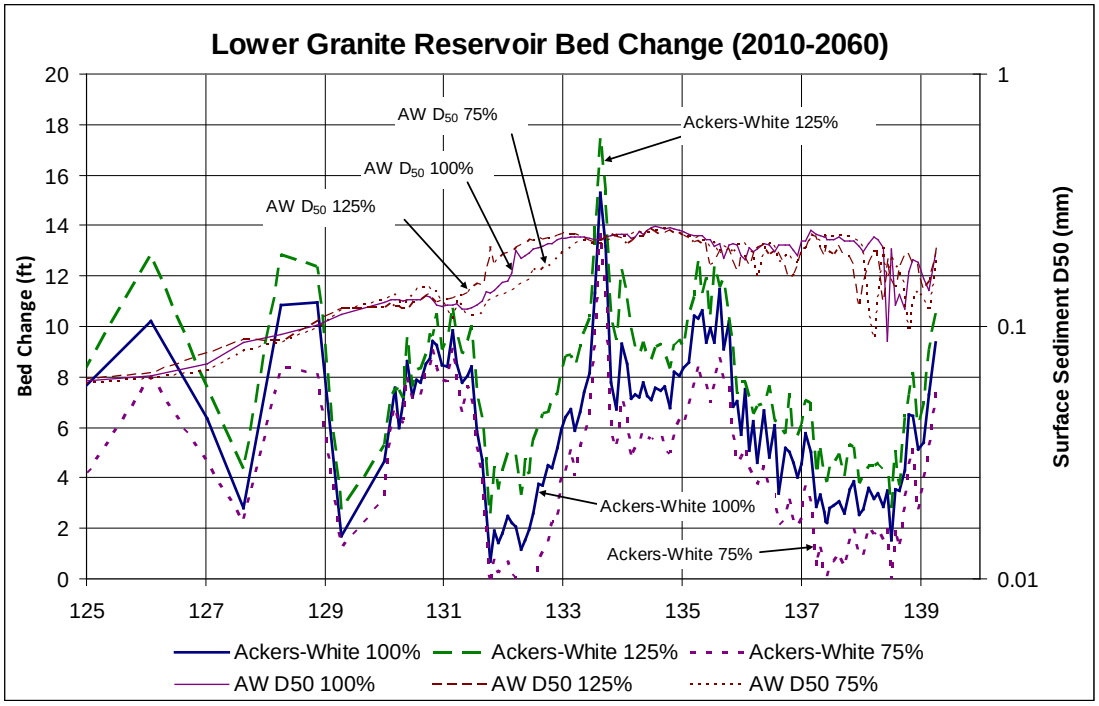


Figure 65. Simulated Bed change in Lower Granite Reservoir for alternative sediment loads.

Cross sections of the adjusted channels at the end of the 2010-2060 for the 100 percent load simulation were exported from the HEC-RAS sediment transport module and incorporated into hydraulic models to represent the 50-year future channel condition. As noted in Section 10.12, the most important cross section properties for flood model are wetted-area and hydraulic radius. Unreasonable or inconsistent adjustments in these parameters can indicate a poor sediment transport solution. The wetted-area and hydraulic radius for the year simulated year 2060 cross sections are compared to the same parameters for the actual 2009 channel geometry in Figure 66 through Figure 69. The wetted-area and hydraulic radius was computed for the 8 June 2010 calibration discharge of 214,200 cfs. Below RM 130, the wetted-area of the simulated channel decreased by an average of about 9800 ft^2 from 2009 to 2060 and above Silcott the wetted-area of the channel decreased by about 5300 ft^2. On average, the hydraulic radius of the simulated channel below RM 130 decreased by 1.5 ft and above RM 130 the hydraulic radius decreased by 0.9 ft. The plot of wetted-area in Figure 67 indicates that the sediment transport solution oscillated slightly between cross sections in the segment from RM 135 to RM 137. The oscillations might be dampened by adjustment of the computation parameters in the HEC-RAS sediment module and increase of cross section spacing (with loss of channel information), but the effect of the oscillations on the performance of the hydraulic model is minimal. Long-term sediment transport simulations with cross section spaced at greater intervals confirmed that

general deposition patterns and accumulation volumes were not sensitive to cross section spacing. Simulated 50-year sediment accumulation depths in Lower Granite Reservoir for HEC-RAS sediment transport models developed with cross sections spaced at 400 ft and 1600 ft are compared in Figure 70. The simulation based on a 1600 ft cross section spacing evens out the variability produced the simulation based on the 400 ft spacing.

The year 2060 wetted-area between RM 134 and the confluence averages 42,300 ft^2, which agrees very well with the 41,500 ft^2 equilibrium wetted-area estimated from the Parker hydraulic geometry relationships. The good agreement between the simulated year 2060 wetted-area and the equilibrium hydraulic geometry further validates the use of Ackers-White function for prediction of future channel condition, and it indicates that the segment above RM 134 will approach equilibrium in the 50-year future analysis period. This also suggests that monitoring of sediment accumulation and channel geometry in this segment would be a means to confirm the accuracy of the prediction of future channel condition.

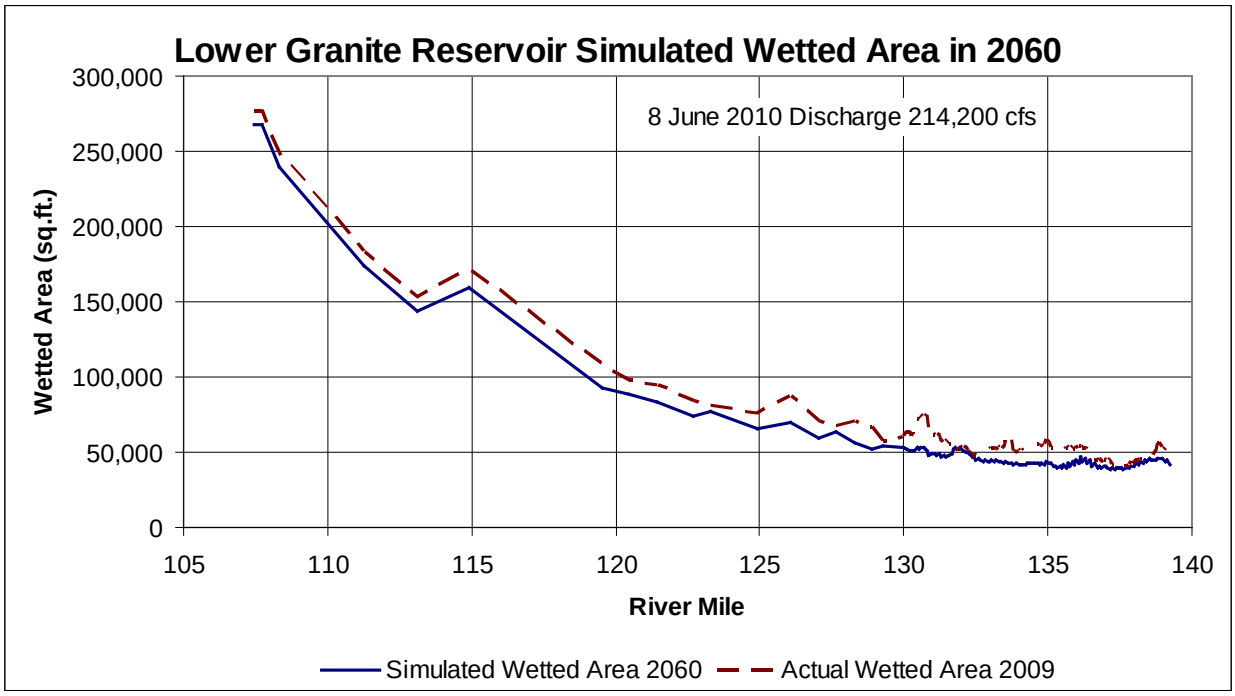


Figure 66. Simulated wetted-area in Lower Granite Reservoir in 2060.

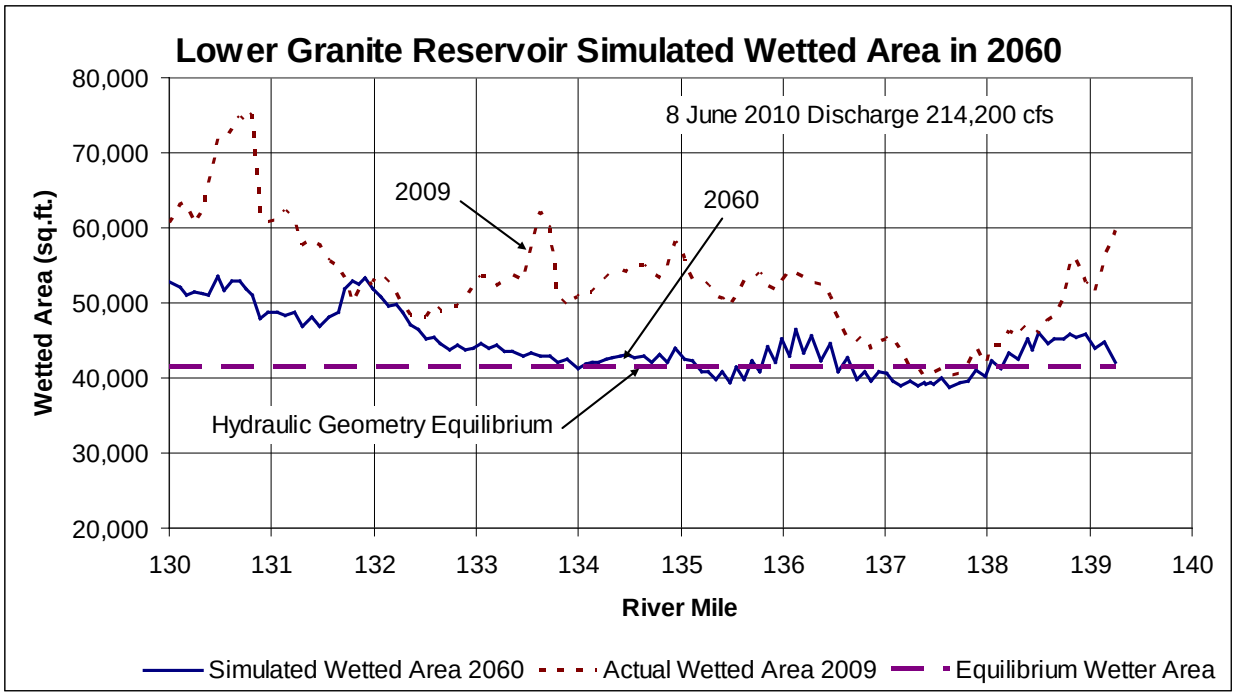


Figure 67. Simulated wetted-area Silcott to the confluence in 2060.

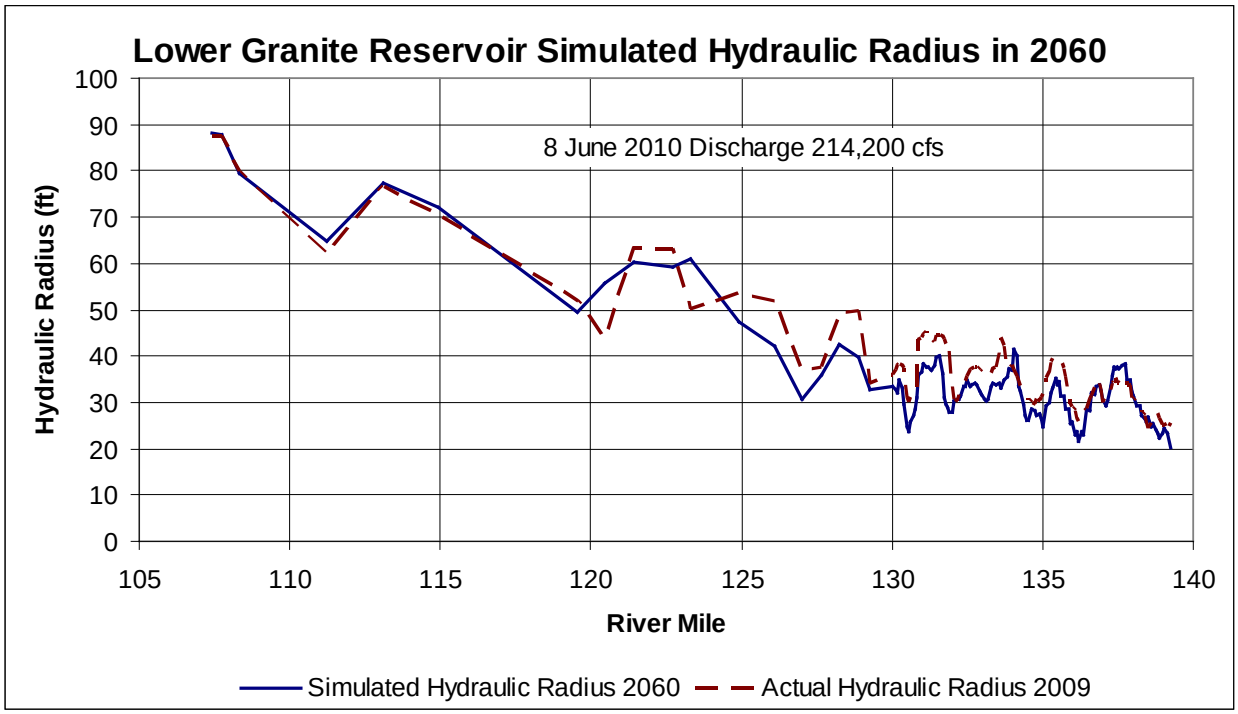


Figure 68. Simulated hydraulic radius in Lower Granite Reservoir in 2060.

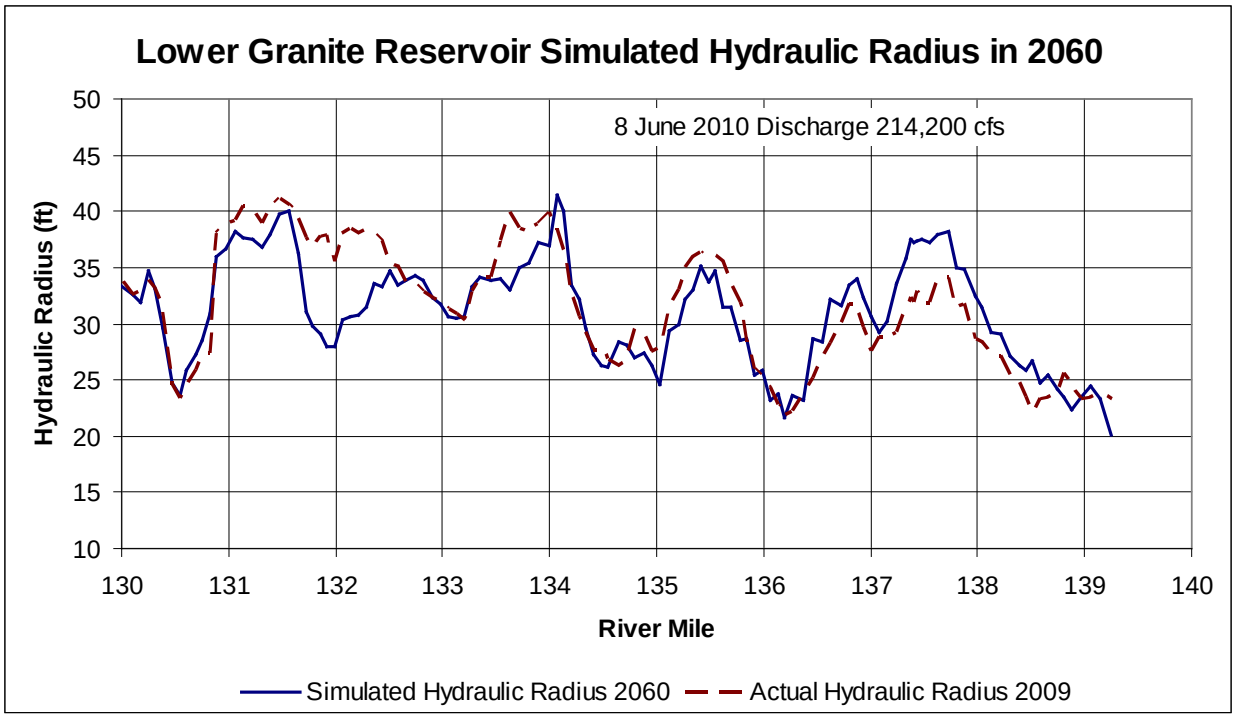


Figure 69. Simulated hydraulic radius Silcott to the confluence in 2060.

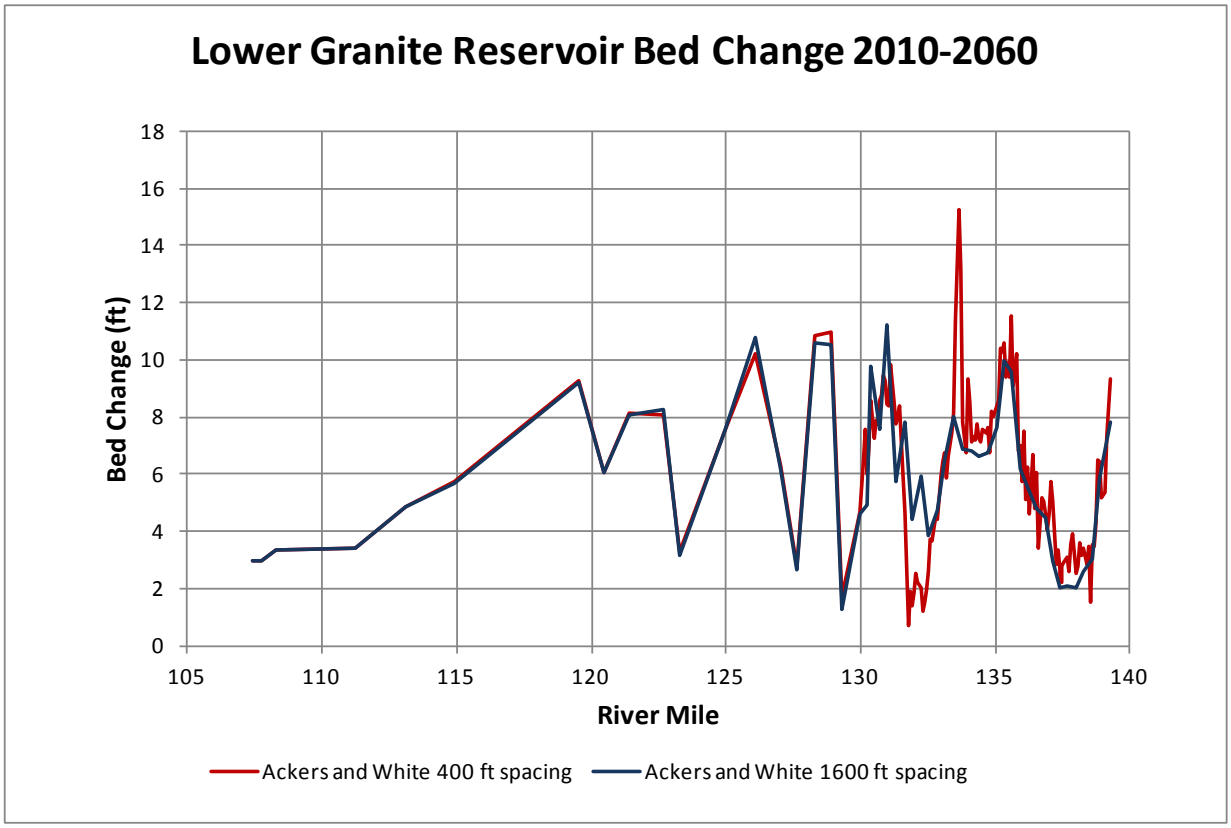


Figure 70. Effect of cross section spacing on long-term simulation of sediment accumulation.

Simulation of expected sediment load was continued for another 50 year period to produce a total of 100 years of sediment accumulation in Lower Granite Reservoir. Again, the daily quasi-unsteady flow time series for the Snake and Clearwater Rivers for the future 50-year period was comprised of the historic discharge record from 1 October 1974 through 30 September 2010 for the first 36 years, plus the repeated period 1 October 1974 to 30 September 1988 for the latter 14 years (18263 daily values). The 50 year discharge series was repeated in the extended analysis rather than continued from 1 October 1988 and then cycled back to 1 October 1974 so that the influx of sediment would be the same for both 50 year periods.

The 50-year and 100-year cumulative sediment volumes are plotted in Figure 71 and Figure 72. Sediment transport in the extended simulation was computed with the Ackers-White function. In Figure 71, total sediment volume at RM 107 at the end of the 100 year simulation was 139.5 mcy, and as expected is about 200 percent of the 50-year load. At RM 130, the 100-year sediment volume is 27.9 mcy, which is 168 percent of the 50-year volume. The reduced ratio between 100-year and 50-year volumes at RM 130 indicates that more sediment is transported to the lower reservoir. The rescaled plot in Figure 72 shows little additional accumulation in the upper segment of the reservoir. Plots of the 50-year and 100-year mean effective bed elevations and surface sediment D_{50} in Figure 73 for RM 125 to the confluence show segments that have maintained near equilibrium and that the surface sediment is becoming coarser below RM 135 and sand is transported further into the reservoir.

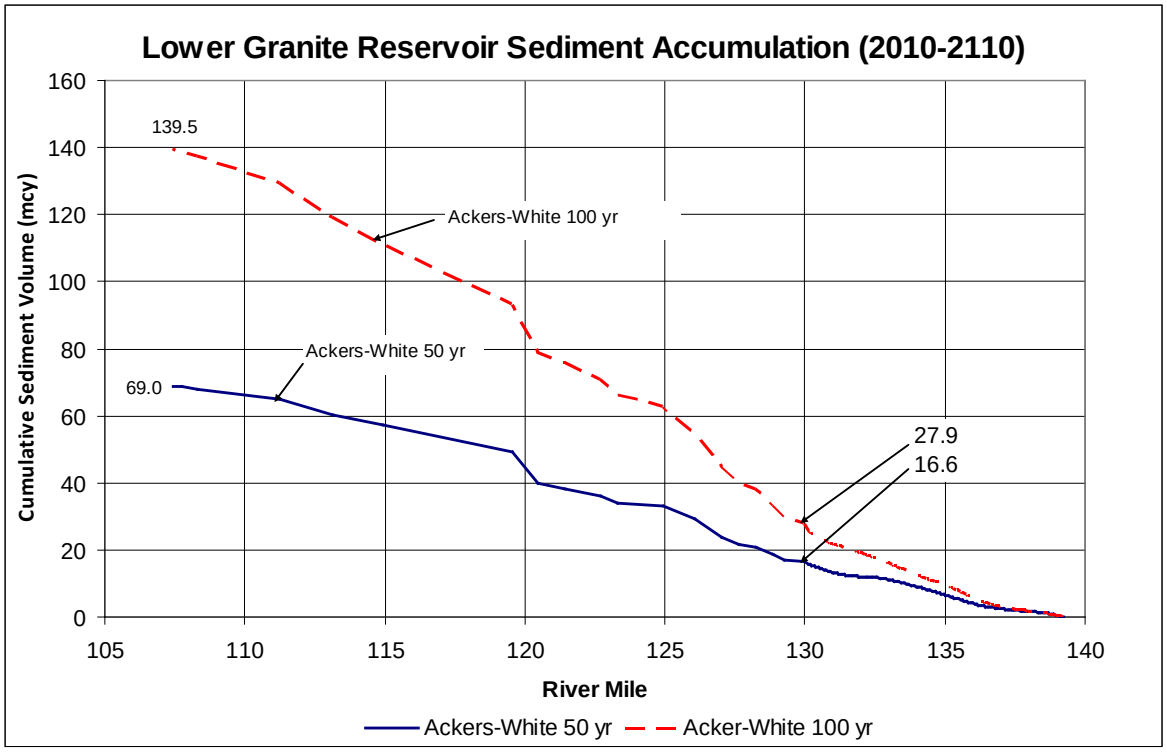


Figure 71. 50-year and 100-year sediment accumulation volumes in Lower Granite Reservoir.

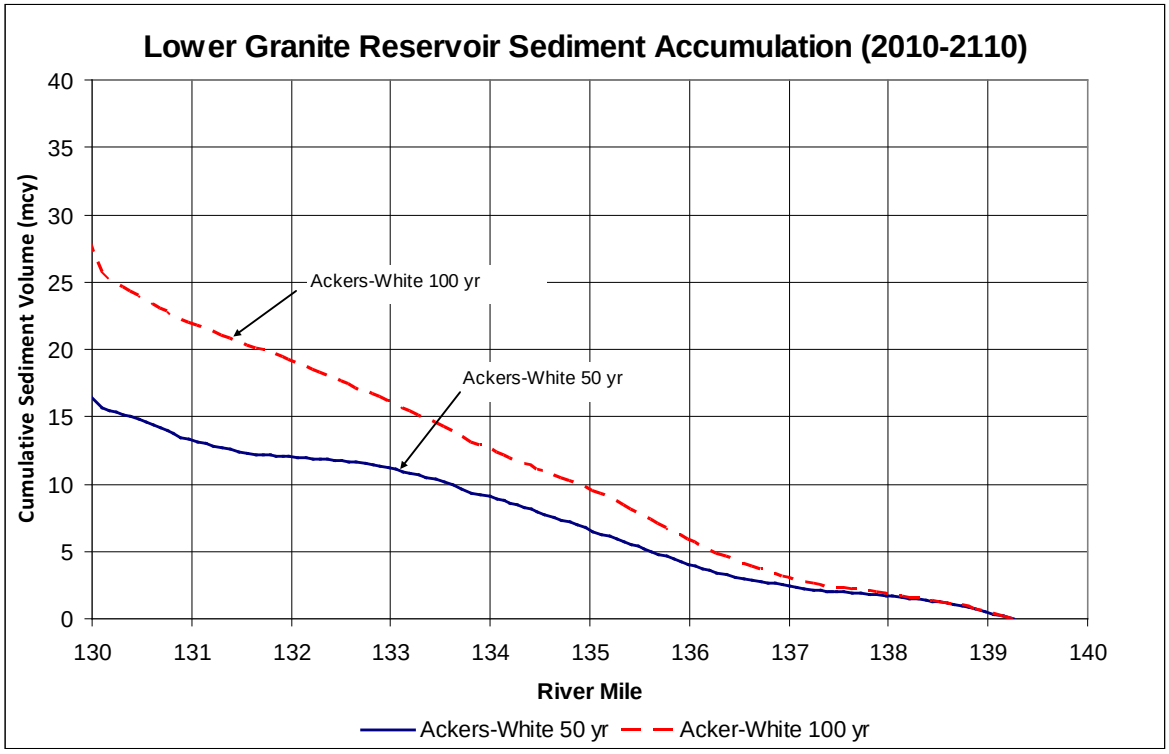


Figure 72. 50-year and 100-year sediment accumulation volumes from Silcott to the confluence in Lower Granite Reservoir.

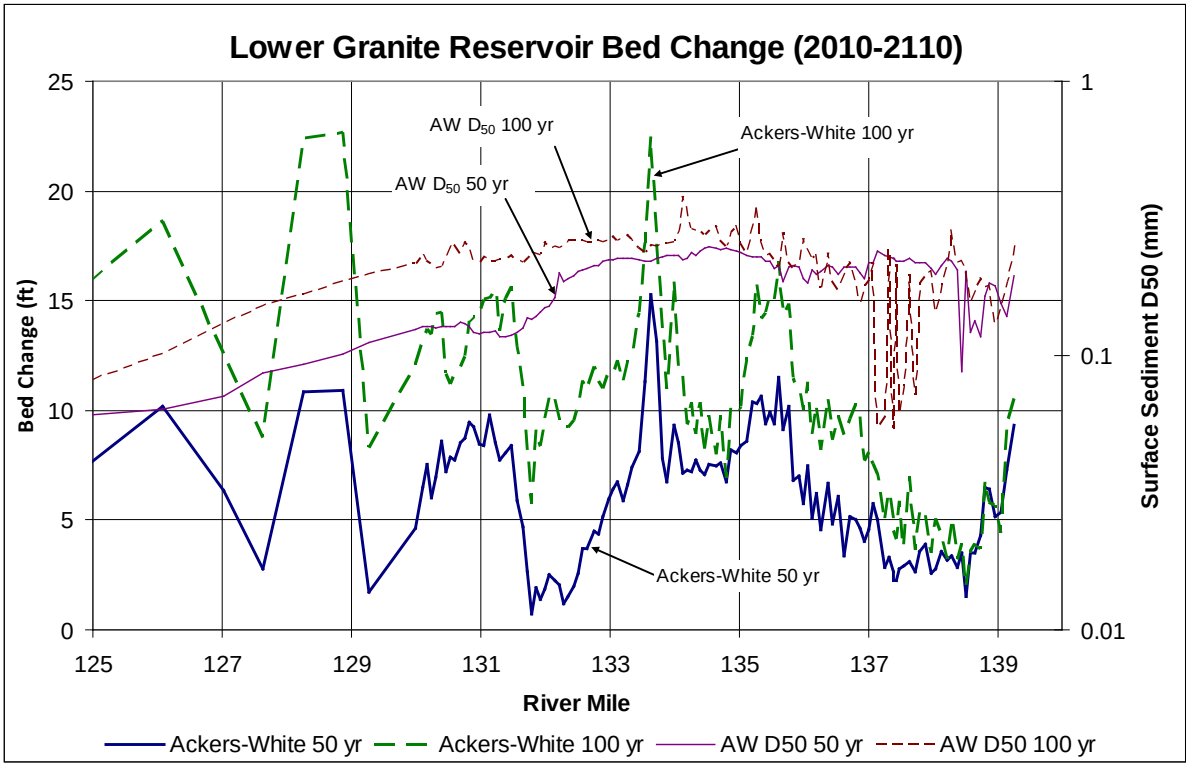


Figure 73. 50-yr and 100-year mean effective bed change and surface D50 for Lower Granite Reservoir RM 125 to the confluence.

11. Mobile-bed Flood Risk Analysis of the Future Channel

In the previous section, the sediment accumulation and hydraulic properties of the channels in Lower Granite Reservoir at the end of the 50-year future analysis period were predicted by simulating sediment transport with the Ackers-White and Toffaleti transport functions. The cross sections at the end of the 50-year simulation period become the geometry used in the analysis of flood risk of the future condition. The hydraulic performance for the flood risk analysis of the year 2060 channel can be evaluated in two ways:

1. Partial mobile-bed approach, a fixed-bed hydraulic model is developed from the year-2060 cross sections and the hydraulic performance of the year-2060 geometry is evaluated in a steady-flow analysis using the same set of extreme discharges as was used for the fixed-bed hydraulic model of the 2009 channel geometry. In the fixed-bed model the hydraulic effects of sediment mobility during extreme discharges are represented by appropriate Manning's *n* values for bed regime as discussed in Section 10.9. No bed adjustment during extreme discharges is simulated.
2. Full mobile-bed approach, a sediment transport model is developed with the year-2060 cross sections to allow the channel to adjust by scour and deposition during extreme discharges. An unsteady flow time series is developed by the balanced hydrograph method to proportion the inflow hydrographs so they are consistent with the exceedance probability of the extreme discharges.

11.1. Partial Mobile-Bed approach

Both approaches require that initial channel geometry and a hydraulic model be developed from the year-2060 cross sections. The hydraulic model for the partial mobile-bed approach was developed in several steps:

1. Cross sections from the Ackers-White and Toffaleti simulations were imported into a basic channel model. Cross sections from the Toffaleti simulation were imported to replace the Ackers-White cross sections below RM 120 in Lower Granite Reservoir.
2. Bridge geometries were imported from the 2009 fixed-bed model.

3. Separate fixed-bed models were developed from the initial geometry to represent the lower and upper bed regime conditions. The only difference between the models is the specifications of Manning's *n*.

4. For the upper bed regime model, the original Manning's *n* values from the calibrated 2009 fixed-bed model were used throughout the model because they are nearly equivalent to the values estimated from the Brownlie relationship for upper regime.

5. For the lower bed regime model, the original Manning's *n* values from the calibrated 2009 fixed-bed model were adjusted so that the Manning's *n* values were not less than the 0.028 value assumed in the historic channel models, which is somewhat greater than the 0.026 value computed by the Brownlie method for lower bed regime flow.

6. The steady flow discharges and downstream boundary water surface elevations (Table 4) were the same as the annual peak discharges used in the FDA analysis of the 2009 channel geometry.

HEC-RAS Estimated Annual Peak Steady Flow Discharges for FDA Risk Analysis											
			Exceedance Probability (Percent)								
River	Reach	RS	50	20	10	4	2	1	0.4	0.2	SPF
Clearwater	Lewiston	7.85	49433	65967	75799	87138	94905	102167	111124	117587	125000
Snake	Clarkston	148.83	110991	148115	170189	195650	213089	229394	249505	264016	295000
Snake	Lower Granite	139.254	160423	214082	245988	282788	307995	331562	360629	381603	420000
Lower Granite forebay elevation (feet)			733.78	732.00	730.66	729.32	728.40	728.21	727.98	727.81	727.40

Table 4. HEC-RAS annual peak steady flow discharges for FDA risk analysis.

The steady flow models for upper and lower bed regimes were executed in HEC-RAS 4.1.0. Froude numbers at all cross sections for all runs were subcritical; the highest Froude number was 0.46 for the SPF discharge. The runs terminated normally and the only warnings issued were related to conveyance changes, which prior testing showed had negligible influence on the water surface profile. It is important to acknowledge that hydraulic models cannot be calibrated because the channel geometry is a predicted future condition.

Flow profiles for the 1-percent, 0.2 percent and SPF discharges and the upper regime bed (lower Manning's *n*) are plotted in Figure 74 through Figure 78. Hydraulic parameters and levee margins (freeboard) for the Clearwater and Snake Rivers for the upper regime bed are listed in Table 5 and Table 6. Freeboard is greater than 3 feet at all locations for the 1-percent exceedance discharge. On the Clearwater River the left bank levee freeboard is less than 1 foot from the confluence to RM 0.686.

Flow profiles for the lower regime (higher Manning's *n*) are plotted in Figure 79, through Figure 82. Hydraulic parameters and levee margins (freeboard) for the Clearwater and Snake Rivers for the upper regime bed are listed in Table 7 and Table 8. Freeboard at the left bank levee on the Clearwater River is greater than 2 feet at all locations for the 1-percent exceedance discharge. The SPF water surface exceeds the height of the left bank levee on the Clearwater River between the confluence and RM 0.967. The SPF water surface also exceeds the height of the right bank levee on the Snake River between the confluence and RM 140.324.

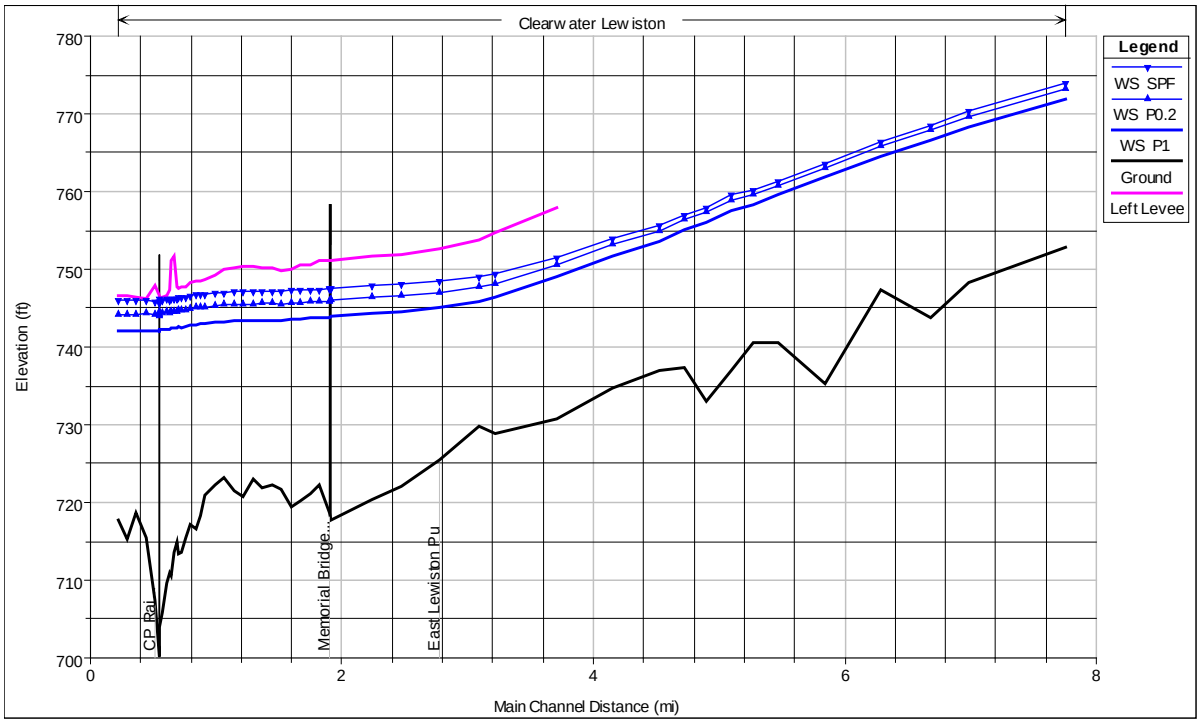


Figure 74. HEC-RAS 2060 upper regime fixed-bed steady flow profiles for Clearwater River.

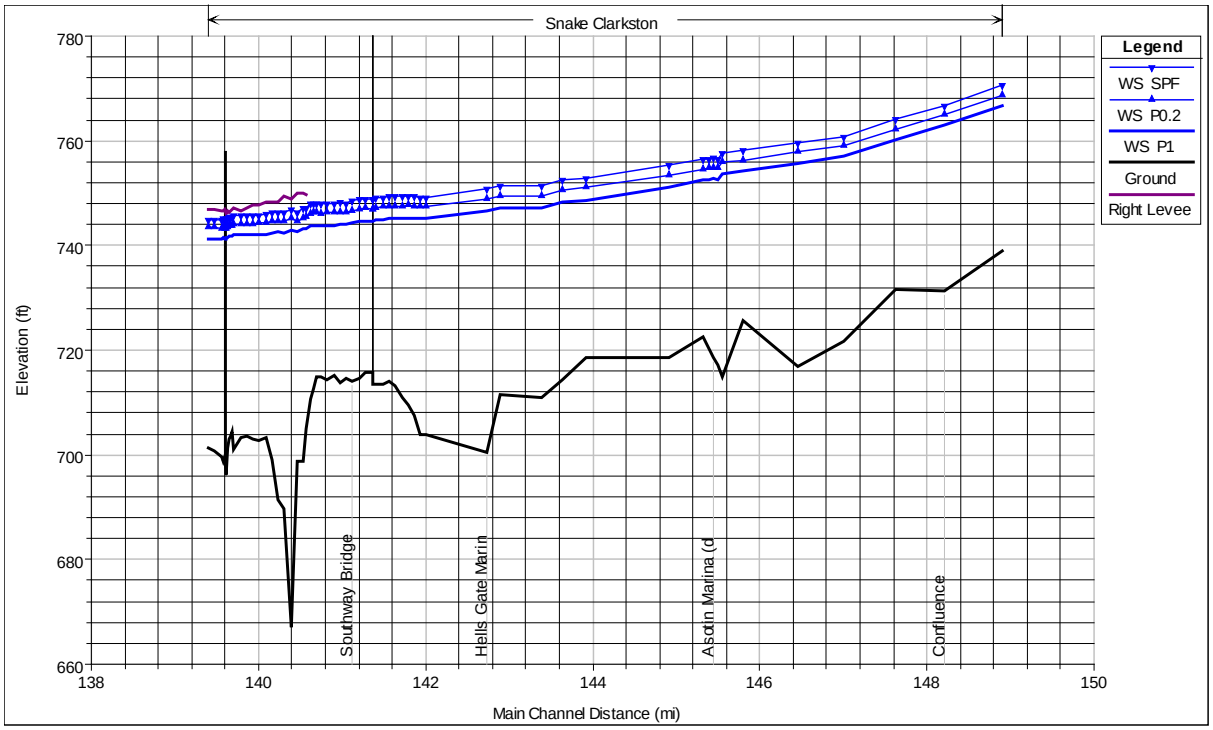


Figure 75. HEC-RAS 2060 upper regime fixed-bed steady flow profiles for Snake River above confluence.

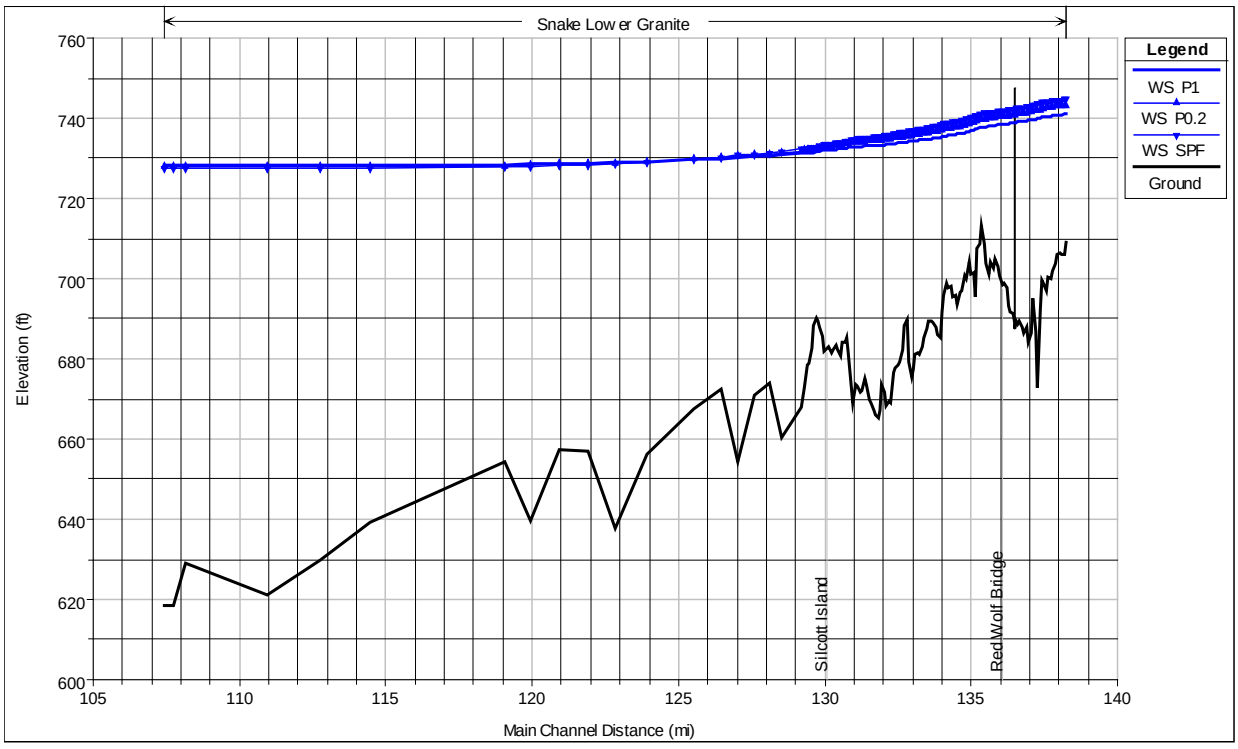


Figure 76. HEC-RAS 2060 upper regime fixed-bed steady flow profiles for Snake River below the confluence (Lower Granite Reservoir).

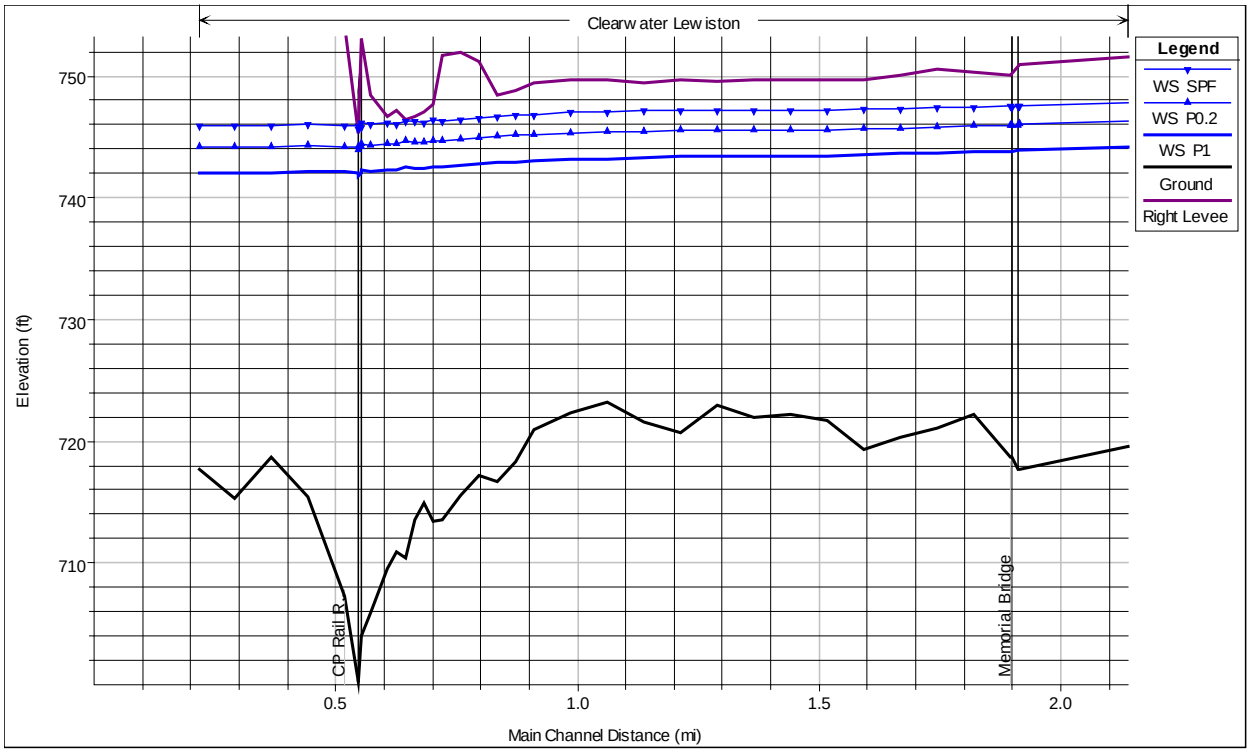


Figure 77. HEC-RAS 2060 upper regime fixed-bed steady flow profiles for Clearwater River near the CPRR bridge.

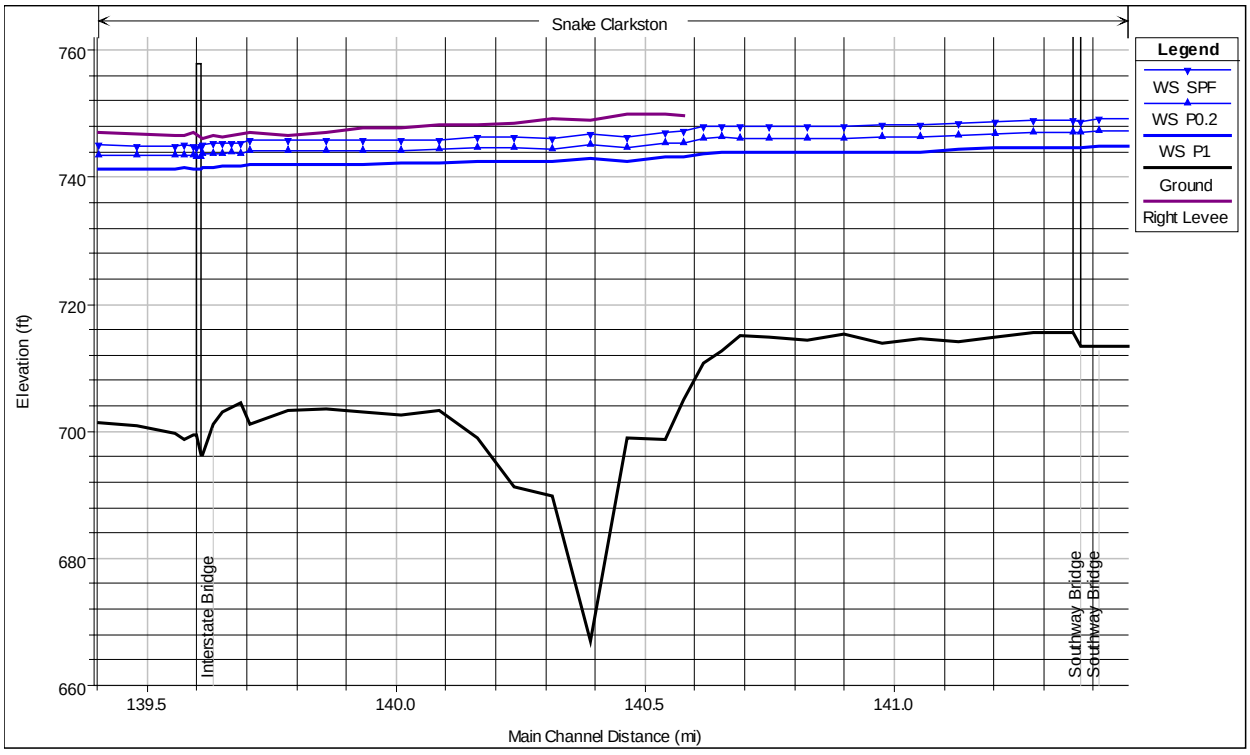


Figure 78. HEC-RAS 2060 upper regime fixed-bed steady flow profiles for Snake River near Interstate Bridge.

HEC-RAS 2060 Fixed-Bed Water Surface Profile for Upper Bed Regime (Calibrated Manning's *n*) - Clearwater River near the Confluence											
				Water Surface		Mean		Levee Elevations		Levee Freeboard	
			Discharge	Elevation	Energy	Velocity		Left	Right	Left	Right
Reach	River Sta	Profile	cfs	ft NAVD88	Slope	ft/s	Froude No.	ft NAVD88	ft NAVD88	ft	ft
Lewiston	0.217	P1	102,167	741.98	0.000203	5.08	0.25	746.56	758.95	4.58	16.97
Lewiston	0.217	P0.2	117,587	744.18	0.000160	5.00	0.23	746.56	758.95	2.38	14.77
Lewiston	0.217	SPF	125,000	745.94	0.000125	4.76	0.20	746.56	758.95	0.62	13.01
Lewiston	0.299	P1	102,167	742.06	0.000134	4.99	0.21	746.57	759.21	4.51	17.15
Lewiston	0.299	P0.2	117,587	744.22	0.000120	5.10	0.20	746.57	759.21	2.35	14.99
Lewiston	0.299	SPF	125,000	745.97	0.000103	4.97	0.19	746.57	759.21	0.60	13.24
Lewiston	0.373	P1	102,167	742.05	0.000177	5.60	0.24	746.41	756.90	4.36	14.85
Lewiston	0.373	P0.2	117,587	744.21	0.000158	5.71	0.23	746.41	756.90	2.20	12.69
Lewiston	0.373	SPF	125,000	745.94	0.000134	5.55	0.22	746.41	756.90	0.47	10.96
Lewiston	0.461	P1	102,167	742.15	0.000123	5.38	0.21	746.23	753.76	4.08	11.61
Lewiston	0.461	P0.2	117,587	744.28	0.000118	5.61	0.21	746.23	753.76	1.95	9.48
Lewiston	0.461	SPF	125,000	746.00	0.000104	5.53	0.20	746.23	753.76	0.23	7.76
Lewiston	0.59	P1	102,167	742.05	0.000189	6.77	0.26	746.70	745.28	4.65	3.23
Lewiston	0.59	P0.2	117,587	744.16	0.000186	7.09	0.26	746.70	745.28	2.54	1.12
Lewiston	0.59	SPF	125,000	745.87	0.000169	7.01	0.25	746.70	745.28	0.83	-0.59
Lewiston	0.6	P1	102,167	742.36	0.000145	6.13	0.23	746.23	753.06	3.87	10.70
Lewiston	0.6	P0.2	117,587	744.48	0.000144	6.45	0.23	746.23	753.06	1.75	8.58
Lewiston	0.6	SPF	125,000	746.17	0.000131	6.42	0.22	746.23	753.06	0.06	6.89
Lewiston	0.65	P1	102,167	742.23	0.000184	7.15	0.26	746.36	748.40	4.13	6.17
Lewiston	0.65	P0.2	117,587	744.34	0.000185	7.55	0.26	746.36	748.40	2.02	4.06
Lewiston	0.65	SPF	125,000	746.03	0.000171	7.53	0.25	746.36	748.40	0.33	2.37
Lewiston	0.686	P1	102,167	742.34	0.000178	6.80	0.25	746.52	746.74	4.18	4.40
Lewiston	0.686	P0.2	117,587	744.46	0.000178	7.15	0.26	746.52	746.74	2.06	2.28
Lewiston	0.686	SPF	125,000	746.15	0.000161	7.11	0.25	746.52	746.74	0.37	0.59
Lewiston	0.701	P1	102,167	742.29	0.000195	7.24	0.27	747.39	747.23	5.10	4.94
Lewiston	0.701	P0.2	117,587	744.41	0.000194	7.61	0.27	747.39	747.23	2.98	2.82
Lewiston	0.701	SPF	125,000	746.10	0.000177	7.57	0.26	747.39	747.23	1.29	1.13

Table 5. HEC-RAS 2060 Fixed-Bed Upper Regime Water Surface Profile - Clearwater River near the Confluence.

HEC-RAS 2060 Fixed-Bed Water Surface Profile for Upper Bed Regime (Calibrated Manning's n) - Snake River near the Confluence											
				Water Surface		Mean			Levee Elevations		Levee Freeboard	
			Discharge	Elevation	Energy	Velocity			Left	Right	Left	Right
Reach	River Sta	Profile	cfs	ft NAVD88	Slope	ft/s	Froude No.		ft NAVD88	ft NAVD88	ft	ft
Clarkston	139.404	P1	229,394	741.31	0.000232	8.21	0.29			747.02		5.71
Clarkston	139.404	P0.2	264,016	743.40	0.000235	8.69	0.30			747.02		3.62
Clarkston	139.404	SPF	295,000	745.03	0.000241	9.14	0.31			747.02		1.99
Clarkston	139.475	P1	229,394	741.30	0.000233	8.92	0.30			746.93		5.63
Clarkston	139.475	P0.2	264,016	743.37	0.000239	9.49	0.31			746.93		3.56
Clarkston	139.475	SPF	295,000	744.99	0.000248	10.02	0.32			746.93		1.94
Clarkston	139.535	P1	229,394	741.29	0.000226	9.29	0.30			746.49		5.20
Clarkston	139.535	P0.2	264,016	743.33	0.000239	10.00	0.31			746.49		3.16
Clarkston	139.535	SPF	295,000	744.92	0.000253	10.63	0.32			746.49		1.57
Clarkston	139.55	P1	229,394	741.47	0.000210	8.76	0.29			746.61		5.14
Clarkston	139.55	P0.2	264,016	743.54	0.000222	9.40	0.30			746.61		3.07
Clarkston	139.55	SPF	295,000	745.16	0.000235	9.98	0.31			746.61		1.45
Clarkston	139.565	P1	229,394	741.36	0.000236	9.52	0.31			746.95		5.59
Clarkston	139.565	P0.2	264,016	743.40	0.000250	10.24	0.32			746.95		3.55
Clarkston	139.565	SPF	295,000	745.00	0.000265	10.89	0.33			746.95		1.95
Clarkston	139.58	P1	229,394	741.50	0.000253	9.56	0.31			746.08		4.58
Clarkston	139.58	P0.2	264,016	743.57	0.000267	10.24	0.32			746.08		2.51
Clarkston	139.58	SPF	295,000	745.20	0.000281	10.84	0.33			746.08		0.88
Clarkston	139.595	P1	229,394	741.54	0.000245	9.52	0.31			746.49		4.95
Clarkston	139.595	P0.2	264,016	743.62	0.000256	10.18	0.32			746.49		2.87
Clarkston	139.595	SPF	295,000	745.25	0.000268	10.79	0.33			746.49		1.24
Clarkston	139.61	P1	229,394	741.67	0.000229	9.12	0.30			746.39		4.72
Clarkston	139.61	P0.2	264,016	743.77	0.000239	9.77	0.31			746.39		2.62
Clarkston	139.61	SPF	295,000	745.41	0.000250	10.35	0.32			746.39		0.98
Clarkston	139.625	P1	229,394	741.74	0.000218	8.99	0.29			746.62		4.88
Clarkston	139.625	P0.2	264,016	743.84	0.000228	9.63	0.30			746.62		2.78
Clarkston	139.625	SPF	295,000	745.48	0.000240	10.22	0.31			746.62		1.14
Clarkston	139.659	P1	229,394	741.68	0.000258	9.43	0.32			746.89		5.21
Clarkston	139.659	P0.2	264,016	743.77	0.000267	10.07	0.33			746.89		3.12
Clarkston	139.659	SPF	295,000	745.41	0.000278	10.66	0.34			746.89		1.48
Clarkston	139.679	P1	229,394	742.03	0.000170	8.31	0.26			747.08		5.05
Clarkston	139.679	P0.2	264,016	744.15	0.000180	8.95	0.27			747.08		2.93
Clarkston	139.679	SPF	295,000	745.82	0.000191	9.52	0.28			747.08		1.26
Clarkston	139.756	P1	229,394	742.02	0.000193	8.78	0.28			746.67		4.65
Clarkston	139.756	P0.2	264,016	744.13	0.000204	9.45	0.29			746.67		2.54
Clarkston	139.756	SPF	295,000	745.79	0.000216	10.04	0.30			746.67		0.88
Clarkston	139.833	P1	229,394	742.07	0.000189	8.90	0.28			747.07		5.00
Clarkston	139.833	P0.2	264,016	744.18	0.000202	9.59	0.29			747.07		2.89
Clarkston	139.833	SPF	295,000	745.84	0.000215	10.21	0.30			747.07		1.23
Clarkston	139.925	P1	229,394	742.08	0.000203	9.23	0.29			747.71		5.63
Clarkston	139.925	P0.2	264,016	744.18	0.000220	9.97	0.30			747.71		3.53
Clarkston	139.925	SPF	295,000	745.84	0.000236	10.62	0.31			747.71		1.87
Clarkston	139.984	P1	229,394	742.14	0.000194	9.33	0.28			747.86		5.72
Clarkston	139.984	P0.2	264,016	744.24	0.000210	10.10	0.30			747.86		3.62
Clarkston	139.984	SPF	295,000	745.89	0.000225	10.77	0.31			747.86		1.97
Clarkston	140.043	P1	229,394	742.20	0.000211	9.43	0.29			748.36		6.16
Clarkston	140.043	P0.2	264,016	744.31	0.000226	10.19	0.31			748.36		4.05
Clarkston	140.043	SPF	295,000	745.97	0.000241	10.85	0.32			748.36		2.39
Clarkston	140.102	P1	229,394	742.46	0.000181	8.86	0.27			748.33		5.87
Clarkston	140.102	P0.2	264,016	744.59	0.000196	9.57	0.29			748.33		3.74
Clarkston	140.102	SPF	295,000	746.28	0.000211	10.20	0.30			748.33		2.05
Clarkston	140.161	P1	229,394	742.53	0.000161	8.85	0.26			748.41		5.88
Clarkston	140.161	P0.2	264,016	744.66	0.000176	9.61	0.27			748.41		3.75
Clarkston	140.161	SPF	295,000	746.35	0.000190	10.27	0.29			748.41		2.06
Clarkston	140.241	P1	229,394	742.41	0.000202	9.83	0.29			749.32		6.91
Clarkston	140.241	P0.2	264,016	744.52	0.000220	10.65	0.31			749.32		4.80
Clarkston	140.241	SPF	295,000	746.19	0.000237	11.37	0.32			749.32		3.13
Clarkston	140.324	P1	229,394	743.01	0.000096	8.00	0.20			748.94		5.93
Clarkston	140.324	P0.2	264,016	745.18	0.000109	8.80	0.22			748.94		3.76
Clarkston	140.324	SPF	295,000	746.90	0.000122	9.50	0.23			748.94		2.04
Clarkston	140.406	P1	229,394	742.58	0.000280	10.48	0.33			749.92		7.34
Clarkston	140.406	P0.2	264,016	744.71	0.000297	11.28	0.35			749.92		5.21
Clarkston	140.406	SPF	295,000	746.41	0.000314	11.98	0.36			749.92		3.51
Clarkston	140.489	P1	229,394	743.10	0.000194	9.18	0.28			749.91		6.81
Clarkston	140.489	P0.2	264,016	745.30	0.000208	9.90	0.29			749.91		4.61
Clarkston	140.489	SPF	295,000	747.06	0.000220	10.52	0.31			749.91		2.85
Clarkston	140.544	P1	229,394	743.13	0.000259	9.24	0.31			749.79		6.66
Clarkston	140.544	P0.2	264,016	745.38	0.000265	9.81	0.32			749.79		4.41
Clarkston	140.544	SPF	295,000	747.18	0.000273	10.31	0.33			749.79		2.61

Table 6. HEC-RAS 2060 Fixed-Bed Upper Regime Water Surface Profile - Snake River near the Confluence.

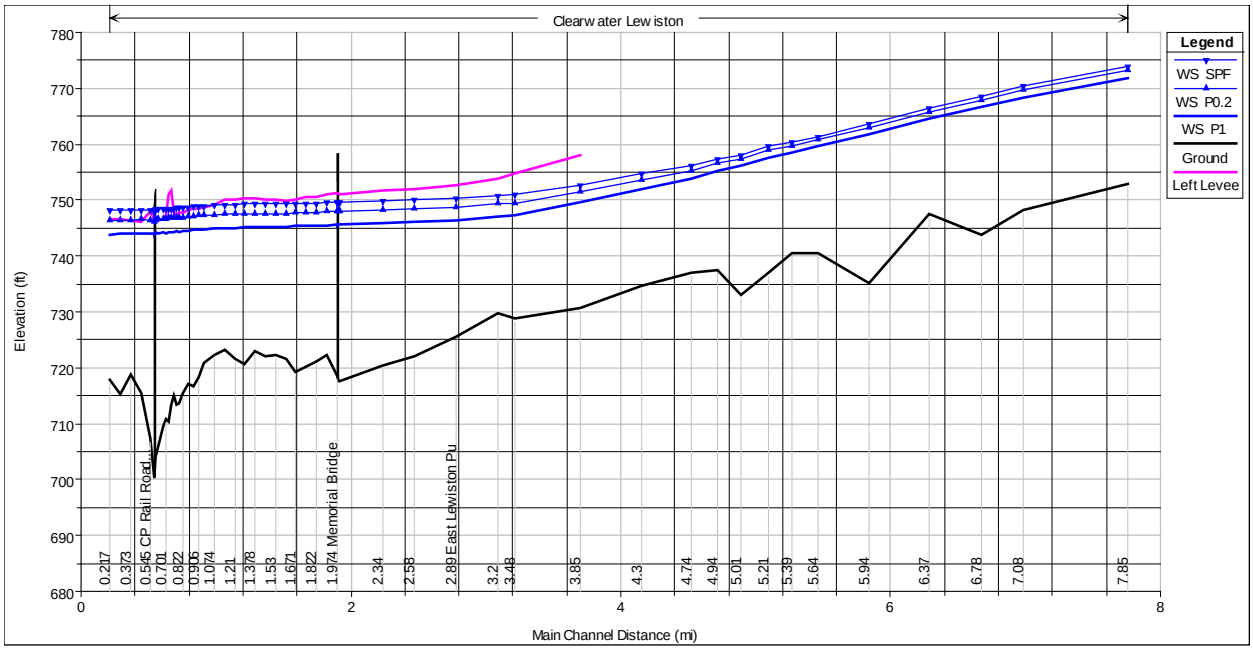


Figure 79. HEC-RAS 2060 lower regime fixed-bed steady flow profiles for Clearwater River.

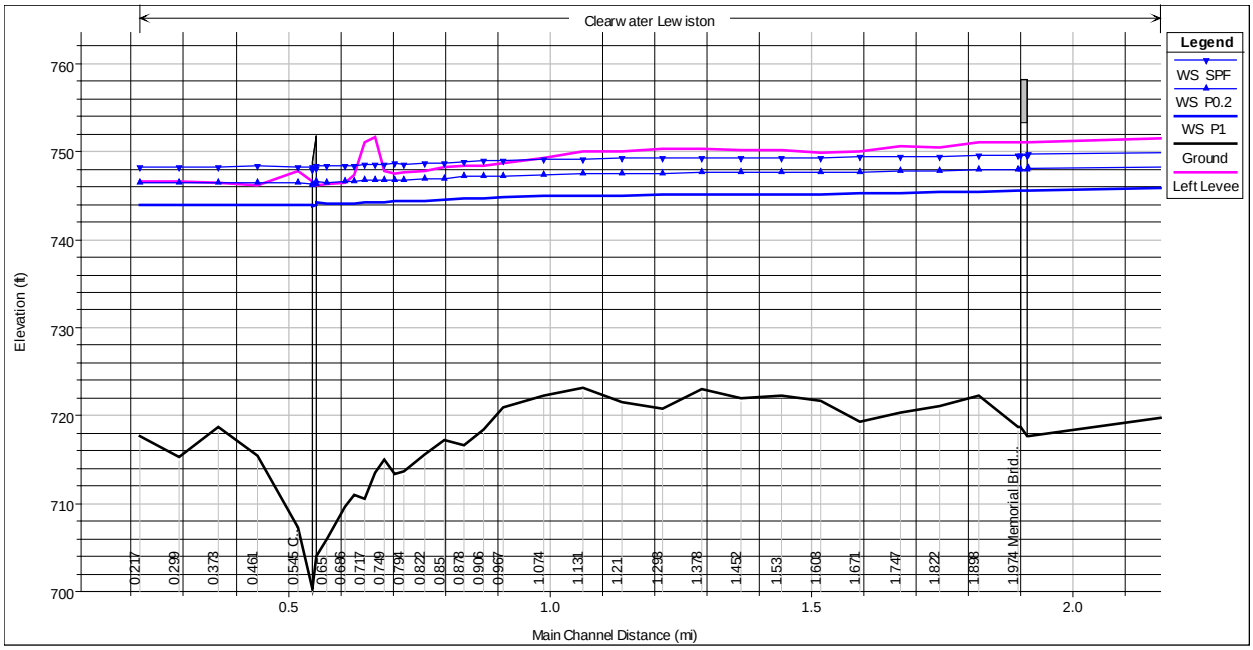


Figure 80. HEC-RAS 2060 lower regime fixed-bed steady flow profiles for Clearwater River near CPRR Bridge.

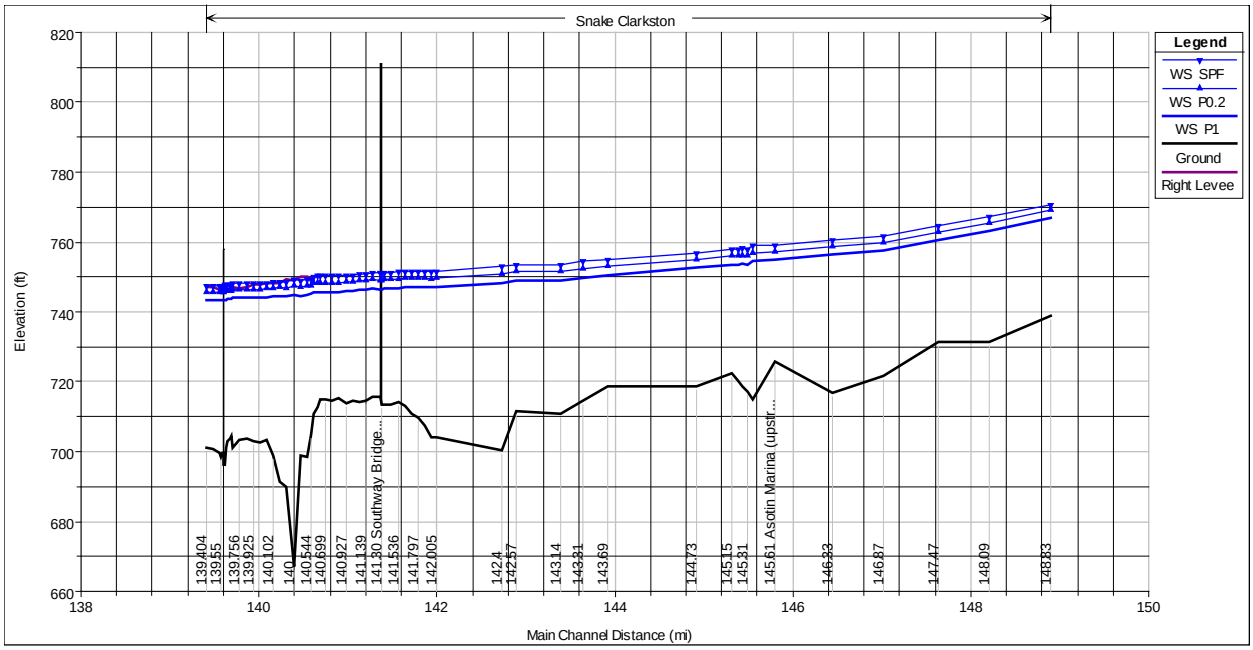


Figure 81. HEC-RAS 2060 lower regime fixed-bed steady flow profiles for Snake River above confluence.

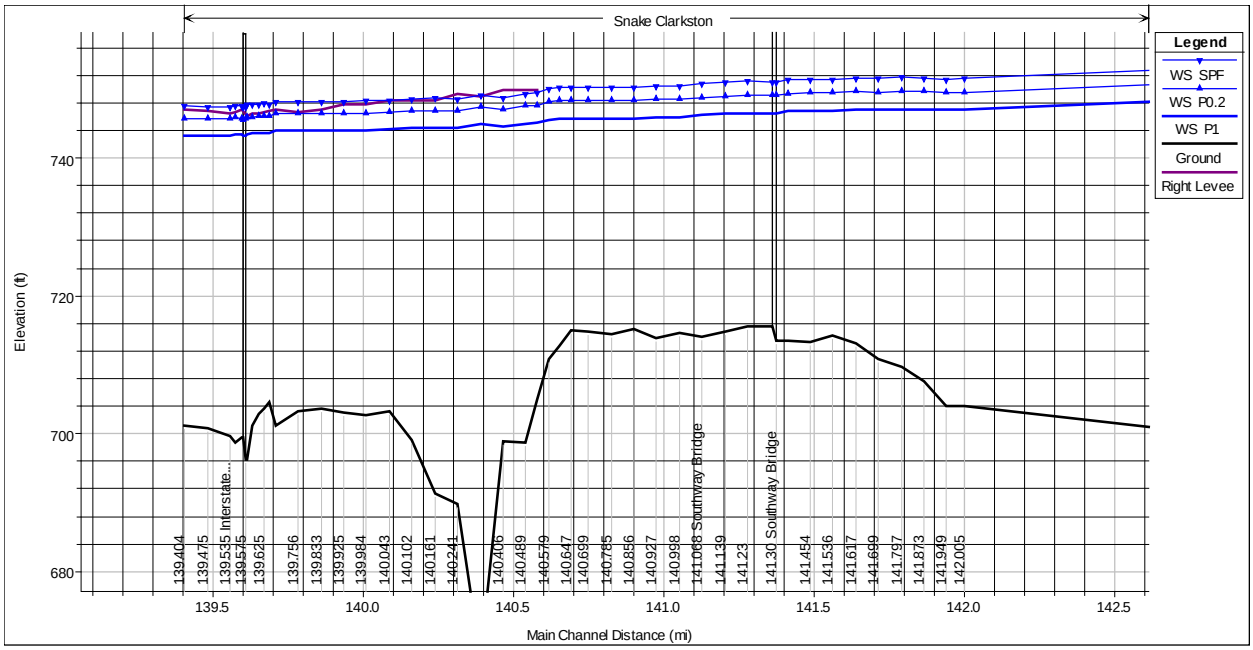


Figure 82 HEC-RAS 2060 lower regime fixed-bed steady flow profiles for Snake River near Interstate Bridge.

HEC-RAS 2060 Fixed-Bed Water Surface Profile for Lower Bed Regime - Clearwater River near the Confluence											
				Water Surface		Mean		Levee Elevations		Levee Freeboard	
			Discharge	Elevation	Energy	Velocity		Left	Right	Left	Right
Reach	River Sta	Profile	cfs	ft NAVD88	Slope	ft/s	Froude No.	ft NAVD88	ft NAVD88	ft	ft
Lewiston	0.217	P1	102,167	743.89	0.000164	4.42	0.20	746.56	758.95	2.67	15.06
Lewiston	0.217	P0.2	117,587	746.41	0.000129	4.35	0.18	746.56	758.95	0.15	12.54
Lewiston	0.217	SPF	125,000	748.30	0.000098	4.07	0.16	746.56	758.95	-1.74	10.65
Lewiston	0.299	P1	102,167	743.94	0.000122	4.50	0.18	746.57	759.21	2.63	15.27
Lewiston	0.299	P0.2	117,587	746.44	0.000108	4.57	0.17	746.57	759.21	0.13	12.77
Lewiston	0.299	SPF	125,000	748.30	0.000090	4.41	0.16	746.57	759.21	-1.73	10.91
Lewiston	0.373	P1	102,167	743.94	0.000160	5.03	0.21	746.41	756.90	2.47	12.96
Lewiston	0.373	P0.2	117,587	746.44	0.000135	5.02	0.19	746.41	756.90	-0.03	10.46
Lewiston	0.373	SPF	125,000	748.29	0.000115	4.90	0.18	746.41	756.90	-1.88	8.61
Lewiston	0.461	P1	102,167	744.02	0.000118	4.93	0.18	746.23	753.76	2.21	9.74
Lewiston	0.461	P0.2	117,587	746.49	0.000107	5.02	0.18	746.23	753.76	-0.26	7.27
Lewiston	0.461	SPF	125,000	748.33	0.000094	4.92	0.17	746.23	753.76	-2.10	5.43
Lewiston	0.545	P1	102,167	743.99	0.000153	5.65	0.21	747.88	754.89	3.89	10.90
Lewiston	0.545	P0.2	117,587	746.44	0.000145	5.85	0.21	747.88	754.89	1.44	8.45
Lewiston	0.545	SPF	125,000	748.29	0.000123	5.66	0.19	747.88	754.89	-0.41	6.60
Lewiston	0.59	P1	102,167	743.94	0.000185	6.21	0.23	746.70	745.28	2.76	1.34
Lewiston	0.59	P0.2	117,587	746.38	0.000178	6.45	0.23	746.70	745.28	0.32	-1.10
Lewiston	0.59	SPF	125,000	748.22	0.000159	6.34	0.22	746.70	745.28	-1.52	-2.94
Lewiston	0.6	P1	102,167	744.18	0.000144	5.67	0.20	746.23	753.06	2.05	8.88
Lewiston	0.6	P0.2	117,587	746.65	0.000145	5.84	0.20	746.23	753.06	-0.42	6.41
Lewiston	0.6	SPF	125,000	748.45	0.000131	5.80	0.19	746.23	753.06	-2.22	4.61
Lewiston	0.65	P1	102,167	744.08	0.000184	6.62	0.23	746.36	748.40	2.28	4.32
Lewiston	0.65	P0.2	117,587	746.55	0.000176	6.84	0.23	746.36	748.40	-0.19	1.85
Lewiston	0.65	SPF	125,000	748.35	0.000161	6.80	0.22	746.36	748.40	-1.99	0.05
Lewiston	0.686	P1	102,167	744.18	0.000178	6.29	0.23	746.52	746.74	2.34	2.56
Lewiston	0.686	P0.2	117,587	746.64	0.000168	6.51	0.22	746.52	746.74	-0.12	0.10
Lewiston	0.686	SPF	125,000	748.43	0.000152	6.47	0.21	746.52	746.74	-1.91	-1.69
Lewiston	0.701	P1	102,167	744.14	0.000193	6.68	0.24	747.39	747.23	3.25	3.09
Lewiston	0.701	P0.2	117,587	746.59	0.000188	6.97	0.24	747.39	747.23	0.80	0.64
Lewiston	0.701	SPF	125,000	748.40	0.000167	6.84	0.23	747.39	747.23	-1.01	-1.17
Lewiston	0.717	P1	102,167	744.31	0.000153	5.95	0.21	751.12	746.44	6.81	2.13
Lewiston	0.717	P0.2	117,587	746.77	0.000151	6.23	0.21	751.12	746.44	4.35	-0.33
Lewiston	0.717	SPF	125,000	748.54	0.000139	6.20	0.21	751.12	746.44	2.58	-2.10
Lewiston	0.733	P1	102,167	744.29	0.000182	6.27	0.23	751.66	746.74	7.37	2.45
Lewiston	0.733	P0.2	117,587	746.74	0.000178	6.53	0.23	751.66	746.74	4.92	0.00
Lewiston	0.733	SPF	125,000	748.52	0.000162	6.48	0.22	751.66	746.74	3.14	-1.78
Lewiston	0.749	P1	102,167	744.28	0.000189	6.49	0.23	747.77	747.03	3.49	2.75
Lewiston	0.749	P0.2	117,587	746.73	0.000183	6.76	0.23	747.77	747.03	1.04	0.30
Lewiston	0.749	SPF	125,000	748.53	0.000160	6.62	0.22	747.77	747.03	-0.76	-1.50
Lewiston	0.764	P1	102,167	744.41	0.000151	5.94	0.21	747.57	747.67	3.16	3.26
Lewiston	0.764	P0.2	117,587	746.86	0.000149	6.22	0.21	747.57	747.67	0.71	0.81
Lewiston	0.764	SPF	125,000	748.65	0.000132	6.10	0.20	747.57	747.67	-1.08	-0.98
Lewiston	0.794	P1	102,167	744.35	0.000195	6.49	0.24	747.72	751.76	3.37	7.41
Lewiston	0.794	P0.2	117,587	746.80	0.000189	6.76	0.24	747.72	751.76	0.92	4.96
Lewiston	0.794	SPF	125,000	748.59	0.000165	6.59	0.22	747.72	751.76	-0.87	3.17
Lewiston	0.822	P1	102,167	744.47	0.000163	6.08	0.22	747.83	751.90	3.36	7.43
Lewiston	0.822	P0.2	117,587	746.93	0.000156	6.35	0.22	747.83	751.90	0.90	4.97
Lewiston	0.822	SPF	125,000	748.69	0.000139	6.26	0.21	747.83	751.90	-0.86	3.21
Lewiston	0.85	P1	102,167	744.55	0.000163	5.89	0.22	748.29	751.20	3.74	6.65
Lewiston	0.85	P0.2	117,587	747.01	0.000154	6.12	0.21	748.29	751.20	1.28	4.19
Lewiston	0.85	SPF	125,000	748.77	0.000137	6.04	0.20	748.29	751.20	-0.48	2.43
Lewiston	0.878	P1	102,167	744.69	0.000127	5.27	0.19	748.47	748.41	3.78	3.72
Lewiston	0.878	P0.2	117,587	747.16	0.000121	5.48	0.19	748.47	748.41	1.31	1.25
Lewiston	0.878	SPF	125,000	748.92	0.000106	5.38	0.18	748.47	748.41	-0.45	-0.51
Lewiston	0.906	P1	102,167	744.74	0.000138	5.18	0.20	748.48	748.87	3.74	4.13
Lewiston	0.906	P0.2	117,587	747.21	0.000127	5.34	0.19	748.48	748.87	1.27	1.66
Lewiston	0.906	SPF	125,000	748.96	0.000112	5.25	0.18	748.48	748.87	-0.48	-0.09
Lewiston	0.967	P1	102,167	744.78	0.000153	5.06	0.20	748.75	749.40	3.97	4.62
Lewiston	0.967	P0.2	117,587	747.27	0.000137	5.16	0.20	748.75	749.40	1.48	2.13
Lewiston	0.967	SPF	125,000	749.02	0.000118	5.04	0.18	748.75	749.40	-0.27	0.38

Table 7. HEC-RAS 2060 Fixed-Bed Lower Regime Water Surface Profile - Clearwater River near the Confluence.

HEC-RAS 2060 Fixed-Bed Water Surface Profile for Lower Bed Regime - Snake River near the Confluence											
				Water Surface		Mean			Levee Elevations		Levee Freeboard	
			Discharge	Elevation	Energy	Velocity			Left	Right	Left	Right
Reach	River Sta	Profile	cfs	ft NAVD88	Slope	ft/s	Froude No.		ft NAVD88	ft NAVD88	ft	ft
Clarkston	139.404	P1	229,394	743.31	0.000229	7.58	0.26			747.02		3.71
Clarkston	139.404	P0.2	264,016	745.74	0.000227	7.97	0.26			747.02		1.28
Clarkston	139.404	SPF	295,000	747.53	0.000227	8.31	0.27			747.02		-0.51
Clarkston	139.475	P1	229,394	743.32	0.000230	8.22	0.27			746.93		3.61
Clarkston	139.475	P0.2	264,016	745.74	0.000231	8.69	0.27			746.93		1.19
Clarkston	139.475	SPF	295,000	747.50	0.000237	9.13	0.28			746.93		-0.57
Clarkston	139.535	P1	229,394	743.30	0.000231	8.69	0.27			746.49		3.19
Clarkston	139.535	P0.2	264,016	745.69	0.000241	9.30	0.28			746.49		0.80
Clarkston	139.535	SPF	295,000	747.44	0.000249	9.78	0.29			746.49		-0.95
Clarkston	139.55	P1	229,394	743.46	0.000216	8.19	0.26			746.61		3.15
Clarkston	139.55	P0.2	264,016	745.87	0.000224	8.74	0.27			746.61		0.74
Clarkston	139.55	SPF	295,000	747.65	0.000231	9.18	0.27			746.61		-1.04
Clarkston	139.565	P1	229,394	743.36	0.000241	8.89	0.28			746.95		3.59
Clarkston	139.565	P0.2	264,016	745.76	0.000251	9.52	0.29			746.95		1.19
Clarkston	139.565	SPF	295,000	747.52	0.000259	9.99	0.29			746.95		-0.57
Clarkston	139.58	P1	229,394	743.50	0.000258	8.90	0.28			746.08		2.58
Clarkston	139.58	P0.2	264,016	745.93	0.000266	9.46	0.29			746.08		0.15
Clarkston	139.58	SPF	295,000	747.72	0.000270	9.87	0.29			746.08		-1.64
Clarkston	139.595	P1	229,394	743.54	0.000248	8.85	0.28			746.49		2.95
Clarkston	139.595	P0.2	264,016	745.97	0.000253	9.41	0.29			746.49		0.52
Clarkston	139.595	SPF	295,000	747.77	0.000257	9.82	0.29			746.49		-1.28
Clarkston	139.61	P1	229,394	743.65	0.000233	8.52	0.27			746.39		2.74
Clarkston	139.61	P0.2	264,016	746.08	0.000238	9.06	0.28			746.39		0.31
Clarkston	139.61	SPF	295,000	747.88	0.000243	9.48	0.28			746.39		-1.49
Clarkston	139.625	P1	229,394	743.71	0.000223	8.40	0.27			746.62		2.91
Clarkston	139.625	P0.2	264,016	746.14	0.000229	8.95	0.27			746.62		0.48
Clarkston	139.625	SPF	295,000	747.93	0.000235	9.39	0.28			746.62		-1.31
Clarkston	139.659	P1	229,394	743.66	0.000260	8.78	0.28			746.89		3.23
Clarkston	139.659	P0.2	264,016	746.09	0.000264	9.32	0.29			746.89		0.80
Clarkston	139.659	SPF	295,000	747.87	0.000270	9.77	0.30			746.89		-0.98
Clarkston	139.679	P1	229,394	743.95	0.000177	7.82	0.24			747.08		3.13
Clarkston	139.679	P0.2	264,016	746.40	0.000185	8.37	0.25			747.08		0.68
Clarkston	139.679	SPF	295,000	748.17	0.000194	8.85	0.26			747.08		-1.09
Clarkston	139.756	P1	229,394	743.95	0.000200	8.25	0.25			746.67		2.72
Clarkston	139.756	P0.2	264,016	746.39	0.000208	8.82	0.26			746.67		0.28
Clarkston	139.756	SPF	295,000	748.17	0.000217	9.31	0.27			746.67		-1.50
Clarkston	139.833	P1	229,394	744.00	0.000198	8.38	0.25			747.07		3.07
Clarkston	139.833	P0.2	264,016	746.44	0.000208	8.98	0.26			747.07		0.63
Clarkston	139.833	SPF	295,000	748.22	0.000218	9.49	0.27			747.07		-1.15
Clarkston	139.925	P1	229,394	744.03	0.000215	8.70	0.26			747.71		3.68
Clarkston	139.925	P0.2	264,016	746.46	0.000228	9.33	0.27			747.71		1.25
Clarkston	139.925	SPF	295,000	748.23	0.000241	9.88	0.28			747.71		-0.52
Clarkston	139.984	P1	229,394	744.09	0.000205	8.81	0.26			747.86		3.77
Clarkston	139.984	P0.2	264,016	746.52	0.000217	9.47	0.27			747.86		1.34
Clarkston	139.984	SPF	295,000	748.28	0.000231	10.07	0.28			747.86		-0.42
Clarkston	140.043	P1	229,394	744.16	0.000221	8.89	0.27			748.36		4.20
Clarkston	140.043	P0.2	264,016	746.60	0.000232	9.53	0.28			748.36		1.76
Clarkston	140.043	SPF	295,000	748.37	0.000245	10.10	0.29			748.36		-0.01
Clarkston	140.102	P1	229,394	744.39	0.000193	8.36	0.25			748.33		3.94
Clarkston	140.102	P0.2	264,016	746.85	0.000205	8.98	0.26			748.33		1.48
Clarkston	140.102	SPF	295,000	748.64	0.000217	9.54	0.27			748.33		-0.31
Clarkston	140.161	P1	229,394	744.46	0.000173	8.39	0.24			748.41		3.95
Clarkston	140.161	P0.2	264,016	746.92	0.000185	9.05	0.25			748.41		1.49
Clarkston	140.161	SPF	295,000	748.71	0.000197	9.62	0.26			748.41		-0.30
Clarkston	140.241	P1	229,394	744.37	0.000215	9.28	0.27			749.32		4.95
Clarkston	140.241	P0.2	264,016	746.81	0.000229	10.01	0.28			749.32		2.51
Clarkston	140.241	SPF	295,000	748.57	0.000246	10.67	0.29			749.32		0.75
Clarkston	140.324	P1	229,394	744.88	0.000107	7.69	0.19			748.94		4.06
Clarkston	140.324	P0.2	264,016	747.36	0.000121	8.42	0.21			748.94		1.58
Clarkston	140.324	SPF	295,000	749.18	0.000133	9.03	0.22			748.94		-0.24
Clarkston	140.406	P1	229,394	744.54	0.000291	9.84	0.30			749.92		5.38
Clarkston	140.406	P0.2	264,016	747.01	0.000302	10.52	0.31			749.92		2.91
Clarkston	140.406	SPF	295,000	748.79	0.000319	11.17	0.32			749.92		1.13
Clarkston	140.489	P1	229,394	745.01	0.000206	8.67	0.26			749.91		4.90
Clarkston	140.489	P0.2	264,016	747.52	0.000216	9.29	0.27			749.91		2.39
Clarkston	140.489	SPF	295,000	749.35	0.000229	9.88	0.28			749.91		0.56
Clarkston	140.544	P1	229,394	745.07	0.000265	8.62	0.28			749.79		4.72
Clarkston	140.544	P0.2	264,016	747.62	0.000267	9.09	0.29			749.79		2.17
Clarkston	140.544	SPF	295,000	749.50	0.000276	9.57	0.30			749.79		0.29

Table 8. HEC-RAS 2060 Fixed-Bed Lower Regime Water Surface Profile - Snake River near the Confluence.

11.2. Index Sections for the FDA Flood Risk Analysis

Index cross sections for the FDA analysis were located at low points throughout the levee system (Figure 83). Index sections on the Clearwater River were located at the confluence on the left bank levee at RM 0.30, near the CPRR Bridge at RM 0.60 on the left bank levee and at RM 0.72 on the right bank levee, above the boat turning basin on the left and right bank levees at RM 1.67, and above Memorial Bridge on the left and right bank levees at RM 2.34. An index section was also located on the Snake River right bank levee near the Interstate Bridge at RM 139.58.

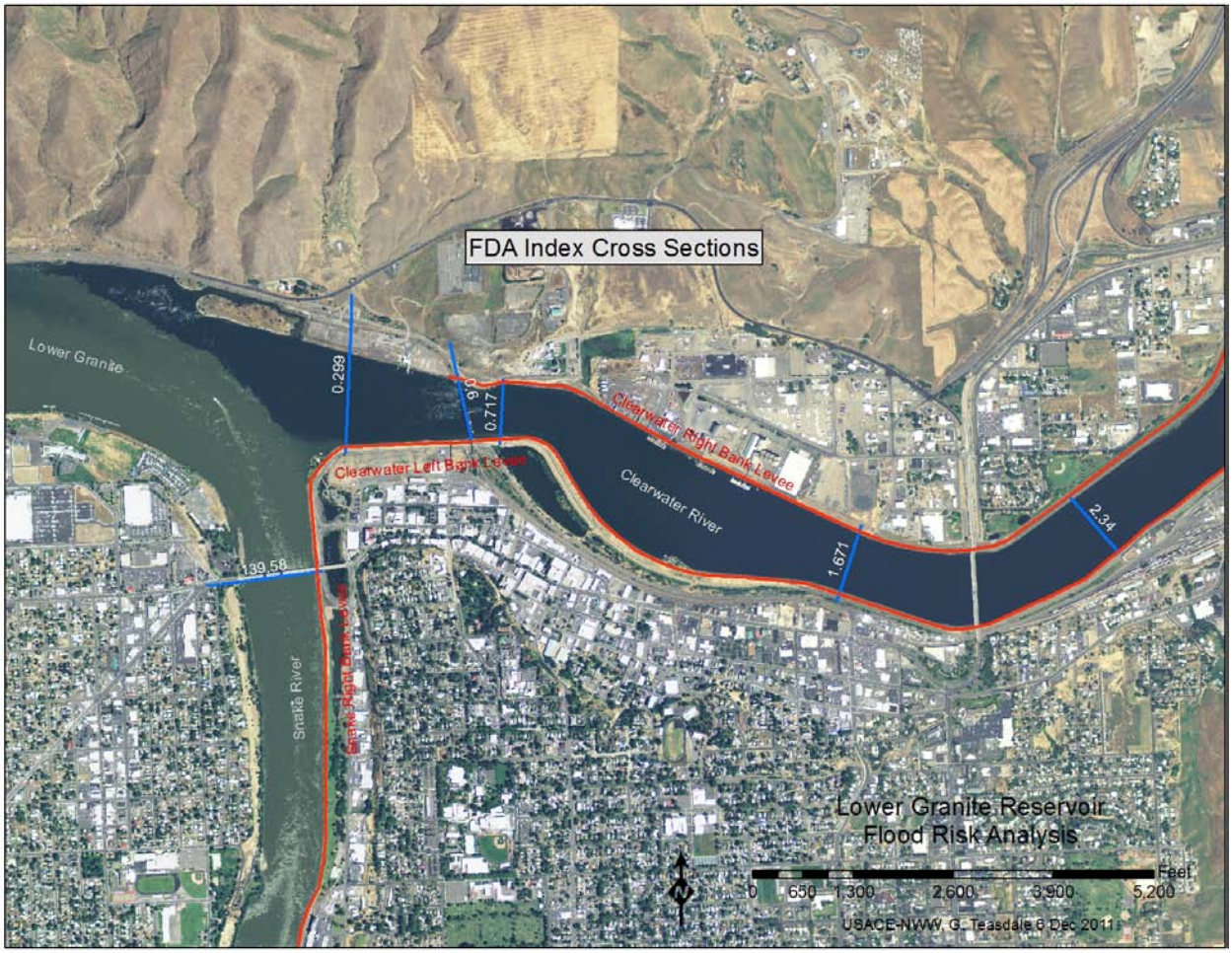


Figure 83. FDA Index cross section locations.

11.3. Conditional Non-Exceedance Probabilities – 2060 Partial Mobile-Bed Analysis of Upper and Lower Bed Regime

The water surface profiles from the year 2060 fixed bed hydraulic models of the upper and lower bed regimes discussed in Section 10 were exported from HEC-RAS into the format required by FDA. Flood risk for the upper and lower bed regime conditions were evaluated in FDA for 0.5 and 2.0 standard deviations of stage uncertainty. Except for the change in channel geometry, other aspects and limitations of the FDA analysis are the same as those discussed in Section 5 in Part 1. The 50-year long-term risk and conditional nonexceedance probabilities (CNP) from the FDA risk analysis are summarized in Table 9 for Clearwater RM 0.3 and in Table 10 for Snake RM 139.58.

For the upper regime bed condition at year 2060, the CNP for the 1-percent exceedance discharge at Clearwater RM 0.3 is 0.9855 for a 0.5 standard deviation of stage uncertainty, and 0.9460 for a stage standard deviation of 2.0. The 50-year long-term risk varies from 0.0492 to 0.0991 this range of stage uncertainty. The index section rating curves were extended by method 2 in which the flows in the Clearwater and Snake Rivers are 30% and 70% of the total discharge below the confluence. For the lower regime bed condition at year-2060, the CNP for the 1- percent exceedance discharge at Snake RM 139.58 is 0.9931 for a 0.5 standard deviation stage uncertainty, and 0.9646 for a stage standard deviation of 2.0. The 50-year long-term risk varies from 0.0311 to 0.0695.

Water levels for the lower bed regime condition at year-2060 are significantly higher than those for the upper bed regime condition. The CNP for the 1- percent exceedance discharge at Clearwater RM 0.3 is 0.8971 for a 0.5 standard deviation stage uncertainty, and 0.7926 for a stage standard deviation of 2.0. The 50-year long-term risk varies from 0.1672 to 0.2944. For Snake RM 139.58 and the upper regime bed condition at year-2060, the CNP for the 1- percent exceedance discharge is 0.9258 for a 0.5 standard deviation stage uncertainty, and 0.8260 for a stage standard deviation of 2.0. The 50-year long-term risk varies from 0.1350 to 0.2542.

Year 2060 Conditional Non-Exceedance Probabilities and Long-term Risk at Clearwater RM 0.3, Curve Extension 2								
	Standard	50-year	Flood Frequency					
	Deviation	Long-Term	10.0%	4.0%	2.0%	1.0%	0.4%	0.2%
Hydraulic Resistance	Stage (ft)	Risk	Conditional Non-Exceedance Probabilities					
Upper Regime	0.5	0.0492	1.0000	1.0000	0.9986	0.9855	0.8941	0.7358
Lower Regime	0.5	0.1672	1.0000	0.9990	0.9824	0.8971	0.6264	0.3839
Upper Regime	2.0	0.0991	0.9997	0.9964	0.9837	0.9460	0.8249	0.6792
Lower Regime	2.0	0.2944	0.9966	0.9734	0.9124	0.7926	0.5687	0.3924

Table 9. Year 2060 fixed-bed conditional non-exceedance probabilities at Clearwater RM 0.3.

Year 2060 Conditional Non-Exceedance Probabilities and Long-term Risk at Snake RM 139.58, Curve Extension 2								
	Standard	50-year	Flood Frequency					
	Deviation	Long-Term	10.0%	4.0%	2.0%	1.0%	0.4%	0.2%
Hydraulic Resistance	Stage (ft)	Risk	Conditional Non-Exceedance Probabilities					
Upper Regime	0.5	0.0311	1.0000	1.0000	0.9994	0.9931	0.9375	0.8189
Lower Regime	0.5	0.1350	1.0000	0.9995	0.9889	0.9258	0.6946	0.4565
Upper Regime	2.0	0.0695	0.9998	0.9978	0.9898	0.9646	0.8783	0.7659
Lower Regime	2.0	0.2542	0.9973	0.9795	0.9300	0.8260	0.6170	0.4404

Table 10. Year 2060 fixed-bed conditional non-exceedance probabilities at Snake RM 139.58.

11.4. Balanced Hydrograph Development

An unsteady flow time series is necessary to perform the mobile-bed sediment transport simulation of scour and deposition during the extreme discharges considered in the flood risk analysis. The discharge time series is developed by the balanced hydrograph (flood) method which proportions the inflow hydrographs so they are consistent with the exceedance probability of the extreme discharges. A balanced hydrograph, also called a balanced flood, is one that is of equal severity for all possible critical durations[40]. In the balanced hydrograph method, the shape of a large historic flood is adjusted to that the peak discharge and flood volumes for various durations have the same exceedance probability.

Historic floods at Lower Granite Reservoir are discussed in Section 1. The June 1974 snowmelt flood was selected as the basis of the development the balanced hydrograph because it is the largest flood that has occurred since the reservoir was filled and its shape is representative of other snowmelt floods for Lower Granite and the Snake and Clearwater Rivers. The 1974 flood hydrograph at Lower Granite Reservoir is plotted in Figure 84.

Volume-frequency statistics for total flow at Lower Granite Reservoir for durations 1 through 90 days were computed HEC-SSP 2.0. Total flow at Lower Granite Reservoir was computed as the sum of the daily average discharges for the Snake River at Anatone and the Clearwater River at Spalding. The volume-frequency statistics were computed by fitting a log Pearson type 3 (LP3) distribution to the daily discharge data. Exceedance probabilities ranged from 0.99 to 0.002. The fitted LP3 curves were adjusted to prevent overlap at the ends of the fitted distributions. This was done by adjusting the individual standard deviation and skew parameters to provide a smooth

[40] Beard, Leo R. (1975). "Hypothetical Floods", *Hydrologic Engineering Methods for Water Resources Development, International Hydrological Decade, HEC-IHD-0500*. Hydrologic Engineering Center, U.S. Army Corps of Engineers, Davis CA.

monotonic relationship as discussed in the HEC-SSP manual[41]. Volume-frequency curves for Lower Granite Reservoir are plotted in Figure 85 and the volume-duration values are listed in Table 11 . It is recognized that the LP3 distribution departs from the regulated discharge data near the 50 percent probability. A graphical analysis would provide better overall fit to the volume duration data, but the fit of the LP3 distribution is reasonable at the low probabilities important in the flood risk analysis and is adequate for development balanced hydrographs for the sediment transport simulation.

For reasons discussed in discharge frequency analysis in Section 1, it is not practical to develop a probabilistic analysis of coincident volume-frequencies for a joint balanced hydrograph of the Snake and Clearwater Rivers. Instead, the total balanced hydrograph for Lower Granite Reservoir was proportioned to the Snake and Clearwater Rivers by factors derived from the Snake River discharges that occurred on the date of the annual volume duration value listed in the HEC-SSP data. In other words, the average was computed of the ratio of the daily Snake River discharge to total Lower Granite discharge on the dates listed in the SSP volume-frequency data. The resulting proportioning factors are listed in Table 12. The ratio does not vary significantly between durations and averages about 0.66 across all durations. This proportioning factor agrees well with the factor derived in the multivariate frequency analysis.

Essentially, the balanced hydrograph method sets the peak of the pattern hydrograph, in this case the peak discharge of the 1974 flood, equal to the desired exceedance discharge then adjusts the shape of the hydrograph so that the flood volumes for the desired durations are equal to the volumes associated with the same exceedance value. Thus, a 1-percent peak exceedance discharge that is the peak of a balanced hydrograph also incorporates all 1-percent exceedance flood volumes for the durations between 1 and 90 days. The exceedance discharges fit to the Lower Granite reservoir balanced hydrograph are the FDA peak discharges listed in Table 4. The procedure maintains the volumes of the volume-duration frequencies for reasonably shaped hydrographs single-peaked hydrographs, but requires some smoothing for more complicated shapes. Currently, the balanced hydrograph is not incorporated in HEC-SSP. A simple balanced hydrograph method is implemented in HEC1 legacy software. Beard provided Fortran computed code that implements the method[40]. In this study, the balanced hydrograph was developed with custom Matlab™ scripts. The resulting balanced hydrographs for Lower Granite are plotted in Figure 86. The balanced hydrographs follow the pattern of the original flood and reproduce the original exceedance duration-volumes within 1 percent.

[41] USACE (2010). *HEC-SSP Statistical Software Package, CPD-86,* Hydrologic Engineering Center, U.S. Army Corps of Engineers, Davis, CA.

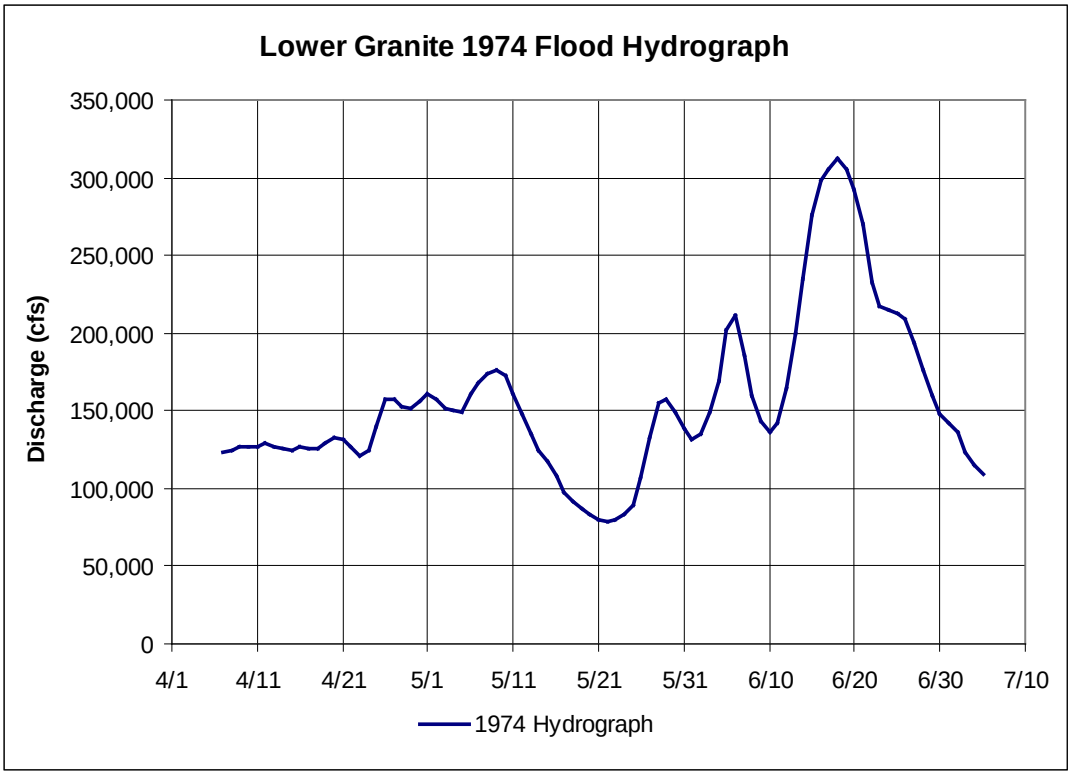


Figure 84. 1974 Flood Hydrograph at Lower Granite Reservoir.

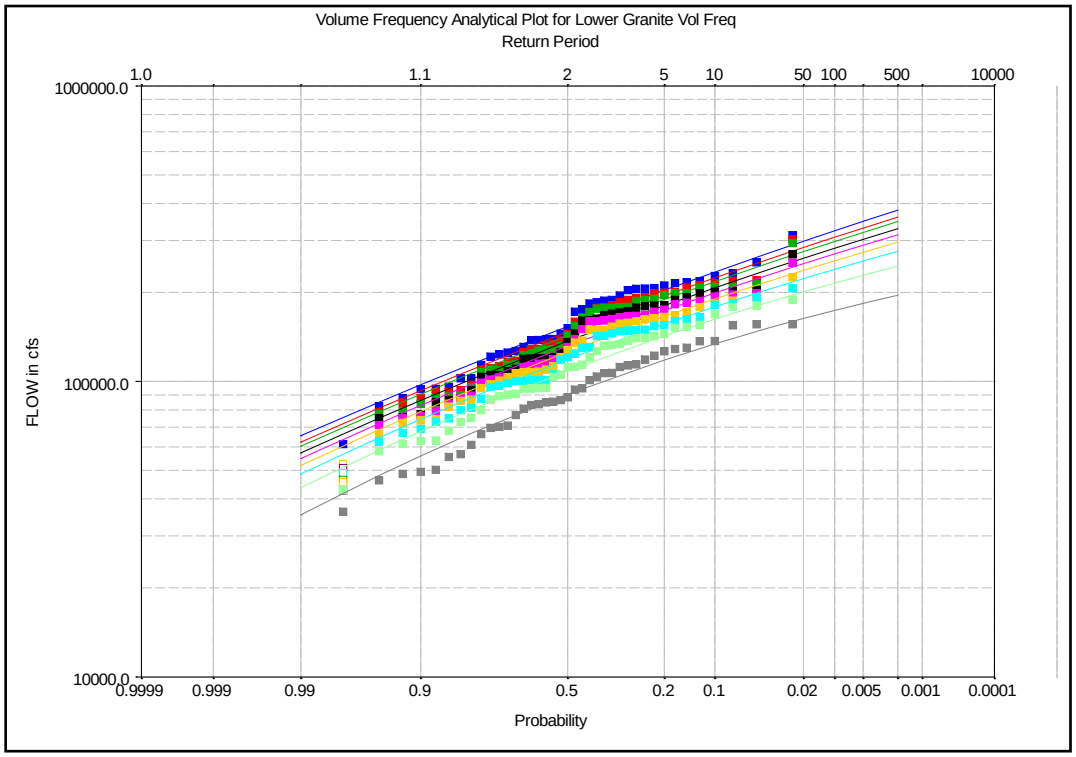


Figure 85. Volume-frequency curves for Lower Granite Reservoir.

Lower Granite Volume-Duration-Frequency (1972-2010)										
Percent	Adjusted Total Volume (cfs-day) for Duration (day)									
Exceedance	1	5	7	11	15	21	30	45	60	90
0.2	381603	1799446	2432951	3612197	4697778	6213167	8260143	11046600	13584864	17607654
0.4	360629	1687838	2284465	3397310	4424117	5860842	7807854	10474848	12910326	16797429
1	331562	1536888	2083109	3104707	4050216	5377365	7183722	9678821	11964966	15648480
2	307995	1418331	1924434	2872909	3752732	4990553	6680793	9030020	11187918	14689755
4	282788	1294814	1758653	2629634	3439364	4581165	6145266	8332488	10346568	13638348
10	245988	1120112	1523342	2282404	2990057	3990773	5367177	7306893	9098748	12054285
20	214082	973514	1325135	1988172	2607471	3484944	4695210	6409917	7997400	10632834
50	160423	735545	1001960	1505061	1975730	2643709	3567306	4882104	6101712	8138898
One day duration discharge adjusted to be equal to the peak discharge										

Table 11. Volume-duration-frequency statistics for Lower Granite Reservoir.

Lower Granite Volume-Duration-Frequency (1972-2010)										
	Discharge Ratio for Duration (day)									
	1	5	7	11	15	21	30	45	60	90
Flow Ratio	63.7	65.4	65.4	65.5	66.5	67.2	67.5	67.8	67.6	67.6

Table 12. Discharge ratios for proportioning the Lower Granite Reservoir balanced hydrograph.

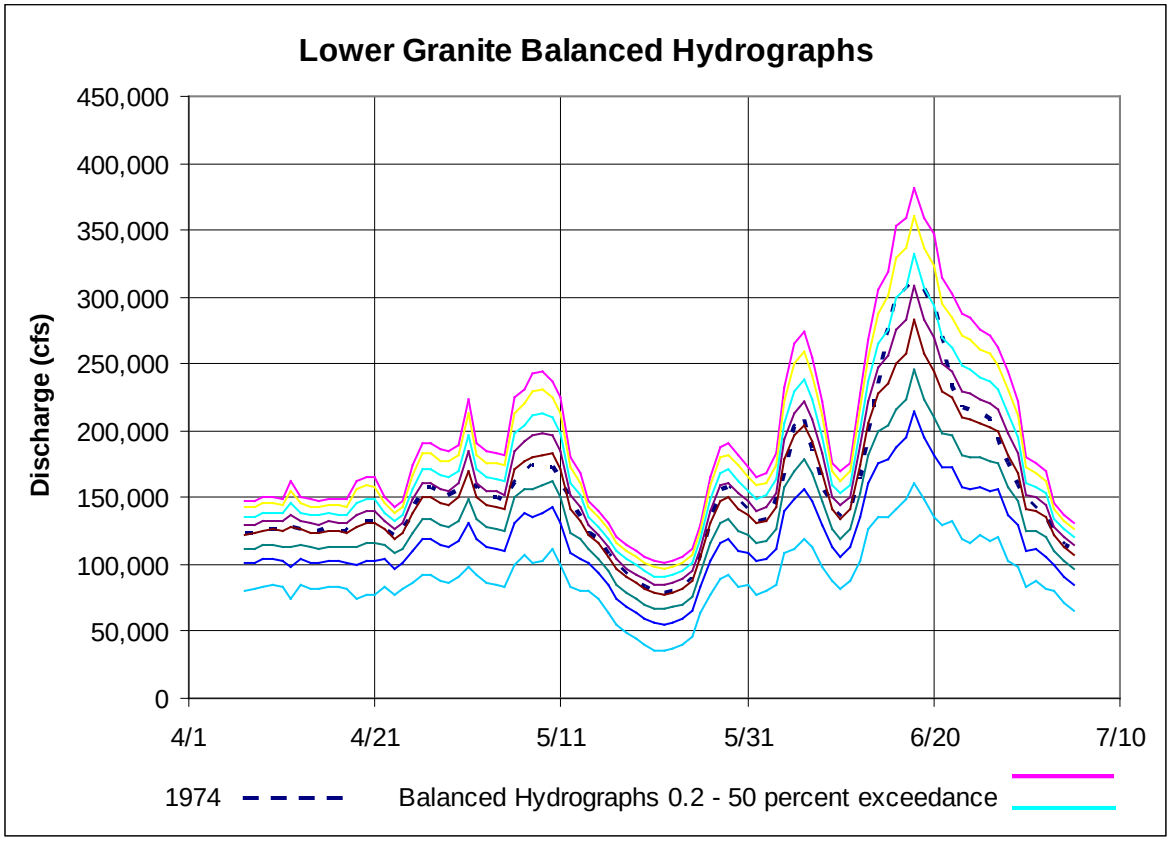


Figure 86. Balanced hydrograph floods for Lower Granite Reservoir.

11.5. Full Mobile-Bed Approach

In the full mobile-bed approach, a sediment transport model is developed with the year-2060 cross sections to allow the channel to adjust by scour and deposition during extreme discharges. The hydraulic model for the full mobile-bed approach was developed with the following steps:

1. The basic geometry model geometry from the partial mobile-bed approach is serves as the initial geometry for the sediment transport analysis.
2. Bed material designations and boundary conditions are specified for the Ackers-White transport function. Bed material designations are listed in Table 13.
3. As for the partial mobile-bed approach, the initial geometry is duplicated so that individual mobile-bed hydraulic models represent the lower and upper bed regime conditions.
4. For the upper bed regime model, the original Manning's *n* values from the calibrated 2009 fixed-bed model were used throughout the model because they were nearly equivalent to the values estimated from the Brownlie relationship for upper regime.
5. For the lower bed regime model, the original Manning's *n* values from the calibrated 2009 fixed-bed model were adjusted so that the Manning's *n* values were not less than the 0.026 value computed by the Brownlie method for lower bed regime flow.
6. Balanced hydrographs developed by the procedure discussed in Section 11.4 for the Snake and Clearwater Rivers are input as the boundary conditions for the exceedance discharges in the FDA analysis.
7. The sediment load boundary condition is the same as the sediment rating table used in the long-duration sediment transport analysis of Section 10.13 except that the rating curve is extended to beyond the extreme flows with loads determined from the adjusted power fit of the measured sediment data as described in Section 6.

Sediment transport simulations must be performed separately for each exceedance discharge as an individual model run. Each balanced hydrograph flow series sediment transport analysis is 87 days long and was assigned a start date of April 7 based on the original 1974 pattern hydrograph. The Ackers-White sediment transport function was used for all simulations. Sediment unit weights were 90 $lbft^2$ for

sand, 70 $lbft^2$ for silt and 30 bft^2 for clay. For comparison, balanced hydrograph simulations were also performed with the year-2009 cross sections.

Many trial simulations were performed to observe the effect of adjustment on sediment computation parameters. While all simulations were stable at default settings, the boundary condition weighting factors were changed slightly to dampen oscillation at the confluence. An unreasonable amount of deposition occurred at the CPRR Bridge on the Clearwater River. It is known from the sediment range cross sections that medium sand sediment does not deposit at the bridge so the cross sections at the bridge were set as pass-through nodes in the model sediment data. Transients in the simulation caused by initial bed gradation adjustment did not significantly affect the water surface profile at the peak of the hydrograph. The addition of a bed initialization period (warm-up) of several months at the beginning of the simulation did not significantly change the water surface profile at the peak of the hydrograph. As a further test, bed gradation hotstart initialization was implemented with a beta version of HEC-RAS 4.2 beta. The warm-up initialization of the bed for the M1 profile is somewhat arbitrary and depends on the steady flow assumed during the startup period. The approach was to simulate a long (254 days) constant discharge that is the same as the starting values in the balanced hydrographs. The discharges are high enough to transport sediment into the reservoir from the regression curve boundary condition. Plots of D_{50}, D_{90}, and D10 grain sizes show that the gradation stabilized about half way through the warm-up period. The most abrupt changes in gradation occur in the first few days, which confirmed that the month long warm-up period in the original model was adequate.

The general pattern of scour and deposition was similar for all simulations. Scour and deposition at the peak of the 1-percent exceedance balanced hydrograph on 19 June for the upper regime (low *n*) bed condition is shown in Figure 87. Scour begins just above the confluence in both the Snake and Clearwater Rivers and continues at a decreasing rate to about RM 138. A moderate amount of deposition occurs from RM 138 to RM 137, followed by additional scour from RM 137 to RM 135. Most of the deposition occurs downstream of RM 135. Maximum scour depth, as represented by mean effective channel invert change, was 6 feet and the maximum deposition depth was about 5 feet.

The plot of sediment discharge in Figure 88 shows that sediment inflows at the peak of the balanced hydrograph was about 60,000 tons per day (tpd) on the Clearwater River and about 262,000 tpd on the Snake River. Sediment discharge peaks at RM 134 at about 625,000 tpd. The plot of longitudinal cumulative mass change of the bed in Figure 89 shows that about 1.5 million tons of sediment was eroded from the confluence to RM 135 and that most of the sediment is deposited between RM130 and RM 135. The pattern of cumulative bed change is similar for the

upper bed regime 0.2 percent exceedance balanced hydrograph in Figure 90 and the lower bed regime 0.2 percent exceedance balanced hydrograph Figure 91.

Bed Material Designation for Balanced Hydrograph Sediment Transport Geometry					
River	Reach	Upstream Station	Downstream Station	Bed Material	D_{50} mm
Clearwater	Lewiston	7.850	1.603	Large Cobble	128
Clearwater	Lewiston	1.530	0.967	Medium Sand	0.5
Clearwater	Lewiston	0.906	0.545	Large Cobble	128
Clearwater	Lewiston	0.461	0.217	Medium Sand	0.5
Snake	Clarkston	148.83	142.005	Small boulder	512
Snake	Clarkston	141.949	139.58	Large Cobble	128
Snake	Clarkston	139.565	139.404	Large Cobble	128
Snake	Lower Granite	139.254	134.066	Medium Sand	0.5
Snake	Lower Granite	133.997	130.106	Fine Sand	0.25
Snake	Lower Granite	129.989	107.43	Silt	0.016

Table 13. Bed material designations for the balanced hydrograph sediment transport model.

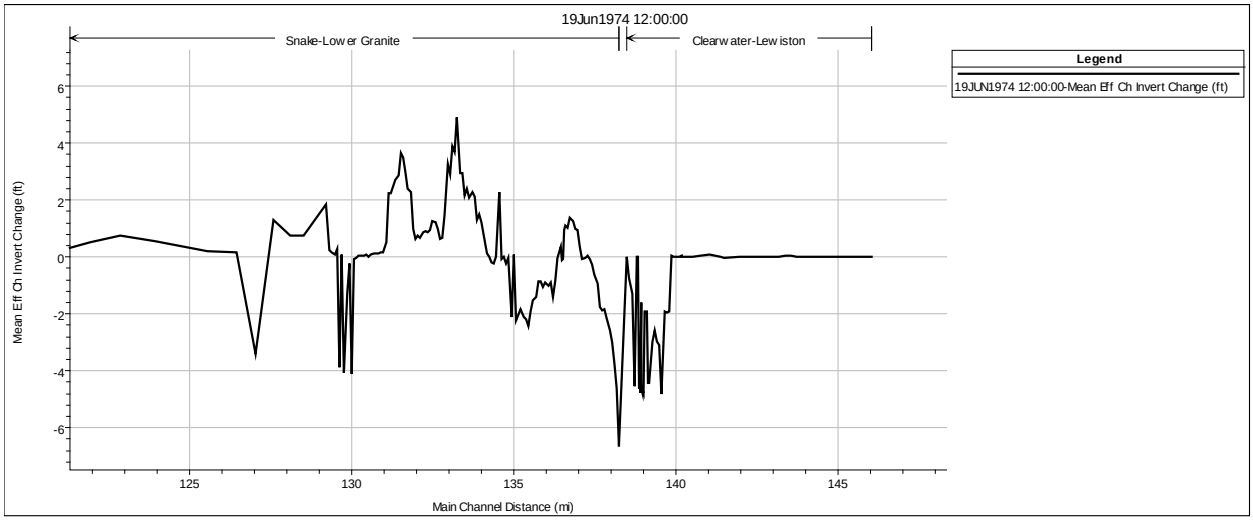


Figure 87. Deposition and scour during 1-percent exceedance balanced hydrograph.

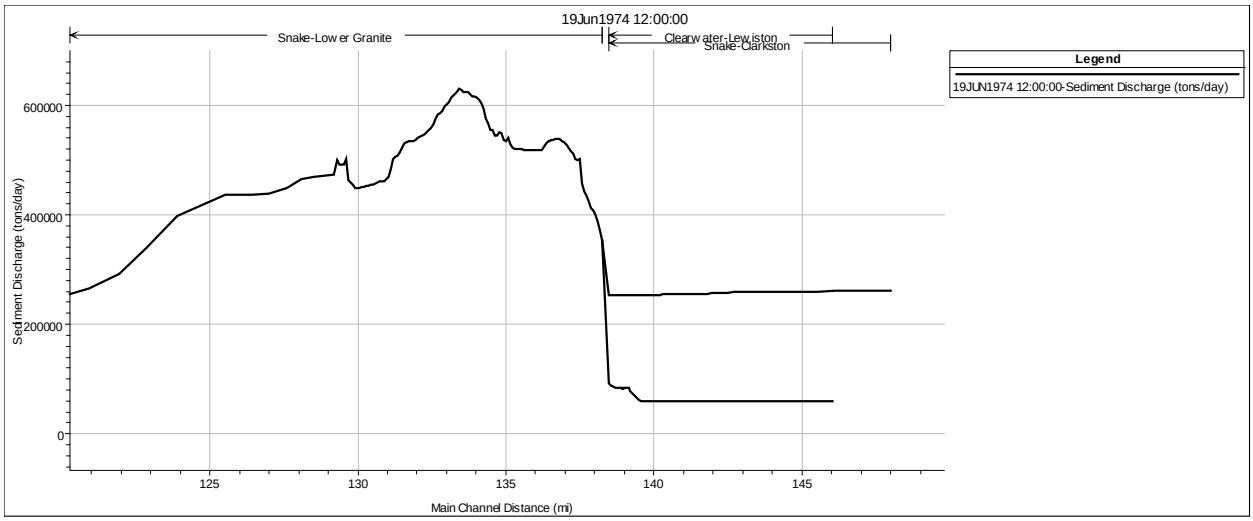


Figure 88. Sediment discharge at peak of 1-percent exceedance balanced hydrograph.

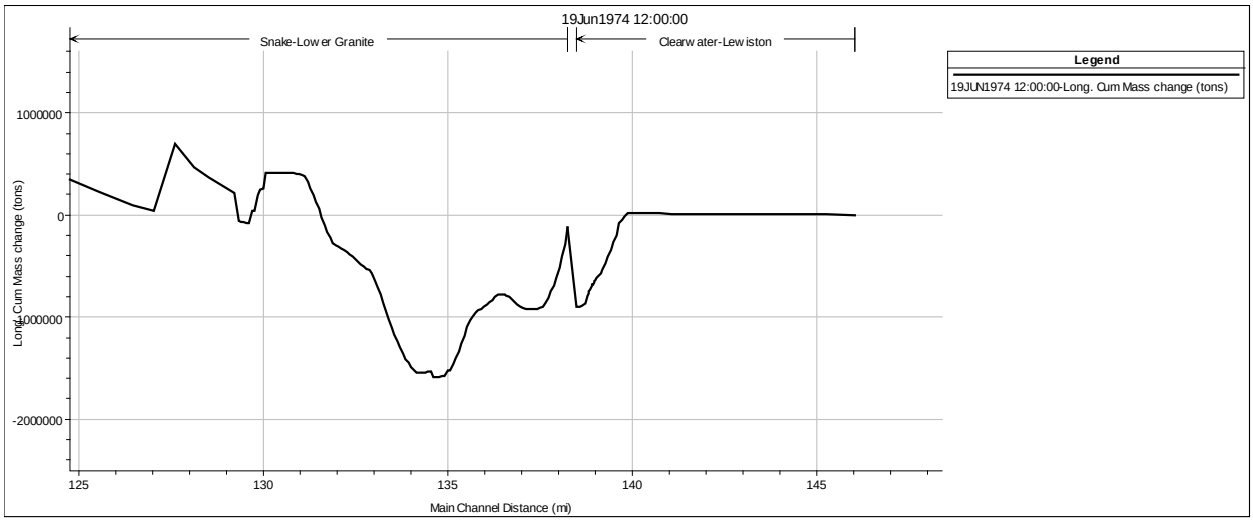


Figure 89. Longitudinal cumulative mass change at peak of 1-percent exceedance balanced hydrograph.

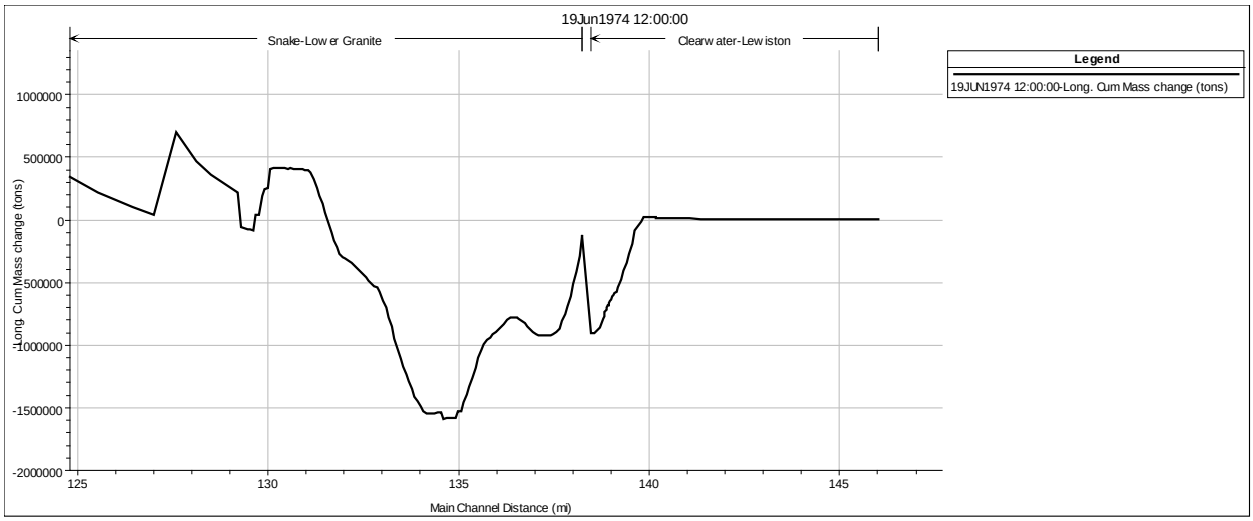


Figure 90 Longitudinal cumulative mass change at peak of 0.2-percent exceedance balanced hydrograph for the upper regime bed condition.

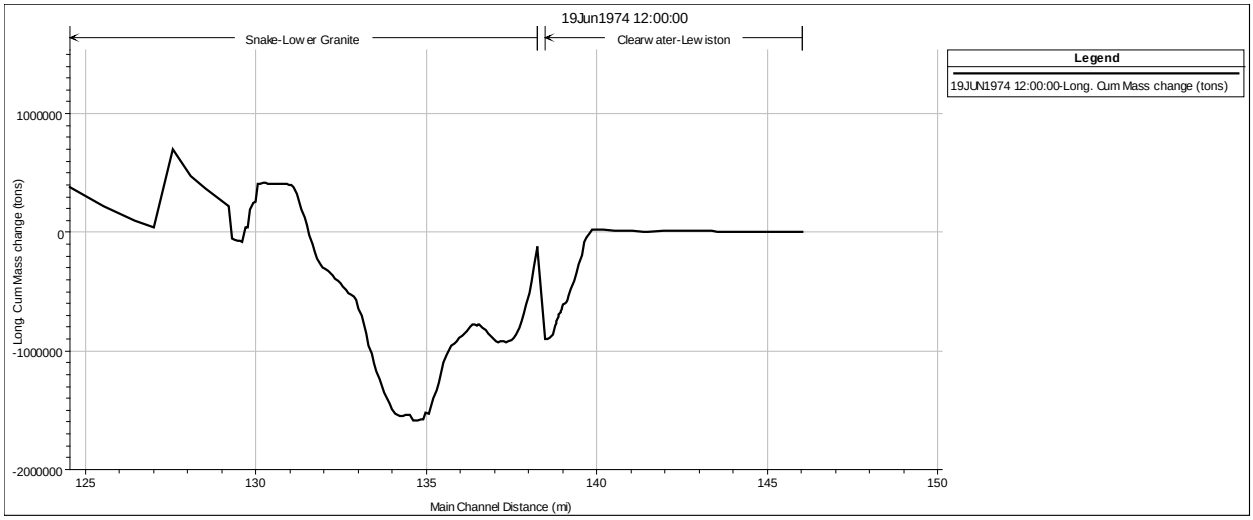


Figure 91. Longitudinal cumulative mass change at peak of 0.2-percent exceedance balanced hydrograph for the upper regime bed condition.

The peak water surface elevation is found by inspection of the water surface profiles generated by the sediment transport simulation. Since the shape of the balanced hydrograph and general pattern of bed change was similar for all simulations, the peak water surface at the confluence occurred on 19 June in all simulations. Peak water surface elevations at Clearwater RM 0.217 for the full mobile-bed analysis are summarized and compared to the partial mobile-bed analysis in Table 14 and Table 15.

Peak water surface elevations at the confluence (Clearwater RM 0.217) for both the partial mobile-bed and full mobile-bed analyses of the year-2060 channel are very similar even though the methods and assumptions embodied in the approaches are

very different, except for the initial channel geometry and Manning's roughness. Peak discharges for the steady flow partial mobile-bed analysis are significantly less than the peak discharges for the balanced hydrograph full mobile bed analysis. This is due to proportioning of the flows between the Snake and Clearwater Rivers in the balanced hydrograph method. The sediment transport analysis shows that a large amount of sediment is eroded from the confluence area, but that most of the sediment is retained in the upper reach of Lower Granite Reservoir where it still has significant influence on the flood water surface profile. Simulation of the SPF discharge with a two-dimensional ADH sediment transport model of the upper segment of Lower Granite Reservoir corroborates this finding. The ADH simulation is discussed in Section 12.

For the upper regime bed condition, the 1-percent exceedance flood stage for the full mobile-bed was less than 0.2 ft below bed stage determined with the partial mobile approach. Differences for the upper regime stages for the 0.4 percent and 0.2 exceedance discharges were negligible. For the lower regime bed condition, the 1-percent exceedance flood stage for the full mobile-bed was also about 0.2 ft below the partial mobile-bed stage. The full mobile-bed stages for upper regime for the 0.4 percent and 0.2 exceedance discharges less than 0.3 ft below the corresponding stages for the partial mobile-bed analysis.

Water surface elevations from the fixed-bed analysis of the 2009 channel geometry are also listed in Table 14 and Table 15. The water surface elevations listed for the fixed-bed 2009 upper regime analysis are directly comparable to the upper regime water surface elevations for the full mobile-bed balanced hydrograph method and do not differ significantly. The water surface elevations for the lower regime by the balanced hydrograph method are substantially less than for the fixed-bed analysis, primarily because greater values of Manning's *n* (0.028 to 0.03) were used in the "historic *n*" fixed-bed analysis.

Peak Water Surface Elevation at Clearwater River Mile 0.217										
	Partial Mobile-Bed Approach - Steady Flow					Full Mobile Bed Approach - Balanced Hydrograph				
	Steady Flow	Water Surface Elevation (feet NAVD88)				Unsteady Peak	Water Surface Elevation (feet NAVD88)			
Percent	Discharge	2009		2060		Discharge	2009		2060	
Exceedance	cfs	Upper Reg	Lower Regime	Upper Regime	Lower Regime	cfs	Upper Regime	Lower Regime	Upper Regime	Lower Regime
SPF	125,000	741.57	744.96	745.94	748.30	133,122	741.72	743.48	745.82	748.13
0.2	117,587	740.11	743.25	744.18	746.41	138,603	740.12	741.96	744.17	746.26
0.4	111,124	739.30	742.32	743.26	745.39	130,985	739.03	741.04	742.98	745.14
1	102,167	738.16	741.03	741.98	743.89	120,427	737.79	739.69	741.73	743.67

Table 14. Water surface elevations at Clearwater RM 0.217 for partial and full mobile-bed computation methods.

Peak Water Surface Elevation at Clearwater River Mile 0.217										
	Partial Mobile-Bed Approach - Steady Flow					Full Mobile Bed Approach - Balanced Hydrograph				
	Steady Flow	Water Surface Elevation (feet NAVD88)				Unsteady Peak	Water Surface Elevation Difference (feet)			
Percent	Discharge	2009		2060		Discharge	2009		2060	
Exceedance	cfs	Upper Reg	Lower Regime	Upper Regime	Lower Regime	cfs	Upper Regime	Lower Regime	Upper Regime	Lower Regime
SPF	125,000	741.57	744.96	745.94	748.30	133,122	0.15	-1.48	-0.12	-0.17
0.2	117,587	740.11	743.25	744.18	746.41	138,603	0.01	-1.29	-0.01	-0.15
0.4	111,124	739.30	742.32	743.26	745.39	130,985	-0.27	-1.28	-0.28	-0.25
1	102,167	738.16	741.03	741.98	743.89	120,427	-0.37	-1.34	-0.25	-0.22

Table 15. Water surface elevation difference at Clearwater RM 0.217 for partial and full mobile-bed computation methods.

11.6. Conditional Non-Exceedance Probabilities – 2060 Full Mobile-Bed Analysis of Upper and Lower Bed Regime

The water surface elevations from the partial mobile-bed approach and the full mobile-bed approach were similar, so the conditional non-exceedance probabilities and long-term risk probabilities for the full mobile-bed analysis would be nearly the same as those for the partial mobile-bed analysis in Section 11.3.

11.7. Added Levee Height for SPF Freeboard

The Lewiston Levee system was constructed with 5 ft of freeboard above the SPF water surface elevation. As discussed previously, the hydraulic performance of levee systems are now generally evaluated with the risk-based methods employed above. In traditional design, freeboard provided a margin above the flood water surface to account for uncertainties in hydrologic data and analysis methods. These uncertainties are now directly incorporated in the risk-based analysis. The concept of levee freeboard has been an important in the public discussion of the Lewiston Levee system. To facilitate continued discussion of flood risk reduction and dam safety, it is worthwhile to determine the height that would have to be added to the existing levee embankment to provide 5 feet of freeboard for the SPF. Table 16 and Table 17 list the heights that are added to the current top-of-levee elevations to provide 5 ft of freeboard above the median (50 percent) water surface elevation for the Standard Project Flood (SPF). The tables include the heights for the current (2009) and 50-year future (2060) channel condition computed for both lower and upper bed regimes. The heights were derived from the results of water surface computations and models discussed previously.

For the 2009 channel condition in upper bed regime, 5 ft of freeboard exists during the SPF on the Clearwater River except near the Camas Prairie Rail Road (CPRR) Bridge at RM 0.6 where the maximum difference is 1.1 feet for the left bank levee and 1.2 for the right bank levee. The 5 ft of freeboard exists at all points on the Snake River right bank levee for the 2009 channel condition. As discussed previously, the upper bed regime is the likely bed condition during extreme discharges. For the

2009 lower bed regime condition on the Clearwater River, the maximum added height is 4.3 ft for the left bank levee and 4.5 ft for the right bank levee near the CPRR Bridge. The added height decreases to near 0 ft at the upstream end of the levee system. The maximum added height for the Snake River levee in a lower bed regime condition is 3.1 ft at RM 139.61 above the Interstate Bridge.

For the 2060 (year-50) channel condition in upper bed regime on the Clearwater River, added levee heights to obtain the 5 ft of freeboard for the SPF varies from 0.9 ft at the upstream end of the left bank levee to a maximum of 4.9 ft near the CPRR Bridge. The maximum added height for the Clearwater River right bank levee is 5.6 ft near the CPRR Bridge. Maximum height for the Snake River levee is 4.1 ft for the upper bed regime condition. For the 2060 lower bed regime condition, the maximum added height is 7.0 ft for the left bank levee and 7.9 ft for the right bank levee near the CPRR Bridge. The maximum added height for the Snake River levee for the 2060 lower bed regime condition is 6.6 ft.

Clearwater River Added Levee Height for 5 ft Freeboard During SPF								
	Year 2009 Added Height (feet)				Year 2060 Added Height (feet)			
River	Upper Regime		Lower Regime		Upper Regime		Lower Regime	
Mile	Left Levee	Right Levee	Left Levee	Right Levee	Left Levee	Right Levee	Left Levee	Right Levee
2.890	0.0	0.0	0.5	0.0	0.9	0.2	2.7	2.0
2.580	0.0	0.0	0.6	0.0	1.1	0.0	3.1	1.4
2.340	0.0	0.0	0.5	0.4	1.1	1.1	3.2	3.1
1.993	0.0	0.0	0.8	1.3	1.6	2.1	3.7	4.2
1.974	0.0	0.0	0.7	1.8	1.4	2.5	3.5	4.6
1.898	0.0	0.0	0.7	1.4	1.4	2.1	3.5	4.2
1.822	0.0	0.0	1.1	1.1	1.9	1.9	4.0	4.0
1.747	0.0	0.0	0.8	1.4	1.7	2.3	3.8	4.4
1.671	0.0	0.0	1.3	1.7	2.2	2.6	4.3	4.7
1.603	0.0	0.0	1.5	1.7	2.3	2.5	4.4	4.6
1.530	0.0	0.0	1.3	1.7	2.1	2.5	4.2	4.6
1.452	0.0	0.0	1.3	1.8	2.1	2.6	4.2	4.7
1.378	0.0	0.0	1.0	1.7	1.8	2.6	4.0	4.7
1.293	0.0	0.0	1.0	1.6	1.9	2.5	4.0	4.6
1.210	0.0	0.0	1.2	1.9	2.0	2.7	4.2	4.8
1.131	0.0	0.0	1.2	1.6	2.0	2.4	4.1	4.5
1.074	0.0	0.0	2.0	1.6	2.8	2.3	4.9	4.5
0.967	0.0	0.0	2.4	1.7	3.1	2.5	5.3	4.6
0.906	0.0	0.0	2.5	2.2	3.3	2.9	5.5	5.1
0.878	0.0	0.0	2.5	2.5	3.3	3.3	5.5	5.5
0.850	0.0	0.0	2.6	0.0	3.3	0.4	5.5	2.6
0.822	0.0	0.0	2.9	0.0	3.6	0.0	5.9	1.8
0.794	0.0	0.0	2.9	0.0	3.6	0.0	5.9	1.8
0.764	0.0	0.0	3.0	2.9	3.8	3.7	6.1	6.0
0.749	0.0	0.2	2.8	3.5	3.5	4.2	5.8	6.5
0.733	0.0	0.5	0.0	3.8	0.0	4.5	1.9	6.8
0.717	0.0	0.7	0.0	4.1	0.2	4.9	2.4	7.1
0.701	0.0	0.0	3.1	3.2	3.7	3.9	6.0	6.2
0.686	0.5	0.3	3.9	3.7	4.6	4.4	6.9	6.7
0.650	0.7	0.0	4.0	2.0	4.7	2.6	7.0	5.0
0.600	1.1	0.0	4.4	0.0	4.9	0.0	7.2	0.4
0.590	0.0	1.2	3.1	4.5	4.2	5.6	6.5	7.9
0.545	0.0	0.0	1.9	0.0	3.1	0.0	5.4	0.0
0.461	0.3	0.0	3.5	0.0	4.8	0.0	7.1	0.0
0.373	0.1	0.0	3.3	0.0	4.5	0.0	6.9	0.0
0.299	0.0	0.0	3.2	0.0	4.4	0.0	6.7	0.0
0.217	0.0	0.0	3.2	0.0	4.4	0.0	6.7	0.0

Table 16. Added height to Clearwater River levee to provide 5 ft freeboard during SPF.

Snake River Added Levee Height for 5 ft Freeboard During SPF				
	Year 2009 Added Height (feet)		Year 2060 Added Height (feet)	
River Mile	Upper Regime Right Levee	Lower Regime Right Levee	Upper Regime Right Levee	Lower Regime Right Levee
140.544	0.0	1.6	2.4	4.7
140.489	0.0	1.2	2.2	4.4
140.406	0.0	0.8	1.5	3.9
140.324	0.0	2.1	3.0	5.2
140.241	0.0	1.5	1.9	4.3
140.161	0.0	2.3	2.9	5.3
140.102	0.0	2.1	3.0	5.3
140.043	0.0	1.9	2.6	5.0
139.984	0.0	2.1	3.0	5.4
139.925	0.0	2.1	3.1	5.5
139.833	0.0	2.7	3.8	6.2
139.756	0.0	3.0	4.1	6.5
139.679	0.0	2.5	3.7	6.1
139.659	0.0	2.7	3.5	6.0
139.625	0.0	2.9	3.9	6.3
139.610	0.0	3.1	4.0	6.5
139.595	0.0	2.8	3.8	6.3
139.580	0.0	3.1	4.1	6.6
139.550	0.0	2.1	3.1	5.6
139.535	0.0	2.6	3.6	6.0
139.475	0.0	2.6	3.4	6.0
139.404	0.0	2.2	3.1	5.6

Table 17. Added height to Snake River levee to provide 5 ft freeboard during SPF.

11.8. Summary of the Flood Risk Analysis for the year 2060 future Channel Condition.

The partial and full mobile-bed analyses of the year 2060 channel geometry produced similar estimates of flood water surface elevations at the confluence and in the Lewiston Levee system. The FDA flood risk computations in Section 11.3 showed that the conditional non-exceedance probabilities were greater than 94 percent for the 1-percent exceedance discharge and the 50-year long-term risk of overtopping was about 10 percent for the left bank levee on the Clearwater River at the confluence for the condition of upper bed regime and a large (2.0) standard deviation of stage uncertainty. The bed regime analysis in Section 10.8 indicates that the lower roughness upper bed regime condition is more likely than the higher roughness lower bed regime during extreme discharges. Section 15 includes additional discussion and analysis of bed regime in Lower Granite Reservoir. Taken together, these findings

support an understanding that the flood risk at the end of the 50-year analysis period, while higher than at present, remains sufficiently low so that immediate corrective action is not justified based solely on the expected short-term increase in flood risk. The long-term increase in flood risk for the future channel condition does indicate that sediment accumulation in Lower Granite Reservoir must be managed to maintain the current levels of flood risk reduction. Sediment management alternatives are discussed in Section 12.

It should be recognized that the prediction of the transition from lower regime to upper regime is not precise and the application of empirical regime analysis to the scouring conditions at the confluence during extreme discharges is not directly implemented in the risk-based methods employed in this study. Furthermore, while the analysis of the existing condition in Section 5 showed that flood risk is presently low, even for lower bed regime conditions, flood risk will continue to increase as sediment accumulates in Lower Granite Reservoir. It should be understood that the flood risk computations show an unacceptable level of flood risk if the bed remains in lower regime after sufficient sediment accumulates, even though the credible methods employed in this study indicate that the transition to upper regime will most likely occur before the peak of extreme discharges that pose the most flood risk. The uncertainty in the rate of discharge at which the upper segment of Lower Granite Reservoir transitions from lower to upper bed regime cannot be completely resolved with the available data and current analysis methods. Further monitoring of sediment load, continued acquisition of detailed bathymetry, more measurements of bedload sediment and suspended load transport within the reservoir, and perhaps physical modeling of the confluence, is recommended to better understand how flow resistance and bed regime affect flood water surfaces during extreme discharge at Lower Granite Reservoir.

The acquisition of data to better define the response of the mobile bed of Lower Granite was begun in May 2011. Section 12 discusses bathymetry data and sand wave bedload transport data that were measured near the peak of the seasonal hydrograph when sand bed-load was being transported through the reservoir. The May 2011 bathymetry shows that the height and wavelength of dunes were less than those observed in low flow bathymetry acquired in 2009 and 2010, which further indicates that a transition to upper bed regime would likely occur before the peak of the extreme discharges adopted in the flood risk analysis.

12. Alternatives for Sediment Management in Lower Granite Reservoir

The historic sediment range data, the hydraulic geometry analysis and the sediment transport analysis above showed that some segments of the channel in the upper reach of Lower Granite Reservoir are tending towards a state of relative morphological equilibrium under the prevailing sediment loads and discharges. During equilibrium transport, flow velocity and bed shear stress are great enough that sediment erosion balances sediment deposition so that there is no net change in the equilibrium depth of the channel cross section. At even higher velocities, if sediment inflow remains constant, the rate of sediment erosion will exceed deposition and a channel section will tend to erode to reestablish a new deeper equilibrium depth. In-reservoir sediment management measures can take advantage of this sediment dynamic to promote sediment transport in the upper reach of Lower Granite to help maintain navigation depth and hydraulic conveyance. Potential sediment management measures, besides dredging, include river training structures, such as spur dikes; manipulation of the hydraulic grade line of the reservoir such as with seasonal draw-downs of the reservoir pool; and trapping of sediment upstream of the confluence.

12.1. Sediment Management with Spur Dike Fields

River training structures are constructed features that alter channel hydrodynamics and sediment transport to produce desired channel conditions or alleviate problems caused by channel instability. River training structures have been devised for various purposes including grade stabilization, bank protection, reduced shoaling, and creation of fisheries habitat. Common structures constructed in medium and large rivers including spur dikes, bendway weirs and submerged vanes. Spur dikes are rockfilled or piling structures that extend outward from the bank part way into the channel. Spur dikes confine the flow to a narrower cross section, which increases the discharge per unit width and in alluvial channels establishes a deeper equilibrium depth in the unobstructed portion of the channel. Spur dikes may have disadvantages which include increased hydraulic resistance and the creation of habitat that may encourage predation of juvenile salmonids. Spur dikes can also change navigational and recreational use of a reservoir.

Possible spur dike fields are shown in Figure 92. Optimum spacing of spur dikes is in the range of 2 to 5 times the length of the dike[42,43]. Spur dikes are located in the turning basin of the Clearwater River at the Port of Lewiston, across from the Port of Clarkston, across from the Port of Wilma, and downstream from the Port of Wilma. A longitudinal dike is located at Red Wolf Marina. The design and placement of spur dikes depend on field conditions, so the configuration of the dikes shown in Figure 92 may change in a detailed design study. The intent of this study was to evaluate the long-term potential of spur dikes to maintain greater depths in the navigation channels and promote transport of sediment away from the confluence into deeper segments of the reservoir. Since the spur dikes partially obstruct flow and add boundary roughness, it is necessary to determine the effect of spur dikes on the flood water surface profile and flood risk.

The hydraulic and sediment transport effects of spur dike fields were evaluated with HEC-RAS one-dimensional models and ADH two-dimensional models. Spur dikes were added to the 2009 channel geometry that was used in the long-term sediment transport simulation of the year-2060 channel condition. Spur dikes were modeled as blocked obstructions. The left bank spur dike at Clearwater RM 1.131 is shown in Figure 93. Tops of the spur dikes were set above the flood water surface level (full depth spur dikes) to maximize the effect of the added hydraulic resistance. Blocked obstructions were added to all model cross sections within a dike field even though the actual spacing of the dikes would be greater than the model cross section spacing. This assures that HEC-RAS simulates the condition when sediment has filled the interior of the dike field. Roughness coefficients, boundary conditions, and bed parameters in the long-term simulation of sediment transport for the dikes was the same as the previous simulations. Sediment transport was computed with the Ackers-White function.

[42] Berger, R.C. and Alexander M.P. (1993). *Design Criteria for Lateral Dikes in Estuaries, Technical Report REMR-HY-9, Waterways Experiment Station*, U.S. Army Corps of Engineers, Vicksburg, MS.

[43] USACE (2006). *Environmental Design Handbook, Upper Mississippi River Environmental Management Program*, http://www.mvn.usace.army.mil/EMP/designhandbook.htm.

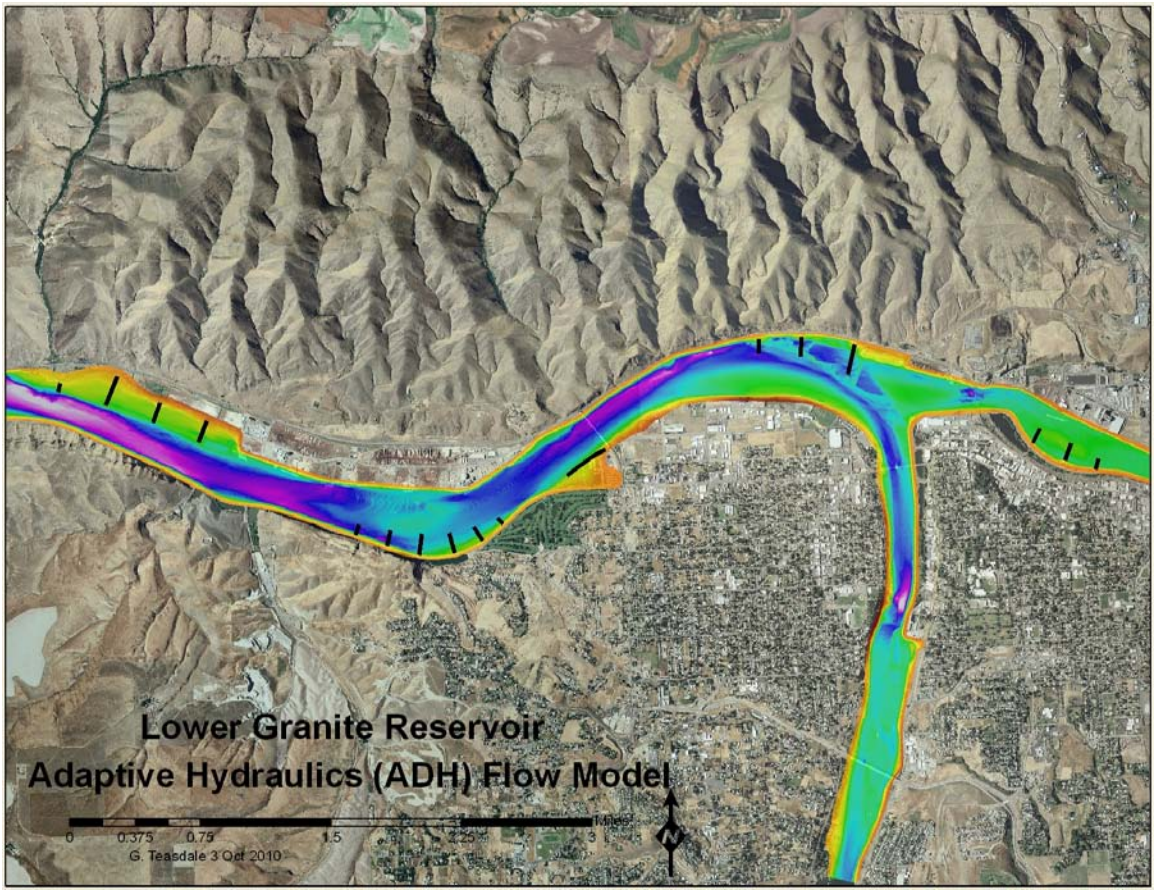


Figure 92. Location of potential spur dikes in Lower Granite Reservoir.

The longitudinal accumulation volumes and surface D_{50} at year 2060 for Lower Granite Reservoir above RM 130 are plotted in Figure 94 for simulations performed with and without spur dikes. Cumulative sediment volumes at RM 134 are about 3 mcy or 33 percent less for the simulation that included spur dike fields. Total accumulation at RM 130 is about the same in both simulations, indicating that sediment transported through the dike fields is mostly re-deposited in the segment above Silcott. The surface D_{50} plots show that coarser sediment is transported further into the reservoir in the simulation that included dikes.

Bed change plots in Figure 95 show that the simulation computed 3 to 5 ft of scour in the dike field between RM 138.4 and RM 139.0 and the dike field between RM 135.8 and RM 136.5 prevented about 5 ft of deposition. The dike field between RM 134.0 and RM 134.9 helped reduce extra accumulation that would have occurred because of the greater amount of sediment passed by the upper dike fields. A more aggressive dike field in this location could further reduce sediment accumulation.

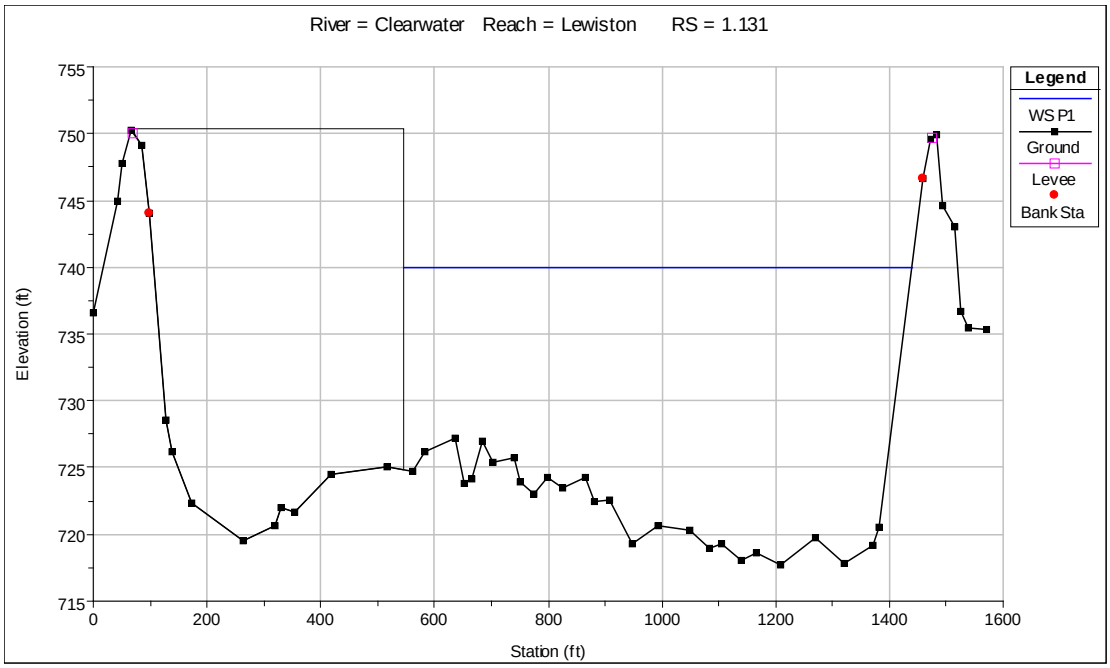


Figure 93. Spur dike at Clearwater RM 1.131 represented in HEC-RAS.

The longitudinal accumulation volumes and surface D_{50} at year 2060 for the Clearwater River turning basin are plotted in Figure 96 for simulations performed with and without spur dikes. Cumulative sediment volumes at RM 0.9 are about 0.5 mcy (42 percent) less for the simulation that included the spur dikes. Total accumulation at RM 0.2 is also about 0.5 mcy less for the simulation with spur dikes, so the sediment does not re-deposit in the Clearwater River and is transported into Lower Granite Reservoir. The surface D_{50} plots show no change in the surface sediment distributions with and without dikes. Bed change plots in Figure 97 show that in the simulation with dikes, between 2 and 4 feet of sand was prevented from depositing in the turning basin.

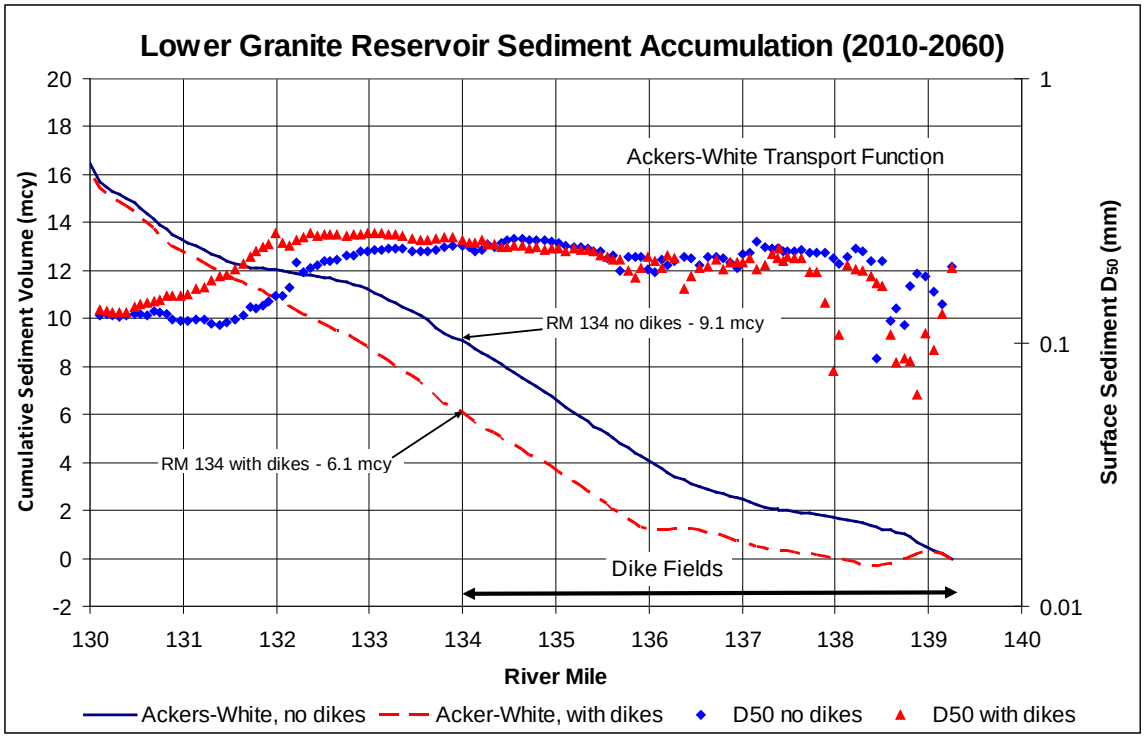


Figure 94. Ackers-White sediment accumulation volumes at year 2060 in Lower Granite Reservoir with and without spur dikes.

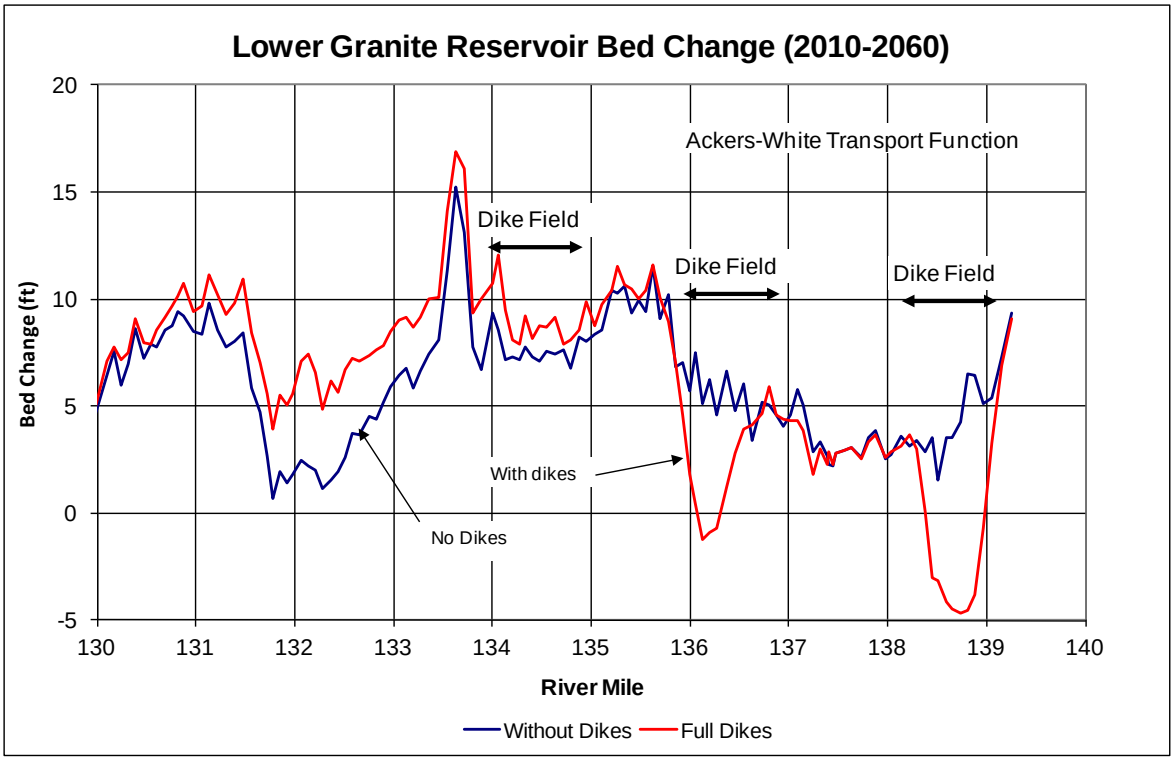


Figure 95. Ackers-White sediment bed change at year 2060 in Lower Granite Reservoir with and without spur dikes.

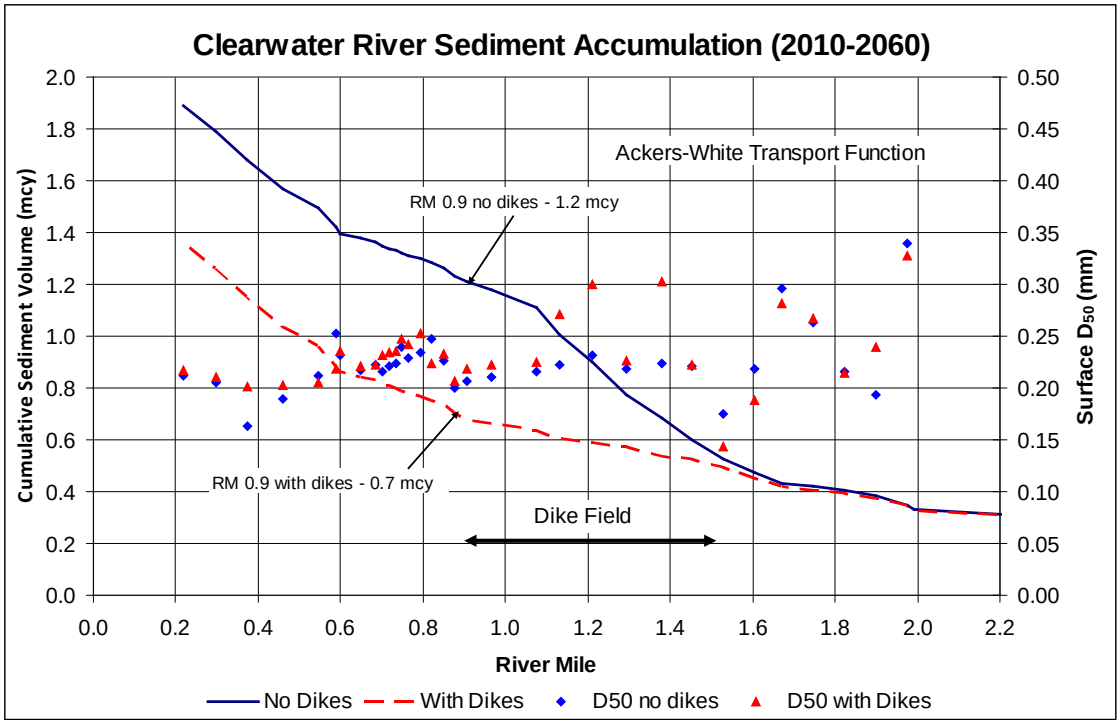


Figure 96. Ackers-White sediment accumulation volumes at year 2060 in Clearwater River with and without spur dikes.

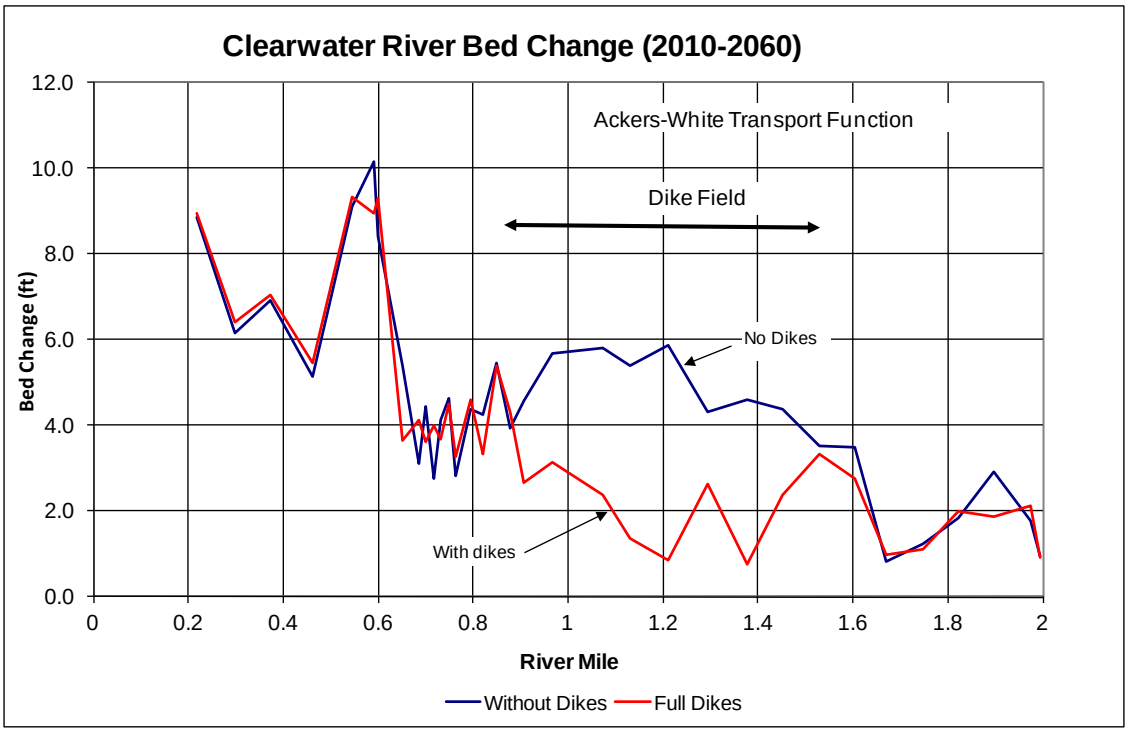


Figure 97. Ackers-White sediment bed change at year 2060 in the Clearwater River with and without spur dikes.

Bendway weirs and sediment vanes generally do not extend above the flood water surface and may lie below navigation depth. Less of the wetted channel area is obstructed by the submerged features, so less sediment will be eroded from the modified channel, but the effect on channel conveyance during flood discharge will be less. The effect of submerged training structures was modeled in HEC-RAS by reducing the height of the spur dikes to about half the depth of the channel during the 1-percent discharge. As before, the one-dimensional model only approximates the complex two and three-dimensional flow patterns around the training structures, so the simulated long-term channel adjustments at a particular cross section are not expected to be precise.

Longitudinal sediment accumulation volumes for Lower Granite Reservoir above RM 130 are compared in Figure 98 for full-height spur dikes, half-height spur dikes and the channel without spur dikes for the long-term simulation of sediment transport. The half-height spur dikes cause about 21 percent less channel erosion over the 50-year period than the full height spur dikes at the end of the spur dike field at RM 134. The plots of bed change in Figure 99 show that the half-height spur dikes produce about half the channel adjustment as the full-height spur dikes. Half-height spur dikes maintain the current depth of the channel at the confluence and allow the about the same accumulation as the channel without spur dikes between RM 134 and RM 135.

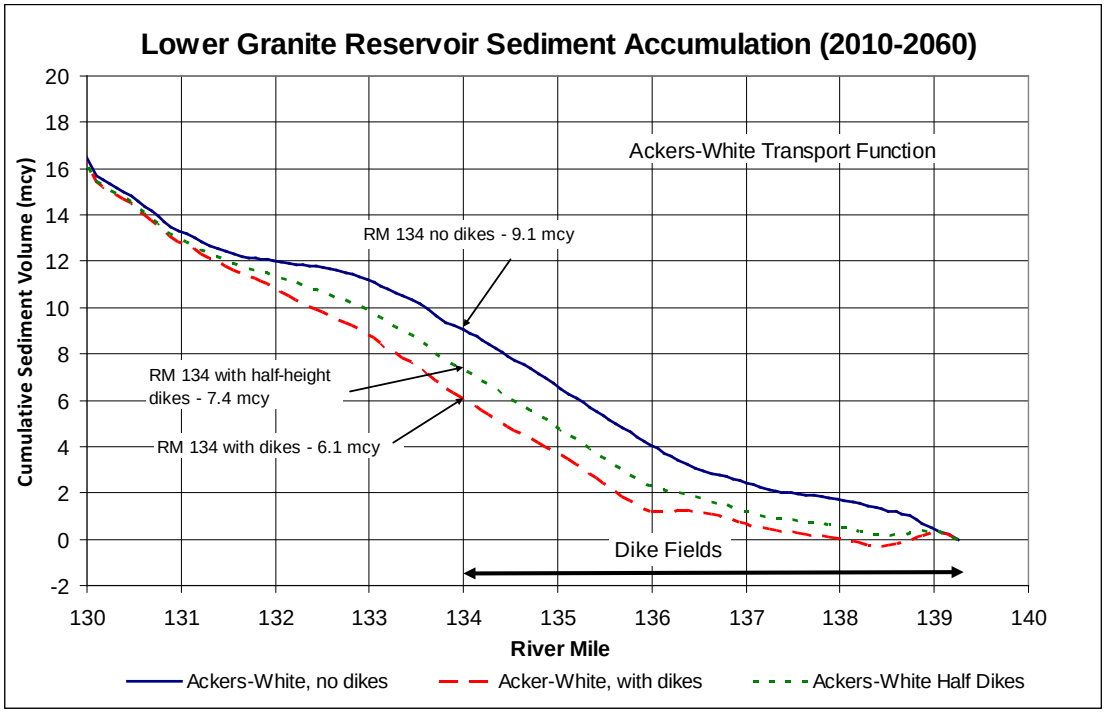


Figure 98. Ackers-White sediment accumulation volumes at year 2060 in Lower Granite Reservoir with half-height spur dikes.

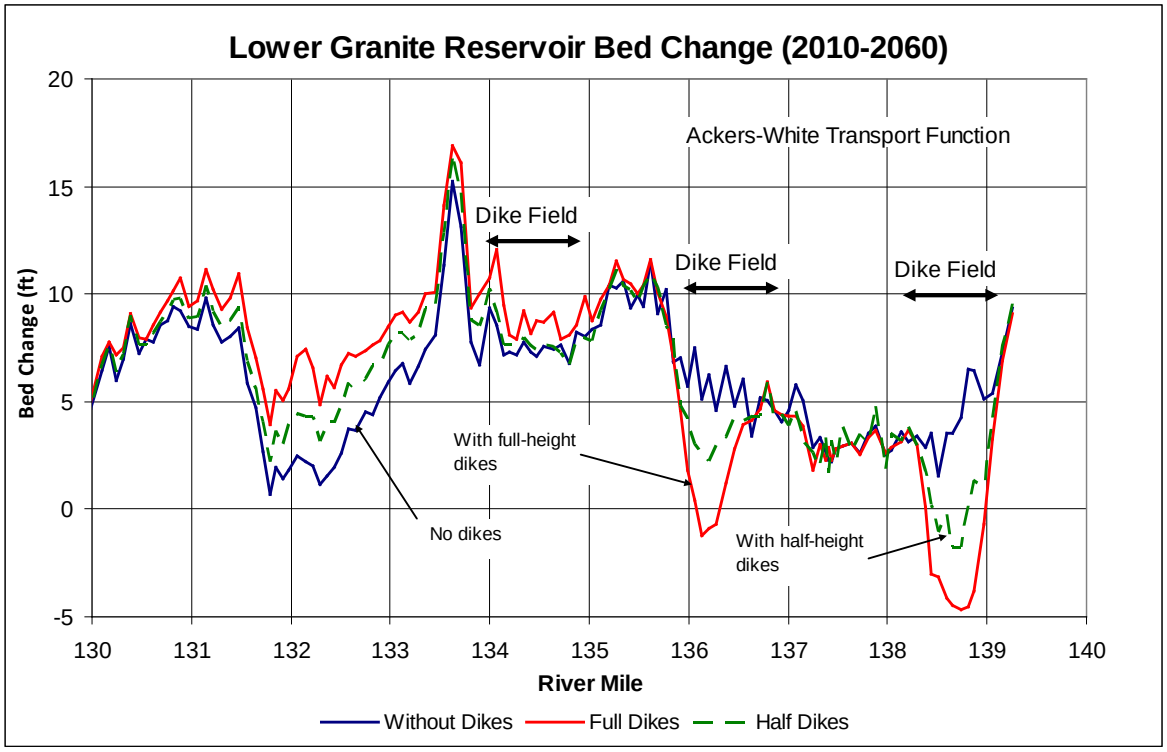


Figure 99. Ackers-White sediment bed change at year 2060 in the Lower Granite Reservoir with half-height spur dikes.

Spur dikes add hydraulic roughness to the channel and initially reduce the conveyance (wetted area) of the channel, so the water surface profile during extreme discharges will be greater in a channel that has spur dikes than in one without spur dikes. As sediment is eroded from the channel, conveyance through the spur dike field is recovered and the water surface profile will decrease, but it may not completely recover to the original profile. Adjusted channel geometries for the full-height spur dike and the half-height spur dike configurations at the end of the 50-year simulation were exported from the sediment transport module and incorporated into HEC-RAS channel models for evaluation of the extreme discharges used in the FDA analysis. The water surface profiles were computed for upper and lower bed regimes with the partial mobile-bed steady flow and full mobile-bed balanced hydrograph approaches. Water surface elevations at the confluence (Clearwater RM 0.2) for the different channel configurations, computation methods and bed regimes for the 2009 and 2006 conditions are compared in Table 18 and Table 19.

Spur dikes raised the flood water surface at the confluence by between 1.3 and 1.6 ft for the year-2009 channel with the partial mobile-bed approach and between 0.7 and 1.1 ft for the full mobile-bed approach. The long-term simulation showed that 2009 initial channel geometry was scoured to a new equilibrium depth within a few flood cycles, so the partial mobile-bed model of the 2009 condition gives a relatively

conservative estimate of the effect of the spur dikes. For the year-2060 channel, Spur dikes raised the flood water surface at the confluence by between 0.1 and 0.4 ft with the partial mobile-bed approach and between -0.1 and 0.4 ft for the full mobile-bed approach. The relative increase in water surface elevation for the year 2060 channel with spur dikes is less because the channel has adjusted to the presence of the spur dikes in the long-term simulation. Half-height spur dikes produce about half as much relative increase in flood water surface as caused by the full-height spur dikes.

Water Surface Elevation With and Without Spur Dikes at Clearwater River Mile 0.217 - Upper Bed Regime											
	Partial Mobile-Bed Approach - Steady Flow						Full Mobile Bed Approach - Balanced Hydrograph				
	Steady Flow	Water Surface Elevation (feet NAVD88)					Unsteady Peak	Water Surface Elevation (feet NAVD88)			
Percent	Discharge	2009			2060		Discharge	2009		2060	
Exceedance	cfs	No Dikes	With Dikes	Half-height Dikes	No Dikes	With Dikes	cfs	No Dikes	With Dikes	No Dikes	With Dikes
SPF	125,000	741.57	743.21	742.36	745.94	746.13	133,122	741.72	742.11	745.82	746.24
0.2	117,587	740.11	741.66	740.91	744.18	744.33	138,603	740.12	741.08	744.17	744.29
0.4	111,124	739.30	740.80	740.11	743.26	743.35	130,985	739.03	740.13	742.98	743.41
1	102,167	738.16	739.62	739.01	741.98	741.99	120,427	737.79	738.78	741.73	741.88

Table 18. Upper bed regime water surface elevations at Clearwater RM for simulations with spur dikes.

Water Surface Elevation at Clearwater River Mile 0.217 - Lower Bed Regime											
	Partial Mobile-Bed Approach - Steady Flow						Full Mobile Bed Approach - Balanced Hydrograph				
	Steady Flow	Water Surface Elevation (feet NAVD88)					Unsteady Peak	Water Surface Elevation (feet NAVD88)			
Percent	Discharge	2009			2060		Discharge	2009		2060	
Exceedance	cfs	No Dikes	With Dikes	Half-height Dikes	No Dikes	With Dikes	cfs	No Dikes	With Dikes	No Dikes	With Dikes
SPF	125,000	744.78	746.26	745.42	748.30	748.65	133,122	743.48	744.18	748.13	748.77
0.2	117,587	743.13	744.55	743.81	746.41	746.64	138,603	741.96	742.87	746.26	746.66
0.4	111,124	742.22	743.59	742.91	745.39	745.54	130,985	741.04	741.93	745.14	745.47
1	102,167	740.90	742.22	741.62	743.89	744.04	120,427	739.69	740.37	743.67	743.54

Table 19. Lower bed regime water surface elevations at Clearwater RM for simulations with spur dikes.

12.2. Flood Risk Analysis of Current and Future Channels with Spur Dikes

Conditional non-exceedance probabilities (CNP) and long-term risk (LTR) for the year-2009 and year-2060 channels with and without full-height spur dikes were computed with FDA software version 2.5.1 for the upper and lower bed regimes and stage uncertainties at 0.5 and 2.0 standard deviations. The FDA analysis was based on the year-2009 and year-2060 fixed-bed channel geometries (partial mobile-bed approach). Use of these geometries is conservative because the flood water surface elevations produced by these models are somewhat higher than those produced by the full mobile-bed approach. The 2.0 standard deviation of stage is a very conservative estimate of stage uncertainty because bed regime is directly incorporated in the comparison. The FDA project performance is summarized in Table 20 and Table 21 for Clearwater RM 0.3. For the 2009 channel with spur dikes, the CNP and LTR for the 1-percent exceedance discharge is 0.9991 and 0.0084 for a channel condition of upper bed regime and 0.5 standard deviations of stage uncertainty. With the more

conservative channel condition of lower bed regime and 2.0 standard deviations of stage uncertainty, the CNP and LTR for the 1-percent exceedance discharge is 0.9355 and 0.1129. For the 2060 channel with spur dikes, the CNP and LTR for the 1-percent exceedance discharge is 0.9820 and 0.0557 for a channel condition of upper bed regime and 0.5 standard deviations of stage uncertainty. With the more conservative channel condition of lower bed regime and 2.0 standard deviations of stage uncertainty, the CNP and LTR for the 1-percent exceedance discharge is 0.7737 and 0.3124.

Year 2009 Conditional Non-Exceedance Probabilities and Long-term Risk with Spur Dikes at Clearwater RM 0.3, Curve Extension 2

	Standard	50-year	Flood Frequency					
	Deviation	Long-Term	10.0%	4.0%	2.0%	1.0%	0.4%	0.2%
Hydraulic Resistance	Stage (ft)	Risk	Conditional Non-Exceedance Probabilities					
Upper Regime	0.5	0.0084	1.0000	1.0000	1.0000	0.9991	0.9891	0.9584
Lower Regime	0.5	0.0566	1.0000	1.0000	0.9981	0.9815	0.8759	0.7039
Upper Regime	2.0	0.0207	1.0000	0.9999	0.9991	0.9940	0.9638	0.9080
Lower Regime	2.0	0.1129	0.9997	0.9960	0.9860	0.9355	0.7989	0.6429

Table 20. Year 2009 CNP and LTR for channel with spur dikes at Clearwater RM 0.3.

Year 2060 Conditional Non-Exceedance Probabilities and Long-term Risk with Spur Dikes at Clearwater RM 0.3, Curve Extension 2

	Standard	50-year	Flood Frequency					
	Deviation	Long-Term	10.0%	4.0%	2.0%	1.0%	0.4%	0.2%
Hydraulic Resistance	Stage (ft)	Risk	Conditional Non-Exceedance Probabilities					
Upper Regime	0.5	0.0557	1.0000	1.0000	0.9982	0.9820	0.8773	0.7088
Lower Regime	0.5	0.1866	1.0000	0.9987	0.9780	0.8784	0.5860	0.3429
Upper Regime	2.0	0.1063	0.9997	0.9965	0.9828	0.9408	0.8075	0.6496
Lower Regime	2.0	0.3124	0.9965	0.9709	0.9032	0.7737	0.5398	0.3616

Table 21. Year 2060 CNP and LTR for channel with spur dikes at Clearwater RM 0.3.

More detailed hydraulic modeling and design studies are necessary to determine the actual location, orientation and length of spur dikes or other river training structures. Initial two-dimensional ADH modeling results of potential spur dikes fields are shown in Figure 100 and Figure 101. The erosion and deposition depicted in the Figure 100 is the bed displacement computed by the ADH model for a bed of medium sand (0.33 mm). Sediment loads were defined by equilibrium load boundary conditions on both the Snake and Clearwater Rivers for the observed 29 hour long hydrograph May 25-26, 2011. Similarly, the possible spur dike field in the turning basin at the Port of Lewiston on the Clearwater River constricts the channel and erodes a bed of medium sand during 24 hours in the same hydrograph. While relatively high seasonal discharges and extraordinarily high sediment loads were simulated, it demonstrates the rapid response of accumulated sand to erosive forces even under a high sediment load. Additional discussion of the development of ADH models of Lower Granite Reservoir is in Section 17.

The effect of spur dikes on existing facilities such as the effluent lines shown in Figure 100 and Figure 101 must be evaluated during design studies. Particle tracking modeling of the spur dike field at the confluence indicates that this spur dike configuration would somewhat change the zone of initial dilution of the paper mill effluent diffuser.

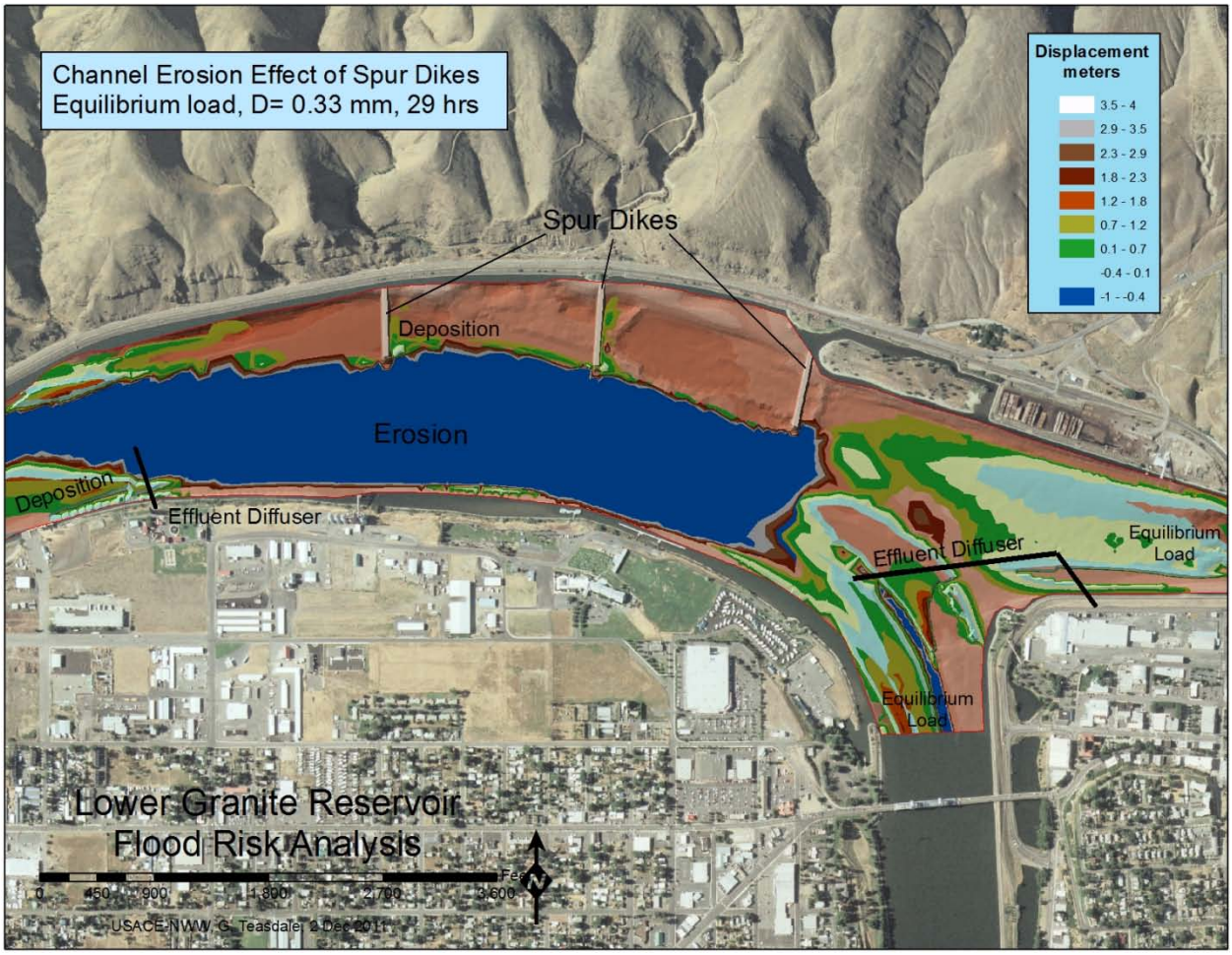


Figure 100. Erosion and deposition predicted by an ADH 2D model of a confluence spur dike field.

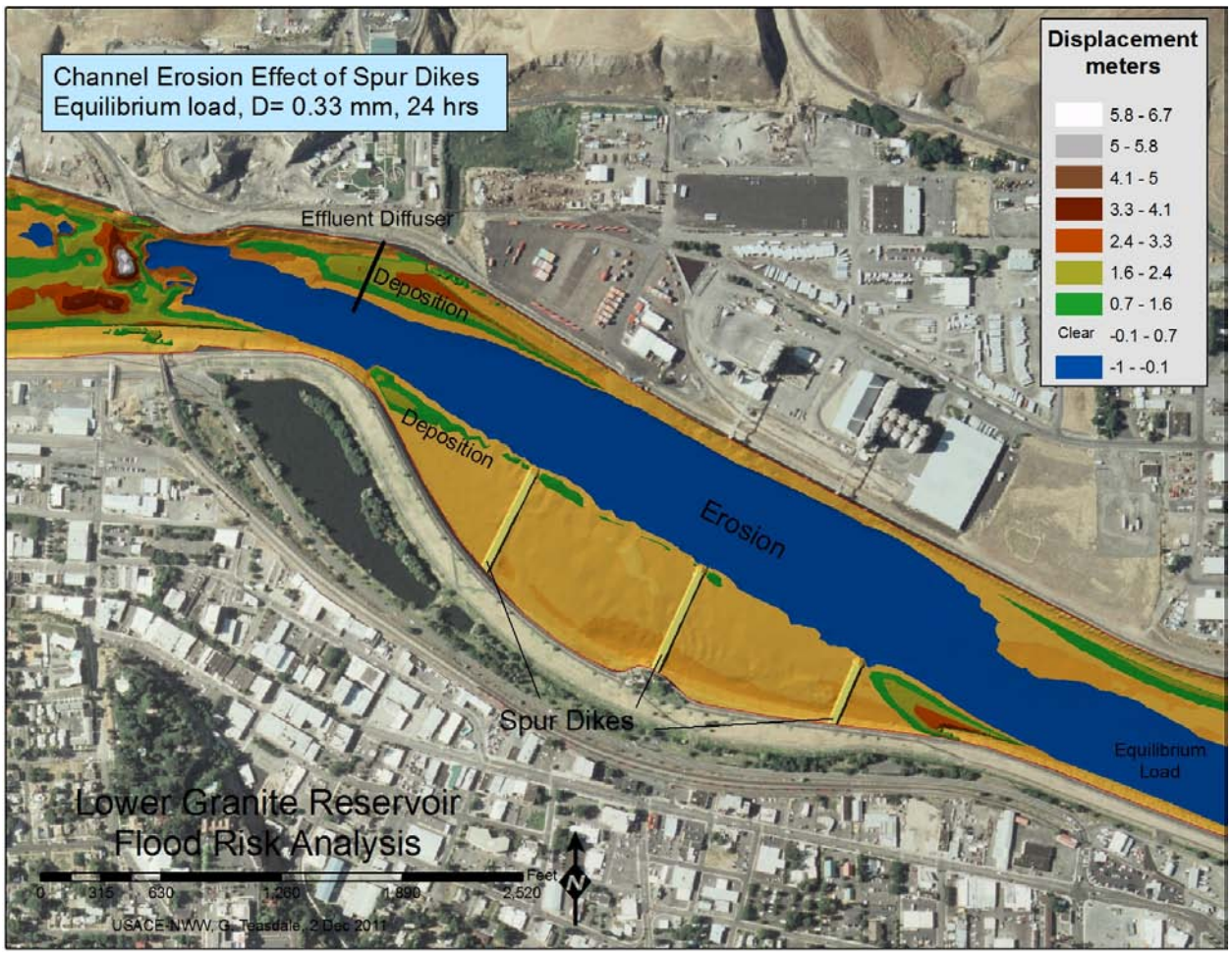


Figure 101. Erosion and deposition predicted by an ADH 2D model of a Clearwater turning basin spur dike field.

12.3. Seasonal Drawdown of Reservoir Water Surface

Seasonal drawdown of the Lower Granite Reservoir water surface is another in-reservoir management action that can re-mobilize sediment from the confluence area and transport it further into the reservoir where it has less effect on the flood water surface level in the levee system. Drawdown of the reservoir water surface, which concentrates the flow in a smaller channel cross section, increases flow velocity and bed shear stress, erodes sediment deposits, and increases sediment transport rates. The Snake and Clearwater River channels near the confluence approach free-flow conditions when the drawdown level in Lower Granite Reservoir is low enough to eliminate the backwater effect of the dam.

A drawdown test of Lower Granite Reservoir was performed in March 1992[44] during which the forebay water surface at Lower Granite Dam was lowered 37 feet from near full pool 739.4 ft to 702.7 ft (NAVD88). The drawdown lasted 41 days from 23 February to 3 April. Total Inflow discharge to Lower Granite Reservoir was relatively low and averaged about 30,000 cfs. Sediment transport rates were measured at several locations in the reservoir and reached about 68,000 tons per day at the peak of the inflow hydrograph. Over 1 million tons of sediment (about 0.8 mcy at 90 pcf) were likely eroded from the confluence area during the 15 days period when the reservoir water surface was lowest. Measured sediment transport rates at the upper limit of the residual pool near Silcott (RM 130) were less than 5,000 tons per day, indicating that most of the sediment eroded from the confluence was re-deposited in the reach above Silcott Island.

Bed change during drawdown conditions can be simulated with sediment transport modeling to predict the effectiveness of drawdown as a sediment management technique. Possible drawdown scenarios range from drawdown in the winter during minimum inflow to drawdown at the height of the seasonal peak discharge in spring and early summer. For a given drawdown level and duration, higher inflows increase sediment transport rates and scour more sediment from the confluence area. Three scenarios were evaluated to demonstrate the potential of drawdown to erode sediment from the confluence area. These include drawdown during the low inflow discharges that occurred in February and March 2010, drawdown during the typical seasonal peak discharge in May and June 2010, and drawdown during the early season peak discharge of March and April 2011. Each scenario assumed the same pattern of forebay control employed in the 1992 test.

Discharge hydrographs for the Snake and Clearwater Rivers and the Lower Granite Dam forebay elevation time series for the three scenarios are plotted in Figure 102, Figure 103, and Figure 104. Sediment transport for the drawdown scenarios was simulated with the Ackers-White transport function in HEC-RAS. The initial 2009 channel geometry, bed material specifications and sediment load rating tables were the same as those used in the long-term sediment transport simulation. Sediment transport algorithms in HEC-RAS do not simulate bank erosion and sloughing; processes that are likely important during drawdown. Vertical cut banks and mass failures are seen in the 1992 aerial photographs of the confluence such as that in Figure 105. The bank processes entrain substantial amounts of sediment that are not included in typical sediment transport functions. Bed change volumes computed by HEC-RAS for the drawdown scenarios are likely low estimates.

[44] USACE (1992). 1992 *Reservoir Drawdown Test, Lower Granite and Little Goose Dams*. Walla Walla District, U.S. Army Corps of Engineers.

Longitudinal cumulative change in bed sediment volume for each of the scenarios for Lower Granite Reservoir and the Clearwater River are plotted in Figure 106 and Figure 107. In the February-March 2010 scenario, total inflow to Lower Granite Reservoir was relatively low and averaged 25,500 cfs during the 41 day drawdown period from 1 February to 13 March (Figure 102). Bed erosion in this simulation was the least of the three scenarios because of the low inflow discharge. About 69,900 cubic yards (cy) was eroded from the boat turning basin on the Clearwater River and an additional 347,600 cy was eroded from the Snake River channel above RM 136. Total simulated volume eroded from the bed is about half the actual erosion volume estimated for the 1992 drawdown test even though inflow conditions are similar. The difference is likely due to the simple treatment of lateral erosion processes in the simulation, differences between bed topographies between 1992 and 2009, choice of transport function, characterization of the grain size of the bed sediment in the model, and imprecision of the 1992 volume estimate.

Other sediment transport functions provide higher estimates of total bed change volume than the Ackers-White function, but there is insufficient data in the 1992 drawdown test report to calibrate a transport function specifically for the drawdown condition. With the stereo aerial photography of the exposed channel was obtained during the 1992 drawdown test, it may be possible in future work to measure the change in bed topography with photogrammetric methods and develop more precise estimates of erosion volumes for calibration of a sediment transport model. Sediment transport modeling approaches are being developed to simulate erosion and deposition following dam removal[45]. The new approaches might be applied to the hydraulically similar conditions during drawdown to improve sediment transport estimates.

In the second simulation, the 1992 forebay elevation sequence spans the June 2010 seasonal peak discharge from 4 May 2010 to 13 June 2010 (Figure 103). This scenario likely represents conditions that maximize erosion from the confluence during a typical high flow year. Total inflow to Lower Granite Reservoir averaged 98,700 cfs during this period and peaked at 216,100 cfs on 6 June. Bed erosion in this simulation totaled about 2.5 million cubic yards (mcy) and was the maximum of the three scenarios. About 0.46 mcy was eroded from the boat turning basin on the Clearwater River and 2.11 mcy was eroded from the Snake River channel above RM 135.8.

[45] Cui, Y and Wilcox, A. (2008). "*Development and application of numerical models of sediment transport associated with dam removal*." *Sedimentation Engineering, Processes, Measurements, Modeling and Practice*, ASCE Manuals and Reports of Engineering Practice No. 110.

In the third simulation, the drawdown sequence spanned the discharge that peaked on in April 2011 (Figure 104). Total inflow to Lower Granite Reservoir averaged 84,900 cfs during this period and peaked at 137,000 cfs on 3 April. Bed erosion in this simulation totaled about 2.1 million cubic yards (mcy). About 0.54 mcy was eroded from the boat turning basin on the Clearwater River and 1.5 mcy was eroded from the Snake River channel above RM 135.8.

Longitudinal accumulated bed change for the three drawdown simulations are plotted for Lower Granite Reservoir in Figure 106 and for the Clearwater River in Figure 107. Similar to the 1992 drawdown observations, the simulations indicate that most of the sediment eroded from the confluence is re-deposited above Silcott Island. Total volume of sediment erosion in the second and third simulations is about equivalent to the average annual volume of sediment accumulation measured in Lower Granite Reservoir, which suggests that drawdown actions would have to be frequent to be an effective sediment management technique.

Channel cross section geometry at the end of the June 2010 drawdown simulation was exported from the sediment module and incorporated into a fixed-bed steady flow model. The water surface elevation at the confluence (Clearwater RM 0.217) for 1-percent exceedance discharge computed with the post-drawdown channel geometry was about 0.7 feet higher than the water surface computed with the 2009 channel geometry before drawdown. This result suggests that drawdown of the reservoir may have to be greater than the 1992 drawdown sequence to transport sediment further into Lower Granite Reservoir and reduce flood water surface elevation at the confluence.

More detailed studies of drawdown scenarios should be developed in future work. The drawdown in 1992 caused adverse impacts to infrastructure in the upper segment of Lower Granite Reservoir. The potential for adverse impacts and possible mitigation actions should also be investigated in future work.

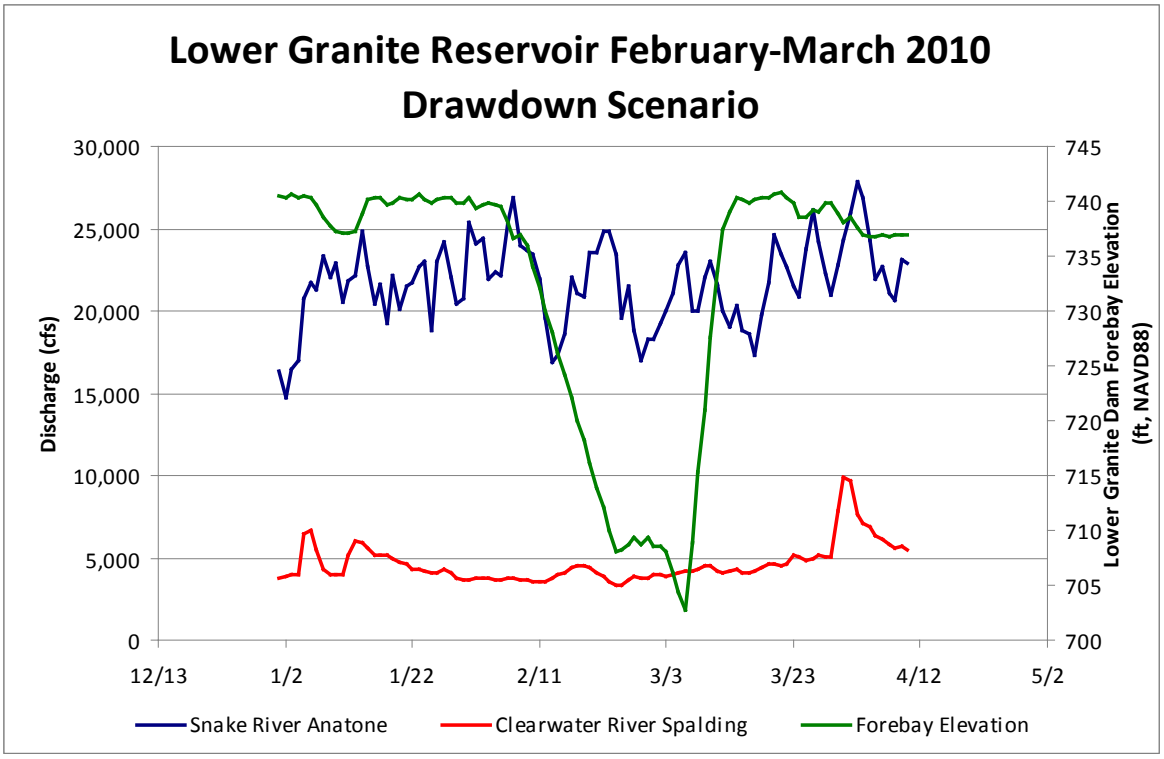


Figure 102. February-March 2010 Drawdown Scenario.

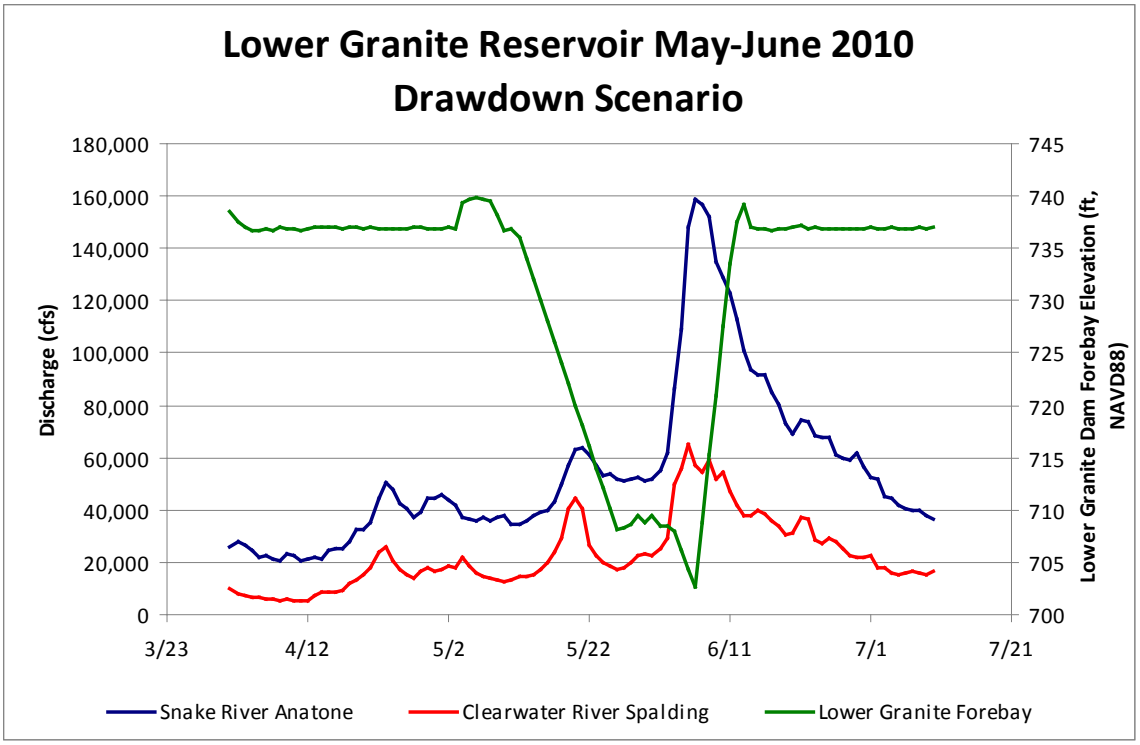


Figure 103. May-June 2010 Drawdown Scenario.

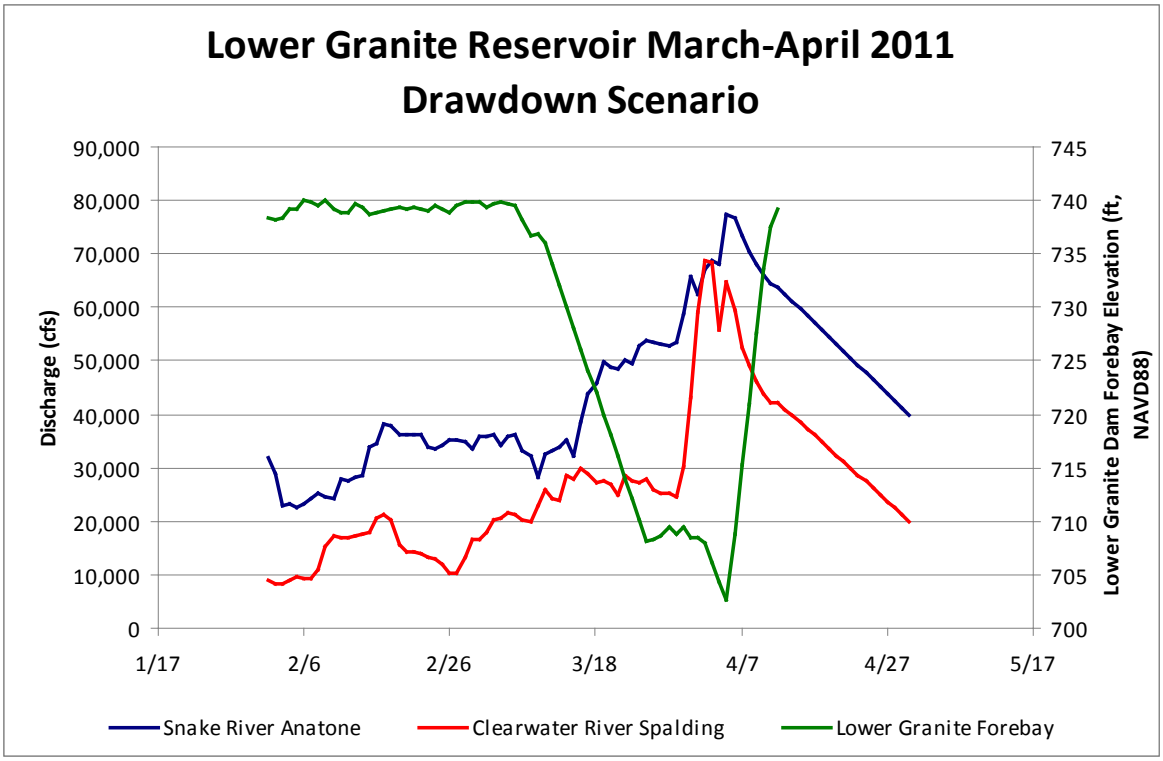


Figure 104. March-April 2011 Drawdown Scenario.



Figure 105. March 17, 1992 aerial photograph of confluence during drawdown.

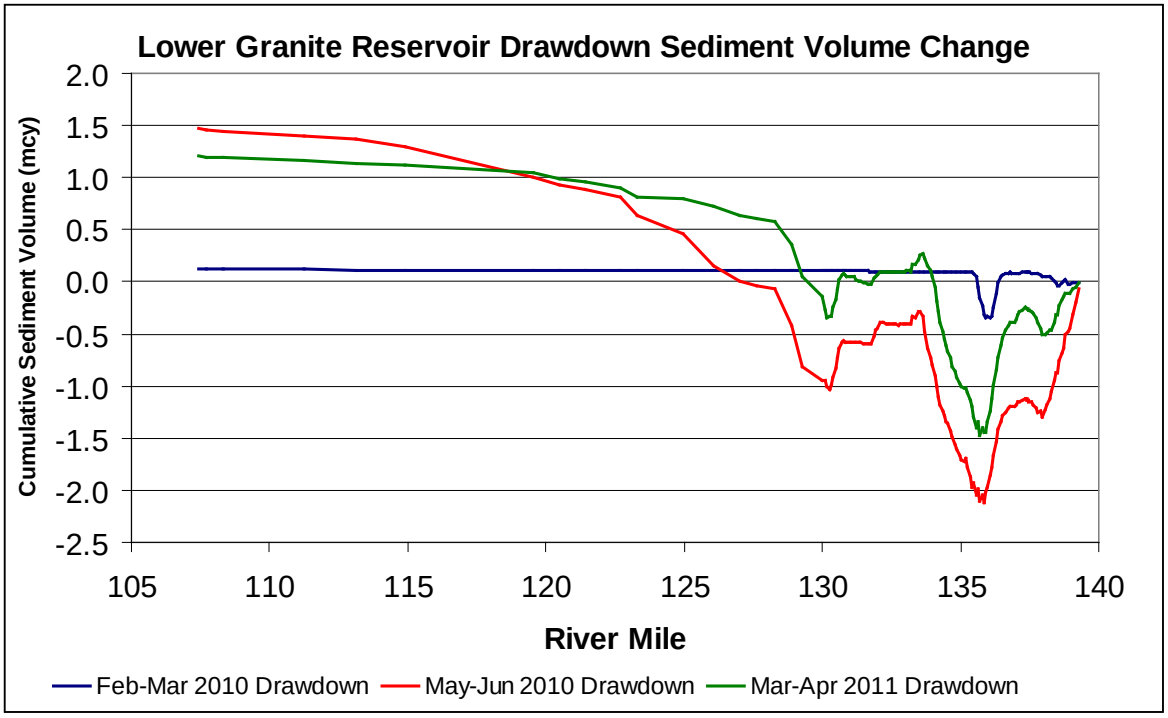


Figure 106. Lower Granite Reservoir drawdown sediment accumulation.

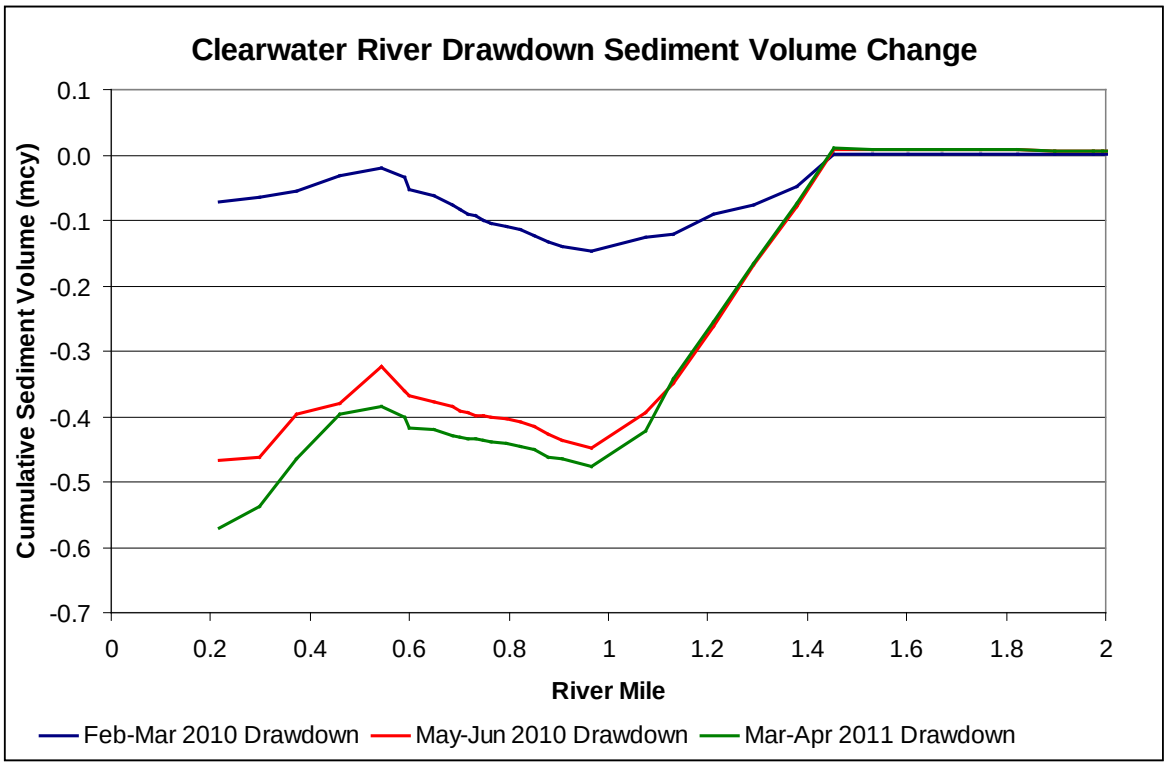


Figure 107. Clearwater River drawdown sediment accumulation.

12.4. Sediment Trap in the Snake River

The sediment load analysis in Section 8 showed that the volume of sand delivered to Lower Granite Reservoir from the Snake River is about 0.6 mcy per year. A large part of this load is bedload which is evident from the sand waves that form upstream from the Lewiston Levee System on the Snake River as seen in the 2009 and 2011 bathymetries. Potentially, substantial volumes of sand bedload can be trapped and harvested in the channel, thereby reducing the amount of sediment that accumulates below the confluence. A possible location for a sediment trap is immediately upstream from the right bank levee on the Snake River at RM 140.7 (Figure 108). This location is advantageous because narrowing of the channel produces a local backwater effect that reduces the amount of sand carried in suspension.

The efficiency of a sand trap at this location was evaluated with a HEC-RAS sediment transport model in which the 2009 channel geometry was modified by modifying the channel cross section geometry between RM 140.544 and RM 140.785 to simulate a sediment trap that has a flat bottom at elevation 700 ft NAVD88 across most

of the channel. This lowers the bed in this segment by about 10 ft. Total length of the trap is about 1900 ft and the volume of the trap relative to the 2009 channel geometry is 0.77 mcy. Sediment loads were simulated for the average daily discharges for water year 2010 and 2011. The total mass of sand trapped by size fraction is determined from the difference of the cumulative mass passing the cross sections upstream and downstream from the sediment trap. Plot of cumulative mass-passing curves and trapping efficiency curves in Figure 109 and Figure 110 show that the trapping efficiencies of medium sand (0.5 mm) and fine sand (0.25 mm) are 89 percent and 49 percent while only about 6 percent of the very fine sand (0.125 mm) is trapped. Total volume of medium sand and fine sand trapped for the two year period was 0.3 mcy. The trapping efficiency curve shows that the trapping efficiency was decreasing as the trap filled with sediment during the second year. Sediment would have to be removed from the trap annually either by dredging or by a permanently installed mechanical sand extraction system. Further analysis and detailed hydraulic modeling of alternative sediment trap configurations would needed before an actual sediment trap could be designed and constructed.

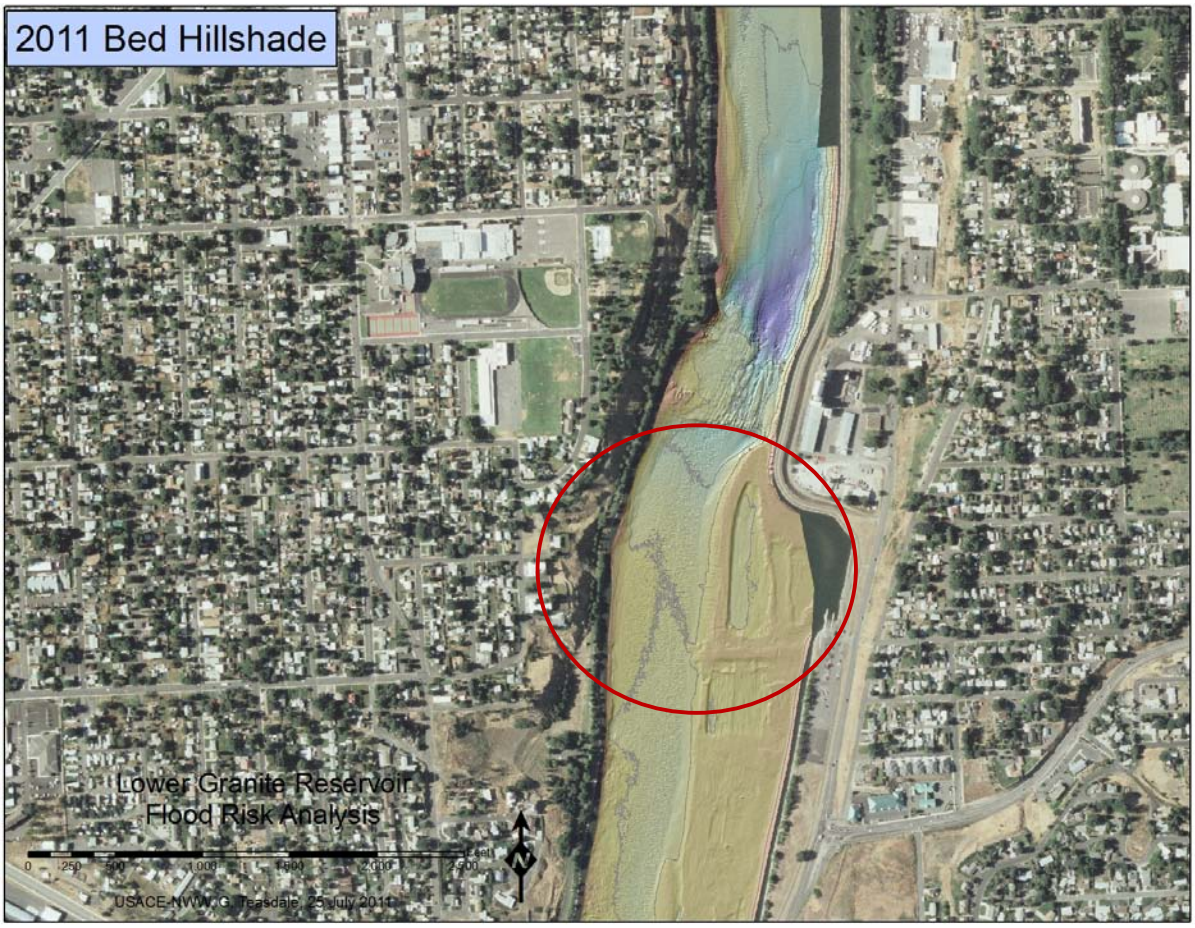


Figure 108. Location of a potential sediment trap on the Snake River.

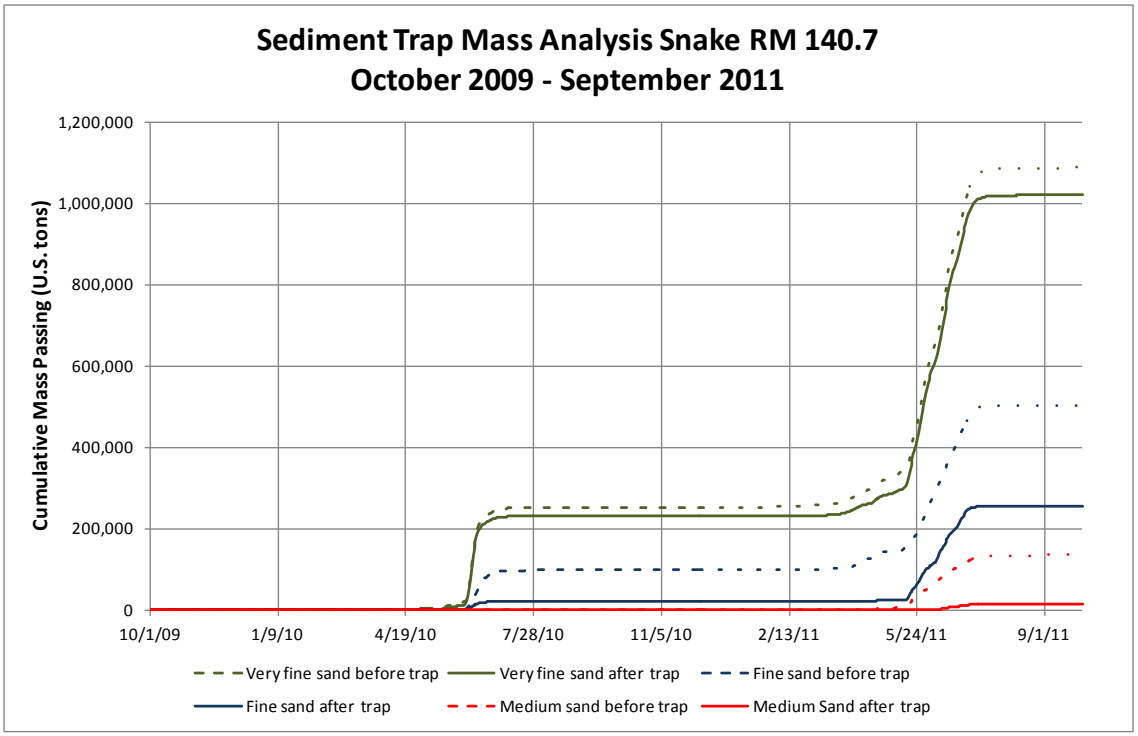


Figure 109. Snake River sediment trap mass analysis, WY 2010-2011.

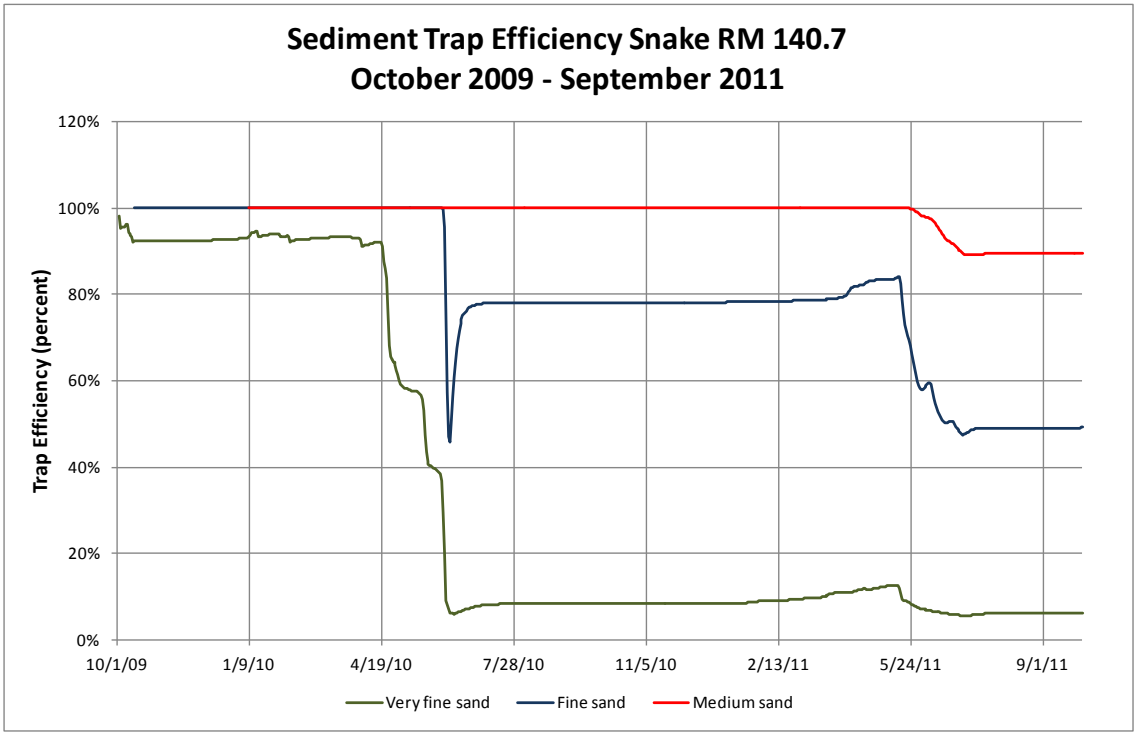


Figure 110. Snake River sediment trap efficiency.

12.5. Extreme Drawdown During Floods

Conceptually, Lower Granite Dam could be modified so that the water surface at the forebay could be drawn down to very low levels during an extreme flood in an attempt to reduce the water surface elevation at the confluence. Figure 111 shows a conceptual forebay operation that draws the reservoir down to the lowest elevation reached in the 1992 drawdown study. Maximum drawdown occurs about 1 month prior to the peak of the flood to allow the greatest amount of sediment to be eroded from the upper reservoir during the rising limb of the hydrograph.

The water surface profile for the 0.2 percent (500 yr) exceedance discharge balanced hydrograph for the year-50 channel condition was computed with the mobile-bed HEC-RAS model as described above for the fully-mobile approach. Computed water surface profiles for the currently approved forebay flood control operation and the conceptual extreme drawdown operation are plotted in Figure 112. Though extreme drawdown of the reservoir eroded substantial sediment from the confluence area, it lowered the flood water surface less than 2 ft. Extreme drawdown (or breaching of the dam) of the reservoir is not an effective long-term strategy to reduce flood risk as sediment accumulates in the upper segment of the reservoir. The one-dimensional sediment transport simulation for the extreme drawdown scenario has the same limitations as those discussed above. Additional one and two dimensional model analysis, and perhaps physical modeling, of the extreme drawdown scenario should be performed in future work.

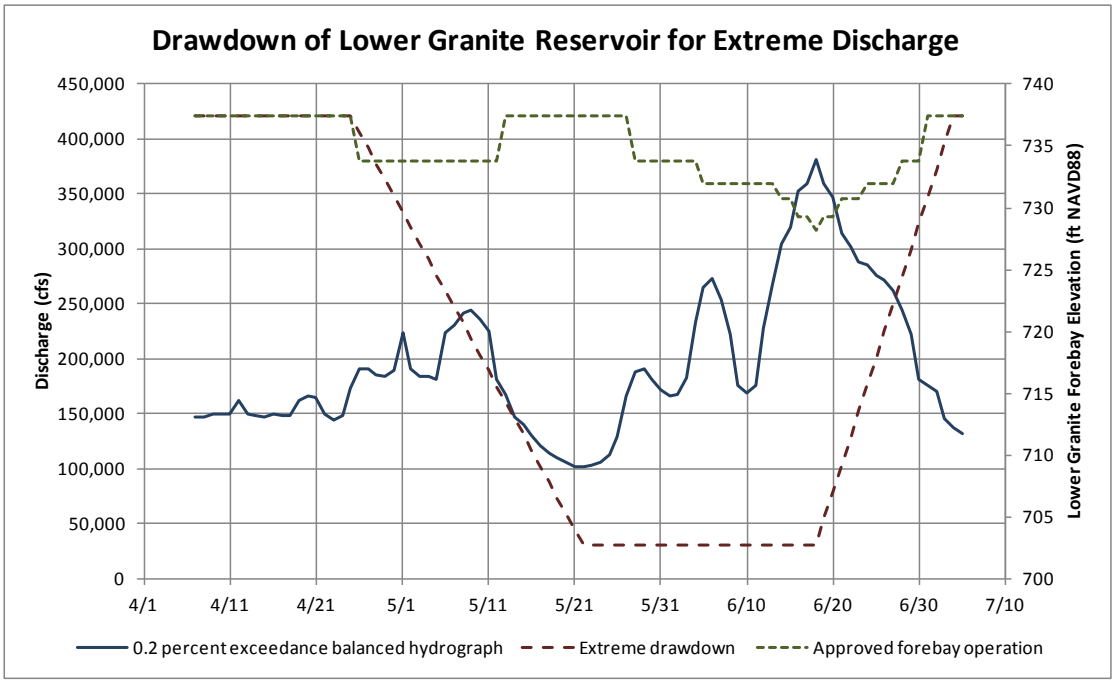


Figure 111. Conceptual extreme drawdown of forebay for flood control.

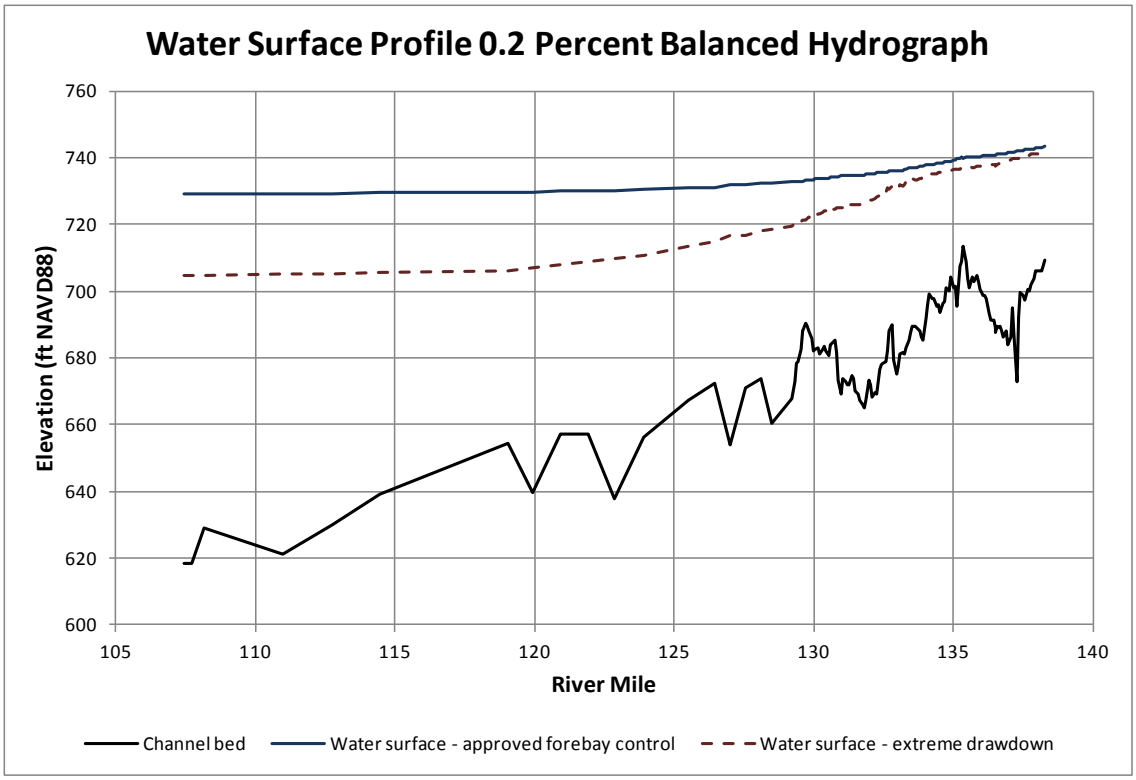


Figure 112. Flood water surface profile for extreme forebay drawdown.

12.6. Dredging to Preserve the 2009 Level of Flood Risk Reduction

The longitudinal sediment accumulation curves for the 2010-2060 period plotted in Figure 57 show that the predicted sediment accumulation above RM 130 in Lower Granite Reservoir is about 0.33 mcy per year. Toward the end of the 50-yr analysis period the center of mass of the accumulated sediment shifts downstream as the upper segment of the reservoir adjusts towards an equilibrium hydraulic geometry, but the enough sediment still accumulates to reduce flood capacity (flow conveyance) at the Lewiston Levee system. On average about 0.33 mcy per year of sand sediment must be dredged from the channel between RM 130 and the confluence to maintain the current level of flood risk reduction at the Lewiston Levee.

The 50-year accumulation curve for the Clearwater River shows that on average 0.04 mcy per year was retained in the Clearwater River as the channel approached equilibrium. This amount of accumulation provides a low estimate of annual dredging volumes on the Clearwater River. Additional sediment must be removed to maintain navigation depth. If sediment is periodically dredged from the turning basin and at the mouth of the Clearwater River more sediment will deposit in the dredged area. The sediment load analysis showed that sand load in the Clearwater River averages about

0.1 mcy per year. This provides a more conservative estimate of the annual dredging volume to maintain the current level of flood risk reduction and navigation depth in the Clearwater River. A 0.1 mcy per year volume is about the historic average annual dredging volumes in the Clearwater River.

12.7. Dredging to Recover Hydraulic Capacity

As demonstrated by the hydraulic modeling discussed in Section 10.10, sediment that accumulates near the confluence has greater effect on the flood water surface elevation in the levee system. Sediment that accumulates near the confluence should have a higher priority for removal when the dredging objective is to preserve the flood risk reduction benefit of the levee system. Priority dredging areas are shown in Figure 113. A total of 380 acres of channel area is delineated. Priority areas 1, 2 and 3 include the authorized navigation channel. Dredged sediment should be deposited below RM 125 to minimize the effect of the dredge placements on the flood water surface at the confluence.

Dredging of the upper reservoir channel is a certain action that can recover hydraulic capacity (flow conveyance) that has been lost to sediment accumulation. Two scenarios illustrate the amount of dredging required to recover substantial capacity. In the first scenario, a HEC-RAS model was developed from the September 2011 bathymetry and was modified to simulate dredging of the upper reservoir to approximately the 1974 bed elevation. About 2.84 mcy of sediment was removed from the channel between the confluence and RM 132.7, which is slightly more than the estimated sand load that was delivered by the Snake River during water year 2011. A fixed-bed model that was developed from the modified geometry reduced the SPF water surface elevation at the confluence by 0.5 ft, or about the same as the SPF elevation computed with the 2009 calibrated HEC-RAS model.

In the second example, the 2011 channel geometry was modified to simulate excavation of the submerged island at the Port of Wilma (RM 136) The excavation would remove a high point in the channel of Lower Granite Reservoir. Excavation of the island to the elevation shown in Figure 114 removes about 9.2 mcy of sediment from the channel and would help promote transport of sediment through the upper segment of the reservoir. Part of the volume excavated is material in the original river channel. A HEC-RAS model developed from the modified geometry reduced the SPF elevation at the confluence by about 1 ft.

These examples demonstrate that dredging in the upper segment of Lower Granite Reservoir can reduced the flood water surface at the confluence, but that relatively large volumes of material must be removed to produce a substantial reduction in the elevation of the flood water surface. As noted in the discussion of sediment

transport above, sand bedload is transported further into the reservoir now than in the past. This likely makes dredging of recent deposits to improve capacity and flow conveyance more difficult, costly and less feasible than in the past.

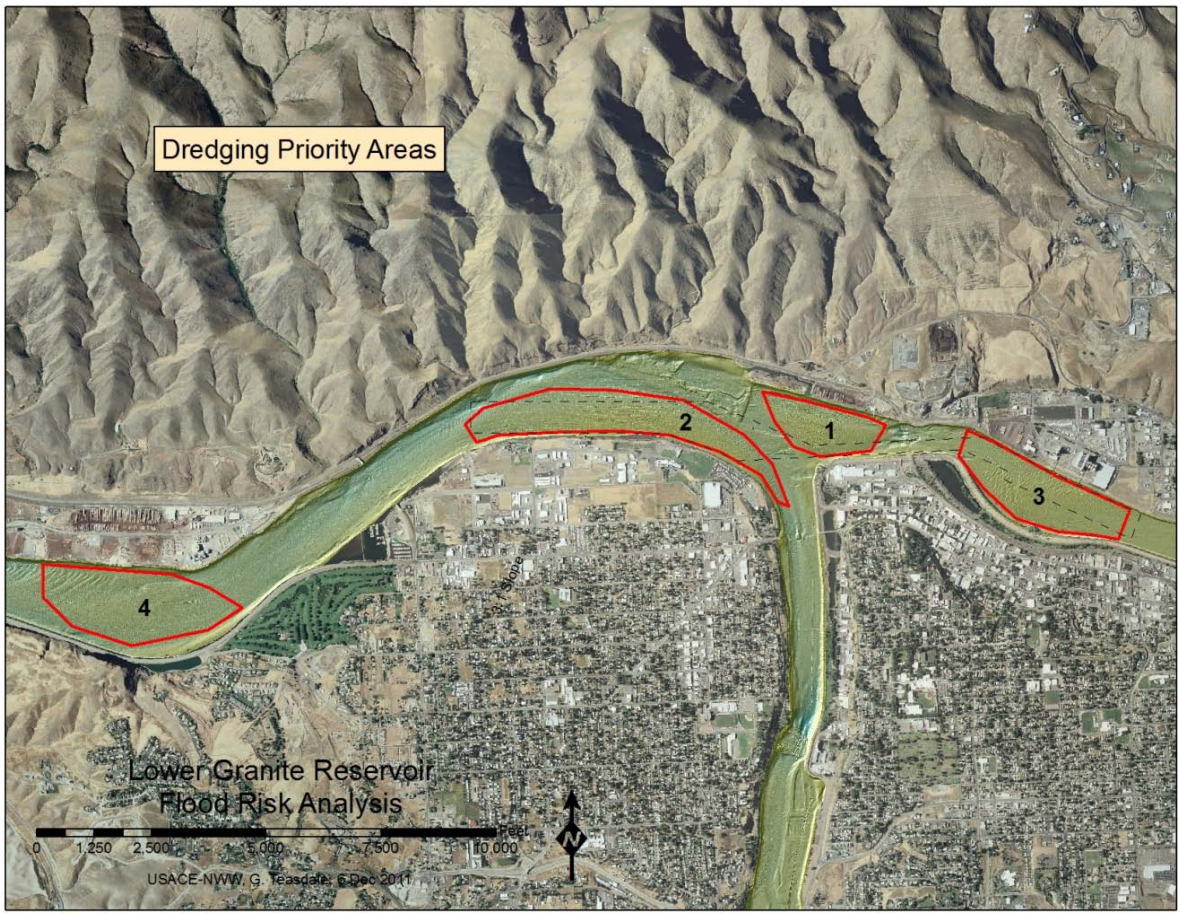


Figure 113. Dredging priority areas for flow conveyance.

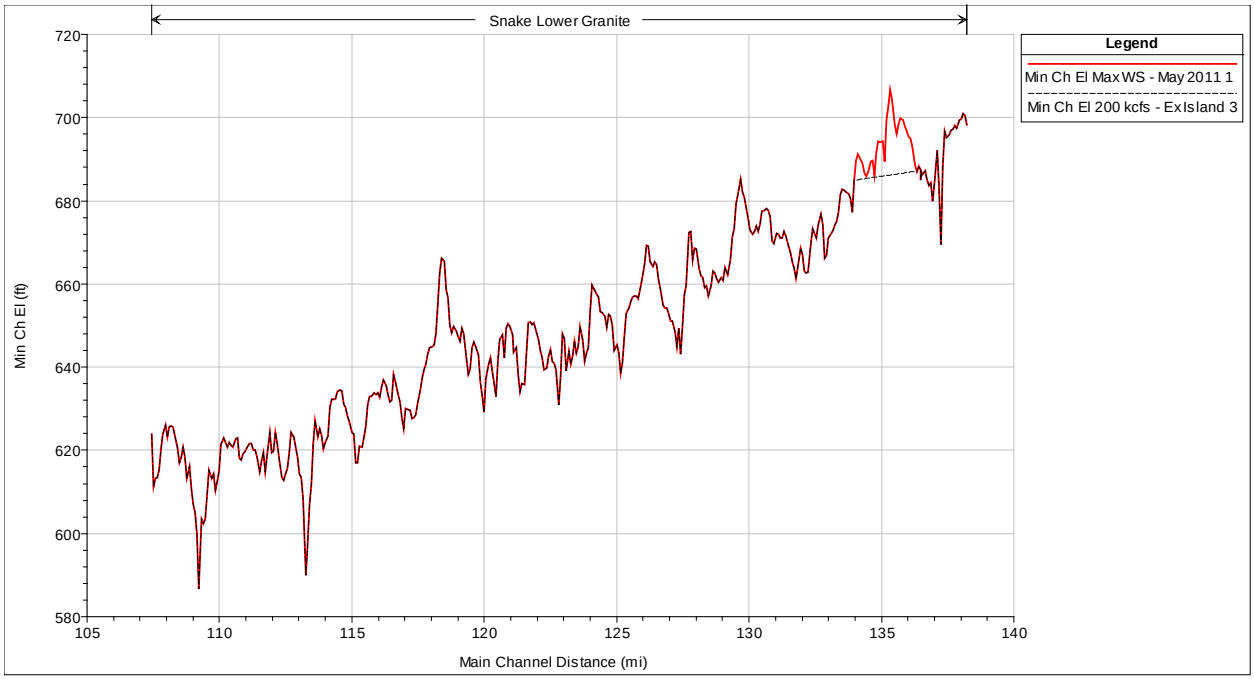


Figure 114. Removal of the submerged island at the Port of Wilma.

12.8. Stability of Dredge Material Placement

Material that was dredged from the navigation channels and port areas in past dredging actions was placed in Lower Granite Reservoir to construct shallow water habitat. It is likely that this method of beneficial use of dredge material will be adopted in future dredging actions. To function as habitat, the dredge material must be placed so that it is stable and resistant to water erosion. The sediment transport modeling in this study showed that sand is not transported much beyond RM 126 during normal seasonal flows, and it follows that sand material placed lower in the reservoir should resist erosion. This assumption can be verified by computations of incipient particle motion and by examining the displacement of shallow water habitat constructed with dredge material in 2006.

About 340,000 cubic yards of dredge material was placed in the winter of 2005-2006 near Noxway Canyon (RM 117) in Lower Granite Reservoir to form about 15 acres of shallow water habitat. Material placed as shown in Figure 115 increased the height of an existing bench on the left side of the reservoir channel. Bathymetry of the site was surveyed before and after the material was placed. Comparison of the bathymetry grids in Figure 116 and Figure 117 show that the thickness of the placement averages about 14 feet and the depth to the surface of the placement is between 10 and 12 feet at normal pool elevations. The 2D velocity field for a discharge of 200,000 cfs was computed with an ADH model developed from the September 2011 bathymetry (Figure 118). Velocities over the shallow water habitat are less than 1.5 ft/s. This velocity is

high enough to initiate motion in fine sand, but not sufficient to cause general upset and movement of the mass of the placement. The Shields stress diagram for incipient motion in Figure 119 shows that medium sand (0.5 mm) and fine sand (0.25 mm) plot in the region where little or no movement of sediment in this size range is expected at this discharge. Some fine surface material is expected to move as ripples which could gradually erode the surface of the bench, perhaps to diminish habitat quality over several years (decades). The wind fetch at this location is about 1 mile, so orbital velocities induced by wave motion should not significantly contribute to erosion of the placement.

Comparison of the September 2011 bathymetry and the 2006 bathymetry confirms some movement of surface material. The profile of the longitudinal transect of the placement in Figure 120 shows that the surface of the placement was smoothed and that material has moved slightly downstream. The observed movement is consistent with the movement expected from the hydraulic analysis.

This method of analysis can be employed in the planning of future dredge material placements. Dredge material placement sites should be monitored to determine if material must be added to recover habitat quality lost to surface erosion.

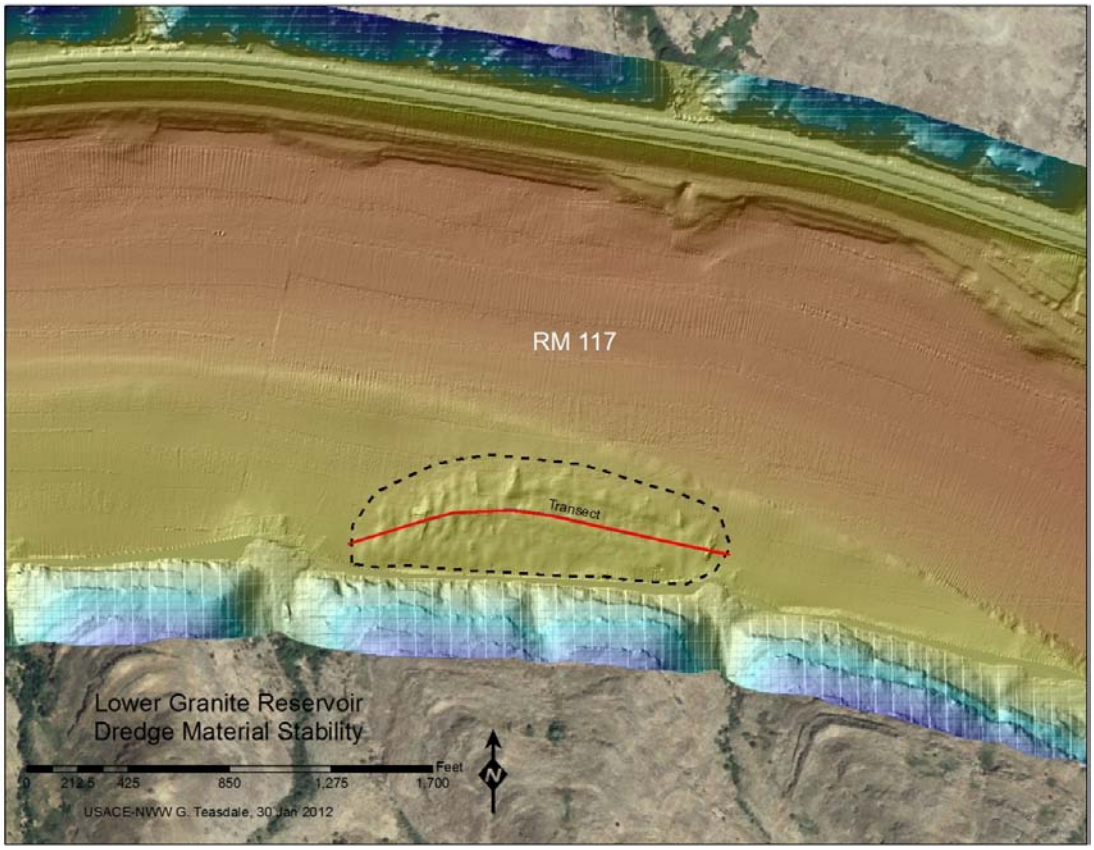


Figure 115. Dredge material placement site at Snake RM 117.

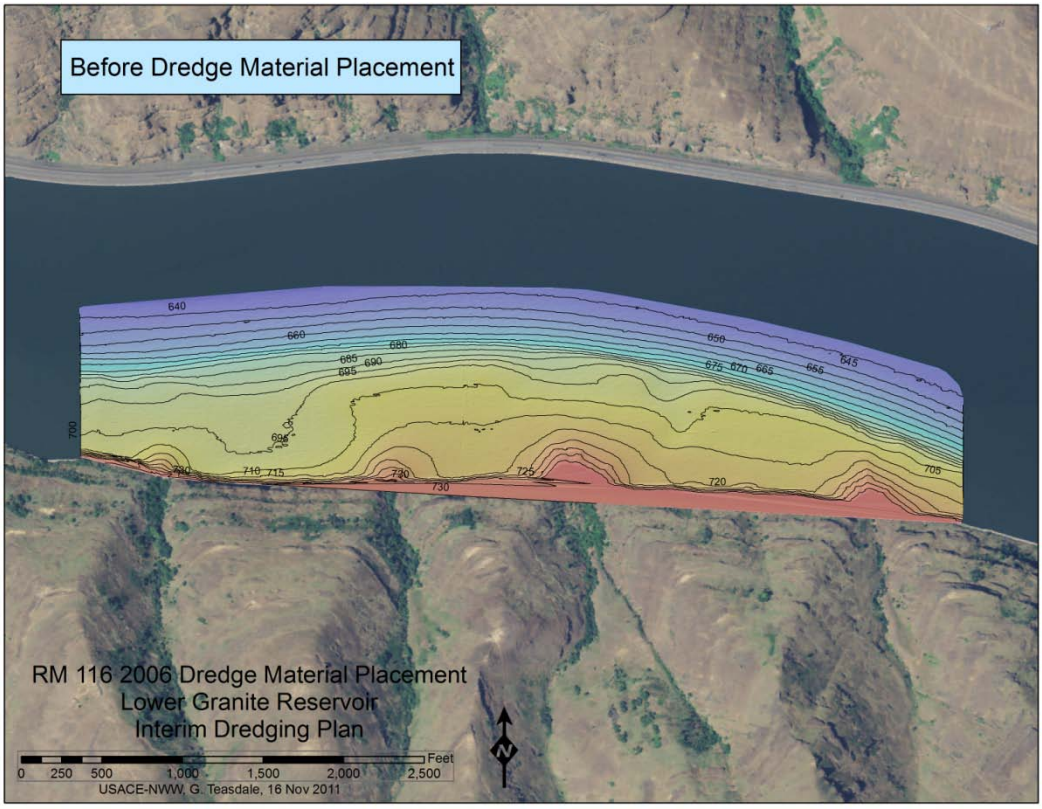


Figure 116. Shallow water habitat site before dredge material placement.

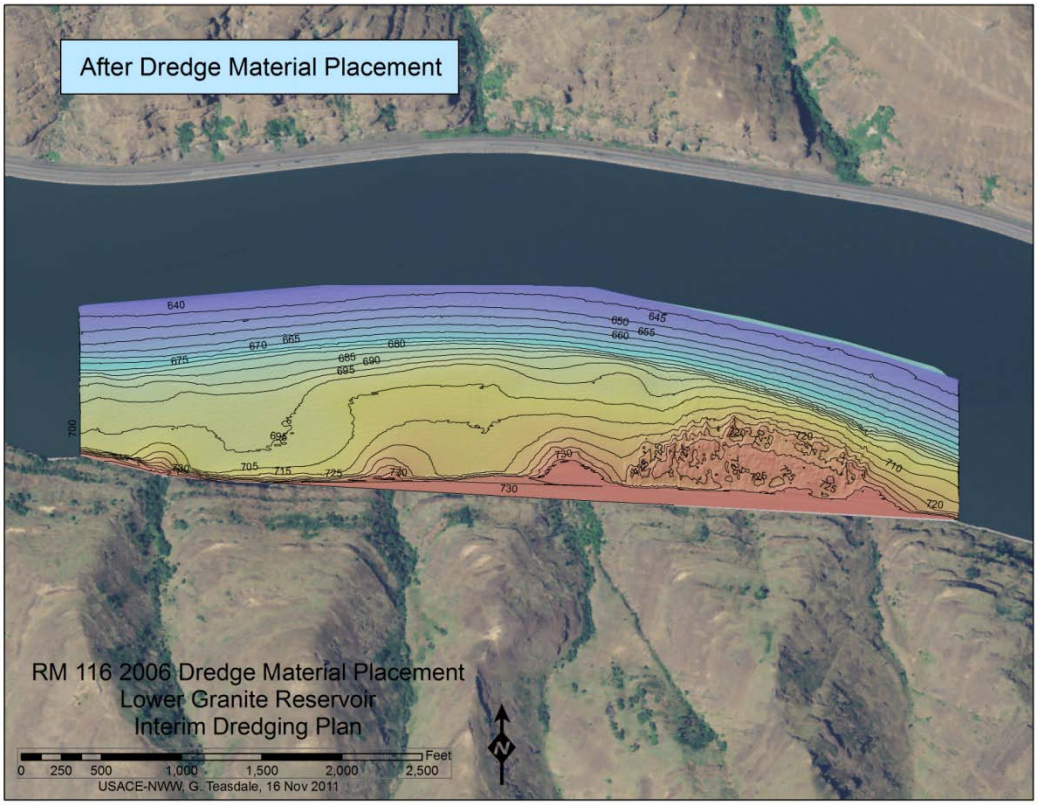


Figure 117. Shallow water habitat site after dredge material placement.

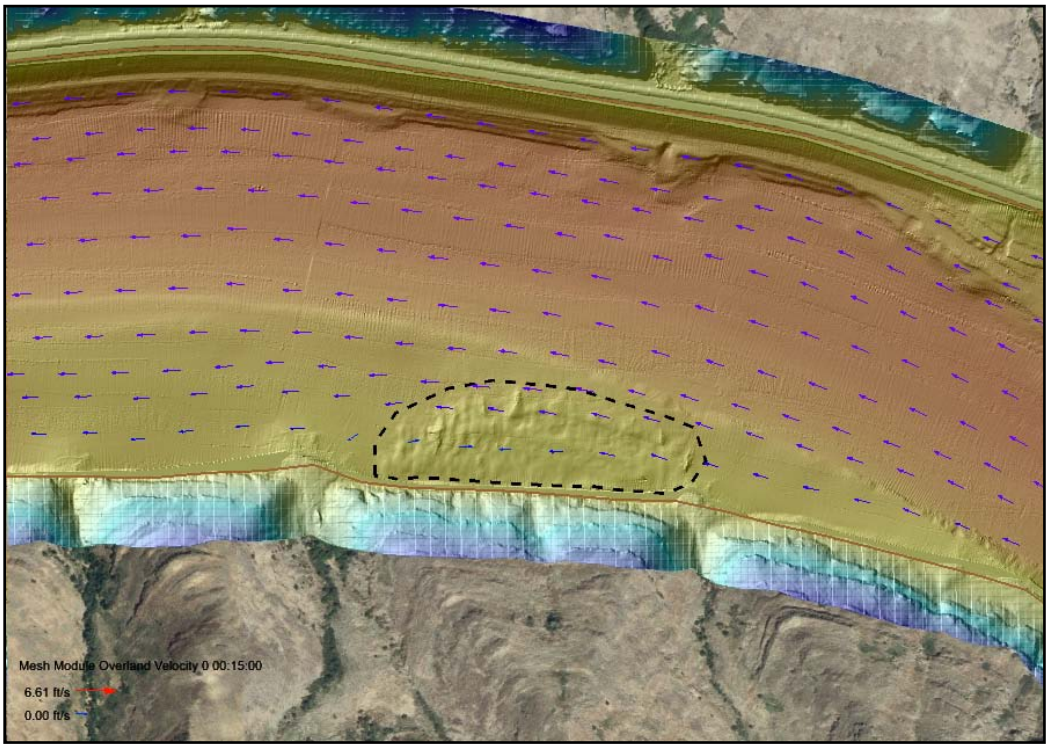


Figure 118. 2D velocity field at the dredge material placement site at 200 kcfs.

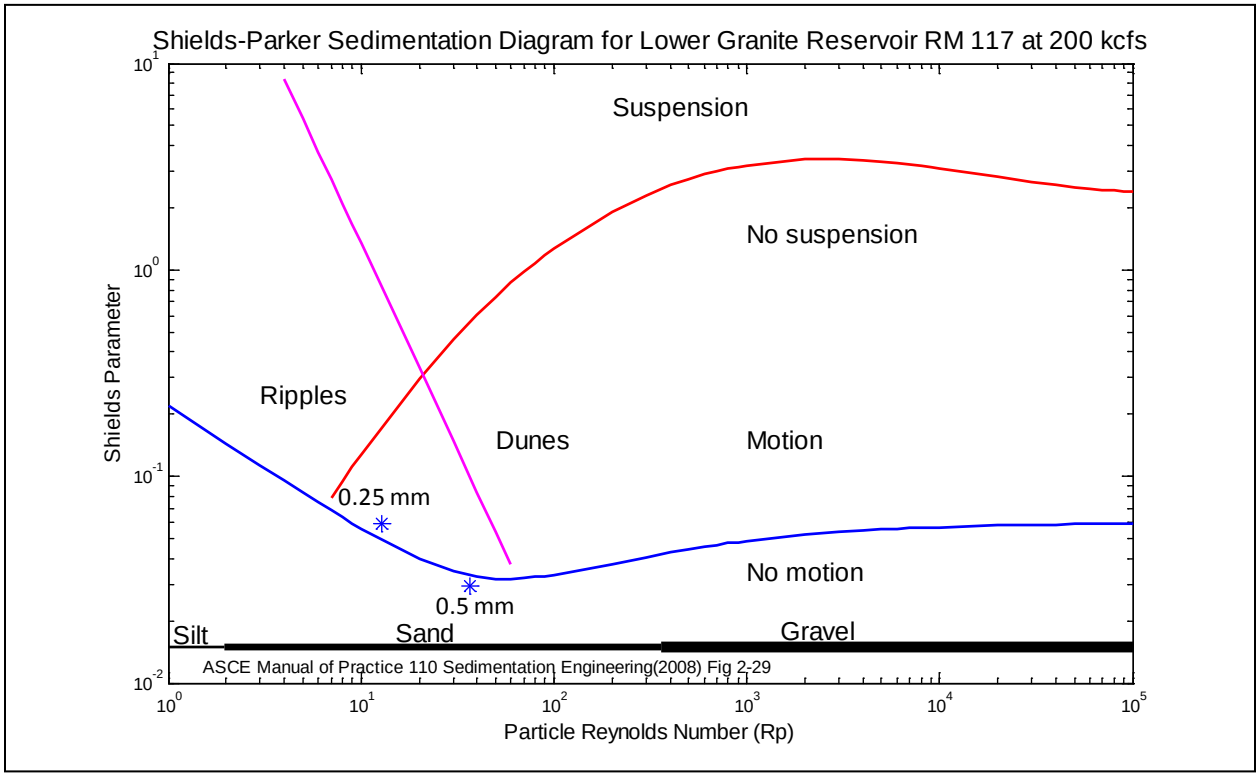


Figure 119. Shields-Parker sedimentation diagram for RM 117 at 200 kcfs.

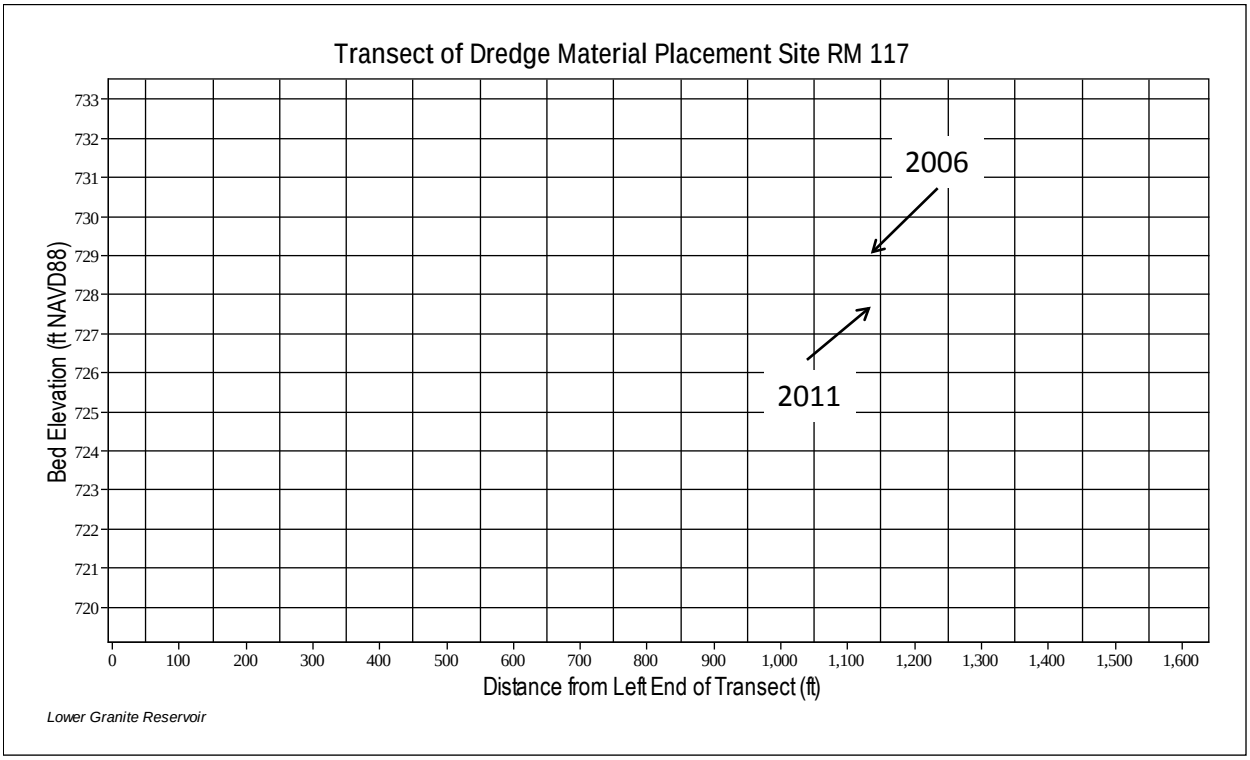


Figure 120. Comparison of bed elevation transects at the dredge material placement site at RM 117.

12.9. Management of Sediment at Boat Basins in Lower Granite Reservoir

Sediment deposition in the boat basins in Lower Granite Reservoir impairs the normal recreational use of public and private boat ramps and marinas. During the course of the study, sedimentation problems at several boat basins were evaluated during field inspections and by hydraulic and sediment transport modeling. Affected locations include the Asotin, WA Boat Basin in Chief Looking Glass Park (Snake RM 145), Hells Gate Marina (Snake RM 142), Swallows Nest Park (RM 741), and Red Wolf Marina (Snake RM 137). Sediment impacts are the most severe at the Asotin Boat Basin. The following description and approach to analysis and management of sedimentation in boat basins illustrate the process that would be followed in implementation of the Programmatic Sediment Management Plan.

Sand deposits block the inlet to the Asotin, WA Boat Basin in Chief Looking Glass Park on the Snake River at RM 145 so that the boat ramp or marina are unusable. Figure 121 and Figure 122 show that the top of the sand bar is between 3 and 5 ft above the low flow water surface. Fine sediment fills the interior of boat basin

so that it could not function as a marina even if the bar at the inlet were removed (Figure 123).

Two-dimensional ADH hydraulic models and field observations confirm that a strong eddy forms at the mouth of the inlet and that fine sediment circulates through the basin (Figure 124). The bar is formed by suspended sand that settles in the lower velocity of the eddy. Sand bedforms are not present in the river channel outside the inlet, which also indicates that sand is carried into the inlet in suspension.

Possible management actions at the Asotin Boat include dredging, alteration of of the inlet and construction of a gated relief channel to flush fine sediment from the basin. Several alternative inlets were evaluated by hydraulic modeling (Figure 125 and Figure 126) and discussed with local officials. There is strong local interest in restoring the marina to normal use and possible sources of funding are being considered.



Figure 121. Sediment deposition at inlet to the Asotin Boat Basin.



Figure 122. Sand bar at the inlet to the Asotin Boat Basin.

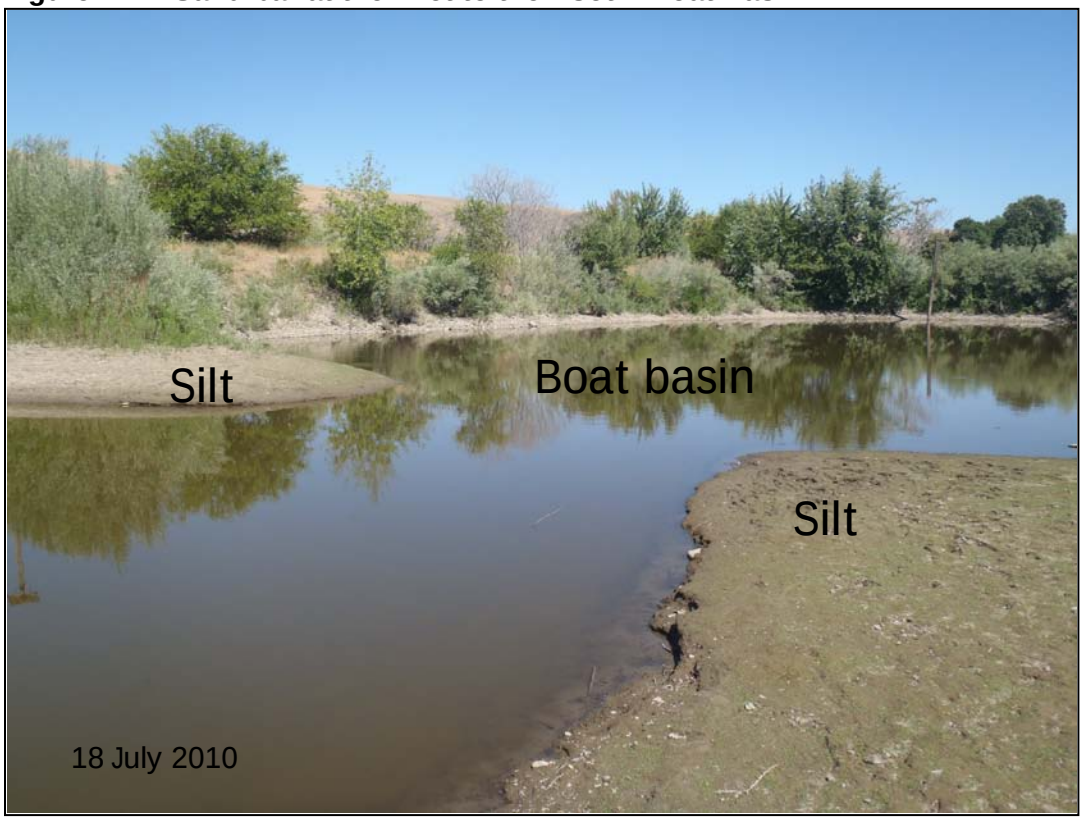


Figure 123. Silt deposits in the Asotin Boat Basin.

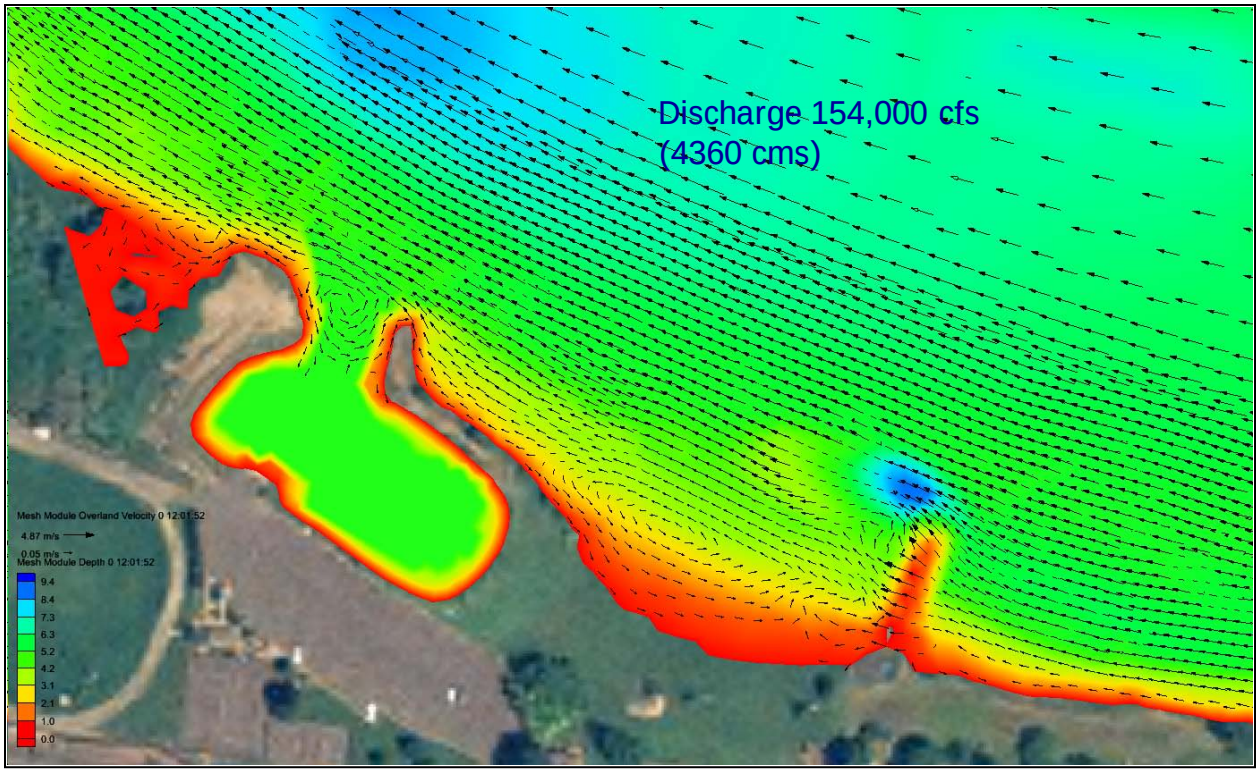


Figure 124. Velocity vectors and eddy at the inlet of the Asotin Boat Basin.

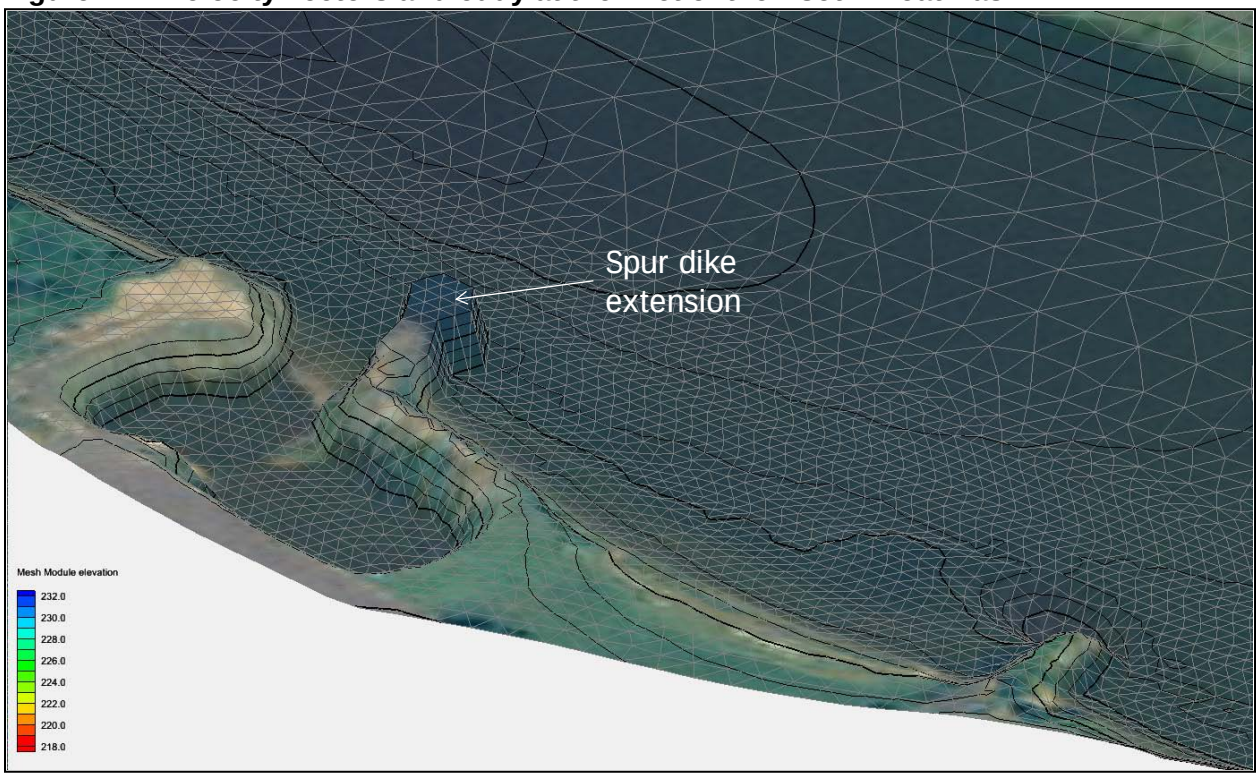


Figure 125. Potential spur dike extension at the inlet of the Asotin Boat Basin.

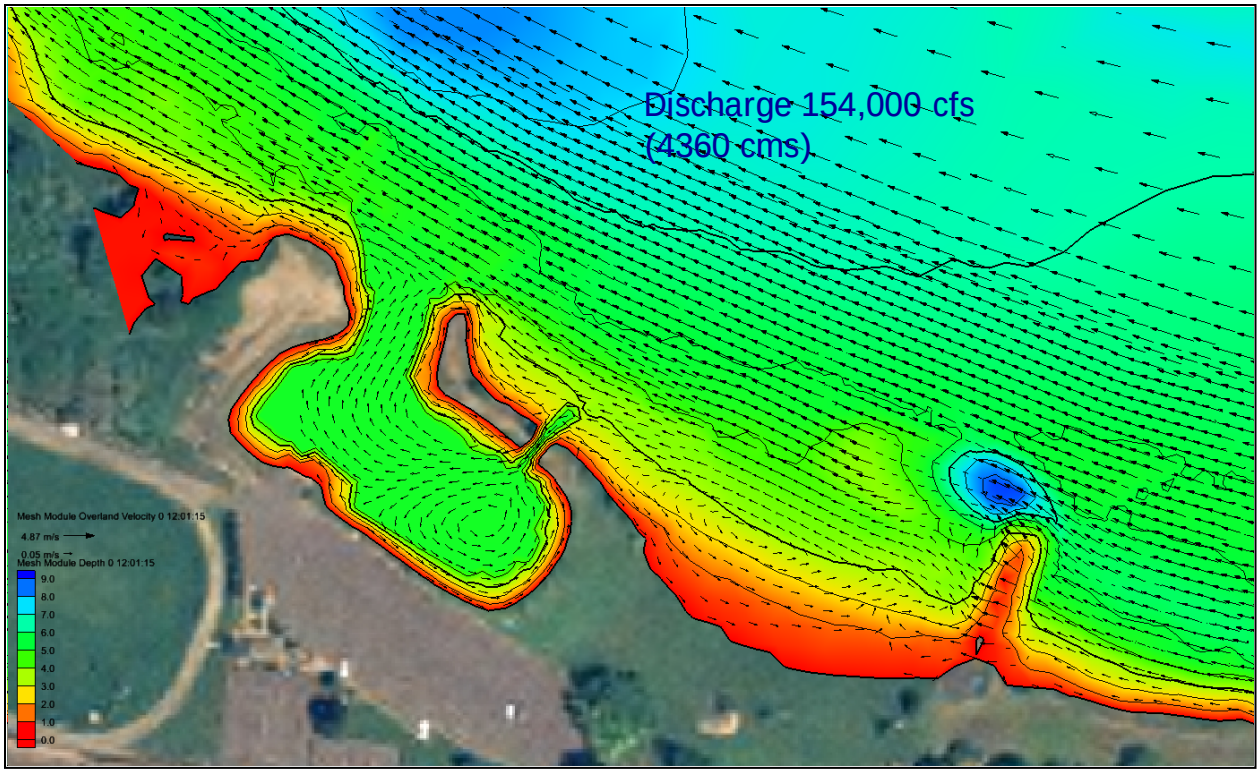


Figure 126. Potential relief channel at the Asotin Boat Basin.

13. Flood Risk due to Wind Waves at the Confluence

Strong winds increase the risk that levees situated next to open water will overtop during extreme floods. Waves momentarily add to the height of the water surface and may intermittently overtop a levee even though the still water surface lies below the crest of the levee. A rise in the mean water surface near a levee may also be caused by a sustained wind that pushes water to one end of a large body of water (wind set-up). Flood risk due to wind waves is discussed in Corps guidance for levee system valuation[46] and computation of wave heights and wave periods are described in Engineering Manual 1110-2-1100[47].

Surface waves occur in a series or spectra of individual waves of varying height and wavelength. A wave series is characterized by an energy-based significant wave height and spectral peak wave period. Significant wave heights are usually defined as the average of the highest one-third of the waves and can be determined from the spectral distribution of the wave series. Occasional waves may have heights (crest to trough distance) that are nearly twice the significant wave height. Momentum carries an impinging wave up the sloping surface of a levee embankment. The extra height gained by a wave as it breaks upon the embankment is called run-up and is computed separately from the significant wave height. Most waves that break upon a levee over a period of several minutes have heights that are much less than the significant wave height. The largest waves in a series may overtop top a levee during an extreme flood, but if the waves are infrequent the overtopping flow may not cause interior flooding or threaten the integrity of the levee. Low rates of overtopping can be intercepted by the interior drainage system and pumped back outside the levee.

13.1. Computational Method for Wave Height, Run-up and Set-up

Computational methods for wave dynamics vary from simple empirical relationships to three-dimensional computer simulations with meteorological forcing. Selection of a computational method depends on the physical setting, complexity of the meteorology and modeling objectives. In this study, significant wave height, run-up and overtopping rates were computed by the USACE Automated Coastal Engineering System (ACES) module in the Coastal Engineering Design and Analysis System

[46] USACE (2010). EC 1110-2-6067 *USACE Process for the National Flood Insurance Program (NFIP) Levee System Evaluation*, 31 August 2010 (Expires 31 August 2012), U.S. Army Corps of Engineers, Washington, DC., 104p.

[47] U.S. Army Corps of Engineers. 2002. Coastal Engineering Manual. Engineer Manual 1110-2-1100, U.S. Army Corps of Engineers, Washington, D.C. (in 6 volumes).

(CEDAS) software[48]. The ACES method provides reliable estimates of wave parameters for well defined conditions and is the preferred methodology for the analysis of Corps projects[47]. A method for computing wind set-up in run-of-river reservoirs does not currently exist in Corps guidance, so a simple two step procedure was developed.

The wind wave analysis has six main elements 1) evaluation of fetch length, 2) statistical analysis of wind data, 3) computation of significant wave height and wave period, 4) computation of wind set-up, 5) computation of wave run-up and overtopping rate, and 6) assessment of the added flood risk due to waves. Straight line fetch lengths at the Lewiston Levee system are not extraordinarily long, so a fetch-limited wind analysis can adequately characterize wave heights for the flood risk analysis.

13.2. Fetch Length and Depth

Wave heights in a fetch-limited location are primarily dependent on wind speed and fetch length. The levee near the confluence of the Snake and Clearwater Rivers is exposed to the longest fetch in the westerly direction. Fetch lines at the confluence are plotted in Figure 127 and listed in Table 22. An array of fetch lines is preferred over a single long fetch line because the ACES methodology computes an average fetch distance that provides a more realistic estimate of wave height and direction. The longest fetch line is about 8,300 ft on an azimuth of 280° from the confluence. An average depth of 33 ft in the area bounded by the fetch lines was determined from the 2009 bathymetry at a water surface elevation of 744.5 ft NAVD88.

Fetch Lengths at the Confluence		
	Length	Direction
ID	ft	deg
1	1,920	260
2	2,464	270
3	8,264	280
4	6,429	290
5	4,853	300
6	3,709	310
7	2,847	320
8	2,320	330

Table 22. Fetch lengths at the confluence of the Snake and Clearwater Rivers.

[48] http://chl.erdc.usace.army.mil/cedas

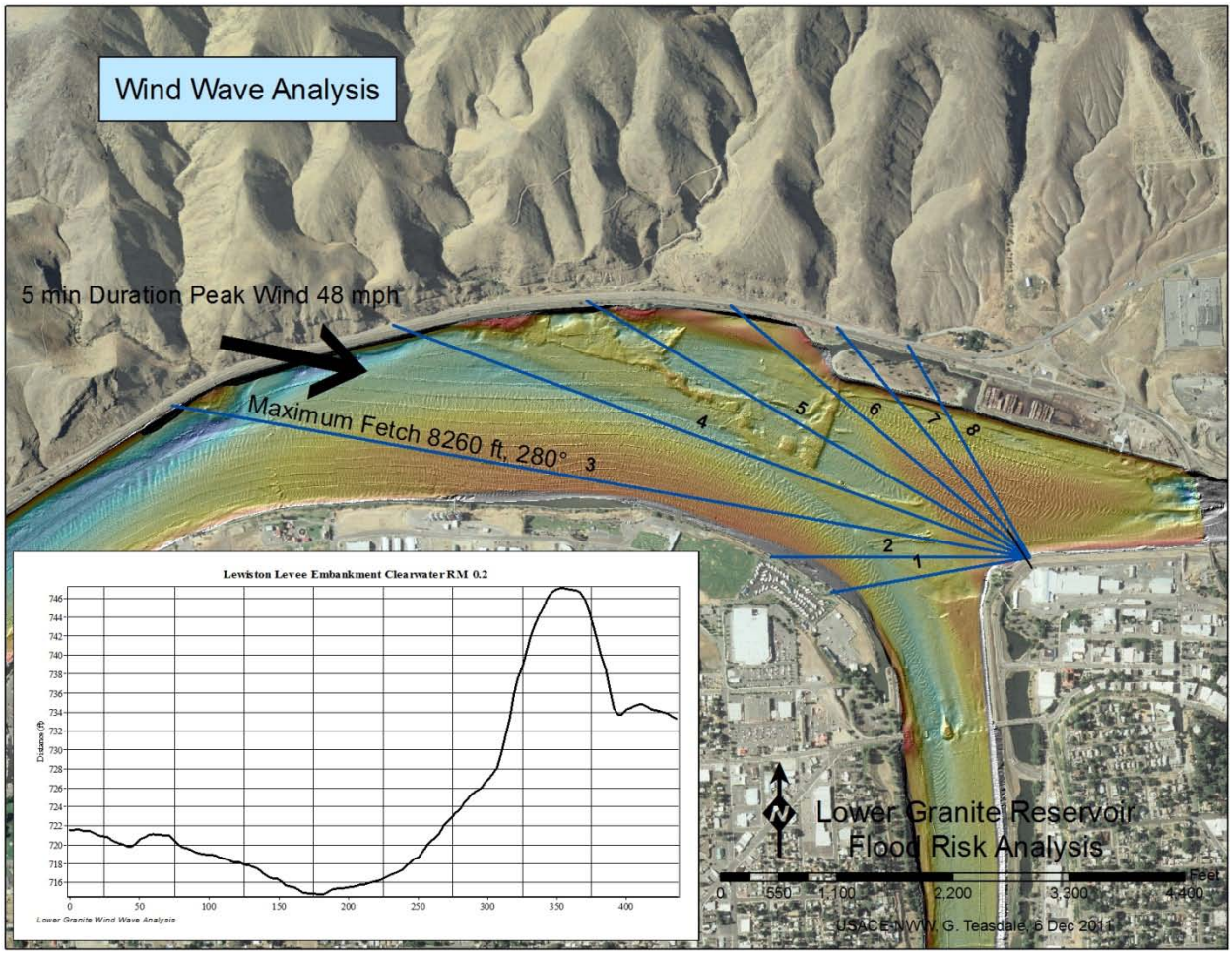


Figure 127. Confluence fetch diagram.

13.3. Wind Speed Frequency Analysis

The nearest meteorological station to the confluence of the Snake and Clearwater River with a long record of wind data is at the Lewiston, ID airport (Coop ID 105241) which is located about 3.5 miles southeast of the confluence. Other stations include the U.S. Bureau of Reclamation Agrimet meteorological station on Silcott Island (RM 130)[49] and a corporate meteorological station at Clearwater Paper Corporation in Lewiston which is located about 2.5 miles east of the confluence. Daily maximum 2-minute average wind speeds were obtained from the U.S. Department of Commerce, National Weather Service (NWS), National Climate Data Center online data distribution system[50]. The NWS wind dataset includes calendar date and wind direction. Extreme

[49] http://www.usbr.gov/pn/agrimet/

[50] http://www.ncdc.noaa.gov/oa/ncdc.html

discharges in the Snake and Clearwater River occur from November through June, so an annual maximum wind speed series was developed from the 2-minute duration maximum daily wind speed data for November through June. The selected analysis period was 1995 to 2010. The annual maximum 2-minute duration wind speeds for all directions and the southerly direction (90°-270°) are plotted in Figure 128 and listed in Table 23. The greatest measured 2-minute duration wind speed was 46 mph in December from a direction of 260°. For conservatism, the maximum wind speeds from any direction were used in the analysis, though restricting wind direction to westerly or southerly winds did not significantly reduce the expected 2-minute duration wind speed.

It is necessary to select an appropriate exceedance frequency for wind speed for the risk analysis. The guidance suggests a maximum value of wind speed should be used in a conservative wave analysis. A log Pearson Type 3 (LP3) distribution was fit to the annual maximum 2-minute duration (all direction) wind speed series using Bulletin 17B procedures in the HEC-SSP software. The frequency curve in Figure 129 shows that the LP3 distribution fit the annual maximum series reasonably well. The expected 1-percent exceedance wind speed, 48 mph (21.5 m/s), was selected for the wave height and run-up analysis at the confluence. The maximum 2-minute duration wind speed for November through June in the period 1995-2010 was 46 mph while for all months the maximum 2-minute duration wind speed was 51 mph. The selected value of wind speed is conservative for the flood risk analysis, especially since wind speed and annual maximum day discharge in Lower Granite are not correlated (Figure 130).

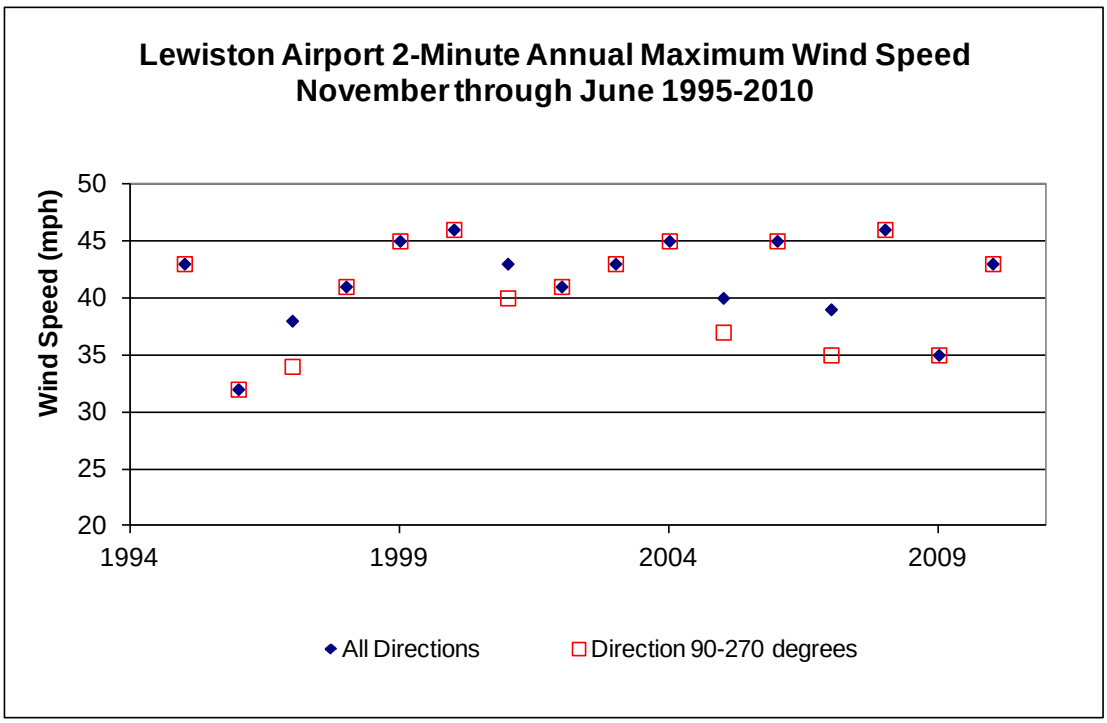


Figure 128. 2-minute annual maximum wind speed at the Lewiston Airport.

Annual Maximum 2-min Duration Wind Speed		
	Wind Speed (mph)	
Year	All Directions	90° - 270°
1995	43	43
1996	32	32
1997	38	34
1998	41	41
1999	45	45
2000	46	46
2001	43	40
2002	41	41
2003	43	43
2004	45	45
2005	40	37
2006	45	45
2007	39	35
2008	46	46
2009	35	35
2010	43	43

Table 23. Annual maximum 2-minute duration wind speed.

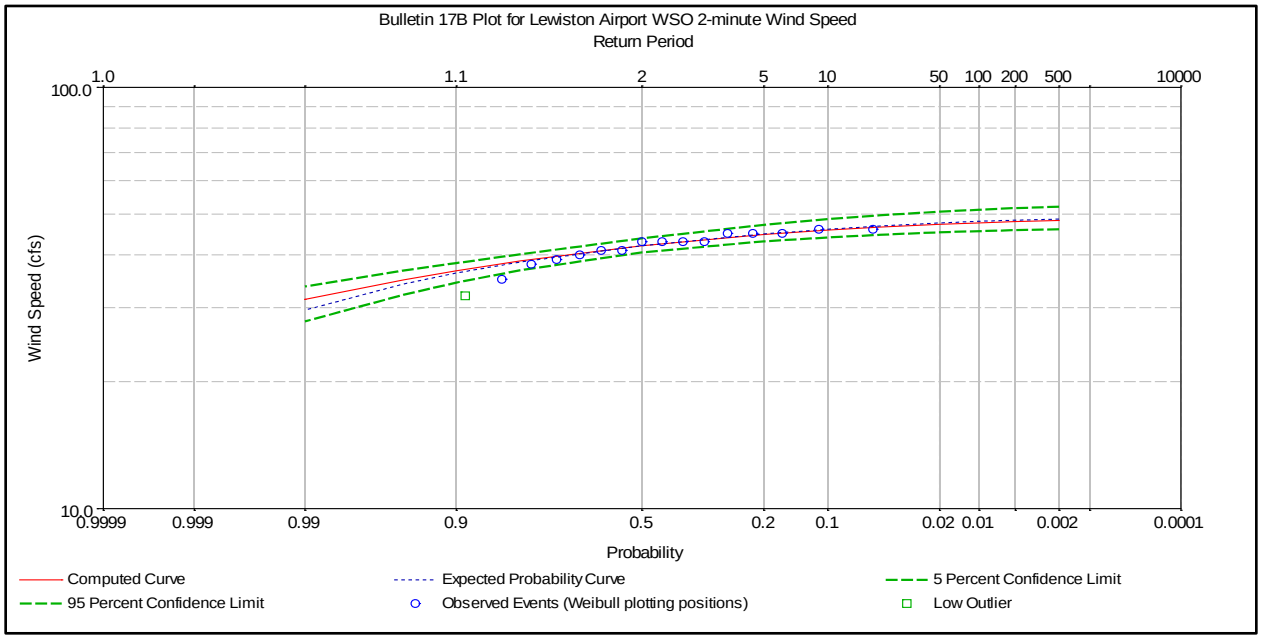


Figure 129. Frequency curve for 2-minute duration maximum annual seasonal (Nov-Jun) wind speed at the Lewiston, ID Airport.

Annual Seasonal Maximum 2-minute Duration Wind Speed at the Lewiston,ID Airport for November - June. Data from 1995 - 2010.					
Percent Chance Exceedance	Return Period	Computed Velocity mph	Expected Velocity mph	Confidence Limits 5% mph	95% mph
0.2	500	48.3	48.7	52.1	46.0
0.5	200	48.0	48.4	51.6	45.8
1	100	47.7	48.0	51.2	45.5
2	50	47.3	47.6	50.6	45.2
5	20	46.6	46.9	49.7	44.6
10	10	45.8	46.0	48.6	44.0
20	5	44.7	44.8	47.1	43.1
50	2	42.1	42.1	43.8	40.5
80	1.25	38.7	38.5	40.2	36.8
90	1.11	36.7	36.2	38.3	34.4
95	1.05	34.9	34.1	36.7	32.2
99	1.01	31.4	29.6	33.7	27.8

Table 24. Wind speed - frequency values for the Lewiston, ID Airport.

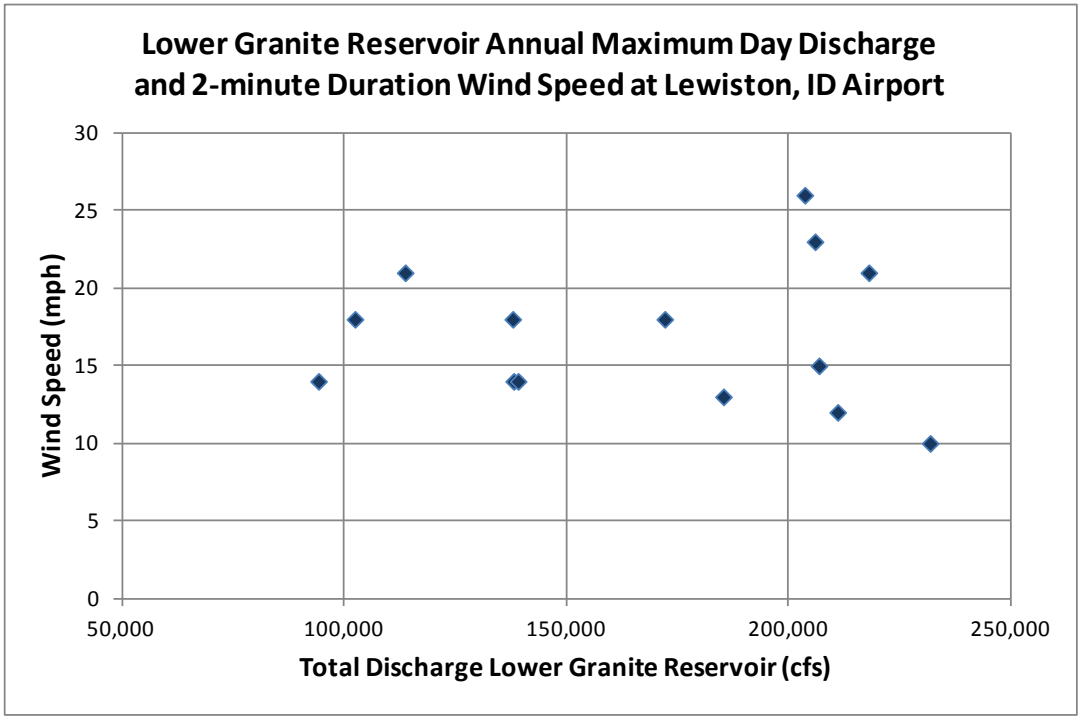


Figure 130. Correlation between annual maximum discharge and wind speed.

13.4. Significant Wave Height

The ACES module of the CEDAS software system was used to compute significant wave height, run-up and overtopping rate. Computations and methods performed by the software are described in EM 1110-2-1100[47]. It is necessary to specify wind duration for the wave calculation to maximize wave growth along the fetch. Wind duration for the computation of wave height at the confluence was estimated with fetch-limited wave growth time equation II-2-35 from EM 1110-2-1100:

$$t_{x,u} = 77.23\frac{X^{0.67}}{u^{0.34}g^{0.33}} = 77.23\frac{(2519)^{0.67}}{(20.45)^{0.34}(9.81)^{0.33}} = 2436\,\text{s} = 0.68\,\text{hours}$$

where $t_{x,u}$ is time required for waves crossing a fetch of length X under a wind of velocity u to become fetch-limited. In this calculation the longest fetch length of 8,264 ft in Table 22 was converted to meters and the selected wind speed 48 mph was converted to m/s.

The array of fetch lines and azimuths were entered into the ACES program and the significant wave height was computed for the shallow and restricted condition. The ACES software adjusted the wind speed both for duration and by a short fetch factor discussed in the documentation. The final adjusted wind speed was 55.9 mph for the duration of 0.68 hours. The weighted fetch length was 7227 feet and the mean wave direction was 284°. The significant wave height at the confluence computed by ACES for these parameters is 1.81 ft and the wave period is 2.45 s. The ACES computation agreed well with manual computations using the procedure in EM 1110-2-1100[47].

Restricted Shallow Fetch-Limited Significant Wave Height Lower Granite Reservoir at the Confluence	
El of Observed Wind (Zobs)	33 feet
Observed Wind Speed (Uobs)	48 mph
Air Sea Temp. Diff. (dT)	0 deg F
Dur of Observed Wind (DurO)	0.1 hours
Dur of Final Wind (DurF)	0.68 hours
Lat. of Observation (LAT)	46.4 deg
Wind Fetch Length (F)	7227 FEET
Avg Fetch Depth (d)	33 feet
Wind Direction (WDIR)	280 deg
Eq Neutral Wind Speed (Ue)	40.03 mph
Adjusted Wind Speed (Ua)	55.89 mph
Mean Wave Direction (THETA)	284 deg
Wave Height (Hmo)	1.81 feet
Wave Period (Tp)	2.45 sec

Table 25. Significant wave height and period at confluence computed with ACES.

13.5. Wind Set-up at the Confluence

Lower Granite Reservoir between the dam and the confluence of the Snake and Clearwater Rivers is 30.8 miles long and is roughly aligned in the direction of the westerly winds that are typical of the interior Columbia River Basin during early winter and spring. Sustained westerly winds exert shear stress on the water surface and cause the surface to slope upward towards the confluence. Superelevation of the water surface from one end of the reservoir to the other is called wind set-up. The slope of the water surface due to wind is in addition to the hydraulic gradient of the flowing water.

Wind set-up at the confluence was estimated with measured stage data at the confluence and hydraulic computations. Wind data from the Agrimet station at Silcott Island (RM 130) showed that the highest sustained winds on Lower Granite Reservoir since the station was installed in 2002 occurred on 7 February 2008. Wind speeds peaked at 67 mph at 7:00 am and averaged 39 mph for over an hour. During this time the discharge in Lower Granite Reservoir was very low, total inflow only averaged about 27,000 cfs, but the discharge varied because of power releases at Hells Canyon Dam. Forebay elevations at Lower Granite Dam and water surface elevations at the confluence varied about 1 ft during the period. Water surface elevations and discharge in Lower Granite Reservoir for February 5-9, 2008 are plotted in Figure 131.

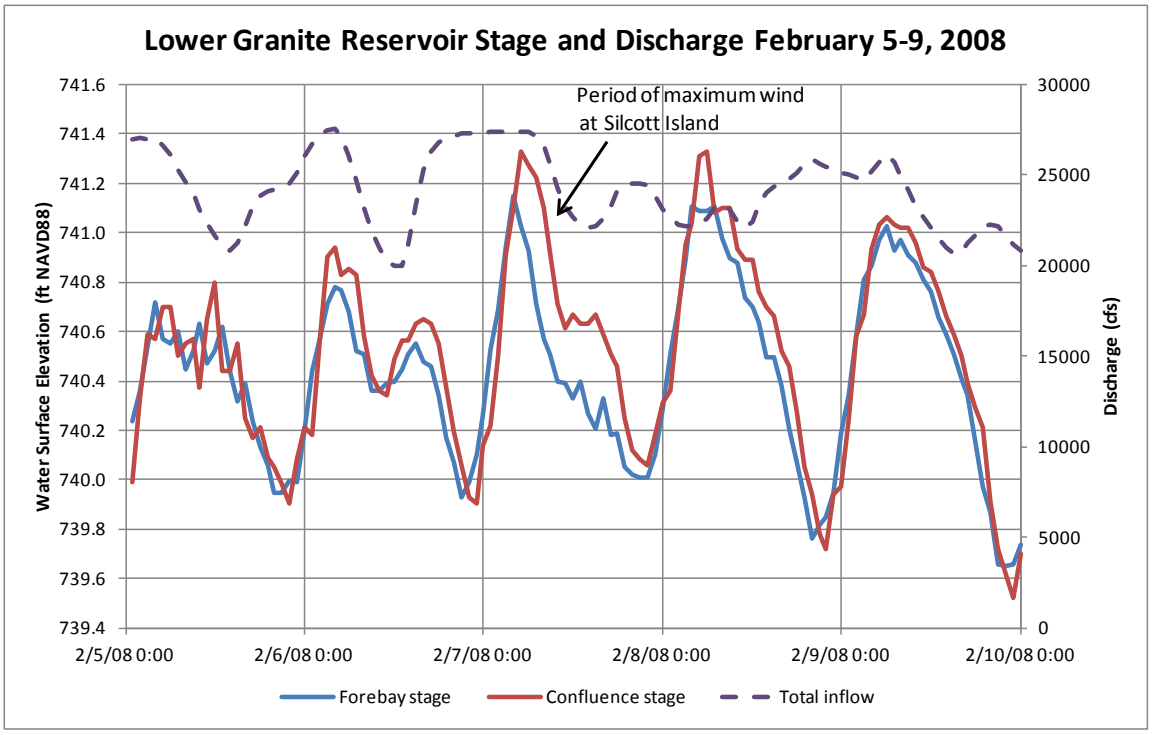


Figure 131. Stage and discharge in Lower Granite Reservoir February 5-9, 2008.

The figure shows that the difference between the water surface elevation at the confluence and the forebay on the morning of 7 February was greater than in the preceding and following periods even though discharge was decreasing. This indicates that part of the difference can be attributed to wind set-up caused by the sustained westerly wind. Wind speed is plotted with the difference between the confluence and forebay water surface elevations in Figure 132. The elevation difference in Figure 132 before and after 7 February averaged about 0.1 ft and the greatest difference during morning of 7 February was about 0.65 ft, which indicates a wind set-up of about 0.5 ft was due to the 39 mph wind.

Wind data for the NWS meteorological station at the Lewiston, ID Airport and at the Clearwater Paper Corporation meteorological station are also plotted in Figure 132. The 1-hour average wind speeds at the Lewiston Airport were somewhat higher than the 15-minute wind speeds at Silcott, and the 1-hour average wind speed reported at the Clearwater Paper Corporation station were substantially lower during the time of the strongest winds. There is good agreement between the meteorological stations when wind speeds were below about 30 mph, which suggests that wind speeds above this value are more strongly influenced by local terrain. A meteorological station should be installed at the confluence for a more detailed study of winds and waves.

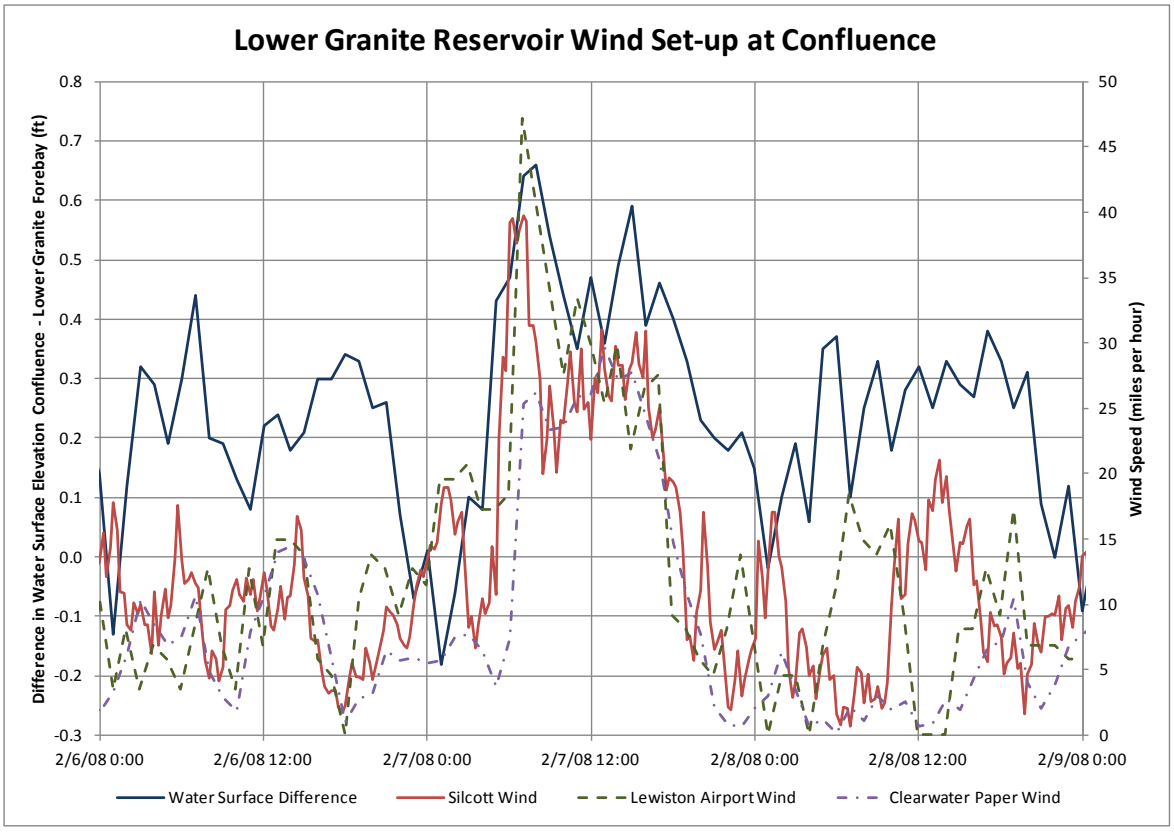


Figure 132. Wind set-up conditions in Lower Granite Reservoir February 6-9, 2008.

It is difficult to visually separate superelevation caused by wind set-up from changes in water surface elevation due to the variability in forebay stage and inflow. The amount of change in the water surface due to flow and forebay control can be determined with the calibrated fixed-bed HEC-RAS unsteady flow model of Lower Granite Reservoir. Since the HEC-RAS simulation does not simulate wind drag, the difference between the computed water surface elevation and the measured water surface elevation at the confluence during peak wind period will provide an estimate of wind set-up. The computed and measured water surface elevations at the confluence are plotted in Figure 133 along with wind speed at Silcott Island. There is good agreement between the computed and measured water surface elevations during the periods of light winds before and after the peak wind period on 7 February, showing that the calibration is acceptable for low flow. Immediately after the peak wind period at 7:00 am, the maximum difference between the computed and measured water surface elevations is 0.6 feet, which becomes the estimate of wind set-up during this period. By this analysis, a reasonable estimate of wind set-up at the confluence for a sustained 39 mph is about 0.6 ft.

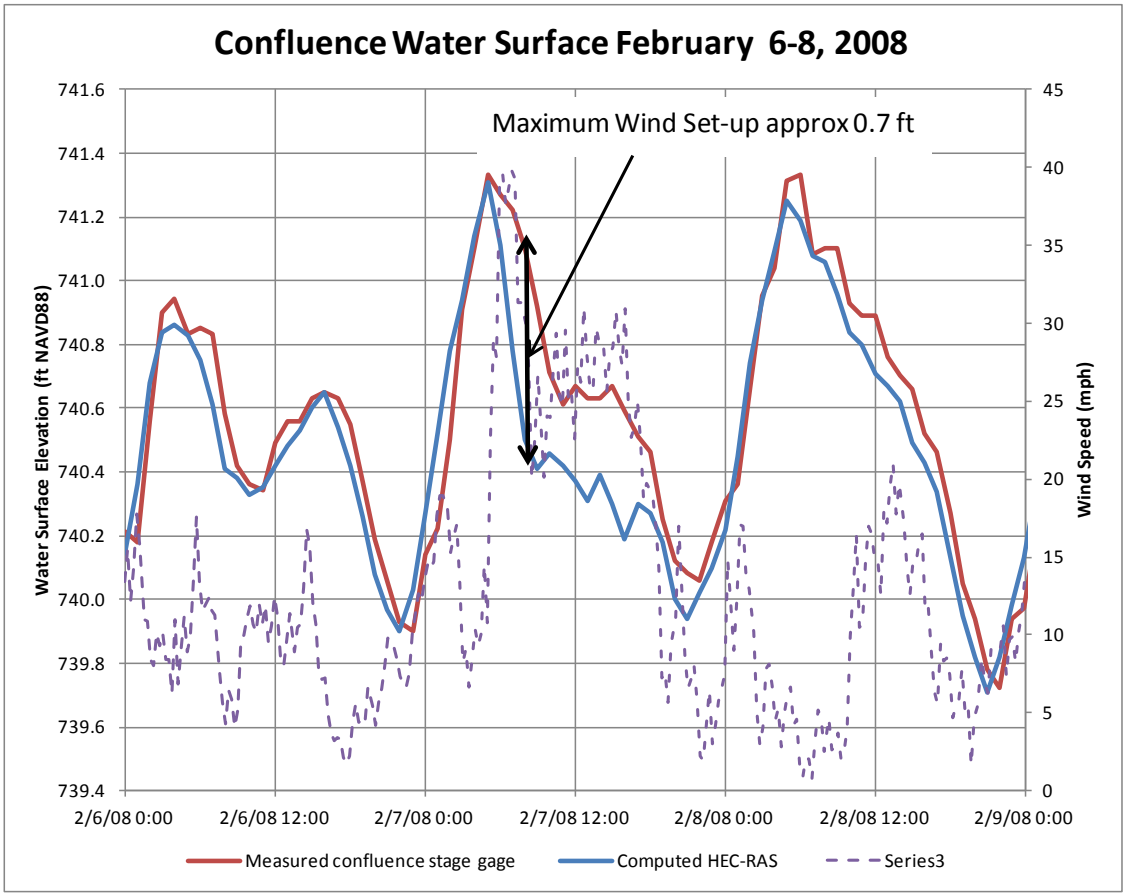


Figure 133. Wind set-up derived from HEC-RAS computation of water surface at the confluence.

Having obtained a reliable estimate of wind set-up for known conditions from the measured stage at the confluence and the unsteady HEC-RAS model (step 1), wind set-up can be estimated with a hydraulic equation which has wind an independent variable and the results confirmed by comparison with the measured value set-up. If the measured and predicted values of wind set-up agree, then the hydraulic equation can be used to predict set-up for the extreme wind condition in the flood risk analysis (step 2).

The unsteady one-dimensional hydrodynamic equation for storm surge[51] can be simplified for steady state conditions and negligible bottom stress to

$$0 = -gD\frac{\partial z}{\partial x} + \frac{\tau_{sx}}{\rho}$$

where D is the water depth, x is the distance along the waterbody, z is the elevation of the water surface, τ_{sx} is the wind shear stress, ρ is the density of water, and g is the acceleration of gravity. The shear stress of the wind on the surface of the water is

$$\tau_s = \rho_a C_D U_w^2$$

$$C_D = 0.001(1.1 + 0.035U_{10})$$ Equation II-2-36, EM 1110-2-1100

where ρ_a is the density of air, C_D is the coefficient of drag, and U_w is the wind speed over the water, and U_{10} is the wind speed over the water at a height of 10 m. Combining the equations and solving for the water slope gives

$$\frac{\partial z}{\partial x} = \frac{\rho_a C_D U_w^2}{\rho g D} \ .$$

It is reasonable that during high wind conditions, wind is channeled by the canyon topography along the length of Lower Granite Reservoir and that wind speed along the reservoir can be approximated by the wind speed measured at Silcott Island. Substituting a wind speed of 39 mph (17.4 m/s), an air density of 1.225 kg/m^3, a water density of 1000 kg/m^3, and average depth of 51 ft (16 m), into the equation gives the slope of the water surface as,

$$C_D = 0.001(1.1 + 0.035U_{10}) = 0.001\big(1.1 + 0.035(17.4)\big) = 0.0017$$

$$\frac{\partial z}{\partial x} = \frac{\rho_a C_D U_w^2}{\rho g D} = \frac{(1.225)(0.0017)\big(17.4\big)^2}{(1000)(9.81)(16)} = 4.017\times10^{-6} \ .$$

[51] USACE (1984). *Shore Protection Manual*, 4th Ed, Equation 3-77, U.S. Army Corps of Engineers, Washington, DC.

Assuming that the forebay elevation remains constant at Lower Granite Dam (set-down is offset by forebay control) the wind set-up at the confluence is computed,

$$\Delta z = \frac{\Delta z}{\Delta x} L = \left(4.017 \times 10^{-6}\right)\left(30.8 \text{ mi}\right)\left(5280 \frac{\text{ft}}{\text{mi}}\right) = 0.65 \text{ ft}.$$

The computed wind set-up agrees very well with the wind set-up estimated from the confluence stage data and the calibrated unsteady HEC-RAS model. Having confirmed that the simple hydraulic equation can estimate wind set-up for a known event, wind set-up can be predicted for higher wind velocities that do not greatly exceed the measured condition. For the flood risk analysis, a sustained wind speed of 48 mph for the 1-percent exceedance wind event gives a computed wind set-up at the confluence of 1.1 ft.

13.6. Wave Run-up and Overtopping Rate

Wind-generated waves have wave periods which trigger wave breaking on almost all sloping structures. The breaking wave causes run-up and run-down which is defined as the maximum and minimum water-surface elevation measured vertically from the still-water level[52]. Wave run-up was computed with the ACES software. Run-up height depends on the slope and roughness of the levee embankment. Elements of the geometry of the levee embankment that are input into the ACES wave run-up module are shown in Figure 134. Levee geometry was determined from the combined 2009 bathymetry, 2009 levee profile survey and the 2010 LiDAR data (Figure 135). The embankment slope (θ) is 3:1 (horizontal to vertical) at Clearwater RM 0.2. The approach slope angle (ϕ) was specified as 10:1. The height of the levee crest (which determines height h_s) is 746.56 ft NAVD88 and the elevation of the toe of the levee (which defines depth d_s) is 728 ft NAVD 88. The overtopping coefficient α was set to 0.076 and coefficient Q^*_0 was set to 0.01. Levee embankment roughness coefficients and breaking criteria were set at default.

[52] USACE (2002). Volume VI, Chap 5, Coastal Engineering Manual. Engineer Manual 1110-2-1100, U.S. Army Corps of Engineers, Washington, D.C.

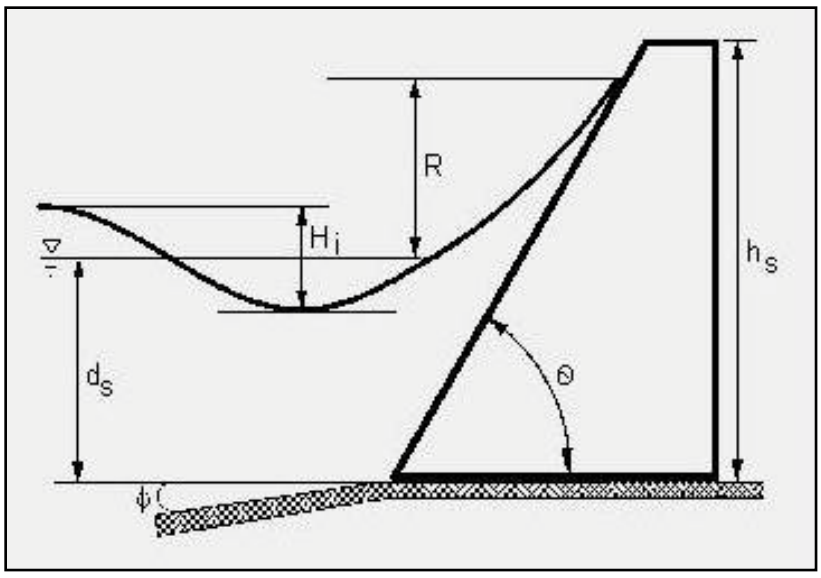


Figure 134. ACES wave run-up diagram.

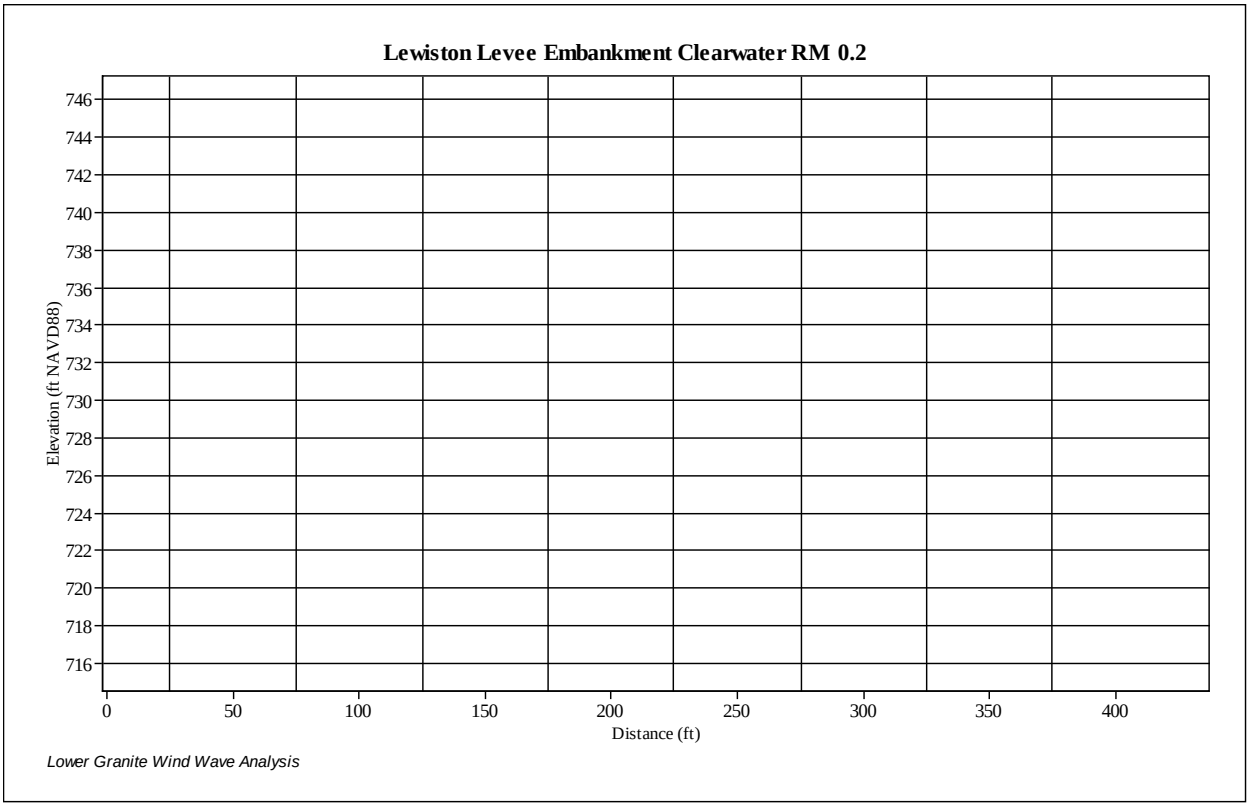


Figure 135. Geometry of the levee at Clearwater RM 0.21.

Wind set-up and wave run-up are added to the still water level determined by hydraulic modeling of the flood discharges. The non-probabilistic equation for flood stage becomes,

$$WSE_{fw} = WSE_f + H_{ws} + H_{wr}$$

where WSE_{fw} is the flood water surface elevation due to flood discharge and wind, WSE_f is the water surface elevation due only to flood discharge, H_{ws} is the height of wind set-up, and H_{wr} is the height of wave run-up. Significant wave height is not included in the above equation because it is a parameter in the wave run-up computation. The addition of the wave set-up height produces a conservative (very) estimate of total run-up height, overtopping elevation and interior overtopping discharge rate.

Median probability water surface elevations for extreme discharges at year-2009 and year-2060 were computed previously in the flood risk analysis and are listed in Table 26.

Clearwater RM 0.21 Water Surface Elevation feet NAVD88				
Exceedance percent	Discharge cfs	Year 2009 ft NAVD88	Year 2060 ft NAVD88	Levee Elevation ft NAVD88
1	102,167	738.16	741.98	746.56
0.4	111,124	739.27	743.26	746.56
0.2	117,587	740.09	744.18	746.56
SPF	125,000	741.57	745.94	746.56

Table 26. Water surface elevations at Clearwater RM 0.21 for year-2009 and year-2060.

Run-up height and overtopping rates were computed with ACES for the exceedance discharges listed in Table 26 and the run-up parameters given above. Results of the run-up computations for the year-2009 and year-2060 channel conditions are listed in Table 27 and Table 28. Wave run-up does not cause overtopping of the levee at Clearwater RM 0.21 for the year-2009 channel even for the Standard Project Flood (SPF) discharge. With continued sediment deposition, at year-60 the flood water surface rises so that wave run-up causes overtopping during the SPF and substantial overtopping during the 0.2 percent (500 year) exceedance discharge. Overtopping discharge for 0.4 percent (250 year) discharge is 0.005 cfs per foot of levee or about 5 cfs (2000 gallons per minute) per 1000 ft of levee. It is likely that the levee interior drainage system could be improved to accommodate this discharge. The average depth of the channel was not reduced in the computation of the year-60 significant wave height and run-up because as shown previously it is likely that sediment will be eroded from the confluence area during extreme discharges.

Clearwater RM 0.21 Wave Run-up and Levee Overtopping Discharge for Year-2009												
Exceedance percent	Discharge cfs	Water Surface ft NAVD88	Levee Elevation ft NAVD88	Toe Elevation ft NAVD88	Set-up ft	ds ft	hs ft	Hmo ft	Run-up ft	Run-up Elevation ft NAVD88	Freeboard ft	Overtopping Rate cfs
1	102,167	738.16	746.56	728	1.1	11.26	18.56	1.82	1.54	740.80	5.76	0
0.4	111,124	739.27	746.56	728	1.1	12.37	18.56	1.82	1.54	741.91	4.65	0
0.2	117,587	740.09	746.56	728	1.1	13.19	18.56	1.82	1.54	742.73	3.83	0
SPF	125,000	741.57	746.56	728	1.1	14.67	18.56	1.82	1.54	744.21	2.35	0

Table 27. Wave run-up at the confluence for the year-2009 channel.

Clearwater RM 0.21 Wave Run-up and Levee Overtopping Discharge for Year-2060												
Exceedance percent	Discharge cfs	Water Surface ft NAVD88	Levee Elevation ft NAVD88	Toe Elevation ft NAVD88	Set-up ft	ds ft	hs ft	Hmo ft	Run-up ft	Run-up Elevation ft NAVD88	Freeboard ft	Overtopping Rate cfs/ft
1	102,167	741.98	746.56	728	1.1	15.08	18.56	1.82	1.54	744.62	1.94	0
0.4	111,124	743.26	746.56	728	1.1	16.36	18.56	1.82	1.54	745.90	0.66	0.005
0.2	117,587	744.18	746.56	728	1.1	17.28	18.56	1.82	1.54	746.82	-0.26	0.13
SPF	125,000	745.94	746.56	728	1.1	19.04	18.56	1.82	1.54	748.58	-2.02	Submerged

Table 28. Wave run-up at the confluence for the year 2060 channel.

13.7. Summary of the Wind Wave Analysis

Strong winds increase the risk that levees situated next to open water will overtop during extreme floods. Winds can increase the height of the water surface at a levee by the action of wind set-up and wave run-up. The superelevated water surface may intermittently overtop a levee even though the still water surface lies below the crest of the levee. The potential for wind set-up in Lower Granite Reservoir was evaluated by examination of confluence stage records, simulation of the reservoir water surface profile, and a simple hydraulic formulation. Significant wave height and wave run-up were computed with the ACES module of the USACE Coastal Engineering Design and Analysis System (CEDAS) software. Results of the analysis indicate that wave overtopping does not occur in the year-2009 channel up to and including the SPF discharge. Continuous overtopping occurs at the confluence during the SPF discharge in the year 2060 channel and substantial intermittent overtopping flow occurs during the 0.2 percent discharge.

14. Summary of the Flood Risk Analysis

This section summarizes and compares the FDA conditional non-exceedance probabilities and long-term risk of the different channel configurations discussed in the previous sections. The 8 channel configurations listed in Table 29 were evaluated at 8 index sections (Figure 136) to demonstrate the effect of epistemic uncertainty on the outcome of the FDA analysis. The main sources of epistemic uncertainty are the future sediment loads, the sediment transport models that predict the future channel condition, and the hydraulic response of the channel at extreme discharge.

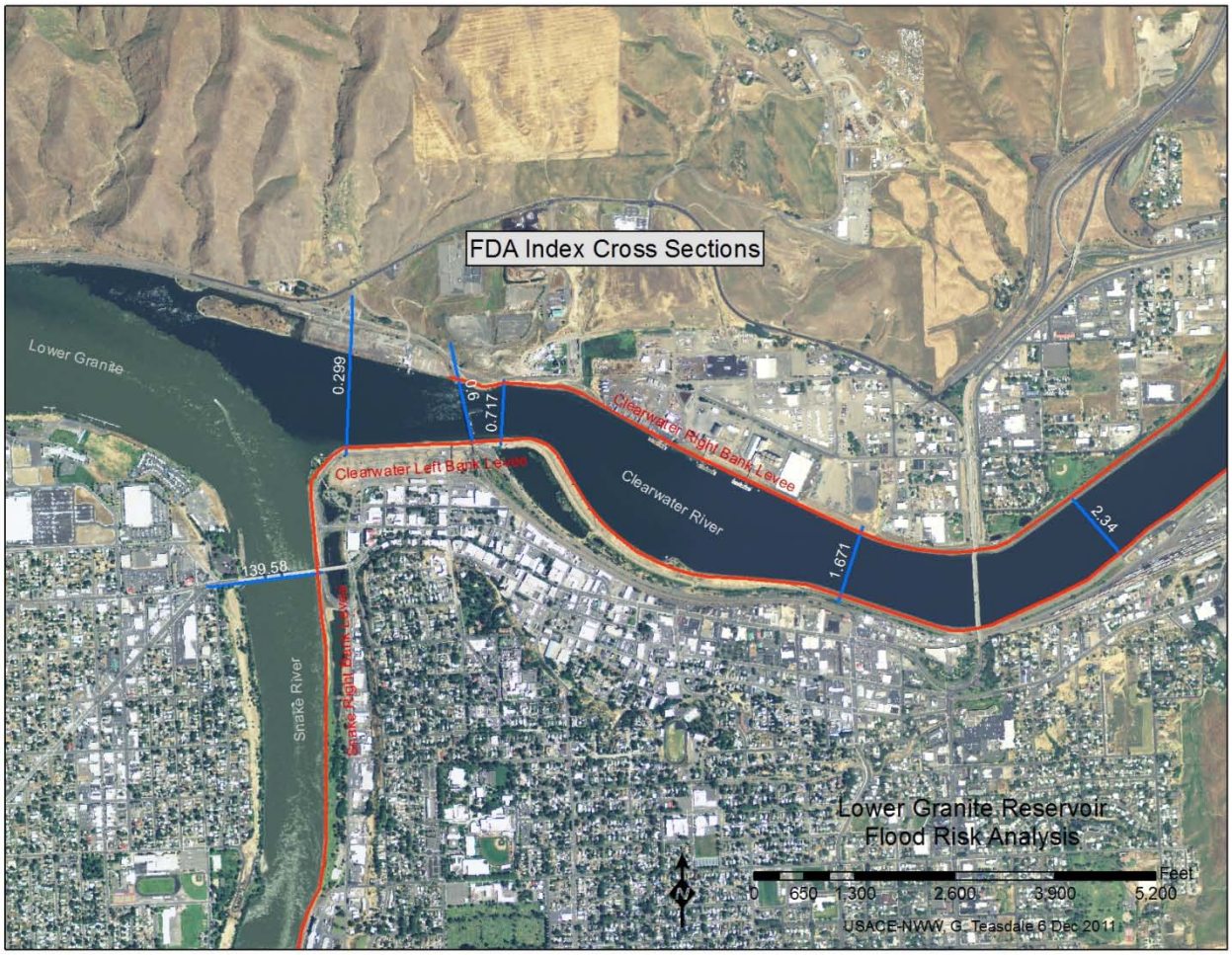


Figure 136. FDA Index Cross sections at the Lewiston levee system.

The basic data and approach for the analysis, and limitations of the current FDA analysis are discussed in Part 1, Section 5 for the current (year 2009) channel condition. These essential considerations apply to all the channel configurations. Flood risk due to potential misoperation of the spillway gates at Lower Granite Dam, blockage

of the CPRR Bridge by debris, and wind waves are also sources of epistemic uncertainty, but are not directly incorporated into the probabilistic analysis. Instead, misoperation and blockage potentials are treated as a separate element of risk in Part 1, Section 5.12. Flood risk due to wind waves was evaluated in Section 13.

Lower Granite Reservoir - Lewiston Levee Flood Risk - Evaluated Channel Configurations	
1	2009 channel geometry with lower bed regime flow resistance with no channel modifications.
2	2009 channel geometry with upper bed regime flow resistance with no channel modifications.
3	2009 channel geometry with lower bed regime flow resistance with spur dikes.
4	2009 channel geometry with upper bed regime flow resistance with spur dikes.
5	2060 channel geometry with lower bed regime flow resistance with no channel modifications.
6	2060 channel geometry with upper bed regime flow resistance with no channel modifications.
7	2060 channel geometry with lower bed regime flow resistance with spur dikes.
8	2060 channel geometry with upper bed regime flow resistance with spur dikes.

Table 29. Channel configurations evaluated for the Lewiston levee flood risk analysis.

The channel configurations were evaluated at two levels of stage uncertainty represented by standard deviations of 0.5 and 2.0. As discussed in Section 10, the effect of bed regime on flow resistance affects stage is specifically evaluated in separate hydraulic model simulations external to FDA rather than incorporate this uncertainty into the stage uncertainty specified in FDA. The stage uncertainty added in FDA represents other sources of uncertainty including normal spillway operation variation, unsteady flow effects, and variability in sediment loads. The data analysis indicates that the 0.5 standard deviation of stage uncertainty is the most realistic, at least for the current year 2009 channel configuration. The 2.0 standard deviation of stage uncertainty provides greater conservatism to account for the greater uncertainty in the future channel condition. As discussed in Section 5, two methods of extending the index section rating curve were evaluated including 1) if the total discharge in Lower Granite below the confluence for the extreme discharge is limited to the SPF of 420,000 cfs and 2) if the total discharge in Lower Granite Reservoir is defined by the 70 percent and 30 percent flow-split of the Snake and Clearwater Rivers with forebay water surface elevations obtained from the free-flow rating curve for the spillway. As discussed Section 5, simple curve extension does not eliminate the bias caused by the uncorrelated simulation of the Clearwater and Snake River discharges in the FDA analysis.

Conditional non-exceedance probabilities for the 1-percent exceedance discharge and long-term risk for the channel configurations are compared for the current (year 2009) and future (year 2060) channel conditions in Table 30 and Table 31. The evaluations show a range of CNP and LTR that vary from high assurance in year 2009 to unacceptable risk levels in year 2060. The most realistic risk evaluations are

highlighted with light-blue shading and the most conservative evaluations are highlighted with light-orange shading. For the year 2009 channel condition without modification, CNP values exceed 0.95 at all index sections for all configurations. The most realistic year 2009 configuration is upper bed regime, 0.5 standard deviations of stage uncertainty, and curve extension method 1. The most conservative year 2009 configuration is lower bed regime, 2.0 standard deviations of stage uncertainty, and curve extension method 2. The most realistic future channel condition in year 2060 is represented by upper bed regime, 2.0 standard deviations of stage uncertainty, and curve extension method 1, has CNP values for the 1-percent exceedance discharge that are greater than 0.94 at all index sections. However, the CNP values reduce to 0.75 near the CPRR Bridge with the more conservative assumption of lower bed regime. The conclusion from flood risk analysis is that the risk of overtopping the levees during the 50-year planning period is unacceptable and effective sediment management is needed to maintain flow conveyance and levee performance as sediment continues to accumulate in Lower Granite Reservoir. Spur dikes reduce deposition in the navigation channels, but do not significantly change the levels of flood risk.

			Lower Regime, Current Condition (Year 2009) Stage Uncertainty 0.5 Standard Deviation				Upper Regime, Current Condition (Year 2009) Stage Uncertainty 0.5 Standard Deviation			
			Index Section Curve Extension - Method 1				Index Section Curve Extension - Method 1			
			CNP 1-percent		50-yr Long-term Risk		CNP 1-percent		50-yr Long-term Risk	
River	Index Location	Description	No Dikes	With Dikes	No Dikes	With Dikes	No Dikes	With Dikes	No Dikes	With Dikes
Clearwater	Confluence	Confl RM 0.299	0.999	0.999	0.005	0.006	0.999	0.999	0.005	0.005
	CPRR Brg	CPRR RM 0.6	0.999	0.988	0.005	0.035	0.999	0.999	0.005	0.005
	Right Low	L RM 1.671	0.999	0.995	0.005	0.020	0.999	0.999	0.005	0.005
	Left Turn Basin	L RM 2.34	0.999	0.999	0.005	0.005	0.999	0.999	0.005	0.005
	Port	R RM 1.671	0.999	0.999	0.005	0.005	0.999	0.999	0.005	0.005
	R North Lewiston	R RM 2.34	0.999	0.999	0.005	0.005	0.999	0.999	0.005	0.005
	Left WTP	R RM 0.717	0.999	0.999	0.005	0.005	0.999	0.999	0.005	0.005
Snake	Clarkston	R RM 139.58	0.999	0.999	0.005	0.005	0.999	0.999	0.005	0.005
			Lower Regime, Current Condition (Year 2009) Stage Uncertainty 2.0 Standard Deviation				Upper Regime, Current Condition (Year 2009) Stage Uncertainty 2.0 Standard Deviation			
			Index Section Curve Extension - Method 1				Index Section Curve Extension - Method 1			
			CNP 1-percent		50-yr Long-term Risk		CNP 1-percent		50-yr Long-term Risk	
River	Index Location	Description	No Dikes	With Dikes	No Dikes	With Dikes	No Dikes	With Dikes	No Dikes	With Dikes
Clearwater	Confluence	Confl RM 0.299	0.986	0.948	0.027	0.084	0.999	0.998	0.005	0.009
	CPRR Brg	CPRR RM 0.6	0.967	0.892	0.055	0.162	0.999	0.993	0.006	0.017
	Right Low	L RM 1.671	0.975	0.911	0.043	0.136	0.999	0.995	0.006	0.013
	Left Turn Basin	L RM 2.34	0.999	0.993	0.006	0.017	0.999	0.999	0.005	0.005
	Port	R RM 1.671	0.999	0.989	0.007	0.023	0.999	0.999	0.005	0.005
	R North Lewiston	R RM 2.34	0.999	0.998	0.006	0.009	0.999	0.999	0.005	0.005
	Left WTP	R RM 0.717	0.999	0.998	0.006	0.009	0.999	0.999	0.005	0.005
Snake	Clarkston	R RM 139.58	0.991	0.958	0.020	0.068	0.999	0.999	0.005	0.007
			Lower Regime, Current Condition (Year 2009) Stage Uncertainty 0.5 Standard Deviation				Upper Regime, Current Condition (Year 2009) Stage Uncertainty 0.5 Standard Deviation			
			Index Section Curve Extension - Method 2				Index Section Curve Extension - Method 2			
			CNP 1-percent		50-yr Long-term Risk		CNP 1-percent		50-yr Long-term Risk	
River	Index Location	Description	No Dikes	With Dikes	No Dikes	With Dikes	No Dikes	With Dikes	No Dikes	With Dikes
Clearwater	Confluence	Confl RM 0.299	0.994	0.982	0.029	0.057	0.999	0.999	0.005	0.008
	CPRR Brg	CPRR RM 0.6	0.988	0.960	0.044	0.092	0.999	0.997	0.005	0.017
	Right Low	L RM 1.671	0.990	0.968	0.039	0.080	0.999	0.998	0.005	0.013
	Left Turn Basin	L RM 2.34	0.999	0.997	0.005	0.019	0.999	0.999	0.005	0.005
	Port	R RM 1.671	0.999	0.995	0.007	0.026	0.999	0.999	0.005	0.005
	R North Lewiston	R RM 2.34	0.999	0.999	0.005	0.008	0.999	0.999	0.005	0.005
	Left WTP	R RM 0.717	0.999	0.999	0.005	0.008	0.999	0.999	0.005	0.005
Snake	Clarkston	R RM 139.58	0.998	0.989	0.015	0.043	0.999	0.999	0.005	0.005
			Lower Regime, Current Condition (Year 2009) Stage Uncertainty 2.0 Standard Deviation				Upper Regime, Current Condition (Year 2009) Stage Uncertainty 2.0 Standard Deviation			
			Index Section Curve Extension - Method 2				Index Section Curve Extension - Method 2			
			CNP 1-percent		50-yr Long-term Risk		CNP 1-percent		50-yr Long-term Risk	
River	Index Location	Description	No Dikes	With Dikes	No Dikes	With Dikes	No Dikes	With Dikes	No Dikes	With Dikes
Clearwater	Confluence	Confl RM 0.299	0.978	0.936	0.051	0.113	0.999	0.994	0.009	0.021
	CPRR Brg	CPRR RM 0.6	0.956	0.879	0.085	0.187	0.997	0.987	0.014	0.034
	Right Low	L RM 1.671	0.965	0.898	0.070	0.162	0.998	0.990	0.011	0.028
	Left Turn Basin	L RM 2.34	0.998	0.987	0.011	0.034	0.999	0.999	0.005	0.007
	Port	R RM 1.671	0.996	0.982	0.017	0.044	0.999	0.999	0.006	0.008
	R North Lewiston	R RM 2.34	0.999	0.995	0.009	0.020	0.999	0.999	0.005	0.006
	Left WTP	R RM 0.717	0.999	0.994	0.009	0.020	0.999	0.999	0.005	0.006
Snake	Clarkston	R RM 139.58	0.985	0.949	0.036	0.093	0.999	0.997	0.007	0.012

Table 30. Lewiston levee CNP and LTR evaluations for year 2009 channel condition.

			Lower Regime, Future Condition (Year 2060) Stage Uncertainty 0.5 Standard Deviation				Upper Regime, Future Condition (Year 2060) Stage Uncertainty 0.5 Standard Deviation			
			Index Section Curve Extension - Method 1				Index Section Curve Extension - Method 1			
			CNP 1-percent		50-yr Long-term Risk		CNP 1-percent		50-yr Long-term Risk	
River	Index Location	Description	No Dikes	With Dikes	No Dikes	With Dikes	No Dikes	With Dikes	No Dikes	With Dikes
Clearwater	Confluence	Confl RM 0.299	0.910	0.887	0.151	0.177	0.999	0.999	0.005	0.005
	CPRR Brg	CPRR RM 0.6	0.873	0.883	0.191	0.181	0.999	0.999	0.005	0.005
	Right Low	L RM 1.671	0.890	0.909	0.174	0.152	0.999	0.999	0.005	0.005
	Left Turn Basin	L RM 2.34	0.999	0.999	0.008	0.007	0.999	0.999	0.005	0.005
	Port	R RM 1.671	0.998	0.999	0.015	0.005	0.999	0.999	0.005	0.005
	R North Lewiston	R RM 2.34	0.999	0.999	0.005	0.005	0.999	0.999	0.005	0.005
	Left WTP	R RM 0.717	0.999	0.999	0.005	0.005	0.999	0.999	0.005	0.005
Snake	Clarkston	R RM 139.58	0.948	0.923	0.102	0.134	0.999	0.999	0.005	0.005
			Lower Regime, Future Condition (Year 2060) Stage Uncertainty 2.0 Standard Deviation				Upper Regime, Future Condition (Year 2060) Stage Uncertainty 2.0 Standard Deviation			
			Index Section Curve Extension - Method 1				Index Section Curve Extension - Method 1			
			CNP 1-percent		50-yr Long-term Risk		CNP 1-percent		50-yr Long-term Risk	
River	Index Location	Description	No Dikes	With Dikes	No Dikes	With Dikes	No Dikes	With Dikes	No Dikes	With Dikes
Clearwater	Confluence	Confl RM 0.299	0.803	0.784	0.277	0.297	0.955	0.955	0.070	0.072
	CPRR Brg	CPRR RM 0.6	0.765	0.776	0.330	0.309	0.943	0.952	0.093	0.079
	Right Low	L RM 1.671	0.781	0.802	0.308	0.277	0.948	0.960	0.086	0.065
	Left Turn Basin	L RM 2.34	0.969	0.971	0.055	0.050	0.997	0.997	0.011	0.010
	Port	R RM 1.671	0.956	0.959	0.076	0.069	0.994	0.995	0.014	0.013
	R North Lewiston	R RM 2.34	0.990	0.991	0.023	0.021	0.999	0.999	0.007	0.006
	Left WTP	R RM 0.717	0.989	0.990	0.024	0.021	0.999	0.999	0.007	0.006
Snake	Clarkston	R RM 139.58	0.837	0.819	0.234	0.255	0.973	0.970	0.048	0.051
			Lower Regime, Future Condition (Year 2060) Stage Uncertainty 0.5 Standard Deviation				Upper Regime, Future Condition (Year 2060) Stage Uncertainty 0.5 Standard Deviation			
			Index Section Curve Extension - Method 2				Index Section Curve Extension - Method 2			
			CNP 1-percent		50-yr Long-term Risk		CNP 1-percent		50-yr Long-term Risk	
River	Index Location	Description	No Dikes	With Dikes	No Dikes	With Dikes	No Dikes	With Dikes	No Dikes	With Dikes
Clearwater	Confluence	Confl RM 0.299	0.897	0.878	0.167	0.187	0.986	0.982	0.049	0.056
	CPRR Brg	CPRR RM 0.6	0.868	0.875	0.196	0.190	0.979	0.982	0.061	0.056
	Right Low	L RM 1.671	0.883	0.896	0.182	0.169	0.981	0.985	0.058	0.051
	Left Turn Basin	L RM 2.34	0.987	0.988	0.047	0.045	0.998	0.998	0.015	0.012
	Port	R RM 1.671	0.983	0.983	0.055	0.053	0.997	0.997	0.020	0.016
	R North Lewiston	R RM 2.34	0.994	0.999	0.028	0.005	0.999	0.999	0.006	0.005
	Left WTP	R RM 0.717	0.994	0.999	0.029	0.005	0.999	0.999	0.006	0.005
Snake	Clarkston	R RM 139.58	0.926	0.909	0.135	0.154	0.993	0.990	0.031	0.039
			Lower Regime, Future Condition (Year 2060) Stage Uncertainty 2.0 Standard Deviation				Upper Regime, Future Condition (Year 2060) Stage Uncertainty 2.0 Standard Deviation			
			Index Section Curve Extension - Method 2				Index Section Curve Extension - Method 2			
			CNP 1-percent		50-yr Long-term Risk		CNP 1-percent		50-yr Long-term Risk	
River	Index Location	Description	No Dikes	With Dikes	No Dikes	With Dikes	No Dikes	With Dikes	No Dikes	With Dikes
Clearwater	Confluence	Confl RM 0.299	0.793	0.774	0.294	0.312	0.946	0.941	0.099	0.106
	CPRR Brg	CPRR RM 0.6	0.757	0.766	0.341	0.325	0.928	0.939	0.125	0.110
	Right Low	L RM 1.671	0.773	0.791	0.320	0.294	0.934	0.948	0.117	0.096
	Left Turn Basin	L RM 2.34	0.960	0.961	0.080	0.077	0.992	0.993	0.026	0.023
	Port	R RM 1.671	0.946	0.947	0.100	0.096	0.988	0.990	0.033	0.029
	R North Lewiston	R RM 2.34	0.983	0.991	0.044	0.021	0.997	0.997	0.015	0.013
	Left WTP	R RM 0.717	0.982	0.990	0.044	0.021	0.997	0.997	0.015	0.013
Snake	Clarkston	R RM 139.58	0.826	0.809	0.254	0.272	0.965	0.960	0.070	0.077

Table 31. Lewiston levee CNP and LTR evaluations for year 2060 channel condition.

Lower Snake River Programmatic Sediment Management Plan Environmental Impact Statement

Appendix F

Hydrology and Hydraulics
Lower Granite Reservoir Sedimentation Analysis and Lewiston Levee Flood Risk Analysis

Part 3

Prepared by:

U.S. Army Corps of Engineers
Walla Walla District

August 2014

Table of Contents

15. Evolution of Sand Bedforms and Sedimentation in Navigation Channels 11
15.1. Bathymetry Acquisition and Processing 12
15.2. Fixed-bed One-dimensional Sediment Range Hydraulic Model 15
15.3. Calibrated HEC-RAS One-dimensional Hydraulic Model 17
15.4. Hillshade Maps of Bedforms and Bed Change 22
15.4.1. Confluence Hillshade Bathymetry Maps 23
15.4.2. Port of Clarkston Hillshade Bathymetry Map 26
15.4.3. Port of Wilma Hillshade Bathymetry Map 28
15.4.4. Silcott Island Hillshade Bathymetry Map 30
15.4.5. Snake River Hillshade Bathymetry Map 33
15.5. Dune Transect Profiles 36
15.5.1. Confluence Bedform Profiles 36
15.5.2. Clearwater Turning Basin Bedform Profiles 43
15.5.3. Port of Clarkston Bedform Profiles 46
15.5.4. Red Wolf Bedform Profile 51
15.5.5. Port of Wilma Bedform Profiles 53
15.5.6. Silcott Bedform Profile 57
15.5.7. Snake River Bedform Profile 59
15.6. Bathymetry Difference Mapping 62
15.6.1. Confluence Bathymetry Difference Maps 62
15.6.2. Port of Clarkston Bathymetry Difference Maps 65
15.6.3. Port of Lewiston Bathymetry Difference Maps 67
15.6.4. Snake River 2011-2009 Bathymetry Difference Maps 69
15.6.5. Red Wolf 2011-2009 Bathymetry Difference Maps 72
15.6.6. Port of Wilma 2011-2009 Bathymetry Difference Maps 73
15.6.7. Below-Wilma 2011-2009 Bathymetry Difference Maps 76
15.6.8. Silcott Island 2011-2009 Bathymetry Difference Maps 78
15.7. Sediment Transport Modeling of the May 2011 Channel 81
15.7.1. May 2011 Sediment Rating Curve Simulation 81
15.7.2. Simulated Bed Change September 2009 to May 2011 85
15.8. Analysis of Bed Regime Conditions 88

15.8.1. Two-Dimensional ADH Model of Lower Granite Reservoir 89
15.8.2. Spatial Analysis of Bed Regime with the Brownlie Relationships 94
15.8.3. Spatial Analysis of Bed Regime with the Karim Relationships 97
15.8.4. Spatial Analysis of Bed Regime with the Simons and Richardson Relationship 99
15.8.5. Comparison with Bed Regime of the Lower Columbia River 100
15.8.6. Bed Displacement during SPF Estimated with ADH 102
15.9. Summary and Conclusions of the Bed-form and Bed Regime Analysis 103
16. Sediment Deposition in Navigation Channels 105
16.1. Recent Sediment Encroachment in Navigation Channels 105
16.2. Long-Term Sediment Encroachment in Navigation Channels 108
17. Hydraulic Modeling of Environmental Flows 113
17.1. Water Travel Time 113
17.1.7. One-dimensional Model Development 113
17.1.8. Steady Flow Travel Time and Reach Transit Time 116
17.1.9. Reach Transit Times for WY 2011 and WY 2007 118
17.2. Two-dimensional Depth-Velocity Distribution in Lower Granite Reservoir 122
17.2.10. Development of the ADH Two-dimensional Model 122
17.2.11. Discharge and Stage for the Depth and Velocity Analysis 123
17.2.12. Model Calibration 128
17.2.13. Depth and Velocity Grids 128
18. Fire, Climate Variation and Sediment Yield 134
18.1. Watershed Characterization for Sediment Yield Modeling 137
18.1.14. Digital Elevation Data 137
18.1.15. Land Cover Data 137
18.1.16. Surface Soils Data 145
18.2. Meteorology and Climate Projections 147
Meteorological Stations 147
18.2.17. Climate Projections 149
18.3. Wildfire Area in the Lower Granite Sediment Yield Watershed 151
18.3.18. Historic Fire Perimeters 151
18.3.19. Future Fire Potential 157
18.4. Selection of a Sediment Yield Model 163

18.5. Sediment Yield Subbasin Models 164
18.5.1. Salmon River at Whitebird Subbasin SWAT model 165
18.5.2. Selway River Subbasin SWAT model 170
18.5.3. Potlatch River Subbasin SWAT Model 171
18.5.4. Other Subbasin SWAT Models 173
18.6. Effect of Increased Fire Area in the Salmon River Basin 173
18.7. Effect of Climate at Year 2060 on Sediment Yield 175

List of Figures

Figure 1. Bathymetry survey area May 2011. 13
Figure 2. September 2011 bathymetry Snake RM 117 at dredge material disposal site. 14
Figure 3. Bathymetry survey area September 2010. 15
Figure 4. Updated historic water surface elevation estimates at the confluence during the Standard Project Flood. 17
Figure 5. Cross section locations for calibrated fixed-bed HEC-RAS model. 19
Figure 6. Lower Granite Reservoir stage and discharge 26 May 2011. 20
Figure 7. May 17, 2011 highwater marks measured by the City of Lewiston, ID. 20
Figure 8. Calibrated 17 May 2011 water surface profile of the Clearwater River. 21
Figure 9. Calibrated 17 May 2011 water surface profile of the Snake River. 21
Figure 10. Daily average discharge in Lower Granite Reservoir 2009-2011. 23
Figure 11. Bedforms at the confluence September 2009. 24
Figure 12. Bedforms at the confluence September 2010. 25
Figure 13. Bedforms at the confluence 26 May 2011. 25
Figure 14. Bedforms at the confluence September 2011. 26
Figure 15. Bedforms at the Port of Clarkston September 2009. 27
Figure 16. Bedforms at the Port of Clarkston 26 May 2011. 27
Figure 17. Bedforms at the Port of Clarkston September 2011. 28
Figure 18. Bedforms at the Port of Wilma September 2009. 29
Figure 19. Bedforms at the Port of Wilma 26 May 2011. 29
Figure 20. Bedforms at the Port of Wilma September 2011. 30
Figure 21. Bedforms near Silcott September 2009. 31
Figure 22. Bedforms near Silcott 26 May 2011. 31
Figure 23. Bedforms near Silcott September 2011. 32
Figure 24. Bedforms below Silcott September 2011. 32
Figure 25. Bedforms near RM 128.5 September 2011. 33
Figure 26. Bedforms Snake River near above the confluence September 2009. 34
Figure 27. Bedforms Snake River near above the confluence May 2011. 35
Figure 28. Bedforms Snake River near above the confluence September 2011. 35
Figure 29. Dune profile transect lines at the confluence. 38

Figure 30. Comparison of September 2009 and May 2011 dune profiles at transect A. 38
Figure 31. Comparison of September 2009 and May 2011 dune profiles at transect B. 39
Figure 32. Comparison of September 2009 and May 2011 dune profiles at transect C. 39
Figure 33. Fourier analysis of September 2009 dune profile at confluence transect line A. 40
Figure 34. Fourier analysis of May 2011 dune profile at confluence transect line A. 40
Figure 35. Fourier analysis of Sep 2011 dune profile at confluence transect line A. 41
Figure 36. Comparison of September 2009 and May 2011 amplitude coefficients for dune profiles at transect A at the confluence. 41
Figure 37. Trend of September 2009 and May 2011 dune profile amplitude coefficients at confluence transect line A. 42
Figure 38. Trend of September 2009 and May 2011 dune profile amplitude coefficients at confluence transect line B. 42
Figure 39. Trend of September 2009 and May 2011 dune profile amplitude coefficients at confluence transect line C. 43
Figure 40. Dune profile transect lines in the Clearwater River turning basin. 44
Figure 41. Dune profiles September 2009 through 2011 in the Clearwater River turning basin at transect A. 44
Figure 42. Fourier amplitude coefficient trends for September 2009, September 2010 and May 2011 in the Clearwater River turning basin at transect A. 45
Figure 43. Dune profiles 2009 through 2011 in the Clearwater River turning basin at transect B. 45
Figure 44. Fourier amplitude coefficient trends for September 2009, September 2010 and May 2011 in the Clearwater River turning basin at transect B. 46
Figure 45. Dune profile transect lines at the Port of Clarkston. 47
Figure 46. Dune profiles for September 2009 and May 2011 at the Port of Clarkston transect A. 48
Figure 47. Fourier amplitude coefficient trends for September 2009 and May 2011 at the Port of Clarkston at transect A. 48
Figure 48. Dune profiles for September 2009 and May 2011 at the Port of Clarkston transect B. 49
Figure 49. Fourier amplitude coefficient trends for September 2009 and May 2011 at the Port of Clarkston at transect B. 49
Figure 50. Dune profiles for September 2009 and May 2011 at the Port of Clarkston transect C. 50
Figure 51. Fourier amplitude coefficient trends for September 2009 and May 2011 at the Port of Clarkston at transect C. 50
Figure 52. Dune profile transect line at Red Wolf. 51
Figure 53. Dune profiles for September 2009 and May 2011 at Red Wolf transect A. 52
Figure 54. Fourier amplitude coefficient trends for September 2009 and May 2011 at Red Wolf transect A. 52
Figure 55. Dune profile transect lines at the Port of Wilma. 53
Figure 56. Dune profiles for September 2009 and May 2011 at the Port of Wilma transect A. 54
Figure 57. Fourier amplitude coefficient trends for September 2009 and May 2011 at the Port of Wilma at transect A. 54
Figure 58. Dune profiles for September 2009 and May 2011 at Port of Wilma transect B. 55

Figure 59. Fourier amplitude coefficient trends for September 2009 and May 2011 at Port of Wilma at transect B. 55
Figure 60. Dune profiles for September 2009 and May 2011 at Port of Wilma transect C. 56
Figure 61. Fourier amplitude coefficient trends for September 2009 and May 2011 at the Port of Wilma at transect C. 56
Figure 62. Dune profile transect line at Silcott. 57
Figure 63. Dune profiles for September 2009 and May 2011 at Silcott transect C. 58
Figure 64. Fourier amplitude coefficient trends for September 2009 and May 2011 at Silcott at transect C. 58
Figure 65. Dune profile transect line in the Snake River near the Interstate Bridge. 59
Figure 66. Dune profiles for September 2009 and May 2011 at Snake River transect A. 60
Figure 67. Fourier amplitude coefficient trends for September 2009 and May 2011 at Snake River transect A. 60
Figure 68. Dune profiles for September 2009 and May 2011 at Snake River transect B. 61
Figure 69. Fourier amplitude coefficient trends for September 2009 and May 2011 at Snake River transect B. 61
Figure 70. Bathymetry difference September 2010 - September 2009 at the confluence. 63
Figure 71. Bathymetry difference May 2011 - September 2010 at the confluence. 63
Figure 72. Bathymetry difference September 2011 - May 2010 at the confluence. 64
Figure 73. Bathymetry difference September 2011- September 2009 at the confluence. 64
Figure 74. Bathymetry difference September 2010- September 2009 at the Port of Clarkston. 65
Figure 75. Bathymetry difference May 2011- September 2010 at the Port of Clarkston. 66
Figure 76. Bathymetry difference September 2011 - September 2009 at the Port of Clarkston. 66
Figure 77. Bathymetry difference September 2010- September 2009 at the Clearwater turning basin. 67
Figure 78. Bathymetry difference May 2011 - September 2010 at the Clearwater turning basin. 68
Figure 79. Bathymetry difference September 2011 - September 2010 at the Clearwater turning basin. 68
Figure 80. Bathymetry difference September 2011 - September 2009 at the Clearwater turning basin. 69
Figure 81. Bathymetry difference May 2011- September 2009, Snake River at upstream end of levee. 70
Figure 82. Bathymetry difference September 2011- September 2009, Snake River at upstream end of levee. 70
Figure 83. Bathymetry difference May 2011- September 2009 at Interstate Bridge. 71
Figure 84. Bathymetry difference September 2011- September 2009 at Interstate Bridge. 71
Figure 85. Bathymetry difference May 2011- September 2009 at Red Wolf Bridge. 72
Figure 86. Bathymetry difference September 2011- September 2009 at Red Wolf Bridge. 73
Figure 87. Bathymetry difference May 2011- September 2009 at the Port of Wilma (1). 74
Figure 88. Bathymetry difference September 2011- September 2009 at the Port of Wilma (1). 74
Figure 89. Bathymetry difference May 2011- September 2009 at the Port of Wilma (2). 75
Figure 90. Bathymetry difference September 2011- September 2009 at the Port of Wilma (2). 75
Figure 91. Bathymetry difference May 2011- September 2009 below Wilma. 76
Figure 92. Bathymetry difference May 2011- September 2009 below Wilma. 77
Figure 93. Bathymetry difference May 2011 - September 2009 above Silcott. 77
Figure 94. Bathymetry difference September 2011 - September 2009 above Silcott. 78

Figure 95. Bathymetry difference May 2011- September 2009 at upper Silcott Island. 79
Figure 96. Bathymetry difference September 2011- September 2009 at upper Silcott Island. 79
Figure 97. Bathymetry difference May 2011 - September 2009 at Lower Silcott Island. 80
Figure 98. Bathymetry difference September 2011 - September 2009 at Lower Silcott Island. 80
Figure 99. Bed-load measurement site above Red Wolf Bridge at Snake RM 137.6. 83
Figure 100. Inflow hydrographs for May 2011 sediment transport simulation. 83
Figure 101. Measured sand wave bed-load at Snake RM 137.6. 84
Figure 102. Comparison of simulated sediment rating curves with measured sand wave bed-load transport for May 2011. 84
Figure 103. Comparison of the Toffaleti transport function rating curve with measured sand wave bed-load transport after partial model calibration. 85
Figure 104. Lower Granite Reservoir discharge and forebay elevation 2009-2011. 86
Figure 105. Simulated and actual average bed change in Lower Granite Reservoir 2009-2011. 87
Figure 106. Comparison of simulated sediment rating curves for 2009-2011 with measured sand wave bed-load transport. 87
Figure 107. Domain of the ADH model of Lower Granite Reservoir. 91
Figure 108. ADH model mesh near the confluence. 91
Figure 109. 3D view of ADH Model mesh near the confluence. 92
Figure 110. 3D view of ADH Model mesh near Silcott Island. 92
Figure 111. Shields stress computed with ADH model for discharge on 26 May 2011. 93
Figure 112. Bed shear stress computed with ADH model for 1-percent chance discharge. 94
Figure 113. Stream power computed with ADH model for SPF discharge. 94
Figure 114. Brownlie bed regime for the 1-percent exceedance discharge. 96
Figure 115. Brownlie bed regime for the SPF discharge. 96
Figure 116. Karim bed regime for the 1-percent exceedance discharge. 98
Figure 117. Karim bed regime for the SPF discharge. 98
Figure 118. Simons and Richardson bed regime for the 1-percent chance discharge. 99
Figure 119. Simons and Richardson bed regime for the SPF discharge. 100
Figure 120. Sand bedforms in the Lower Columbia River at the Port of Kalama. 101
Figure 121. Analysis of bed regime in the Lower Columbia River at the Port of Kalama. 101
Figure 122. Bed displacement estimated with an ADH model during the SPF. 102
Figure 123. Deposition in the navigation channel at the confluence in September 2009. 106
Figure 124. Deposition in the navigation channel at the confluence in September 2010. 106
Figure 125. Deposition in the navigation channel at the confluence in May 2011. 107
Figure 126. Deposition in the navigation channel at the confluence in September 2011. 107
Figure 127. Stable channel cross section at Clearwater RM 1.66. 110
Figure 128. Stable channel cross section at Clearwater RM 1.99. 110
Figure 129. Simulation of 50-year effective channel depth in the Clearwater turning basin. 111
Figure 130. Simulation of 2060 mean active bed elevation in the Clearwater turning basin. 111
Figure 131. Simulation of 50-year effective channel depth at the Port of Clarkston. 112
Figure 132. Simulation of 2060 mean active bed elevation in Snake River at confluence. 112
Figure 133. WY 2011 inflow hydrograph for Lower Granite Reservoir. 114

Figure 134. WY 2007 inflow hydrograph for Lower Granite Reservoir. 115
Figure 135. Calibration of the September 2011 HEC-RAS model. 115
Figure 136. Steady flow travel time in Lower Granite Reservoir for 17 May 2011. 116
Figure 137. Steady flow travel time rating curve for reach RM 139.25 to 107.43. 117
Figure 138. Flow-duration travel time rating curve for reach RM 139.25 to 107.43. 117
Figure 139. Unsteady flow reach transit times for Lower Granite Reservoir in WY 2011. 119
Figure 140. Unsteady flow reach transit times for Lower Granite Reservoir in WY 2007. 120
Figure 141. Unsteady flow reach transit times for Lower Granite Reservoir in WY 2011 with alternative forebay operations. 120
Figure 142. Reach transit time frequency curve for Lower Granite Reservoir in WY 2011 and WY 2007. 121
Figure 143. September 2011 bathymetry near Silcott Island. 124
Figure 144. September 2011 bathymetry and USGS 2010 shallow water bed elevation lines. 125
Figure 145. ADH 100 ft nominal mesh resolution. 125
Figure 146. ADH 2011 model mesh in Lower Granite Reservoir near Silcott Island. 126
Figure 147. ADH 2011 model mesh at the confluence of the Snake and Clearwater Rivers. 126
Figure 148. WY 2009-2011 stage and discharge hydrographs for Lower Granite Reservoir. 127
Figure 149. Comparison of ADH and HEC-RAS water surface profiles for Lower Granite Reservoir. 129
Figure 150. Comparison of ADH and HEC-RAS velocity profiles for Lower Granite Reservoir. 130
Figure 151. May 2011 ADCP transects at the confluence. 130
Figure 152. Comparison of ADH and ADCP velocities at Snake RM 138.9. 131
Figure 153. Comparison of ADH and ADCP velocities at Clearwater RM 0.2. 131
Figure 154. Comparison of ADH and ADCP velocities at Snake RM 138.3. 132
Figure 155. ADH depth grid for a discharge of 200 kcfs at Snake RM 128. 132
Figure 156. ADH velocity grid for a discharge of 200 kcfs at Snake RM 128. 133
Figure 157. 2001 National Land Cover Dataset of the Lower Granite sediment yield watershed. 139
Figure 158. 2006 National Land Cover Dataset of the Lower Granite sediment yield watershed. 139
Figure 159. 2006 NLCD grid for the Potlatch River basin. 141
Figure 160. NASS 2010 crop data layer for the Potlatch River basin. 142
Figure 161. Landfire Existing Vegetation Type (EVT) grid for the Selway River basin. 144
Figure 162. Landfire Existing Vegetation Cover (EVC) grid for the Salmon River basin. 144
Figure 163. 2011 Landsat 5 visible near-infrared images and recent fires in the Lower Granite sediment yield watershed. 146
Figure 164. 3 September 2011 MODIS imagery of active fires in the Lower Granite sediment yield watershed. 147
Figure 165. Meteorological and climate stations in the lower Snake and Clearwater River basins. 149
Figure 166. GFDL year 2060 February precipitation grid for the Pacific Northwest. 150
Figure 167. GFDL year 2060 February maximum temperature grid for the Pacific Northwest. 151
Figure 168. 1971-1980 fire perimeter polygons for the Lower Granite Reservoir sediment yield watershed. 153
Figure 169. 1981-1990 fire perimeter polygons for the Lower Granite Reservoir sediment yield watershed. 154

Figure 170. 1991-2000 fire perimeter polygons for the Lower Granite Reservoir sediment yield watershed. 154
Figure 171. 2001-2010 fire perimeter polygons for the Lower Granite Reservoir sediment yield watershed. 155
Figure 172. Chart of wildfire area in the Lower Granite Reservoir sediment yield watershed. 155
Figure 173. 1971-2010 annual mapped fire area in the Lower Granite sediment yield watershed. 156
Figure 174. 1889-2010 annual mapped fire area in the Lower Granite sediment yield watershed. 156
Figure 175. Relationship of difference in discharge and mapped fire area. 157
Figure 176. Recurrent fire areas decades 1991-2000 and 2001-2010. 159
Figure 177. 5 September 1994 Landsat 5 image of active fire areas. 159
Figure 178. 23 July 2007 Landsat 5 image of active fire areas. 160
Figure 179. 2007 fire perimeter polygons for the Lower Granite Reservoir sediment yield watershed. 160
Figure 180. 1971-2010 combined fire perimeter polygons for the Lower Granite Reservoir sediment yield watershed. 161
Figure 181. Fire Regime Group (FRG) with fire return period less than 35 years. 161
Figure 182. Relative likelihood of wildfire in the Lower Granite sediment yield watershed from data by of fire by Parisien et al. (2012). 162
Figure 183. Potential fire erosion index for Salmon River basin. 162
Figure 184. 2012 Wildfires in the lower Snake River watershed. 163
Figure 185. Subbasins of the Lower Granite Basin sediment yield model. 165
Figure 186. Salmon River at Whitebird SWAT model catchments without wildfire areas. 168
Figure 187. Salmon River at Whitebird SWAT model catchments with wildfire areas. 169
Figure 188. Selway River subbasin SWAT model catchments without wildfire areas. 170
Figure 189. Selway River subbasin SWAT model catchments with wildfire areas. 171
Figure 190. Potlatch River subbasin SWAT model catchments. 172
Figure 191. Salmon River at Whitebird SWAT model catchments with potential wildfire areas. 174

List of Tables

Table 1. Comparison of computed SPF water surface elevations at the confluence. 22
Table 2. Discharges in Lower Granite Reservoir when bedforms in bathymetry were formed. 23
Table 3. Annual peak steady flow discharges for FDA risk analysis. 95
Table 4. Unsteady flow travel time computation. 118
Table 5. Summary of reach transit times in Lower Granite Reservoir. 121
Table 6. Discharges for Lower Granite Reservor depth-velocity analysis. 127
Table 7. Mass balance and watershed sediment yield for Lower Granite Reservoir WY 2009-2011. 136
Table 8. Land cover types and proportional areas in the Lower Granite sediment yield watershed. 140
Table 9. Change between NLCD 2001 and NLCD 2006. 140
Table 10. Land cover areas in the SWAT model of Salmon River at Whitebird. 168
Table 11. Land cover areas in the SWAT model of the Potlatch River basin. 172
Table 12. Summary of other initial SWAT subbasins models in the lower Snake and Clearwater River basin. 173
Table 13. Summary of year 2060 GFDL climate change projection for the lower Snake and Clearwater River Basin. 175

THIS PAGE INTENTIONALLY LEFT BLANK

15. Evolution of Sand Bedforms and Sedimentation in Navigation Channels

Sand bedforms alter the flow resistance of Lower Granite Reservoir and affect flood stage at the confluence of the Snake and Clearwater Rivers. As flows increase to extreme discharges that pose the most flood risk, the channel of Lower Granite Reservoir becomes highly mobile and likely will transition from lower bed regime, characterized by large dunes and greater roughness, to upper bed regime which offers substantially less hydraulic resistance as bedforms washout and flatten. Whether or not the bed transitions to upper regime is important because if it does, the flood stage elevation at the confluence will be lower and the risk of overtopping the levees in Lewiston will be less. The point of transition from lower to upper bed regime is indefinite in discharge and location, and cannot be determined precisely by current sediment transport theory and computational methods. The flood risk analysis described in the previous sections incorporated the uncertainty due to bed regime by evaluating flood risk for both bed conditions. It was found that while flood risk was acceptably low for both bed regimes in the year-2009 channel, persistence of lower bed regime in the year-2060 channel would increase flood risk to unacceptable levels. All analysis performed to this point indicates the likelihood of a transition to upper regime during extreme discharges, but it also must be recognized that a transition to upper regime has not been observed or documented in historic data for Lower Granite Reservoir. Further studies of bedforms and bedload transport are needed to better define the uncertainty of the transition between bed regimes in Lower Granite Reservoir.

With the assistance of the USACE Coastal and Hydraulic Laboratory, Engineering Research and Development Center (CHL-ERDC), an investigation of sand wave development and in-reservoir bedload transport was begun in May 2011. High resolution bathymetry of Lower Granite Reservoir was acquired during peak flows of May 2011 that captured the state of sand bedforms as they moved through the reservoir. Bedforms near the confluence in the May 2011 bathymetry were generally smaller than those observed in bathymetry obtained during the low flow in 2009, 2010 and 2011 indicating that sand bedforms had diminished during high flow and that the bed was beginning to transition to upper bed regime. This apparent transition was occurring at discharges less than empirical methods for equilibrium channels predict, which suggests that the conditions of partial disequilibrium sediment transport that prevail in Lower Granite Reservoir may promote an early transition in bed regime.

Though not widely investigated, apparent early transitions in bed regime have been observed in other studies[1].

The mobility of the bed in Lower Granite Reservoir and its effect are examined with six approaches 1) development of calibrated hydraulic models with bathymetry acquired during the high discharge of May 2011, 2) comparison of hillshade maps made from the September 2009, September 2010 and May 2011 bathymetries, 3) Fourier analysis of dune profile transects, 4) comparison of bathymetry difference maps, 5) sediment transport simulation during the peak of the May 2011 discharge and from 2009 to 2011, and 6) spatial analysis of bed regime with several empirical relationships.

15.1. Bathymetry Acquisition and Processing

Bathymetry of the upper reach of Lower Granite Reservoir was acquired by the USACE Engineering Research and Development Center (ERDC) Coastal and Hydraulics Laboratory in late May 2011 and in August and September 2011. High resolution multibeam bathymetry was acquired with a 250 KHz Geoswath echo sounder installed in a 24 foot SeaArk survey boat. The echosounder is RTK GPS positioned and compensated for pitch, heave and roll. Horizontal accuracy is stated as +/- 2 cm and vertical resolution of bathymetric elevations is approximately 3 cm in 50 meter of water[2]. The May 2011 survey area included the Snake River from river mile 130 to river mile 141 and on the Clearwater River from the confluence to river mile 0.59 (Figure 1). Sediment transport measurements and acoustic Doppler velocity measurements were also obtained at selected locations in a second vessel. Multibeam bathymetry of the entire reservoir was acquired during low flow in August and September. The bathymetry depicts details of sediment features in the lower reservoir such as the dredge material placement site (Knoxway Canyon) near Snake RM 117 in Figure 2.

Echosounder data was processed with Hypack© hydrographic survey software. Bathymetry point data was processed to a resolution of 2 feet. Triangulated irregular network (TIN) datasets were generated from the point data with ESRI Arcmap 3D analyst software. To be comparable with previous bathymetry datasets, the 2011 TIN datasets were converted to ESRI grids that have a horizontal resolution of 3 feet. Comparisons between channel bed profiles extracted from the TIN datasets and grids showed that re-sampling to a 3 foot grid did not significantly change the shape and

[1] Prent, M. T. H., and E. J. Hickin.(2001). Annual regime of bedforms, roughness and flow resistance, Lillooet River, British Columbia, BC. Geomorphology 41(4):369-390.

[2] Abraham,D., Pratt, T., Sharp, J. (2010). "Measuring bedload transport on the Missouri River using time sequenced bathymetric data", 2nd Joint Federal Interagency Conference, Las Vegas, NV, June 27-July 1, 2010.

dimensions of the sand dune bedforms. Hydraulic model geometries and bed change grids were generated from the 3-foot resolution grids.

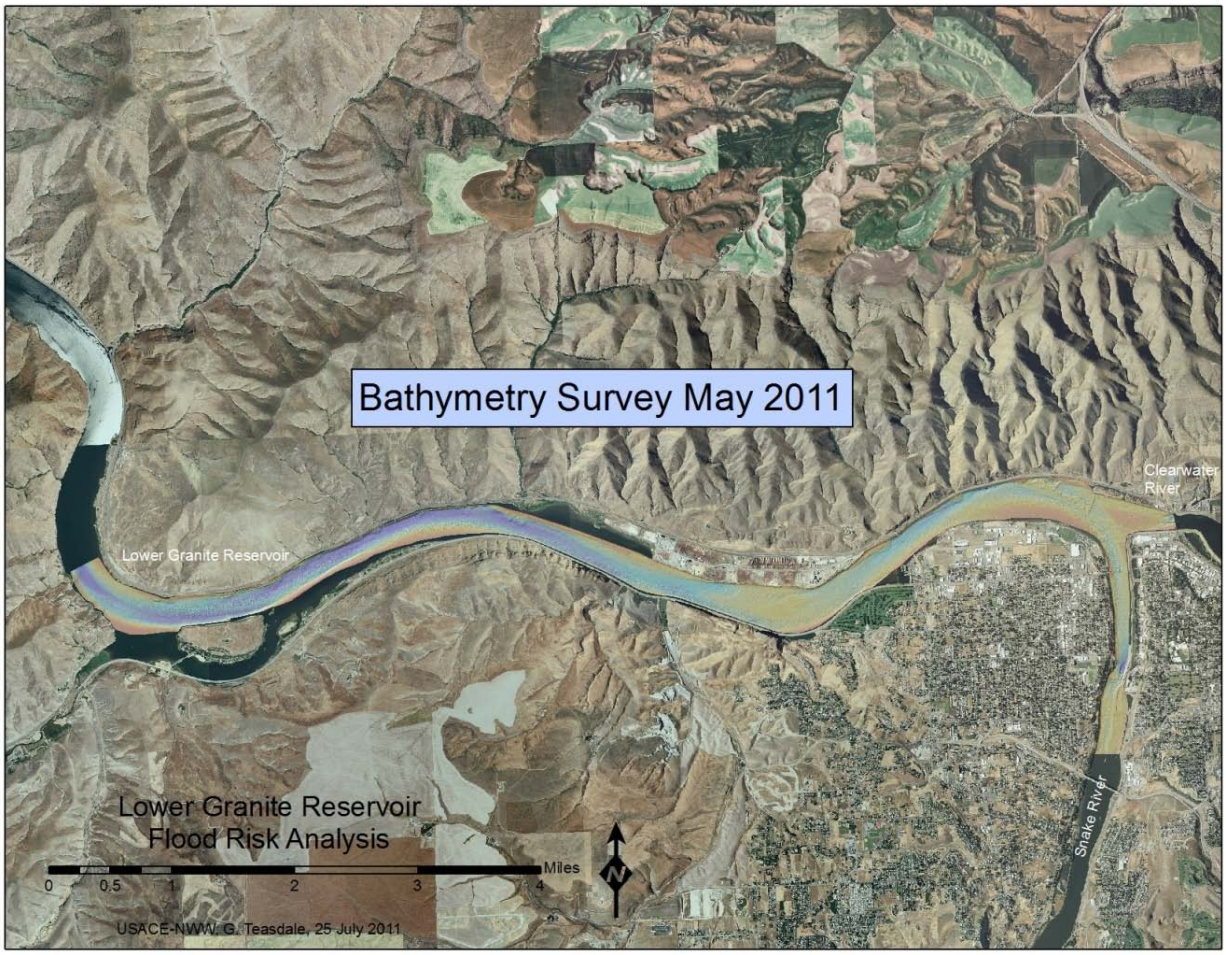


Figure 1. Bathymetry survey area May 2011.

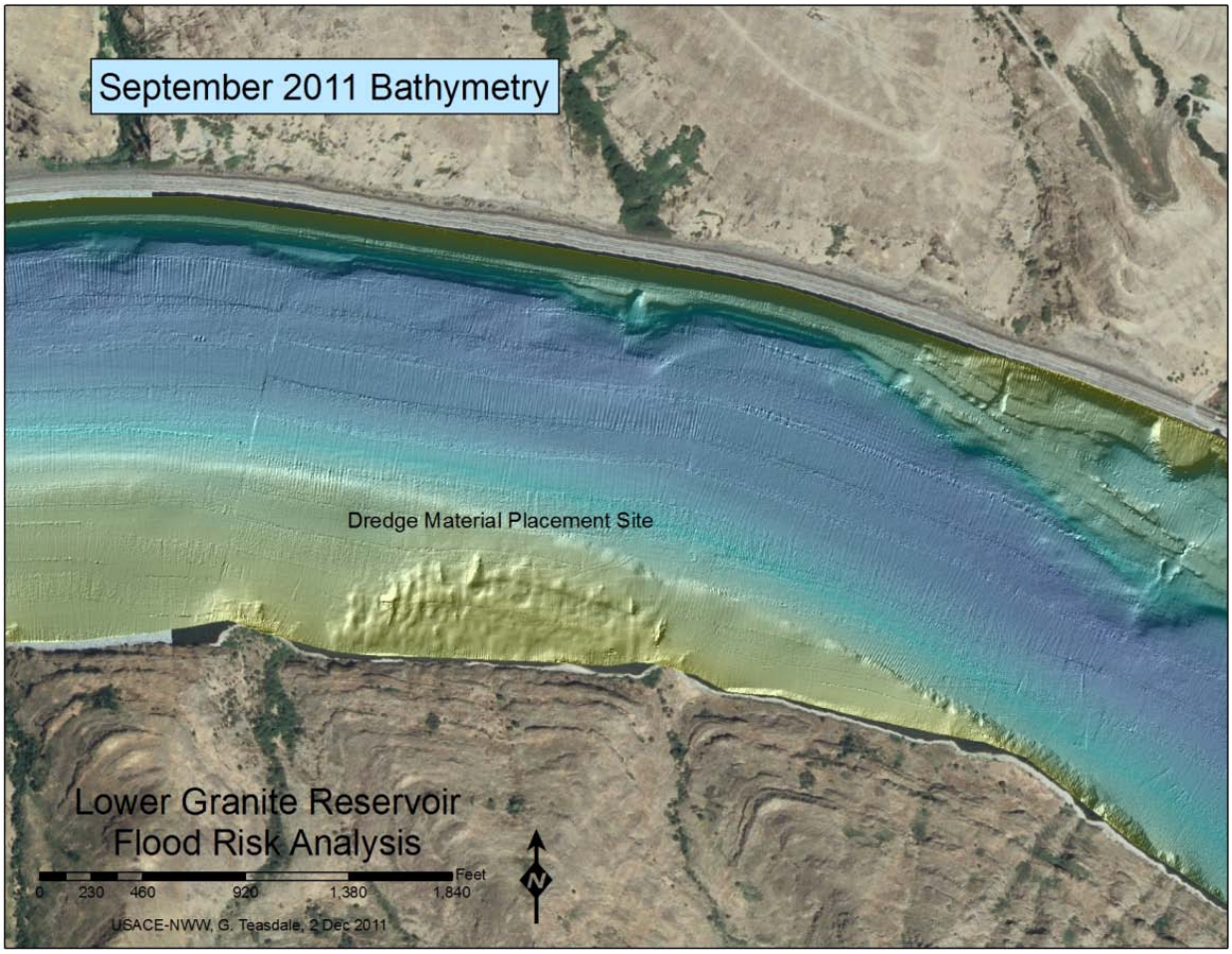


Figure 2. September 2011 bathymetry Snake RM 117 at dredge material disposal site.

Bathymetry of the confluence area was acquired by a hydrographic survey contractor for USACE in late summer and early fall 2010 for the annual navigation channel condition survey and sediment range survey. The equipment and methods are described in contract submittal documents[3] and are of similar accuracy as the ERDC bathymetry. Multi-beam echosounding bathymetry was acquired from mile 137.7 to 139.6 on the Snake River and from mile 0 to 1.9 on the Clearwater River (Figure 3). Single beam echosounding cross sections were also acquired at the historic sediment ranges throughout Lower Granite Reservoir.

[3] NWW (2011). Contract W912EF-10-D-0002, Terresond, Seattle, WA.

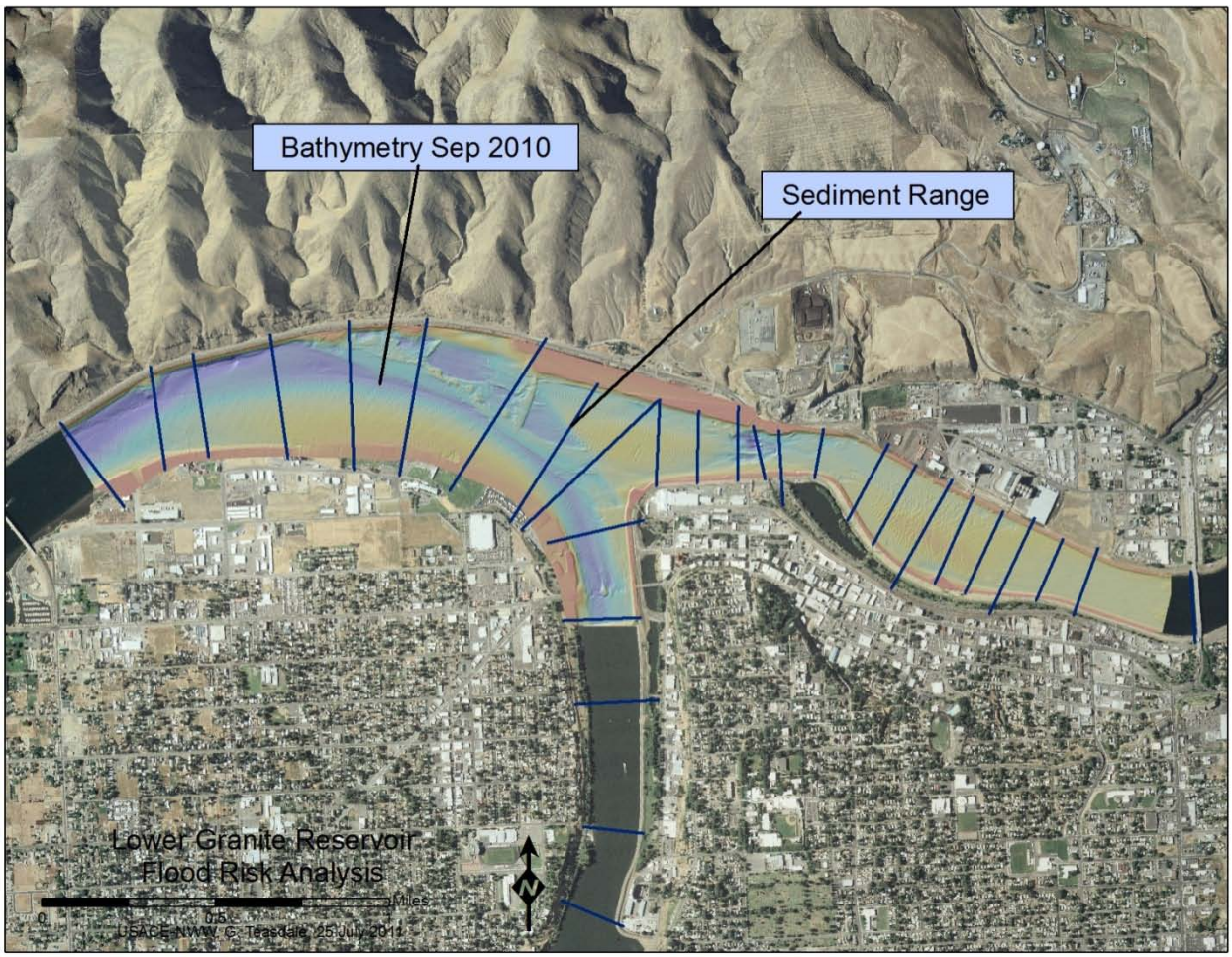


Figure 3. Bathymetry survey area September 2010.

15.2. Fixed-bed One-dimensional Sediment Range Hydraulic Model

One dimensional HEC-RAS and two dimensional ADH models of Lower Granite Reservoir were developed from the new bathymetry. The hydraulic models developed for the flood risk analysis discussed in the previous sections were developed from the 2009 bathymetry acquired by USGS and sediment range cross sections in the lower part of Lower Granite Reservoir. The new hydraulic models developed from the May and September bathymetry acquired by ERDC provide a check on the previous model results and show the changes in hydraulic performance caused by the inflow of a substantial amount of sediment during 2011. In particular, the cross sectional area of the channel in the May 2011 bathymetry provides a more realistic representation of channel conveyance during high discharge without the need to estimate effect of bed mobility. Calibration of hydraulic models developed from this functionally mobile geometry provided a best-estimate of the flow resistance (Manning's *n*) of the active channel. It is shown below that computed water surface profiles at the confluence for extreme discharges based on the May 2011 bathymetry are less than those based on

the static 2009 and 2010 bathymetry. The new hydraulic modeling does not invalidate the previous modeling for the flood risk analysis, but is a significant extension of the previous work that also demonstrates the ongoing process of periodic reevaluation of the hydraulic performance of the Lewiston Levee system under the Programmatic Sediment Management Plan.

Fixed-bed one-dimensional HEC-RAS hydraulic models were developed with sediment range cross sections derived from the 2010 condition survey and 2011 ERDC bathymetry. These models implement the historical fixed-bed analysis methods used in previous studies and were developed with procedures described in Section 3.7. Water surface profiles were computed for the Standard Project Flood (SPF) discharge assuming the relatively high (as compared to calibrated values) Manning's *n* roughness values adopted in the historic fixed bed modeling. The 2010 model geometry downstream of Snake River mile 137.7 was developed from sediment ranges measured in 2010 and the multibeam bathymetry through the condition survey area. The 2009 sediment range cross sections were used in the 2010 model geometries upstream of the 2010 condition survey area. Cross section elevation data at the sediment range locations for the 2011 model geometry were extracted from the 2011 bathymetry through 2011 survey area and the 2010 sediment range cross sections were used below River Mile 130. The 2009 sediment range cross sections above the 2011 survey area were used in the 2011 model geometry. Use of 2009 cross sections above the confluence in the 2010 and 2011 model geometries has no effect on the water surface elevation at the confluence because hydraulic control is governed by the Lower Granite forebay elevation for the M1 backwater surface profile.

The SPF water surface elevations at Clearwater River Mile 0.22 (Snake River Mile 139.29) from the historic and current hydraulic models are plotted in Figure 4 and is similar to the plot in Section 3. The computed water surface elevation at the confluence increased from 2009 to 2011 from 744.43 to 744.78. It is important to note that the 2009 and 2010 bathymetry was collected during low discharge when the channel bed was immobile. It is shown below that the conveyance of the channel near the confluence was greater in the may 2011 model geometry when the bed was mobile. This would reduce the water surface elevation at the confluence even if the Manning's *n* is held constant. Water surfaces for the SPF discharge computed with the calibrated models are also plotted in Figure 3. The 2011 SPF water surface elevation at the confluence is about 0.6 ft less with the high discharge geometry than with the low flow geometry.

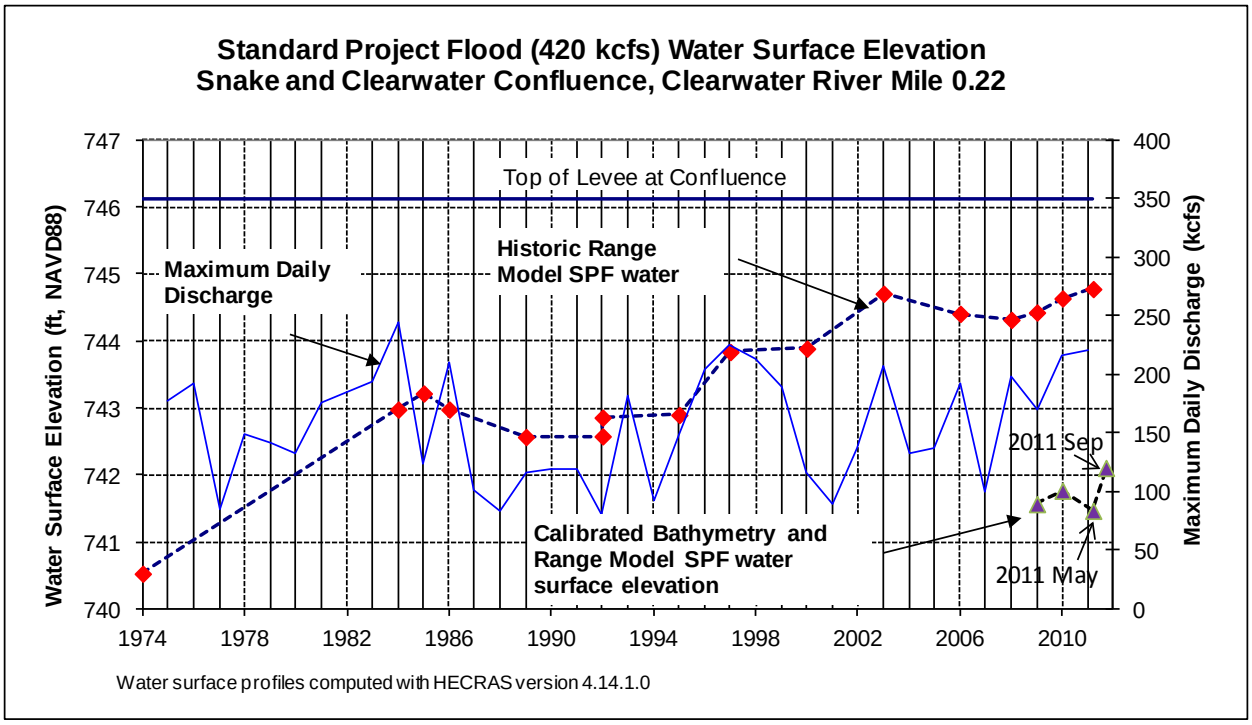


Figure 4. Updated historic water surface elevation estimates at the confluence during the Standard Project Flood.

15.3. Calibrated HEC-RAS One-dimensional Hydraulic Model

Fixed-bed one-dimensional HEC-RAS hydraulic models for 2010 and 2011 were developed with the more closely spaced cross sections and procedures used in the calibrated hydraulic model employed in the flood risk analysis discussed in Section 3.8. Channel elevation data was derived from the bathymetry datasets as described in the previous section. Overbank cross section data was extracted from the 2010 LiDAR elevation data. To facilitate cross section generation in HEC-GeoRAS, the 2010 LiDAR grid was merged with the 2010 and 2011 bathymetry grids (Figure 5).

The 2010 hydraulic model was calibrated to the high discharge of 8 June 2010 by the procedures described in Section 3.9. Calibrated Manning's *n* values for the 2010 model were not significantly different from those derived for the 2009 calibrated model. The computed water surface elevation at Clearwater RM 0.22 (Snake RM 13.29) for the 8 June 2010 discharge was only 0.06 ft higher for the 2010 model when the unaltered Manning's *n* values from the 2009 model were adopted in the 2010 model.

The May 2011 model was calibrated to the high discharge and confluence stage on 26 May 2011 (Figure 6). Again, the calibrated Manning's *n* values were not significantly different than those in the 2009 model. The computed water surface elevation at Clearwater RM 0.22 for the 26 May 2011 discharge was only 0.07 ft higher

for the 2011 model when the unaltered Manning's *n* values from the 2009 model were adopted in the 2011 model. It is likely that the actual Manning's *n* for the May 2011 channel model is slightly lower than the 2009 (and 2010) values because new sediment accumulation was not measured below RM 130 during the May 2011 survey. New sediment accumulation below RM 130 would slightly decrease the cross section area of the channel in the lower reach of the reservoir, requiring that an offsetting higher values of Manning's *n* be used in calibration to match the water surface elevation at the confluence (because the 2010 cross sections below RM 130 were used in the 2011 model).

Calibration of the May 2011 channel model was checked with high water marks surveyed by the City of Lewiston, Idaho Public Works Department on 17 May 2011 when discharge in the Snake River was 128,000 cfs and discharge on the Clearwater was 66,200 cfs. Elevation of the forebay at Lower Granite was 736.69 ft NAVD88. The City of Lewiston dataset includes 45 high water measurements along the right bank of the Snake River and the left bank of the Clearwater River. Locations of the high water marks along the Lewiston levee system are shown in Figure 7. The close spacing of the high water measurements enabled refined calibration of roughness values between the bridges on the Snake and Clearwater Rivers. The September 2011 channel model was initially calibrated to the 26 May 2011 gage data and refined with the City of Lewiston 17 May 2011 high water marks. The water surface profile generated by the calibrated September 2011 channel model is a good fit of the 17 May high water marks on the Clearwater River (Figure 8) and the Snake River (Figure 9).

The differences between the calibrated Manning's *n* values for the May 2011 channel geometry and the September 2011 channel geometry are not significant, only 0.005 units with the September 2011 channel geometry having a Manning's *n* value of 0.022 throughout the reservoir below the confluence. Manning's *n* values along the Clearwater River were 0.023 below Memorial Bridge at RM 1.99, and then varied from 0.028 to 0.032 above RM 1.99. Manning's *n* values on the Snake River were 0.025 between the confluence and Interstate Bridge at RM 139.6. Above RM 139.6 the *n*-values were 0.026 to RM 145.15 at Asotin. Above Asotin *n*-values were assumed to increase to 0.035, but there was no calibration data to confirm this specification.

The SPF water surface elevation at the confluence was computed with the calibrated 2010 and 2011 HEC-RAS fixed bed models and are compared to the 2009 model results in Table 1. The computed SPF elevation based on the 2010 model is 0.2 ft higher than the SPF elevation computed by the 2009 model. With the May 2011 high flow geometry model, the SPF water surface is negligibly less (0.04 ft) than that computed with the 2009 model and the SPF water surface is 0.5 ft higher for the September 2011 low flow geometry model. The SPF water surfaces based on the

calibrated models are plotted in Figure 4. Minimum freeboard at the confluence is about 4.5 ft based on the calibrated models.

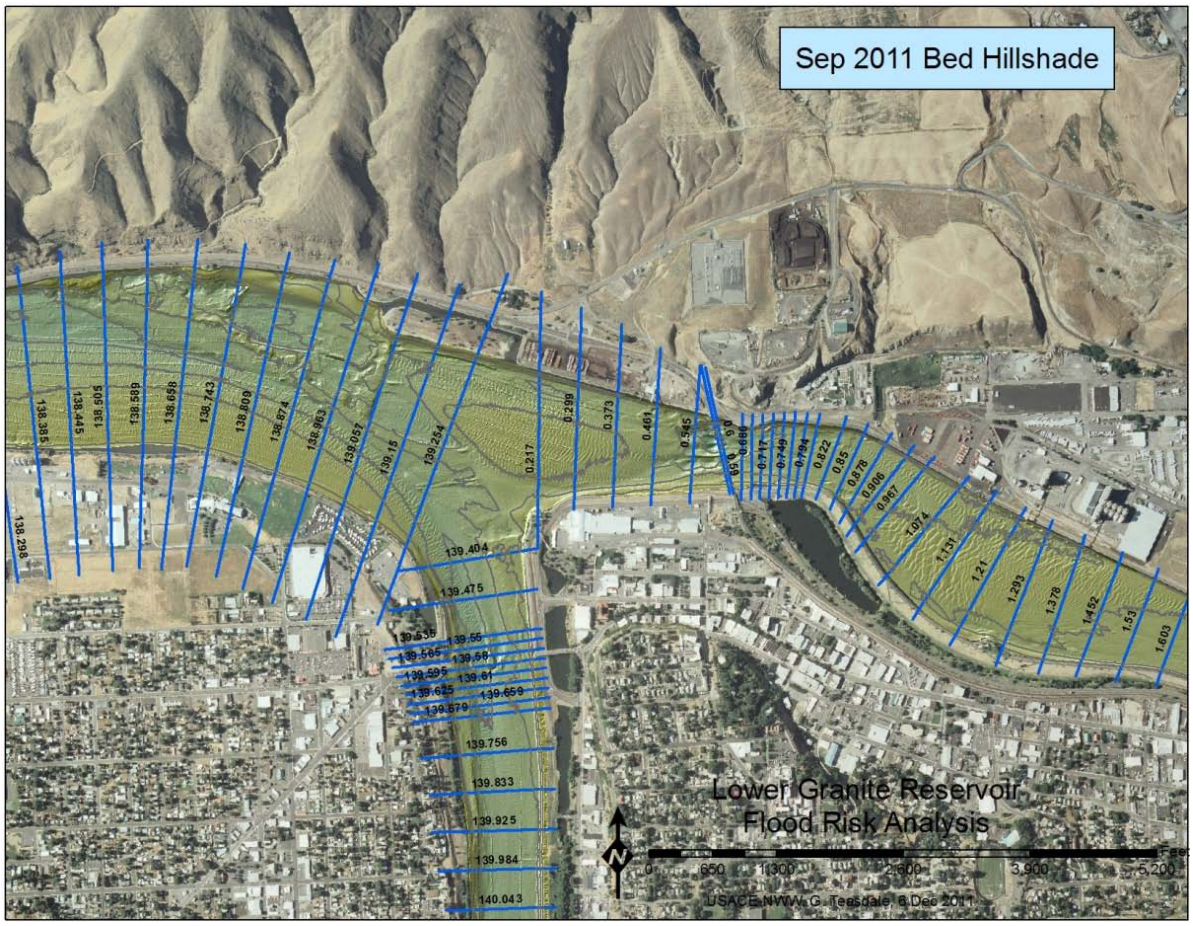


Figure 5. Cross section locations for calibrated fixed-bed HEC-RAS model.

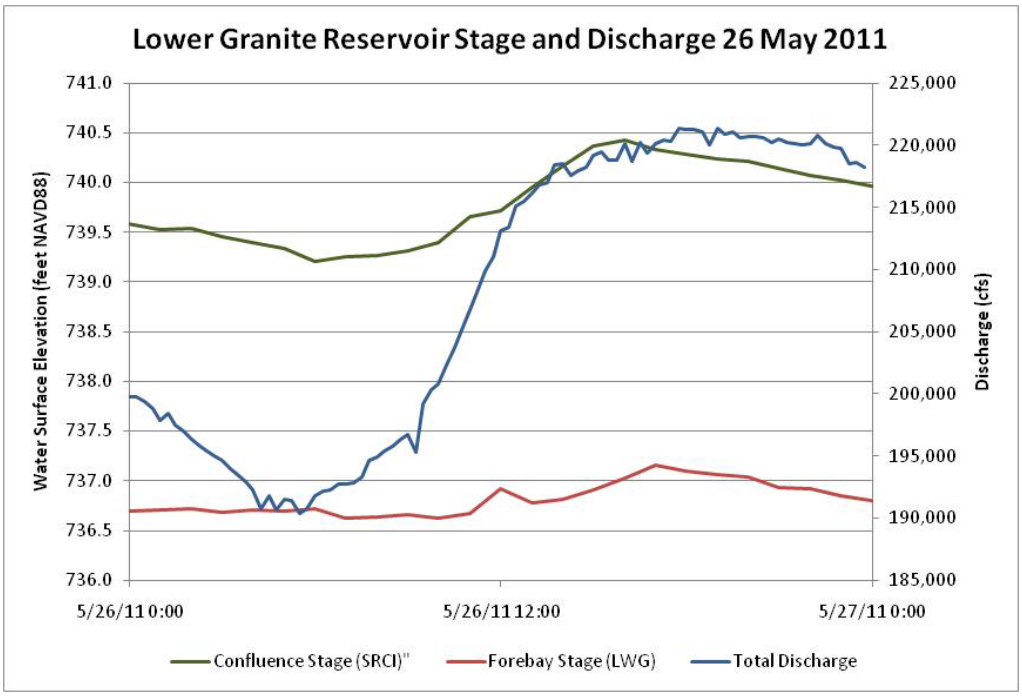


Figure 6. Lower Granite Reservoir stage and discharge 26 May 2011.



Figure 7. May 17, 2011 highwater marks measured by the City of Lewiston, ID.

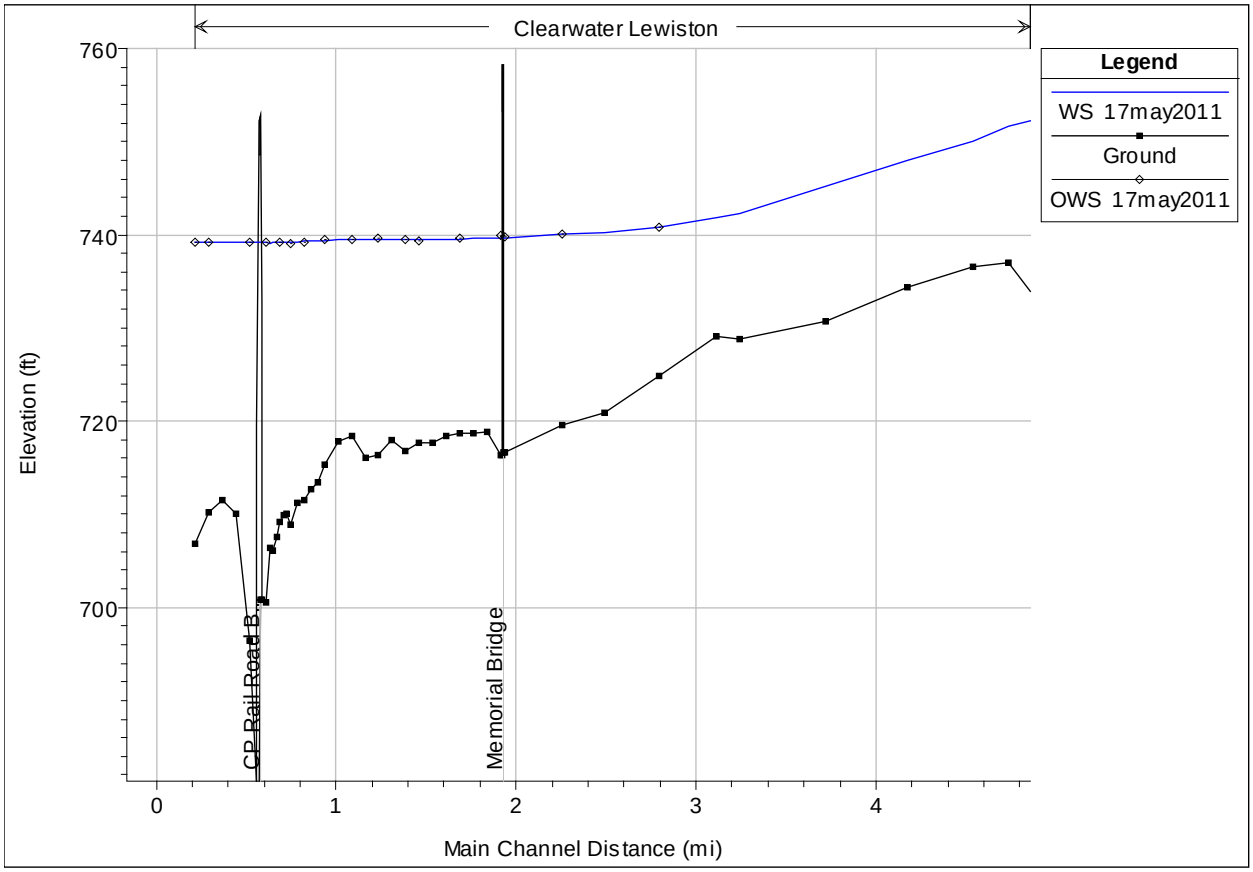


Figure 8. Calibrated 17 May 2011 water surface profile of the Clearwater River.

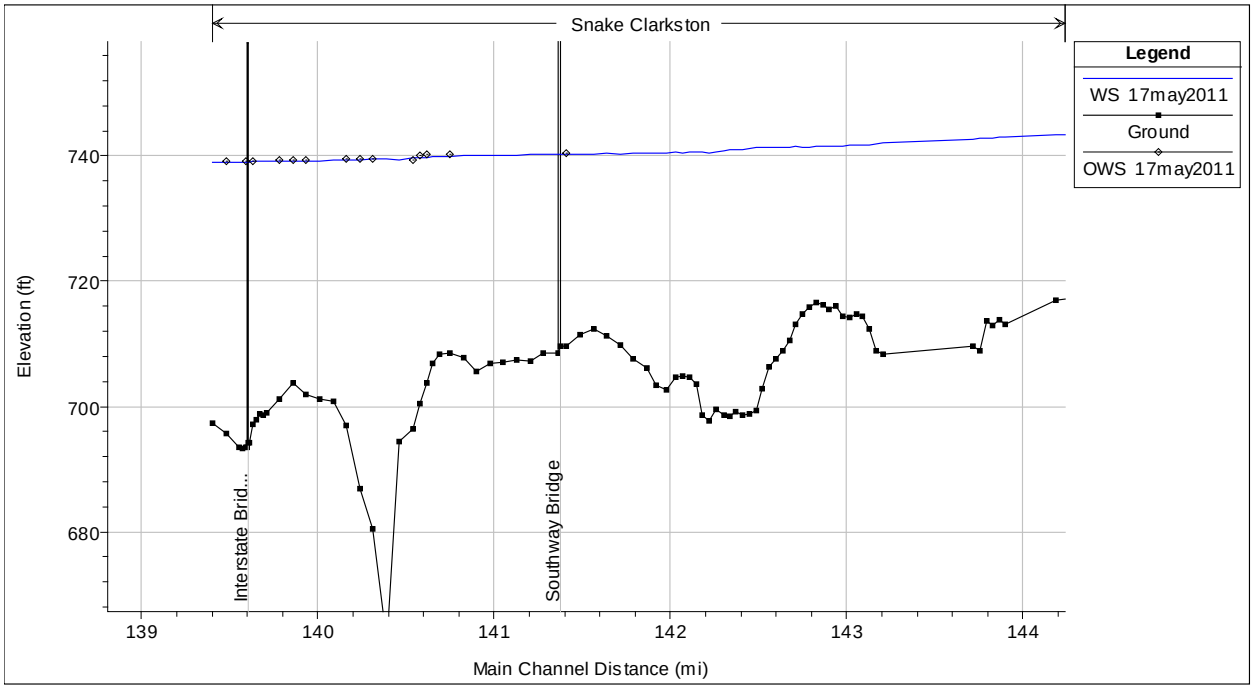


Figure 9. Calibrated 17 May 2011 water surface profile of the Snake River.

Comparison SPF HEC-RAS 2009-2010 Fixed-Bed Water Surface Profile (Calibrated Manning's *n*) - Clearwater River near the Confluence											
				Water Surface		Mean			Levee Elevations		Levee Freeboard	
			Discharge	Elevation	Energy	Velocity			Left	Right	Left	Right
Reach	River Sta	Geometry	cfs	ft NAVD88	Slope	ft/s	Froude No.		ft NAVD88	ft NAVD88	ft	ft
Lewiston	0.217	2009	125,000	741.57	0.000055	3.87	0.14		746.56	758.95	4.99	17.38
Lewiston	0.217	2010	125,000	741.77	0.000052	3.77	0.14		746.56	758.95	4.79	17.18
Lewiston	0.217	2011 May	125,000	741.47	0.000051	3.62	0.14		746.56	758.95	5.09	17.48
Lewiston	0.217	2011 Sep	125,000	742.11	0.000060	3.96	0.15		746.56	758.95	4.45	16.84

Table 1. Comparison of computed SPF water surface elevations at the confluence.

15.4. Hillshade Maps of Bedforms and Bed Change

Bed forms in Lower Granite Reservoir were measured, mapped and compared in the high-resolution bathymetry acquired in 2009, 2010 and 2011. Hillshade maps of the Lower Granite Reservoir channels were developed from the bed elevation bathymetry grids. Hillshade maps are an accessible means to qualitatively assess morphodynamic change. It is visually apparent in the hillshade images below that the dunes in the 2009 imagery are larger than in 2010 and especially May 2011 in the upper part of the reservoir. Following the high discharge in May 2011, the bedforms (dunes) again increased in size during recession of the hydrograph so that residual bedforms in the September 2011 bathymetry were nearly as large as those in the September 2009 bathymetry.

As discussed in Section 10, in lower bed regime the size and spacing of sand dunes increase with increasing discharge until the dunes begin to washout as the bed transitions to upper regime. Since the bathymetries in 2009 and 2010 were collected during low flow in late summer and fall, the dunes recorded in the bathymetries are residual bedforms that retain the approximate size, shape and arrangement of the largest dunes that formed in lower bed regime near or after the peak of the seasonal hydrographs in Lower Granite Reservoir. Even if the transition to upper regime occurred near the peak of the hydrograph and bedforms were washed out, dunes will reform during the recession of the hydrograph as the bed reenters lower regime, provided discharge is not terminated abruptly so that the recession flow in adequate to rework the bed morphology or secondary flow patterns do not substantially alter normal bed form development. The largest dunes (mega-dunes) that form at the peak or during hydrograph recession will persist through the recession, perhaps with smaller dunes superimposed.

The peak discharges Lower Granite Reservoir when the bedforms in the bathymetry were formed are listed in Table 2. The highest discharges on the Clearwater River and in Lower Granite Reservoir below the confluence occurred in 2011. The peak discharge in the Snake River in 2010 was greater than the discharge when the bathymetry was acquired on 26 May 2011. The plot of daily average

discharge for Lower Granite in Figure 10 shows that the seasonal hydrographs in 2009 and 2011 were longer in duration than in 2010.

Reach	2009		2010		2011	
	Date	Discharge	Date	Discharge	Date	Discharge
Snake River (Peak at Anatone)	7-Jun-09	126,000	5-Jun-10	173,000	26-May-11	144,000
Clearwater River (Peak at Spalding)	31-May-09	67,000	5-Jun-10	70,100	26-May-11	77,400
Lower Granite Reservoir (maximum day)	31-May-09	170,600	6-Jun-10	216,100	26-May-11	221,000

Table 2. Discharges in Lower Granite Reservoir when bedforms in bathymetry were formed.

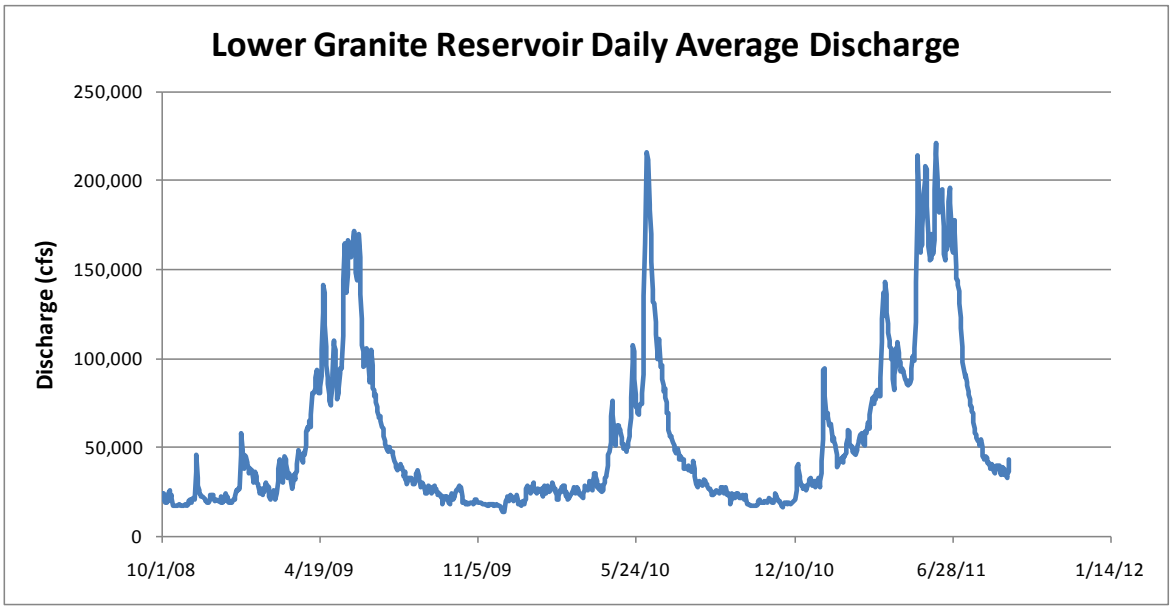


Figure 10. Daily average discharge in Lower Granite Reservoir 2009-2011.

15.4.1. Confluence Hillshade Bathymetry Maps

Hillshade bathymetry maps of the confluence area in Figure 11 through Figure 14 show distinct changes in the size and spacing of the sand dune bedforms due to the difference in flow conditions between 2009 and 2011. Most noticeable is the reduction in the heights and spacing of the dune field that curves around the bend of the Snake River channel near the Port of Clarkston in the May 2011 bathymetry. Similarly, the bedforms are nearly washed out on the top of the sediment mound at the Mouth of the Clearwater River in the May 2011 bathymetry. The dunes at these locations reformed during recession of the hydrograph and appear again in the September 2011 bathymetry. The heights of the dunes in the Snake River channel below Interstate Bridge appear larger in the 2011 hillshade map than those in the 2009 and 2011 hillshade maps. The elevation contours that are superimposed on the bathymetry have

a 10 ft interval. The edges of the multibeam echo swaths are more pronounced in the 2011 bathymetry because the analysts at ERDC were asked to perform minimal of processing to retain more detail in the dune fields.

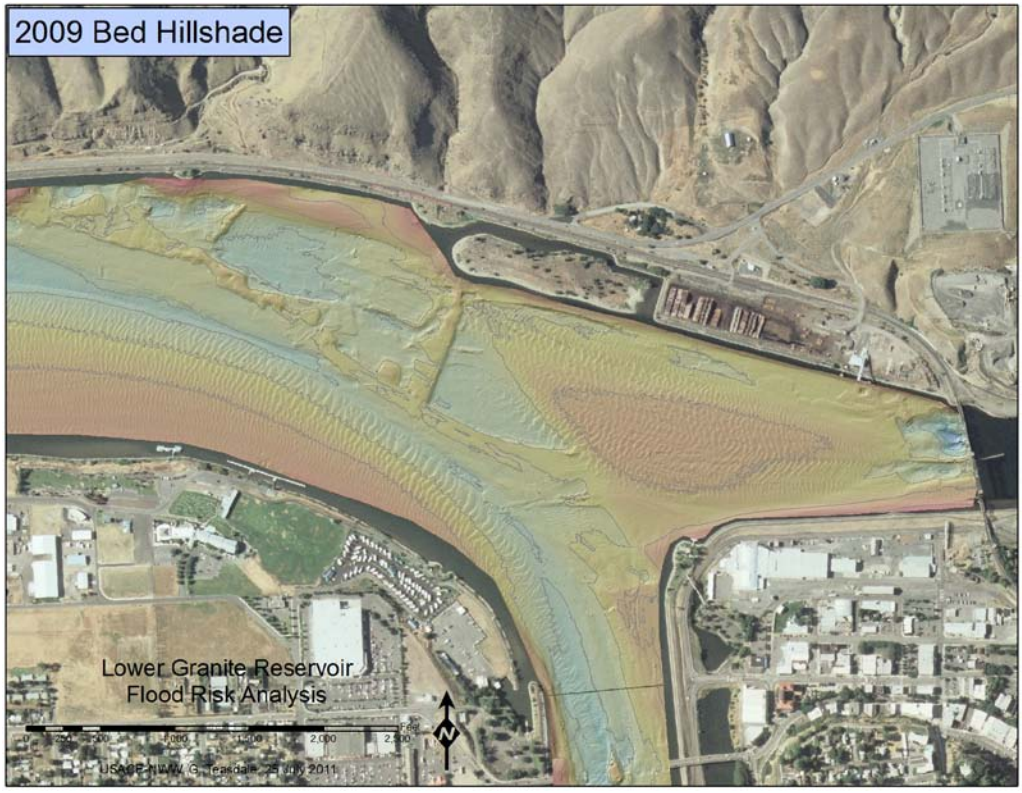


Figure 11. Bedforms at the confluence September 2009.

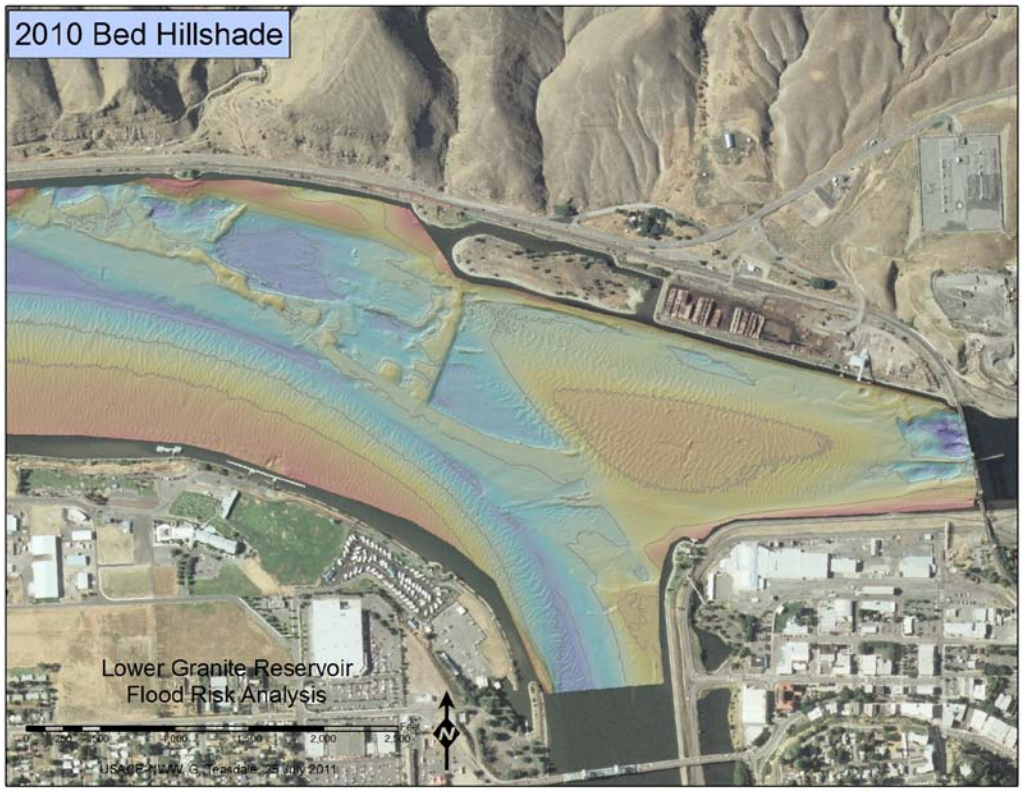


Figure 12. Bedforms at the confluence September 2010.

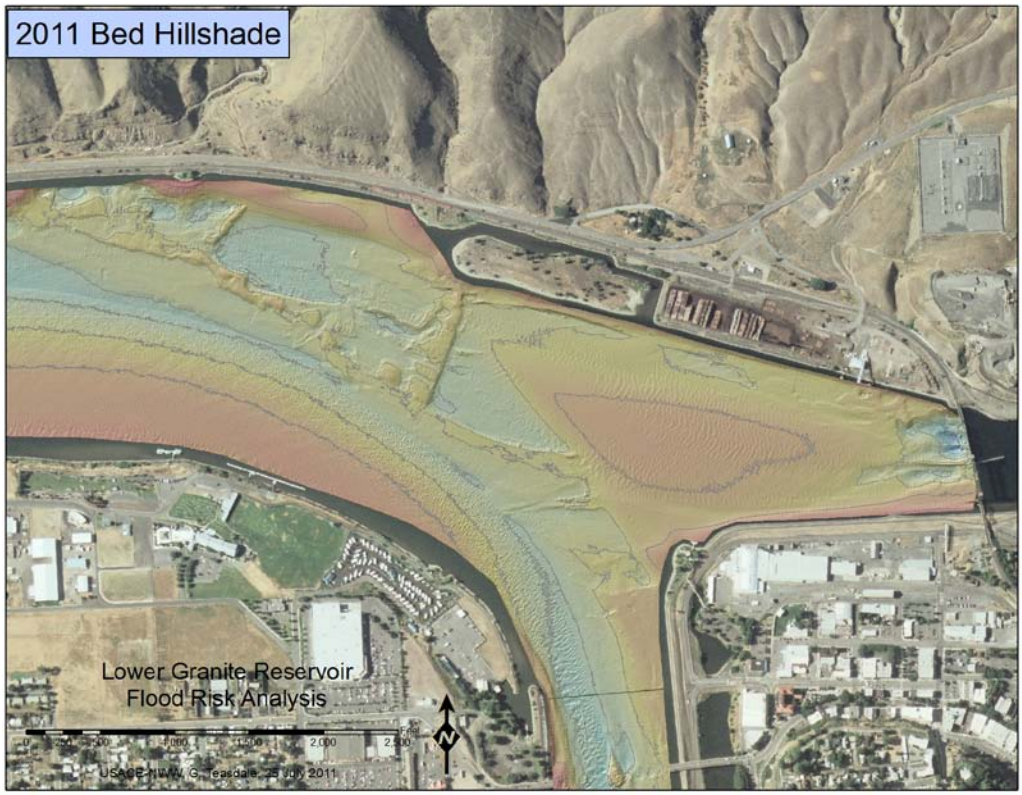


Figure 13. Bedforms at the confluence 26 May 2011.



Figure 14. Bedforms at the confluence September 2011.

15.4.2. Port of Clarkston Hillshade Bathymetry Map

At the Port of Clarkston, the bedforms in the deepest part of the channel are smaller at high discharge in the May 2011 bathymetry (Figure 16) than in the September 2009 bathymetry (Figure 15). Along the left bank, in front of the port facilities, a lane of dunes forms close to the bank on the inside of the bend. The dunes near shore are somewhat larger in the May 2011 bathymetry than in the 2009 bathymetry, likely because the velocities and bed shear stress were greater in May 2011 than at the peak of the discharge in 2009. Dunes are again larger and more defined in the September 2011 bathymetry (Figure 17).

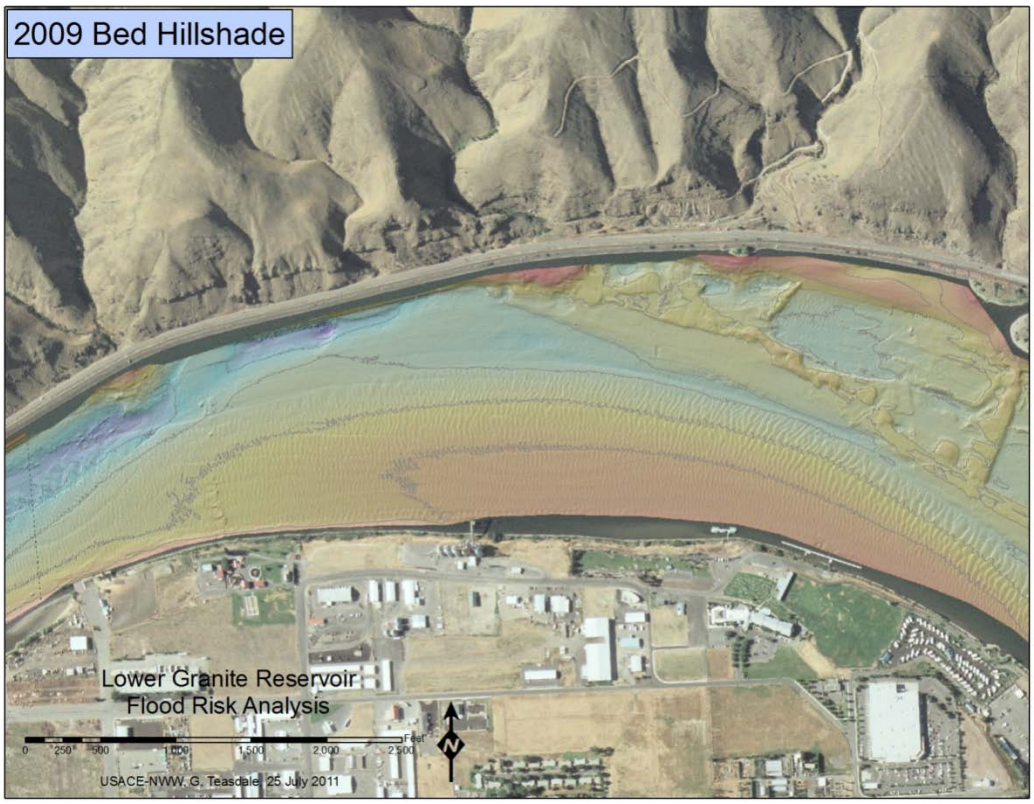


Figure 15. Bedforms at the Port of Clarkston September 2009.

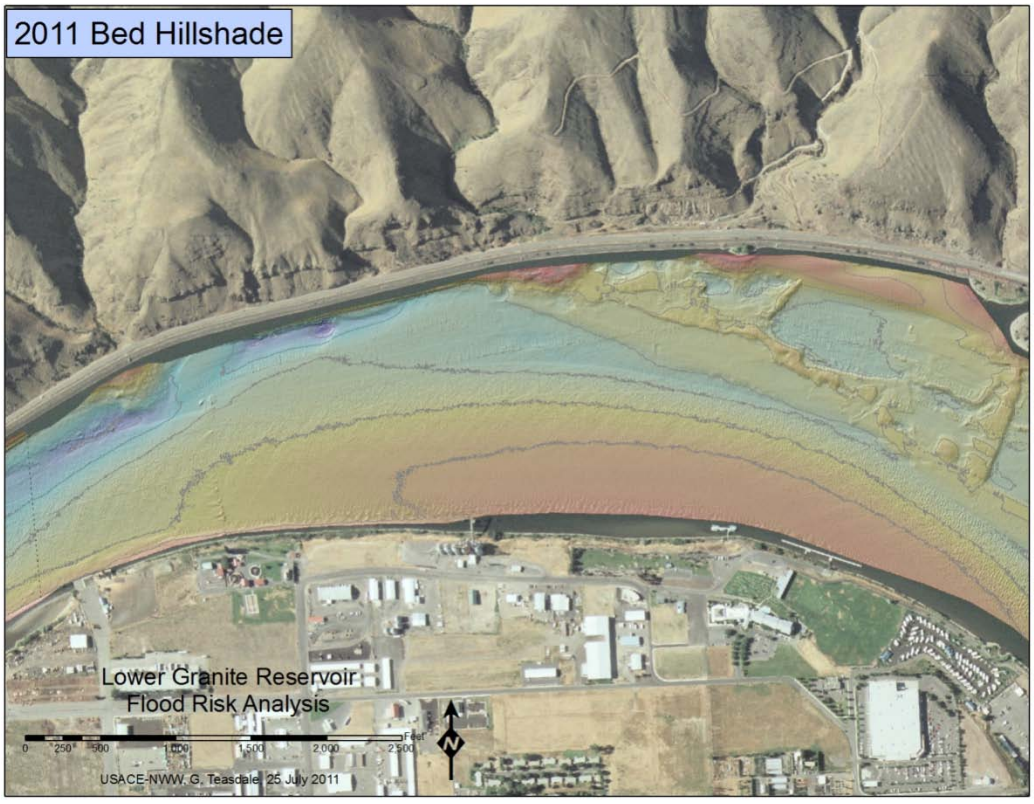


Figure 16. Bedforms at the Port of Clarkston 26 May 2011.



Figure 17. Bedforms at the Port of Clarkston September 2011.

15.4.3. Port of Wilma Hillshade Bathymetry Map

By the Port of Wilma, the very large dunes in the middle of the channel below Red Wolf Bridge in the September 2009 (Figure 18) bathymetry are washed out in the 26 May 2011 bathymetry (Figure 19). Downstream along the right bank, dunes are wider in the downstream direction and more flattened in the May 2011 bathymetry than in the September 2009 bathymetry. Small dunes in the center of the channel and along the left bank are also smaller in the 2011 bathymetry. Dunes have reformed by the time the September 2011 bathymetry was acquired (Figure 20). Bedforms on the outside of the bend are smaller in the September 2011 bathymetry than in the September 2009 and May 2011 bathymetries. This suggests that secondary flow patterns in the band and around the submerged island affect the recovery of the dune field (and flow resistance).

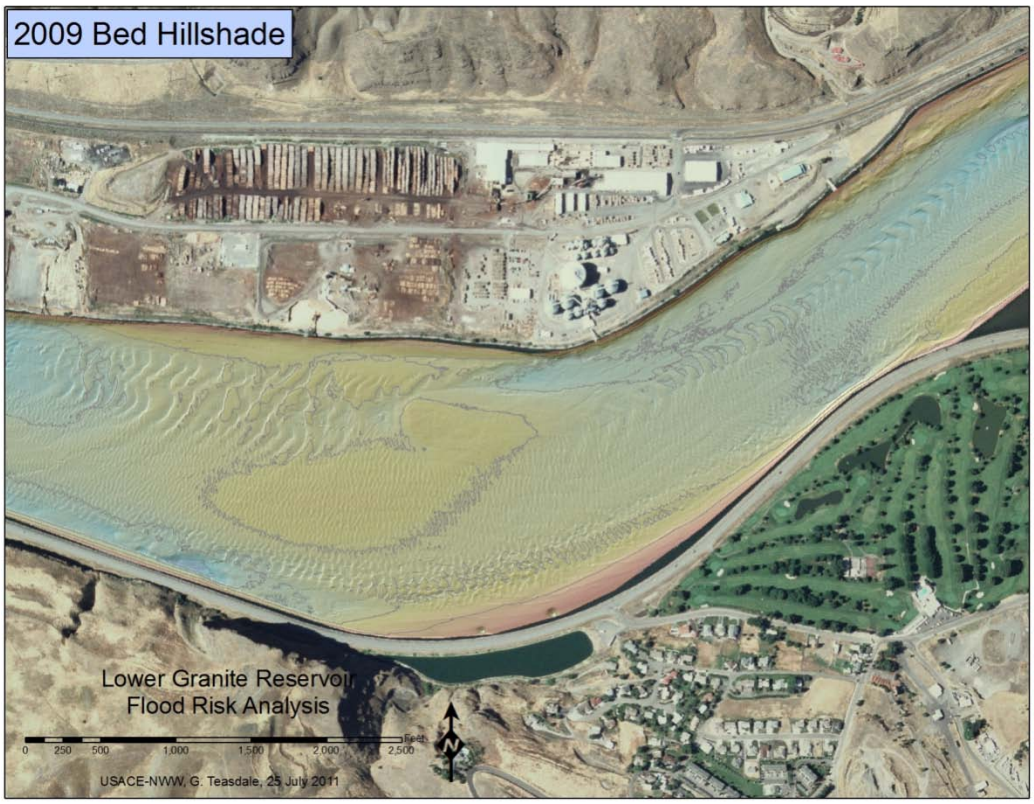


Figure 18. Bedforms at the Port of Wilma September 2009.

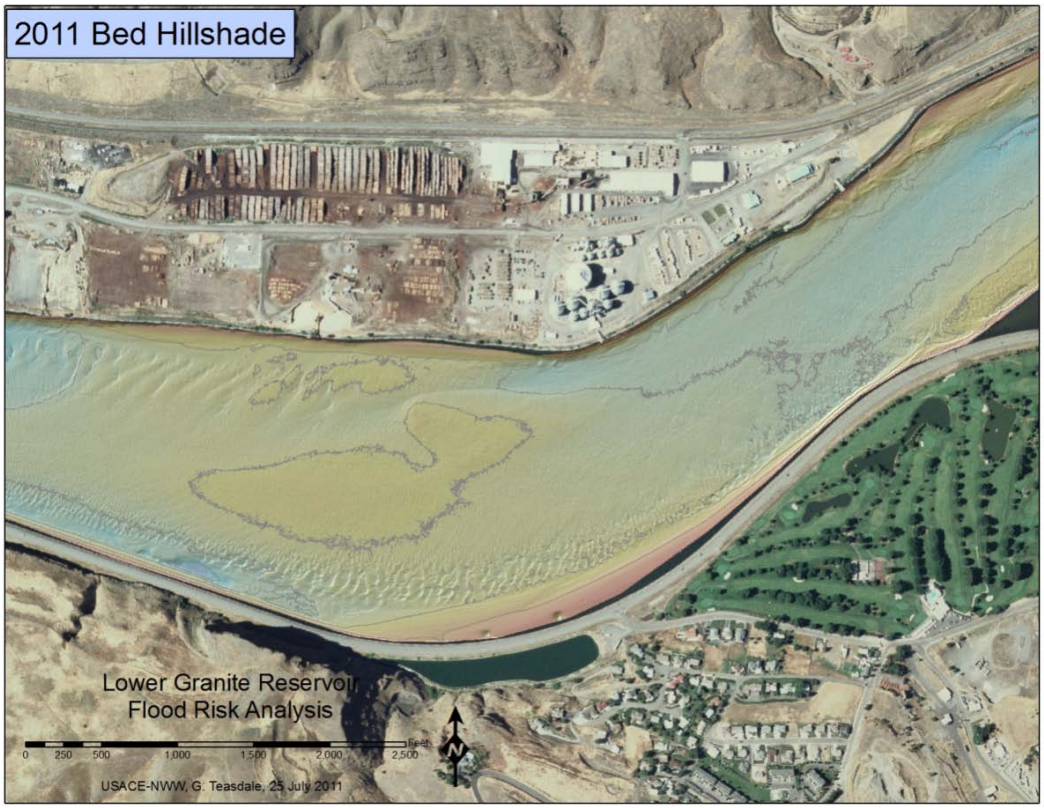


Figure 19. Bedforms at the Port of Wilma 26 May 2011.

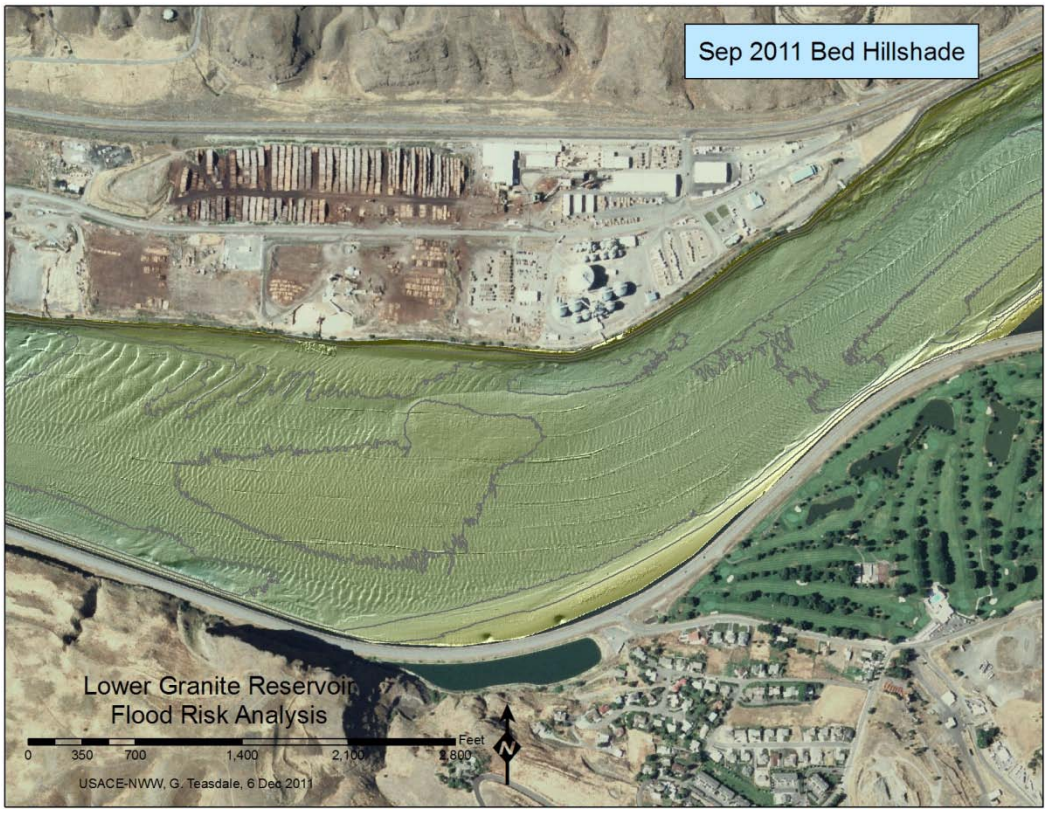


Figure 20. Bedforms at the Port of Wilma September 2011.

15.4.4. Silcott Island Hillshade Bathymetry Map

Near Silcott Island the trend of bedform change during the high discharge of May 2011 is opposite to that upstream. At this location the reservoir begins to substantially widen and deepen so the bed shear stress is reduced. The dune field in the May 2011 (Figure 22) and September 2011 (Figure 23) bathymetries are larger and extend further into the lower reservoir than those in the 2009 (Figure 21). Dune bedforms vanish at about RM 128.5 in the September 2011 bathymetry, about 2 miles further downstream than in September 2009. The bathymetry comparison confirms that sand bed-load is transported deeper into the reservoir during higher discharge and will continue to migrate further downstream as predicted by the sediment transport analysis.

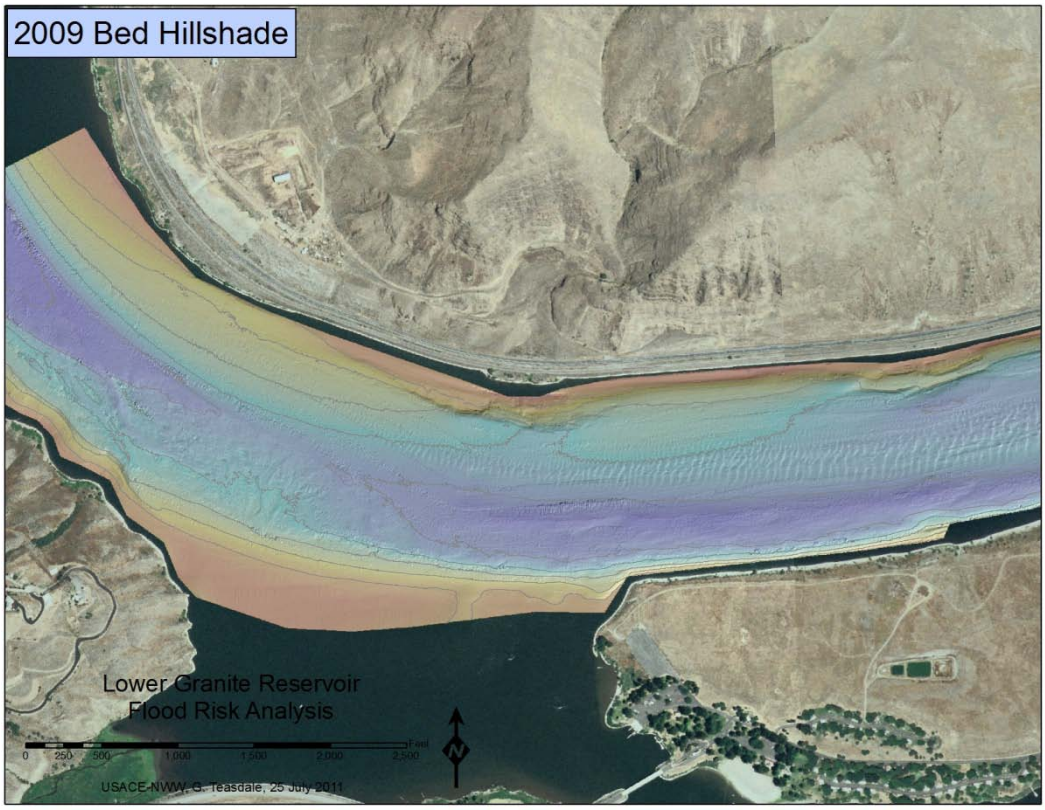


Figure 21. Bedforms near Silcott September 2009.

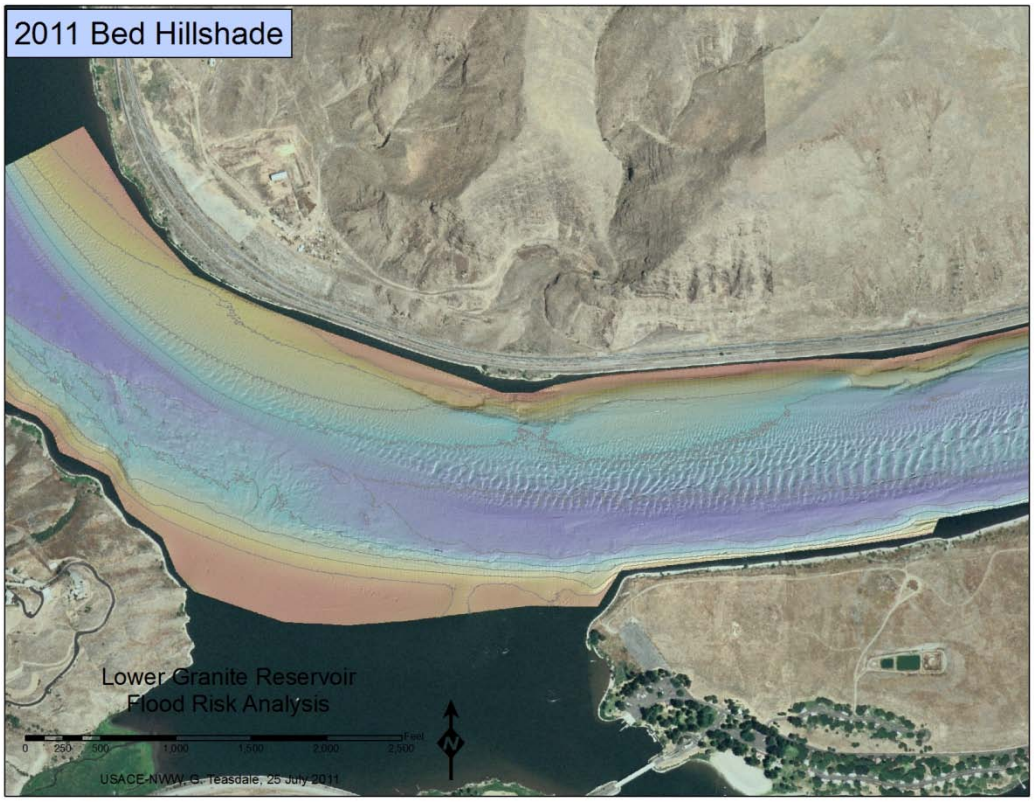


Figure 22. Bedforms near Silcott 26 May 2011.



Figure 23. Bedforms near Silcott September 2011.

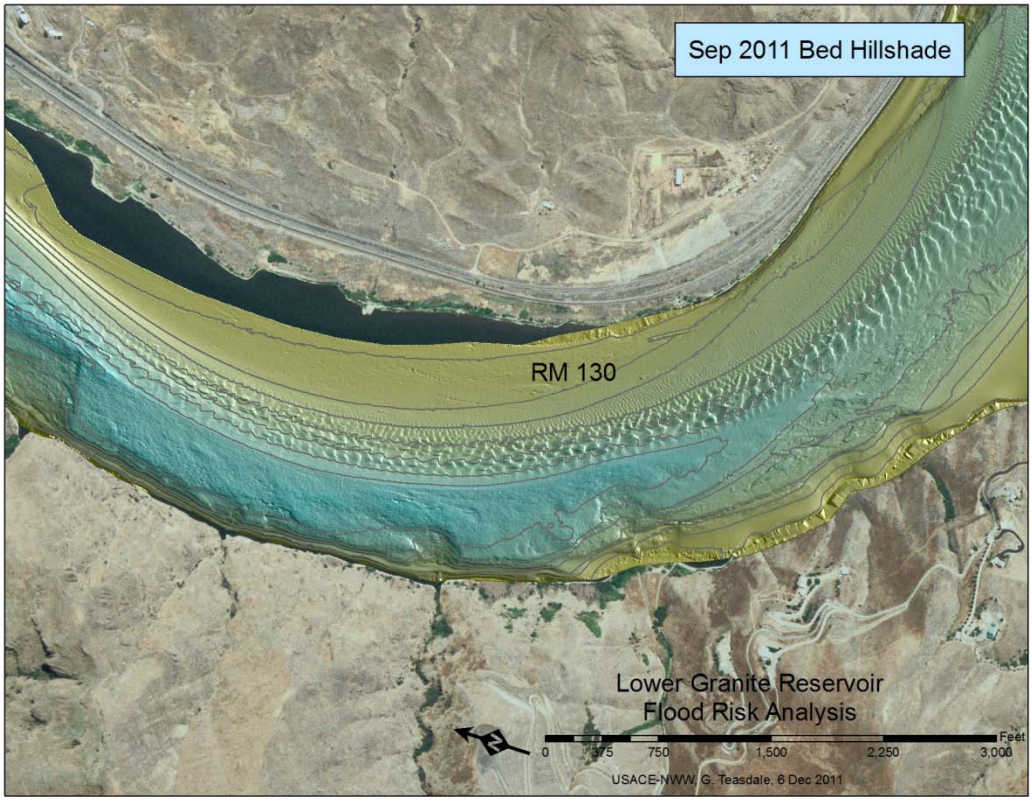


Figure 24. Bedforms below Silcott September 2011.

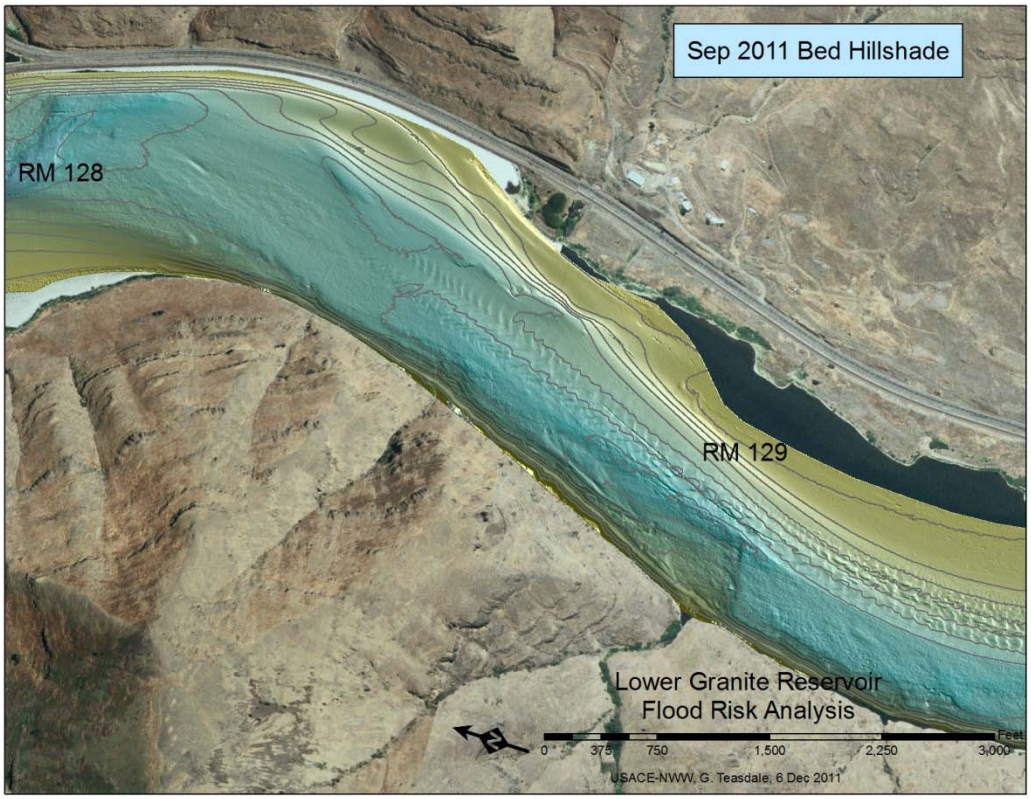


Figure 25. Bedforms near RM 128.5 September 2011.

15.4.5. Snake River Hillshade Bathymetry Map

A dune fields in the Snake River upstream of the levee system follows the progression or bed regime transition from large dunes in the September 2009 bathymetry (Figure 26) to a nearly planar bed with very small dunes in May 2011bathymetry (Figure 27) to larger dunes again in the September 2011bathymetry (Figure 28). A second dune field between the deep hole at RM 140.3 and Interstate Bridge at RM 139.6 also showed substantial flatten of the bedforms in the May 2011 bathymetry but not complete elimination of the dunes near the bridge.

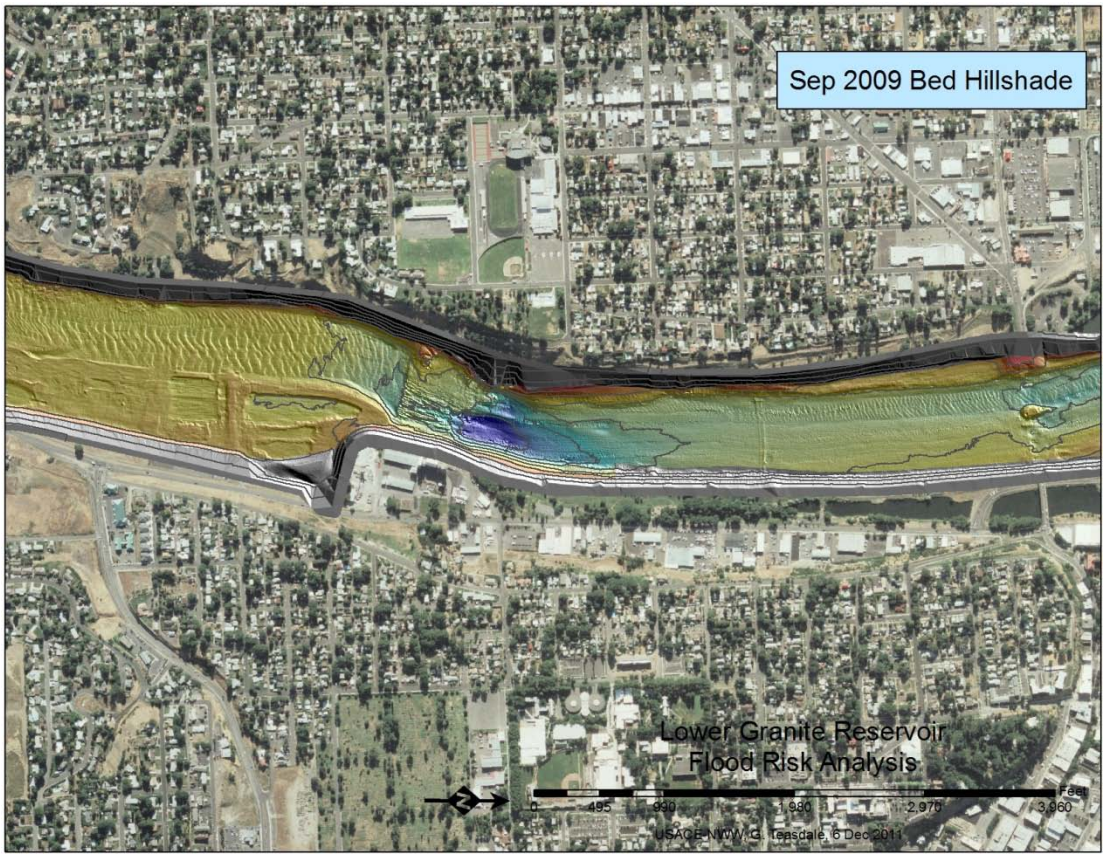


Figure 26. Bedforms Snake River near above the confluence September 2009.

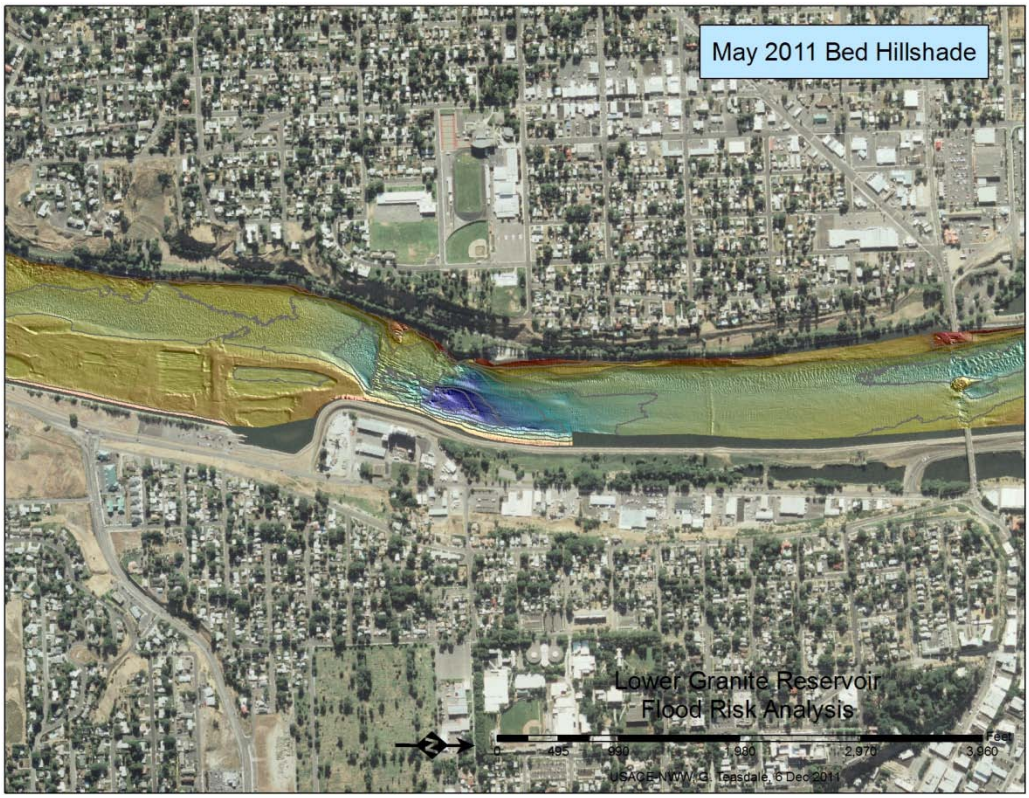


Figure 27. Bedforms Snake River near above the confluence May 2011.



Figure 28. Bedforms Snake River near above the confluence September 2011.

15.5. Dune Transect Profiles

Changes in dune fields can be measured directly in transect profiles obtained at different times and discharges. Few techniques of direct analysis have been published. In this study dominant wave lengths and amplitudes of the dune longitudinal profiles were determined with a Fourier series analysis of dune bed waveform. A Fourier analysis fits amplitude coefficients for a selected number of harmonics to a waveform and is commonly applied in electronic signal analysis and stochastic hydrology. In the analysis of a dune profile, the most significant harmonics indicate wavelengths and amplitudes of the dominant dunes. Changes in the amplitude coefficients between profiles acquired at different times indicate altered dune morphology and provide a rational method to quantify the degree of change. As a check on the quality of the Fourier analysis, the amplitude coefficients can be applied to a summation of sine and cosine terms to reproduce the original bed transect waveform. The Fourier analysis procedure was implemented with a Matlab script and is an adaptation of formulations presented by Salas[4] for hydrologic time serie analysis. Importantly, the actual bed elevation difference between dune profiles do not affect the Fourier analysis, so elevation datum discrepancies or a net elevation change of the bed due to general deposition or erosion does not affect the comparison of amplitude coefficients.

15.5.1. Confluence Bedform Profiles

Bedform transect lines at the confluence of the Snake and Clearwater Rivers at the locations in Figure 29 were extracted from the September 2009, May 2011 and September 2011 bathymetry. The dune profiles are plotted in Figure 30, Figure 31 and Figure 32. The spacing and height of the dunes in May 2011 during the high discharge were smaller and more closely spaced, and appear more irregular than those in September 2009. This indicates that the dunes were beginning to washout as the bed transitioned from lower regime to upper regime. The dunes heights and wavelengths are again larger in the September 2011 profiles which show that the bed was recovering to a well developed lower bed regime condition during recession of the hydrograph.

Graphical outputs from the Fourier analysis of the 2009 and 2011 dune profiles at transect line A at the confluence are shown in Figure 33, Figure 34 and Figure 34. The top subplot in each figure shows the original dune profile and the fit of the Fourier series. The second subplot shows the error between the Fourier series fit and the original profile. The bottom subplot is a plot of the amplitude coefficients versus the

[4] Salas, J.D., Delleur, J.W., Yevjevich, V., and Lane, W.L. (1997). Applied Modeling of Hydrologic Time Series. Water Resources Publications, LLC. Littleton, CO.

Fourier harmonic expressed as a bed wavelength distance. Peaks in the plot of the amplitude coefficients indicate the dominant wavelengths of the dune profile.

The September 2009 dune profile has a very dominant wavelength at about 45 feet which has an amplitude coefficient of about 0.4 ft. The actual heights of the dominant dunes in the profile are somewhat greater than twice the dominant amplitude coefficient. Actual heights of the dunes are not equivalent to the amplitude coefficients because of the summation of terms involved in the Fourier series, though maximum dune heights can be obtained from the Fourier series.

The Fourier analysis of the May 2011 dune profile does not indicate a dominant amplitude at 45 ft and all amplitude coefficients are less than those in September 2009 up to a wavelength of about 75 feet. The dominant amplitude coefficient for transect A in September 2011 again increases to about 0.4 feet with a wavelength somewhat over 100 ft. Amplitude coefficients are more easily compared when plotted together as in Figure 36. Wavelength longer than 75 ft in the May 2011 profile has greater amplitude coefficients than the 2009 profile, but are still less than the peak amplitudes in the 2009 profile, which shows that the dunes in September 2009 have been washed out into a shallower and longer bedform. Amplitude coefficients for very long wavelengths, greater than about 300 ft at this location, reflect the underlying bed topography.

The Fourier series amplitude coefficients for September 2009 and May 2011 dune profiles at transect line A in the confluence follow a power equation trend as shown in Figure 37. Both the amplitude coefficients and wavelengths are plotted on log scales. The power equation trend, which plots as a straight line in log-log space, is a common characteristic of nearly all the dune profiles in Lower Granite Reservoir and reflects the sediment transport process of dune formation and sand wave movement. The amplitude coefficient trend line for a bed profile that is upper regime or in transition to upper regime should plot below or have less slope than the trend line for a bed that is in lower regime. A trend line that plots below another because its dune heights are smaller and a trend line with less slope exhibits a decreased trend in dune heights with wave length. When the discharge associated with the comparison trend line is greater, both conditions indicate washing out of the dune field and a transition to upper bed regime. This relationship is seen in the September 2009 and May 2011 profiles in Figure 37. Trend line comparisons for the Fourier amplitude coefficients for the September 2009 and May 2011 dune profiles at the confluence are plotted in Figure 38 and Figure 39. The amplitude coefficient trends at both transect B and C also indicate a reduction in bedform size and a transition to upper bed regime.

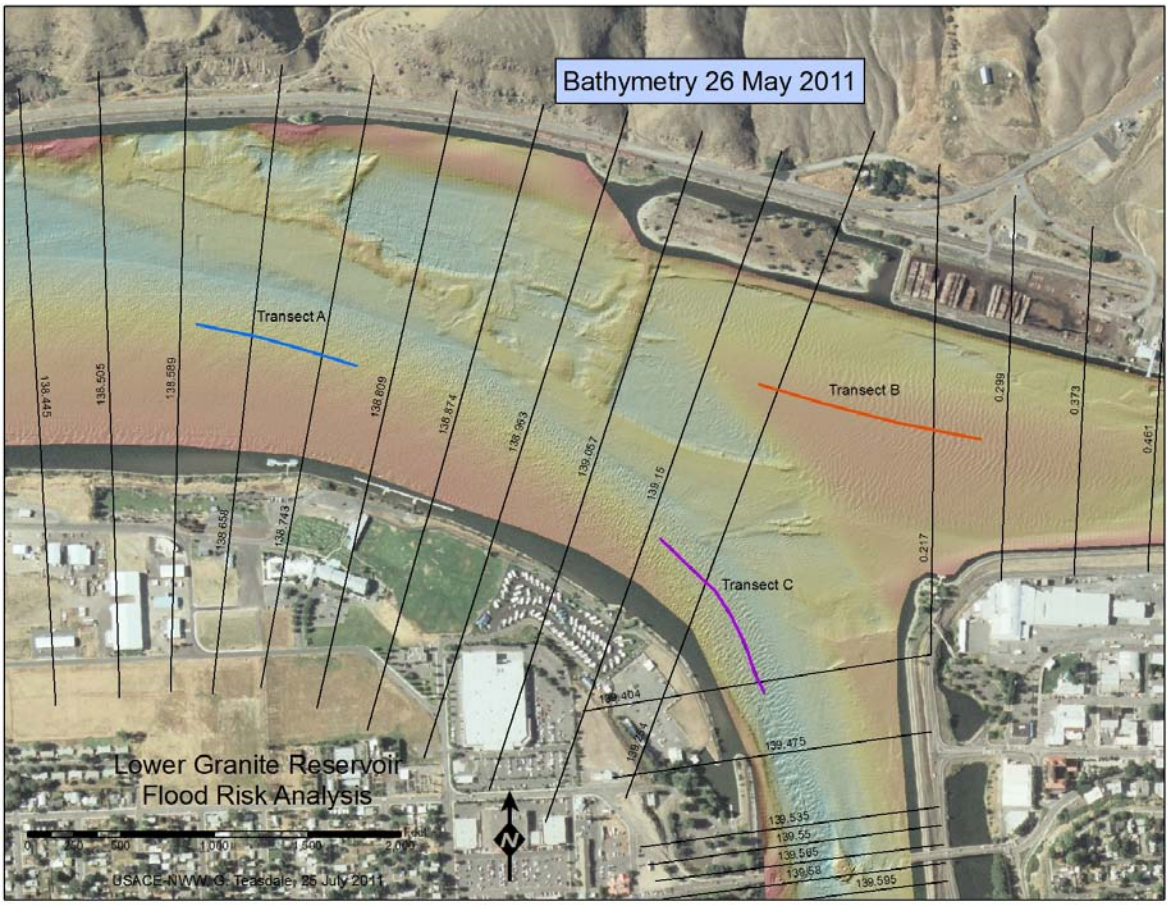


Figure 29. Dune profile transect lines at the confluence.

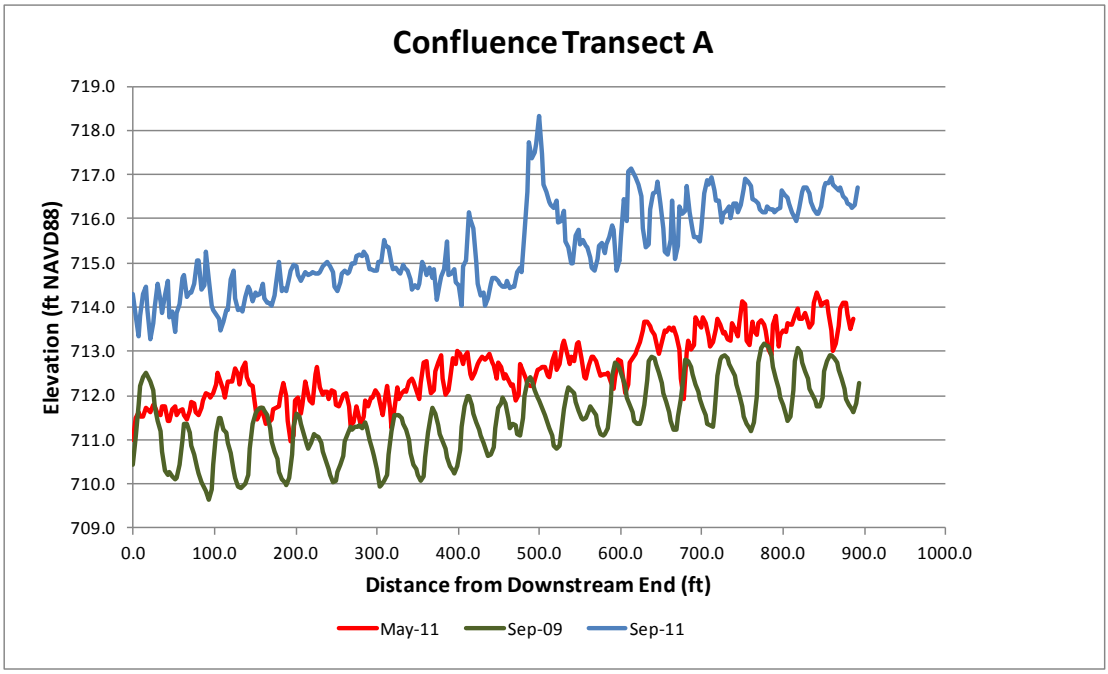


Figure 30. Comparison of September 2009 and May 2011 dune profiles at transect A.

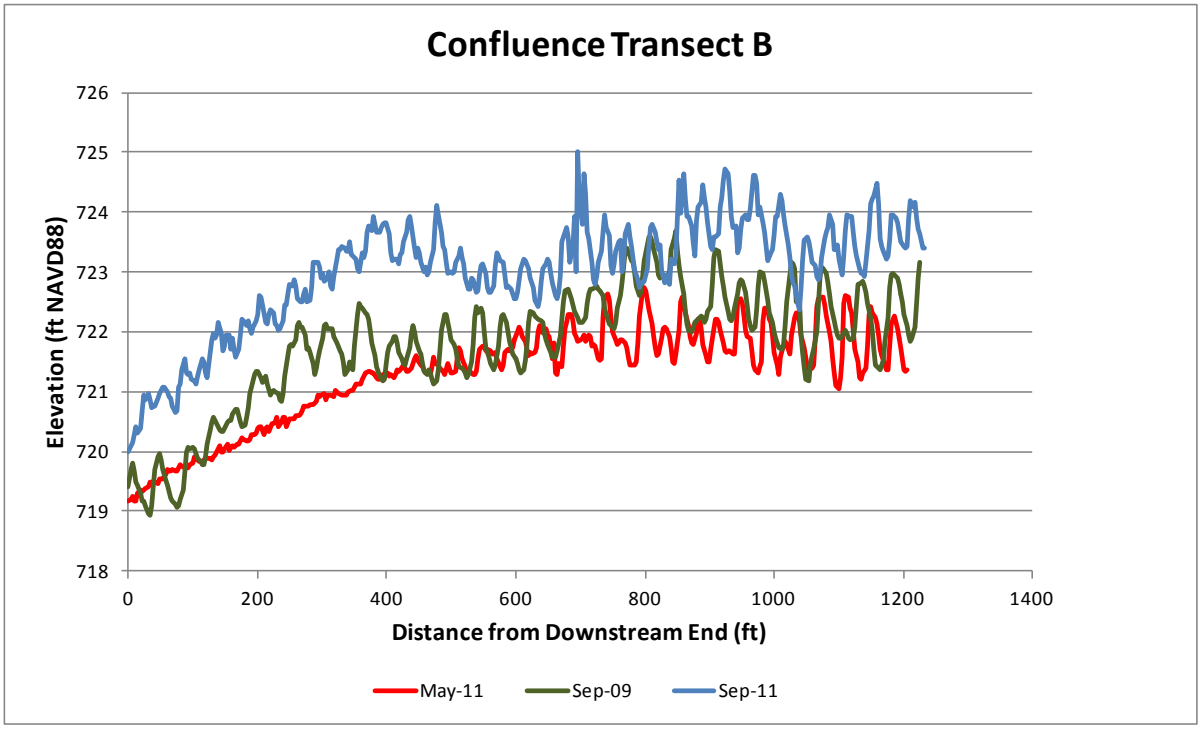


Figure 31. Comparison of September 2009 and May 2011 dune profiles at transect B.

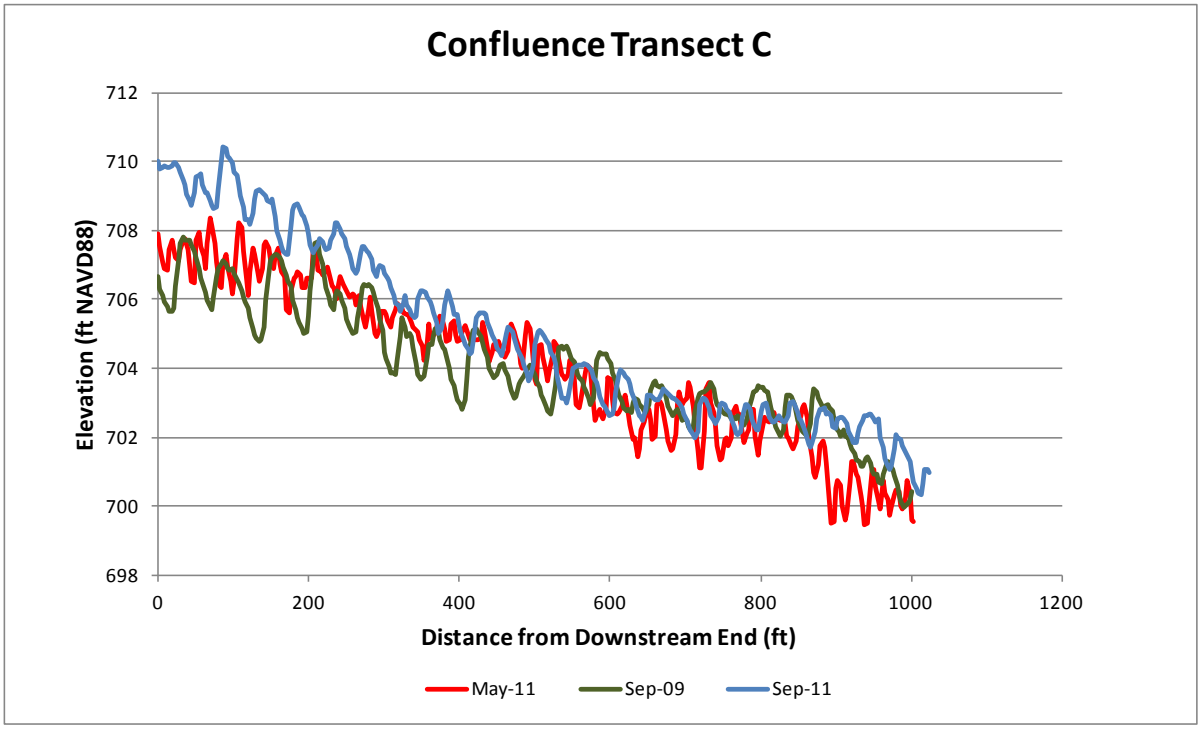


Figure 32. Comparison of September 2009 and May 2011 dune profiles at transect C.

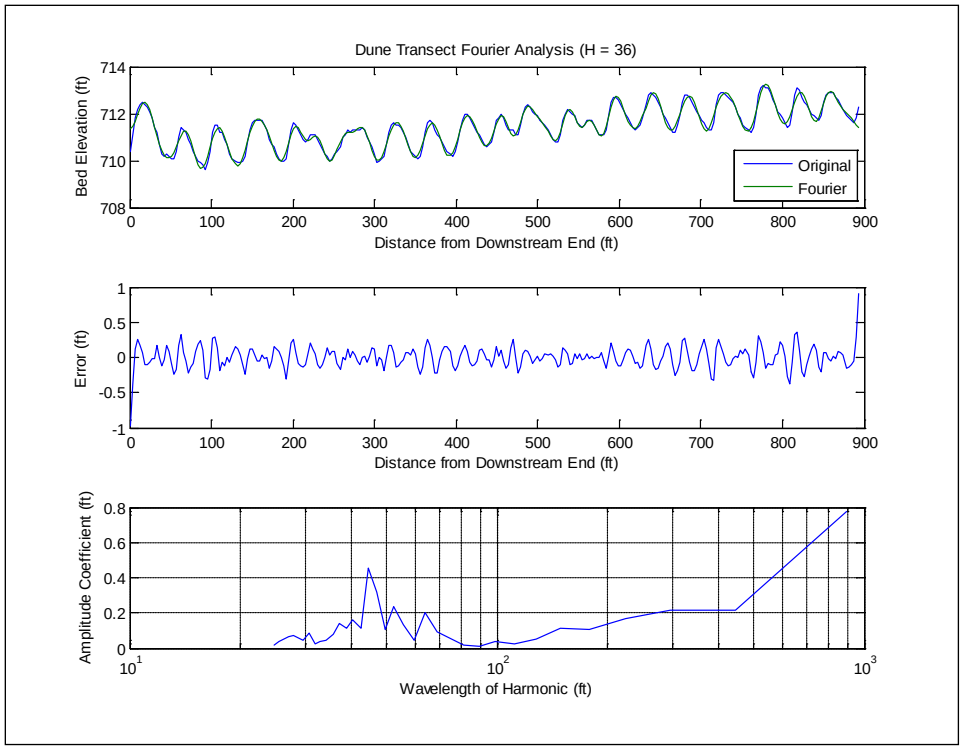


Figure 33. Fourier analysis of September 2009 dune profile at confluence transect line A.

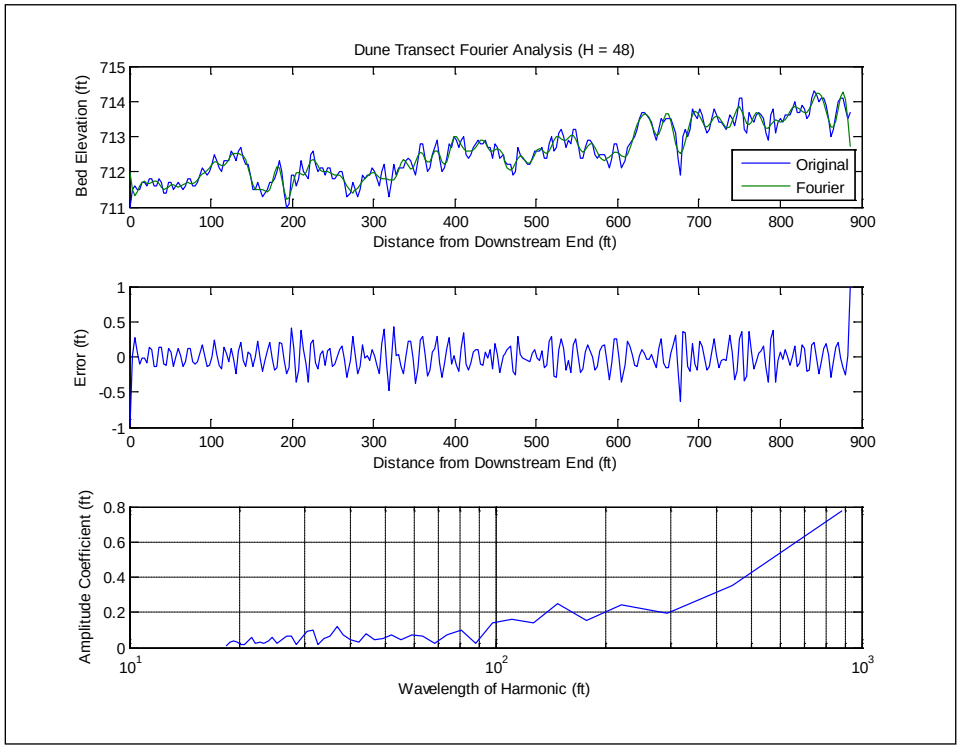


Figure 34. Fourier analysis of May 2011 dune profile at confluence transect line A.

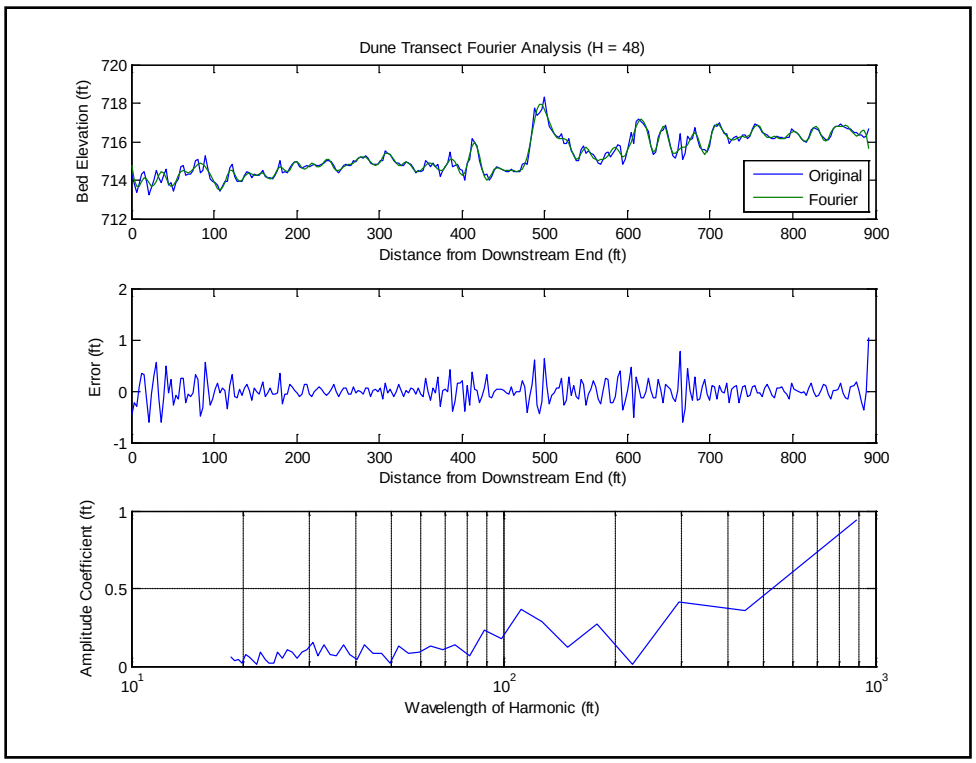


Figure 35. Fourier analysis of Sep 2011 dune profile at confluence transect line A.

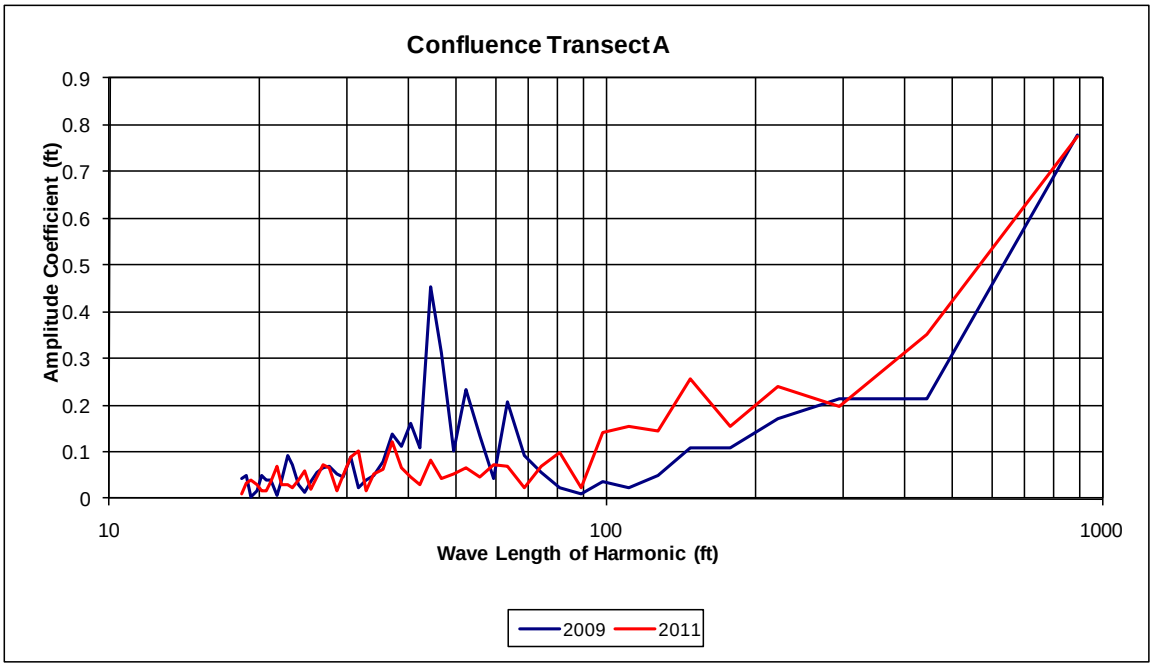


Figure 36. Comparison of September 2009 and May 2011 amplitude coefficients for dune profiles at transect A at the confluence.

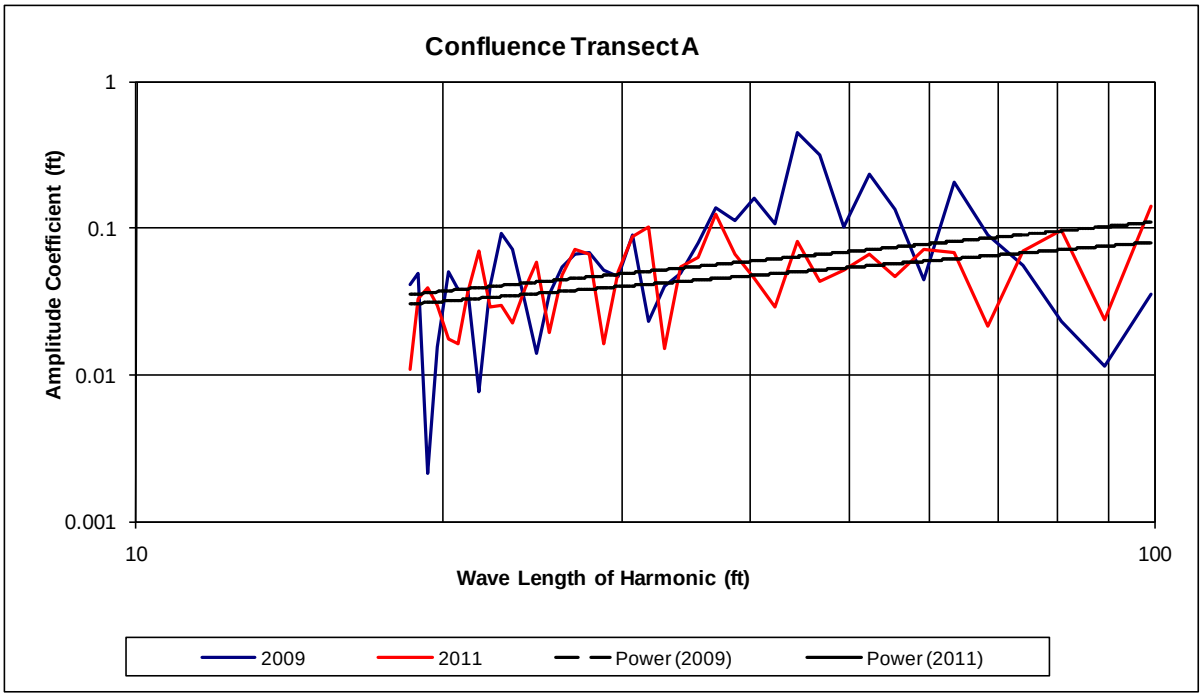


Figure 37. Trend of September 2009 and May 2011 dune profile amplitude coefficients at confluence transect line A.

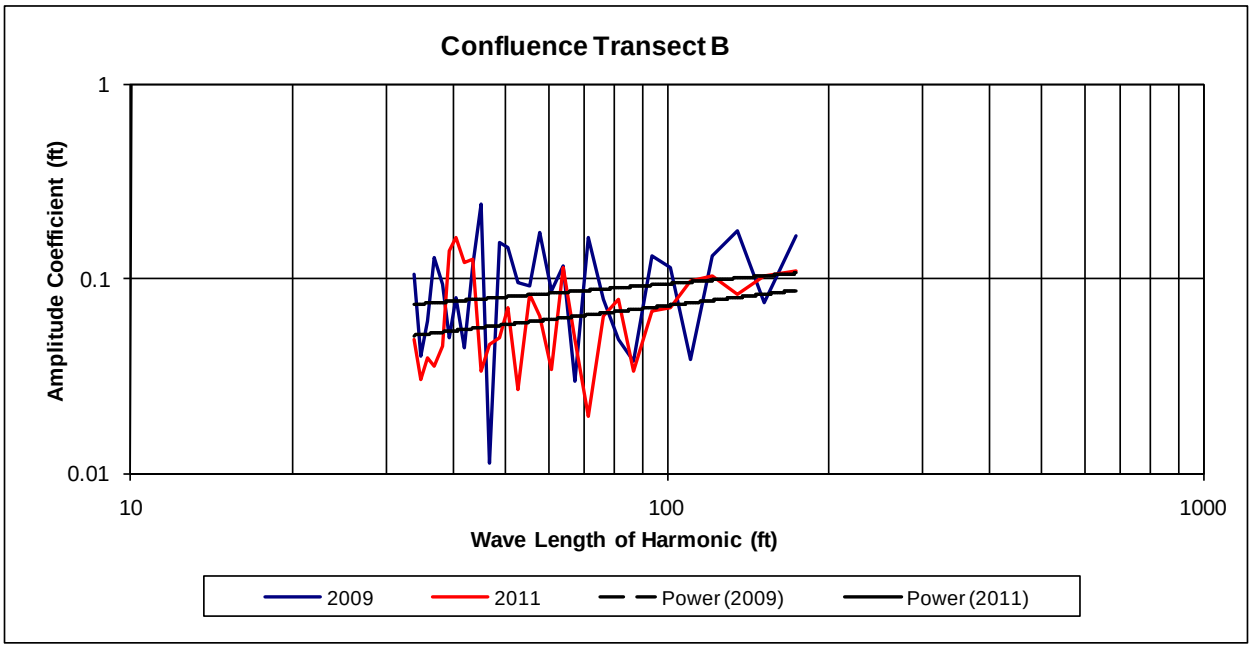


Figure 38. Trend of September 2009 and May 2011 dune profile amplitude coefficients at confluence transect line B.

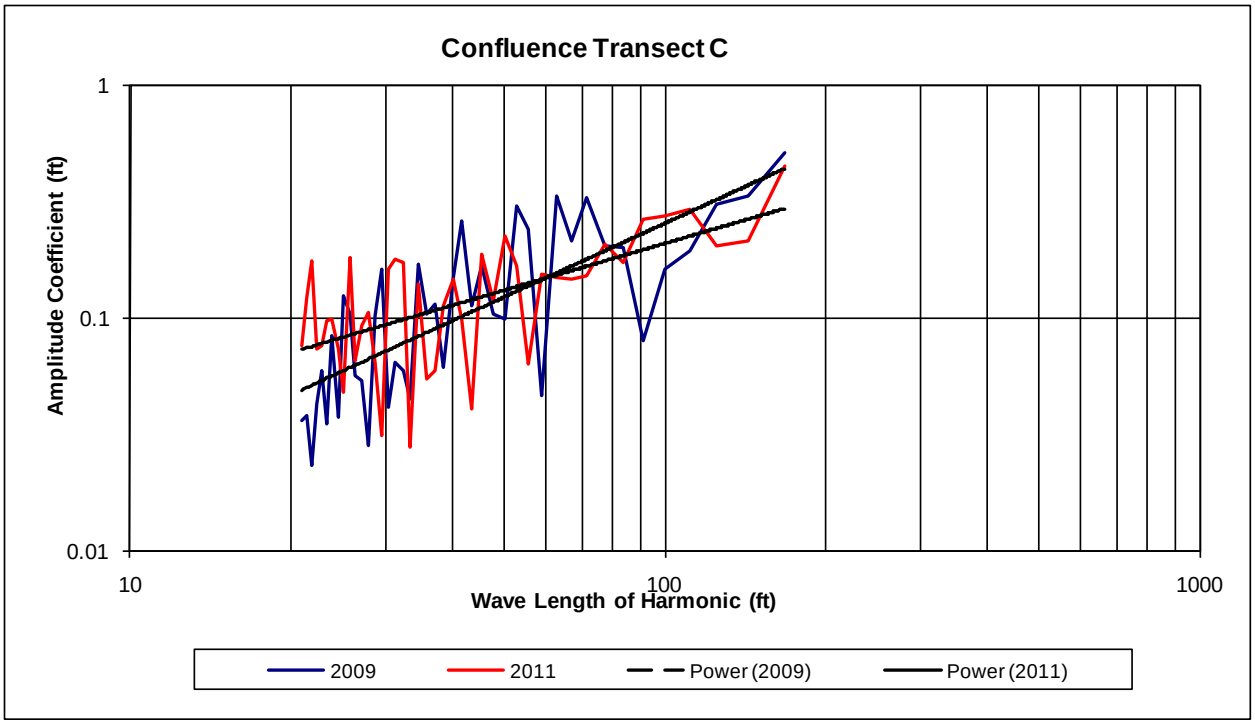


Figure 39. Trend of September 2009 and May 2011 dune profile amplitude coefficients at confluence transect line C.

15.5.2. Clearwater Turning Basin Bedform Profiles

Bedform profiles for the Clearwater River turning basin were extracted from the bathymetries acquired in September 2009, September 2010, May 2011, and September 2011 at the locations in Figure 40. Dune profiles and amplitude coefficients are plotted in Figure 41 through Figure 44. Dune profiles along both transect lines indicate that the Clearwater River channel was in transition to upper bed regime when the 26 May 2011 bathymetry was acquired. Large dunes are again well developed in the September 2011 profile.

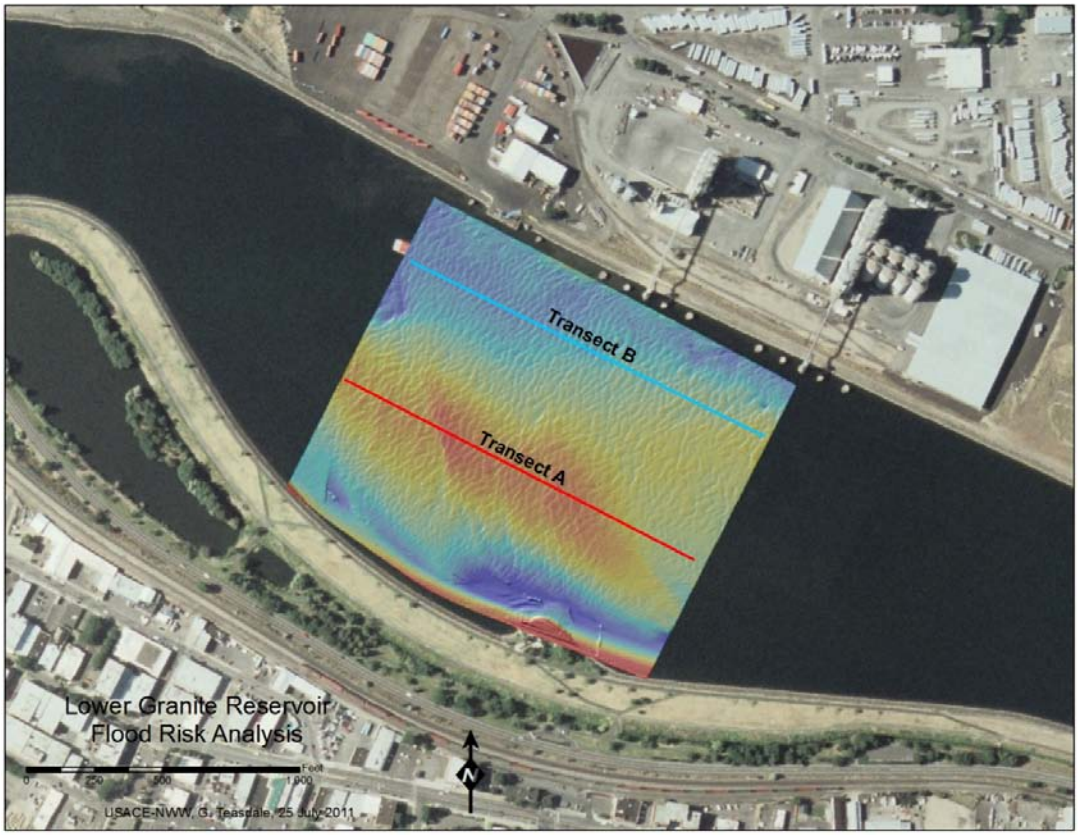


Figure 40. Dune profile transect lines in the Clearwater River turning basin.

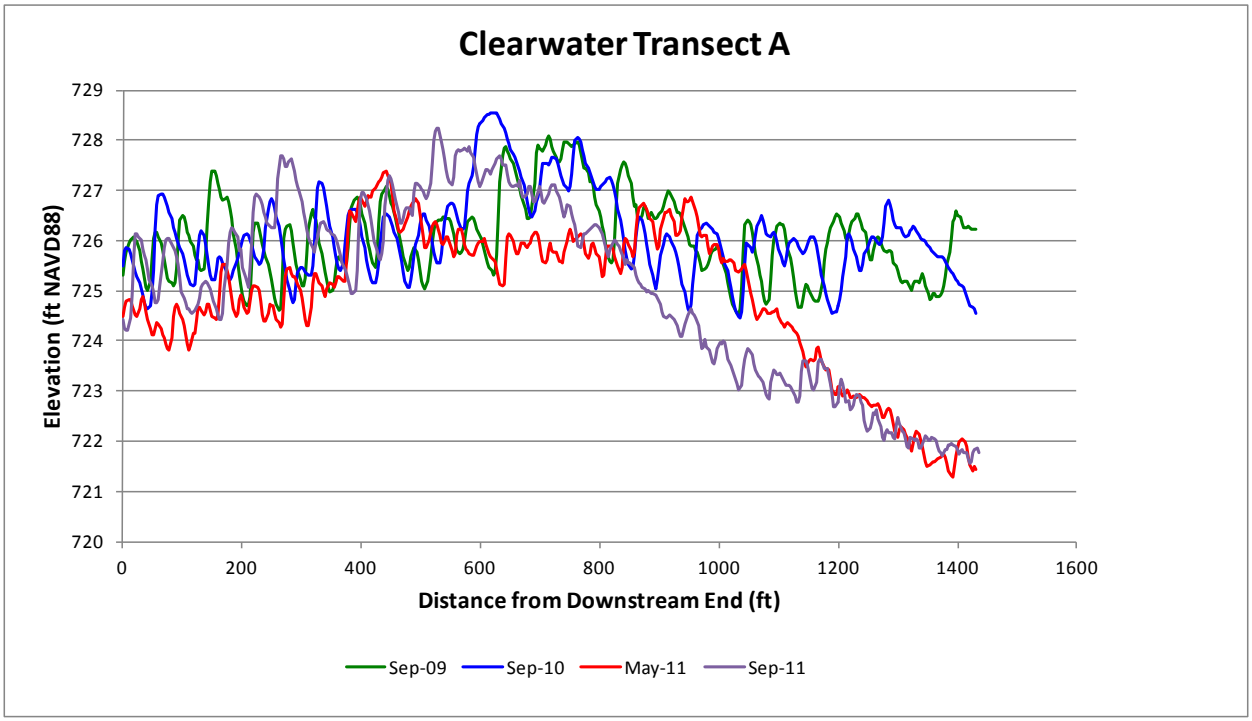


Figure 41. Dune profiles September 2009 through 2011 in the Clearwater River turning basin at transect A.

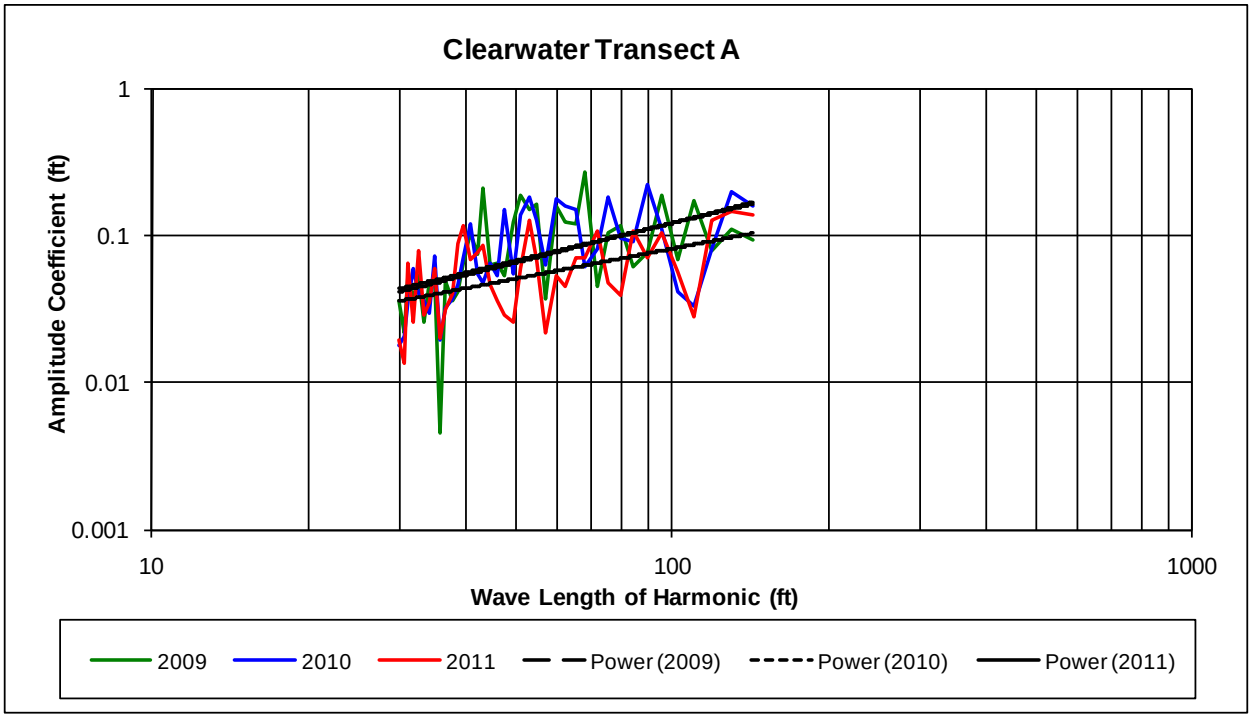


Figure 42. Fourier amplitude coefficient trends for September 2009, September 2010 and May 2011 in the Clearwater River turning basin at transect A.

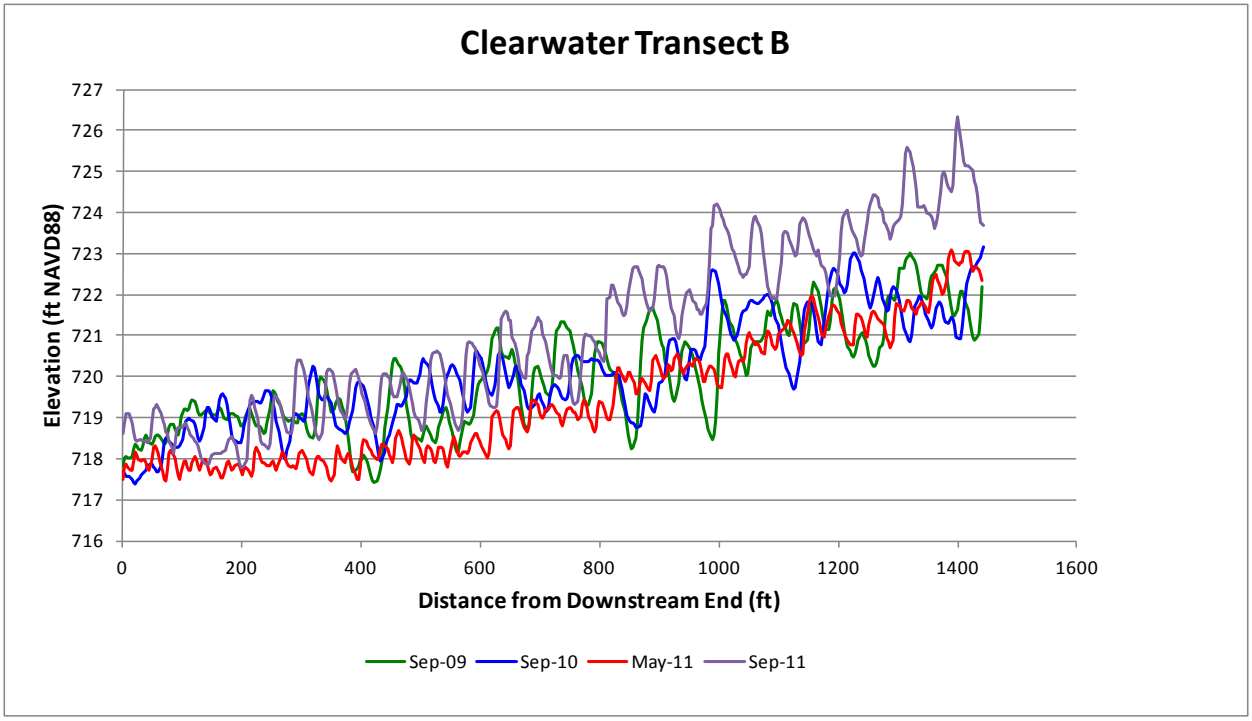


Figure 43. Dune profiles 2009 through 2011 in the Clearwater River turning basin at transect B.

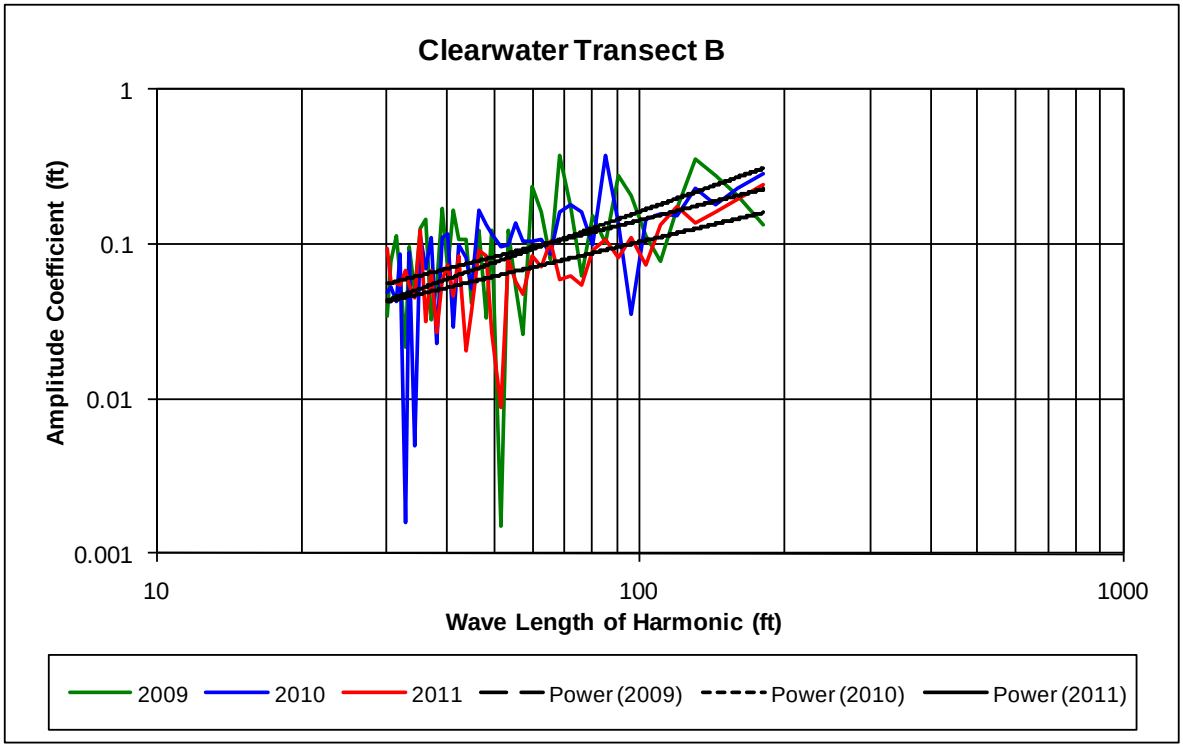


Figure 44. Fourier amplitude coefficient trends for September 2009, September 2010 and May 2011 in the Clearwater River turning basin at transect B.

15.5.3. Port of Clarkston Bedform Profiles

Bedform profiles for the Lower Granite Reservoir at the Port of Clarkston were extracted from the September 2009 and May 2011 bathymetry at the locations in Figure 45. Dune profiles and amplitude coefficients are plotted in Figure 46 through Figure 51. Dune profiles along the three transect lines indicate that the Snake River channel was in transition to upper bed regime when the 26 May 2011 bathymetry was acquired.

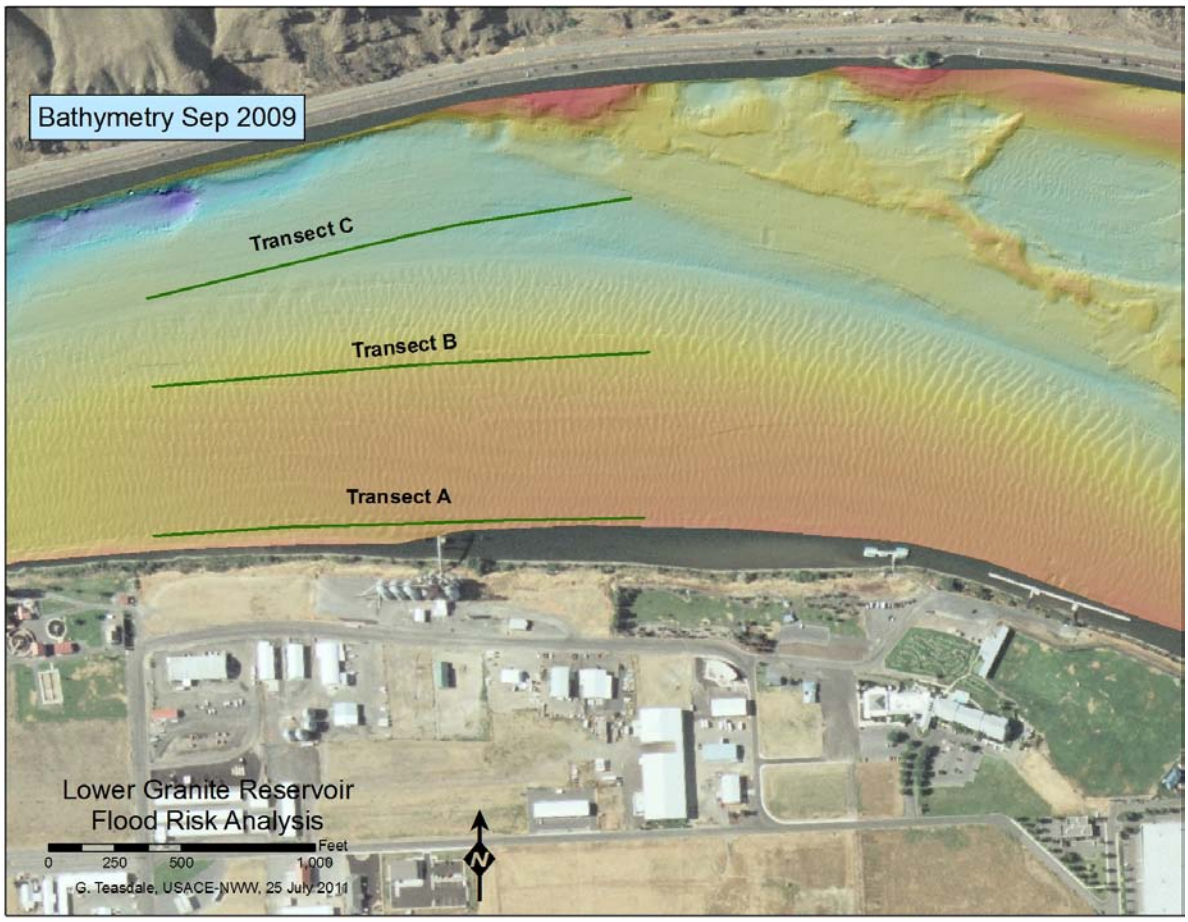


Figure 45. Dune profile transect lines at the Port of Clarkston.

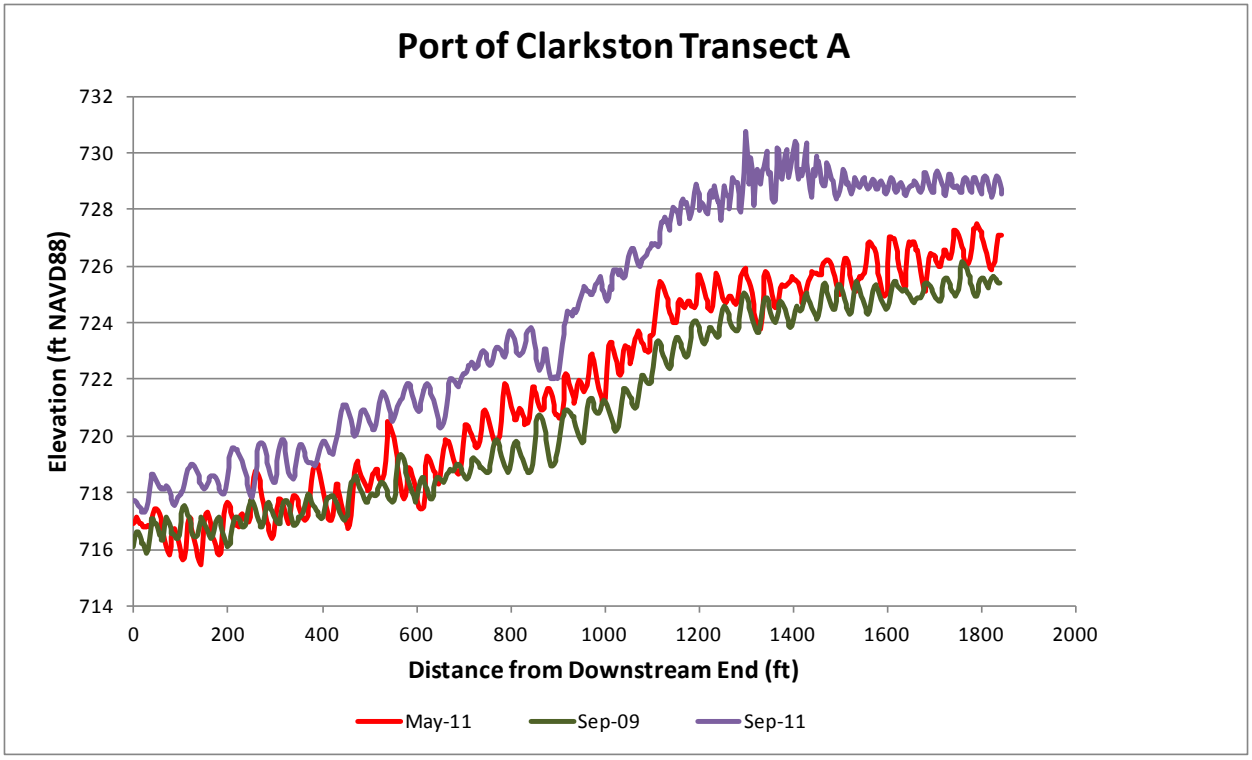


Figure 46. Dune profiles for September 2009 and May 2011 at the Port of Clarkston transect A.

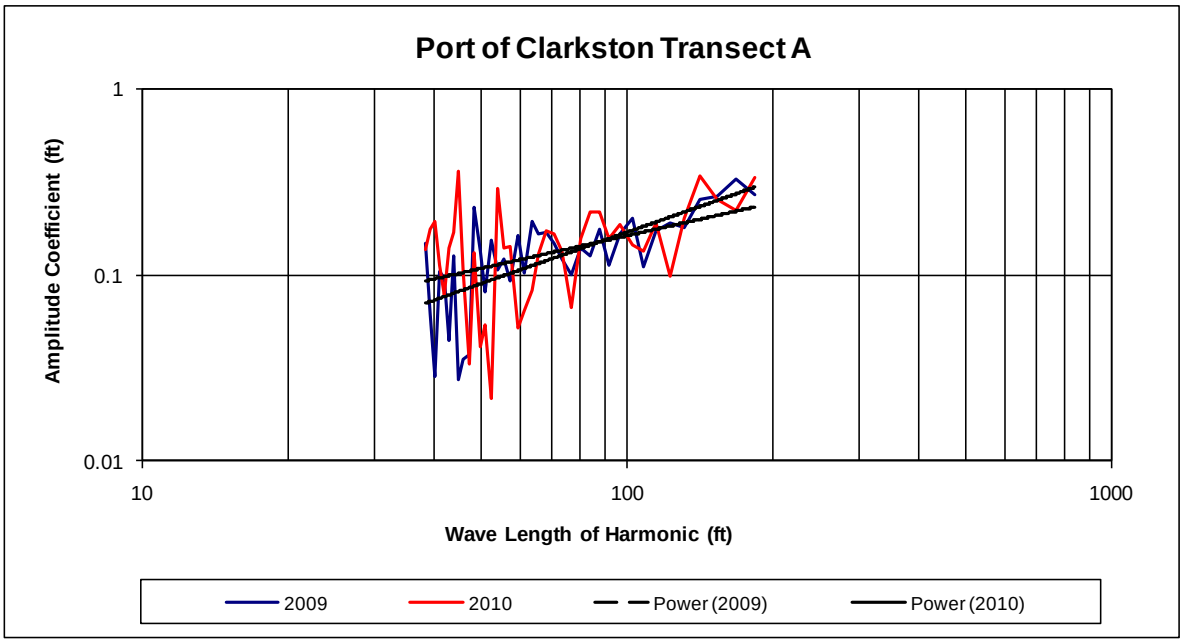


Figure 47. Fourier amplitude coefficient trends for September 2009 and May 2011 at the Port of Clarkston at transect A.

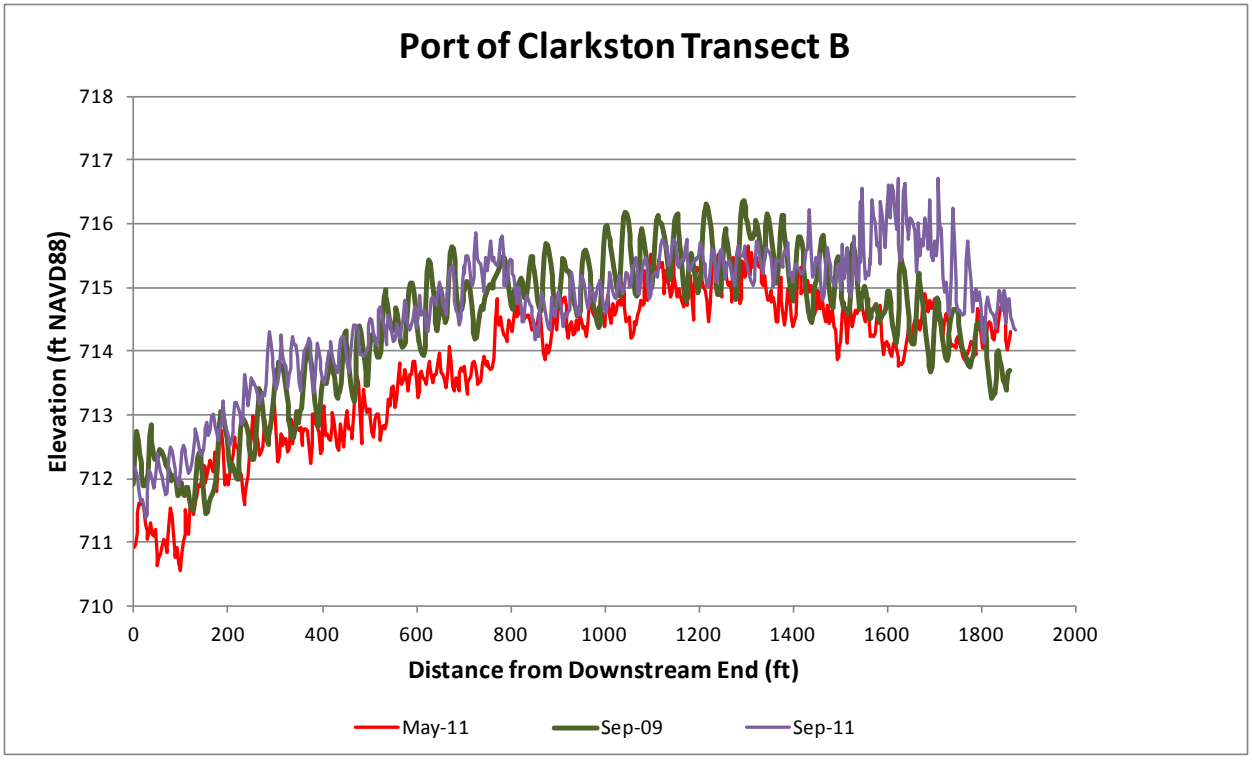


Figure 48. Dune profiles for September 2009 and May 2011 at the Port of Clarkston transect B.

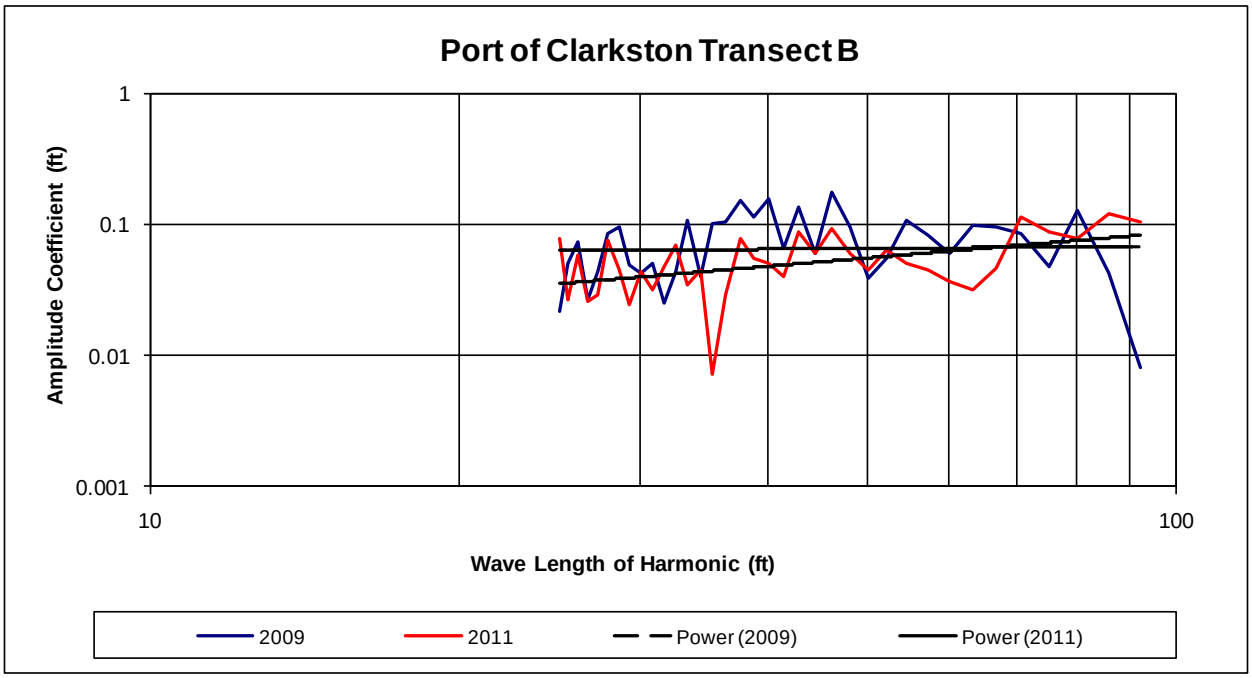


Figure 49. Fourier amplitude coefficient trends for September 2009 and May 2011 at the Port of Clarkston at transect B.

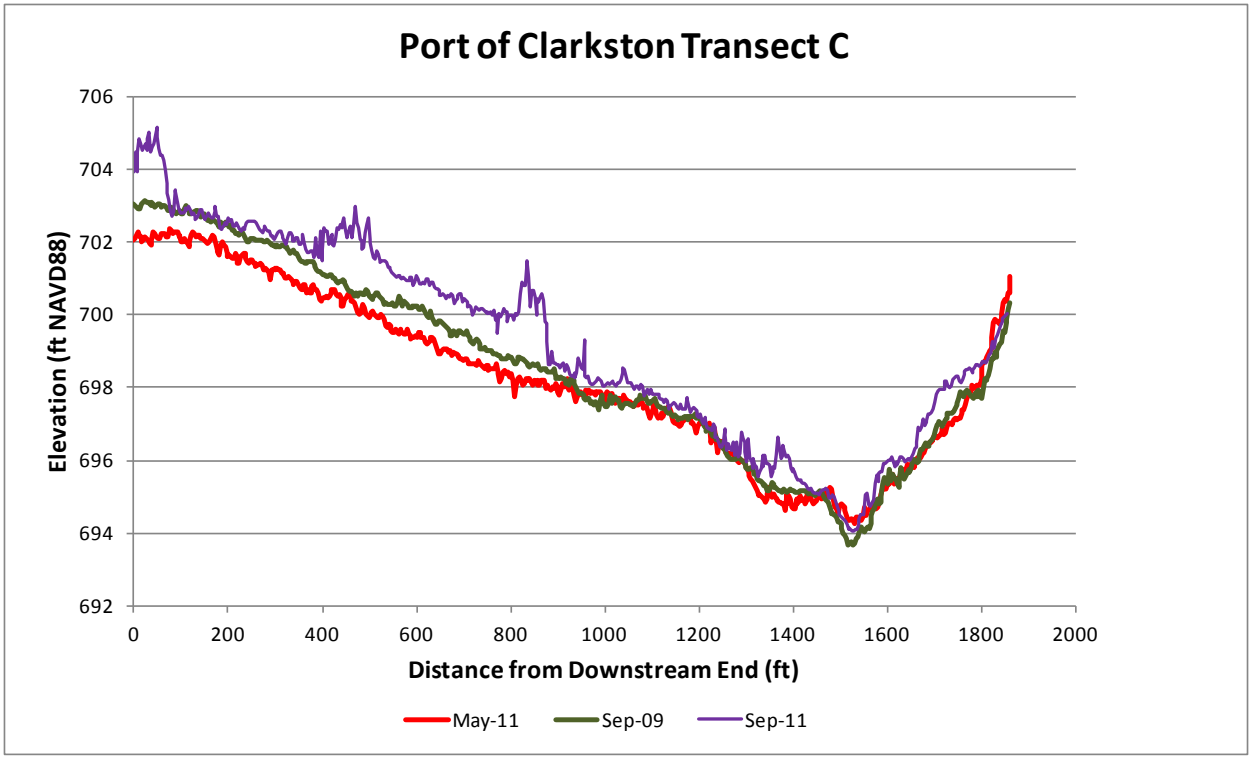


Figure 50. Dune profiles for September 2009 and May 2011 at the Port of Clarkston transect C.

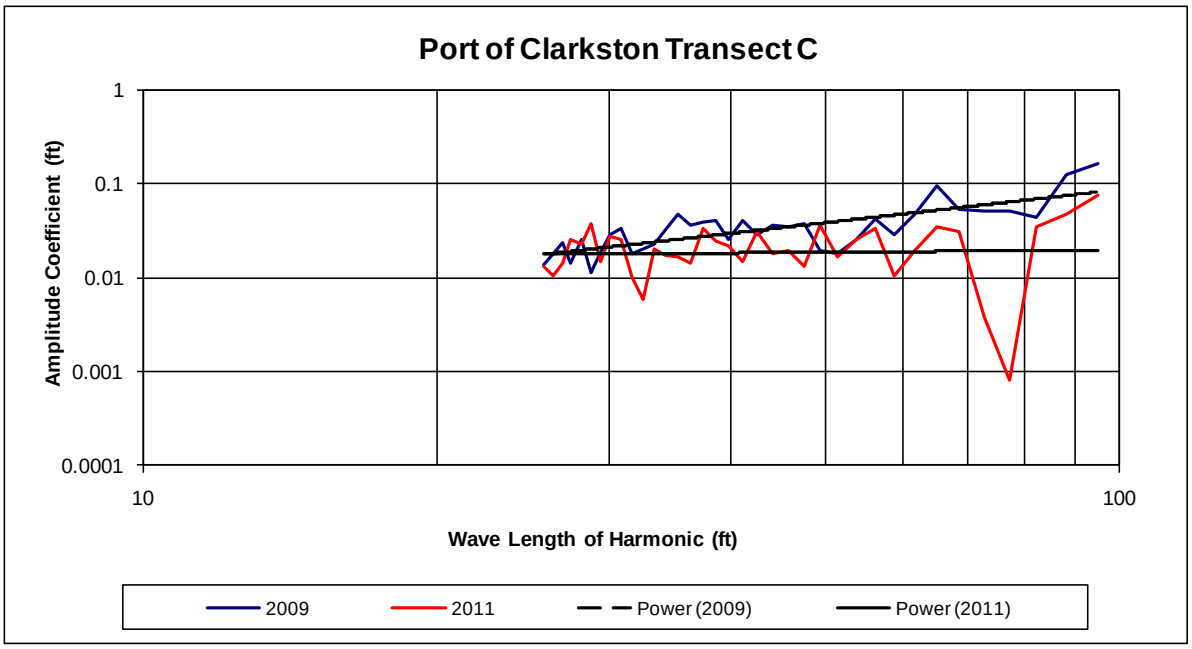


Figure 51. Fourier amplitude coefficient trends for September 2009 and May 2011 at the Port of Clarkston at transect C.

15.5.4. Red Wolf Bedform Profile

Bedform profiles for the Lower Granite Reservoir below Red Wolf Bridge were extracted from the September 2009 and May 2011 bathymetry at the locations in Figure 52. Dune profiles and amplitude coefficients are plotted in Figure 53 and Figure 54. The dune profiles indicate that the Snake River channel had transitioned to upper bed regime when the 26 May 2011 bathymetry was acquired.

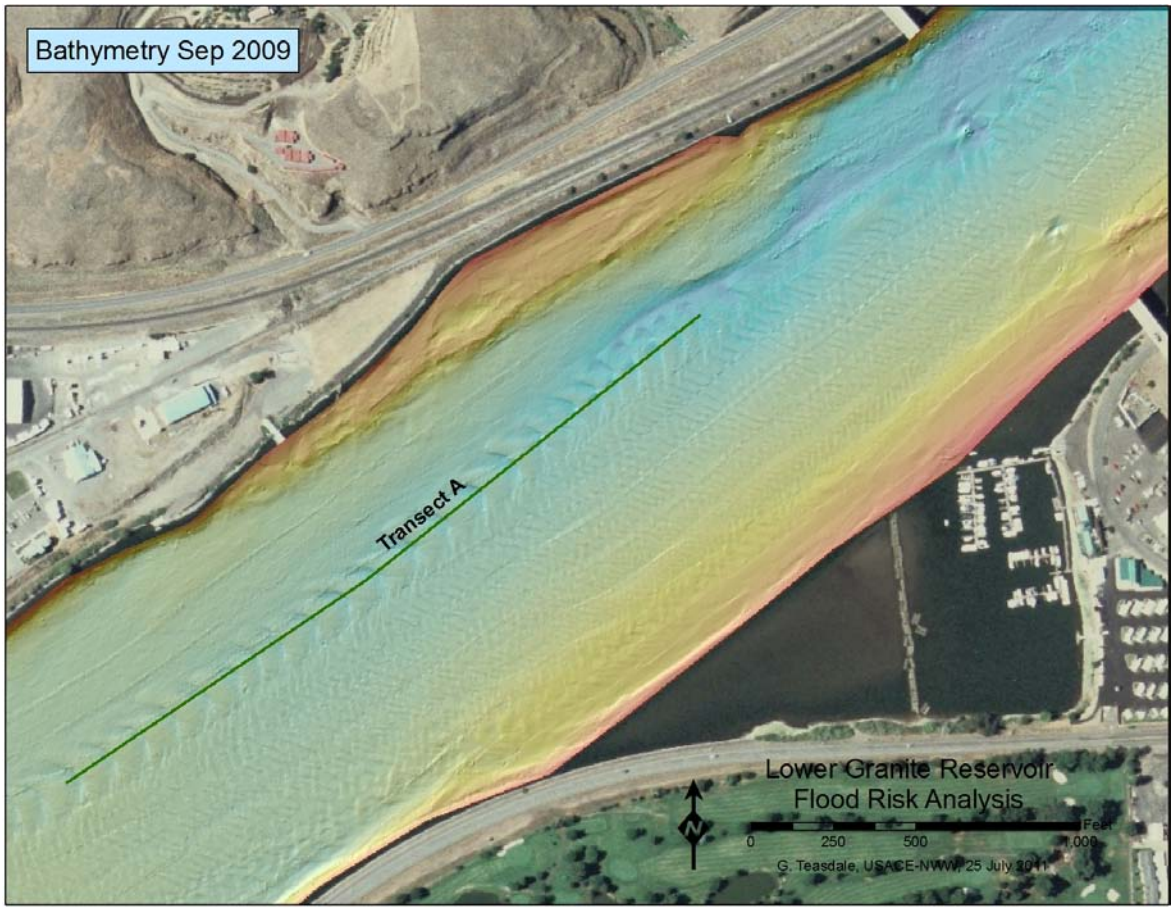


Figure 52. Dune profile transect line at Red Wolf.

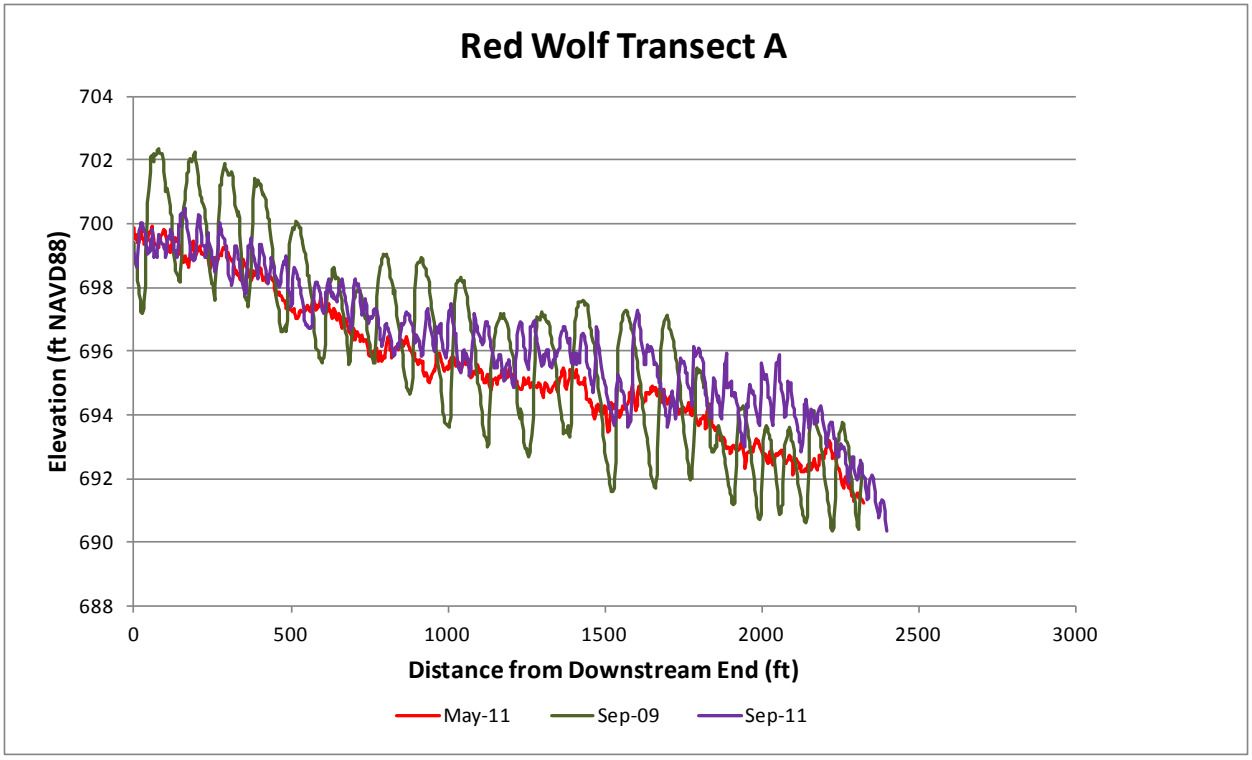


Figure 53. Dune profiles for September 2009 and May 2011 at Red Wolf transect A.

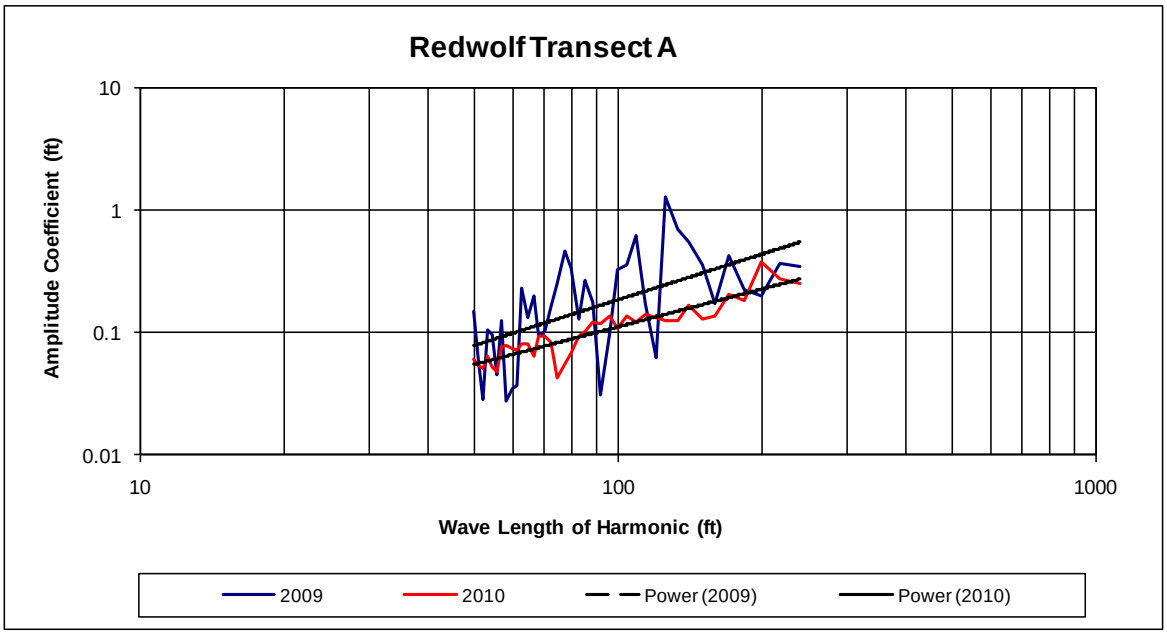


Figure 54. Fourier amplitude coefficient trends for September 2009 and May 2011 at Red Wolf transect A.

15.5.5. Port of Wilma Bedform Profiles

Bedform profiles for the Lower Granite Reservoir at the Port of Wilma were extracted from the September 2009 and May 2011 bathymetry at the locations in Figure 55. Dune profiles and amplitude coefficients are plotted in Figure 56 through Figure 61. Dune profiles along transect A and B lines indicate that the Snake River channel was in transition to upper bed regime when the 26 May 2011 bathymetry was acquired. The channel bed at transect C, which is in the outside of the bend, had not transitioned to upper regime. Dunes in the 26 May 2011 bathymetry are larger than those in the September 2009 bathymetry at transect C.

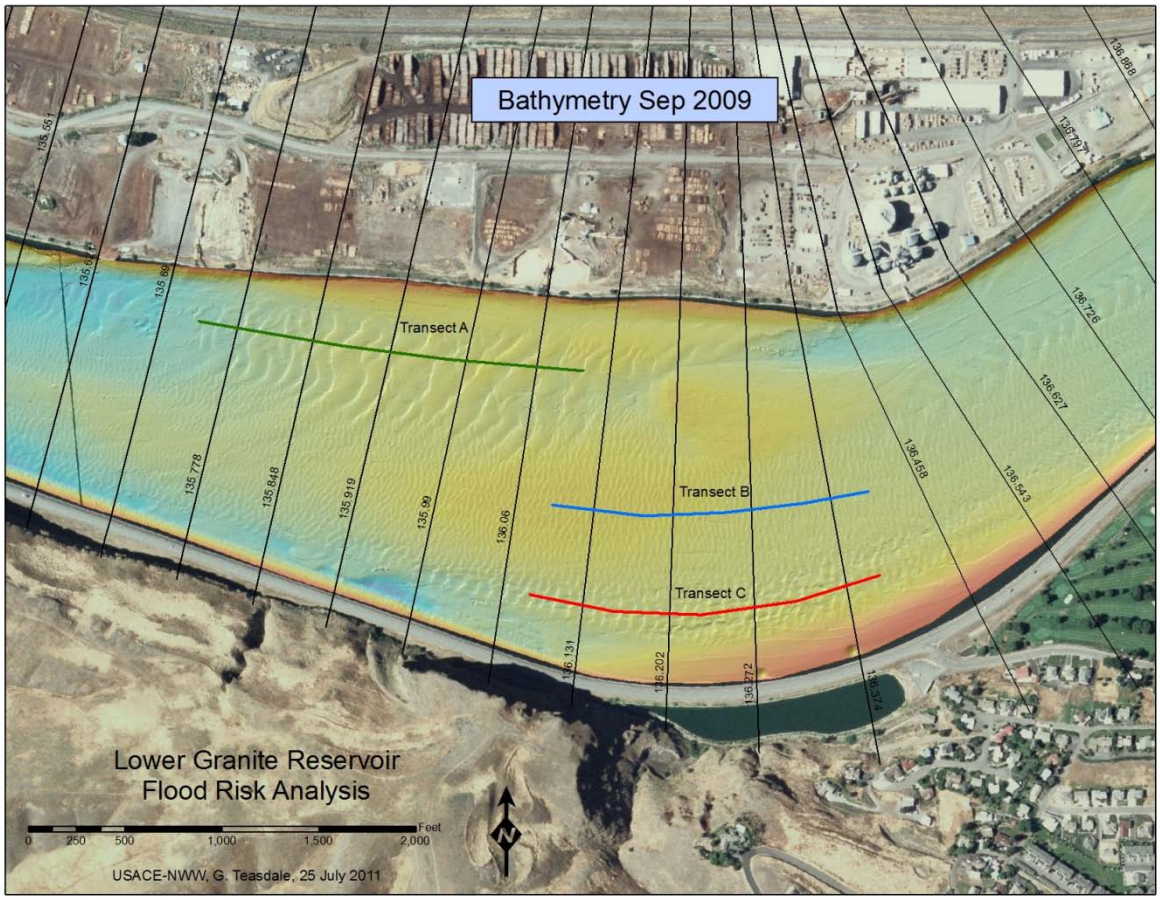


Figure 55. Dune profile transect lines at the Port of Wilma.

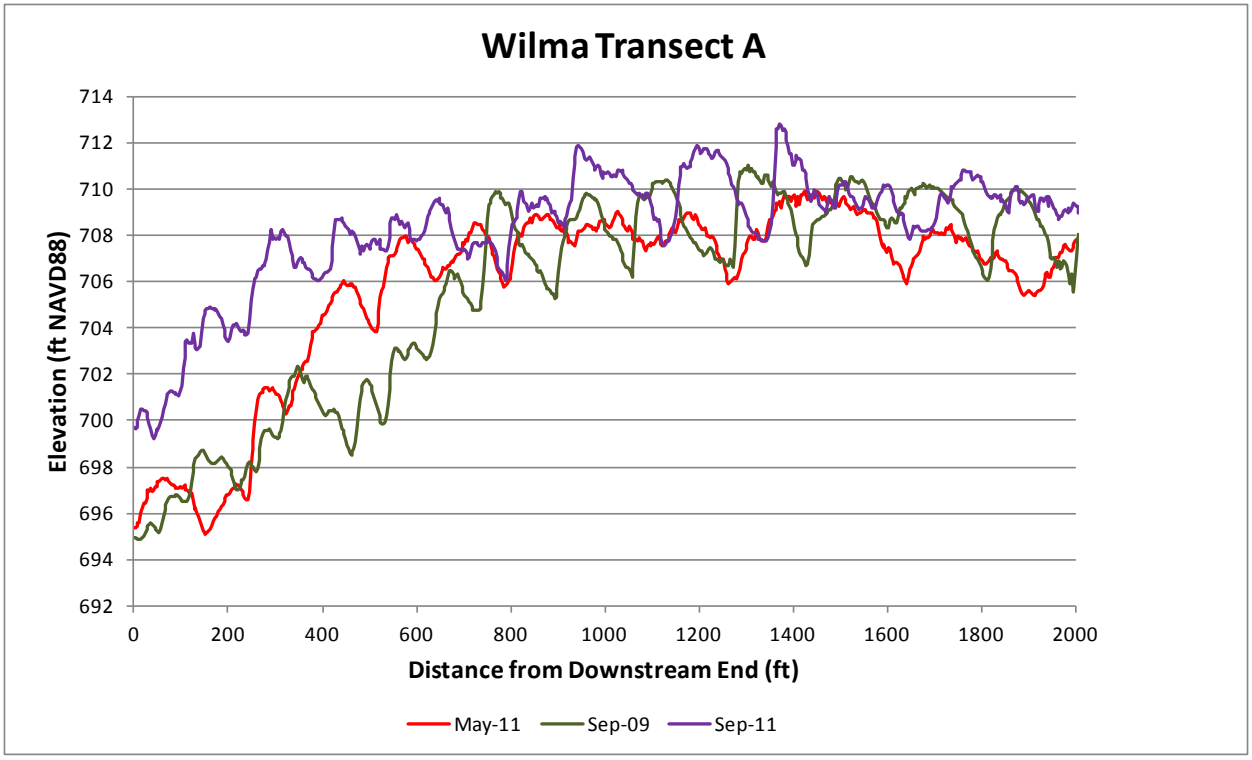


Figure 56. Dune profiles for September 2009 and May 2011 at the Port of Wilma transect A.

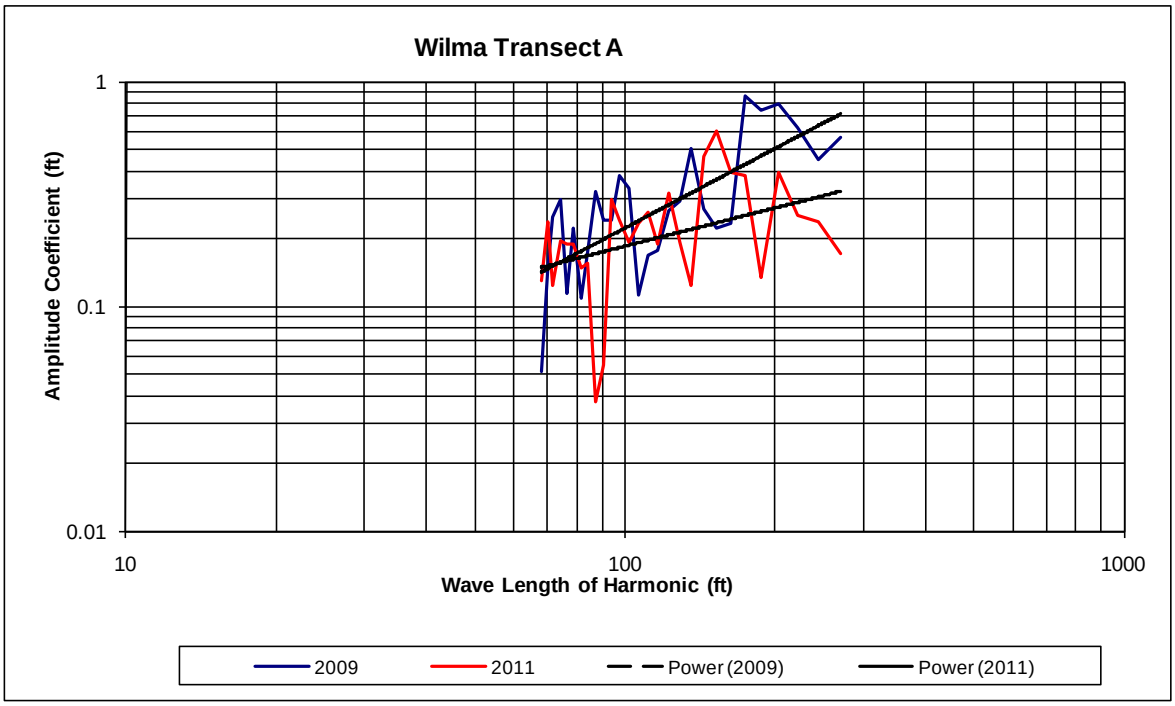


Figure 57. Fourier amplitude coefficient trends for September 2009 and May 2011 at the Port of Wilma at transect A.

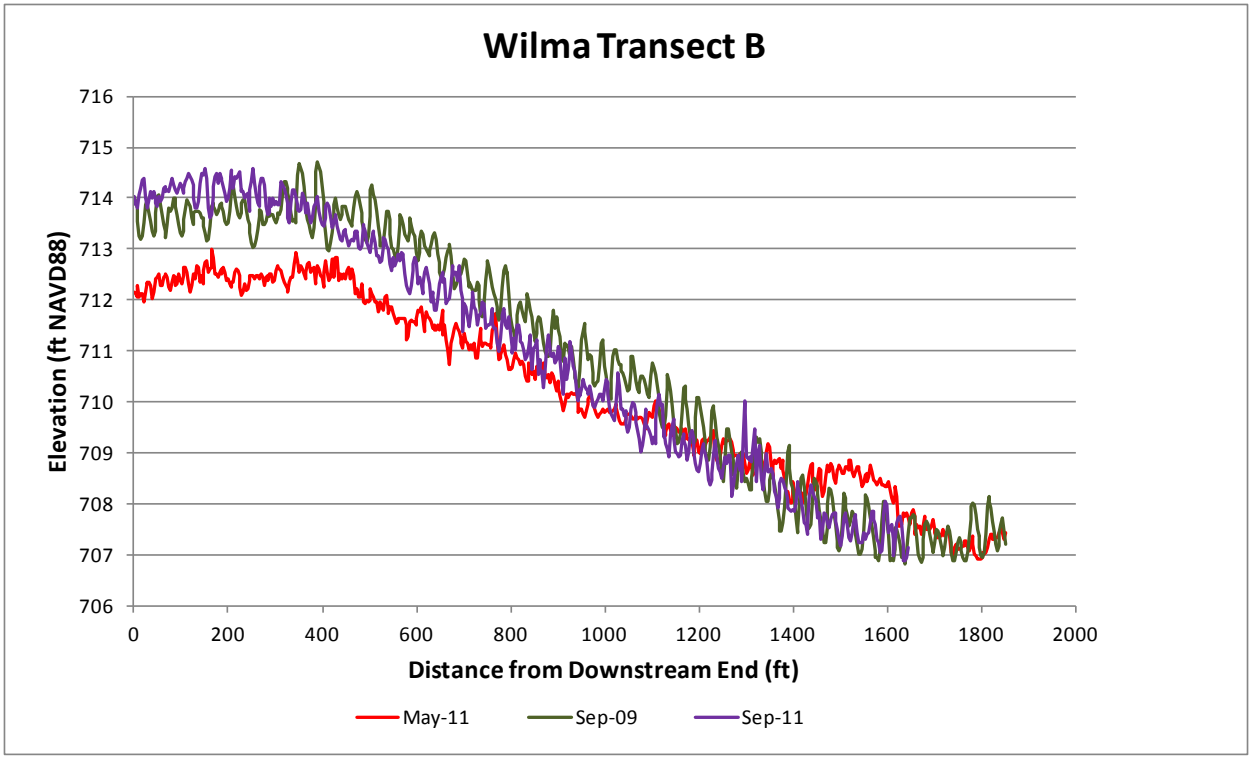


Figure 58. Dune profiles for September 2009 and May 2011 at Port of Wilma transect B.

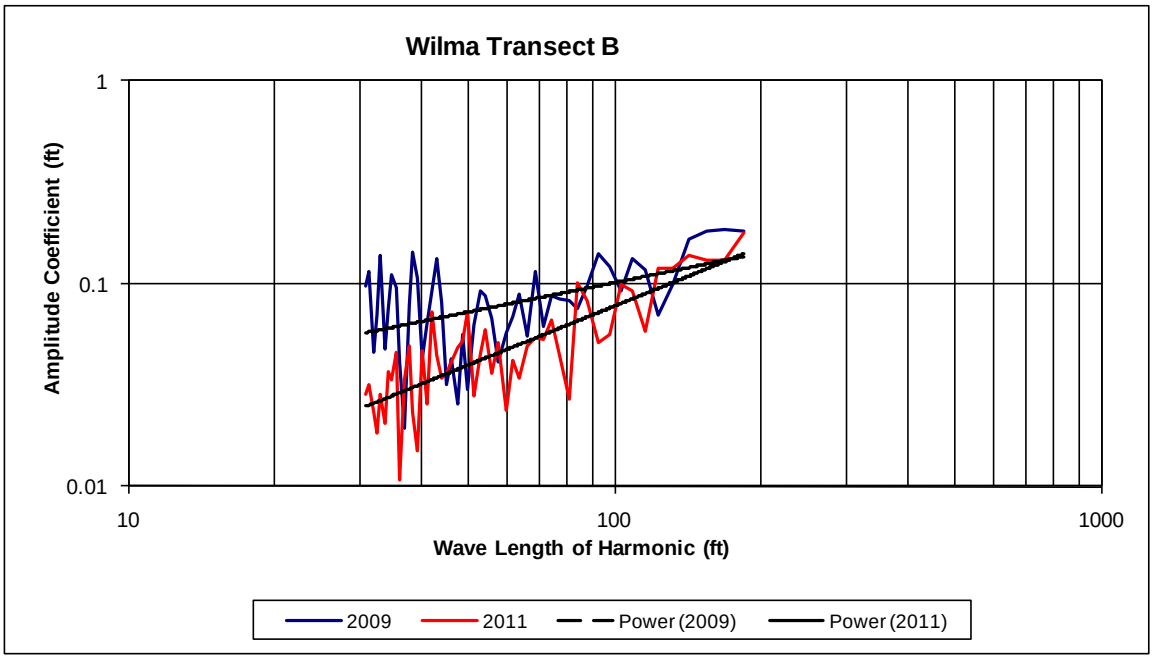


Figure 59. Fourier amplitude coefficient trends for September 2009 and May 2011 at Port of Wilma at transect B.

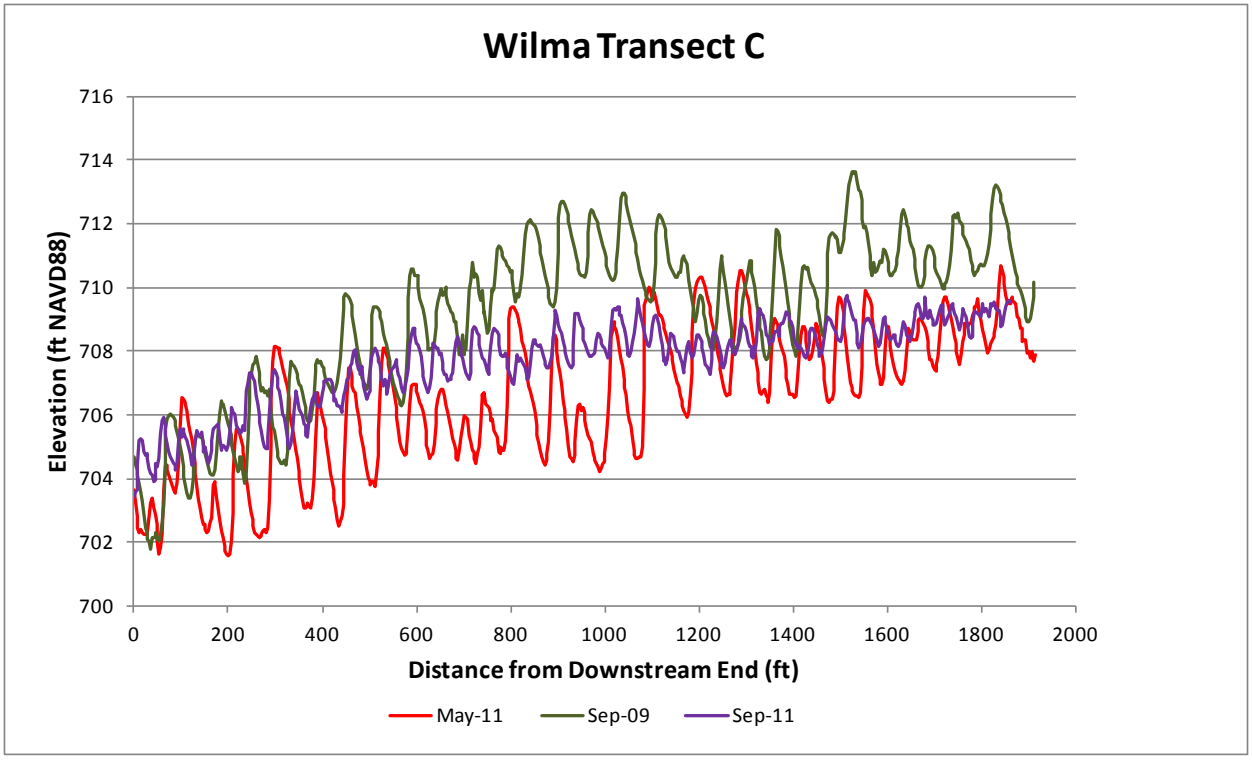


Figure 60. Dune profiles for September 2009 and May 2011 at Port of Wilma transect C.

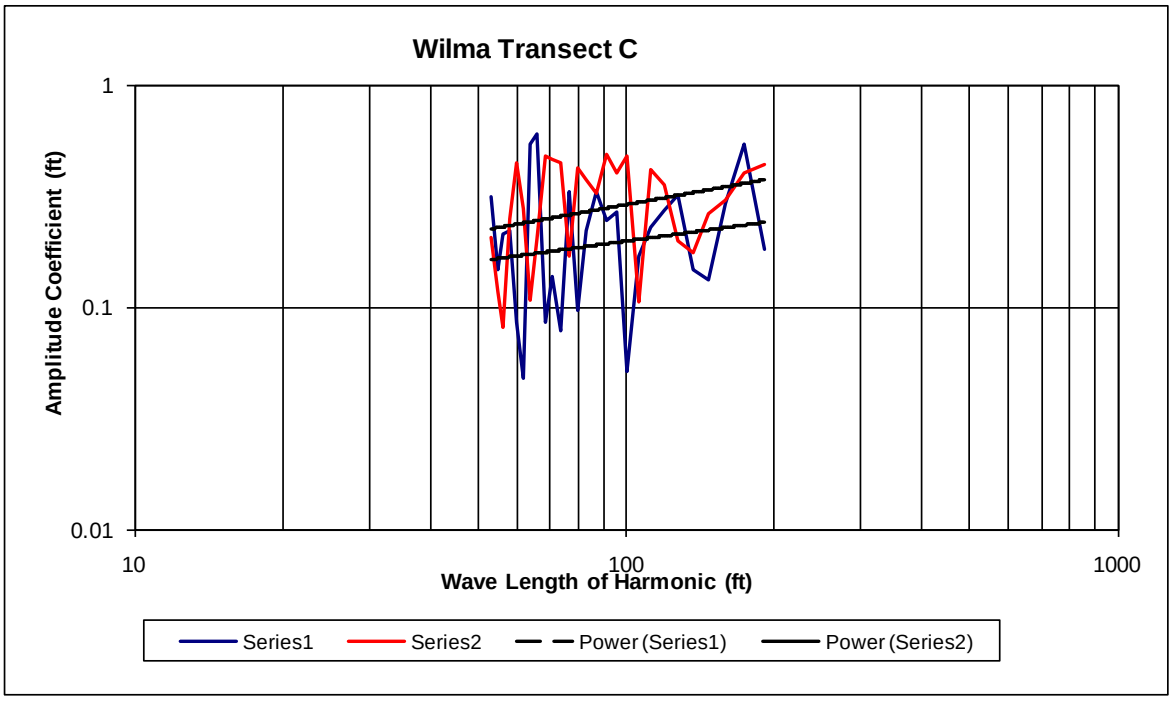


Figure 61. Fourier amplitude coefficient trends for September 2009 and May 2011 at the Port of Wilma at transect C.

15.5.6. Silcott Bedform Profile

Bedform profiles for the Lower Granite Reservoir at Silcott were extracted from the September 2009 and May 2011 bathymetry at the location in Figure 62. Dune profiles and amplitude coefficients are plotted in Figure 63 and Figure 64. The dune profiles indicate that the Snake River channel at this location was not transitioning to upper bed regime when the May 2011 bathymetry was acquired. Dunes in the May 2011 bathymetry are substantially larger than those in the September 2009 bathymetry. The large size of the dunes indicates a relatively high rate of sand transport into the lower reservoir. The residual dunes in the September 2011 bathymetry are about as large as the dunes in the May 2011 bathymetry. The Fourier amplitude plot (Figure 64) for the September 2011 profile agrees well with the amplitude plot for the May 2011 profile, which supports the assumption that residual dunes in the low flow bathymetry approximately represent the largest dunes that develop during recession of the hydrograph.

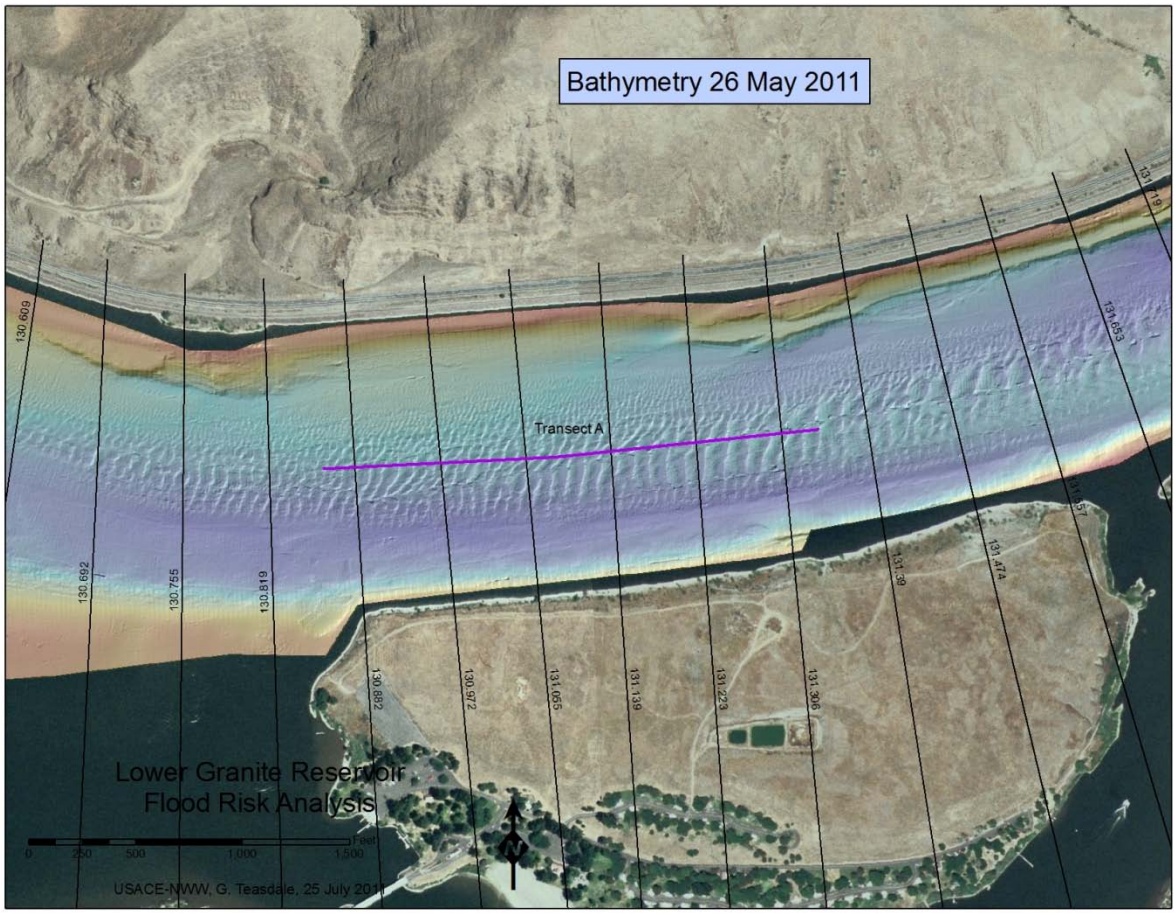


Figure 62. Dune profile transect line at Silcott.

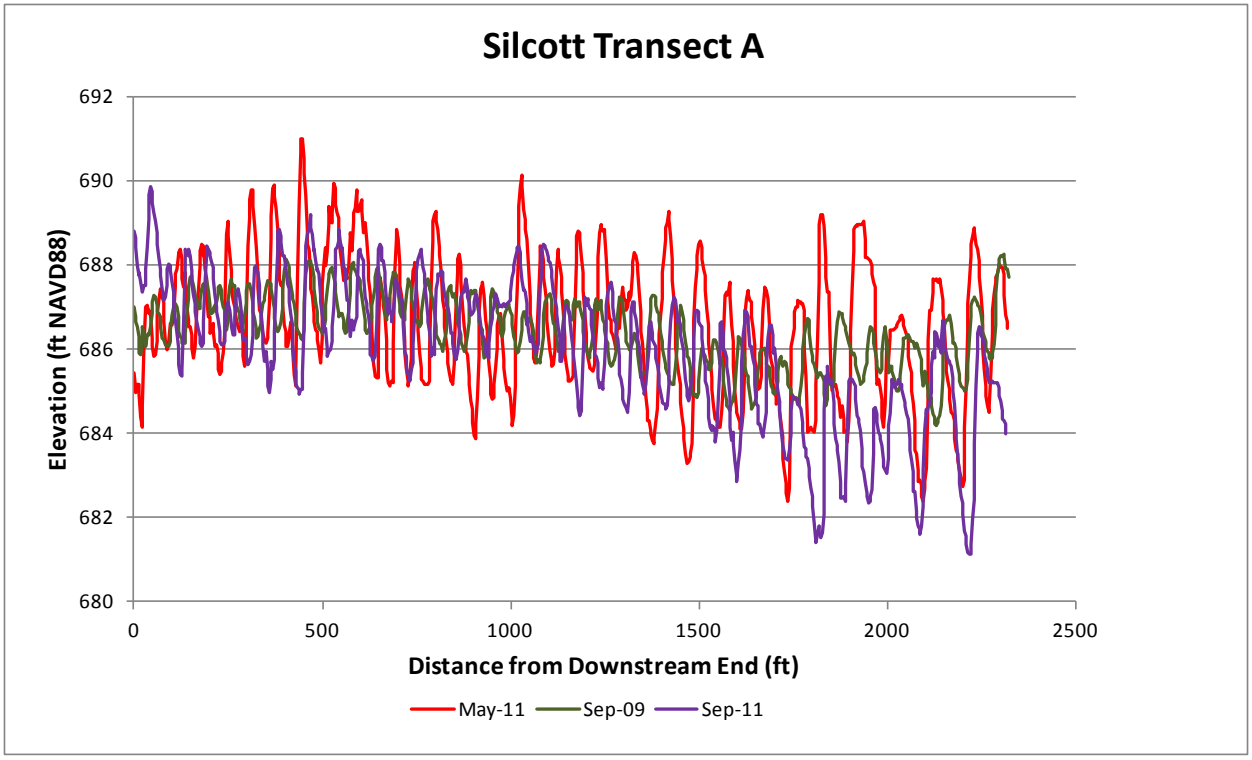


Figure 63. Dune profiles for September 2009 and May 2011 at Silcott transect C.

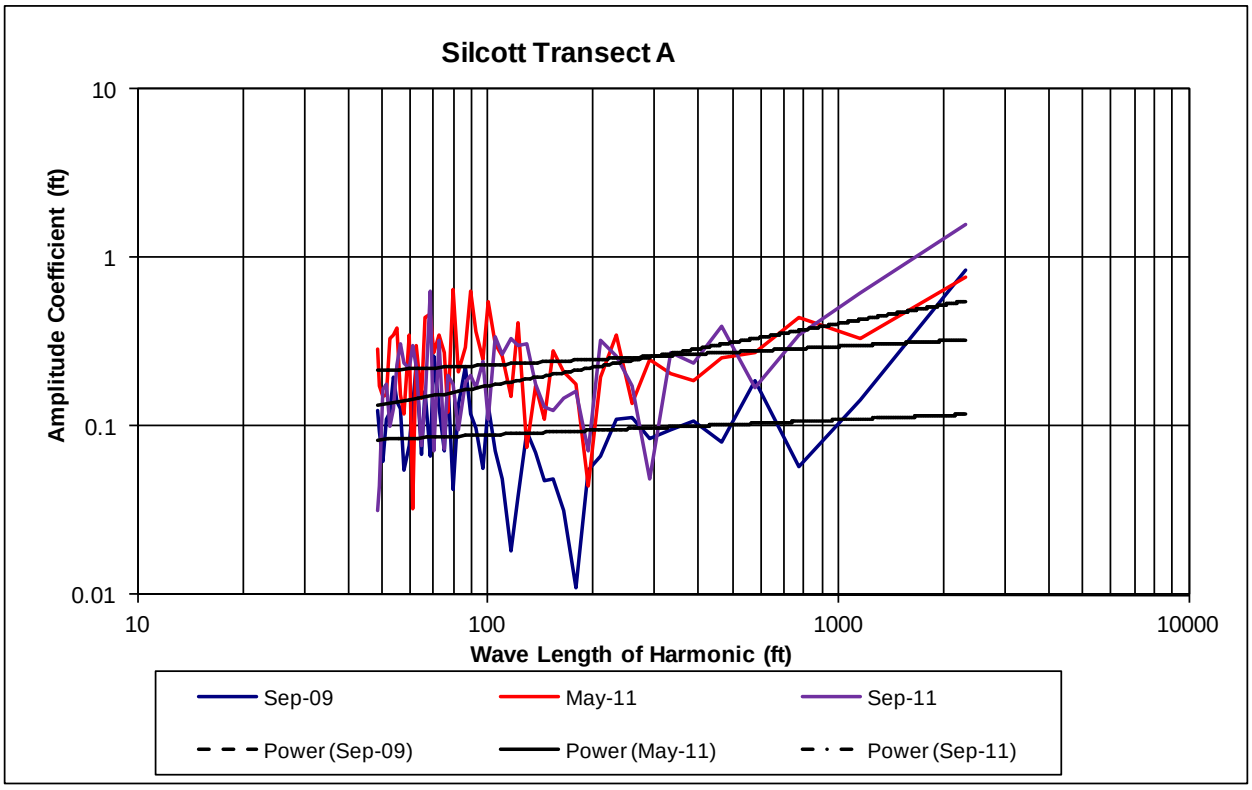


Figure 64. Fourier amplitude coefficient trends for September 2009 and May 2011 at Silcott at transect C.

15.5.7. Snake River Bedform Profile

Bedform profiles for the Snake River near the Interstate Bridge were extracted from the September 2009, May 2011 and September 2011 bathymetry at the locations in Figure 65. Dune profiles and amplitude coefficients are plotted in Figure 66 through Figure 69. The dune profiles indicate that the Snake River was transitioning to upper bed regime above the bridge when the May 2011 bathymetry was acquired and then recovered to lower regime before collection of the September 2011 bathymetry. The plot of transect B in Figure 68 indicates that the bed below Interstate Bridge remained in lower regime. Flow patterns immediately below the bridge likely influence the development of bedforms during recession of the hydrograph because the dunes in the September 2011 bathymetry are not as large as the dunes in the May 2011 bathymetry.

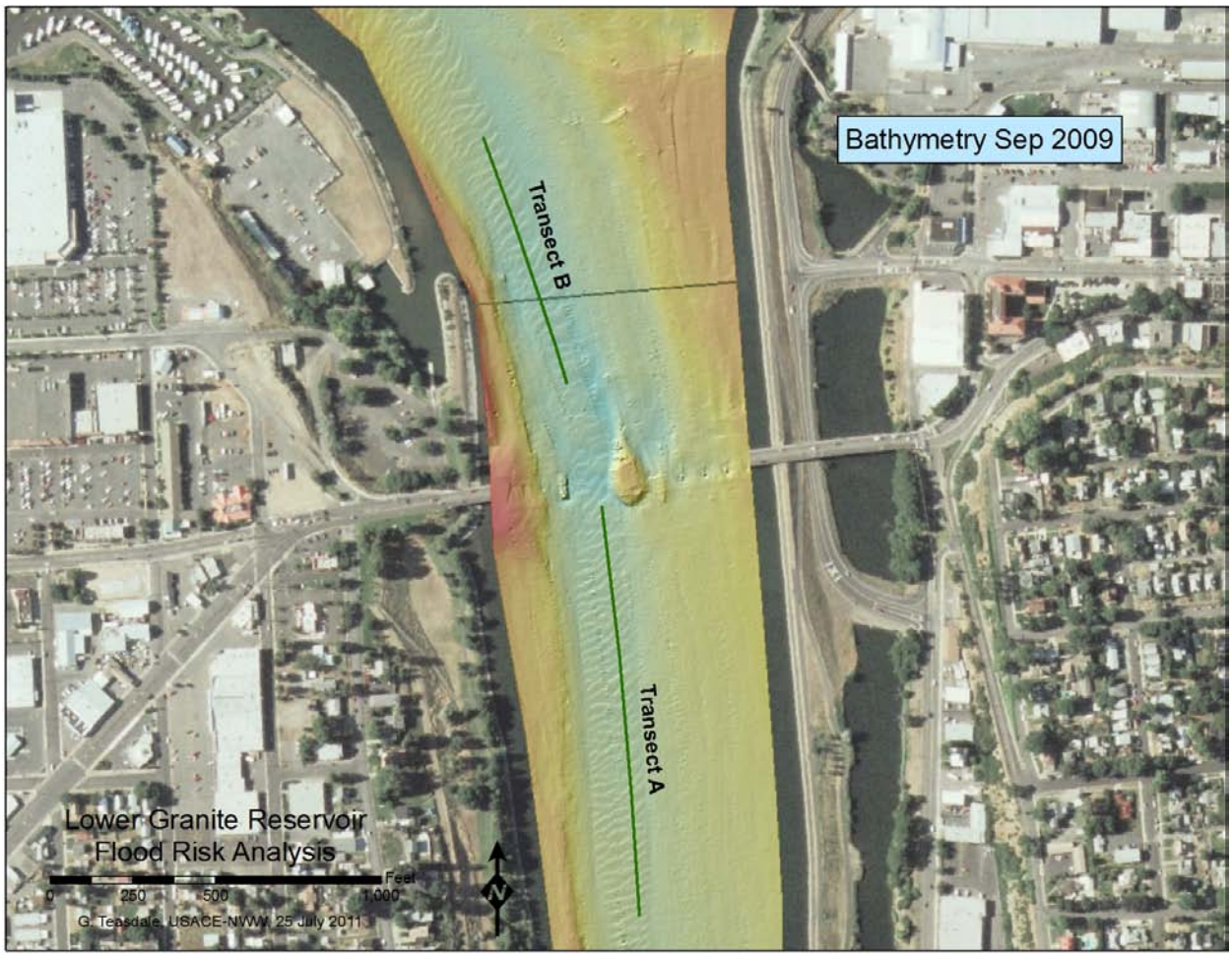


Figure 65. Dune profile transect line in the Snake River near the Interstate Bridge.

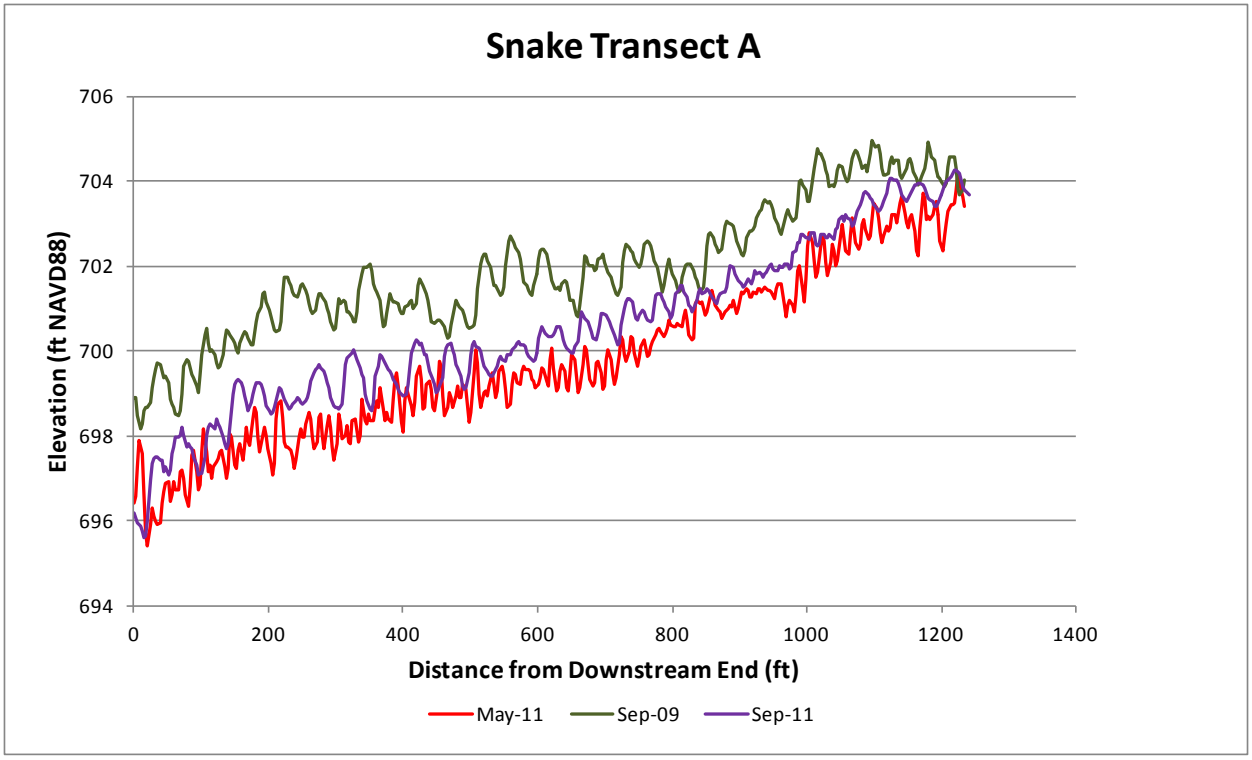


Figure 66. Dune profiles for September 2009 and May 2011 at Snake River transect A.

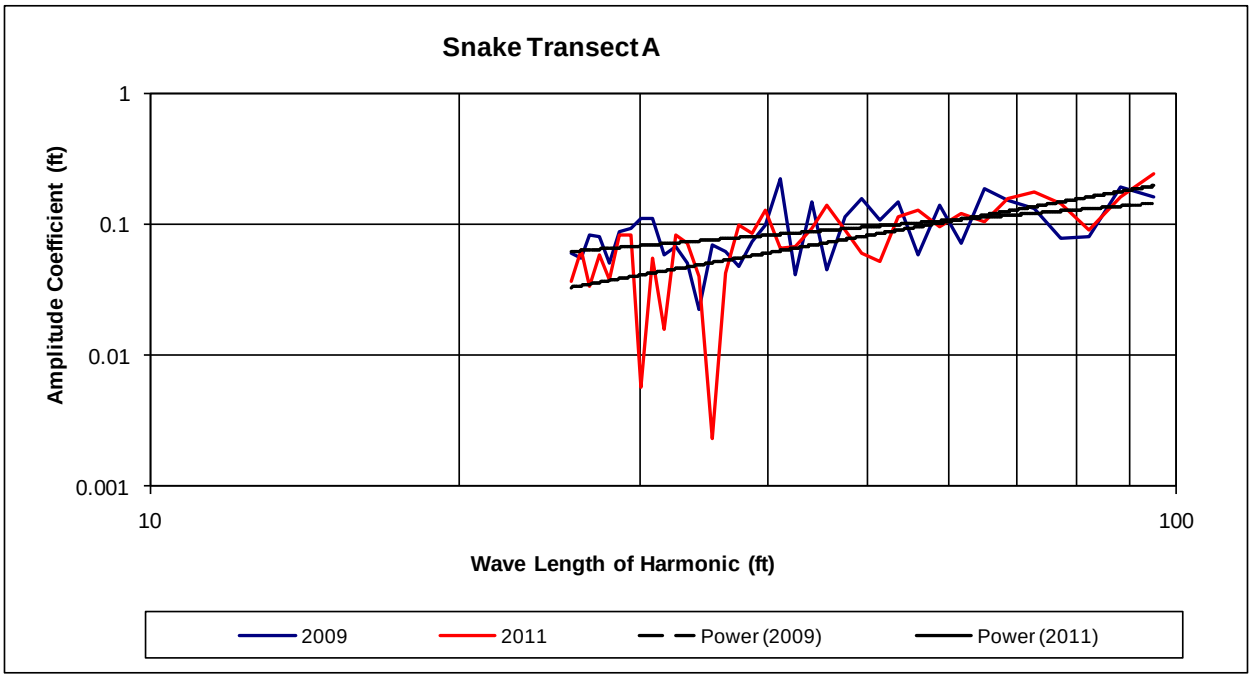


Figure 67. Fourier amplitude coefficient trends for September 2009 and May 2011 at Snake River transect A.

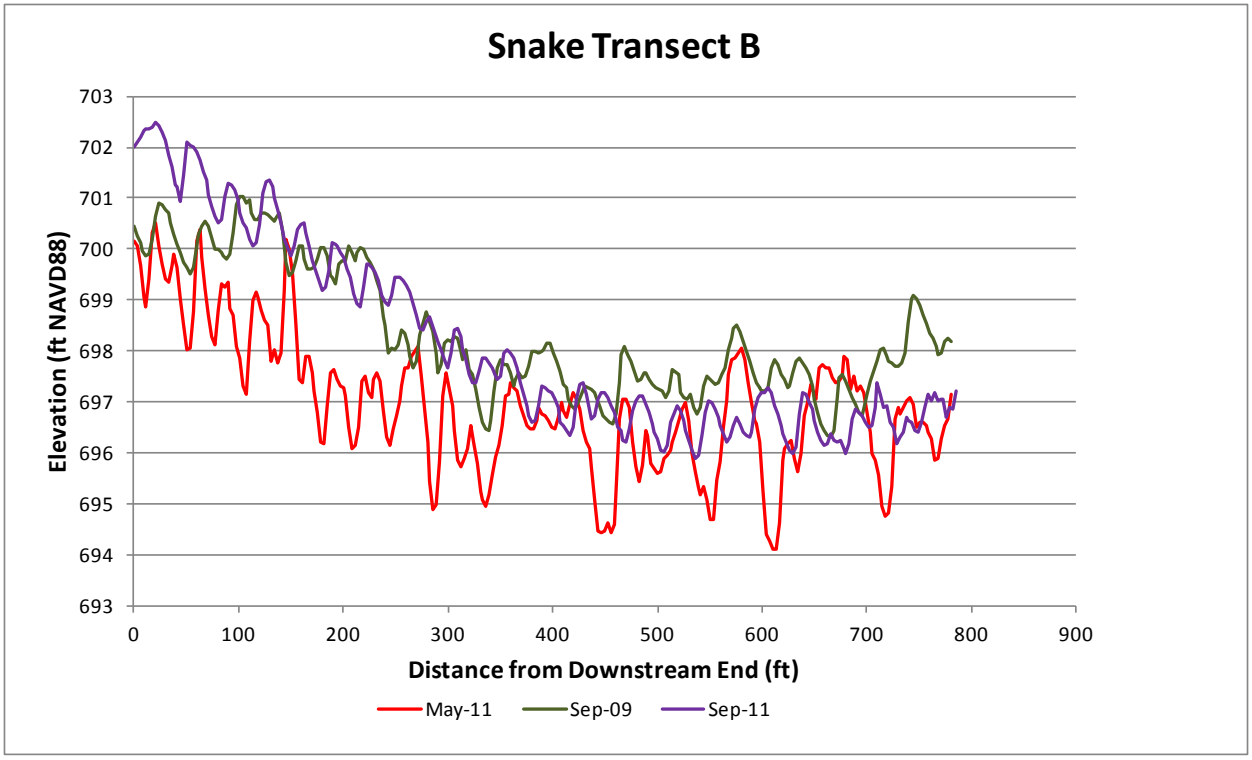


Figure 68. Dune profiles for September 2009 and May 2011 at Snake River transect B.

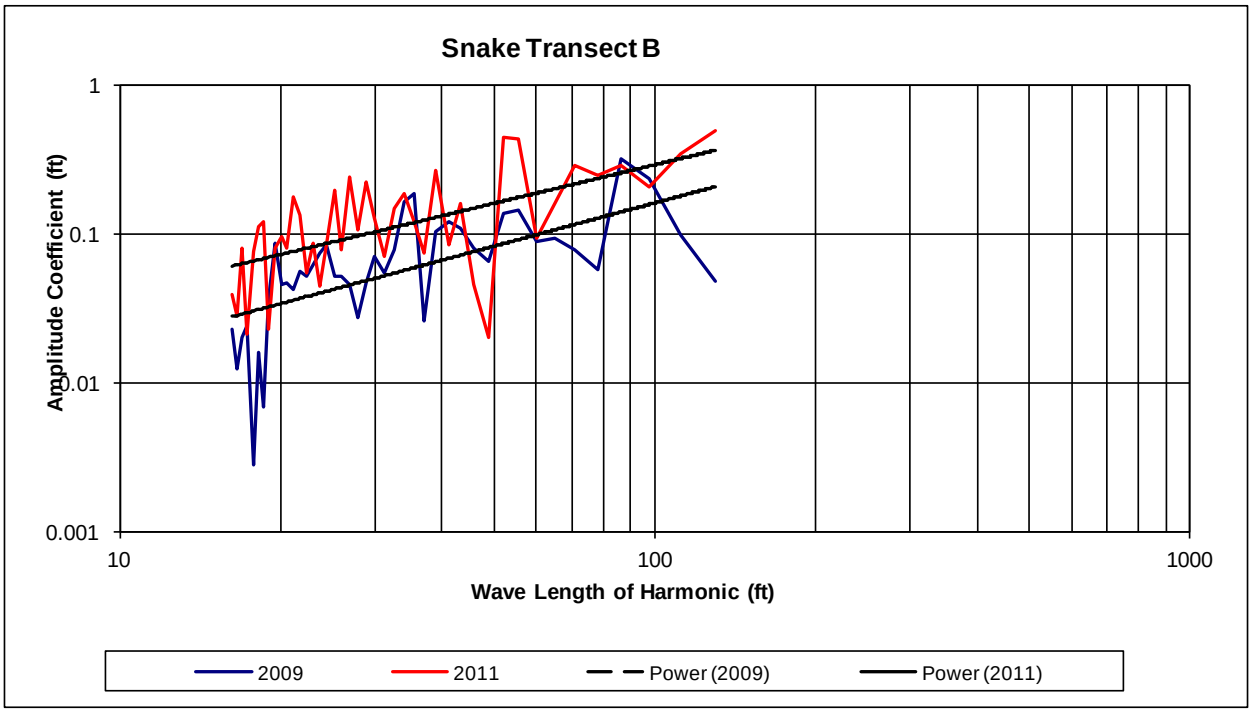


Figure 69. Fourier amplitude coefficient trends for September 2009 and May 2011 at Snake River transect B.

15.6. Bathymetry Difference Mapping

Quantitative changes in channel bathymetry caused by sediment erosion and deposition were computed and mapped by differencing of bathymetry grids. The series of images below show the difference between the September 2009, September 2010, May 2011, and September 2011 bathymetries. Bathymetry acquired in September was during low flow when the bed of the channel was immobile. The May 2011 bathymetry was acquired during high flow when the bed was active. The 2010 bathymetry for the navigation channel condition survey was acquired only in the confluence area and the Clearwater River turning basin. The September 2009 and May 2011 bathymetries were obtained of the Lower Granite Reservoir channel from Silcott Island to the confluence, and from the confluence to the upstream end of the Lewiston levee system on the Snake River. The September 2011 bathymetry was of the entire reservoir from Lower Granite Dam to about RM 141.2 on the Snake River and RM 1.99 on the Clearwater River. Only the main section of the Clearwater turning basin was measured in the May 2011 bathymetry survey.

Differences are depicted in the difference maps below as a classified depth range that varies from - 3 ft to + 3.5 ft. Differences greater or less than this range were depicted as the least or greatest value in the scale range. The legend depicts deposition as shades of yellow and orange, no net change as gray, and scour as shades of green and blue. In all comparisons the bathymetry difference was computed by subtracting the earlier bathymetry grid from the later bathymetry grid.

15.6.1. Confluence Bathymetry Difference Maps

At the confluence, the difference between September 2010 and September 2009 in Figure 70 shows varied erosion and deposition for the main channels and substantial deposition in front of the docking facility near the Quality Inn in Clarkston. In the May 2011 - September 2010 difference map in Figure 71, the high discharge in May 2011 mostly eroded the main channels, but still deposited some sediment in front of the berthing area. The bed eroded an average of 0.35 feet between September 2009 and May 2011 in the area covered by the image. There was substantial erosion of the Snake River channel near the inlet to the USACE Resource Office boat landing in the May 2011- 2010 map which removed the sediment deposited between 2009 and 2010. The difference between the September 2011 and September 2009 bathymetries in Figure 73 shows an average deposition of 1.5 ft, with several feet of new sediment accumulation at the Port of Clarkston. In two-dimensional hydraulic and sediment transport modeling of the confluence the distinct line formed by the dune field on the inside of the bend follows the interface of the merging flows of the Snake and Clearwater Rivers during moderate to high discharge.

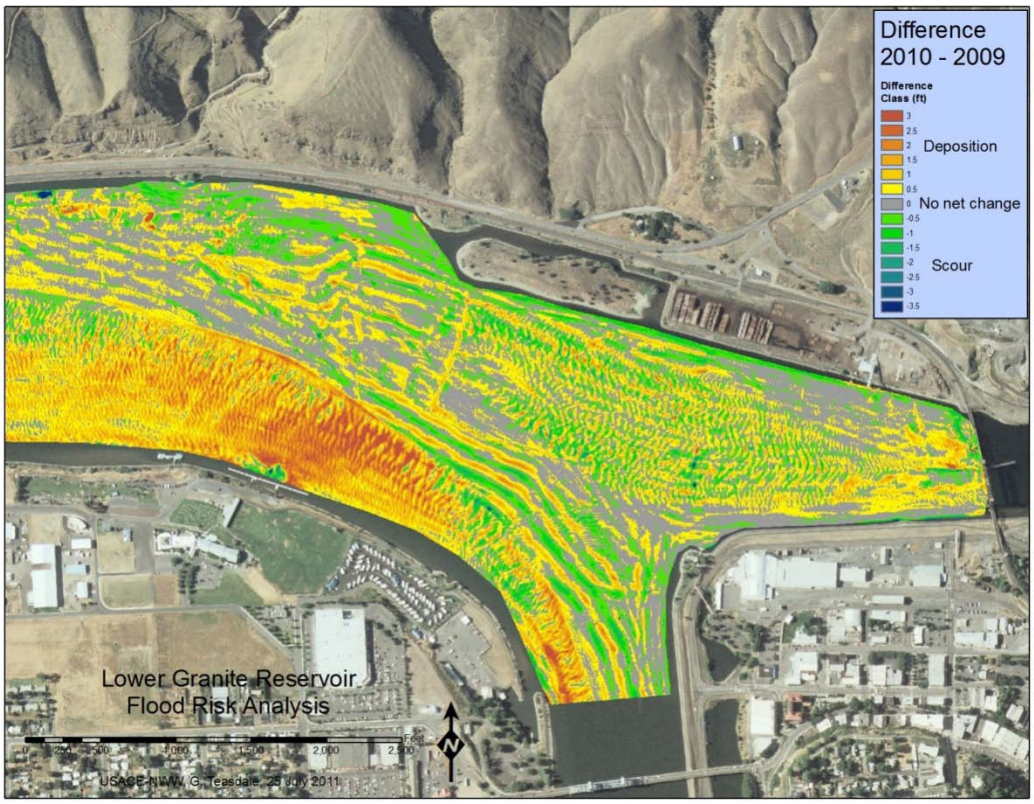


Figure 70. Bathymetry difference September 2010 - September 2009 at the confluence.

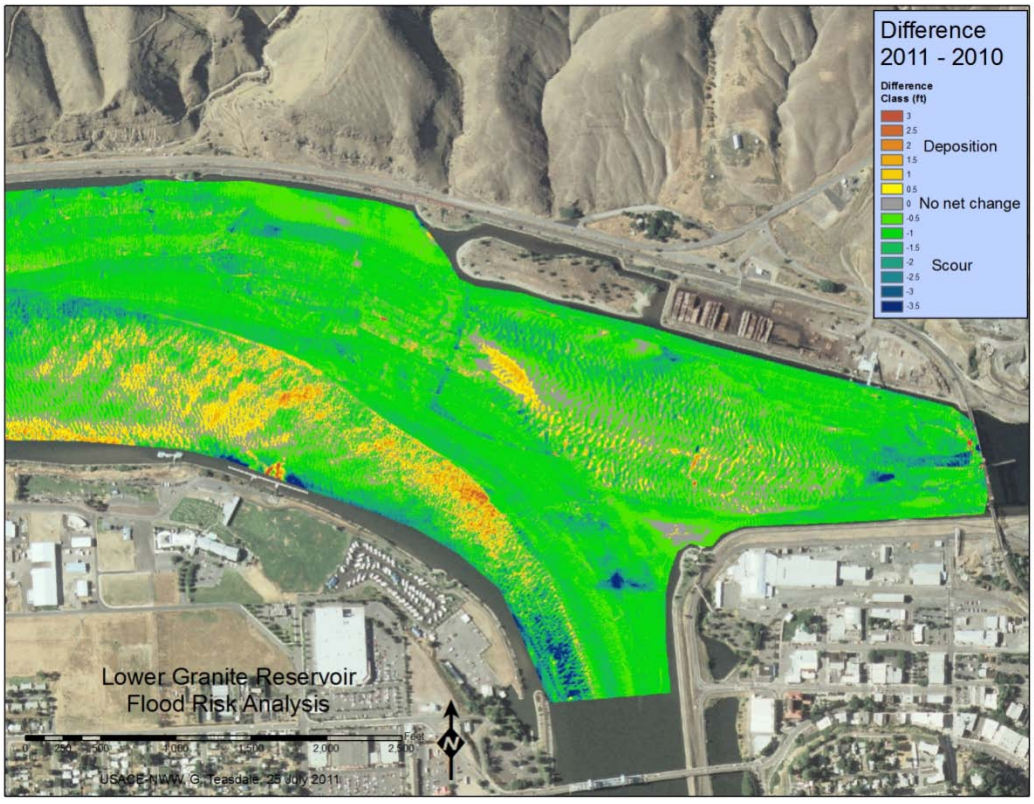


Figure 71. Bathymetry difference May 2011 - September 2010 at the confluence.

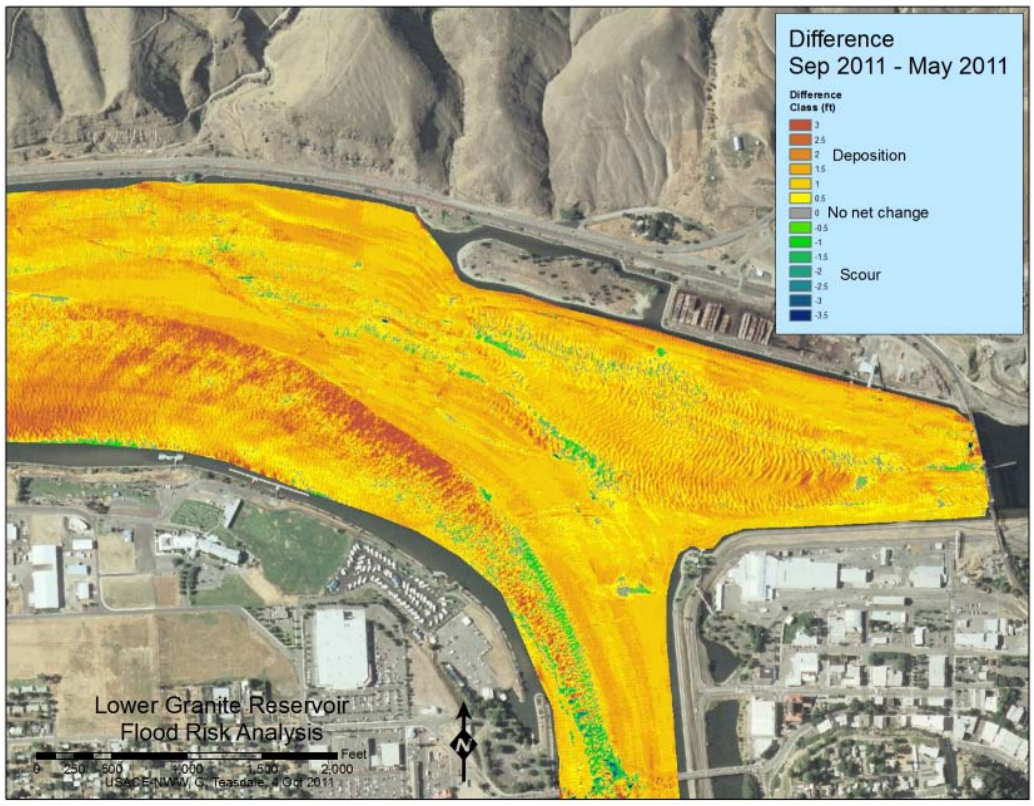


Figure 72. Bathymetry difference September 2011 - May 2010 at the confluence.

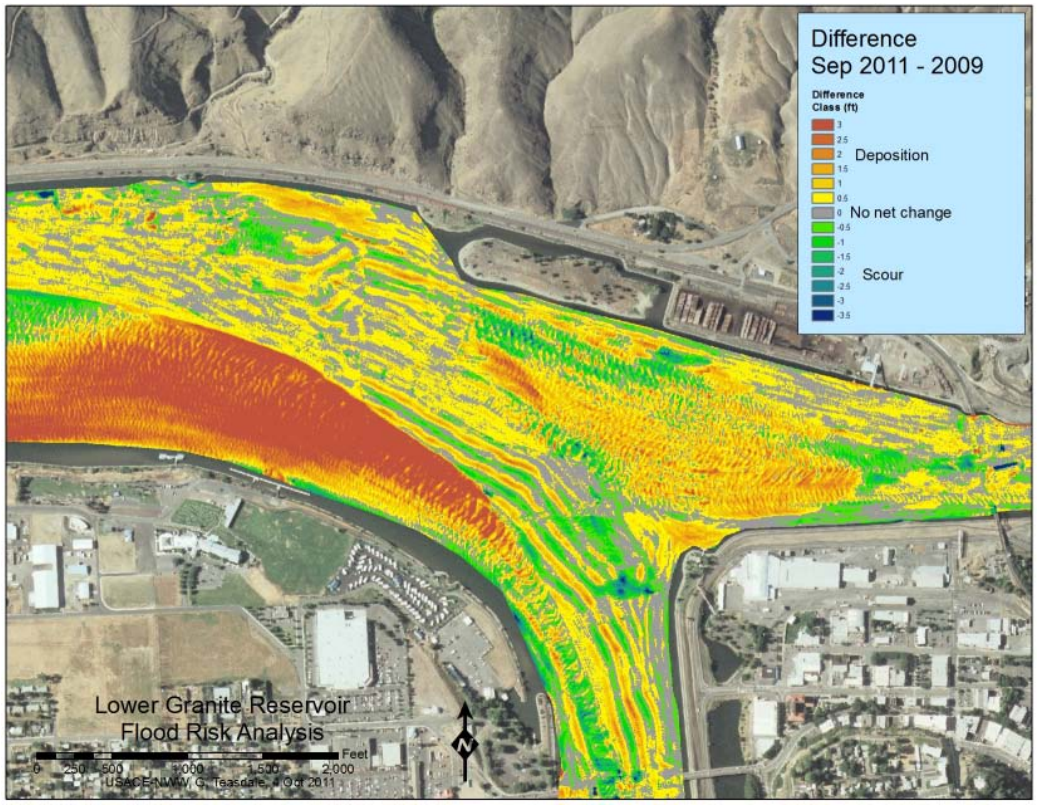


Figure 73. Bathymetry difference September 2011- September 2009 at the confluence.

15.6.2. Port of Clarkston Bathymetry Difference Maps

The bathymetry difference maps at the Port of Clarkston in Figure 74, Figure 75 and Figure 76 show deposition in the main channel between September 2009 and September 2010 and erosion of the accumulated sediment in May 2011. Average bed erosion from September 2009 to May 2011 was 0.3 ft. Following peak flows May 2011, sediment again accumulated and by September 2011 the average depth of deposition was 1.3 ft. Sediment was deposited along the left bank near the port facilities in both 2010 and 2011. There was net erosion of sediment between September 2011 and September 2009 in the middle of the channel downstream from the port.

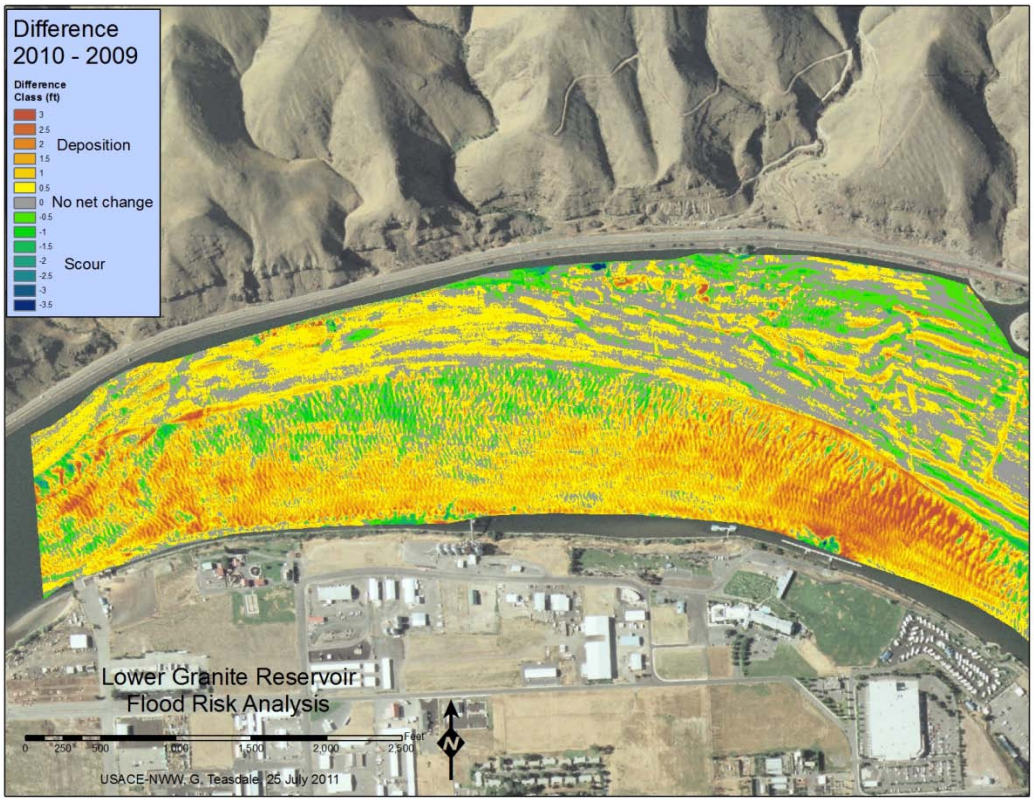


Figure 74. Bathymetry difference September 2010- September 2009 at the Port of Clarkston.

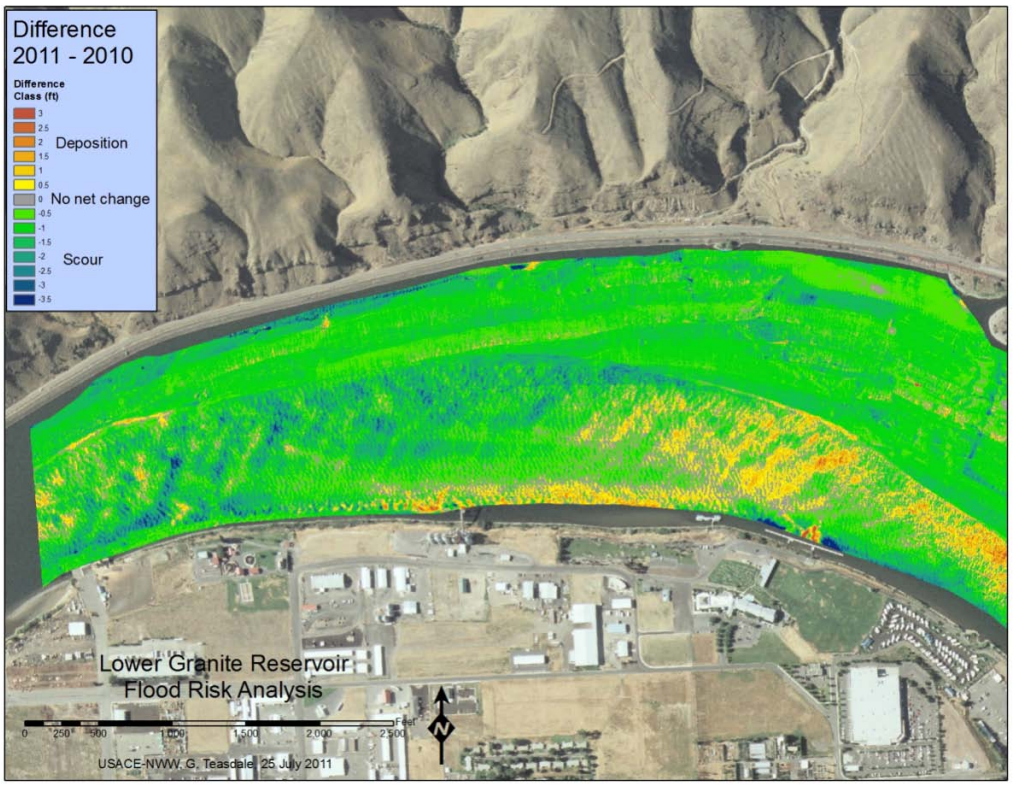


Figure 75. Bathymetry difference May 2011- September 2010 at the Port of Clarkston.

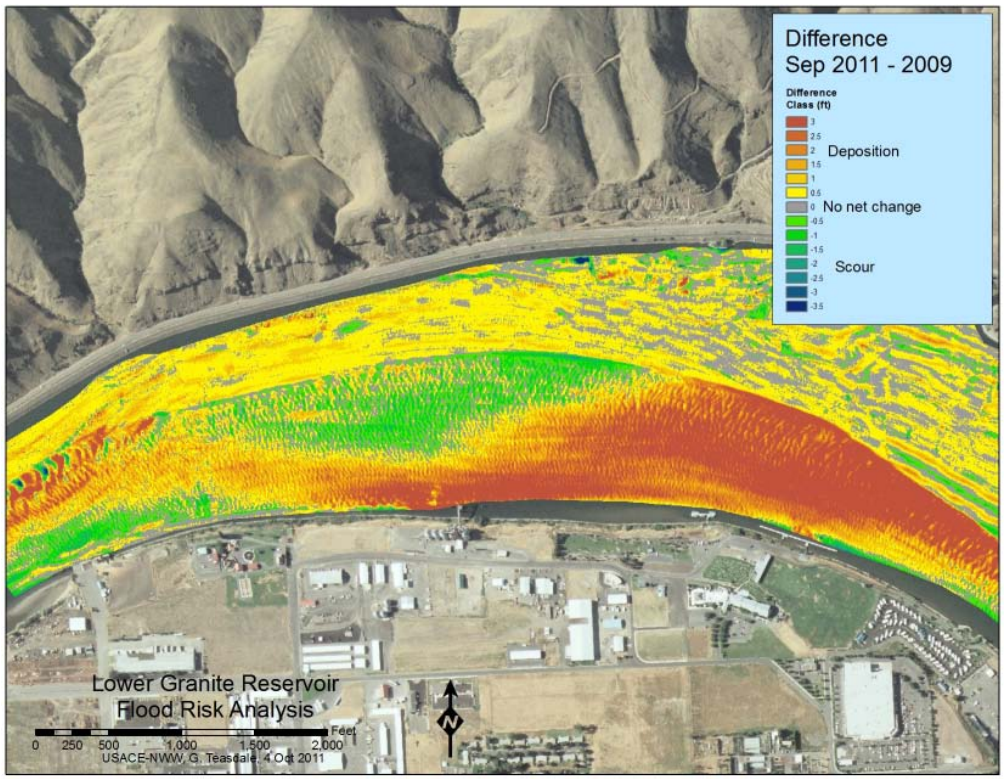


Figure 76. Bathymetry difference September 2011 - September 2009 at the Port of Clarkston.

15.6.3. Port of Lewiston Bathymetry Difference Maps

The bathymetry difference maps for the Clearwater at the Port of Lewiston in Figure 77 through Figure 80 show a redistribution of sand waves within the turning basin from 2009 to 2011 and a small net deposition of less than 0.1 ft by September 2011. The relatively narrow segments of the channel upstream and downstream from the turning basin are dynamically stable and show no net gain or loss of sediment.

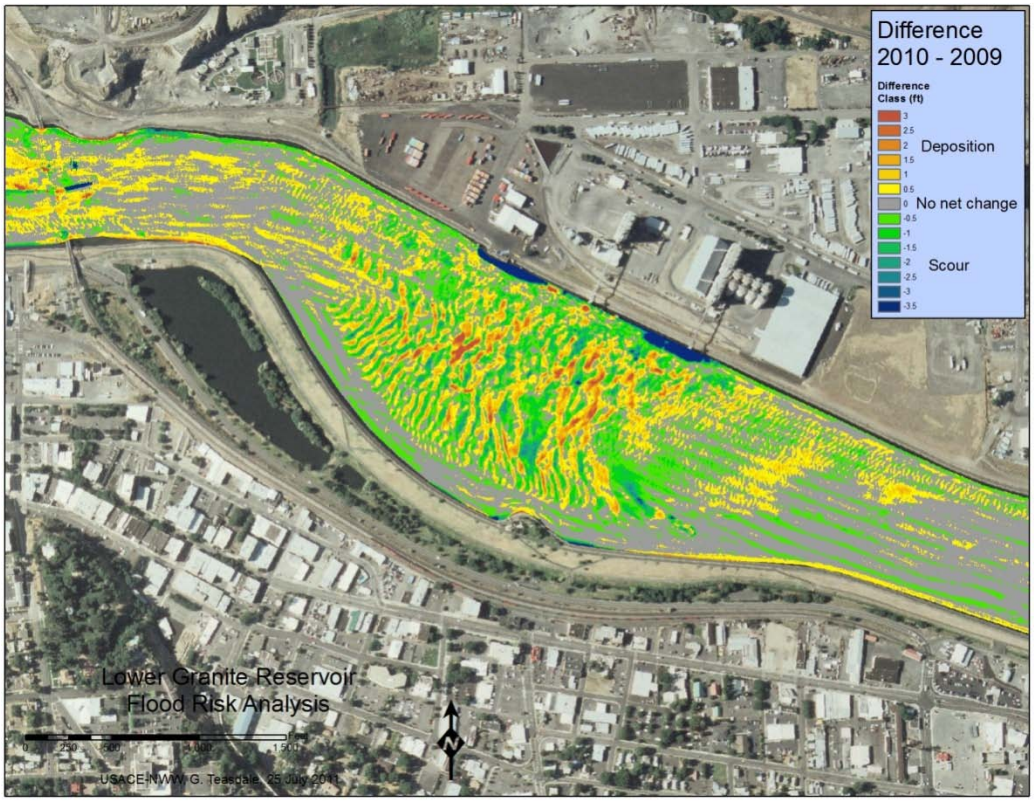


Figure 77. Bathymetry difference September 2010- September 2009 at the Clearwater turning basin.

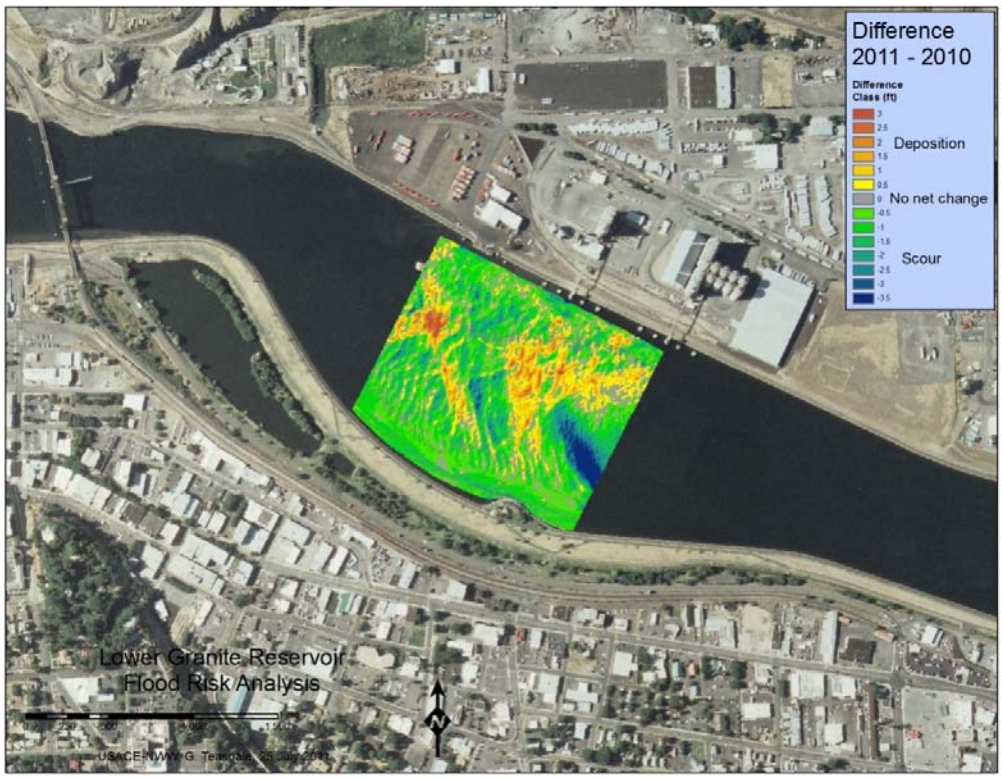


Figure 78. Bathymetry difference May 2011 - September 2010 at the Clearwater turning basin.

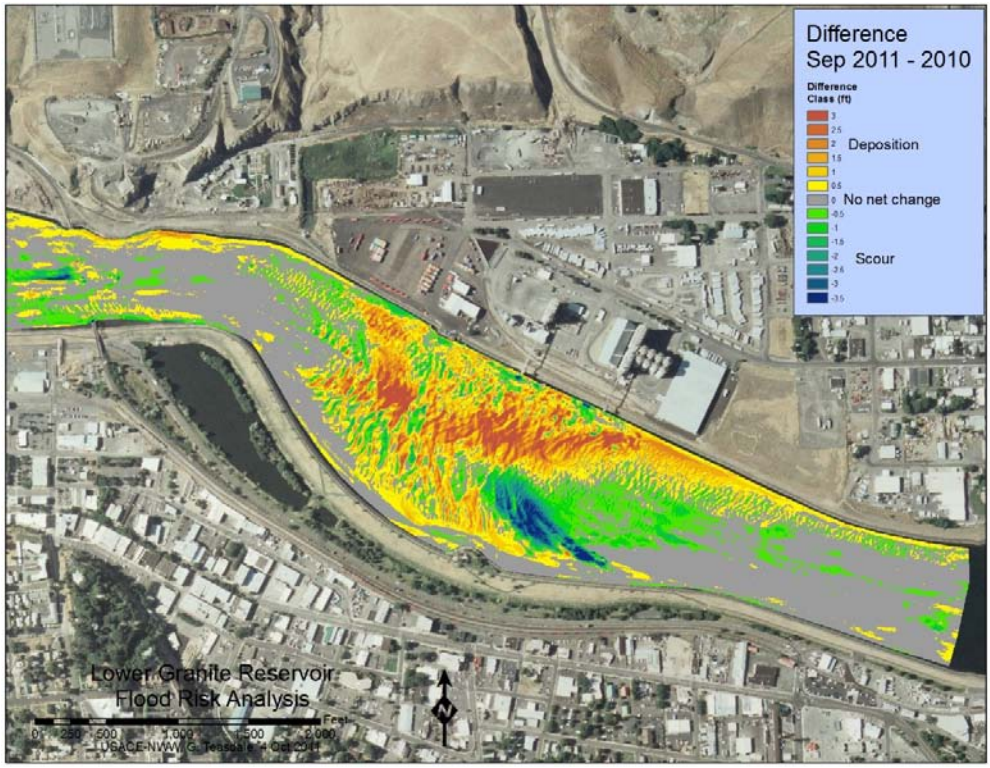


Figure 79. Bathymetry difference September 2011 - September 2010 at the Clearwater turning basin.

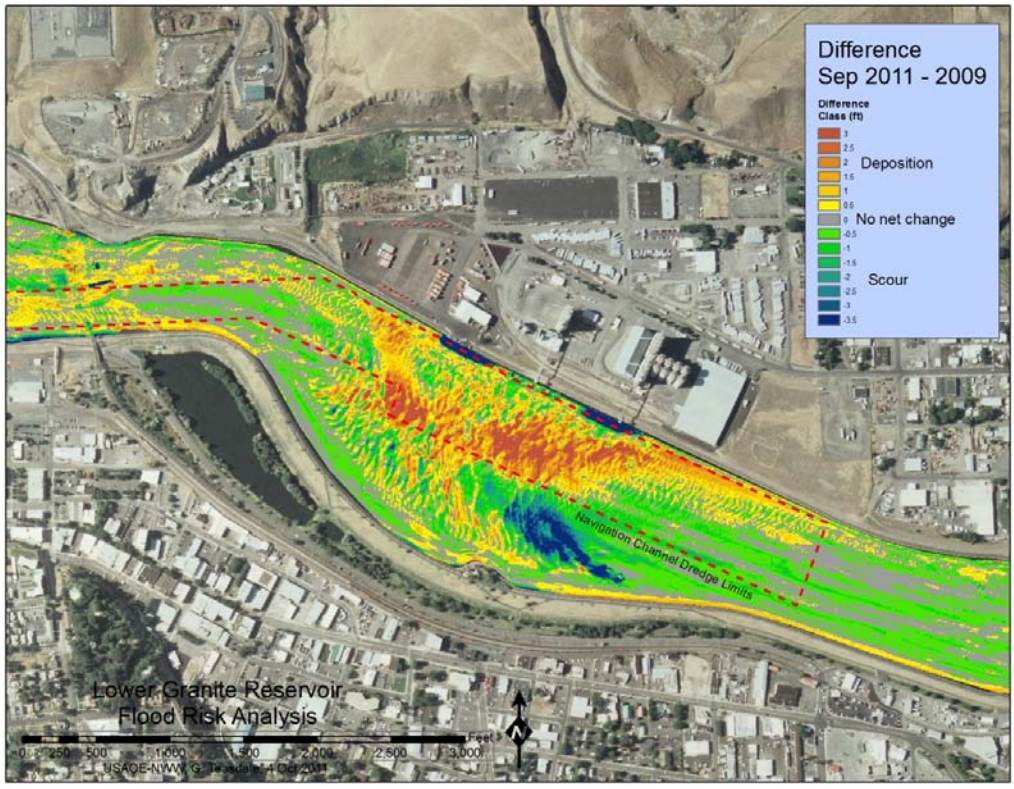


Figure 80. Bathymetry difference September 2011 - September 2009 at the Clearwater turning basin.

15.6.4. Snake River 2011-2009 Bathymetry Difference Maps

Difference maps computed with the 2011 and 2009 bathymetry for the Snake River above the confluence are in Figure 81 through Figure 84. Substantial erosion of the main channel shown on the map occurred during the peak discharge in June 2010 and May 2011. Average bed erosion between September 2009 and May 2011 was 1.49 ft. Erosion of the main channel continues to Interstate Bridge. Below interstate bridge, some deposition was measured in the May 2011 bathymetry. By September 2011 the average depth of erosion had decreased to 0.8 ft.

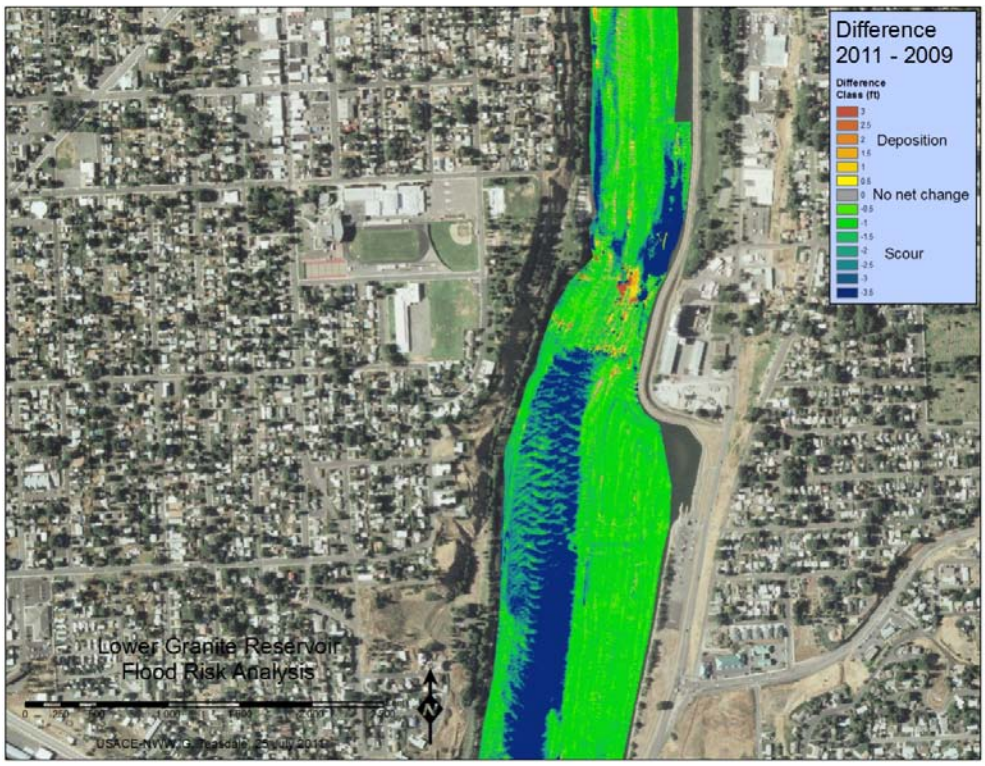


Figure 81. Bathymetry difference May 2011- September 2009, Snake River at upstream end of levee.

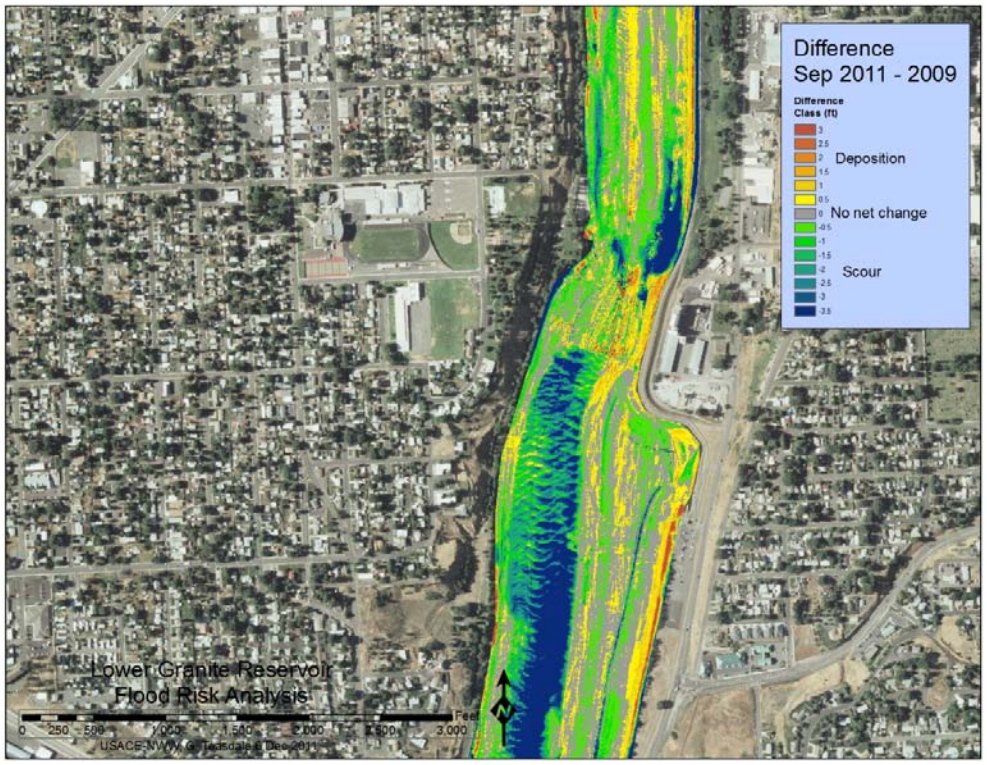


Figure 82. Bathymetry difference September 2011- September 2009, Snake River at upstream end of levee.

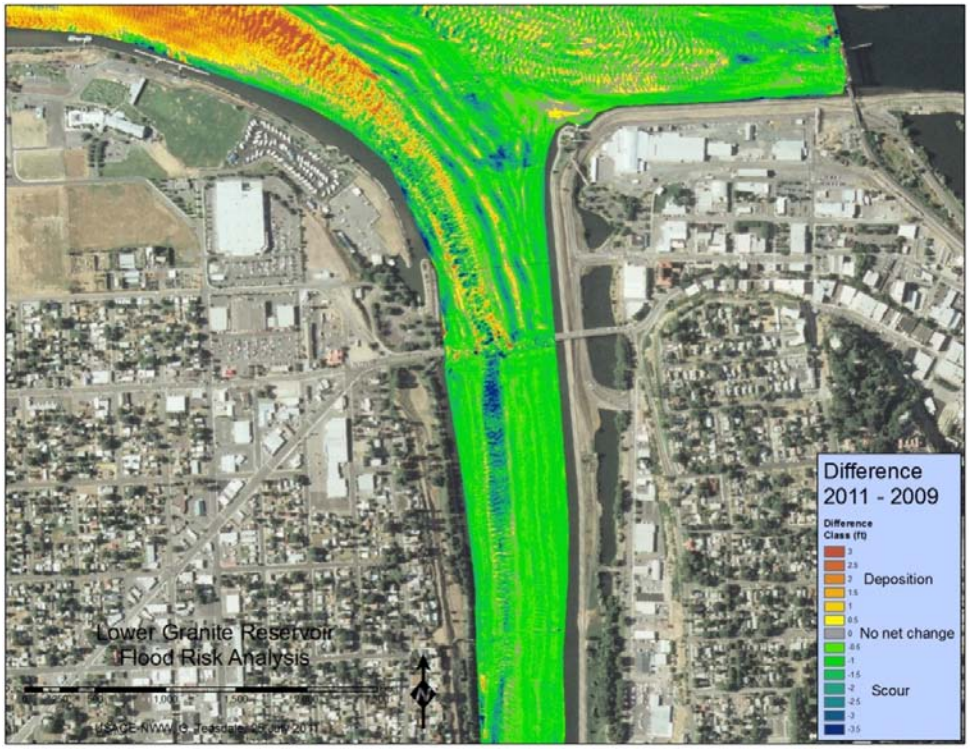


Figure 83. Bathymetry difference May 2011- September 2009 at Interstate Bridge.

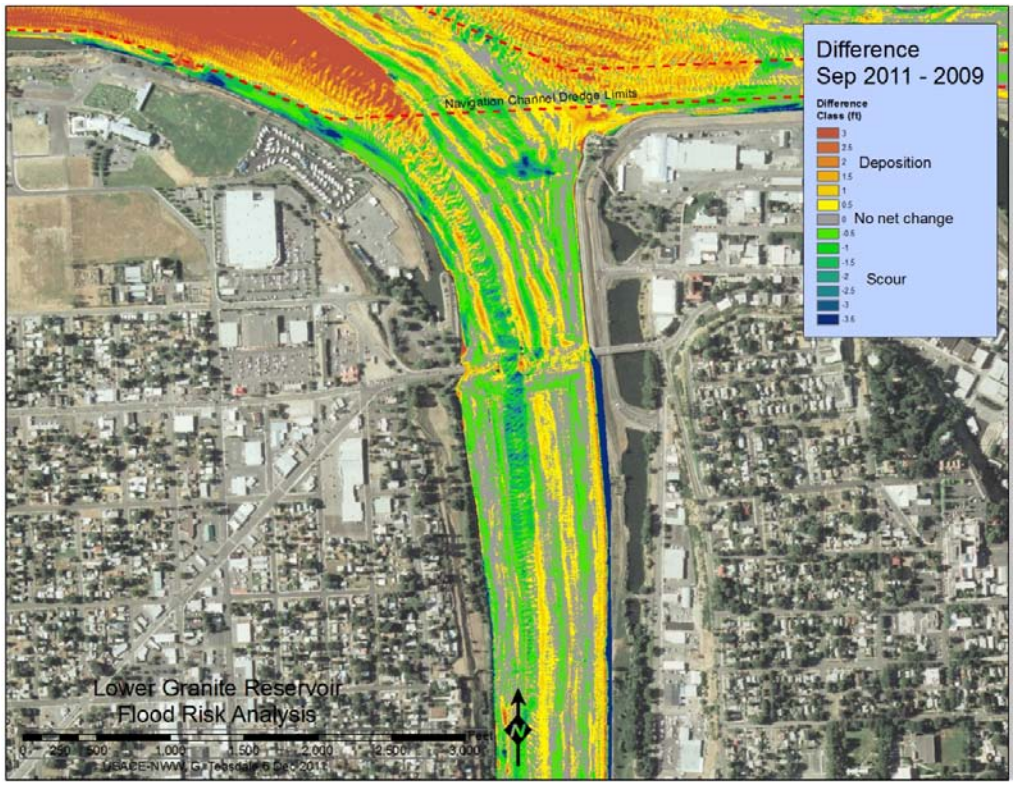


Figure 84. Bathymetry difference September 2011- September 2009 at Interstate Bridge.

15.6.5. Red Wolf 2011-2009 Bathymetry Difference Maps

The May 2011 - September 2009 bathymetry difference map for the Lower Granite Reservoir near Red Wolf bridge in Figure 85 mostly shows erosion of the main channel. Erosion depths are about 0.5 ft. Some deposition occurred along the left bank of the channel near the Red Wolf Marina. The shallow areas of the marina were not surveyed in May 2011, but likely continued to accumulate fine sediment. Sediment again accumulated by September 2011. The difference between the September 2011 bathymetry and September 2009 bathymetry averages 0.7 ft over the channel area in Figure 86.

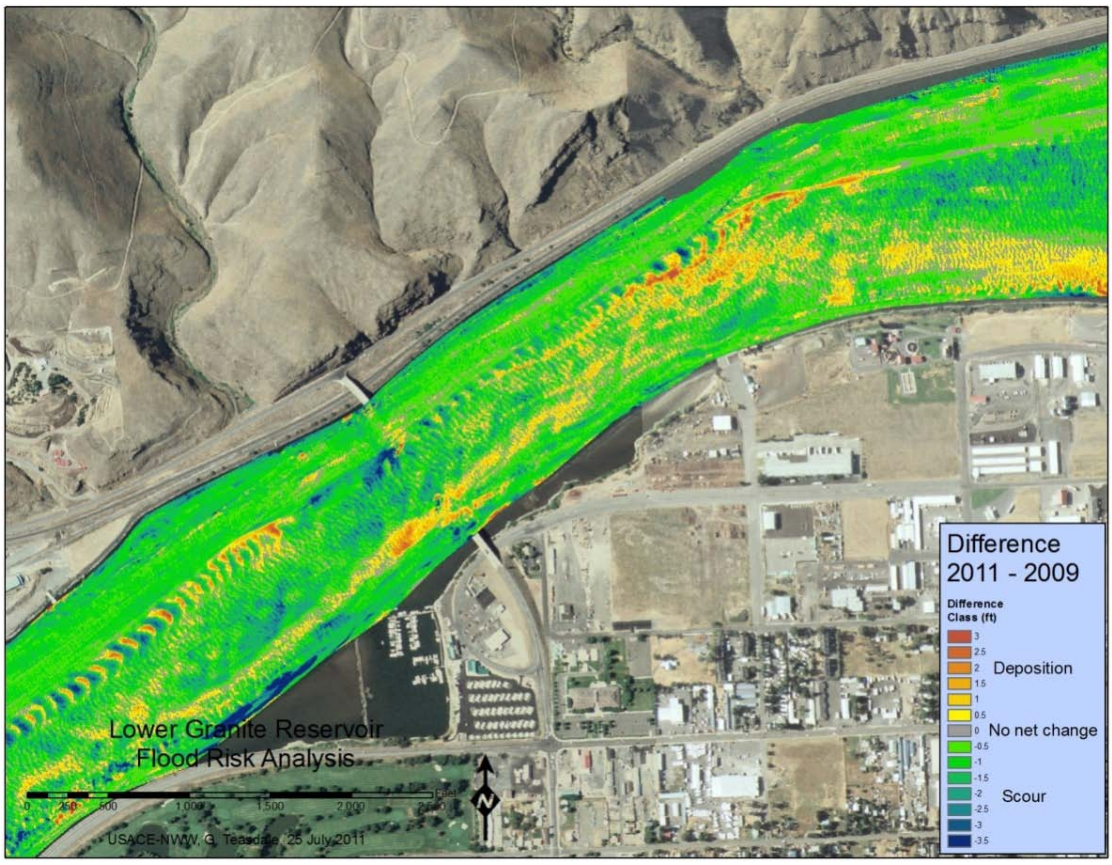


Figure 85. Bathymetry difference May 2011- September 2009 at Red Wolf Bridge.

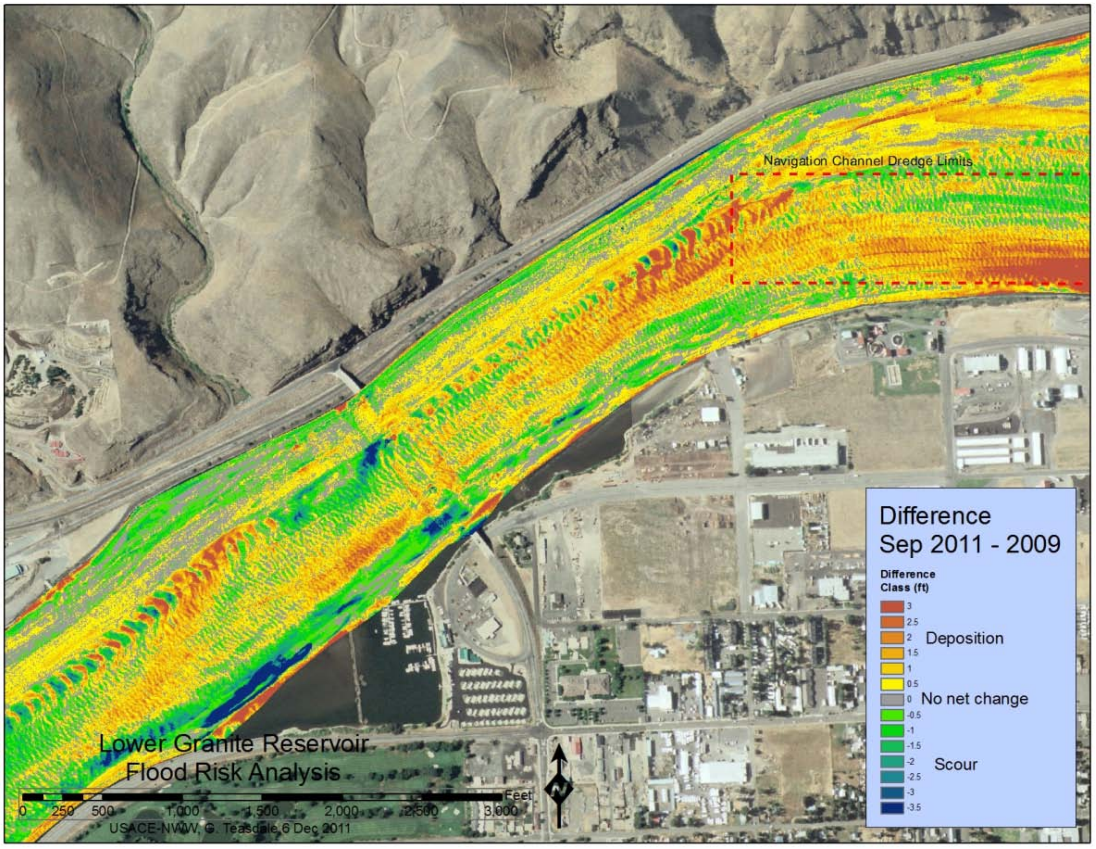


Figure 86. Bathymetry difference September 2011- September 2009 at Red Wolf Bridge.

15.6.6. Port of Wilma 2011-2009 Bathymetry Difference Maps

The 2011-2009 bathymetry difference maps for the Lower Granite Reservoir at the Port of Wilma are shown in Figure 87 through Figure 90. The main channel was eroded and sediment deposition occurred in middle of the channel at the bend and downstream of the high point of the channel caused by the submerged island. An average of 0.6 feet of sediment was eroded from the channel between September 2009 and May 2011 in the area covered by the figures. By September 2011 an average of 1.0 feet had again deposited in this segment of the reservoir.

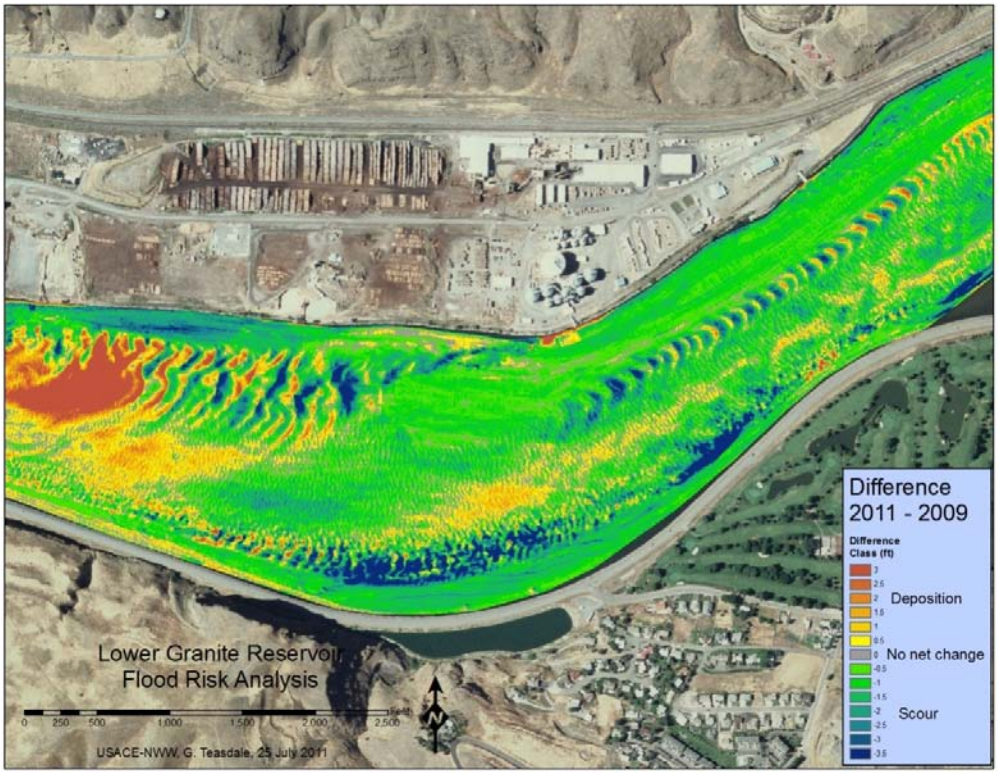


Figure 87. Bathymetry difference May 2011- September 2009 at the Port of Wilma (1).

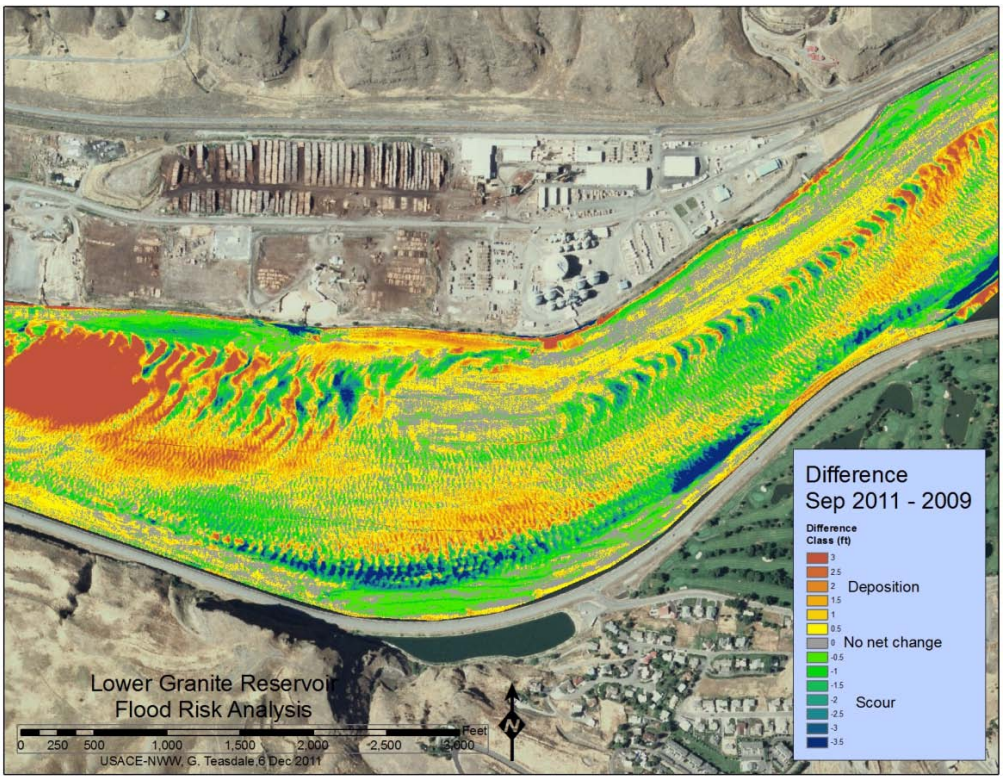


Figure 88. Bathymetry difference September 2011- September 2009 at the Port of Wilma (1).

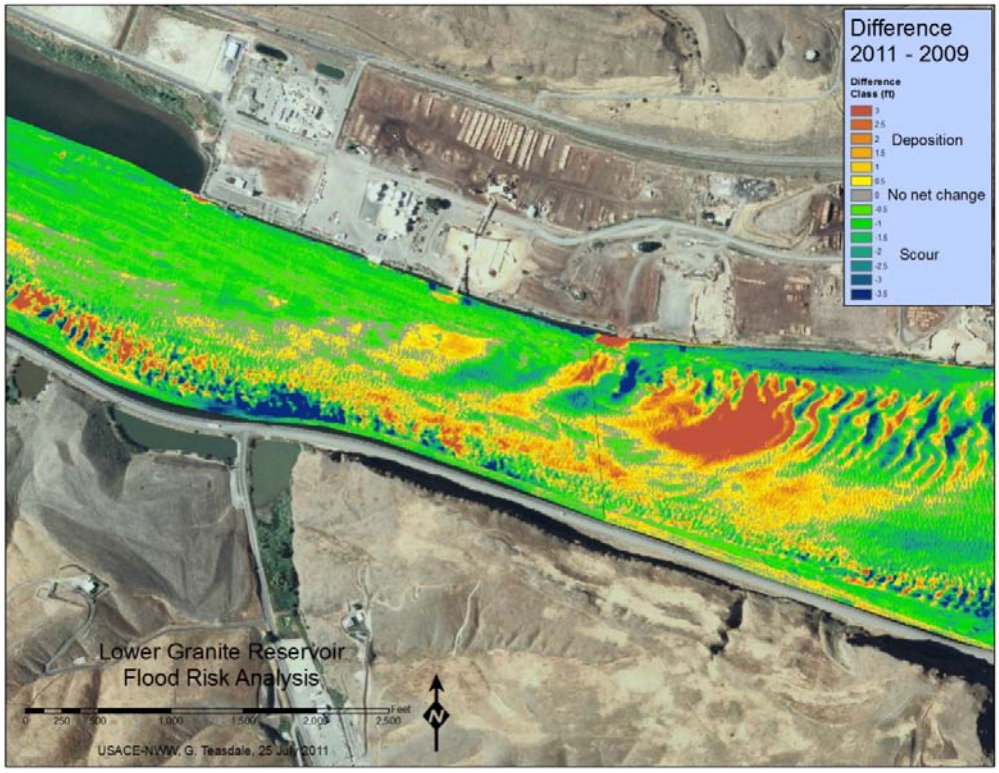


Figure 89. Bathymetry difference May 2011- September 2009 at the Port of Wilma (2).

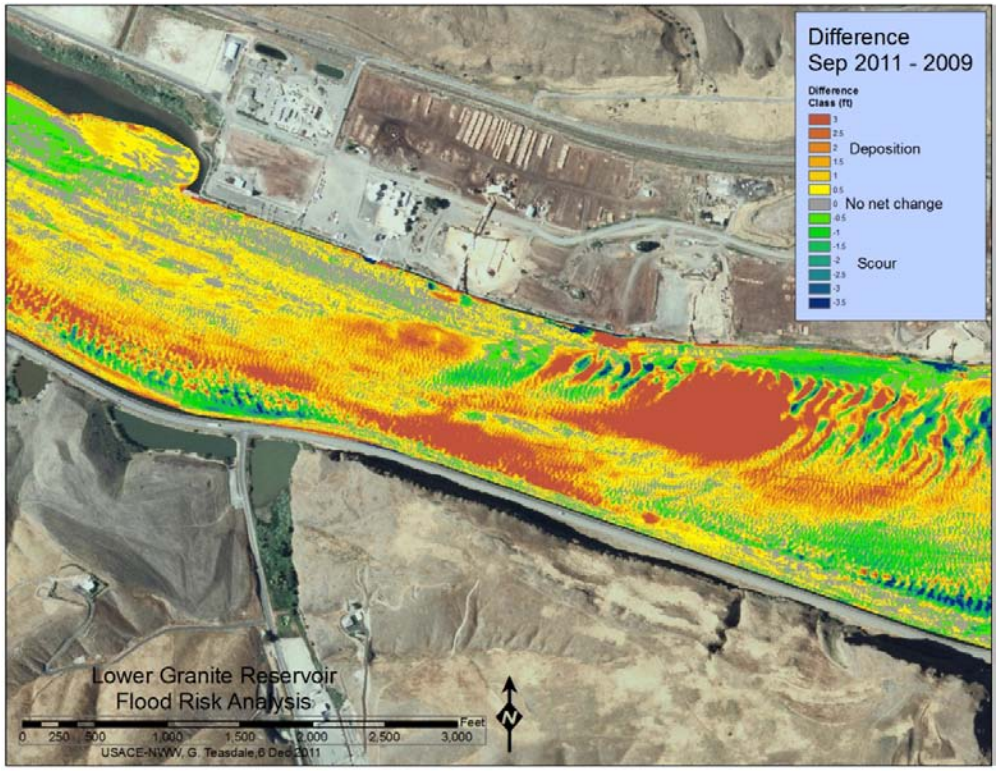


Figure 90. Bathymetry difference September 2011- September 2009 at the Port of Wilma (2).

15.6.7. Below-Wilma 2011-2009 Bathymetry Difference Maps

The 2011-2009 bathymetry difference maps for the channel of Lower Granite Reservoir between the Port of Wilma and Silcott Island are in Figure 91 through Figure 94. Below the Port of Wilma, between September 2009 and May 2011 sediment deposited in the left half of the main channel while the right half of the channel showed a slight amount of scour, and above Silcott Island sediment deposition occurs across most of the channel. Overall about 0.5 ft of sediment eroded from this segment of the reservoir. By September 2011 an average of 0.7 ft of sediment had deposited since May 2009.

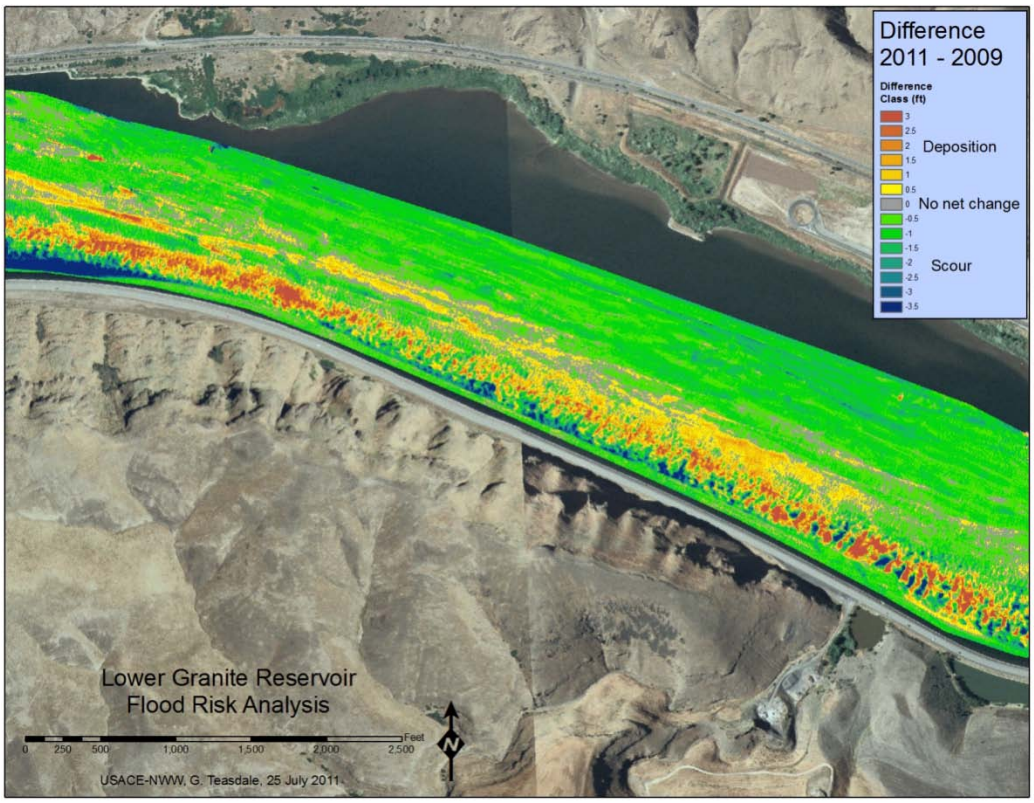


Figure 91. Bathymetry difference May 2011- September 2009 below Wilma.

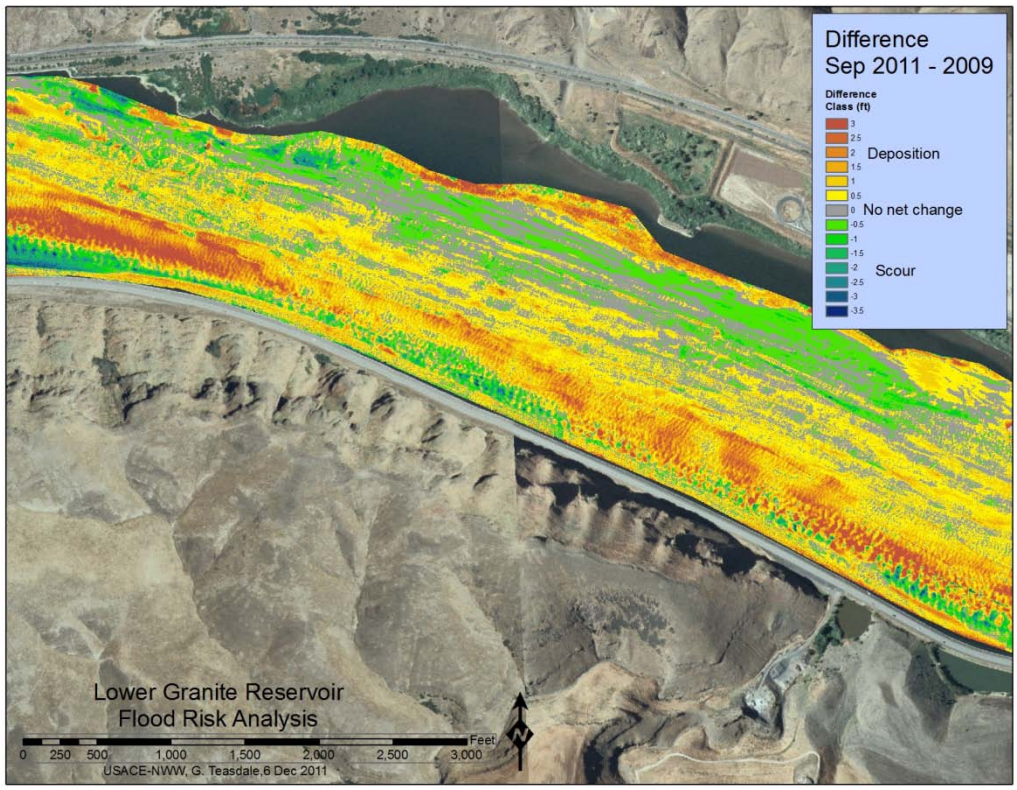


Figure 92. Bathymetry difference May 2011- September 2009 below Wilma.

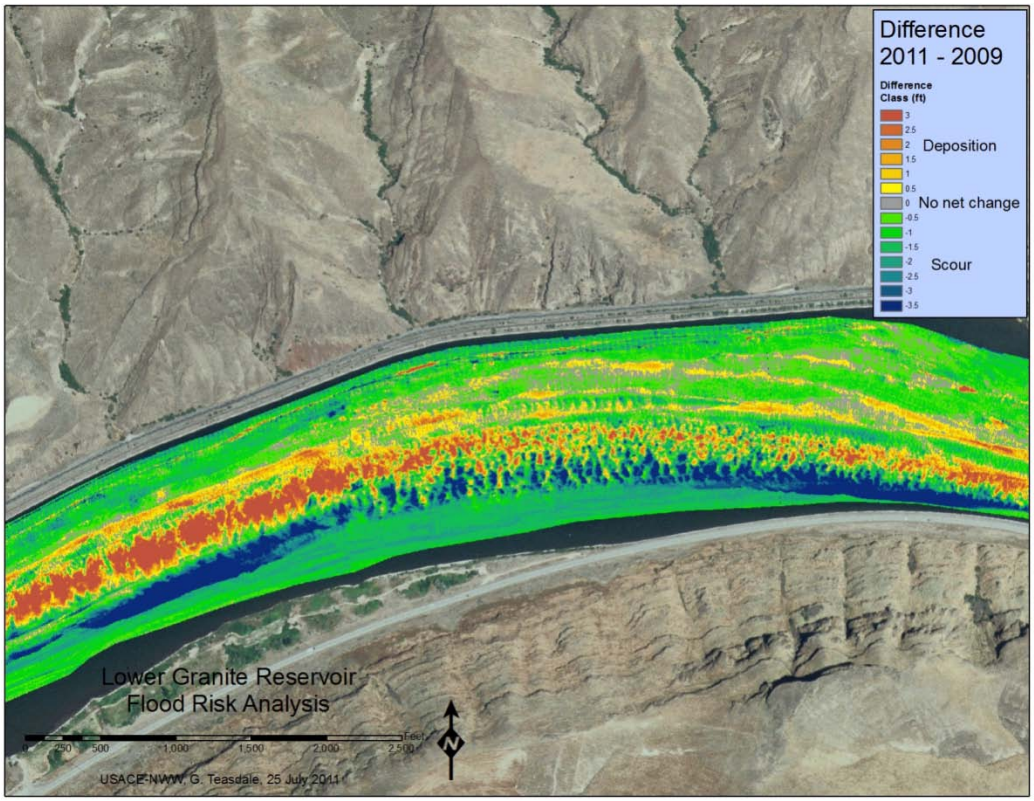


Figure 93. Bathymetry difference May 2011 - September 2009 above Silcott.

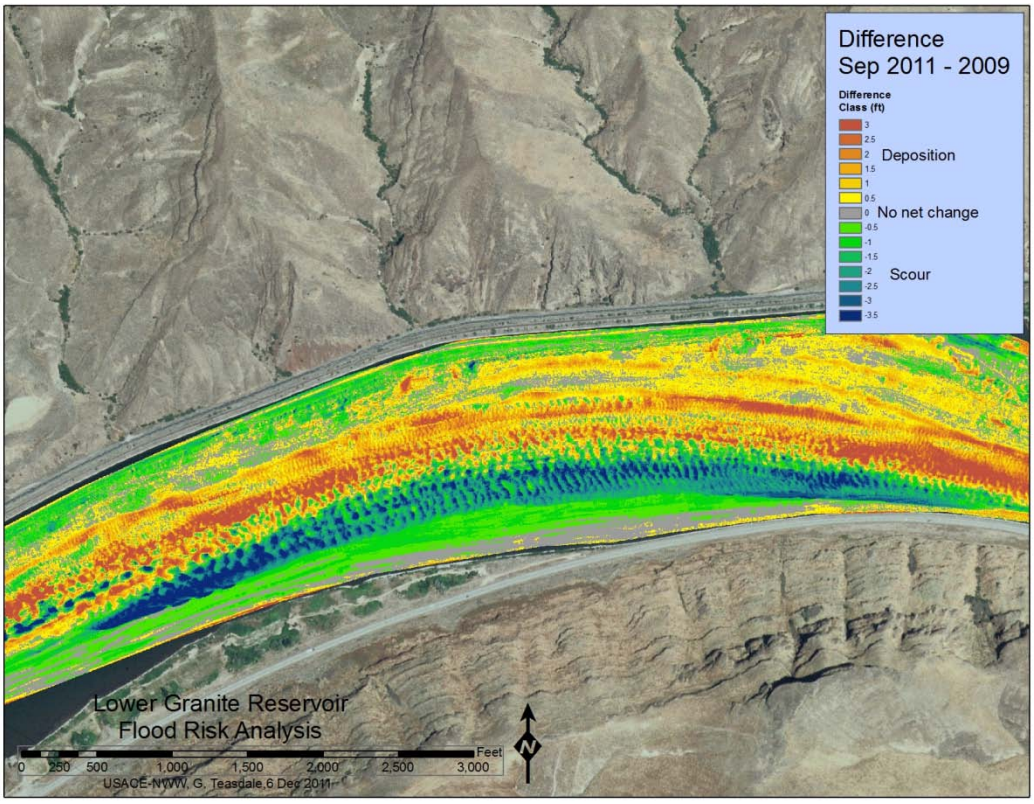


Figure 94. Bathymetry difference September 2011 - September 2009 above Silcott.

15.6.8. Silcott Island 2011-2009 Bathymetry Difference Maps

The 2011-2009 bathymetry difference maps for the Lower Granite Reservoir near Silcott Island are in Figure 95 through Figure 98. From September 2009 to May 2011 an average of 0.3 feet was eroded from the channel near Silcott Island. Sediment deposited in the middle of the channel and erosion occurred along the shallower bed near the banks. As indicated by the bed-forms, the mid-channel sediment deposition is sand bed-load, while the erosion along the margins is the scour of fine silt and sand material that was deposited prior to 2011 during lower discharges. The prolonged high discharge in May and June 2011 carried a large volume of sediment into this segment and further into the reservoir. Deposition since September 2009 averaged 3.8 feet by September 2011.

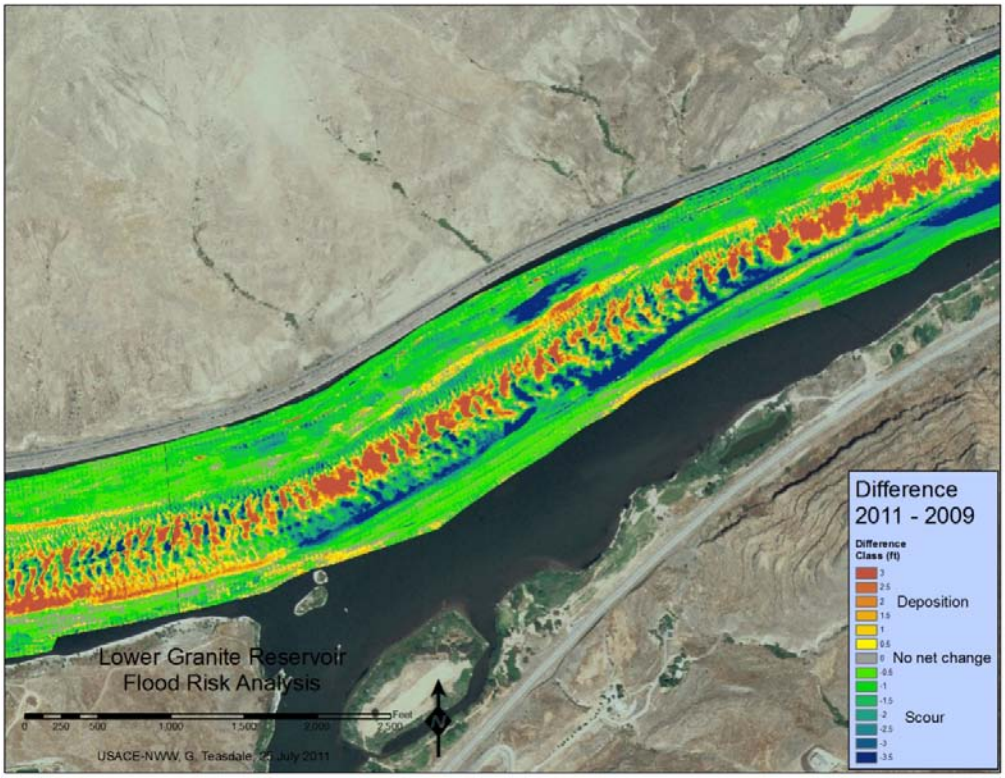


Figure 95. Bathymetry difference May 2011- September 2009 at upper Silcott Island.

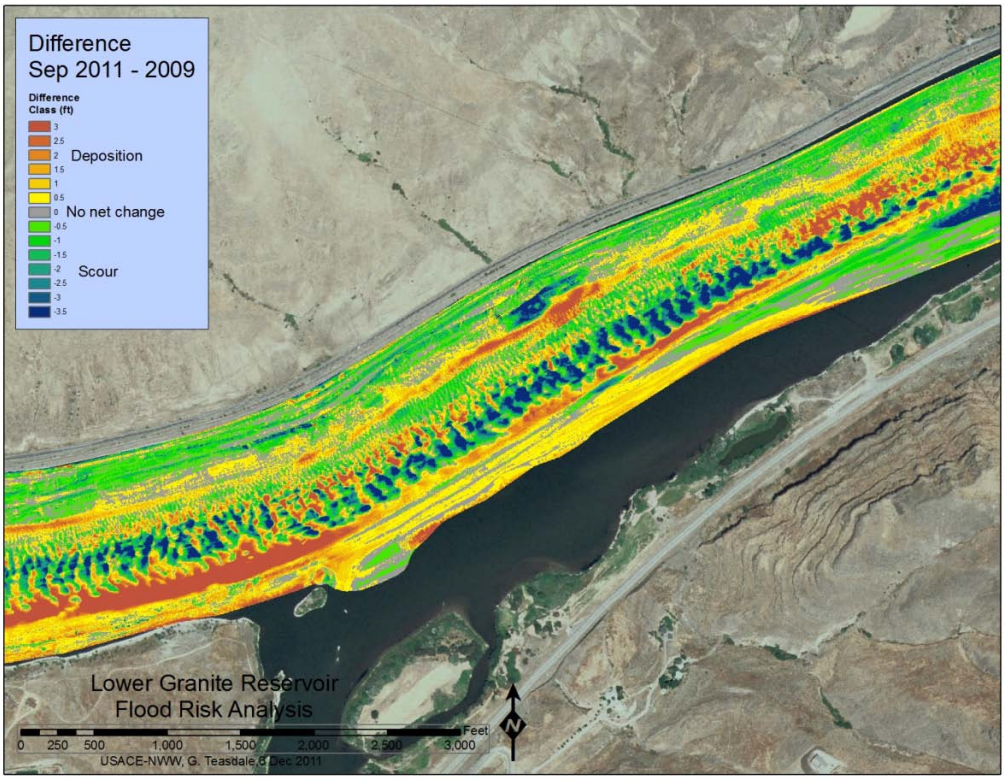


Figure 96. Bathymetry difference September 2011- September 2009 at upper Silcott Island.

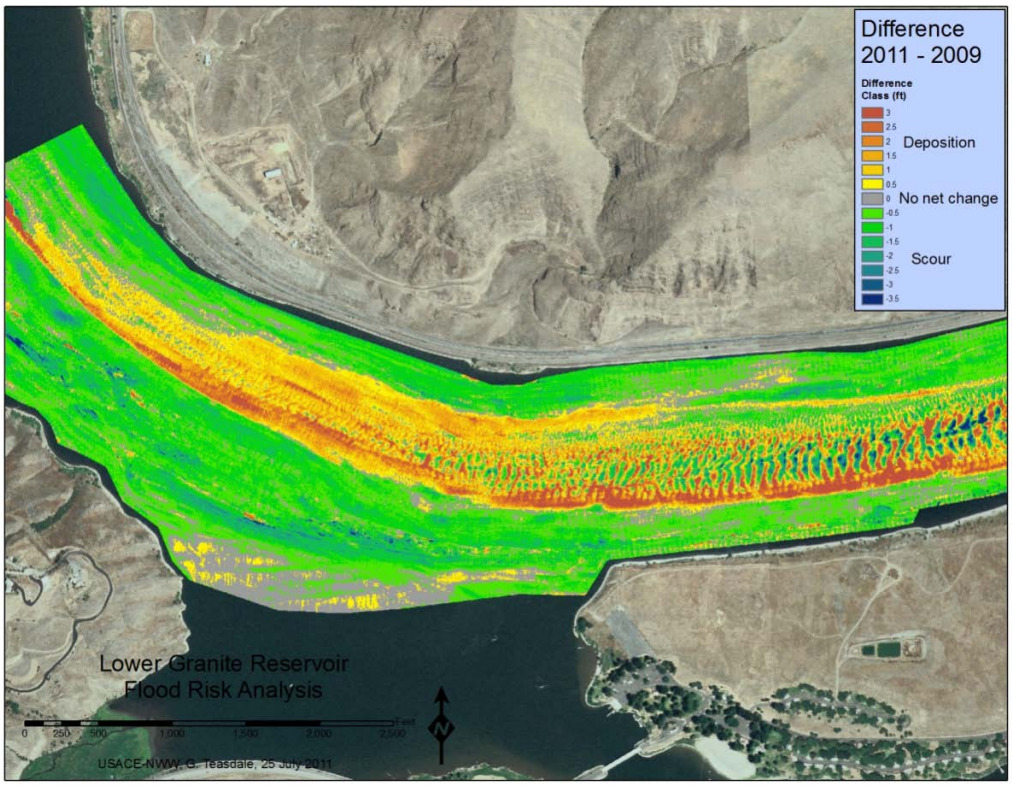


Figure 97. Bathymetry difference May 2011 - September 2009 at Lower Silcott Island.

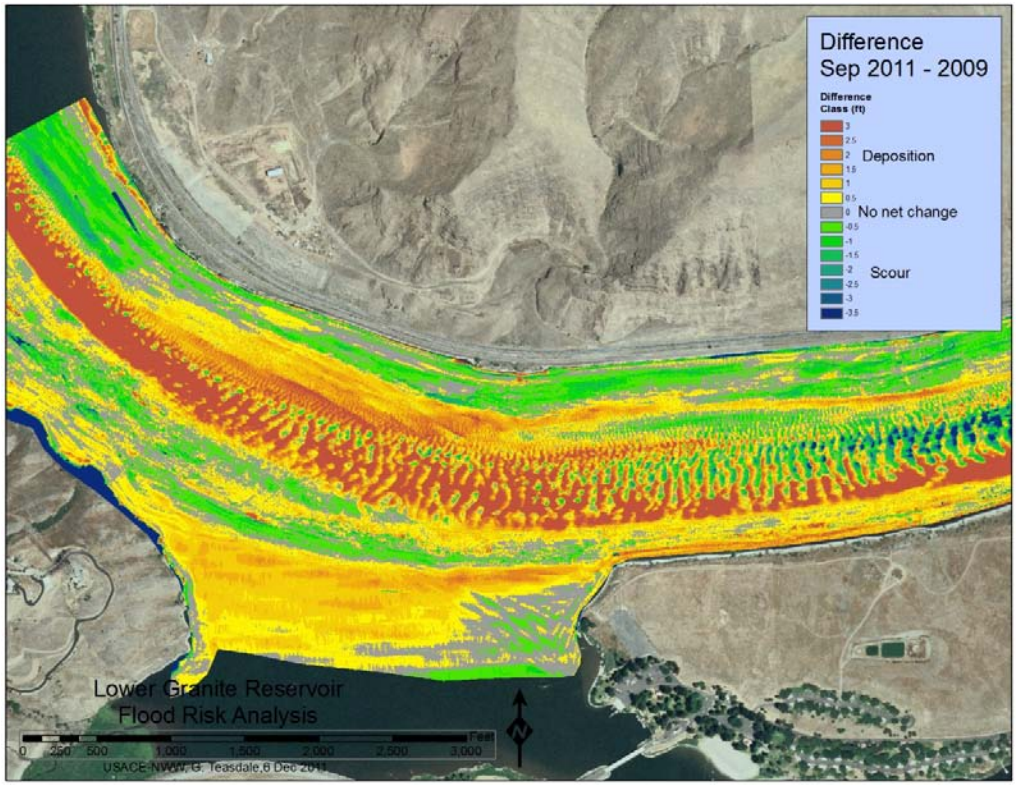


Figure 98. Bathymetry difference September 2011 - September 2009 at Lower Silcott Island.

15.7. Sediment Transport Modeling of the May 2011 Channel

The May 2011 bathymetry provides an opportunity to examine the performance of sediment transport models of the upper part of Lower Granite Reservoir. Results of these simulations are not employed directly in the long-term flood risk analysis, but useful for identifying the direction of future sediment studies and sediment transport model development for the reservoir. Sediment transport for the May 2011 period was simulated with the calibrated one-dimensional HEC-RAS model geometry developed from the May 2011 bathymetry that was described in Section 9. Two general simulation scenarios were developed based on the calibrated September 2009 and May 2011 HEC-RAS model geometries. In the first scenario, sediment transport rating curves were developed from the May 2011 geometry at the site where sand wave bed-load load was measured near the peak discharge in late May 2011. The sediment transport function for the model was selected based on a comparison of the measured and simulated bed-load discharge rates. In the second scenario, sediment transport and bed change was simulated for the period October 2009 to May 2011 to examine how well the sediment transport model predicted erosion and scour observed in the May 2011 bathymetry relative to the 2009 bathymetry.

15.7.1. May 2011 Sediment Rating Curve Simulation

Sand wave bed-load transport was measured by ERDC[5] above Red Wolf Bridge (Figure 99) during the bathymetry survey near Snake RM 137.6. Bed-load was measured before, after and near the peak of the discharge hydrograph at the times and discharges indicated in Figure 100. The measured sand wave bed-load discharge[6] plotted in Figure 101 is fit well with a linear or power relationship with water discharge (no bias correction). As discussed in Section 8 power equation relationships fit the measured sediment loads in the Snake and Clearwater Rivers (and other rivers) , so the power fit is preferred over the linear fit even though the correlation coefficient for the power fit is slightly less.

Sediment transport at the bed-load measurement site was simulated with a simplified HEC-RAS model to validate selection of an equilibrium transport function by comparing computed sediment discharge with the measured bed-load discharge. The simplified model only included the cross sections in Lower Granite Reservoir near the location of the bed-load measurement site. Sediment load at the upstream boundary of the bed-load measurement site was defined by an equilibrium condition and the

[5] Abraham,D., Pratt, T., Sharp, J. (2010). "Measuring bedload transport on the Missouri River using time sequenced bathymetric data", 2nd Joint Federal Interagency Conference, Las Vegas, NV, June 27-July 1, 2010.

[6] Abraham, D. (2011). Personal communication, May 2011.

sediment of the erodible channel bed was defined as uniform medium sand. Inflow hydrographs were extracted from the hourly discharge series for the stream gages at Spalding on the Clearwater River and at Anatone on the Snake River for the period May 22 through May 30, 2011 (Figure 100). The computation interval in the quasi-unsteady flow time series was 15 minutes and the temperature was kept constant at 50 degrees Fahrenheit. The downstream tailwater time series for the simplified model was computed with the full fixed-bed HEC-RAS model which used the hourly time series of water surface elevations at the forebay of Lower Granite Dam as the downstream boundary condition.

Sediment rating curves produced by the simplified model at Snake RM 137.632 for several equilibrium transport functions are compared to the bed-load measurements in Figure 102. The rating curve based on the Toffaleti transport function agree well with the bed-load measurements, though the function departs somewhat from the measured bed-load at greater discharges, likely in part because of supply-limited partial transport in the channel. Bed-forms observed in the May 2011 bathymetry and earlier bathymetries show that only part of the channel width transports substantial bed-load during high discharge. It was noted in Section 9 that the Toffaleti transport function reproduced the long-term accumulation of sediment in Lower Granite Reservoir reasonably well. Sediment discharge with the Ackers-White total transport function for the uniform sediment greatly exceeded the measured bed-load transport for the high discharge condition even with adjustment of the function parameters in HEC-RAS.

The simplified model was partially calibrated by adjustment of the erodible widths of the model cross sections, slight coarsening of the bed grain size distribution in the vicinity of the bed-load site and inclusion all cross sections up to the confluence in the sediment transport model. Partial calibration results in Figure 103 show a reduction in the upper part of the rating curve but an increase in the scatter of the rating curve because of the more variable sediment load. Additional bed-load and suspended sediment measurements in Lower Granite should be obtained in future work to support development of a calibrated sediment transport function specifically for the partial transport conditions in Lower Granite Reservoir.

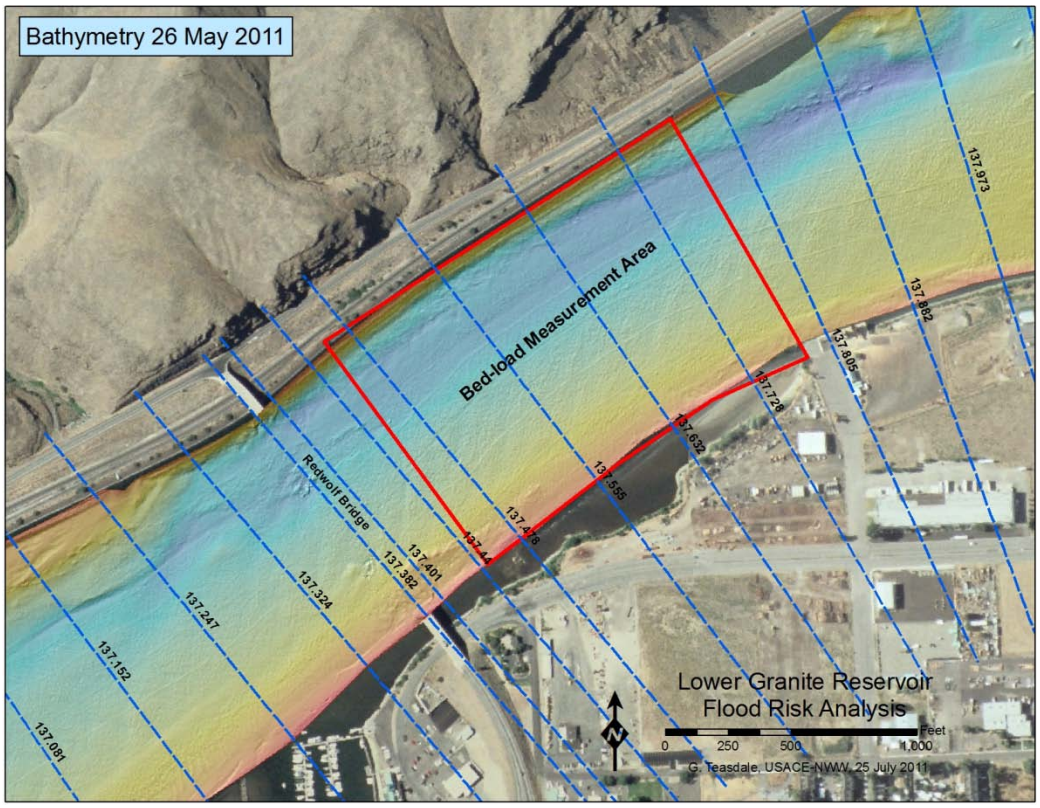


Figure 99. Bed-load measurement site above Red Wolf Bridge at Snake RM 137.6.

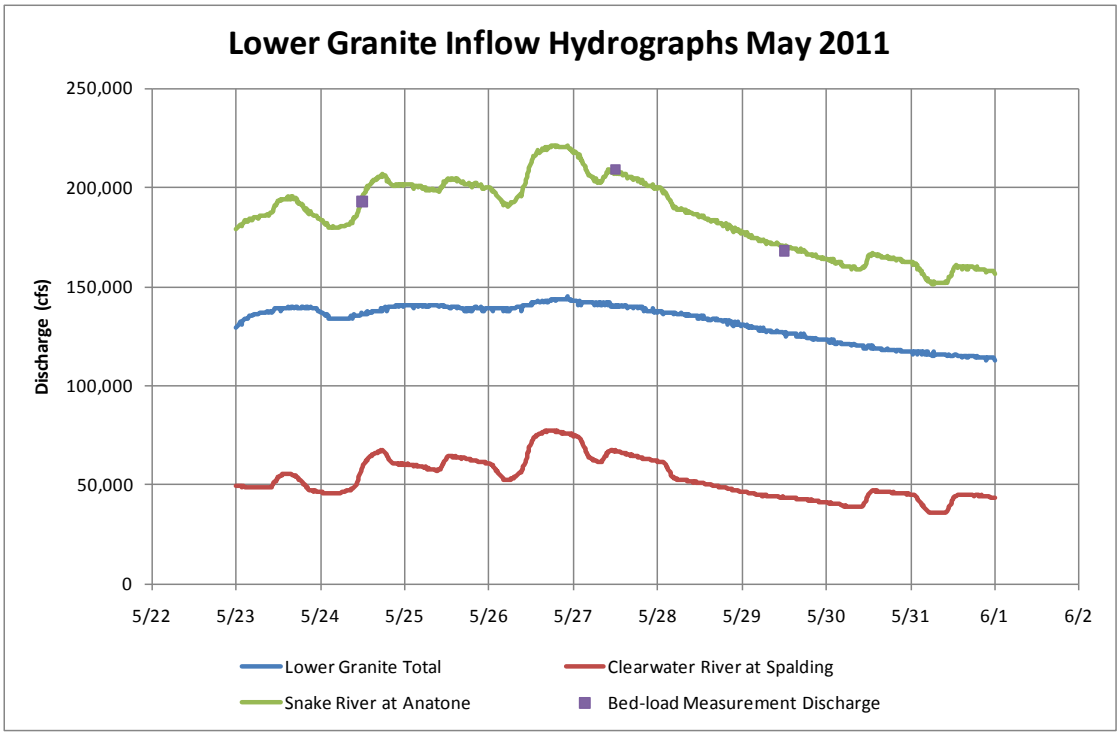


Figure 100. Inflow hydrographs for May 2011 sediment transport simulation.

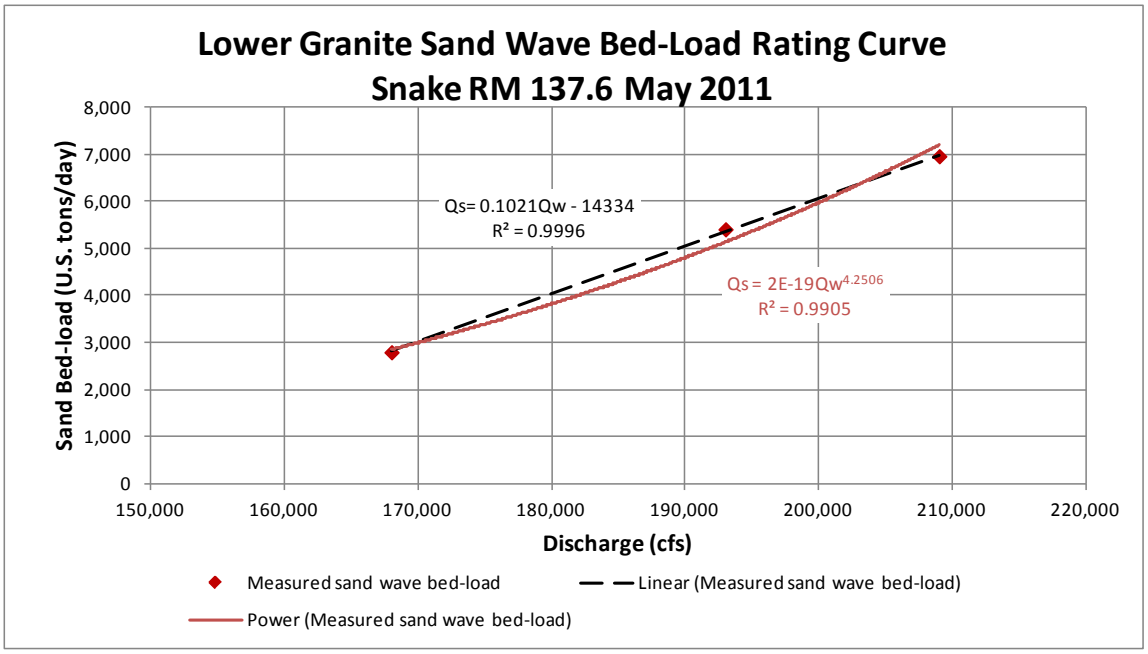


Figure 101. Measured sand wave bed-load at Snake RM 137.6.

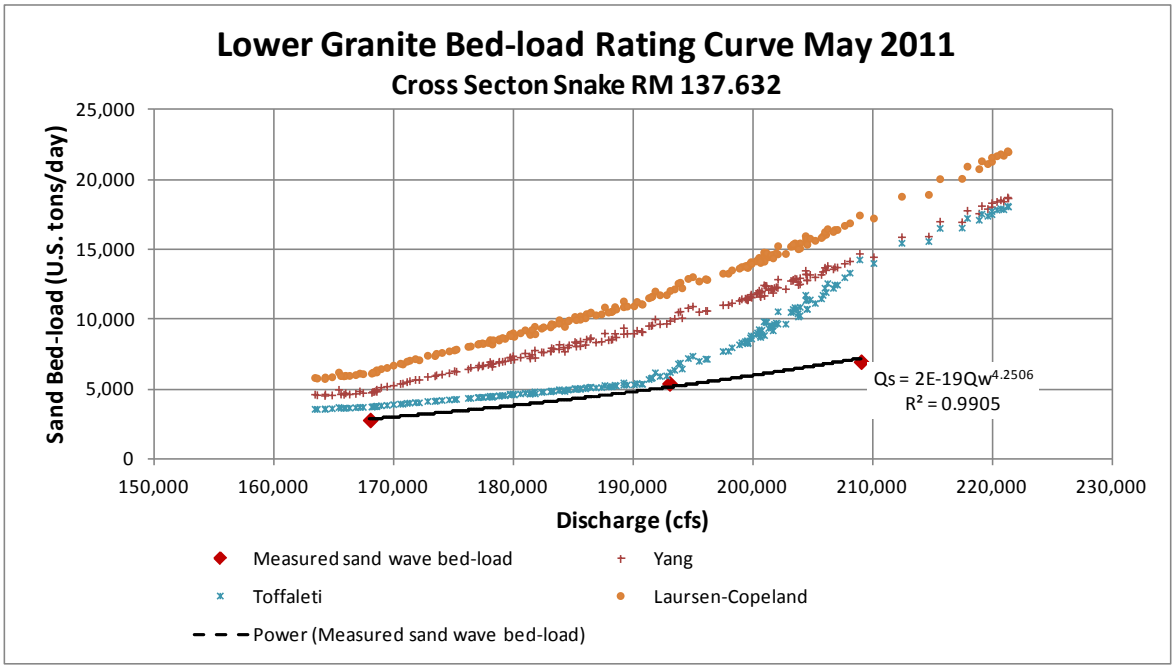


Figure 102. Comparison of simulated sediment rating curves with measured sand wave bed-load transport for May 2011.

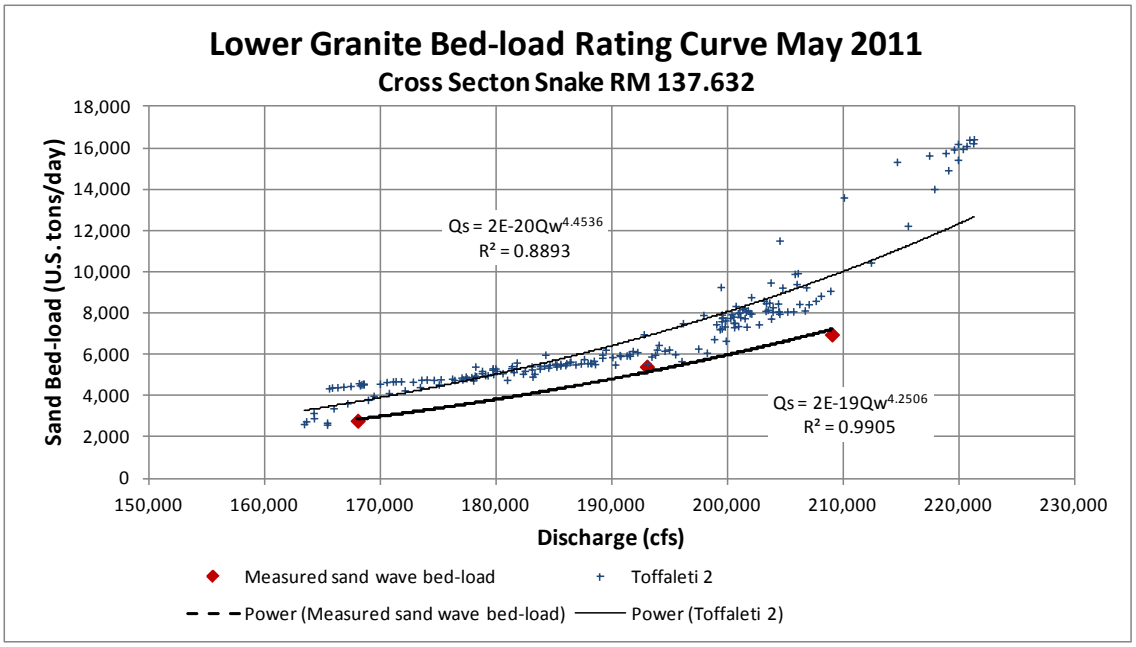


Figure 103. Comparison of the Toffaleti transport function rating curve with measured sand wave bed-load transport after partial model calibration.

15.7.2. Simulated Bed Change September 2009 to May 2011

In the second scenario, sediment transport and channel bed change from October 2009 to May 30, 2011 was simulated with HEC-RAS using as the initial geometry the calibrated 2009 bathymetry and sediment range cross sections discussed in Section 9. Simulated bed change was then compared to the actual bed change in the May 2011 bathymetry to judge the performance of the sediment transport model.

Inflow hydrographs were extracted from the daily discharge series for the stream gages at Spalding on the Clearwater River and at Anatone on the Snake River for the time period from October 1, 2009 through May 30, 2011. The downstream boundary condition was defined by the time series of daily average water surface elevations at the forebay of Lower Granite Dam. The computation interval in the quasi-unsteady flow time series was 6 hours and the temperature was kept constant at 50 degrees Fahrenheit. Forebay elevations and the inflow time series are plotted in Figure 104. Bed sediment grain size distributions were set according to the guidelines in Table 69. Sediment loads in the Clearwater and Snake Rivers were defined by the sediment rating curves given in Table 62 and Table 63.

Simulated and measured bed changes for Lower Granite Reservoir from the confluence to Snake RM 130 are plotted in Figure 105. As discussed above, the bathymetry difference maps showed that the bed of Lower Granite Reservoir eroded slightly from 2009 to May 2011. Actual bed erosion between the confluence and RM 130 in Figure 105 averages about 0.5 ft. The actual bed change profile was computed

from the 2009-2011 bathymetry difference maps by averaging the difference in bed elevation along each model cross section. Bed change simulated with the Toffaleti transport function averaged 0.1 ft from RM 130 to the confluence and the range of the differences is approximately equal to the heights of the largest bed-forms. Differences between the simulated and measured bed change, while not extreme, are attributed to the accuracy of the transport function (a total bed material load function), the sediment load boundary condition based on the long-term sediment regression relationships, the assumptions of the spatial variability of the bed sediment grain size distribution, and simplification of secondary flow and partial bed processes in the one-dimensional sediment transport model. The greatest departures between the simulated and measured bed change occur at the widening of the Lower Granite channel near Red Wolf Marina at Snake RM 137.1, near RM 133.7 below the Port of Wilma, and below Silcott Island at RM 130.8. The model over-predicted deposition at these locations which have strong secondary currents because of the expansion of the flow field.

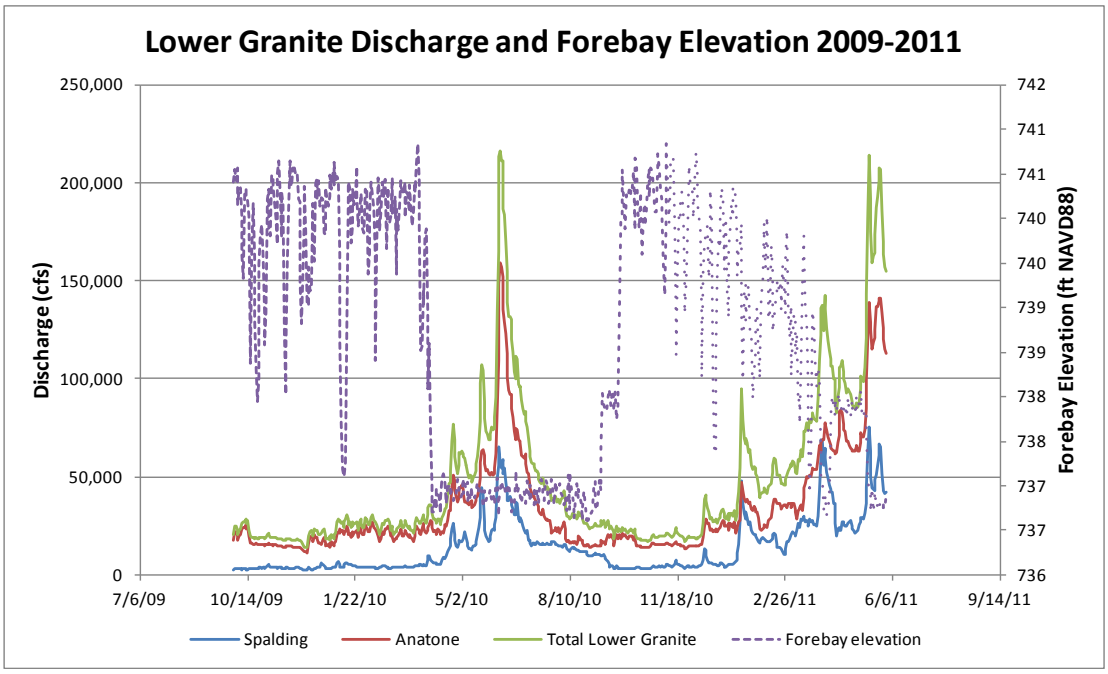


Figure 104. Lower Granite Reservoir discharge and forebay elevation 2009-2011.

The average sediment rating curve at cross section at RM 137.632 from the October 2009-May 2011 simulation plotted in Figure 106 agrees well with the measured sand wave bed-load rating curve for the medium sand fraction computed by the Toffaleti total load function. The rating curve of medium sand for the 2009-2011 simulation is less than the rating curve for the May 2011 simulation because the sediment load boundary condition is defined by the long-term sediment load regression equations rather than an equilibrium bed condition. The sediment load regression equation better

represents the partial transport condition in Lower Granite reservoir. The intent of this comparison is to suggest possible future directions in the development of refined methods sediment transport estimation and prediction within Lower Granite Reservoir.

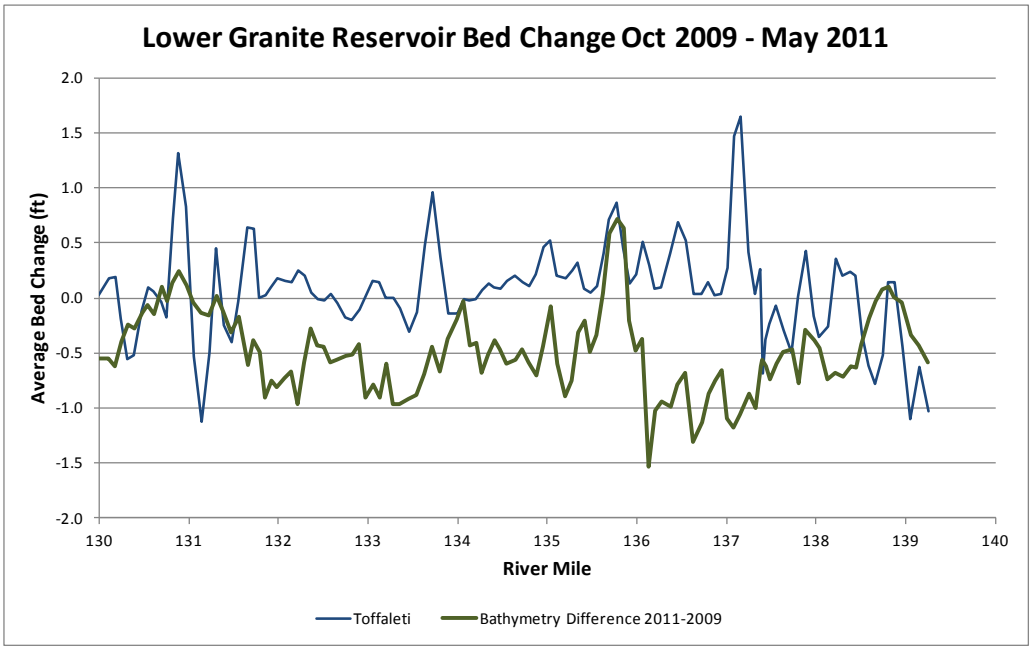


Figure 105. Simulated and actual average bed change in Lower Granite Reservoir 2009-2011.

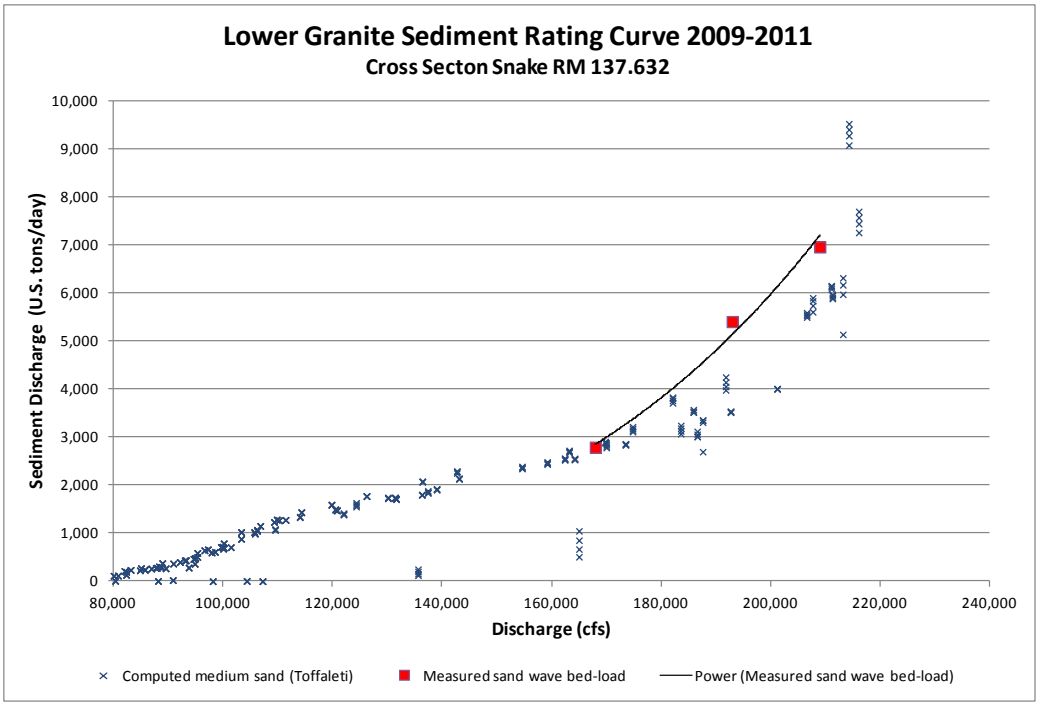


Figure 106. Comparison of simulated sediment rating curves for 2009-2011 with measured sand wave bed-load transport.

15.8. Analysis of Bed Regime Conditions

Hydraulic resistance of the mobile bed of Lower Granite Reservoir depends on the size and extent of sand bed-forms. The progression of bed-form development and its effect on flow resistance is discussed in Section 9. The hillshade bathymetry maps, dune profile analysis and bathymetry difference maps presented above all show that the sand bed-forms had generally decreased in size in the upper reach of Lower Granite Reservoir when the bathymetry was acquired during high discharge in May 2011 as compared to the bathymetry acquired in September 2009, September 2010 and September 2011.

Sand bed-forms decrease in size during high discharge if 1) the mobile sand is scoured down to a immobile bed layer, or 2) there is insufficient sand bed-load on a threshold channel of immobile substrate to support bed-form development, or 3) the sand bed-forms are washed out as the bed changes from lower sediment bed regime to upper sediment bed regime, or 4) a combination of both conditions. Given the expected sediment loads discussed in Section 8, it is very unlikely that the rate of sand load entering the reservoir could be so reduced that sand is eroded from the upper reservoir down to the original gravel and cobble bed of the pre-dam river channel except in the known equilibrium segments. Sand bed-load transport rates measured by ERDC during the bathymetry survey were as high as 7000 tons per day during the May 2011 discharge which is well below the sediment transport capacity predicted by equilibrium sediment transport equations for sand bed channels of similar size and energy slope. Therefore, it is most likely that a transition in bed regime, perhaps accelerated by conditions of supply-limited partial transport, is the primary cause of the reduction in the size of sand bed-forms in the May 2011 bathymetry.

The Brownlie regime analysis presented in Section 9.7 demonstrated that it is likely that the sand bed of Lower Granite Reservoir and the Clearwater and Snake River channels transition from lower bed regime to upper bed regime during very high discharge. It is noted again that the energy slope of reservoir is controlled by operation of the outlets and spillway at Lower Granite Lock and Dam and that free-flow river conditions with substantial overbank flow do not occur in the reservoir. Rivers with substantial overbank flow during high discharge tend to remain in lower bed regime.

The high-resolution bathymetry acquired during the high discharge in May 2011 enabled the development of two-dimensional channel hydraulic models that more realistically represent the flow conditions when substantial bed-load is transported in the reservoir. Better estimates of depth averaged velocities, bed shear stress and transverse energy gradient can be obtained from the high-discharge channel model, which then supports a refined bed regime analysis.

15.8.1. Two-Dimensional ADH Model of Lower Granite Reservoir

A two-dimensional depth-average model of Lower Granite Reservoir was developed with the Adaptive Hydraulics hydraulic (ADH) modeling software developed by the USACE Coastal and Hydraulics Laboratory, Engineering Research Center[7]. The domain of the model, shown in Figure 107, extends from river mile 130 to 142 on the Snake River and from mile 0 to 2 on the Clearwater River. It includes the Lewiston levee system, the Port of Lewiston, Port of Clarkston, and the Port of Wilma.

The mesh of the model is triangulated network of 92,500 elements and covers an area of 1,196 ha. Average element size is 129 m^2. The ADH mesh at the confluence is shown in Figure 108. The mesh was developed in units of meters and projected to the UTM 11 North datum. Sizes of the mesh elements vary to represent the channel topography and maintain computational efficiency. The mesh resolution varies from about 10 meters at the channel edge and in areas of complex bathymetry to a resolution of 40 meters in relatively flat areas of the deep channel. Main channel features, in the three dimensional views of the mesh in Figure 109 and Figure 110, are represented well for the subcritical flow conditions of the Lower Granite Reservoir simulations. Constructed features such as bridge piers and docking facilities are not represented in the version of the ADH model used in the regime analysis.

Elevations of the nodes at the intersections of the mesh elements were extracted from the May 2011 bathymetry grid. Initial test simulations identified stability problems at selected nodes in the mesh that were then manual adjusted. Relatively few, much less than 0.1 percent of the nodes were adjusted, and most of these were near the wet-dry boundary at the banks and islands. Ground elevations for the mesh nodes above the normal pool elevation were extracted from the 2010 LiDAR elevation data. Node elevations in shallow water areas that were not covered by the bathymetry survey were interpolated from a TIN produced by combining the LiDAR data and bathymetry data.

The upstream boundary condition for the ADH model was defined by a discharge time series at node strings at the edges of the model domain on the Snake River and Clearwater River. The downstream boundary condition at the edge of the model domain below Silcott Island was defined by a time series of tailwater elevations. Since the model does not extend to Lower Granite Dam, tailwater elevations were obtained from corresponding simulations with the calibrated HEC-RAS model.

[7] Berger, R.C., Tate, J.N., Brown, G.L., Savant, G. (2010). Adaptive Hydraulics Users Manual, AdH Version 3.2, Coastal and Hydraulics Laboratory, Engineering Research and Development Center, U.S. Army Corps of Engineers, Vicksburg, MS.

Simulations of the 26 May 2011 discharge, one-percent chance exceedance discharge and Standard Project Flood (SPF) discharge used in the bed regime analysis were performed by increasing the inflow discharges from 0 to the maximum flow. The maximum flow was held steady for four hours in the model run to dampen the seich response of the reservoir. Time series of water surface elevations at selected points were checked to verify steady flow conditions. Sediment transport was not modeled in initial simulations as the modeling objective was to obtain depth averaged velocities and bed shear stress at the extreme discharge based on the May 2011 bathymetry which had measured the channel geometry while sediment was actively transported. A uniform Manning's *n* value of 0.023 based on the calibrated HEC-RAS model was assigned to the channel elements in the model domain below the confluence. Two levels of mesh adaption were generally allowed in the simulation. Water surface elevations at the confluence computed with the ADH model agreed well with results of the calibrated HEC-RAS model.

Outputs from the ADH simulation include water depth and velocity magnitudes and vectors. Water surface elevation is computed by adding the water depth to the bathymetry elevation at the mesh node. Other hydraulic parameters including point estimates of energy slope, bed shear stress, stream power, and shear velocity are derived from the depth, water surface elevation and velocity parameters. Dimensionless Shields stress is computed by also selecting a representative sediment grain size and sediment density. Hydraulic parameters computed by ADH were imported into GIS for further analysis and display. Example spatial map outputs of Shields stress, bed shear stress and stream power for the confluence are shown in Figure 111 and Figure 112 and Figure 113. Point estimates were interpolated to ESRI grids using the Spatial Analyst extension.

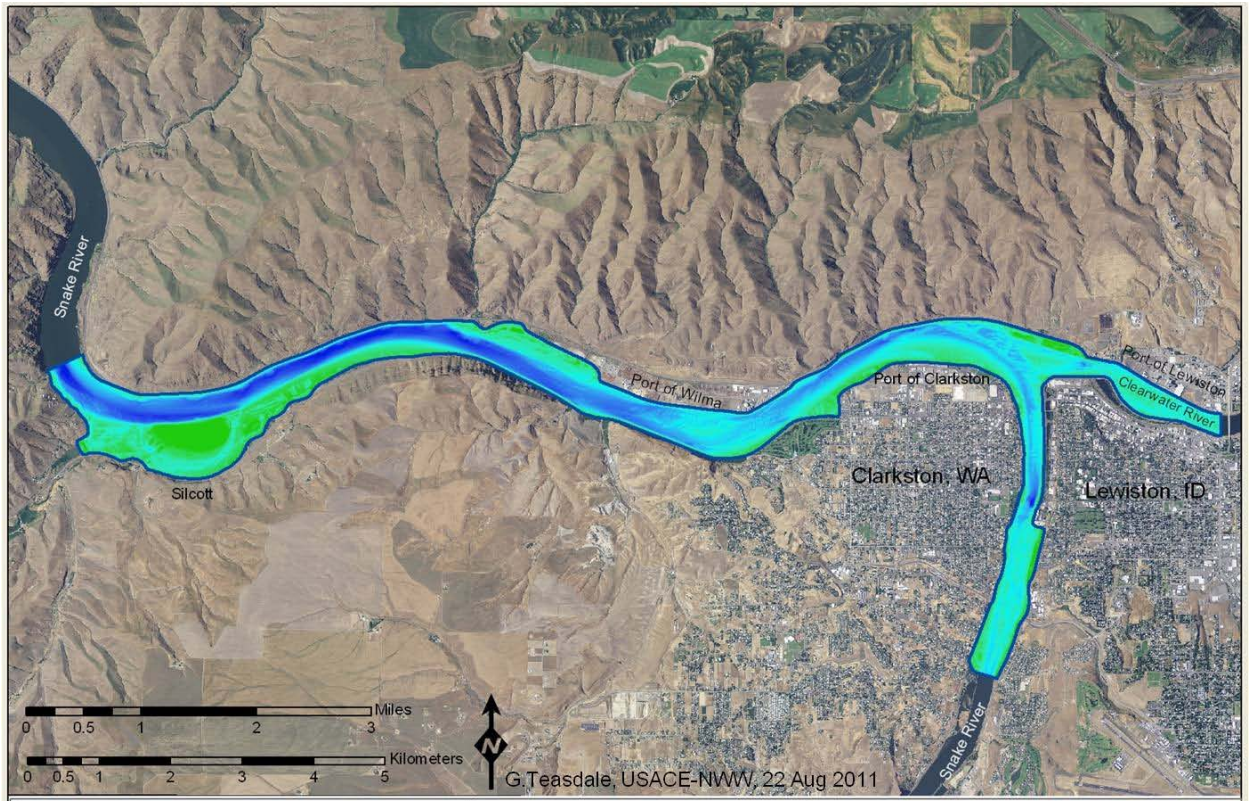


Figure 107. Domain of the ADH model of Lower Granite Reservoir.

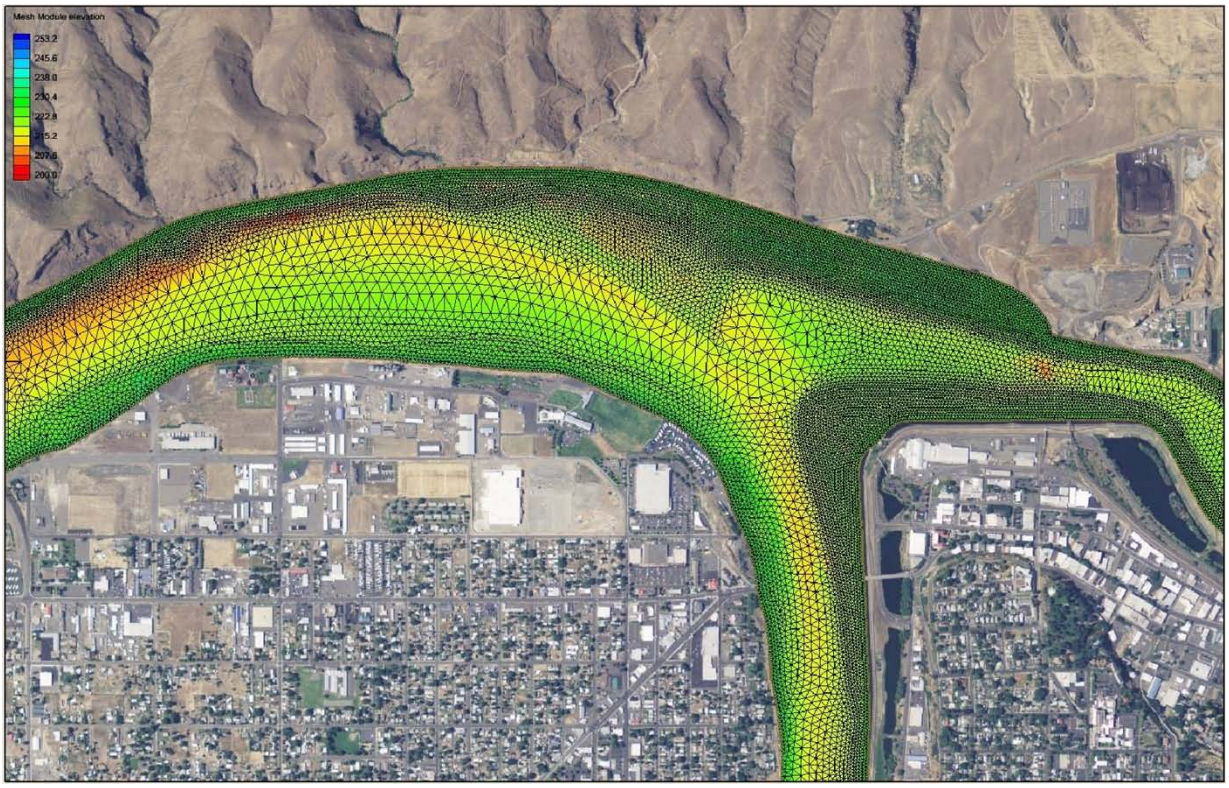


Figure 108. ADH model mesh near the confluence.

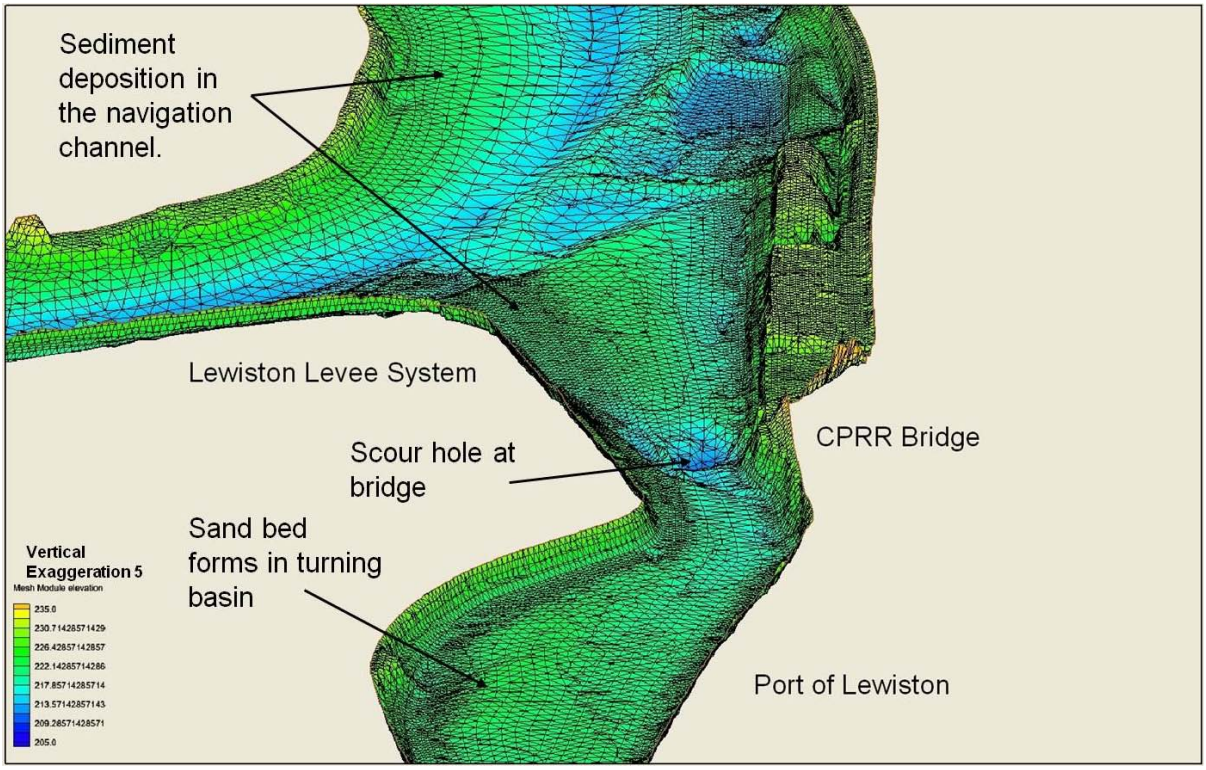


Figure 109. 3D view of ADH Model mesh near the confluence.

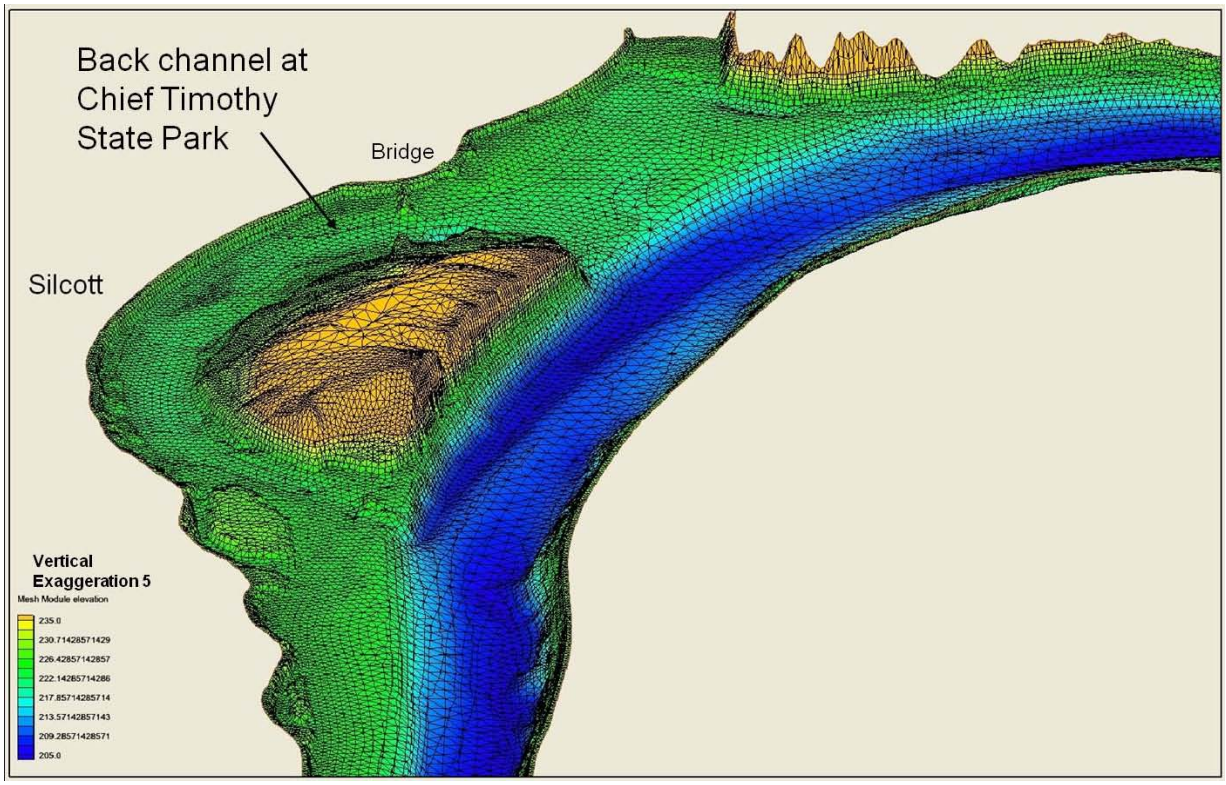


Figure 110. 3D view of ADH Model mesh near Silcott Island.

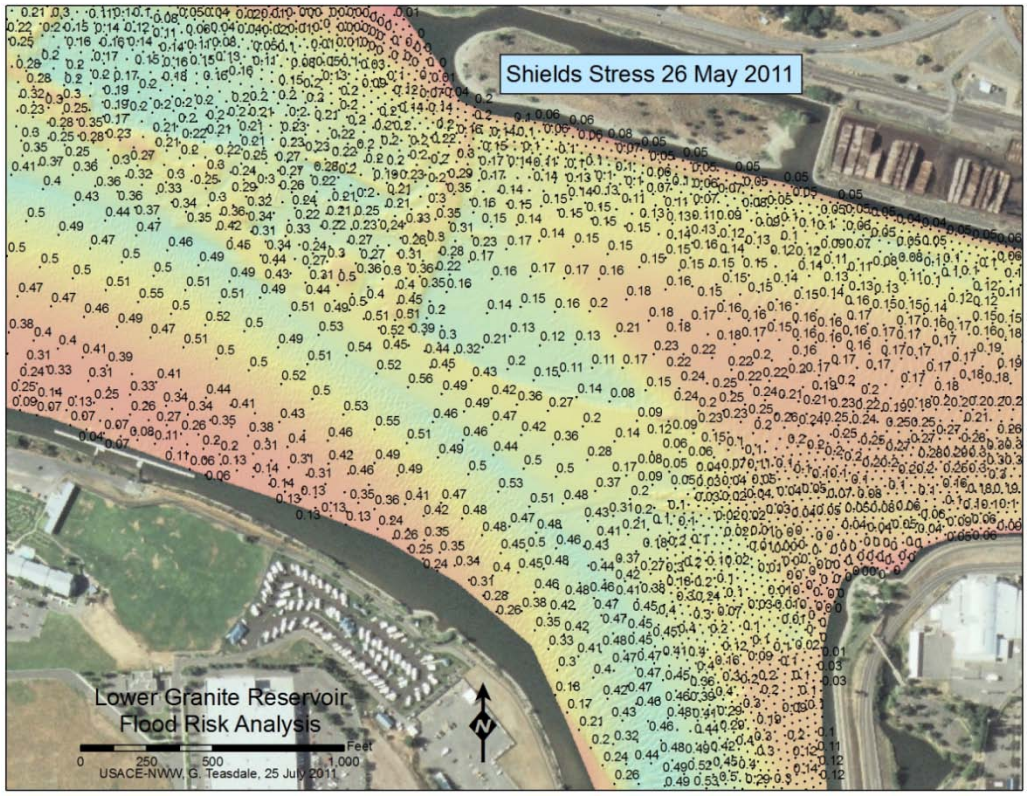


Figure 111. Shields stress computed with ADH model for discharge on 26 May 2011.

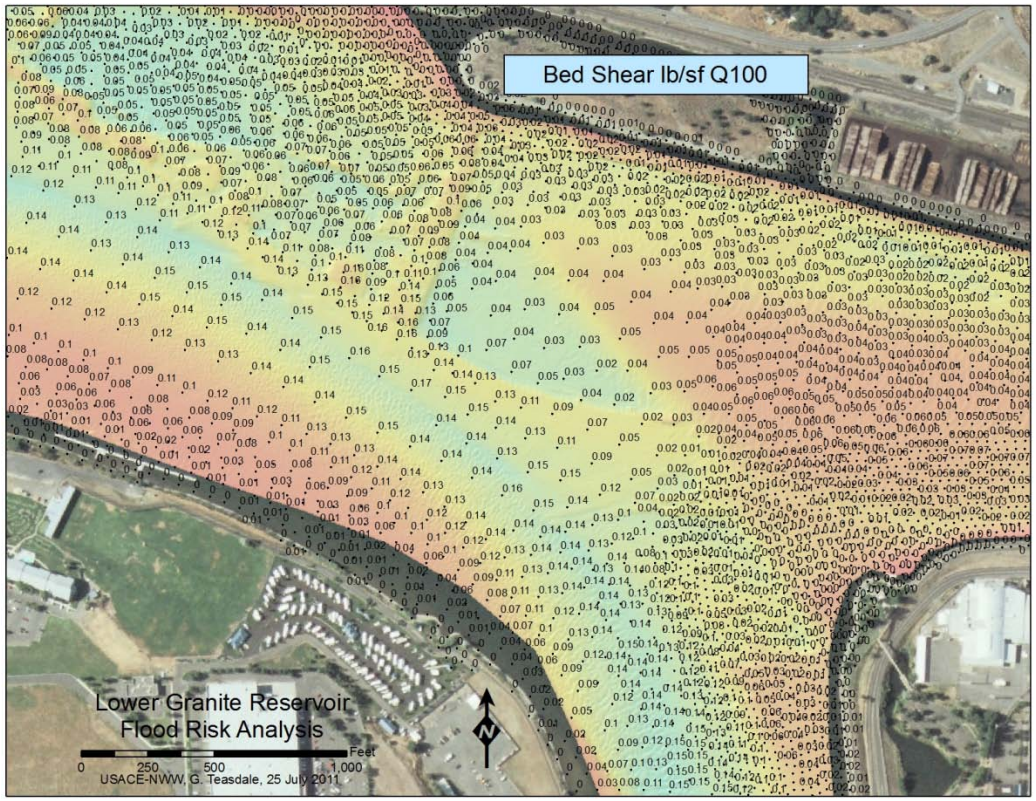


Figure 112. Bed shear stress computed with ADH model for 1-percent chance discharge.

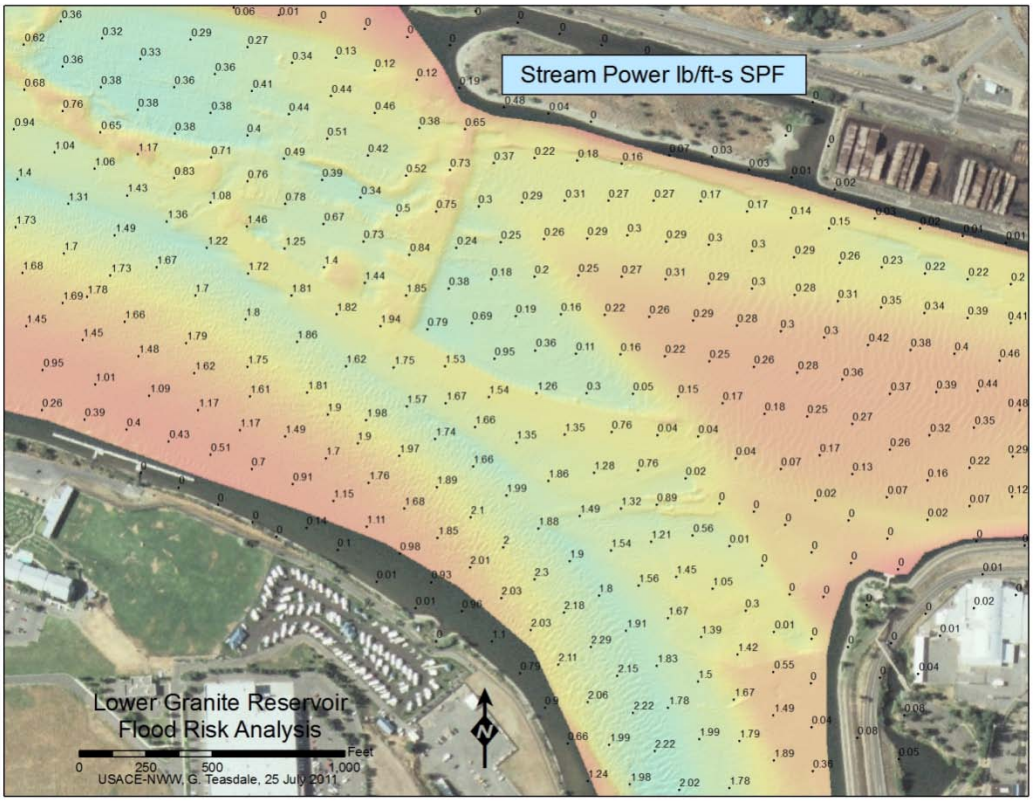


Figure 113. Stream power computed with ADH model for SPF discharge.

15.8.2. Spatial Analysis of Bed Regime with the Brownlie Relationships

The Brownlie analysis discussed in Section 9.7 can be adapted to a grid-based analysis of bed regime throughout the ADH model domain. Brownlie found that the transition from lower to upper regime is a function of grain Froude number,

$$\text{If } F_g \le \frac{1.74}{S^{1/3}}, \text{ then the channel is in lower regime}$$

$$\text{If } F_g > \frac{1.74}{S^{1/3}}, \text{ then the channel is in upper regime}$$

The grain Froude number is computed,

$$F_g = \frac{V}{\left[(s_s - 1) g d_{50}\right]^{0.5}}$$

where F_g is the grain Froude number, V is the flow velocity (ft s^{-1}), s_s is the specific gravity of the sediment particles, g is the acceleration of gravity (ft^3 s^{-1}). The maximum slope at which lower regime occurred in Brownlie's dataset was about 0.006 (0.6%), which implies that there is a high degree of certainty that channels with bed gradients greater than 0.6% will be in upper bed regime.

In the spatial analysis, Brownlie's relationships are applied by computing the grain Froude number at each cell in the grid from the grid of cell velocities and a grid of sediment grain size. Grid cell velocities were derived from the ADH simulation results as described above and the grain size distribution in the model domain was defined by the results of the sediment core survey described in Section 7. Once the grain Froude number is computed it is compared to the Brownlie energy slope relationships prescribed above. The value of the grid cell is computed as the ratio of the grain Froude number to the energy slope limit:

$$R_B = \frac{F_g}{1.74\ S^{-1/3}}$$

where a value of R_b greater than 1.25 indicates the bed is in upper bed regime and a value less than 0.8 indicates the bed is in lower regime. Values of R_b between 0.8 and 1.25 indicate the bed is in transition from lower bed regime to upper regime. Brownlie developed more complex relationships that included viscous (temperature) effects for the transition zone between lower regime and upper regime. The relationships above are appropriate for this analysis bed regime in Lower Granite Reservoir.

Results of the Brownlie spatial analysis are shown in Figure 114 and Figure 115 for the 1-percent chance exceedance discharge and the SPF discharge. The 1-percent chance exceedance and SPF discharges for the Clearwater and Snake Rivers from Section 4 are listed in Section 1. The Brownlie analysis indicates that during the 1-percent chance exceedance discharge most of Snake River channel through Lower Granite Reservoir to Silcott Island is in transition to upper regime and is in upper regime near the confluence. The Clearwater River above the confluence remains in lower regime according to the Brownlie analysis. During the SPF discharge, transition and upper regime bed conditions are indicated throughout the Snake River channel above Silcott Island. The Clearwater River is indicated as remaining in lower regime because the SPF discharge is not much greater than the 1-percent exceedance discharge because of flood regulation by Dworshak Reservoir (Section 1).

HEC-RAS Estimated Annual Peak Steady Flow Discharges for FDA Risk Analysis											
			Exceedance Probability (Percent)								
River	Reach	RS	50	20	10	4	2	1	0.4	0.2	SPF
Clearwater	Lewiston	7.85	49433	65967	75799	87138	94905	102167	111124	117587	125000
Snake	Clarkston	148.83	110991	148115	170189	195650	213089	229394	249505	264016	295000
Snake	Lower Granite	139.254	160423	214082	245988	282788	307995	331562	360629	381603	420000
Lower Granite forebay elevation (feet)			733.78	732.00	730.66	729.32	728.40	728.21	727.98	727.81	727.40

Table 3. Annual peak steady flow discharges for FDA risk analysis.

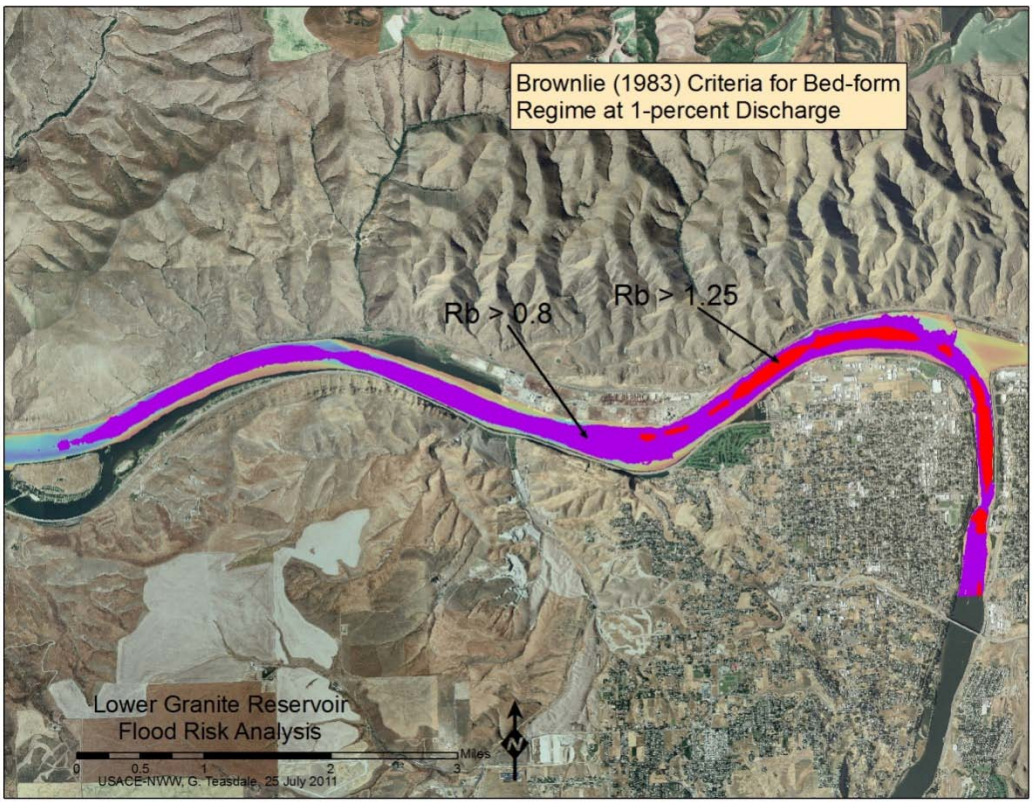


Figure 114. Brownlie bed regime for the 1-percent exceedance discharge.

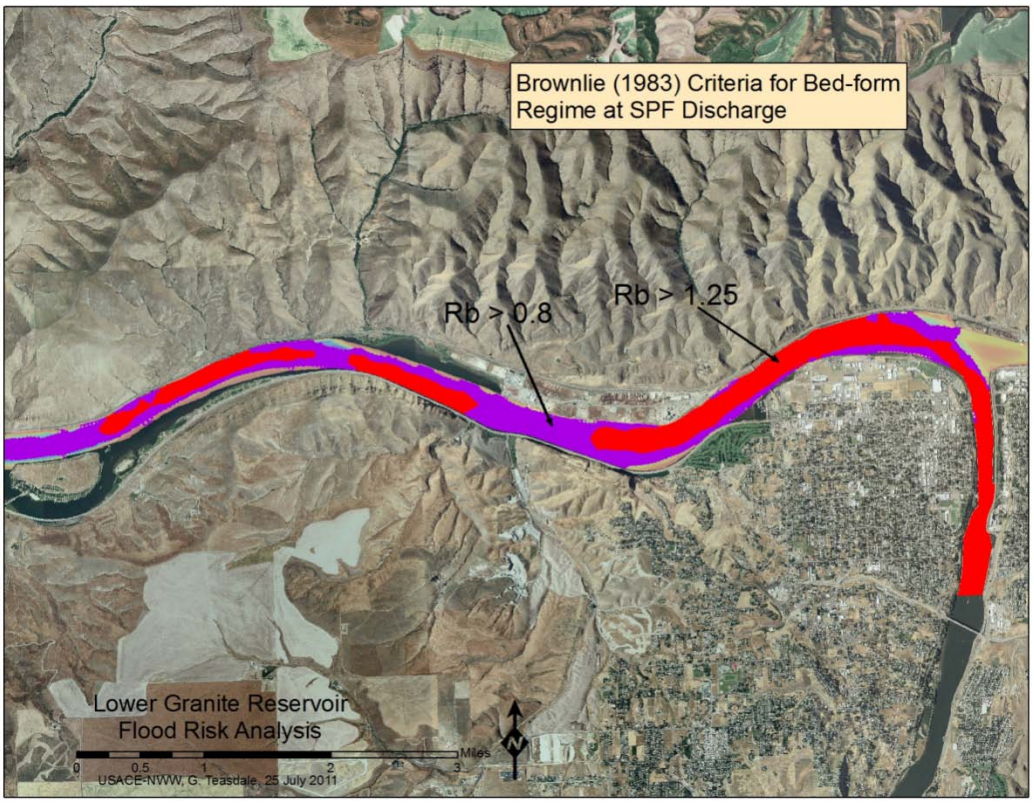


Figure 115. Brownlie bed regime for the SPF discharge.

15.8.3. Spatial Analysis of Bed Regime with the Karim Relationships

Spatial analysis of bed regime can also be developed from relationships developed by Karim[8]. Karim predicted the beginning of the transition to upper regime and the beginning of upper regime as functions of the Froude number:

$$F_t = 2.716\left(\frac{H}{D_{50}}\right)^{-0.25}$$

$$F_u = 4.785\left(\frac{H}{D_{50}}\right)^{-0.27}$$

where F_t is the limiting Froude number for the beginning of the transition to upper regime, F_u is the Froude number for the beginning of upper, H is the flow depth, and D_{50} is the median grain size of the sediment. The Froude number is computed:

$$Fr = \frac{U}{\sqrt{gH}}$$

where Fr is the Froude number, U is the water velocity, g is the acceleration of gravity.

In the spatial analysis with the Karim relationships, grid cell values are computed by each of the equations above using the flow depth and water velocity from the ADH simulations. As with the Brownlie analysis, the final grid cell value is a ratio, in this case computed as Fr/F_t or Fr/F_u.

Results of the Karim analysis for the 1-percent chance exceedance discharge and the SPF discharge are very similar to the Brownlie analysis. The Karim analysis indicates that during the 1-percent chance exceedance discharge most of Snake River channel through Lower Granite Reservoir to Silcott Island is in transition to upper regime and is in upper regime near the confluence. Most of the Clearwater River channel above the confluence is again predicted to remains in lower regime. During the SPF discharge, transition and upper regime bed conditions are indicated throughout the Snake River channel above Silcott Island.

[8] Karim, F. (1995). "Bed configuration and flow resistance in alluvial-channel flows." Journal of Hydraulic Engineering, 121(1), 15-25.

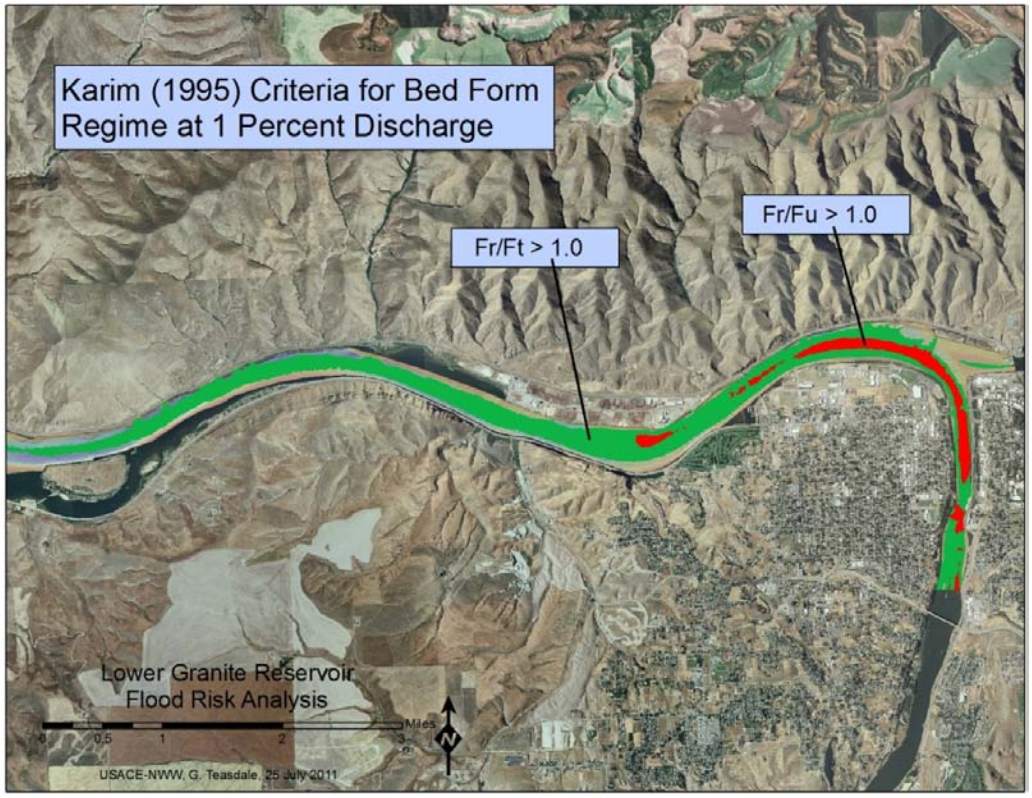


Figure 116. Karim bed regime for the 1-percent exceedance discharge.

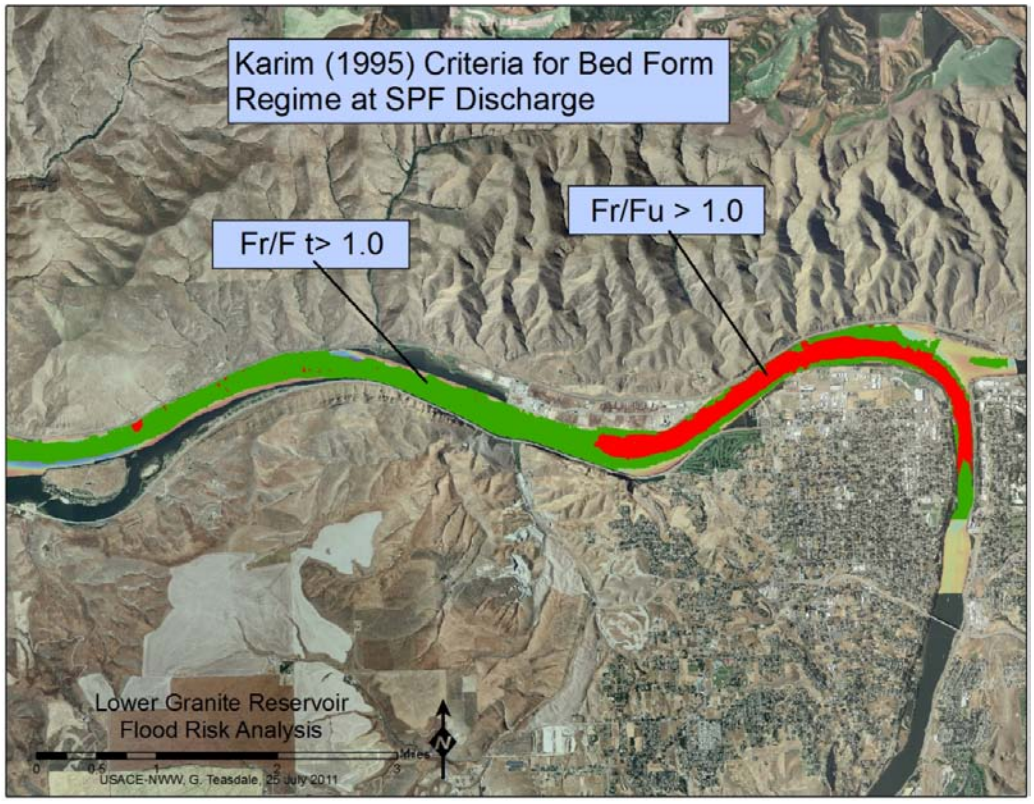


Figure 117. Karim bed regime for the SPF discharge.

15.8.4. Spatial Analysis of Bed Regime with the Simons and Richardson Relationship

An early and still widely applied indicator of bed regime is a diagram based on steam power developed by Simons and Richardson[9]. The diagram[10] indicates that the bed will be in upper regime when stream power is greater than about 0.6 lb/ft-s for sediment with a median grain size between 0.3 and 0.4 mm. Stream power is computed as the product of the grid cell velocity and the grid cell bed shear stress. In a spatial analysis, the Simons and Richardson predictor is applied by identifying all grid cells in the model domain that exceed the 0.6 lb/ft-s criteria. The results of the Simons and Richardson analysis for the 1-percent chance exceedance discharge and the SPF are show in Figure 118 and Figure 119. Almost all the Snake River channel for both the 1-percent chance exceedance discharge and SPF discharge is indicated as being in upper regime by the Simons and Richardson criteria.



Figure 118. Simons and Richardson bed regime for the 1-percent chance discharge.

[9] Simons, D.B. and Richardson, E.V. (1966) Resistance to flow in alluvial channels. Professional Paper 422J, U.S. Geological Survey, Washington, DC.

[10] Simons, D.B. and F. Senturk (1976). *Sediment Transport Technology*, Water Resources Publications, Littleton, CO.

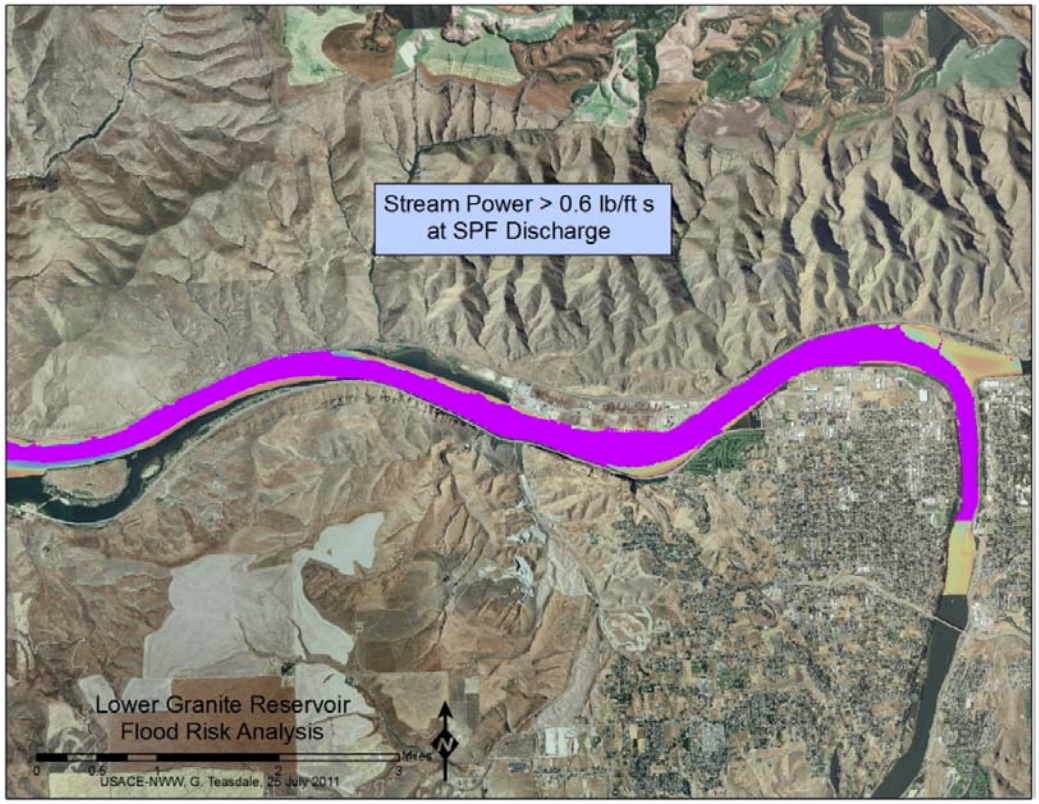


Figure 119. Simons and Richardson bed regime for the SPF discharge.

15.8.5. Comparison with Bed Regime of the Lower Columbia River

It is informative to compare the analysis of bed regime of the hypothetical 420,000 cfs SPF discharge in Lower Granite Reservoir with an actual discharge of this magnitude in a sand bed channel in the Columbia River system. The geometry of large sand bed-forms and the effective channel were obtained from bathymetry of the lower Columbia River near Kalama, OR acquired by the USACE Portland District during November 2011when discharge peaked at about 460,000 cfs. The bed profile in Figure 120 of the channel near the Port of Kalama shows dunes as high as 12 feet and wavelengths of several hundred feet.

A one-dimensional HEC-RAS model was developed from the November 2011 bathymetry for the reach from the Beaver Army terminal at RM 53 to Columbia City, OR at RM 85. The bed regime analysis methods described above all predicted that the channel bed would be in lower regime at the 460,000 cfs discharge. Froude number ratios from the Karim analysis are plotted in Figure 121. Interestingly, there are undocumented reports that hydrographic surveyors have observed large sand dunes beginning to flatten and washout during very high discharge on the Lower Columbia

River. Bathymetric data of the lower Columbia River could be investigated in future work to improve regime prediction methods.

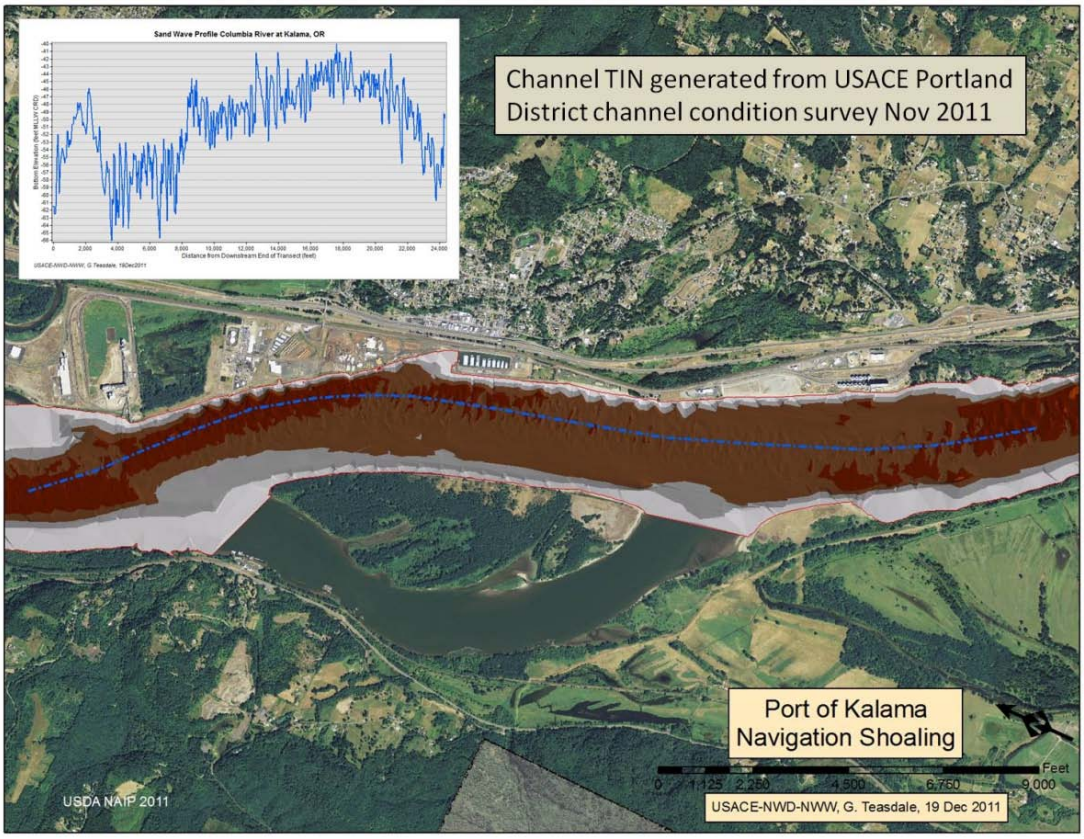


Figure 120. Sand bedforms in the Lower Columbia River at the Port of Kalama.

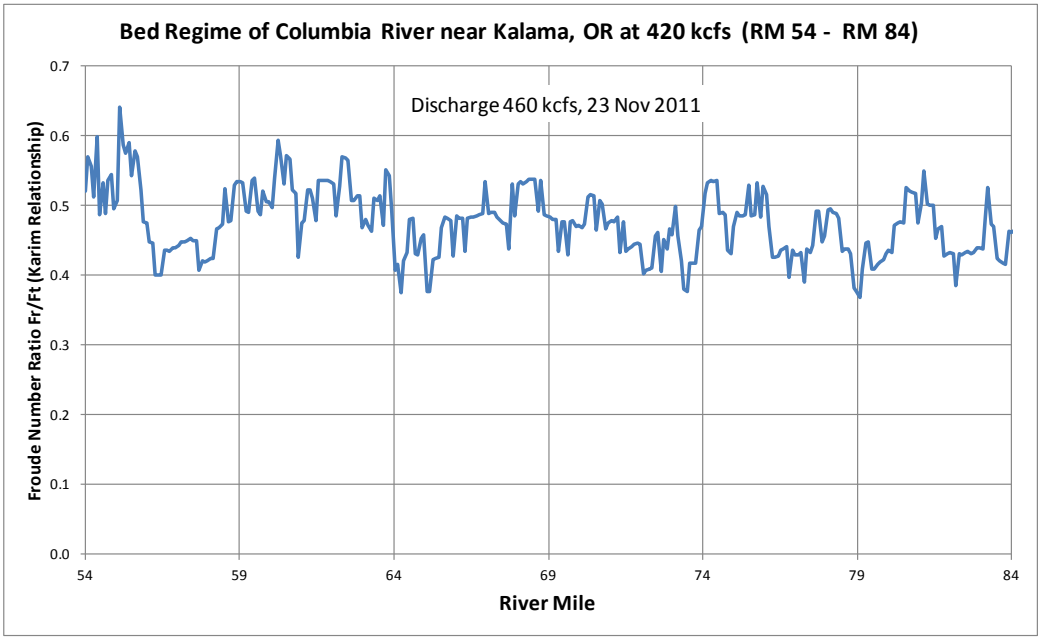


Figure 121. Analysis of bed regime in the Lower Columbia River at the Port of Kalama.

15.8.6. Bed Displacement during SPF Estimated with ADH

While most operational sediment transport models do not model bed-forms directly, some sand bed-load transport functions were derived from data that include upper regime bed conditions. Bed displacement during the SPF was computed with the ADH model of Lower Granite Reservoir. The ADH model does not directly account for reduction in flow resistance due to bed regime, but transport rates computed by ADH may reasonably approximate transport rates expected during upper bed regime conditions. Sediment erosion and deposition computed with the two-dimensional model are shown in Figure 122. Sediment eroded in the deepest parts of the channel to the bed limit specified in the model (1 m). A single grain size of medium sand (0.5 mm) was specified and the discharge was held steady at 420,000 cfs (11,890 cms) for 2 hours. The pattern of erosion agrees reasonably well with the pattern of upper bed regime predicted by the Brownlie relationship in Figure 115.

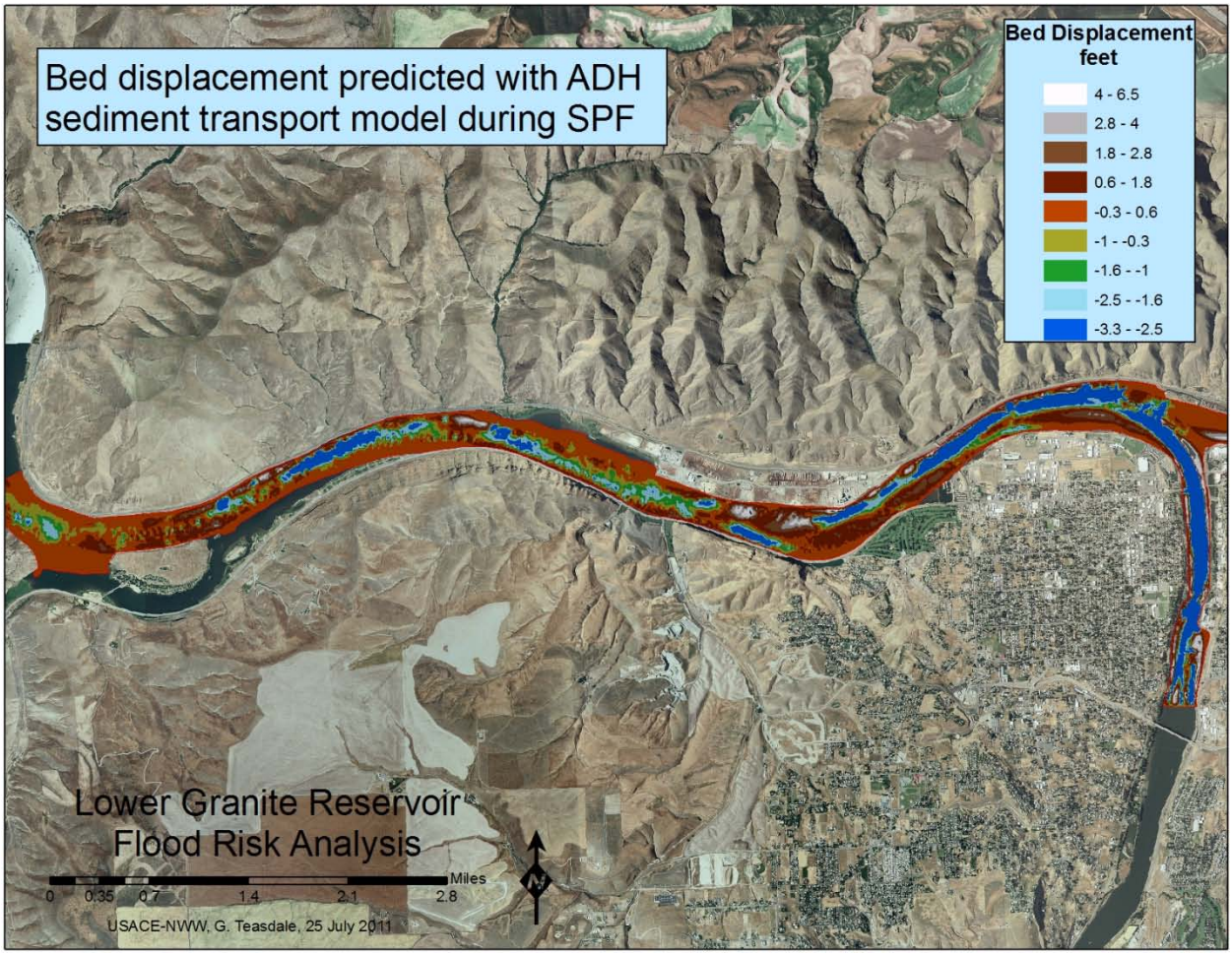


Figure 122. Bed displacement estimated with an ADH model during the SPF.

15.9. Summary and Conclusions of the Bed-form and Bed Regime Analysis

Bathymetry of Lower Granite Reservoir above Silcott Island was measured near the peak discharge in May 2011. At the time of the survey sand bed-load was being transported through the upper segments of the reservoir and the geometry of the active mobile sand bed-forms was captured in the high resolution bathymetry. The high-discharge bathymetry was compared directly with bathymetry datasets acquired in September 2009, September 2010 and September 2011 when the bed was immobile. The May 2011 survey was the first direct measurement of active bed-forms in the reservoir.

One dimensional HEC-RAS and two dimensional ADH models of Lower Granite Reservoir were developed from the May 2011 bathymetry. The cross sectional area of the channel in the May 2011 bathymetry provides a more realistic representation of channel conveyance during high discharge without the need to estimate channel geometry changes due to sediment transport. Calibrated hydraulic models developed from this functionally mobile geometry provide best-estimates of the flow resistance (Manning's *n*) of the active channel. It was found that the Manning's *n* values for the calibrated HEC-RAS hydraulic model based on the 2011 bathymetry were not significantly different from the calibrated HEC-RAS hydraulic model based on the 2009 bathymetry. This is an important finding because hydraulics models developed in previous studies of Lower Granite Reservoir assumed greater Manning's *n* values at high discharge. It was shown that computed water surface profiles at the confluence for extreme discharges based on the functionally mobile May 2011 bathymetry are less than those based on the static 2009 and 2010 bathymetry.

The mobility of the bed in Lower Granite Reservoir and its effect were examined with six approaches 1) development of calibrated hydraulic models with bathymetry acquired during the high discharge of May 2011, 2) comparison of hillshade maps made from the September 2009, September 2010 and May 2011 bathymetries, 3) Fourier analysis of dune profile transects, 4) comparison of bathymetry difference maps, 5) sediment transport simulation during the peak of the May 2011 discharge and from 2009 to 2011, and 6) spatial analysis of bed regime with several empirical relationships. Bed-forms above Silcott Island and the confluence in the May 2011 bathymetry were generally smaller than those observed in the low discharge bathymetry of 2009 and 2010, indicating that sand bed-forms were washing-out and that the bed was beginning to transition to upper regime bed. Overall, sediment was eroded near the confluence and deposited lower in the reservoir near and below Silcott Island.

A method of evaluating dune profile transects with Fourier waveform analysis was presented and shown to be an effective means to compare and quantify bed-form changes. The dune profiles throughout the upper part of the reservoir showed that the

Lower Granite Reservoir channel was transitioning to upper bed regime when the May 2011 bathymetry was acquired.

Difference maps that compared the 2009, 2010 and 2011 bathymetry showed widespread erosion of sediment from the Snake River channel near and below the confluence when the May 2011 bathymetry was acquired. Bed elevation differences were approximately the height of the dominant bed-forms, which again indicates that the channel was in transition to upper bed regime. Sediment again accumulated during recession of the seasonal hydrograph in 2011.

Sediment discharge rating curves computed by the HEC-RAS sediment transport model with the Toffaleti transport function agreed reasonably well with the measured rates of bed-load transport. The sediment transport model predicted a small increase in sediment deposition between Snake RM 130 and the confluence between October 2009 and May 2011 when the measured bed change showed a small average decrease. The results indicate that regression based sediment load boundary conditions and the HEC-RAS sediment transport model provide reasonable predictions of sediment transport and accumulation in Lower Granite Reservoir. Additional sediment studies and model tests are recommended to improve sediment transport models for Lower Granite Reservoir.

Spatial analyses of bed regime for the 1-percent chance exceedance discharge and the Standard Project Flood were developed by adapting empirical bed regime relationships to a grid-based spatial analysis. The bed regime maps of the three empirical relationships all indicated that most of the Snake River channel in Lower Granite Reservoir is either transitioning from lower bed regime to upper regime or is in upper regime at the extreme discharges.

Jointly, these analyses support the earlier finding that transition and upper regime bed conditions prevail in the regulated Lower Granite Reservoir channel during high discharge and that the flow resistance of the channel does not substantially increase, and likely decreases, during extreme discharges in Lower Granite Reservoir. The transition to upper bed regime is important because the flood stage elevation at the confluence will be lower and the risk of overtopping the levees in Lewiston will be less than if the bed remains in lower regime. The FDA computations based on upper bed regime conditions presented earlier likely provide the best representation of flood risk at the Lewiston levees.

16. Sediment Deposition in Navigation Channels

A navigation channel depth of 14 feet is authorized for Lower Granite Reservoir. Sediment deposition in the navigation channel in 2009, 2010 and 2011 was computed from the bathymetry datasets and is mapped in Figure 123 through Figure 126. The authorized navigation channel depth is defined relative to a fixed water surface elevation which may vary depending on the time of year and flow conditions. To improve fish passage the authorized channel depth has been referenced to the minimum operating pool (MOP) elevation for Lower Granite Reservoir at 733 ft NGVD29. In most years sediment deposits in the navigation channel at the Port of Lewiston on the Clearwater River and at the Port of Clarkston on the Snake River. Past dredging actions periodically removed sediment from the navigation channels, but since suspension of dredging operations sediment deposits have partially obstructed the navigation channel. To compensate, the target operating pool elevation was recently raised by 2 ft in consultation with cooperating agencies to temporarily recover navigation depth at the ports.

16.1. Recent Sediment Encroachment in Navigation Channels

The figures show the areas of sediment that encroach into the navigation channel for three pool elevations: 733 ft (MOP), 734 ft and 735 ft. Sediment encroaches into the navigation channel in all three years at all pool depths. While the net change of accumulated sediment across the full width of the channel at the Port of Lewiston between September 2009 and September 2011 was small, new sediment deposited within the navigation channel was substantial and further impacts navigation.

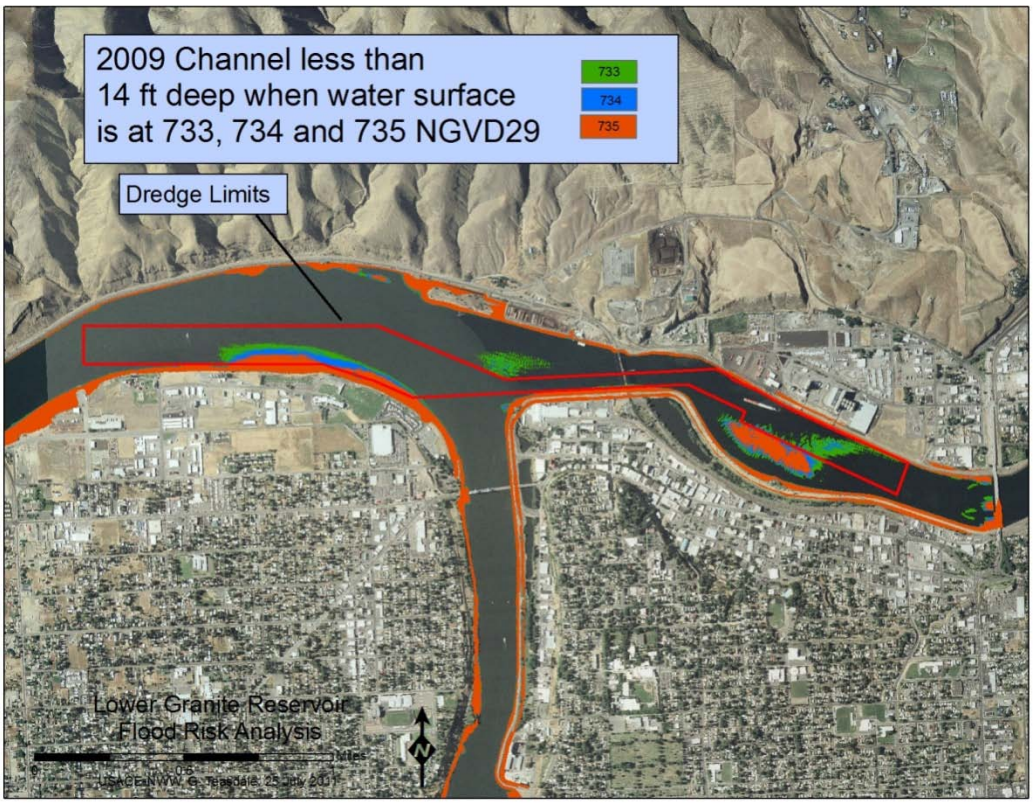


Figure 123. Deposition in the navigation channel at the confluence in September 2009.

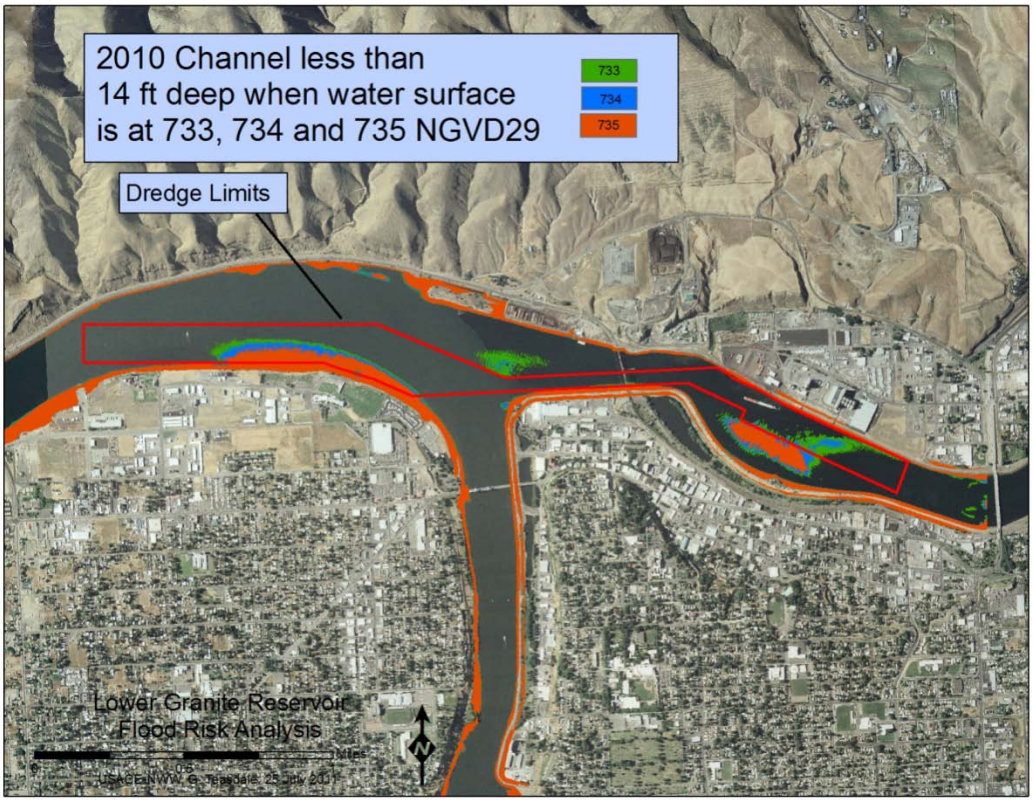


Figure 124. Deposition in the navigation channel at the confluence in September 2010.

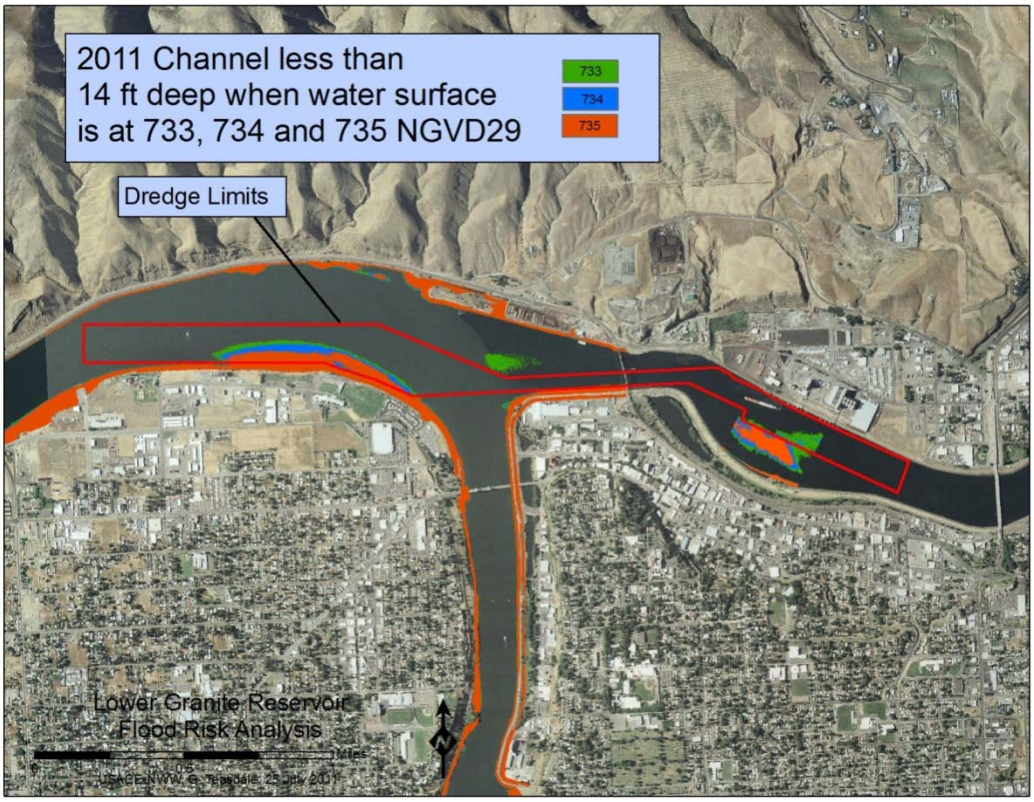


Figure 125. Deposition in the navigation channel at the confluence in May 2011.

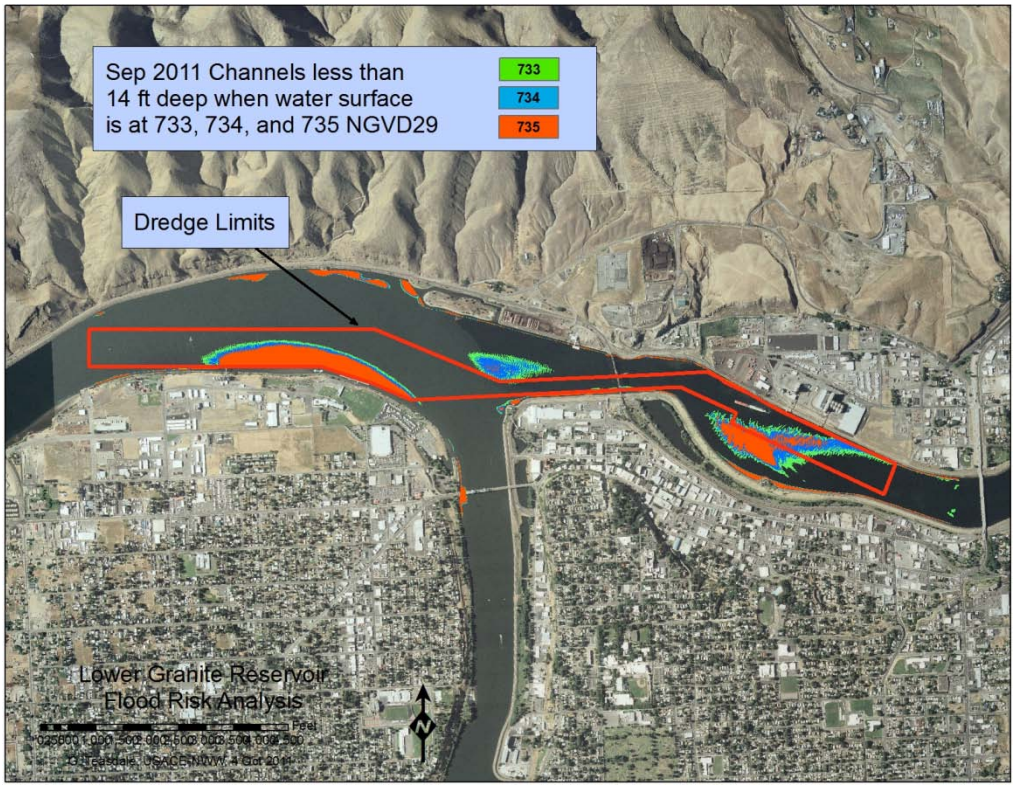


Figure 126. Deposition in the navigation channel at the confluence in September 2011.

16.2. Long-Term Sediment Encroachment in Navigation Channels

Previous sections show that current watershed sediment load rates will persist and may increase, so sediment will continue to accumulate in the navigation channel during the 50-year future analysis period unless sediment deposits are removed or reduced by 1) reduction of sediment influx to the navigation channel, 2) dredging, 3) river training structures, 4) reservoir flow modification, or 5) a combination of the methods. These methods are discussed in subsequent sections.

Long-term equilibrium depths of the Clearwater and Snake River navigation channels can be estimated with the alluvial hydraulic geometry relationships discussed in Section 4 and the effective discharges presented in Section 8. Effective discharge is the discharge-duration combination that transports the most sediment over a long period of time so is most effective in shaping an alluvial channel. The effective discharge for the Clearwater River is about 45,000 cfs (1274 cms). Substituting this discharge and adopting a median grain size of 0.3 mm in the sand channel relationships developed by Parker gives an equilibrium depth of 14 feet:

$$\hat{Q} = \frac{Q_{bf}}{\sqrt{gD_{50}}D_{50}{}^{2}} = \frac{1274}{\sqrt{9.81(0.0003)}(0.0003)^{2}} = 2.61\times10^{11}$$

$$\text{Depth, } H = 3.01\hat{Q}^{0.321}D_{50} = 3.01(2.61\times10^{11})^{0.321}(0.0003) = 4.17 \text{ m or } 14 \text{ ft}$$

$$\text{Width, } B = 0.274\hat{Q}^{0.565}D_{50} = 0.274(2.61\times10^{11})^{0.565}(0.0003) = 232 \text{ m or } 760 \text{ ft.}$$

The predicted equilibrium channel depth is about equal to the authorized navigation channel depth which indicates that sediment removal would be necessary to maintain the channel through the turning basin because of non-uniform deposition and the movement of sand bedforms.

The equilibrium channel depth predicted by the Parker relationship agrees reasonably well with the actual depth of the Clearwater River channel upstream from the turning basin. Historical sediment ranges discussed in Section 6 show no sediment accumulation in the channel between RM 1.66 (Figure 127) above the turning basin to RM 1.99 (Figure 128) at Memorial Bridge. The average channel depth and width in this segment are 16.1 ft and 770 ft at the 50 percent chance exceedance (2-year) discharge.

Another method for predicting equilibrium channel depths is to simulate long-term sediment accumulation with the one-dimensional HEC-RAS sediment transport model

discussed in Section 10. Figure 129 shows the progressive change in effective depth in the Clearwater turning basin at RM 1.21 during the simulation of the 50-year future period. The predicted equilibrium depth is approximately 14 ft, which agrees with the equilibrium depth predicted with the Parker relationships. Without periodic removal of sediment, the simulation predicts that the channel will reach equilibrium in about 20 years under current sediment load and discharge conditions. Longitudinal bed profiles through the turning basin for the existing 2009 bed and the year-50 simulated bed are plotted in Figure 130. This figure shows that raising the pool to the maximum operating elevation 738 ft NGVD29 would not recover the navigation depth lost due to long-term sediment deposition.

Similarly, the properties of the equilibrium channel of the Snake River below the confluence can be predicted with the alluvial hydraulic geometry relationships and sediment transport modeling. The equilibrium depth and width predicted by the Parker relationships are 19 ft and 1290 ft based on an effective discharge of 115,000 cfs and a median grain size of 0.3 mm. As discussed in Section 4, the current geometry of the Snake River channel below the confluence is formed in part by the backwater of Lower Granite Dam so the functional channel is wider and deeper than a self-formed alluvial channel. The 50-year simulation of effective channel depth at Snake RM 138.809 in Figure 131 shows the equilibrium channel depth reduces to a depth of 29 feet in about 20 years under the regulated flow conditions of the reservoir.

Longitudinal bed profiles of the channel below the confluence for the existing 2009 bed and the year-50 simulated bed are plotted in Figure 132 and show that the mean equilibrium channel is deeper than the 14 ft authorized navigation channel. While the predicted mean equilibrium depth below the confluence is greater than the authorized channel depth (14 ft), shoaling at the Port of Clarkston still occurs because the strong secondary flow circulation pattern deposits sediment on the inside of the bend below the confluence.

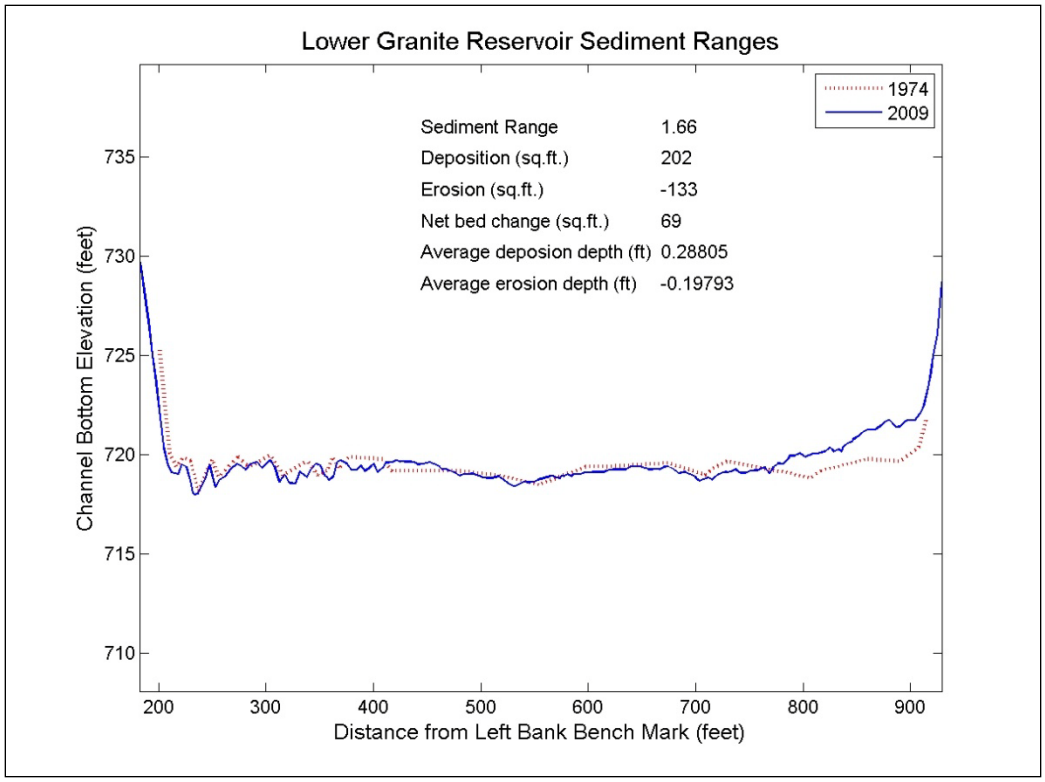


Figure 127. Stable channel cross section at Clearwater RM 1.66.

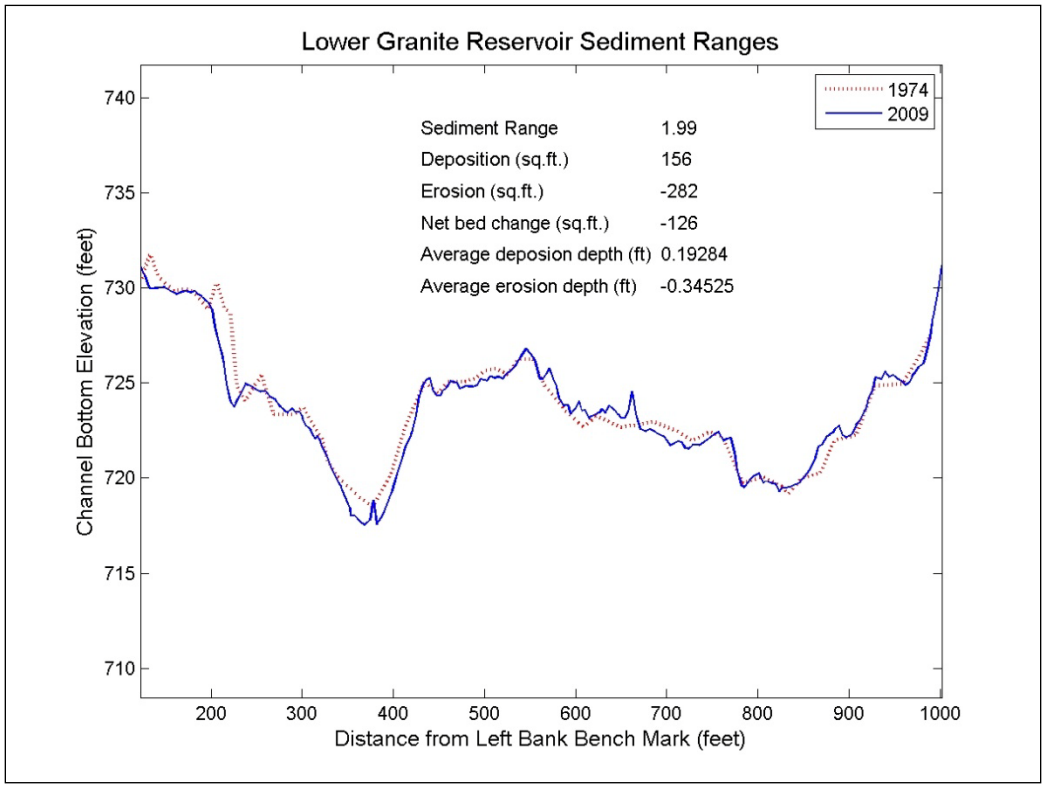


Figure 128. Stable channel cross section at Clearwater RM 1.99.

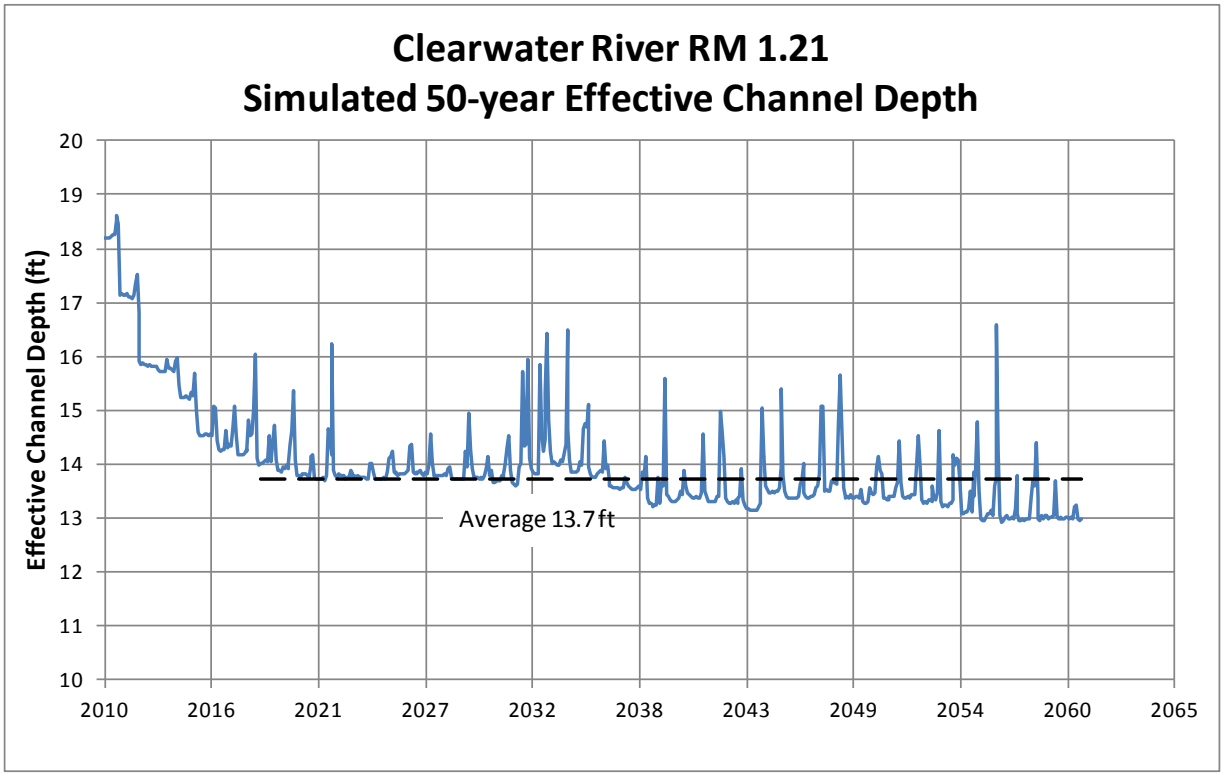


Figure 129. Simulation of 50-year effective channel depth in the Clearwater turning basin.

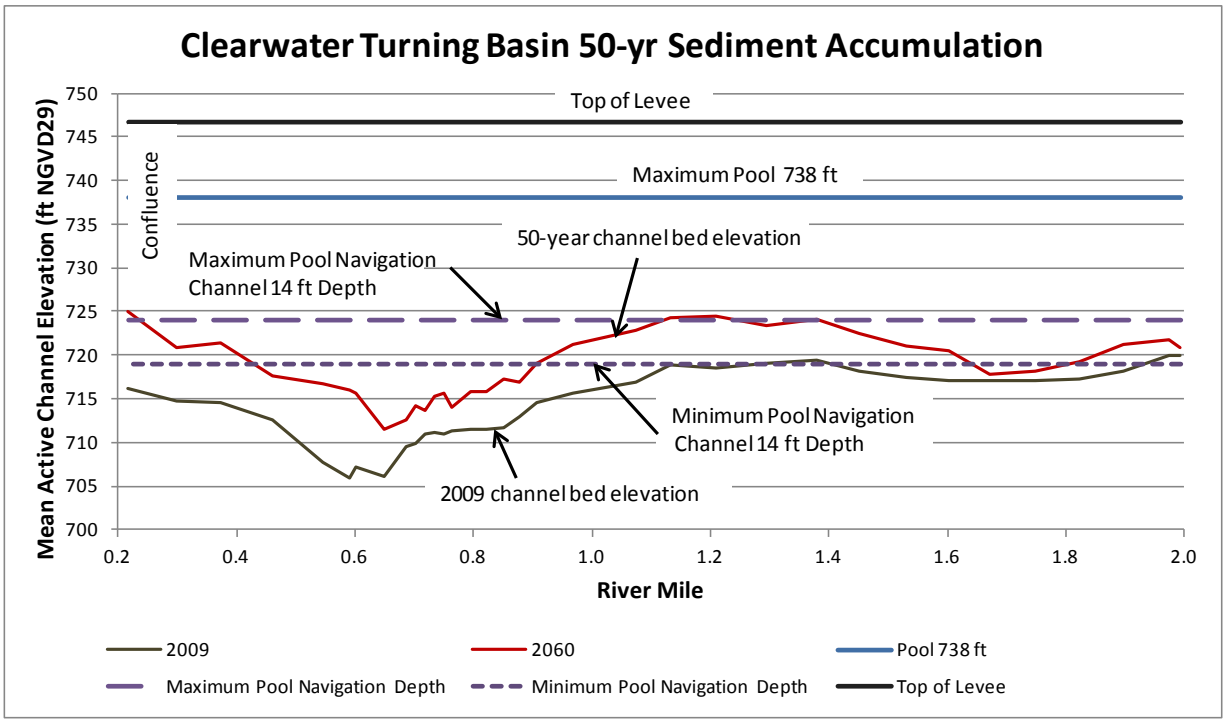


Figure 130. Simulation of 2060 mean active bed elevation in the Clearwater turning basin.

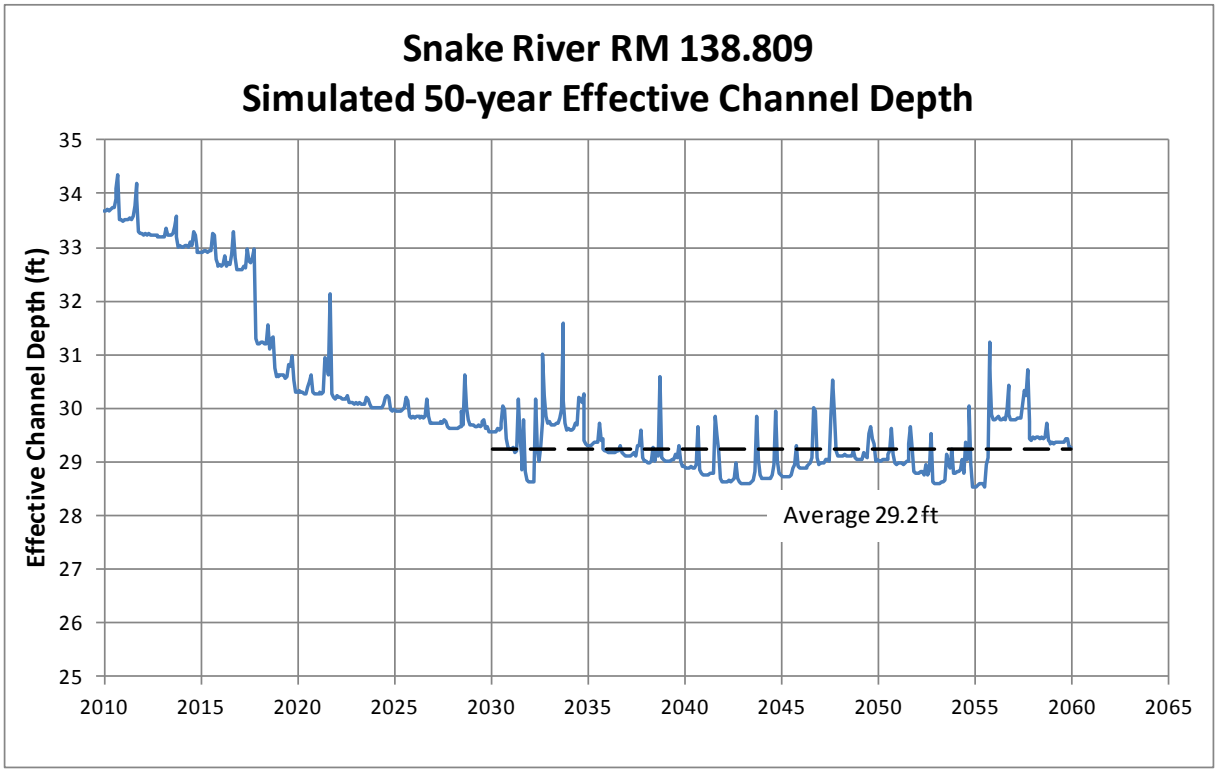


Figure 131. Simulation of 50-year effective channel depth at the Port of Clarkston.

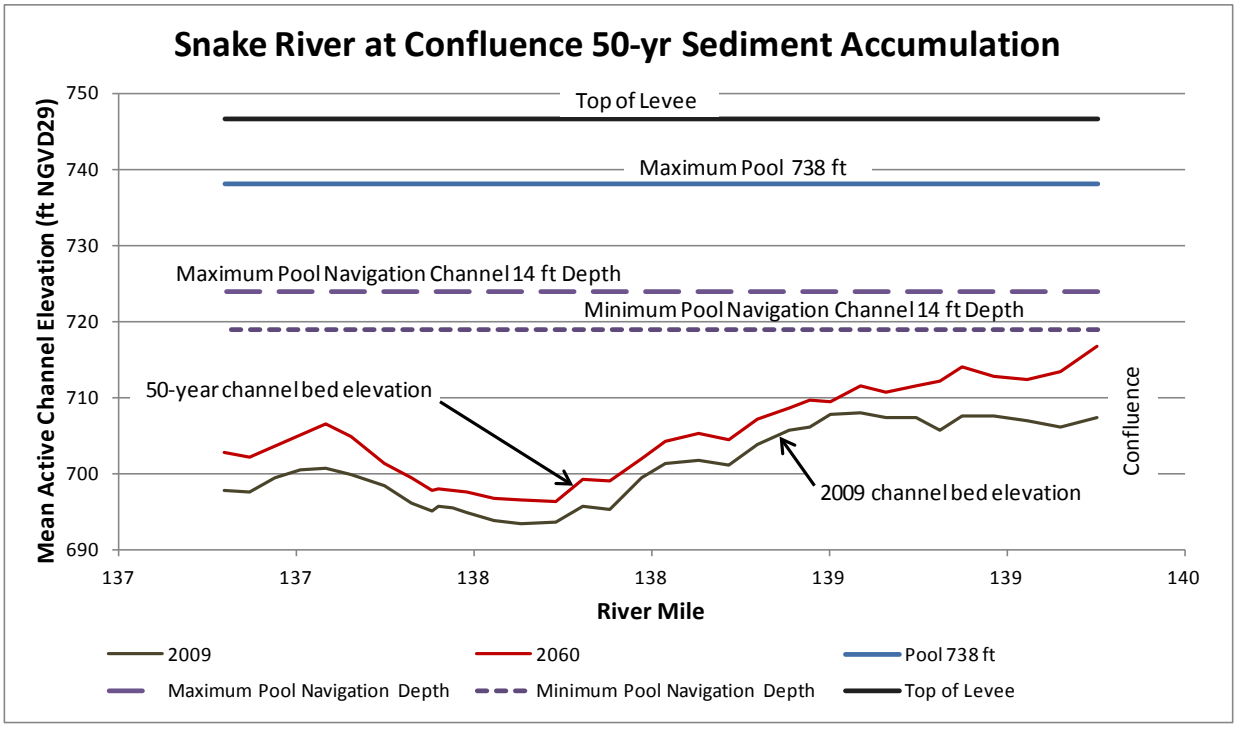


Figure 132. Simulation of 2060 mean active bed elevation in Snake River at confluence.

17. Hydraulic Modeling of Environmental Flows

The movement of water greatly affects the physical, chemical and biological processes of natural lakes and reservoirs[11,12]. The magnitude, frequency, timing, duration, rate of change, and predictability of environmental flows are key factors in freshwater biodiversity which require careful evaluation[13]. While a thorough analysis of far-field[14] environmental flow hydraulics of Lower Granite Reservoir and the other reservoirs of the lower Snake River reservoir system is beyond the scope of the PSMP-EIS, two aspects were evaluated to support characterization of the quality of fishery habitat. These are water travel time and the two-dimensional depth-velocity distribution of Lower Granite Reservoir.

17.1. Water Travel Time

The travel time of water through Lower Granite reservoir is a measure of the amount of time that juvenile fish spend in the reservoir during downstream migration. The objective of the hydraulic analysis was to estimate the total water travel time through the reservoir under current forebay operations and for hypothetical operations at higher than normal pool elevations.

17.1.7. One-dimensional Model Development

Travel time was computed with a calibrated one-dimensional unsteady flow HEC-RAS model that was developed from the September 2011 multibeam echosounding bathymetry of the reservoir. The domain of the model included Lower Granite Reservoir from RM 107.43 to RM 129.25, the Clearwater River from RM 0 to 1.99 and the Snake River from RM 129.25 to 141.23. Model cross sections in the reservoir were spaced at 400 ft intervals to provide accurate estimates of water volume and mean water velocity.

Boundary conditions for the unsteady flow simulation were developed from the daily average inflow discharge series and the daily average water surface elevations at the forebay of Lower Granite Dam for water years 2011 and 2007 (October to

[11] Wetzel, R.G. (1983). *Limnology*, 2nd Ed., Saunders College Publishing, Fort Worth.

[12] Chapra, S. (1997). *Surface Water-Quality Modeling*, McGraw-Hill, NY.

[13] Arthington, A.H., Bunn, S.E., Poff, N.L., nd Naiman, R.J. (2006). "The challenge of providing environmental flow rules to sustain river ecosystems." Ecological Applications, 16(4), 1311-1318.

[14] Far-field is a term used in hydraulics to describe the general region of flow that is far enough from major structures, such as dams and pump stations, so that the pattern flow is not directly affected by the local hydrodynamics of the structure.

September). Flows during water year 2011 were unusually high (Figure 133), while in WY 2007 flows were relatively low (Figure 134). Peak discharge in WY 2011 was over 200,000 cfs, while in WY 2007 is was about 100,000 cfs. The two years provide a good contrast in seasonal hydrographs for comparison of reservoir water travel times.

Alternative forebay operations were simulated by adjusting the elevation of the tailwater boundary condition in the model. The alternatives included 1) the actual forebay elevations in WY 2011, 2) WY 2011 forebay elevations plus 1 foot, 3) WY 2011 forebay elevations plus 2 feet for all discharges over 120 kcfs and plus 1 foot for all other discharges. Operations were constrained so that the elevation at the confluence did not greatly exceed 738 feet (NGVD29). The 2011 HEC-RAS model was calibrated to the 17 May 2011 high water marks discussed previously. The unsteady flow water surface elevations computed with the calibrated HEC-RAS model agreed well with measured stage at the confluence of the Snake and Clearwater Rivers (Figure 135). Products of the model analysis included steady flow travel time rating curves, unsteady flow reach transit times for WY 2011 and WY 2007, unsteady flow reach transit time for alternative forebay operations, and unsteady flow travel time frequency curves

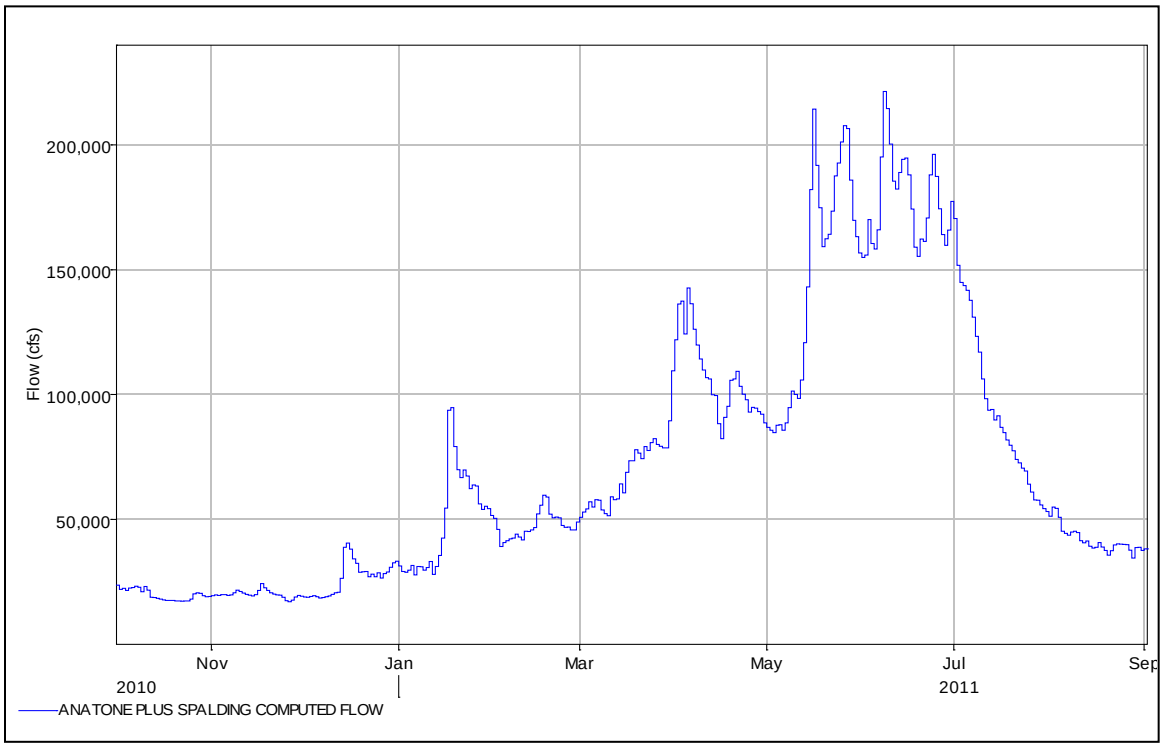


Figure 133. WY 2011 inflow hydrograph for Lower Granite Reservoir.



Figure 134. WY 2007 inflow hydrograph for Lower Granite Reservoir.

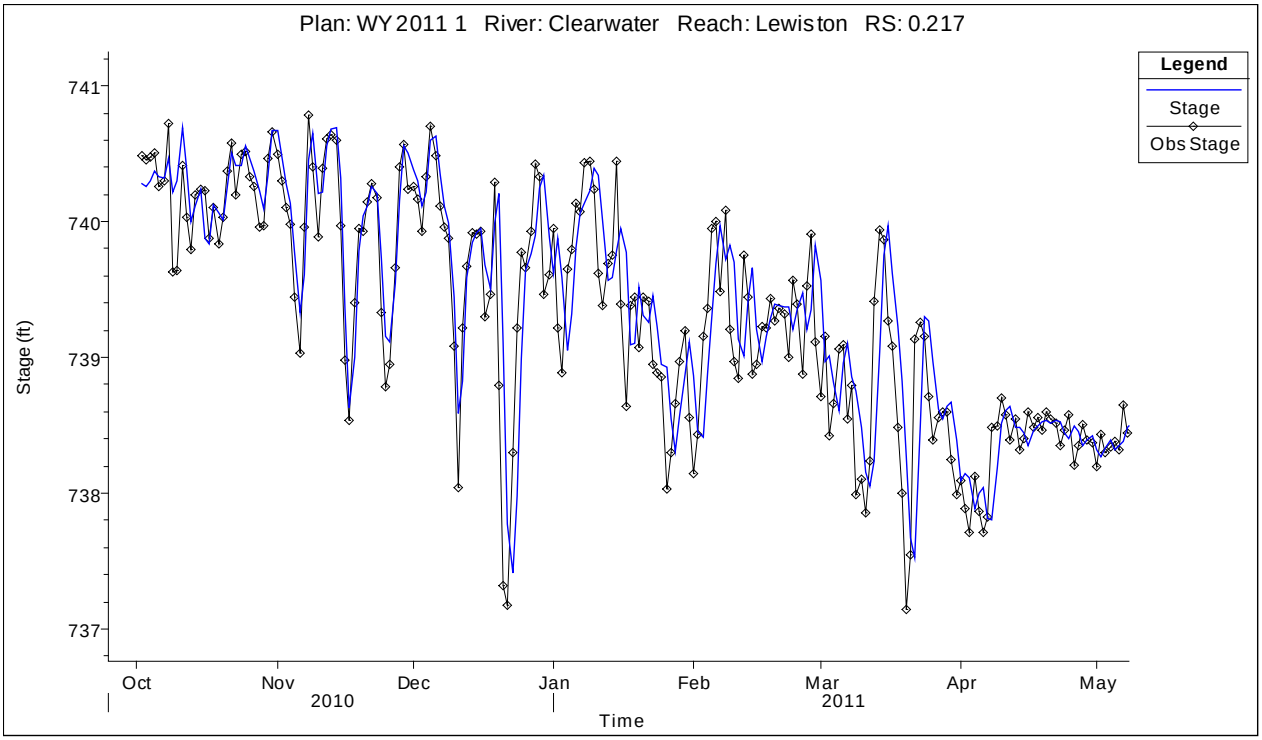


Figure 135. Calibration of the September 2011 HEC-RAS model.

17.1.8. Steady Flow Travel Time and Reach Transit Time

The HEC-RAS software computes the steady flow travel time of individual segments (between individual cross sections) by dividing segment length by the average water velocity in the segment. Total steady flow travel time of a reach is computed directly by HEC-RAS as the sum of travel times through the individual segments in the reach assuming flow remains steady (Figure 136). A steady flow travel time rating curve can be developed from the steady flow travel times for a range of discharges. Figure 137 is a plot and statistical fit of the steady flow rating curve for the reach of Lower Granite Reservoir between RM 139.25 and 107.43. Steady flow travel time rating curves can also be developed with steady-flow flow-duration discharge values such as in Figure 138. In WY 2011, steady flow travel time varied from 0.9 to 12.6 days and was influenced more by variation in discharge than variation in the forebay elevation of the alternatives.

The HEC-RAS software reports travel time for an unsteady flow series as a series of steady flow reach travel times. Steady flow travel times are of limited use, because during low flows the discharge does not remain constant long enough for a water parcel to transit the length of the reach during the steady flow period. For example, if flow is steady for one day, the travel time for a reach reported by HEC-RAS in effect assumes that the flow remains steady long enough for water to transit the full length of the reach even if the velocity is so low that it would actually take several days for a water parcel to transit the reach. In this case, the steady flow reach travel times would not give an accurate representation of the travel time of a water parcel through a reach. Unsteady flow reach *transit* times may be derived from HEC-RAS data with a supplemental analysis.

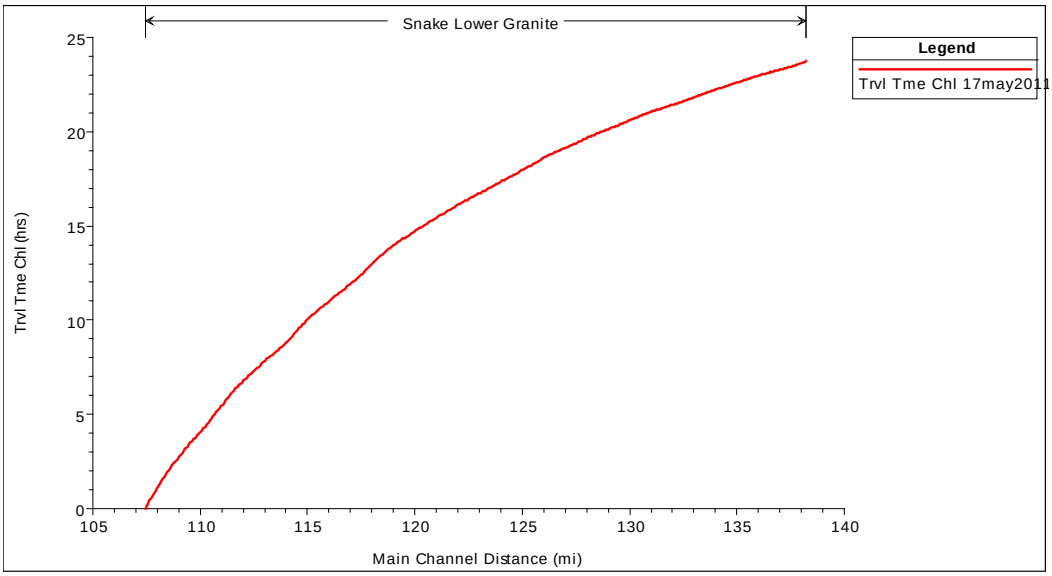


Figure 136. Steady flow travel time in Lower Granite Reservoir for 17 May 2011.

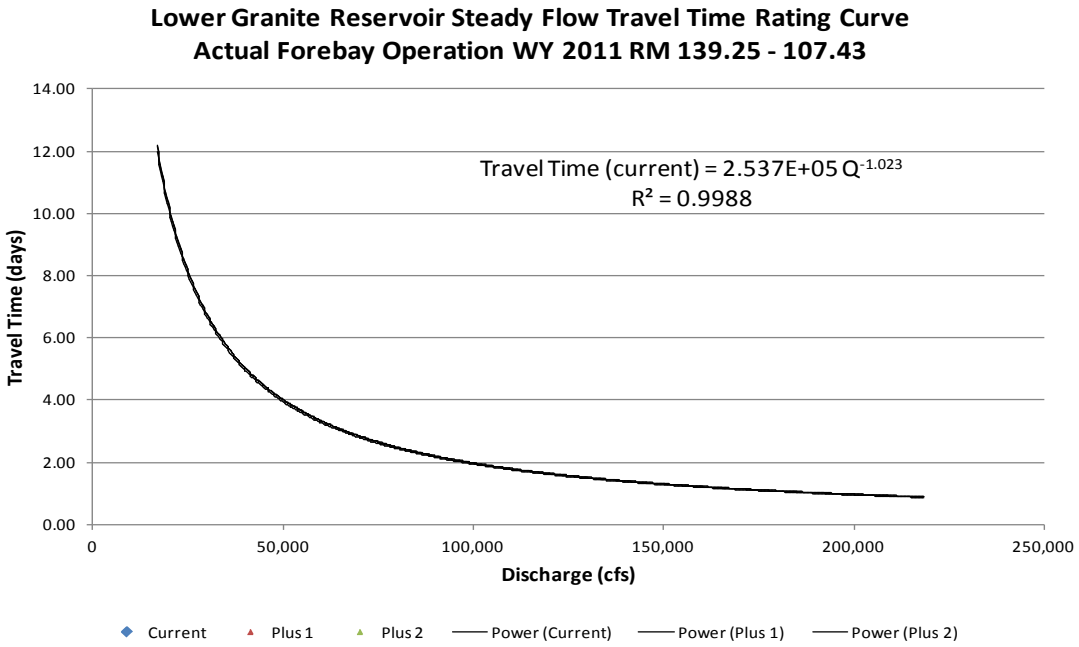


Figure 137. Steady flow travel time rating curve for reach RM 139.25 to 107.43.

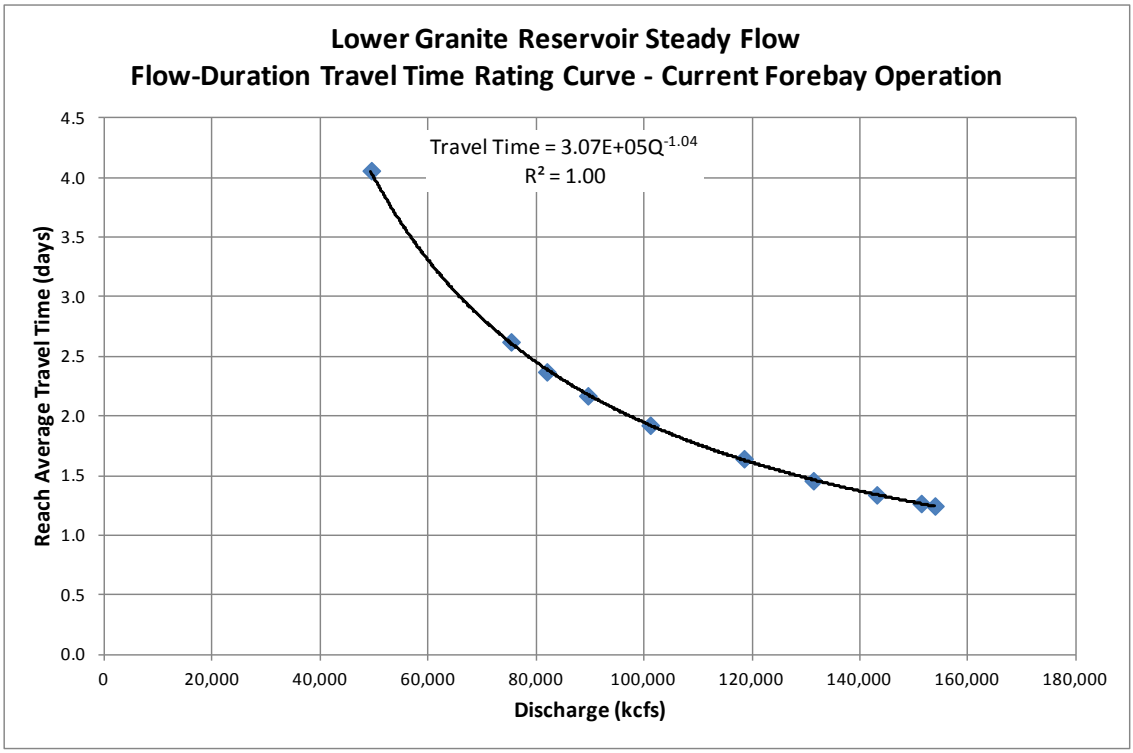


Figure 138. Flow-duration travel time rating curve for reach RM 139.25 to 107.43.

Unsteady reach transit times are computed from the incremental difference between the HEC-RAS steady flow travel times. The computation was performed with a Matlab script and is illustrated in Table 4. Reach transit times were computed for each day of the unsteady flow hydrograph. The method can be extended to discharge averaging periods of shorter duration.

Day	Total Distance ft	Travel Time hr	Velocity ft/s	Distance in one day ft	Cumulative Distance ft
1	158,400	200.0	0.22	19,008	19,008
2	158,400	180.0	0.24	21,120	40,128
3	158,400	160.0	0.28	23,760	63,888
4	158,400	150.0	0.29	25,344	89,232
5	158,400	150.0	0.29	25,344	114,576
6	158,400	160.0	0.28	23,760	138,336
7	158,400	180.0	0.24	21,120	159,456
Average	158,400	168.6	0.26		
			Last day distance adjustment	1,056 ft	
			Last day time adjustment	4320 s	
			Last day time adjustment	0.05 day	
			Adjusted total transit time	6.95 day	

Table 4. Unsteady flow travel time computation.

17.1.9. Reach Transit Times for WY 2011 and WY 2007

Unsteady flow reach transit times for WY 2011 are plotted in Figure 139 and for WY 2007 in Figure 140 along with the discharge hydrographs and series of daily steady flow travel times. In WY 2011, the estimate of reach transit time for the actual forebay operation varied from 0.88 days to 11.52 days and averaged 4.69 days. In WY 2007, transit time for actual forebay operations varied from 1.88 days to 12.29 days and averaged 6.46 days. The difference between years of the average daily transit time was 1.78 days or about a 38 percent difference. The unsteady flow reach transit times for the hypothetical alternative forebay operations in WY 2011 are plotted in Figure 141. Elevation of the pool had a small effect on the daily average transit time, 0.1 days or about a 2 percent difference. Reach transit times for WY 2011 and WY 2007 are summarized in Table 5.

Reach transit time duration curves can be developed from the transit time data such as those for WY 2011 and WY 2007 plotted in Figure 142. The difference in transit times between years is apparent. The analysis could be extended to more years

and the annual exceedance statistics developed for transit time variables. Reach transit times could also be evaluated with a two-dimensional model of the reservoir, Lagrangian particle tracking and calibrated with dye tracing measurements. These analyses may be pursued in the future.

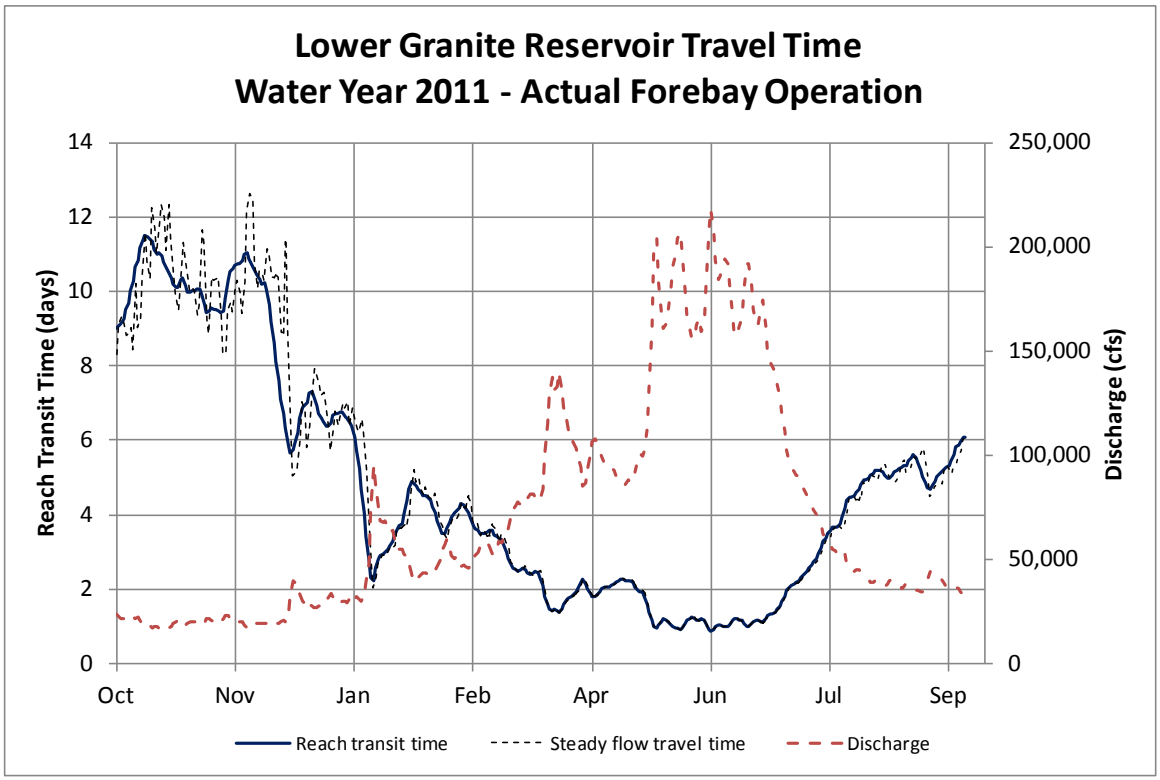


Figure 139. Unsteady flow reach transit times for Lower Granite Reservoir in WY 2011.

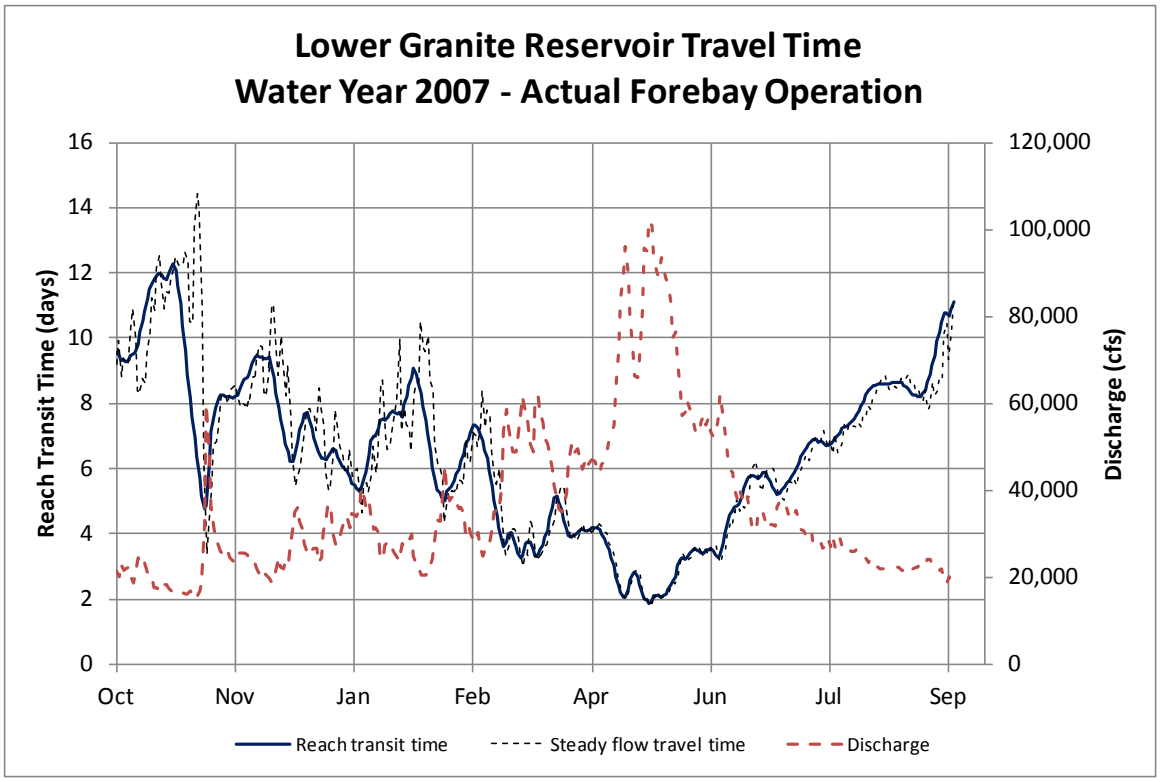


Figure 140. Unsteady flow reach transit times for Lower Granite Reservoir in WY 2007.

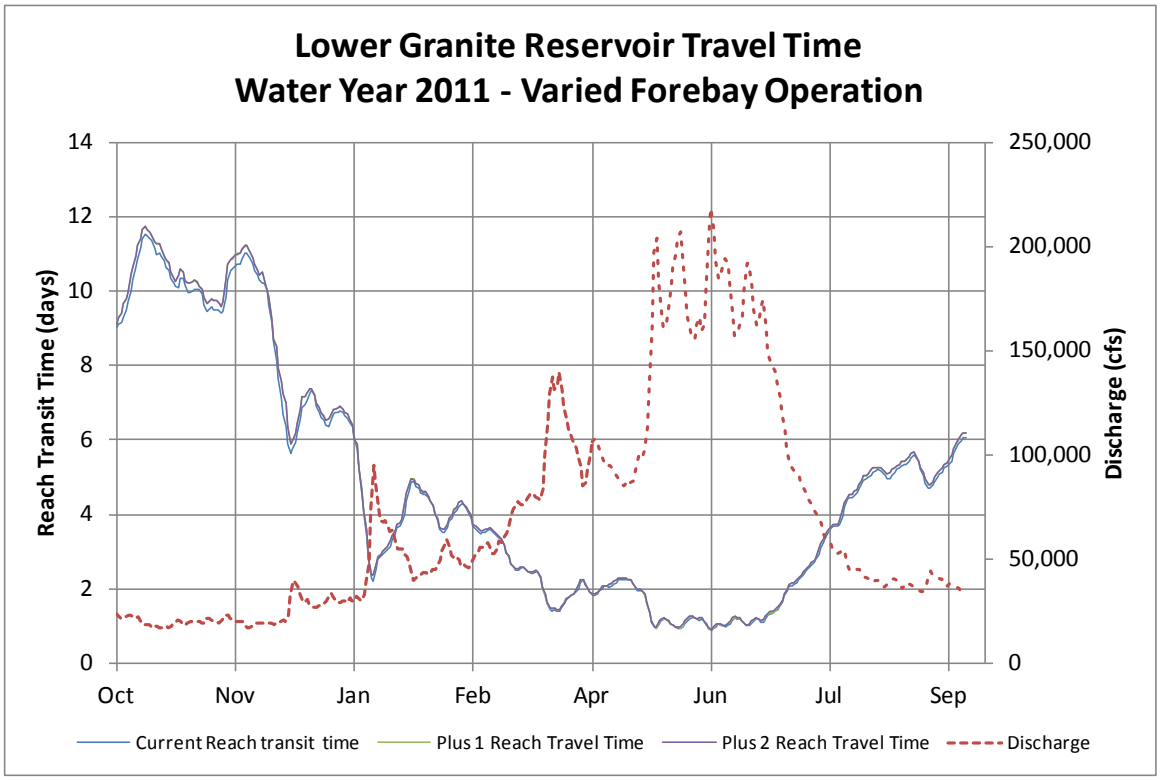


Figure 141. Unsteady flow reach transit times for Lower Granite Reservoir in WY 2011 with alternative forebay operations.

Lower Granite Unsteady Flow Reach Transit Time (days)				
	WY 2011 Forebay Operation			WY 2007
	Actual	Plus 1	Plus 2	Actual
Maximum day	11.52	11.74	11.73	12.29
Minimum day	0.88	0.90	0.91	1.88
Average daily	4.69	4.79	4.79	6.46

Table 5. Summary of reach transit times in Lower Granite Reservoir.

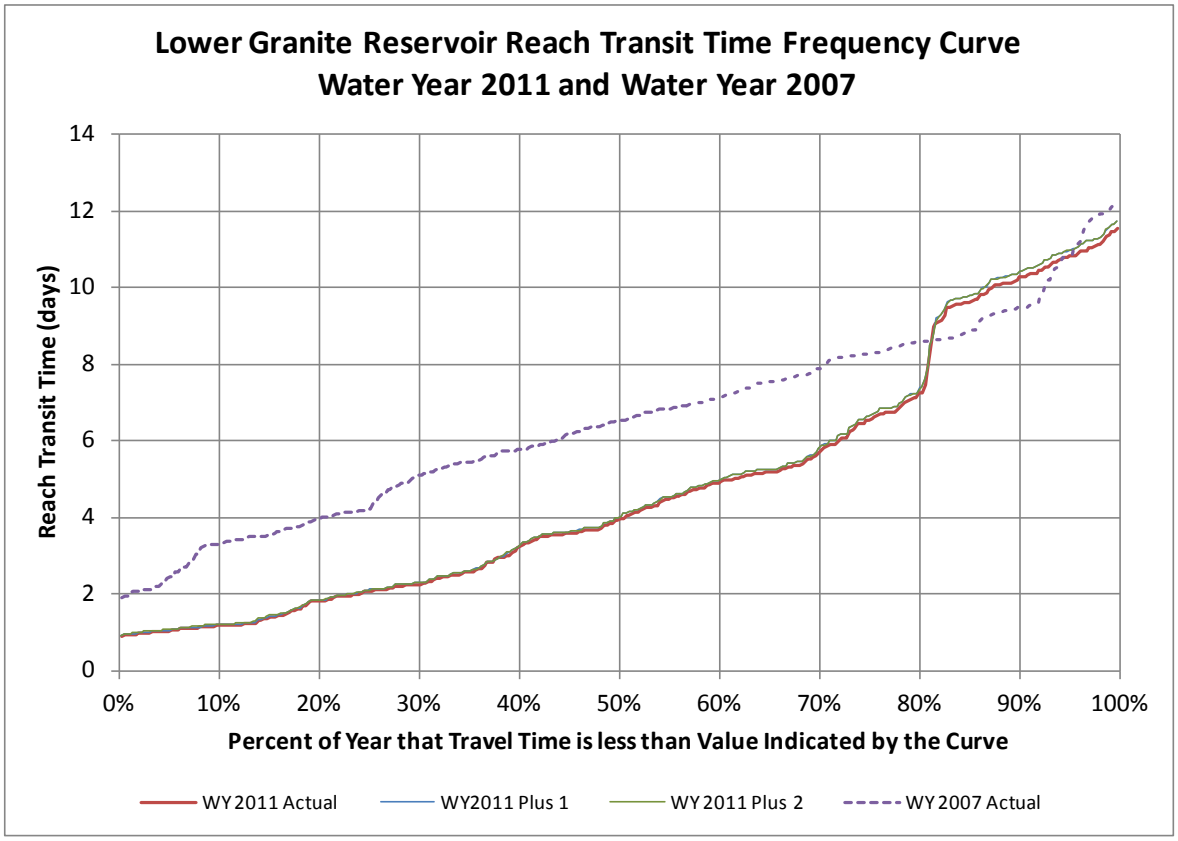


Figure 142. Reach transit time frequency curve for Lower Granite Reservoir in WY 2011 and WY 2007.

17.2. Two-dimensional Depth-Velocity Distribution in Lower Granite Reservoir

Water depth and velocity are important factors that influence the quality of fishery habitat and are required by certain habitat evaluation methods[15,16]. The characteristics of rearing and migratory habitat in Lower Granite Reservoir are being evaluated in PSMP-EIS study[17] and depth-velocity distributions of reservoir were developed to support the analysis. Shallow water, mostly the near-shore, is the main interest in the habitat analysis, so the flow depth and velocity are best estimated with two-dimensional hydraulic model. Study objectives could be met with 10 foot resolution grids of depth and velocity.

17.2.10. Development of the ADH Two-dimensional Model

Depth and velocity distributions were computed with the USACE Adaptive Hydraulics (ADH) modeling software. The analysis area included the Snake River from the forebay of Lower Granite Dam (RM 107.5) to Southway Bridge (RM 141.23) and the Clearwater River from the confluence to Memorial Bridge (RM 1.99). The reservoir was divided into two model domains: Lower Granite Dam to just below the confluence and from just below the confluence to the upstream limit of the analysis areas on both the Snake and Clearwater Rivers. The separate model domains decreased overall model development time, decreased simulation runtimes, and increased flexibility in simulating discharges.

The ADH two-dimensional models were developed from the September 2011 multibeam echosounding bathymetry acquired by ERDC-CHL using the equipment and methods described above. The bathymetry provides a very high resolution representation of channel topography (Figure 143). A very shallow area the near left shore above Silcott Island was not surveyed in September 2011, so bathymetry of this area was obtained from the 2009 USGS survey. Elevation transects of the near-shore areas of Lower Granite Reservoir below Silcott Island was obtained by USGS in 2010. This elevation data was used to augment the 2011 multibeam bathymetry in some shallow areas of the lower model domain (Figure 144).

[15] Waddle, T.J. (2001). *PHABSIM for Windows user's manual and exercises: U.S. Geological Survey Open-File Report* 2001-340. 288 p.

[16] Hickey, J. (2011). *HEC-EFM: A Spatial Accessory for HEC-EFM (Ecosystem Functions Model) Users Manual, Ver 1.0*, U.S. Army Corps of Engineers, Hydrologic Engineering Center, Davis, CA.

[17] Tiffan, K.F., Garland, R.D. and Rondorf, D.W. (2006). "Predicting changes in subyearling Fall Chinook Salmon rearing and migratory habitat under two drawdown scenarios for John Day Reservoir, Columbia River." *North American Journal of Fisheries Management*, 26, 894-907.

Optimum resolution of the ADH model meshes were determined by trial simulations and previous experience with the ADH model that was developed for sediment transport analysis at the confluence. Trial ADH models were developed of the segment of Lower Granite Reservoir between RM 127.5 and RM 130.2. A steady flow of 200,000 cfs was simulated with models that had nominal mesh resolutions of 100 ft and 50 ft. Figure 145 shows that even the100 ft nominal mesh closely follows the shore line. Differences between the computed water surface, velocity and depth grids for the two meshes were minor and negligible in the lower model domain. Average simulated depths over the 2.7 mile reach were the same for both meshes and the standard deviation of the differences in depth between individual grid cells was 0.01 ft. Average velocity in the test reach only differed by 0.01 ft/s and the standard deviation of the differences between grid cells was 0.17 ft/s. Differences were minor because the ADH model refines the mesh to control inaccuracies in the simulation. Simulation results should be comparable when changes in channel topography are gradual so that meshes of different resolutions essentially represent the same bed geometry.

Differences in runtimes between the models were significant; simulations with the 100 ft resolution mesh were completed about five times faster than for the 50 ft resolution mesh. Based on this test and prior experience, the 100 ft nominal resolution mesh was selected for the final simulations of the lower model domain (Figure 146). An ADH model with a near-shore mesh resolution of 50 ft represented the variability of the channel better near the confluence, so was selected for the final simulations of the upper model domain (Figure 147).

17.2.11. Discharge and Stage for the Depth and Velocity Analysis

Habitat characteristics were to be evaluated over the range of normal seasonal discharges. Steady flows selected for simulation included mean annual discharge, the median probability flow-duration (exceedance) discharges for 30-day, 7-day, 1-day, and a nominal seasonal peak discharge of 200,000 cfs. Volume-frequency (flow-duration exceedance) statistics for total daily average flow in Lower Granite Reservoir and the daily average flow in the Snake River upstream of the confluence were computed with HEC-SSP 2.0 software. Median probabilities were determined by graphical analysis because parametric relationships did not fit the regulated flow data. Discharges in the Clearwater were adjusted so that the flow-duration discharge on the Snake River occurred simultaneously with the corresponding flow-duration discharge in Lower Granite Reservoir. Discharges used in the ADH depth and velocity simulations are listed in Table 6. Steady flows were simulated by increasing the unsteady flow hydrograph from 0 to the desired discharge over a period of two hours, then holding the discharge constant for four to eight hours to allow time for the dynamic wave to

dampen. At the lower discharges, the dynamic wave persisted in the lower model domain because of the long reservoir length and the mild slope. Two levels of mesh adaption were allowed throughout the model domains during the simulation run.

A constant forebay elevation of 736.9 ft NAVD88 was specified for all simulations of the lower model domain. A forebay elevation of 736.9 closely approximates the actual forebay elevation during moderate and high flow discharge periods in water years 2010 and 2011 (Figure 148). Since steady flows were being simulated, tailwater elevations for the upper domain model were set to match the simulated water surface elevations from the lower domain model for similar discharges.

The hydraulic roughness throughout the ADH model domains were set based on the Manning's *n* values for the calibrated HEC-RAS model. Manning's n for the central part of the channel was set to 0.0225 for all simulations. Manning's *n* values of mesh elements at the channel banks and shoreline of islands were set to 0.040. Manning's *n* values of the cobble bed areas in the upper domain model were set to 0.032. Bridges were not simulated in the ADH model.

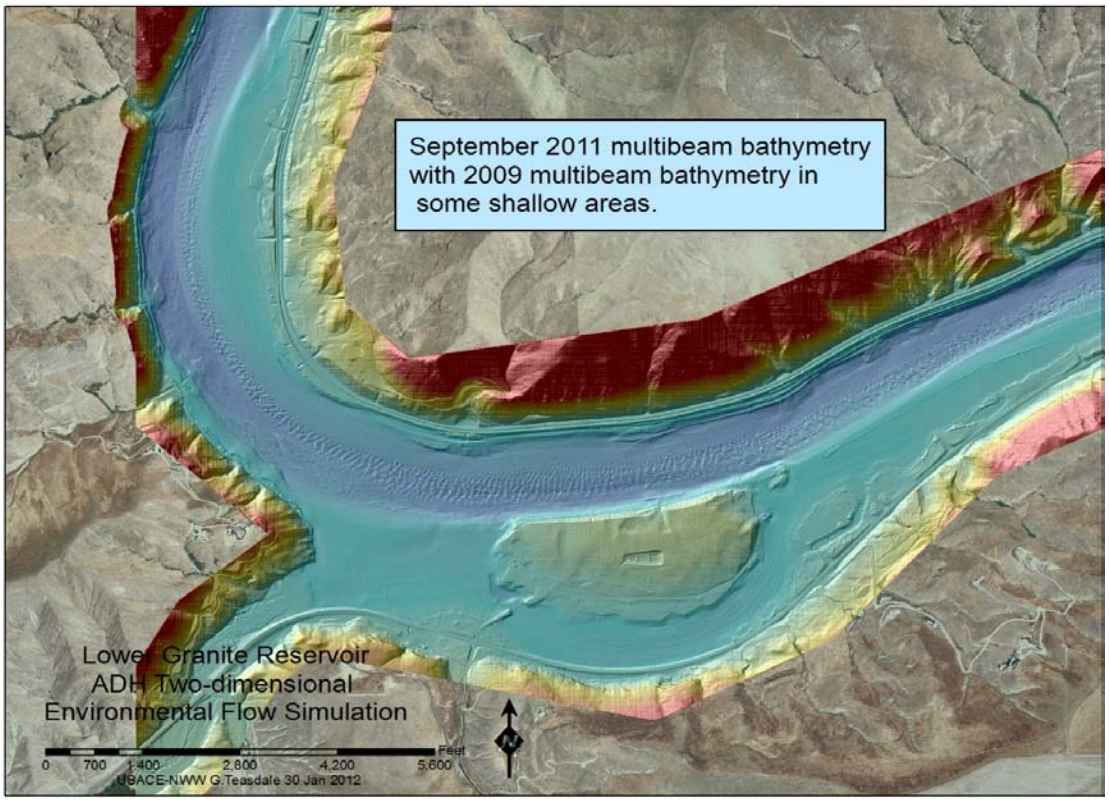


Figure 143. September 2011 bathymetry near Silcott Island.

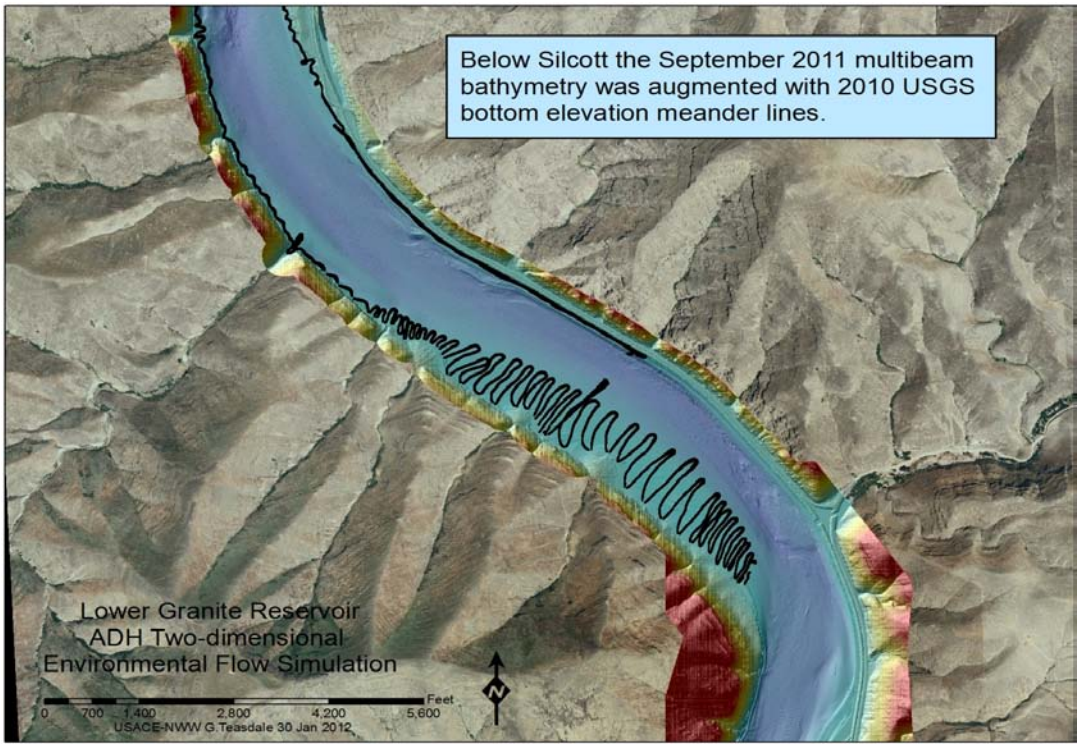


Figure 144. September 2011 bathymetry and USGS 2010 shallow water bed elevation lines.

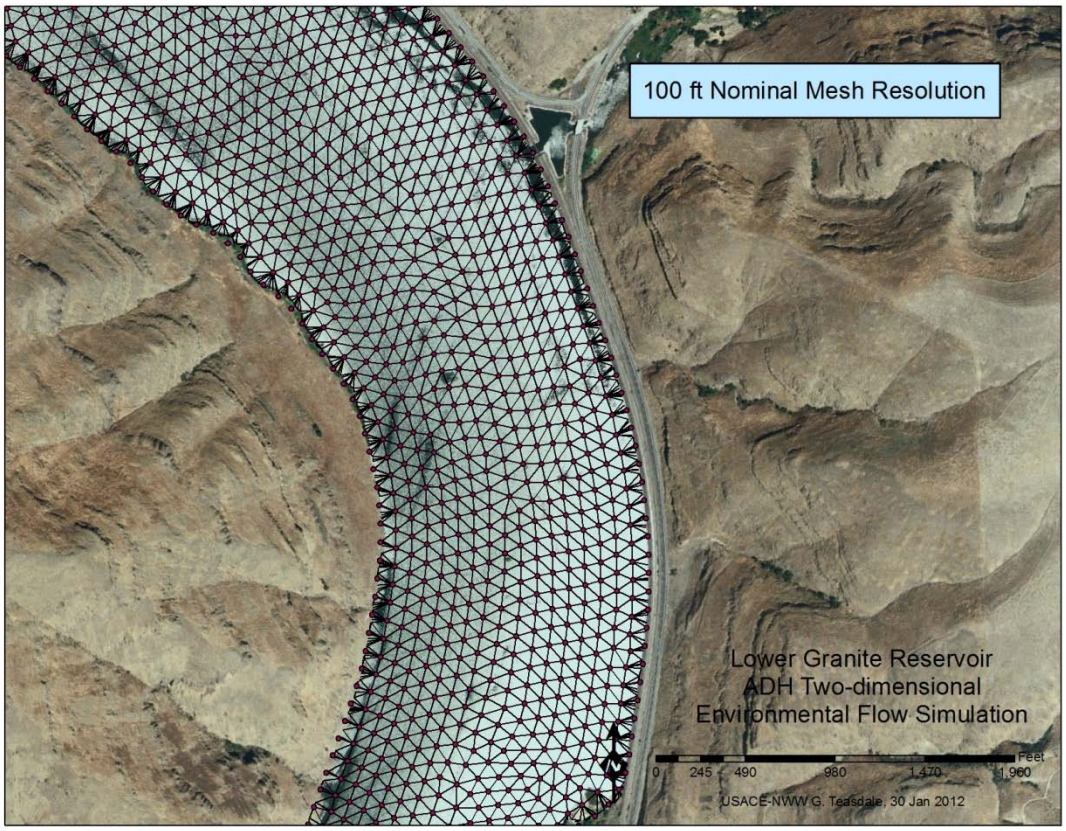


Figure 145. ADH 100 ft nominal mesh resolution.



Figure 146. ADH 2011 model mesh in Lower Granite Reservoir near Silcott Island.

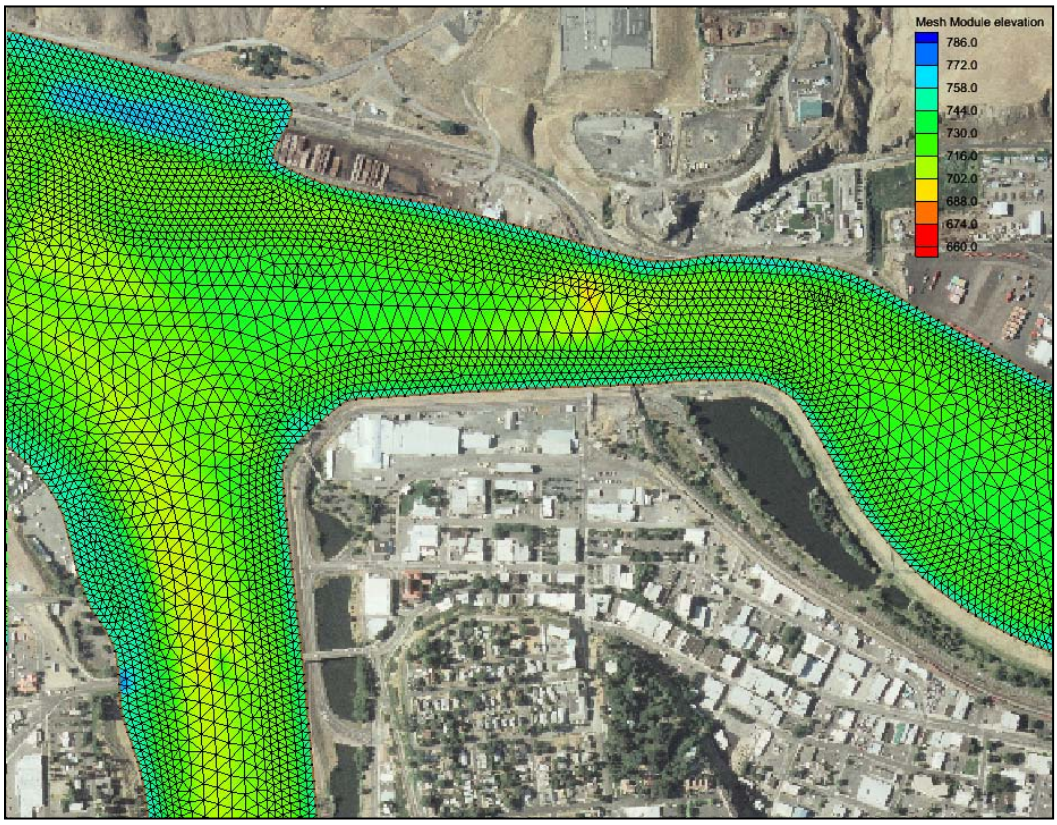


Figure 147. ADH 2011 model mesh at the confluence of the Snake and Clearwater Rivers.

Discharges for Lower Granite Reservoir Depth-Velocity Analysis					
	Discharge in cubic feet per second (cfs)				
	Nominal	Flow-Duration Discharge			Annual
Reach	Peak	1-day	7-day	30-day	Mean
Clearwater[1]	62,000	35,848	36,073	34,485	34,474
Snake	138,000	118,000	107,000	84,000	14,943
Lower Granite	200,000	153,848	143,073	118,485	49,417
[1] Clearwater River discharges are set to balance the flow-duration discharges for the Snake River and Lower Granite Reservoir.					

Table 6. Discharges for Lower Granite Reservor depth-velocity analysis.

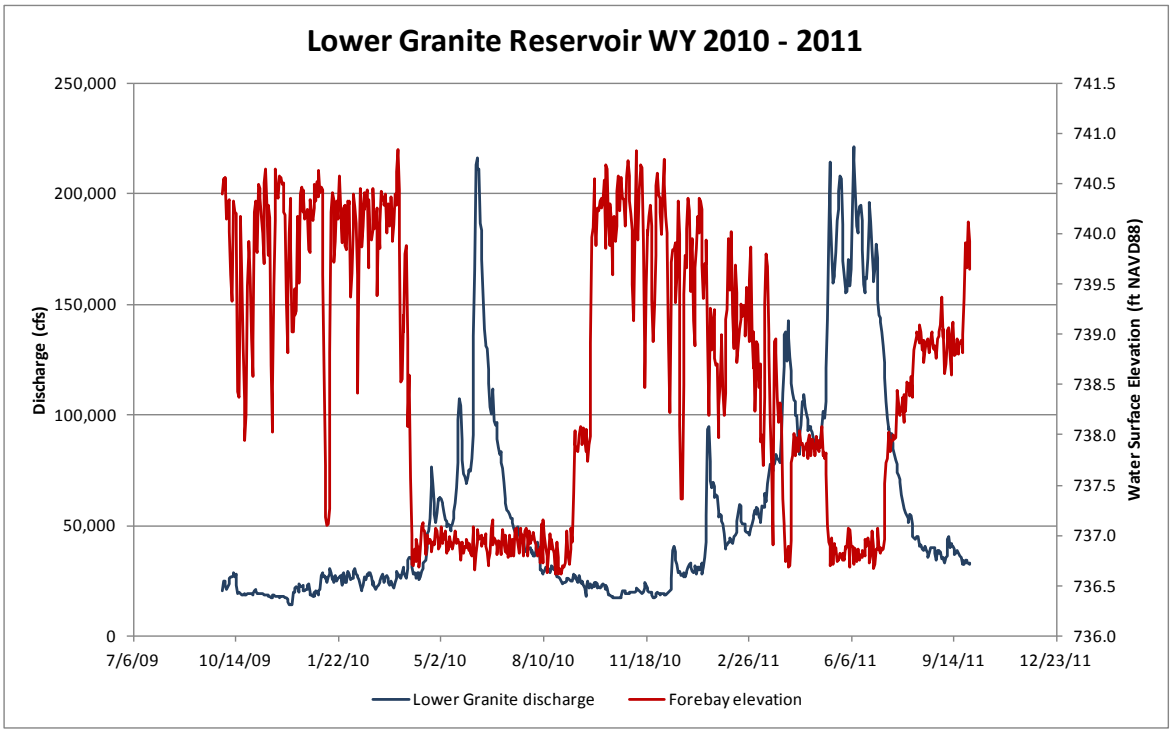


Figure 148. WY 2009-2011 stage and discharge hydrographs for Lower Granite Reservoir.

17.2.12. Model Calibration

At present there is insufficient water surface elevation and velocity data to fully calibrate two-dimensional models of Lower Granite Reservoir. The reasonableness of the ADH depth and velocity estimates for the environmental flow simulations were judged by comparison with the calibrated one-dimensional HEC-RAS model discussed above and with limited acoustic Doppler current profiler (ADCP) measurements obtained near the confluence in May 2011. The water surface profile from the ADH steady flow simulation of 200 kcfs in the lower model domain plotted in Figure 149 agree well with the HEC-RAS profile. The ADH water surface profile differs somewhat from the HEC-RAS one-dimensional profile because it was obtained from the center of the channel and because the dynamic wave caused by ramping of the discharge was not fully dampened. Water velocities computed by the ADH model plotted in Figure 150 also agree well with the average channel velocity computed by the HEC-RAS model. Velocities for the ADH profile were obtained from the center of the channel and should be higher than the average channel velocity.

In May 2011, the ERDC bathymetry survey crew obtained ADCP velocity transects near the confluence of the Snake and Clearwater Rivers. Velocities and depths of the three ADCP transects shown in Figure 151 were compared to ADH depths and velocities for similar steady flow discharges. Velocities from the ADH model of the upper domain at Snake RM 138.9 and Clearwater RM 0.2 are plotted in Figure 152 and Figure 153 and agree well with the ADCP velocities. Velocities at Snake RM 138.3 from the ADH model of the lower domain also agree reasonably well with ADCP velocities in Figure 154. Water depths simulated by the ADH model also agree well with the depths measured at the ADCP transects. Differences in the measured and simulated velocities could be reduced by adjusting the Manning's *n* values of the model and performing the calibration for a continuous unsteady flow hydrograph. These comparisons show that the ADH models provide reasonable estimates of depth averaged two-dimensional water depths and velocities for the characterization of shallow water habitat.

17.2.13. Depth and Velocity Grids

Depth and velocity grids were derived from the ADH simulations with a multistep process that includes:

1. Export the water surface elevations and velocities at the nodes of the model meshes for each of the desired discharges. The results are exported as georeferenced text (x,y,z) data.
2. Import the depth and velocity text data into ESRI Arcmap as georeferenced point data.

3. Produce Triangulated Irregular Networks (TIN) and ESRI grids for each of the depth and velocity point datasets. Specify a grid resolution of 10 ft during conversion from TINs to grids.
4. Produce 10 ft resolution water depth grids by subtracting the September 2011 bathymetry grid from the simulated water surface elevation grid.
5. Set to null all values in the depth grid less than 0. Negative depths are produced because the ADH model projects the water surface outside the wetted area of the model domain (to simulate groundwater).
6. Use the processed depth grid to mask the water velocity grid.
7. Merge the processed depth and velocity grids for both model domains for each of the desired flows to produce the final depth and velocity grids.

The final depth and velocity grids are a seamless data layer from Lower Granite Dam to upper boundary of the upper model domain. Minor velocity differences in the overlap areas between the lower and upper model domain were averaged by creating a patching TIN by combining the velocity points from both models. Depth and velocity grids near Snake RM 128 are shown in Figure 155 and Figure 156. A bed slope grid was also produced from the September 2011 bathymetry using ESRI Spatial Analyst.

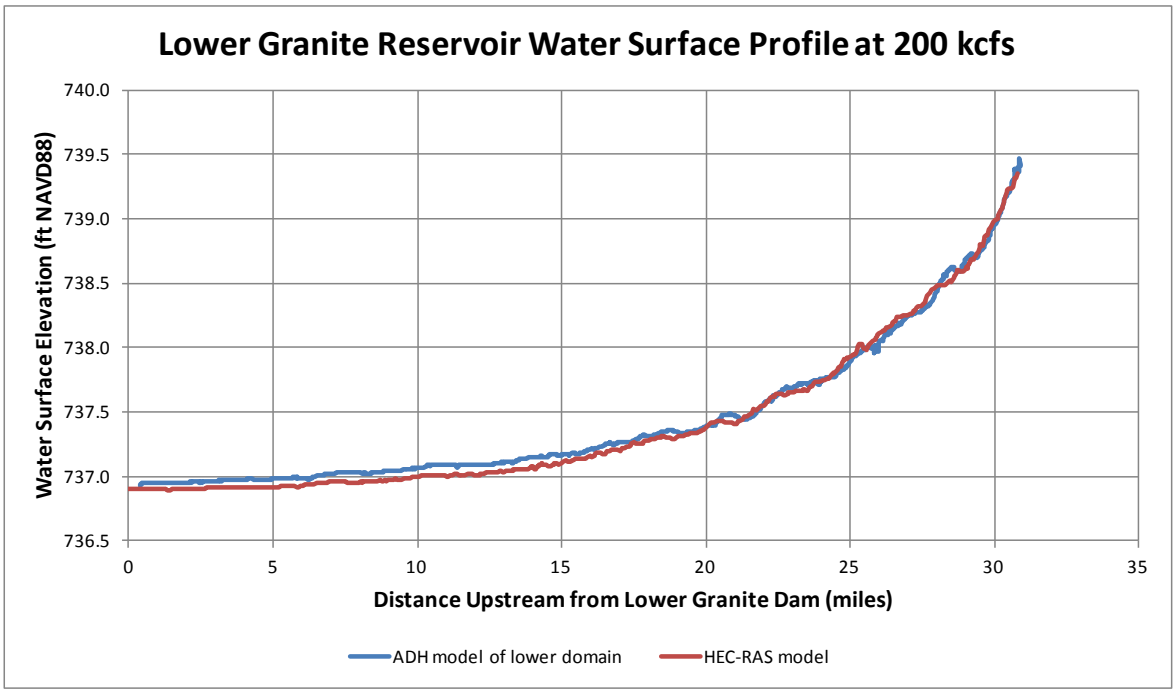


Figure 149. Comparison of ADH and HEC-RAS water surface profiles for Lower Granite Reservoir.

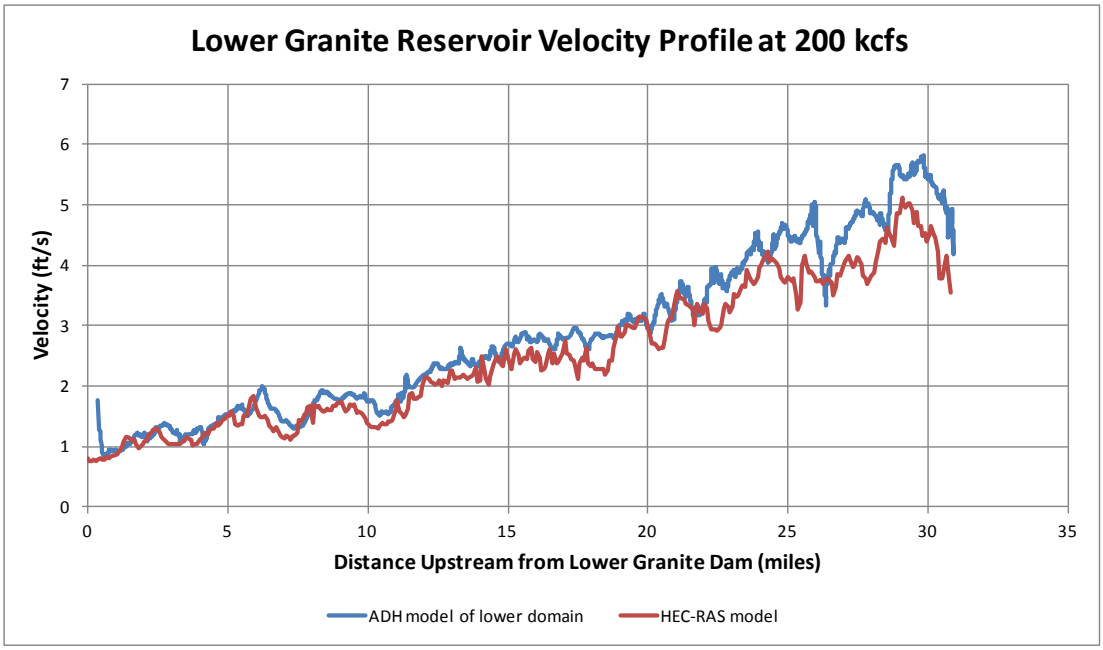


Figure 150. Comparison of ADH and HEC-RAS velocity profiles for Lower Granite Reservoir.

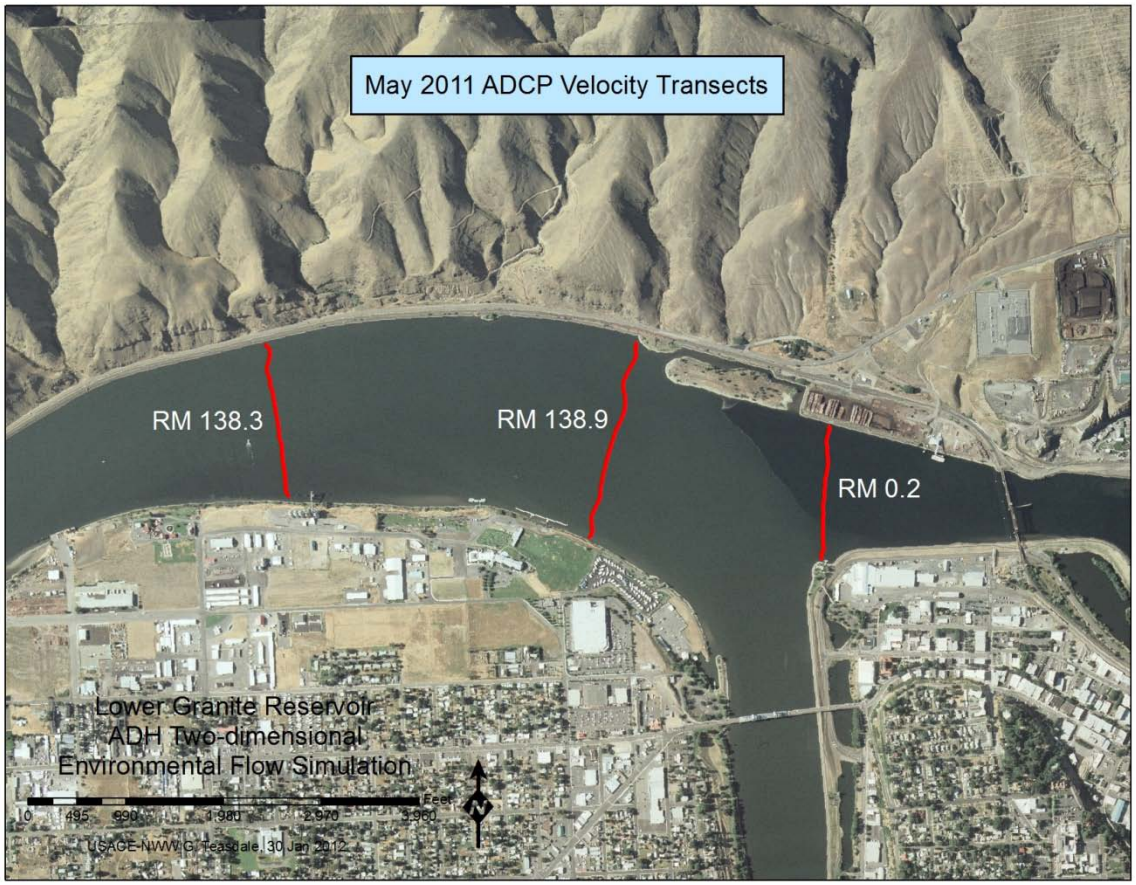


Figure 151. May 2011 ADCP transects at the confluence.

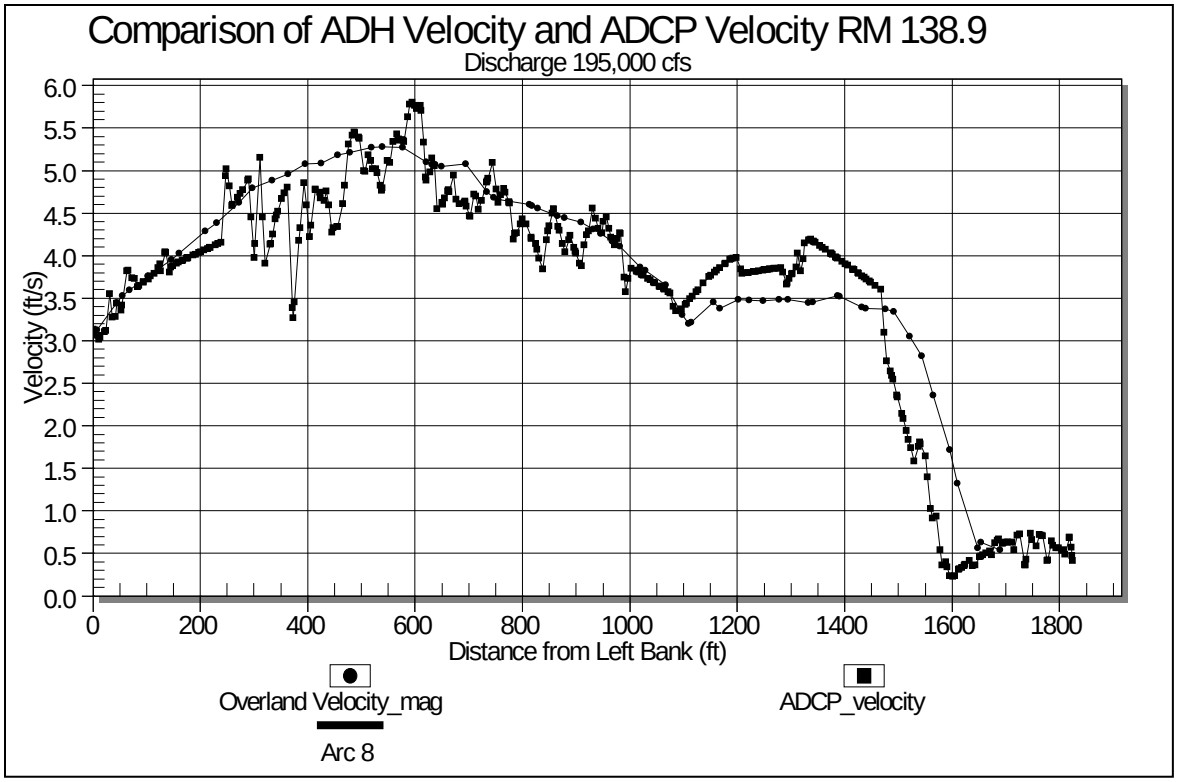


Figure 152. Comparison of ADH and ADCP velocities at Snake RM 138.9.

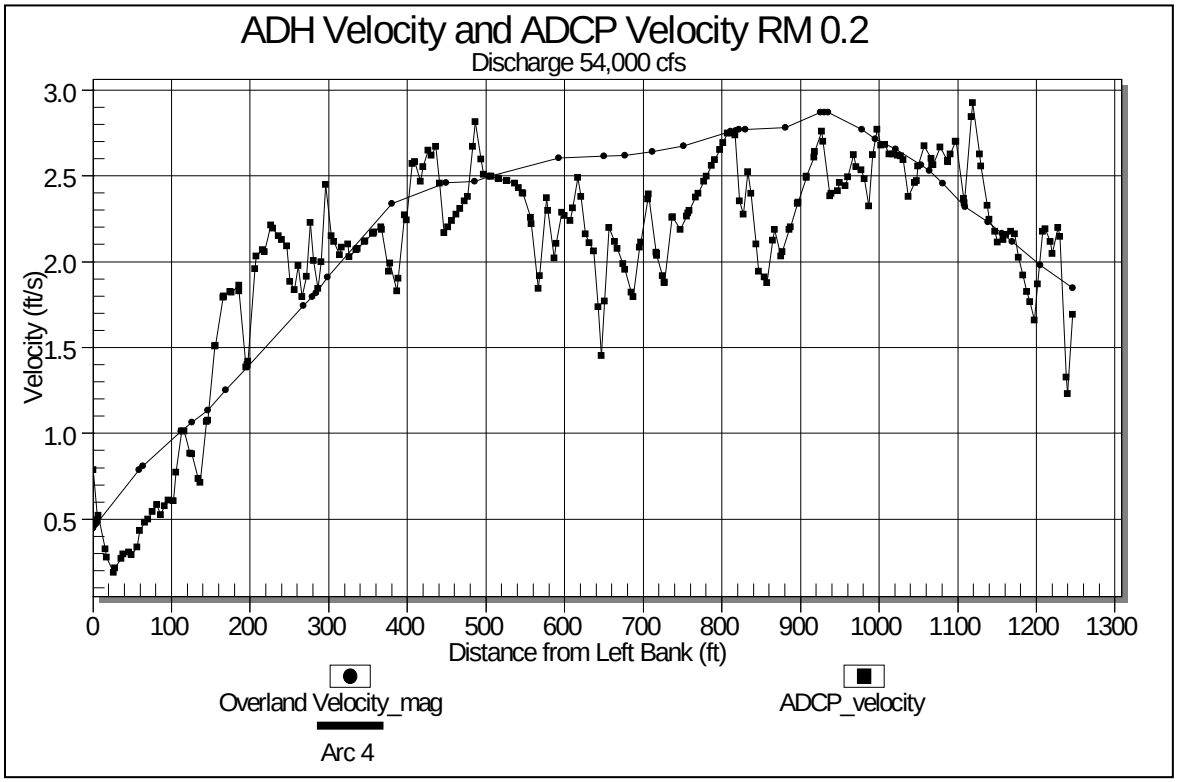


Figure 153. Comparison of ADH and ADCP velocities at Clearwater RM 0.2.

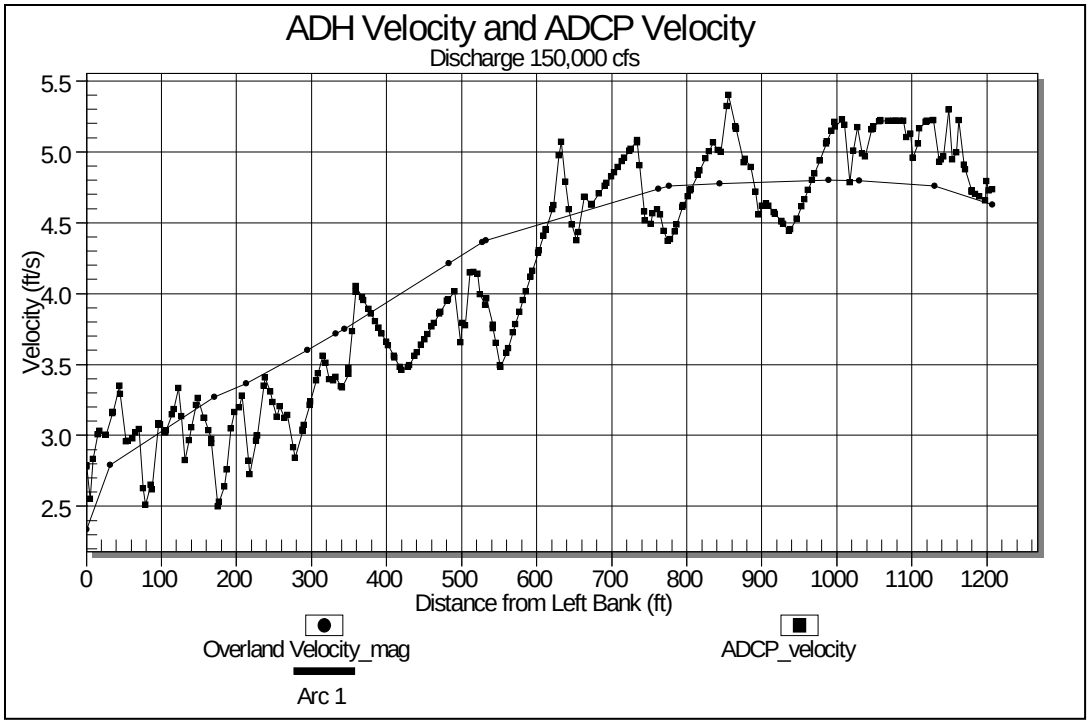


Figure 154. Comparison of ADH and ADCP velocities at Snake RM 138.3.

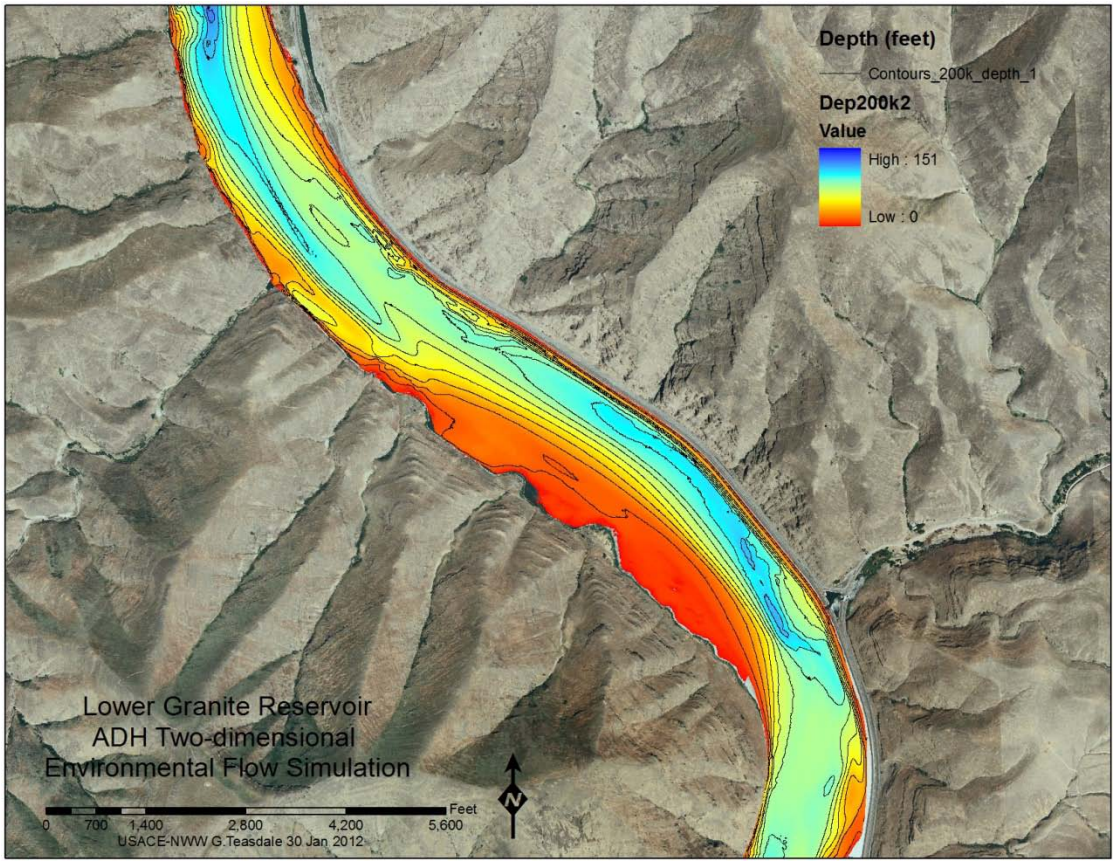


Figure 155. ADH depth grid for a discharge of 200 kcfs at Snake RM 128.

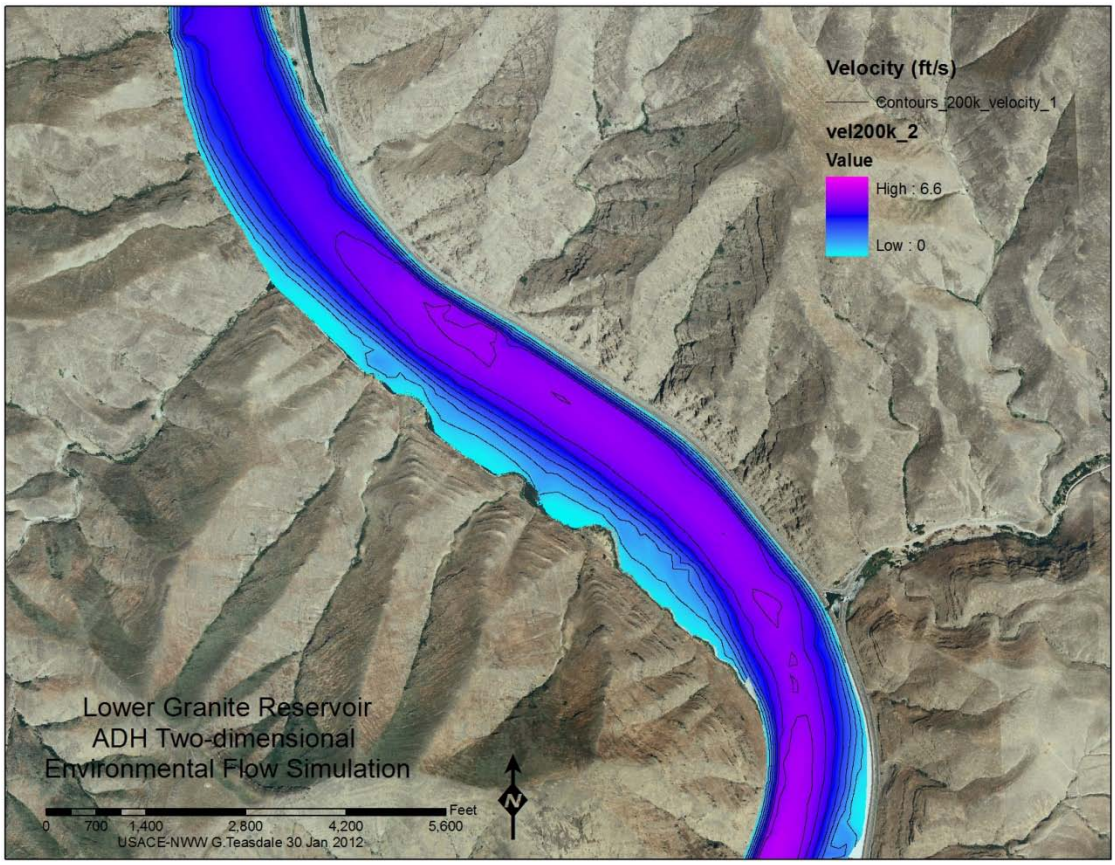


Figure 156. ADH velocity grid for a discharge of 200 kcfs at Snake RM 128.

18. Fire, Climate Variation and Sediment Yield

Sediment yield is the total sediment outflow from a watershed, measured at a cross section of reference and in a specified period of time[18]. Measurements of the volume of sediment that has accumulated in Lower Granite Reservoir since 1974 (Section 7) showed that the sediment yield of the Lower Granite sediment yield watershed averages 0.15 U.S. tons per acre per year (ton/ac/yr). In Section 9, the sediment yield at Lower Granite Reservoir was estimated at 0.19 ton/ac/yr with regression equations developed from sediment loads in the Snake and Clearwater Rivers measured from 2008 to 2011. The independent estimates agree very well. Both estimates were developed using credible methods and assumptions, so together the estimates show that the current sediment yield at Lower Granite Reservoir is known with good certainty.

Sediment yield varies substantially between years because of variation in meteorological and land surface conditions. Temporal variability of sediment yield is reflected in the differences of sediment accumulation rates in Section 7.5 and the variability of the sediment load data in Section 9. Sediment yield also varies substantially between subbasins as seen in the sediment mass balance summarized in Table 74 in Section 9.16 (included below as Table 7). Spatial variability is caused by differences in meteorological inputs, land cover and hydrologic condition.

Meteorology and land cover change with time. There is no assurance that average sediment yield rates at Lower Granite Reservoir and in the basin will remain constant through the 50-year analysis period of the PSMP. The analysis of trends in Section 9.16 suggests that sediment load in the Snake River may now be increasing. Characterization of sediment yield from forestland by USFS scientists for the PSMP-

[18] Piest, R.F. and Miller, C.R. (1975) "Sediment sources and sediment yields.", *Sedimentation Engineering, ASCE Manuals and Reports on Engineering Practice No. 54*, Ed. V.A. Vanoni, American Society of Civil Engineers, Reston, VA.

EIS[19,20] and other recent evaluations[21,22,23,24] indicate strong potential that sediment yield will increase because of more extensive and frequent wildfires perhaps promoted by a warming climate. The effect of wildfire on sediment yield in the Snake and Clearwater basins is evident[25]. Extensive and frequent wildfires expose the watershed to erosion by intense storms. Widespread wildfire followed by an extreme regional storm would drastically increase short-term sediment yield and disturb the drainage system. Cosmogenic analysis of sediment yield in the mountains of central Idaho by Kirchner et al. strongly suggests that such extreme events define the long-term sediment balance of the Lower Snake and Clearwater basins, and that current rates of sediment yield are less than long-term rates by an order of magnitude. Synchronous events of extensive wildfire and extreme storms are difficult to predict, and the erosion that would occur in the aftermath would be difficult, likely impossible, to control with current resources and technology. The relationships between climate, wildfire and sediment yield are therefore important to consider when planning a strategy to meet extreme sediment inflows and manage long-term sediment accumulation in Lower Granite Reservoir.

Descriptions of climate and the fire-affected landscape translate to estimates of sediment yield by means of a watershed hydrologic model. Sediment yield hydrologic models are complex, with many interdependent components that simulate hydrology, snowmelt and rainfall runoff, soil erosion, stream flow routing, groundwater interactions, and vegetation life cycles. While it is not realistic to expect precise quantification of the effect of climate variability and fire, first-order estimates of watershed sediment yield

[19] Goode, J.R., Luce, C. and Buffington, J.M. (2010) *Enhanced Sediment Delivery to large basins in a Changing Climate: Implications for management and habitat*.

[20] Elliot, W.J., Foltz, R.B. and Miller, S. (2010) *Upland Erosion Processes in Northern Idaho Forests*.

[21] Morgan, P., Heyerdahl, E.K., and Gibson, C.E. (2008). Multi-season Climate Synchronized Forest Fires Throughout the 20th Century, Northern Rockies, USA Ecology, 89(3), 717–728.

[22] Kirchner, J. W., R. C. Finkel, C. S. Riebe, D. E. Granger, J.L. Clayton, J. G. King and W. F. Megahan (2001) "Mountain erosion over 10 yr, 10 k.y., and 10 m.y. time scales." *Geology* 29(7): 591-594.

[23] Littell, J.S., Gwozdz, R. (2011) Climatic water balance and regional fire years in the Pacific Northwest, USA: linking regional climate and fire at landscape scales. In 'The Landscape Ecology of Fire, Ecological Studies 213'. (Eds D McKenzie, C Miller, DA Falk) pp. 117–139. (Springer ScienceþBusiness Media)

[24] Littell J.S., McKenzie D., Peterson D.L., Westerling A.L. (2009) "Climate and wildfire area burned in western US ecoprovinces.", 1916–2003. *Ecological Applications* 19, 1003–1021. doi:10.1890/07-1183.1

[25] See reports by the USFS in this EIS.

can be obtained with appropriately formulated hydrologic models[26,27], especially when calibrated with sediment load measurements at the scale of interest. Reasonably comprehensive datasets are now available that characterize the terrain, soil, hydrology, meteorology, climate, land cover, fire-affected area, and river channel system for a basin-scale sediment yield and routing model of the Lower Granite Reservoir watershed. The recent sediment load measurements in the tributary rivers in the lower Snake and Clearwater River provide the data to calibrate the sediment yield model at the scale of the major subbasins.

Total Suspended Sediment Mass Balance Water Years 2009-2011							
Source Watershed	Suspended Sediment tons	Watershed Area mi2	Sediment Yield ton/mi^2/yr	Sediment Yield ton/ac/yr	Percent of Spalding	Percent of Anatone	Percent of Lower Granite
Selway River	359,154	1,916	62.5	0.10	28.4%		3.6%
Lochsa River	132,258	1,178	37.4	0.06	10.5%		1.3%
Lower Middle Fork (computed)[1]	-58,786	313	-62.6	-0.10	-4.7%		-0.6%
S.F. Clearwater above Harpster	152,876	878	58.0	0.09	12.1%		1.5%
Lower S.F. Clearwater (computed)[2]	16,862	291	19.3	0.03	1.3%		0.2%
Above Orofino (computed)[3]	330,043	931	118.1	0.18	26.1%		3.3%
Potlatch River	285,316	594	160.2	0.25	22.6%		2.8%
Lower Clearwater (computed)[4]	44,940	738	20.3	0.03	3.6%		0.4%
Total at Spalding	1,262,662	6,839	61.5	0.10	100.0%		12.5%
Salmon River at Whitebird	5,406,912	13,424	134.3	0.21		61.1%	53.5%
Grande Ronde River at mouth	589,980	4,101	48.0	0.07		6.7%	5.8%
Lower Snake River (computed)[5]	2,851,571	2,108	451.0	0.70		32.2%	28.2%
Total at Anatone	8,848,463	19,633	150.2	0.23		100.0%	87.5%
Total at Lower Granite	10,111,125	27,137	124.2	0.19			100.0%

[1] Kooskia - (Selway + Lochsa)
[2] Stites - Harpster
[3] Orofino - (Kooskia + Stites)
[4] Spalding - (Orofino + Potlatch)
[5] Anatone - (Whitebird + Grande Ronde)
[6] Anatone + Spalding

Table 7. Mass balance and watershed sediment yield for Lower Granite Reservoir WY 2009-2011.

[26] Miller, M.E., MacDonald, L.H., Robichaud, P.R., Elliot, W.J. (2011) "Predicting post-fire hillslope erosion in forest lands of the western United States." *International Journal of Wildland Fire* 20, 982–999.

[27] Bacmort, K.S., Arabi, M., Frankenberger, J.R., Engle, B.A. and Arnold, J.G. (2006) "Modeling long-term water quality impact of structural BMPs.", *Trans. ASABE*, 49(2), 367-374.

18.1. Watershed Characterization for Sediment Yield Modeling

Physically-based sediment yield models require extensive and consistent spatially distributed data that characterize the terrain, land cover, soils, and hydrology at a level of detail that is appropriate for the scale of the model domain. The subbasin models discussed below were parameterized with the best data that is reasonably accessible to the public. Higher resolution and more current characterizations of hydrologic condition and soil erosion can be produced for extensive areas with current technology[28] , but development of new extensive datasets was beyond the time frame and budget of the PSMP-EIS. High resolution land cover data also quickly lose temporal accuracy unless updated frequently. The primary datasets used in development of the subbasin sediment yield models are briefly described below. It is expected that the land cover and fire data used in the analysis will be updated in routine work by the resource management agencies.

18.1.14. Digital Elevation Data

Subbasin catchments, drainage networks and terrain elevations were derived from the USGS 30-meter resolution National Elevation Dataset (NED)[29]. The 30-meter resolution NED was used instead of the higher resolution 10-meter NED because initial tests showed negligible differences in sediment yield estimates for the size of subbasins employed in this study. All NED data was obtained from the USGS Seamless Data Warehouse (now the National Map)[30].

18.1.15. Land Cover Data

Land cover datasets considered for subbasin characterization included the Multi-Resolution Land Characterization (MRLC) consortium 2001 and 2006 National Land Cover Datasets (NLCD)[31], the U.S. Department of Agriculture National Agricultural Statistics Service (NASS) Cropland Data Layer[32] and land cover data from the U.S.

[28] Teasdale, G.N. (2005) Satellite and Aerial Imaging in Characterization, Hydrologic Analysis and Modeling of Inland Watersheds and Streams, Ph.D. thesis, Department of Civil and Environmental Engineering, Washington State University, Pullman, WA.

[29] Gesch, D., Evans, G., Mauck, J., Hutchinson, J., Carswell Jr., W.J., 2009, The National Map—Elevation: U.S. Geological Survey Fact Sheet 2009-3053, 4 p. http://ned.usgs.gov/.

[30] http://seamless.usgs.gov/

[31] http://www.mrlc.gov/nlcd06_data.php

[32] http://www.nass.usda.gov/research/Cropland/SARS1a.htm

Department of Interior and USDA Forest Service Landfire[33] program. Landsat 5, Landsat 7 and MODIS satellite imagery was also examined to verify the occurrence and extent of recent wildfires. There is a strong interest and commitment by these agencies to monitor land cover change and update these datasets. Continuity of the Landsat program[34], assures that the necessary land cover information will be available to these agencies and other organizations for land cover assessment.

National Land Cover Dataset (NLCD)

The National Land Cover Dataset 2006 (NLCD2006) is a 16-class land cover classification scheme that has been applied consistently across the conterminous United States at a spatial resolution of 30 meters[35]. NLCD2006 is based primarily on the unsupervised classification of Landsat Enhanced Thematic Mapper+ (ETM+) imagery acquired around 2006. NLCD2006 also quantifies land cover change between the years 2001 to 2006. A formal accuracy assessment of the NLCD2006 land cover change product is planned for 2011. A previous version, NLCD2001, was developed from satellite imagery from the late 1990's[36] and had good accuracy at the scale of intended use.

The NLCD grids for 2001 and 2006 for the Lower Granite Reservoir sediment yield watershed are shown in Figure 157 and Figure 158. Land cover percentages in NLCD2006 by Hydrologic Unit Code level 8 basins are given in Table 8. Forestland is the most extensive land cover type (55%) followed by shrubland (21%) and grassland (16%). Cultivated crops are the fourth largest type at 5 percent of the total area. Relative proportions of land cover types have changed somewhat from 2001 to 2006, notably in the Salmon River basin. Overall, there is a gain of about 260 sq. mi. of shrubland and a loss of about 220 sq. mi. of forestland (Table 9). Some change can attributed to better classification methods, but some change can be correlated to recent wildfire data.

[33] http://www.landfire.gov/

[34] http://ldcm.nasa.gov/index.html

[35] Fry, J., Xian, G., Jin, S., Dewitz, J., Homer, C., Yang, L., Barnes, C., Herold, N., and Wickham, J. (2011) "Completion of the 2006 National Land Cover Database for the Conterminous United States." *PE&RS*, Vol. 77(9):858-864.

[36] Wickham, J. D., S. V. Stehman, J. A. Fry, J. H. Smith, and C. G. Homer. (2010) "Thematic accuracy of the NLCD 2001 land cover for the conterminous United States." *Remote Sensing of Environment* 114 (6):1286-1296.

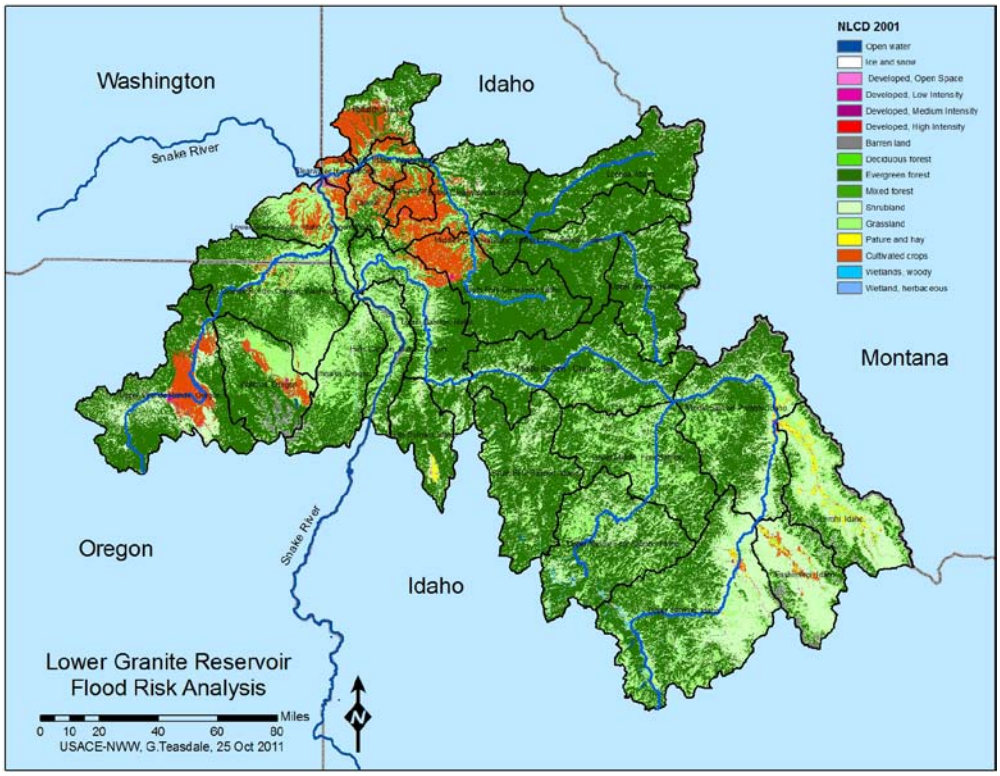


Figure 157. 2001 National Land Cover Dataset of the Lower Granite sediment yield watershed.

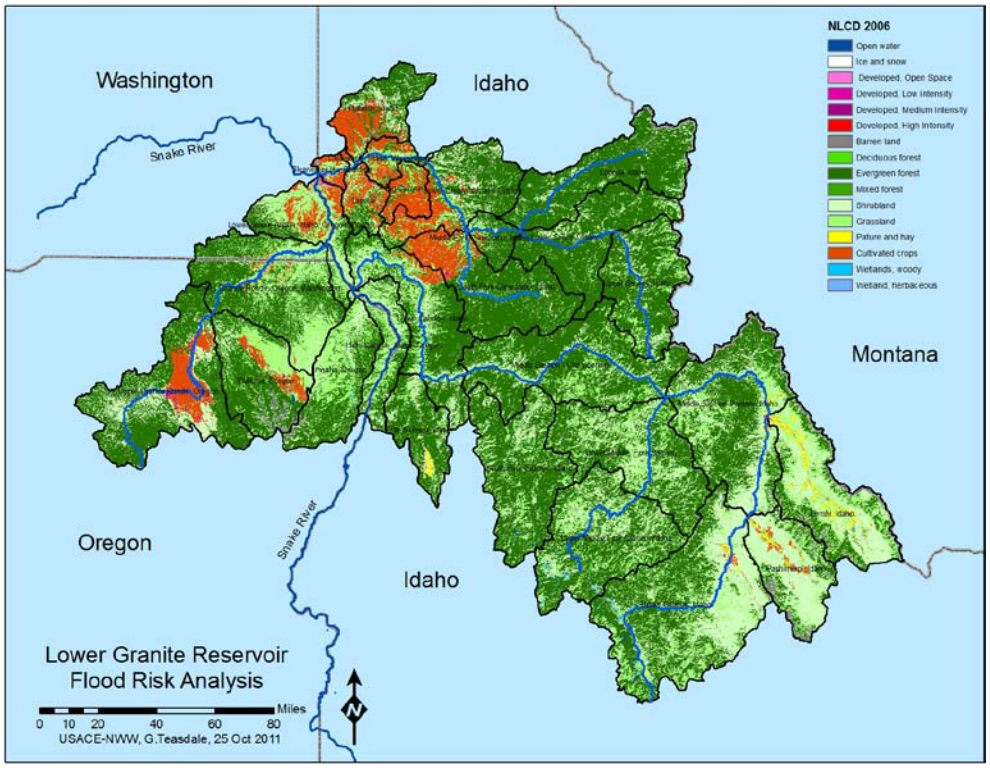


Figure 158. 2006 National Land Cover Dataset of the Lower Granite sediment yield watershed.

Lower Granite Reservoir Sediment Yield Watershed 2006 NLCD Summary																	
	Percent of Total Watershed Area by National Land Cover Database Class																
Watershed HUC 8	11 Open Water	12 Perennial Ice/Snow	21 Developed, Open Space	22 Developed, Low Intensity	23 Developed, Medium Intensity	24 Developed, High Intensity	31 Barren Land	41 Deciduous Forest	42 Evergreen Forest	43 Mixed Forest	52 Shrubland	71 Grassland - Herbaceous	81 Pasture - Hay	82 Cultivated Crops	90 Woody Wetlands	95 Emergent Herbaceous Wetlands	Total
Hells Canyon	0.6%	0.0%	0.0%	0.0%	0.0%	0.0%	0.1%	0.0%	39.4%	0.0%	24.4%	35.2%	0.1%	0.0%	0.1%	0.0%	100%
Imnaha	0.0%	0.0%	0.3%	0.0%	0.0%	0.0%	1.7%	0.0%	48.7%	0.0%	15.5%	33.3%	0.0%	0.1%	0.3%	0.0%	100%
Lower Snake-Asotin	0.8%	0.0%	2.4%	1.0%	0.2%	0.0%	0.0%	0.1%	22.3%	0.0%	16.8%	39.5%	0.0%	16.8%	0.0%	0.0%	100%
Upper Grande Ronde	0.1%	0.0%	1.1%	0.5%	0.1%	0.0%	0.0%	0.0%	59.2%	0.0%	21.8%	2.5%	0.1%	14.5%	0.0%	0.1%	100%
Wallowa. Oregon.	0.4%	0.0%	0.8%	0.2%	0.0%	0.0%	5.2%	0.0%	52.6%	0.0%	9.9%	22.8%	0.3%	7.7%	0.0%	0.0%	100%
Lower Grande Ronde	0.2%	0.0%	0.1%	0.0%	0.0%	0.0%	0.0%	0.0%	54.6%	0.0%	14.1%	29.1%	0.2%	1.7%	0.0%	0.0%	100%
Upper Salmon	0.4%	0.4%	0.2%	0.2%	0.1%	0.0%	0.8%	0.0%	42.6%	0.0%	34.2%	18.8%	1.0%	0.3%	0.4%	0.7%	100%
Pashimeroi	0.0%	0.0%	0.5%	0.3%	0.3%	0.0%	7.9%	0.0%	15.8%	0.0%	51.2%	18.3%	2.5%	3.0%	0.2%	0.0%	100%
Middle Salmon-Panther	0.1%	0.0%	0.3%	0.2%	0.1%	0.0%	0.4%	0.0%	54.7%	0.0%	27.2%	15.5%	1.0%	0.1%	0.2%	0.2%	100%
Lemhi	0.0%	0.0%	0.7%	0.3%	0.1%	0.0%	2.6%	0.0%	23.9%	0.0%	35.8%	30.2%	5.9%	0.1%	0.2%	0.2%	100%
Upper Middle Fork Salmon	0.1%	0.0%	0.0%	0.0%	0.0%	0.0%	0.1%	0.0%	58.1%	0.0%	24.4%	16.1%	0.0%	0.0%	0.5%	0.7%	100%
Lower Middle Fork Salmon	0.1%	0.0%	0.0%	0.0%	0.0%	0.0%	0.1%	0.0%	56.3%	0.0%	23.2%	20.1%	0.0%	0.0%	0.1%	0.0%	100%
Middle Salmon - Chamberlain	0.2%	0.0%	0.0%	0.0%	0.0%	0.0%	0.0%	0.0%	72.7%	0.0%	16.0%	11.1%	0.0%	0.0%	0.0%	0.0%	100%
South Fork Salmon	0.2%	0.0%	0.0%	0.0%	0.0%	0.0%	0.1%	0.1%	71.9%	0.0%	18.9%	8.4%	0.0%	0.0%	0.3%	0.1%	100%
Lower Salmon	0.4%	0.0%	0.4%	0.1%	0.0%	0.0%	0.0%	0.0%	54.0%	0.0%	20.2%	20.5%	0.2%	3.9%	0.1%	0.0%	100%
Little Salmon	0.3%	0.0%	0.6%	0.2%	0.0%	0.0%	0.3%	0.1%	68.9%	0.0%	17.7%	9.4%	2.2%	0.0%	0.1%	0.1%	100%
Upper Selway	0.1%	0.0%	0.0%	0.0%	0.0%	0.0%	0.1%	0.0%	74.1%	0.0%	15.4%	10.2%	0.0%	0.0%	0.0%	0.0%	100%
Lower Selway	0.1%	0.0%	0.0%	0.0%	0.0%	0.0%	0.0%	0.0%	85.3%	0.1%	11.9%	2.5%	0.0%	0.0%	0.0%	0.0%	100%
Lochsa	0.2%	0.0%	0.4%	0.1%	0.0%	0.0%	0.0%	0.0%	86.1%	0.2%	10.2%	2.7%	0.0%	0.0%	0.1%	0.1%	100%
Middle Fork Clearwater	0.6%	0.0%	0.9%	0.1%	0.0%	0.0%	0.0%	0.4%	73.4%	0.2%	12.7%	7.1%	0.0%	4.5%	0.1%	0.1%	100%
South Fork Clearwater	0.0%	0.0%	0.8%	0.1%	0.0%	0.0%	0.0%	0.0%	70.2%	0.0%	6.4%	5.7%	0.1%	16.5%	0.1%	0.1%	100%
Potlatch	0.0%	0.0%	1.8%	0.3%	0.0%	0.0%	0.0%	0.3%	47.5%	0.0%	18.0%	3.2%	0.0%	28.1%	0.4%	0.3%	100%
Lower Clearwater abv Orofino	0.2%	0.0%	1.4%	0.3%	0.0%	0.0%	0.0%	0.0%	52.2%	0.0%	18.7%	9.1%	0.0%	17.6%	0.2%	0.2%	100%
Big Canyon	0.0%	0.0%	2.8%	0.1%	0.0%	0.0%	0.0%	0.0%	12.7%	0.0%	1.2%	17.4%	0.0%	65.7%	0.0%	0.0%	100%
Lapwai	0.1%	0.0%	4.3%	0.2%	0.0%	0.0%	0.0%	0.6%	27.8%	0.2%	5.9%	23.5%	0.0%	36.9%	0.2%	0.2%	100%
Clearwater blw Spalding	1.8%	0.0%	5.5%	3.6%	2.2%	0.3%	0.0%	0.2%	1.4%	0.0%	7.7%	27.3%	0.5%	49.3%	0.1%	0.1%	100%
Clearwater	0.8%	0.0%	4.0%	0.3%	0.1%	0.0%	0.0%	1.8%	20.6%	0.2%	8.1%	24.5%	0.0%	39.3%	0.1%	0.2%	100%
Class Total	0.2%	0.0%	0.6%	0.2%	0.1%	0.0%	0.7%	0.0%	55.0%	0.0%	20.7%	16.1%	0.6%	5.4%	0.2%	0.2%	100%

Table 8. Land cover types and proportional areas in the Lower Granite sediment yield watershed.

Lower Granite Reservoir Sediment Yield Watershed 2006 NLCD Summary																	
	Area Change in Square Miles from NLCD 2001 to NLCD 2006 by National Land Cover Database Class																
Watershed HUC 8	11 Open Water	12 Perennial Ice/Snow	21 Developed, Open Space	22 Developed, Low Intensity	23 Developed, Medium Intensity	24 Developed, High Intensity	31 Barren Land	41 Deciduous Forest	42 Evergreen Forest	43 Mixed Forest	52 Shrubland	71 Grassland - Herbaceous	81 Pasture - Hay	82 Cultivated Crops	90 Woody Wetlands	95 Emergent Herbaceous Wetlands	Total
Hells Canyon	0.0	-0.1	0.0	0.0	0.0	0.0	0.0	0.0	-16.9	0.0	-4.4	21.3	0.0	0.0	0.0	0.0	0
Imnaha	0.0	0.0	0.0	0.0	0.0	0.0	0.0	0.0	-1.7	0.0	1.5	0.1	0.0	0.1	-0.2	0.0	0
Lower Snake-Asotin	0.0	0.0	0.1	0.0	0.0	0.0	0.0	0.0	-0.2	0.0	0.0	-0.4	0.0	0.4	0.0	0.0	0
Upper Grande Ronde	0.0	0.0	0.0	0.0	0.0	0.0	0.0	0.0	-7.8	0.0	1.7	4.7	0.0	0.7	0.1	0.6	0
Wallowa. Oregon.	0.0	0.0	0.0	0.0	0.0	0.0	0.0	0.0	-4.4	0.0	-0.3	3.9	0.0	0.9	0.0	-0.1	0
Lower Grande Ronde	0.0	0.0	0.0	0.0	0.0	0.0	-0.2	0.0	-8.4	0.0	-0.3	8.2	0.0	0.8	0.0	0.0	0
Upper Salmon	0.0	-2.1	0.0	0.0	0.0	0.0	0.9	0.0	-7.1	0.0	8.9	0.1	-0.6	-0.4	0.1	0.2	0
Pashimeroi	0.0	0.0	0.0	0.0	0.0	0.0	0.4	0.0	-1.6	0.0	0.7	-0.1	0.3	-0.2	0.2	0.3	0
Middle Salmon-Panther	-0.1	0.0	0.0	0.0	0.0	0.0	0.1	0.0	-27.7	0.0	63.1	-35.2	-0.4	0.0	0.1	0.1	0
Lemhi	0.0	0.0	0.0	0.0	0.0	0.0	0.1	0.0	-5.1	0.3	4.2	-1.4	-0.7	-0.1	0.6	2.1	0
Upper Middle Fork Salmon	0.0	-0.4	0.0	0.0	0.0	0.0	0.1	0.0	-14.3	0.0	36.2	-21.6	0.0	0.0	0.0	0.0	0
Lower Middle Fork Salmon	0.0	-0.3	0.0	0.0	0.0	0.0	0.2	0.0	-31.7	0.0	74.1	-42.3	0.0	0.0	0.0	0.0	0
Middle Salmon - Chamberlain	-0.4	-0.1	0.0	0.0	0.0	0.0	0.0	0.0	-21.0	0.0	18.2	3.2	0.0	0.0	0.0	0.0	0
South Fork Salmon	0.0	-0.1	0.0	0.0	0.0	0.0	0.1	0.0	-13.1	0.0	12.9	0.2	0.0	0.0	0.0	0.1	0
Lower Salmon	0.0	0.0	0.0	0.0	0.0	0.0	0.0	0.0	-5.1	0.0	0.8	4.3	-0.1	0.1	0.0	0.1	0
Little Salmon	0.0	-0.1	0.0	0.0	0.0	0.0	0.0	0.0	-2.4	0.0	1.7	0.1	0.6	0.0	0.0	0.0	0
Upper Selway	0.0	-0.2	0.0	0.0	0.0	0.0	0.0	0.0	-15.7	0.0	5.0	10.8	0.0	0.0	0.0	0.0	0
Lower Selway	-0.1	-0.1	0.0	0.0	0.0	0.0	0.0	0.0	-4.1	-0.1	4.1	0.2	0.0	0.0	0.0	0.0	0
Lochsa	0.0	-0.1	0.0	0.0	0.0	0.0	0.0	0.0	-8.9	0.0	6.5	2.5	0.0	0.0	0.0	0.0	0
Middle Fork Clearwater	-0.1	0.0	0.0	0.0	0.0	0.0	0.0	0.0	-1.8	0.0	1.9	-0.2	0.0	0.3	0.0	0.0	0
South Fork Clearwater	0.0	0.0	0.0	0.0	0.0	0.0	0.0	0.0	-7.2	0.0	2.5	4.5	0.0	0.2	0.0	0.0	0
Potlatch	0.0	0.0	0.0	0.0	0.0	0.0	0.0	-0.1	-7.9	0.0	10.2	-0.3	0.0	-1.8	-0.1	0.0	0
Lower Clearwater abv Orofino	0.0	0.0	0.0	0.0	0.0	0.0	0.0	0.1	-11.4	0.0	9.9	1.2	0.0	0.3	0.0	0.1	0
Big Canyon	0.0	0.0	0.0	0.0	0.0	0.0	0.0	0.0	-0.1	0.0	0.0	-0.3	0.0	0.3	0.0	0.0	0
Lapwai	0.0	0.0	0.0	0.0	0.0	0.0	0.0	0.0	-0.7	0.0	-0.1	0.6	0.0	0.3	0.0	0.0	0
Clearwater blw Spalding	0.0	0.0	0.0	0.0	0.0	0.0	0.0	0.0	0.0	0.0	0.0	0.0	0.0	0.0	0.0	0.0	0
Clearwater	0.0	0.0	0.0	0.0	0.0	0.0	0.0	-0.1	-0.3	0.0	1.4	-0.6	0.0	-0.3	0.0	0.0	0
Class Total	-0.9	-3.5	0.2	0.1	0.0	0.0	1.7	-0.1	-226.6	0.2	260.4	-36.4	-1.0	1.4	0.9	3.4	0

Table 9. Change between NLCD 2001 and NLCD 2006.

NASS Cropland Data Layer

The NASS Cropland Data Layer (CDL) is a raster-based, geo-referenced, crop-specific land cover data layer[37]. The CDL has a ground resolution of 30 meters. The CDL is produced from satellite imagery acquired by Landsat 5, Landsat 7, and the

[37] http://www.nass.usda.gov/research/Cropland/metadata

Indian Remote Sensing RESOURCESAT-1 (IRS-P6) during the growing season. The CDL is updated annually. Some states use additional satellite imagery and ancillary inputs to supplement and improve the classification. Agricultural training and validation data are derived from the Farm Service Agency (FSA) Common Land Unit (CLU) Program. The NLCD 2001 is used as non-agricultural training and validation data. User accuracies of the crop classifications for the major cultivated crops in the lower Snake and Clearwater River basins are typically 80 percent and higher.

The NASS cropland data is more detailed than the cultivated land classes in the NLCD. While the total area of cultivated land in the Potlatch River basin is about the same for the NLCD and NASS CDL in Figure 159 and Figure 160, the NASS-CDL is much more refined and the annual grids show the change in specific crop types. The NASS-CDL was used to define land cover types in the agricultural areas of the sediment yield models.

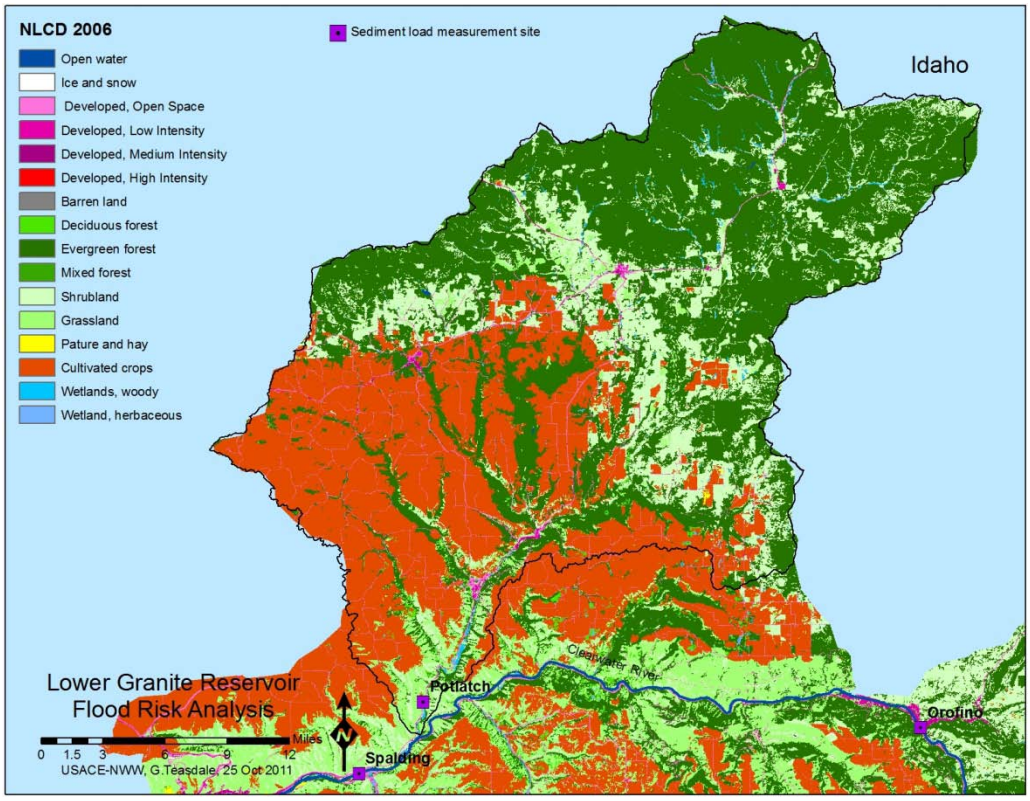


Figure 159. 2006 NLCD grid for the Potlatch River basin.

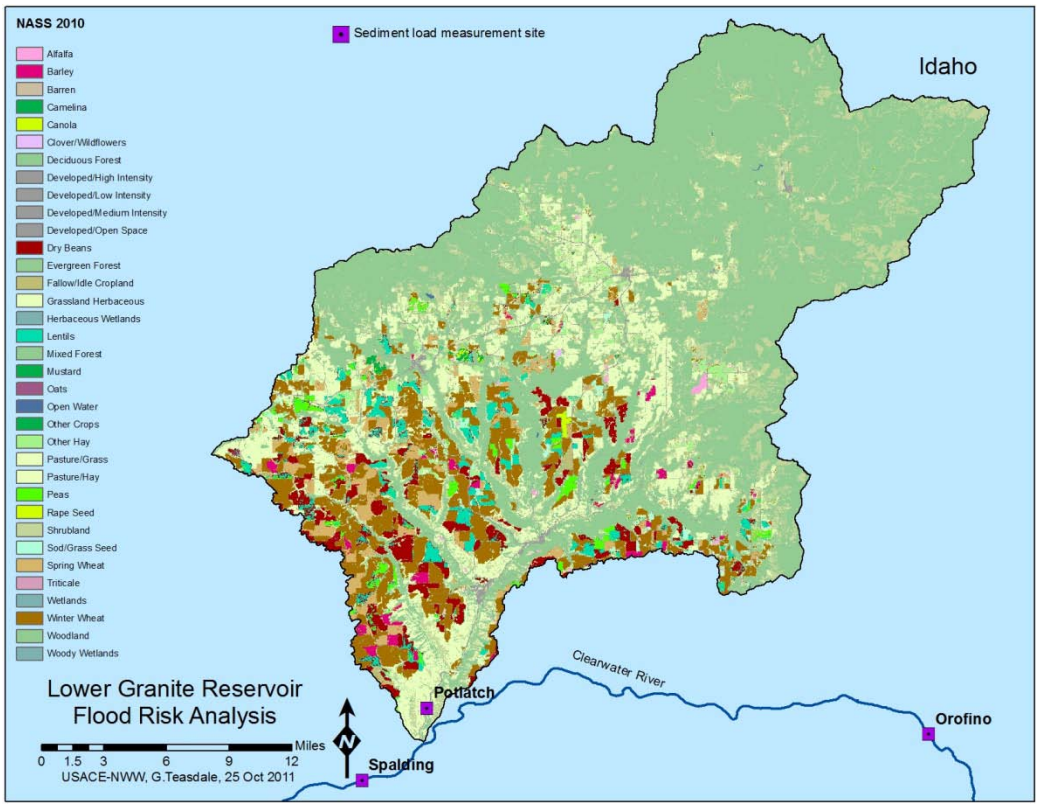


Figure 160. NASS 2010 crop data layer for the Potlatch River basin.

Landfire Land Cover and Fire Regime Data

Several land cover datasets are produced by the U.S. Department of Agriculture Forest Service and U.S. Department of the Interior Landfire program including the Existing Vegetation Type (EVT), Existing Vegetation Cover (EVC), and multiple classifications related to fire regime[38]. The objective of the Landfire Prototype Project was to produce comprehensive digital data layers of current vegetation composition and structure, wildland fuel, historical fire regimes, and fire regime condition class (FRCC) across the United States at a 30-meter spatial resolution[39]. The Landfire project was performed in two large study areas: the highlands of central Utah and the second in the northern Rocky Mountains of Idaho and Montana.

The Existing Vegetation Type (EVT) layer represents species composition of the land cover. Vegetation map units are primarily derived from NatureServe's Ecological

[38] Metadata for Landfire products.

[39] Rollins, Matthew G.; Frame, Christine K., tech. eds. 2006. *The LANDFIRE Prototype Project: nationally consistent and locally relevant geospatial data for wildland fire management*. Gen. Tech. Rep. RMRS-GTR-175. Fort Collins: U.S. Department of Agriculture, Forest Service, Rocky Mountain Research Station. 416 p.

Systems classification, which is a nationally consistent set of mid-scale ecological units. Additional units are derived from NLCD, National Vegetation Classification Standard (NVCS) Alliances, and LANDFIRE specific types. EVTs are mapped using decision tree models, field data, Landsat imagery, elevation, and biophysical gradient data. The EVT data provides very detailed land cover types in areas that are dominated by forestland and rangeland. Figure 161 shows the EVT layer in the vicinity of the Selway River basin. Agricultural classifications in the EVT are adopted from the NASS-CDL. The last update of the EVT was in 2008. It is uncertain if future updates are planned.

The Existing Vegetation Cover (EVC) layer represents the vertically projected percent cover of the live canopy layer for a 30-m grid cell. EVC is generated separately for tree, shrub and herbaceous cover lifeforms using training data and other supporting data. Percentage tree, shrub, and herbaceous canopy cover training data are generated using plot-level ground-based visual assessments. Once the training data are developed, relationships are established separately for each lifeform between the training data and combination of Landsat, elevation, and ancillary data. Each of the derived data layers (tree, shrub, herbaceous) has a potential range from 0-100 percent which are merged into a single composite EVC layer. Figure 162 shows the EVC grid for the Salmon River basin.

The Fire Regime Groups (FRG) were intended to characterize the presumed historical fire regimes within landscapes based on interactions between vegetation dynamics, fire spread, fire effects, and spatial context. The Mean Fire Return Interval (MFRI) layer quantifies the average period between fires under the presumed historical fire regime.

In general, the Landfire land cover classifications are more detailed than necessary for the hydrologic modeling of first-order sediment yield at the scale of the subbasins in this study. There is insufficient regional data to discriminate the differences in hydrologic response between the diverse vegetation types in the EVT classification. Considerable research level work would be necessary to correlate Landfire vegetation classifications with hydrologic parameters. In this initial work the Landfire data was used to confirm the more general land cover types of the 2006 NLCD and to gain a better appreciation of the role of fire in the hydrologic and sediment regimes of the basin.

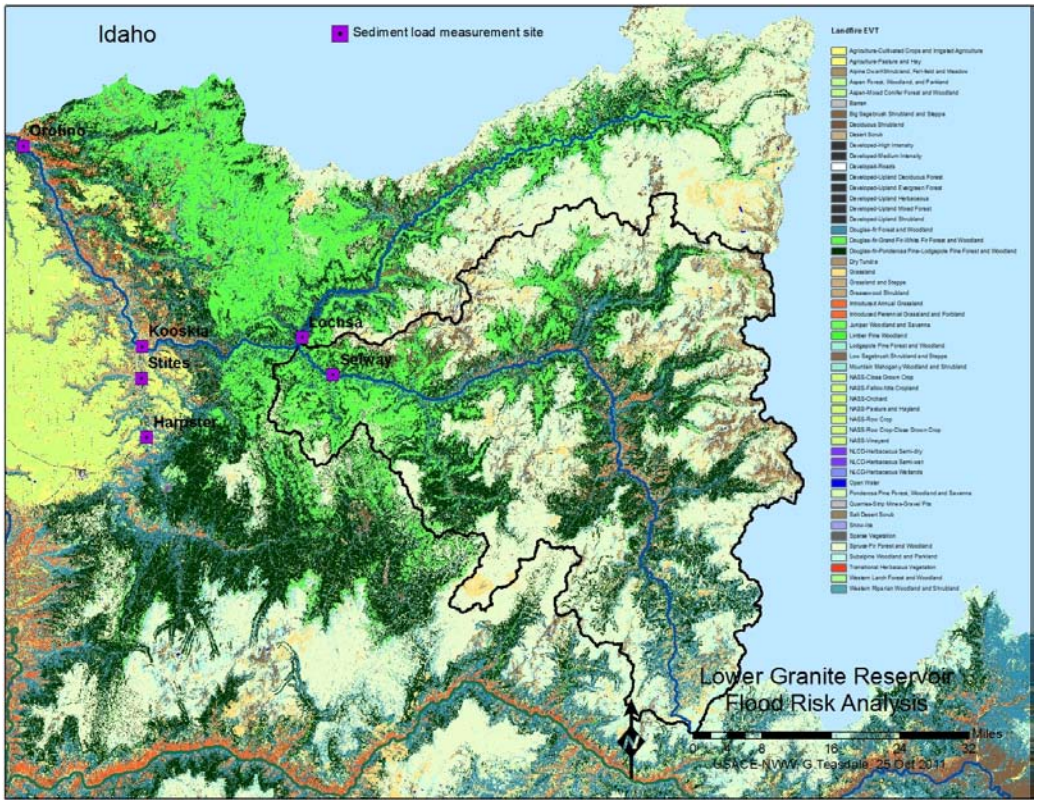


Figure 161. Landfire Existing Vegetation Type (EVT) grid for the Selway River basin.

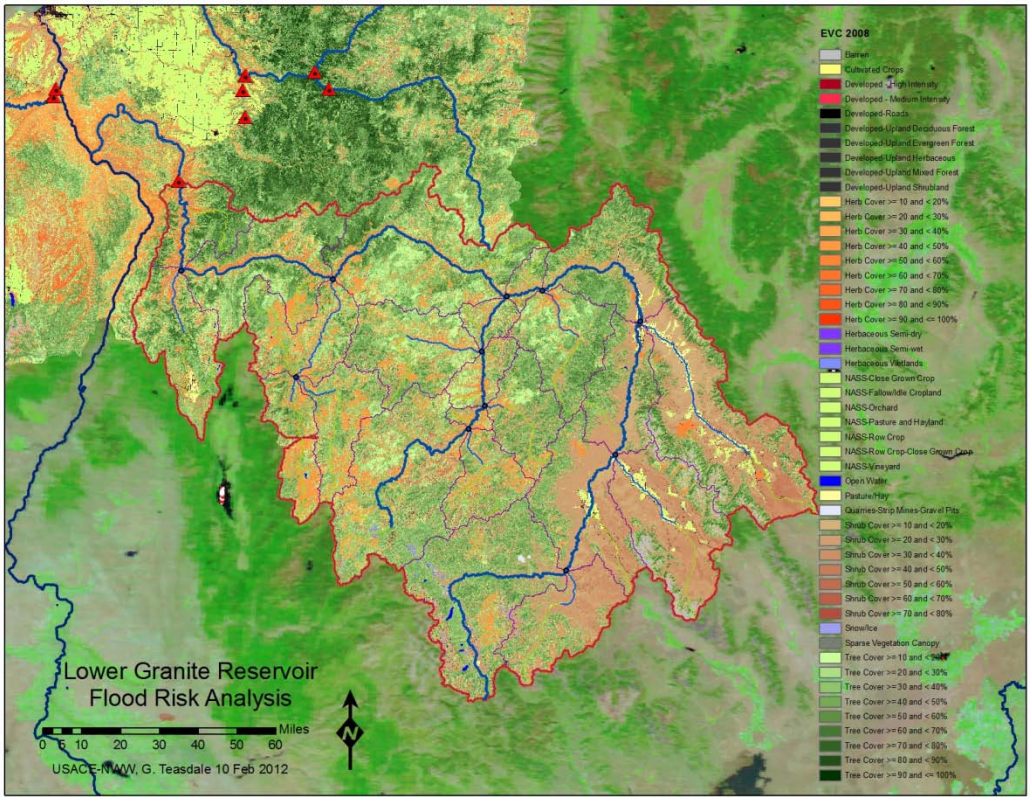


Figure 162. Landfire Existing Vegetation Cover (EVC) grid for the Salmon River basin.

Satellite Imagery

Georeferenced multi-band images from Landsat satellites[40] for late summer and fall 2011 were obtained from the USGS Global Visualization View archive[41]. Daily MODIS (Moderate Resolution Imaging Spectroradiometer) imagery[42] is available from the USFS Remote Sensing Applications Center[43]. Visible and near-infrared bands were composited to produce a nearly cloud-free coverage of the Lower Granite sediment yield watershed. The burn areas (scars) of recent wildfire areas are identified in the September 2011 imagery in Figure 163. Active fires in the Salmon and Selway River basins are visible in the 3 September 2011 MODIS imagery in Figure 164. Burn areas derived from satellite imagery can be compared to fire data layers produced by the fire management agencies discussed below. In future work, burn severity may be evaluated in the images and considered along with hydrologic conditions parameters to define the potential for erosion and sediment delivery. Recover of burn areas could be monitored in a time sequence of Landsat images and possibly correlated with sediment load and accumulation. Other space-borne imagers could aid in the study the hydrologic condition of the lower Snake and Clearwater River basins[28].

18.1.16. Surface Soils Data

Surface soil parameters were derived from the USDA U.S. General Soil Map (STATSGO2) formerly known as the State Soil Geographic Database and the Soil Survey Geographic (SSURGO) database[44]. Some high resolution soil classifications were available from the USFS, but the extent of coverage was so limited that it could not be used efficiently in the subbasin models.

The U.S. General Soil Map consists of general soil association units. It was developed by the National Cooperative Soil Survey and supersedes the State Soil Geographic (STATSGO) dataset published in 1994. It consists of a broad-based inventory of soils and non-soil areas that can be cartographically shown at the scale mapped. The dataset was created by generalizing more detailed soil survey maps. Where more detailed soil survey maps were not available, the probable classification and extent of soil type was determined based on geology, topography, vegetation, and climate, and Landsat images.

[40] http://landsat.gsfc.nasa.gov/

[41] http://glovis.usgs.gov/

[42] http://modis.gsfc.nasa.gov/

[43] http://activefiremaps.fs.fed.us/imagery.php

[44] Soil survey data is online at http://soildatamart.nrcs.usda.gov/.

The Soil Survey Geographic (SSURGO) database was developed with field mapping methods and standards used to develop the original soil survey maps. Mapping scales generally range from 1:12,000 to 1:63,360; SSURGO is the most detailed level of soil mapping done by the Natural Resources Conservation Service (NRCS).

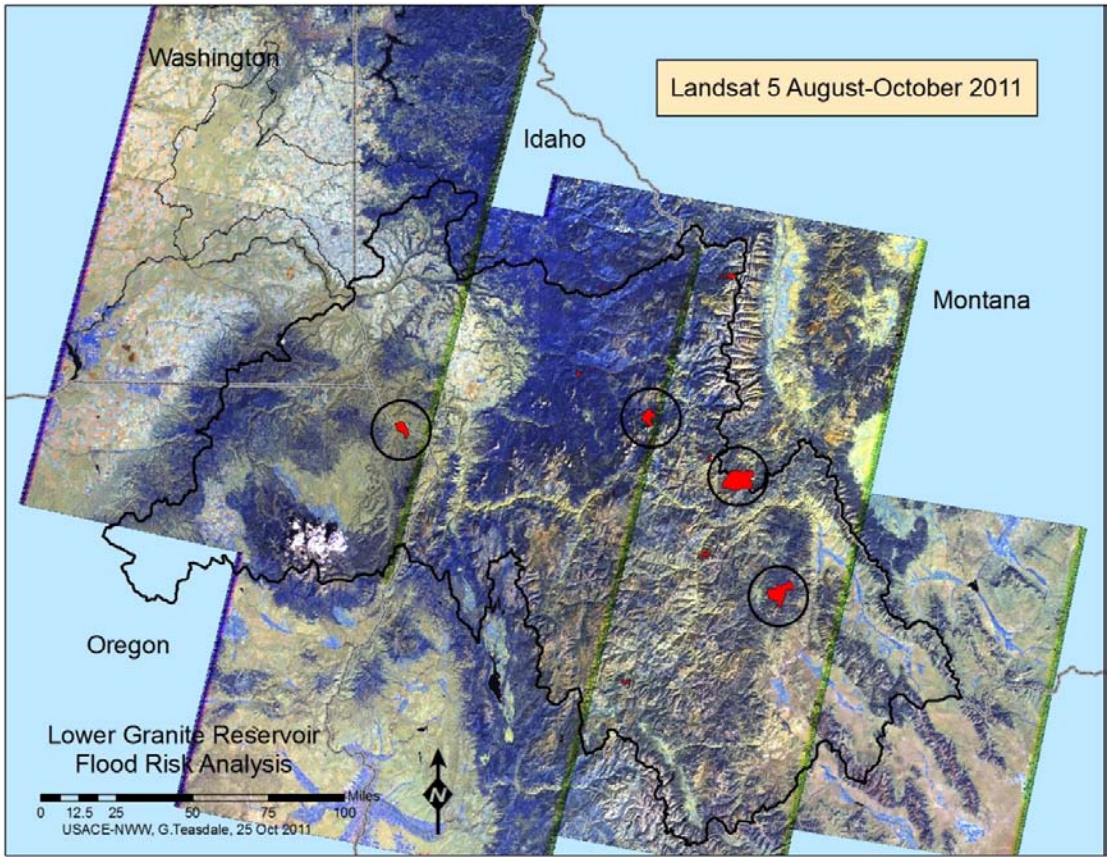


Figure 163. 2011 Landsat 5 visible near-infrared images and recent fires in the Lower Granite sediment yield watershed.

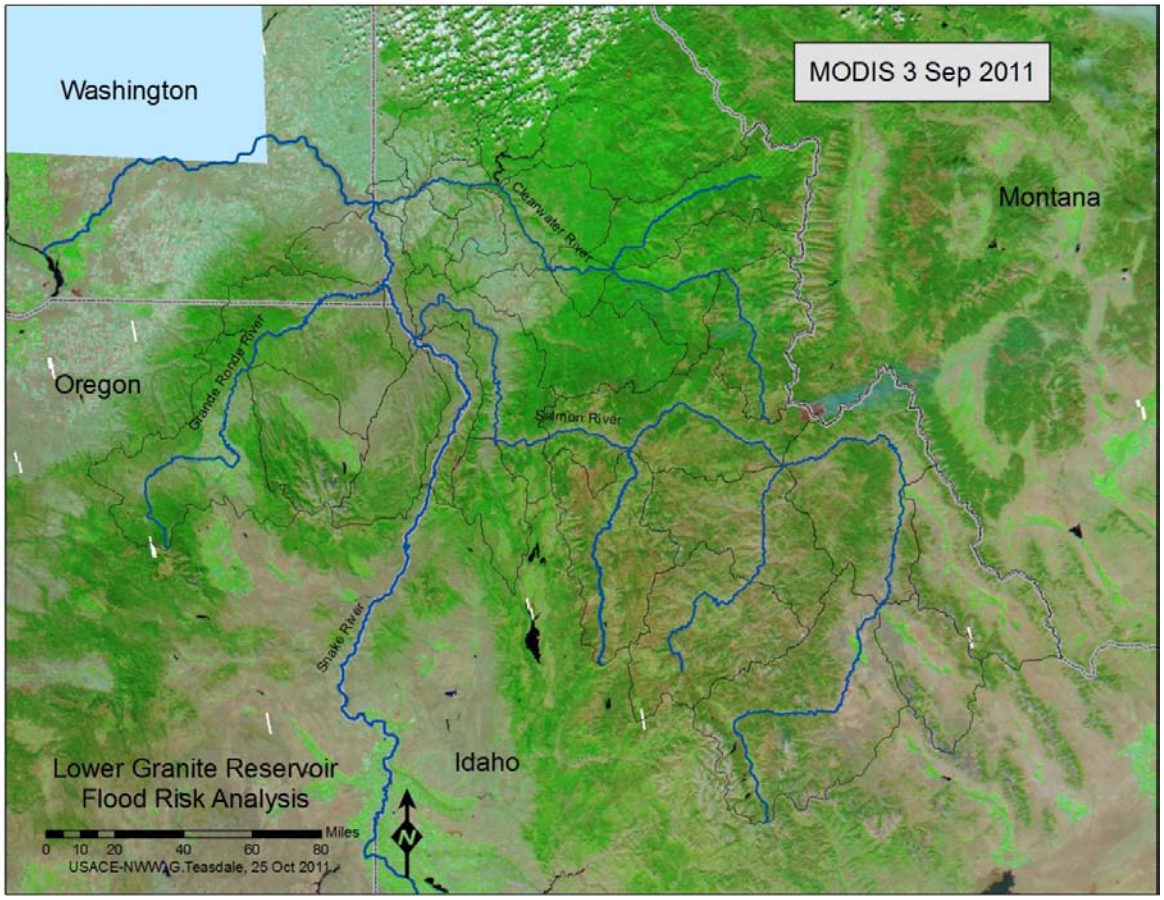


Figure 164. 3 September 2011 MODIS imagery of active fires in the Lower Granite sediment yield watershed.

18.2. Meteorology and Climate Projections

Soil erosion by surface water and landslides in saturated soils are the dominant processes that deliver sediment to rivers and streams in the lower Snake and Clearwater River basins. The rates and frequency of soil delivery events strongly depend on the hydrology of the basin. Representative long-term meteorological and climate data is necessary to model and simulate sediment yield. Soil erosion by wind was assumed to be negligible and not considered in development of the sediment yield models.

Meteorological Stations

Much of the area of the basin is relatively high altitude forestland and shrubland where snowmelt is a major factor in the hydrologic regime. The forested headwaters of the basin are sparsely populated where there are relatively few long-term meteorological stations. The Natural Resources Conservation Service Snotel

stations[45] are the primary source of meteorological data in upper elevations of the basin. The Snotel stations other meteorological stations in the lower Snake and Clearwater River basins are shown in Figure 165.

Climate parameters for hydrologic modeling have been derived by USDA from long-term records from stations throughout the US. The SWAT model weather generator uses the climate parameters to simulate meteorological inputs for extended simulations[46]. In SWAT, actual weather data may be substituted for all or some of the meteorological parameters. In this initial work, the SWAT climate stations were used, but some climate parameters were modified to better represent higher elevation conditions. Additional work is planned to improve the representation the meteorology, hydrology, snow water equivalent, and snow covered area in the forested basins.

Data on current climate conditions was also obtained from other published sources. Long-term climate averages for selected stations were obtained from the University of Idaho, College of Agriculture Bulletin 784[47]. Current normal (1971-2000) precipitation and temperature grids was acquired from the PRISM Climate Group at Oregon State University[48].

[45] http://www.wcc.nrcs.usda.gov/snow/

[46] Neitch, S.L., Arnold, J.G., Kiniry, J.R. and Williams, J.R. (2005) *Soil and Water Assessment Tool Theoretical Documentation, Version 2005*. Grassland, Soil and Water Research Laboratory, USDA Agricultural Research Service, Temple, TX.

[47] Abramovich, R., Molnau, M., and Craine, C. (1998), Climates of Idaho: University of Idaho, Moscow, ID, College of Agriculture Bull 784.

[48] http://www.prism.oregonstate.edu/

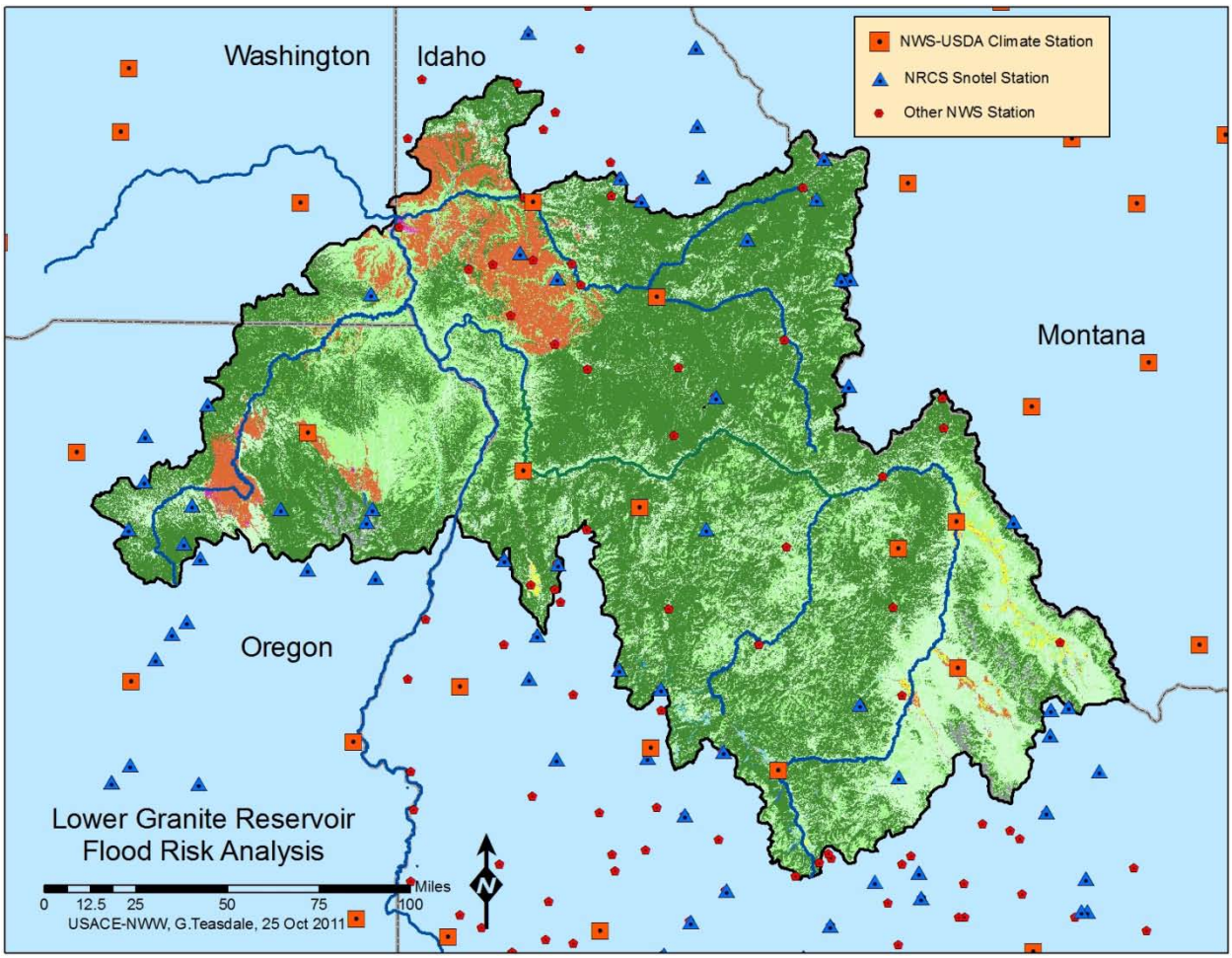


Figure 165. Meteorological and climate stations in the lower Snake and Clearwater River basins.

18.2.17. Climate Projections

Future climate conditions for the Snake and Clearwater River basins were derived from bias corrected and downscaled WCRP CMIP3 climate and hydrology projections[49]. The downscaled climate data was developed by the U.S. Department of the Interior's Bureau of Reclamation (Research and Development Office) and the Lawrence Livermore National Laboratory, the Bureau of Reclamation's Technical Service Center, Santa Clara University Civil Engineering Department, Climate Central, Scripps Institution of Oceanography, and U.S. Geological Survey. The work is supported in part by the U.S. Army Corps of Engineers Institute for Water Resources.

[49] http://gdo-dcp.ucllnl.org/downscaled_cmip3_projections/#Welcome

The data archive contains moderate resolution (12 km) translations of climate projections over the contiguous U.S. based on global climate projections from the World Climate Research Programme's (WCRP's) Coupled Model Inter-comparison Project phase 3 (CMIP3) multi-model dataset[50]. Projections from many climate models are available in the archive. Climate projections for the sediment yield analysis were derived from outputs of the GFDL 2.1 model developed by the U.S. Dept. of Commerce, National Oceanic and Atmospheric Agency, Geophysical Fluid Dynamics Laboratory[51].

The climate projections selected for the sediment yield analysis are for the SRES A2 scenario which represents higher emissions with more fragmented technological change and economic growth. Monthly grids of precipitation, minimum temperature and maximum temperature for the years 2056 to 2065 were aggregated to produce a 10 year average of monthly and annual values that centered on year 2060. Figure 166 and Figure 167 show the precipitation and maximum temperature grids for the Pacific Northwest from the GFDL 2.1 SRES A2 scenario.

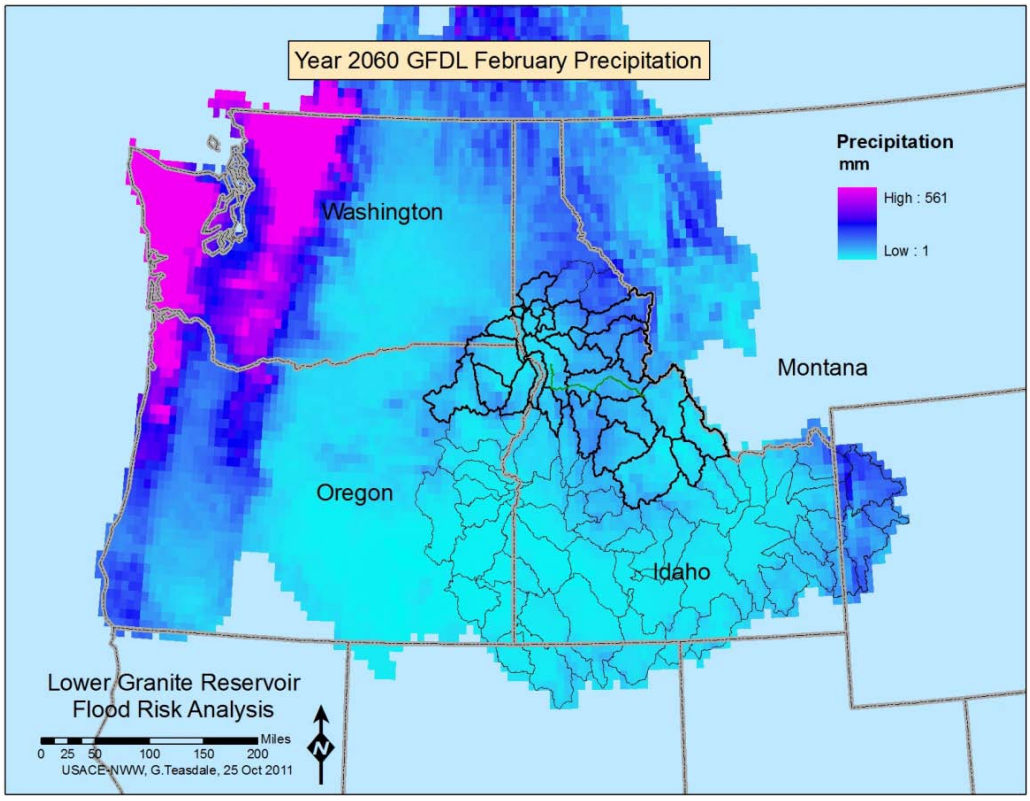


Figure 166. GFDL year 2060 February precipitation grid for the Pacific Northwest.

[50] http://www.ipcc.ch/

[51] Delworth, T.L. et al (2006) GFDL's CM2 global coupled climate models part 1: formulation and simulation characteristics. *J Climate* 19:643-674.

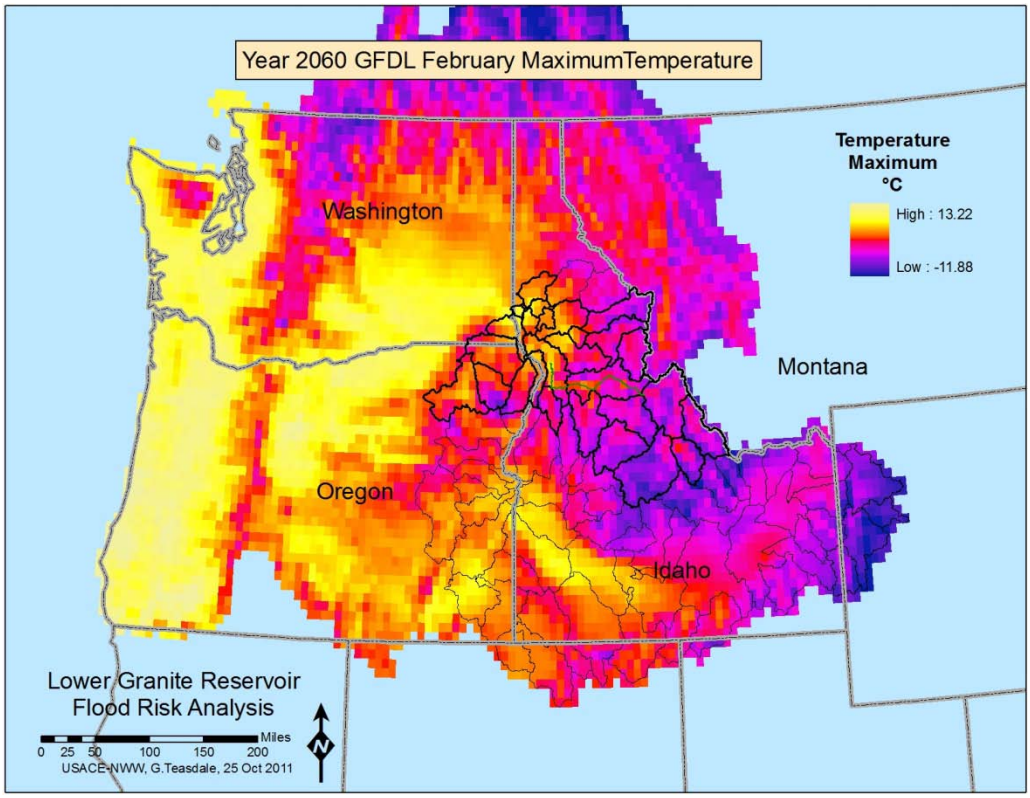


Figure 167. GFDL year 2060 February maximum temperature grid for the Pacific Northwest.

18.3. Wildfire Area in the Lower Granite Sediment Yield Watershed

Wildfire increases the exposure of soils to rainfall and runoff and substantially increases the potential for erosion and delivery of sediment to the stream channel system[19, 20]. The extent and timing of large fires must be considered in the development of a sediment yield model for the Lower Granite sediment yield watershed. Federal and state agencies record information about wildfire occurrence and extent. Annual fire data has been compiled since about 1916 and this extensive dataset has allowed analyses of longer-term wildfire-climate relationships[24]. Accessible fire data for the Lower Granite sediment yield watershed is reviewed below from the perspective of its relationship to sediment yield.

18.3.18. Historic Fire Perimeters

Fire perimeter data is available from the Geospatial Multi-Agency Coordination Group (GeoMAC)[52]. The GeoMAC website provides access to GIS shapefiles of current fire locations and perimeters in the conterminous 48 states and Alaska. Fire

[52] http://www.geomac.gov/index.shtml and http://rmgsc.cr.usgs.gov/outgoing/GeoMAC/historic_fire_data/

perimeters are submitted to GeoMAC by member organizations and then posted to an FTP site for downloading.

Historic fire perimeters produced by the fire management agencies are available as ESRI shapefiles and file geo-databases from the USFS[53,54]. Gibson[55] describes the origin and characteristics of the historic fire perimeter data for the Northern Rocky Mountains dating back to 1889. Historic fire perimeters for the Grande Ronde basins are available from the USFS Region 6[56]. Fire perimeter data is available directly from GeoMAC beginning in the year 2000. The target scale of recent fire perimeter data is 1:24,000 and conforms to National Wildfire Coordinating Group (NWCG) standards[57]. GeoMAC wildland fire perimeters are added to the historic layer dataset on a quarterly basis. Multiple polygons for the same fire are combined and the acreage of the combined polygon is recalculated to show only one polygon per fire[58].

Annual fire perimeter polygons for the Lower Granite sediment yield watershed were combined into the decadal polygons (all mapped fire areas for a 10-year period) shown in Figure 168 through Figure 171. Fire perimeter polygons prior to 2000 were obtained from the historic data assembled by Gibson and Morgan for the Northern Rocky region and the Blue Mountain fire history polygons for the Grande Ronde basin. Fire perimeters polygons for 2000 through 2010 were obtained from GeoMAC for all basins. The images show a striking increase in the extent of wildfire in the last two decades. During the decade 1971-1980 mapped fire area totaled only 242 sq. mi. In the current (2001-2010) decade, mapped fire area increased to 3025 sq. mi. Mapped fire areas by decade are summarized in Figure 172. Fire areas for each year are plotted in Figure 173 and show that wildfire was most extensive in 2000 and 2007. Similar to figure by Littell et al[24], the 2000 and 2007 fire areas standout in the full record of fire data dating back to 1889 in Figure 174. Comparisons of current fire perimeters with the very early fire data are mostly qualitative because of the changing methods of

[53] http://www.fs.fed.us/r1/gis/thematic_data/fire_history_r1_1985_2009_poly.htm

[54] Gibson, C. E. and Morgan, P. (2009). *Atlas of digital polygon fire extents for Idaho and western Montana (1889-2003)*. [Online]. Fort Collins, CO: U.S. Department of Agriculture, Forest Service, Rocky Mountain Research Station. Available: http://www.fs.fed.us/rm/data_archive [2009, May 7].

[55]Gibson, C.E. (2006) *A Northern Rocky Mountain polygon fire history: Accuracy, limitations, strengths, applications, and recommended protocol of digital fire perimeter data*. M.S. thesis. Moscow, ID: University of Idaho.

[56] http://www.fs.fed.us/r6/data-library/gis/umatilla/

[57] http://www.nwcg.gov/pmu/pmo-archive/products/stds/gdl_fire_perimeter/cover.htm

[58] http://rmgsc.cr.usgs.gov/outgoing/GeoMAC/historic_fire_data/us_hist_fire_perimeters_dd83_METADATA.htm

delineating burn areas. Gibson gives a detailed discussion of the relative accuracy of the fire perimeter data[55]. Good potential exists to augment the fire perimeter data with assessments of hydrologic condition from satellite imagery and hydrologic records since the beginning of the Landsat 5 program in 1984.

There is an apparent relationship between discharge in the Salmon River basin and fire-affected area. Figure 175 is a plot of the difference between the mean annual discharges for the Salmon River at Whitebird and the Clearwater River at Orofino along with the annual mapped fire area since 1974. If meteorological factors remain relatively constant, large areas affected by fire will increase the rate of surface runoff of a basin by reducing surface water retention, evapotranspiration and possibly infiltration. Since the Clearwater basin was not as affected by fire, the difference between the Salmon River discharge and the Clearwater River discharge should increase with the area of recent fire. Using the difference between the Salmon River and Clearwater River discharges in the analysis reduces the effect of annual precipitation variation in basin. The relationship between water supply and fire in the Lower Granite watershed should be examined in future work and would likely be best evaluated with hydrologic modeling.

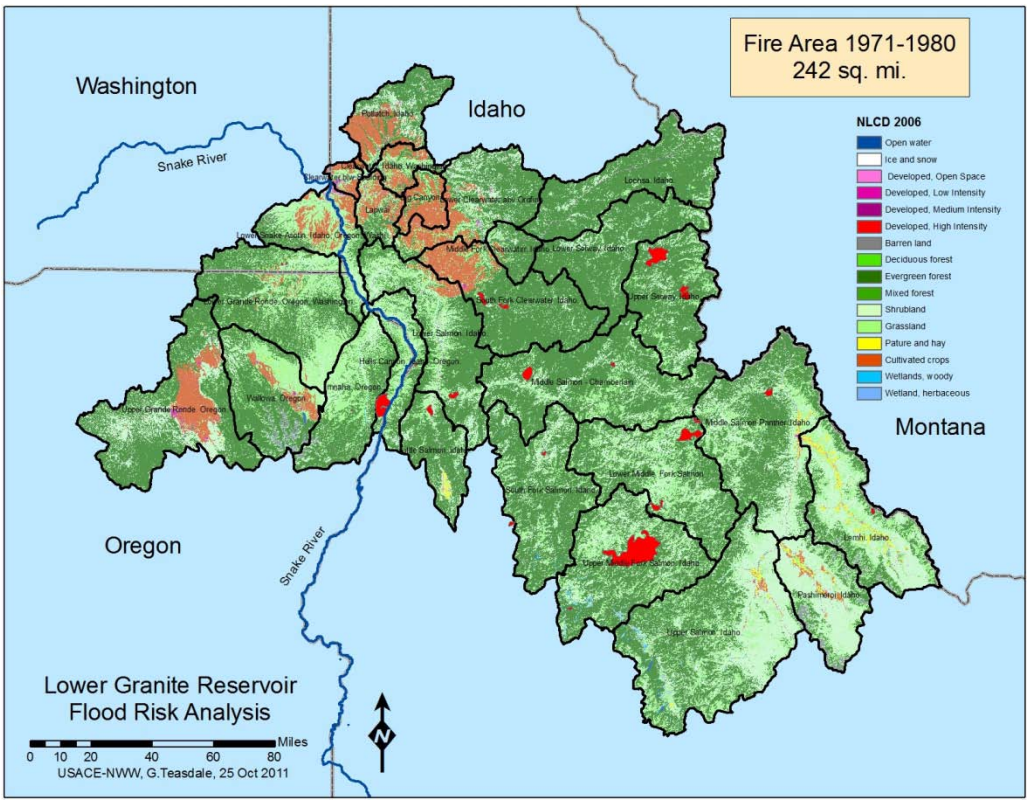


Figure 168. 1971-1980 fire perimeter polygons for the Lower Granite Reservoir sediment yield watershed.

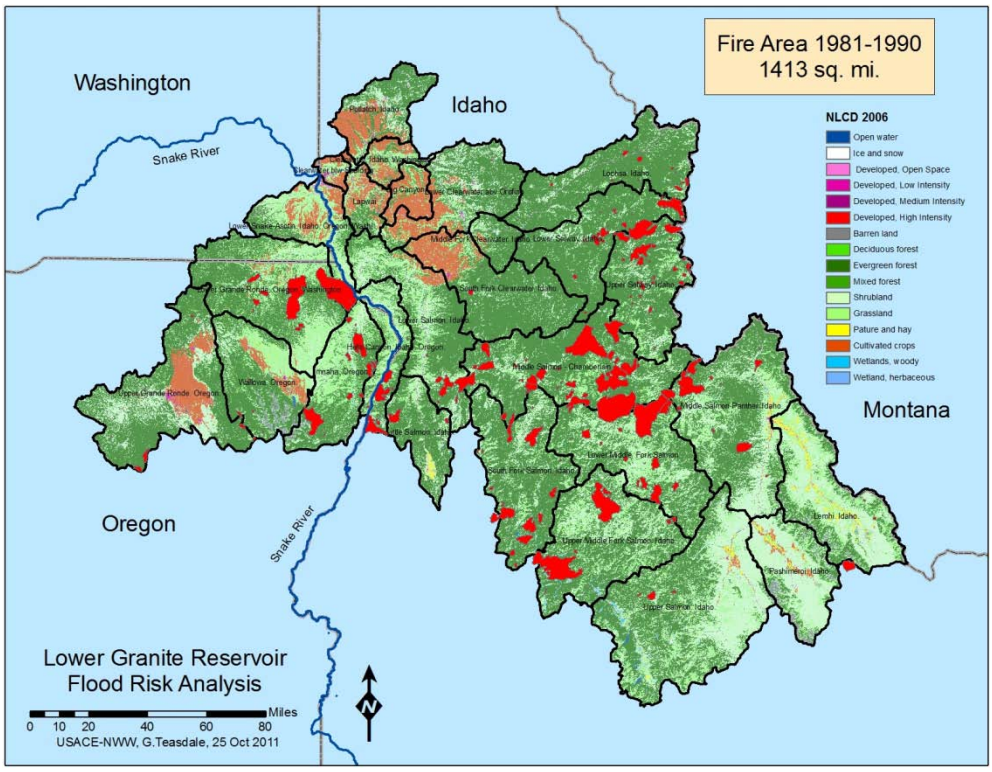


Figure 169. 1981-1990 fire perimeter polygons for the Lower Granite Reservoir sediment yield watershed.

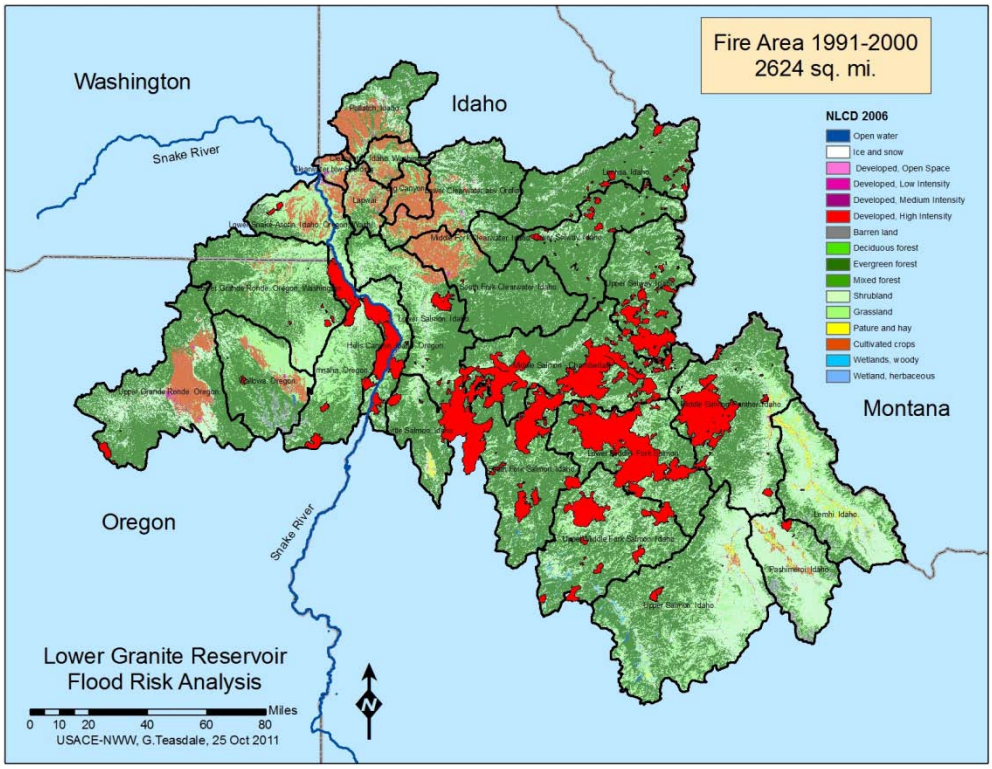


Figure 170. 1991-2000 fire perimeter polygons for the Lower Granite Reservoir sediment yield watershed.

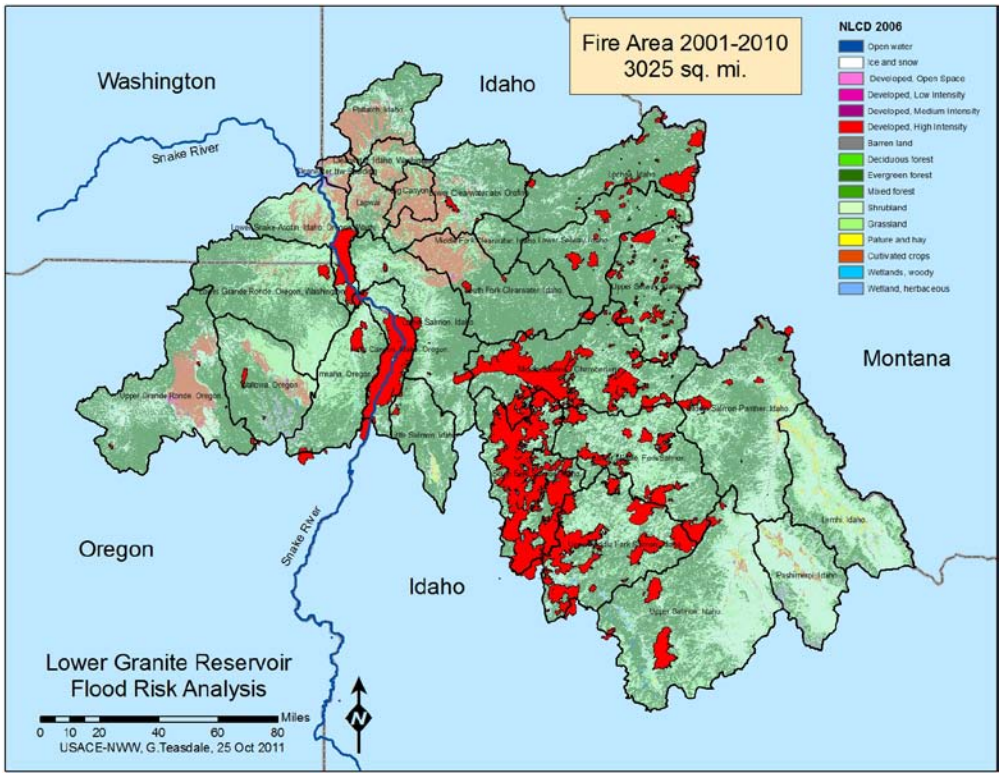


Figure 171. 2001-2010 fire perimeter polygons for the Lower Granite Reservoir sediment yield watershed.

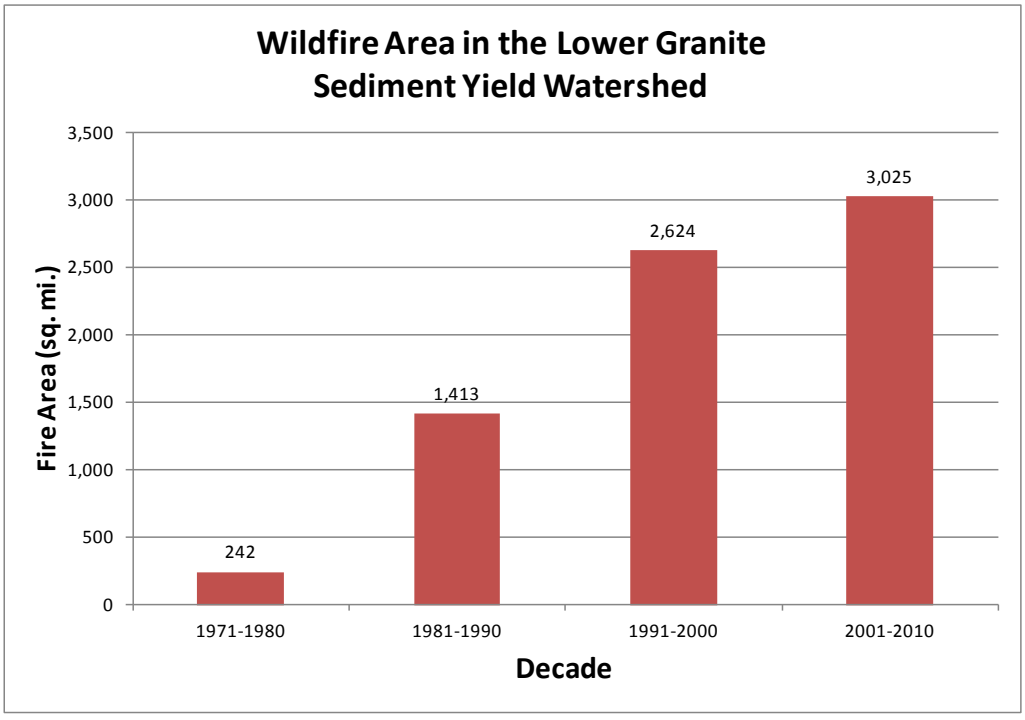


Figure 172. Chart of wildfire area in the Lower Granite Reservoir sediment yield watershed.

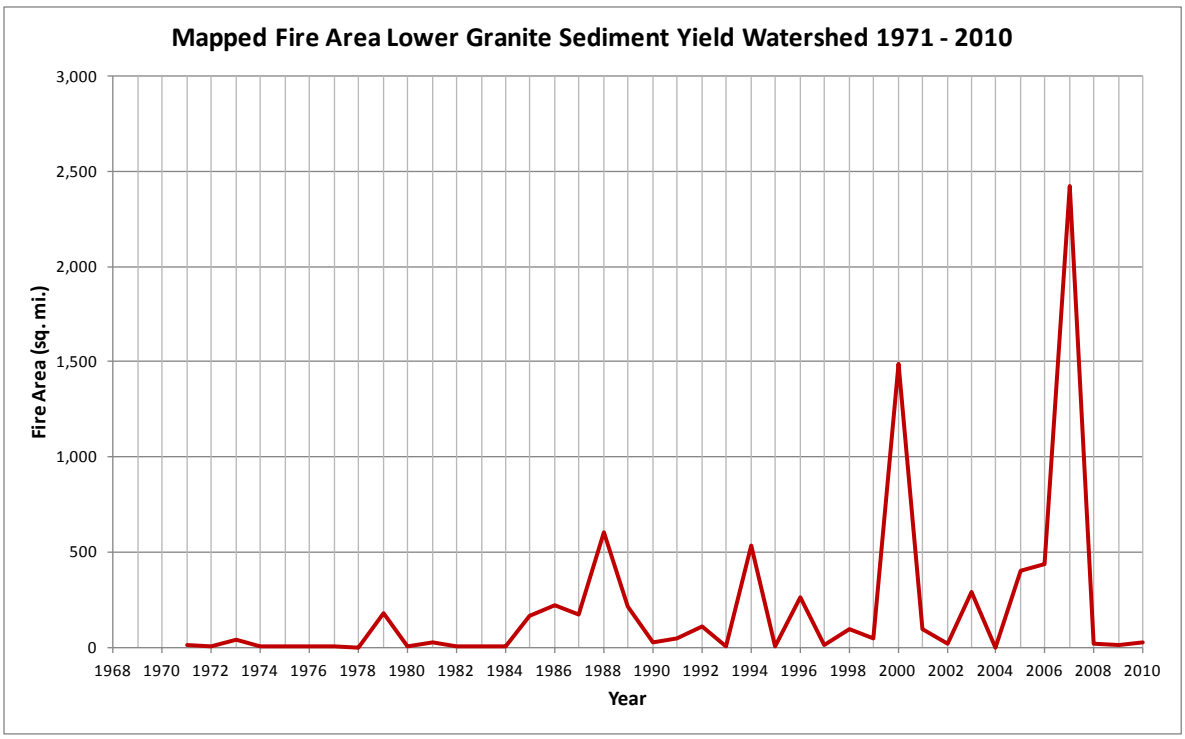


Figure 173. 1971-2010 annual mapped fire area in the Lower Granite sediment yield watershed.

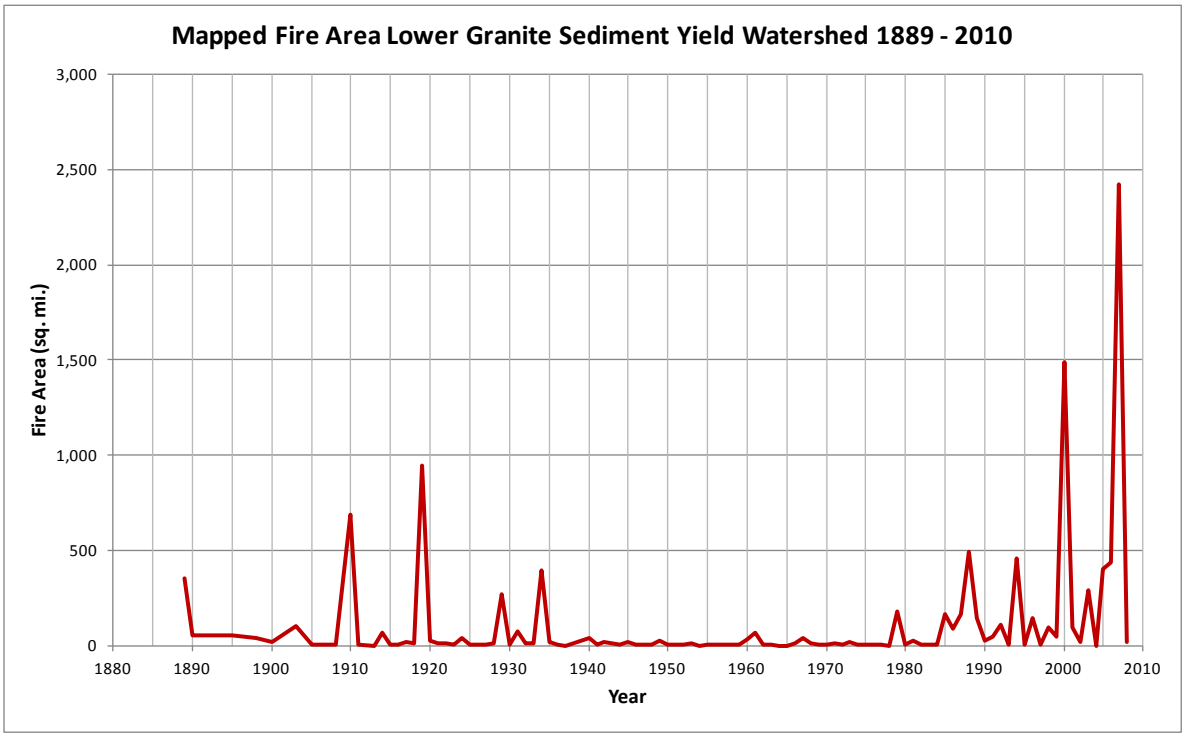


Figure 174. 1889-2010 annual mapped fire area in the Lower Granite sediment yield watershed.

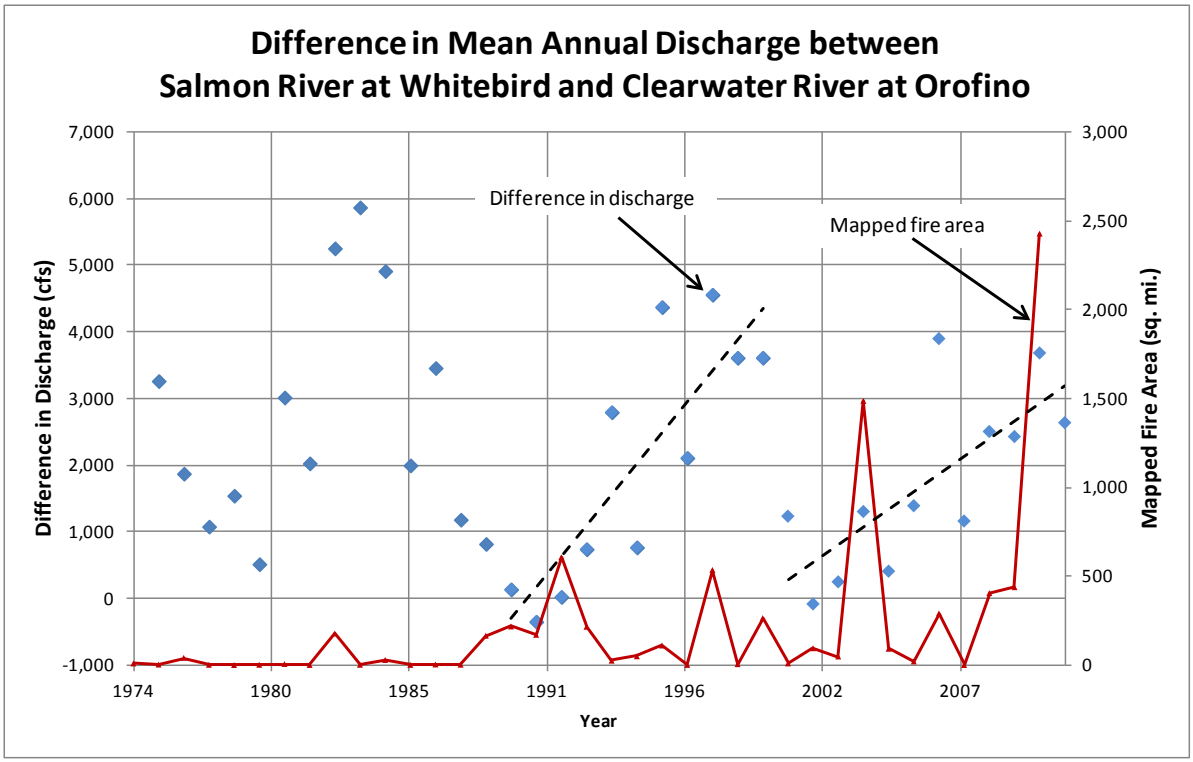


Figure 175. Relationship of difference in discharge and mapped fire area.

18.3.19. Future Fire Potential

Fire severity and loss of vegetative cover cannot be obtained directly from fire perimeter data. Fires may recur within a few years in areas where sufficient fuel remains or where new growth is able to sustain combustion. In the 2001-2010 decade, fire recurred on 473 sq. mi. that was burned in the previous decade (Figure 176). The largest area of overlap is in the Salmon River and Snake River canyons. Landsat 5 images in Figure 177 and Figure 178 confirms that the areas in the Salmon River canyon and the South Fork of the Salmon River canyon were burned in 1994 and 2007. Landsat imagery also showed that large areas in the Snake River canyon burned in 1996 and 2007.

The year 2007 was a severe year for wildfire throughout the northern Rocky Mountains. Total fire perimeter area in 2007 in the Lower Granite sediment yield watershed was 2427 sq. mi (Figure 179) which was 16 percent of the total fire perimeter area mapped in 2007 for the contiguous U.S. and Alaska. The total area affected by fire since 1971, not including overlap areas, is 6220 sq. mi. or about 23 percent of the 27,137 total area of the Lower Granite sediment yield watershed (Figure 180). Fire density is greatest in the Salmon River basin, Hells Canyon and to a lesser extent in the Selway River basin. Fire return periods of less than 35 years as indicated by the Landfire Fire Regime Group data layer (Figure 181) occur throughout the basin.

As this report was being updated in October 2012, wildfires are again burning across large areas of the lower Snake River basin. New and active burn scar areas in Figure 184 total 1169 sq. mi. as of 4 October 2012. The Mustang Complex fire (530 sq. mi.) and the Sheep fire (75 sq. mi.) are adjacent to the Salmon River which increases the potential that large amount of sediment will be delivered directly to the main channel system.

There is an apparent disparity between the fire return period classification and the extent of fire mapped in the Grande Ronde basin. Some disparity is because historical fire perimeters may not have been completely compiled for this basin. However, the disparity may also indicate that sediment yield from forestland and rangeland in the Grande Ronde basin may substantially increase in the future due to wildfire.

Methods are being developed to evaluate the spatial distribution of the probability of wildfire across the western U.S using spatial modeling and statistical analysis[59]. Figure 182 shows a subset of the relative-likelihood-of-fire grid developed by Parisien et al. (full model) for the Lower Granite sediment yield watershed. The relative likelihood of fire is high across the Salmon and Selway basins. The likelihood grid was developed from the fire perimeter data for 1984-2008 so would reflect weaknesses in that data. The relative likelihood grids by Parisen et al. do not correspond directly to probability and frequency as employed in hydrologic analysis, but they do indicate subbasins with a higher risk of wildfire and long-term potential to deliver sediment to the channel network.

Various metrics of short-term soil erosion hazard following wildfire can be derived from the spatial datasets described above. An example is in Figure 183 in which the grid cells indicate where the land slope is greater than 20 percent, annual precipitation is greater than 15 inches, tree and shrub cover is greater than 50 percent, and the relative likelihood of fire is greater than 0.5. Also shown is the total fire perimeter area for the decade 2001-2010. By this index, the lower and middle Salmon River basin would be expected to deliver substantial quantities of sediment to the Salmon River. Research is needed to determine the best short-term indicators of sediment delivery potential.

[59] Parisien, M-A, Snetsinger, S., Greenberg, J.A., Nelson, C.R., Schoennagel, T., Dobrowski, S.Z., and Moritz, M. A. (2012) "Spatial variability in wildfire probability across the western United States.", *International Journal of Wildland Fire*, early online publication.

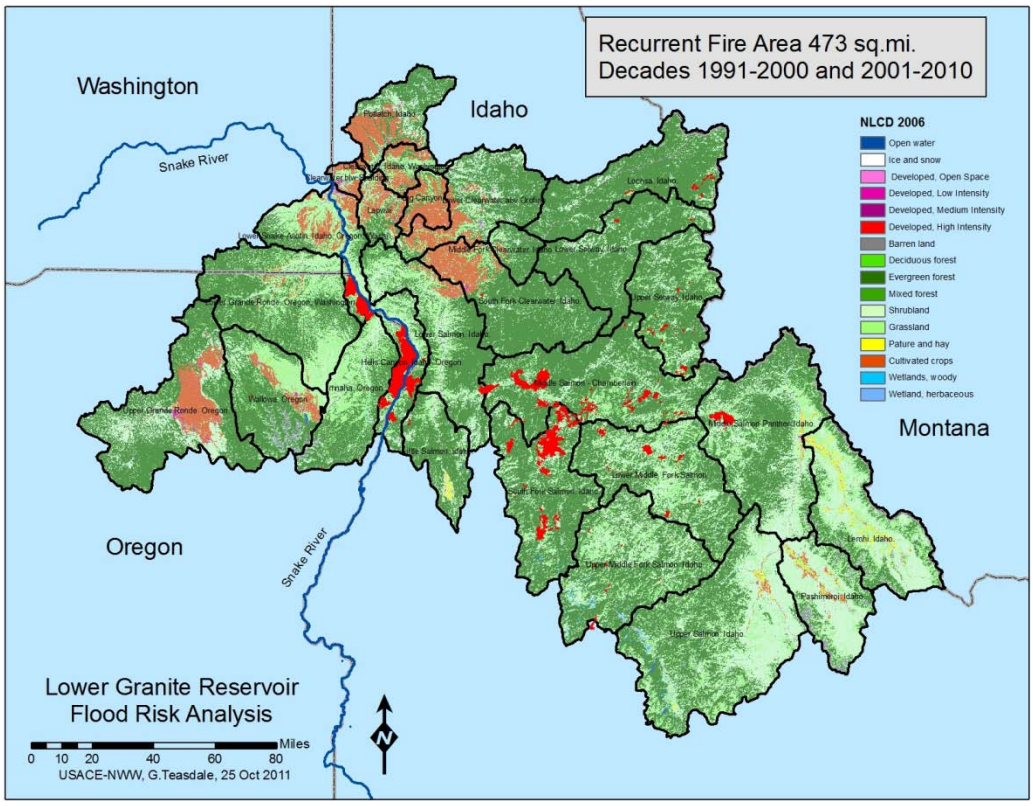


Figure 176. Recurrent fire areas decades 1991-2000 and 2001-2010.

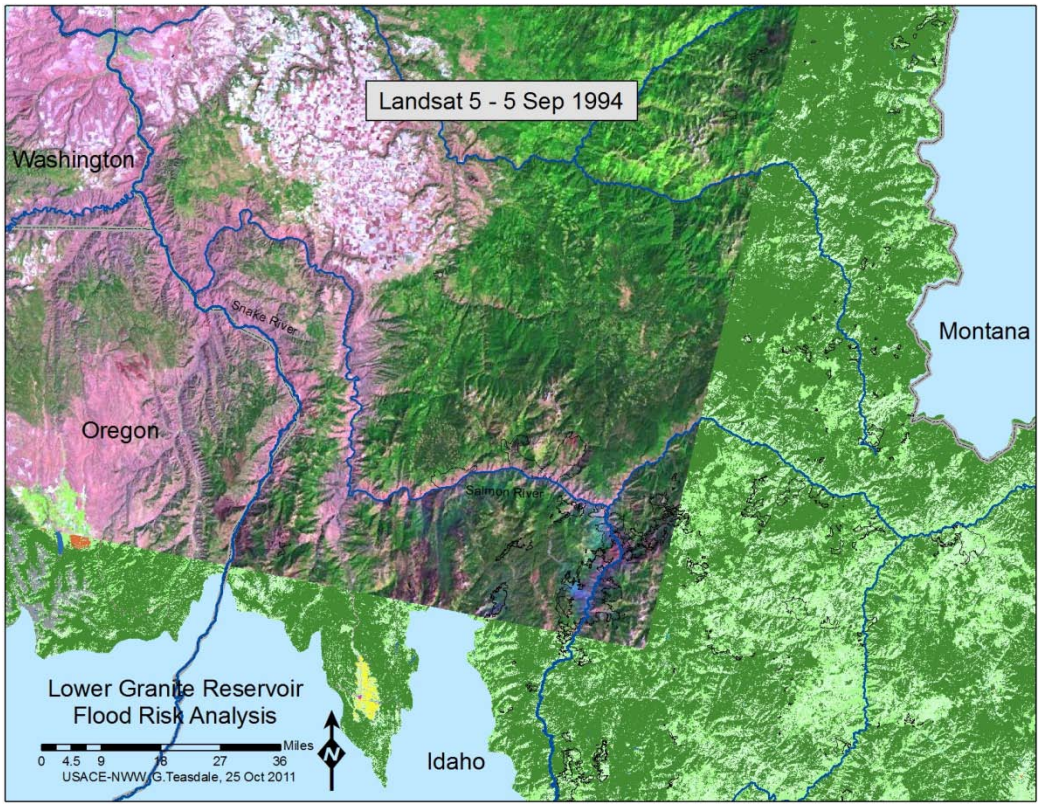


Figure 177. 5 September 1994 Landsat 5 image of active fire areas.

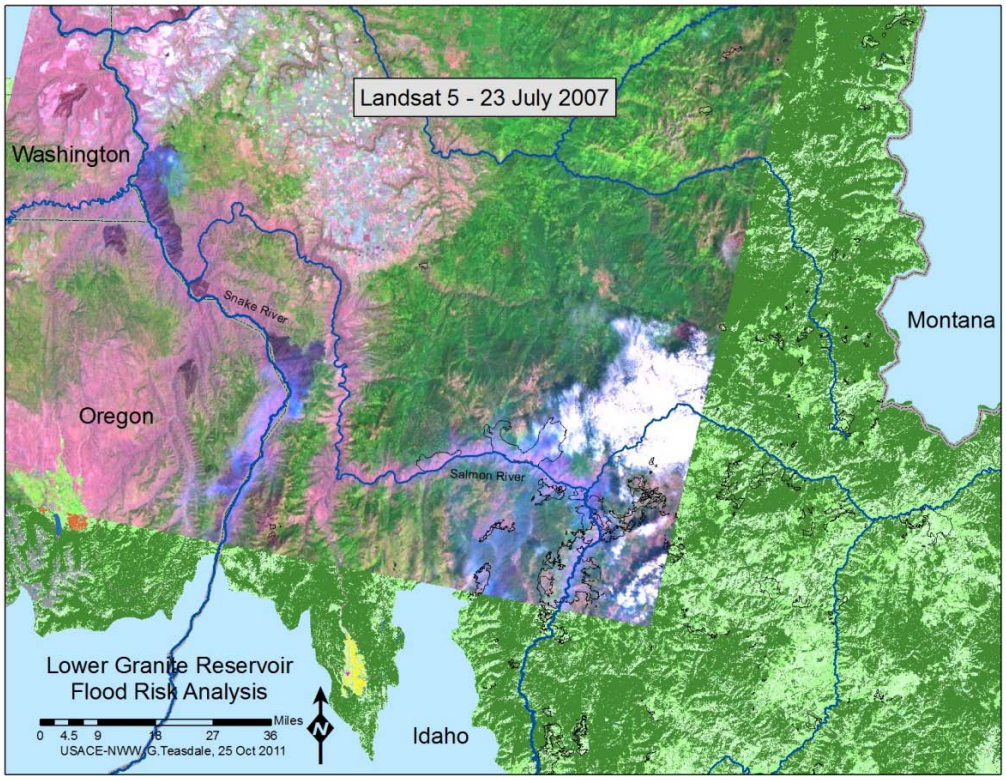


Figure 178. 23 July 2007 Landsat 5 image of active fire areas.

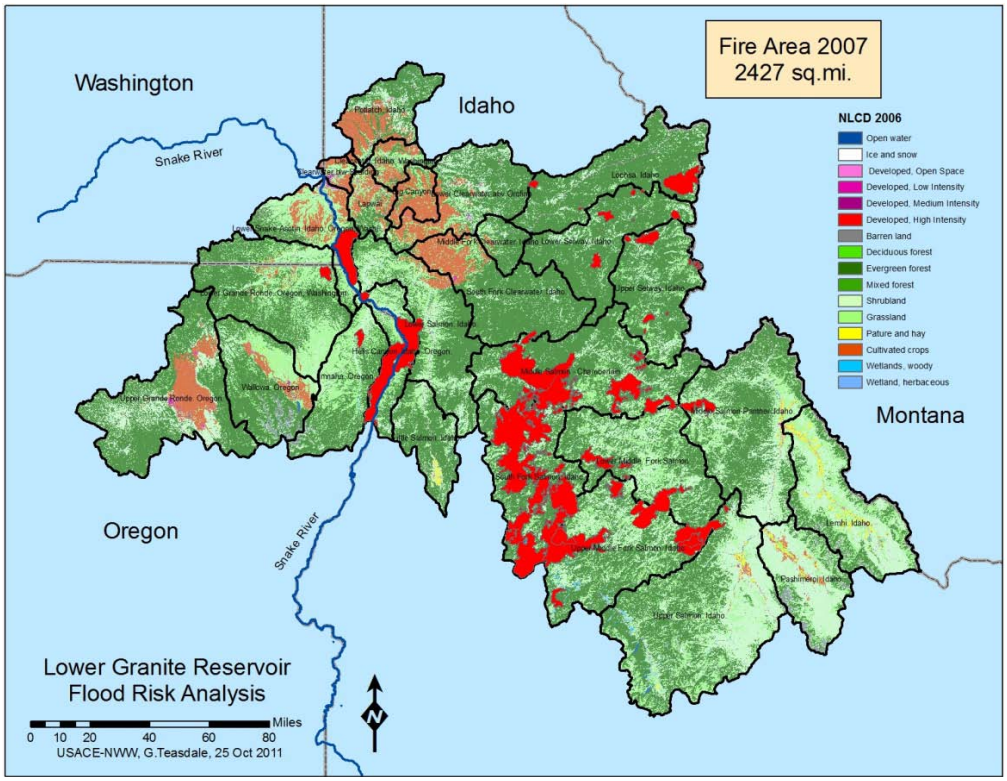


Figure 179. 2007 fire perimeter polygons for the Lower Granite Reservoir sediment yield watershed.

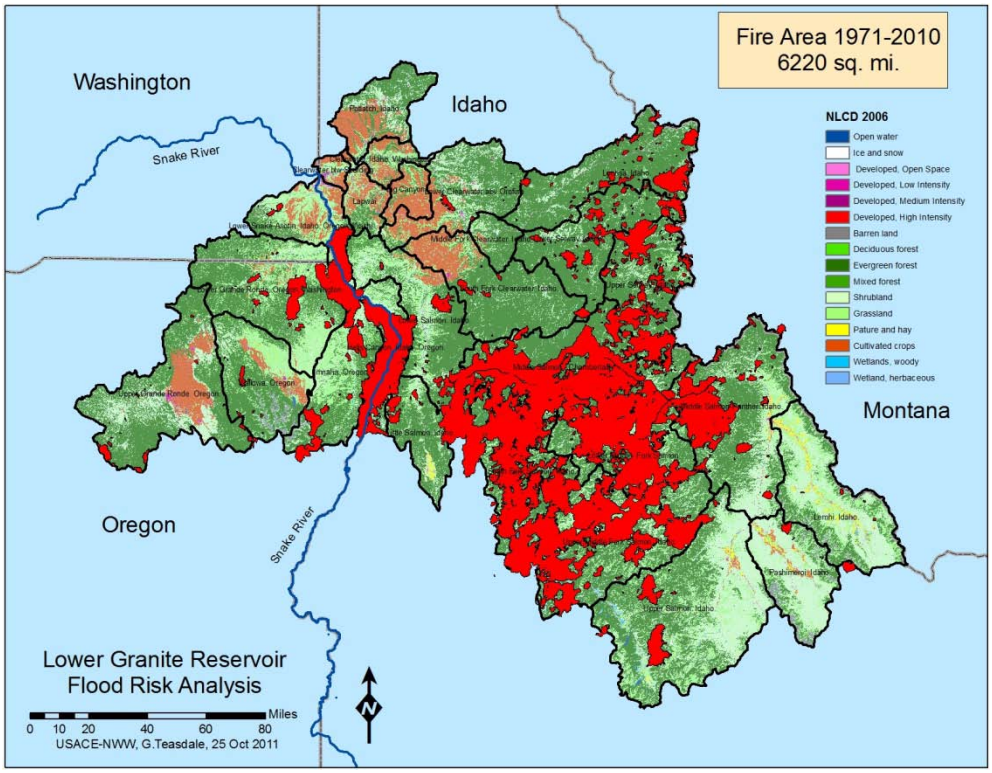


Figure 180. 1971-2010 combined fire perimeter polygons for the Lower Granite Reservoir sediment yield watershed.

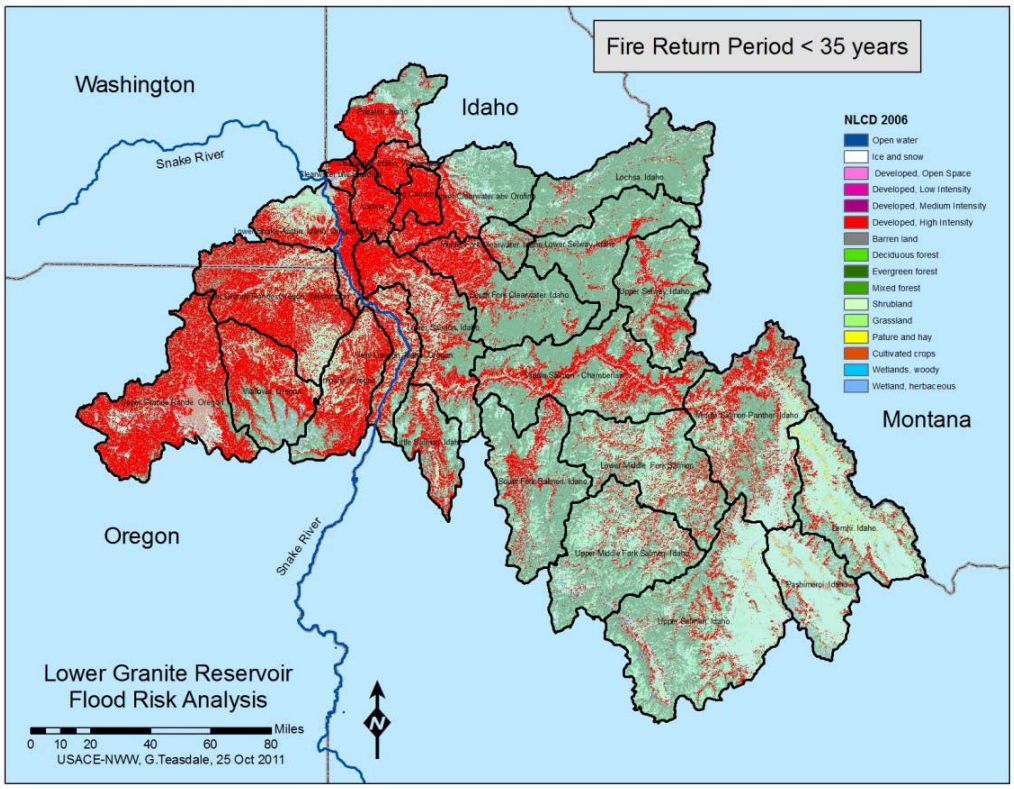


Figure 181. Fire Regime Group (FRG) with fire return period less than 35 years.

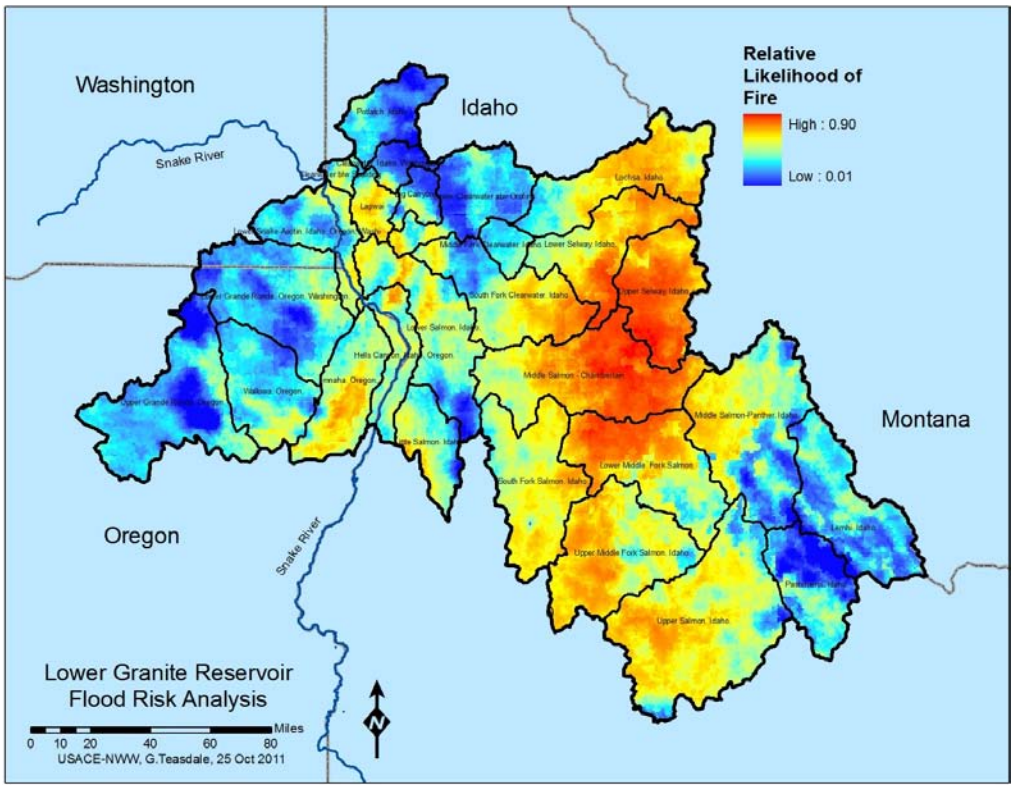


Figure 182. Relative likelihood of wildfire in the Lower Granite sediment yield watershed from data by of fire by Parisien et al. (2012).

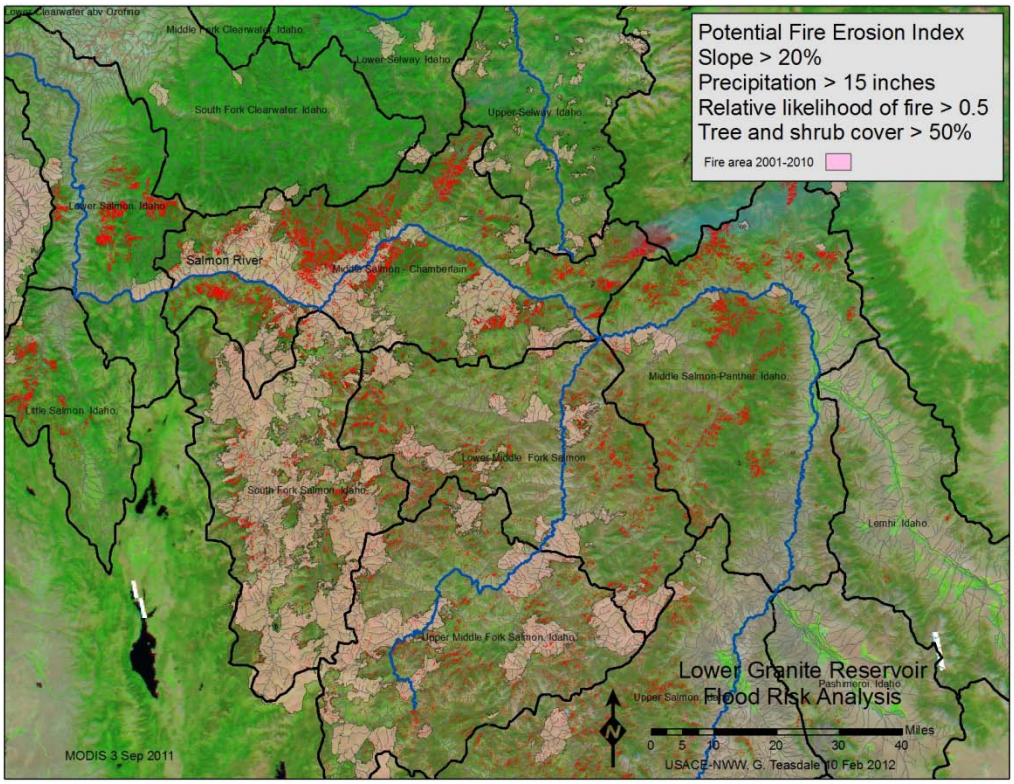


Figure 183. Potential fire erosion index for Salmon River basin.

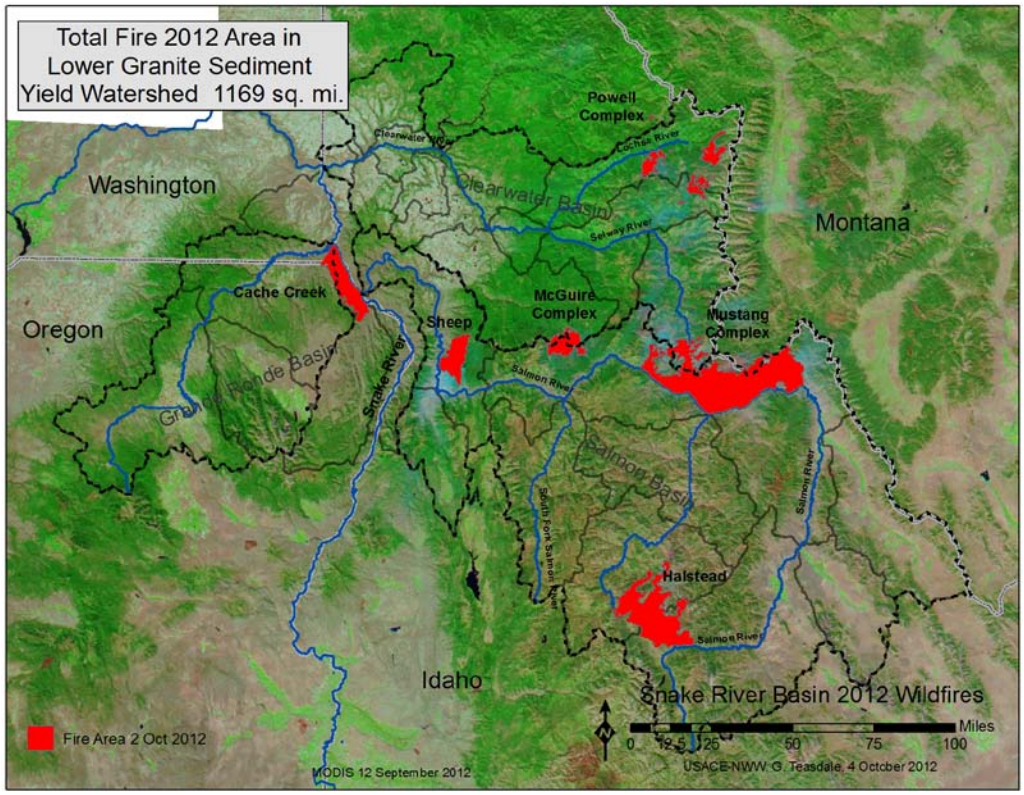


Figure 184. 2012 Wildfires in the lower Snake River watershed.

18.4. Selection of a Sediment Yield Model

It is challenging to develop physically-based sediment yield models for the many subbasins of the 27,000 square mile sediment yield watershed of Lower Granite Reservoir. The task is more difficult when the overriding objective is to evaluate the effect of climate variability and fire on both short-term and long-term sediment yield. Neither aspect of sediment yield have yet received sufficient attention in scientific and engineer research.

Several potential watershed scale modeling systems are available including the Soil and Water Assessment Tool (SWAT)[60], the Hydrological Simulation Program-Fortran (HSPF)[61] and the Geo-spatial interface for the Water Erosion Prediction Project (GeoWEPP)[26,62]. The semi physically-based SWAT model was selected because its physical and biological functions are sensitive to the meteorological variables necessary

[60] http://swatmodel.tamu.edu/documentation/

[61] http://www.epa.gov/ceampubl/swater/hspf/

[62] http://www.geog.buffalo.edu/~rensch/geowepp/

to simulate a realistic response in long-term sediment yield under climate forcing. While fire-affected land cover types are not currently defined in the default SWAT database, existing land cover parameterizations can be adapted to simulate first-order fire effects. Model components in SWAT include weather generation, surface runoff, return flow, percolation, evapotranspiration, transmission losses, pond and reservoir storage, crop growth and irrigation, groundwater flow, reach routing, nutrient and pesticide loading, water transfer. The SWAT model is widely applied in research and operational watershed hydrologic and water quality simulation[63], and it is one of the models supported in the U.S. Environmental Protection Agency Better Assessment Science Integrating point and nonpoint Sources (BASINS) system[64].

18.5. Sediment Yield Subbasin Models

Sediment yield models were developed for the major subbasins in the sediment delivery watershed for Lower Granite Reservoir and the Palouse River basin (Figure 185). To aid calibration, the outlets of the initial subbasin models coincide with the sediment load measurement sites. Eventually, subbasins in the operational model will be delineated to coincide with the Hydrologic Unit Code (HUC) level 8 boundaries. The initial subbasin models were developed as individual SWAT models. Sediment and flow routing in the main tributary rivers is with HEC-RAS. The individual subbasins SWAT models are discussed below.

[63] There nearly 1000 peer-reviewed journal articles in the SWAT literature database (https://www.card.iastate.edu/swat_articles/)

[64] http://water.epa.gov/scitech/datait/models/basins/index.cfm

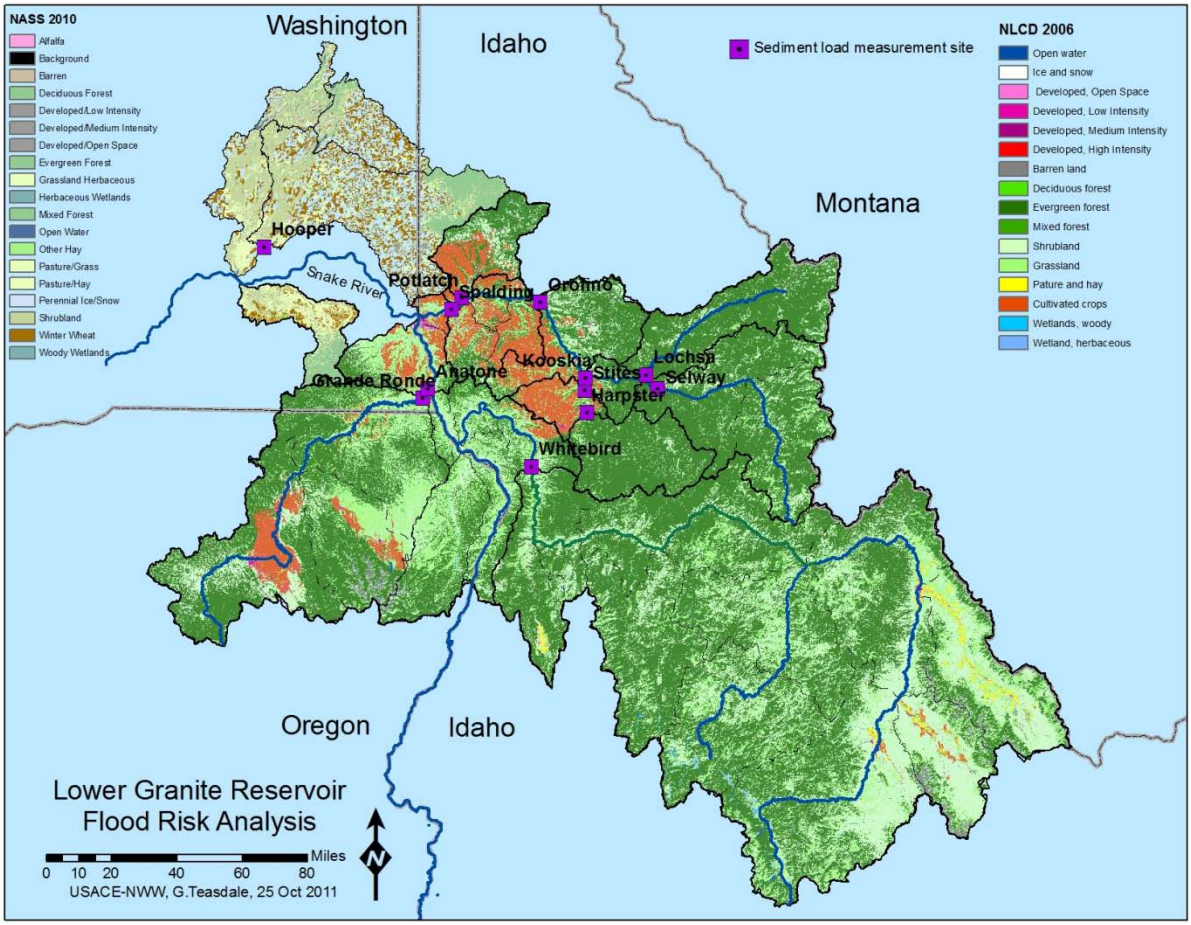


Figure 185. Subbasins of the Lower Granite Basin sediment yield model.

18.5.1. Salmon River at Whitebird Subbasin SWAT model

Catchments for the SWAT model of the Salmon River watershed above Whitebird (SRWB) were derived by semi-automatic analysis of the 30-meter digital elevation model (DEM) in the SWAT modeling system. Processing of terrain data is similar to those employed in HEC-HMS and is described in the SWAT model documentation. The SRWB is represented by 23 catchments. The average size of the catchments is 582 sq.mi. Channels in the catchments were extracted from the DEM so only approximate the hydraulic properties of the actual stream system. Accurate representation of the channel system is less important when evaluating sediment yield over a period of several years and decades. Stream channels in the Lower Granite sediment yield watershed may temporarily store transient sediment, but are generally supply limited so over a period of a few years will transport all sediment delivered from upland sources. The subbasins and channels of the SRWB model are shown in Figure 186.

Land use in the SRWB subbasin based on the NLCD2006 is 53 percent forestland (Forest-Evergreen), 27 percent shrubland (Range-Brush), 17 percent grassland (Range-Grasses) and 4 percent other land cover types. Land cover areas for the SRWB subbasin are summarized in Table 10. A conversion table is used to assign NLCD classifications to SWAT land use classes that better represent erosion potential, conservation practices and crop growth. Land use classes that are pre-defined in the SWAT modeling system that correspond to the dominant land cover types are FRSE, RNGB and RNGE. Threshold values that define model hydrologic response units (HRU) in the catchments were generally set at 25 percent for slope, 25 percent for land use and 25 percent for soil type in the forested subbasins. Lower thresholds were set for HRU development in agricultural subbasins (more HRUs) and were determined by the actual areas of the dominant cultivated agricultural classes. Fire affected area is not directly represented in the pre-defined SWAT land use classes.

Climate and meteorology for initial simulations for the SRWB subbasin model is derived from the climate stations included in the SWAT modeling system. There are 11 climate stations in the SRWB area. Meteorological variables in the SWAT data generally agreed well with climate summaries for Idaho[47].

Runoff in the SWAT model is determined by the curve number method[65] and soil erosion is computed with the Modified Universal Soil Loss Equation (MUSLE)[66]. Sediment yields for hydrologic response units are computed by the MUSLE equation,

$$S_y = 95\left(Q \times q_p\right)^{0.56} K\ LS\ C\ P\ F$$

where

[65] Hawkins, R.H., Ward, T.J., Woodward, D.E., Van Mullem, J.A. (2009) *Curve Number Hydrology - State of the Practice*, ASCE Press, Reston, VA

[66] Williams, J.R. (1975) Sediment-yield prediction with universal equation using runoff energy factor. In Present and prospective technology for predicting sediment yield and sources: Proceedings of the sediment yield workshop, USDA Sedimentatio Lab., Oxford, MS, November 28-30, 1972. ARS-S-40.

S_y = sediment yield, tons

Q = runoff volume, acft

q_p = peak flow rate, cfs

K = soil erosion factor (USLE/RUSLE)

LS = Slope gradient and length factor (USLE/RUSLE)

C = cover and management factor (USLE/RUSLE)

P = supporting conservation practice factor (USLE/RUSLE)

F = soil coarse fragment factor

Values for the hydrologic variables (Q, q_p) are determined from the curve number runoff analysis. The exponent of the hydrologic variables group may not represent rainfall and runoff energy in the best manner for the Lower Granite sediment yield basin, but was found to be acceptable for the multi-year simulations in this initial modeling. Soil parameters (K, F) are derived from the Statsgo and SSURGO soil data. The slope gradient and length factor (LS) is determined from the SWAT analysis of the DEM. The effect of land cover (land use) on sediment yield is represented by the cover and management factor (C) and the supporting conservation practice factor (P). For a given meteorological series, the C and P factors are the main calibration parameters for sediment yield.

The SWAT model simulates the life cycles of natural cover and cultivated crops based on the meteorology inputs and growth and crop management factors specified in the SWAT land use database. It is recommended practice[46] to not modify the pre-defined factors for specific land use types unless supported by field studies. The land use growth and crop management factors were not adjusted in the simulations of the Lower Granite sediment yield watershed. Simulated crops yields in the agricultural subbasins compared well with published data[67].

Initial scenarios of sediment yield were for a period of 30 years to simulate the long-term sediment yield of the subbasins under constant land cover and climate conditions. Simulated subbasin period average yields of water and sediment were compared to measured values at the outlet of the subbasin model. Accuracy of plus or minus 20 percent were desired for both water and sediment yield simulated by the initial subbasin models.

Sediment yield for the SRWB was simulated with and without fire-affected area included in the land cover representation. The first 30-year simulation subbasin produced a water yield that was 17 percent less than the average yield of 10.9 inches

[67] NASS (2011) "Washington's 2011 Winter Wheat Yield Second Highest on Record", *Press Release*, National Agricultural Statistics Service, Washington Field Office, Olympia, WA.

as determined from the USGS stream gage on the Salmon River at Whitebird for the period 1980 to 2011. No adjustment was made to the meteorological parameters or the runoff curve numbers. Sediment yield for the first simulation averaged 0.06 ton/ac/yr, which is 73 percent less than the 0.21 tons/ac/yr measured at Whitebird for the period 2009-2011 (Table 7). The first simulation did not include fire affected area so the sediment yield would be expected to be lower than that measured.

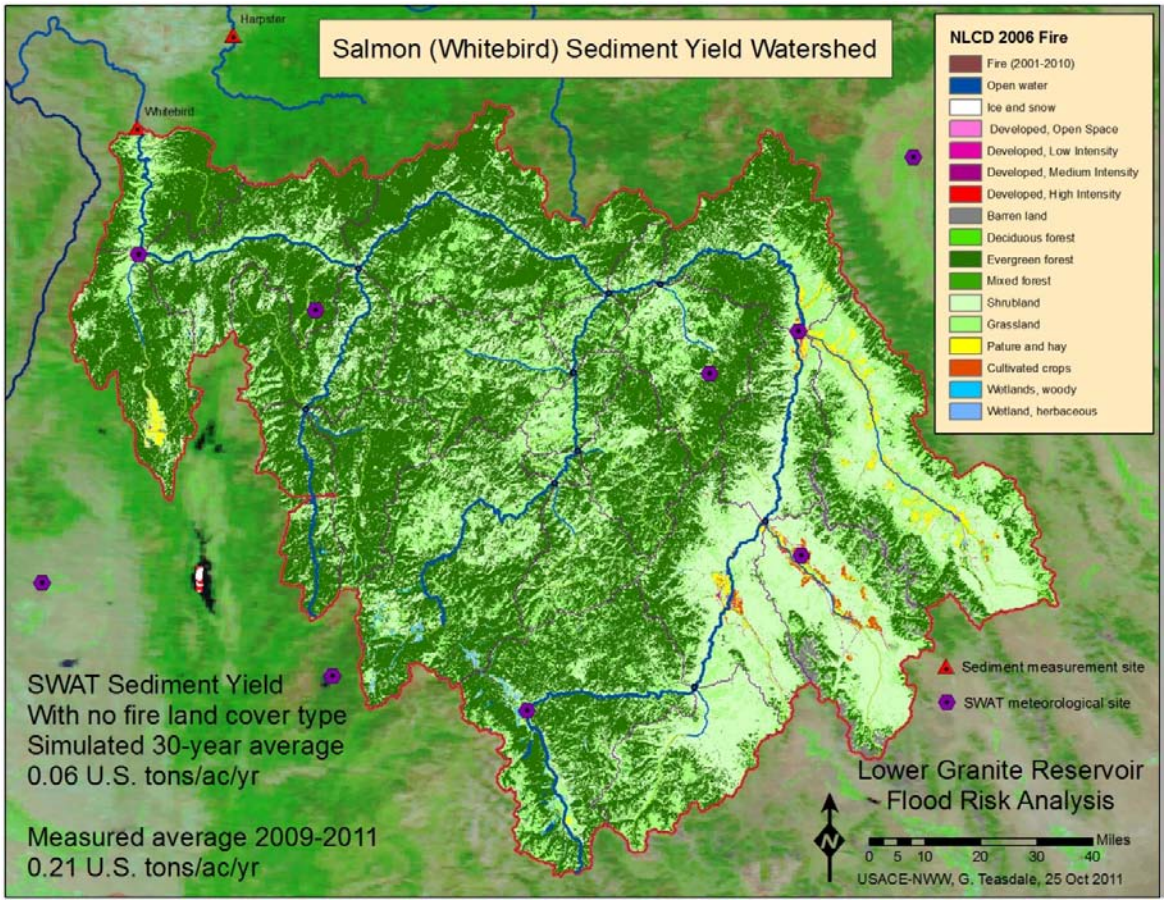


Figure 186. Salmon River at Whitebird SWAT model catchments without wildfire areas.

Land Cover Areas in Salmon River at Whitebird SWAT Model			
NLCD 2006 Land Cover	SWAT Class	Area sq. mi.	Area percent
Forest-Evergreen	FRSE	7,078	52.87
Range-Brush	RNGB	3,625	27.08
Range-Grasses	RNGE	2,212	16.52
Other		473	3.53
Total		13,387	100

Table 10. Land cover areas in the SWAT model of Salmon River at Whitebird.

Fire affected area was included in a second 30-year simulation of sediment yield in the SRWB subbasin. A grid of the fire perimeter area for the period 2001-2010 was merged with the NLCD2006 grid to produce a composite land cover grid shown in Figure 187. A SWAT land use type for fire area in forestland and rangeland was defined based on the land use type for evergreen forest (FRSE). The only change to the FRSE type was to increase the cover and management factor (USLE_C) from 0.001 to 0.01. For comparison, a C value of 0.01 is one third of the pre-defined value for winter wheat and so represents a more exposed soil condition. With inclusion of fire-affected land cover, the simulated sediment yield for the SRWB subbasin for the 30-year period was 0.24 ton/ac/yr, which is 12 percent more than the measured sediment yield. This reasonable agreement between the simulated and measured values of long-term sediment yield shows that the SWAT model is capable of reproducing water and sediment yield with sufficient accuracy to characterize the response of the Lower Granite sediment yield basin to changes in fire-affected area and climate. However, considerable more work would be necessary to accurately simulate annual and event sediment yields.

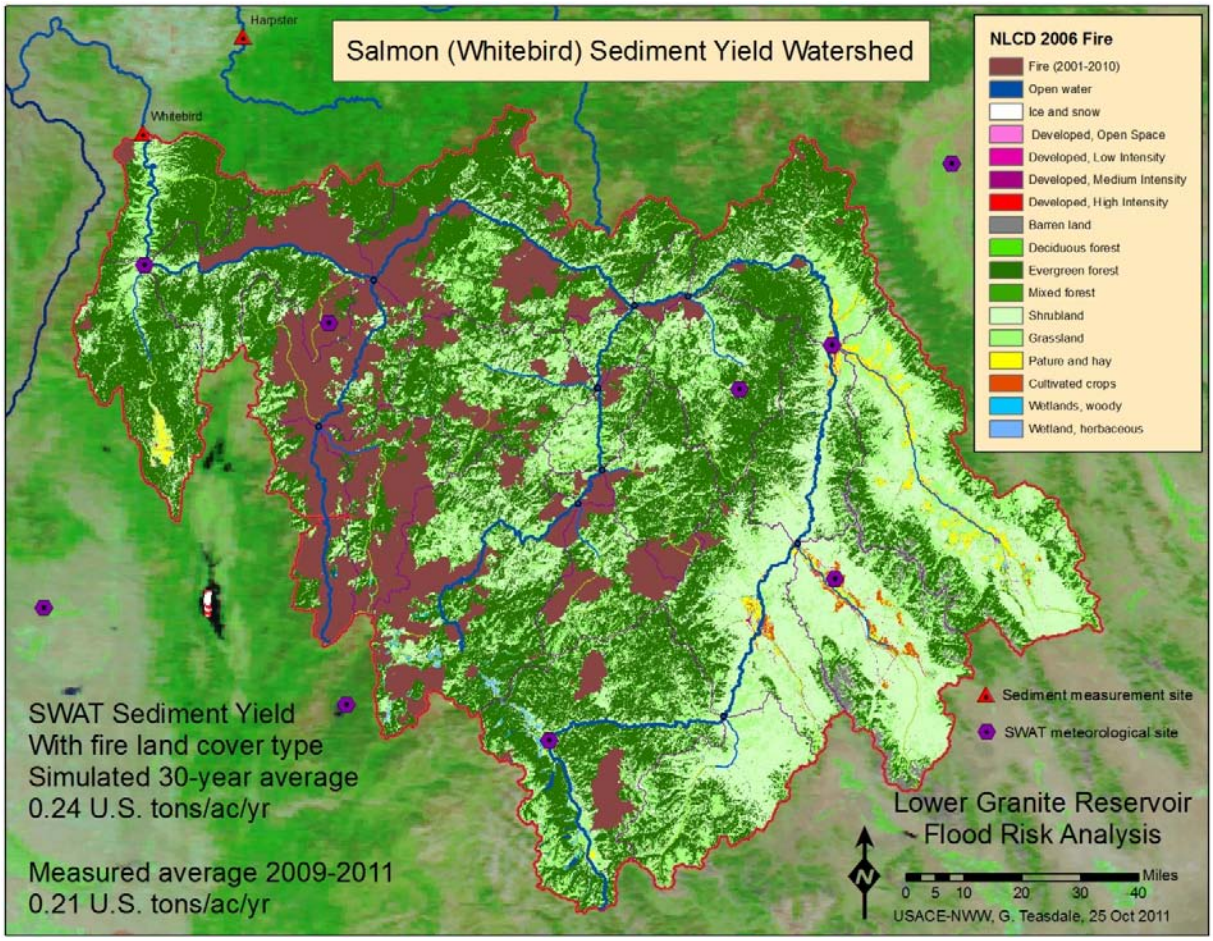


Figure 187. Salmon River at Whitebird SWAT model catchments with wildfire areas.

18.5.2. Selway River Subbasin SWAT model

A SWAT model of the Selway River subbasin was developed using procedures similar to those described for the Salmon River at Whitebird subbasin. Sediment yield from a 30-year simulation without fire-affected area included in the land cover was 40 percent less than the 0.10 ton/ac/yr measured during 2009-2011. Simulated water yield was 11 percent greater than the measured yield (26.2 in) at the USGS stream gage on the Selway River. Slight adjustments were made to the SWAT climate parameters to better represent higher elevation conditions. When fire-affected area was included, the simulated sediment yield matched the measured sediment yield. As with the SRWB subbasin model, the crop and management factor (USLE_C) for the fire land use type was 0.01. No other changes were made to the land use parameters.

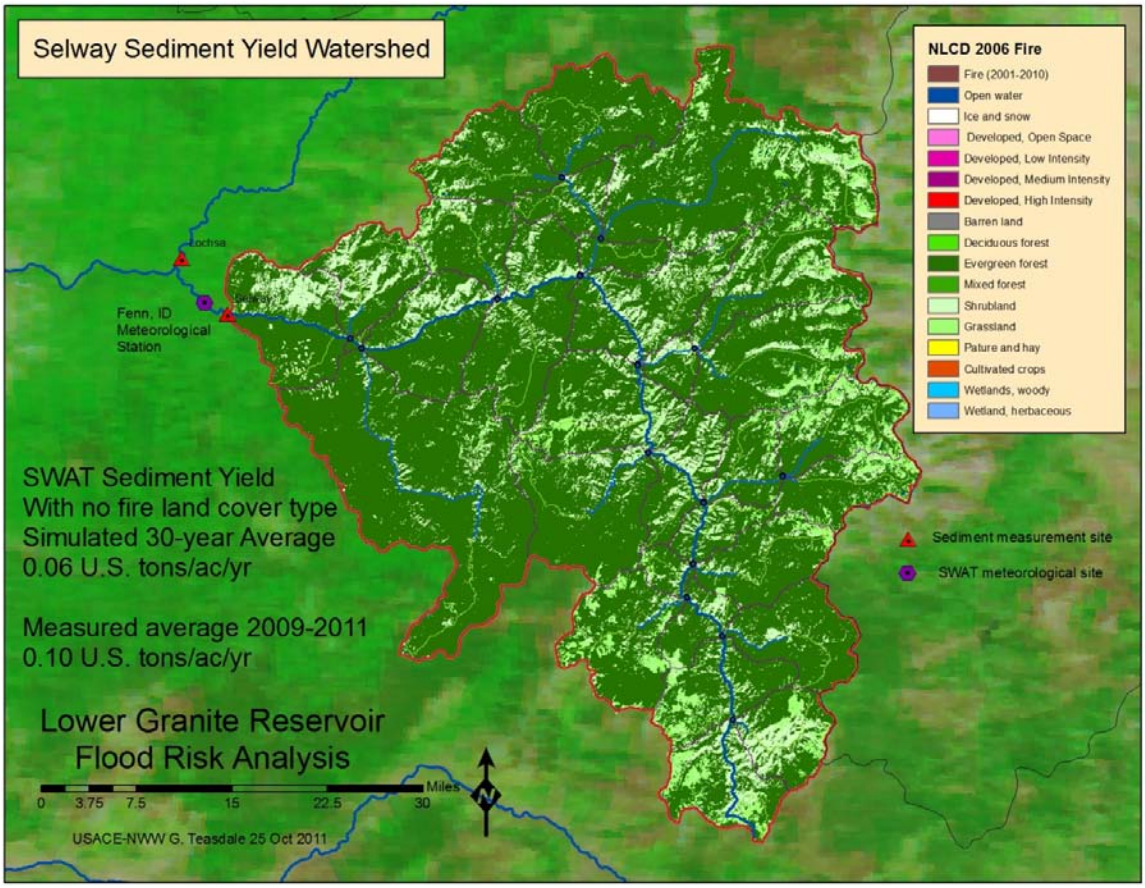


Figure 188. Selway River subbasin SWAT model catchments without wildfire areas.

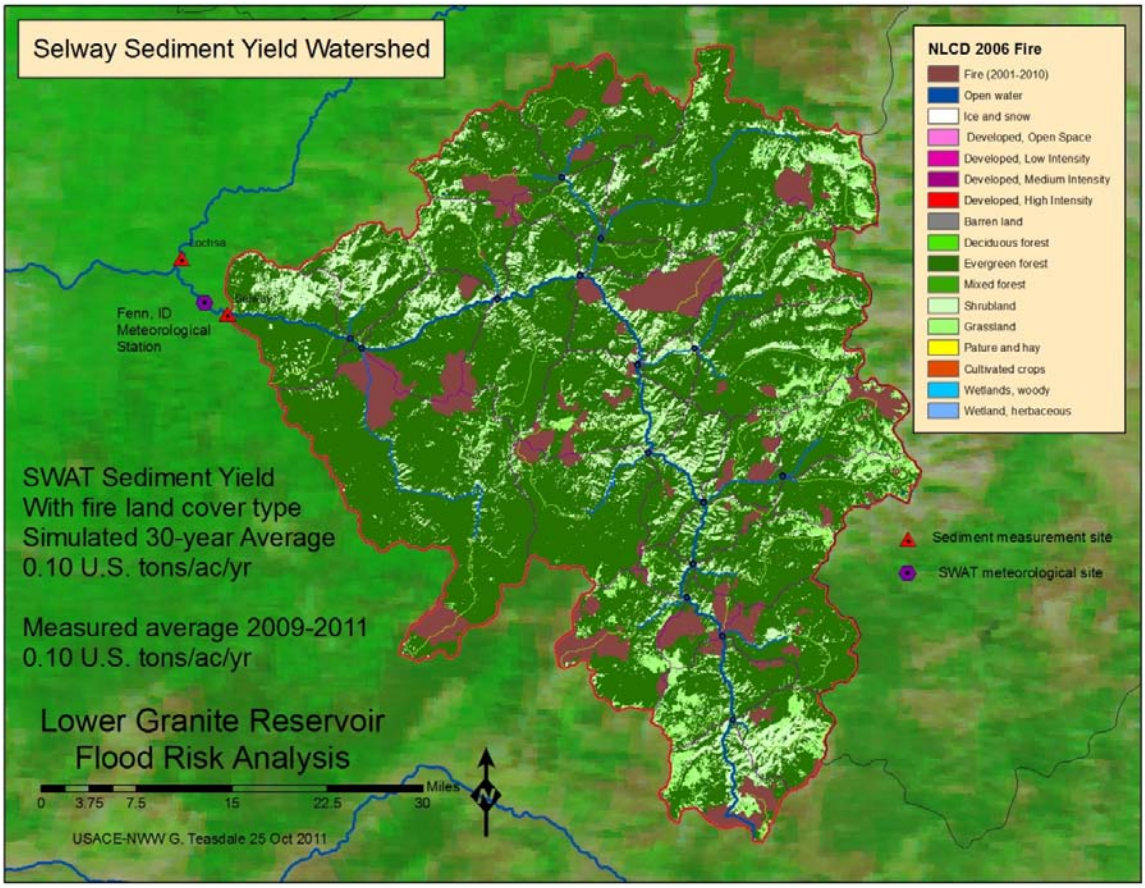


Figure 189. Selway River subbasin SWAT model catchments with wildfire areas.

18.5.3. Potlatch River Subbasin SWAT Model

The Potlatch River basin has substantial areas of forestland and cultivated agricultural land. There are 25 catchments in the SWAT model of the Potlatch subbasin shown in Figure 190. Land use in the Potlatch subbasin based on the NLCD2006 is 51 percent forestland; 11 percent shrubland; 10 percent pasture; 17 percent cultivated agriculture comprised of winter wheat, spring wheat and field peas; and about 11 percent other land cover types. Land cover areas are summarized in Table 11. There is no mapped fire area in the Potlatch basin in the historic fire perimeter data.

The 30-year average sediment yield was simulated for the Potlatch subbasin. Simulated water yield was 18 percent greater than the 8.85 inch water yield measured at the USGS stream gage on the Potlatch River. The stream gage was established in 2003, so the measured water yield is based on a relatively short gage record. The simulated sediment yield is 0.23 tons/ac/yr, which is 8 percent less than the 0.25 tons/ac/yr measured during 2009-2011. No adjustments were made to the SWAT pre-defined land use parameters, except that the supporting conservation practice factor (USLE_P) for winter wheat and spring wheat were change to 0.7 and the filter width,

which represents vegetation buffers, was specified at 5 m (16 ft). These changes were made to represent the effect of soil conservation practices in the basin.

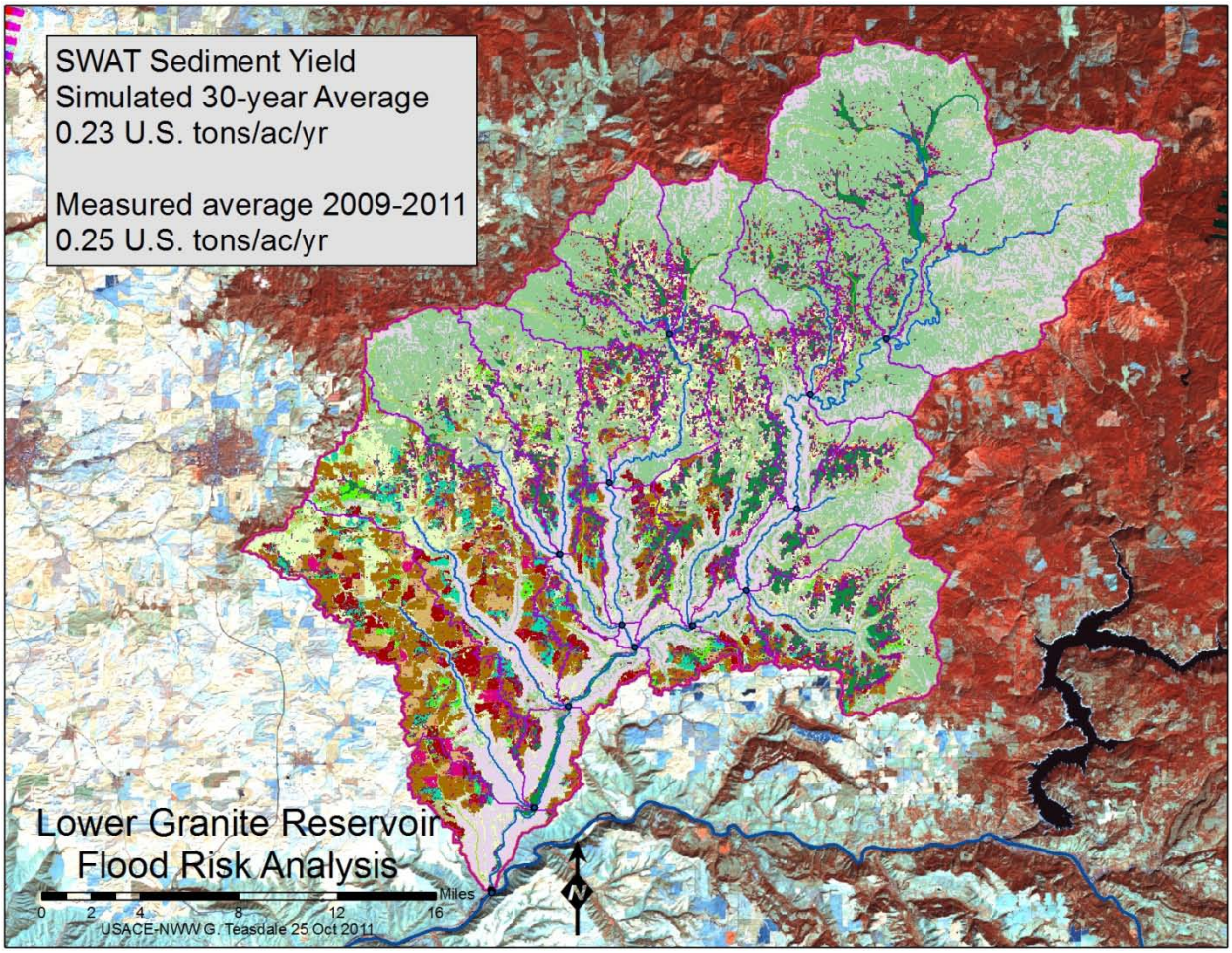


Figure 190. Potlatch River subbasin SWAT model catchments.

Land Cover Areas in Potlatch River SWAT Model			
NLCD 2006 Land Cover	SWAT Class	Area sq. mi.	Area percent
Forest-Evergreen	FRSE	305	51.38
Range-Brush	RNGB	64	10.76
Pasture	PAST	61	10.34
Winter Wheat High Residue	WWHR	55	9.35
Field Peas	FPEA	25	4.17
Range-Grasses	RNGE	19	3.24
Spring Wheat	SWHT	18	3.03
Other		46	7.73
Total		593	100

Table 11. Land cover areas in the SWAT model of the Potlatch River basin.

18.5.4. Other Subbasin SWAT Models

Sediment yield models were developed for other main subbasins in the lower Snake River and Clearwater River basins. Model development procedures were similar to those described above. The sediment yield models were calibrated to the measured sediment loads without having to make extraordinary adjustments to the SWAT meteorology and land use parameters. Results of 30-year simulations are summarized in Table 12. In general, when fire-affected area is included in the land cover parameterization the SWAT subbasin models simulate long-term sediment yield reasonably well with only small adjustments of land use parameters. The 20 percent accuracy objectives were met except for the Lochsa River and the Harpster and Stites subbasin models for the South Fork of the Clearwater River. The accuracy of these models can likely be improved with further refinement of the hydrology and land use parameters. Additional subbasin models may be developed in future work for the PSMP as funding becomes available.

Watershed	Area Mi^2	Measured Sediment Yield U.S. tons ac^{-1} yr^{-1}	Simulated Sediment Yield U.S. tons ac^{-1} yr^{-1}	Error	Actual Water Yield in	Simulated Water Yield Error Percent	Forestland Fire Area (2001-2010) mi^2	Conservation Practice Adjustment for WWHR and SWHT		
								CN2	USLE P	Filter W (m)
Asotin[1]	326	0.08	0.08	0%	4.0	16.3%		75	0.6	10
Palouse-Hooper	1,940	0.42	0.45	7%	4.1	2.8			0.7	2
Selway	1,904	0.10	0.10	0%	26.3	-9.6%	185			
Lochsa	1,130	0.08	0.20	150%	33.0	-36.2%	115			
Potlatch	593	0.25	0.23	-8%	8.85	17.9%			0.7	5
Salmon Whitebird	13,387	0.21	0.24	14%	10.9	-17.2%	2,105			
SF Clearwater Harpster	870	0.09	0.06	-33%						
SF Clearwater Stites	1,163	0.08	0.12	50%	11.7	23.5%		70	0.6	5
Lapwai[2]	269		0.21		3.9	6.7%			0.7	0
Tucannon	504		0.13		4.6	-6.5%				

[1] Asotin sediment measured as total suspended solids (TSS)
[2] Diversion for irrigation above gage.

Table 12. Summary of other initial SWAT subbasins models in the lower Snake and Clearwater River basin.

18.6. Effect of Increased Fire Area in the Salmon River Basin

Increased area of fire-affected land cover would be expected to increase the sediment yield in the Salmon River basin. It is plausible that the fire-affected area could expand to the remaining forestland and shrubland that has moderate to high cover density and high relative likelihood of fire. Expected fire-affected areas were identified in Salmon River basin as grid cells that had greater than 50 percent cover for the forest and shrub class in Landfire EVC grid and had a greater than 50 percent relative likelihood of wildfire in the Parisien et al. full-model grid. With this criteria, the fire-affected area increased from 16 percent to 22 percent of the SRWB subbasin and the 30-year average sediment yield increased from 0.21 ton/ac/yr to 0.31 ton/ac/yr, a 48

percent increase. The resulting land cover grid for the SRWB SWAT subbasin model is shown in Figure 191.

This simulation of the effect of increase fire-affected area on sediment yield is likely conservative. As vegetation recovers in older fire-affected areas, the exposure to surface erosion decreases. Wildfire will eventually affect all the areas identified, but the annual rate of increase in fire-affected area may be offset by the recovery of previously burned areas so that annual sediment yield remains relatively constant. This benign projection seems less plausible given the recent history of fire in the Lower Granite sediment yield watershed. The 2012 Mustang Complex fire and Sheep fire in Figure 184 are in areas outside the classified as having high fire potential in Figure 191, indicating that rating scheme may be too simple.

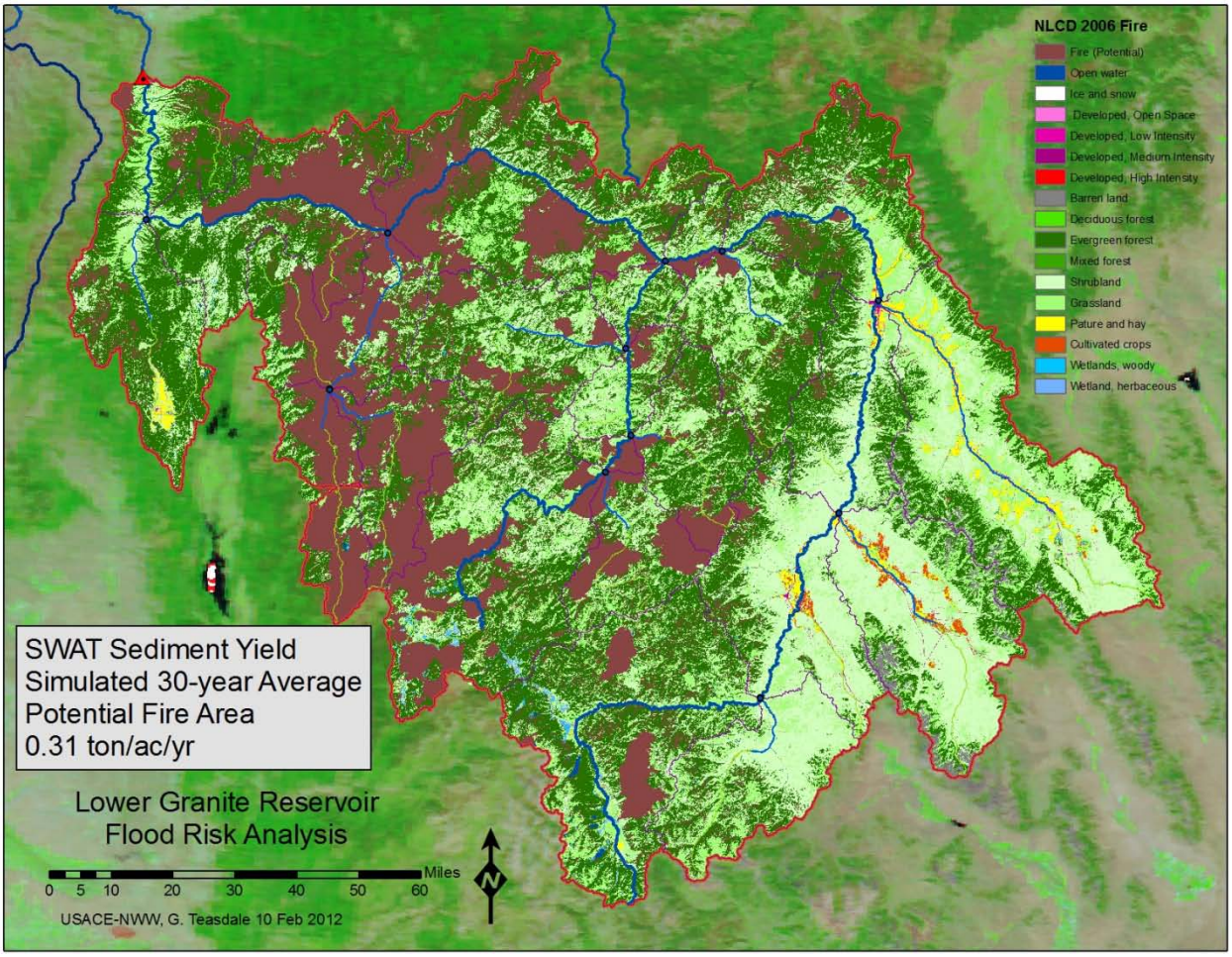


Figure 191. Salmon River at Whitebird SWAT model catchments with potential wildfire areas.

18.7. Effect of Climate at Year 2060 on Sediment Yield

The potential effect of climate change on sediment yield in the Lower Granite basin was characterized with the aid of the GFDL climate projections[51]. Monthly grids of precipitation, minimum temperature and maximum temperature for the years 2056 to 2065 were aggregated to produce a 10 year average of monthly and annual values that centered on year 2060. The average annual grids of current (1971-2000) normal precipitation and temperature were extracted from grids developed by the PRISM group[48] for the U.S. Using GIS methods, the basin average annual precipitation and temperatures were derived for each of the HUC8 subbasins in the Lower Granite sediment yield watershed and for the main river basins. The differences between the projected and current precipitation and temperatures are summarized in Table 13. The values in Table 13 agree with recent descriptions of expected climate trends in the Pacific Northwest[68].

As noted above, a warming climate will likely increase the extent of fire-affected area. According to the GFDL model, total annual precipitation in the Lower Granite sediment yield watershed will not change substantially. With the warming trend, proportionally more precipitation will occur as rainfall upon a land surface that is less protected by vegetative cover and snowpack resulting in increased sediment yield. Snowpack and snowmelt regimes will change as a result of both climate warming and loss of vegetative cover. Simulation of these changes will require refined meteorological parameterization and more detailed subbasin parameters than those currently in the initial subbasin models discussed above. This more detailed modeling may be pursued in future work for the PSMP as funding becomes available.

Summary of GFDL Climate Change at Year 2060 for Lower Snake and Clearwater River Basin								
	Precipitation		Temperature Minimum		Temperture Maximum		Temperature Average	
	Difference 2060-2010		Difference 2060-2010		Difference 2060-2010		Difference 2060-2010	
Basin	mm	Percent	°C	Percent	°C	Percent	°C	Percent
Salmon River	17.8	1.7%	-0.68	45%	6.68	66%	3.00	93%
Clearwater River	-53.2	-6.0%	1.38	51%	7.09	59%	4.23	74%
Grande Ronde River	8.5	-0.06%	0.53	201%	6.96	54%	3.74	57%
Lower Granite	-1.6	-0.6%	0.18	62%	6.92	62%	3.55	80%
Year 2010 defined as average precipitation and temperature for years 1970 - 2001								

Table 13. Summary of year 2060 GFDL climate change projection for the lower Snake and Clearwater River Basin.

[68] RMJOC (2011) *Climate and Hydrology Datasets for Use in the River Management Joint Operating Committee (RMJOC) Agencies' Longer-Term Planning Studies Part IV – Summary*, River Management Joint Operating Committee, online http://www.bpa.gov/power/pgf/ClimateChange/Final_PartIV_091611.pdf.

THIS PAGE INTENTIONALLY LEFT BLANK